The petrology and geochemistry of the Igaliko Dyke swarm, south Greenland.

Pearce, Nicholas John Geoffrey

THE PETROLOGY AND GEOCHEMISTRY

OF THE

IGALIKO DYKE SWARM,

SOUTH GREENLAND.

VOLUME 1

N. J. G. PEARCE, BSc., FGS.

A thesis submitted for the degree of
Doctor of Philosophy, at
The Department of Geological Sciences
Durham University
February 1988

ABSTRACT

The dykes from the Igaliko Nepheline Syenite complex belong to at least 3 individual swarms (i) a Mid-Gardar swarm in the Østfjordsdal valley, (ii) a Late-Gardar, Si-oversaturated swarm associated with the Younger Giant Dykes of Tugtutôq and (iii) a Si-undersaturated swarm intimately associated with the Late Gardar Igaliko Nepheline Syenite Central Complexes. In addition Early Gardar activity is recorded by the presence of some ultramafic lamprophyres which predate the Motzfeldt centre, sparse trachytes which are truncated by intrusions within the Motzfeldt centre and a possible BD_0 dolerite which is also cut by the Motzfeldt centre. Most dykes however are bracketed between the Early and Late Igdlerfigssalik syenite intrusions.

The main oversaturated and undersaturated suites can be separated on their Zr/Nb ratios ($\approx$6.4 and 3.9 respectively). In addition, the undersaturated basic rocks have smooth chondrite normalised incompatible element spidergrams whereas the oversaturated basic rocks are characterised by negative Nb and positive P anomalies.

Evolution of both suites can be modelled in terms of fractional crystallisation of feldspar, clinopyroxene, olivine, apatite and opaques from basaltic parents to either phonolitic or rhyolitic minimum compositions. In each instance these evolved compositions are extremely rich in incompatible trace elements (REE, Nb, Zr, Rb).

In some cases a high CO_2 content in the undersaturated rocks may lead to the formation (by liquid immiscibility) of late stage carbonatite magmas. High CO_2 also produces high fo_2 in these magmas and it is argued that in some cases this can suppress the development of negative Eu anomalies on feldspar fractionation.

The undersaturated swarm may have evolved from lamprophyric parental magmas, eg. camptonites, which are relatively abundant basic dykes. Ultramafic lamprophyres, often early, may have formed as extremely small degree partial melts at the onset of Gardar rifting. In the Late Gardar, magma genesis is related to the different extensional tectonic regimes which were operative at that time.

Mineralogical evolution follows paths similar to several other Gardar suites and records a higher fo_2 in the undersaturated rocks. Zr becomes concentrated in interstitial residual liquids in benmoreites and substitutes into amphibole as the newly proposed end-member zirconian-arfvedsonite.

CONTENTS

Abstract	i
Contents	ii
Copyright	vi
List of Tables	vii
List of Figures	ix
List of Plates	xiii
Acknowledgements	xvi
SECTION 1: INTRODUCTION AND STRUCTURE	
CHAPTER 1:INTRODUCTION	
1.1: General Features	1
1.2: Gardar Geology	2
1.3: History of Research	5
1.4: Aims	8
1.5: Sampling and Mapping	9
CHAPTER 2: STRUCTURE	
2.1: Introduction	11
2.2: Faulting	11
2.3: Gardar Rift Setting	11
2.4: Tectonic Setting	13
2.5: Dyke Morphology	15
2.6: Strikes	16
2.7: Stratigraphy	18
2.8: Fingered Sheets and Echelon Cracks	22
2.9: Igaliko Dyke Features	24
2.10: Internal Features	28
2.11: Crustal Extension	34
SECTION 2: ROCKS OF COMPOSITIONS RANGING FROM BASALT TO PHONOLITE AND RHYOLITE	
CHAPTER 3: PETROGRAPHY	
3.1: Introduction	35
3.2: Giant Dyke and possible BD_0	35
3.3: Basalt and Dolerite	37
3.4: Hawaiite and Mugearite	38
3.5: Benmoreite	40
3.6: Phonolites	44
3.7: Quartz Porphyries	47
3.8: Syeno-gabbros and 'Late' Dolerites	47
3.9: Sperulitic Trachytes, Quenched and Glassy Rocks	49
3.10: Rhomb Porphyries	50
3.11: Trachytes *(s.s)* and Trachy-andesites	37
3.12: Summary	52

CHAPTER 4: MINERALOGY

4.1: Introduction 54

4.2: Pyroxenes 55

4.2.A: General 55

4.2.B: Recalculation, Nomenclature and Projection 55

4.2.C: Site Occupancy 57

4.2.D: Pyroxene Variation 58

4.2.E: Minor Element Variation 60

4.3: Olivine 63

4.3.A: General 63

4.3.B: Compositional Variation 64

4.4: Amphiboles 65

4.4.A: General 65

4.4.B: Recalculation and Classification 66

4.4.C: Amphibole Chemistry 69

4.4.D: Recrystallisation 73

4.5: Biotite 74

4.5.A: Introduction 74

4.5.B: Chemical Variation 75

4.6: Fe-Ti oxides 77

4.7: Nephelines 78

4.7.A: Introduction 78

4.7.B: Compositional Variation 79

4.8: Feldspars 81

4.8.A: General 81

4.8.B: X-ray Studies 81

4.8.C: Compositional Variation 86

4.8.D: Comparison with Central Complex Feldspars 90

4.8.E: Sub-solidus Unmixing 91

4.9: Sodalite 94

4.10: Analcite 95

4.11: Cancrinite 96

4.12: Sphene 98

4.13: Other Minerals 99

Chlorite 99

Scapolite 99

Gieseckite 100

'Glass' 101

Pseudoleucite 102

Garnet 103

Sundries 103

4.14: Mineral - Mineral Geothermometers 103
4.14.A: Fe-Ti Oxide 103
4.14.B: Olivine - Clinopyroxene 104
4.14.C: Nepheline - Alkali Feldspar 105
4.14.D: Conclusions 106
4.15: Brief Conclusions from Mineralogical Evolution 108
CHAPTER 5: GEOCHEMISTRY
5.1: Introduction 110
5.2: Classification and Presentation of Data 110
5.3: Element Variation 112
5.4: K/Rb, Zr/Nb and Ce/Y 126
5.5: Magmatic Evolution 135
5.5.A: High Zr/Nb Suite 136
5.5.B: Liquidus Assemblages 137
5.5.C: Mineral Extract Calculations 138
5.5.D: Incompatible Element Variation 141
5.6: Low Zr/Nb Suite (excluding Østfjordsdal Swarm) 147
5.6.B: Liquidus Assemblages 149
5.6.C: Mineral Extract Calculations 149
5.6.D: Incompatible Element Variation 152
5.7: Further consideration of Incompatible Elements 156
5.8: Normative Mineralogy 162
5.9: Peralkaline Residua System and AFM 165
5.10: Mineralogical Differences 167
CHAPTER 6: RARE EARTH ELEMENT GEOCHEMISTRY
6.1: Introduction 169
6.2: Basaltic Rocks and 'Mantle Metasomatism' 171
6.3: Tephrites/Basanites 179
6.4: Intermediate Rocks 181
6.5: Benmoreites 182
6.6: Trachytes 185
6.7: Phonolites 186
6.8: Igdlerfigssalik Syenite 6 187
6.9: Conclusions 187
SECTION 3: OTHER OCCURRENCES
CHAPTER 7: CARBONATITES
7.1: Introduction and Field Occurrence 189
7.2: Petrography 190
7.3: Mineralogy 193
7.3.A: Pyroxene 193
7.3.B: Phlogopite 194
7.3.C: Oxides 196
7.3.D: Amphibole 197

7.3.E: Garnet 197
7.3.F: Chlorite 198
7.3.G: Olivine 198
7.3.H: Perovskite 199
7.3.I: Partially analysed minerals 199
Carbonates 199
Apatite 201
Fluorite 202
Allanite 203
Baryte 204
REE Minerals 204
7.3.J: Mineralogical Conclusions 205
7.4: Geochemistry 205
7.4.A: Introduction 205
7.4.B: Chemical Variation 206
7.4.C: Incompatible Element Variation 208
7.5: Models of Carbonatite Petrogenesis 209
7.6: Geochemistry, REE and Petrogenesis 215
7.7: Melting Studies 220
CHAPTER 8: LAMPROPHYRES
8.1: Introduction 221
8.2: Petrography 224
8.2.A: Alkaline Lamprophyres (AL) 224
8.2.B: Calc-alkaline Lamprophyres (CAL) 225
8.2.C: Ultramafic Lamprophyres (UML) 228
8.2.D: Breccia Dykes 231
8.3: Mineralogy 232
8.3.A: Pyroxenes 232
8.3.B: Amphiboles 235
8.3.C: Phlogopite/Biotite 236
8.3.D: Oxides and Sphene 238
8.3.E: Felsic Mineralogy 240
8.4.F: Garnet 242
8.4: Geochemistry 244
8.5: Conclusions and Occurrence 256
CHAPTER 9: ØSTFJORDSDAL DYKE SWARM
9.1: Introduction 259
9.2: Petrography and Field Occurrence 260
9.3: Mineralogy 266
9.4: Geochemistry 269
9.5: Conclusions 273
CHAPTER 10: BIG FELDSPAR DYKES
10.1: Introduction 274

10.2: Petrology 274
10.3: Geochemistry 276
10.4: Anorthosites – General Statement 279
10.5: Conclusions 280
CHAPTER 11: CONCLUSIONS
11.1: Introduction 283
11.2: Component Dyke Swarms 283
11.3: Chemical Evolution 285
11.4: Mineralogical Evolution 289
11.5: Significance of Carbonatites 290
11.6: Significance of Lamprophyres 292
11.7: Relationship of BFD's 294
11.8: Stratigraphy 294
11.9: Fault Geometry and Rifting 295
11.10: Rifting and Magma Genesis 296
11.11: Summary 299
REFERENCES 302

LIST OF TABLES

Table 2.7.1	Stratigraphy of the Igaliko Nepheline Syenite complex	21
Table 3.10.1	Range of Composition of some anorthoclase phenocrysts	51
Table 3.12.1	Summary mineralogy of the petrographic groups described in Chapter 3	53
Table 4.7.1	Nepheline equilibration temperatures from Hamilton (1961)	80
Table 4.8.1A	Alkali feldspar cell parameters	84
Table 4.8.1B	Alkali feldspar composition from 2θ $\bar{2}01$	84
Table 4.8.2	Temperature-distance variation from feldspar recrystallisation, dyke 58291-8	93
Table 4.13.1	Comparison of average 'glass' and whole rock major element compositions	101
Table 4.14.1	Temperatures calculated from olivine - clinopyroxene geothermometer of Powell and Powell (1978)	105
Table 4.14.2	Temperatures calculated from nepheline - alkali feldspar geothermometer of Powell and Powell (1977)	106
Table 5.3.1	Correlation coefficient matricies for major elements	119
Table 5.3.2	Basalt compositions – high Zr/Nb	121
Table 5.3.3A	Correlation matricies for trace elements – high Zr/Nb	127
Table 5.3.3B	Correlation matricies for trace elements – low Zr/Nb	128
Table 5.4.1	Number of analysed samples of different rock types with differing Zr/Nb ratios	131
Table 5.5.1	Average composition of TAS classified high Zr/Nb rocks – 2 pages	138
Table 5.5.2	Liquidus mineral assemblages calculated from Nathan and VanKirk (1978) model	139
Table 5.5.3	Results of mineral extract calculations – high Zr/Nb suite	140
Table 5.6.1	Average composition of TAS classified low Zr/Nb rocks – 2 pages	147
Table 5.6.2	Liquidus mineral assemblages calculated from Nathan and Van Kirk (1978) model	150
Table 5.6.3	Results of mineral extract calculations – low Zr/Nb suite	151
Table 5.7.1	Table of distribution coefficients for partial melting model	161
Table 6.1.1	REE concentrations (ppm) in chondrites commonly used for normalisation	170
Table 6.2.1	Distribution coefficients and other parameters used in melting/fractional crystallisation modelling	172
Table 7.3.1	Partial analyses of calcite – atoms per formula unit	200
Table 7.3.2	Partial anlayses of apatites from the carbonatite dykes (wt%)	202
Table 7.3.3	Partial analyses of allanite (wt%)	203
Table 7.3.4	Partial analyses of baryte from carbonatites (wt%)	205
Table 7.6.1	Average major and selected trace element data from carbonatite etc. (unscaled)	217
Table 8.1.1	Summary of major petrological contrasts between the four lamprophyre branches (excluding kimberlites), from Rock (1987a)	222
Table 8.1.2	Mineralogical classification of lamprophyres, excluding Lamproites	223
Table 8.3.1	Selected fassaite analyses from UML and AL	235
Table 8.3.1	Analyses of sphene from lamprophyres as atoms per 20 oxygens	240
Table 8.3.2	Cr-spinel anlayses from UML 325392	241
Table 8.3.3	Garnet analyses from 41906 as atoms per 12 oxygens	243

Table 8.4.1	Average lamprophyre compositions compared to averages from Rock (1987a)	248
Table 9.3.1	Andradite analyses from 326289	269
Table 9.4.1	Selected chemical analyses from Østfjordsdal phonolitic dykes	271
Table 10.3.1	Analyses of plagioclase xenocrysts from BFD's	277
Table 11.3.1	Major element ratios of average basic rocks from the Igaliko Dyke Swarm	286
Table 11.8.1	Cross-cutting relationships from analysed dykes	295

LIST OF FIGURES

		Follows Page
Figure 1.1.1	Geographical sketch map of the Igaliko -Narssarssuaq area.	1
Figure 1.2.1	General geological map of the Gardar Province	2
Figure 1.2.2	Geological sketch map of the Igaliko Nepheline Syenite complex.	2
Figure 2.3.1A	Geometry of experiments shearing clay blocks (from Wilcox *et al.* 1973)	12
Figure 2.3.1B	Shearing experiments: Geometry – Sanderson and Marchini (1984)	12
Figure 2.3.1C	Transtension shearing experiments: Geometry – Sanderson and Marchini (1984)	12
Figure 2.6.1	Histogram of strikes of Igaliko dykes	16
Figure 2.6.2	Orientation of major (E-W) Gardar faults	18
Figure 2.7.1	Geological sketch map of the Østfjordsdal area	19
Figure 2.7.2	Sketch map of dyke intersections,970m summit Narssarssuaq peninsula	20
Figure 2.7.3	Sketch map of dyke intersections, Lower Flink's Dal	20
Figure 2.7.4	View of Qôrqup Qâqai showing dykes in Giesecke's Dal fault zone	20
Figure 2.8.1	Schematic representation of fingered sheet (after Pollard *et al.* 1975)	23
Figure 2.8.2	'Geometry of parent and echelon cracks' (from Lutton 1971)	23
Figure 2.8.3	'Three-dimensional form of a segmented dyke' (from Delaney and Pollard 1981)	23
Figure 2.8.4A	Schematic representation of echelon cracks that grow along straight propagation paths	23
Figure 2.8.4B	Schematic representation of echelon cracks that grow along curved propagation cracks	23
Figure 2.9.1	Field sketches representing a sequence of increasing dilation	24
Figure 2.9.2A,B	Field sketch of dyke 326217	24
Figure 2.9.2C,D	Field sketch showing large scale echelon features	24
Figure 2.9.3	Field sketch of dyke at Storelv	25
Figure 2.9.4	Field sketch of dyke at Storelv	25
Figure 2.9.5A	'Geometry of fractures produced in shear zone (after Segall and Pollard 1980)	26
Figure 2.9.5B	Superimposition of left and right stepping echelon arrays on a regional echelon set	26
Figure 2.9.6A	R and P fractures in a fault zone (from Gamond 1983)	27
Figure 2.9.6B	Igaliko dyke ocupying R fracture	27
Figure 2.10.1	Relative magma viscosity vs. melt volume percent (from Arzi 1978)	29
Figure 4.2.1	Pyroxene nomenclature	55
Figure 4.2.2	Pyroxene trends in phonolites, Mg - Fe^{2+}+Mn - Na compared to Di-Hd-Ac	56
Figure 4.2.3	Variation of pyroxene composition (2 pages)	57
Figure 4.2.4	Comparison of pyroxene trends from Igaliko with other alkali rock suites	59
Figure 4.2.5	Pyroxene chemical variation against of Na-Mg –3 pages	60
Figure 4.3.1	Olivine analyses	63

Figure 4.4.1	Amphibole classifications – 2 pages (from Leake 1978)	68
Figure 4.4.2A	Al vs. Ca for amphiboles	68
Figure 4.4.2B	Part of Phillips (1961) amphibole classification	68
Figure 4.4.3	Amphibole chemical variation against Na^B - Al^T – 3 pages	69
Figure 4.4.4	Amphibole chemical variation	70
Figure 4.4.5A	Ti vs. Zr in amphiboles	71
Figure 4.4.5B	Magnesium number vs. Zr in amphiboles	71
Figure 4.4.6	Amphibole chemical variations	72
Figure 4.4.7	Amphibole chemical variation against distance from Igdlerfigssalik syenite in a metamorphosed dyke	73
Figure 4.5.1	Biotite variation from the Igaliko dykes	75
Figure 4.5.2	Biotite variation from the Igaliko dykes	76
Figure 4.6.1	Iron-titanium oxide analyses	77
Figure 4.6.2	Mn variation in iron-titanium oxides	77
Figure 4.7.1	Nepheline analyses on Hamilton (1961) gheothermometer	79
Figure 4.8.1	Feldspar nomenclature (after Smith 1974)	81
Figure 4.8.2A	Feldspar cell parameter bÅvs. cÅ	83
Figure 4.8.2B	Feldspars, 2θ $\bar{2}04$ vs. 2θ 060	83
Figure 4.8.3	Feldspar compositions – Ca-Na-K atomic% – 2 pages	86
Figure 4.8.4	Zoning within feldspar phenocrysts – Ca-Na-K atomic%	87
Figure 4.8.5	Feldspar, nepheline and whole rock data in Petrogeny's residua system – 2 pages	88
Figure 4.8.6	Ba and Fe in feldspars vs. Ca-K	89
Figure 4.8.7	Alkali feldspars from recrystallised phonolite plotted on 2 feldspar solvus	92
Figure 4.9.1	Sodalite and analcite chemical variation	94
Figure 5.2.1A	TAS classification (Cox *et al.* 1979)	111
Figure 5.2.1B	TAS classification (Le Bas *et al.* 1986)	111
Figure 5.2.1C	TAS plot of Igaliko analyses	111
Figure 5.3.1	Major elements vs. Fractionation Index – 3 pages	112
Figure 5.3.2	SiO_2 wt% vs. Molecular $Na_2O/(Na_2+K_2O)$ – alkali loss	115
Figure 5.3.3	Trace elements vs. F.I. – 6 pages	119
Figure 5.3.4	Trace elements vs. F.I. – 2 pages	119
Figure 5.3.5	Ba vs. Ce, samples with MgO>3.0 wt%	122
Figure 5.4.1	K_2O wt% vs. Rb ppm	129
Figure 5.4.2	Histograms of Zr/Nb data	130
Figure 5.4.3A	Histogram of F.I., low and high Zr.Nb suites	132
Figure 5.4.3B	Histogram of F.I., Tugtutôq-Ilímaussaq dykes (from Martin 1985)	132
Figure 5.4.4	Zr vs. Nb	133
Figure 5.4.5	Zr/Nb vs. Nb for selected basaltic rocks	134
Figure 5.5.1	Chondrite normalised incompatible element 'spidergrams' – high Zr/Nb basaltic rocks	141
Figure 5.5.2	Chondrite mormalised incompatible element 'spidergrams' – all average groups of high Zr/Nb dykes	141

Figure 5.6.1	Histograms of Zr/Nb from South Qôroq and Motzfeldt centres	148
Figure 5.6.2	Chondrite normalised incompatible element 'spidergrams' – all average low Zr/Nb dykes	152
Figure 5.7.1	Incompatible element variation – 4 pages	156
Figure 5.7.2	Nb/Y vs. Nb, Zr/Y vs. Zr, La/Y vs. La, Nb/Zr vs. Nb – 4 pages	158
Figure 5.7.3	Histograms of ratios of incompatible elements	159
Figure 5.7.4	Zr/Nb vs. Ce/Y	160
Figure 5.8.1	'Exploded norm' diagrams (*Ne - Di - Ol - Hy - Qz*) – 2 pages	163
Figure 5.8.2	Normative *Ne - Ks - Qz*, Petrogeney's Residua System – 2 pages	164
Figure 5.9.1	Peralkaline residua system – 2 pages	165
Figure 5.9.2	A–F–M diagrams	167
Figure 5.10.1	Na-Mg vs. Mg (atoms per 6 oxygens) in pyroxenes	168
Figure 6.1.1	Ce ppm vs. $(La/Lu)_{cn}$	169
Figure 6.1.2	$(Gd.Lu)_{cn}$ vs. $(La/Sm)_{cn}$	170
Figure 6.2.1	Chondrite normalised REE 'spidergrams' – basaltic rocks, high Zr/Nb	171
Figure 6.2.2	Chondrite normalised REE 'spidergrams' – picrites and late basalt low Zr/Nb	176
Figure 6.2.3	Chondrite normalised REE 'spidergrams' – alkali gabbro, high Zr/Nb	177
Figure 6.3.1	Chondrite normalised REE 'spidergrams' – tephrite, basanite and camptonite	179
Figure 6.4.1	Chondrite normalised REE 'spidergrams' – intermediate rocks	181
Figure 6.5.1	Chondrite normalised REE 'spidergrams' – benmoreites, high Zr/Nb	182
Figure 6.5.2	Chondrite normalised REE 'spidergrams' – benmoreites, low Zr/Nb – 2 pages	183
Figure 6.5.3	Eu/Eu^* vs. $(Sr/Ce)_{cn}$	184
Figure 6.6.1	Chondrite normalised REE 'spidergrams' – trachytes, high Zr/Nb	185
Figure 6.6.2	Chondrite normalised REE 'spidergrams' – trachytres cut by Motzfeldt foyaite	185
Figure 6.7.1	Chondrite normalised REE 'spidergrams' – phonolites	186
Figure 6.8.1	Chondrite normalised REE 'spidergrams' – Igdlerfigssalik Syenite 6	187
Figure 7.3.1	Pyroxene anlyses from carbonatite dykes	194
Figure 7.3.2	Mica compositions from carbonatites – 2 pages	195
Figure 7.3.3	$Fe^{2+}+Fe^{3+}$ vs. Mn in magnetites	196
Figure 7.3.4	Olivine compositions from carbonatite 41958	196
Figure 7.4.1	Carbonatite whole rock analyses	206
Figure 7.4.2	Carbonatite geochemistry vs. SiO_2 – 3 pages	206
Figure 7.4.3	Chondrite normalised REE 'spidergrams' for all carbonatites – 3 pages	208
Figure 7.5.1A	Average carbonatite dyke compositions based on TAS classification	212
Figure 7.5.1B	2-liquid field (Freestone and Hamilton 1980)	212
Figure 7.5.2	Distribution coefficients – 2 pages	213
Figure 7.5.3A,B	Distribution coefficient	214
Figure 7.5.3C	REE partitioning (Wendlandet and Harrison 1980)	214
Figure 7.6.1	Chondrite normalised REE 'spidergrams' – carbonatites – 2 pages	216

Figure 7.6.2	Chondrite normalised REE 'spidergrams' – carbonatites compared to phonolites and UML	218
Figure 8.3.1	Lamprophyre pyroxene compostions	232
Figure 8.3.2	Pyroxenes from lamprophyres cf. fields from Rock (1987a)	232
Figure 8.3.3	Pyroxenes from lamprophyres – Ti and Al vs. $Fe^{2+}/Fe^{2+}+Mg$	233
Figure 8.3.4	Zoning in pyroxenes from AL 325943	234
Figure 8.3.5A	Calcic amphibole compositions from lamprophyres	235
Figure 8.3.5B	Alkali amphibole compositions from lamprophyres	235
Figure 8.3.6	Amphibole composition from lamprophyres cf. fields from Rock (1987a)	235
Figure 8.3.7	Amphibole composition from lamprophyres – Mg-Fe+Mn-Na+K and Mg-Fe^{2+}+Mn-Ti	235
Figure 8.3.8	Mica composition from lamprophyres – Al^{iv} vs. Fe/Fe+Mg and Al^{iv} vs. Ti	236
Figure 8.3.9	Mica composition from lamprophyres	237
Figure 8.3.10	Mica composition from lamprophyres cf. fields from Rock (1987a)	237
Figure 8.3.11	Opaque oxide composition from lamprophyres	238
Figure 8.3.12	Feldspar composition from lamprophyres – Ca-Na-K atomic	240
Figure 8.4.1A	Major element variation from lamprophyres against MgO wt%	244
Figure 8.4.1B	Trace element variation from lamprophyres – 2 pages	244
Figure 8.4.2	Lamprophyre discriminant plots, based on major elements – 2 pages	246
Figure 8.4.3	Incompatible element variation in lamprophyres	247
Figure 8.4.4	Chondrite normalised REE 'spidergrams' – lamprophyres – 6 pages	247
Figure 8.4.5	Average lamprophyre compositions	251
Figure 8.4.6	REE 'spidergrams' – UML	252
Figure 8.4.7	REE 'spidergrams' – AL and CAL	254
Figure 8.4.8	REE 'spidergrams' – carbonatite/UML	255
Figure 8.4.9	REE 'spidergrams' – altered UML	256
Figure 9.2.1	Alkali feldspar exsolution textures from 326289	263
Figure 9.3.1	Østfjordsdal feldspars on 2-feldspar solvii at 1kb	267
Figure 9.4.1	A–F–M variation in Østfjordsdal dykes	271
Figure 9.4.2	Incompatible elemet variation from Østfjordsdal dykes – 2 pages	271
Figure 9.4.3	Chondrite normalised REE 'spidergrams' – Østfjordsdal phonolites and trachyandesite	272
Figure 10.3.1	Chondrite normalised REE 'spidergrams' – BFD	278

LIST OF PLATES

		Follows Page
Frontispiece	Dykes in Lower Flink's Dal	xvii
Plate 1.1	Aerial view across southern part of Igaliko Nepheline Syenite complex	1
Plate 2.1	View across Avanardleq, Motzfeldt centre, of dyke	25
Plate 2.2	Broken *bridge* in a spherulitic dyke	25
Plate 2.3	Narrow apophysis of dyke 326205-10	25
Plate 2.4	Lobate margin to dyke 236205-10	25
Plate 2.5	Shear zone crossing dyke 326205-10	25
Plate 2.6	Multiple dykes intruded into fault zone (325615)	25
Plate 2.7	Xenoliths of BFD material and syenite in microsyenite dyke	30
Plate 2.9	Disaggregating syenite xenolith in dyke 326502-10	31
Plate 2.10	Breccia dyke 41947, 326250	31
Plate 2.11	Drag folding in a dyke cutting the Østfjordsdal syenite	33
Plate 2.12	Drag fold in dyke 326322	33
Plate 3.1	63778, Alkali Gabbro Giant Dyke, XPL	36
Plate 3.2	325992, Dolerite, XPL	36
Plate 3.3	63845B, Recrystallised Basalt, XPL	37
Plate 3.4	43902, Syeno-gabbro, XPL	37
Plate 3.5	325986, Benmoreite, PPL	40
Plate 3.6	325986, Benmoreite, XPL	40
Plate 3.7	58294, Recrystallised Benmoreite, XPL	42
Plate 3.8	326331, Recrystallised Phonolite, XPL	42
Plate 3.8A	326207, Phonolite, PPL	44
Plate 3.8B	326207, Phonolite, XPL	44
Plate 3.9A	325928, Phonolite, PPL	45
Plate 3.9B	325928, Phonolite, XPL	45
Plate 3.10	325964, Porphyritic Phonolite, XPL	45
Plate 3.11	304022, Porphyritic Phonolite, XPL	45
Plate 3.12	63895, Quartz Porphyry, XPL	47
Plate 3.13	58139, Porphyritic Benmoreite, XPL	47
Plate 3.14	304034, Spherulitic Trachyte, XPL	49
Plate 3.15	58086, Spherulitic Trachyte, PPL	49
Plate 3.16	58051, Rhomb Porphyry, XPL	50
Plate 3.17	325931, Rhomb Porphyry, XPL	50
Plate 3.18	58063, Phonolite, XPL	50
Plate 3.19	Hand specimen of spherulitic trachyte	50
Plate 4.1	Margin of dyke 325923	102
Plate 4.2	Large pseudoleucites in phonolite.	102
Plate 7.1	Flow-banding in carbonatite dyke (54243/4, 326329)	191
Plate 7.2	Carbonatite/mica carbonatite dyke (326358/9)	191
Plate 7.3	Flow-banding in fluorite-carbonatite (325910)	191

Plate 7.4	Close up of surface of 325910 with fluorite cubes	191
Plate 7.5	Carbonatite/UML sill in Lower Flink's Dal (326258-60)	191
Plate 7.6	Hand specimen of 326333, fresh surface	191
Plate 7.7A	326333, Carbonatite, PPL	191
Plate 7.7B	326333, Carbonatite, XPL	191
Plate 7.8	326336, Carbonatite, XPL	191
Plate 7.9	326302, Carbonatite, XPL	191
Plate 7.10	326358, Carbonatite, XPL	191
Plate 7.11	326359, Mica-rich Carbonatite, XPL	191
Plate 7.12	325388, Fluorite-carbonatite, XPL	191
Plate 7.13	326395, Fluorite rock, PPL	191
Plate 7.14	Product of experimental run of 43802 and 325908 in 50-50 w/w mix	220
Plate 7.15	Product of experimental run of 43802 and 326333 in 50-50 w/w mix	220
Plate 8.1A	52285, Camptonite, PPL	224
Plate 8.1B	52285, Camptonite, XPL	224
Plate 8.2	326308, Camptonite, PPL	224
Plate 8.3	52274, Camptonite, XPL	224
Plate 8.4A	325943, Camptonite, hand specimen	224
Plate 8.4B	325943, Camptonite, PPL	224
Plate 8.5	43887, Minette, XPL	227
Plate 8.6A	326281, Vogesite, hand specimen	227
Plate 8.6B	326281, Vogesite, PPL	227
Plate 8.6C	326281, Vogesite, XPL	227
Plate 8.7A	326318, Vogesite, PPL	227
Plate 8.7B	326318, Vogesite, XPL	227
Plate 8.8	326301, Ultramafic Lamprophyre, hand specimen	229
Plate 8.9	326301, UML, PPL	229
Plate 8.10A	326303, UML, PPL	229
Plate 8.10B	326303, UML, XPL	229
Plate 8.11	326314, UML, PPL	229
Plate 8.12	326222, Altered Ultrabasic Lamprophyre, PPL	229
Plate 8.13	325960-1, Breccia Dyke, SW end of Motzfeldt Sø	231
Plate 8.14	41947, Breccia Dyke, Iganaq, XPL	231
Plate 9.1	326309, Recrystallised Phonolite, hand specimen	262
Plate 9.2	326275, Recrystallised Phonolite, XPL	262
Plate 9.3	326289, Recrystallised Phonolite	262
Plate 9.4	326289, Recrystallised Phonolite, XPL	262
Plate 9.5	Porphyritic Syenite, fresh surface	264
Plate 9.6	Porphyritic Syenite, weathered surface	264
Plate 9.7	52267, Porphyritic Syenite, XPL	264
Plate 9.8	Sheared Porphyritic Syenite	264
Plate 9.9	Alkali metasomatism at dyke margins	264
Plate 10.1	325901-3, BFD from Igaliko village	275

Plate 10.2	325901-3, BFD from Igaliko village	275
Plate 10.3	63828, BFD, XPL	275
Plate 10.4	325902, BFD, XPL	275
Plate 10.5	A selection of BFD including xenoliths/xenocrysts	275
Plate 10.6	325903, BFD	275
Plate 10.7	326370/304150, BFD, XPL	275
Plate 10.8	326370/304150, BFD, hand specimen	275

XPL or PPL indicates photomicrograph

ACKNOWLEDGEMENTS

I am very grateful to NERC for financing this research through grant GT4/83/GS/-17. At Durham I would like to thank Dr. C. H. Emeleus for introducing me to Gardar geology and for continued support and assistance throughout the course of this project. I would also like to thank Dr. A. Peckett who helped greatly with aspects of the mineralogy. Ron Hardy helped in explaining the running of the XRF for both major and trace element analyses and prepared/checked over the data used in the new trace element programs written during the course of this study. John Faithfull, Colin Bradshaw, Nick Smith, Simon Day and Chris Bedford provided interesting discussion on aspects of igneous petrology at various times. Richard England was kind enough to check through drafts of Chapters 2 and 6. Dr. Phil Leat helped out with some of the geochemistry. Use of facilities at Durham was made available by Professors J. F. Dewey and R. N. Thompson (who also provided some useful ideas on basalts) for which I am very grateful. Ron Lambert and George Randall expertly produced large numbers of thin and polished sections. Thanks are also due to Dave Schofield and Dave Asbery for sundry favours and to Paul Laverick for assistance in the Geochemistry Laboratory.

At Manchester I would like to thank Dr. C. M. B. Henderson who provided facilities for conducting XRD studies on some feldspars and helped with their interpretation. Tim Hopkins and Dave Plant provided electron-microprobe facilities at Manchester giving me a fairly free hand with the booking system. Bruce Kjaersgaard was good enough to carry out a few melting experiments on carbonatite - phonolite mixtures for me.

At Leicester I would like to thank Dr. Niel Hodgson (now at BP, Aberdeen), Nick Marsh and Adelaide Holmes for analysing the carbonatites for me, some of which they also prepared on my behalf. Nick Marsh also introduced me to REE separations for ICP and provided me with a 'shopping list' and assorted other information enabling me to set up a similar system at Durham. Thanks also to Bob Tarzey for accommodation in Leicester.

I am grateful to Dr. Nick Walsh and Alison Warren for instruction in the use of the NERC ICP at Kings College/Royal Holloway and Bedford New College.

Fieldwork in Greenland was carried out under the wing of GGU. Thanks are due particularly to Jorgen Lau, the basecamp manager for organising supplies etc. whilst we were in the field. The company of Tapsa, Lotte, Torsten, Gitte, Michael *et al.* in the field made 9 weeks in South Greenland more enjoyable than it could have been.

Finally, my deepest thanks to Fiona Smith for patiently typing, retyping and correcting Chapters 4 onwards and preparing/tidying up many of the diagrams: without her help this thesis would have taken considerably longer to complete.

FRONTISPIECE: A swarm of trachytic dykes cutting the easily weathered syenites of the Motzfeldt centre in Lower Flink's Dal.

SECTION 1: INTRODUCTION AND STRUCTURE

CHAPTER 1: INTRODUCTION

1.1: General Features.

The Igaliko Nepheline Syenite complex occupies an area of some 1000 square kilometres in the area to the east of Narssarssuaq airport (61° 10'N, 45° 26'W), south Greenland (figure 1). The complex comprises four major and a few minor (satellitic) nepheline syenite bodies and an associated dyke swarm of mid-Proterozoic (Gardar) age. These are intruded into basement granite (ca. 1760 Ma) and Gardar age supracrustal rocks (lavas and sediments).

The area is bounded to the north and east by the inland ice sheet. It is essentially a deeply dissected plateau cut by steep sided, glacial valleys, and fjords which open to the sea some 80 km to the south-west. Daunting cliffs up to 1400m in height bound these valleys, their bases clad in vast scree fans several hundred metres in height. The heights of the peaks in the area around Motzfeldt Sø, and farther inland towards the ice sheet, are remarkably uniform at about 1500m, with the ground to the south-west of the complex (around Igaliko village) becoming less rugged (see Figure 1.1.1).

The only settlements in the area other than small farms scattered along the shores of Tunugdliarfik are at Narssarssuaq airport; at Qagssiarssuk, the Viking settlement established by Erik the Red; and at Igaliko, an attractive fishing village at the head of Igaliko Fjord. Igaliko is the site of a former Norse cathedral and bishopric, Garður, now in ruins, which gave its name to the Gardar period of igneous activity in south Greenland.

A field season of 9 weeks was undertaken between late June and early September 1984 working in conjunction with the Greenland Geological Survey (GGU). Field work was centred on nine small camps of two to four people, established with the help of helicopters.

Summer weather conditions in south Greenland are similar to those of north-west Scotland in March. Clear, still daytime temperatures can reach ca. 20° C at low altitudes, with a drop to below freezing at night. Rain (or snow at high levels) and

Figure 1.1.1 Geographical sketch map of the Igaliko - Narssarssuaq area, showing the camp sites used during the 1984 field season.

1. Storelv
2. Lower Flink's Dal
3. Østfjordsdal
4. Igaliko (ca. 4 km north of Igaliko village)
5. Lejrelv
6. Narssarssuaq (north of river at Narssarssuaq)
7. 'Harry's Dal'
8. 'Hotel Motzfeldt' (south-west corner of Motzfeldt Sø)
9. 475 m lake, Mellemlandet

Figure 1.1.1

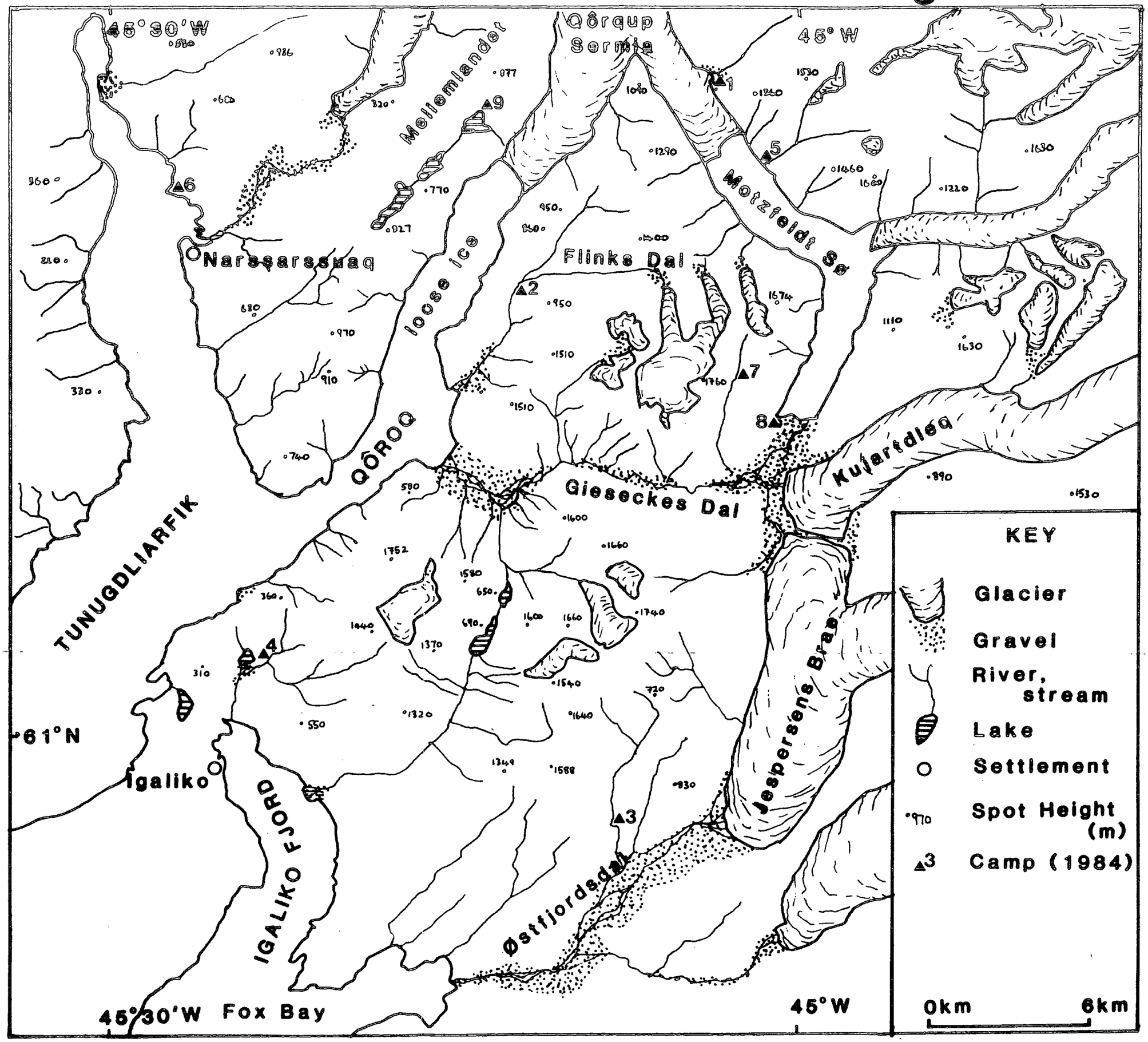
45°30'W
45°W
Qôrqup Sermia
Mellemlænder
Narssarssuaq
Flinks Dal
Motzfeldt Sø
loose ice
QÔROQ
Giesecke Dal
Kujarfdleq
TUNUGDLIARFIK
IGALIKO FJORD
Igaliko
61°N
Østfjordsdal
Jespersens Brae
Fox Bay
KEY
Glacier
Gravel
River, stream
Lake
Settlement
Spot Height (m)
Camp (1984)
0km
6km

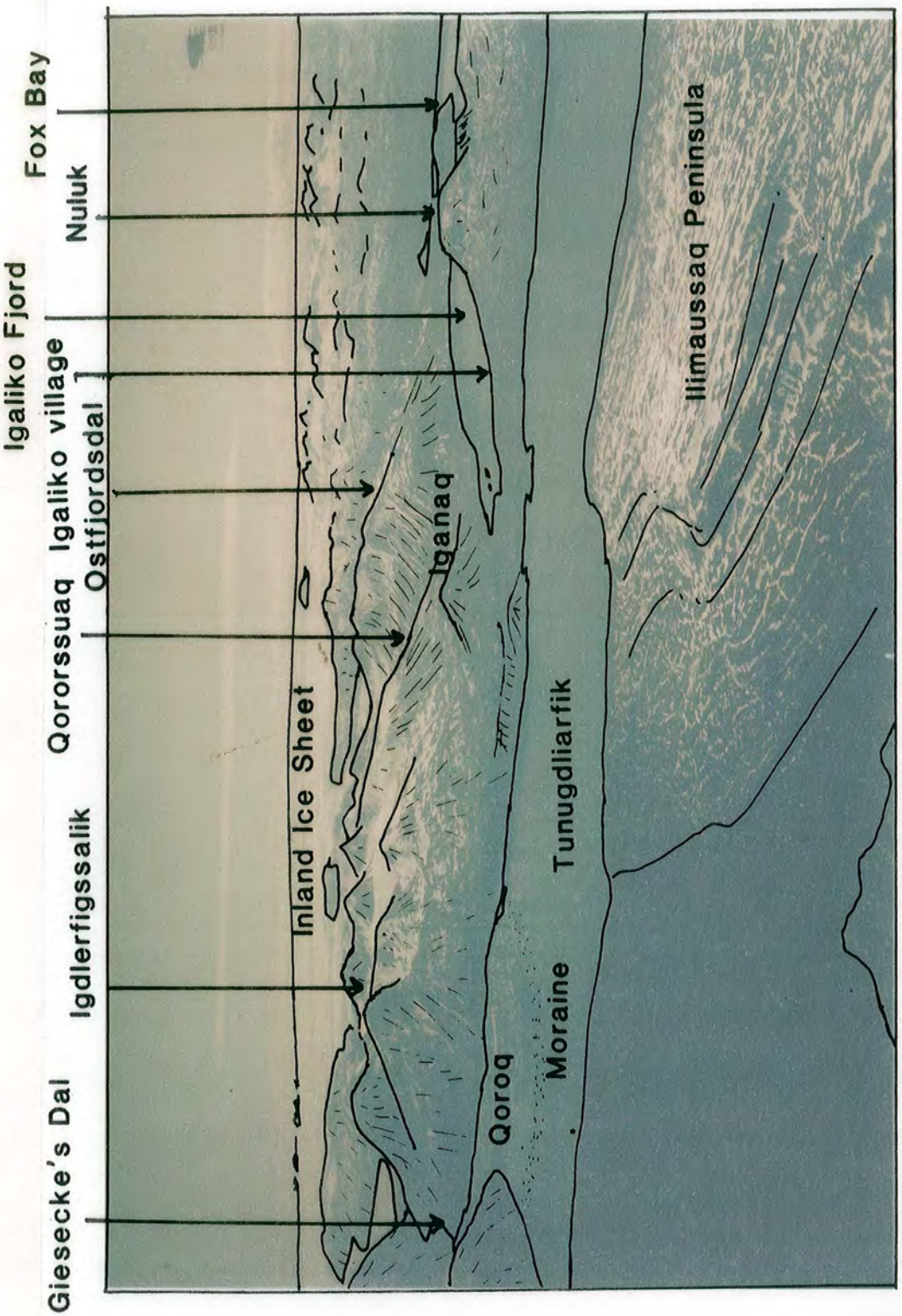

Plate 1.1 Aerial view across the southern part of the Igaliko Nepheline Syenite complex.

fog (low cloud) were common causing the loss of about half the working days in the field. Violent, warm winds (Föhn) occur as an area of high atmospheric pressure, which has built up over the inland ice sheet, empties into a depression approaching from the sea. These winds are unpredictable, springing up rapidly they can demolish even well prepared field camps. Fortunately they were infrequent during the summer of 1984.

Vegetation is scarce, especially on the syenites where the crumbly weathering of these rocks inhibits the formation of a soil. Where plants have been able to establish a hold, usually in sheltered niches or on leeward slopes, the vegetation consists of small arctic flowers (eg. gentians) and mosses; and stunted trees such as birch and willow. These trees tend to hug the ground although in rare cases they attain heights of up to 2 metres. Passage through this type of woodland is tortuous. Fauna is also, not surprisingly, scarce although several ptarmigan, arctic hares, an eagle, assorted species of small birds and a young arctic fox were seen.

1.2: Gardar Geology

The geology of the Gardar province has recently been summarised in a comprehensive account by Upton and Emeleus (1987) . This updates similar overviews of Gardar geology by Upton (1974) and Emeleus and Upton (1976) . Only a brief account of Gardar geology, with emphasis on parts of direct relevance to this thesis will be given here.

The evolution of the Gardar province is related to repeated episodes of continental rifting and the associated generation of large volumes of alkali basaltic magma starting at ca. 1350 Ma and continuing for about 200 million years. Three main cycles can be recognised, Early, Mid and Late Gardar, each of which commenced with the uprising of large quantities of alkali basalt or hawaiitic magma during periods of crustal thinning and terminated in the emplacement of central complexes towards the end of the extensional phases. There are of course exceptions to this general rule, with, for example, the emplacement of the South Qôroq centre and early units of the Igdlerfigssalik centre being emplaced at the start of the Late Gardar cycle. Figure 1.2.1 (slightly modified after Stephenson 1976b) shows the geology of the Gardar province and Figure 1.2.2 (slightly modified after Emeleus and Harry 1970) shows the geology of the Igaliko Nepheline

Figure 1.2.1 General geological map of the Gardar Province (slightly modified after Stephenson 1976b) showing major faults, positions of main dyke swarms and major intrusive complexes.

1. Kûngnât
2. Ivigtut
3. Grønnedal-Íka
4. Nunarssuit
5. Puklen
6. Central Tugtutôq
7. Dyrnaes-Narssaq
8. Ilímaussaq
9. Igaliko
10. Klokken

Figure 1.2.1

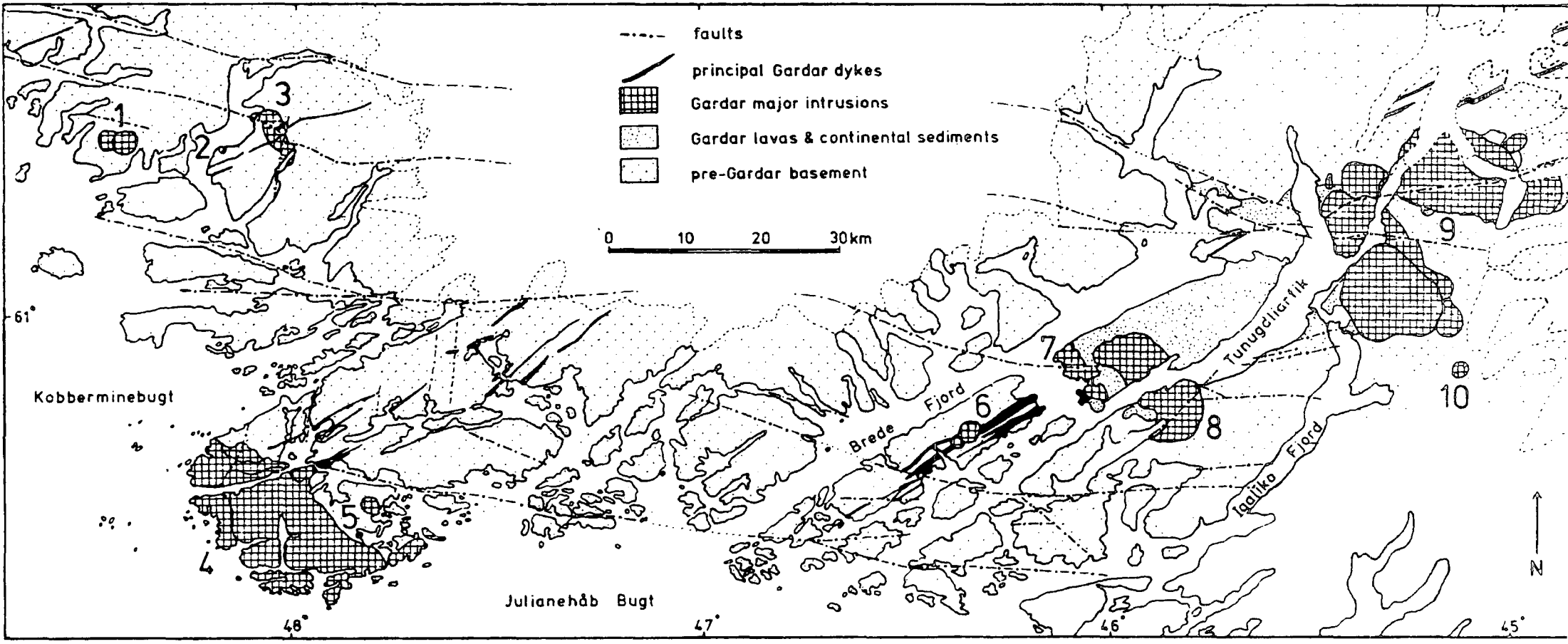
faults
principal Gardar dykes
Gardar major intrusions
Gardar lavas & continental sediments
pre-Gardar basement
0 10 20 30km
1
2
3
4
5
6
7
8
9
10
Kobberminebugt
Julianehåb Bugt
Brede Fjord
Tunugdliarfik
Igaliko Fjord
61°
48°
47°
46°
45°
N

Figure 1.2.2 Sketch map of the geology of the Igaliko Nepheline Syenite complex (slightly modified after Emeleus and Harry 1970).

Figure 1.2.2

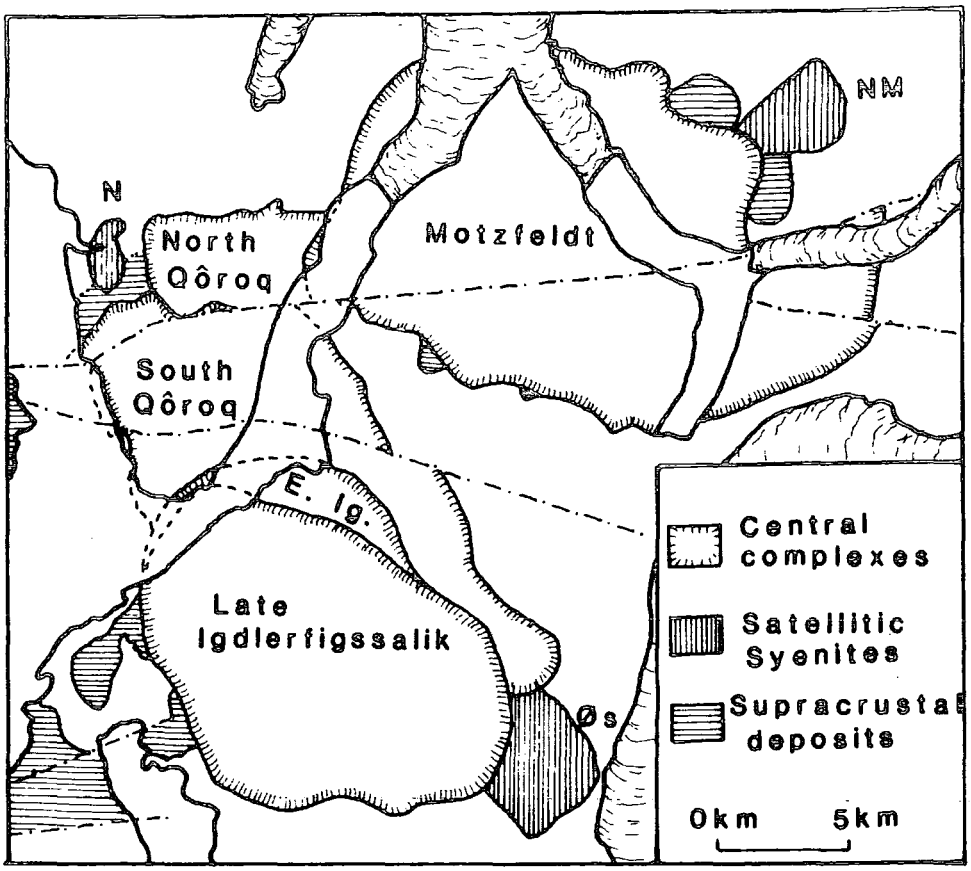
NM
N
North
Qôroq
Motzfeldt
South
Qôroq
E. Ig.
Late
Igdlerfigssalik
Øs
Central
complexes
Satellitic
Syenites
Supracrustal
deposits
0km
5km

Syenite complex.

Early Gardar: Lavas of the Eriksfjord Formation represent the earliest Gardar igneous activity. These are preserved interbedded with sandstones in fault-bounded blocks; the lavas accounting for about half of the 3000m of preserved supracrustal material. The Eriksfjord Formation rests unconformably on (early Proterozoic) Ketilidian granites (*sensu lato*) dated at 1850-1600 Ma and is cut by the Motzfeldt and North Qôroq nepheline syenite central complexes (1282 ± 31 Ma and 1286 ± 61 Ma respectively, Blaxland *et al.* 1978 *), from which the youngest lavas may have been erupted (Upton and Blundell 1978; Jones 1980). The lavas tend to become more evolved with time.

Near the base of the Eriksfjord Formation at Qagssiarssuk, carbonatitic and lamprophyric tuffs crop out (Stewart 1970). These occurrences mark the site of an Early Gardar volcano. Carbonate pseudomorphs may be after melilite (Stewart 1970) or nyerereite, $Na_2Ca(CO_3)_2$ (Deans and Robert 1984). In the west of the province the Grønnedal-Íka complex was emplaced at 1299 ± 17 Ma (Blaxland *et al.* 1978).

Mid Gardar: Mid Gardar activity commenced with the emplacement of swarms of basic dykes (Berthelsen and Henriksen 1975). Early types were lamprophyric followed by more abundant doleritic and trachy-doleritic dykes, some up to 200m in width. These younger dykes (the so called Brown Dykes) have been divided into 4 generations - 0, 1, 2 and 3. Brown dykes of the first generation, 0, (BD_0's) trend east-west whilst groups BD_1 to BD_3 become more north-east south-west trending as they become younger. BD's of generations 0, 1 and 2 cut the Grønnedal-Íka complex which constrains their older age limit.

Although the BD's are generally sparse in the Igaliko area, in Mellemlandet a 30m dolerite dyke, 325610-11, (possibly BD_0,Emeleus and Harry (1970)) is cut by early units of the (Early Gardar) Motzfeldt centre, indicating a 'transgressive' Early to Mid

---

* *Upton and Emeleus (1987) recalculated the Rb-Sr isochron ages of Blaxland et al. (1978) using the decay constant of* ^{87}Rb *as* $\lambda^{87}Rb = 1.42 \times 10^{-11}\ yr^{-1}$ *(Steiger and Jäger 1977) instead of* $\lambda^{87}Rb = 1.39 \times 10^{-11}\ yr^{-1}$ *used in 1978. All ages cited here as Blaxland et al. (1978) are the recalculated ages from Upton and Emeleus (1987) .*

Gardar boundary across the province, with the Early Gardar activity ending earlier in the west of the province. Mid Gardar 'Brown Dyke' injection may have spread eastwards across the region from a focus in the west (west of Kûngnât), reaching the Igaliko region before the termination of the Early Gardar activity in this area. If this is the case, the BD_0 generation can be bracketed between 1299 ± 17 Ma and 1282 ± 31 Ma.

An important swarm of phonolitic and syenitic dykes extends from Fox Bay (near the head of Igaliko Fjord) north-eastwards beyond the Østfjordsdal syenite. The swarm is about 10 km. in width. These dykes are unlike any other Gardar dykes seen in the Igaliko area and include several large porphyritic syenite members (up to 20m wide) which were termed the Fox Bay nepheline porphyries by Ussing (1912). This swarm is truncated by the Østfjordsdal syenite (possibly older than or contemporaneous with the South Qôroq centre) and can be regarded as Mid or Early Gardar, its older age limit being unconstrained.

Mid Gardar activity may be regarded as a local manifestation of a large scale magmatic event that affected much of the pre-Grenville cratonic regions of Canada and Fennoscandia (Patchett *et al.* 1978). This phase of activity ended with the emplacement of the Kûngnât Fjeld complex (1219 ± 16 Ma, Patchett *et al.* 1978) and Ivigtut (1222 ± 25 Ma, Blaxland *et al.* 1978). With the possible exception of the Østfjordsdal syenite, there are no Mid Gardar major intrusions in the Igaliko area.

Late Gardar: Late Gardar activity saw the emplacement of several syenitic and granitic central complexes along with two major ENE-WSW to NE-SW dyke swarms, the centre of activity having moved farther from the cratonic margins than earlier Gardar magmatism.

Intrusions early in the Late Gardar include the South Qôroq centre (1160 ± 8 Ma, Blaxland *et al.* 1978) and the early units of the Igdlerfigssalik centre. These, along with the Tugtutôq Older Giant Dyke, (1154 ± 16 Ma, Upton *et al.* 1985), are cut by one of the major dyke swarms in the province, the Tugtutôq - Ilímaussaq - Nunataq swarm. These dykes are in turn truncated by the late units of the Igdlerfigssalik centre and the Ilímaussaq centre (1143 ± 15 Ma and 1143 ± 21 Ma respectively, Blaxland *et al.* 1978)

and the central Tugtutôq complex (1124 ± 20 Ma, Martin 1985). This constrains the age of the Tugtutôq - Ilímaussaq - Nunataq dyke swarm between 1154 ± 16 Ma and 1143 ± 21 Ma. Many of the dykes in the Igaliko area belong to this larger swarm.

The Tugtutôq - Ilímaussaq - Nunataq zone is separated from the second major dyke swarm, that of the Nunarssuit - Isortoq zone, by about 60 km of ground in which Gardar dykes are scarce. The Nunarssuit - Isortoq zone is assumed to be broadly the same age as the Tugtutôq - Ilímaussaq - Nunataq zone although this is poorly constrained. Giant dykes are common to both zones although the two swarms show marked chemical differences (see Upton and Emeleus (1987) for a detailed account).

Other Late Gardar intrusions include the gabbros and granites from the Nunarssuit area in the west of the province; and the oversaturated Klokken layered syenite intrusion just south-east of the Igaliko complex.

1.3: History of Research

The mineralogist K. L. Giesecke visited the Igaliko Nepheline Syenite complex during each of two visits he made to the Julianehåb district in 1806 and 1809 (Giesecke 1910). He explored the valley off Qôroq Fjord now known as 'Giesecke's Dal' making note of some of the rock types in the area, including granite at Qôroq and sandstone and porphyry at Igaliko. It is these porphyries that seem to have attracted the attention most of the early geologists. Pingel (1843) produced an account of these dykes with subsequent collecting by Laube (1873) and petrography by Vrba (1874).

Steenstrup and Kornerup (1881) and Flink (1898) knew of the presence of a large amount of nepheline syenite east of Igaliko and Tunugdliarfik, but no systematic study was undertaken until Ussing and Bøggild mapped along the shores of Qôroq Fjord and in the area around Igánaq (Ussing 1894, 1912). Ussing identified several different types of syenite and noted the occurrence of syenite porphyry and tinguaite dykes cutting the syenites near 'Flink's Dal', in Qôrorssuaq and south of Narssârssuk. Of particular importance, he noted that many of the dykes pre-date the syenites in the area between Tunugdliarfik and Igánaq.

The pegmatite at Narssârssuk drew geologists to the region towards the end of the

19^{th} century, notable contributions being made by Flink (1898), Flink *et al.* (1899), Bøggild (1906) and Steenstrup (1909). Ussing (1912) summarised current knowledge of the minerals from this locality which encouraged further extensive sampling (Gordon 1924, 1927). Ødum (1927) extended the mapped limits of the syenite as far as Østfjordsdal and discovered the Klokken syenite on the south side of the Østfjordsdal gravel flats.

C. E. Wegmann visited the area prior to the Second World War and observed many dykes cutting the syenites along the coast section between Narssarssuaq and Qôroq. He (Wegmann 1938) envisaged a 'transformationist' origin for the Igaliko syenites (as he had for the Ilímaussaq nepheline syenites), and thought that many of the dykes had also undergone this metasomatising - migmatising event. Bondam (1955) also followed this idea in describing some alkali trachyte dykes from Narssarssuaq. With the demise of the transformationist hypothesis in the genesis of syenites these ideas lost favour.

Regional mapping of South Greenland by GGU started in the late 1950's. As part of this project C. H. Emeleus and the late W. T. Harry carried out systematic mapping of the Igaliko Nepheline Syenite complex between 1961 and 1963. After the death of W. T. Harry in 1964, C. H. Emeleus concluded the mapping of the complex with field seasons in 1966 and 1969. An account of the general geology of the complex along with the first complete map of the complex was published subsequently (Emeleus and Harry 1970).

North of Narssarssuaq Walton (1965) defined the northern extent of the Tugtutôq - Ilímaussaq - Nunataq dyke swarm, while Berrange (1966) demonstrated the presence of Gardar dykes south of Igaliko fjord. Scharbert (1966) published structural data (from X-ray diffraction studies) on alkali feldspars from undersaturated microsyenite dykes in the area and 2 years later produced major element chemical data on similar dykes from the Ilímaussaq peninsula (Scharbert 1968).

J. W. Stewart and V. Poulsen studied the supracrustal materials of the Ilímaussaq peninsula which crop out between Qagssiarssuk and Narssaq. Poulsen (1964) concentrated on the sandstones whilst Stewart (1964,1970) reported many carbonatitic and lamprophyric minor intrusions and eruptives. These are seen outcropping in the vicinity

of Qagssiarssuk at the base of the Eriksfjord Formation.

To the south-west of the Igaliko complex, B. G. J. Upton started a long standing association with the geology of the Island of Tugtutôq (Upton 1962) and in particular a series of giant dykes (Upton 1964a, 1964b; Upton and Thomas 1980; Upton *et al.* 1985). The giant dykes with widths of up to 800m show transverse compositional changes (either gradual or abrupt) with margins of alkali olivine gabbro and cores of syenite, formed either by *in situ* fractionation or by injection into the dyke core from a deeper magma chamber. Cropping out on the northeast end of Tugtutôq and in the vicinity of Narssaq are a series of potassic ultramafic rocks, much richer in elements such as Mg, Ni, Ca and poorer in Al than most other Gardar rocks. Upton and Thomas (1973) considered these rocks to be residual from fractional crystallisation of a very Mg rich magma of kimberlitic type.

In the late 1960's R. Macdonald and others investigated the origins of some of the more evolved (feldspathic) dyke rocks from the Tugtutôq area (Macdonald 1969, 1970; Macdonald and Edge 1970; Macdonald and Parker 1970). These dykes which post-date the Tugtutôq Giant Dyke Complex are mostly *q*-normative and range from trachy-basalts to (quartz) microsyenites and microgranites. Only six dykes containing feldspathoids from this area are reported by Macdonald. Of the 35 published analyses for Zr and Nb from these dykes, 32 samples show a Zr/Nb ratio greater than 5.2. This will be discussed in relation to the Igaliko dykes in a later chapter. A. R. Martin has recently completed a study of the petrogenesis of the Tugtutôq dykes (Martin 1985, Upton *et al.* 1985).

Recently Upton and Fitton (1985) studied the dyke lithologies in the ground between the Igaliko Nepheline Syenite complex and the Inland Ice. These include several giant dykes broadly similar to those of Tugtutôq, and a series of thinner, more evolved dykes, again very similar to the Tugtutôq occurrences. In these smaller dykes a compositional trend from hawaiite through to rhyolite and minor amounts of phonolite was observed. This was attributed to early olivine and plagioclase fractionation, followed by later clino-pyroxene, FeTi oxides, apatite and alkali feldspar. A carbonatite - lamprophyre association was recorded and this will be discussed later with regard to similar rocks from the Igaliko area. For the smaller (ie. not giant) silicic dykes, Zr/Nb ratios are

around 6 to 8, and these rocks are generally *q* or *hy*-normative.

Since the early 1970's attention in the Igaliko Nepheline Syenite complex has turned to a more detailed investigation of the individual nepheline syenite central complexes with several PhD studies being undertaken at Durham and Leeds. D. Stephenson led the way with a definitive study of the petrology, geochemistry and mineralogy of the South Qôroq centre, indicating many of the trends to be expected in such alkaline intrusions (Stephenson 1972, 1973, 1974, 1976). A study of the older North Qôroq centre was undertaken by A. D. Chambers who found broadly similar trends to Stephenson although late stage fluids had complicated the evolutionary history of North Qôroq, and this provided scope for investigations in a slightly different direction (Chambers 1976).

With the petrogenesis now reasonably well defined, M. Powell (at Leeds) directed her investigation of the Igdlerfigssalik centre towards an understanding of phase equilibria and element distribution within these slowly cooled nepheline syenite centres (Powell 1976, 1978). A. P. Jones concluded the initial re-investigation of the central complexes with a study of the Motzfeldt centre, paying particular attention to some of the more 'exotic' rock types such as the lujavrites (Jones 1980, 1984; Jones and Peckett 1980).

In 1982, working in conjunction with GGU's SYDURAN project, C. Bradshaw started a reassessment of the geology of the Motzfeldt centre, with attention being directed towards detailed re-mapping of the centre and assessing its economic (strategic) mineral potential (especially U, Th, Nb, Ta) (Tukiainen *et al.* 1984, Bradshaw 1985, 1987).

The applicability of these individual studies to the rocks of the Igaliko dyke swarm will be discussed later in the relevant chapters.

1.4: Aims

The investigation of the Igaliko Dyke Swarm completes an initial study of the intrusive igneous rocks from the Igaliko Nepheline Syenite complex.

The dykes, predominantly fine grained and carrying variable amounts of phenocrysts, represent fast-cooled liquids, aphyric varieties representing 'true magmatic' com-

positions. This distinction between the dykes and the slow cooled cumulate rocks of the central complexes (which do not necessarily reflect the bulk composition of the magmas from which they crystallised) invites their use in (geochemical) studies of magmatic evolution.

The aim of this project was to complete the sampling of the Igaliko Dyke Swarm and to undertake a detailed petrological and geochemical investigation of this material. The main objectives were to determine the magmatic history and petrogenesis of the swarm from the accumulated data and to try to establish any inter-relationships between the wide variety of rock types found (including the syenites of the central complexes).

The fact that the dykes represent frozen liquids which were available at the time of their emplacement makes this study not only applicable to the dyke swarm itself, but must also relate directly to the large scale availability of magmas for (and derived from) the central complexes.

1.5: Sampling and Mapping

Approximately 400 samples from dykes had been collected by C. H. Emeleus and W. T. Harry during the initial mapping of the complex in the 1960's. This material was available for study at Durham along with their field reports. D. Stephenson donated another 100 samples which he had collected in 1972 and some 30 samples collected by C. Bradshaw in 1982 from the Motzfeldt area were also available.

During the 1984 field season some 320 more samples were collected. The fine grained and generally homogenous nature of the dykes meant that relatively small samples were suitable for geochemical analysis. The dykes are generally very fresh and fist sized samples with weathered crusts removed were collected. All sample numbers used throughout this thesis (either 5 or 6 digit numbers) refer to the numbers of the GGU collection. These are listed, along with some basic information about each sample, in Appendix 1.

Mapping and sample locating was carried out at a scale of 1:20,000 using either aerial photographs or USAF base maps surveyed during World War 2. Figure 1 shows the locations of the areas visited during the 1984 field season. Of these, the camps

at Østfjordsdal and to the north of Narssarssuaq had not been visited previously by workers from Durham. Several areas were revisited, although much new material was collected from these.

Two maps are enclosed in the back flap of this thesis (Maps 1 and 2). Map 1 shows the country between Igaliko village, Tunugdliarfik and Igánaq at a scale of 1:10,000. As well as showing sample locations of the multitude of dykes from this area, it includes information from mapping by C. H. Emeleus and from Harrison and Hesselbo (1984).

Map 2, at a scale of 1:50,000, is a compilation map of the Igaliko Nepheline Syenite complex. It is based upon the map of the region by Emeleus and Harry (1970) , but incorporates all recent changes and additions. These are the results of remapping of the individual complexes, and in the case of the Motzfeldt centre, a complete reclassification (Bradshaw 1987). Improved access, better base maps and more detailed investigations have all added to the knowledge of the geology of the area, although in a broad sense the Emeleus and Harry (1970) map has suffered only minor modification. Map 2 includes all dykes mapped during this study; all dykes mapped previously be C. H. Emeleus and W. T. Harry; and all published data from maps showing Gardar dykes in this area.

CHAPTER 2: STRUCTURE

2.1: Introduction

The Gardar period represents repeated episodes of intra-continental rifting and associated alkali magmatism superimposed on the older Ketilidian basement. Since Gardar times the province has remained virtually unaffected by younger tectonic events.

2.2: Faulting

Two major sets of faults are prominent in the Gardar province. These are oriented WNW-ESE and WSW-ENE (Berthelsen and Noe-Nygaard 1965; Stephenson 1976b; Thrysted *et al.* 1986). The WNW-ESE trending faults are sinistral strike-slip faults with displacements of between 6 and 8 km (Henriksen 1960; Emeleus and Stephenson 1970; Tukiainen *et al.* 1984). As will be seen later these are very important in the evolution of the Gardar province as a whole. The WSW-ENE faults, again strike-slip, have considerably smaller displacements the range of 10's to 100's of metres in a dextral sense.

Vertical movement on these faults has been difficult to determine, although it has been recorded (Emeleus 1964; Emeleus and Stephenson 1970; Boshe *et al.* 1971). The Eriksfjord Formation preserved on the Ilímaussaq peninsula represents a fault-bounded block downthrown by some 2 to 3km. (Emeleus and Upton 1976). In the Motzfeldt area downthrows of 100 to 800 metres can be defined using the base of the Eriksfjord Formation as a guide (Tukiainen *et al.* 1986). At least 500m of downthrow can be seen on the ESE trending Flinks Dal Fault which bisects the Motzfeldt centre (Bradshaw 1987) and more than 300 metres of movement is seen on an ENE trending fault which cuts Igánaq (a small peak near Igaliko) in the south of the Igaliko Nepheline Syenite Complex.

Figure 1.2.1 (slightly modified after Stephenson 1976b) shows the major structural features of the province.

2.3: Gardar Rift Setting

Many of the features of the Gardar province are typical of a continental rift envi-

ronment. These include:-

1. Continental red sandstone/volcanic sequences preserved in fault bounded blocks.

2. Alkali magmatism derived from a mantle source.

3. Marked parallelism of major (intersecting) fault systems with long histories of movement.

4. Subvolcanic central complexes and dyke swarms.

5. An axial gravity 'high' in the southern part of the province (under Tugtutôq). (Sørensen 1970; Stewart 1970; Upton 1974; Blundell 1978; Upton and Blundell 1978).

It has long been realised that the spatial distribution of the central complexes is closely related to the intersections of the ESE-WNW and ENE-WSW trending fault systems (Berthelsen and Noe-Nygaard 1965; Stephenson 1976b). Stephenson (1976b) noted the elliptical plan of many of the major Gardar intrusions (especially South Qôroq, Igdlerfigssalik and Grønnedal-Íka) and attributed this to simple (sinistral) shear along a shear direction of 105°, their outcrops essentially defining simple shear strain ellipsoids.

This type of simple shear can be easily explained by wrench tectonics. In this environment, with ESE-WNW sinistral shearing, the minimum principal stresses (σ_3) occur along a SSE-NNW direction (at roughly 45° to the shear direction) producing extensional features (for example dykes and graben structures) oriented roughly ENE-WSW (perpendicular to σ_3). The actual angle at which these features occur is governed by the internal frictional properties of the rock (see Gamond 1983), with 45° cited here being a reasonable approximation. Experiments by Wilcox *et al.* (1973) who sheared clay blocks produced exactly these types of extensional features (see Figure 2.3.1A). Their results show the same angular relationships between the experimentally produced fractures as their real counterparts seen in the Gardar Province (cf. Bradshaw 1987). Figures 2.3.1B and C show the orientations of Riedel (R and R') shears and extensional features formed in a sinistral shear zone. In B there is no extension of the zone, while in C the shear zone is being extended, ie. transtensional (see Sanderson and Marchini

Figure 2.3.1A Experiments shearing clay blocks from Wilcox *et al.* 1973. Simple shear causes secondary faulting and tension in this basic wrench tectonic environment.

Figure 2.3.1B Sinistral shear with no extension of the shear zone (ie. $\alpha^{-1} = 1$) where α^{-1} is the present width/original width of the shear zone (from Sanderson and Marchini 1984). R and R' (Riedel) shears develop, along with veins (dykes) marked V and graben structures form perpendicular to the direction of maximum extension. C is the axis of maximum compression.

Figure 2.3.1C Sinistral shear with extension of the shear zone (ie. $\alpha^{-1} > 1$, from Sanderson and Marchini 1984). Key as in Figure 2.3.1B. In this transtensional environment the R and R' shears may open. The angular relationships between these, the main axis of dykes (V) and the sinistral faults compares very closely to the orientations of dykes seen in the Igaliko Nepheline Syenite complex (see Chapter 2.6).

Figure 2.3.1

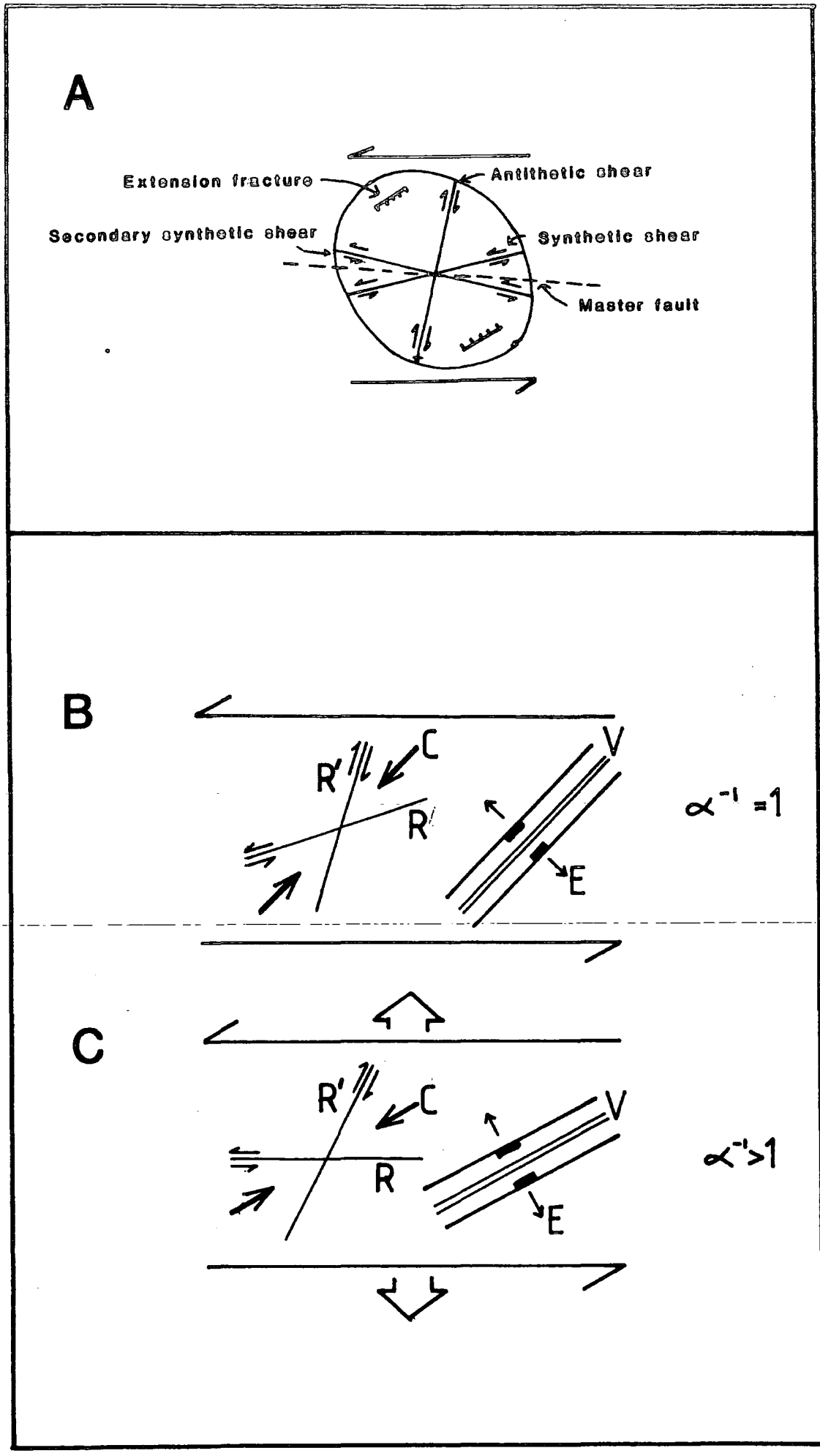
A
Extension fracture
Antithetic shear
Secondary synthetic shear
Synthetic shear
Master fault
B
R'
C
R
V
E
$\alpha^{-1}=1$
C
R'
C
R
V
E
$\alpha^{-1}>1$

1984). In this type of transtensional environment, extension across these Riedel shear zones may occur as well as on the primary extension features (marked V).

Within the Gardar province, the majority of the dykes tend to show an ENE trend. This includes the larger, regional swarms, such as the Tugtutôq - Ilímaussaq - Nunataq zone of dykes as well as the more local occurrences such as the dykes around the Igaliko Nepheline Syenite complex. This indicates tension across much of the province in a SSE direction, although the Mid Gardar Brown Dykes tend not to conform to this general rule (see Chapter 1). As well as the dyke swarms having this ENE trend, a series of horst/graben structures are seen in the Gardar with this orientation. Both can be easily explained as a result of ESE-WNW sinistral shear (see also Chapter 2.6).

Bradshaw (1987), considering the emplacement mechanisms of the Gardar central complexes, showed how the intersections of major and secondary faults formed in a shear zone can produce 'rhombochasms' (Biddle and Christie-Blick 1986). These are fault bounded blocks of rock, fault movement on the major faults having been transferred onto the secondary faults, to produce an isolated block. With continued shearing these isolated rhombs are forced to rotate in the shear direction (anticlockwise for sinistral shear), this rotation producing a roughly circular fracture. Block (cauldron) subsidence, leading to a circular, 'ring dyke' structure then follows accompanied by the rise of salic magma. This produces an outcrop pattern similar to many of the central complexes seen in the Gardar.

2.4: Tectonic Setting

Baragar (in Baer *et al.* 1974; Baragar 1977) has drawn attention to the similarity, timing and lithological sequences between the North American mid-continental rift system (the Keweenawan Supergroup), the Seal Lake Group of Labrador and the Gardar Province and has attributed these features to a major Proterozoic continental rifting event. Palaeomagnetic evidence shows that South Greenland, North America and Northern Europe formed a continuous land mass until the Mesozoic (Piper 1982).

The Keweenawan (1200-1000 Ma) of North America occupies a belt approximately 2000km by 150km, and is composed of mafic (tholeiitic) rocks and red continental sandstones (Halls 1978). The rift comprises several lava plateaux (2.5 to 7km deep

and 100 to 250km across) with some of the earlier lavas being enriched in incompatible elements (Green 1983).

Extension in the Keweenawan must have been considerably greater than in the Gardar (Upton 1974; Upton and Emeleus 1987) despite the likely association of the two rift systems (Baragar 1977), with the Gardar having a network graben structure, a smaller axial gravity high and a more alkaline petrology (Harris 1969).

Bradshaw (1987) proposed a relatively limited amount of crustal extension for the province as a whole, the crustal attenuation being taken up by a series of extensional fault blocks. Major graben formation in the region was not generally achieved with the possible exception of the Tugtutôq - Narssaq zone (Upton and Blundell 1978) where extensive axial dyking above a marked linear gravity high is seen (Blundell 1978). This 'high' of some 300 to 400 mgals above background can be assigned to a gabbroic body of any shape intermediate between a shallow (to 10km depth) 25km wide 'sill' which breaks the surface at Narssaq (and is coincident with gabbroic outcrops there) or a thinner (10km wide) vertical sheet extending to about 40km depth. The latter model is similar to that proposed by Chase and Gilmer (1973) for the North American gravity high, where they also proposed the formation of new oceanic crust in the rift, this having since been convincingly disputed by Green (1983). Of the two models proposed by Blundell (1978), he favours the shallow sill like body.

Burke (1980) suggests that the Keweenawan, Seal Lake and Gardar may represent penetrative aulacogen systems related to the opening of the Grenville ocean. This would involve rifting, alkali magmatism and continental extension along transform faults (possibly reactivating pre-existing structures). Sykes (1978) points out that during an episode of continental fragmentation, rifting will tend to follow the youngest zone of previous orogenesis. This avoids having to disrupt old, cold and strong cratonic areas. Thus, the Ketilidian, only some 350 Ma older than the Early Gardar could be reasonably easily remobilised in comparison to the Greenland craton. Sykes (1978) also adds that reactivated continental transform faults, unlike their oceanic counterparts, will involve only relatively small horizontal displacements (several as opposed to several hundred kilometres). Henriksen (1960) has noted a pre-Gardar history for one of the major ESE sinistral strike-slip faults in the province.

Within the pattern of pre-existing and newly formed structural features, 'hot spots' will occur at the junctions of faults within this system. This compares favourably with the locations of many of the Gardar intrusions (Stephenson 1976b). This type of rifting and magmatism is essentially a 'passive' response to tectonic stresses and not the surface expression of a mantle plume (cf. Burke and Dewey 1973).

Patchett *et al.* (1978) concluded that the Mid-Gardar Brown Dyke activity (between 1260 Ma and 1190 Ma) was caused by the initial stage or stages of a continental separation which led ultimately to the Grenville orogeny. In contrast, Gordon and Hempton (1986) show the Keweenawan rift to have formed in response to the collision of the Grenville plate into the North American plate along a NNE-SSW trending collision zone, producing NW-SE sinistral strike-slip faults. This concurs with the views of Donaldson and Irving (1972) who related the Keweenawan to the (dextral) strike-slip collision of the Grenville plate (from the SSE) with the North American plate. Halls (1978) points out however that there is no visible Grenville suture zone.

There thus seems to be no consensus opinion as to the causes of the Keweenawan and, by inference, the Gardar rifting, although all agree that crustal interaction between the North American and Grenville plates is in some way responsible.

Bradshaw (1987) concluded that intra-plate strain, either caused by Grenvillian impact or continental extension reactivated the Ketilidian mobile belt producing ENE trending extensional fault blocks and several roughly parallel WNW-ESE strike-slip faults in response to sinistral shearing. Crustal thinning and continental extension produced a rise in the geothermal gradient (Mackenzie 1978) and induced partial melting in the upper mantle. At the intersections of the major lineaments 'rhombochasms' developed, allowing the accumulation of salic magmas, these zones being analogous to 'leaky transform faults' in the oceanic lithosphere. Deep fractures allowed rapid rise of magma which followed the ENE zones of tension in the brittle upper crust.

2.5: Dyke Morphology

Recently, much work has been undertaken with a view to understanding the mechanism of intrusion of tabular bodies of rock. These may be igneous bodies such as dykes or sills, or veins infilled with quartz or carbonate for example. These principles apply

regardless of scale, composition or orientation of the sheet like body in the earths crust, the most important factor being its relationship to the stress regime present in its host rock.

Needless to say dykes (sills, veins, inclined sheets etc.) are not the simple sheets of rock they are often assumed to be in basic text books (see for example Billings 1972, pages 331-7). Most texts also fail to show the termination of these bodies, giving no indication as to propagation methods, with the edges of these sheets usually assumed to be simple curves concave towards their centres. Planar marginal contacts (assumed to be the norm) are invariably more complex, undergoing *offsets* (along strike) with the formation of smaller sheets (apophyses or *horns*) at these steps in the sheet walls.

The mechanism of intrusion is commonly thought to be one of simply splitting apart the host rock along a planar fracture (or opening a pre-existing fracture either by crustal extension or forceful injection of magma) and filling this with magma/mineralising fluid which will subsequently crystallise.

2.6: Strikes

Dykes, being common extensional features, will be emplaced in the plane normal to the minimum principal stress (σ_3, Anderson 1951). Figure 2.6.1 shows a histogram of all measured strike directions for the Igaliko Dyke Swarm. As can be seen most of the dykes strike between 050° and 060°, with a slight skew towards higher strikes. The departure from a smooth (Gaussian type distribution) between strikes of 040° and 045° is due to the Østfjordsdal Dyke Swarm, which has an average strike of 043° (with σ_n of 15.6°). This difference in strike between the supposed Mid-Gardar (Østfjordsdal) dykes and the majority of the Igaliko Dykes (of late Gardar age) represents a change in the direction of minimum principal stress of about 10°. The Østfjordsdal Dykes will be discussed in a later chapter.

The groups of dykes striking at 020° to 025° and 090°to 095° represent sets of conjugate (Riedel R and R') shears that have opened up in a transtensional regime (see Figure 2.2.3C, after Sanderson and Marchini 1984). Ideally these fractures would form at the same angle (ca. 30°) either side of the direction of least compressive stress (represented by the extensional features such as dykes and horst/graben structures

Figure 2.6.1 Histogram of strikes of Igaliko Dykes. The majority of the dykes from Igaliko strike at between 050° and 055° and show a slightly skewed distribution. Deviations from a smooth (Gaussian) distribution are seen at 4 strike ranges.

000° to 005°. Dykes on the Narssarssuaq peninsula cutting the South Qôroq syenites have been rotated by the regional shearing into a roughly N-S orientation.

020° to 025° and 090° to 095°. These dykes are occupying Riedel shears (see Figure 2.3.1C) which have been opened during transtensional extension of the region (see text).

040° to 045°. The excess of dykes over a smooth distribution is due to the orientation of the Mid-Gardar Østfjordsdal dyke swarm which has an average strike of 043°.

Figure 2.6.1 HISTOGRAM OF STRIKES OF IGALIKO DYKES

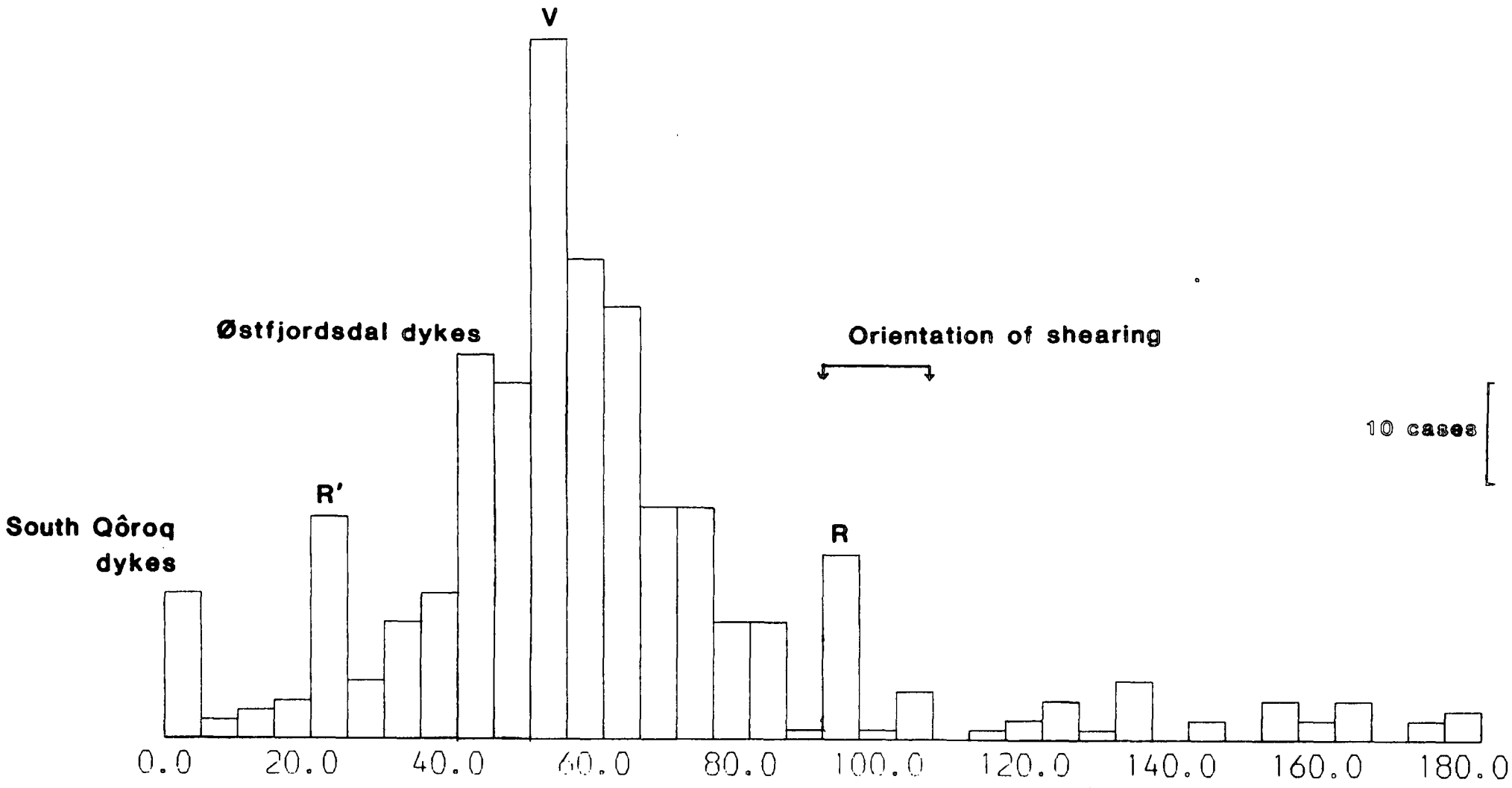

trending in the Gardar case at between 050° and 055°). The same process that caused the skewing of the 'normal' distribution of the strike directions probably accounts for the fact that they occur at -30° and +35° to the major extensional features. From Figure 2.3.1B and C it can be seen that the orientation of Riedel shears changes between a simple shear environment and a transtensional environment, with one of the sets of Riedel shears (R) becoming parallel to the shear direction. The dykes trending at between 090° and 095° are close to the 105° orientation for the shearing calculated by Stephenson (1976b), although not exactly parallel. Simple shear does not however explain their orientations either, with weak transtensional extension of the area being the cause. The internal frictional properties of the country rock will also affect the orientations of secondary extension features formed in a shearing environment (eg. dykes, grabens and Riedel shears, Gamond 1983). This may also be responsible for the difference between calculated and observed features.

Berthelsen and Henriksen (1975) noted a trend of counter-clockwise rotation with increasing youth of the dykes. This is particularly evident in the Brown Dyke (BD) generations with BD_0 striking roughly E-W, BD_1 striking at 060° and BD_2 striking roughly 020°. Upton and Fitton (1985) also noted a slight difference between the strikes of the Giant Dykes (63°±2°) and the later, smaller, more felsic dykes (57°±2°). This they tentatively assigned to a long lived stress producing process (in the asthenosphere) giving ESE-WNW tension, with the Greenland plate undergoing a slow clockwise rotation above this.

As has already been shown, the Gardar province was subjected to roughly E-W faulting throughout its evolution, this having been caused by regional shear induced by relative motions between the Grenville and North American plates (see Chapter 2.4 and Bradshaw 1987). The extensional features such as dykes and graben seen in the region are a result of this tectonic regime. It would seem unlikely then that a persistent asthenospheric process is the cause of the stresses here, and that the rotation of the Greenland plate above this to cause the change in strike of the dykes must also be in doubt. Another explanation must be sought.

Simple shear, such as the model proposed by Stephenson (1976b) to account for the outline of the central complexes, would have the effect of rotating the early formed dykes

in an anticlockwise direction and thus cannot explain the observed changes in strike. This can however explain the fact that most of the dykes within the fault-bounded block of the South Qôroq centre (see Map 2) strike roughly north-south. This is also true of the dykes cutting the early units of the Igdlerfigssalik centre on the southern side of Gieseckes Dal. There may also have been some (anticlockwise) rotation of the fault-bounded block of the South Qôroq centre due to continued movement on these faults, which would have a similar effect.

Major E-W fault orientations (measured from the 1:500,000 Geological Map of South Greenland) are scattered between 080° and 115° (see Figure 2.6.2). There is a fairly distinct group trending at 090° and a cluster (or possibly 2 groups) at 100° and 105°. Relative movements between the North American and Grenville plates has been shown to be the cause of the tectonic stresses operating in the Gardar. This large scale tectonic regime resulted in movements on the major, roughly E-W sinistral faults in the region. If interactions between the Grenville and North American plates, be it either the opening of an ocean (tentatively proposed by Patchett *et al.* 1978) or continental collision (Green 1983), produced crustal stresses of differing orientation with time, movement on faults of different orientations would be favoured. This would also cause variations in σ_3 in the inter-fault regions and may account for the apparent difference in strikes of the varying sets of dykes, eg. the Østfjordsdal swarm, the Tugtutôq - Ilímaussaq - Nunataq Giant Dykes and the later more felsic dykes such as those of the Igaliko province. A change from transtensional extension to simple shear could also have the same effect (see Chapter 2.9).

Within the Igaliko Dyke Swarm, there is no strong evidence for a change of orientation between petrographically distinct groups. BFD, basalts, lamprophyres and trachytes gave average strike directions of between 054° to 058° with the carbonatites giving an average strike of 070°. All types however gave very large standard deviations (σ_n commonly 35°), and thus the apparent difference shown by the carbonatites is meaningless.

2.7: Stratigraphy

From Figure 2.6.1 it can be seen that as a single group, the greatest number of dykes

Figure 2.6.2 Orientation of major (E-W) Gardar faults. The major roughly E-W faults (measured from the 1:500,000 map of S. Greenland) fall into 2 (or possibly 3) groups. See text for explanation.

Figure 2.6.2 ORIENTATION OF MAJOR (E-W) GARDAR FAULTS.

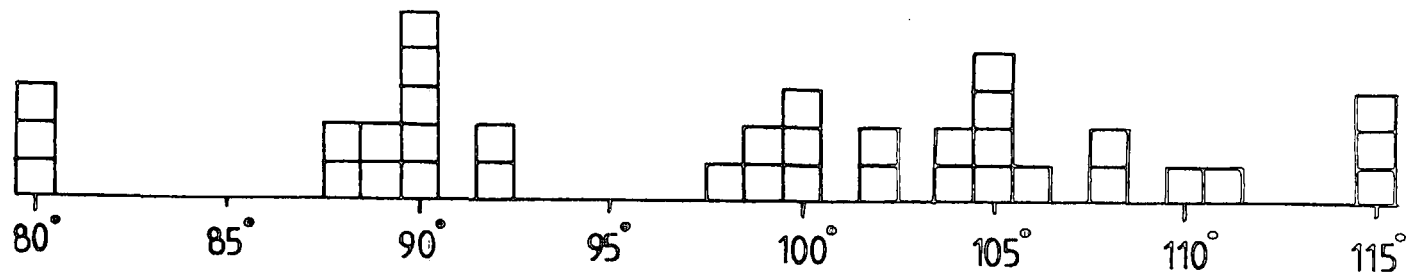

strike between 050° and 055°, with over half of all recorded cases striking between 040° and 065°. This marked (sub-) parallelism means that intersections are fairly rare and a large scale (regional) stratigraphy is difficult to deduce directly. Inevitably, where useful intersections might have been expected from the strikes of separate dykes, lakes, snow patches, scree etc. obscure the vital ground.

Local stratigraphies, however can be reasonably easily erected and from these a broad regional pattern can be drawn. As has already been noted, the age of the majority of the Igaliko Dykes is bracketed between the early and late units of the Igdlerfigssalik centre. The Østfjordsdal swarm predates the Østfjordsdal satellitic syenite which, in turn, is older than or contemporaneous with the South Qôroq centre. This Østfjordsdal swarm is petrographically distinct from any of the other Gardar dykes in the Igaliko Nepheline Syenite complex, containing large (20m +) porphyritic syenite dykes; 'blue-grey' trachytes and phonolites; and basaltic/lamprophyric examples. There are no BFD's in this area, and this in its own right suggests a very different origin for these Mid-Gardar dykes.

A possible BD_0 in Mellemlandet is truncated by the Motzfeldt centre, and within the Motzfeldt centre porphyritic foyaite sheets (Bradshaw 1987) north of Motzfeldt Sø cut 2 trachytic dykes (325913-4) about 500m NW of Lejrelv (Pearce and Emeleus 1985). This indicates that there was a period of dyke emplacement contemporaneous with intrusions within the Motzfeldt centre. Within the other centres no internal boundaries are seen to truncate any dykes (excluding that between early and late Igdlerfigssalik).

Local Stratigraphies.

Figure 2.7.1 shows a sketch map of relationships observed in the Østfjordsdal area. In two clear instances, early lamprophyric dykes are cut by the large porphyritic syenite dykes and these in turn are cut by many trachytic dykes. The 'blue-grey' trachytes sometimes show intimate relationships to the porphyritic syenites, appearing in some cases to be almost a marginal facies, and in other instances to be distinctly later. The whole swarm is also cut by late pegmatite sheets assumed to emanate from the Igdlerfigssalik Centre.

Figure 2.7.2 shows the cross-cutting relationships observed at the 970m summit on

Figure 2.7.1 Geological sketch map of the Østfjordsdal area. Basic dykes marked **lp** are lamprophyres. Cross cutting relations where unclear on the map are marked **y** for the younger dyke, **o** for the older and **?** where the age relations are uncertain.

Figure 2.7.1

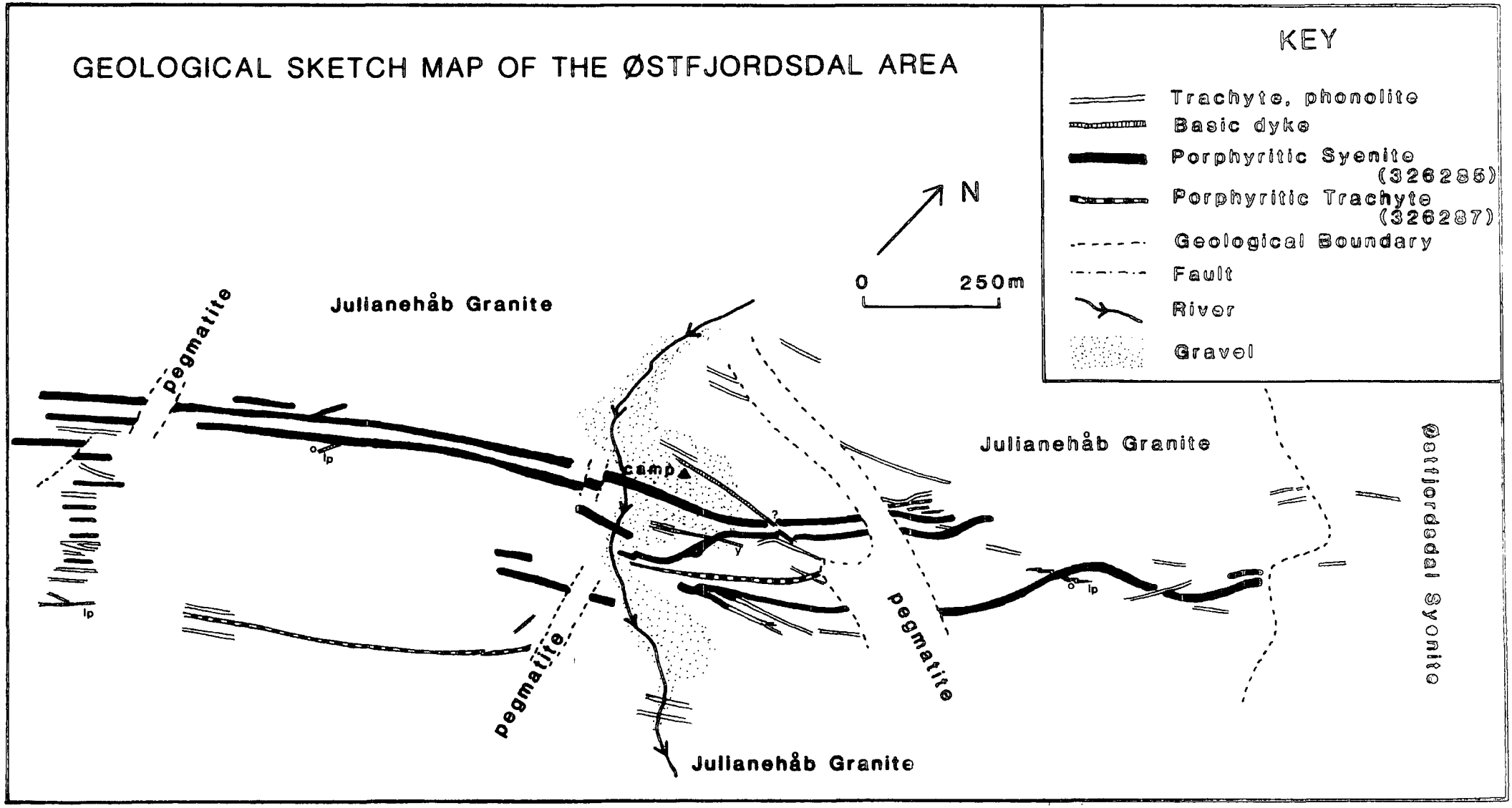
GEOLOGICAL SKETCH MAP OF THE ØSTFJORDSDAL AREA
KEY
Trachyte, phonolite
Basic dyke
Porphyritic Syenite (326285)
Porphyritic Trachyte (326287)
Geological Boundary
Fault
River
Gravel
N
0
250m
Julianehåb Granite
pegmatite
camp
Julianehåb Granite
pegmatite
pegmatite
Julianehåb Granite
Østfjordsdal Syenite

the Narssarssuaq peninsula (within the South Qôroq centre, from Emeleus and Harry 1970). Early BFD's are seen to be cut by successive generations of alkali trachytic dykes. Figure 2.7.3 shows cross-cutting relationships from dykes in Lower Flinks Dal, where several generations of trachytic dykes are seen to intersect.

Throughout the Igaliko complex only one BFD is seen to cut a trachytic dyke (Emeleus and Harry 1970 page 89; and this study), this locality being 1.3km NNW of the 970m summit.

As has already been noted, the majority of the dykes pre-date the late Igdlerfigssalik syenites. Recognition of dykes later than these syenites is limited to those that are seen to cut these late syenites or those that exist in an unmetamorphosed state in the aureole of the late Igdlerfigssalik syenites. Thus, late dykes may not easily be recognised as such elsewhere. These late dykes tend to be evolved phonolites, or, more abundant than had been previously thought, carbonatites, with many examples cropping out in the ground around the SW margin of the Igdlerfigssalik syenite (see Map 1). These carbonatites tend to cut other dykes, although occasionally they are seen to be cut by trachytic or phonolitic dykes, presumably also late. Appendix 1 contains all cross cutting relations observed and can be referenced for more 'local' information.

With these generalisations having been made, it must be noted that alkali basaltic magma is available at a late stage in the evolution of the central complexes (eg. Motzfeldt, Igdlerfigssalik) appearing as late dykes. Also, at Igdlerfigssalik, several late dykes of intermediate composition (between gabbro and phonolite) and one late lamprophyre are seen. Magma of a reasonably unevolved nature must persist at depth until late stages of central complex evolution in some type of stratified magma chamber (cf. Stephenson 1973).

From the local field evidence a broad, and somewhat generalised, regional stratigraphy can be drawn (Table 2.7.1)

The relative ages of the Motzfeldt and North Qôroq centres are unclear. While Jones (1980) considers the Motzfeldt centre to be the younger, A. D. Chambers (pers. comm. 1986) could see no unequivocal evidence for the relative ages of either centre. Map 2 shows the Motzfeldt centre to be the younger of the two. The possible BD_0

Figure 2.7.2 Sketch map of dyke intersections at the 970m summit on the Narssarssuaq peninsula (from Emeleus and Harry 1970). The solid dykes are BFD's, all others are trachytic and phonolitic.

Figure 2.7.3 Sketch map of dyke intersections in Lower Flinks'Dal. Abbreviations used:- **R. P.** Rhomb Porphyry, **Cbt.** Carbonatite. All other dykes are trachytic or phonolitic. Note how the Rhomb Porphyry is offset by a series of smaller faults as it approaches the major Flink's Dal Fault.

Figure 2.7.4 View of the southern face of Qôrqup Qâqai across Giesecke's Dal. Dykes can be seen being smeared out as they enter the Giesecke's Dal Fault zone. The dotted line marks the northern limit of the fault zone (after Emeleus and Harry 1970).

Figure 2.7.2

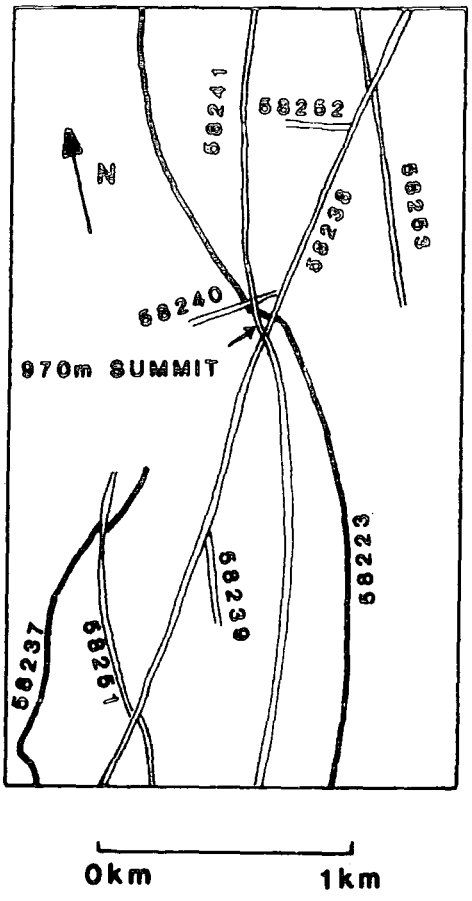

Figure 2.7.3

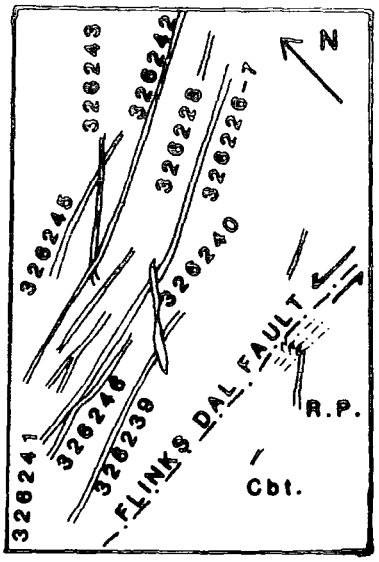

Scale 1:20,000

Figure 2.7.4

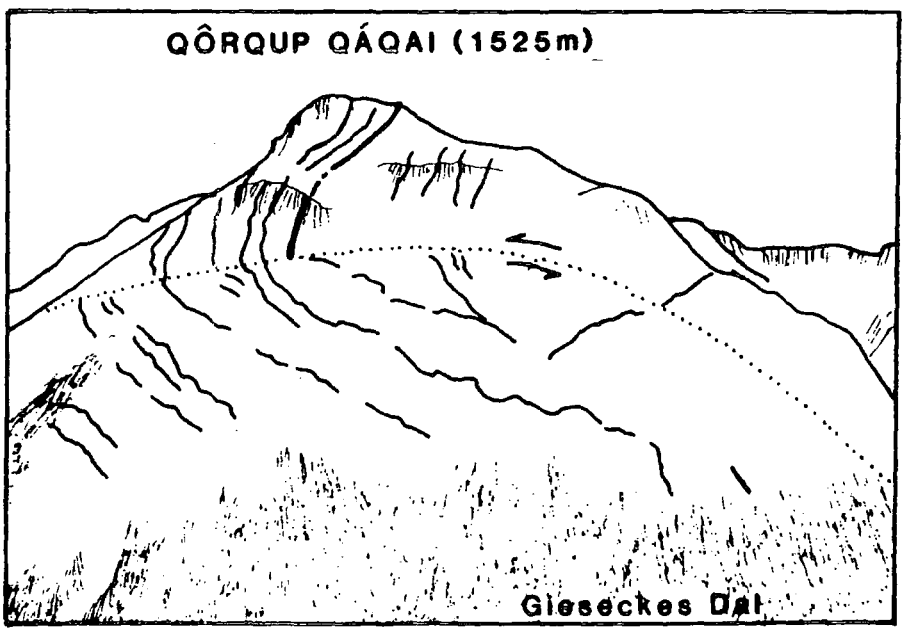

Table 2.7.1

Stratigraphy of the Igaliko Nepheline Syenite complex.

	Late dykes - Carbonatite,phonolite etc
L	**Late Igdlerfigssalik syenites**
A	Trachytic and phonolitic dykes
T	Lamprophyre, basalt and trachybasalt dykes
E	Big Feldspar Dykes
	South Qôroq and **Early Igdlerfigssalik syenites**
M	Østfjordsdal syenite
I	Trachyte and phonolite dykes
D	Østfjordsdal Swarm Porphyritic Syenite and 'blue-grey' trachytes
?	Lamprophyre dykes
E	Motzfeldt Foyaite Sheets
A	Some Porphyritic Trachyte dykes
R	**Motzfeldt syenites**
L	**North Qôroq syenites**
Y	BD_0(?) in Mellemlandet

clearly pre-dates the Motzfeldt centre and thus may or may not pre-date the North Qôroq syenites.

The dykes of the Tugtutôq - Ilímaussaq - Nunataq zone are also late Gardar (see Chapter 1) with many members of this swarm cropping out in the Igaliko region. These dykes are truncated by the Ilímaussaq nepheline syenite complex, and are probably also pre- Late Igdlerfigssalik, suggesting they are roughly the same age as the bulk of the Igaliko dykes.

Faulting.

Major, roughly E-W trending faults with long histories of movement are a result of the regional stress regime across the Gardar province. In the Igaliko region displacements on these faults can reach as much as 6km (shown by the displacement of the eastern margin of the Motzfeldt centre by the Flinks Dal Fault, Tukiainen *et al.* 1985). Offsets of the dykes by these major faults are not as great as this, with dykes on the Narssarssuaq peninsula being offset only some 2km by the same fault (Emeleus and

Harry 1970). The southern of two major faults on the Narssarssuaq peninsula records fault movement occurring while dyke emplacement was active. A 12m wide sparsely porphyritic microsyenite (59774, 58241) is offset sinistrally by about 100m across this fault, whilst the majority of the other dykes are offset by about 400m (see Map 2). The offset of dykes across the Narssarssuaq Peninsula however accounts for about 6km of along strike offset of the swarm across the area, although the offset across faults is much less than this.

Commonly dykes become brecciated as they approach the fault zone being offset along smaller faults parallel to the major fault (see Map 2 on the Narssarssuaq peninsula and Figure 2.7.3) or they become sheared and deformed in the fault zone. A spectacular example of this can be seen on the southern face of Qôrqup Qáqai (on the northern side of Gieseckes Dal) where a swarm of trachytic dykes is strung out for several hundred metres within the fault zone (see Figure 2.7.4, from Emeleus and Harry 1970).

Major faulting thus appears to have occurred intermittently throughout the evolution of the Igaliko Nepheline Syenite complex, with overlap of fault movement and dyke emplacement being evident in some areas. Fault movements continued after the major phase of dyke emplacement, offsetting swarms of dykes by up to 2km (Emeleus and Stephenson 1970). This is consistent with a simple shear model for dyke emplacement where where a continued build up of tension in the crust, after formation of extensional features such as dykes, causes major movement on a master fault (see Figure 2.3.1, Wilcox *et al.* 1973). The southern bounding fault of the supracrustal succession near Igaliko truncates many dykes within the these rocks, although it is unclear whether this movement is pre- or post late Igdlerfigssalik syenite (Emeleus and Harry 1970). There are no examples of dykes postdating the latest fault movements in the area.

2.8: Fingered Sheets and Echelon Cracks

Many workers have reported morphological aspects of the form of sheet intrusions, including fingers emanating into the country rock (Hills 1901; Hurlburt and Griggs 1939; Pollard *et al.* 1975), and offsets (Harker 1909; Anderson 1951; Currie and Ferguson 1970; Pollard 1973; Smith 1973). Both Harker (1909) and Anderson (1951) proposed three dimensional models for the features they had observed, but it was not until

Pollard *et al.* (1975) surveyed in detail slumped blocks in the marginal regions of the Shonkin Sag laccolith that evidence for the three dimensional form of sheet margins was truly observed. They found isolated *fingers* of magma had propagated into the country rock, coalescing some distance (in this case ca. 100m) behind their tips into a discrete sheet (see Figure 2.8.1). Finger initiation is explained by the interaction of two fluids with different viscosities (ie. heated, plastic country rock and magma) forced together under pressure. When one of these fluids is 'pushed' into the other, an irregular interface (wavey or bumpy) develops between them (Saffman and Taylor 1958). Once this irregularity has been established, fingers grow rapidly in length from the protruberances of the less viscous fluid into the more viscous fluid. Fingers will have chilled margins around the whole of their periphery and will deform the country rock between adjacent fingers to eventually form *cusps* as fingers coalesce (see also Nicholson 1985). Pollard *et al.* (1975) discuss in detail a mathematical treatment of the formation of fingered peripheries to sheet intrusions.

En echelon arrays of cracks form and propagate in a very different manner, and the field evidence from Igaliko suggests that emplacement along this type of fracture is the dominant mechanism (see later).

Examples of echelon cracks are quite common in the literature (see Pollard *et al.* 1982 for a review) and they occur on scales from microns to kilometres. This ubiquity attests to their importance in the fracture process. Pollard *et al.* (1982), in a similar approach to fingered sheets, give a very detailed and complex mathematical account of the mechanisms of formation of arrays of en echelon crack segments.

Echelon cracks emanate from the breakdown of a parent crack into an array of smaller fractures (see Figure 2.8.2), often *twisted* away from the orientation of the parent crack. The parent fracture will form in the plane of least compressive stress and, due to stress changes at the tip of the parent crack, rotation of the principal stresses about the axis of propagation of the parent crack will occur on a local scale, inducing the twist in the echelon array (Delaney and Pollard 1981; Pollard *et al* 1982; see Figure 2.8.3). Individual echelon cracks approximate in form to helicoidal cracks (increasing twist away from the parent crack), these requiring less energy to form than a volumetrically similar twisted flat-sided crack (Pollard *et al.* 1982).

Figure 2.8.1 Schematic representation of the periphery of a fingered sheet intrusion (after Pollard *et al.* 1975). Fingers extend into the country rock some distance maintaining a fairly consistent width over most of their length. Coalescence of the fingers into a single sheet leaves cusps of deformed country rock at the sheet margins.

Figure 2.8.2 Idealised block diagram illustrating the geometry of parent and echelon cracks (from Lutton 1971).

Figure 2.8.3 Idealised three-dimensional form of a segmented dyke (from Delaney and Pollard 1981). Segmentation is caused by the rotation of the axis of least principal stress during propagation of the dyke. Note how this rotation increases with increasing distance from the parent crack.

Figure 2.8.1

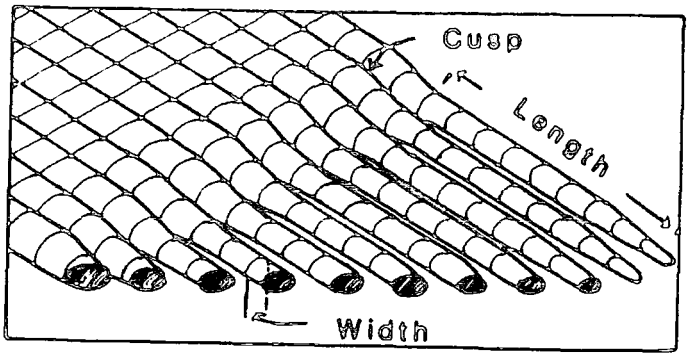

Figure 2.8.2

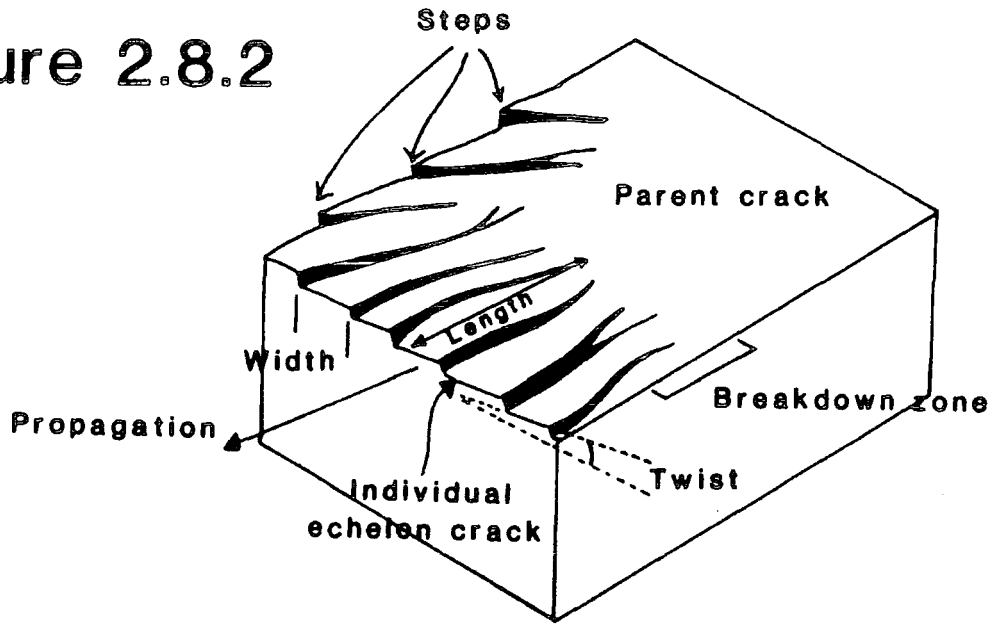

Figure 2.8.3

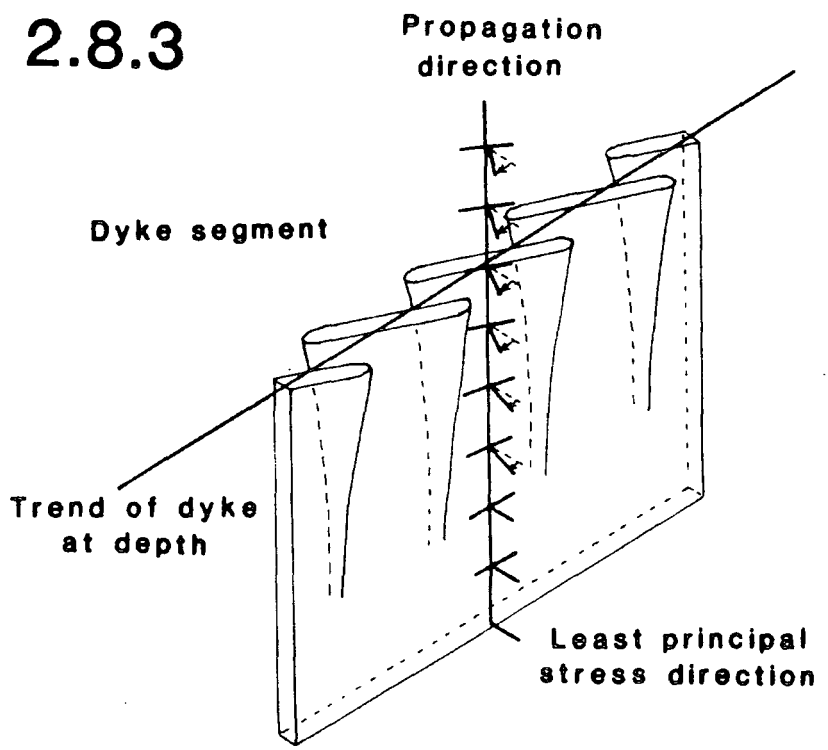

Figure 2.8.4A Schematic illustration of echelon cracks that grow along straight propagation paths.

I Before cracking (ie. no dilation). Broken line represents propagation path.

II After propagation. Some dilation has been accommodated by bending of bridges. Crack walls are divided into a curved inner part and a rectilinear outer part.

III After failure. Failure of bridges along cross fractures causes crack linkage resulting in a considerable increase in dilation.

Figure 2.8.4B Schematic illustration of echelon cracks that grow along curved propagation paths.

I Before cracking (ie. no dilation). Broken line represents propagation path. Mechanical interaction between adjacent cracks causes crack tips to curve toward each other as they propagate.

II After propagation. Some dilation has been accommodated by rotation of bridges. Crack walls are divided into two curved distal parts and one rectilinear central part.

III After failure. Propagation of the crack tip to the crack plane causes separation of the rotated bridge from one side of the crack wall with linkage resulting in a considerable increase in dilation.

Figure 2.8.4

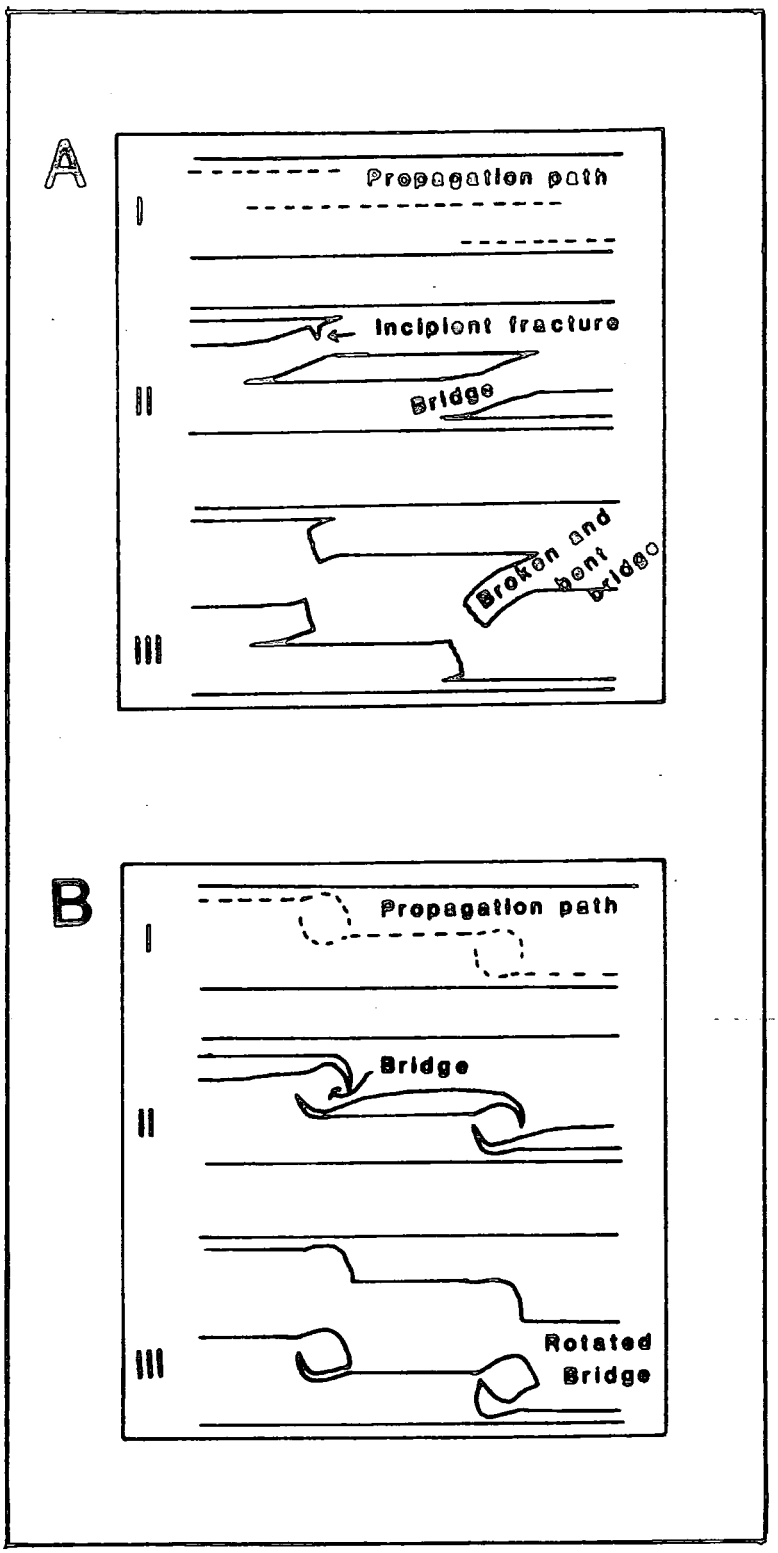
A
Propagation path
I
Incipient fracture
II
Bridge
Broken and bent bridge
III
B
Propagation path
I
Bridge
II
Rotated Bridge
III

Echelon cracks can form along cracks intermediate in shape between either straight or curved (end-member) propagation paths (Nicholson and Pollard 1985), the curvature of the propagation path being caused by mechanical interaction between adjacent crack tips (Pollard *et al.* 1982). Figures 2.8.4A and 2.8.4B (from Nicholson and Pollard 1985) show idealised sketches of the initial dilation and linkage of arrays of echelon cracks with straight and curved propagation paths respectively. Linkage occurs either by cross-fracturing of the *bridge* separating adjacent cracks (for straight propagation paths) or by propagation of crack tips into the adjacent crack (for curved propagation paths). After linkage of adjacent cracks, in both cases dilation increases rapidly (Nicholson and Pollard 1985).

2.9: Igaliko Dyke Features

Figures 2.9.1-4 and Plates 2.1-5 show features of dyke morphology observed in the Igaliko region. From these, the 'echelon array' morphology can be clearly seen with many of the features described in the previous section being easily recognised. Generally the dykes are quite narrow, commonly 3 to 8 metres, with the larger examples rarely exceeding 15 metres. BFD's are among the largest seen in the Igaliko region, with widths of about 15 metres, and as a general rule carbonatites tend to be the narrowest, rarely wider than 2 metres. Wider dykes, not surprisingly, tend to be coarser grained.

Figure 2.9.1 shows a schematic increase in the degree of dilation, from a narrow relatively unbent bridge in 2.9.1A through more curved bridges, followed by the development of a cross fracture in 2.9.1D to bridging blocks which have completely separated from one side-wall of the dyke in 2.9.1E and F (cf. Figure 2.8.2).

Separation of the dykes into several segments is not uncommon with one large fracture breaking up into a zone of several sub-parallel fractures. This produces a small swarm of dykes of essentially the same composition. The swarm of dykes shown in the Frontispiece cutting the Motzfeldt centre are all similar petrographically and chemically, individual members merging, bifurcating and pinching out along the length of the swarm. This can also be seen in Figure 2.9.2A and B, where one dyke splits into 2 smaller dykes.

Curved propagation paths can be seen in the 30cm wide dyke in Figure 2.9.2B.

Figure 2.9.1 Field sketches representing a sequence of increasing dilation from A to F.

A Relatively unbent bridge.

B and C Increased amounts of bending of the bridge.

D Small incipient cross fracture developing in bridge, indicating the onset of breaking.

E and F Complete separation of the broken bridge from one wall of the dyke.

Compare this sequence with Figure 2.8.4A.

Figure 2.9.1

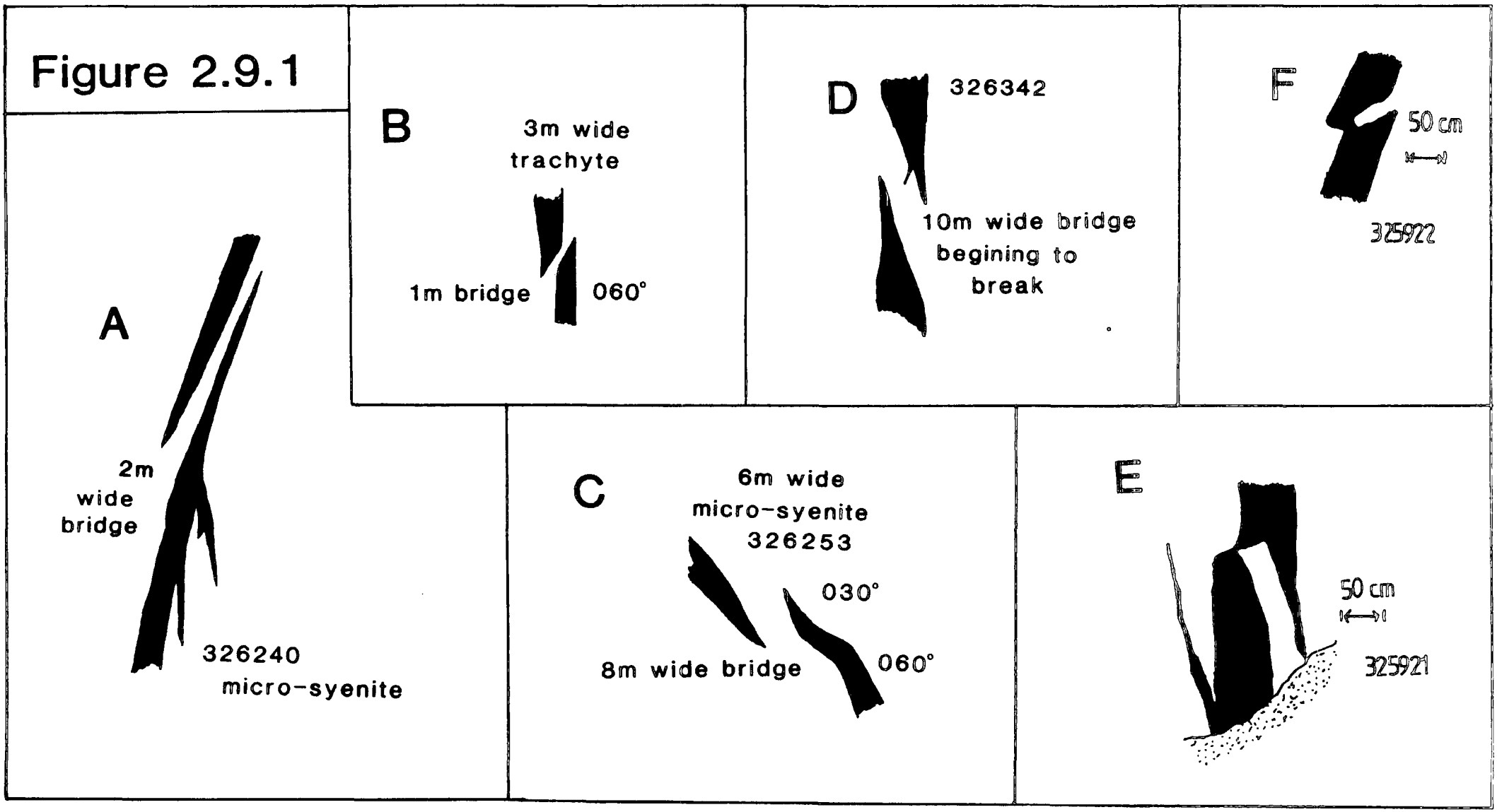
A
2m
wide
bridge
326240
micro-syenite
B
3m wide
trachyte
1m bridge
060°
C
6m wide
micro-syenite
326253
030°
8m wide bridge
060°
D
326342
10m wide bridge
begining to
break
E
50 cm
325921
F
50 cm
325922

Figure 2.9.2A and B Dyke 326217. The 30 cm dyke illustrated in B shows a rotating bridging piece (cf. Figure 2.8.4B) while the steps in the 80 cm dyke (the stumps of broken bridges) may indicate that this part of the dyke propagated along straight paths.

Figure 2.9.2C and D Large scale echelon features. These dykes will have propagated into or out of the page. C appears to have reasonably straight propagation paths whereas D seems to have grown along more curved cracks. Small steps in the lower section of D indicate a smaller en echelon geometry superimposed upon the larger echelon array.

Figure 2.9.2

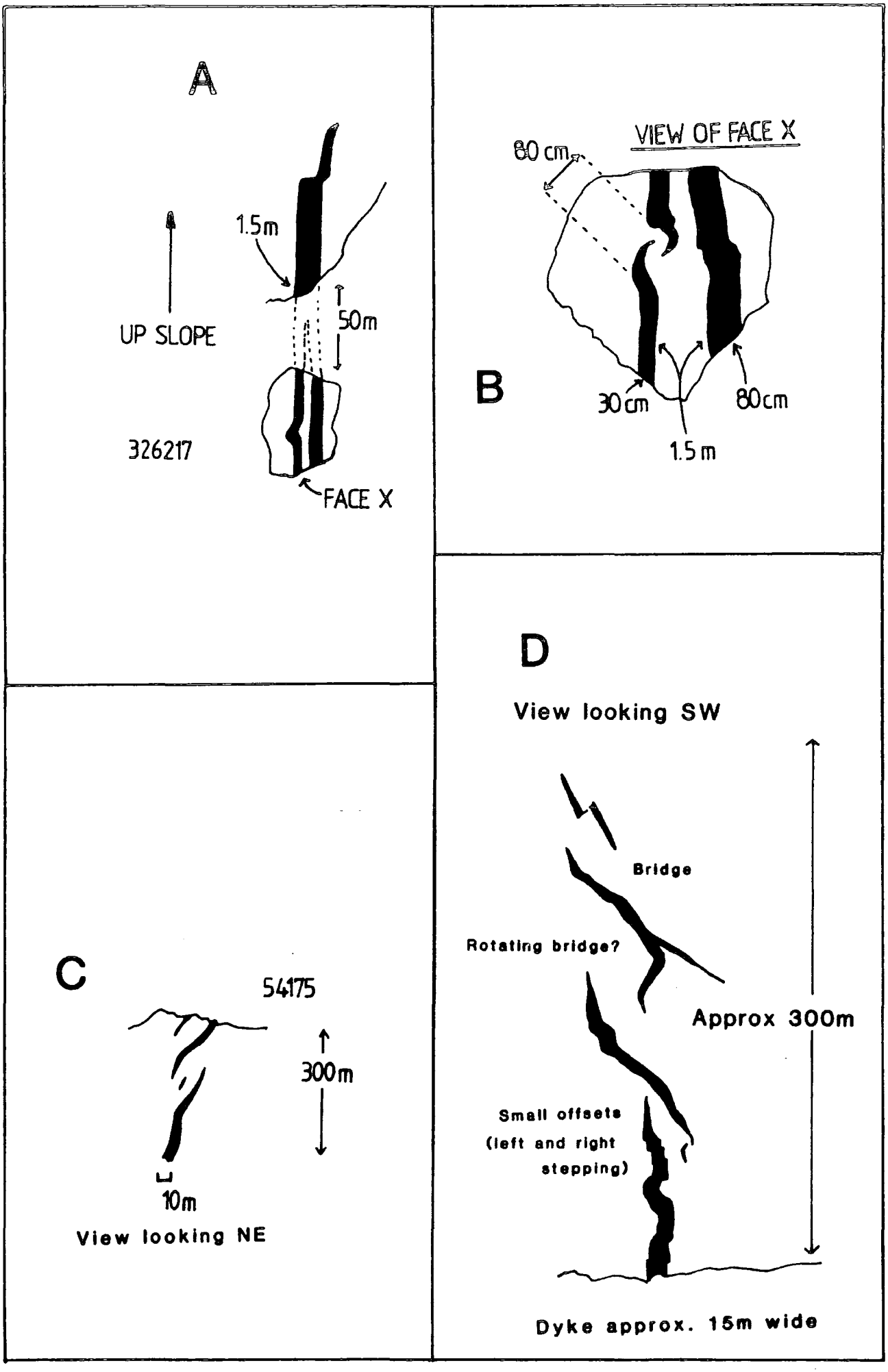
A
1.5m
UP SLOPE
50m
326217
FACE X
B
VIEW OF FACE X
80 cm
30 cm
80cm
1.5 m
C
54175
300m
10m
View looking NE
D
View looking SW
Bridge
Rotating bridge?
Approx 300m
Small offsets
(left and right
stepping)
Dyke approx. 15m wide

These have the effect of rotating the central block of rock between the two crack tips. Increased dilation would separate the rotated block from one side of the dyke. The 80cm dyke in the same figure shows small steps in the walls. These are the residual 'stumps' left after the breaking off and removal of a bridge.

The above echelon features were all on a 'metre' scale. Figures 2.9.2C and D and Plate 2.1. show features of echelon cracks on a 100m scale. The propagation direction of these dykes will have been either into or out of the page. In both cases the the individual echelon cracks have twisted through quite large angles (roughly 30°) from the presumed vertical orientation of the parent crack. Smaller scale echelon features of the dyke in Figure 2.9.2D can be seen as the offsets in opposite walls of the dyke, these being the stumps left from broken bridges. Both examples will be at some distance (several hundred metres to a few kilometres) from their parent cracks.

Figures 2.9.3 and 2.9.4 show detailed maps of two dykes at Storelv. These are well exposed dykes showing a variety of marginal features. In Figure 2.9.3 many bridges are still preserved, indicating an overall *left stepping* echelon crack geometry (see Figure 2.9.5A for terminology, after Segall and Pollard 1980), although the offshoot of the dyke in the lower right has a *right stepping* geometry. The dyke trends roughly 050° overall although it kinks to a roughly N-S trend with the development of some shearing where 2 larger, more continuous 050° fractures are linked. Petrographically all segments of the dyke are identical. Flow banding in very fine grained chilled material is a common feature of the margins of dykes. It can be seen to bend round broken bridges and steps in the walls of the dykes in many places.

In Figure 2.9.4 quite different features associated with dilation of a dyke can be seen. The margins still show the remnants of small broken bridges (see insets) with the emplacement of this dyke also being intimately associated with contemporaneous shearing (see Plate 2.5). A band of xenoliths within the dyke is not offset across the dextral shear zones which offset the dyke margins, this shearing being an early feature of the dilation.

Both left and right stepping echelon arrays are apparent in the field (see Figure 2.9.1 where A,B,C and F are left stepping and D and E are right stepping), although

Plate 2.1 View SW across Avanardleq, Motzfeldt centre, of dyke. The en echelon arrangement of the individual segments is clearly visible. Note the many small irregularities in the dyke walls, especially in the lower segment. The dyke is about 15 metres wide at the base of the picture.

Plate 2.2 Broken bridge in a spherulitic trachyte dyke. The bridge has become completely detached from one side wall of the dyke. Scale on hammer shaft in inches.

Figure 2.9.3 Field sketch of dyke at Storelv. This trachytic dyke showed many of the common features of dykes which form from the dilation and linkage of echelon cracks. Many bent bridges are preserved, with stumps of those which have broken protruding from the dyke walls. Flow banding at the margins of the dyke is also a fairly common feature. Where the dyke makes a marked change of direction (to roughly N-S) some shearing is apparent. this is probably a Riedel type shear induced by regional sinistral shear.

Figure 2.9.3

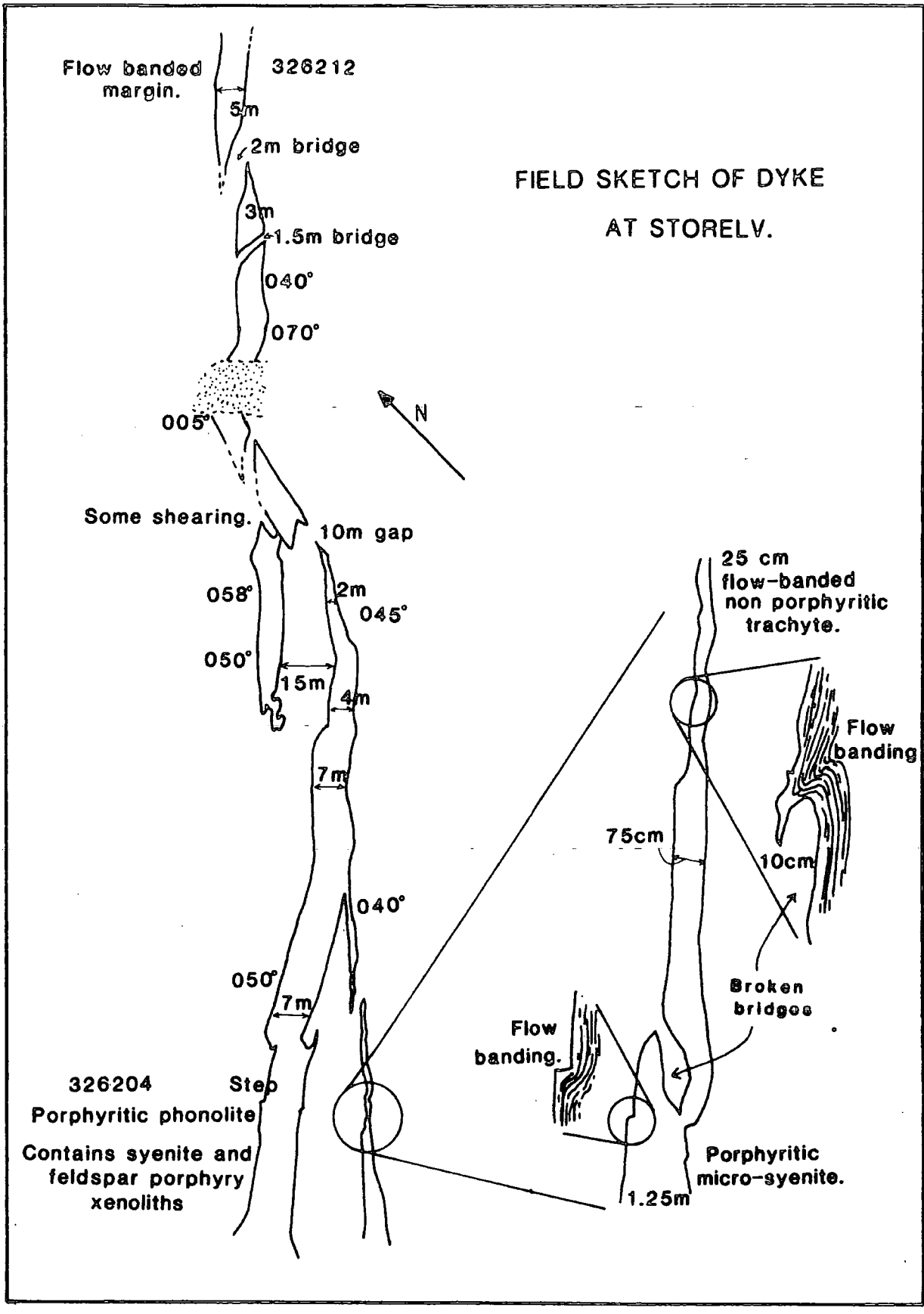
FIELD SKETCH OF DYKE
AT STORELV.
Flow banded margin.
326212
5m
2m bridge
3m
1.5m bridge
040°
070°
005°
N
Some shearing.
10m gap
058°
2m
045°
050°
15m
4m
7m
040°
050°
7m
326204
Step
Porphyritic phonolite
Contains syenite and feldspar porphyry xenoliths
25 cm flow-banded non porphyritic trachyte.
Flow banding
75cm
10cm
Broken bridges
Flow banding.
Porphyritic micro-syenite.
1.25m

Figure 2.9.4 Field sketch of dyke at Storelv. This phonolitic dykes contains many xenoliths concentrated into a distinct band. The emplacement of this dyke is intimately associated with shearing at the dyke margin oriented at 030°. These are probably Riedel shear zones caused by the regional sinistral shearing, and active at the time of emplacement. Steps in the margins and stumps of bridges are shown in the lower 2 insets. The upper inset shows fractures developed at the dyke margins, due to small relative horizontal (along strike) movements of opposite sides of the dyke.

Figure 2.9.4

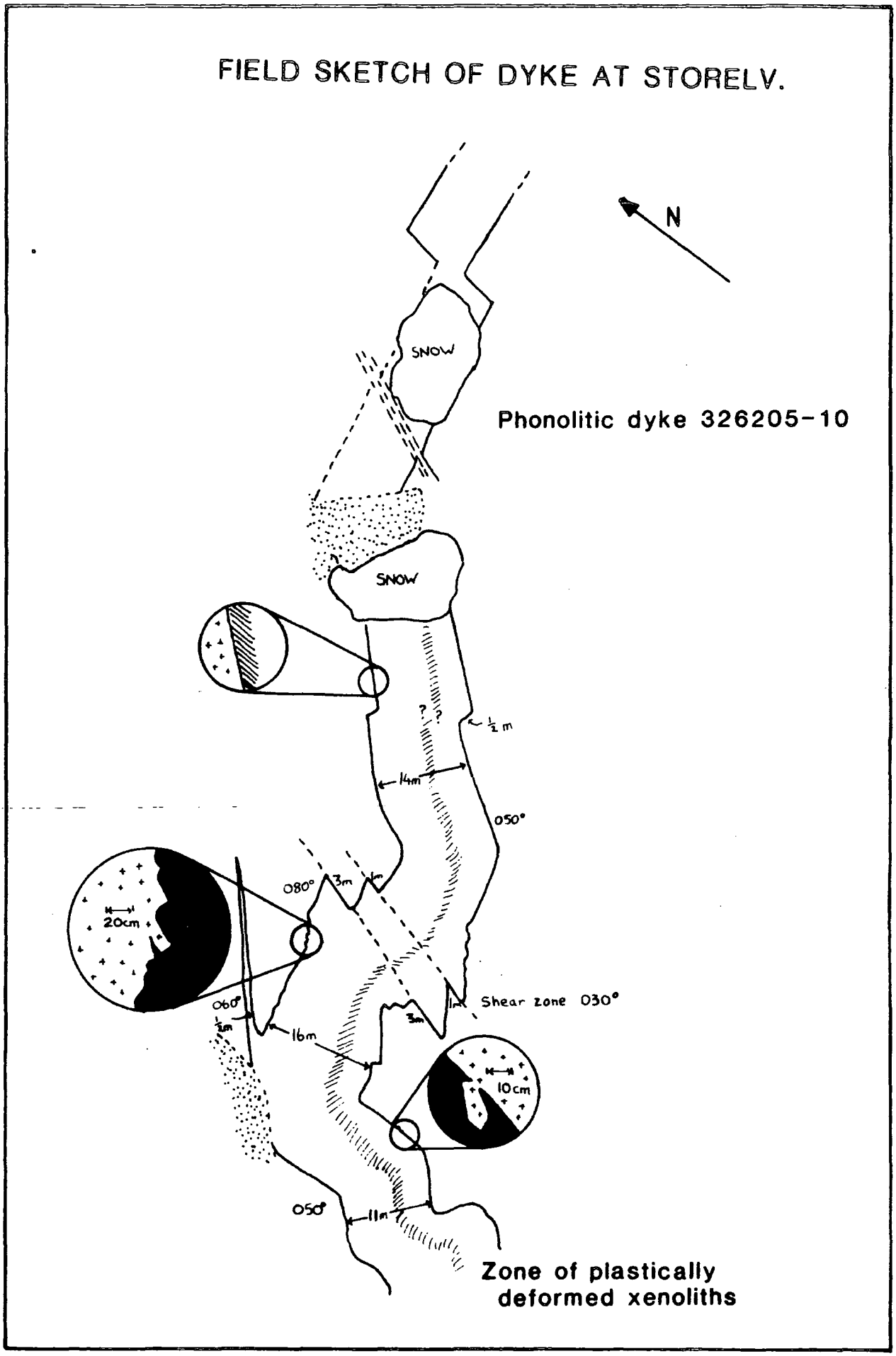
FIELD SKETCH OF DYKE AT STORELV.
N
SNOW
SNOW
Phonolitic dyke 326205-10
½ m
14m
050°
080°
3m
1m
20cm
060°
3m
16m
1m
Shear zone 030°
3m
10cm
050°
11m
Zone of plastically deformed xenoliths

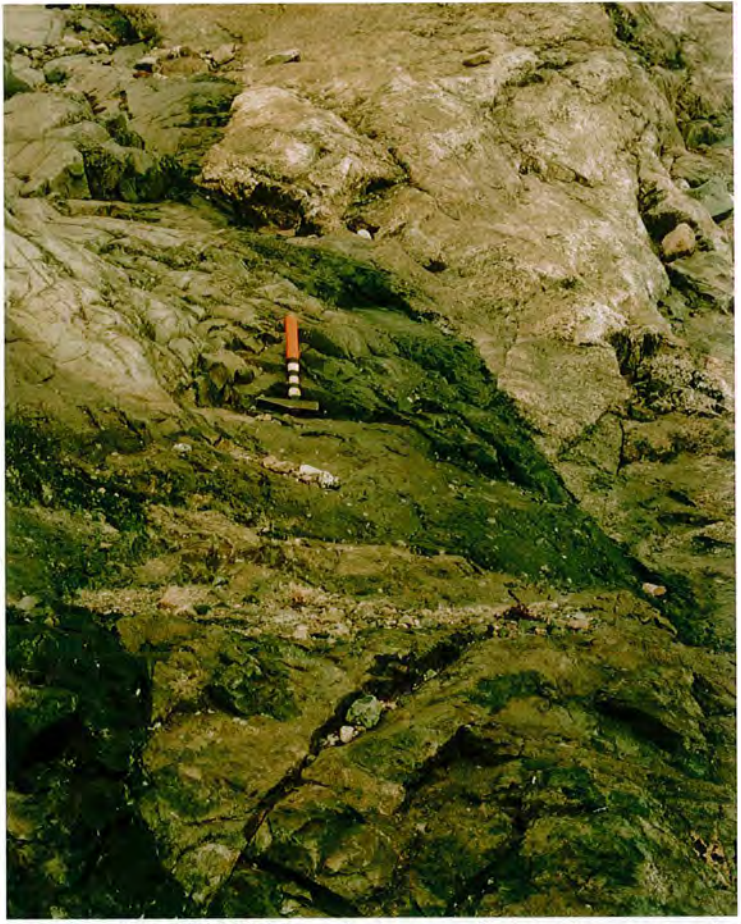

Plate 2.5 Shear zone crossing dyke 326205-10 producing an offset in the margin of about 1 m. The shearing was active at the time of dilation of the dyke, shown by the darker chilled marginal band (ca. 20 cm wide) but ceased before final solidification (see Figure 2.9.4).

Plate 2.6 Multiple narrow (1 to 2.5 m) dykes intruded into a fault zone (Sample 325615). Width of photograph approximately 40 m. Screens of granite separate individual parts of this dyke.

on a regional scale the Gardar dyke swarms have a right stepping geometry induced by (and at 45° to) the regional left lateral shearing (cf. Ramsay 1967, pages 88-91). Figure 2.9.5B shows how left and right stepping arrays of echelon cracks are superimposed on a regional set of right stepping echelon fractures.

However, in a simple shear model, such as Figure 2.9.5A, with no transtensional extension of the shear zone, left stepping fractures would remain closed (unless forced open by high pressure magma) whereas simple sinistral shear would cause the right stepping set to open. This will also be true of the 'secondary' set of echelon cracks superimposed on a regional set by the local secondary shear directions (small arrows, Figure 2.9.5B). If these secondary left stepping sets of echelon cracks do form they will have a higher strike direction than the equivalent right stepping set. When, however, bridge failure and crack linkage occurs the overall strike of the dyke (be it either initially left or right stepping) will be that of the regional set of echelon fractures (see Figure 2.8.3).

In a transtensional environment, the extension of the shear zone (as in Figure 2.3.1B) would, as well as causing dilation on the secondary right stepping fractures and on the Riedel shears, greatly assist in the opening of the secondary left stepping echelon cracks (see Figure 2.9.5B).

Slight variations in the orientation of the tension in the crust (caused perhaps by movement on different faults with time) may also favour/hinder the dilation of any previously formed fractures. Thus if the direction of maximum tension changes, different sets of pre-existing echelon cracks may open (see below).

In the Igaliko region there is a marked structural grain to the Julianehåb Granite. This is clearly seen on aerial photographs and is mirrored to some extent in the orientation of the SW trending fjords in South Greenland. Mapping in the Østfjordsdal area showed that the dykes trend roughly parallel to this structural grain. This however does not exist in the syenites of the Igaliko Nepheline Syenite complex, nor in the supracrustal material in the vicinity of Igaliko and Narssarssuaq.

The orientation of the grain with respect to the tensional stresses induced by the regional shearing may control the development of fractures in the rock, it being much

Figure 2.9.5A Theoretical geometry of fractures produced in a shear zone (after Segall and Pollard 1980).

Figure 2.9.5B Superimposition of left and right stepping en echelon array geometries upon a regional right stepping echelon array (marked by the dashed line). This model would require transtension for the left stepping set to form.

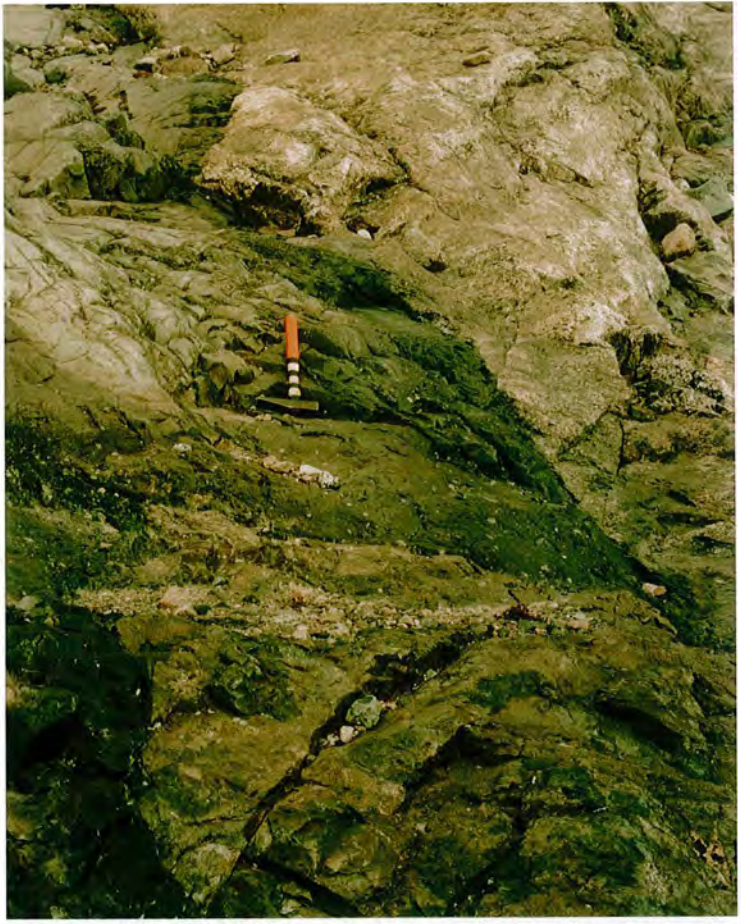

Plate 2.5 Shear zone crossing dyke 326205-10 producing an offset in the margin of about 1 m. The shearing was active at the time of dilation of the dyke, shown by the darker chilled marginal band (ca. 20 cm wide) but ceased before final solidification (see Figure 2.9.4).

Plate 2.6 Multiple narrow (1 to 2.5 m) dykes intruded into a fault zone (Sample 325615). Width of photograph approximately 40 m. Screens of granite separate individual parts of this dyke.

Figure 2.9.5

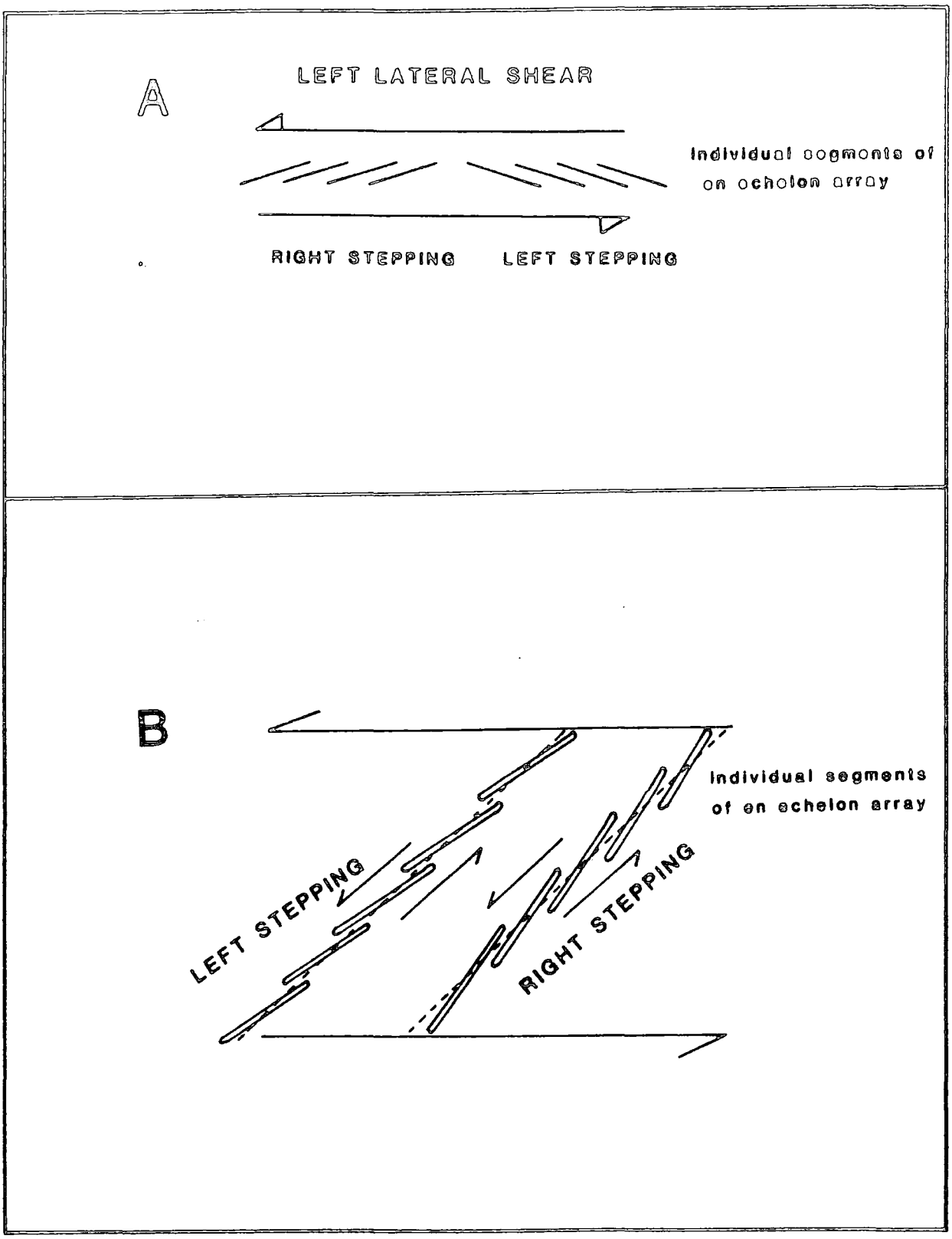
A
LEFT LATERAL SHEAR
individual segments of
an echelon array
RIGHT STEPPING
LEFT STEPPING
B
individual segments
of an echelon array
LEFT STEPPING
RIGHT STEPPING

easier for the rock to fracture along, rather than across, pre-existing lines of weakness. Left or right stepping secondary echelon geometries (such as those in Figure 2.9.5B) could thus form along inhomogeneities in the country rock. Their general orientation would be close to the regional 45° echelon array, the actual strike of individual dyke segments being governed by the angle the country-rock grain makes with this regional en echelon set.

Within the syenites local variations may produce left or right stepping geometries oriented close to the overall 45° orientation induced by the shearing. The syenites are however essentially homogenous when compared to the basement granite, and it may just be fortuitous as to whether left or right stepping echelon fractures develop, with transtensional extension generally favouring the opening of both left and right stepping secondary fractures (where as simple shear promotes the opening of a secondary right stepping set only).

The Giant dykes to the north of the Igaliko Nepheline Syenite complex strike at slightly higher angles than later more evolved dykes (see Chapter 2.6; Upton and Fitton 1985). These Giant Dykes appear to have a left stepping geometry and thus may be expected to have a slightly higher strike than right stepping dykes formed in the same tectonic regime. High extension rates to form these giant dykes may be coupled with transtensional extension of the province assisting in the formation of a left stepping geometry. A subsequently less vigorous transtensional extension of the area may then favour the formation of right stepping arrays, this possibly accounting for the 6° difference in strike between the Giant Dykes and the later more felsic dykes. A change from simple shear (Figure 2.3.1B) to transtensional extension (Figure 2.3.1C) causes a rotation of the orientation of the major extensional features. This may also have had an affect upon the orientations of the Giant Dykes.

Displacement along fault zones can also form arrays of echelon cracks. Figure 2.9.6B (from Gamond 1983) shows the relationship of such fractures (Riedel or R fractures) which open as shearing is initiated. Continued displacement of one side of the shear zone with respect to the other causes the formation of small faults (P fractures) on which slipping occurs, accommodating this extra displacement and causing dilation across the shear zone. Figure 2.9.6B shows one observed example of this type of emplacement

Figure 2.9.6A Association of R (Riedel) Fractures and P fractures in a fault zone (from Gamond 1983). The R fractures will develop under regional shearing, the P fractures will however only develop if the shear zone is allowed to dilate (Vialon 1979) or where displacement is great (Tchalenko and Ambraseys 1970).

Figure 2.9.6B Observed example of dyke from Igaliko occupying R fracture as in **Figure 2.9.6A**.

Figure 2.9.6

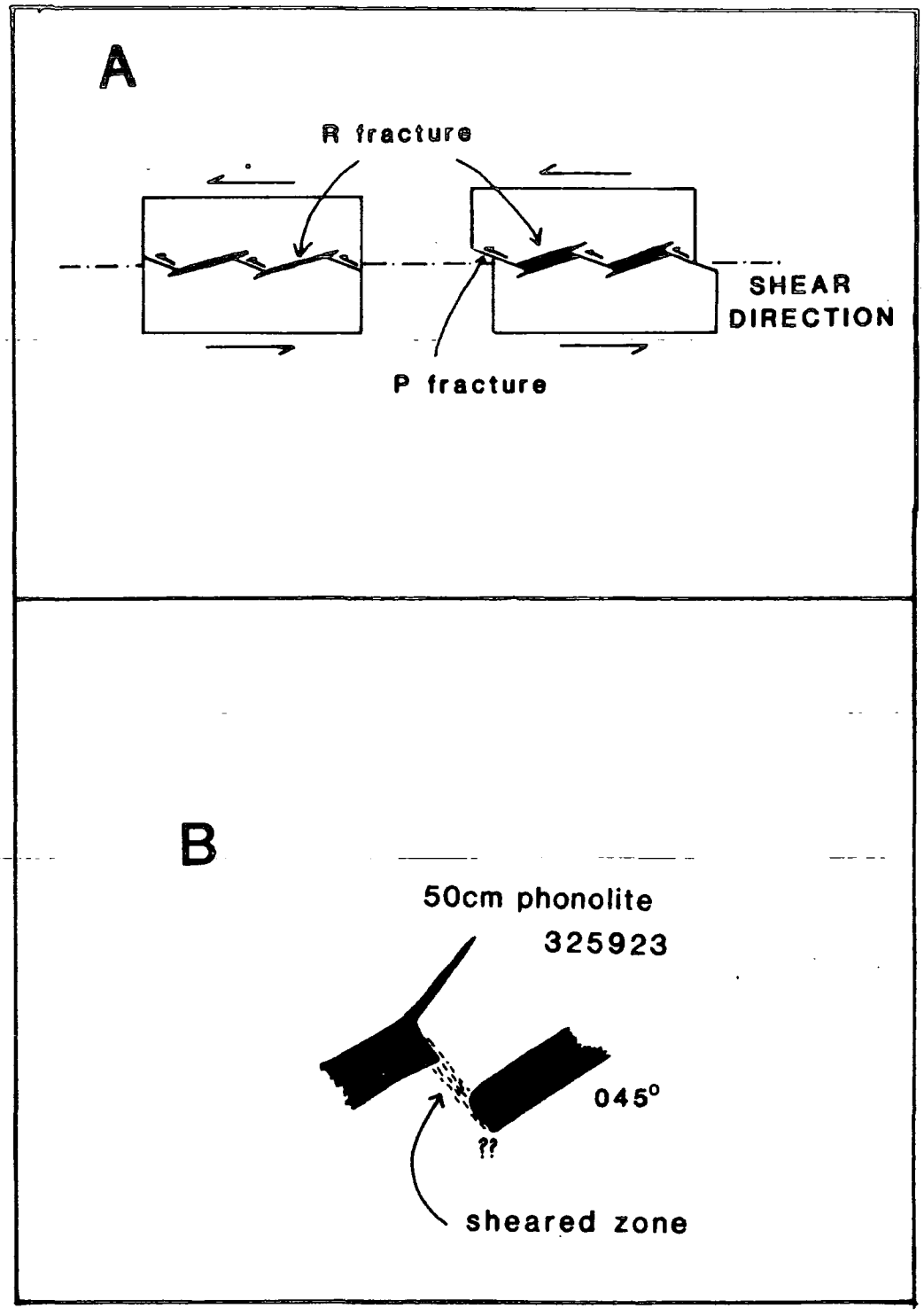
A
R fracture
SHEAR
DIRECTION
P fracture
B
50cm phonolite
325923
045°
??
sheared zone

mechanism, with the dyke sitting in the shear zone.

Another example of a fault zone controlling the emplacement of a dyke was seen on the western shore of the 475m lake in Mellemlandet (see Map 2). A swarm of about ten 1 to 1.5 metre basic dykes occupy a highly brecciated zone some 35 metres wide, with individual dykes separated by screens of granitic material between 1 and 2 metres wide. There seemed to have been little or no vertical or horizontal movement of the granitic material, and the displacement across the fault could not be determined due to lack of a suitable reference horizon. These dykes did not show the typical en echelon geometries (see Plate 2.5) and were probably a reasonably passive feature where basaltic magma seeped up a pre-existing fault zone as it dilated.

In conclusion, the majority of the dykes in this region show en echelon geometries on a variety of scales. Their orientation, in some cases is controlled by the structural grain of the rocks into which they are emplaced. Dyke emplacement along fault zones also occurred in the region although this mechanism is of minor importance. Transtensional extension of the province, coupled perhaps with high magmatic pressures, was responsible for the orientations and geometry of the Giant Dykes of the Tugtutôq - Ilímaussaq - Nunataq zone (and probably also those of the Nunarssuit - Isortoq Zone). Less vigorous transtensional extension (resembling more simple shear conditions) followed this and was operative during the emplacement of the smaller, more felsic dykes. These changes in tectonic regime over the Gardar province were caused by relative motions between the North American and Grenville plates producing large scale changes in crustal stresses across the area. Movements on faults of slightly different orientations resulted from these changes in stress regime. This in turn may have modified dyke orientations. Country rock grain will also have had some control on the orientations of some of the dykes.

2.10: Internal Features

Xenoliths and xenocrysts of crustal material are fairly common in the Gardar dykes, although no examples of mantle material have been recorded from Igaliko.

A notable case of xenolithic and xenocrystic dykes are the Big Feldspar Dykes (BFD's, see Bridgwater and Harry 1968). The petrology and geochemistry of these will

be dealt with in a later chapter although some features will be discussed here. The dykes contain plagioclase crystals up to 30 to 40 cm in length and/or large pieces (sometimes several metres in diameter) of anorthosite presumed to be from fairly high levels in the crust. The xenolithic and xenocrystic assemblage within a BFD tends to be fairly constant along its length (Emeleus and Harry 1970) and this can be useful in identifying dykes which have been displaced across fault zones (Emeleus and Stephenson 1970).

BFD's tend to have non-porphyritic (non-xenocrystic), sometimes flow-banded margins, with an increasing content of xenoclastic material towards the centre of the dyke, there sometimes being a fairly abrupt increase in the content of foreign material. BFD's tend to be among the larger dykes in the region (commonly around 15 metres wide) and often contain extreme amounts of xeno-clastic material (anything between a few to about 70% of clasts by volume). This large content of solid material within the magma will greatly increase its viscosity (see Figure 2.10.1, from Arzi 1978).

Similarly, the so called 'Rhomb Porphyries', trachytic dykes containing many large (1 to 2cm) alkali feldspar phenocrysts (up to 30% by volume commonly), tend to show aphyric margins and densely porphyritic cores. Similar relationships are also developed to a lesser degree in less phenocryst-rich dykes.

Many authors have noted similar features in porphyritic dykes (eg. Drever and Johnston 1958, and Gibb 1968 on dykes from the Isle of Skye; Simkin 1967 on dykes and sills from the Isle of Skye). Experiments by Battacharji and Smith (1964) and Battacharji (1967) using suspensions approximating to porphyritic magmas showed how flowage differentiation could concentrate suspended particles into the central part of a conduit. Three principal mechanisms producing this migration have been identified.

The Wall Effect operates only over a few grain diameters from the walls of the pipe repelling individual crystals. It is poorly understood and only of importance in very narrow conduits (Maude and Whitmore 1956).

The Magnus Effect, acting upon individual grains in laminar flow in a velocity graded profile (ie. with faster flow rates at the core of the dyke), induces a rotation in the grain caused by the different rates of flow on either side of it. This causes inward translation of the grain (Pao 1961).

Figure 2.10.1 Relative viscosity of magma versus percentage of melt by volume (from Arzi 1978). This curve is calculated from

$$\eta_r = (1.35C - 0.35)^{-2.5}$$

where η_r is the relative viscosity and C is the percentage of melt. This indicates the *Rheological critical melt percentage* at 26% (Roscoe 1952). The shaded zone represents a suggested usual range of RCMP of 20± 10% (Arzi 1978).

Figure 2.10.1

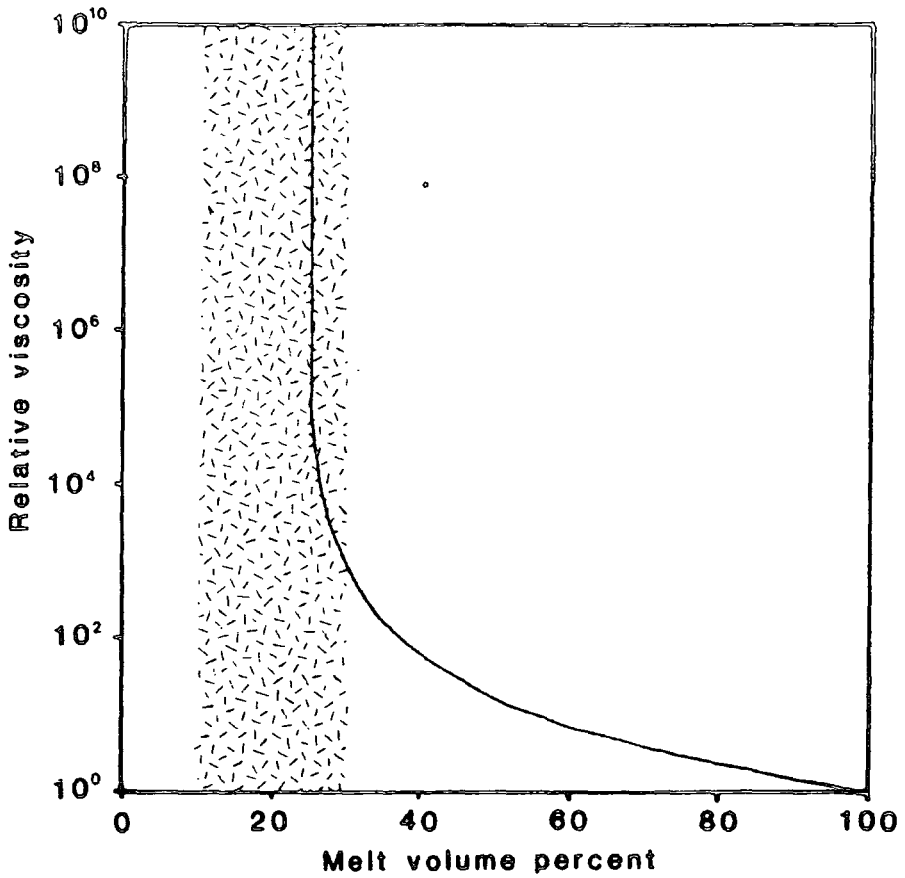
Relative viscosity
10^{10}
10^{8}
10^{6}
10^{4}
10^{2}
10^{0}
0
20
40
60
80
100
Melt volume percent

The Bagnold Effect affects the grain population in contrast to individual grains. In all flowing Newtonian suspensions with more than 13% by volume of spherical grains there is a grain dispersive pressure due to the shear of the suspension and proportional to the rate of shear whether flow is laminar or turbulent (Bagnold 1954). Komar (1972a and b) applied this to flow of porphyritic magma in dykes and showed that, so long as the concentration of crystals is greater than 8%, this grain dispersive pressure is higher at the dyke margins than at the dyke core. This compels the crystals to concentrate towards the centre of the dyke where the rate of shear tends to zero. Komar (1972a) considers this to be approximately 100 times more important than the Magnus effect. In dykes of more than 100 m width however, the Bagnold Effect becomes unimportant (Barrière 1976) and other methods such as gravity stratification etc. must be sought to account for these differentiated intrusions.

Most dykes from the Igaliko Nepheline Syenite complex are in the 3 to 10 metre width range, with only a few dykes exceeding 15 metres and none above 30 metres in width. In the sparsely porphyritic dykes (a rather arbitrary field definition for dykes with phenocrysts less than about 5% by volume), the Wall and Magnus Effects will gradually redistribute the phenocryst load. In those dykes with more than 8% by volume of phenocrysts (which includes those referred to as porphyritic, Rhomb Porphyries and BFD's) the Bagnold Effect will rapidly concentrate more (and larger) phenocrysts towards the central portions of the dyke (Komar 1972a).

However, Bridgwater (1968) and Bridgwater and Harry (1968) assigned the distribution of phenocrysts and xenocrysts in the BFD's to the gradual tapping of a gravity stratified magma chamber in which crystals of different compositions (and densities) had settled to different levels. A horizontal traverse of the dyke thus represents a vertical section through the magma chamber. This is in stark contrast to the flow differentiation model proposed by Battacharji (1967) as a means of producing variations in crystal content across a dyke.

A 15 metre wide BFD cropping out about 200 metres west of the jetty at Igaliko village showed features similar to those shown by Bridgwater (1968). A section from margin to core across the dyke showed a 5cm aphyric chilled margin; 15cm of very sparsely porphyritic chilled material (phenocrysts of alkali feldspar 3 to 5mm across);

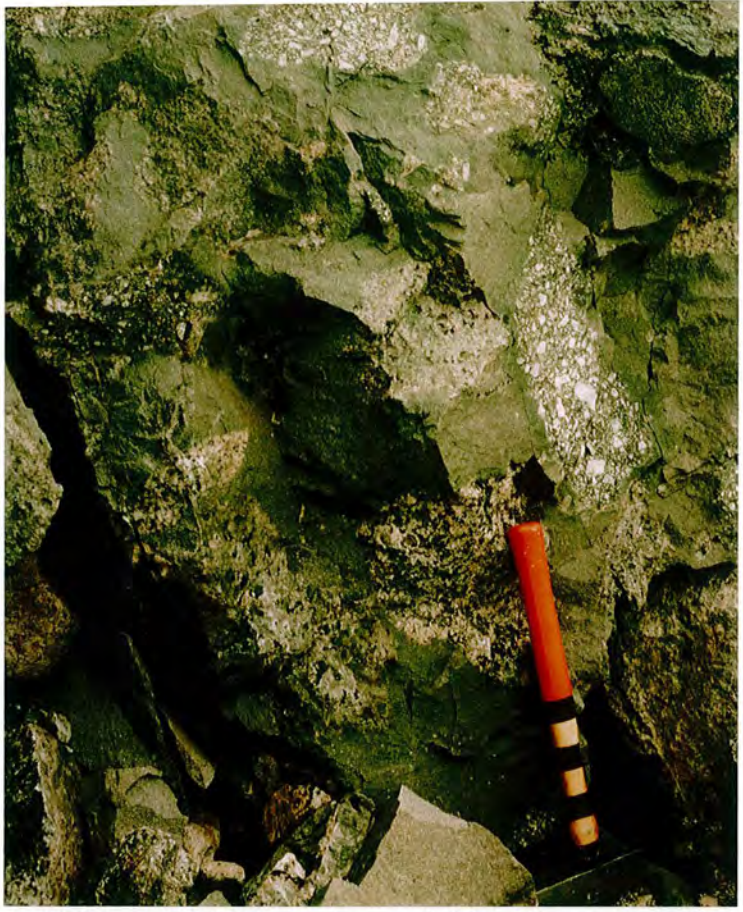

Plate 2.7 Xenoliths of BFD material (10 cm above and right of hammer shaft) and syenite (under end of hammer shaft) entrained in a microsyenite dyke. Scale on hammer shaft in inches.

Plate 2.8 Plastically deformed (dark) xenoliths in phonolitic dyke 326205-10. These are presumed to be a chilled marginal facies to the dyke, wrenched from the dyke walls by continued throughput of magma. Note also large, pale yellow syenite xenolith (upper right).

1.5 metres of porphyritic trachy-dolerite (about 40% by volume of plagioclase (An_{42}) and anorthoclase crystals 2 to5 mm across); and a central core of very coarsely packed plagioclase (An_{52}, 5mm to 5cm) and anorthoclase crystals (5mm to 1.5cm) making about 50% by volume of the rock, in a (trachy-)doleritic matrix. Occasional large (20cm+) anorthosite xenoliths and plagioclase megacrysts occurred in this central zone. These internal boundaries are not sharp but rapidly gradational.

Gravity stratification could explain the compositional variation across the dyke (cf. Bridgwater 1968; Bridgwater and Harry 1968) but not the size variation of the included material, where the larger clasts are concentrated more towards the centre. Flow differentiation, particularly 'Bagnold' forces, would however produce this inward concentration of coarser material (Komar 1972a), but not the compositional variation. It seems likely then, that initial gravitational separation in a magma chamber was modified on intrusion by flow differentiation processes to produce the observed outcrop pattern.

Xenoliths of rocks presently cropping out at the surface in the Gardar region are also fairly widespread, although not especially common. These will, to a large extent, be the remnants of broken and detatched bridges carried along by the magma. They are often distinct from the host rock of the dyke at its present level of exposure. These include fragments of granite, sandstone and syenite with odd instances of BFD (see Plate 2.7) and fine grained igneous material assumed to be a chilled marginal facies, removed from the dyke walls by continued throughput of magma, ie. cognate xenoliths.

The dyke 326205-10 (outcrop illustrated in Figure 2.9.3) showed many interesting features of the occurrence of xenoliths (see Plates 2.8-10). Small dark clasts within the dyke occur exclusively in a distinct band about 2 metres wide close to the south-western margin of the dyke. There is no marked internal chill or visible compositional change separating this zone from the rest of the dyke. The xenoliths are highly contorted having been deformed whilst in a plastic condition. This dyke also contains many syenitic xenoliths. These exist in various stages of disaggregation/assimilation (see Plate 2.8 which shows a complete, pale yellow xenolith and Plate 2.9 where a cluster of separate crystals from a 'dissolving' xenolith can be seen).

This type of assimilation will release crystals, strictly xenocrysts, into the dyke.

Their true origins may therefore be (if no disequilibrium exists between the xenocryst and host) almost impossible to detect directly. With trachyte/phonolite and syenite having similar solidus temperatures, disaggregation of xenoliths would occur fairly rapidly and the recognition of 'ghost' xenoliths in the field may be the only way to observe this process. Rapid cooling of (particularly narrow) dykes would minimise this and the relatively high viscosity of these trachytic melts may prevent distribution of the liberated xenocrysts. Most xenoliths observed in the field were in reasonably complete condition.

Other xenolith types included Julianehåb Granite and sandstone. Granites, with fairly low solidus temperatures, are seen in some examples to be partially melted whereas the only examples of sandstone that were seen remained intact. 326250 and 41947 is a breccia dyke from the flanks of Igánaq (see Map 1) and contains many sandstone xenoliths (see Plate 2.10), being almost grain supported. At this locality the dyke cuts the Julianehåb Granite, and is at least 150 m below the unconformity with the Eriksfjord Formation and over 2 km along strike from down-faulted sandstones on the south-eastern side of Igánaq. It seems likely that this dyke was fed from the south-east, although some vertical movement cannot be ruled out. Again, magma under high pressure must be required to push what must be an extremely viscous mixture of solid and liquid many kilometres.

Bridgwater and Harry (1968) observed some BFD's containing up to 80% by volume of xenocrysts and xenoliths, concluding that in some cases post intrusion (and pre-solidification) narrowing of the dyke must have occurred. Such large contents of solid material within the magma would greatly increase its viscosity placing it at or near its *Rheological Critical Melt Percentage* (RCMP), where shear and deformation of the solids must take place for flow to occur (see Figure 2.10.1, from Arzi 1978). Since most xenoliths in the BFD's are undeformed (as too are the sandstone xenoliths in the breccia dyke above) it would thus seem that in some instances narrowing of the dyke after magma injection may have occurred.

In the Rhomb Porphyries, with perhaps 30% of phenocrysts by volume, magma viscosities would be increased about 7 fold compared to an aphyric magma of the same composition. Intrusion of these magmas would not necessarily require great magmatic

pressures. In contrast, some of the BFD's with 70% or more of xenolithic material will have had viscosities up to 1000 times that of the aphyric equivalent of the host magma, and this must attest to high magmatic pressures and probable forceful intrusion for at least some of the Gardar dykes.

This increase in viscosity will not affect the flow differentiation forces operating on the suspended solid load, the grain dispersive pressures such as the Bagnold forces being directly proportional to the viscosity of the fluid part of the solid-fluid suspension (Bagnold 1954).

Evidence for magma movement can also be seen from mineral alignments and drag folds within the dykes (cf. Tweto 1951). Tabular minerals, such as bladed laths of alkali feldspar are commonly aligned parallel to the dyke margins, this flow banding bending around offsets and steps in the margins of the dyke. Drag folds caused by viscous flow within the dyke are also quite common (see Plates 2.11 and 2.12). Slight variations in the modal mineralogy allow these structures to be picked out, although in some instances, where mineral deformation and shearing has occurred due to the differential flow of parts of the dyke, the end result is more spectacular (Plate 2.12).

Flow banding is also an extremely common feature of the carbonatites. Silicate minerals are loosely concentrated into bands which are more resistant to weathering than the intervening carbonate and these stand proud of the dykes surface. These bands show drag folds etc. (Plates included in Carbonatites chapter).

Several examples of composite dykes are recorded from the Igaliko Dyke Swarm, with the same fracture having been exploited more than once as a conduit for magma flow. Sometimes abrupt margins can be detected between the younger and older parts of the dyke and in other instances the internal contacts are more diffuse. These may separate markedly different compositions or may be just internal chills separating magma pulses from the same source. Generally, the degree of compositional change is slight between pulses, suggesting the time gap between individual injections of magma was relatively small.

2.11: Crustal Extension

Crustal extension due to dyke emplacement was obtained from measured sections across various parts of the dyke swarm. Exposure was generally good and it is estimated that between 80% and 90% of dykes were recorded.

Dilations of about 3% were obtained in both the Østfjordsdal region and the ground between Igánaq and Tunugdliarfik (to the NE of Igaliko village). In the area to the north of Narssarssuaq, where there are many more basaltic and Big Feldspar dykes, crustal extension due to dyke intrusion is about 10% (Pearce and Emeleus 1985). This compares well with the 10% extension recorded on the Ilímaussaq Peninsula by Scharbert (1968).

Crustal extension in the Tugtutôq - Ilímaussaq - Nunataq zone due to dykes (including Giant Dyke lithologies) ranges between 18.7% and 25% (see table below).

Tugtutôq	18.7%	
Mellemlandet	22.7%	ca. 80% exposure
G. F. Holm Nunataq	25%	poorly exposed

(data from Upton and Fitton 1985)

Exclusion of the Giant Dykes from the aggregate width of dykes seen in Mellemlandet gives a crustal extension of 8.8%, comparing favourably with the 10% measured to the north of Narssarssuaq, where no Giant Dykes crop out. 3% extension across the Igaliko Nepheline Syenite complex may seem to be a reasonable background figure for the Gardar province (cf. Bradshaw 1987 and Chapter 2.4), increasing locally to between 10% and 25% along the line of the Tugtutôq - Ilímaussaq - Nunataq zone of dykes. It has already been speculated that extension across the Gardar as a whole was small, with the limited development of graben structures in regions of greater extension (for example, Tugtutôq). Increased dilation in these regions will be marked by increased numbers of dykes.

Plate 2.11 Drag folding in a dyke cutting the Østfjordsdal syenite picked out by differential weathering. Lens cap 5 cm across.

Plate 2.12 Drag fold in dyke 326322. The dark band contains sheared groundmass minerals. The lighter material is mineralogically identical. Lens cap 5 cm across.

SECTION 2: ROCKS OF COMPOSITIONS RANGING FROM BASALT TO PHONOLITE AND RHYOLITE

CHAPTER 3: PETROGRAPHY

3.1: Introduction

This chapter describes the main features of the majority of the dykes seen in the Igaliko area. It deals with the petrology, mineralogy and geochemistry of rocks ranging in composition from basalt (tephrites and basanites also), through to evolved rock types such as phonolites and quartz porphyries (rhyolites). The carbonatitic and lamprophyric dykes are largely excluded from this chapter and will be discussed later in more detail. Petrographically the dykes can be divided into various (obvious) groups either in hand specimen or thin section, although in many cases the name applied to a rock has been obtained from its geochemistry (eg. total alkali-silica plot, Cox *et al.* 1979, see Figure 5.2.1).

The first section of this chapter will deal with petrography and field descriptions of lithologically distinct groups, the later sections dealing *en masse* with the mineralogy and geochemistry of these rocks as an evolving group. On this basis it must be remembered that 'pigeon-holing' of these rocks is done for convenience of description and is not meant to separate chemically and petrogenetically related rock types.

As a general rule these dykes are fairly fresh. The majority are unaffected by later geological events except that many of the dykes in the vicinity of the late Igdlerfigssalik syenites have been thermally metamorphosed. In the petrographic descriptions fresh, unmetamorphosed varieties are considered first followed by altered or recrystallised examples.

3.2: Giant Dyke and possible BD_0

Giant Dykes (Upton 1962) extend from Tugtutôq across the north western edge of the Igaliko Nepheline Syenite complex and disappear under the Inland Ice at G. F. Holm Nunataq (see Figure 1.2.1). Samples of one of these (a 500m wide Giant Dyke, 63777-80) were collected by C. H. Emeleus in 1963 from Mellemlandet (see Map 2). In this dyke, fine grained, dark marginal dolerite grades inwards to a coarser, well layered gabbroic

rock with cumulus platy plagioclase crystals (An_{55}) up to 1cm in length. Interstitial to these are irregular ophitic (Ti-) augites 1 to 2cm diameter, euhedral/subhedral olivine (ca. Fo_{70}, up to 1mm diameter, see Plate 3.1) and apatite needles up to 500μm. Opaque oxides (Fe-Ti) occur as blocky, well formed interstitial crystals (ca. 1mm in diameter) in the core of the dyke whereas in the margins the appear as larger (up to 2mm) skeletal crystals. Where fresh, the olivine contains many extremely small (20μm long) needles of an (exsolved) opaque oxide mineral. 63777, an anorthositic gabbro from the central layered portion of the dyke, is particularly rich in apatite (ca. 8% modally).

Late stage, possibly hydrothermal, alteration has converted most of the feldspar to sericite but has barely affected the ferro-magnesian minerals. Margins of some of the olivine crystals have been altered to iddingsite, chlorite and iron oxide grains but this is generally rare. Upton and Fitton (1985) report similar lithologies from giant dykes on Mellemlandet, Syenitknold and G. F.Holm Nunataq, however, these have evolved through syeno-gabbros to ferro-syenites.

Also in Mellemlandet and to the east of the 475m lake (the author's camp 9, 1984, see Figure 1.1.1) a 30m wide gabbroic dyke (strike 115°, possibly related to the BD_0 generation of dykes, Emeleus and Harry 1970) is seen to be cut by the the Motzfeldt centre. A doleritic margin (325610) grades inwards to a moderately coarse, dark blue-grey gabbro (325611) containing fairly fresh plagioclase laths (An_{52}) up to 1.5mm in length. These, along with fresh augite subhedra (also up to 1.5mm across) are enclosed in a very fine grained, dark greenish-brown felted groundmass of chlorite and iron oxides, probably representing an altered glass phase. Larger opaque oxides occur as blocky crystals (500μm in diameter, probably Ti-magnetite); also present are thin, acicular crystals (up to 500μm in length, possibly ilmenite) which become less abundant towards the core of the dyke. No fresh olivine was observed. Small, rare apatite crystals (400μm by 50μm) also occur. These are sometimes skeletal, tubular and contain altered glass. The alteration of the dyke will have been caused, in part, by the emplacement of the Motzfeldt centre nearby.

This dyke (325610-11) has no counterpart elsewhere within the Igaliko Nepheline Syenite complex as regards age or size and as such is not related to the main (Late-) Gardar phase of dykes. It appears to be faulted out across the NNW trending fault

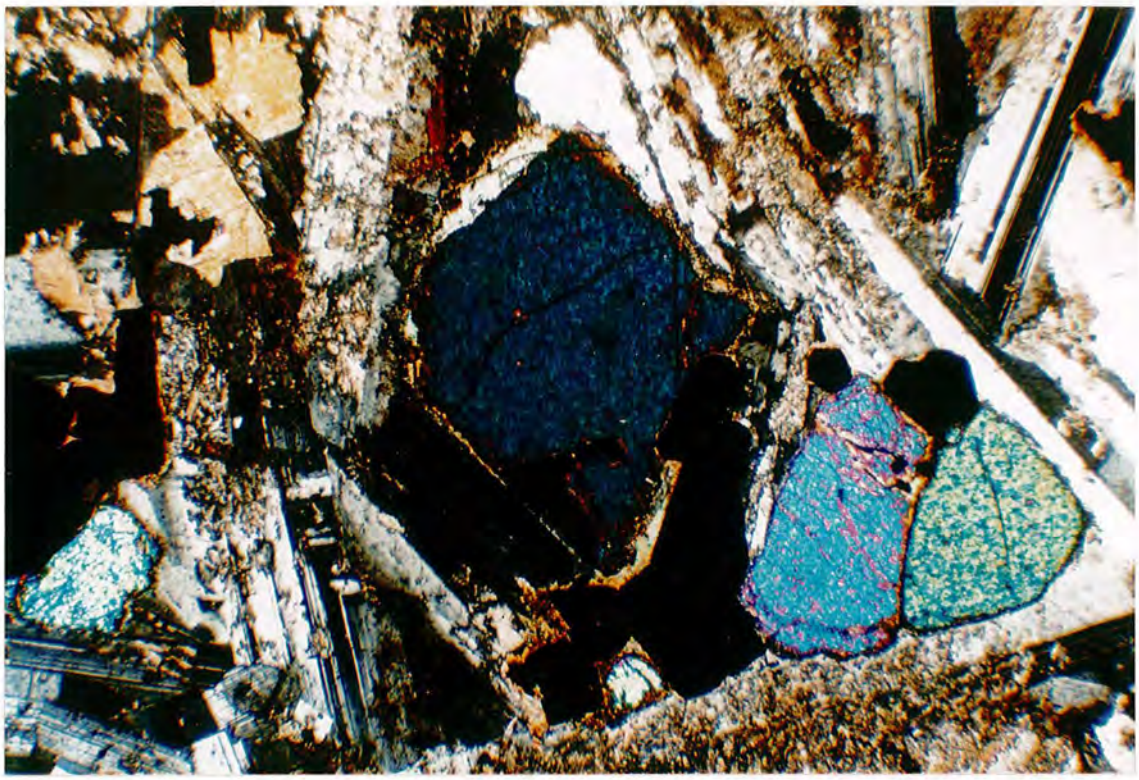

Plate 3.1 63778, Alkali Gabbro Giant Dyke. XPL. ×35. Cumulus olivine and sericitised plagioclase (An_{60}) with interstitial Fe-Ti oxides and ophitic salitic pyroxene (upper left , pale yellow interference colours). Reaction rims of biotite on the oxides, some chlorite rimming the olivine.

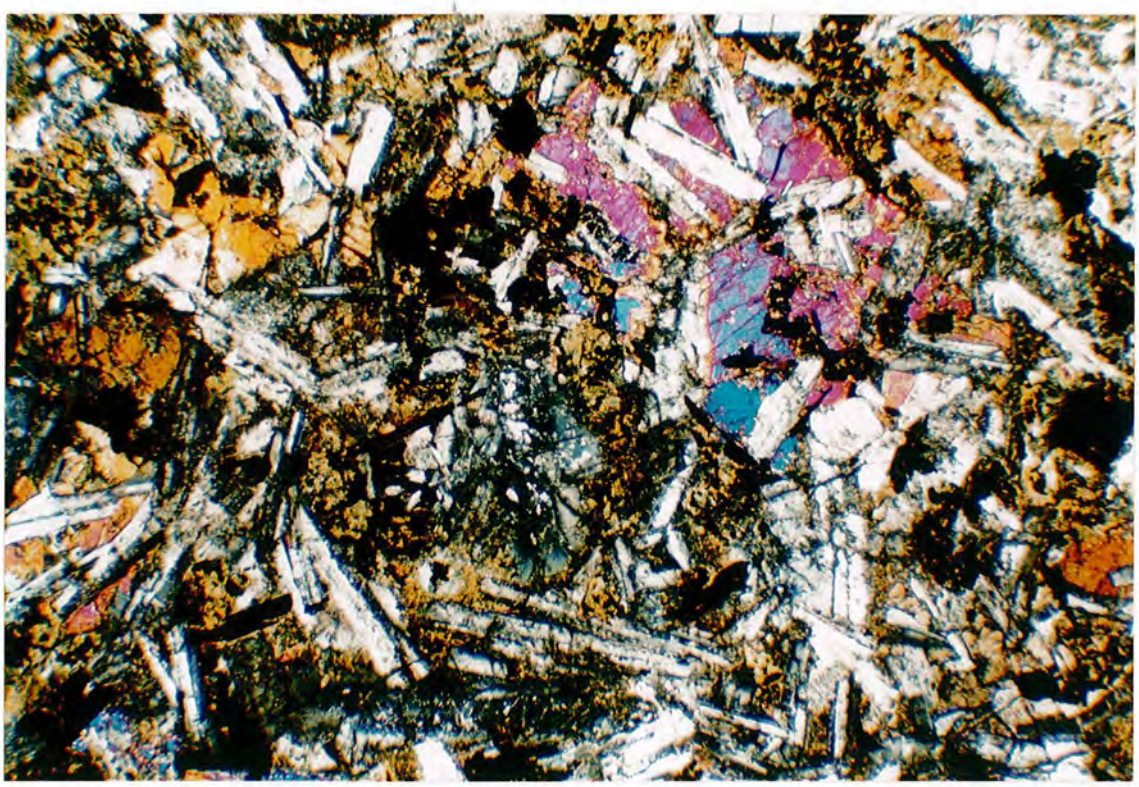

Plate 3.2 325992, Dolerite. XPL. ×35. Ophitic, (sub-ophitic) augitic pyroxenes enclosing plagioclase (An_{60}). Acicular ilmenite grains set in a ground mass of altered glass (chlorite and Fe-oxide grains).

running along the string of lakes from the North Qôroq centre, although from Emeleus and Upton (1976, Figure 170) it would appear to lie along the strike of a BD_0 cropping out some 10km north of Qagssiarssuk. It has not been reported from the intervening ground, and the evidence presented here is not enough to decide whether or not this is a BD_0 generation dyke. The implications of concluding that this a BD_0, with regard to the stratigraphy of the Gardar province would involve a reclassification of the early Igaliko Centres at the least.

3.3: Basalt and Dolerite.

Basaltic and doleritic dykes are most abundant to the north of Narssarssuaq where they crop out along with many BFD's and trachytic dykes (see Map 2). They are relatively scarce across the rest of the Igaliko Nepheline Syenite complex. A swarm of doleritic dykes has been reported to the south east of the Igdlerfigssalik Centre, but no material from these dykes was available for study. Late alkali gabbro dykes occur within both the Motzfeldt and Igdlerfigssalik Centres and these will be discussed in a later section.

Basaltic dykes are generally between 4 and 10 metres wide with well chilled margins. They contain plagioclase, either as large phenocrysts (up to 3cm by 8mm, eg. 325971) or as smaller groundmass crystals (typically 1mm long). Compositions range between typical values of An_{60} to An_{40} for both phenocrysts and groundmass plagioclase with some zoning to more sodic margins in the groundmass crystals being evident.

Alteration has proceeded to varying degrees in the majority of the rocks with plagioclase being partially converted to aggregates of sericite. Clinopyroxene, a pinkish titaniferous augite ($Ca_{42}Mg_{34}Fe_{24}$) generally remains very fresh in most samples, showing a sub-ophitic relationship to the groundmass plagioclase (see Plate 3.2). Fresh olivine is present in some of the samples occurring as small, roughly equant (subhedral) grains of about Fo_{70-75}. Marginal alteration of olivine to chlorite and iron oxides is common, with chlorite pseudomorphs showing olivine was originally present in some more altered specimens. Groundmass aggregates of chlorite and iron oxide are common to all examples, in part produced by the breakdown of olivine and partly produced by the alteration of an interstitial glass phase. Iron oxides (ilmenites in 325990) are abundant,

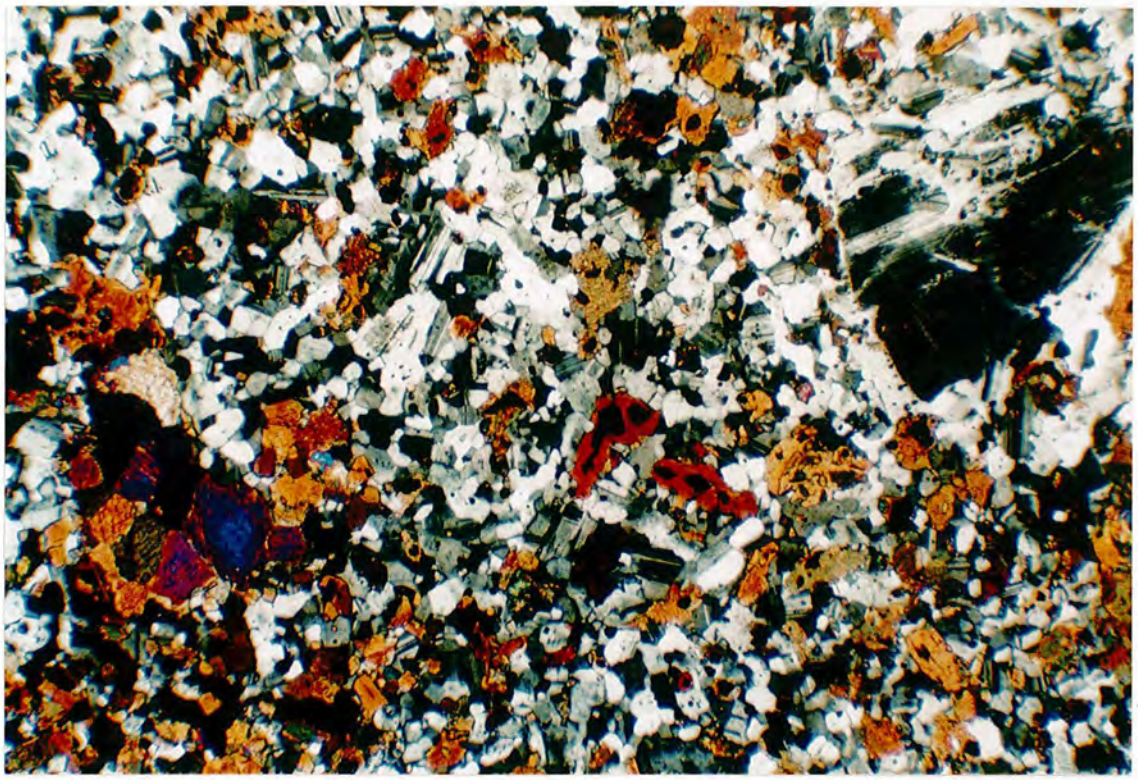

Plate 3.3 63845B, Recrystallised Basalt. XPL. ×35. Granoblastic texture of small pyroxene, plagioclase and olivine grains. Clusters of pyroxene and larger grains of plagioclase suggest a porphyroblastic texture.

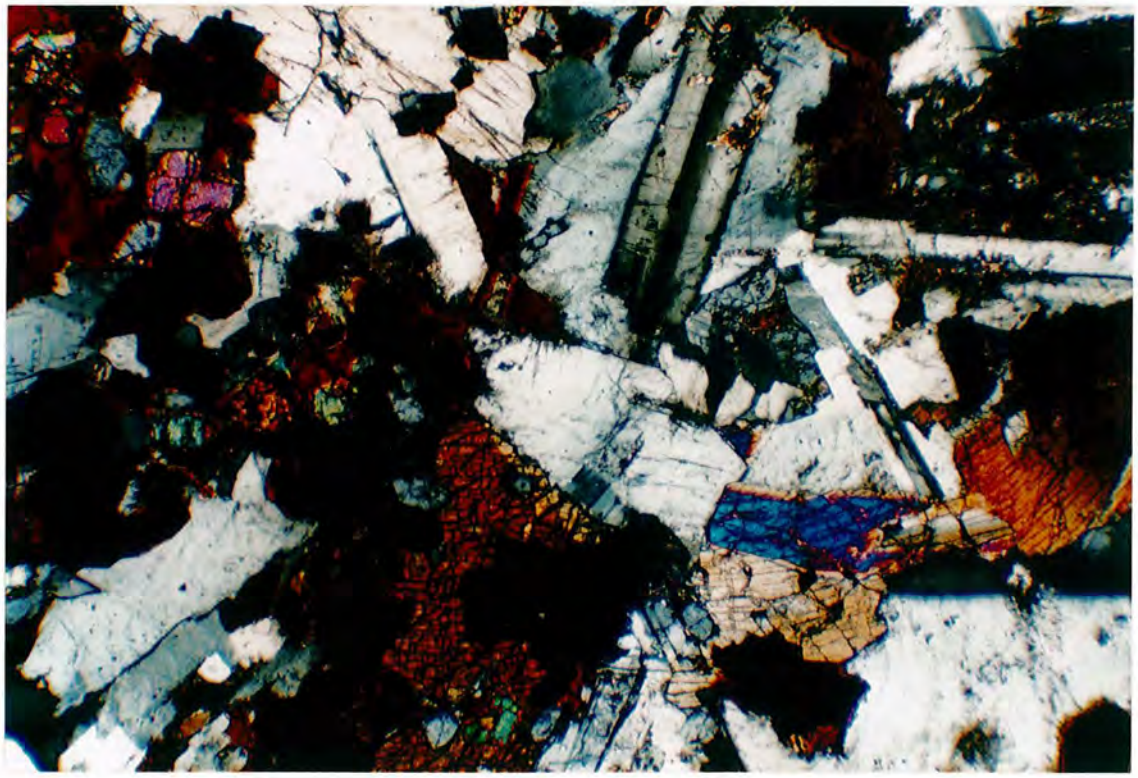

Plate 3.4 43902, Syeno-gabbro. XPL. ×35. Mugearitic syeno-gabbro with both alkali feldspar and plagioclase. Large salitic pyroxenes (bottom centre) and smaller olivine (Fo_{40}, top left). Deep red Ti-rich biotite encloses opaque oxides. Minor apatite.

modally 10% or more, with both blocky (500μm diameter) and acicular (500μm long) varieties present in the same specimen. Pyrite is also present. Apatite is rare, occurring as scattered small (350μm long) crystals or in some samples as small needles (100μm) enclosed in augite and olivine (eg. 325990).

Chemical analysis revealed two picritic basalts, and although altered, clear outlines of large (2.5mm diameter) olivine phenocrysts (now chlorite) can be seen in a flow laminated groundmass of (500μm long or less) plagioclase laths (325618).

Chlorite (after ferro-magnesian minerals or glass), sericite (with islands of fresh plagioclase), iron oxide aggregates and occasional rare biotite comprise the typical alteration assemblage of the basaltic types. This alteration is developed to a greater or lesser degree in all samples.

Recrystallisation

One recrystallised (hornfelsed) 'basalt' (63845B) was found cutting the Early Igdlerfigssalik syenites (see Plate 3.3). It shows a well developed granoblastic texture on a 200-300μm scale with a mineralogy of plagioclase (An_{55}, 45% modally), augite (20-25%), hornblende(20-25%), olivine(5%) and opaque oxides (5%) with reaction rims of biotite. Large aggregates (up to 1.5mm diameter) of small (200μm) individual clinopyroxene crystals contribute to a blasto-porphyritic texture as do some plagioclase rich patches of the groundmass. The texture and mineralogy would suggest medium to high grades of metamorphism (Spry 1969). Complete re-equilibration has not occurred in this sample with large modal differences in mineral contents evident across the sample on a 5mm scale.

3.4: Hawaiite and Mugearite

Hawaiites and mugearites form a group of rocks which are chemically between basalt and benmoreite. Higher alkalis and silica and less magnesium than basalts is reflected mineralogically by a gradual decline in the quantities of plagioclase and ferro-magnesian minerals and an increase in the content of more alkali rich feldspars. They occur more widely across the province than basalts and dolerites, although they are not particularly abundant.

Typically hawaiites, similar in appearance to basalts, contain plagioclase (about An_{35-45}), pinkish Ti-rich augite/salite (no longer showing ophitic relations to the feldspar), iron oxides and olivine (Fo_{50-60}). Alkali feldspar occurs in some of these rocks, either as patches interstitial to the plagioclase or as small blocky crystals. A typical alteration assemblage would be chlorite after ferro-magnesian minerals, sericite or clay minerals after feldspar and reaction/alteration rims of biotite enclosing the iron oxides.

Mugearites contain more discrete alkali feldspar, a less calcic plagioclase (An_{20-30}) and fewer ferro-magnesian minerals than hawaiites. Olivine and pyroxene have both become more Fe rich than in the hawaiites (Fo_{40-30} and salite/augite).

Compared to the basalts, the apatite content increases gradually from hawaiite through to mugearite, reaching perhaps 1-2% modally. Amphibole (?α=light brown, β=dark greenish-brown, γ=dark brown, a ferro-pargasitic hornblende) occurs in some of these trachy-basalts, either as interstitial patches in the groundmass or as alteration/reaction products of pyroxene and olivine at a late stage.

The hawaiites and mugearites are generally aphyric, although occasional rare anorthoclase phenocrysts ($An_{20}Ab_{57}Or_{22}Cn_1$) showing well developed albite and pericline twins are seen. The margins of these phenocrysts are often somewhat corroded and they are commonly overgrown by feldspar of the same composition as that in the groundmass.

The BFD's form part of this group of rocks, their matrices generally being hawaiitic or mugearitic in composition. As a group they will be discussed in a later chapter.

Recrystallisation

Several recrystallised mugearites were found in the vicinity of the Late Igdlerfigssalik syenites. They show granoblastic textures similar to those observed in the basalts, although generally slightly coarser in grain size (ca. 300μm). They are composed predominantly of alkali feldspar and dark brown hornblende, each approximately 40-50% of the mode. Biotite, opaque oxides and apatite occur in subordinate amounts. Relic phenocrysts of alkali feldspar (possibly relic anorthoclase) can be seen in some samples (eg. 326357).

Aggregates of amphibole and biotite may suggest a blasto-porphyritic texture after

pyroxene. Where the grade of recrystallisation is lower, development of a granular texture has been suppressed (eg. 58123). In these less metamorphosed examples original alkali feldspar laths are still visible (although somewhat clouded) and the only mineralogical change is the conversion of ferro-magnesian minerals to aggregates of biotite (200-300μm in diameter).

3.5: Benmoreite

Benmoreites are the largest single rock type from the Igaliko Dyke Swarm and as such show the greatest amount of internal variation. They are common across the whole of the Igaliko Nepheline Syenite complex, and were generally described in the field as 'trachyte'. Their mineralogy remains fairly consistent throughout the group which essentially rests between mugearite and either phonolite or trachyte.

Phenocrysts of feldspar, either anorthoclase or an alkali feldspar such as sanidine are fairly common in these rocks (see Chapter 4.8). The anorthoclase usually shows very well developed pericline and albite twinning (see for example Plates 3.15, 3.17 and 3.18), and may or may not be mantled by a more alkali rich feldspar similar in composition to the groundmass feldspar. The 'sanidine' type feldspars (strictly compositions intermediate between high albite and sanidine) show simple Carlsbad twins. They are sometimes zoned and often develop narrow overgrowths of groundmass feldspar. The feldspars only rarely show microperthitic exsolution textures, which sometimes may be quite coarse although not usually visible in hand specimen (see also Recrystallisation).

Other phenocryst phases include micro-phenocrysts of pinkish titan-augite, generally about 500μm in diameter; and of a pale yellowish fayalitic olivine. These olivines are generally badly corroded around their margins with the production of much opaque oxide. They rarely exceed 300-400μm in diameter.

The groundmass mineralogy is dominated by laths of alkali feldspar, showing simple Carlsbad twins or occasionally multiple (albite) twinning (see Plates 3.5A and B). Their compositions vary across the whole alkali feldspar range, although most are confined between Or_{40} and Or_{60} (see Figure 4.8.1). These feldspar laths are often aligned to produce striking trachytic textures.

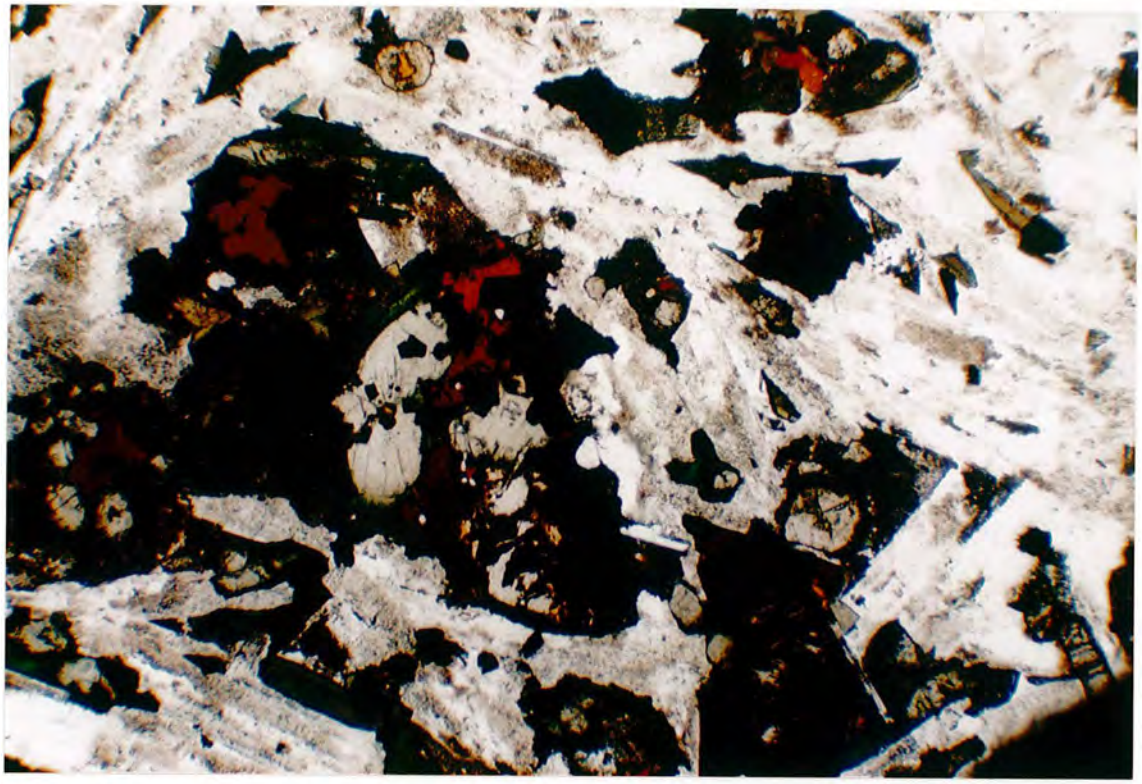

Plate 3.5A 325986, PPL. ×35.

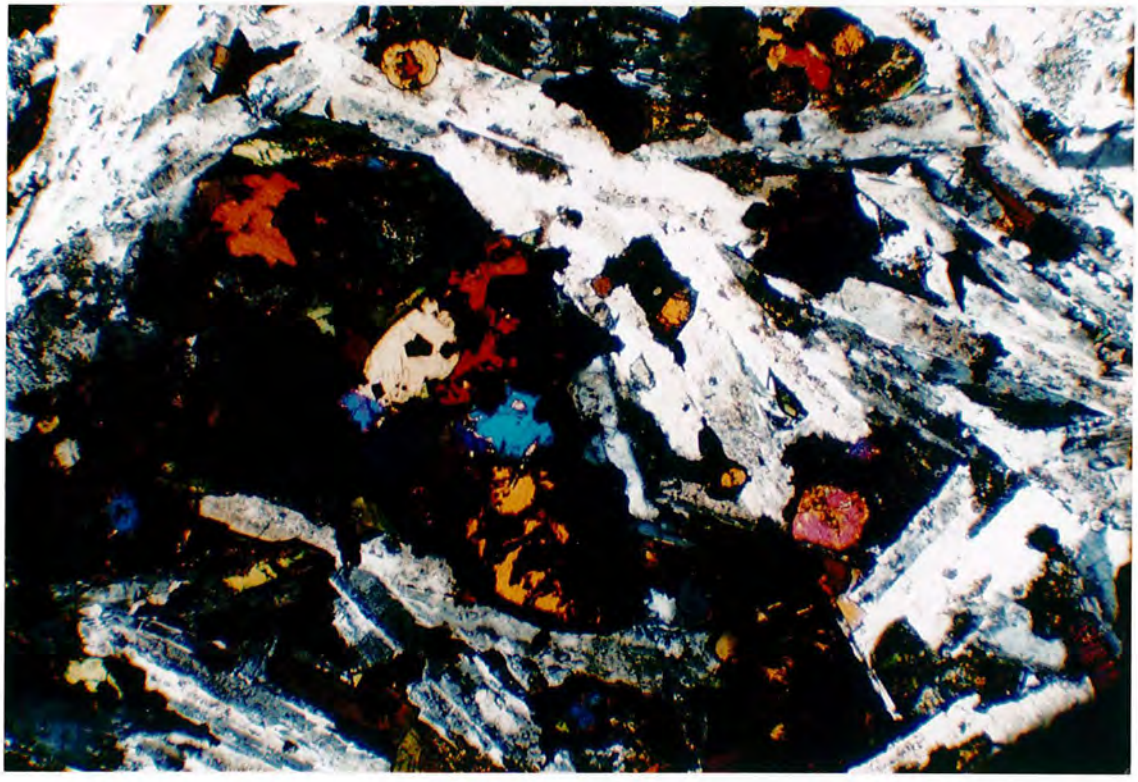

Plate 3.5B 325986, Benmoreite. XPL. ×35. Pale salitic pyroxene cores zone out to green aegirine-augite rims over a narrow width with alkali amphibole (dark green-blue) overgrowths. Also biotite (brown) and corroded olivine with oxide rims (bottom of mafic cluster at centre of picture). Groundmass composed of alkali feldspar and minor apatite.

Benmoreites can be either silica oversaturated, silica saturated or silica undersaturated, (the latter being the more dominant condition in the Igaliko dykes) and is indicated by the presence of quartz, of neither quartz nor nepheline, or the presence of nepheline. Other feldspathoidal minerals such as analcite or sodalite also indicate silica undersaturation. Quartz, nepheline or feldspathoids rarely exceed 10% of the mode, typically occurring in quantities of 3-5% .

Nepheline is the most common felsic mineral after feldspar. It is often altered to gieseckite, a high birefringence, colourless, micaceous mineral. This tends to form either as single 'flakes' (up to 300μm typically) within otherwise unaltered nepheline, or as larger, amorphous aggregates partly or wholly replacing the original nepheline. Nepheline usually occurs as patches interstitial to the feldspar, although in some instances it forms small (a few hundred microns diameter), blocky subhedral/euhedral crystals. Quartz, analcite and sodalite occur exclusively as patches interstitial to the groundmass feldspar.

The mafic mineralogy is dominated by pyroxene and amphibole, constituting between 30 and 40% of the mode. Both minerals are usually present although occasionally only amphibole occurs. The pyroxene typically occurs as small pale pinkish-green crystals with cores of augite/salite or ferro-augite/ferro-salite commonly zoning out to darker bottle/grass-green aegirine-augite margins.

Amphibole, often occurring as reaction rims to the pyroxene, ranges in composition from calcic to alkali (based on the classification of Leake 1979). Where not as an overgrowth on the pyroxene, amphibole occurs as patches interstitial to the feldspar. The following table shows typical pleochroic schemes for the most commonly occurring observed of amphibole.

	α	β	γ
Ferro-richterite	muddy dark brown	olive brown	pale straw brown
Katophorite	pale straw brown	muddy bluish-green	deep olive green
Arfvedsonite	deep inky blue	pale pinkish green	dark brownish-blue

Other amphiboles were also recorded in lesser amounts than the above (eg. ferro-edenite, pleochroic in browns). As a rule, the amphiboles undergo an increase in Na

and Fe from the core to the margin of the crystal, coupled with an decrease in Mg, changing colour from browns and greens to dark inky blues.

The presence in these rocks of alkali rich mafic minerals such as aegirine-augite and arfvedsonite shows that a peralkaline condition (moles Na+K > Al) has been reached.

Small grains of iron oxides are present in all cases, modally up to a few percent and often rimmed by biotite. Biotite also develops as a separate phase in minor amounts in many of these samples. Apatite is common in amounts of a percent or so (modally) in virtually all examples.

Alteration, evident to some degree in most samples, is first manifested by a clouding of the feldspar.As alteration proceeds this becomes more turbid as alteration proceeds with the development of brownish (?iron-stained) clay minerals. Ferro-magnesian minerals alter to iron-stained patches and aggregates of dark greenish-brown (iron rich) chlorite and iron oxides. Nepheline, as already mentioned alters to produce gieseckite.

Recrystallisation

Many dykes of benmoreitic composition have been recrystallised in the thermal aureole of the Late Igdlerfigssalik syenites. The textural and mineralogical changes are best described by tracing one dyke (ie. fixed whole rock composition) towards the syenite margin. Samples 58291-8, collected by C. H. Emeleus at distances of between 700m to 150m from the contact show these changes extremely well. In general there is a gradual textural development to greater degrees of recrystallisation as the contact of the syenite is approached. However, samples 58294 and 58295 differ from this general trend. The following list is compiled to show a gradual change with distance from the contact. To achieve this samples 58294 and 58295 have been listed in reverse order due to their similarities with 58296 and 58293 respectively. This break in a smooth textural development with distance from the Late Igdlerfigssalik syenites is probably due to differences in local conditions (water content?) between 58294 and 58295.

58291 -700m. Texturally extremely similar to an unmetamorphosed benmoreite with well developed trachytic texture. Mineralogy: alkali feldspar (500μm long), amphibole (sub-calcic ferro-edenite), bottle green aegirine-augite. Mafic minerals

Plate 3.6 58294, Recrystallised Benmoreite. XPL ×35. Large poikiloblastic amphibole (hastingsitic hornblende) with a granoblastic ground mass of perthitic alkali feldspar and areas of (brown) altered nepheline (gieseckite?) at left of picture. This texture is typical of high grade thermal metamorphism of these rocks.

Plate 3.7 326331, Recrystallised Phonolite. XPL. ×35. Brown amphibole and green pyroxene cluster in bottom left of picture. Despite the development of a granoblastic texture the rock has still retained a trachytic appearance even though thoroughly recrystallised. The term *trachy-blastic* is suggested for this texture.

are unzoned and the feldspar shows a noticeable perthitic texture. Small amount of high birefringence material within the feldspar due to the development of small (5μm), moderate to high relief inclusions (?pyroxene or amphibole). Both iron oxides and biotite show ragged outlines.

58292 -650m. Fairly similar to 58291. Perthitic exsolution in feldspars has become coarser, with feldspar laths still showing a trachytic texture. More biotite has developed as too has more speckley ?pyroxene or amphibole. Minor amounts of cancrinite developed after nepheline. Amphibole (ferro-edenite and katophorite) and aegirine-augite still present as discrete grains.

58293 -600m. Mineralogy: dark green-dark brown hastingsitic amphibole, alkali feldspar and iron oxide. There is no pyroxene. Trachytic texture has mostly been replaced by a developing grano-blastic texture. Brown altered patches, possibly (stained) gieseckite, have developed in the groundmass (10-15% modally) after ?nepheline. Feldspar is mostly perthitic although some separate albite and orthoclase grains are visible.

58295 -470m. Extremely similar to 58293 both texturally and mineralogically. Some cancrinite has also developed.

58294 -500m. Appearance of large (2.5mm diameter) poikiloblastic amphibole (pleochroism dark green - straw green - straw brown, compositionally hastingsite or hastingsitic hornblende), occasionally containing relic cores of a pinkish-green aegirine-augite. The amphibole contains many small inclusions of feldspar (200-400μm in diameter). Groundmass has a well developed granular texture (on a 500μm scale) and consists of perthitic feldspar with occasional separate grains of albite and orthoclase. Coarsely perthitic phenocrysts of alkali feldspar (4mm in length) still visible. Patches of altered nepheline (gieseckite) occur as muddy rounded grains. Some sphene (up to 200μm diameter) has developed. Iron oxides have aggregated into larger (1mm diameter) rounded grains often rimmed by sphene. This sample is illustrated in Plate 3.6.

58296 -400m. Mineralogy and petrography very similar to 58294. Slightly coarser granoblastic texture than 58294 (600-800μm scale). Many small aegirine-augite

grains (up to 500μm) present with no amphibole overgrowth. Amphiboles (hastingsitic hornblende) slightly smaller than 58294 (ca. 1.5mm diameter). Groundmass contains (400μm) fresh nepheline crystals.

58297 -300m. Groundmass feldspar predominantly albite and orthoclase as separate grains. More altered than 58296, with clouding of the groundmass feldspar. Amphibole still as large dark brown-pale brown pleochroic poikiloblasts, compositionally magnesian hastingsitic hornblende. Minor aegirine-augite occurring only as cores to the amphibole poikiloblasts.

58298 -150m. Large (5mm+ diameter) greenish black-light brown/fawn poikiloblastic amphibole (hastingsitic hornblende) in a groundmass of altered amphibole, nepheline and orthoclase (clouded to a muddy brown colour). Fresh feldspar and nepheline inclusions protected from alteration within the amphibole poikiloblasts. Dark green aegirine-augite occasionally seen as cores to the amphibole. Relic alkali feldspars, altered and coarsely perthitic, are still discernable. Minor amounts of groundmass cancrinite and biotite present. Some (retrograde?) development of chlorite after ferro-magnesian minerals.

In general, the major changes in the benmoreites on thermal metamorphism can be summarised as; (i) exsolution and sub-solvus recrystallisation of the feldspars to albite and orthoclase; (ii) equilibration of initially zoned ferro-magnesian minerals and (iii) consumption of the pyroxene and recrystallisation of the amphibole to form large poikiloblastic crystals. All recrystallised rocks of benmoreitic composition showed textures similar to some of those described above. The compositional development of the amphiboles from these samples is discussed in Chapter 4.3.

3.6: Phonolites

Phonolites are the second most abundant group of analysed rocks and are identified essentially by the appearance of abundant nepheline in thin section. They tend to form fairly narrow dykes (3-5m commonly), which are feldspar-phyric although rarely with large nepheline phenocrysts. They are thus generally referred to as trachytes in the field. Phonolites are common across the whole of the Igaliko Nepheline Syenite complex.

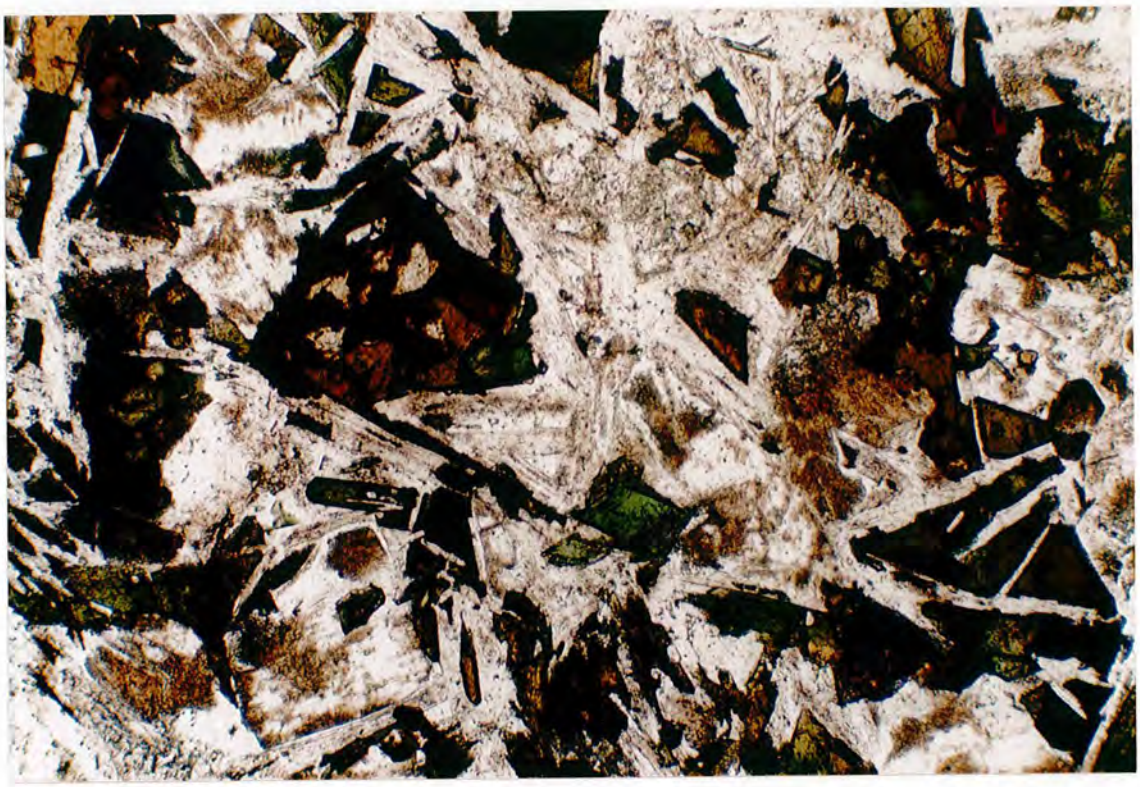

Plate 3.8A 326207, Phonolite. PPL. ×70.

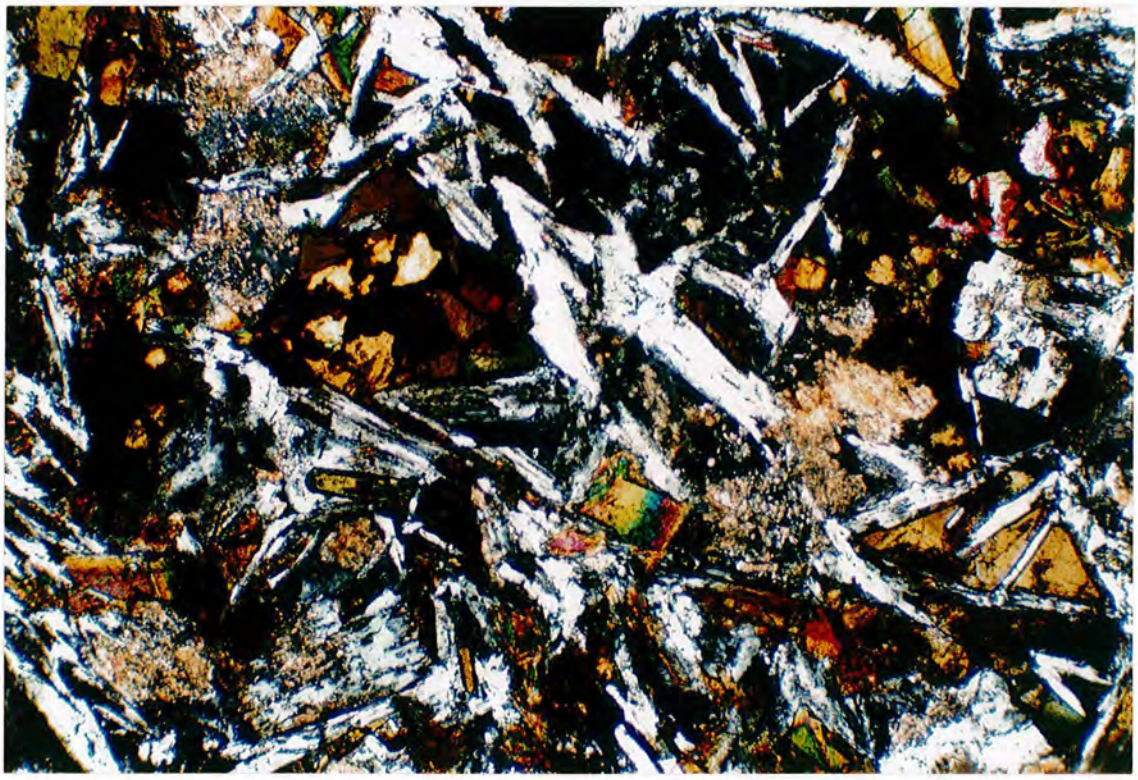

Plate 3.8B 326207, XPL. ×70. Dark blue-green, sodic-calcic amphibole (katophorite) and olivine (with rims of iron oxide, centre left) set in a matrix of alkali feldspar (laths), nepheline (rounded, blocky grains) and analcite (isotropic patch, top centre right). Nepheline, altering to bright flakes of the micaceous mineral giesekite is seen (upper mid left and lower mid right). There is no pyroxene in this slide.

Porphyritic phonolites contain phenocrysts of bladed, high temperature alkali feldspar (eg. sanidine) up to 1.5cm by 2mm, showing simple carlsbad twins and generally lacking any exsolution textures. Large euhedral nepheline phenocrysts (2-4mm in diameter) with well developed square or hexagonal outlines are generally subordinate to feldspar, although occasionally they reach 20% of the mode (eg. 304006, see Plates 3.10 and 3.11). Rarely, small phenocrysts (500μm diameter) of a fayalitic olivine are seen, invariably corroded and rimmed by opaque iron oxides.

Alkali feldspar and nepheline along with alkali rich ferro-magnesian minerals dominate the groundmass. Feldspars (40-60% of the mode) generally occur as lath shaped or bladed crystals with simple carlsbad twins and little or no exsolution textures. Nepheline (up to 25% modally) occurs either as interstitial patches to the feldspar (much as in the benmoreites) or as small, blocky subhedral crystals (a few hundred microns in diameter, see Plates 3.8A and B and 3.9A and B).

Minor amounts of other felsic minerals are seen in many cases. Analcite forms interstitial to the feldspar, generally to the exclusion of nepheline. Sodalite occurs alongside, or sometimes pseudomorphing, nepheline. These minerals rarely exceed 5% of the mode. Gieseckite is present in many samples partially or wholly replacing nepheline.

The groundmass often shows well developed trachytic textures, becoming less obvious in the coarser examples. Some of the finer grained (more rapidly cooled dykes) show a sub-variolitic growth of small (500μm) alkali feldspars.

The most abundant ferro-magnesian minerals are aegirine-augite and sodic-calcic or alkali amphiboles. The pyroxene, occurring as discrete (subhedral) grains, is usually zoned from a pinkish core (salite or titaniferous augite) to bottle green margins of aegirine-augite. These can in turn be overgrown by a dark, inky blue-dark green/brown pleochroic alkali amphibole (arfvedsonite). In some cases no pyroxene is present, the only ferro-magnesian mineral being amphibole. Biotite, although never more than a few percent of the mode is present in many samples, as too are iron oxides (titanomagnetites or deep red hematites) which occur in similar amounts.

Other accessory minerals include purple fluorite (small interstitial grains), clear sphene rimming opaque oxide minerals, zircons (up to several hundred microns in di-

ameter) and in a very few samples almost opaque, deep red-brown aenigmatite (eg. in 43898, 328378).

Many phonolite dykes, due to their narrow width cool rapidly to a very fine grained, green coloured rock. They are composed of very small needles of aegirine-augite and lesser amounts of alkali amphibole (both about 150μm by 30μm). These are enclosed in a very fine grained, felsic groundmass (presumably alkali feldspar and nepheline). Compositionally, these rocks are phonolites, although petrographically it would be difficult to classify them as such. They are quite common across the region and distinctive in thin section.

Alteration produces clouding of the feldspar with the production of assemblages of clay minerals. Nepheline alters fairly readily to aggregates of gieseckite, or in some cases involving the addition of CO_2, to cancrinite. Ferro-magnesian minerals give way to aggregates of chlorite and iron oxides, the liberated iron often giving an overall red stain to the whole sample.

Recrystallisation

Thermal metamorphism of phonolite dykes was observed in the vicinity of the Late Igdlerfigssalik syenites. The textural development of these rocks is similar to the benmoreites and is characterised by the development of granular textures. Exsolution in the feldspars leads to the growth of separate albite and orthoclase grains. Poikiloblastic amphiboles (hastingsitic hornblende) develop by recrystallisation of pre-existing amphibole and digestion of aegirine-augite, although in some samples the pyroxene may remain as small (150μm diameter) grains. Either cancrinite, or sodalite, or both, are present in most recrystallised phonolites as low relief groundmass grains, replacing in part some of the original nepheline.

Sample 326331 shows an alignment of groundmass crystals even though a well developed granular recrystallisation texture has formed, with the growth of large (2mm diameter) poikiloblastic amphibole crystals. This alignment bears a strong resemblance to a residual trachytic texture and the term *trachy-blastic* is suggested (see Plate 3.7).

3.7: Quartz Porphyries

The quartz porphyries are a very limited group of rocks with only two such dykes recorded from the Igaliko Nepheline Syenite complex (63894/5 and 63989). Two others were available for study also, both from the Ilímaussaq peninsula– 141224 from Qagssiarssuk and 63881 from 5km south west of Qagssiarssuk. They are significant as they represent magmas of 'oversaturated minimum' compositions (as opposed to phonolite which represents the undersaturated minimum).

Quartz porphyries are characterised by the presence of high temperature, bi-pyramidal quartz phenocrysts between 1mm and 2mm in diameter (see Plate 3.12). These are usually euhedral/subhedral with some showing embayed crystal margins. Non perthitic alkali feldspar showing simple carlsbad twinning and generally rather clouded is the only other phenocryst phase. These are usually 2-3mm in length by 0.5-1mm in breadth. Large aggregates of iron oxide (600μm diameter) with cores of aegirine occurring in one sample may represent altered pyroxene phenocrysts.

The groundmass is composed predominantly of finely intergrown alkali feldspar and quartz, (grain size 50μm to 200μm typically). In some samples a poorly developed granophyric intergrowth can be seen. Finely disseminated iron oxide is common, as too is a reddish iron staining. Ferro-magnesian minerals, present only in 63895, are small (50-100μm) grains of aegirine-augite/aegirine and a dark blue arfvedsonitic amphibole.

The quartz porphyries from the Igaliko region all have a crystalline (not glassy) groundmass, with flow banding visible in only the margins of the dykes (eg. 63844). These appear petrographically dissimilar to the comendite dykes of Tugtutôq, although they are still both rhyolites.

3.8: Syeno-gabbros and 'Late' dolerites

'Syeno-gabbro' is a field term used to describe coarse-grained rocks of trachy-basaltic composition. Its use also includes rocks described as mafic syenites and some alkali gabbros and dolerites. These tend to occur as quite large dykes (up to 100m wide) and are often related to the late stage evolution of central complexes (for example the arcuate ring dyke and large alkali gabbro dykes in Flink's Dal, Motzfeldt centre, and late

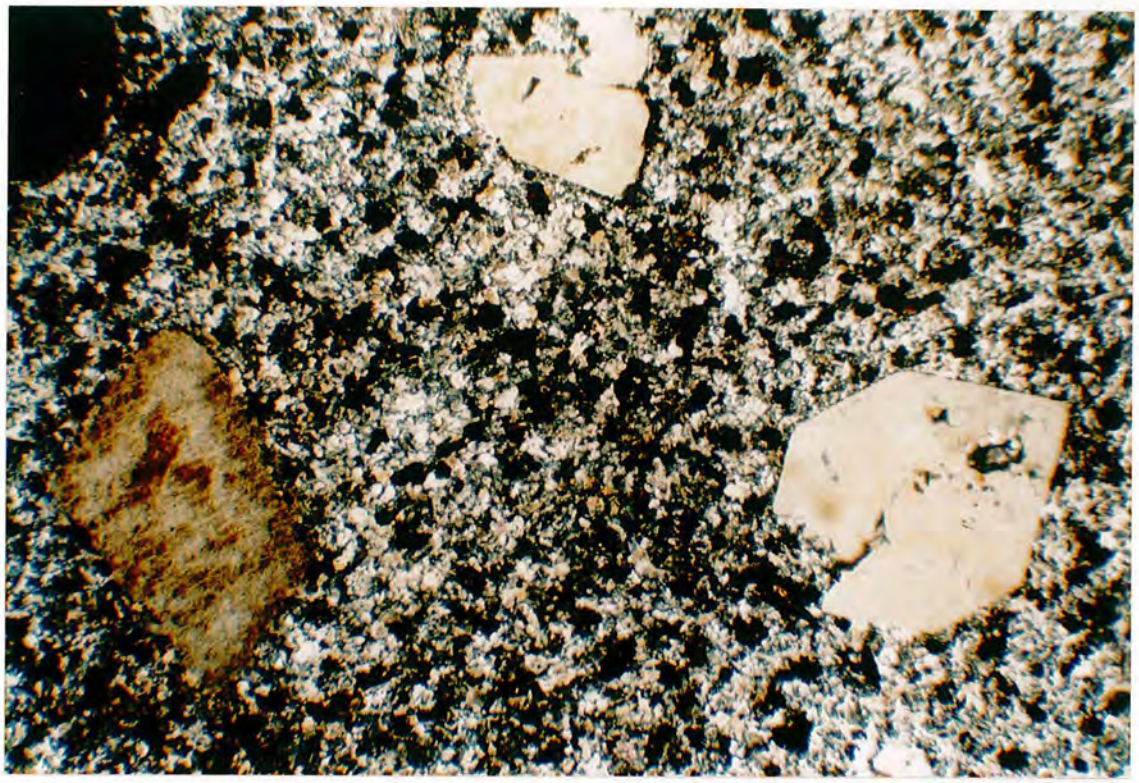

Plate 3.12 63895, Quartz Porphyry. XPL. ×35. Phenocrysts of high temperature, bipyramidal quartz (bottom right) and altered alkali feldspar (bottom left) set in a ground mass of quartz, alkali feldspar and opaque oxides.

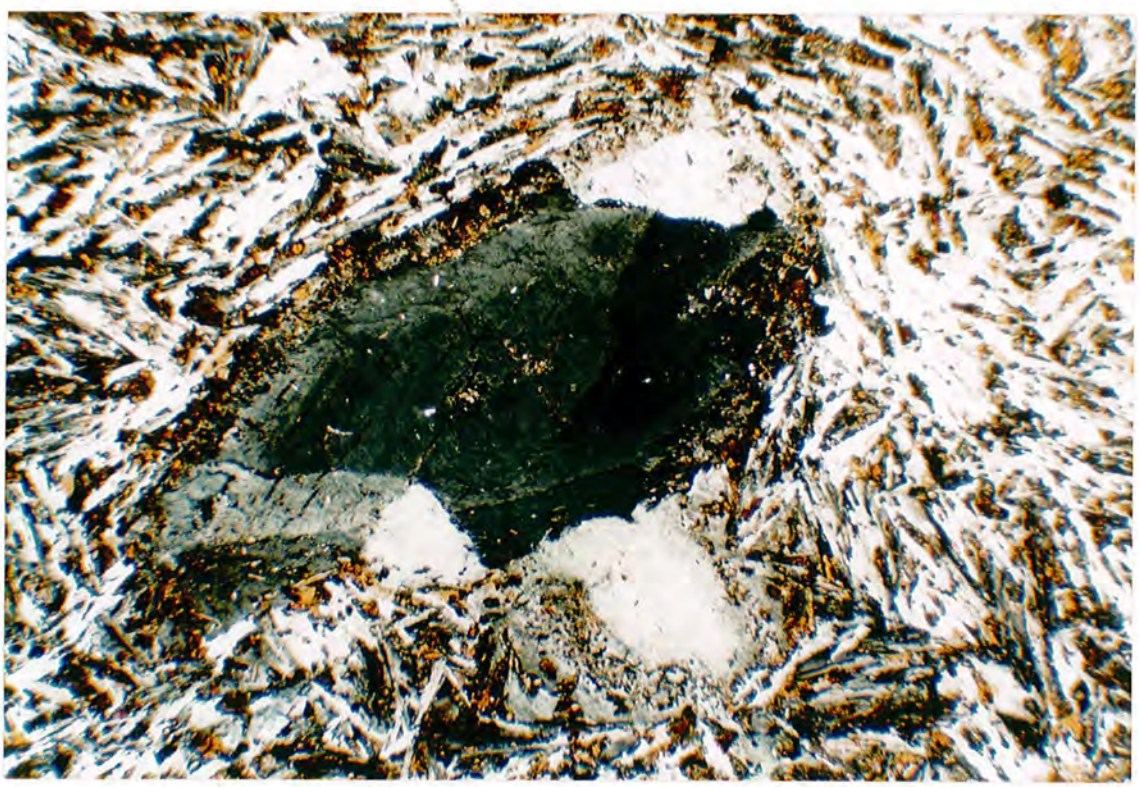

Plate 3.13 58139, Porphyritic Benmoreite. XPL. ×35. Phenocryst of alkali feldspar (possibly relic anorthoclase) set in a fine ground mass of alkali feldspar and pyroxene. Well developed trachytic texture in the ground mass feldspar, flowing around the phenocryst. Note the 'dusty' overgrowth on the rims of the phenocryst (cf. Nash *et al.* 1969).

alkali dolerites/gabbros cutting the Igdlerfigssalik syenites). They also occur as smaller dykes and are sparsely distributed across the Igaliko Nepheline Syenite complex.

The mineralogical variation is essentially similar to that seen in the range of basalt, through hawaiite and mugearite to benmoreite, and is summarised in the list below.

Olivine: Euhedral/subhedral crystals between 10 and 20% modally. Present in most samples. Compositional range Fo_{70} to fayalites.

Pyroxene: Deep pinkish titaniferous augite and salite in gabbros, to pale greenish, possibly slightly alkali rich, hedenbergites in evolved examples. 10-20% of the mode. Ophitic in gabbros, discrete grains in more evolved types. Rare rims of aegirine-augite. Pyroxene present in all samples.

Plagioclase: Phenocrysts of An_{60} in doleritic rocks, An_{50} in hawaiitic examples. Normal zoning to more sodic margins common. Groundmass plagioclase ranges from An_{60} in basalts to ca. An_{20} in mugearites. No plagioclase in benmoreites. Generally lath shaped, occasional hints of flow orientation. Rare examples of oscillatory zoned groundmass plagioclase.

Alkali feldspar: Absent in gabbroic varieties, increasing in content from minor interstitial patches in hawaiitic types through discrete grains to be total feldspar in benmoreites. Some phenocrysts, otherwise hypidiomorphic granular groundmass texture. Perthitic in some cases.

Biotite: Deep red/brown (Ti rich) biotite present in all samples. Increasing abundance from minor quantities as reaction rims to iron oxides in basaltic types through to large (5mm diameter) sub-ophitic crystals (up to 15% modally) in benmoreitic varieties.

Amphibole: Absent from all samples.

Accessories: Abundant, sometimes large (1mm long) apatite, between 2-5% modally. Iron oxides (5-10% modally) usually rimmed or completely enclosed by biotite.

Alteration: Clouding of the feldspar to produce sericite or clay minerals. Alteration of

ferro-magnesian minerals to chlorite and iron oxide aggregates.

Total alkalis-silica classification (Figure 5.2.1) showed many of these syeno-gabbros to be tephritic or basanitic. These are rich in mafic minerals and have plagioclase (where present) subordinate to alkali feldspar. They would appear to be more mugearitic or benmoreitic from their felsic mineral compositions and possess alkali and silica contents that have been diluted by the large amount of mafic material they carry. These 'mafic-benmoreitic' types are generally dykes other than those of the 'late' central complex association. Plate 3.4 illustrates a mugearitic syeno-gabbro.

The larger syeno-gabbroic dykes usually show a compositional variation across their width from more basaltic margins to mugearitic and benmoreitic cores. They attest to the availability of relatively unevolved magma at a late stage in the evolution of the central complexes.

3.9: Spherulitic Trachytes,Quenched and Glassy Rocks

Spherulitic trachyte is a field term applied to a group of rocks with a marked spherulitic texture (see Plates 3.14, 3.15 and 3.19). They are always quite narrow dykes (1-2 metres) and are present across the whole of the Igaliko Nepheline Syenite complex. Compositionally Spherulitic Trachytes tend to be trachybasaltic to phonolitic, with no basaltic examples recorded.

Spherulitic textures (with spherulites generally the size of a pea) develop by devitrification of quenched glass, sometimes nucleated on microphenocrysts of feldspar or apatite. Microscopically, fully devitrified examples show radiating sprays of skeletal microcrystals (probably pyroxene or iron oxides) embedded in a light, felsic matrix. Less devitrified examples show small clusters of radiating microcrysts embedded in an isotropic, apparently glassy matrix. A whole spectrum of intermediate conditions exists. It was not possible to obtain separates of this 'glass' free from obviously crystalline material for study by XRD and, due to its age, it must be assumed to be micro-crystalline, despite its isotropic nature.

Spherulitic textures develop from rapidly cooled (quenched) glasses and thus can be expected to occur in narrower dykes. These textures are also common at the margins

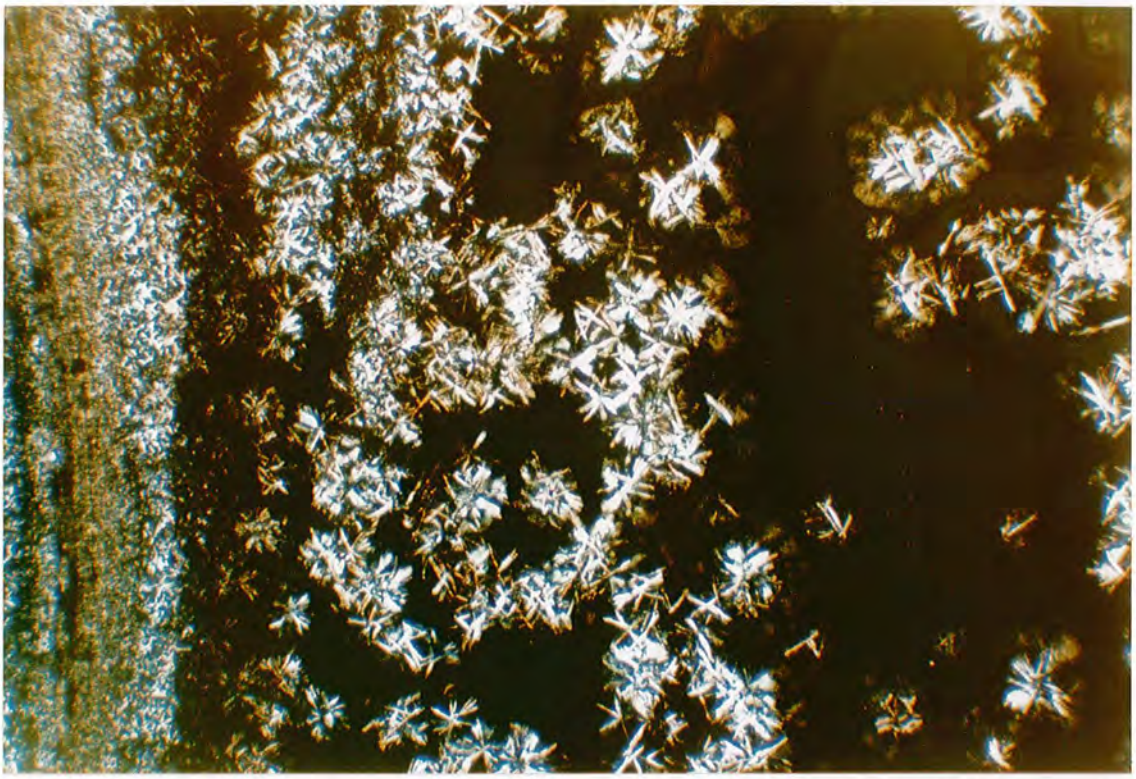

Plate 3.14 304034, Spherulitic Trachyte. XPL. ×35. Small crystallites of alkali feldspar growing in an isotropic, glassy matrix. These crystallite clusters are surrounded by spheres of less crystalline, partially devitrified glass. Flow banding in the glass visible at the left of the picture.

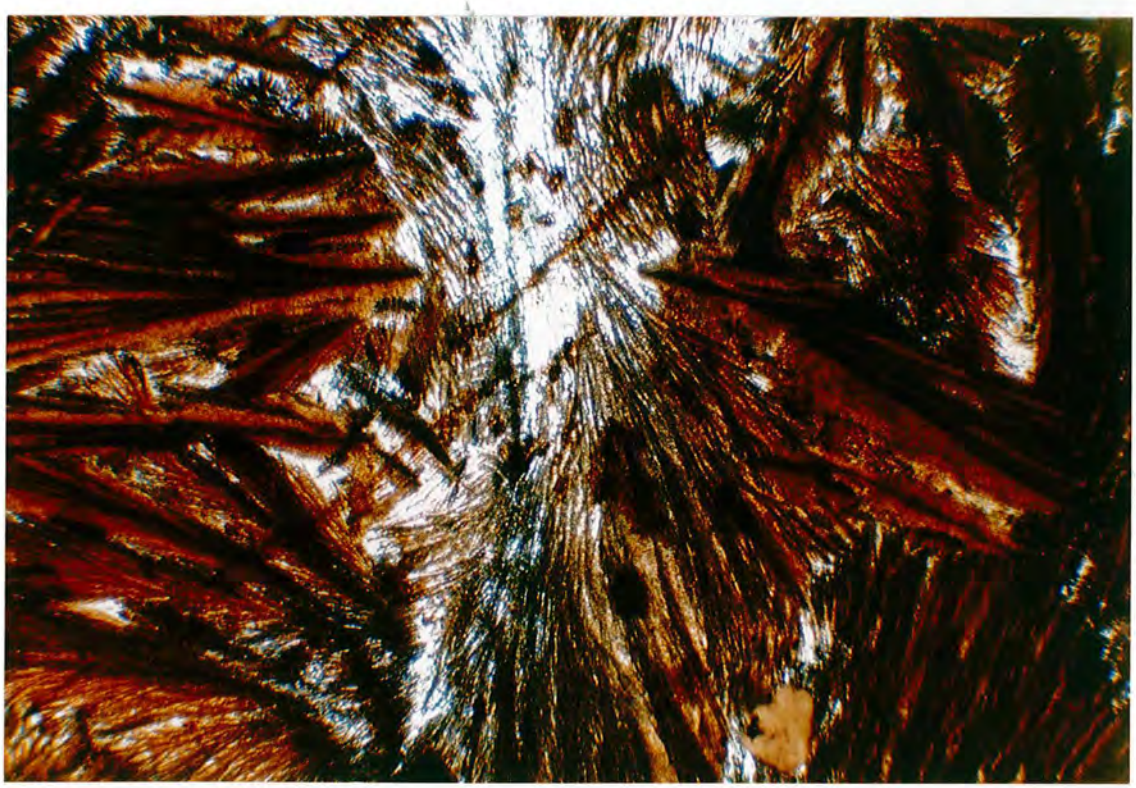

Plate 3.15 58086, Spherulitic Trachyte. PPL. ×35. Large radiating sprays of opaque oxide and ferro-magnesian minerals in a felsic matrix (centre). This is typical of a fully devitrified spherulitic trachyte in thin section, giving an appearance of 'interlocking spheres' in hand specimen.

of larger dykes which often show a few centimetre wide chilled zone, sometimes flow banded and often spherulitic.

Dykes containing abundant fresh 'glass' are very rare. 325923 is a glassy, peralkaline phonolite showing marked 'flow banding' of glassy stringers separated by devitrified patches containing small crystals of feldspar, nepheline and alkali pyroxene (40-50μm).

Variolitic textures are developed in many samples. This texture is also caused by rapid cooling and crystal growth, although the rock was never glassy. This variolitic condition is caused by an intermediate rate of cooling between glassy and more 'normal' (trachytic) fine-medium grained textures. 'Variolites' are generally small radial sprays of elongate feldspar crystals. These rocks tend also to be trachy-basaltic and phonolitic in composition (see Plate 3.18).

3.10: Rhomb Porphyries

Rhomb Porphyries are a group of highly porphyritic 'trachytic' rocks (about 20-30% phenocrysts by volume) distinguished by large (1-2cm in length) rhombic feldspar phenocrysts. They are easily distinguished in the field and occur sparsely throughout the region.

The major phenocryst phase is anorthoclase feldspar, characterised by albite and pericline twins, often developed to a spectacular degree (see Plates 3.16 and 3.17). Cores to these phenocrysts occasionally show only albite twins and these tend to have a slightly more calcic composition (plagioclase). The majority of anorthoclase phenocrysts are overgrown by a feldspar of composition similar to that in the groundmass. Occassionally these are cored by a more alkali-rich feldspar, zoned out at intermediate distances to anorthoclase and then back to rims of alkali feldspar. Some feldspar aggregates appear almost to be 'xenoliths' of granular syenite, showing crystals with mutually interfering margins. Table 3.10.1 shows the range in composition of some anorthoclase phenocrysts, as well as compositional data for olivine and clinopyroxene phenocrysts.

Pyroxene, as a phenocryst phase is always present in these rocks, usually of a salitic or augitic composition (see table) and may be pinkish (Ti-augite). They occur as euhedral crystals up to about 1.5mm in length scattered sparsely through the groundmass.

Table 3.10.1

	Olivine	Pyroxene	Feldspar		
	Fo	Ca-Mg-Fe	Ca-Na-K-Ba		
52293		46-35-19	15-58-24-3	Phenocryst	
46237	47	37-36-27	18-59-21-2	Phenocryst	
			4-49-46-1	Groundmass	
141233		46-32-22	6-51-41-2	Core	
			22-62-16-0	Intermediate	Phenocryst
			6-48-46-0	Rim	
59660	40	47-31-22	22-55-22-1	Phenocryst	
			5-32-62-1	Groundmass	

Phenocrysts of olivine are also present in some samples. They are usually about Fo_{40-50}. The mineral is generally euhedral/subhedral, although in some samples it is quite badly corroded and rimmed by opaque oxides. Olivine crystals rarely exceed 500μm in diameter.

The groundmass mineralogy is typically that of the benmoreites, consisting of alkali feldspar, pyroxene, amphiboles and iron oxides with little or no nepheline and quartz.

The anorthoclase phenocrysts will have crystallised from a relatively high temperature, trachy-basaltic magma. Emplacement at shallower structural levels was followed by rapid cooling. This cooling from a high temperature monoclinic form causes twinning as the crystal inverts to a triclinic habit and produces the cross-hatching so characteristic of anorthoclase. This is also the case for other dykes carrying anorthoclase phenocrysts. The aggregates of feldspar crystals probably represent cognate xenoliths from the walls of the magma chamber entrained during magma flow. Some anorthoclase phenocrysts also show an almost skeletal texture, with well formed rhombic margins, partially 'cored out' and enclosing large amounts of groundmass material (see Plate 3.16).

3.11: Trachytes (*s.s.*) and Trachy-andesites

Field descriptions of most of the feldspar-rich dykes are limited to the term 'trachyte' and, where nepheline is visible, 'phonolite'. The majority of these so called 'trachytes',

with more detailed study, turn out to be either benmoreites or phonolites. Trachytes (*s.s.*) as defined mineralogically or geochemically (eg. in total alkalis-silica space, Cox *et al.* 1979) are quite rare in the Igaliko Dyke Swarm. This is also true of the trachy-andesites (the silica-oversaturated equivalents of the trachy-basalts).

Mineralogically the few trachytes (*s.s.*) and trachy-andesites which occur in the region are very similar to the benmoreites, with a tendency for these to be saturated or oversaturated, (ie. quartz rather than nepheline bearing). They contain more feldspar, and quartz (which may reach 5-10% of the mode) and generally less ferro-magnesian minerals. These quartz-bearing varieties tend to be larger, more persistent dykes with several examples cropping out in the region to the north of Narssarssuaq and cutting the South Qôroq centre. Occasional crystals of aenigmatite are seen in these along with alkali-rich amphiboles and pyroxenes (hedenbergite and aegirine-hedenbergite).

3.12: Summary

Classification on the total alkali-silica basis of Cox *et al.* (1979) named a number of rocks as tephrite/basanite and nephelinite. These types, with the exception of some basanitic syeno-gabbros, are all lamprophyric in character and will be discussed in a later chapter. Mineralogical variation consistent with evolving alkali magma suites was generally observed and Table 3.12.1 (overleaf) shows a summary of typical mineralogical compositions observed in the fine grained rock types.

In general, typical alkali feldspar compositions are in the range Or_{40-60}. In the more slowly cooled varieties (or recrystallised examples such as phonolites) alkali feldspars may have exsolved to give compositions around Or_{10} and Or_{90}. Accessory minerals generally include biotite, apatite, opaque iron oxides with minerals such as zircon and aenigmatite appearing rarely in the more evolved rock types (eg. phonolites). Alteration typically involves clay minerals replacing feldspar, gieseckite after nepheline and chlorite after ferro-magnesian minerals (with some serpentine and iddingsite after olivine also).

Table 3.12.1

Summary mineralogy of the groups described in Chapter 3

Rock Type	Feldspar		Pyroxene (Ca-Mg-Fe)	Olivine	Amphibole	Ne/Qtz
	Plagioclase	Alkali				
Basalt	An_{60-40} Phen & Gm.	Absent	42-34-24 Ophitic	Fo_{70-75}	Absent	
Hawaiite	An_{35-55}	Minor interstitial	40-30-30 Salite	Fo_{50-60}	Absent	
Mugearite	An_{20-30}	Up to 50% total fsp	40-25-35 - Ferro-salite	Fo_{30-40}	Rare. Ferroan pargasitic hbl.	Minor Ne
Benmoreite	Anorthoclase phenoxts with Ab-Or rims. G-mass Ab-Or typically		40-25-35 to aeg-aug rims	Fayalitic Mn rich	Ferro-richterite Katophorite Arfvedsonite	Ne>Qtz usually in gmass.
Phonolite	Absent or albitic	Abundant - >90% of fsp. Some anorthoclase phens but mostly Ab-Or comps.	Salite cores aeg-aug rims	Rare - fayalitic	Arfvedsonite or katophorite (discrete grains or rims to px)	Neph - max. 25%. Also other foids
Rhomb porphyry	Ternary anorthoclase, typically $An_{20}Ab_{58}Or_{20}Cn_2$, rimmed by $Ab_{60}Or_{40}$. Gmass typically $Ab_{60}Or_{40}$		Salitic phenocrysts	Fo_{40} (rare)	Absent in gmass	Minor Q,Ne
Quartz porphyry	Absent	Ab-Or phenocrysts	Rare aegirine	Absent	Riebeckite, (rare)	High temp Qtz phens.
Trachyte (*s. s.*)	Albitic	Anorthoclase or Ab-Or phens	Salite core aeg-aug rims	Rare or absent	Ferro-richterite to Arfvedsonite	Ne rare, Qtz more common
Syeno-gabbro	Coarse grained equivalents of basalts to benmoreites					

CHAPTER 4: MINERALOGY

4.1: Introduction

This chapter deals with the mineralogical trends observed within the Igaliko Dyke Swarm. It excludes mineralogical data from the lamprophyres and carbonatites which are discussed in later chapters but includes data from a group of rocks termed 'other lamprophyres'. These are essentially lamprophyric rocks with tephritic/basanitic and nephelinitic compositions and as such are probably intimately related to the main 'basalt to phonolite and rhyolite' association.

Minerals are treated in no specific order, other than the mafic minerals being dealt with first followed by the iron oxides, felsic minerals and lastly minerals of minor occurrence.

All analyses were carried out using microprobes equipped with an Energy Dispersive Spectrometer (EDS) at Manchester University. Analytical conditions and techniques are described in Appendix II.

Mineral chemistry is plotted throughout the following chapter using a consistent set of different symbols for different rock types. The identification of different groups of rocks is based upon both petrography and whole rock geochemistry. The group labelled 'Trachytes, Syenites' for example is classified on petrographic criteria as no whole rock analyses are available for these felsic samples. The groups of rocks termed 'Benmoreites', 'Hawaiites and Mugearites' and 'Phonolites' have been named using the whole rock total alkali-silica classification of Cox *et al.* (1979). 'Phonolites' also includes unanalysed nepheline-phyric rocks. 'Big Feldspar Dykes' are discriminated from 'Hawaiites and Mugearites' but show overlapping mineral trends and whole rock compositions.

'Recrystallised Trachyte' is used for samples 58291-8, (see Chapter 3) which are chemically benmoreites, but also includes some other recrystallised rocks of unknown felsic composition. 'Syeno-gabbros' applies to coarse grained rocks of trachy-basaltic composition, usually occurring as late dykes.

4.2: Pyroxenes

4.2.A: General

All of the pyroxenes are monoclinic; no members of the (orthorhombic) Enstatite-Ferrosilite series of pyroxenes have been observed. The most magnesian pyroxenes are generally pinkish-lilac, pleochroic salites or rarely pinkish Ti-augites. They occur in the most magnesium-rich dykes such as the basalts/dolerites and hawaiites and mugearites. Minor zoning to Fe-rich margins is present but is only detected by using the microprobe. The greatest modal abundances of pyroxene occur in the magnesian rocks and also in the syenogabbros. There is a distinct tendency for the proportion of pyroxene to decrease with increased fractionation. The grain sizes are greatest in the more magnesian rocks and especially in the gabbros and syenogabbros, where large ophitic crystals occur, and tends to decrease in the more evolved rocks. Compositional zoning is more pronounced in the more evolved group of rocks. The pyroxenes in these rocks have pale pinkish (Ti-augite/salite) cores and are often zoned to more Na-rich (Mg poor), dark green pleochroic margins of aegirine-augite/aegirine-hedenbergite. Small aegirine-augite/aegirine-hedenbergite crystals occur as primary minerals in some evolved examples. In general, analyses were conducted to try to cover the maximum range of mineral composition. Due to the smaller grain size of the groundmass pyroxenes in the more alkali enriched rocks it was only possible to probe core and rim positions. Thus only a minor amount of information of variations within individual, Na enriched crystals is available, the bulk of the trends for the Na-rich varieties being defined from two analyses per groundmass crystal. The larger, more Mg-rich, Na-poor grains in the less evolved rocks tended to show less variation, with only relatively small increases in Fe^{3+} and Na from core to margin, and in some cases showing slight decreases in these elements.

4.2.B: Recalculation, Nomenclature and Projection

Microprobe analysis returns the total iron contents as Fe^{2+}. Estimation of the Fe^{3+}/Fe^{2+} ratio is important and is not merely dependent on Fe^{3+} =Na+K (Carmichael 1967) although this approximation in low Al, Ti and Zr alkali pyroxenes should hold fairly true. Fe^{3+} has been calculated, independent of alkali content, by assuming

Figure 4.2.1 Upper triangle shows the nomenclature of the alkali pyroxenes in terms of end member variation of Diopside - Hedenbergite - Acmite (after Jones 1980). The lower diagram shows part of the nomenclature of pyroxenes from Poldervaart and Hess (1951). It is from these schemes that the pyroxenes from the Igaliko dykes have been classified.

Figure 4.2.1

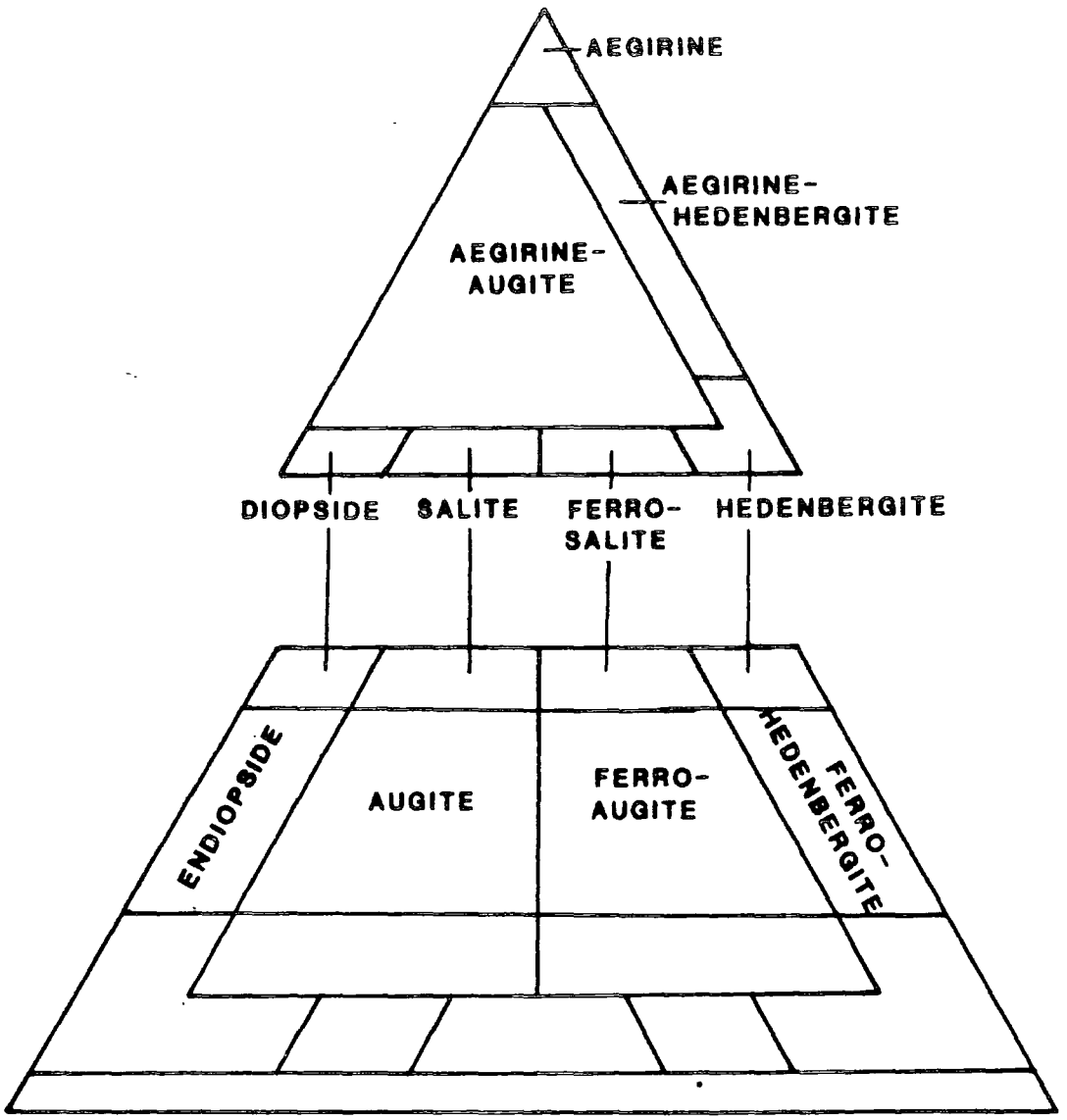
AEGIRINE
AEGIRINE-
HEDENBERGITE
AEGIRINE-
AUGITE
DIOPSIDE
SALITE
FERRO-
SALITE
HEDENBERGITE
ENDIOPSIDE
AUGITE
FERRO-
AUGITE
FERRO-
HEDENBERGITE

stoichiometry of the pyroxene, and recasting the analysis by assuming the deficiency in oxygen atoms in the analysis is due entirely to the presence of Fe^{3+}. This method assumes 4 cations to 6 oxygens and, provided the total of unanalysed elements (Ni, Cr, etc.) is small, provides a good approximation to the Fe^{3+} content (Brooks and Gill 1982).

Alkali pyroxenes involving substitution of $NaFe^{3+} \rightleftharpoons Ca(Fe^{2+}, Mg)$ and $CaMg \rightleftharpoons CaFe^{2+}$ are best described in the system Diopside (Di)–Hedenbergite (Hd)–Acmite (Ac) (see figure 4.2.1).

The term aegirine has been used for pyroxenes containing $Fe^{3+} > 0.8$ atoms per formula unit (Deer *et al.* 1978). Jones (1980) proposed an upper limit of $Fe^{3+} = 0.1$ for pyroxenes of the Diopside-salite-hedenbergite series, with diopside restricted to Mg> 0.8. Hedenbergite was assigned an 'odd polygonal shape' (Jones 1980) in the Fe^{2+} corner of the diagram defined by $Fe^{2+} > 0.8$ where $Fe^{3+} < 0.1$ and $Fe^{2+} > 0.9$ where $0.1 < Fe^{3+} < 0.2$.

Aegirine-augites occupy the space where $Fe^{3+} < 0.8$, Mg> 0.1 and $Fe^{3+} > 0.1$ whilst aegirine-hedenbergites fall in the strip between Fe^{2+} and Na with $0.2 < Fe^{3+} < 0.8$ and $Mg < 0.1$. The above classification (as illustrated in Figure 4.2.1) is partly related to the original classifications of Poldervaart and Hess (1951) in Wo-En-Fs space. This has been modified by Larsen (1976) for compositions of Ac<15, so the iron-rich corner plots as $Fe^{3+}+Fe^{2+}$-Mn-Na, and allows comparison with other trends (see Larsen 1976).

Figure 4.2.2 shows all analyses plotted for each rock group as Mg–$(Fe^{2+}+Mn)$–Na, assumed to represent Di-Hd-Ac. This is a conventional plot used by Stephenson (1972), Chambers (1976) and Jones (1980) and is produced here for comparison. This projection is however strictly incorrect as it does not allow for the presence of other Na-rich end members, (eg. jadeite, $NaAlSi_2O_6$). These Na-rich end members are important constituents of many early-formed, Mg-rich pyroxenes from most dykes. Figure 4.2.3 compares plots of Di-Hd-Ac (as end members) and Mg–$(Fe^{2+}+Mn)$–Na (as atoms per 6 oxygens) for pyroxenes from phonolites. The end member proportions were calculated using the computer program **PYROXENE.F4B** written by Dr. Andrew Peckett of Durham University. The method of the program is outlined in Appendix II.

Figure 4.2.2 Comparison of the pyroxene trend in phonolites when plotted in terms (i) of end member compositions of Di-Hd-Ac and (ii) as atoms of Mg–(Fe^{2+}+Mn)–Na. It can be seen that the most primitive pyroxenes contain no end member acmite (although all contain some Na) and plot on the Di-Hd join. This is due to the assignment of Na to end members such as jadeite. The plot of Mg–(Fe^{2+}+Mn)–Na as atoms may give a misleading impression of the end member compositions as regards acmite, and this should be borne in mind.

IGALIKO DYKE SWARM

Pyroxene analyses

Atomic proportions
(Recalculated to 4 cations
and 6 oxygens)

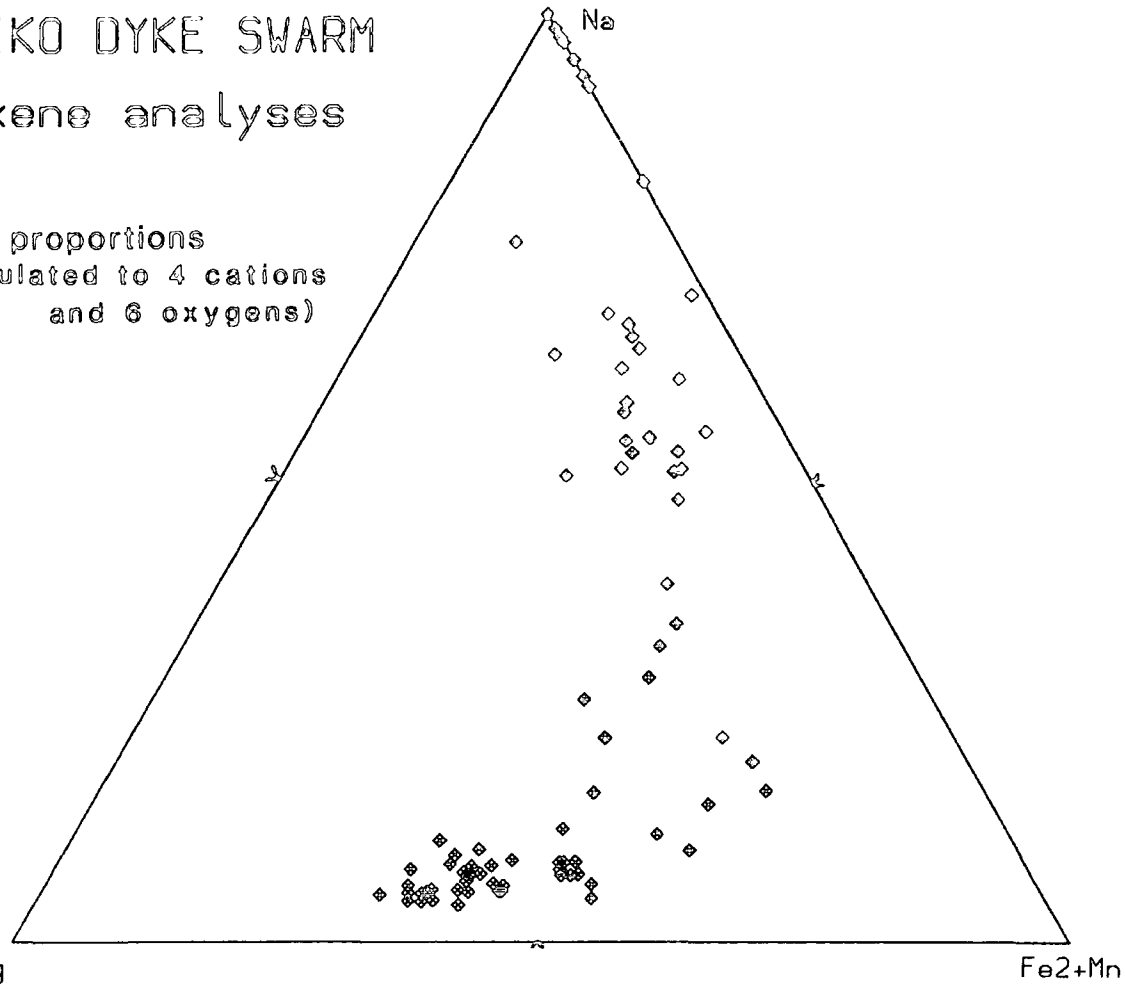

End member
proportions

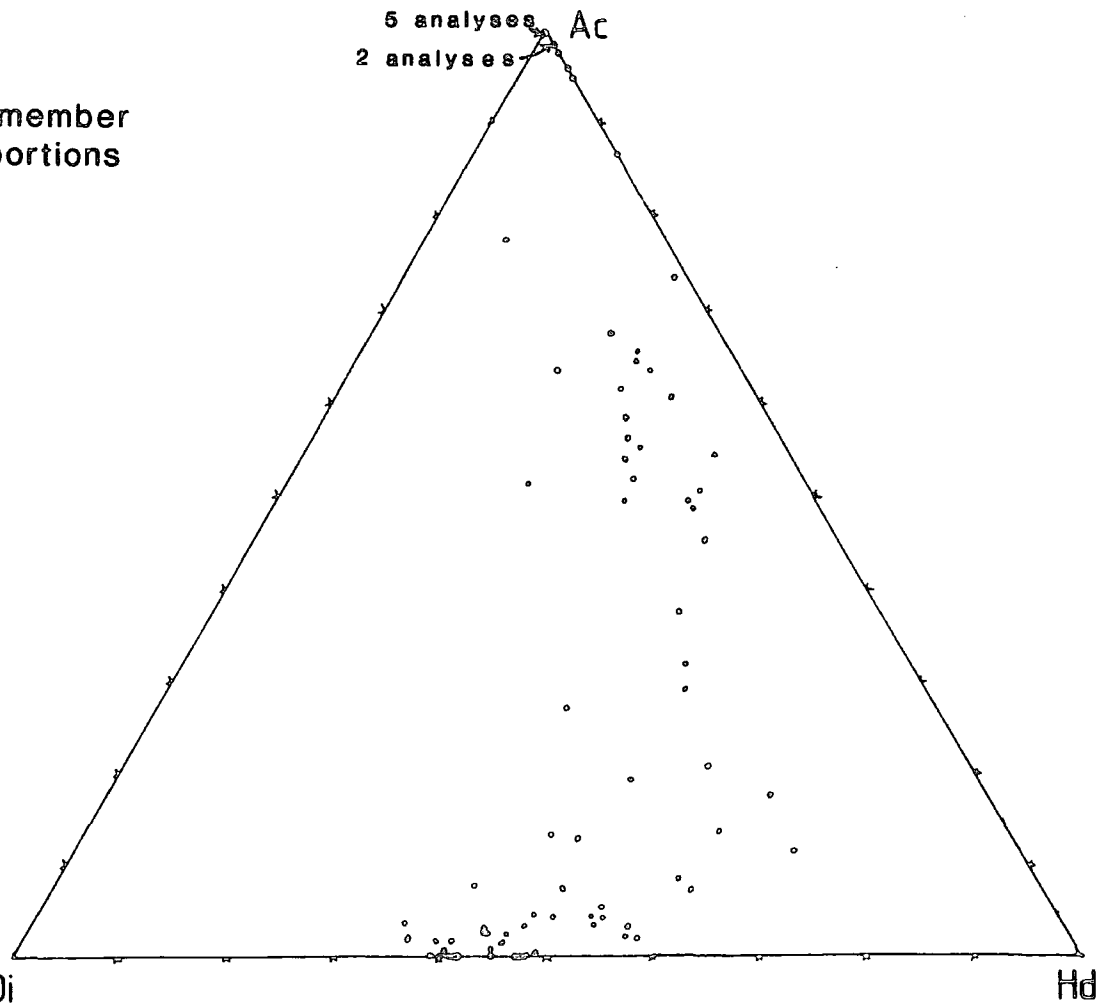

For the more basic Mg, Fe-rich, Na-poor pyroxenes, which also usually contain appreciable Ti and Al, recalculation to end member compositions displaces their position towards the Di-Hd join. This is due to a decrease/absence of the acmite end-member with all the available Na being assigned to either jadeite or $NaTiFMSiO_6$ (FM=Fe^{2+},Mg). Data are however presented in the conventional manner (ie. Mg–(Fe^{2+}+Mn)–Na) for comparative purposes but the effects of Al and Ti on the end member compositions of the pyroxenes should be borne in mind.

4.2.C: Site Occupancy

The general formula of pyroxenes is $X^{vi-viii}Y^{vi}Z^{iv}O_6$. The next section deals with element substitution into the available sites and is based on the general description of pyroxene chemistry by Cameron and Papike (1982).

Z (or T-site): A 4-fold coordinated site, this is essentially occupied by Si and Al. Al/Al+Si decrease with increasing fractionation, (measured by Na -Mg, Stephenson 1972), reflecting a drop in the jadeite component This site can however be occupied by Fe^{3+} under certain P-T-X-fo_2 conditions (Huckenholz *et al.* 1969).

Y (or M1 site): A 6 fold coordinated site, this is essentially occupied by Mg, Fe^{2+} and Mn (as Di, Hd and Johannsenite end members). Other elements that substitute into this site are Al, Ti^{4+} and Fe^{3+} (in a coupled substitution with the X (or M2 site) of $NaFe^{3+} \rightleftharpoons Ca(Mg,Fe^{2+})$).

X (or M2 site): A disordered 6-8 fold coordinated site, generally occupied by Ca and Na with Mn, Fe^{2+}, Mg and minor K. In the (early) salites of the Igaliko Dyke Swarm Ca+Na+K is around 0.92-0.96 increasing to around 1 in the aegirine-augites and aegirines. This deficiency in Ca(+Na+K) is thought to result from minor amounts of (Ca-poor) orthopyroxene in solid solution. K is a minor constituent of many of these pyroxenes, reaching a maximum of 0.322 wt% representing 1.51 mol% of K-Acmite in 54254.65, although more normally K contents are between 0.1 and 0.15 wt% (ca. 0.5 to 0.75 mol% K-acmite).

Figure 4.2.3 (2 pages) Variation of pyroxene composition from individual groups of rocks in terms of atomic Mg–(Fe^{2+}+Mn)–Na. Note how most groups contain pyroxenes in the region of $Mg_{58}(Fe^{2+}+Mn)_{37}Na_5$. It is from this composition that all the different trends of alkali enrichment observed commence.

Figure 4.2.3A

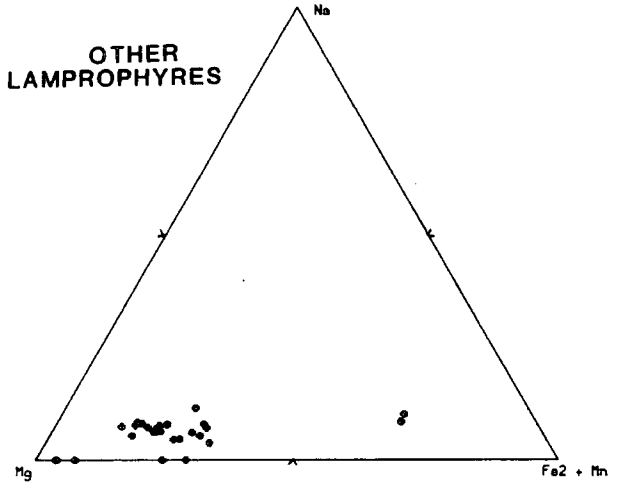
OTHER
LAMPROPHYRES
Na
Mg
Fe2 + Mn

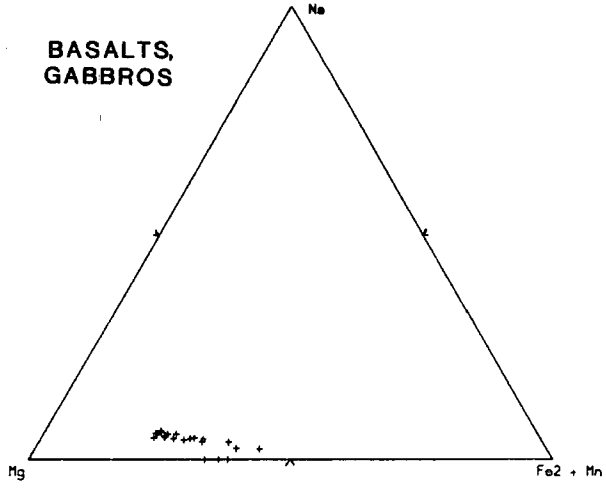
BASALTS,
GABBROS
Na
Mg
Fe2 + Mn

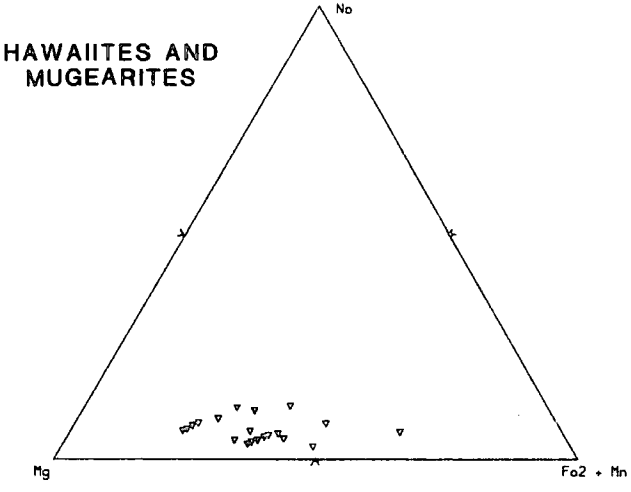
HAWAIITES AND
MUGEARITES
Na
Mg
Fe2 + Mn

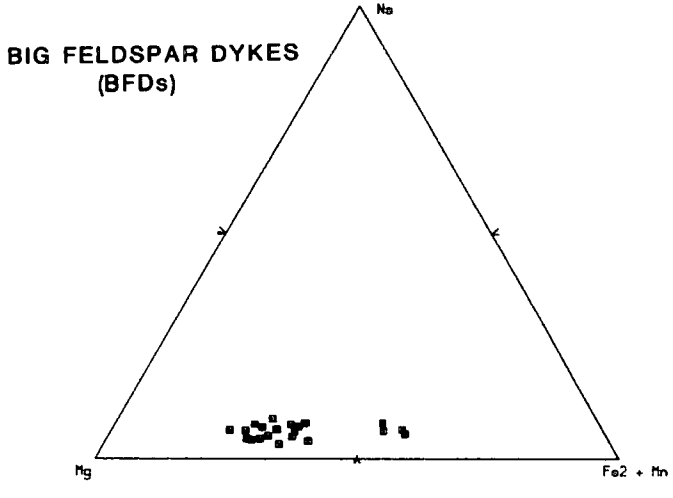
BIG FELDSPAR DYKES
(BFDs)
Na
Mg
Fe2 + Mn

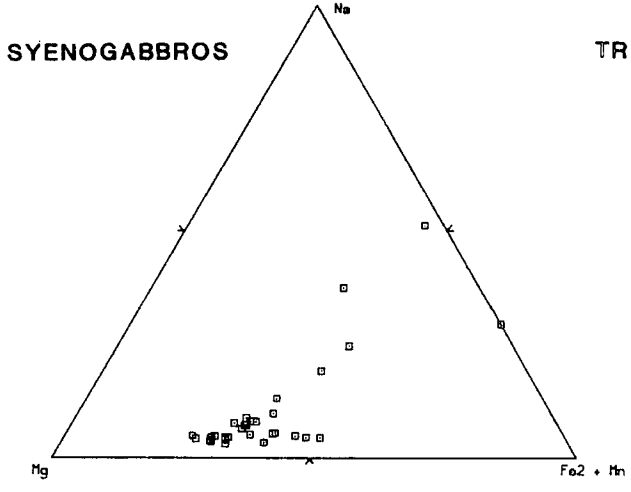
SYENOGABBROS
Na
Mg
Fe2 + Mn

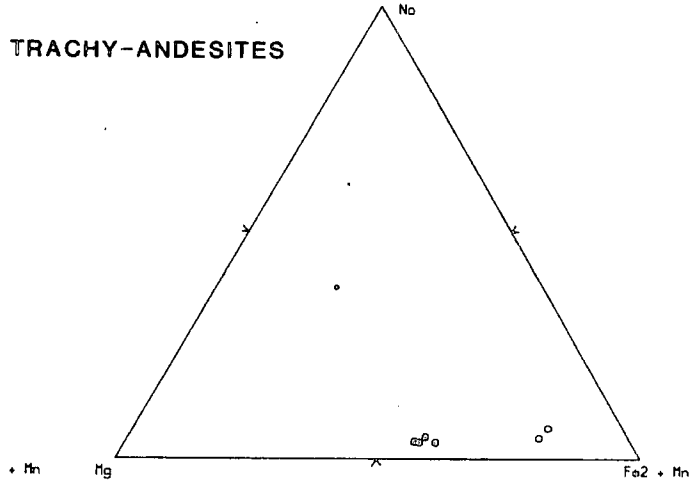
TRACHY-ANDESITES
Na
Mg
Fe2 + Mn

Figure 4.2.3B

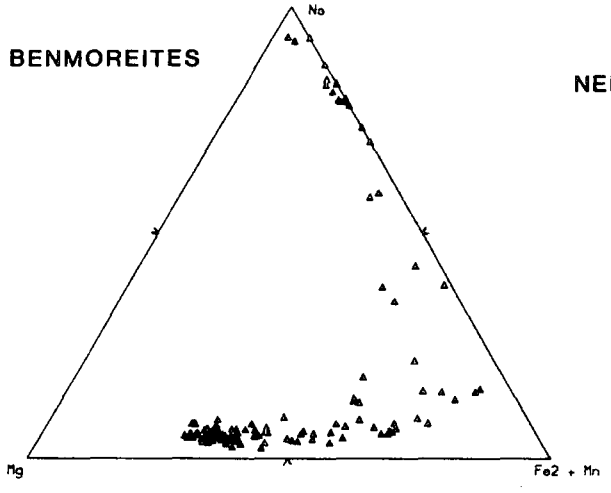
BENMOREITES
Na
Mg
Fe2 + Mn

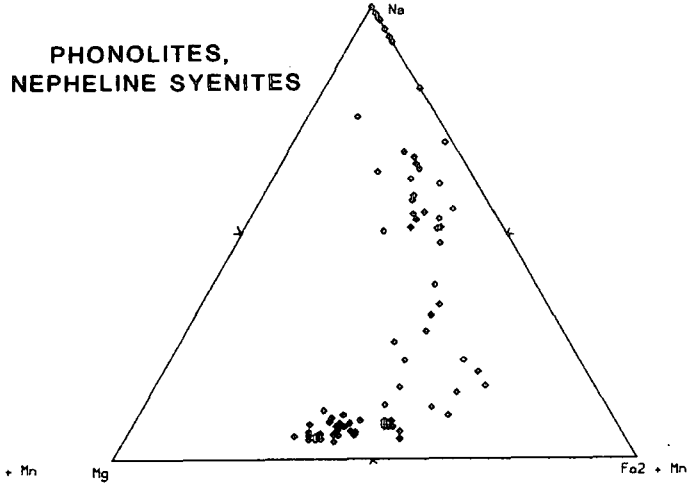
PHONOLITES,
NEPHELINE SYENITES
Na
Mg
Fe2 + Mn

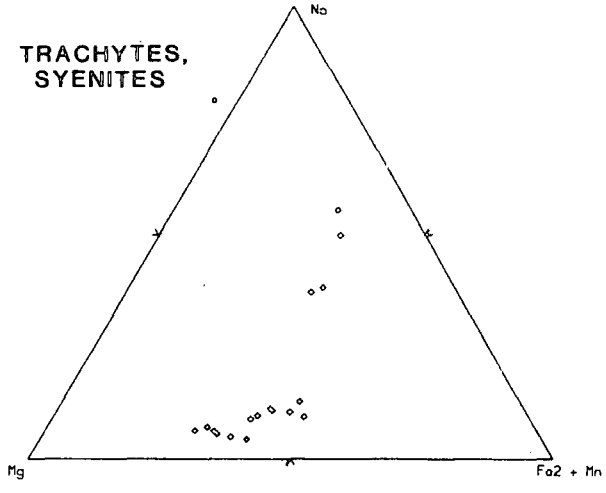
TRACHYTES,
SYENITES
Na
Mg
Fe2 + Mn

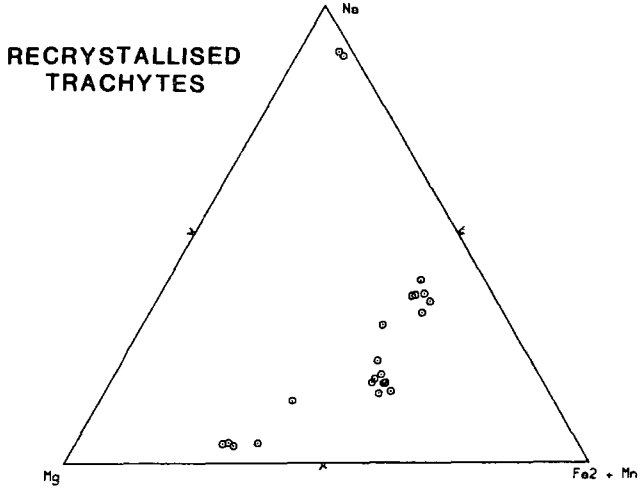
RECRYSTALLISED
TRACHYTES
Na
Mg
Fe2 + Mn

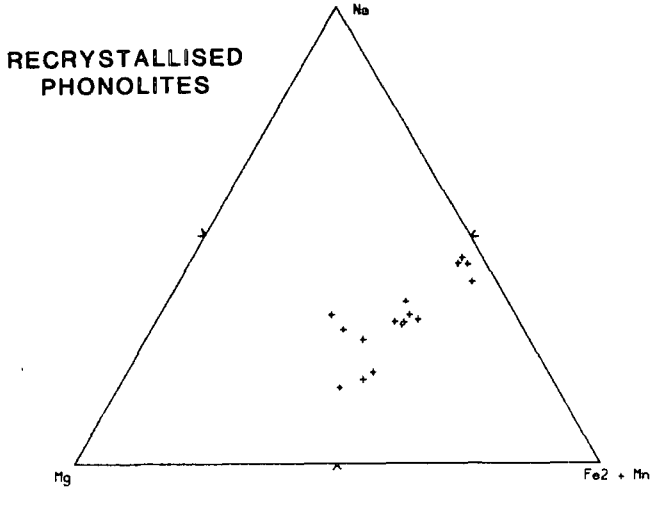
RECRYSTALLISED
PHONOLITES
Na
Mg
Fe2 + Mn

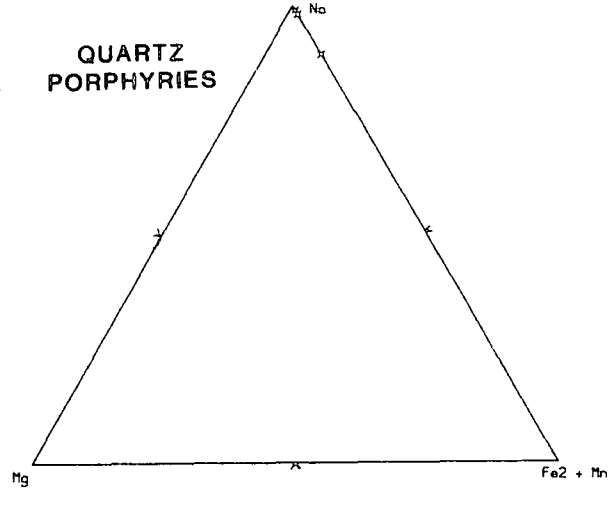
QUARTZ
PORPHYRIES
Na
Mg
Fe2 + Mn

4.2.D: Pyroxene Variation

Figure 4.2.3 shows pyroxene analyses plotted as Mg–(Fe^{2+}+Mn)–Na for each individual rock group. The data roughly reflects the abundance of each rock type present (ie. more phonolites and benmoreites, less basalts and trachybasalts). No volumetric significance should be attached to the distribution of individual analyses within a particular group. Analyses were made with the intention of covering the whole compositional range and not in an attempt to reflect the abundance of a particular composition of pyroxene within each group. The data from each rock type are plotted on Figure 4.2.4 for comparison with trends from other alkaline rock suites.

Basalts (Figure 4.2.3A)

The pyroxenes from the basalts are generally salites or augites and cover a limited compositional range. Pyroxenes from 325611 (the possible BD_0) contain least Na while a cluster of relatively Na-rich pyroxenes (from 63845) plot away from the main trend. TiO_2 and Al_2O_3 appear in quantities up to about 2 wt% and 4 wt% respectively. Ti is present as $NaTiSiAlO_6$ (NATAL, Grapes *et al.* 1979) and $CaTiAl_2O_6$ (Ca-Ti-Tschermak's molecule). Aluminium is generally present as Ca-Tschermak's molecule, $CaAl_2SiO_6$ (Ca-Ts) and not as jadeite, with all the Na having been assigned to Ti bearing end members.

With the exception of 58065, the pyroxenes tend to show atomic Na+Ca≈1, unlike those of both Ilímaussaq and Motzfeldt (Larsen 1976, Jones 1980) with Na+Ca≈0.92-0.96 in the Motzfeldt salites. This has been attributed to solid solution of a Ca-poor pyroxene within the salites and is probably the cause of the low Na+Ca (=0.93) in the pyroxenes from 58065 (which would have ca. 7% of an 'orthopyroxene' component in solution).

Hawaiites, Mugearites and BFD's (Figure 4.2.3A)

The trachy-basaltic rocks continue the trend from salitic pyroxenes towards ferro-salites, maintaining relatively low Na (and low acmite) contents. Like the basalts these rocks tend to contain $NaTiSiAlO_6$, $CaTiAl_2O_6$ and Ca-Ts end member molecules. Na+Ca is around 0.94-.96, having dropped slightly from the basalts and representing

about 5% of 'opx' in solid solution. Na is generally about 0.05-0.09 atoms per formula unit (apfu). There is no marked increase in Na with (Fe^{2+}+Mn).

Syeno-gabbros (Figure 4.2.3A)

These large basaltic and trachybasaltic dykes (which are as evolved as benmoreites in some cases) would seem to show 2 evolutionary trends. Some pyroxenes are trending from salitic compositions to (just) ferro-salites, heading for the Fe^{2+}+Mn corner, with one sample trending from slightly more Na-rich salites across aegirine-augites to aegirine-hedenbergites (58017, a benmoreitic facies of the Late Motzfeldt ring dyke). This is accompanied by an increase in ZrO_2 of up to 6.92 wt% (see later).

Benmoreites (Figure 4.2.3B)

The benmoreites are generally not peralkaline (ie. molar Na_2O+K_2O/Al_2O_3 is less than 1, usually around 0.85 to 0.95). This is reflected in salitic/ferro-salitic cores to the pyroxenes which zone out at quite a late stage to aegirine-augite, aegirine-hedenbergite or aegirine rims. These are often 'mantled' by a rim of sodic-calcic or alkali amphibole (such as katophorite or arfvedsonite).

As crystallisation proceeds, residual interstitial fluids become peralkaline and cause Na to increase towards the crystal margins at a late stage. A minor offshoot from the main benmoreitic trend occurs with some pyroxenes becoming enriched in Na at lower Fe^{2+}+Mn. In general Ca+Na(+K) increases from about 0.98 in the salitic varieties to around 1 in the Na enriched varieties.

Phonolites (Figure 4.2.3B)

The pyroxenes from the phonolites show an increase in Na before appreciable Fe^{2+} and Mn enrichment has occurred. Cores to pyroxenes are usually salites or (just) ferro-salites which zone out across the aegirine-augite field into Na-rich aegirine-hedenbergites and aegirine. Phonolites have peralkalinity indicies between ca. .88-1.05, the peralkaline varieties (molar Na+K>Al) showing the most sodic (early) pyroxenes.

Of particular note are (i) the contrasted evolutionary trends shown by the benmoreites and phonolites, and (ii) that all groups contain salitic/ferro-salitic phenocrysts or

Figure 4.2.4 Comparison of pyroxene trends from other alkali rock suites with the trends observed for different groups of rock from the Igaliko Dyke Swarm.

Figure A: Other Alkali Rock Suites.

1. Uganda (Tyler and King 1967)
2. South Qôroq (Stephenson 1972)
3. Igdlerfigssalik (Powell 1978)
4. Hviddal (from Stephenson and Upton 1982)
5. Klokken (Parsons 1979)
6. Nunarssuit-Alanarssuak (Anderson 1974)
7. Tugtutôq (from Stephenson and Upton 1982)
8. Morotu-Sakhalin (Yagi 1953)
9. Motzfeldt Unit SM4 (Jones 1980)

Figure B: Igaliko Dyke Swarm Pyroxene Trends.

D Field of basalt/gabbros (2 fields).

BFD Field of Big Feldspar Dyke pyroxenes.

L Field of lamprophyre pyroxenes.

H Trend of hawaiite pyroxenes (2 trends at different Na contents).

S Trends from syeno-gabbros. One trend moves towards Fe^{2+}+Mn enrichment, the other trend moves from salite across aegirine-augites.

TA Trachy-andesite trend of Fe^{2+}+Mn enrichment.

B Benmoreite trends. Na enrichment commences at high Fe^{2+}+Mn contents.

P Phonolite trends. Na enrichment occurs at lower Fe^{2+}+Mn than in the benmoreites.

T Trachyte/syenite trend. These felsic rocks named solely by their petrographic character, may in fact be phonolitic on the basis of their pyroxene evolution trend.

RT Recrystallised trachytes/benmoreites. Recrystallisation may be at higher fo_2 than the original crystallisation of benmoreitic rocks and cause a change in the pyroxene compositional trend.

Figure 4.2.4

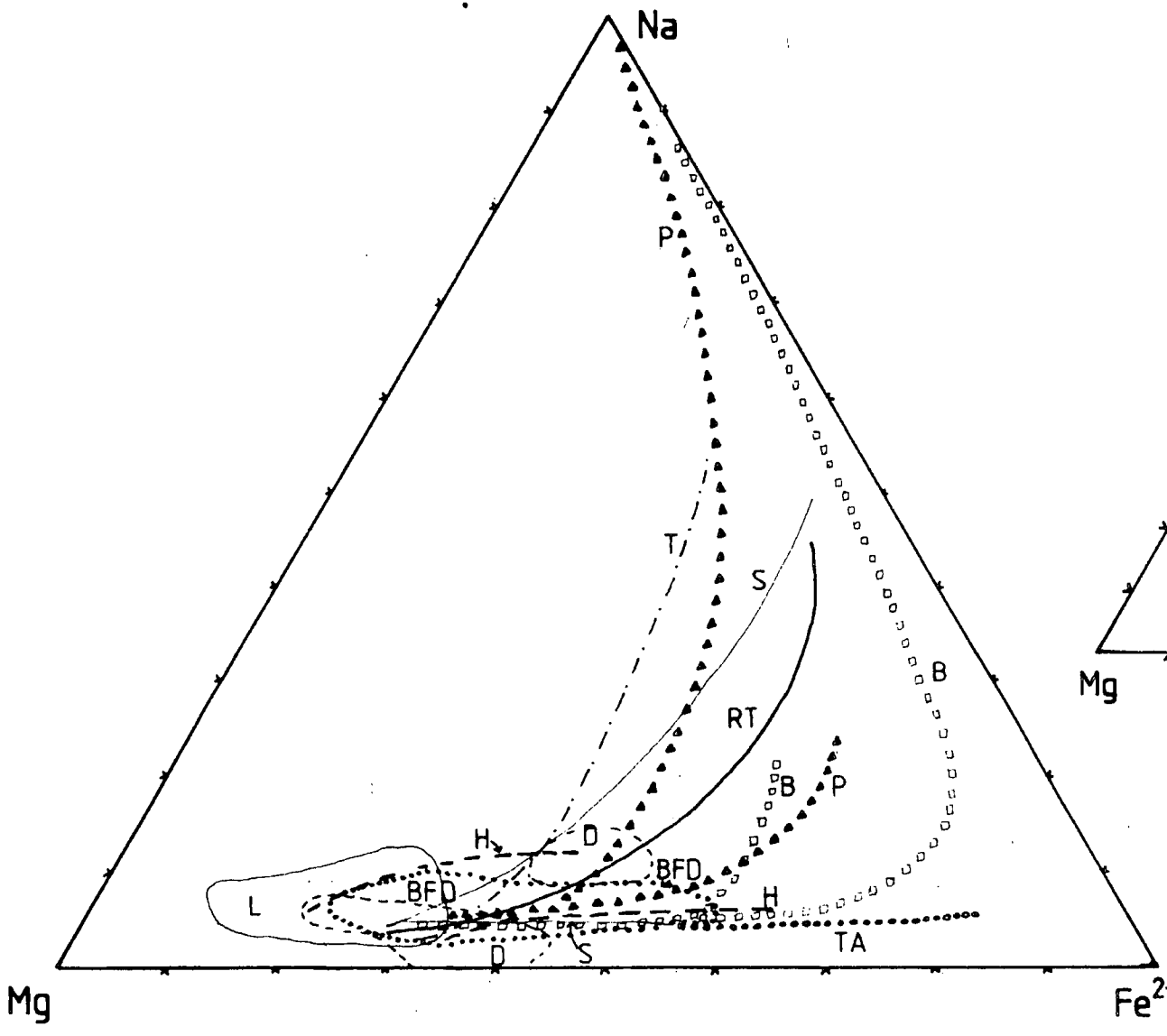

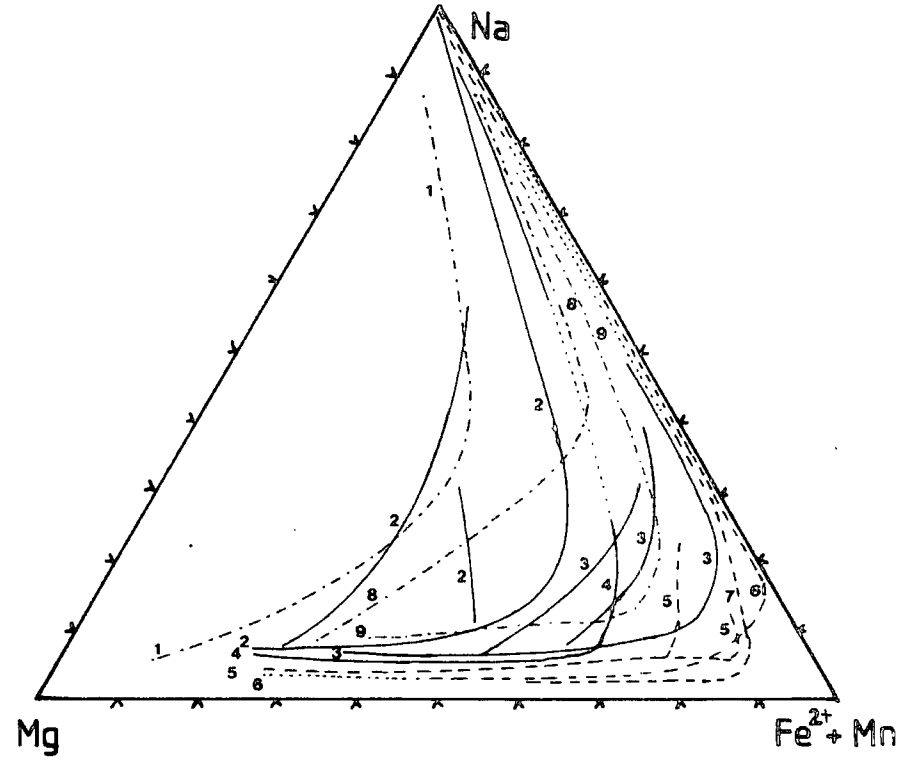

cores to groundmass crystals from which the different trends start.

Many authors have appealed to the fo_2 of the magma as a control on the substitution of $Ca(Fe^{2+},Mg) \rightleftharpoons NaFe^{3+}$ in pyroxenes (eg. Aoki 1964; Yagi 1966; Nash and Wilkinson 1970; Larsen 1976; Chambers 1976; Mitchell and Platt 1978; Jones 1980; Stephenson and Upton 1982). A higher fo_2 will inhibit substantial developement of hedenbergite and allow early $NaFe^{3+} \rightleftharpoons Ca(Mg,Fe^{2+})$ substitution to occur in the pyroxenes. As was noted in Chapter 3, where olivine is present in the benmoreites or phonolites it is always mantled by Fe-rich, Ti-poor opaque oxide, implying an fo_2 above the QFM buffer. The pyroxene trends would imply an increase in fo_2 with increasing fractionation from relatively low fo_2 in the basalts, hawaiites and mugearites, increasing in benmoreites (although still not very high as compared with the Ilímaussaq trend of Larsen 1976) to values above the QFM buffer in phonolites. The presence also of sphene rims on the iron oxides in many cases would also imply an fo_2 above the QFM buffer (Carmichael and Nicholls 1969).

The time at which the liquid becomes peralkaline will have a fundamental control on the generation of Na-enriched pyroxenes. Where peralkalinity occurs early in the crystallisation history, as in the phonolites, the composition of the pyroxene is moved towards Ac at relatively high Mg^{2+} contents, whilst in the benmoreites, peralkalinity in the residual liquid is not achieved until later (ie. after more crystallisation) and the pyroxene evolution proceeds further towards Hd, before Na enrichment commences.

Thus both bulk composition (particularly peralkalinity) and fo_2 would seem to control the compositional trends of these pyroxenes.

4.2.E: Minor Element Variation

Figure 4.2.5 shows the variation of all analysed elements against the pyroxene fractionation index, Na-Mg (Stephenson 1972).

Ti and Al (Figure 4.2.5A)

For most of the pyroxene compositional range Ti and Al show a sympathetic variation with roughly twice as much Al as Ti. Both drop rapidly in content in the range Na-Mg= -0.6 to -0.4 and then remain fairly constant at Ti$\approx$0.02 and Al$\approx$0.5 atoms per

Figure 4.2.5 (3 pages)

Pyroxene chemical variation in terms of Na-Mg (Stephenson 1972). Because of the similar compositions of the most basic pyroxenes from each group there is a large amount of data clustered over the range of Na-Mg from -0.6 to -0.45. This leads to the unfortunate 'black' areas on these plots. The only groups that have no pyroxenes in this range are the recrystallised trachytes and quartz porphyries. All other groups contain pyroxenes with compositions in this range.

Si shows an early increase and continues a gradual rise from about 1.90 in salites at Na-Mg=-0.5 to about 2 in aegirines (at Na-Mg=1).

Ti and Al show an early decrease (cf. Gibb 1973) and remain fairly constant from salites to aegirines. Ti increases in aegirine whilst Al decreases (see text).

Ca, Fe^{2+}, Fe^{3+}, Mn, Mg, Ca and Na all show different trends for phonolites and benmoreites (see text for explanation). Differences in Fe^{2+} and Mn behavior are also evident for the recrystallised phonolites. Comparative trends for Motzfeldt and Ilímaussaq have been inserted on the Fe^{2+} and Mn plots. These are marked so:-

Phonolites —·—·—·—

Benmoreites — — — —

Recrystallised phonolites .....

Motzfeldt ——— MO

Ilímaussaq ——— IL

Zr analyses from the same sample have been joined by tie lines. These lines are not meant to indicate anything other than that these analyses are from the same rock.

Figure 4.2.5A

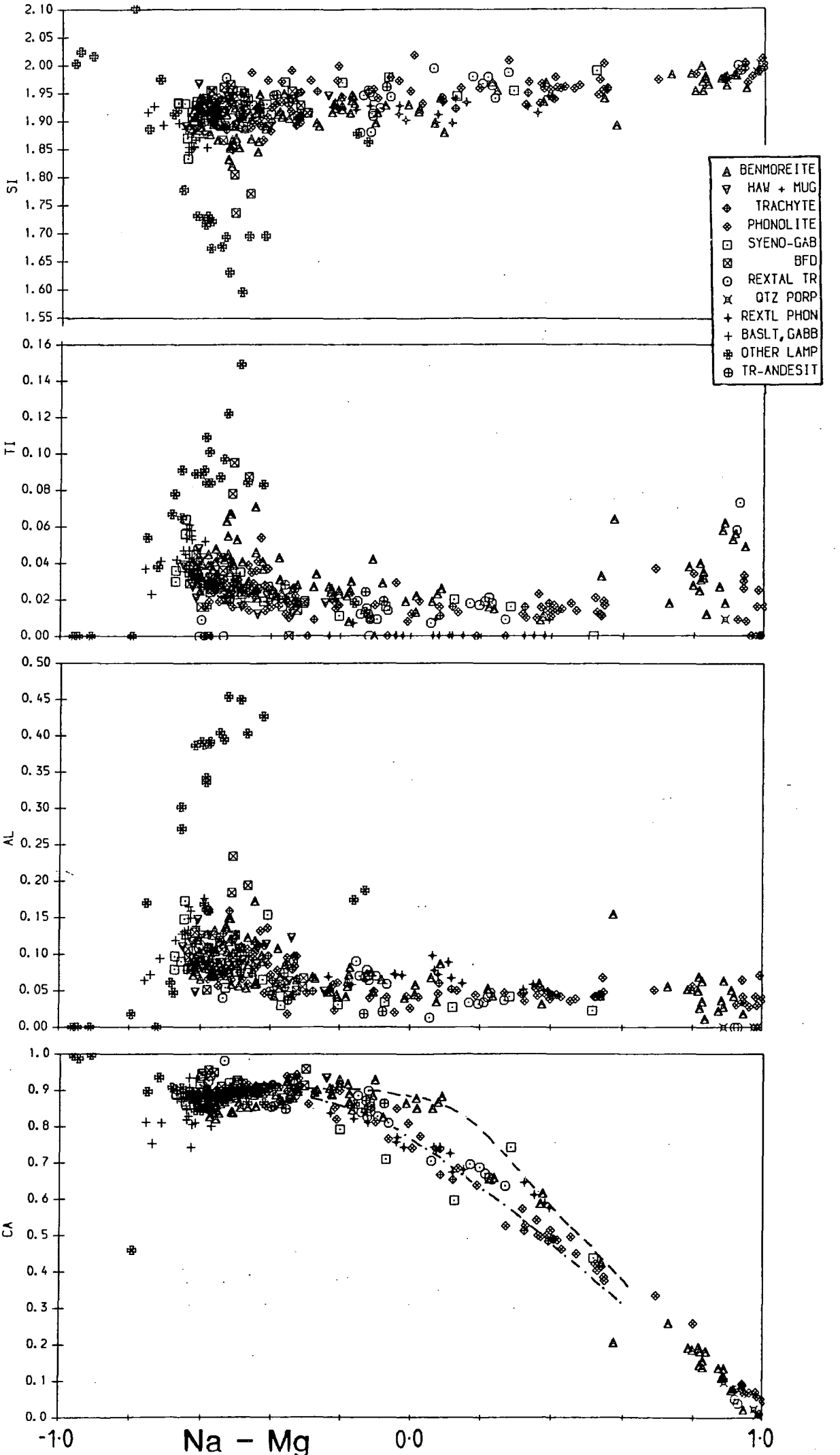
SI
TI
AL
CA
Na – Mg
-1·0
0·0
1·0
BENMOREITE
HAW + MUG
TRACHYTE
PHONOLITE
SYENO-GAB
BFD
REXTAL TR
QTZ PORP
REXTL PHON
BASLT, GABB
OTHER LAMP
TR-ANDESIT

Figure 4.2.5B

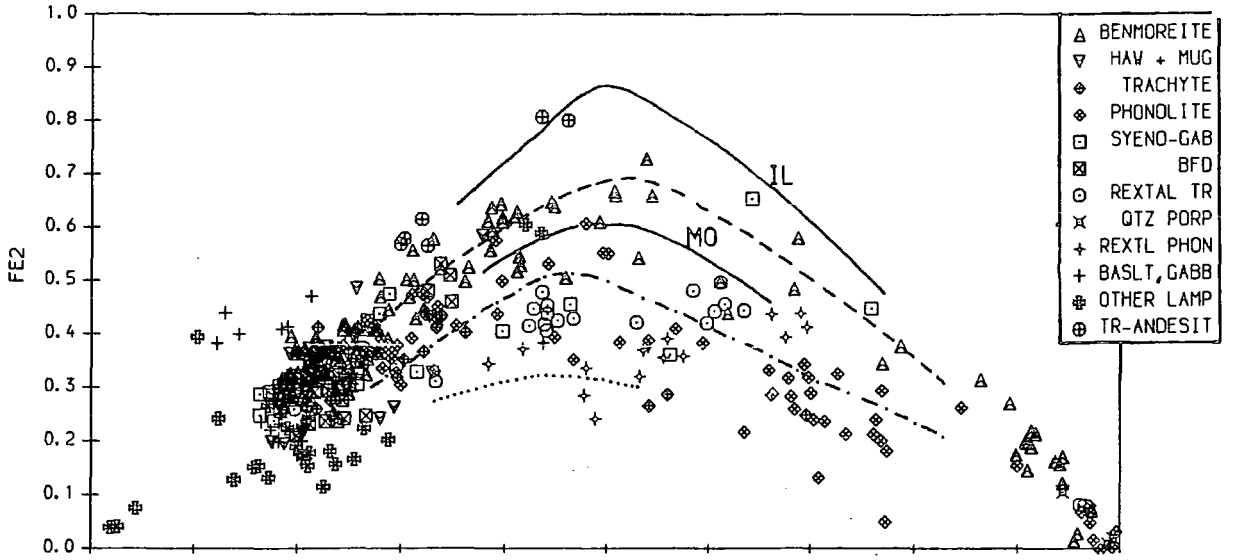
FE2
1.0
0.9
0.8
0.7
0.6
0.5
0.4
0.3
0.2
0.1
0.0
IL
MO
BENMOREITE
HAW + MUG
TRACHYTE
PHONOLITE
SYENO-GAB
BFD
REXTAL TR
QTZ PORP
REXTL PHON
BASLT, GABB
OTHER LAMP
TR-ANDESIT

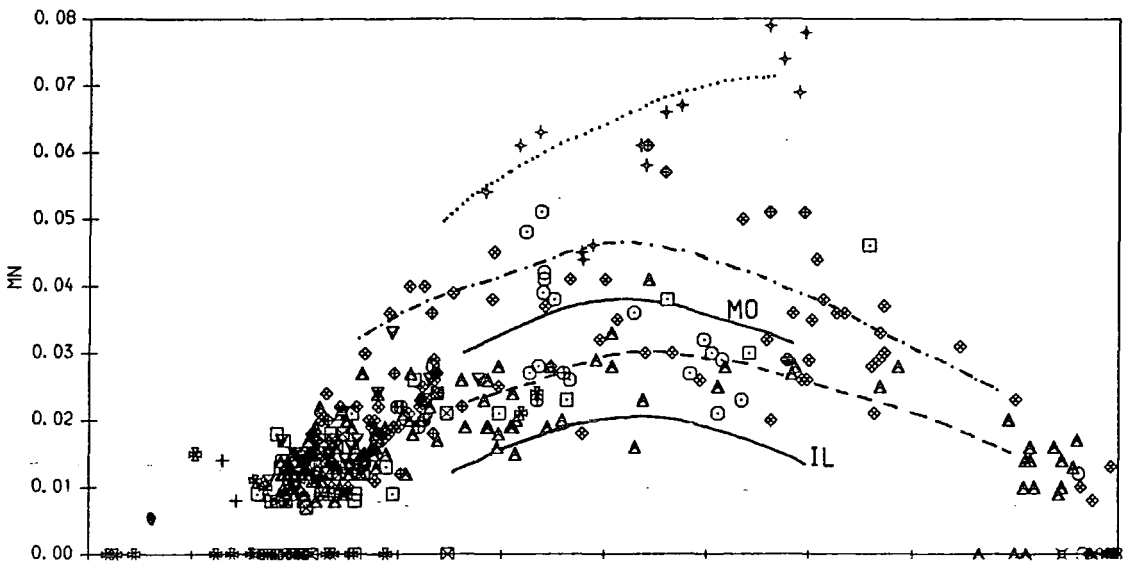
MN
0.08
0.07
0.06
0.05
0.04
0.03
0.02
0.01
0.00
MO
IL

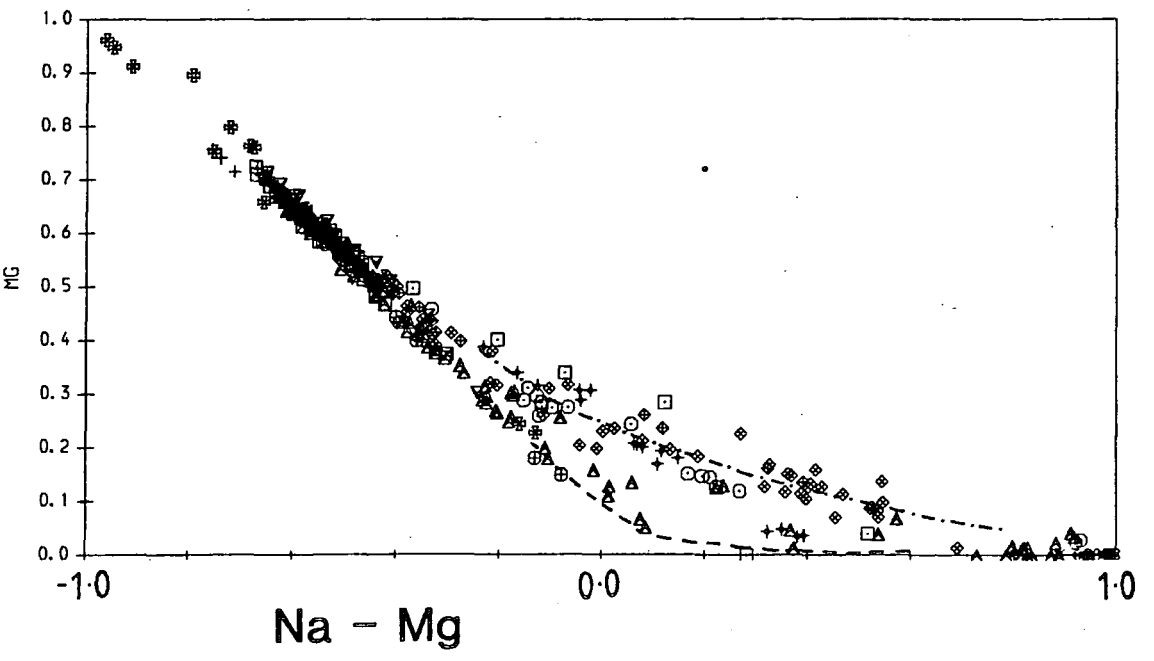
MG
1.0
0.9
0.8
0.7
0.6
0.5
0.4
0.3
0.2
0.1
0.0
-1·0
0·0
1·0
Na - Mg

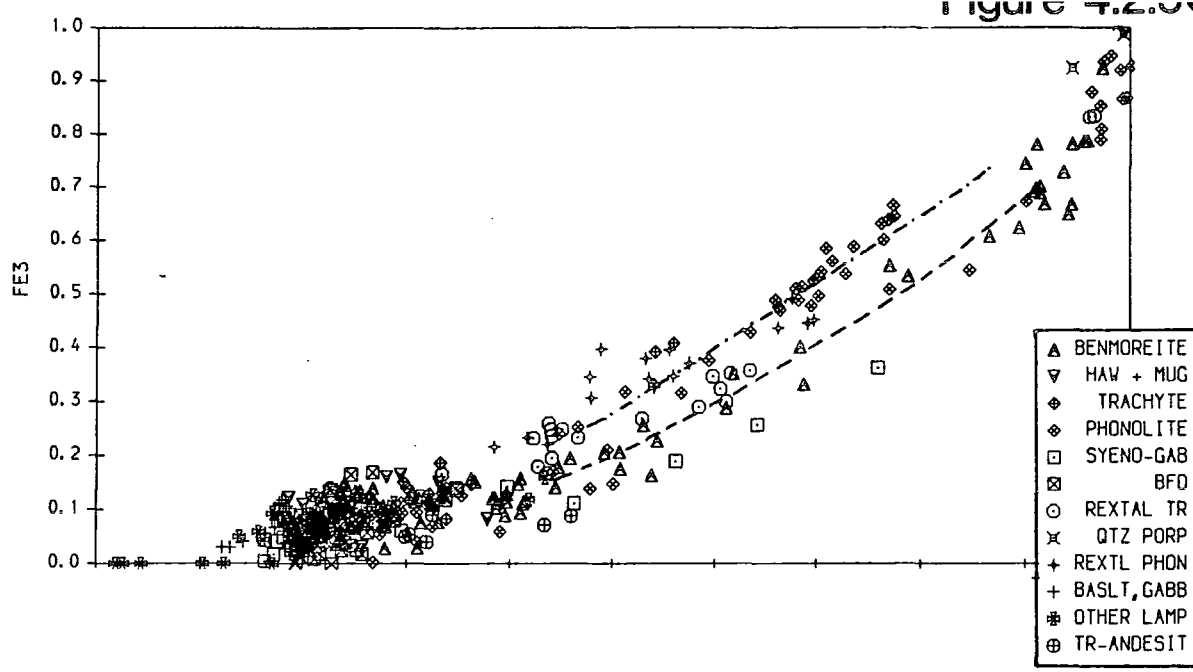
FE3
1.0
0.9
0.8
0.7
0.6
0.5
0.4
0.3
0.2
0.1
0.0
BENMOREITE
HAW + MUG
TRACHYTE
PHONOLITE
SYENO-GAB
BFO
REXTAL TR
QTZ PORP
REXTL PHON
BASLT, GABB
OTHER LAMP
TR-ANDESIT

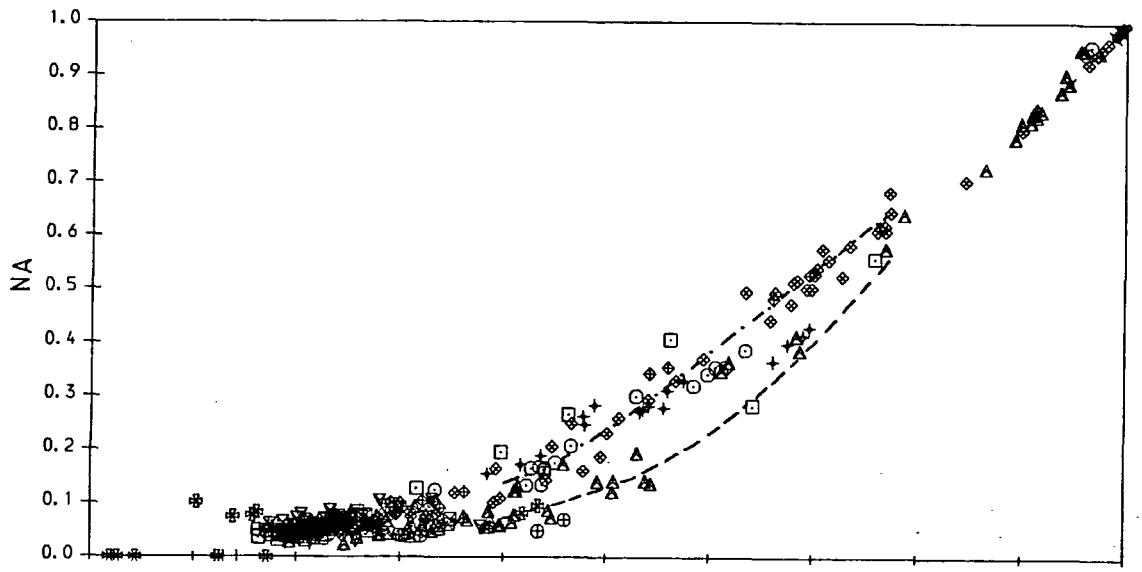
NA
1.0
0.9
0.8
0.7
0.6
0.5
0.4
0.3
0.2
0.1
0.0

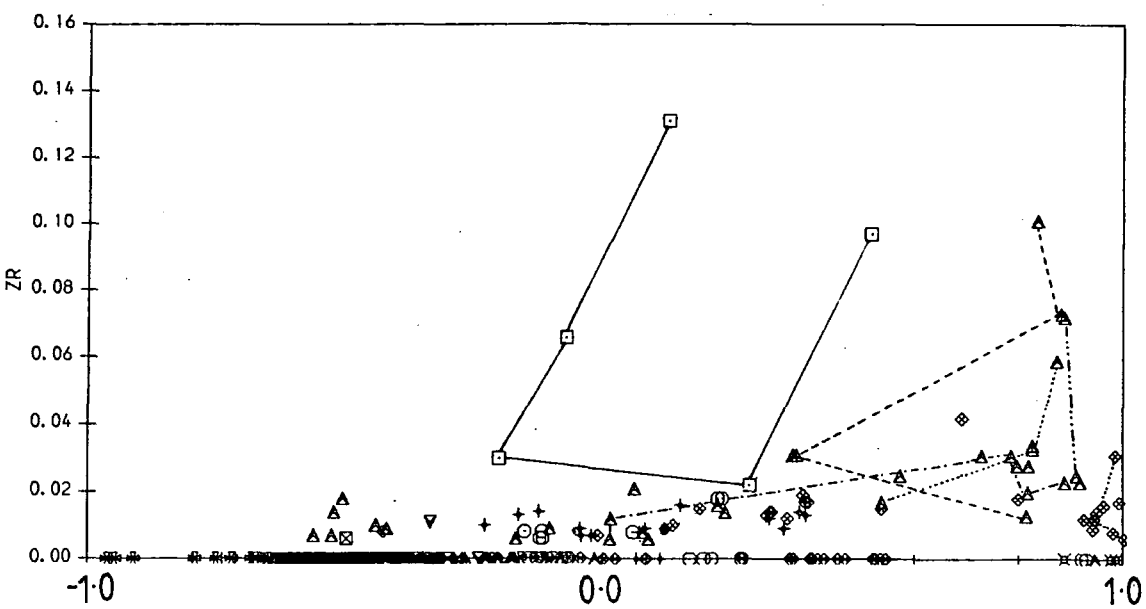
ZR
0.16
0.14
0.12
0.10
0.08
0.06
0.04
0.02
0.00
-1·0
0·0
1·0

Na – Mg

6 oxygens until Ti increases to about 0.06 while Al antithetically drops to 0.00 in the aegirines (ie. at Na-Mg>0.8)

Al is generally present as Ca-Ts in the salite and as jadeite or $NaTiSiAlO_6$ (NATAL) in the aegirines. Ti also occurs in NATAL and also in other end members such as $NaTi_{0.5}(Fe^{2+},Mg)_{0.5}Si_2O_6$ (NAT). Ti-end member nomenclature is taken from Grapes *et al.* (1979) and Nielsen (1979). With increasing Na there is a tendency for Si to increase to approximately 2.0 atoms per 6 oxygens at Na=1.

It would appear that the residual liquids from which the last, Na-rich pyroxenes crystallised were strongly enriched in Ti, Si and Na whilst depleted or completely deficient in Al, as well as being poor in Ca, Mg and Fe^{2+} (ie. strongly peralkaline). This is shown particularly by the benmoreites and trachyandesites, with less clear trends in the phonolites. This trend of late Al deficiency is in contrast to that seen in most alkali pyroxene suites (cf. all previously cited Gardar works, also Platt and Woolley 1986, Brouce and Rançon 1984,Brooks and Gill 1982) where both Ti and Al tend to increase sympathetically at ca. Na-Mg>0.8 atoms (ie. in aegirines). In these Al-free aegirine-bearing rocks crystallisation of feldspar and nepheline would have removed most or all Al from the late stage liquids whilst producing a rise in Na, K and Ti. Thus in the late crystallising pyroxenes Ti would increase but there would be little or no Al available for substitution into the Z (tetrahedral) site and this would antithetically decrease.

Mn and Fe^{2+} (Figure 4.2.5B)

Generally, Mn shows an increase from about 0.015 atoms per formula unit in the salite towards around 0.05 at Na-Mg=0 and then decreases to ca. 0.01 or less (below detection limits) in the aegirines. There is a tendency for the phonolites to show higher Mn than the benmoreites, with the recrystallised phonolites, particularly those from Østfjordsdal, showing almost twice the Mn of other phonolites with similar Na-Mg.

Fe^{2+} shows trends that would be expected from the Mg–(Fe^{2+}+Mn)–Na diagram (Figure 4.2.3), being higher in the benmoreites than the phonolites and peaking in both at around Na-Mg=0. The Fe^{2+} variation is explicable in terms of fo_2 and peralkalinity, however, the Mn, often assumed to go hand-in-hand with Fe^{2+}, seems to follow a different trend. This is not a simple reflection of bulk Mn content of the rock, with

benmoreites and phonolites having similar contents (typically 0.2 to 0.25 wt%) and would seem to be controlled by the olivine content of the sample. Mn will partition preferentially into olivine. Where olivine is present, the Mn content of the pyroxene is lower than where olivine is absent. This is particularly noticeable in the recrystallised phonolites which contain pyroxenes with the highest quantities of Mn and no olivine. Opaque oxides may also exert an effect similar to olivine on the Mn content, these often containing several wt% of Mn (see Chapter 4.6).

Zr

Zirconium end members for the pyroxenes were proposed by Jones and Peckett (1980) as FM-NAZ ($Na(Fe^{2+}\ Mg)_{0.5}Zr_{0.5}Si_2O_6$) and NAZAL ($NaZrSiAlO_6$). These authors were unable to account for the high Zr levels in pyroxenes from the Motzfeldt Centre by coupled substitution such as:

$$Zr^{4+}_{vi} + Al^{3+}_{vi} \rightleftharpoons Fe^{3+}_{vi} + Si^{4+}_{iv}$$

which would only account for about 2.0 wt% ZrO_2. Instead they proposed the Zr end members based on Zr substitution into the 6-fold site alone of

$$(Fe,Mg)^{2+}_{vi} + Zr^{4+}_{vi} \rightleftharpoons 2Fe^{3+}_{vi}$$

and rejected other possibilities such as Zr in the 4-fold site, Zr^{3+} and vacancy substitution such as $\sqcup ZrSiO_6$ or $NaZr_{0.75}\sqcup_{0.25}Si_2O_6$ (where $\sqcup$ indicates a vacancy).

ZrO_2 in pyroxenes has also been reported from Ilímaussaq (Larsen 1976, 1.82 wt%) and the Gardiner Complex (Nielsen 1979, 2.93 wt% from a high Ti-aegirine). The pyroxenes from the Igaliko Dykes show very similar Zr variation to those of Motzfeldt, with contents of 6.92 wt% ZrO_2 from 58017 a benmoreitic facies of the Late Motzfeldt ring dyke and 5.36 wt% from 58206, a benmoreite dyke (representing 26.72 mol% and 20.42 mol% of FM-NAZ respectively).

Watson (1979) showed that Zr solubility in felsic melts was dependent upon peralkalinity and was insensitive of a_{SiO_2}, total Zr or Na_2O/K_2O; thus, the last peralkaline residues of liquid to crystallise would be very Zr-rich, this manifesting itself in high Zr-pyroxenes. Low a_{SiO_2} and high alkali content promote complexes such as $Na_4Zr(SiO_4)_2$

(due to complexing of Zr with Na in the silicate melt, (Watson 1979)) and will militate against formation of other Zr-bearing phases such as zircon, baddeleyite (ZrO_2) or eudialyte.

The Zr content of pyroxenes within one sample is erratic as can be seen from Figure 2.4.5 where the analyses from each sample have been joined. It would also appear that sub-alkali pyroxenes (with relatively little Fe^{3+} and Na) can become strongly enriched in Zr (58017). Jones and Peckett (1980) concluded that small pockets of residual magma with their own particular chemistries (not necessarily the same as other 'pockets' elsewhere within the same sample) were the cause of such variability and this would seem the case here (borne out also by Ti and Al variation in aegirines). Absence of other Zr bearing phases is also needed for Zr-rich aegirine crystallisation (ie. no 'sink' for Zr) and this is shown by all samples from Igaliko containing high Zr pyroxene. The presence of aenigmatite and the absence of Fe-Ti oxides in the Motzfeldt samples indicated fo_2 below the FMQ buffer (see Larsen 1977). However, in the Zr-pyroxene bearing rocks of the Igaliko Swarm no aenigmatite is observed. Fe-Ti oxide and rarely hematite (uniaxial, deep red, overgrowing the opaques in 58206) are seen indicating a higher fo_2 than Jones and Peckett (1980) suggest (ie. above the FMQ buffer) and physico-chemical conditions for the formation of Zr-rich pyroxenes may be less constrained than implied by their results.

In conclusion, the late stage chemistry of a pyroxene is governed by the (often small scale) chemical micro-environment in which it resides. The 'time' at which peralkalinity is achieved and the fo_2 of the liquid determine the general evolutionary trends. The presence or absence of other minerals can also determine certain minor element variations (eg. olivine control on Mn, Zr controlled by other Zr-bearing phases) and chemistry of the last dregs of fractionating liquid controls Ti, Al and Zr contents of the last crystallising pyroxene.

4.3: Olivine

4.3.A: General

Olivine is a common phase in the more basic rocks and becomes less abundant in the more fractionated types. As fractionation increases olivine tends to become less

Figure 4.3.1

A. Olivine analyses in terms of Mg-Fe-Mn. Mn can be seen to increase with increasing Fe. For comparison trends from other rock suites are included.

SQ- South Qôroq (Stephenson 1972).

Il- Ilímaussaq (Larsen 1976).

Sk- Skaergaard (Wager and Deer 1939).

Mo- Motzfeldt (Jones 1980).

B. Olivine analyses in terms of Mg–(Fe+Mn)–(Ca×5). Two trends of Ca enrichment in olivine are apparent from this diagram. The upper trend (marked U) of higher Ca is from olivines in rocks containing normative nepheline. The lower trend (marked S) is from olivines in hypersthene or quartz normative rocks. The a_{SiO_2} would thus seem to control Ca contents in olivines (see text).

IGALIKO DYKE SWARM

Olivine analyses

Atoms per 4 oxygens

Figure 4.3.1

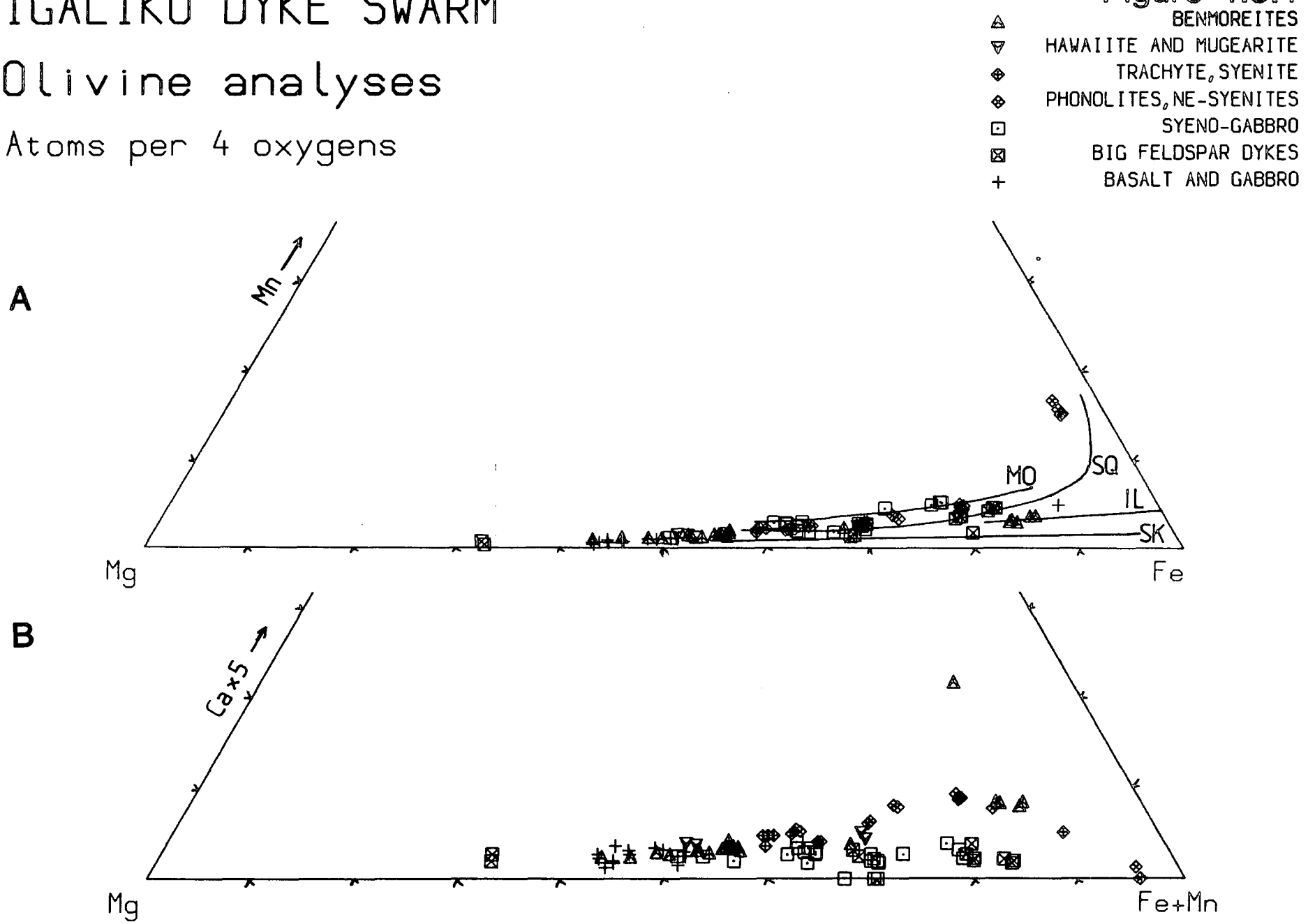

stable and is often corroded with the formation of rims of magnetite.

Magmatic evolution leads to compositional change from relatively Mg-rich, colourless varieties to more Fe and Mn rich, pale yellow types. Pseudomorphing of the olivines by chlorite and/or serpentine is the most common alteration assemblage, with replacement by iddingsite seen in some samples.

4.3.B: Compositional Variation

Ni, Cr or Ti were not detected in any olivines from the Igaliko Dyke Swarm, the major variation being seen in Mg, Fe, Mn and Ca.

Predictably, the fayalite content of olivines rises through basalts to benmoreites and phonolites. This is coupled with a concomitant increase in Mn such that typical compositions range from $Fo_{55}Fa_{44}Tp_1$ (basalts) to ca. $Fo_{15}Fa_{79}Tp_6$ in some BFD's and benmoreites, and up to $Fo_4Fa_{80}Tp_{16}$ in one phonolite. Figure 4.3.1 compares this variation with that observed in certain other rock suites.

The syeno-gabbro trend includes samples from the Motzfeldt ring dyke and late alkali gabbro dyke in Upper Flink's Dal, as well as a syeno-gabbro from Igdlerfigssalik. The trend for these is one of higher Mn than the remainder of the Igaliko dykes and simply reflects marginally higher bulk Mn content of the rock (cf. Simkin and Smith 1970). The general trend is also higher than that found by Stephenson (1973) from South Qôroq and Larsen (1976) from Ilímaussaq.

Ca variation is shown in an exaggerated fashion in Figure 4.3.1B, where two trends are clearly visible, an upper trend of increasing Ca with increasing (Fe+Mn) and a lower trend of constant or slightly decreasing Ca with increasing (Fe+Mn).

Simkin and Smith (1970) hinted at a variation in Ca with increasing Fe content but assigned the bulk of the variation to a pressure control (lower pressure, more Ca) with less emphasis on the bulk rock composition. Ca content of olivine can be related to a larnite component (Ca_2SiO_4), and can be shown by the equation

$$CaFeSi_2O_6 = Ca_2SiO_4 + Fe_2SiO_4 + 2SiO_2$$

ie. Hedenbergite = larnite + fayalite + 2silica. Thus the larnite component may depend

on silica content of the magma, with a low a_{SiO_2} promoting increased Ca in olivine. Low pressure may also produce a similar effect (Nicholls *et al.* 1971; Stormer 1972,1973). Thus the more undersaturated (alkaline with lower a_{SiO_2}) and shallower an igneous body, the higher the Ca content of the olivines. Larsen (1976) noted that Simkin and Smith's data set did not include any strongly peralkaline intrusions and attributed high Ca from Ilímaussaq olivines to the peralkalinity and low silica (as well as the shallow depth of the complex).

In general those samples on the higher Ca trend show normative *ne* while those of the lower trend show normative *hy* (with the rare exceptions to this being due mostly to uncertainties in the estimation of bulk rock Fe^{2+}/Fe^{3+} ratios prior to the calculation of the norm).

It would thus seem that a_{SiO_2} is an important control on larnite content of olivine, with silica deficient rocks crystallising olivines with higher contents of Ca at higher Fe+Mn values, whilst those from more silica saturated rocks contain less Ca. There is no evidence of an antithetic relationship between Ca and Mn.

Na_2O was invariably recorded at between 0.3 and 0.6 wt% and this is considered to be a fault of the microprobe, any Na that may have been present (see Jones 1984) going unrecorded. Al_2O_3 was recorded in amounts from between 0.26 and 0.62 wt% in about one eighth of the samples and one sample showed ZrO_2 at 0.28 wt%.

4.4: Amphiboles

4.4.A: General

Amphiboles increase in abundance with increasing host rock fractionation. They are generally absent from the basalts, becoming abundant in the benmoreites and phonolites, where they may dominate over pyroxene.

This volumetric increase with fractionation is mirrored by a compositional variation, noted by a change in the dominant pleochroic scheme. The more basic amphiboles (pargasitic hornblendes) show dark brown - light brown - dark greenish brown pleochroism (eg. in the mugearites), whilst in the benmoreites shades of brown pleochroism in ferrorichterites pass into darker greens with a hint of blue in katophorites. These grade into

dark inky-blue - pale pinkish brown - dark brown pleochroic schemes in the arfvedsonites (cf. Chambers 1976, Jones 1980). This change in colour is often evident within individual grains, indicating zonation to marginal, alkali enriched compositions.

Amphibole crystallisation is closely related to that of the pyroxenes, with amphiboles commonly seen as overgrowths to pyroxenes, although unlike the Motzfeldt, North Qôroq (Chambers 1976) and Ilímaussaq (Larsen 1976) centres, there appear to be no further overgrowths of alkali pyroxene on the amphibole.

Amphiboles are also common to the recrystallised rocks in the vicinity of the Late Igdlerfigssalik syenites.

4.4.B: Recalculation and Classification

Amphiboles are the most complex and variable group of rock forming minerals studied. This is primarily due to a wide variety of cation sites within the amphibole structure which enable a large range of ionic radii to be accommodated (Ernst 1968).

Analysis by electron-microprobe is unable to distinguish between FeO and Fe_2O_3, with the total iron content usually reported as FeO. Many of the amphiboles studied here contain high total iron and, due to the high fo_2 concluded from the pyroxenes, must contain appreciable Fe^{3+}. Amphiboles may contain between 15 and 16 cations per 23 oxygens (calcic and sodic-calcic/alkali types respectively) and are unlike pyroxenes where stoichiometry can be assumed (Cawthorn and Collerson 1974). Thus recalculation to a fixed number of oxygens for all cations in an attempt to balance Fe^{2+}/Fe^{3+} must be doubtful. On this basis Leake (1978), although not specifically advocating one particular method, suggests that 'calculation on the basis of 23(O) and then adjustment of the total cations, excluding (Ca+Na+K), to 5+8=13 by varying the Fe^{2+}/Fe^{3+}, has much to recommend it'. Leake (1978) reports no Ba-bearing amphiboles, and following the method of Knight (1976), Ba was also excluded from the calculation of T+C cations to 13 (see below).

This method is in contrast to that used by Chambers (1976) and Jones (1980) who recalculated for Fe^{2+}/Fe^{3+} using the computer program `MINDATA5` of Knight (1976). Jones (1984) however, argued that this method was similar to that suggested by Leake

(1978), outlined above. Brooks and Gill (1982) compared the 13 cation based recalculation with wet-chemical results for amphiboles from the Kangerdlugssuaq intrusion, Greenland reported by Kempe and Deer (1970) and concluded that even a rough estimate of Fe^{3+} was better than assuming none was present. Stout (1972) states that recalculation on these lines would provide a crude maximum estimate of Fe^{3+}/Fe^{2+}.

The classification scheme employed here is that proposed by Leake (1978). Standard amphiboles have the general formula $A_{0-1}B_2C_5T_8(OH,F,Cl)_2$ with cations assigned to sites in the order:

T=Si, Al, Fe^{3+}, Ti to total 8.000

C=residual Al, Ti, Fe^{3+} then Zr, Mg, Fe^{2+}, Mn to total 5.000

B=residual Fe^{2+}, Mn, Mg then Ca, Ba, Na to total 2.000

A=residual Na, then K. This should total between 0-1.000

The table below shows a comparison of site names used by Leake (1978) and Phillips (1966) as well as coordination numbers, cation sites and commonly occupying cations. The classification scheme of Phillips (1966) has been used in previous studies of amphiboles from Gardar Complexes.

Leake (1978)	Phillips (1966)	Cation sites	Coordination	No. of cations	Common cations
T	Z		4	8	Si,Al,(Fe^{3+},Ti)
C	Y	M4	6	5	Al,Fe^{3+},Ti,Mg,Fe^{2+},Mn
B	X	M1,M2,M3	6-8	2	Ca,Na,Ba
A	A		10-12	0-1	Na,K

The Leake (1978) classification is based upon a division of amphibole compositional space into 4 categories on Ca+Na occupancy of the B site:-

$(Ca+Na)_B$ <1.34: Iron-magnesium-manganese group

$(Ca+Na)_B \geq 1.34$ and Na_B <0.67: Calcic amphibole group

$(Ca+Na)_B \geq 1.34$ and $0.67 \leq Na_B < 1.34$: Sodic-calcic amphibole group

$Na_B \geq 1.34$: Alkali amphibole group

Each of these groups is then subdivided as shown in Figure 4.4.1A, B and C on the basis of $Mg/Mg+Fe^{2+}$ against either Si atoms in the standard cell or $Fe^{3+}/Fe^{3+}+Al^{vi}$. Plotted on these diagrams are analyses of amphiboles from this study relevant to each category. There are no amphiboles from the iron-magnesium-manganese group in these dykes and this classification scheme is not included.

This method is ideally suited to computer-based classification for easy handling of large quantities of data. Prefices such as potassian, manganoan etc. are also permitted in this scheme for varieties rich in certain non-essential elements.

For comparative purposes a plot of Al^Z vs Na^X is included (Figure 4.4.2B). This forms part of the Phillips (1966) classification scheme. The loci of both Jones (1980) and Chambers (1976) data from Motzfeldt and North Qôroq amphiboles are indicated. Classification by this method alone can produce spurious results. Jones (1980) noted that 'pargasites', as classified by the Phillips (1966) scheme, were in fact ferro-hastingsites. This was due to the low Mg content of these amphiboles which is not considered by the Phillips scheme. Chambers (1976) reported pargasites and ferro-pargasites from North Qôroq and Jones (1980) ascribed the absence of these fairly basic amphiboles from Motzfeldt to the overall more fractionated nature of the Motzfeldt magmas compared to the North Qôroq magmas.

The Phillips (1966) classification scheme also takes no account of Fe^{3+} content. Thus arfvedsonite, an important alkali amphibole end member, is represented by eckermannite due to its low Al content in the C (or Y) site. By considering both $Mg/Mg+Fe^{2+}$ and $Fe^{3+}/Fe^{3+}+Al$, as well as the Ca and Na contents of the B site, Leake's (1978) classification scheme removes such complications and better represents the wide range of amphibole compositional space.

The majority of the amphiboles from the Igaliko dykes are calcic, with progressively lesser amounts of sodic-calcic and alkali amphiboles. There are no very obvious correlations between rock type and amphibole type, this in part reflecting the range of

Figure 4.4.1 (2 pages)

A. (Facing page). Calcic amphibole classification from Leake (1978) with analyses from Igaliko dykes plotted in the relevant compositional ranges.

B. (Overleaf). Sodic-calcic amphibole classification from Leake (1978) with analyses from the Igaliko dykes plotted in the relevant compositional ranges.

C. (Overleaf). Alkali amphibole classification from Leake (1978) with analyses from the Igaliko dykes plotted in the relevant compositional ranges.

CALCIC AMPHIBOLES $(Ca+Na)_B \geq 1.34$, $Na_B < 0.67$

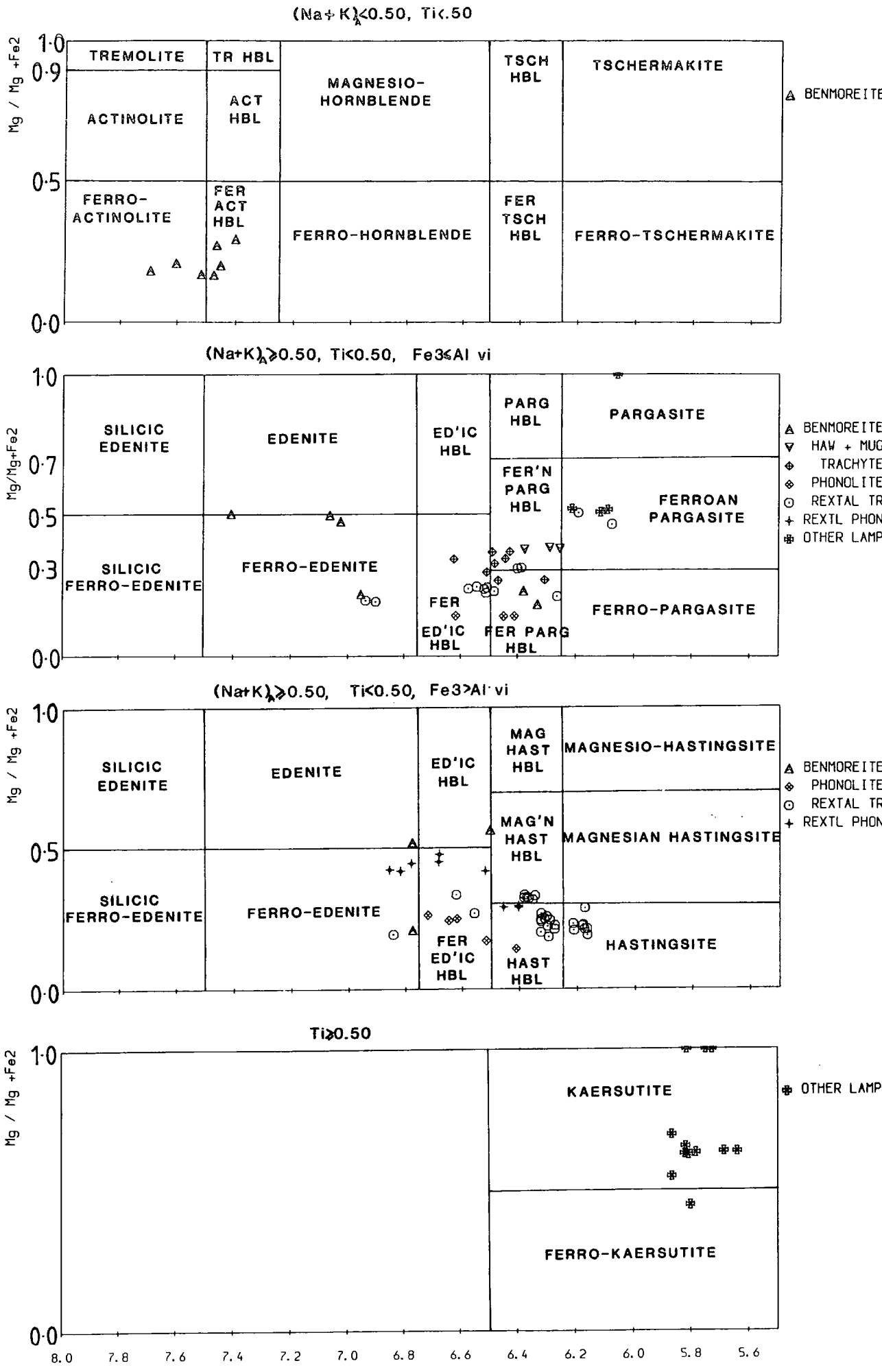

Figure 4.4.1B

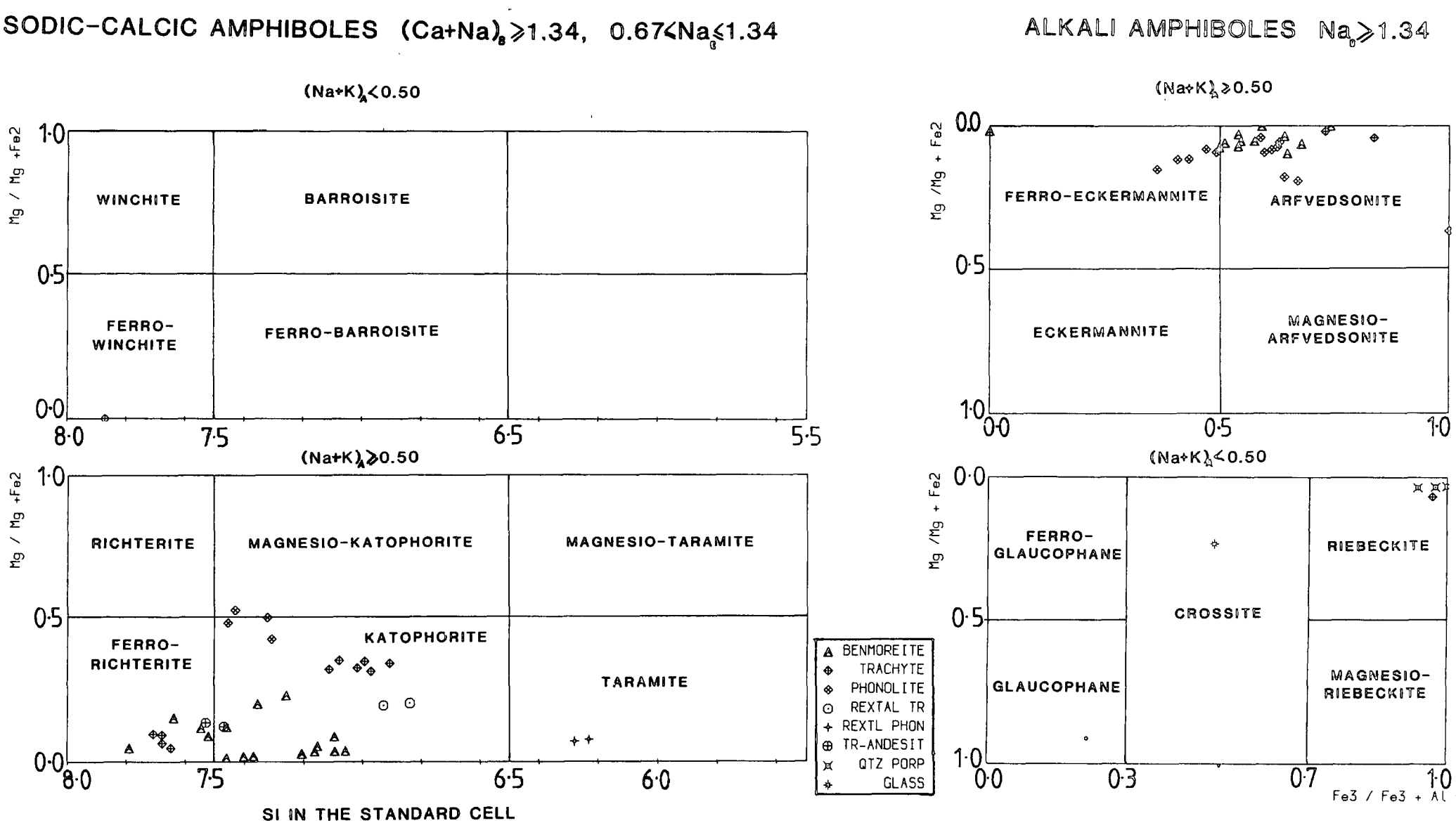
SODIC-CALCIC AMPHIBOLES (Ca+Na)B ≥1.34, 0.67<NaB≤1.34
ALKALI AMPHIBOLES NaB≥1.34
(Na+K)A<0.50
(Na+K)A≥0.50
Mg / Mg +Fe2
WINCHITE
BARROISITE
FERRO-WINCHITE
FERRO-BARROISITE
1·0
0·5
0·0
8·0
7·5
6·5
5·5
(Na+K)A≥0.50
(Na+K)A<0.50
RICHTERITE
MAGNESIO-KATOPHORITE
MAGNESIO-TARAMITE
FERRO-RICHTERITE
KATOPHORITE
TARAMITE
6·0
BENMOREITE
TRACHYTE
PHONOLITE
REXTAL TR
REXTL PHON
TR-ANDESIT
QTZ PORP
GLASS
SI IN THE STANDARD CELL
Mg /Mg + Fe2
0·0
FERRO-ECKERMANNITE
ARFVEDSONITE
ECKERMANNITE
MAGNESIO-ARFVEDSONITE
FERRO-GLAUCOPHANE
CROSSITE
RIEBECKITE
GLAUCOPHANE
MAGNESIO-RIEBECKITE
0·3
0·7
Fe3 / Fe3 + Al vi

Figure 4.4.2

A. Al vs. Ca (atoms per 23 oxygens and T+C=13) for all amphiboles from the Igaliko dykes.The straight line marks a 1:1 correlation between Ca and Al. The dash-dot line marks the trend observed by Larsen (1976) of Al deficiency in katophorites (see page 71/72). This may also be evident from some of the dykes (see text).

Abbreviations: Hast - Hastingsite
Kat - Katophorite
Arf - Arfvedsonite

B. Part of the Phillips (1966) classification scheme for amphiboles with Na^X plotted against Al^Z as atoms per formula unit. The dashed line encloses all analysed North Qôroq amphiboles from Chambers (1976), the dotted line encloses all analyses of amphiboles from Motzfeldt, (Jones 1980).

End member abbreviations:-

Pa	Pargasite	$NaCa_2Mg_4AlSi_6Al_2O_{22}(OH)_2$
Ts	Tschermakite	$Ca_2Mg_3Al_2Si_6Al_2O_{22}(OH)_2$
Ed	Edenite	$NaCa_2Mg_5Si_7AlO_{22}(OH)_2$
Tr	Tremolite	$Ca_2Mg_5Si_8O_{22}(OH)_2$
Su	Sundiusite	$NaNaCaMg_3Al_2Si_6Al_2O_{22}(OH)_2$
R	Richterite	$NaNaCaMgSi_8O_{22}(OH)_2$
M	Miyashiroite	$NaNa_2Mg_3Al_2Si_7AlO_{22}(OH)_2$
Ec	Eckermannite	$NaNa_2Mg_4AlSi_8O_{22}(OH)_2$
G	Glaucophane	$Na_2Mg_3Al_2Si_8O_{22}(OH)_2$

The vertical line from Richterite (R) to Sundiusite (Su) separates alkali amphiboles on the right from non-alkali amphiboles on the left. Na^X is equivalent to Na^B of the Leake (1978) scheme and Al^Z is equivalent to Al^T.

Figure 4.4.2A

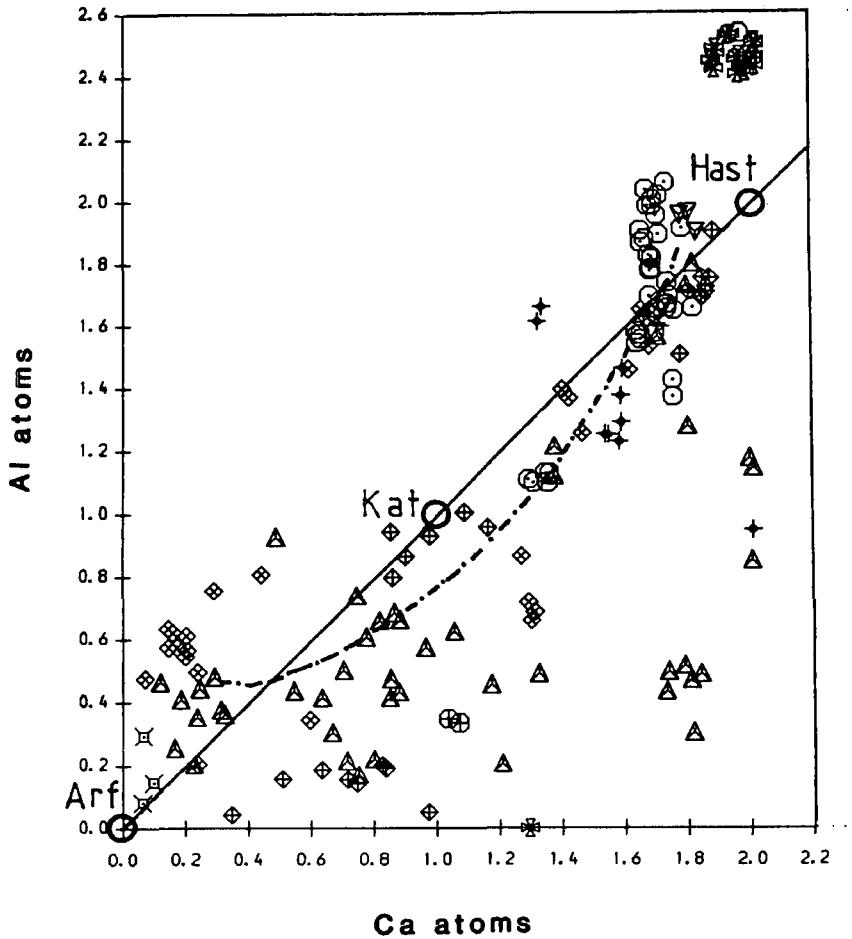

Figure 4.4.2B

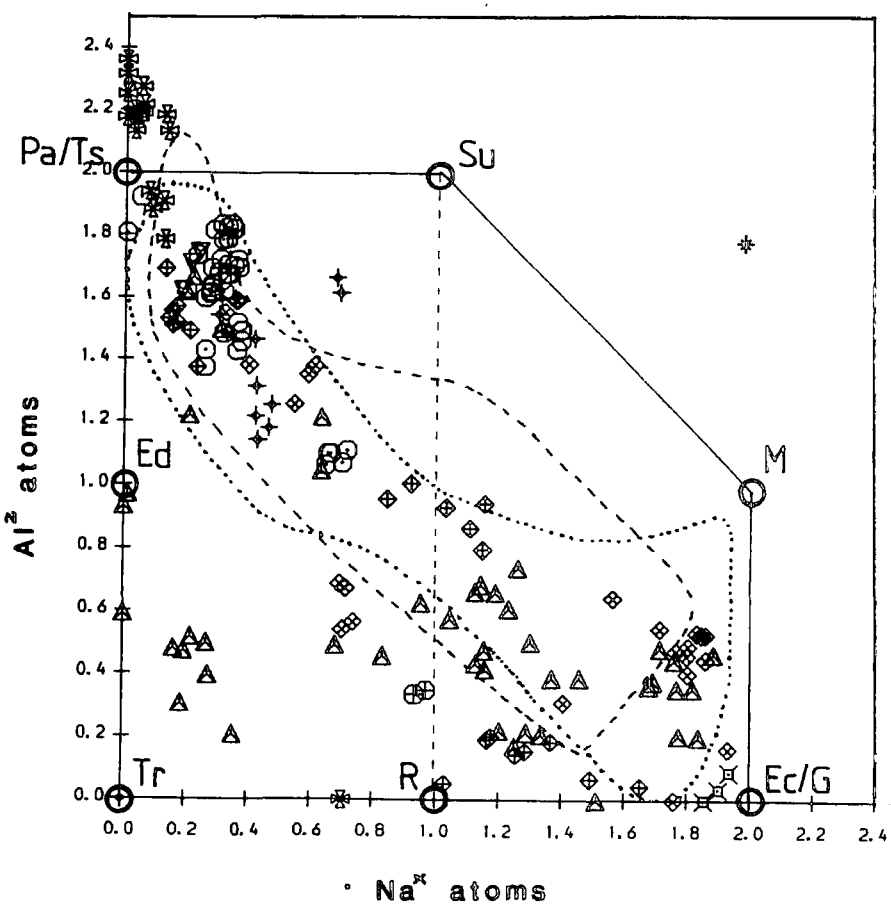

composition that can be seen in zoned crystals from one sample. However, recrystallised trachytes and phonolites, and hawaiites/mugearites do not contain alkali amphiboles, and in general the 'other lamprophyres' contain magnesio-kaersutite (a reddish-brown pleochroic, Si-poor, Ti-rich amphibole). Other Si-poor (Al^{vi}-rich) amphiboles such as pargasite and hastingsite are relatively rare, with examples only from recrystallised trachytes and 'other lamprophyres'. The Igaliko magmas thus appear less fractionated then those of Motzfeldt and North Qôroq where pargasitic amphiboles were recorded.

Amphiboles from the Igaliko dykes range, with increasing alkali content, from ferro-actinolites and ferro-actinolitic hornblende through iron-rich pargasitic hornblendes ($Fe \leq Al^{vi}$) into hastingsitic and edenitic hornblendes ($Fe^{3+} > Al$). With more Na and less Ca in B, compositions grade into katophorites and ferro-richterites and finally, when Na dominates the B-site, into alkali amphiboles such as ferro-eckermannite and arfvedsonite (very Fe^{3+}-rich, Al^{vi}-poor). This change records a progressive decrease in $Mg/Mg+Fe^{2+}$ and Ca, and an increase in Si, Na and Fe^{3+} with fractionation.

4.4.C: Amphibole Chemistry

The major substitution occurring within the amphiboles from the Igaliko dykes is

$$Ca^B + Al^T \rightleftharpoons Na^B + Si^T$$

coupled with an increase in Fe^{2+} and Fe^{3+} and decline in Mg with evolution. This is identical to the substitutions described by Chambers (1976) from North Qôroq and Jones (1980) from Motzfeldt. Larsen (1976) and Anderson (1974) also describe similar substitutions from Ilímaussaq and parts of the Nunarssuit Complex respectively. The index Na^B-Al^T (Na^X-Al^Z) can be used to cover this compositional range (Chambers 1976) and all the analyses from the dykes are plotted against this index. Consequently, against this fractionation index, it can be seen that Si gradually increases to ca. 8 atoms per formula unit in the alkali rich amphiboles (ie. at Na^B-Al^T=2) and Ca gradually decreases to around 0.

The A site occupancy ranges from almost empty (ie. very little Na or K in A) to 1 or greater (up to ca. 1.22). This excess of Na+K in A will in part be due to the recalculation procedure used for Fe^{3+}, but may also be an analytical problem. Micro-

Figure 4.4.3 (3 pages)

Amphibole chemical variation as atoms per formula unit plotted against Na^B-Al^T (Chambers 1976).

Amphiboles show a gradual increase in Si from <6 in kaersutite (Na^B-$Al^T \approx$ -2.2), ca. 6.2 in hastingsitic amphiboles (Na^B-$Al^T \approx$ -1.5), to about 8 in the alkali amphiboles (at Na^B-$Al^T \approx 2$).

Ti drops rapidly from kaersutites (at Na^B-Al^T <-2.0) and stays below 0.5 atoms as Na^B-Al^T rises to 2.

Ca gradually drops from 2.0 $\longrightarrow$ 0.0 as Na^B-Al^T rises from -2 to 2.

Fe^{2+}, Fe^{3+}, Mn, and Mg all show a wide range of composition at any particular Na^B-Al^T. Fe^{2+}, Fe^{3+} and Mn show an increase with Na^B-Al^T whilst Mg decreases.

Na and K show relatively constant concentrations across the whole range of Na^B-Al^T. As K is greater than 0.25 atoms in most analyses the prefix potassian should strictly be used (Leake 1978). This has been omitted from amphibole names in the text for brevity. Similarly about half of the analyses contain >0.25 atoms Ti and the prefix titanian should be applied to the name (except in the kaersutites). Similarly, this has been omitted for ease.

Zr shows an increase from about Na^B-Al^T=0.0. It is noticable that benmoreites contain a more Zr-rich amphibole than the phonolites. This may be an effect of the lower fo_2 in the benmoreites. Zr is assigned to a newly proposed amphibole end member - zirconian arfvedsonite (see text).

Figure 4.4.3A

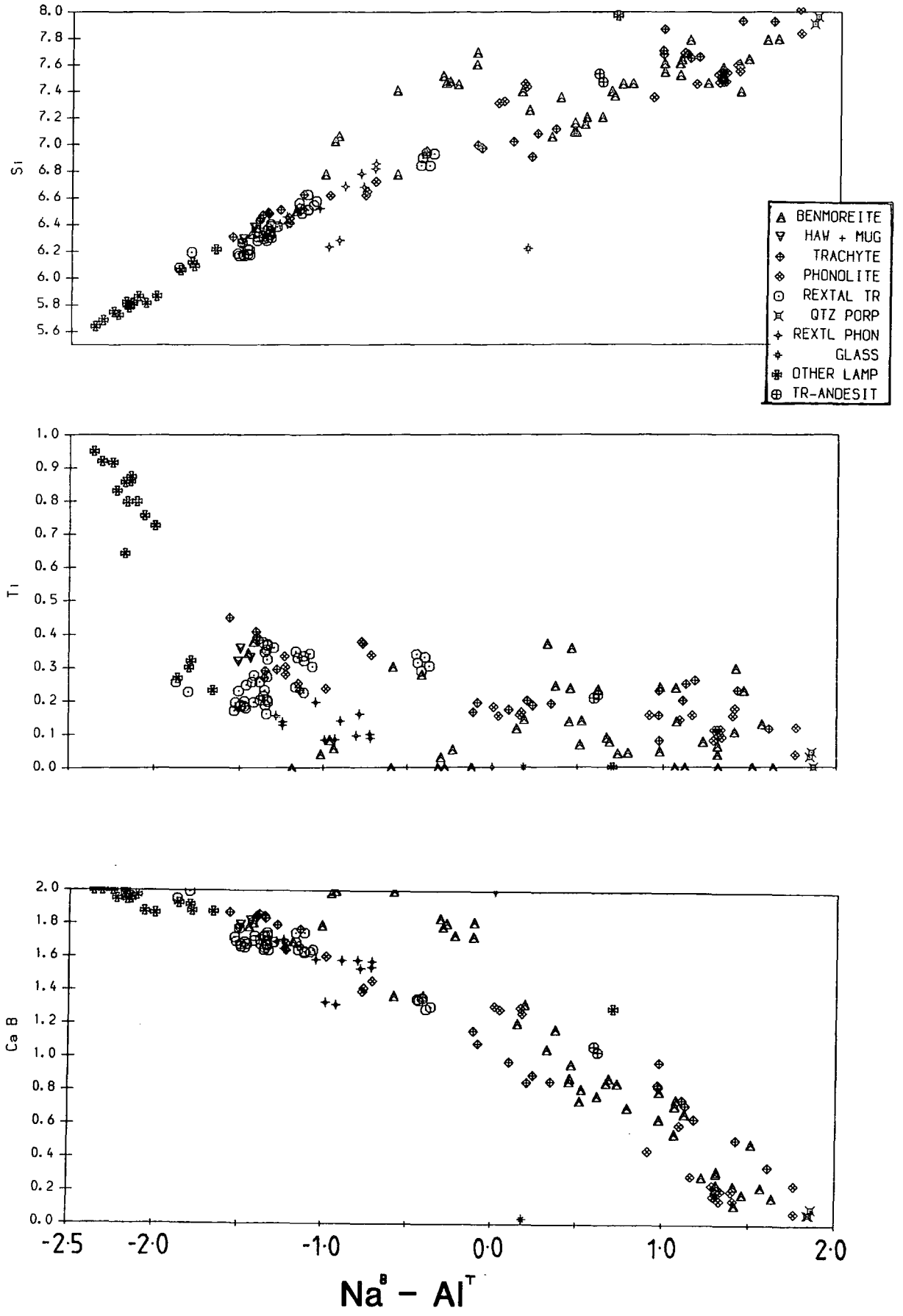
Si
8.0
7.8
7.6
7.4
7.2
7.0
6.8
6.6
6.4
6.2
6.0
5.8
5.6
BENMOREITE
HAW + MUG
TRACHYTE
PHONOLITE
REXTAL TR
QTZ PORP
REXTL PHON
GLASS
OTHER LAMP
TR-ANDESIT
Ti
1.0
0.9
0.8
0.7
0.6
0.5
0.4
0.3
0.2
0.1
0.0
Ca B
2.0
1.8
1.6
1.4
1.2
1.0
0.8
0.6
0.4
0.2
0.0
-2·5
-2·0
-1·0
0·0
1·0
2·0
Na^B − Al^T

Figure 4.4.3B

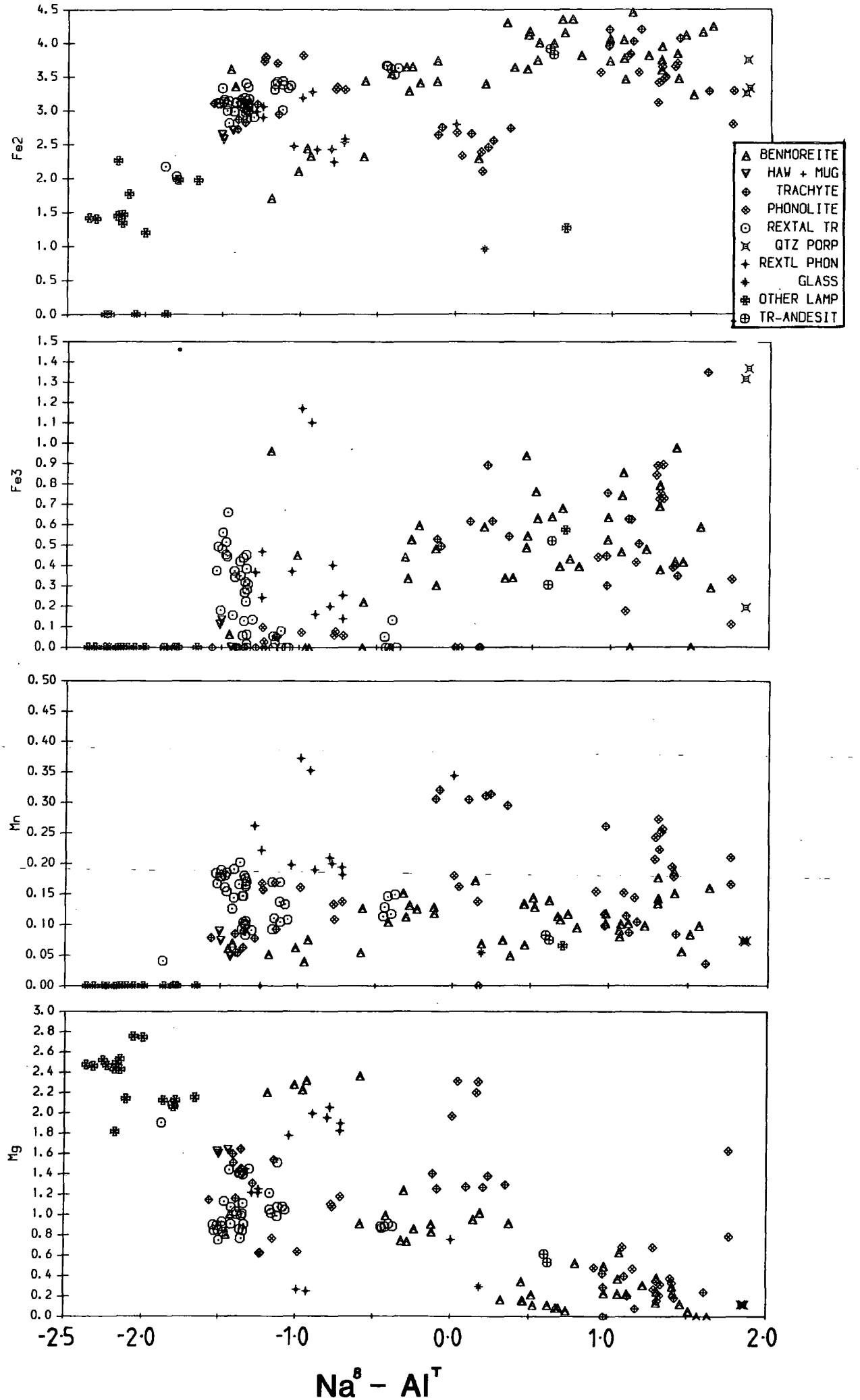
Fe2
Fe3
Mn
Mg
BENMOREITE
HAW + MUG
TRACHYTE
PHONOLITE
REXTAL TR
QTZ PORP
REXTL PHON
GLASS
OTHER LAMP
TR-ANDESIT
-2·5
-2·0
-1·0
0·0
1·0
2·0
Na^B − Al^T

Figure 4.4.3C

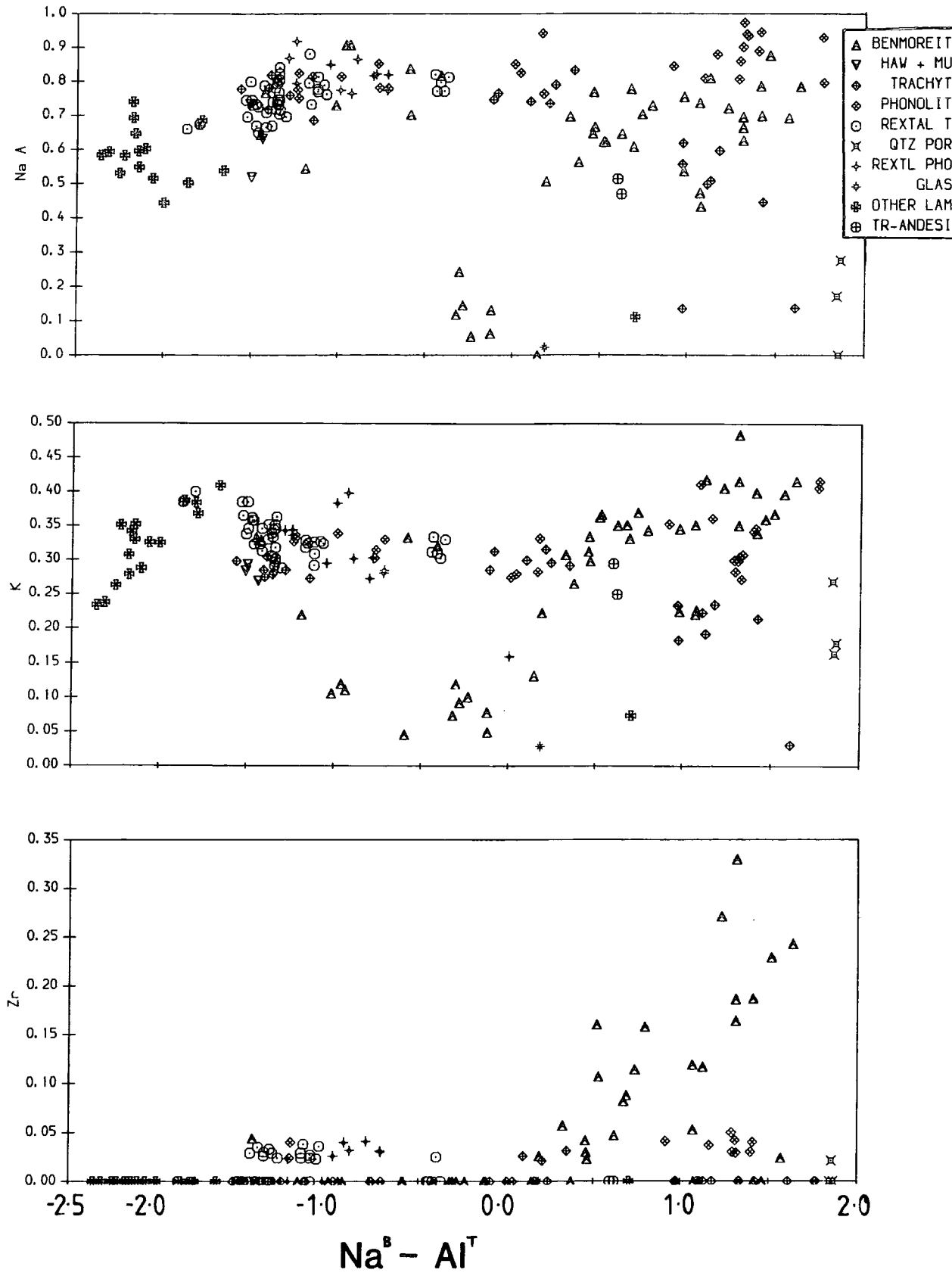
Na A
K
Zr
BENMOREIT
HAW + MU
TRACHYT
PHONOLIT
REXTAL T
QTZ POR
REXTL PHO
GLAS
OTHER LAM
TR-ANDESI
-2·5
-2·0
-1·0
0·0
1·0
2·0
Na^B – Al^T

probe analyses of alkali rich ferro-magnesian minerals often show excess Na, a feature apparently more pronounced in amphiboles than in pyroxenes (Dr. K. Pendlebury, Manchester University, pers. comm. 1986). The Na contents of the amphiboles correlate with the total alkali content of the whole rock (cf. Helz 1973; Jakes and White 1972; Wills 1974), with the less alkali rich amphiboles occurring in the less alkaline rocks.

As with the pyroxenes, late crystallising interstitial amphiboles become more alkali enriched, with an associated decrease of Mg and Al. A wide range of compositions can occur in a single zoned crystal, this being due to progressive compositional changes within the late magmatic fluids.

Ti shows an early decrease with Al^T (to Na^B-$Al^T \approx$-1.5) and then a gradual slow decline in contrast to trends observed in Motzfeldt. Helz (1973) relates lower Ti to lower crystallisation temperature in more fractionated magmas, with fo_2 possibly having the same effect. The rapid cooling of the magmas from relatively high temperatures may arrest this behaviour. The gradual decline in Ti may also be due to crystallisation of Ti-bearing oxide minerals at lower temperatures (Beddoe-Stephens 1977).

With increasing (Na^B-Al^T), Mg declines and there is a corresponding increase in Fe^{2+}, Fe^{3+} and Mn although all of these show a somewhat erratic distribution. Mn reaches its highest concentration in recrystallised phonolites (up to 2.71 wt%). This is possibly due to the consumption of other Mn-bearing phases such as pyroxene to produce the amphibole during thermal metamorphism (see Chapter 4.3).

K maintains a relatively uniform concentration in the amphiboles, rising slightly from ca. 0.35 atoms per formula unit to 0.45 atoms per formula unit in the more Na-rich (arfvedsonitic) amphiboles. Na^A shows a gradual increase as Al^T drops (see Figure 4.4.4) and Ca decreases with decreasing Al^T.

Cawthorne (1976) contends that high Na_2O and high Na_2O/K_2O as well as low Ti (with TiO_2 being proportional to total pressure) are all indicators of low pressure crystallisation of amphibole.

Zirconium becomes increasingly abundant in amphiboles with higher (Na^B-Al^T),

Figure 4.4.4

Amphibole variation in terms of Ca against K, Ca and N^T. Comparative trends from the Si-oversaturated Kûngnât Complex (marked K) and the Si-undersaturated South Qôroq Complex (marked SQ) are also shown (from Stephenson and Upton 1982). Stephenson and Upton (1982) describe the effect of Si saturation on the various trends observed from these different complexes.

K remains relatively constant as Ca increases and Na decreases rapidly with increasing Ca. Al^T also shows a relatively steady decrease with decreasing Ca. The above variation would be expected if the major change is

$$Ca^B + Al^T \rightleftharpoons Na^B + Si^T$$

as has been assumed (see Chapter 4.4.C).

Figure 4.4.4

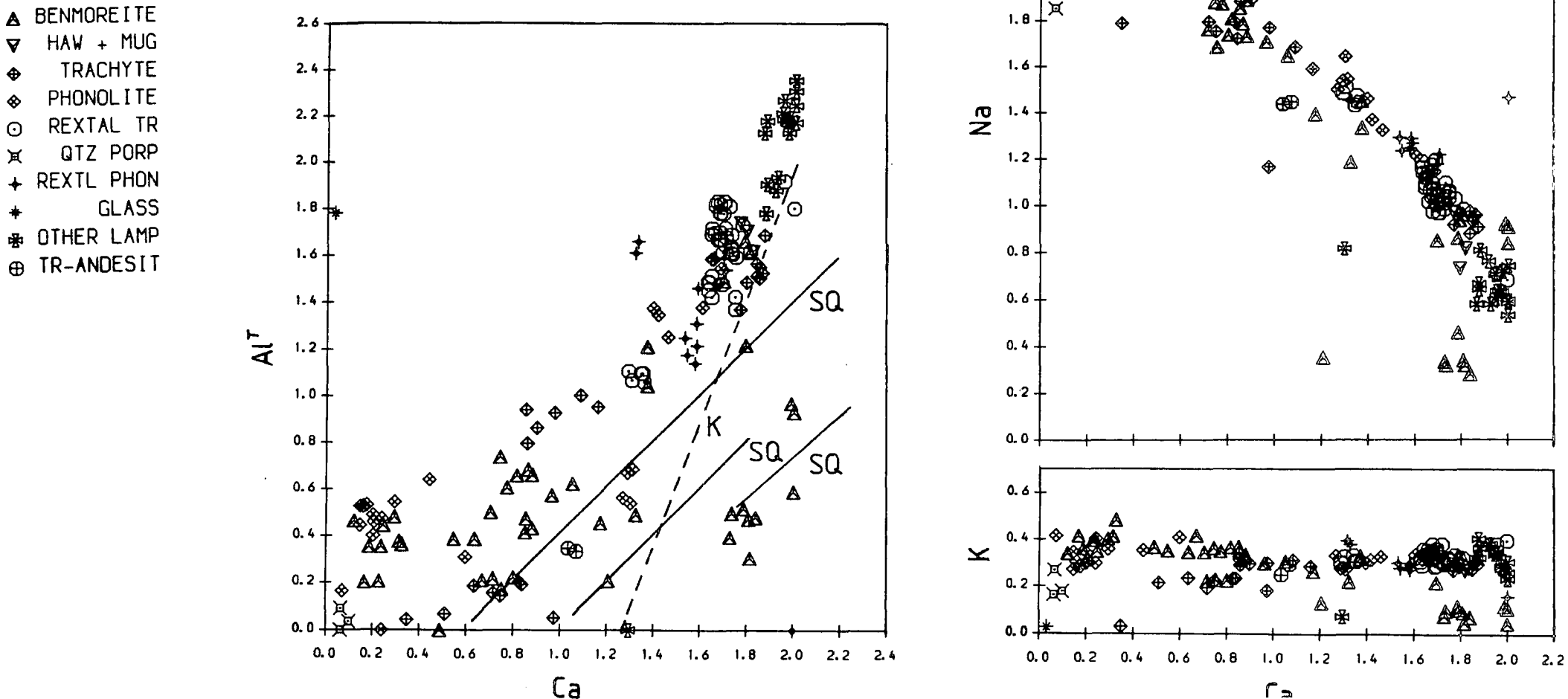
BENMOREITE
HAW + MUG
TRACHYTE
PHONOLITE
REXTAL TR
QTZ PORP
REXTL PHON
GLASS
OTHER LAMP
TR-ANDESIT
Al^T
Ca
SQ
K
SQ
SQ
Na
K
Ca

reaching up to 4.13 wt% ZrO_2 in an arfvedsonite from 325986, (a benmoreite). Both Larsen (1976) and Jones (1980) report up to 0.75 wt% ZrO_2 from Ilímaussaq and Motzfeldt amphiboles respectively. These would appear to be the only two recent citations of Zr in amphiboles, Dana (1892) lists an analysis (p.400) of 0.75 % ZrO_2 from a riebeckite.

Leake (1978) however, makes no mention of Zr bearing amphiboles and the only Ti end member mentioned is kaersutite. On the classification of Leake (1978) these Zr-rich amphiboles would correctly be termed zirconian-katophorites or zirconian-arfvedsonites. Zr can only substitute into the C site, a site commonly occupied by Ti, Al, Fe^{3+},Mg and Fe^{2+}.

Unlike Ilímaussaq (Larsen 1976), there is a marked 1:1 negative correlation between Ti and Zr (see Figure 4.4.5) in the Igaliko dykes and may imply an exchange reaction similar to $2Fe^{3+} \longrightarrow Fe^{2+} + Ti^{4+}$ as suggested by Larsen (1976) to account for high Ti in the Ilímaussaq amphiboles. Substitution of $2Fe^{3+} \longrightarrow Fe^{2+} + Zr^{4+}$ in the C site could produce Zr-rich equivalents to both katophorite and arfvedsonite. The limits of Zr substitution into these would give compositions of $Na_2CaFe^{2+}_{4.5}Zr_{0.5}AlSi_7O_{22}(OH)_2$ - the Zr-rich katophorite, and $Na_3Fe^{2+}_{4.5}Zr_{0.5}Si_8O_{22}(OH)_2$ - the Zr-rich arfvedsonite. However, in many of the Zr enriched amphiboles Zr≈Al. With this in mind a more probable exchange would involve the coupled substitution,

$$Zr^{4+}_C + Al^{3+}_T \rightleftharpoons Fe^{3+}_C + Si^{4+}_T$$

into arfvedsonite. The limit of this substitution would give a zirconian-arfvedsonite of composition $Na_3(Fe^{2+},Mg)_4ZrSi_7AlO_{22}(OH)_2$, and this is proposed as a new amphibole end member.

On the basis of the negative correlation between Ti and Zr (Figure 4.4.5) there may be a fairly straight forward Zr ⇌ Ti exchange in the C site, giving a Zr-Ti arfvedsonite of composition $Na_3(Fe^{2+},Mg)_4(Zr,Ti)Si_7AlO_{22}(OH)_2$. If Zr>Al, the Fe^{3+} must be substituted into the T site such that $Fe^{3+}_C + Si^{4+}_T \rightleftharpoons Zr^{4+}_C + Fe^{3+}_T$. In some analyses Si+Al<8 and Fe^{3+} in T would seem likely in these cases.

In the alkali enriched amphiboles from these rocks, the zirconian-arfvedsonite end

Figure 4.4.5

A. Ti vs. Zr in amphiboles. Note the marked 1:1 negative correlation suggesting an exchange of Ti $\rightleftharpoons$ Zr.

B. Magnesium number ($Mg/(Fe^{2+} + Mg)$) vs. Zr in amphiboles. Zr is only enriched in the more Fe-rich (Mg-poor) amphiboles, and also only apparently in rocks of benmoreitic composition.

Figure 4.4.5

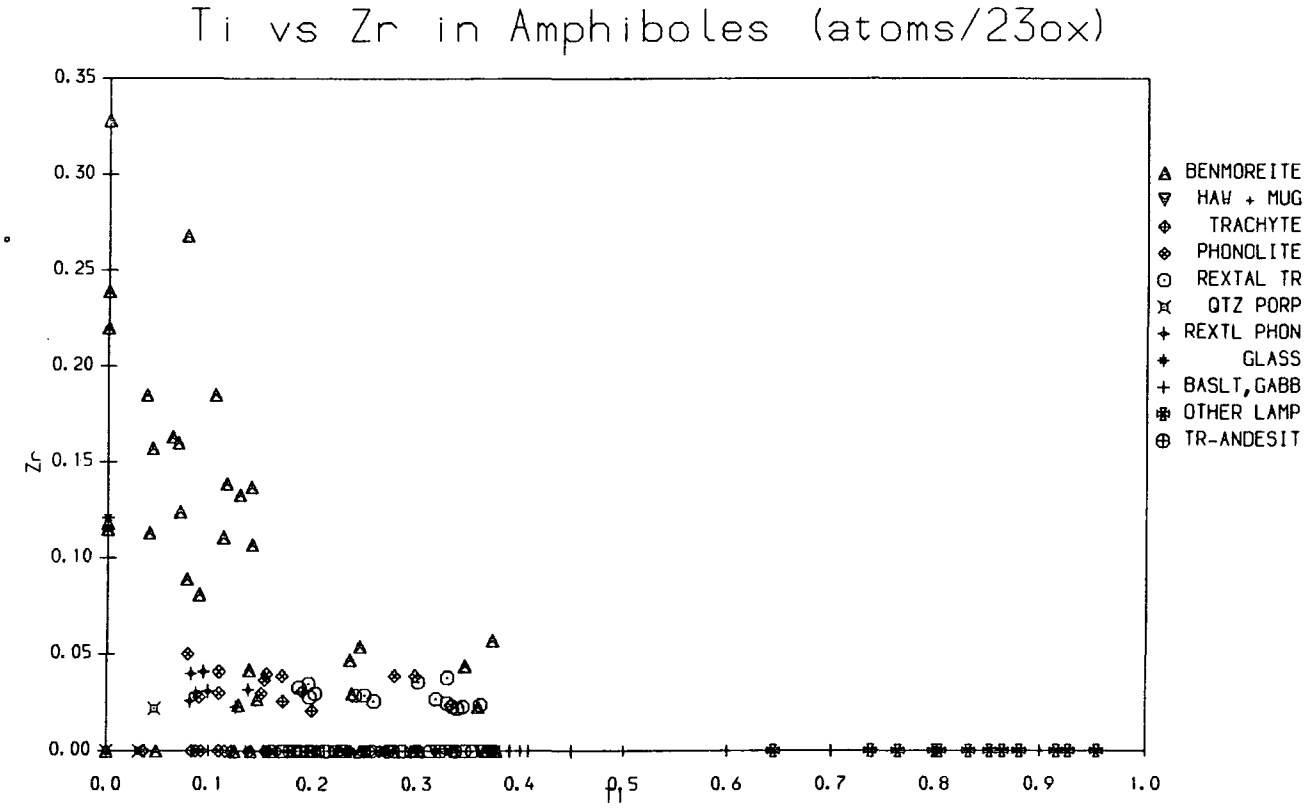
Ti vs Zr in Amphiboles (atoms/23ox)
Zr
Ti
0.35
0.30
0.25
0.20
0.15
0.10
0.05
0.00
0.0
0.1
0.2
0.3
0.4
0.5
0.6
0.7
0.8
0.9
1.0
BENMOREITE
HAW + MUG
TRACHYTE
PHONOLITE
REXTAL TR
QTZ PORP
REXTL PHON
GLASS
BASLT,GABB
OTHER LAMP
TR-ANDESIT

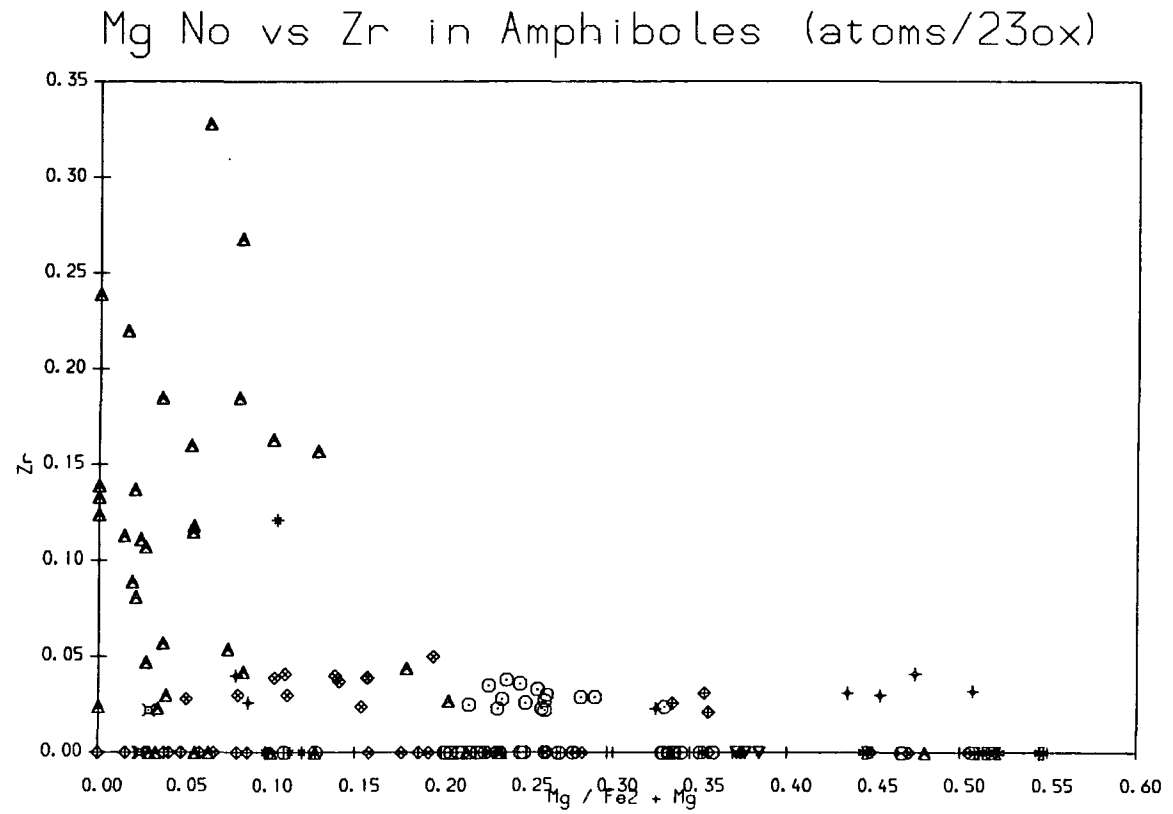
Mg No vs Zr in Amphiboles (atoms/23ox)
Zr
Mg / Fe2 + Mg
0.35
0.30
0.25
0.20
0.15
0.10
0.05
0.00
0.00
0.05
0.10
0.15
0.20
0.25
0.30
0.35
0.40
0.45
0.50
0.55
0.60

member is present in quantities up to 33.0 mol% (325986.45, 4.130 wt% ZrO_2) and the Zr-Ti arfvedsonite end member up to 34.8 mol% (325986.46, 3.390 wt% ZrO_2 and 0.629 wt% TiO_2). Zr-amphiboles are almost exclusively late crystallising groundmass crystals or overgrowths on pyroxenes. Similar micro-chemical environments to those which prevailed during formation of Zr-rich pyroxenes, will have caused the Zr enrichment in the amphiboles. These micro-environments will have needed higher water contents to allow amphibole formation either by direct crystallisation or by reaction of alkali pyroxene (which is unstable at high water content, Yagi 1953), and will have been the cause of late stage Zr amphibole crystallisation. As with the pyroxenes, formation of Zr-rich amphibole will require no other Zr-bearing phase to crystallise and act as a sink for Zr. Late stage Fe-Ti oxide crystallisation would absorb the majority of residual Ti. This would remove competition for the amphibole C site, thus leaving Zr free to partition into the late crystallising mineral. Prior to Fe-Ti oxide crystallisation both Ti and Zr would enter the late stage amphibole in quantities governed by their distribution coefficients, leading to the Zr-Ti arfvedsonite end member compositions (see above). As Fe-Ti oxide crystallisation commences, Ti is removed and Zr builds up in amphiboles at the expense of Ti.

The coexisting pyroxenes and amphiboles show erratic relationships between their Zr contents, sometimes they have similar concentrations, while in other instances one phase may be virtually Zr free. Larsen (1976) observed approximately twice as much Zr in pyroxene as in coexisting amphiboles (at similar Na/Ca ratios) from Ilímaussaq. A similar relationship was not observed from the amphiboles from the Igaliko dykes.

Figure 4.4.6A shows all analyses plotted on Mg-Ca-Na (analogous to Mg–(Fe^{2+}-+Mn)–Na for pyroxenes). There is a continuous trend of amphibole evolution from relatively Mg-rich compositions through to alkali-rich varieties. Stephenson (1973) noted a 'discontinuous reaction series' relationship between the pyroxenes and amphiboles where aegirine-hedenbergite reacts to form arfvedsonite with increased fractionation of the residual liquid. This type of relationship was not observed in this investigation. In the dykes, amphiboles from individual groups of rocks show a wide variety of compositions. There are no obvious different trends of amphibole evolution (cf. pyroxenes) from different rock types, except perhaps that the phonolite amphiboles become en-

Figure 4.4.6

A. Amphibole variation in terms of Mg-Ca-Na as atoms recalculated to T+C=13. There is a continuous trend of amphibole evolution, unlike that noted by Stephenson (1973), where amphibole chemistry covered a 'gap' in the pyroxene evolutionary trends.

B. Amphibole compositions in terms of Mg, total Fe+Mn, Na+K as atoms recalculated to 23 oxygens. A minor oversaturated trend moves off towards Fe+Mn, whereas the majority of analyses follow an undersaturated trend similar to that observed in South Qôroq or Ilímaussaq.

Figure 4.4.6

IGALIKO DYKE SWARM

Amphibole analyses

T+C cations=13.000

A

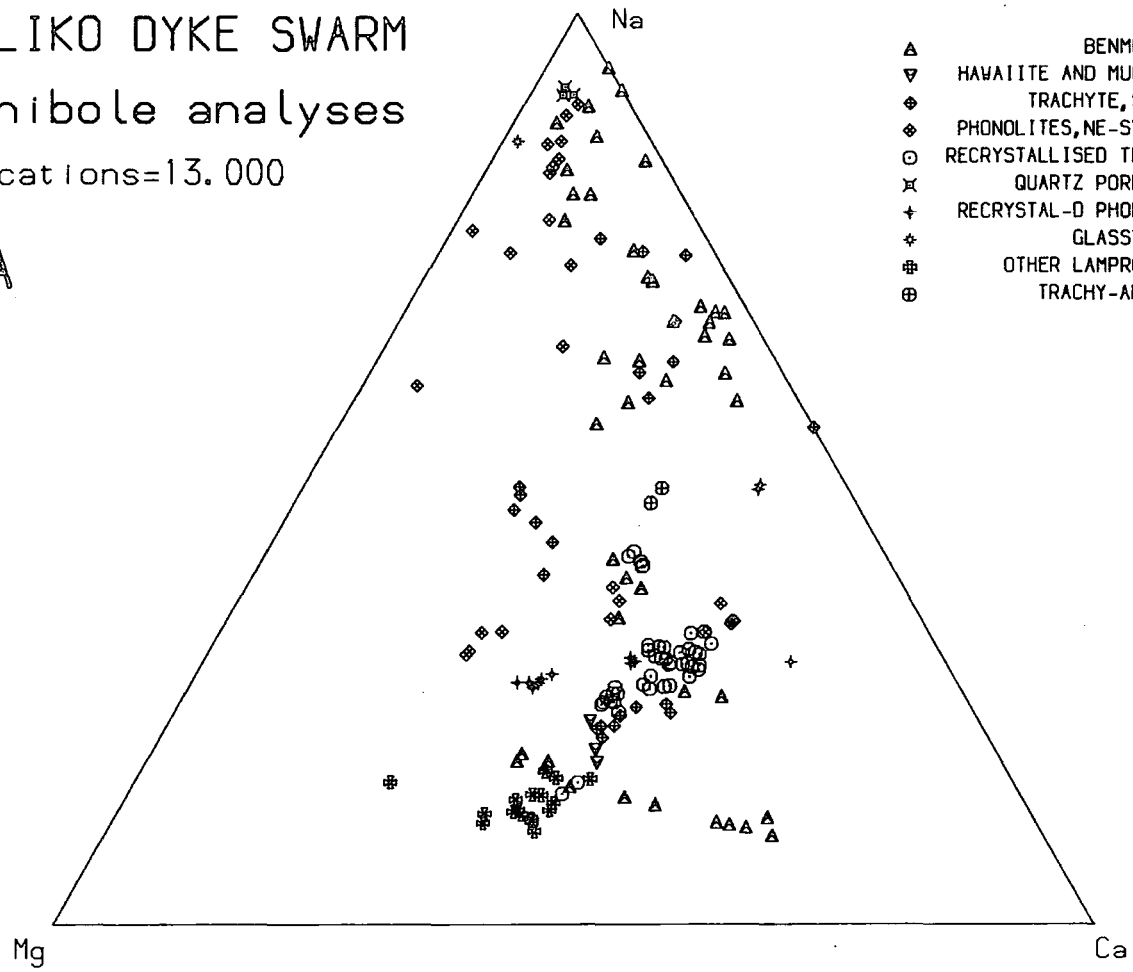

BENMOREITES
HAWAIITE AND MUGEARITE
TRACHYTE, SYENITE
PHONOLITES, NE-SYENITES
RECRYSTALLISED TRACHYTE
QUARTZ PORPHYRIES
RECRYSTAL-D PHONOLITES
GLASSY DYKES
OTHER LAMPROPHYRES
TRACHY-ANDESITE

IGALIKO DYKE SWARM

Amphibole analyses

Fe as Total Fe

Cations per 23 oxygens

B

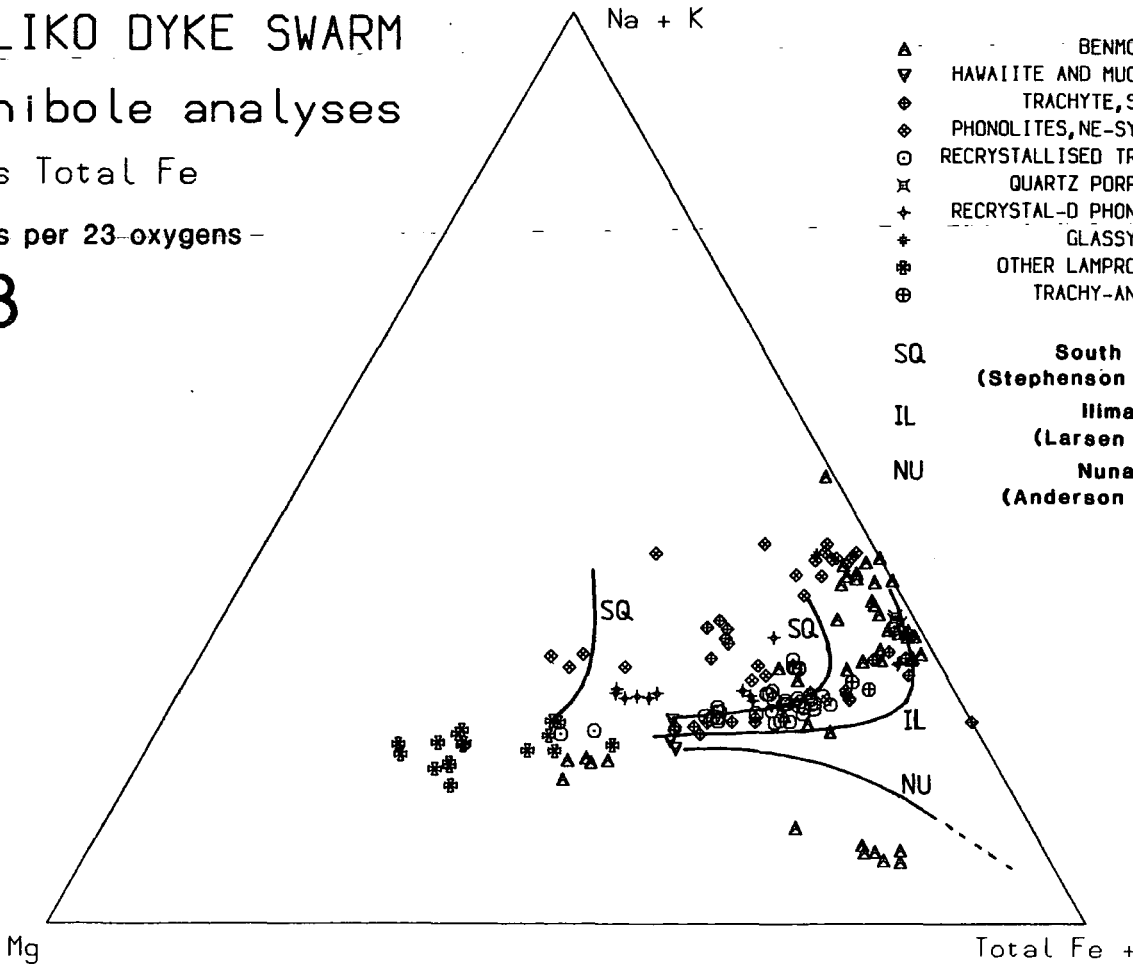

BENMOREITES
HAWAIITE AND MUGEARITE
TRACHYTE, SYENITE
PHONOLITES, NE-SYENITES
RECRYSTALLISED TRACHYTE
QUARTZ PORPHYRIES
RECRYSTAL-D PHONOLITES
GLASSY DYKES
OTHER LAMPROPHYRES
TRACHY-ANDESITE

SQ South Qoroq (Stephenson 1972)

IL Ilimaussaq (Larsen 1976)

NU Nunarssuit (Anderson 1974)

riched in Na at lower Ca contents than the benmoreite amphiboles. This probably reflects differences in bulk rock Ca and Na contents, and, as with the pyroxenes, the time at which the liquids becomes peralkaline. This will be later in the less alkaline benmoreites than the phonolites, allowing more Fe+Mn enrichment to occur before Na enrichment becomes important (cf. pyroxenes).

Larsen (1976) noted an Al deficiency in the katophorites from Ilímaussaq but not in the arfvedsonites or hastingsites. A similar trend is faintly evident from the Igaliko dykes although the scatter of data may hide this (see Figure 4.4.2A). This deficiency is caused by the relatively low activity of both Al and Si in undersaturated, peralkaline magmas, and only at later stages of crystallisation was more Al allowed into the crystal structure, possibly an effect of lower temperatures (Larsen 1976).

Figure 4.4.6B shows comparative trends of amphibole compositional evolution for other alkaline rock suites, with all data from the Igaliko Dyke amphiboles plotted in terms of Mg–Total Fe+Mn–Na+K. A slight trend of earlier alkali enrichment in the phonolites is evident compared to the benmoreites (see above).

Stephenson and Upton (1982) described different trends of amphibole compositional evolution from the Si-undersaturated South Qôroq Centre and the Si-oversaturated Kûngnât Complex. The South Qôroq amphiboles evolve from hastingsite through katophorite to arfvedsonite, whilst Kûngnât evolves from hastingsite through ferro-edenite to ferro-actinolite. The majority of the Igaliko Dyke Swarm amphiboles mirror the undersaturated South Qôroq trend, although a minor trend tends towards Fe+Mn enrichment (Figure 4.4.5A and B) is shown by ferro-actinolites from benmoreite 63896. This overall evolutionary trend is comparable to that seen in the pyroxenes where alkali enrichment trends are dependent on the degree of silica saturation, the stage at which peralkalinity is achieved and fo_2, with higher fo_2 promoting earlier alkali enrichment.

4.4.D: Recrystallisation

58291-298 are samples from an undersaturated benmoreitic dyke which is cut by the Late Igdlerfigssalik syenites (see Chapter 3.5). Figure 4.4.7 shows the change in whole rock and amphibole compositions in terms of Mg, Ca, Na and K along the length of the dyke.

Figure 4.4.7 Variation in Ca, Mg, Na and K in the whole rock (as wt%) and amphiboles (as atoms per formula unit) in samples 58291-298. These samples were collected between 700 and 150m from the contact of the Late Igdlerfigssalik syenites, which truncate the dyke. Amphibole composition is seen to change rapidly at about 625m from the contact. This is some 100-150m farther from the contact than any major sign of textural change. See text for discussion.

Figure 4.4.7

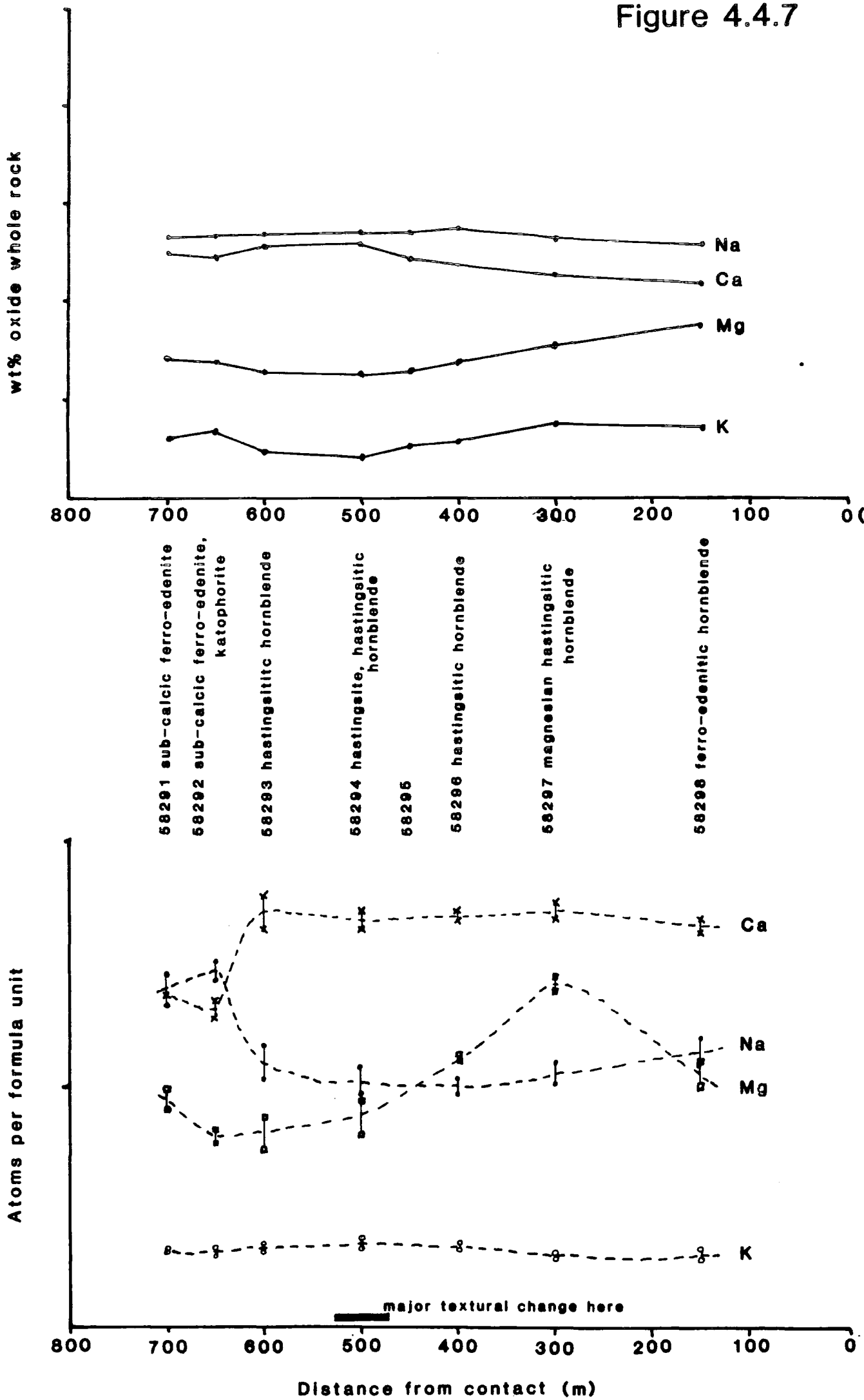
wt% oxide whole rock
Na
Ca
Mg
K
800
700
600
500
400
300
200
100
0
58291 sub-calcic ferro-edenite
58292 sub-calcic ferro-edenite, katophorite
58293 hastingsitic hornblende
58294 hastingsite, hastingsitic hornblende
58295
58296 hastingsitic hornblende
58297 magnesian hastingsitic hornblende
58298 ferro-edenitic hornblende
Atoms per formula unit
Ca
Na
Mg
K
major textural change here
800
700
600
500
400
300
200
100
0
Distance from contact (m)

There is a marked compositional change in the amphiboles at about 625m from the syenite contact. At this distance the amphibole changes from a sub-calcic ferro-edenite to a hastingsitic hornblende. From 625m to 150m Ca remains fairly constant and Na increases slightly towards the contact. Between these distances the only major change is an increase in Mg to a peak at about 300m. Between 300m and 150m Mg decreases despite a continued increase in whole rock MgO. The increase in Mg seems to start at the same distance at which the major textural change is observed (at about 500m). This textural change does not affect the Ca, Na and K contents of the amphiboles which became reset at a greater distance from the contact (ie. at a lower temperature). It is apparent that the bulk rock chemistry starts to change slightly at the same time as major textural change occurs. This change will be a metasomatic effect with ground water leaching out some elements from the dyke (possibly Ca) and introducing others (eg. Mg). The country rocks in the vicinity if the dyke are Julianehåb Granite and basal members of the Eriksfjord Formation which include basalts and sandstones. Ground water circulation through these rocks may pick up elements such as Mg and could thus introduce these into the dyke. The presence of hot fluids circulating throughout the dyke would make diffusion easier and assist in the textural change from a normal igneous texture to a granoblastic (poikiloblastic) texture.

The increase in Mg in the amphiboles between 500m and 300m will be a reflection of increasing bulk rock MgO. However, in 58298 (at 150m) small aegirine-augites have become stable having all but disappeared from 58297 (300m) and the presence of these may account for the decline in Mg in the amphiboles despite a continued increase in bulk rock MgO. Thus whole rock chemistry is not solely responsible for the chemical variation seen within the amphiboles. Recrystallisation of feldspar at about 650m (see Chapter 4.8.E) would liberate Ca and absorb Na. This would be likely to control the compositional change in the amphiboles at these distances. The presence of other ferro-magnesian minerals (aegirine-augite) would affect the Mg content of the amphiboles.

4.5: Biotite

4.5.A: Introduction

Biotite is an important accessory phase and is present in most groups of rocks

in quantities of a few percent. In the syeno-gabbros it may reach up to about 15% modally. Biotites are all pleochroic and range in colour from common dark brown - straw brown varieties to bright red-brown - orange-brown types typical of some syeno-gabbros and rarely very dark (almost black) green - pale (olive) green examples. Deer *et al.* (1966) consider Ti to be responsible for the red colouration and high Fe^{3+} contents may produce a deep green colour, the relative amounts determining the overall shade. This is borne out by the high-Ti biotites from the syeno-gabbros being deep red-brown (see Figure 4.5.1).

Biotite is found either as rims to opaque oxides or as discrete crystals in unrecrystallised rocks; or as aggregates (often with amphibole) in hornfelsed samples. Unlike other ferro-magnesian minerals it is not possible to estimate accurately Fe^{2+}/Fe^{3+} ratios for biotites, thus all Fe is reported as Fe^{2+}. No analyses for (OH) or F were undertaken. Cl was detected in only 2 samples. Analyses are recalculated on a 22 oxygen, anhydrous basis.

4.5.B: Chemical Variation

The general formula of the micas is $X_2Y_{4-6}Z_8O_{22}(OH,F)_4$. K, Na and Ba will occupy the 12 coordinated X site; Fe^{2+}, Mg, Fe^{3+}, Ti and Al, the octahedral Y site and Si and Al, possibly with some Fe^{3+} , the tetrahedral Z site.

Si and Al generally total between 7.7 and 8 atoms per 22 oxygens leaving little or no excess Al available for the octahedral site. The deficit in the tetrahedral site is presumably due to Fe^{3+}, with Ti prefering octahedral coordination.

Increasing fractionation of the biotites is generally marked by an increase in the Fe/Mg ratio and a decrease in Al^{iv}. Figure 4.5.1 shows all analyses plotted as Al^{iv} against Fe/Fe+Mg, this diagram covering the 4 mica end members, annite, siderophyllite, phlogopite and eastonite.

Most micas from these rocks are biotites with the exception of those from the lamprophyres (ie. the nephelinites and tephrites) which are phlogopitic. These also tend to be deficient in Al^{iv} and thus appear, somewhat falsely, to be more fractionated. Increased fractionation produces micas compositionally close to annite-siderophyllite (ie.

Figure 4.5.1: Biotite variation from the Igaliko dykes.

A. Mn is seen to increase with Fe/Fe+Mg following a similar trend to that observed by Jones (1980) from Motzfeldt.

B. Classification of biotites in terms of Al^{iv} against Fe/Fe+Mg. The 4 end members, annite, siderophyllite, phlogopite and eastonite are marked. Increasing fractionation causes a decrease in Al^{iv} with increased Fe/Fe+Mg. Phonolite biotites contain less Mg than those from benmoreites, a reflection of higher fo_2 (Wones and Eugster 1965).

C. As Al drops with increasing Fe/Fe+Mg so too does Al/Al+Si. Phonolite micas may appear to be less aluminous than those from benmoreites, possibly reflecting higher peralkalininty in the phonolites. Trends from Klokken (Parsons 1979) and Motzfeldt (Jones 1980) are marked for comparison.

D. Mg - total Fe - Al.

E. Mg - total Fe - Ti. The 'other lamprophyres' contain low Ti micas, in contrast to their content of kaersutite, probably a reflection of the relevant partition coefficients. Ti shows a slight decrease in micas with increased fractionation.

Figure 4.5.1

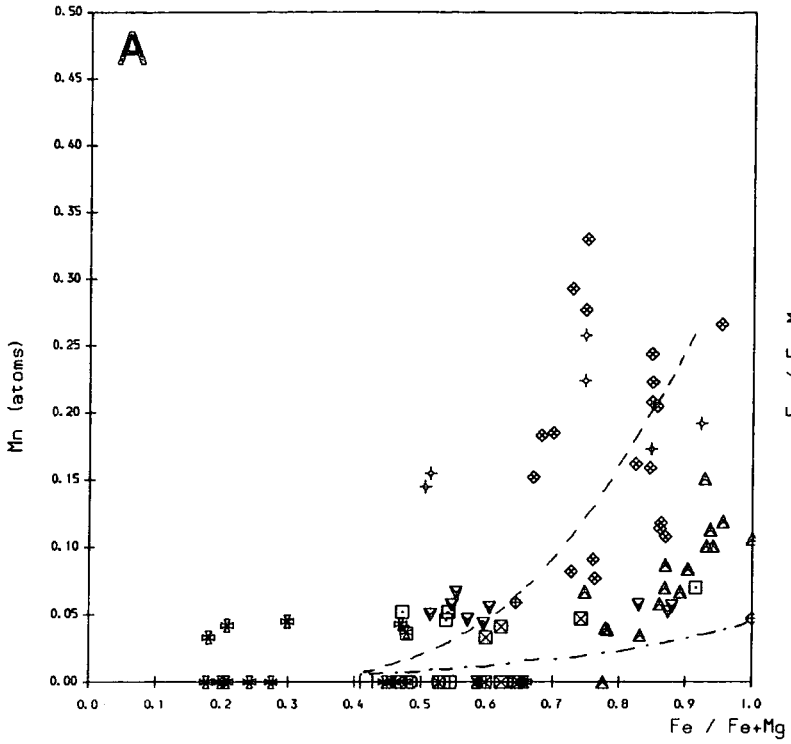

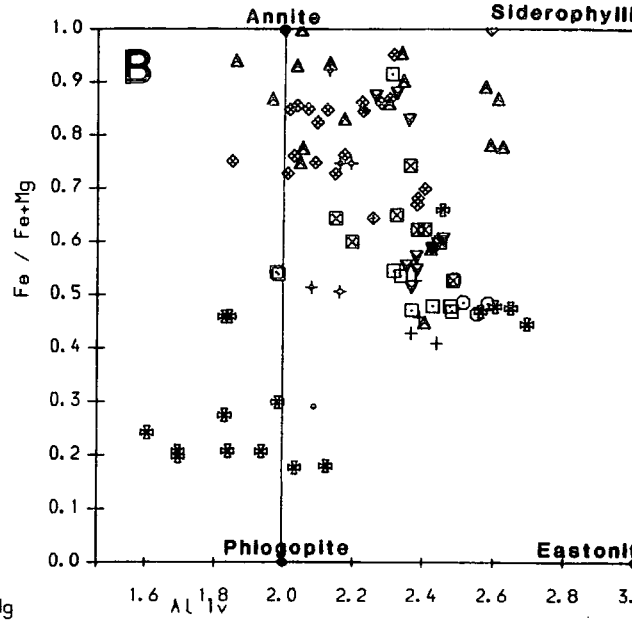

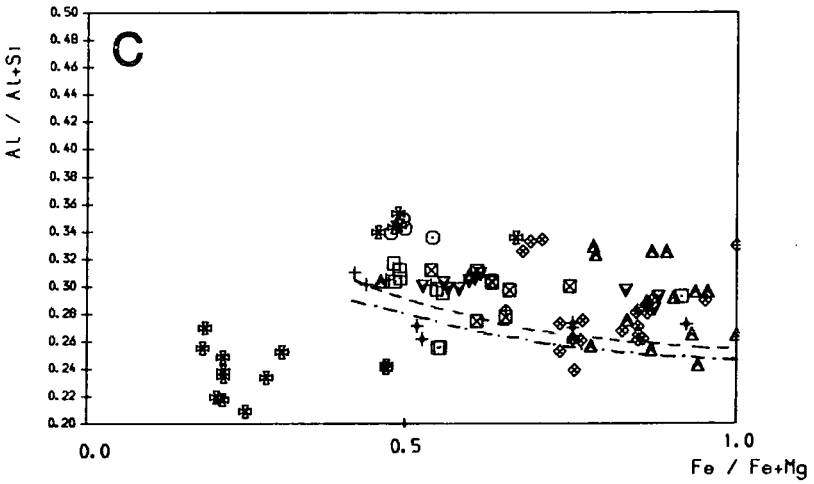

IGALIKO DYKE SWARM

Biotite analyses

Atoms per 22 oxygens
Fe as total Fe

- BENMOREITES
- HAWAIITE AND MUGEARITE
- TRACHYTE, SYENITE
- PHONOLITES, NE-SYENITES
- SYENO-GABBRO
- BIG FELDSPAR DYKES
- RECRYSTALLISED TRACHYTE
- RECRYSTAL-D PHONOLITES
- BASALT AND GABBRO
- OTHER LAMPROPHYRES
- Jones (1980)
- Parsons (1979)

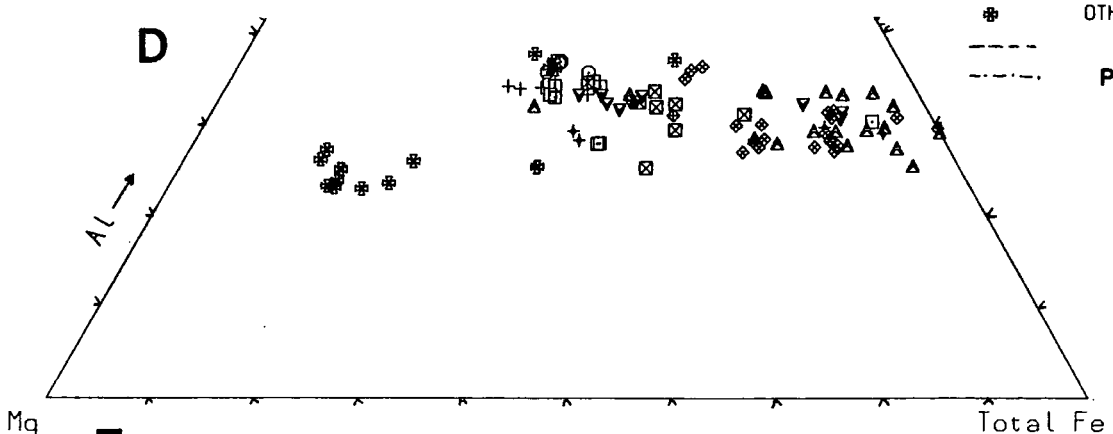

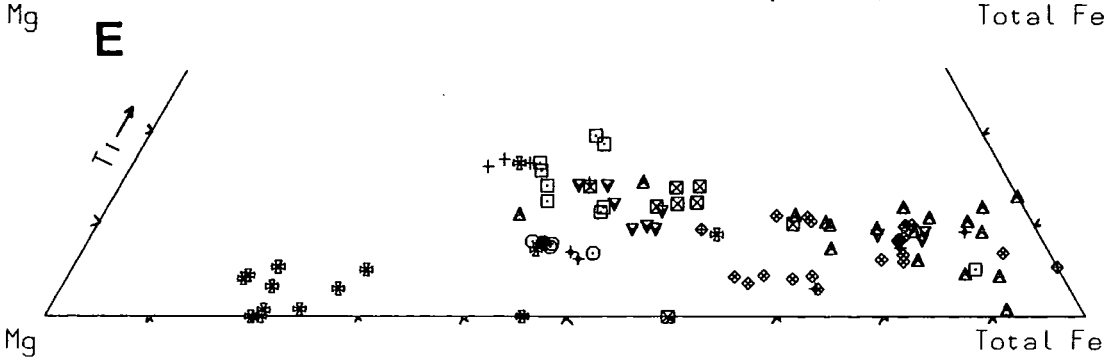

Fe enriched).

Broadly speaking the mica compositions reflect the bulk rock Fe/Mg ratio, giving a range from phlogopites in the lamprophyres (high Mg), through intermediate Fe/Fe+Mg ratios in the basalts, BFDs, hawaiites and mugearites to Fe enriched biotites from the benmoreites. The phonolites however, tend to contain more magnesian micas than the benmoreites (see Figure 4.5.1A), this being consistent with a higher fo_2 in these rocks (Wones and Eugster 1965) and this is also shown by the pyroxenes and amphiboles.

As Al decreases with fractionation, so too does Al/Al+Si and Figure 4.5.1B. compares the data from the Igaliko Dyke Swarm with those of Parsons (1979) from the Si-oversaturated Klokken complex and Jones (1980) from Motzfeldt.

Mn shows an overall increase with host rock fractionation and follows a similar path to the Motzfeldt micas. There is a very obvious difference between the Mn contents of biotites from the phonolites (high Mn) and those from the benmoreites (low Mn, see Figure 4.5.1 and 4.5.2A). This is similar to the trends seen in the pyroxenes where higher fo_2 causes a higher Mn content in the crystallising phases. MnO reaches 2.34 wt% and represents 6.05 mole% of the mangophyllite end member compared with up to 45 mole% mangophyllite recorded from Shonkin Sag biotites (Nash and Wilkinson 1970) and 1 mole% mangophyllite from Klokken (Parsons 1979). Micas from Kûngnât contain generally less than 0.43 wt% MnO with 3 analyses from a pegmatite sheet reaching up to 0.82 wt % (Stephenson and Upton 1982).

K and Na tend to show an antithetic relationship in the biotites. Micas from the phonolites contain more K and less Na than those from the trachybasaltic rocks. Na tends to decrease, somewhat loosely, with decreasing Al^{iv} (see Figure 4.5.2B).

TiO_2 tends to show a decrease with increased fractionation (see Figure 4.5.2C) with high Ti in more basic rocks (up to 9.88 wt% TiO_2 from a syeno-gabbro, ca. 8.2 wt% from gabbroic rocks) dropping to around 1-2 wt% in micas from the phonolites. The lamprophyre biotites however, already noted for being low in Al^{iv} are also, in many cases, relatively low in TiO_2 (3 wt% to 0 wt%). This, along with the Al deficiency, will be caused by partitioning of these elements into coexisting pyroxenes which are particularly rich in both Ti and Al in these rocks (see Chapter 4.2).

Figure 4.5.2: Biotite variation from the Igaliko dykes.

A. Al^{iv} vs MnO (wt%). Mn increases markedly with fractionation, the phonolites having the highest MnO contents (higher fo_2).

B. Al^{iv} vs TiO_2 (wt%). The syeno-gabbros can be seen to contain very Ti-rich micas (almost 10 wt%). this gives these micas a distinct red colour in thin section. Ti generally decreases with increased fractionation. Fields of data from North Qôroq (Chambers 1976) and Motzfeldt (Jones 1980) marked as A and B for comparison.

C. Al^{iv} vs Na_2O (wt%). Na seems to show a general decrease with increased fractionation (lower Al^{iv}).

D. Na vs Ba.

E. The maximum of 2K:Ba shown by any of the micas implies an exchange of $2K^+ \rightleftharpoons Ba^+ + \sqcup$ (where $\sqcup$ represents a vacancy) into the large 12-coordinated site of the mica.

Figure 4.5.2

IGALIKO DYKE SWARM

Biotite analyses

Atoms per 22 oxygens
Fe as total Fe

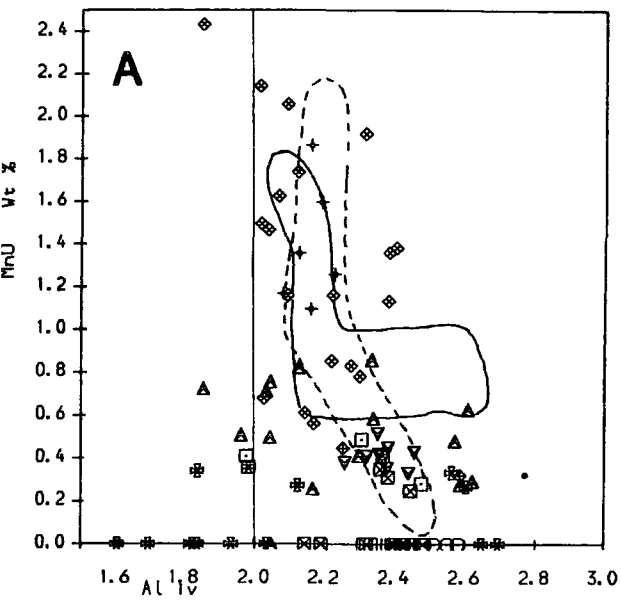

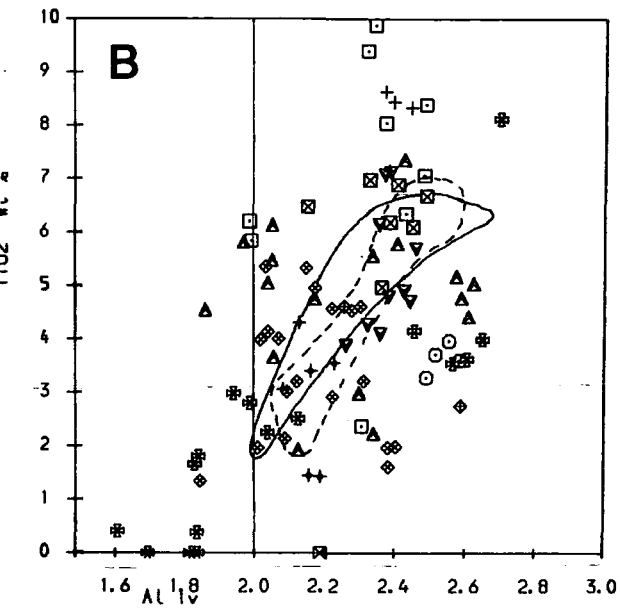

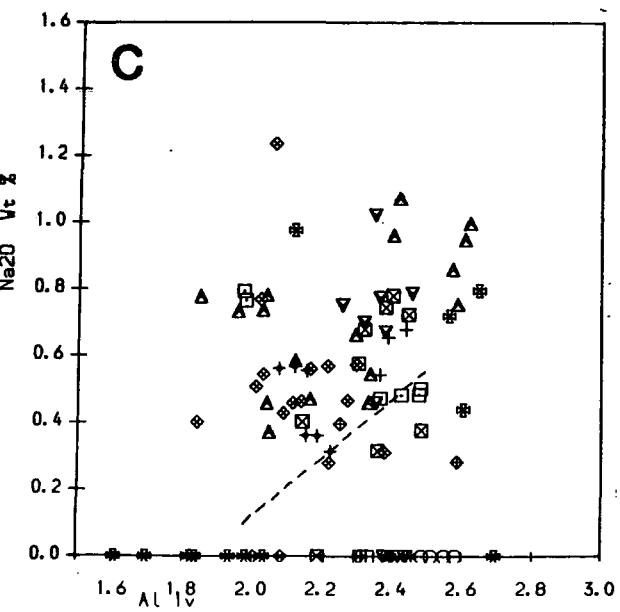

BENMOREITES
HAWAIITE AND MUGEARITE
TRACHYTE, SYENITE
PHONOLITES, NE-SYENITES
SYENO-GABBRO
BIG FELDSPAR DYKES
RECRYSTALLISED TRACHYTE
RECRYSTAL-D PHONOLITES
BASALT AND GABBRO
OTHER LAMPROPHYRES
Chambers (1976)
Jones (1980)

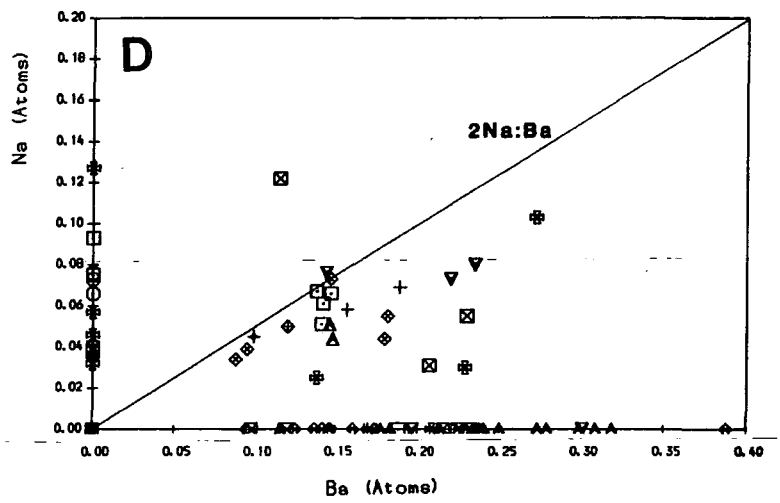

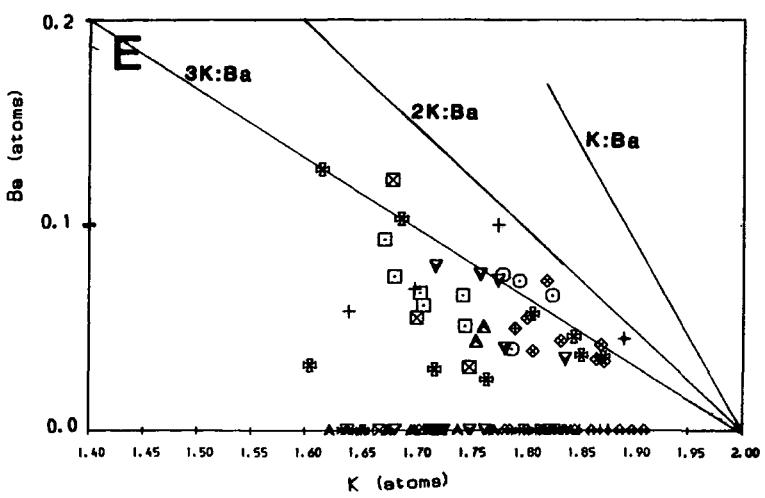

Ba was detected in approximately half the analysed samples reaching 2.156 wt% BaO and its presence appears to be related to the substitution of Ba^{2+} for K^{+} (see Figure 4.5.2D). The overall trend of Ba and K variation shown in Figures 4.5.2D and 4.5.2E would suggest an exchange reaction of $2(K^{+},Na^{+}) \rightleftharpoons Ba^{2+} + \sqcup$ (where $\sqcup$ represents a vacancy in the large, 12 coordinated X site). However, Gaspar and Wyllie (1982) considered a coupled substitution of $(K^{+},Si^{4+}) \rightleftharpoons (Ba^{2+},Al^{3+})$ - Al substituting for Si in the tetrahedral site - in Ba-rich phlogopites from the Jacupiranga Carbonatite. Less Ba occurs in biotites from the more fractionated rocks as a result of the lower bulk rock Ba caused by feldspar fractionation.

4.6: Fe-Ti oxides

Iron-titanium oxides are relatively common constituents of rocks from the Igaliko Dyke Swarm. 45 analyses of both Ti-magnetite and ilmenite were made. These minerals were not however studied in the same detail as the silicate phases due to analytical problems caused by exsolution textures which produced large differences in Fe and Ti contents. Those grains that were analysed were checked at at several points for 'homogeneity' by observing the spectrum produced, a rather arbitrary method, but nonetheless one which distinguished exsolved from unexsolved grains. No attempt was made to obtain 'bulk analyses' of exsolved grains. If the exsolution was coarse enough to be noticed under the poor reflected light optics of the microprobe, analyses of separate phases were made. Coarsely exsolved ilmenite lamellae in magnetite from 141244 were analysed, this being one of only three samples in which ilmenite and magnetite were found to coexist. Most samples contain only magnetite, and a few only ilmenite.

Ilmenite has been recorded from basalts, lamprophyres, syeno-gabbros, a trachy-andesite and a phonolite. Magnetites are recorded from nearly all groups. Figure 4.6.1 shows all data plotted as end member molecules of FeO(+MnO, MgO and CaO), Fe_2O_3(+Al_2O_3) and TiO_2(+SiO_2). Tie lines join analyses of ilmenite and magnetite from the same sample.

Recently much doubt has been cast upon the validity of different methods of calibrating the Fe-Ti oxide geothermometer - oxygen barometer (Buddington and Lindsley 1964; Powell and Powell 1977; Spencer and Lindsley 1981). Large differences in fo_2

Figure 4.6.1 Iron-titanium oxides plotted in terms of molecular $FeO(+MnO+MgO+CaO) - Fe_2O_3(+Al_2O_3) - TiO_2(+SiO_2)$. Tie lines join analyses of ilmenites and magnetites from the same sample. These 'pairs' are usually outside the range of published Fe-Ti oxide geothermometers - oxygen barometers (see text).

Figure 4.6.1

IGALIKO DYKE SWARM

Oxide analyses

Recast after method of Carmichael (1967).
Molecular end-members

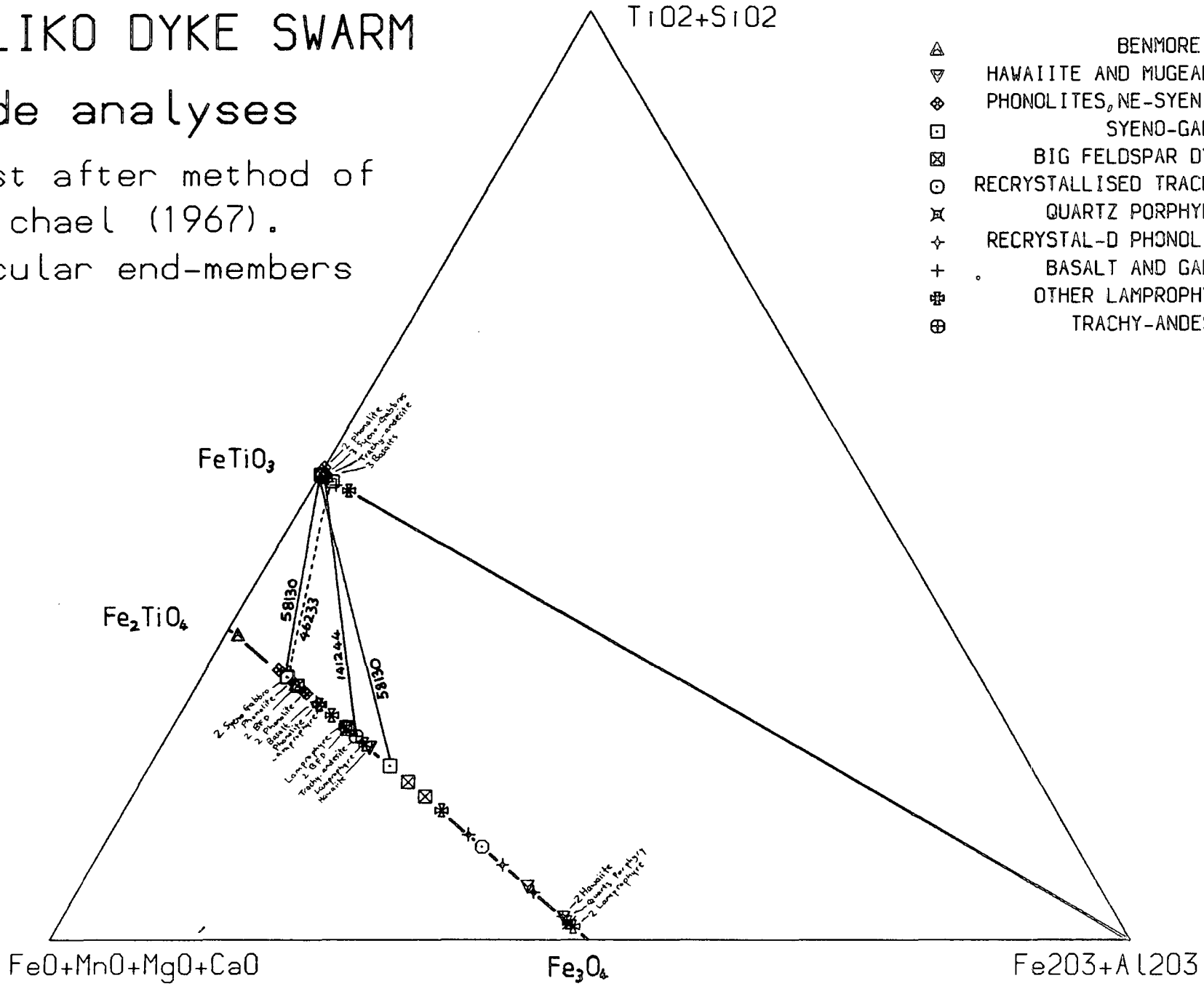

Figure 4.6.2 Variation in Mn with Ti, Fe^{3+} and Fe^{2+} from magnetites and ilmenites. Ilmenites have been recast to 3 oxygens and magnetites to 4 oxygens in the calculation of Fe^{3+}. The dotted line bounds the field of ilmenite analyses. Dashed lines join analyses from the same sample. In magnetites Mn variation is achieved by substitution of Mn for Ti and Fe^{2+} , with Fe^{3+} and Mn showing a sympathetic relationship. This may suggest a complex coupled substitution mechanism of Mn^{2+} and Fe^{3+} for Fe^{2+} and Ti^{4+} (in undetermined ratios). In ilmenites Mn substitution is achieved simply by $Mn^{2+} \rightleftharpoons Fe^{2+}$.

Figure 4.6.2 MAGNETITE AND ILMENITE

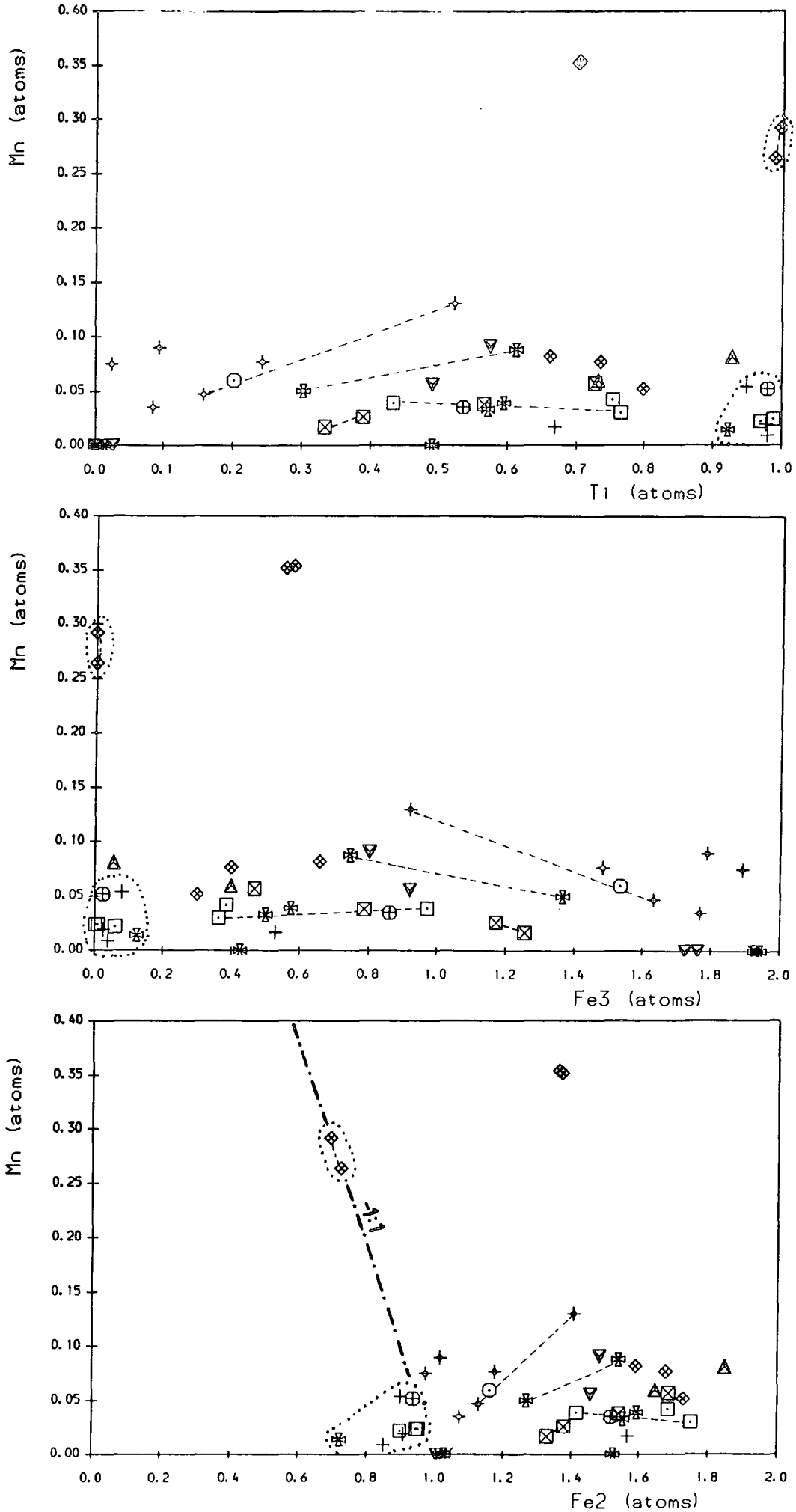

and temperature are commonly recorded from different methods and the assignment of minor oxides (eg. Mn, Al) can also have a large effect on the result (Stormer 1983). End members were calculated by the method of Carmichael (1967) and the only coexisting ilmenite-magnetite pair that was within the range of *any* of the geothermometers - oxygen barometers mentioned above was from a coarsely exsolved ilmenite-magnetite grain and thus is of no use as a liquidus temperature/fo_2 indicator. Those out of range indicate low temperature, low fo_2 equilibration.

Of the minor elements only Mn was detected, although samples were often analysed for V, Cr and Ni. Mn showed enrichment in both ilmenites (up to 13.68 wt% MnO) and magnetites (up to 11.08 wt% MnO) and showed a wide range of concentrations, even within the same sample. Typical contents are of the order of 1-3 wt% MnO. The available data might suggest an increase in the content of Mn with Fe^{2+} and Ti in magnetites and an exchange of $Fe^{2+} \rightleftharpoons Mn^{2+}$ in ilmenites, although this is not particularly obvious (see Figure 4.6.2). There is clear indication of an increase in Mn/Fe^{2+} with increasing whole rock fractionation for either magnetite or ilmenite (cf. Platt and Woolley 1986) although in both cases the highest contents occur in examples from phonolites. Neumann (1974) found that Mn/Fe^{2+} in opaque oxides decreased with whole rock fractionation.

4.7: Nephelines

4.7.A: Introduction

Nepheline is a common phase in the more evolved rock types although it is also recorded in minor amounts from some lamprophyres, BFDs and syeno-gabbros. Its habit changes from small, interstitial patches in the more basic rock types to small, blocky groundmass crystals in both benmoreites and phonolites. It also occurs as relatively large phenocrysts in many porphyritic phonolites.

Alteration of nepheline is fairly common, either to cancrinite, (with the addition of CO_2) or the micaceous mineral, gieseckite, which imparts a pinkish colour in hand specimen.

4.7.B: Compositional Variation

All analysed nephelines have been plotted in the system *Ne-Ks-Qz* on a molecular weight percent basis. This involved recalculation of the nepheline analysis to a molecular formula and assignment of all Na to nepheline (*Ne*), K to kalsilite (*Ks*), Ca to anorthite. Any excess SiO_2 after allocation to these molecules represents *Qz*. Molecular proportions were then converted to weight percent (by multiplication by molecular weights) and *Ne*, *Ks* and *Qz* scaled to 100% for plotting. The results are plotted on Figure 4.7.1 which also shows the Hamilton (1961) geothermometer.

Nepheline has the general formula $(Na,K)AlSiO_4$ and its composition in volcanic rocks is governed by a combination of the bulk rock composition and the temperature of crystallisation. In lower temperature assemblages however, most nephelines tend to fall between the Morozewicz composition ($Na_{6.1}K_{1.52}\square_{0.38}Al_{7.62}Si_{8.32}O_{32}$) and the Buerger ideal composition of $Na_3KAl_4Si_4O_{16}$.

Compositional change in nepheline is dominated by a decrease in Si/Al and sub-solidus exchange of Na for K with falling temperature (Tilley 1954). Thus slow cooling allows exchange of Na and K between coexisting nephelines and feldspar bringing plutonic nephelines into the Morozewicz-Buerger convergence field (Tilley 1954). This convergence is not seen in nephelines from South Qôroq (Stephenson 1972), North Qôroq (Chambers 1976) or Motzfeldt (Jones 1980) and indicates little sub-solidus re-equilibration of nepheline in these centres.

Rapidly cooled rocks do not undergo much sub-solidus re-equilibration with fast cooling to low temperatures essentially 'freezing in' the liquidus composition of nepheline. Thus nephelines from dykes should be a relatively accurate indication of liquidus temperatures of their host magmas. From Figure 4.7.1 it can be seen that the majority of the nephelines equilibrated at temperatures between 700°C and 1068°C (see also Table 4.7.1).

Of these the temperature recorded from recrystallised phonolites would seem to be anomalous (too high for rocks which re-equilibrated at sub-(feldspar) solvus temperatures). In the recrystallised phonolites, mostly from the Østfjordsdal area, nepheline tends to coexist with sodalite and/or cancrinite. Nash *et al.* (1969) suggested that the

Figure 4.7.1: Nepheline analyses for individual groups of rocks, recalculated in terms of end member Nepheline, Kalsilite and excess Quartz (see text for method). Each plot shows the nepheline equilibration isotherms from Hamilton (1961). Also indicated are the theoretical Morozewicz and Buerger compositions. These compositions are often obtained by slowly cooled nephelines (Tilley 1954). See text for interpretation.

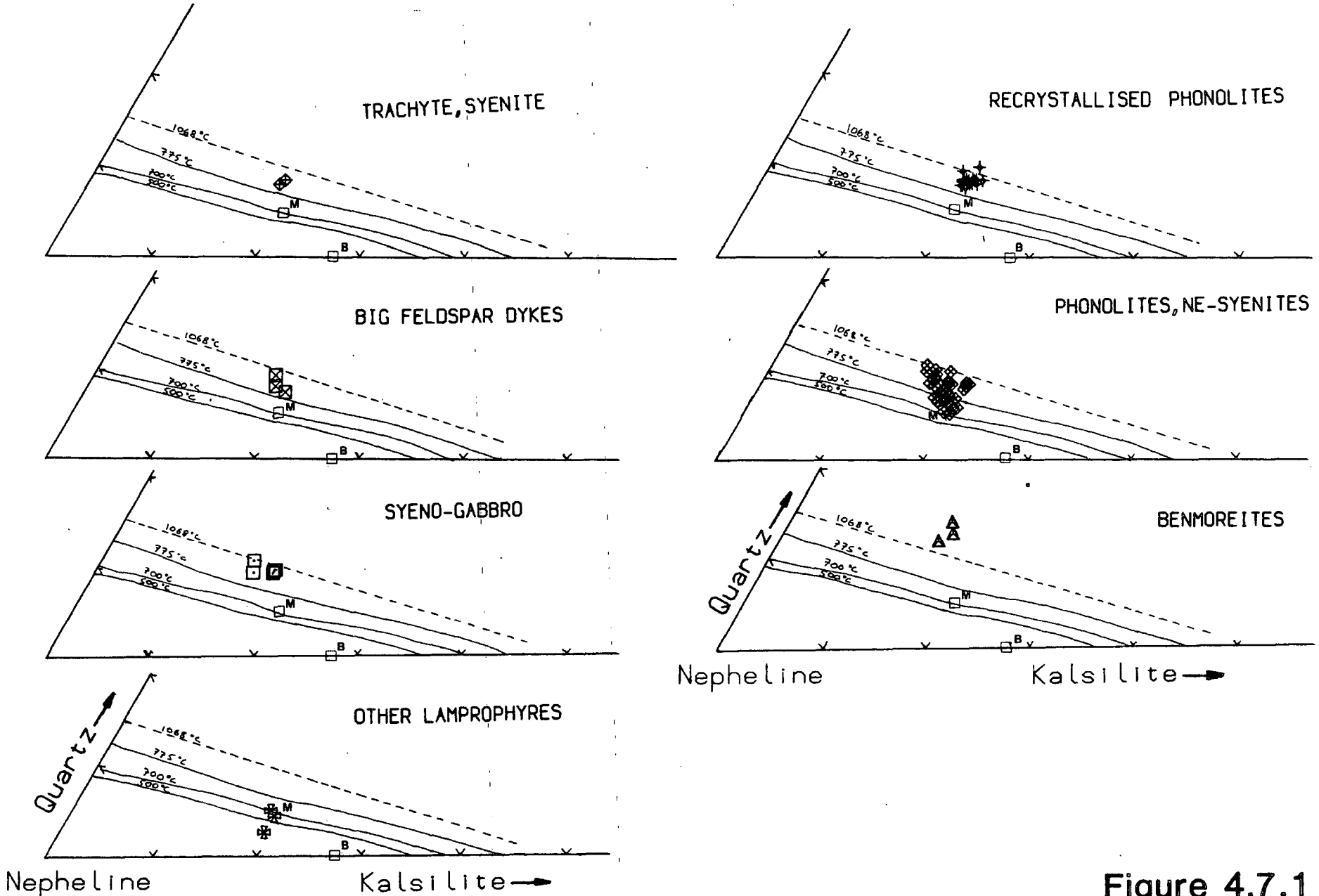
TRACHYTE, SYENITE
RECRYSTALLISED PHONOLITES
BIG FELDSPAR DYKES
PHONOLITES, NE-SYENITES
SYENO-GABBRO
BENMOREITES
OTHER LAMPROPHYRES
Quartz
Nepheline
Kalsilite
1068°C
775°C
700°C
590°C
M
B

Figure 4.7.1

Table 4.7.1

Nepheline equilibration temperatures from Hamilton (1961)

BFDs	1000-800°C
Syeno-gabbros	1050-850°C
Benmoreites	>1068°C(≈1150°C?)
Trachytes/Syenites	900-850°C
Phonolites	1068-700°C (large range near Morozewicz composition)
Recrystallised phonolites	ca. 1000-800°C with some up to ca. 1100°C

presence of sodalite would invalidate the nepheline geothermometer, producing higher excess silica than would be expected and this would seem to be the case for these recrystallised rocks. These rocks will have crystallised at temperatures below 700°C (Smith and Parsons 1974), perhaps as low as 450°C (see Chapter 4.8). The temperatures obtained from the other rocks (excluding perhaps BFDs, see below) are all consistent with a decrease in temperature of crystallisation as the rock becomes more fractionated.

The Hamilton (1961) model, valid for felsic igneous rocks is not applicable as a geothermometer for more basic rocks, which tend to show trends of increasing excess Si (Qz) in nephelines with later crystallisation (Henderson and Gibb 1983). As magma becomes more silica rich and nepheline is joined by alkali feldspar as a crystallising phase the Hamilton (1961) trend of decreasing Qz and increasing Ks with decreasing temperature takes over and the geothermometer can be applied. The nephelines from the lamprophyric rocks are thus inapplicable as geothermometers. The nephelines from the benmoreite record temperatures of approximately 1150°C, which are probably too high for liquidus temperatures of these rocks. The reason for the anomalous temperatures from this sample is unclear, but it may be due to slight alteration to gieseckite, by loss of alkalis causing an increase in the Qz component of the residue.

Nephelines are usually poor in minor and trace elements. CaO was recorded in less than one third of the analyses, reaching a maximum of 1.44 wt% (0.072 atoms/8 oxygens) from the lamprophyre nephelines and 0.993 wt% (0.048 atoms/8 oxygens) in the more evolved rocks, typical contents lying between 0.2 and 0.7 wt%.

Iron, presumably Fe^{3+}, was recorded from most samples, up to 1.35 wt% as Fe_2O_3.

This probably substitutes for Al and tends to be more abundant in the more evolved rock types (cf. Stephenson 1976). MgO was recorded in 10 analyses (up to 0.54 wt%). Of the trace elements, TiO_2 (0.24 wt% and 0.25 wt%) was detected in 2 samples and BaO (0.31 wt%) from one sample.

Zoning

Several nepheline phenocrysts were analysed and zoning tended to be slight and rather variable. Of the minor elements, iron tended to decrease from core to rim and Ca increased.

Na, K, Si and Al and *Qz* showed no systematic changes from core to rim of individual phenocrysts, with separate crystals from the same sample showing different trends. The zoning will be controlled by the presence/absence and composition of other felsic minerals and relative partitioning of metal ions into each of these other phases (eg. feldspar). A trend of decreasing *Qz* in nephelines results from the onset of feldspar crystallisation (Hamilton 1961). Thus, zoned nephelines with increasing *Qz* from core to rim will have crystallised prior to feldspar (ie. in the nepheline crystallisation field) and *vice versa*. Relationships similar to this were recorded by Henderson and Gibb (1983) from alkali basaltic rocks.

4.8: Feldspars

4.8.A: General

Feldspar is the most abundant mineral in the rocks from the Igaliko Dyke Swarm. Feldspars of the plagioclase series occur in the basaltic rocks. In intermediate rocks 'anorthoclase' becomes abundant which gives way to members of the alkali feldspar series in the benmoreitic and phonolitic rock types. Feldspar occurs as both phenocryst and groundmass phases, as well as xenocrysts in the BFD's which will be discussed in a later chapter.

Unlike the alkali feldspars of the slowly cooled Gardar central complexes, relatively little, or no sub-solidus unmixing (on a scale resolvable by a microprobe – see below) has occurred in the dykes, mostly due to rapid cooling from high temperatures. This has distinct advantages when analysing alkali feldspars with an electron microprobe.

Figure 4.8.1: Feldspar nomenclature for 'high temperature' feldspars from Smith (1974).

Figure 4.8.1

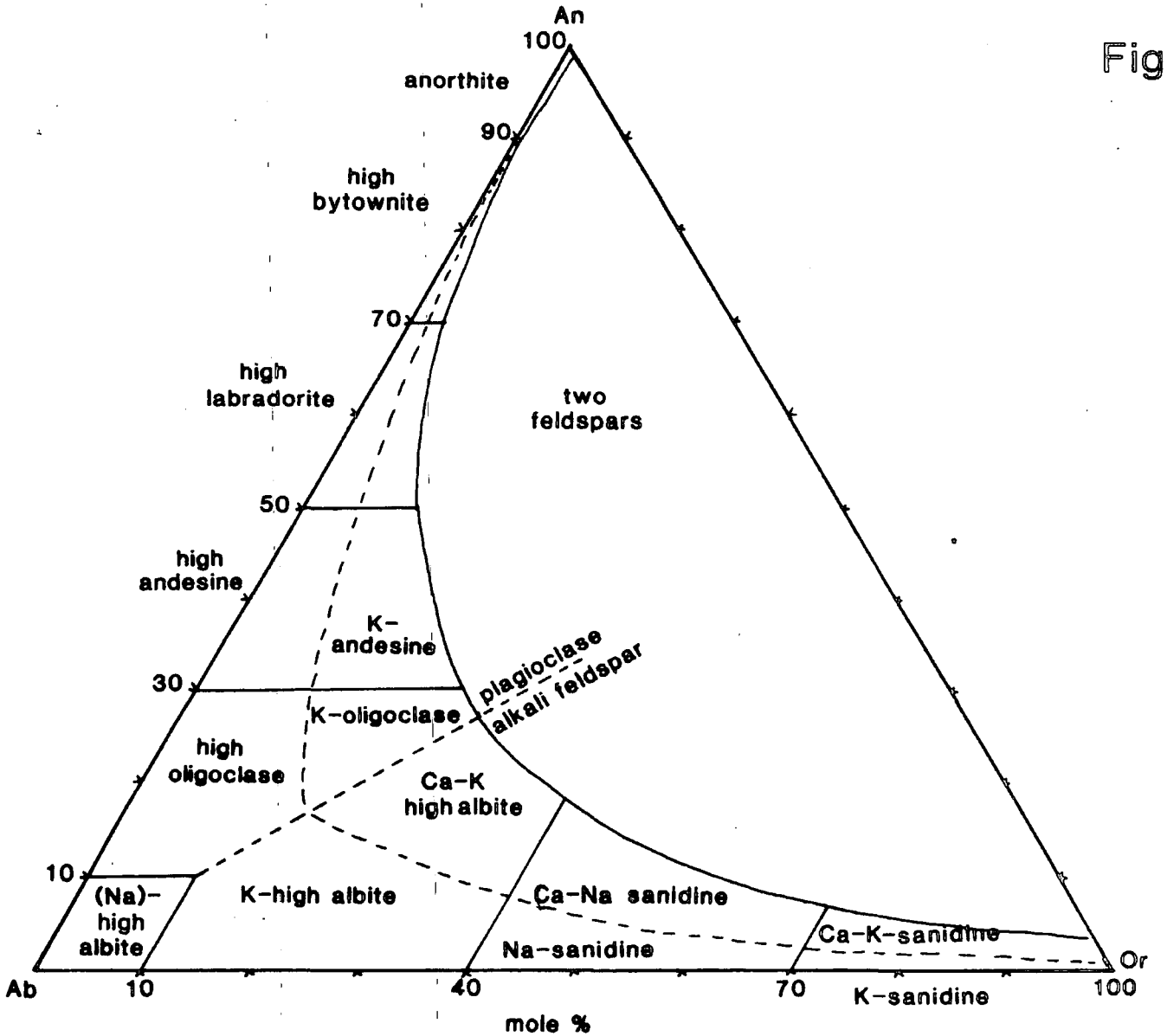
An
100
anorthite
90
high
bytownite
70
high
labradorite
two
feldspars
50
high
andesine
K-
andesine
30
plagioclase
alkali feldspar
K-oligoclase
high
oligoclase
Ca-K
high albite
10
(Na)-
high
albite
K-high albite
Ca-Na sanidine
Ca-K-sanidine
Na-sanidine
Or
Ab
10
40
70
K-sanidine
100
mole %

By using a slightly defocussed electron beam a 'bulk analysis' of that region of the feldspar grain can be obtained from a relatively small area, instead of having to raster the beam across most of a coarsely perthitic grain to average the analysis. In this way zoning across a grain can be defined more accurately. Minor variation may be introduced by some cryptoperthitic samples but will not affect the general conclusions. Chambers (1976) points out that the Ca content of feldspar exerts some control on exsolution processes. Diffusion of Ca into the Na-rich part of the feldspar will require a reconstruction of the alumino-silicate framework. This is a relatively 'high-energy' process where as simple Na-K unmixing is not and operates despite a rise in the solvus (and hence temperature at which unmixing begins) caused by increased Ca. As will be seen later many of the analysed feldspars are rich in Ca and this process too may have inhibited exsolution. Perthitic feldspars were not analysed by microprobe although some were studied by X-ray diffraction methods.

As can be seen from Figure 4.8.3 feldspar evolution follows a predictable compositional change from basalts (containing exclusively plagioclase) through trachy-basalts (with both plagioclase and high temperature, ternary alkali feldspar) to phonolites (exclusively binary alkali feldspar). Figure 4.8.1 shows the nomenclature of high temperature feldspars proposed by Smith (1974). The feldspars are notably K-rich in the basic rocks, a direct result of the alkaline nature of the parent magmas.

4.8.B: X-ray Studies

Several phenocrysts of alkali feldspar from a selection of dykes were studied by X-Ray Diffraction methods. Grains were hand picked, ground under acetone in an agate mortar and separated into two aliquots. One of these portions was then heated (in Au tubing) in a furnace at 900°C for 2 hours and these samples are suffixed H in Table 4.8.1. This has the effect of redistributing the Na and K evenly throughout the feldspar (homogenising the feldspar) without changing the Si/Al ordering and effectively removes complications introduced by the feldspar being perthitic.

XRD patterns were then produced using a Phillips Powder Diffractometer fitted with a Cu K_α X-ray tube, from thin films of powder washed onto a glass slide in acetone. An internal standard (silicon) was used in all runs. The range of 2θ scanned was

from 19° to 58°. All charts were indexed although some produced far better patterns than others, due, in most cases to slight alteration of phenocrysts and production of associated clay minerals. From these charts the 'cleaner' samples were measured using an optical ruler (accurate to 0.001°2θ). 2θ angles were then corrected by reference to the positions of the three Si peaks in this angular range. Peak and 2θ data were then processed by a least squared iterative computer program written by Dr. M.J. Dempsey of Manchester University Geology Department which calculates cell parameters (a, b and c) and interaxial angles (α, β and γ). Acceptable errors are in the range of ±0.010 Å (good errors ±0.005 Å) for cell edges and ±0.05° for α, β or γ. Results within these ranges were achieved by removal of observed peaks that gave large relative angular deviations from their 'calculated' 2θ. These peaks tended to be either smaller and less precisely measured reflections; incorrectly indexed feldspar reflections or peaks produced by other minerals, such as clays. A minimum of 8 peaks was used in all calculations, with some cell parameters being derived from up to 14 peaks.

Certain peaks were necessary to the calculation of cell parameters, such as the $\bar{2}04$, 060 and $\bar{2}01$ peaks which exert a strong effect within the computer program on the results (see Wright 1968). Either monoclinic or triclinic cell parameters were calculated dependent on the absence or presence of both 131 and $1\bar{3}1$ reflections respectively.

Wright (1968) defined a method whereby the *structural state* of a feldspar could be determined from three peaks ($\bar{2}04$, 060 and $\bar{2}01$). The composition of the feldspar governs the position of the $\bar{2}01$ reflection. Table 4.8.1A gives the cell parameters as calculated for those feldspars which gave acceptable errors and Table 4.8.1B gives the composition as determined from the $\bar{2}01$ reflection of all studied feldspars.

Cell-parameter data are plotted on Figure 4.8.2A (after Wright and Stewart 1968) and 2θ $\bar{2}04$ is plotted against 2θ 060 on Figure 4.8.2B (Wright 1968). Both methods give an indication of the structural state of the feldspar. From this it can be seen that the alkali feldspars exist in a variety of structural states, from fully disordered members of the high albite - high sanidine series through increased degrees of Si and Al ordering to fully ordered feldspars of the low albite - maximum microcline series. The Si/Al ordering does not appear to correlate with bulk rock composition. In some cases increased ordering seems to be a feature of more altered feldspars (eg. 54321, a

Figure 4.8.2

A. Feldspar cell parameter data plotted in terms of b(Å) vs. C(Å) (after Wright and Stewart 1968). Crosses indicate limits of errors (see Table 4.8.1). The feldspars can be seen to range from almost fully ordered to fully disordered structures. M indicates the feldspar is monoclinic (showing only the 131 reflection and not both the 131 and $1\bar{3}1$ peaks).

Key:

1. 304006H
2. 41939
3. 46252
4. 46253H
5. 58003
6. 46248H
7. 46252H

B. Feldspars plotted in terms of 2θ $\bar{2}04$ and 2θ 060 for Cu K_α (after Wright 1968). This simple plot can give an accurate idea of the structural state of the feldspar (see text).

Figure 4.8.2

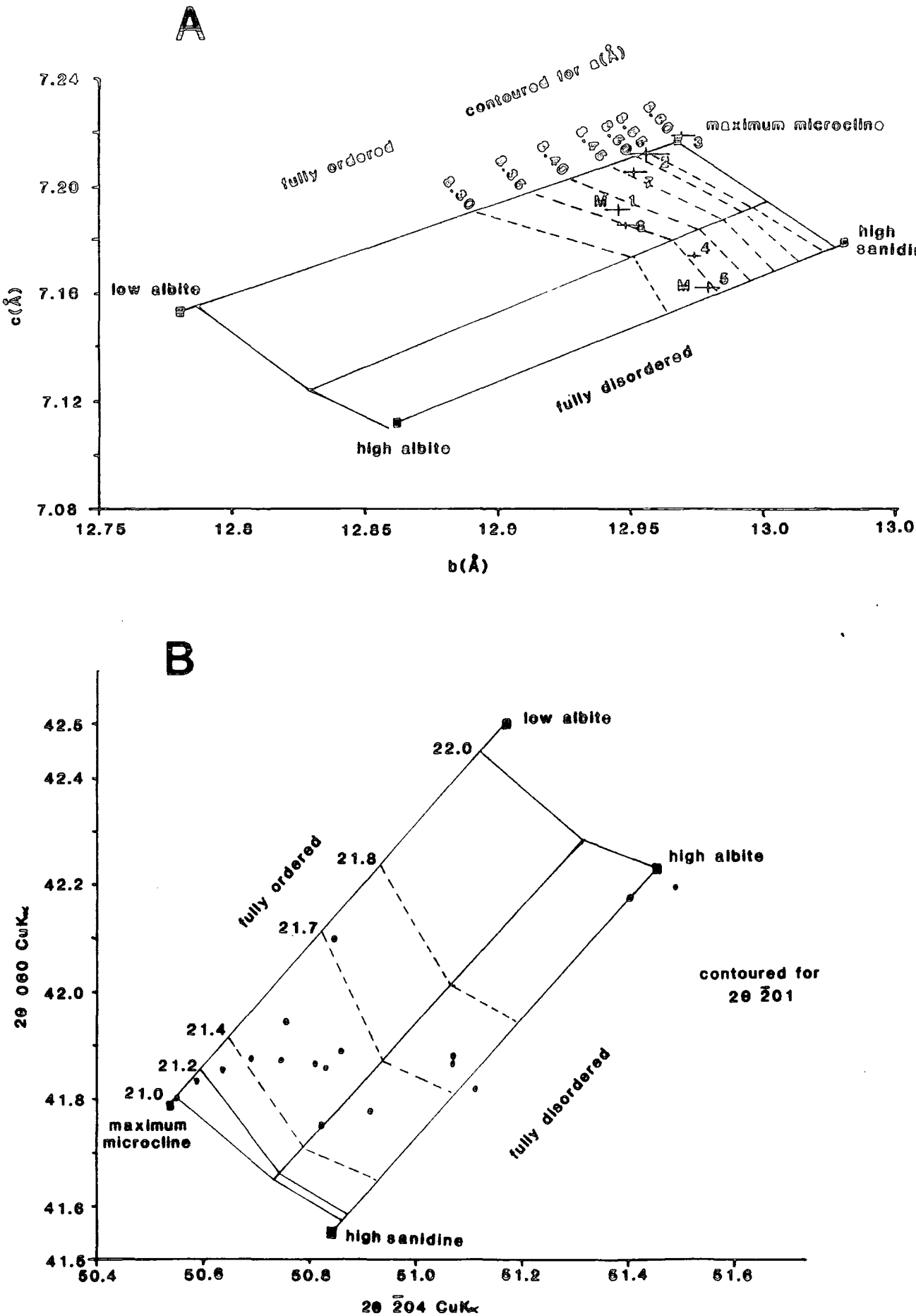
A
contoured for a(Å)
fully ordered
maximum microcline
low albite
high albite
fully disordered
high sanidi
c(Å)
b(Å)
7.24
7.20
7.16
7.12
7.08
12.75
12.8
12.85
12.9
12.95
13.0
B
low albite
high albite
high sanidine
maximum microcline
fully ordered
fully disordered
contoured for
2θ 201
2θ 060 CuKα
2θ 204 CuKα
22.0
21.8
21.7
21.4
21.2
21.0
42.6
42.4
42.2
42.0
41.8
41.6
41.5
50.4
50.6
50.8
51.0
51.2
51.4
51.6

Table 4.8.1A

Alkali Feldspar Cell Parameters

Sample	Monoclinic/ Triclinic	a Å	b Å	c Å	Volume Å^3	$\alpha°$	$\beta°$	$\gamma°$
304006H	Mon	8.5394 ±.0037	12.9499 ±.0050	7.1906 ±.0021	713.00 ±.41		116.23 ±.03	
41939	Tri	8.5849 ±.0001	12.9535 ±.0001	7.2123 ±.0000	721.80 ±.01	89.26 ±.00	115.81 ±.00	89.29 ±.00
46252	Tri	8.6011 ±.0104	12.9686 ±.0045	7.2188 ±.0018	723.74 ±.86	90.73 ±.08	115.91 ±.07	87.79 ±.09
46252H	Tri	8.4784 ±.0088	12.9509 ±.0053	7.2049 ±.0023	701.54 ±.62	90.98 ±.06	116.12 ±.04	87.78 ±.05
46253H	Tri	8.3490 ±.0070	12.9737 ±.0027	7.1741 ±.0010	697.73 ±.54	90.03 ±.03	116.11 ±.04	89.88 ±.05
58003	Mon	8.3356 ±.0104	12.9783 ±.0050	7.1622 ±.0021	696.60 ±.84		115.96 ±.08	
46248H	Tri	8.3983 ±.0088	12.9486 ±.0053	7.1857 ±.0023	701.54 ±.62	90.11 ±.06	116.12 ±.04	89.83 ±.05

Table 4.8.1B

Alkali Feldspar composition from $\bar{2}01$

Sample	2θ $\bar{2}01$	Or%	Rock	Sample	2θ $\bar{2}01$	Or%	Rock
59880H	21.938	8	Phon	126757H	20.436	55	Phon
59880	21.974	6	-"-	126757	20.537	48	-"-
46252H	21.292	71	Ben	54321H	22.14	0	BFD
46252	20.993	97	-"-	54321	22.083	0	-"-
41939H	21.685	32	-"-	58003H	21.576	35	Phon
41939	21.019	95	-"-	58003	21.62	41	-"-
46253H	21.550	45	-"-	304006H	21.352	62	-"-
46242H	21.413	85	Phon	304007	21.352	85	-"-
43846H	20.97	93	Sy	43970	21.28	67	-"-
46248	21.43	55	Phon				

badly altered phenocryst from a BFD and 126757, a slightly altered phenocryst from a phonolite). These do not however, show any marked perthitic texture (cf. Parsons 1978) and the majority are very fresh.

Of these feldspars, the highly disordered feldspars of monoclinic high sanidine type must have quenched from temperatures of the order of 1000°C (Stewart and Wright 1974). Increased ordering with decreasing temperature of crystallisation occurs down to a structural inversion (to triclinic) at about 450°C. High albite type feldspars invert to triclinic structures below 978°C (from monoclinic monalbite, Laves 1952) and remain triclinic on cooling. Rapid cooling prevents Si/Al ordering occurring and it would thus appear that several of the Igaliko feldspars must have quenched from temperatures around 1000°C as they show high albite - high sanidine structures. Increased ordering will result from lower temperature equilibration, as exhibited by the feldspars of the maximum microcline - low albite series (perhaps temperatures of the order of 700-800°C, possibly assisted by a late stage fluid phase).

Exsolution within feldspars gives rise to sets of reflections from the albite and orthoclase phases, particularly from the composition-dependant plane $\bar{2}01$. Heating (homogenising) the sample merges these two sets of reflections. Invariably, where two $\bar{2}01$ peaks are seen, the $Or_{\bar{2}01}$ peak is dominant with smaller $Ab_{\bar{2}01}$ peaks (implying perthitic not anti-perthitic feldspar). Thus, measurements of the larger $\bar{2}01$ peak from the unheated sample gives K-rich compositions whereas the heated $\bar{2}01$ peak gives a more Na-rich composition due to drawing together of the Ab and Or $\bar{2}01$ reflections. Optically no perthitic exsolution is visible in these feldspars (ie. crypto-perthitic). In some cases (eg. 58003, 126757) unheated samples produced very 'clean' single phase diffraction patterns, (ie. only one $\bar{2}01$ peak) with compositions around Or_{40-50}, these being immediately above the middle of the feldspar solvus. The single $\bar{2}01$ peak shows that these samples are unexsolved on a scale resolvable by X-rays and must be interpreted as having quenched extremely quickly to ambient temperatures from their equilibration temperature. 58003 shows a highly disordered structure, whilst 126757 shows a nearly fully ordered Si/Al framework. 126757 would thus appear to have quenched from a lower temperature than 58003. They must also have remained cold enough for the last 1150Ma to prevent any sub-solvus unmixing, an indication of the general stability of

the region. Anorthoclases from some of the rhomb porphyry dykes have retained very fine, high temperature morphologies (see for example Plates 3.16 and 3.17) and also imply that low temperatures have prevailed since initial solidification.

These results agree in general with those of Scharbert (1966) who described many high temperature (crypto-perthitic) alkali feldspars from dykes from the Ilímaussaq Peninsula and Igaliko swarm.

4.8.C: Compositional Variation

From Figure 4.8.3 the various feldspar compositional ranges can be seen for particular groups of rocks, and these tend to follow predictable patterns for their respective host rock type.

The most basic rocks contain the most Ca-rich feldspars ($An_{61}Ab_{37}Or_2$) as cores to some phenocrysts with very similar ($An_{62}Ab_{36}Or_2$) groundmass feldspars. There is a gradual change through hawaiites and benmoreites (and also some BFD's) of increasing Na and K across the high temperature feldspar range (Smith 1974, see Figure 4.8.3) from high andesine through the anorthoclase field (K-oligoclase and Ca-K high albite), crossing the 5kb cotectic of Yoder *et al.* (1957), to soda sanidines. Syeno-gabbros also show a similar range to these with almost all analyses lying above the 5kb cotectic. Benmoreites contain minor plagioclase although most feldspar is more alkaline in composition ranging from anorthoclase (Ca-K high albite) through to Na-sanidines and a few K-sanidines. Phonolites, with the lowest bulk rock Ca and greatest alkalis, contain no plagioclase (save albite in some exsolved feldspars) and the feldspars are mostly Na- and K-sanidines, the latter more abundant in benmoreites. Both phonolites and benmoreites contain feldspars which straddle the 5kb cotectic. Those feldspars from BFD's clustering around $An_{50}Ab_{45}Or_5$ represent xenocryst phases and these will be discussed in a later chapter.

Zoning

Many of the analysed phenocryst phases are strongly zoned as indicated in Figure 4.8.4 which shows most of the phenocrysts encountered from these rocks plotted in terms of An, Ab and Or. Tie lines join analyses from each phenocryst and indi-

Figure 4.8.3 A and B (2 pages)

Feldspar compositions in terms of atomic Ca, Na and K for individual groups of rock type. The 5kb cotectic of Yoder *et al.* (1957) is shown for comparison. The maximum limits of solid solution for feldspars from basalts, hawaiites and mugearites, benmoreites and phonolites closely follow the maximum limits defined by Smith (1974) for high temperature feldspar nomenclature (Figure 4.8.1). The recrystallised feldspars show almost no solid solution of Ca indicating relatively low temperature recrystallisation.

Figure 4.8.3A

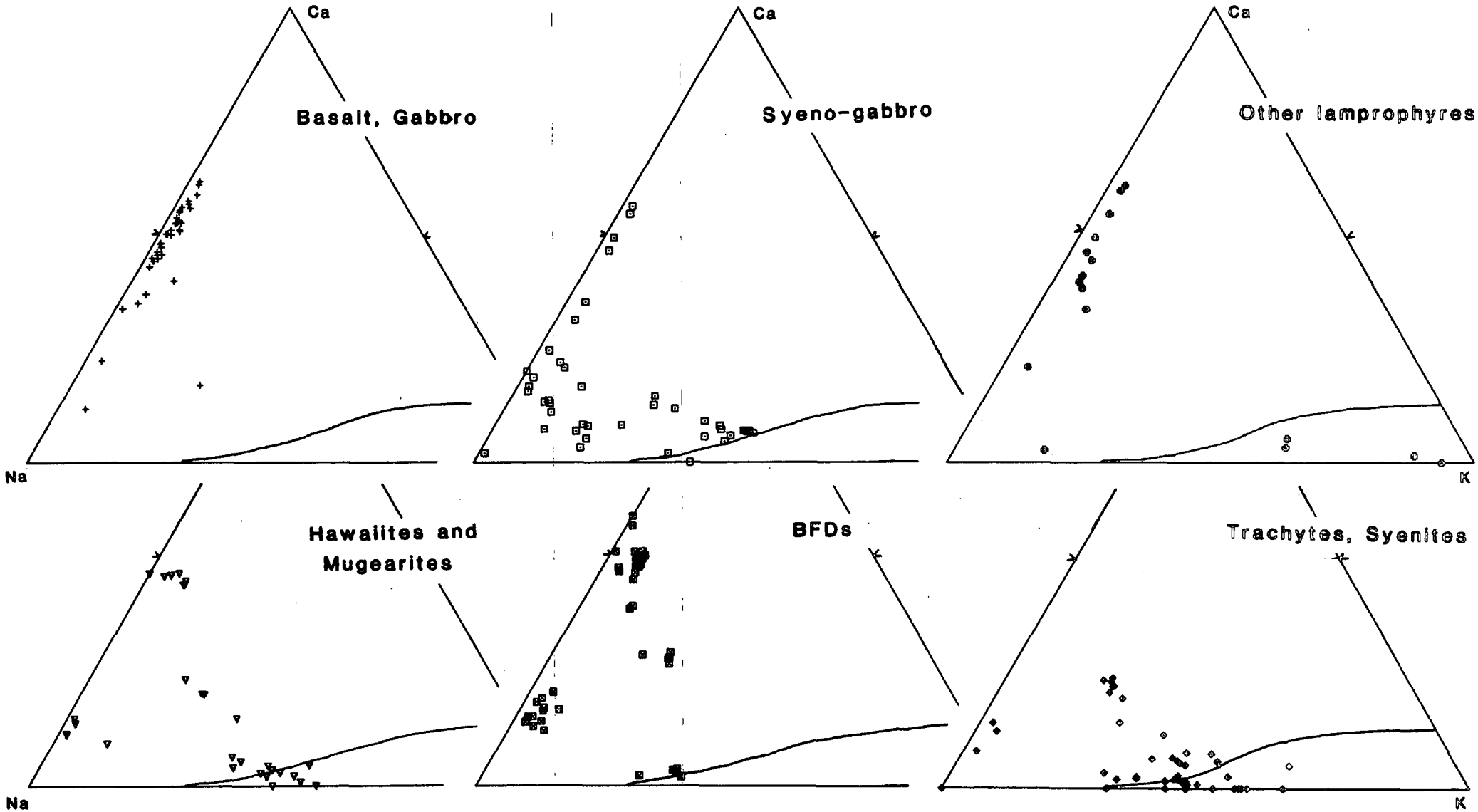
Ca
Basalt, Gabbro
Na
Ca
Syeno-gabbro
Ca
Other lamprophyres
K
Hawaiites and
Mugearites
Na
BFDs
Trachytes, Syenites
K

Figure 4.8.3B

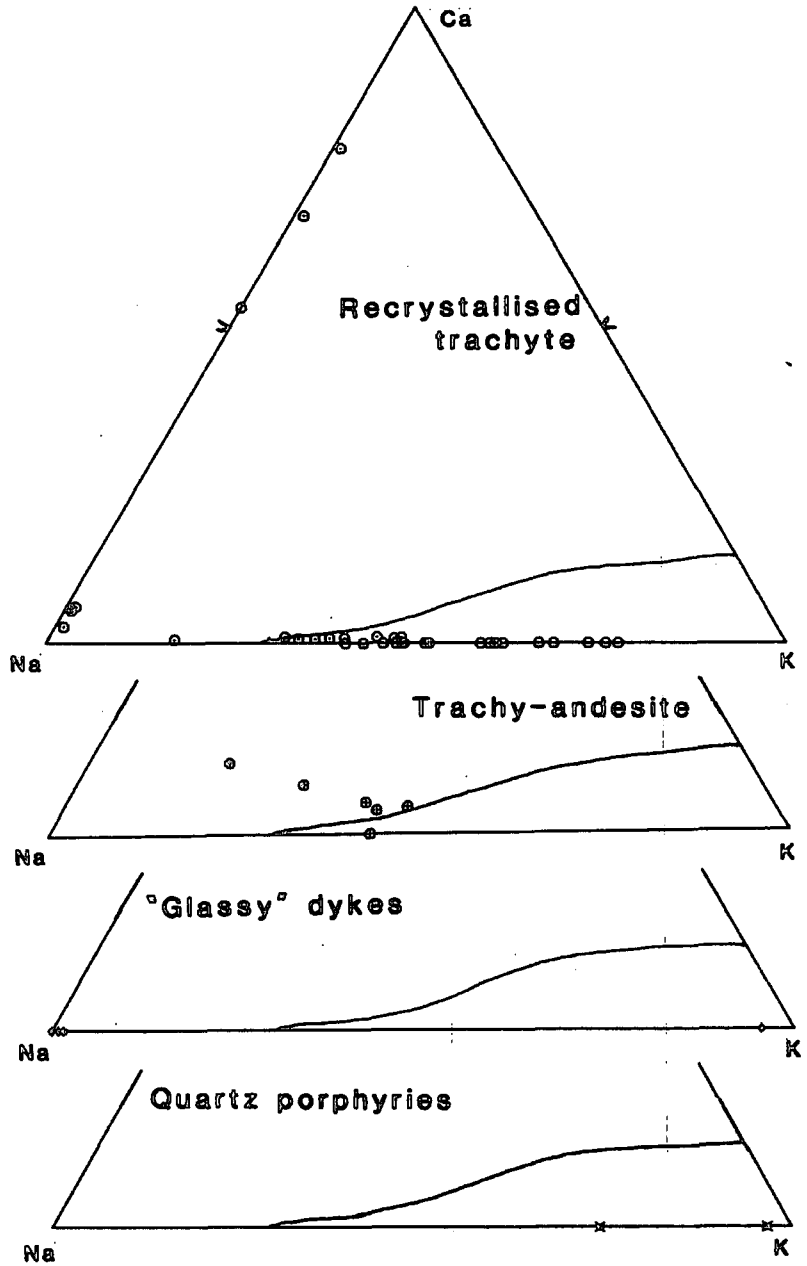
Ca
Recrystallised trachyte
Na
K
Trachy-andesite
Na
K
"Glassy" dykes
Na
K
Quartz porphyries
Na
K

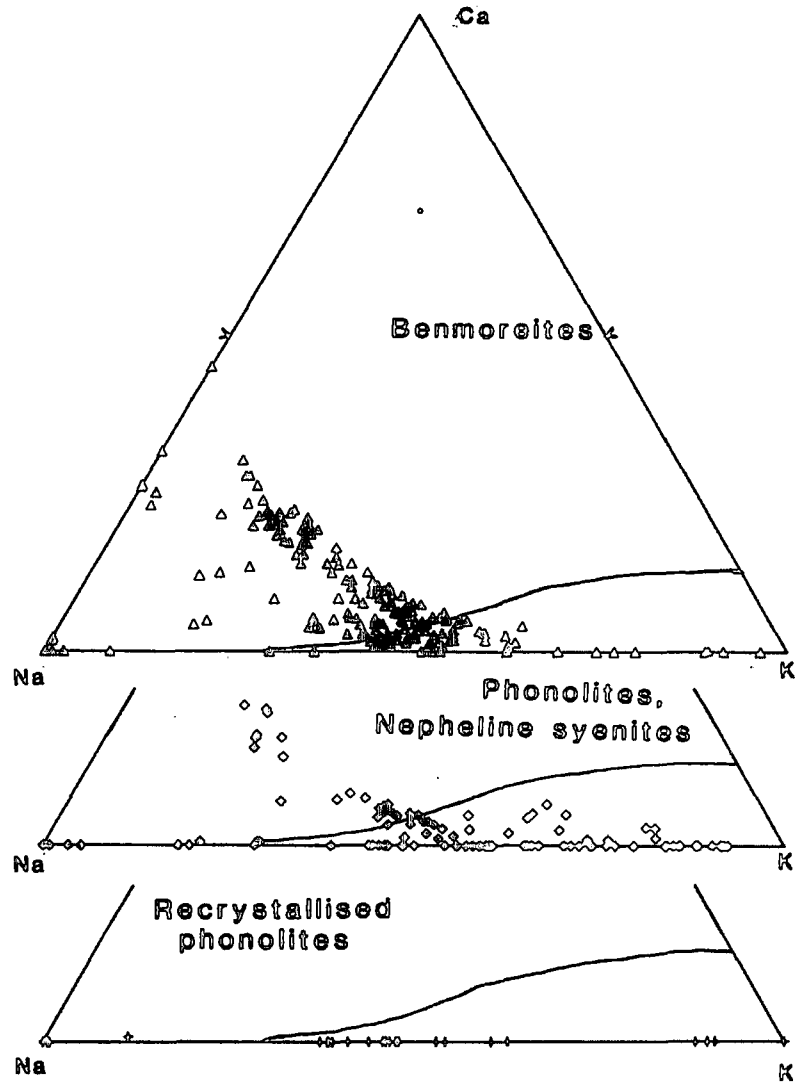
Ca
Benmoreites
Na
K
Phonolites, Nepheline syenites
Na
K
Recrystallised phonolites
Na
K

cate the direction of zoning with the crystal. Clearly, the style and range of zoning within individual phenocrysts is complex and rather erratic. However, certain points are immediately apparent.

(1) Zoning in feldspars from mugearites and BFD's is generally slight (10 compositional units at the most).

(2) Normal zoning (ie. to more Na-rich composition) is common in the basalts and gabbros with minor trends of reverse or oscillatory zoning evident (not visible in thin section).

(3) Zoning in the BFD xenocrysts is very limited (5 compositional units at most).

(4) Benmoreites show the widest and most erratic zoning with a range from K-oligoclase cores to Na-sanidine rims being common from individual crystals. Some phenocrysts also show zoning from Ca-K-high albite to Na-high albite. Pure Ab-Or (binary) phenocrysts are rare.

(5) Phonolites show slightly less extreme zoning than the benmoreites (from K-oligoclase to Na-sanidine), and also show trends of Na or K enrichment within binary alkali feldspars.

Zoning can be either normal or reverse (ie. from Ca-rich to Na+K-rich types or vice versa) in the ternary feldspars, and either K or Na enrichment is seen in the binary alkali feldspars. Some of the minor reverse zoning trends in the ternary feldspars may be a result of the orientation of the crystal within the slide. Thus, the compositional 'core' of the crystal may not be at the geometric centre of the slice of the crystal within the section. Analysis of several points from the centre to the rim of the crystal may thus cross the 'core' at some intermediate position.

Rapid changes of composition are common in the outer regions of the ternary feldspars which have fairly uniform cores (in the region of $An_{20}Ab_{60}Or_{20}$) and narrow rims of $An_{2-4}Ab_{46-48}Or_{50}$. These often have a dusty appearance in thin section, reminiscent of the Group 4 feldspars from Mt. Suswa (Nash *et al.* 1969). (See Plate 3.18). In hand specimen the change can be seen as clear, white cores to the crystals which give way to thin, pinkish rims.

Figure 4.8.4: Zoning within feldspar phenocrysts from various groups of rock types.

Zoning from 'anorthoclase' cores to binary feldspar rims is a common feature of the benmoreites and trachytes and syenites. In the phonolites, there are some anorthoclase phenocrysts but also abundant binary alkali feldspars which show normal and reverse zoning. Cores to the 'anorthoclase' phenocrysts in the phonolites are generally less calcic than anorthoclases from the benmoreites. See text for explanation.

Figure 4.8.4

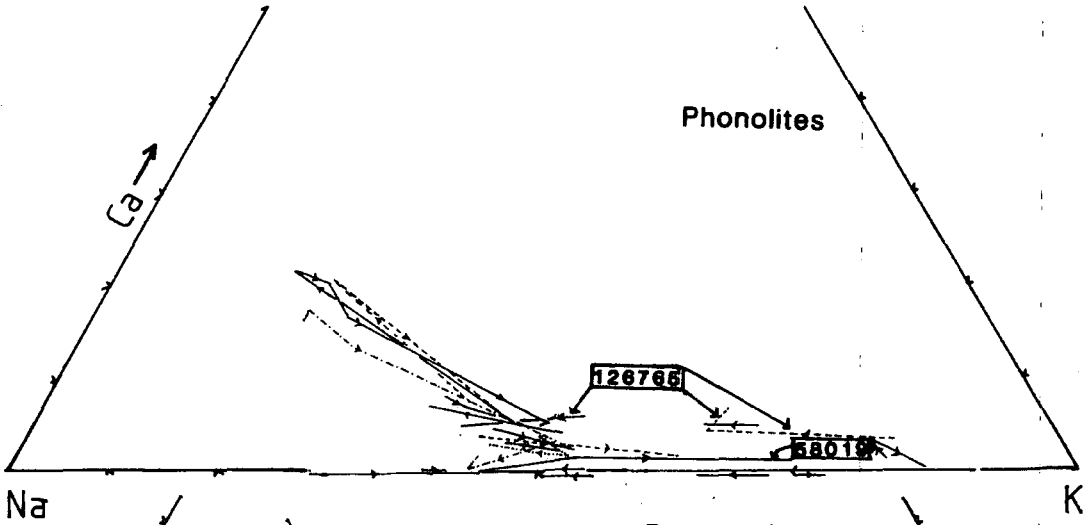
Phonolites
Ca
126766
58019
Na
K

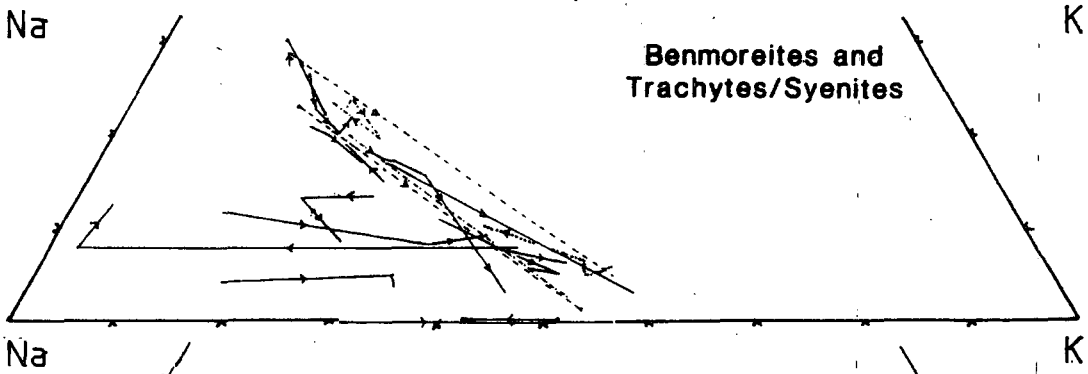
Benmoreites and
Trachytes/Syenites
Na
K

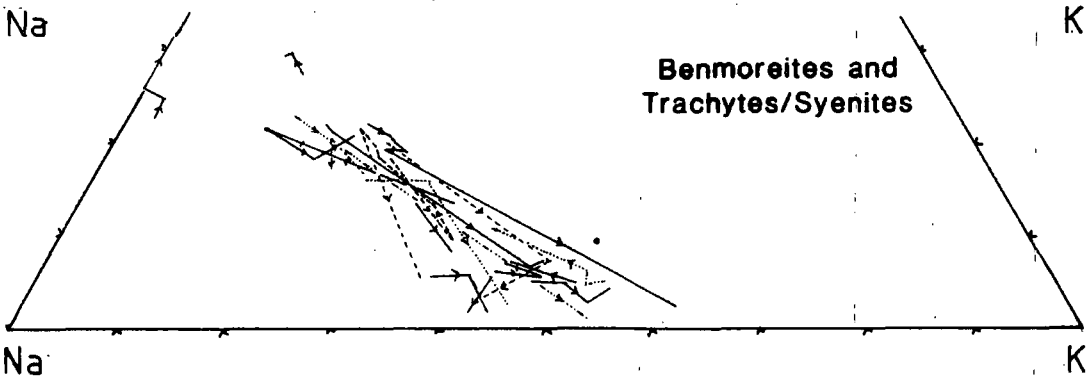
Benmoreites and
Trachytes/Syenites
Na
K

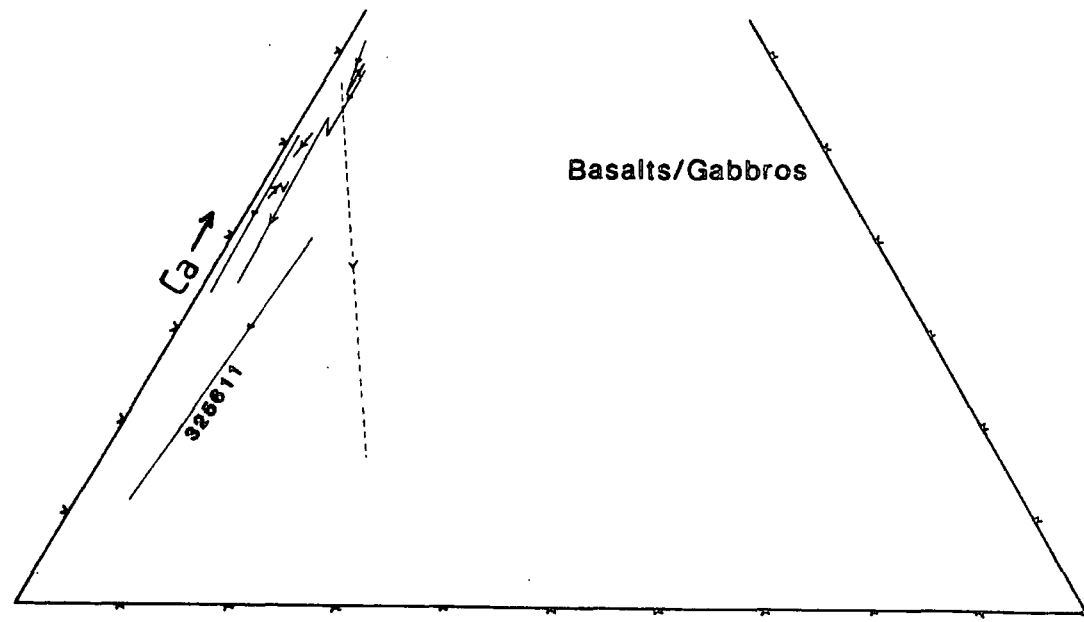
Basalts/Gabbros
Ca
326611
Na
K

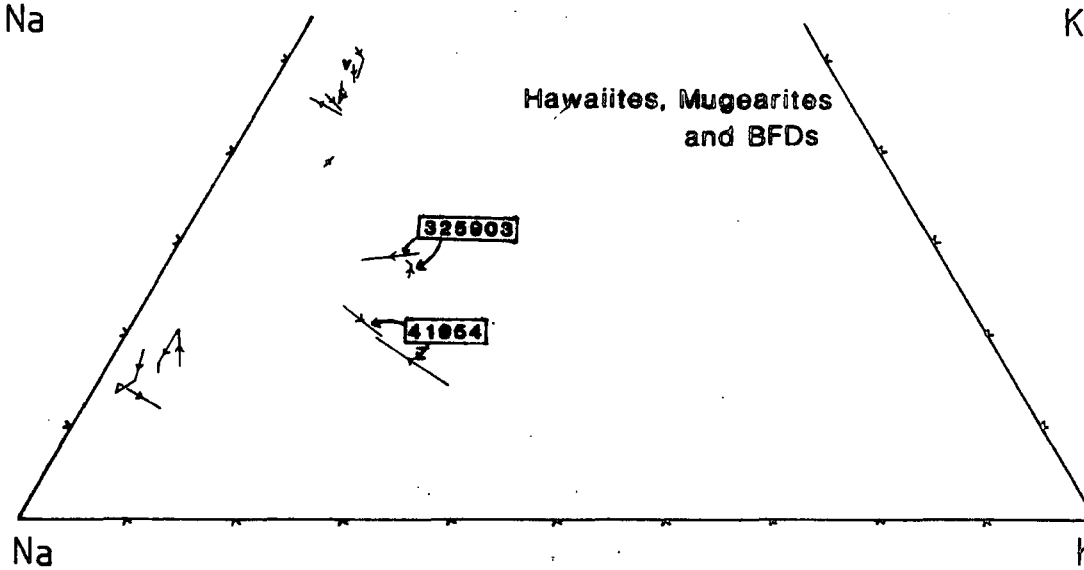
Hawaiites, Mugearites
and BFDs
325903
41064
Na

The cores of the feldspar phenocrysts appear to have formed at depth, crystallising from a magma of benmoreite/augite syenite composition. Chambers (1976) suggests that oligoclase crystallising at depth which is suddenly emplaced to higher levels, may be removed from the liquidus surface. When feldspar reappears on the liquidus, after some crystallisation of other phases has occurred, its composition is near that of an alkali feldspar. Jorgensen (1971) suggests a similar model for plagioclase crystallisation in the system An-Ab-Di. A drop in pressure moves the plagioclase-diopside phase boundary such that a liquid originally crystallising plagioclase would, at lower pressures, crystallise pyroxene. When, after a period of pyroxene crystallisation, plagioclase finally reappears on the liquidus, its composition is much more sodic. The dusty nature of the boundary between core and rim of these crystals will represent small crystals (possibly pyroxene) trapped as feldspar resumed crystallisation. Some of the 'anorthoclase' cores to these K-oligoclase crystals do have slightly ragged/corroded margins, suggesting a period of no crystal growth and/or possible resorbtion (see Plates 3.13 and 3.17). The euhedral nature and common occurrence of pyroxenes found alongside anorthoclase crystals also adds weight to this argument.

Zoning in some of the low Ca feldspars may show either Na or K enrichment from core to margin of the grain. This is particularly evident from feldspars within the phonolites (with An< 8 or so) where both trends are equally abundant. It is also seen to a lesser extent in the benmoreites, (where one sample shows a marked enrichment in Na, the remainder tending to K enrichment from Na contents of around Ab_{20}). Normal zoning in the alkali feldspars would be for low-K alkali feldspars to increase in K and high-K alkali feldspars to decrease in K. The reverse zoning of relatively K-rich feldspar cores to higher K margins seen in phonolites may seem unusual. Co-precipitation of nepheline, into which Na would preferentially partition, would cause an increase in the K/Na of the residual liquid and a complementary rise in the K/Na of the crystallising feldspar, and this may in part explain the observed trends in the phonolites.

Figure 4.8.5 shows feldspars and whole rock data plotted in the system Ne-Ks-Q (termed Petrogeny's Residua System by Bowen 1928). The recalculation of the feldspars into this system is the same as that used for the nephelines (see Chapter 4.7) which are also plotted. From these it was possible to construct feldspar fractionation paths

Figure 4.8.5 (2 pages)

Feldspar and nepheline analyses and whole rock data plotted in 'Petrogeny's residua System' (Bowen 1928). The lines join phenocryst - whole rock data for the same sample. Phase relationships from Hamilton and MacKenzie (1965). Both phenocryst and ground mass data for the feldspars and nephelines are plotted as indicated. Overleaf, liquid lines of descent are illustrated, defined by the individual mineral - whole rock data (cf. Nash *et al.* 1969).

Figure 4.8.5A

Syeno-gabbro
Phenocrysts

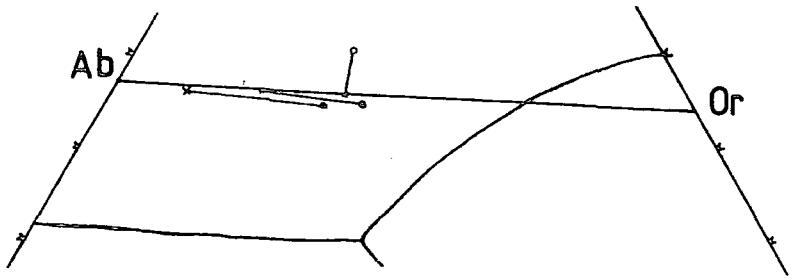

Quartz porphyry
Recrystallised phonolite
Syeno-gabbro
Groundmass

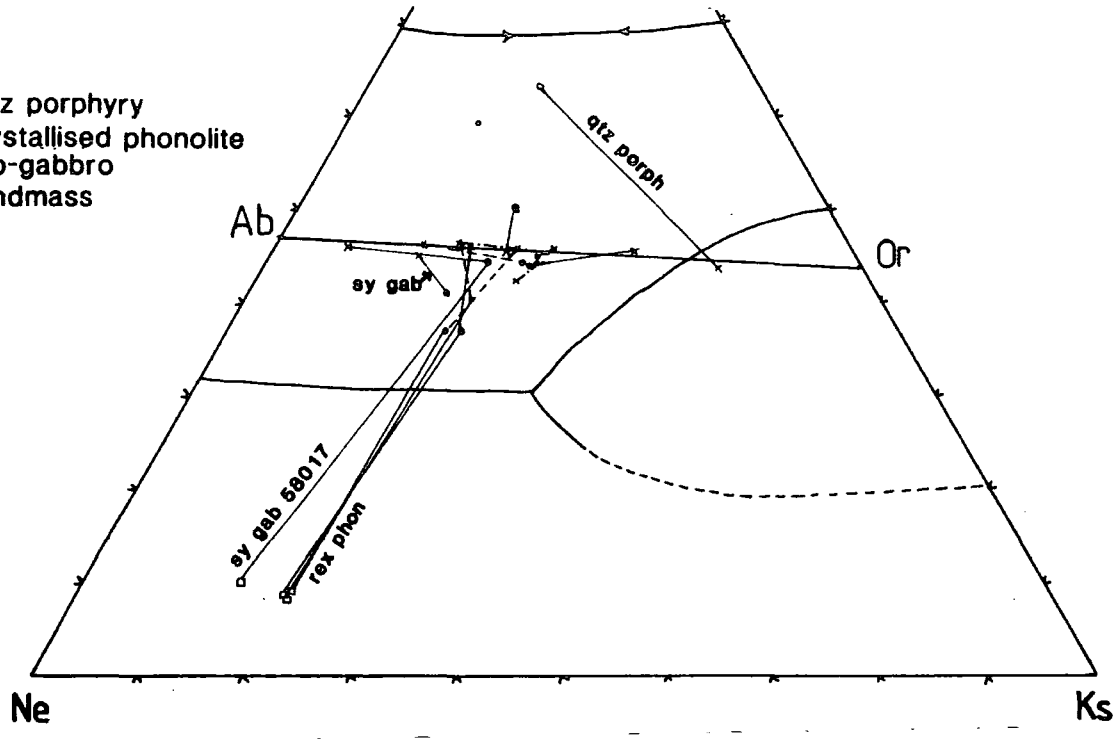

Trachytes
Benmoreites
Phenocrysts

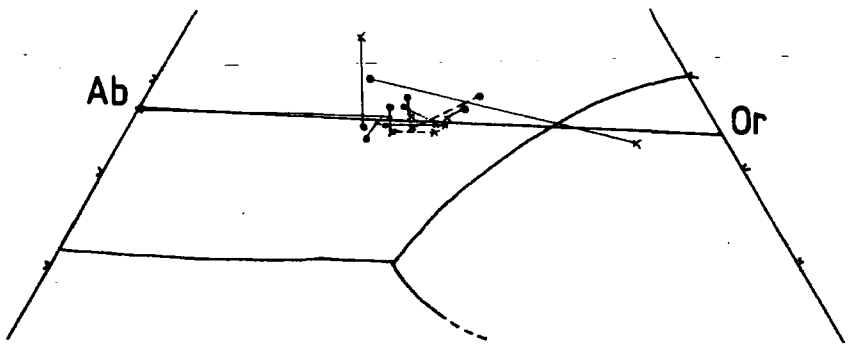

Trachytes
Benmoreites
Groundmass

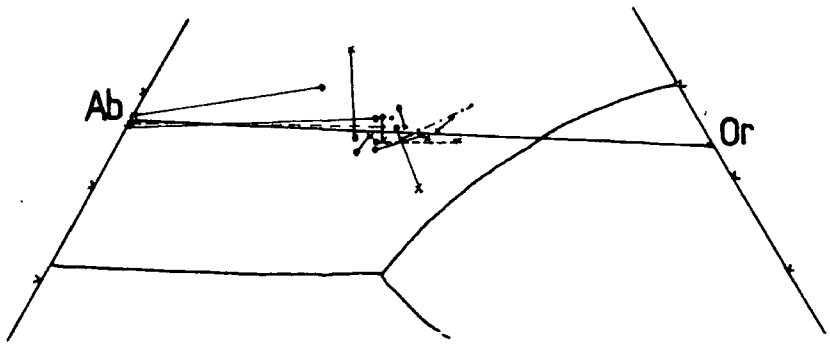

Figure 4.8.5B

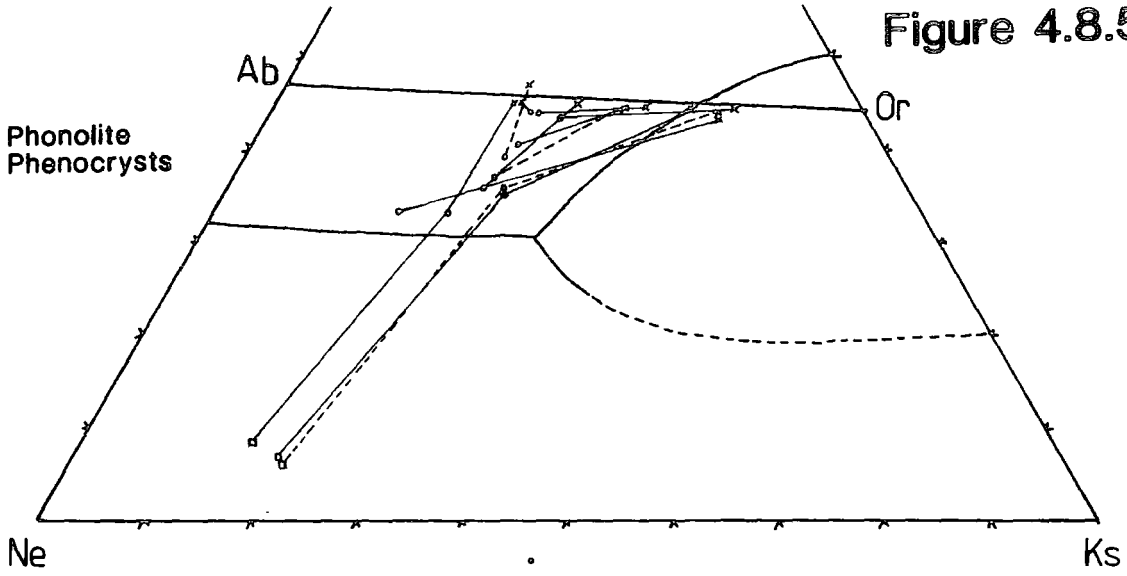
Ab
Or
Phonolite
Phenocrysts
Ne
Ks

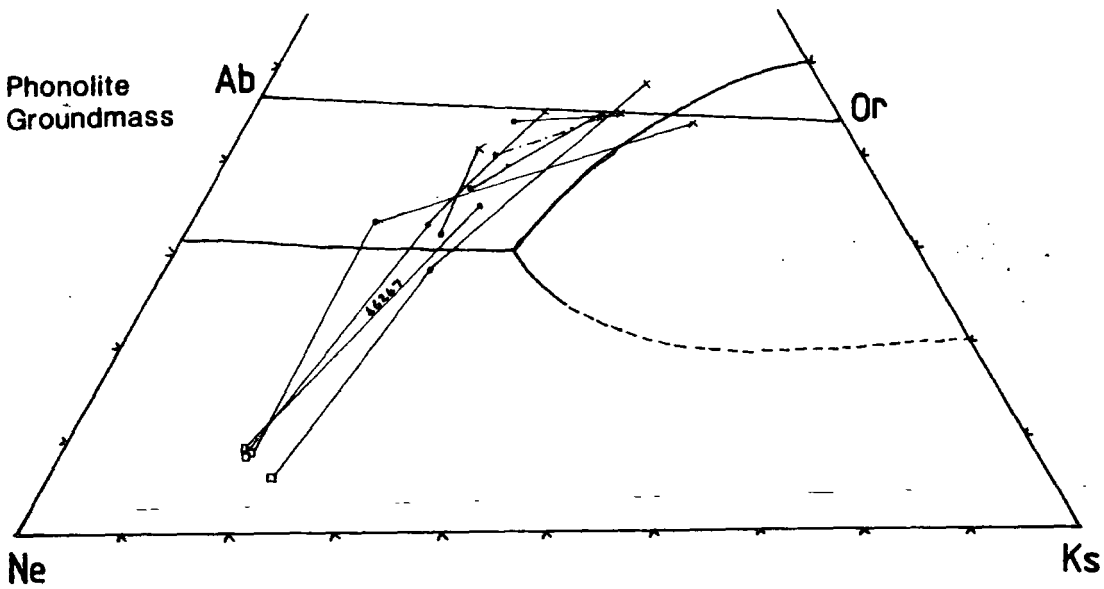
Phonolite
Groundmass
Ab
Or
Ne
Ks

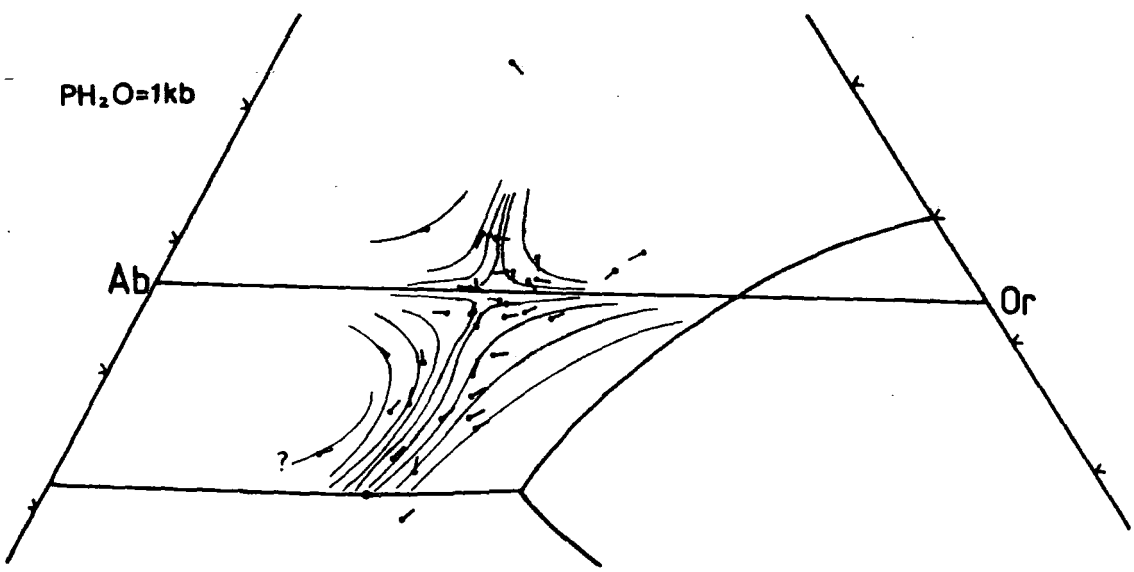
PH₂O=1kb
Ab
Or
?

(Figure 4.8.4F). These show a very similar pattern to those obtained from Mt. Suswa (Nash *et al.* 1969), showing similar inflection points. Thus, magmas lying on the sodic side of the fractionation paths will precipitate feldspars which become more potassic with time. However, those magmas on the potassic side, will initially crystallise a feldspar which becomes more sodic until the liquid composition passes the inflection points, whereby a trend of K enrichment in the feldspar will take over and 'reverse' zoning will occur.

Ba was detected in approximately one third of the analysed feldspars, and in one exceptional case (326276) reaches 5.12 wt% BaO ($An_{5.5}Ab_{44.4}Or_{40.4}Cn_{9.7}$). Generally however, BaO tends not to be greater than1.9 wt% and is usually between 0.5 and 1.2 wt%.

Figure 4.8.6A shows Ba variation against Ca-K atoms (cf. Na-Mg for pyroxenes). The Ba content of the plagioclase is fairly low, rising to a peak (excluding those analyses from 326276 which are >0.050 atoms Ba) at about Ca-K=0.0 to -0.4 and then decreasing towards the K-rich alkali feldspars. This peak in Ba corresponds to compositions ranging from K-oligoclase/Ca-K high albite through to Ca-Na and Ca sanidine. The highest Ba contents are typical of the anorthoclase phenocrysts. The high temperature, disordered structure of these anorthoclase phenocrysts would be more accommodating of the large Ba cation, which substitutes for K. For Ca>K, there is a tendency for Ba to increase with K, however, for Ca<K, Ba decreases with increasing K. This will be due in the most part to the bulk rock Ba and the variation in distribution coefficients of these elements with the changing composition of the crystallising feldspar (see below).

Plagioclase crystallisation concentrates Ba into the residual liquid. As the composition becomes more sodic and potassic (K-oligoclase compositions) Ba starts to partition preferentially into feldspar. This has the effect of depleteing the residual liquid in Ba, and even though the partition coefficient for Ba into feldspar continues to increase with increasing K content, the magma is now too deficient in Ba for its content in feldspar to keep increasing. Thus the Ba content of feldspar declines towards orthoclase. This type of relationship can be seen commonly in the 'dusty' rims of some of the anorthoclase phenocrysts. These rims are commonly Ba-poor, binary feldspars (around Or_{40-50}), surrounding relatively Ba-rich, ternary feldspar cores (around $An_{20}Ab_{60}Or_{18}Cn_2$), al-

Figure 4.8.6

Ba and Fe in Feldspars plotted against Ca-K (atoms) (cf. pyroxenes). Thus anorthite plots at 1.0 on the x axis, Albite (and a line separating plagioclases from alkali feldspars – see Figure 4.8.1) at 0.0 and orthoclase at -1.0.

Fe appears to show a decrease from plagioclase to albite, perhaps increasing slightly to orthoclases.

Ba increases from plagioclases to Ca-K=0 (albites, anorthoclases) where it reaches a peak and then declines to orthoclases. See text for explanation.

Figure 4.8.6

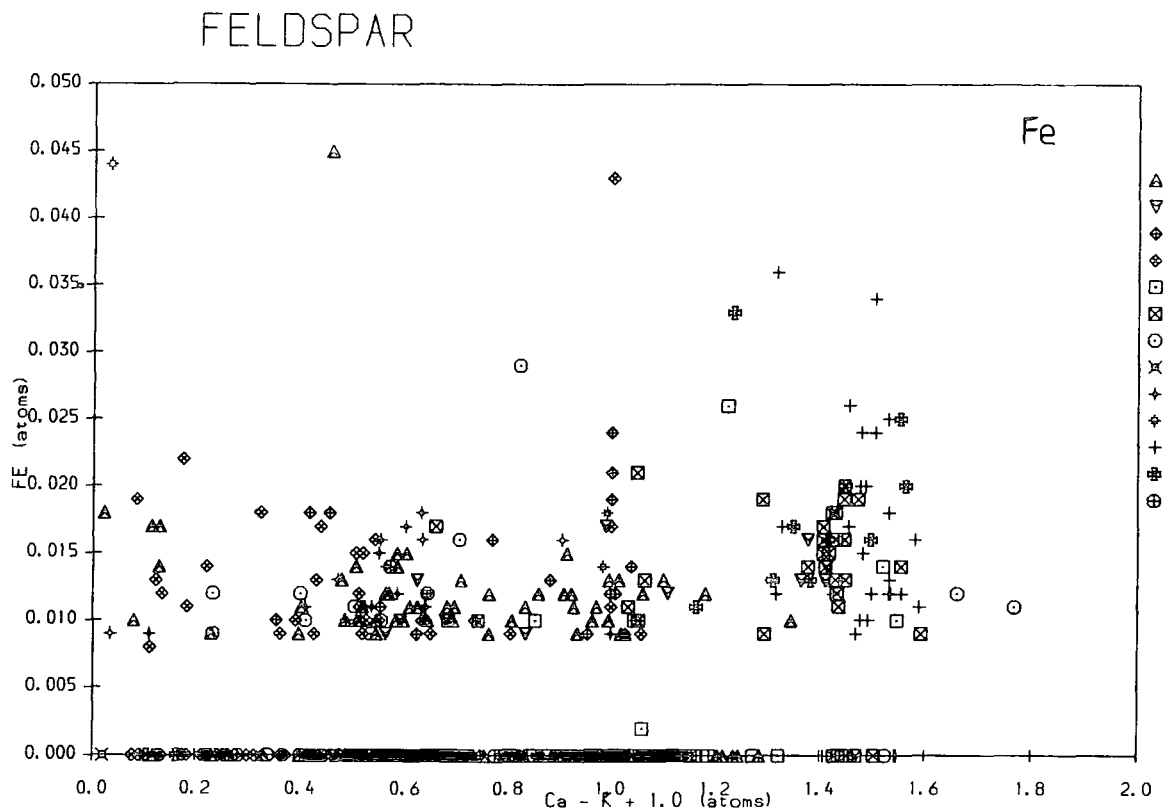
FELDSPAR
Fe
FE (atoms)
0.050
0.045
0.040
0.035
0.030
0.025
0.020
0.015
0.010
0.005
0.000
0.0
0.2
0.4
0.6
0.8
1.0
1.2
1.4
1.6
1.8
2.0
Ca - K + 1.0 (atoms)
BENMOREITE
HAW + MUG
TRACHYTE
PHONOLITE
SYENO-GAB
BFD
REXTAL TR
QTZ PORP
REXTL PHON
GLASS
BASLT,GABB
OTHER LAMP
TR-ANDESIT

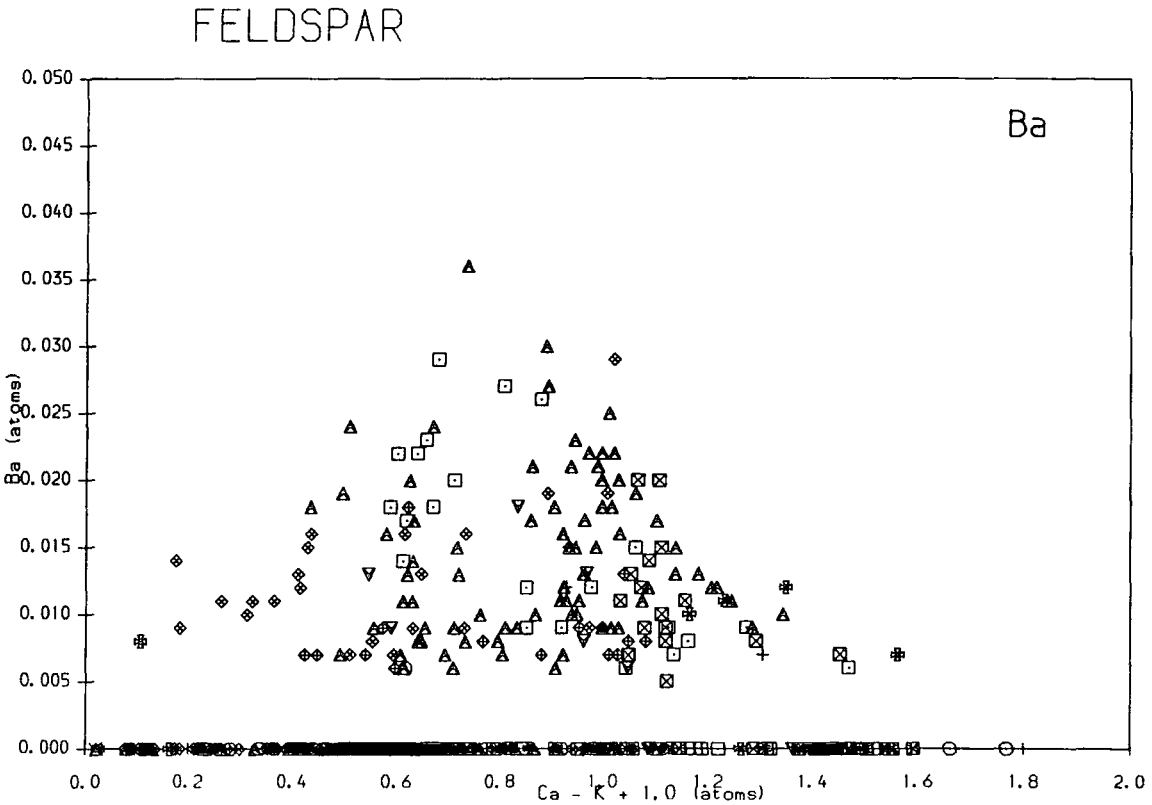
FELDSPAR
Ba
Ba (atoms)
0.050
0.045
0.040
0.035
0.030
0.025
0.020
0.015
0.010
0.005
0.000
0.0
0.2
0.4
0.6
0.8
1.0
1.2
1.4
1.6
1.8
2.0
Ca - K + 1.0 (atoms)

though in rare instances the rims may be Ba enriched.

Afonina and Shmakin (1970) claimed that Ba substitution into K-feldspars inhibited ordering. This was based on observations of the 131 triclinicity index and BaO content. Shmakin (1967), and Makagon and Shmakin (1971) also report confirmatory results although Rhodes (1969) could find no difference in Ba content between'anorthoclases' and microclines from Australian granitic rocks. Only two of the samples of feldspar examined by XRD contained detectable Ba: 58003 (Or_{42}) with 0.58 wt% BaO is monoclinic and 46253 (around Or_{45}) with between 0.48 and 0.95 wt% BaO is triclinic. Both are binary alkali feldspars showing disordered structures and, although there is barely enough data to confirm the results of Afonina and Shmakin (1970), Ba might appear to be another factor that inhibits ordering.

Smith (1974) concluded "that there are no simple answers concerning the substitution of Ba into the feldspar structure."

Iron was the only other minor element detected regularly in the feldspars, and its variation (recalculated as Fe^{2+}) is plotted on figure 4.8.6B. Generally between about 0.3 and 0.7 wt%, FeO reaches a maximum of 1.154% from a benmoreite and 2.751 wt% from the rim of a phenocryst in 325611, the possible BD_0 from Mellemlandet.

Fe is probably present as Fe^{3+} in alkali feldspars substituting for Al, whereas in the plagioclases Fe is probably distributed evenly between Fe^{2+} and Fe^{3+} (with fo_2 having an effect on the Fe^{2+}/Fe^{3+} ratio, Smith 1982).

From the Igaliko dyke feldspars, Fe shows an early decrease with increasing Na, levelling off at around Ca-K=0, and possibly shows a gradual increase as K increases to orthoclase, although the trends are not particularly well defined. Zoning of Fe in feldspar phenocrysts shows no systematic patterns although it is consistently in the same direction within one crystal (ie. not oscillatory). These inconsistent trends of zoning are seen even in phenocrysts of very similar compositions.

4.8.D: Comparison with Central Complex Feldspars

Stephenson (1973), Chambers (1976) and Jones (1980) produced feldspar analyses from the South Qôroq, North Qôroq and Motzfeldt centres respectively. Most of these

are binary alkali feldspars, lying below the Yoder *et al.* (1957) 5kb cotectic. They all however, report minor amounts of ternary feldspar from certain parts of these central complexes (usually oligoclase cores to alkali feldspars). Chambers (1976) considered these to be early formed plagioclases which had not re-equilibrated. If equilibrium had persisted these would have become lime-rich alkali feldspars.

Chambers (1976) also detected Ba and K-rich zones within these oligoclases, although Stephenson (1973) detected no Ba in any feldspars from South Qôroq. Stephenson did however, record minor amounts of oligoclase. It would seem likely that feldspars similar to the anorthoclases found in the dykes would be precursors to the more equilibrated (low temperature) oligoclase and Na-rich alkali feldspars found in the central complexes.

The feldspars of these nepheline syenite central complexes are predominantly large, lath shaped alkali feldspars, with the augite syenite members containing the only Ca-rich feldspars. It appears that the rhombic habit of the 'anorthoclase' feldspars gives over to a lath shaped form with continued evolution to less calcic compositions. A parallel change in feldspar morphology is seen in the dykes also, with rhombic anorthoclase phenocrysts most common in the benmoreitic dykes, these becoming less abundant and giving way to tabular alkali feldspars in the phonolites. This type of change has been noted by Upton (1964a, b) from foyaites on Tugtutôq, from Kangerdlugssuaq (Kempe and Deer 1970) and in the Mt. Suswa lavas (Nash *et al.* 1969), and this may be a useful field indicator of whether the host dyke is benmoreitic or phonolitic.

4.8.E: Sub-solidus unmixing

Although the feldspars from most of the Igaliko dykes are relatively homogenous, many feldspars from the recrystallised rock have undergone sub-solidus unmixing (see for example the progressive changes occurring during recrystallisation, Chapter 3.5).

Feldspars from recrystallised rocks generally plot very close to the binary joins in the An-Ab-Or system, indicating relatively low temperature re-equilibration. They are also free from Ba although many still contain appreciable Fe.

Recrystallisation involves a re-ordering of the feldspar structure by migration of Na

and K ions, and also of Si and Al within the framework, producing a more fully ordered structure (see Chapter 4.8.B). This increase in ordering of the structure will make it less able to accommodate the large Ba^{2+} ion and this will be expelled from the feldspar.

Recently, experimental studies have accurately located the alkali feldspar solvus (eg. Orville 1963; Thompson and Waldbaum 1969; Smith and Parsons 1974). These various results agree closely after correction for pressure differences between experiments (a factors of +16°C/kb increase in pressure). The anorthite content of binary alkali feldspars has a large effect on the position of the solvus, increasing it by 33°C per mole % of anorthite. Thus good data exist for positions of the alkali feldspar solvus at a range of pressures and An contents. Figure 4.8.4 shows Smith and Parson's (1974) solvus at 1kb onto which have been plotted data from the unmixed feldspars from the recrystallised benmoreite dyke 58291-298 (tie lines join analyses from the same sample). Where several analyses plot close together an average analysis has been calculated. The K-rich feldspars are all Ca free but the Na-rich members may contain up to 5 mol% An. Most analyses from 58291 (@ 700m from the syenite) plot at the crest of the solvus. These are probably not affected by metamorphism (although one analysis of Or_{32} intersects the solvus at a temperature of 560°C) and these feldspars will have equilibrated above 700°C on initial crystallisation of the rock. Recrystallisation to two feldspars is evident in samples 58292-297 and the Table 4.8.2 shows the temperatures at which individual feldspars intersect the solvus against the distance of their host rock from the contact.

Recrystallisation in the feldspars may have started at about 650m from the contact (around 450°C), these analyses recording the lowest temperatures. Feldspars further from the contact than this remain almost unaffected (58291). As the contact is approached increasingly high temperatures are recorded for the exsolution and have been 'frozen in' on later cooling, which must have been either relatively rapid compared with diffusion rates or relatively 'dry'.

Temperature - distance data (for the 2kb data above) are plotted on Figure 4.8.7. Projection of this data onto the contact as a straight line gives a minimum temperature of the contact 890°C. However, heatflow calculations from a cooling body in a homogenous medium give curved, 'exponential' type temperature-distance curves (see

Figure 4.8.7

Alkali feldspar compositions from the recrystallised benmoreite 58291-8 plotted on the feldspar solvus of Smith and Parsons (1974) in Figure A. The temperatures of recrystallisation indicated in Figure A are plotted against the distance of the sample from the contact of the Igdlerfigssalik Syenite in Figure B. These data suggest a minimum temperature of the contact of ≈880°C (straight line through data). A rough curve fitted through the data (similar to the thermal gradient calculated by Hart (1964) for the quartz monzonite Eldora Stock) may suggest temperatures for the contact of the Igdlerfigssalik syenites of 960-980°C. This data may suggest that recrystallisation of feldspars does not occur below about 450°C.

Figure 4.8.7

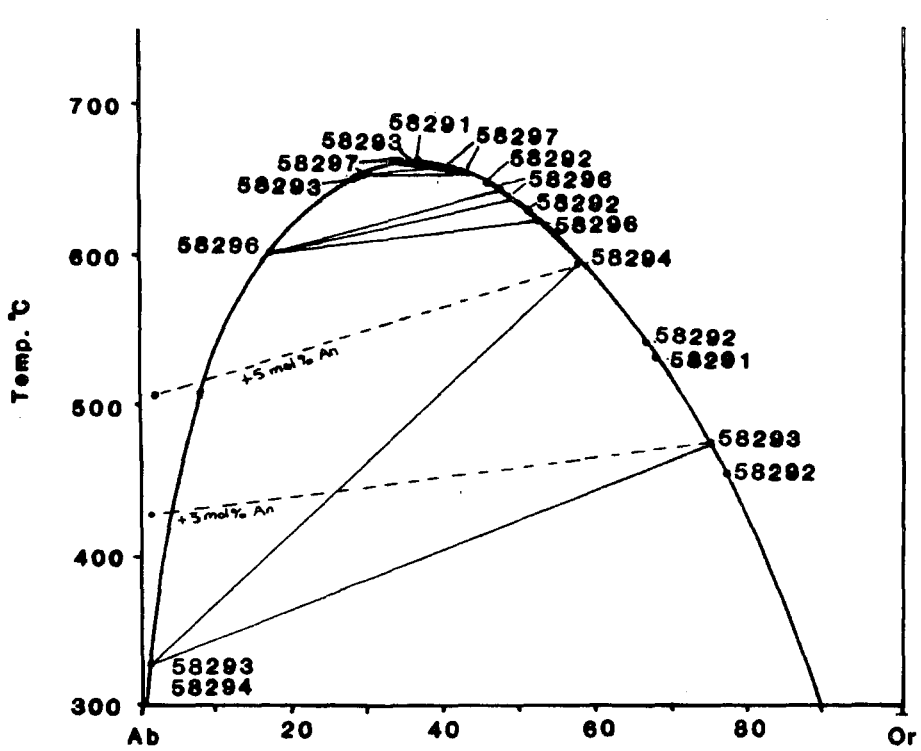
Temp. °C
700
600
500
400
300
Ab
20
40
60
80
Or
58291
58293
58297
58297
58293
58292
58296
58292
58296
58296
58294
58292
58291
58293
58292
58293
58294
+5 mol% An
+5 mol% An

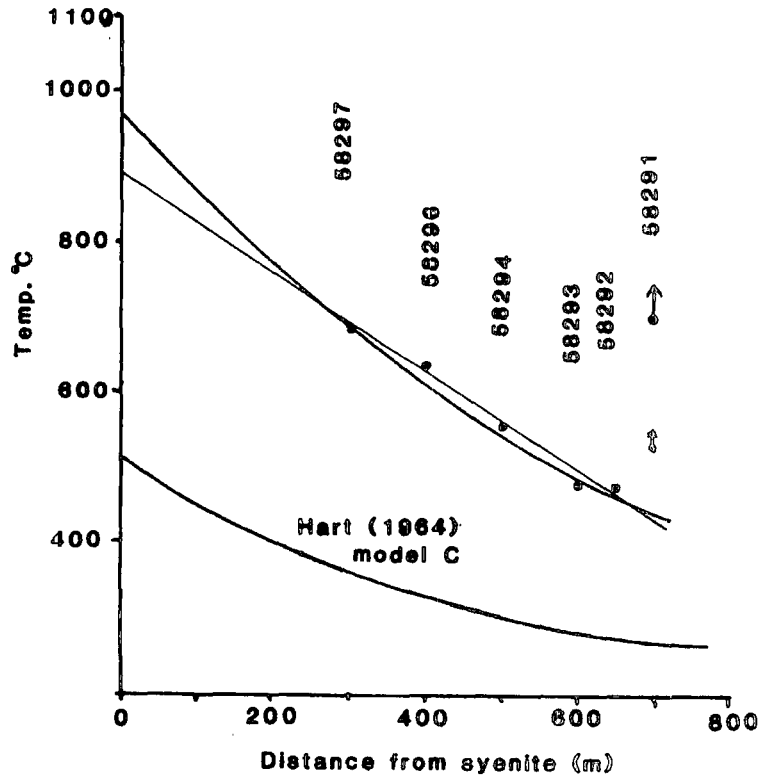
Temp. °C
1100
1000
800
600
400
0
200
400
600
800
Distance from syenite (m)
58297
58296
58294
58293
58292
58291
Hart (1964)
model C

Table 4.8.2

Temperature-distance results of feldspar recrystallisation from dyke 58291-8.

Sample	Distance	Na-Fsp	K-Fsp	Average Temp at 1kb	2kb	
58291	700m	One	feldspar	>670°	>686°	Unaffected
58292	650m	—	lowest 455°	455°	471°	Ksp range 645°-455°
58293	600m	455°	475°	465°	481°	Ab contains 3 mol% An
58294	500m	515°	595°	545°	561°	Ab contains 5 mol% an
58296	400m	605°	625°-645°	620°	636°	
58297	300m	680°	655°-660°	668°	684°	

for example Hart 1964 who based calculations of thermal gradients around a monzonite stock on the heatflow model and equations of Lovering 1935). Temperature at a distance from an intruded mass of rock essentially depends on the form of the body, its temperature (and latent heat of crystallisation) and the conductivity and initial temperature of the rock into which it is intruded. Hart (1964) modelled heatflow around the quartz monzonite Eldora Stock in 'granodioritic' schistose basement. This is a similar physical environment to the region around the Late Igdlerfigssalik syenites, although the Eldora Stock is a much smaller intrusion, and was intruded to within 1000m of the surface at its present exposure levels. Hart's model C is shown on Figure 4.8.4 for comparison.

The temperature of the country rock around the Eldora Stock was assumed to be about 35°C on intrusion. Around the Late Igdlerfigssalik syenites, with perhaps as much as 6km of supracrustal cover, the country rock may have been at about 150-200°C. With large intrusions such as the Late Igdlerfigssalik syenites having been emplaced in virtually the same place as the Early Igdlerfigssalik centre, only perhaps 10Ma later, the country rock temperature may have been even higher. Larger intrusions will also have a greater heating effect on the country rock. With additions of all these factors to Hart's (1964) model C temperature - distance curve, the data obtained from the feldspars of 58291-8 would seem to fit a curve of this type. Constructing a rough exponential curve

through these data points gives a contact temperature of around 970°C, closely agreeing with the feldspar - nepheline equilibration temperatures for SI.4 of about 940-960°C (Powell 1978). It would appear from the data from 58291-8 that feldspar unmixing does not occur at temperatures less than ca. 450°C with higher temperatures required to produce separate 'Ab' and 'Or' grains in this environment.

It is also at about this temperature (450°C, 650m from the contact) at which the amphibole chemistry markedly changes with respect to Ca, Na and K. This is a much lower temperature than that which causes the major textural change (see Figure 4.4.7). Thus it would seem that the change in amphibole chemistry, particularly the changes in Ca, is governed by the recrystallisation of the feldspar at a temperature of about 450°C. Major textural change does not occur in this dyke until the temperature reaches about 550°C, and may possibly be accompanied by a fluid phase (see Chapter 4.4.D).

4.9: Sodalite

Sodalite is reasonably common in rocks from the Igaliko Dyke Swarm. It occurs in particular abundance in the recrystallised phonolites from the Østfjordsdal swarm where it is common as rounded groundmass grains. Sodalite is also recorded from lamprophyric rocks as well as phonolites, recrystallised trachytes and a breccia dyke.

It is easily recognised under ultra-violet light where it fluoresces a vivid orange colour, probably due to the presence of minor quantities of sodium mono- and poly-sulphide (Kirk 1955).

In general the sodalite from the dykes contain slightly less Na and slightly more Cl than those from the North Qôroq and South Qôroq centres (Chambers 1976, Stephenson 1973). Sulphur was detected in some analyses (up to 0.23 wt%). Other minor elements detected included FeO up to 0.48 wt%, MgO to 0.49 wt % and CaO to 0.20 wt%. K_2O was not detected.

Figure 4.9.1 shows sodalite compositions plotted in terms of Cl vs. Si and Na vs. Cl. Na shows a range of between 6.171 and 7.185 atoms per 24 oxygens with slightly higher Si contents evident in the more sodic types. There is also a slight tendency for the lower Cl varieties to have higher Si. There is some bulk rock compositional

Figure 4.9.1: Sodalite and analcite chemical variation.

Sodalite

Si vs. Cl atoms per 21 oxygens and Si vs. Na atoms per 21 oxygens. The most Cl-rich sodalites contain least Si and most Na.

Analcite

Analcite chemical variation recalculated into *Ne-Ks-Qz*. Analcite may form either by alteration of nepheline or by alteration of plagioclase (albite, Henderson and Gibb 1983). See text for explanation.

Analcite analyses

projected into the Residua System.

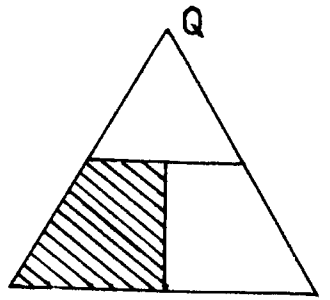

▲ BENMOREITES

⊡ SYENO-GABBRO

✙ OTHER LAMPROPHYRES

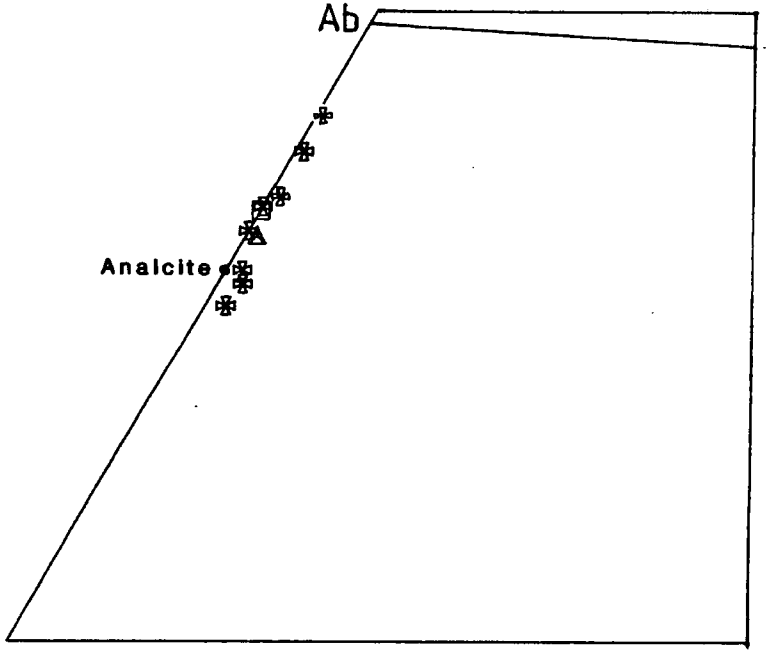

Sodalite Atoms per 21 oxygens

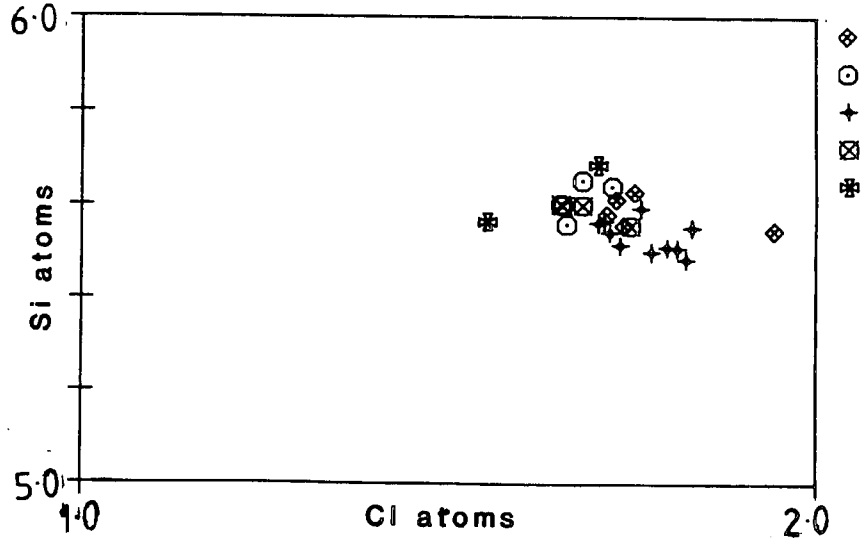

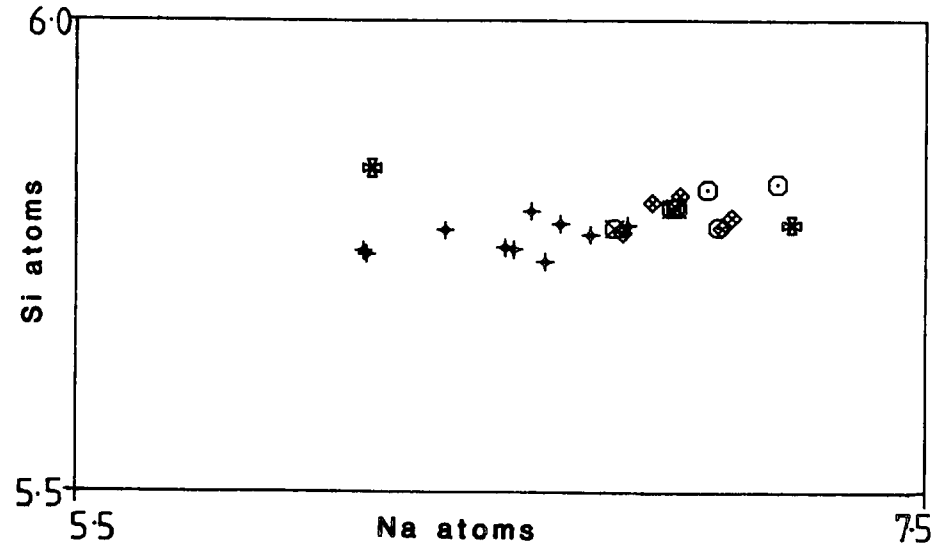

dependence on the sodalite composition with the recrystallised phonolites containing sodalites with the lowest Na and Si, these elements increasing through phonolites to recrystallised trachytes. Cl shows a slight decrease over this compositional range. The Cl data are consistent with a decrease in bulk rock Cl over this range and the Si content may possibly reflect a decreasing a_{SiO_2} (see below). The lower Na contents in sodalites from the seemingly more evolved rocks may be caused by Na partitioning preferentially into nepheline, a common phase in these sodalite bearing rocks.

Stormer and Carmichael (1971) determined the effect of a_{SiO_2} on sodalite stability. From the reaction $Na_4Al_3Si_3O_{12}Cl + 6SiO_2 \rightleftharpoons 3NaAlSi_3O_8 + NaCl$, it can be seen that low a_{SiO_2} favours the formation of sodalite, whilst high a_{SiO_2} would favour albite formation with Cl being lost as a part of a fluid phase. Using this reaction Stormer and Carmichael (1971) demonstrated that in undersaturated liquids, sodalite may even precede nepheline in the crystallisation sequence, depending on the feldspar composition. The fact that sodalite is present need not reflect exceptionally high Cl contents of these magmas but reflects low silica activity in the magmas.

Wellman (1970) studied stability in the system Ab-Or-Ne-Ks-NaCl-H_2O and concluded that the late stage fluids in these systems are essentially aqueous alkali chloride solutions. If this fluid phase is sufficiently enriched in Cl sodalite may crystallise alongside nepheline and feldspar.

Stephenson (1973) notes sodalite rims to some nepheline crystals, presumably a late stage alteration product, by Cl enriched fluids. Analysis 326273.18 (from a recrystallised phonolite) has characteristics intermediate between nepheline and sodalite and may be a late formed alteration product. The metamorphic event that recrystallised the Østfjordsdal dykes may also have been accompanied by fluids rich in water, Cl and CO_2 (for cancrinite). These, as well as aiding elemental diffusion (and thus easing exsolution in the feldspars) may have caused alteration of nepheline to sodalite and cancrinite.

4.10: Analcite

Analcite was analysed from 5 samples. It seems to be more common in the lamprophyric rock types than in the evolved, felsic samples, where it forms as late stage,

interstitial patches.

Chemical variation in the analcites is limited, the most variation being seen in the SiO_2 content which varies from 50.36 to 57.20 wt%. Na ranges from between 11.59 and 13.82 wt% and Al_2O_3 varies between 21.68 and 24.56 wt%. The variation in SiO_2 causes a change in excess *Qz* when analcite analyses are recalculated into the residua system (Figure 4.10.1). All analcites contain less than 0.5 wt% K_2O and thus plot close to the *Ne-Qz* join in this system. Most of the analcites plot between end member analcite ($NaAlSi_2O_6.H_2O$) and albite ($NaAlSi_3O_8$).

Kim and Burley (1971) showed analcite was stable only at temperatures and pressures well below nepheline - alkali feldspar minimum melt compositions. Roux and Hamilton (1976) subsequently showed that analcite was a liquidus mineral between 5-13kb and 640-600°C only. Analcite thus could not have crystallised as a primary mineral from the magmas of the Igaliko Dyke Swarm, which probably crystallised at pressures of around 2kb.

Henderson and Gibb (1977) suggested that analcite forming interstitial patches in the Dippin Sill, Isle of Arran, was formed by late stage alteration of early crystallised nepheline, as well as noting analcite forming as an alteration product of plagioclase. Henderson and Gibb (1983) subsequently showed that their earlier suggestions were probably correct and that Si-rich nepheline may convert, almost isochemically, to analcite. Analcites from the Igaliko Dyke Swarm with less *Qz* than end member analcite ($NaAlSi_2O_6.H_2O$) may have formed in such a way. Those with higher *Qz* however, may have formed by reaction of plagioclase (albite) with alkali and water-rich fluids at a late stage. Textural evidence indicates the late stage origin in all cases but it is not clear what altered/reacted with the residual fluids to form the analcite.

4.11: Cancrinite

Cancrinite is a relatively common phase in some phonolites and recrystallised phonolites being particularly abundant in some members of the Østfjordsdal dyke swarm. Plate 3.11 shows cancrinite replacing nepheline phenocrysts and Plate 3.10 shows cancrinite as a groundmass mineral. It commonly occurs by replacement of nepheline (cf. Chambers 1976), which may be only a minor alteration of the nepheline crystal margins

or wholesale alteration of the grain.

The presence of cancrinite points to a build up of CO_2 in the magma. Chambers (1976) noted calcite as interstitial patches in cancrinite bearing units of the North Qôroq syenite. Emeleus (1964) observed a sequence of increasing CO_2 marked by increasing cancrinite content in nepheline syenites from Grønnedal-Íka. Saether (1957) described a reaction series where nepheline is rimmed by cancrinite which in turn is rimmed by calcite although no relationships of this type were observed from the Igaliko samples.

The major substitution between cancrinites and vishnevites is $CO_2 \rightleftharpoons SO_4$. As S was not detected in any of these analyses it can be assumed that the samples studied here are close to end member cancrinite. There is a considerable variation in Ca and Na contents between individual samples, Ca $\rightleftharpoons$ Na being the major exchange. Cancrinites from the recrystallised phonolites show little variation in Na and Ca within individual samples (around 0.05 atoms per 24 oxygens excluding OH of both Na and Ca), whereas cancrinites from un-recrystallised rocks can show variations of up to 0.7 atoms Na and 0.1 atoms Ca within the same sample. The variation within the un-recrystallised phonolites will be due to differences in CO_2, Na and Ca contents of the late stage fluids from which they formed by alteration of nepheline. This is consistent with the incongruent melting of cancrinite to nepheline and liquid at a-P_{CO_2} of 110 bars (Deer *et al.* 1966).

From the limited data available, cancrinites from recrystallised phonolites have higher Ca than those from the unrecrystallised rocks. This is probably caused by Ca that has been liberated from feldspar (all low or free from Ca) being incorporated into cancrinite as recrystallisation proceeds. If the fluid phase present on recrystallisation is CO_2-rich, the Ca may complex with this and fluid reaction with nepheline may cause the higher Ca in cancrinites.

All but one of the analysed cancrinites are K-free (326289.19 which contains 0.143 wt% K_2O). Minor MgO (up to 0.437 wt%) was detected in 2 samples and FeO (0.283 wt%) was detected from only one.

4.12: Sphene

Sphene is a relatively common mineral occurring throughout the Igaliko Dyke Swarm. It is most common as discrete grains in the ultra-mafic lamprophyre (mica-pyroxenites etc.) but also occurs commonly in other lamprophyres (eg. those of nephelinitic and tephritic/benmoreitic compositions), BFDs and hawaiites/mugearites, benmoreites and phonolites. In these more evolved rocks it is usually observed as a clear rim to opaque oxide grains, this being indicative of relatively high fo_2 (Carmichael and Nicholls 1969). These rims will have formed by reaction/oxidation of the oxide at a late stage.

Many analyses (see Appendix II) appear to have components of both sphene and iron oxide. This is probably due to either a partial replacement of the original oxide grain by sphene along fractures etc. or an analysis which overlapped both sphene and oxide. Those sphenes showing more than about 2 atoms per 20 oxygen of Fe will be such analyses. 46256.36 with 7.5 atoms of Ti and ca. 1.4 atoms of Ca and Si, would appear to be a rutile which has reacted in a similar way. In these cases Si≈Ca and a sphene component can be removed from the analysis leaving an iron oxide residue.

Sphene may be an important host for minor elements such as Nb, Ta and Rare Earth Elements (REE). Analysis by EDS microprobe showed several grains contained appreciable amounts of Nb. This was visible from the 'running display' of the X-ray spectrum generated at the time of the analysis, but as the probe used was not calibrated for Nb, it could not be analysed.

Crystal Chemistry

Ideally sphene should have the formula $CaTiSiO_4(O,OH,F)$. Ca can be substituted by Na usually in minor amounts. K also may substitute for Ca although this is rarely reported (Smith 1970). The analyses from the dykes, by comparison to those reported by Smith (1970), show considerably greater contents of Na and K and this may be an artefact of EDS analysis.

REEs will also occupy the Ca site. Exley (1980) found that in REE-rich sphenes (titanites) from Skye granites a coupled substitution of $Ca^{2+}_{2n} + Ti^{4+}_{n} \rightleftharpoons REE^{2+}_{2n} + Fe^{2+}_{n}$ was required. U and Th will also substitute into the 7-coordinated Ca site.

Al is often assigned to the tetrahedral site along with Si. Ribbe (1982) contends that this is for the most part unjustified. Rosenberg (1974) suggested that synthetic sphenes may hydroxylate with decreasing temperature by $\sqcup + 4H^+ \rightleftharpoons Si^{4+}$ (where $\sqcup$ represents a vacancy) or by $Al^{3+} + H^+ \rightleftharpoons Ti^{4+}$. This exchange mechanism may account for the low Si in some of the sphenes from the dykes. In many cases however, where Si<4 atoms and Ti+Al>4, then Si+Ti+Al≈8 which may imply tetrahedrally coordinated Al, as well as Al substituting for Ti with hydroxylation.

The Ti site can also be occupied by Nb^{5+} and Ta^{5+} with charge balancing being achieved by substitution of Al and Fe^{3+} into the Ti site. Thus, sphenes may be the host for many of the rarer elements throughout the range of compositions of the dykes.

Mg was detected in those analyses that showed high iron contents and is thus probably part of the iron oxide component of the analysis.

Zr was detected in about a quarter of the samples, occurring in quantities up to 2.49 wt%. Zr is assumed to substitute for Ti.

4.13: Others minerals

Chlorite

Chlorite is a relatively common alteration product caused by hydrothermal breakdown of many of the ferro-magnesian minerals. It occurs throughout the whole range of dyke compositions. Chlorite is often seen as a pale green rim to many of the ferromagnesian minerals, especially biotite, where its origins may be very late stage magmatic. Chlorite generally reflects the Fe/Mg ratio of the mineral it replaces. In some of the more iron-rich chlorites, the normal pale green colouration has been replaced by a pale brown pleochroic scheme. Mn contents tend to be higher in the chlorite of the more fractionated rock types reflecting, to an extent, bulk rock Mn content. Some analyses contain up to 3.67 wt% K_2O and this presumably results from incomplete alteration of biotite to chlorite.

Scapolite

3 analyses of scapolite were made, 2 from a recrystallised trachyte and one from a

phonolite. These analyses are all devoid of K and contain about 15 wt% CaO and 5 wt% Na_2O. Scapolite is not a primary mineral of igneous rocks, being more common in medium and high grade metamorphic rocks such as amphibolites and gneisses. In these environments its formation would seem to be controlled by the presence of CO_2 in a reaction with plagioclase:-

$$3CaAl_2Si_2O_8 + CaCO_3 \longrightarrow Ca_2Al_6Si_6O_{24}CO_3$$

ie. anorthite + calcite $\longrightarrow$ meionite. A late stage build up of CO_2 in the phonolite (evidenced in some by the presence of cancrinite) may react with any plagioclase (oligoclase/albite) to produce scapolite. A similar mechanism, with Ca being liberated in the recrystallisation of feldspars (and possible addition of volatiles in the thermal aureole of the Late Igdlerfigssalik syenites) may produce scapolite in the recrystallised trachyte. An exchange of CaAl $\rightleftharpoons$ NaSi as in plagioclases will cause variation in Ca and Na contents.

Gieseckite

Gieseckite is a common alteration product of nepheline (see Chapter 3). Of the 12 analysed gieseckites, 11 are from recrystallised rocks. Si and Al contents are similar to those of nepheline (44-49 wt% SiO_2 and 30-34 wt% Al_2O_3). The major difference from the composition of nepheline is a change in alkali metal content. Nephelines contain approximately 16 wt% Na_2O and 5-6 wt% K_2O. In gieseckites the alkali contents are erratic with K_2O almost always greater than Na_2O. K_2O ranges from 6-9 wt% and Na_2O from 2-9 wt% in gieseckites. Ca contents are higher than those of nepheline, with CaO being detected in all analysed samples to a maximum of 1.11 wt%. Compositionally, gieseckite approaches muscovite by the removal of Na and an increase in K and $(OH)^-$ from nepheline. Hot, hydrous fluids introduced into the recrystallised dykes during the metamorphic event will be the cause of this hydration/alteration. Late magmatic fluids may also cause similar compositional change in nephelines. The increase in K_2O over nephelines may imply that these fluids are K enriched and Na depleted, effecting Na removal as well as perhaps K$\rightleftharpoons$Na exchange in the altering nepheline. Gieseckite is often stained a rust-brown colour, presumably caused by the minor contents of Fe detected in nearly all analyses.

'Glass'

325923 is a phonolitic rock which contains 'stringers' of a devitrified glassy material enclosed in a groundmass of very fine-grained feldspar, amphibole and chlorite. The margin of the dyke is illustrated in Plate 4.1.

The 'glass' is pale brown and almost isotropic. No separation of 'glass' could be obtained for study by XRD to determine any microcrystalline mineralogy. 8 microprobe analyses of this glass were made. Its composition is generally that of phonolite or phonolitic tephrite with one analysis (325923.16) of phonolitic nephelinite composition (by total alkalis - silica classification of Cox *et al.* 1979).

There is a significant difference between the 'glass' composition and the whole rock composition. Table 4.13.1 compares average compositions of the 'glass' analyses with the whole rock major element compositions.

Table 4.13.1

	Whole rock	Avg. Excluding 325923.16	Avg. Including 325923.16
SiO_2	56.66	53.424	52.227
TiO_2	0.48	0.360	0.360
Al_2O_3	20.13	22.131	22.023
FeO	6.28	2.27	3.839
MnO	0.34	0.0	0.0
MgO	0.59	0.0	0.532
CaO	0.80	0.219	0.218
Na_2O	7.35	11.177	10.92
K_2O	4.57	0.839	0.777

These glassy 'stringers' probably represent rapidly quenched residual liquids after crystallisation of about 50% of the liquid (from modal evidence) to K-rich feldspar and Fe-rich amphibole (subsequently altered to chlorite). These minerals would, depending on the proportions crystallising, deplete the magma in Si, Ca, K, Mg, Fe and enrich the residual liquid in Na and Al. Textural evidence suggests some brecciation of the 'glass'. Quenching could have been achieved by rapid emplacement after some

crystallisation elsewhere and this may have entrained the 'stringers' of 'glass' in a crystalline mush. Spherical 'holes' in the 'glass' suggest vesiculation and it is very tempting to apply ignimbrite terminology to these 'glassy stringers'. These 'stringers' bear a striking resemblance to the explosively intruded felsites seen in many of the British Tertiary Volcanic Centres (eg. Rhum), although none possess typical cuspate 'shard' morphologies.

Pseudoleucite

Pseudoleucite has been described from a phonolite dyke cropping out ca. 0.8km WSW of Igaliko village (Hesselbo, 1983, 1986). Samples were collected from this dyke by this author and brief description will be given. For more detail the reader is referred to Hesselbo (1986).

The pseudoleucites show icositetrahedral faces, ie. from the cubic system. They are up to about 10cm in diameter and are quite abundant within the sampled dyke, (325905A - pseudoleucites, 325905 - host phonolite dyke, see Plate 4.2).

Petrographically these pseudoleucites consist of radial intergrowths of feldspar and nepheline (now altered to sericite and K-rich cancrinite), some white mica (possibly muscovite or gieseckite), minor amphibole and scapolite. Small blebs of groundmass material have been enclosed by these large crystals. Iron oxides, with chlorite rims, occur as irregular patches possibly replacing ferro-magnesian minerals.

Hesselbo (1986) reports a loss of alkalis with little or no change in Si/Al/O ratio from the original leucite. He concluded that a sub-solidus reaction took place in the leucite to cause nucleation of nepheline and alkali feldspar from cracks, crystal faces and inclusions within the crystal. This occurred after the matrix of the dyke had solidified and was probably a response to increasing fluid pressure, these fluids being responsible for the change in alkali content.

Pseudoleucites were not seen in any other members of the Igaliko Dyke Swarm, their occurrence being limited to this dyke only.

Plate 4.1: Margin of Dyke 325923 showing its contact with syenite in Motzfeldt. 'Glassy' stringers are visible running parallel to the contact. Coin approximately 1cm diameter.

Plate 4.2: Large pseudoleucites (white 'balls') in host phonolite 325905, about 0.8km WSW of Igaliko village. Scale on hammer shaft in inches.

Garnet

Garnet was found in 3 samples - a carbonatite (326333), an ultra-mafic lamprophyre (41906) and a recrystallised phonolite from Østfjordsdal (326289). Each occurrence will be dealt with in the relevant chapter later.

Sundries

Apatite was only rarely analysed. Pyrite occurs in several of the more basic samples, as do Fe-Ni-Zn-Cu sulphides in some of the lamprophyres. Perovskite was identified in lamprophyres and is discussed later.

Zircon occurs sporadically in some phonolites, usually containing detectable (by EDS) quantities of Hf.

Full analyses of these and other accessory minerals are given in Appendix II.

4.14: Mineral - Mineral Geothermometers

4.14A: Fe-Ti oxide

One of the most widely used geothermometers for fast cooled rocks is an iron - titanium geothermometer - oxygen barometer such as that of Buddington and Lindsley (1964). In Chapter 4.6 it was shown that the only coexisting magnetite - ilmenite pair within the range of the Buddington and Lindsley geothermometer - oxygen barometer was from a coarsely exsolved grain and thus is of no use as an indicator of liquidus temperature and fo_2. Much doubt has recently been cast upon the use of the Fe-Ti oxide geothermometer as different methods of recalculation or different geothermometers produce grossly different results. The results from the only sample within the range of ant of these geothermometers (46233, a syeno-gabbro) gave the following results:-

Buddington and Lindsley (1964)	965°C	$fo_2=10^{-12.8}$
Powell and Powell (1977)	910°C	$fo_2=10^{-29}$
Spencer and Lindsley (1981)	760°C	$fo_2=10^{-17.4}$

and confirm the variation between models (see also Stephenson and Upton 1982). No conclusions can be drawn from this other than the temperature of the liquid magma may have been above 780°C, 910°C or 965°C and the fo_2 may have been greater than

$10^{-12.8}$ on emplacement.

4.14.B: Olivine - Clinopyroxene

An indication of the likely liquidus temperature of several of the dykes can be obtained where olivine exists with clinopyroxene. Powell and Powell (1974) developed a geothermometer based on a regular solution model of the iron - magnesium exchange reaction between olivine and Ca-rich pyroxene. This reaction is partly dependent on the trivalent cations in the pyroxene and thus the analyses should be recalculated after the method of Powell and Powell (1974). This method has been criticised by Wood (1976) who considers that there are considerable uncertainties in the calibration of this geothermometer. However, Powell (1978) defends her use of this for the olivines and pyroxenes from Igdlerfigssalik maintaining that these data are within the range of the calibration data (with the exception of Mn which should have little effect). Chambers (1976) and Jones (1980) employed this geothermometer to obtain estimates of liquidus temperatures of North Qôroq and Motzfeldt magma respectively. This geothermometer has a pressure dependence of about 5°C/kb and an estimate of pressure is required in the calculation. For all results reported in Table 4.14.1 a pressure of 2kb was selected. Minimum and maximum estimates of temperature were calculated for those samples where zoned crystals coexisted by using core and rim compositions or phenocryst and groundmass. This geothermometer is not applicable to high Na clinopyroxenes and thus aegirine-augite/aegirine-hedenbergite crystals were not considered in any of the calculations.

From Table 4.14.1 a wide range of temperatures is recorded for each group although almost all temperatures are in excess of 1000°C. As olivine and pyroxene are generally early phases to crystallise these temperatures may represent minimum liquidus temperatures.

Average temperatures for each group show an expected decrease in liquidus temperature from basaltic magmas through to phonolitic magmas, although this may seem quite a narrow range between the least and most evolved magmas.

Table 4.14.1

Temperatures calculated using olivine - clinopyroxene geothermometer of Powell and Powell (1978).

Sample	Rock type	Temp. (C)	Sample	Rock type	Temp. (C)
59631	gabbro	1043°-1036°	325980	BFD	1040°
58065	gabbro	1062°-1058°	58290	BFD	1030°-1019°
58017	sy-gab	1019°-1018°	63810	BFD	1020°-1018°
46233	sy-gab	1024°-1022°	58224	phon	1007°
59632	sy-gab	1036°	58003	phon	1019°
326241	haw/mug	1030°-1030°	141233	phon	1029°
41954	haw/mug	1029°	63751	phon	1028°-1027°
126772	ben	1036°-1035°	326256	phon	1010°
46237	ben	1050°	average	gabbro	1050°±12°
52298	ben	1038°	average	sy-gab	1024°±7°
59779	ben	1021°-989°	average	haw/mug	1030°±1°
59741	ben	1033°	average	BFD	1025°±9°
46253	ben	1000°-987°	average	ben	1024°±19°
59660	ben	1031°-1029°	average	phon	1020°±10°
52247	ben	1033°-1027°			

Abbreviations. ben: benmoreite, sy-gab: syeno-gabbro, haw/mug: hawaiite/mugearite, phon: phonolite.

4.14.C: Nepheline - Alkali Feldspar

Powell and Powell (1977) also developed a geothermometer based upon equilibration between nepheline and alkali feldspar. This requires recalculation of nepheline analyses into *Ks* and *Qz* and comparison of *Qz* for nephelines against X_{Na} for feldspar at the given *Ks* content of the nepheline. Powell and Powell (1977) consider errors in this method to be in the range ±70-130°C and thus the data must be regarded accordingly. Table 4.14.2 shows the calculated equilibration temperatures using this geothermometer.

Many of the nephelines contained *Ks* above the range of the geothermometer quoted by Powell and Powell. The geothermometer is only applicable where Ca is >1.00 wt% in

Table 4.14.2

Temperatures calculated using the nepheline - alkali feldspar geothermometer of Powell and Powell (1977).

Sample	Nepheline	Alk. Fsp.	Temp (C)	Rock Type
59636	Ph	Ph	880°	Phonolite
304006	Ph1	Ph1	780°	Phonolite
	Ph1	Ph2	890°	
58224	Ph1	Ph2	810°	Phonolite
	Ph1	Ph2	760°	
58015	Gm	Gm	850°	Tephrite
326207	Gm	Gm	950°	Haw/Mug
58019	Gm	Gm	740°	Phonolite
	Ph1	Ph1	680°	Average Ph-Ph
	Ph2	Ph1	850°	temp 770°
	Ph3	Ph1	780°	
Average Phonolite Temperature.....			797°± 68°	

Abbreviations. Ph1: phenocryst 1 etc., Gm: groundmass crystal.

the feldspars. All temperatures from coexisting nepheline - alkali feldspar pairs within the range of the geothermometer are listed in Table 4.14.2. Core compositions of crystals were used in the calculations. Table 4.14.2 also shows 'equilibration' temperatures for groundmass nepheline - alkali feldspar pairs. These may not have been in complete equilibration but may give an idea of the crystallisation temperatures of the late interstitial magmatic liquids.

A fairly wide scatter of temperatures is evident from this geothermometer within one particular group as well as from different phenocrysts within individual samples.

4.14.D: Conclusions

If the cumulus temperatures obtained from olivine and clinopyroxene approximate to the liquidus temperature and those from the nephelines - alkali feldspars are close to the solidus temperature (particularly the groundmass pairs), a combination of these results

might indicate the solidus - liquidus interval for rock types where all 4 minerals co-exist. The only rock group where this is satisfied and the analyses fall within the range of the geothermometers are the phonolites. These indicate a wide solidus - liquidus interval of about 270°C, between 1020°C (for olivine - clinopyroxene) and 750°C (typical lower temperatures from nepheline - alkali feldspar phenocryst pair). Equilibration of nepheline - alkali feldspar may have continued to around 680°C (58019), and the solidus - liquidus interval may have been as much as ca. 350°C.

Narrower solidus - liquidus intervals are shown by the hawaiites/mugearites, which would appear to be of the order of 80°C from the temperatures calculated here. Various experimental studies have shown that the melting interval (liquidus - solidus) is related to peralkalinity (eg. Sood and Edgar 1970; Piotrowski and Edgar 1970; Edgar and Parker 1974) with the more peralkaline rocks having larger melting intervals. These experiments were however conducted using natural, coarse grained cumulates, and thus would be expected to have a large liquidus - solidus interval. Intercumulus liquid, presumably highly evolved, would start melting at relatively low temperatures whereas the high-temperature cumulus mineral phases would not commence melting until considerably higher temperatures. The phenocryst temperatures obtained by various geothermometers represent the early history of the parent magma chamber, and thus crystallisation of these may have prevailed over roughly 300°C of cooling (this data). Dykes however, will cool rapidly and freeze in the inherited chemical characteristics of their constituent phenocrysts, and the results of the above melting experiments would not be directly comparable. There appear to be no similar melting studies on phonolitic rocks for comparison.

The olivine - clinopyroxene temperatures from benmoreite dykes are about 60°C higher than an average SI.4 (augite syenite Unit 4, Igdlerfigssalik centre) temperature and the phonolite dykes are about 80° higher than an average of temperatures obtained from SI.5, SI.6 and SI.7 (nepheline syenites, Powell 1978). This difference may reflect a greater degree of sub-solidus reequilibration within the central complexes. Similar temperatures to those calculated by Powell (1978) were reported by Jones (1980) from olivine - clinopyroxene pairs from Motzfeldt, and Chambers (1976) from North Qôroq.

Feldspar - nepheline equilibration temperatures reported from Igdlerfigssalik (Powell

1978) range between 1100°C to 650°C. These lower temperatures must reflect considerable re-equilibration with falling temperature. The nepheline - feldspar temperatures from the dykes range from between 890°C-680°C, with the 3 phenocryst pairs giving temperatures of between 760-780°C. Thus, with the exclusion of the unusually low 680°C temperature from 58019, most nepheline and feldspar phenocrysts did not undergo as much re-equilibration as the feldspars from Igdlerfigssalik, this reflecting the more rapid cooling of the dykes. More, lower temperature re-equilibration will be the cause of the lower temperature from 58019.

4.15: Brief Conclusions from Mineralogical Evolution

The pyroxene - amphibole mineralogy records an overall decrease in Mg/Mg+Fe with increased evolution and a general increase in Fe^{3+} and alkali content. This is consistent with a gradual increase in fo_2 from basalts through to benmoreites and thence to phonolites. Higher Mg in the biotites from phonolites than those in the benmoreites is also consistent with a higher fo_2 in the phonolites (Wones and Eugster 1965).

The stage at which peralkalinity is achieved in the magma also governs the evolution of pyroxene and amphibole. Zr builds up in the late interstitial fluids and enters pyroxenes as FM-NAZ or NAZAL end members (Jones and Peckett 1980) and amphibole as the newly defined zirconian-arfvedsonite end member.

Olivines become greatly enriched in Mn with increased Fa contents. The larnite component of olivine is shown to be dependant upon a_{SiO_2}, rocks with normative nepheline containing more Ca-rich olivines than *hy* or *qz* normative samples. The presence of olivine (and Fe-oxide) may also control the Mn content of pyroxenes and amphiboles particularly in recrystallised rocks.

The disordered structure of some alkali feldspars implies high temperature crystallisation and rapid cooling. The absence of perthitic exsolution in some of the feldspar phenocrysts (on an X-ray scale) must indicate no reheating or sub-solidus exsolution subsequent to initial crystallisation. Feldspar chemistry from unmetamorphosed rocks also implies high temperature crystallisation with little or no sub-solidus re-equilibration. In the recrystallised rocks, the alkali feldspars exsolve to separate Na and K-rich phases, expelling Ca and Ba. This Ca appears to be taken into amphibole before any obvious

signs of thermal metamorphism (such as textural change) have occurred.

Nepheline analyses show crystallisation temperatures (Hamilton 1961) in the region of 1000-700°C for various groups of rocks and these agree reasonably well with nepheline - alkali feldspar geothermometry (Powell and Powell 1977). Olivine - clinopyroxene geothermometers (Powell and Powell 1974) gives initial liquidus temperatures in the range of 1050°C (basalts) to about 1020°C (phonolites). Fe-Ti-oxides could not give any indication of liquidus temperature or fo_2. Sphene rims to many Fe-Ti oxides, once again, indicate higher fo_2 conditions in the phonolites than the benmoreites, where sphene is less common.

The presence of minerals such as cancrinite, sodalite and analcite attests to the presence of a significant volatile phase (CO_2, Cl and H_2O respectively) and low a_{SiO_2} in the more evolved rocks. Fluorite as an accessory mineral in many phonolites and benmoreites attests to a build up of F at a late stage.

CHAPTER 5: GEOCHEMISTRY

5.1: Introduction

Fine grained, igneous rocks, such as those from the Igaliko dykes, cool rapidly with little or no *in situ* fractionation or sub-solidus re-equilibration. Thus, the Igaliko dykes represent frozen magmas available in the area at the time of their emplacement. A geochemical study of the dykes can yield information about the overall magmatic evolution of the region, information which is more difficult to extract from the rocks of the central complexes due to complications introduced by post-emplacement crystal fractionation and sub-solidus re-equilibration.

The dykes analysed were in general aphyric or sparsely-phyric (5% or so modally of phenocrysts) and can almost be regarded as unmodified magmatic compositions (see Alkali Loss, Chapter 5.3). Phenocryst phases are usually higher temperature representatives of solid solution series than their groundmass equivalents. Their small volumes in the analysed samples will make little difference to the overall abundances of elements (see for example Larsen and Steenfelt 1974).

Appendix III describes analytical techniques used (major, trace and REE analyses) and tables are presented of all data acquired. REE data and its implications are considered in Chapter 6.

5.2: Classification and Presentation of Data

Fine grained igneous rocks can be difficult to classify by modal mineralogical methods such as the QAPF 'double triangle' of Streckeisen (1967, 1976, 1979). Chemical parameters, such as the total alkalis - silica (TAS) content of igneous rocks have been used in attempts to produce a classification of (particularly fine grained) igneous rocks. These TAS classification schemes should be used where no modal mineralogical data is available, which must remain as the primary method of classification if possible (Le Bas *et al.* 1986). Due to the large numbers of samples studied in this work, it was decided to classify these rocks by a TAS method.

Cox *et al.* (1979) proposed one such scheme that has been used widely in recent years, but this was based on a relatively small data set. Le Bas *et al.* (1986) acting

on behalf of the IUGS Subcommision on the Systematics of Igneous Rocks, proposed a different TAS classification based on the CLAIR and PETROS data bases (Le Maitre 1982) which contain some 24000 chemical analyses of fresh volcanic rocks.

The major differences in these schemes are in the classification of trachy-basaltic and trachy-andesitic rock types. Both classification schemes are illustrated in Figure 5.2.1, with all analyses from the Igaliko dykes plotted on each diagram.

From Figure 5.2.1 it can be seen that the analyses of the Igaliko dykes fit more 'neatly' into the Cox *et al.* (1979) TAS classification scheme. The Cox *et al.* scheme returns most of the dykes from Igaliko as benmoreites and phonolites, whereas the Le Bas *et al.* scheme would classify these clusters as trachy-andesite (Na-rich = Benmoreite), Tephri-phonolite, Phonolite and Trachyte - an all round more cumbersome nomenclature, despite its better statistical foundations. Both schemes possess 'sub-root' names to be assigned within one group, dependant on K/Na - eg. the K-rich equivalent of benmoreite is latite, K-rich mugearite is shoshonite. For simplicity, and due to the limited number of symbols available in computerised graph plotting packages, only the Na-rich names have been used. These tend to be the dominant varieties encountered.

Most of the newly acquired geochemical data are presented as X-Y, or triangular diagrams of 2 or 3 variables/ratios, or as 'spidergrams'. A Fractionation Index (F.I.) is used, based essentially on the Thornton and Tuttle (1960) Differentiation Index plus normative acmite and quartz (Macdonald 1969). This F.I. has been used by previous workers (Stephenson 1973, Chambers 1976, Jones 1980). This is a better indicator of fractionation than SiO_2 (eg. Harker diagrams) for these alkaline rocks as SiO_2 does not necessarily increase (and may decrease) with increasing fractionation, particularly from benmoreite to phonolite. The inclusions of normative acmite in the F.I. recognises the importance of increasing peralkalinity with increased fractionation.

Normative mineralogy is dependent on the Fe_2O_3/FeO ratio of the rock. A selection of the dykes covering the compositional range observed were selected for FeO determination. These results were coupled with the Fe_2O_3/FeO ratios determined by Stephenson (1972), Chambers (1976), Jones (1980), Larsen and Steenfelt (1974) and Macdonald (1969, 1970) to produce a grid of Fe_2O_3/FeO in TAS space. The Le Bas *et al.* (1986)

Figure 5.2.1. – (3 pages)

A. TAS classification of Cox *et al.* (1979). This scheme has been used for classification of the fine grained rock types of the Igaliko dykes. Additional to this scheme, the Si-poor range has been divided upon petrography into carbonatites (group 17) and ultramafic lamprophyres (UML, group 16). The 4 UMLs with $SiO_2 \approx 15$ wt% are carbonate - biotite - oxide - clinopyroxene assemblages.

Key:-

1. Basalt
1a. Picritic Basalt
2. Hawaiite
3. Mugearite
4. Benmoreite
5. Trachyte
6. Phonolite
7. Rhyolite
8. Basaltic Andesite
9. Andesite
10. Dacite
11. Trachy-andesite
12. Tephrite/Basanite
13. Phonolitic Tephrite
14. Nephelinite
15. Phonolitic Nephelinite
16. Ultramafic Lamprophyre
17. Carbonatite

'Basaltic andesite' represents the plagioclase xenoliths from the BFD's.

B. TAS classification of Le Bas *et al.* (1986) – overleaf.

Key:-

B Basalt (0.2)
P_c Picro-basalt (0.1)
O_1 Basaltic andesite (0.5)
O_2 Andesite (0.6)
O_3 Dacite (0.65)
R Rhyolite (0.75,1.4)
S_1 Trachy-basalt (0.3)
S_2 Basaltic trachy-andesite (0.51)
S_3 Trachy-andesite (0.58)
T Trachyte (0.66)
U_1 Basanite/Tephrite (0.36)
U_2 Phonotephrite (0.5)
U_3 Tephri-phonolite (0.6,1.5,2.0)
Ph_a Phonolite (0.8,1.5,2.0)
Ph_b Phonolite (1.0,1.5,2.0)
F Foidite (2.0)

This scheme was used to assign Fe_2O_3/FeO ratios to individual samples. The line separating S fields from U fields closely parallels the critical plane of Si saturation for Gardar rocks (Upton 1974). As Fe_2O_3/FeO ratio is controlled to some extent by degree of alkalinity (and Si-saturation) this scheme may better represent changes in Fe_2O_3/FeO through an evolving rock suite and thus was chosen to assign Fe_2O_3/FeO. The values of the Fe_2O_3/FeO ratio used are shown in the above table. This first figure is for non-peralkaline samples, the second for $1 <$ peralkalinity < 1.2, and the third for peralkalinity > 1.2. The division of phonolite into *a* and *b* is done solely for assignment of Fe_2O_3/FeO ratios and is not part of the Le Bas *et al.* (1986) scheme.

C. – Third page. TAS plot of all analyses from Igaliko with compositions of typical mineral phases from these rocks (after Upton 1974). Also shown are the oversaturated and undersaturated minima in the system Ne - Ks - Qz (from Hamilton and Mackenzie 1965).

Figure 5.2.1A

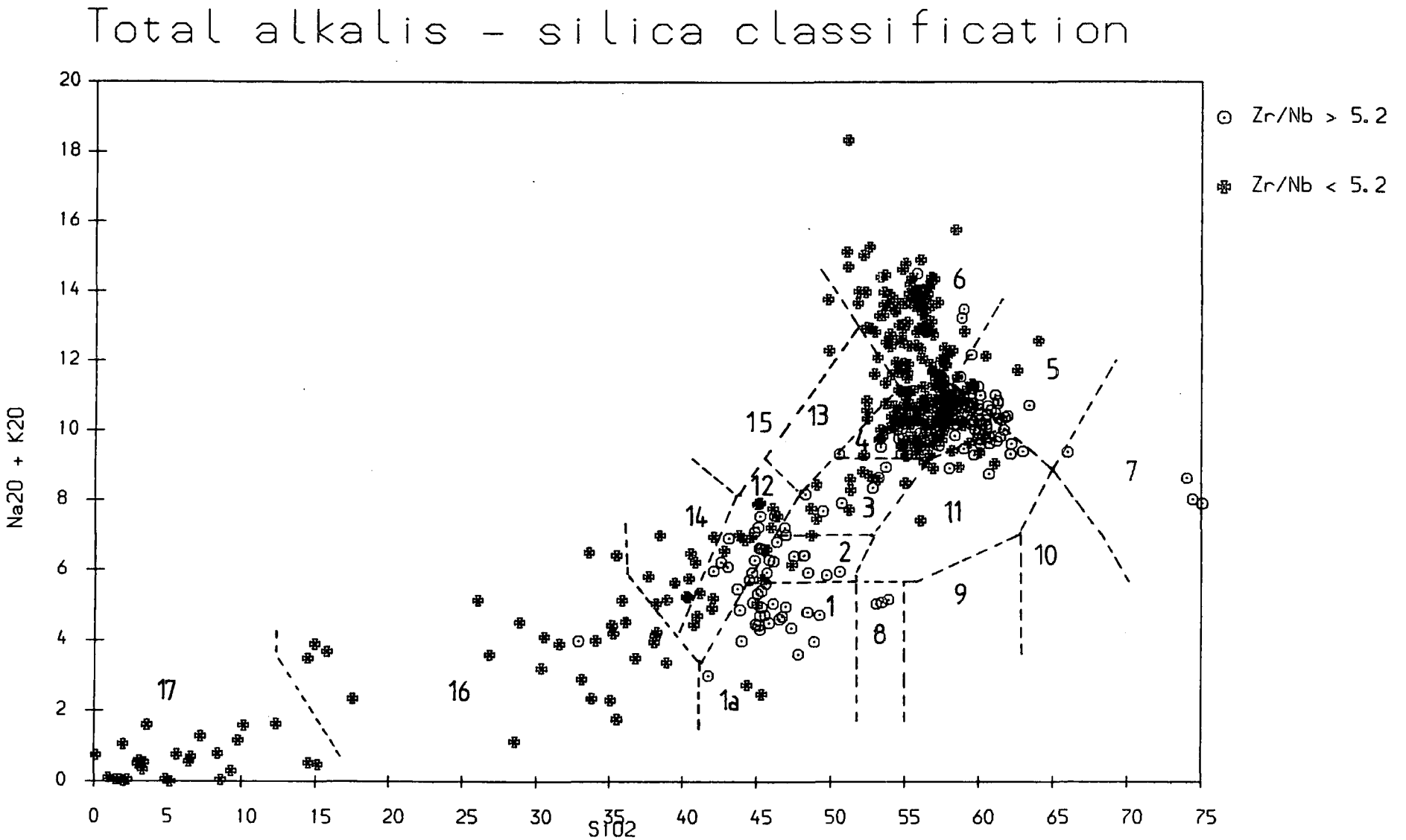
Total alkalis - silica classification
Na2O + K2O
SiO2
Zr/Nb > 5.2
Zr/Nb < 5.2
0
2
4
6
8
10
12
14
16
18
20
0
5
10
15
20
25
30
35
40
45
50
55
60
65
70
75
1
1a
2
3
4
5
6
7
8
9
10
11
12
13
14
15
16
17

Figure 5.2.1B

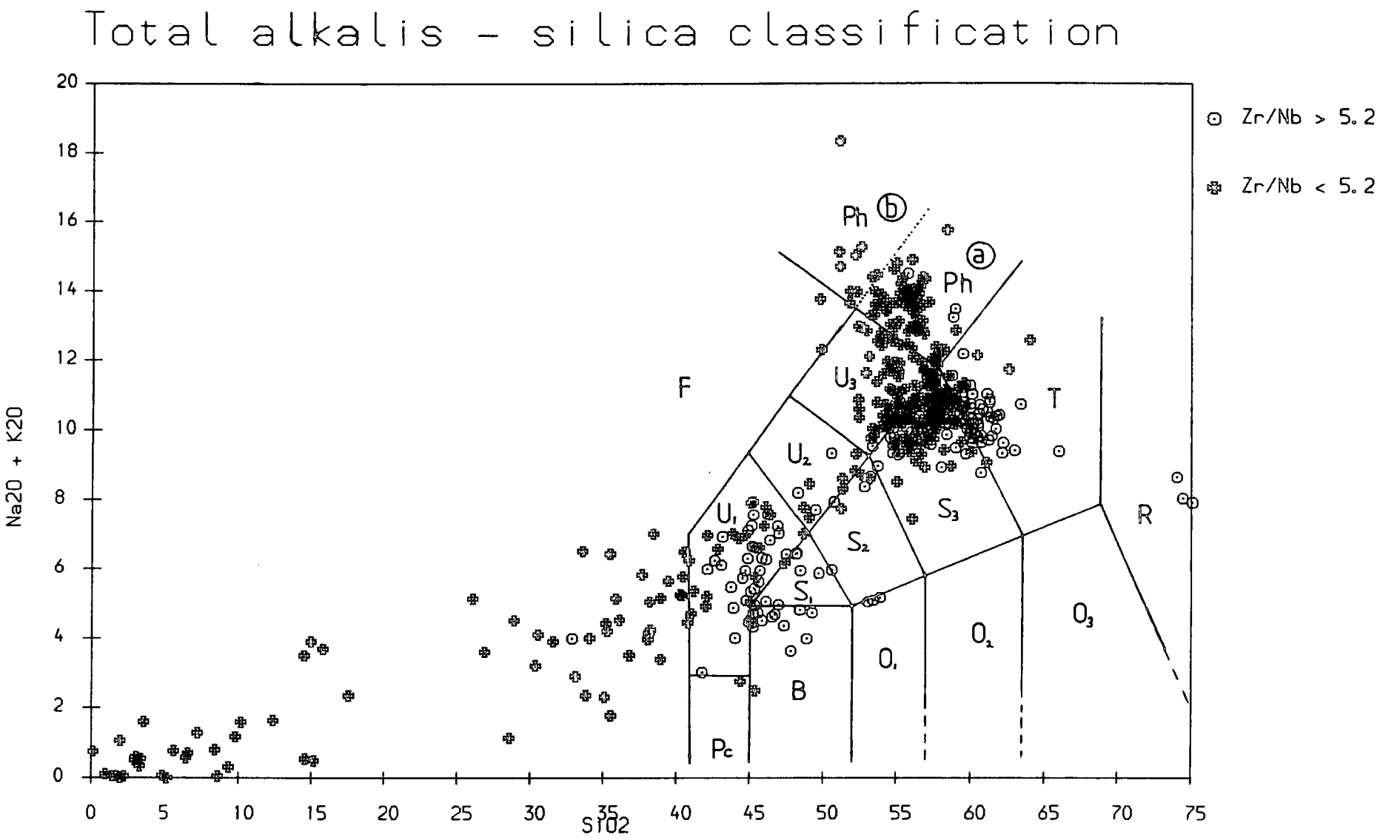
Total alkalis - silica classification
Zr/Nb > 5.2
Zr/Nb < 5.2
Na20 + K20
SiO2
Ph
b
a
Ph
F
U3
T
U2
U1
S3
S2
S1
R
B
Pc
O1
O2
O3
0
2
4
6
8
10
12
14
16
18
20
0
5
10
15
20
25
30
35
40
45
50
55
60
65
70
75

Figure 5.2.1C

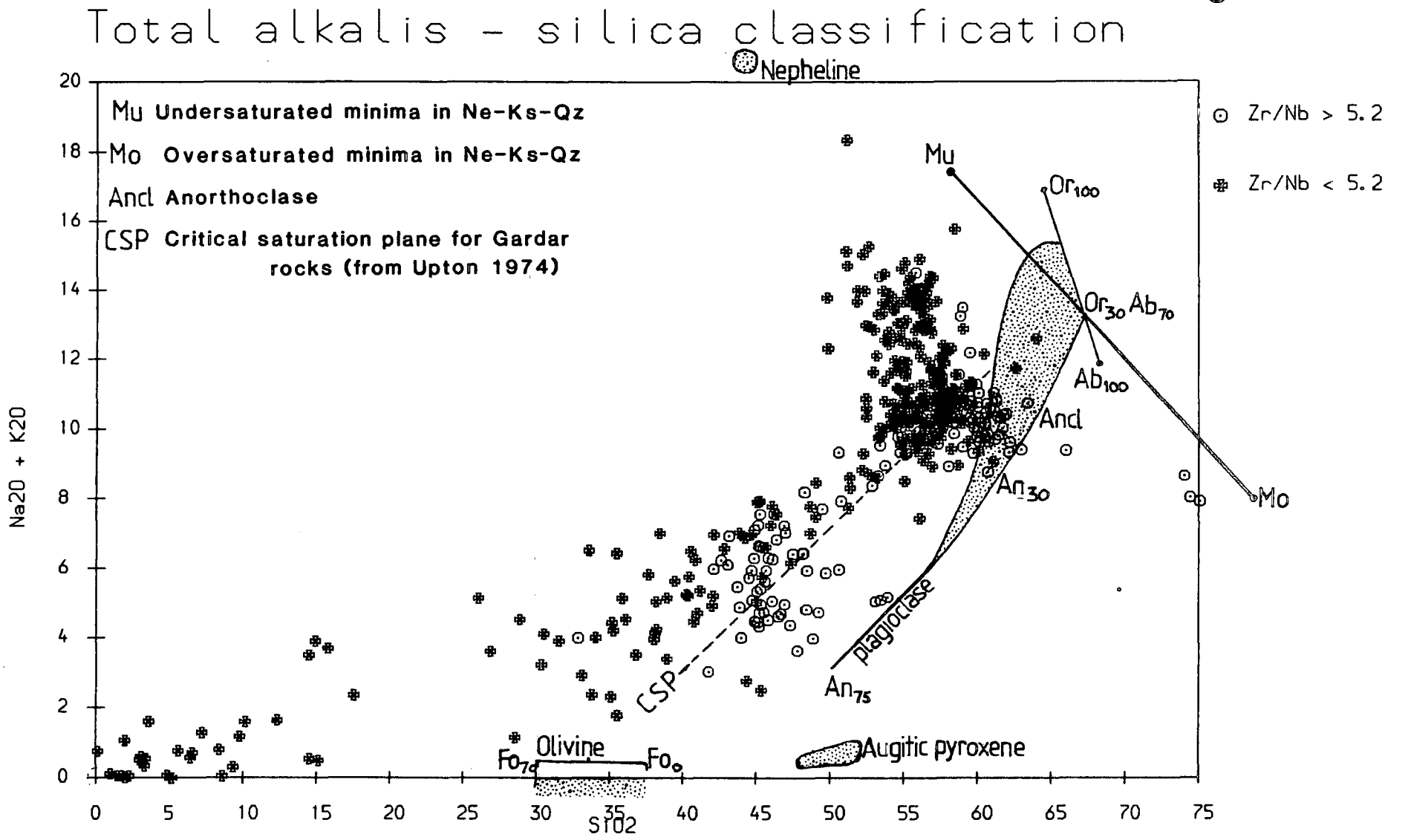
Total alkalis – silica classification
Nepheline
Mu Undersaturated minima in Ne-Ks-Qz
Mo Oversaturated minima in Ne-Ks-Qz
Ancl Anorthoclase
CSP Critical saturation plane for Gardar rocks (from Upton 1974)
Zr/Nb > 5.2
Zr/Nb < 5.2
Mu
Or100
Or30 Ab70
Ab100
Ancl
An30
Mo
plagioclase
An75
CSP
Olivine
Fo70
Fo0
Augitic pyroxene
Na2O + K2O
SiO2
0
2
4
6
8
10
12
14
16
18
20
0
5
10
15
20
25
30
35
40
45
50
55
60
65
70
75

TAS classification (unlike that of Cox *et al.*, 1979) effectively separates undersaturated, saturated and oversaturated rock types, with the undersaturated/saturated boundary comparing closely with the trace of the critical saturation plane for Gardar rocks (from Upton 1974, see Figure 5.2.1). Thus, the Le Bas *et al.* (1986) classification was used to assign an Fe_2O_3/FeO ratio averaged for each Le Bas *et al.* compositional range from the above mentioned data. Higher Fe_2O_3/FeO ratios were assigned to peralkaline rocks within certain groups, these being separated into miaskitic ($1<$peralkalinity<1.2) and agpaitic (peralkalinity≥ 1.2) varieties. Where data were absent for a particular group interpolations were made from the nearest neighbours with similar degrees of silica saturation. In this way reasonably representative CIPW Norms could be calculated.

Despite the general heading of this section – 'Basalts to Phonolite and Rhyolite' – all rock groups will be plotted on many of the following diagrams to aid comparison and remove the need to repeat certain diagrams in later chapters. The name given to a sample is that of the sodic Cox *et al.* (1979) TAS classification. The 3 samples which classify as basaltic-andesites in this scheme are plagioclase xenocrysts from BFD's. BFD hosts have not been discriminated – they are almost entirely hawaiites or mugearites, with minor tephritic and mugearitic compositions reported.

5.3: Element Variation

Figure 5.3.1 shows all major element data plotted against the Fractionation Index of Macdonald (1969), ie. normative $Ab + Or + Ne + Q + Ac + Ns$, rather than against SiO_2 or MgO which show a very restricted range in the more fractionated rocks.

It is no surprise that elements such as Si, Al, Na and K increase and Mg, Fe and Ca decrease with increasing F.I. as it is these elements which govern the normative quantities of felsic and mafic minerals respectively and thus F.I.. They must therefore behave in this manner by the very nature of the index against which they are plotted. These diagrams serve however, to indicate the ranges of these elements found and the abundance of the variously fractionated rock types. Similar diagrams were used by Stephenson (1972) and Chambers (1976) – with all of their data ranging between F.I.'s of 53-94 and 66-94 respectively. Figure 5.2.1C shows TAS data from the dykes with the compositional fields of typical phenocryst phases marked. Also shown is the critical

Figure 5.3.1 (3 pages)

Major elements plotted against Fractionation Index (F.I.) for all samples (including carbonatites and lamprophyres). The F.I. is taken from Macdonald (1969) and is defined as the sum of the normative components FI = $ab + or + ne + q + ac + ns$. The range of F.I.'s shown by individual groups of rocks is shown at the foot of the first page. Certain elements are included twice (eg. TiO_2, P_2O_5) so that the whole range can be covered and observed relatively clearly. Due to the large amount of data from the evolved groups some 'blacking out' of the range of FI 70-90 is observed. Inferences as to the rock types involved can be made from the diagram showing the range of FI's observed within each group. F and Cl are also included with the major elements, and peralkalinity is also plotted against FI. There are only a very few rocks with peralkalinity > 1.3.

Figure 5.3.1A

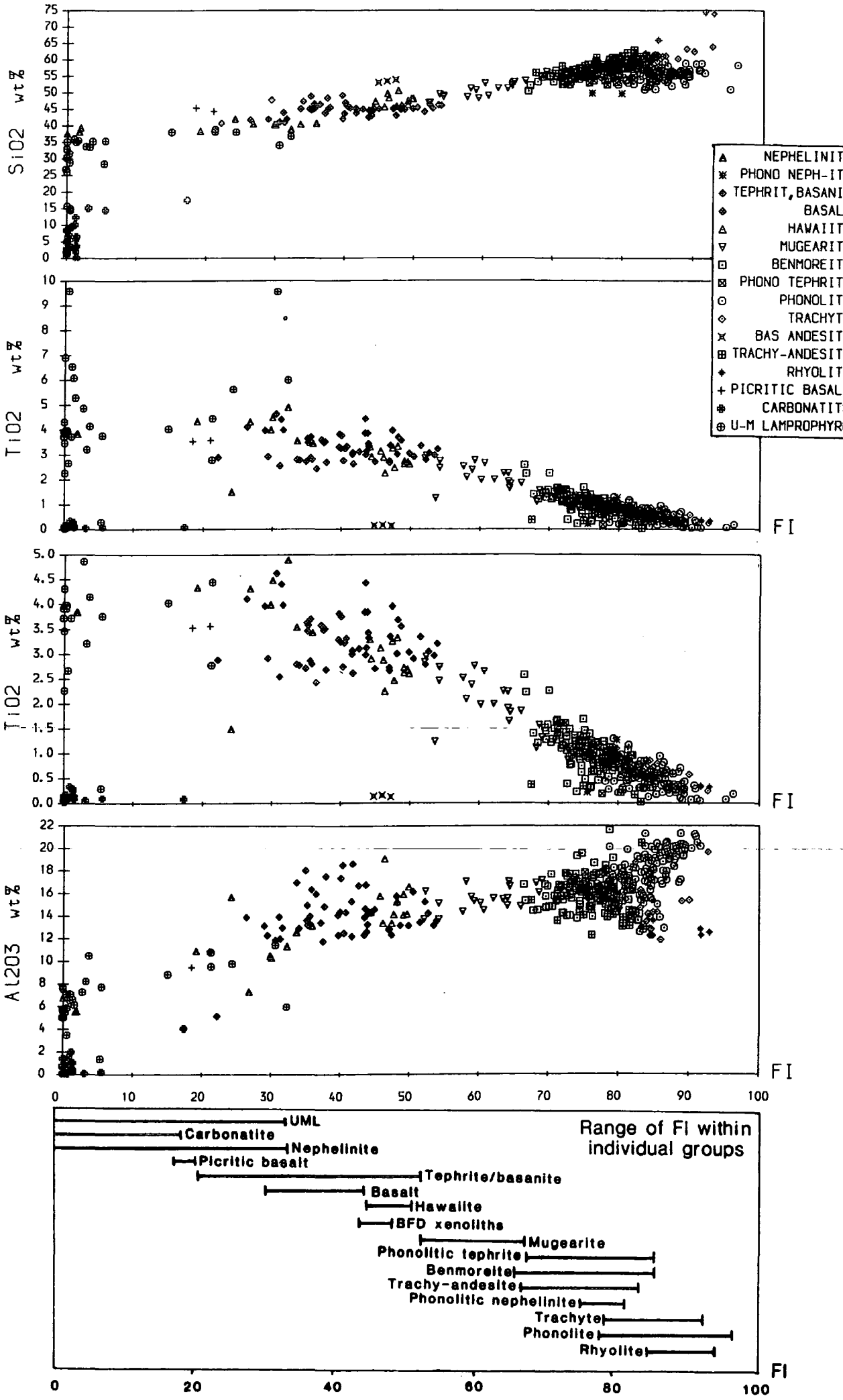
SiO2 wt%
TiO2 wt%
TiO2 wt%
Al2O3 wt%
FI
NEPHELINIT
PHONO NEPH-IT
TEPHRIT, BASANI
BASAL
HAWAIIT
MUGEARIT
BENMOREIT
PHONO TEPHRIT
PHONOLIT
TRACHYT
BAS ANDESIT
TRACHY-ANDESIT
RHYOLIT
PICRITIC BASAL
CARBONATIT
U-M LAMPROPHYR
Range of FI within individual groups
UML
Carbonatite
Nephelinite
Picritic basalt
Tephrite/basanite
Basalt
Hawaiite
BFD xenoliths
Mugearite
Phonolitic tephrite
Benmoreite
Trachy-andesite
Phonolitic nephelinite
Trachyte
Phonolite
Rhyolite

Figure 5.3.1b

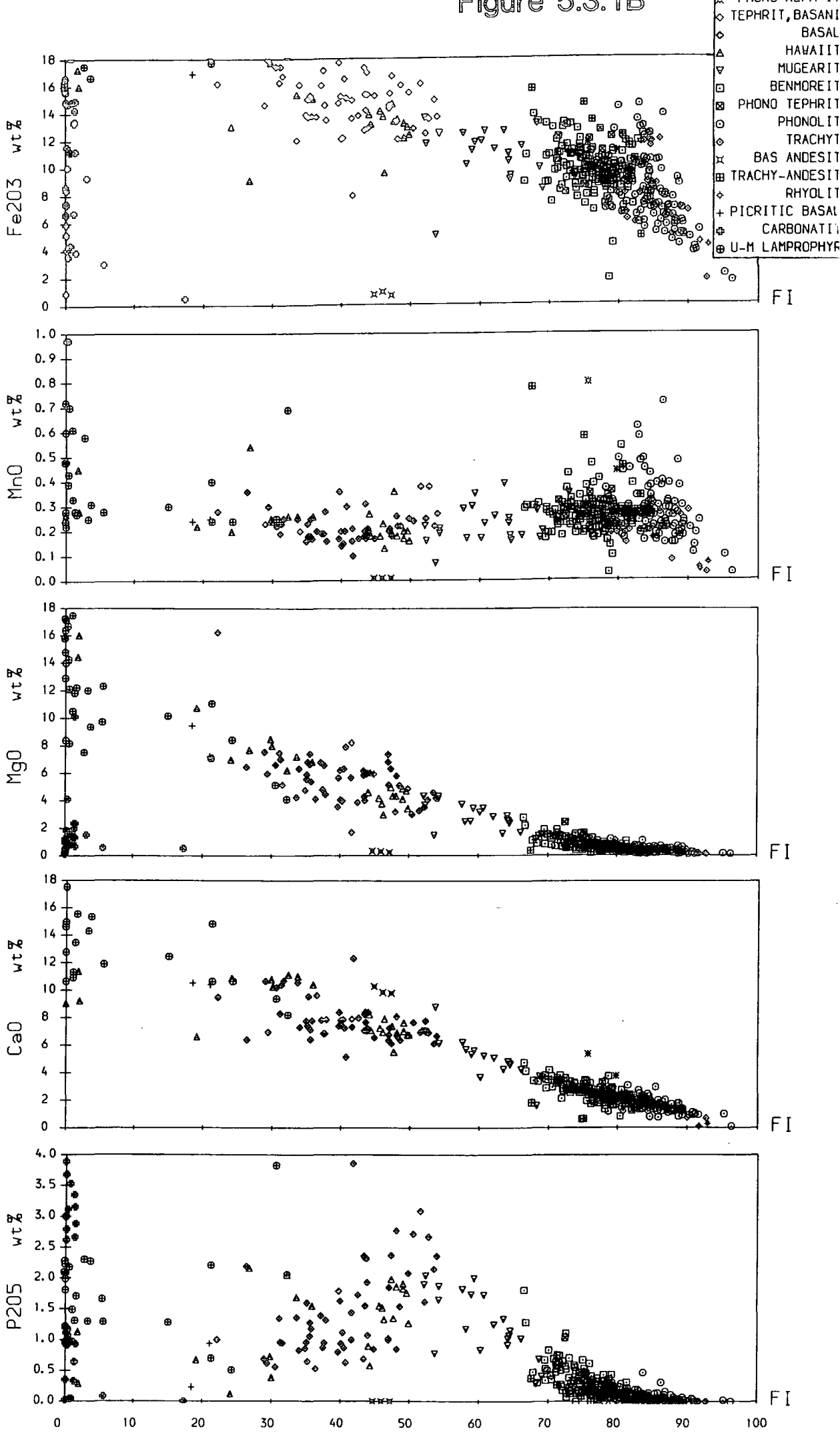
TEPHRIT, BASANI
BASAL
HAWAIIT
MUGEARIT
BENMOREIT
PHONO TEPHRIT
PHONOLIT
TRACHYT
BAS ANDESIT
TRACHY-ANDESIT
RHYOLIT
PICRITIC BASAL
CARBONATI
U-M LAMPROPHYR
Fe2O3 wt%
MnO wt%
MgO wt%
CaO wt%
P2O5 wt%
FI

Figure 5.3.1C

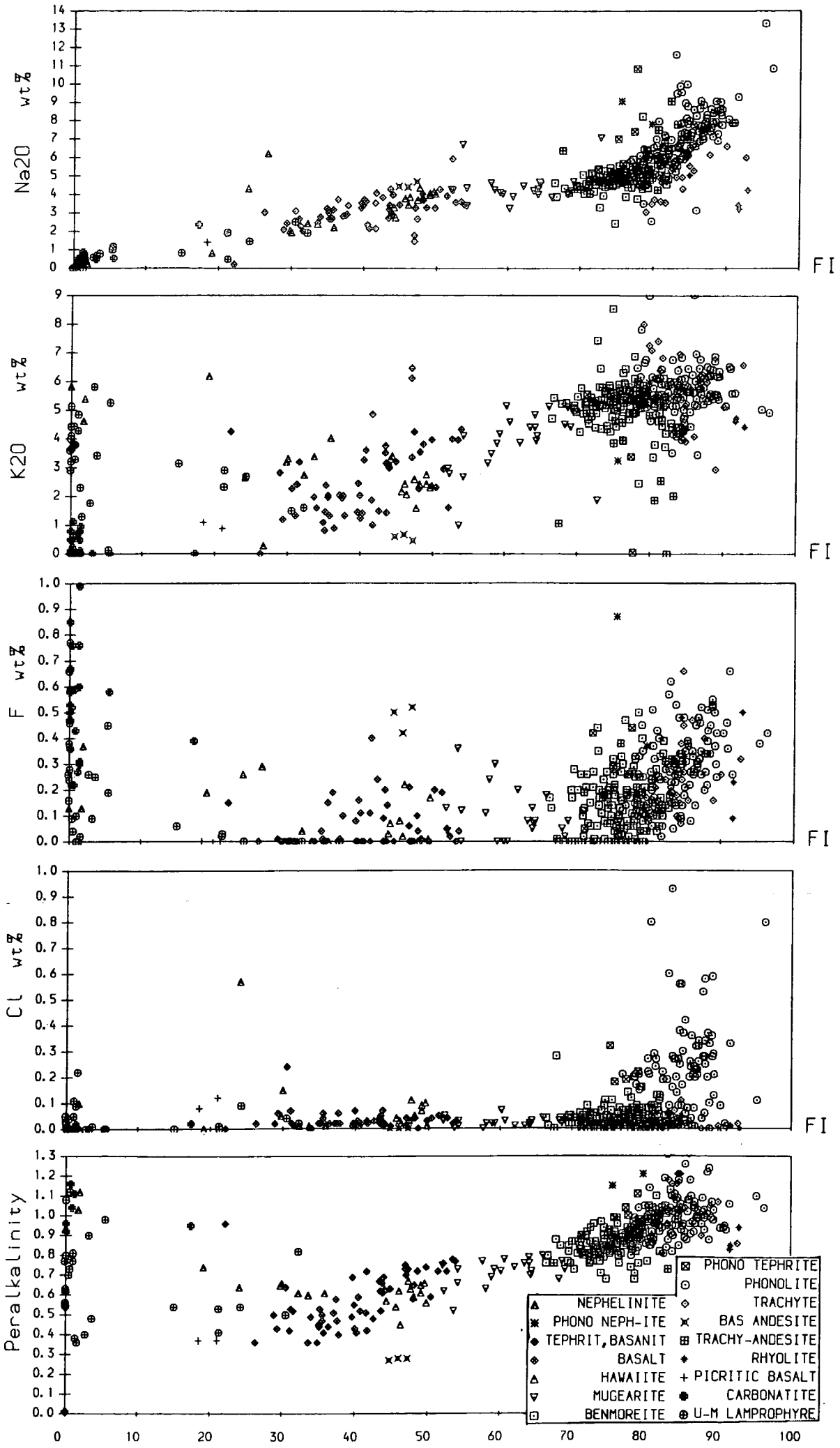
Na2O wt%
K2O wt%
F wt%
Cl wt%
Peralkalinity
FI
PHONO TEPHRITE
PHONOLITE
NEPHELINITE
TRACHYTE
PHONO NEPH-ITE
BAS ANDESITE
TEPHRIT,BASANIT
TRACHY-ANDESITE
BASALT
RHYOLITE
HAWAIITE
PICRITIC BASALT
MUGEARITE
CARBONATITE
BENMOREITE
U-M LAMPROPHYRE

saturation plane for Gardar rocks (from Upton 1974). These phases are assumed to be the major cause of variation within the dyke swarm.

In Chapter 5.4 it is shown that members of 2 dyke swarms crop out in the Igaliko region, and these can effectively be discriminated upon their Zr/Nb ratios - a high Zr/Nb suite trending to Si-oversaturation and a low Zr/Nb suite trending to Si-undersaturation.

Major element correlation matrices are shown in Table 5.3.1 for the high and low Zr/Nb suites, for 3 ranges of F.I., ie. F.I.<50, 50<F.I.<70 and F.I.>70. Tables 5.3.3A and 5.3.3B present trace element correlation matrices for high and low Zr/Nb suites over the same F.I. ranges.

SiO_2

SiO_2 generally increases with F.I.. Two trends become evident at F.I.>70. A higher trend evolves through trachy-andesites and trachytes to rhyolites; and a lower trend (a cluster at around F.I.=88, SiO_2=66%) evolves through benmoreites and phonolitic tephrites to phonolites. The lower trend is closely similar to the data from South Qôroq (Stephenson 1972). The two trends evident from SiO_2 represent evolution towards Si-oversaturated and Si-undersaturated minima and are separated by a thermal barrier in Petrogeny's Residua System (Hamilton and Mackenzie 1965). Fractionation of ferro-magnesian minerals as well as ilmenite/magnetite at low F.I.s will increase SiO_2 gradually. The trend to oversaturated and undersaturated minima is achieved as feldspar fractionation becomes important for rocks on either side of the critical silica saturation plane (see Upton 1974 and Figure 5.2.1C). From Figure 5.2.1C, a combination of alkali feldspar (anorthoclase) with lesser augite and olivine (may be 70-80% feldspar) would have bulk SiO_2 and total alkalis in the region of the critical saturation plane at around SiO_2 $\approx$55 wt%. This corresponds roughly to D.I.$\approx$70. Extraction of this mixture from critically Si-undersaturated rocks would cause an increase in Si and a decrease in the total alkalis, producing a rhyolitic trend (see Chapters 5.5, 5.6 and 5.8).

Al_2O_3

Al_2O_3 shows a gradual increase with F.I. with F.I.>70, two trends are again evident (cf. SiO_2). A trend of increasing Al with F.I. passes through benmoreites to phonolites and a trend of decreasing Al runs through trachy-andesites and trachytes to rhyolites. The upper trend is similar to that seen in South Qôroq. Fractionation of Al free ferro-magnesian phases from the basic to intermediate rocks, along with some plagioclase, will cause the early increase in Al. As with SiO_2, at F.I.>70 alkali feldspar fractionation will be largely responsible for the divergence in the Al_2O_3 contents towards oversaturated and undersaturated minima (see Table 5.3.1).

Fe_2O_3

Fe_2O_3 shows a wide scatter, but a relatively steady decrease with increasing F.I. is evident. This is consistent with the removal of Fe in early crystallising ferro-magnesian phases such as olivine and clinopyroxene. Total iron is reported as Fe_2O_3, however the ratio of Fe_2O_3/FeO increases gradually with increased fractionation. The Fe_2O_3/FeO ratio also increases with increased peralkalinity, Fe^{3+} being accommodated in alkali pyroxenes and alkali amphiboles, as well as more usual occurrence in magnetite and biotite.

MgO

MgO shows a closely constrained decrease with increased fractionation consistent with the early removal of Mg in phases such as olivine and clinopyroxene. The highest MgO contents are from the UML's (up to ca. 16 wt%) with the tephrites and the basalts containing only approximately half of this quantity (ca. 8 wt%) as a typical maximum. Upton and Emeleus (1987) report that typical MgO contents for Gardar basaltic rocks do not exceed ≈8 wt%, these compositions probably representing residues after some early crystal fractionation. High Al_2O_3/CaO ratios may also reflect early olivine and clinopyroxene extraction (see also Ni) and it would seem that the most basic 'gabbros' seen in the region are themselves products of some earlier crystal fractionation. Sparks and Huppert (1984) report a density minimum typically in the range 7-10 wt% MgO during 'dry' olivine and clinopyroxene fractionation of a basaltic magma.

CaO

CaO also shows an un-scattered decrease with increasing F.I., similar to that of MgO. Low pressure fractionation of plagioclase, and also clinopyroxene (along with minor apatite at later stages) will account for the gradual decline in Ca towards the benmoreites and phonolites. The early fractionation of clinopyroxene will account for the high Al_2O_3/CaO ratio seen in the basalts.

Na_2O

Na_2O shows an early increase through the basalts and tephrites/basanites to about 4 wt% at F.I.≈45. Na will be excluded from early crystallising phases (olivine and clinopyroxene). Na_2O remains fairly constant between F.I.≈48-70, this corresponds with a rapid change in composition associated with the onset of Fe oxide crystallisation (see Chapter 5.5), although, with crystallisation of a sodic plagioclase in the intermediate rocks, Na_2O may become 'buffered' in the liquid. At higher F.I., with the onset of alkali feldspar crystallisation, Na is seen to increase towards phonolite in the undersaturated trend whereas in the oversaturated rocks Na tends to decrease towards rhyolite. (See also *K_2O* and *Peralkalinity*).

K_2O

K_2O shows an irregular but relatively steady increase with F.I.. K_2O will not be incorporated into any of the crystallising mineral phases in any great quantity until 'anorthoclase' becomes the dominant feldspar (at F.I.≈70). With continued fractionation of an increasingly alkali feldspar K_2O is elevated in the undersaturated residue and reduced in the oversaturated residue, an effect similar to Na_2O.

Alkali loss

Loss of alkalis may be an important phenomenonin fine grained alkaline rocks. Alkali loss as nepheline alters to gieseckite has already been mentioned, and in extreme cases this can lead to the rocks becoming corundum-normative. This alteration process tends to affect Na to a greater extent than K.

Macdonald (1969) identified 4 major causes of alkali loss from dykes in the Tugtutôq

Figure 5.3.2 SiO_2 wt% vs. Molecular $Na_2O/(Na_2+K_2O)$.

Minor variation in Na/(Na+K) may be caused by alkali loss. This occurs essentially at constant SiO_2. All analyses are plotted as dyke core (C) and dyke margin (M). Alkali loss does not tend to follow any particular trend (cf. Macdonald 1969 who found Na to be lost preferentially, and Martin (1985) who reports K loss as the most important). The larger variations in Na/(Na+K) with SiO_2 are from composite dykes and can vary from basaltic margins to trachytic cores in extreme cases (wide SiO_2 range).

Figure 5.3.2

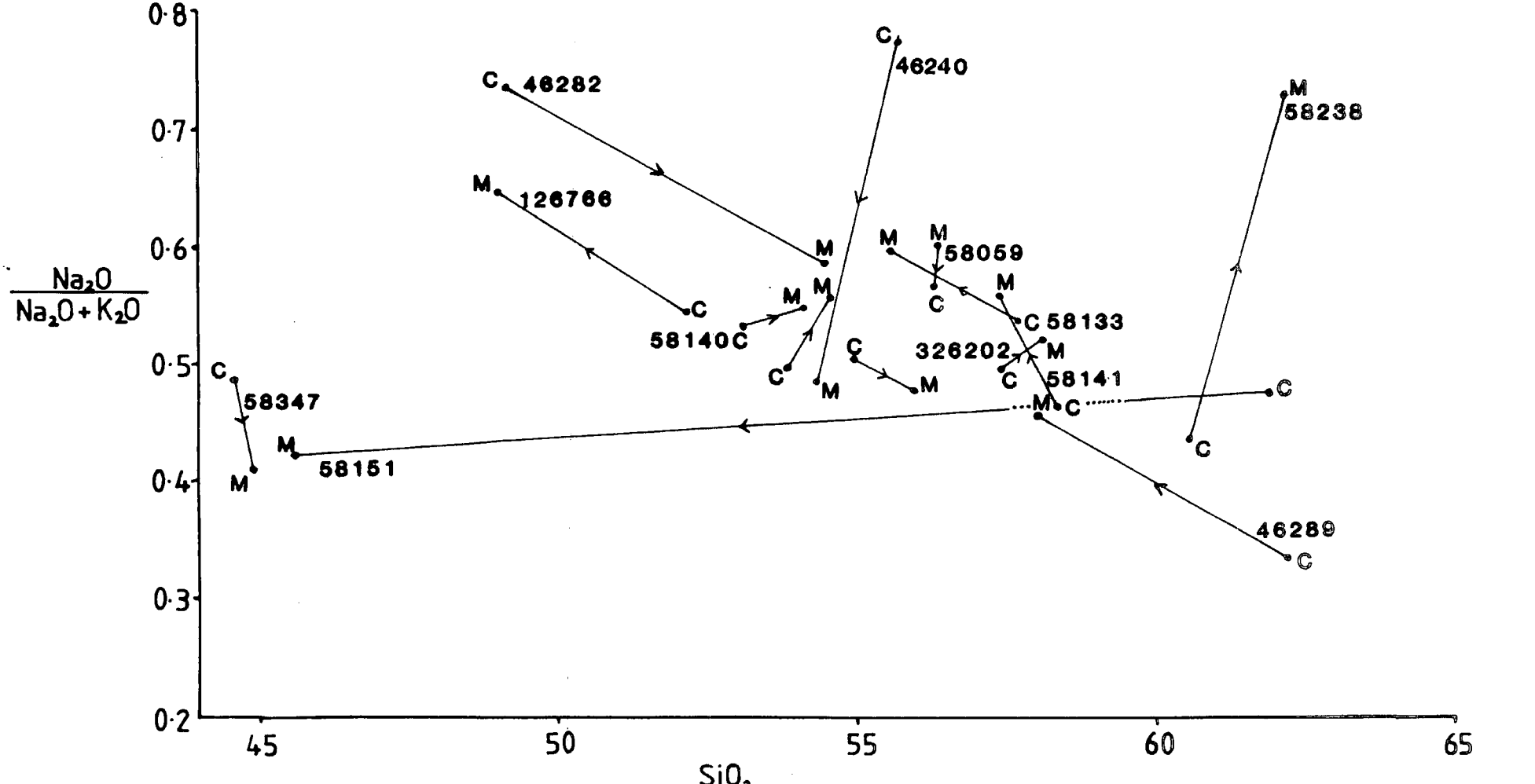
0·8
0·7
0·6
0·5
0·4
0·3
0·2
$\frac{Na_2O}{Na_2O+K_2O}$
45
50
55
60
65
SiO₂
C 46282
C 46240
M 126766
M 58238
M 58059
C 58140
C 58133
326202
58141
C 58347
M 58151
46289

area:-

(i) Alkali removal during escape of a late stage vapour phase.

(ii) Loss of a second vapour phase during devitrification processes – essentially similar to (i) but at a lower temperature.

(iii) Alkali exchange between core and rim of the dyke – presumably in response to the changing thermal gradient on cooling – will modify overall distribution of alkalis in the dyke.

(iv) Loss of Na by alteration of alkali amphibole.

Additional to this, for undersaturated rocks only, can be added

(v) Loss of Na (and possibly gain of K) as nepheline alters to gieseckite. This type of alteration is seen in samples 58291-8, the recrystallised benmoreite cut by the Late Igdlerfigssalik Syenites (see Figure 4.4.7) where Na_2O gradually decreases in the whole rock approaching the contact whilst K_2O remains effectively constant.

Figure 5.3.2 shows analyses from all core-rim pairs of analysed dykes in terms of $Na_2O/(Na_2O+K_2O)$. Large compositional differences reflect 'composite' dykes with major changes in chemistry of the magma between pulses. These changes in Si and alkalis are also mirrored by trace element data, often indicating feldspar and nepheline as the major crystallising phases, although in some cases the core is less fractionated than the rim, indicating possible magma chamber stratification.

The minor variations evident in both Si and $Na_2O/(Na_2O+K_2O)$ may be the result of alkali loss between core and margin of the dyke, but there is no unique sense to the change in the ratio of alkalis with SiO_2. Thus, from core to margin, there seems from this data, to be no preferred migration of alkalis, nor is the variation particularly great.

Martin (1985) contends however that whereas most workers cite Na loss as the greater effect (eg. Macdonald 1969, Rock 1978) the dykes from the Tugtutôq-Ilímaussaq zone suffer preferential K loss. This may be achieved by K and F-rich fluids such as those described by Macdonald *et al.* (1973) from Kûngnât.

Larsen and Steenfelt (1974) described the alkali loss from a micro-kakortokite near Ilímaussaq. High and low alkali facies of this dyke are evident, with different mineralogies. The high alkali samples contain typical agpaitic mineral assemblages including eudialyte, aegirine, arfvedsonite and 2 feldspars. The low alkali samples have magnetite in place of some aegirine hedenbergite, a single (perthitic) feldspar, some hjortdalite (a Zr-silicate) and even zircon. Loss of alkalis causes the change in mineralogy, particularly the increase in magnetite. Normative mineralogies from the 2 facies differ greatly in terms of *ac* and *mt*, but addition of 4% Na_2O to the low alkali analyses produces very similar norms. In this case it would seem that Na is the dominant lost phase, and may amount to about one third of the initial Na_2O content.

The effects of alkali loss must therefore be borne in mind when considering data from (particularly) devitrified or altered samples.

MnO

MnO shows relatively constant compositions of ≈0.25 wt% up to F.I.≈70. MnO will be buffered by its inclusion in the crystallising ferro-magnesian phases (such as olivine, clinopyroxene and opaque oxide minerals). As ferro-magnesian minerals become less important in the fractionating assemblage, MnO will start to increase in the residual magmas. This effect will be countered to some extent by the elevated contents of Mn in olivines and clinopyroxenes. MnO reaches considerably higher contents in the phonolites than in the rhyolites and this may be a reflection of fo_2 (see Chapter 4).

TiO_2

TiO_2 shows relatively level contents through from F.I.≈30-50 (at ≈3 wt%) from where it gradually declines through mugearites into the benmoreitic and more evolved rocks. Ti contents will be 'buffered' early by ilmenite and magnetite crystallisation. At later stages, when titano-magnetite starts to crystallise in abundance (in the hawaiites, see Chapter 5.5) Ti contents will drop more rapidly in the more evolved rocks. This is noted by a relatively rapid decline in Ti against SiO_2 at F.I.≈50 (see Table 5.3.1).

P_2O_5

P_2O_5 shows a relatively steady increase from the less evolved rocks (at F.I.≈30, 0.5

wt% P_2O_5) to rocks of intermediate compositions (F.I.≈55, P_2O_5 ≈3 wt%). Minor apatite is evident in these relatively unfractionated rocks. As the magma becomes more evolved (F.I.>55), apatite becomes an important fractionating phase. This effects a rapid decline of P_2O_5 through benmoreites, leading to complete (or near-complete) depletion of P_2O_5 in many phonolites, trachytes and rhyolites.

F, Cl

F and Cl were both analysed by XRF (see Appendix III) and are reported as weight per cent. Both F and Cl show gradually increasing contents with F.I.. Whilst the undersaturated and oversaturated rocks show similar contents of F, the undersaturated rocks contain appreciably more Cl. This probably reflects the different hosts for these elements. Sodalite will host Cl and amphibole F. Thus with both sodalite and amphibole in phonolites, F and Cl will be high, but with only amphibole in the rhyolites, F will be high but Cl low. The 'saturated' rocks such as the trachy-andesites, trachytes and rhyolites are all marked by low Cl contents. This may be lost in a late stage aqueous solution, whilst in the undersaturated rocks, reaction of nepheline with this fluid would cause reaction to sodalite (see Chapter 4.9). Macdonald (1969) and Macdonald *et al.* (1973) report aqueous alkali halide solutions as agents affecting alkali loss (see above).

Peralkalinity

Peralkalinity (moles Na+K/Al) shows a steady increase with F.I.. 'Peralkalinity' can be divided into two groups, miaskitic, where $1 <$ peralkalinity < 1.2 and agpaitic, where peralkalinity ≥ 1.2. Most of the peralkaline rocks from the dyke swarm are therefore miaskitic, with only a small number of very alkali-rich, agpaitic examples observed. There is no very obvious distinction between peralkalinity and degree of silica saturation. Bowen (1945) described how the peralkalinity in a liquid residue would be increased by the fractionation of plagioclase. This removes Al and Ca with lesser Na from the liquid which leaves the residue richer in both Na and K compared to Al thus increasing the peralkalinity. This he termed the 'plagioclase effect'. A similar process operates in more fractionated rocks in which alkali feldspar crystallises instead of plagioclase. This has been termed the 'orthoclase effect' (cf. 'plagioclase effect') by

Table 5.3.1

Correlation matrices for major elements at F.I. ranges of <50, 50-70 and > 70 for the undersaturated (low Zr/Nb) and oversaturated (high Zr/Nb) suites of dykes (see Chapter 5.4).

Low Zr/Nb – Negative correlations between Ca, Mg and Fe with Si indicate ferromagnesian extraction, at F.I.<50. Al increases with increasing Si, hinting against abundant feldspar fractionation. Between F.I. 50-70, a strong negative correlation between both Ti and P with Si is seen. This marks the onset of major iron oxide and apatite fractionation. Al still increases with increasing Si showing that feldspar fractionation is still not abundant. Alkalis increase with Si and Al, K more so than Na which will be incorporated into plagioclase. Ca shows a stronger negative correlation with Si as too do Fe and Mg, largely a result of clinopyroxene fractionation. At F.I. 50 to 70 Mg and Fe also show stronger negative correlations. At F.I.>70, Al shows little variation with Si, both of these being extracted by now abundant feldspar (see also Sr vs. Zr, Table 5.3.2). K shows a similar relationship to Al. Si remains essentially constant above F.I.=70 (see Figures 5.2.1 and 5.3.1).

High Zr/Nb – At F.I.<50 both Al and Ca increase with SiO_2, and this may imply little or no feldspar fractionation (buffering Ca). Fe and Mg sharply decrease, caused by fractionation of ferromagnesian minerals (mostly olivine as Ca shows little variation). Between F.I. 50-70, Ca, P and Ti all decrease rapidly, indicating the onset of abundant clinopyroxene, plagioclase feldspar, apatite and magnetite fractionation. Al shows no covariance with Si, being essentially constant across this range (buffered by feldspar). Na shows a similar behavior to Al, again a consequence of feldspar, whilst K increases with increasing Si. At F.I.>70, Na, and K decrease with increasing Si, a consequence of removal of an alkali feldspar. Fe, Mg, Ca all continue a decreasing trend with increasing Si caused by minor ferromagnesian fractionation.

Table 5.3.1

Low Zr/Nb
F.I. < 50

VARIABLE	3 SI	4 AL	5 FE	6 MG	7 CA	8 NA	9 K	10 TI	11 MN	12 P	13 F	14 CL
3.SI	1.0000											
4.AL	.6388	1.0000										
5.FE	-.4795	-.3125	1.0000									
6.MG	-.5706	-.8680	.2858	1.0000								
7.CA	-.4430	-.4161	-.1664	.0528	1.0000							
8.NA	.3581	.5404	-.6747	-.7142	.3899	1.0000						
9.K	-.1722	-.1248	.1489	.4121	-.6160	-.5986	1.0000					
10.TI	-.4668	-.3182	.3745	.0590	.3240	-.0763	-.1981	1.0000				
11.MN	-.4259	-.5565	-.1651	.2955	.6802	.1570	-.2421	.2305	1.0000			
12.P	-.2324	-.0307	-.1690	-.2158	.3761	.2983	-.1185	.1506	.5104	1.0000		
13.F	-.2756	-.4214	-.3263	.4853	.2203	-.0000	.2858	-.1882	.3114	-.0802	1.0000	
14.CL	-.1454	-.1907	-.4976	-.0657	.7847	.6413	-.4894	.0336	.6498	.2645	.4401	1.0000

Low Zr/Nb
F.I. 50-70

VARIABLE	3 SI	4 AL	5 FE	6 MG	7 CA	8 NA	9 K	10 TI	11 MN	12 P	13 F	14 CL
3.SI	1.0000											
4.AL	.7766	1.0000										
5.FE	-.5736	-.7085	1.0000									
6.MG	-.8545	-.6713	.2472	1.0000								
7.CA	-.9029	-.6005	.2265	.8883	1.0000							
8.NA	.2562	.2963	.0892	-.3981	-.1880	1.0000						
9.K	.3681	.2342	-.5970	-.1790	-.3079	-.6947	1.0000					
10.TI	-.9340	-.7335	.3342	.8723	.9031	-.4927	-.0543	1.0000				
11.MN	.0622	-.2574	.6862	-.3760	-.3182	.5267	-.5547	-.3052	1.0000			
12.P	-.9572	-.8067	.5592	.8038	.8452	-.3653	-.2656	.9231	-.0310	1.0000		
13.F	.1072	.2060	-.3349	-.1145	.0198	-.1716	.2805	.0208	-.2433	-.0358	1.0000	
14.CL	-.1623	.0377	-.1019	.0904	.1886	-.1866	.1594	.2468	-.3605	.1868	.3302	1.0000

Low Zr/Nb
F.I. > 70

VARIABLE	3 SI	4 AL	5 FE	6 MG	7 CA	8 NA	9 K	10 TI	11 MN	12 P	13 F	14 CL
3.SI	1.0000											
4.AL	-.0270	1.0000										
5.FE	-.3414	-.8561	1.0000									
6.MG	-.1814	-.2489	.1750	1.0000								
7.CA	-.4133	-.4981	.4936	.6256	1.0000							
8.NA	-.3550	.3521	-.2188	-.5610	-.3815	1.0000						
9.K	-.0053	.4186	-.4228	.0062	-.2579	-.2886	1.0000					
10.TI	-.1206	-.4585	.3100	.8204	.7033	-.6426	.0297	1.0000				
11.MN	-.2897	-.4190	.5718	-.1139	.1582	.2638	-.5665	-.1771	1.0000			
12.P	-.2622	-.3014	.2338	.8830	.7365	-.4622	-.1141	.8362	-.0939	1.0000		
13.F	-.2384	.4024	-.3445	-.2719	-.1601	.5561	.0155	-.3998	.1260	-.2055	1.0000	
14.CL	-.4146	.0984	.0249	-.3056	-.2069	.6630	-.0659	-.3902	.1276	-.2476	.3774	1.0000

High Zr/Nb
F.I. < 50

VARIABLE	3 SI	4 AL	5 FE	6 MG	7 CA	8 NA	9 K	10 TI	11 MN	12 P	13 F	14 CL
3.SI	1.0000											
4.AL	.6505	1.0000										
5.FE	-.7534	-.9448	1.0000									
6.MG	-.6946	-.8299	.8734	1.0000								
7.CA	.2279	.6436	-.6535	-.6068	1.0000							
8.NA	.5195	.6356	-.6912	-.7906	.3136	1.0000						
9.K	-.4085	-.5439	.4195	.3742	-.4722	-.2902	1.0000					
10.TI	-.7863	-.8793	.8942	.7657	-.5650	-.5968	.4382	1.0000				
11.MN	-.4988	-.7468	.7649	.6324	-.5292	-.4274	.2211	.6700	1.0000			
12.P	-.6428	-.4528	-.3759	-.2038	-.0461	-.0442	-.4210	.5265	-.3114	1.0000		
13.F	.5779	.8968	-.8728	-.8527	.7086	.6582	-.5295	-.7777	-.7435	-.2856	1.0000	
14.CL	-.1168	-.3511	.2575	.3113	-.3945	.0768	.1562	.1994	.3907	.2901	-.4028	1.0000

High Zr/Nb
F.I. 50-70

VARIABLE	3 SI	4 AL	5 FE	6 MG	7 CA	8 NA	9 K	10 TI	11 MN	12 P	13 F	14 CL
3.SI	1.0000											
4.AL	.0002	1.0000										
5.FE	-.1369	-.9273	1.0000									
6.MG	-.8290	-.3091	.2890	1.0000								
7.CA	-.8436	.4738	-.3062	.5321	1.0000							
8.NA	.0254	.8979	-.7965	-.3869	.4483	1.0000						
9.K	.6446	-.6542	.4603	-.2940	-.9330	-.6521	1.0000					
10.TI	-.8604	-.3321	.3145	.9191	.5271	-.4045	-.2776	1.0000				
11.MN	-.0503	-.5811	.5532	.0435	-.3228	-.4897	.4979	.2248	1.0000			
12.P	-.9100	-.1666	.1925	.8315	.6570	-.2437	-.4236	.9559	.2186	1.0000		
13.F	-.1295	.6880	-.6829	-.1430	.5152	.6501	-.6145	-.0593	-.4166	.1071	1.0000	
14.CL	.3106	-.2524	.3229	-.3311	-.4297	-.1324	.4043	-.3057	.2118	-.3561	-.3554	1.0000

High Zr/Nb
F.I. > 70

VARIABLE	3 SI	4 AL	5 FE	6 MG	7 CA	8 NA	9 K	10 TI	11 MN	12 P	13 F	14 CL
3.SI	1.0000											
4.AL	-.3207	1.0000										
5.FE	-.4886	-.6183	1.0000									
6.MG	-.3928	.0394	.1527	1.0000								
7.CA	-.6931	.0480	.4307	.5789	1.0000							
8.NA	-.1785	.3745	-.1118	-.5891	-.1616	1.0000						
9.K	-.2231	.0837	-.0780	.4561	.0874	-.6152	1.0000					
10.TI	-.4186	-.2915	.4663	.8576	.6657	-.6653	.4464	1.0000				
11.MN	-.5029	-.0720	.6075	-.1461	.1736	.3768	-.3313	-.0583	1.0000			
12.P	-.4040	.1603	0795	.8259	.6136	-.5147	.3863	.8056	-.2366	1.0000		
13.F	.1864	.2608	-.3788	-.5016	-.2395	.5296	-.2511	-.6406	-.1262	-.4376	1.0000	
14.CL	-.2598	.2171	- 0218	-.0350	.0121	.2949	.0682	-.1080	.0658	-.0569	.0543	1.0000

Figure 5.3.3 (6 pages) Trace elements vs. F.I.

All trace element data is presented against F.I. The range of trace element concentration for the ordinate axis has been chosen to exclude a relatively small number of 'extreme' compositions which are illustrated in Figure 5.3.4.

Also included with the trace elements are plots of Zr/Nb, Ce/Y and K/Rb against F.I. Ce/Y is seen to increase gradually with F.I. due most probably to pyroxene fractionation (see text). K/Rb increases gradually through tephrites into basalts (at F.I.$\approx$50) where it levels off slightly and starts to drop fairly rapidly at F.I.$\approx$65, the onset of major K-bearing feldspar (anorthoclase) crystallisation. Zr/Nb has been divided at 5.2 into high Zr/Nb and low Zr/Nb ranges (see Figure 5.4.2). Certain differences in the abundances of individual rock types between low and high Zr/Nb ranges can be seen from this diagram (see also Chapter 5.4).

Figure 5.3.3A

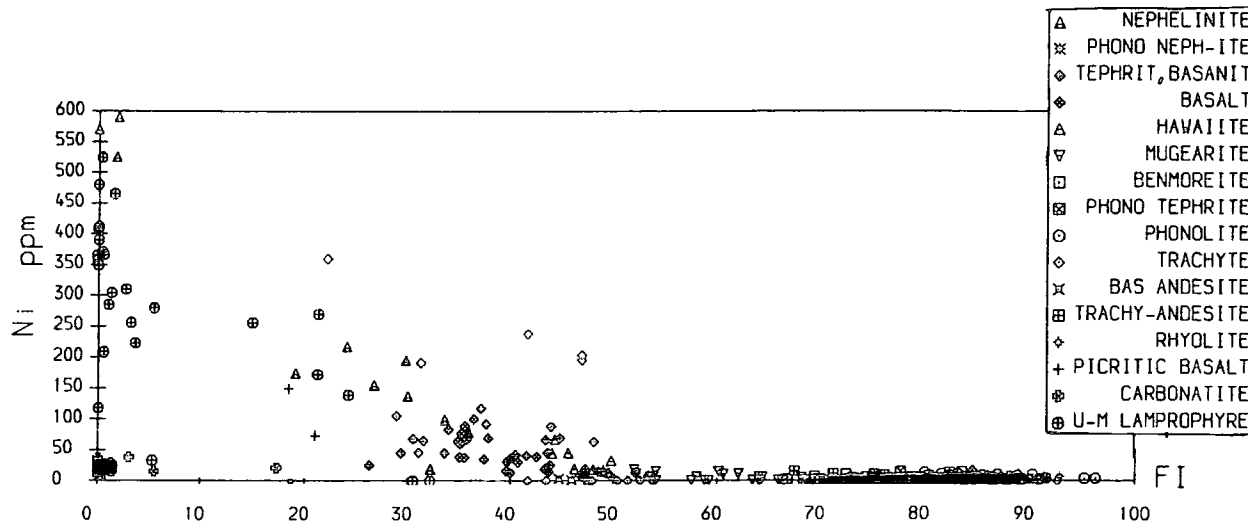
NEPHELINITE
PHONO NEPH-ITE
TEPHRIT, BASANIT
BASALT
HAWAIITE
MUGEARITE
BENMOREITE
PHONO TEPHRITE
PHONOLITE
TRACHYTE
BAS ANDESITE
TRACHY-ANDESITE
RHYOLITE
PICRITIC BASALT
CARBONATITE
U-M LAMPROPHYRE
Ni ppm
FI

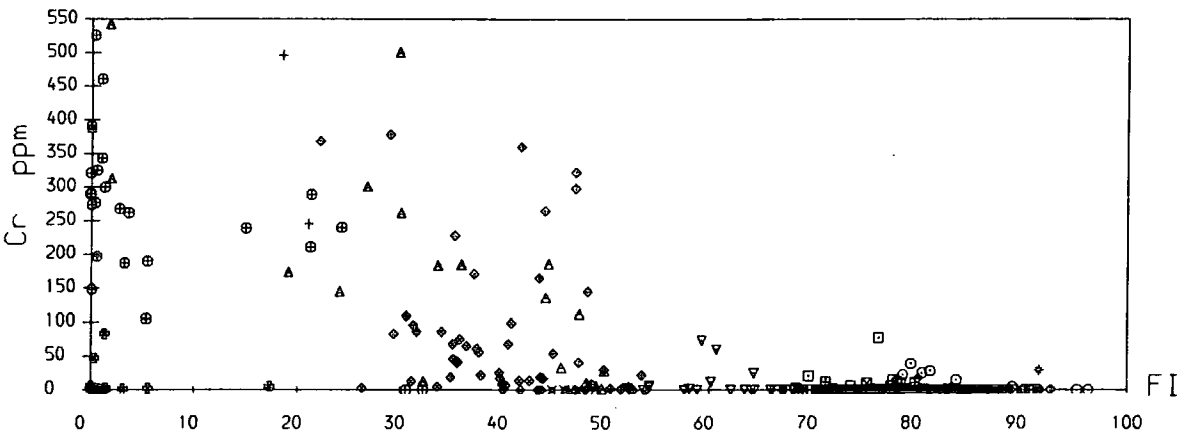
Cr ppm
FI

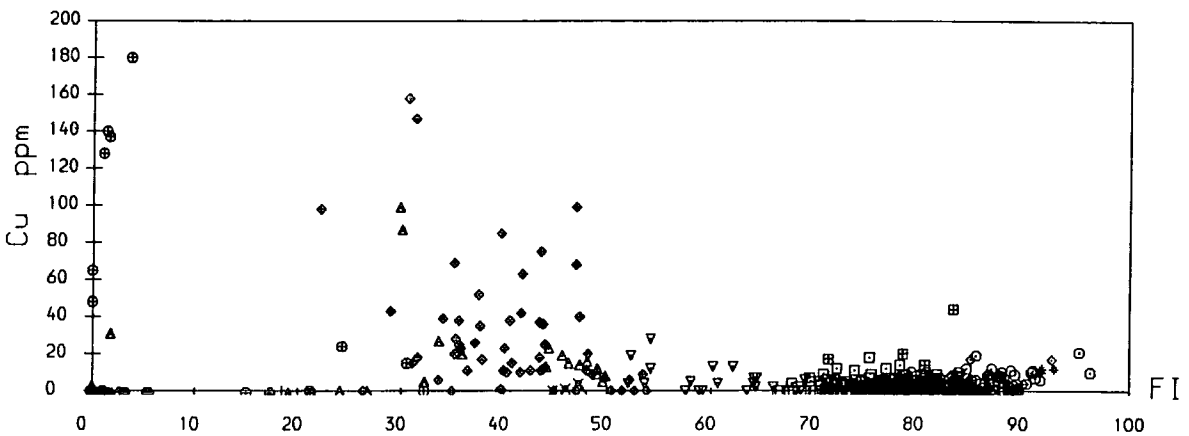
Cu ppm
FI

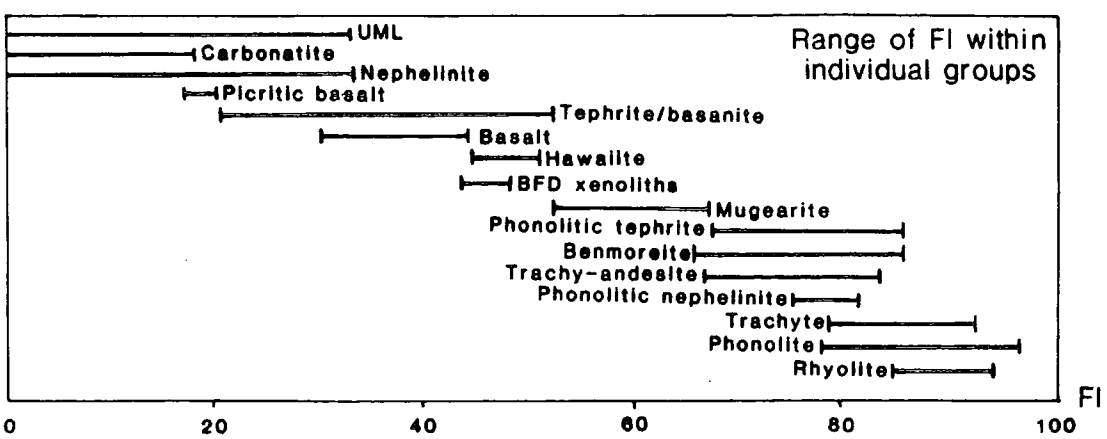
Range of FI within individual groups
UML
Carbonatite
Nephelinite
Picritic basalt
Tephrite/basanite
Basalt
Hawaiite
BFD xenoliths
Mugearite
Phonolitic tephrite
Benmoreite
Trachy-andesite
Phonolitic nephelinite
Trachyte
Phonolite
Rhyolite
FI

Figure 5.3.3B

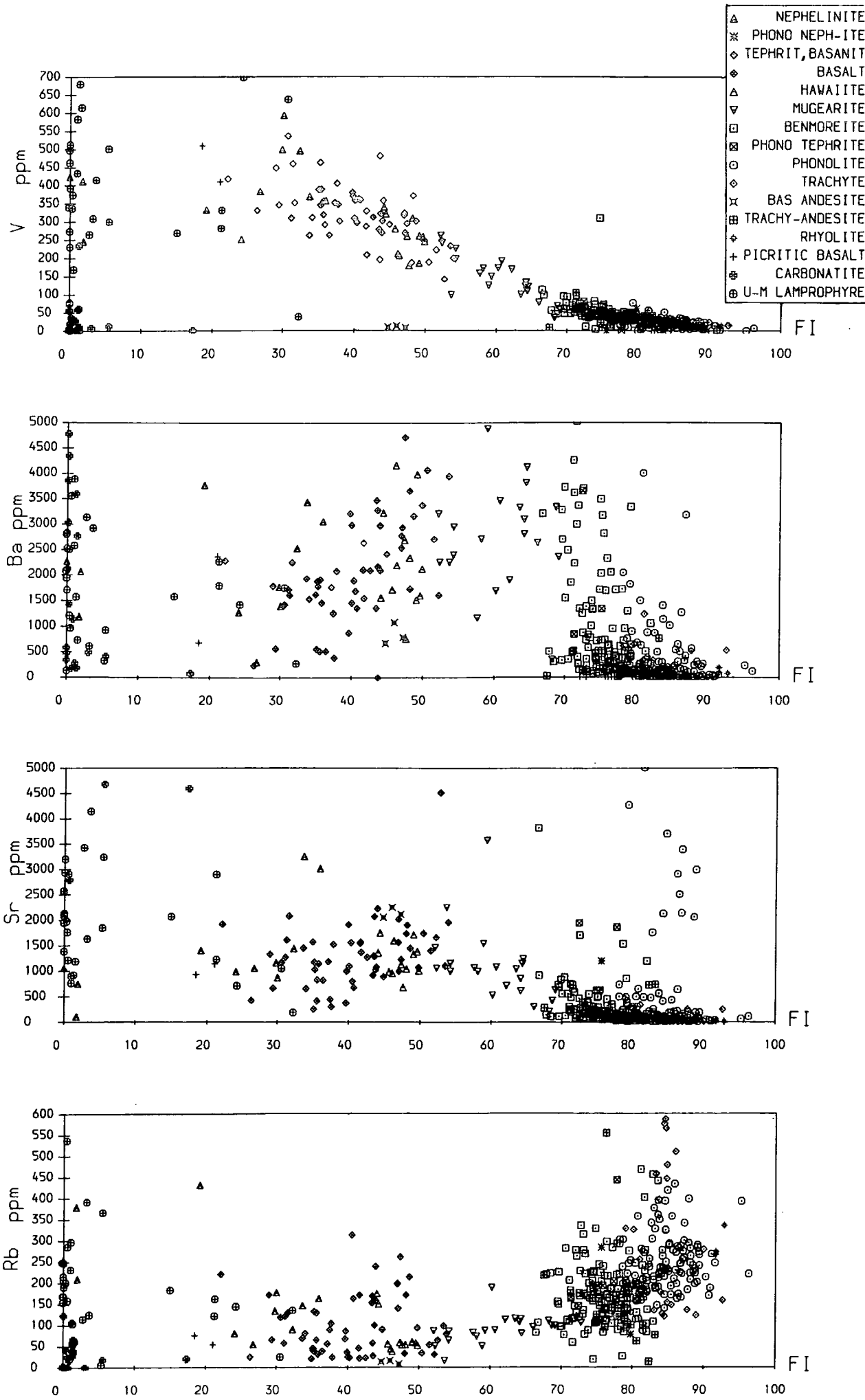
NEPHELINITE
PHONO NEPH-ITE
TEPHRIT, BASANIT
BASALT
HAWAIITE
MUGEARITE
BENMOREITE
PHONO TEPHRITE
PHONOLITE
TRACHYTE
BAS ANDESITE
TRACHY-ANDESITE
RHYOLITE
PICRITIC BASALT
CARBONATITE
U-M LAMPROPHYRE
V ppm
Ba ppm
Sr ppm
Rb ppm
FI

Figure 5.3.3C

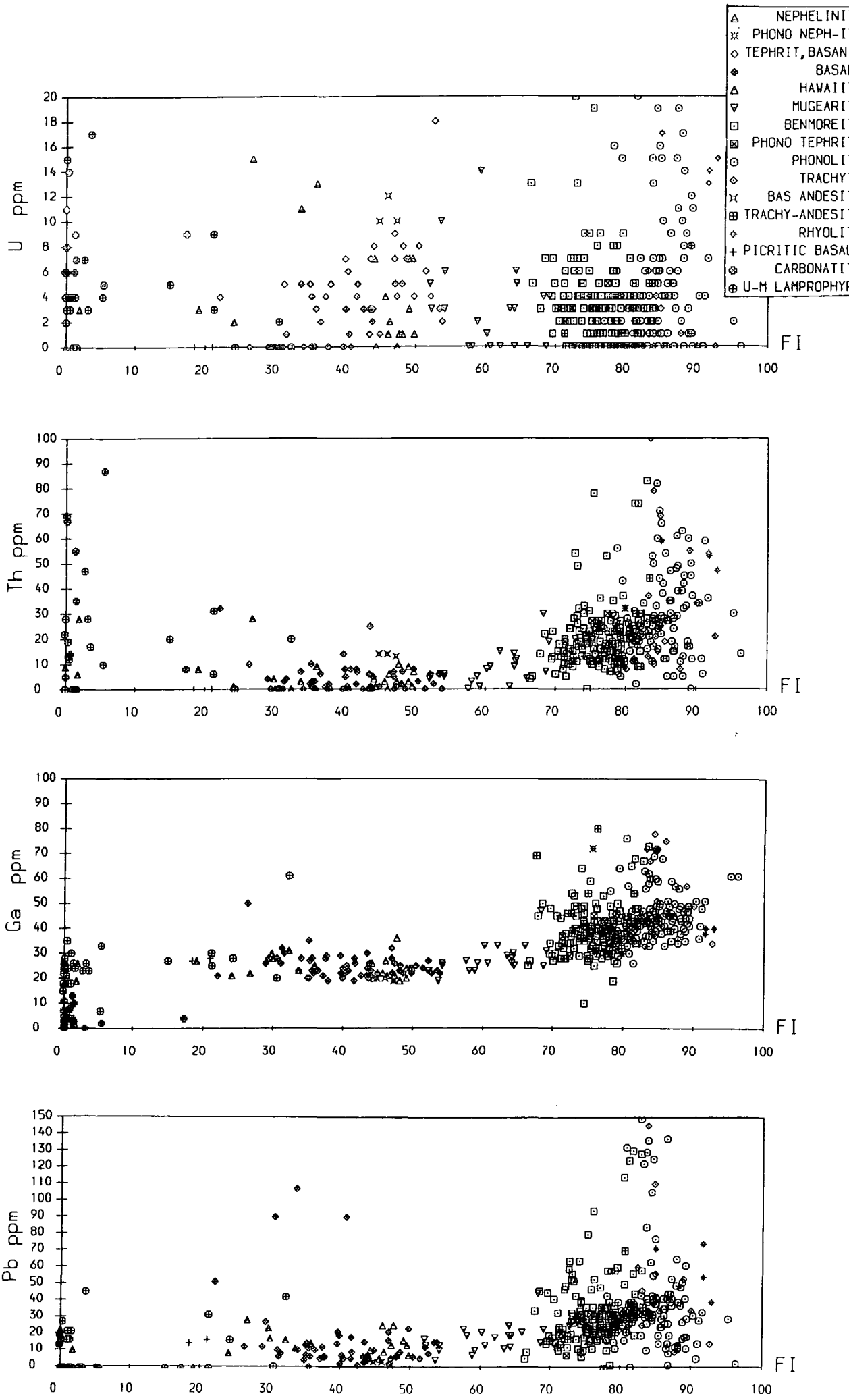
NEPHELINI
PHONO NEPH-I
TEPHRIT, BASAN
BASA
HAWAII
MUGEARI
BENMOREI
PHONO TEPHRI
PHONOLI
TRACHY
BAS ANDESI
TRACHY-ANDESI
RHYOLI
PICRITIC BASA
CARBONATI
U-M LAMPROPHYR
U ppm
Th ppm
Ga ppm
Pb ppm
FI

Figure 5.3.3D

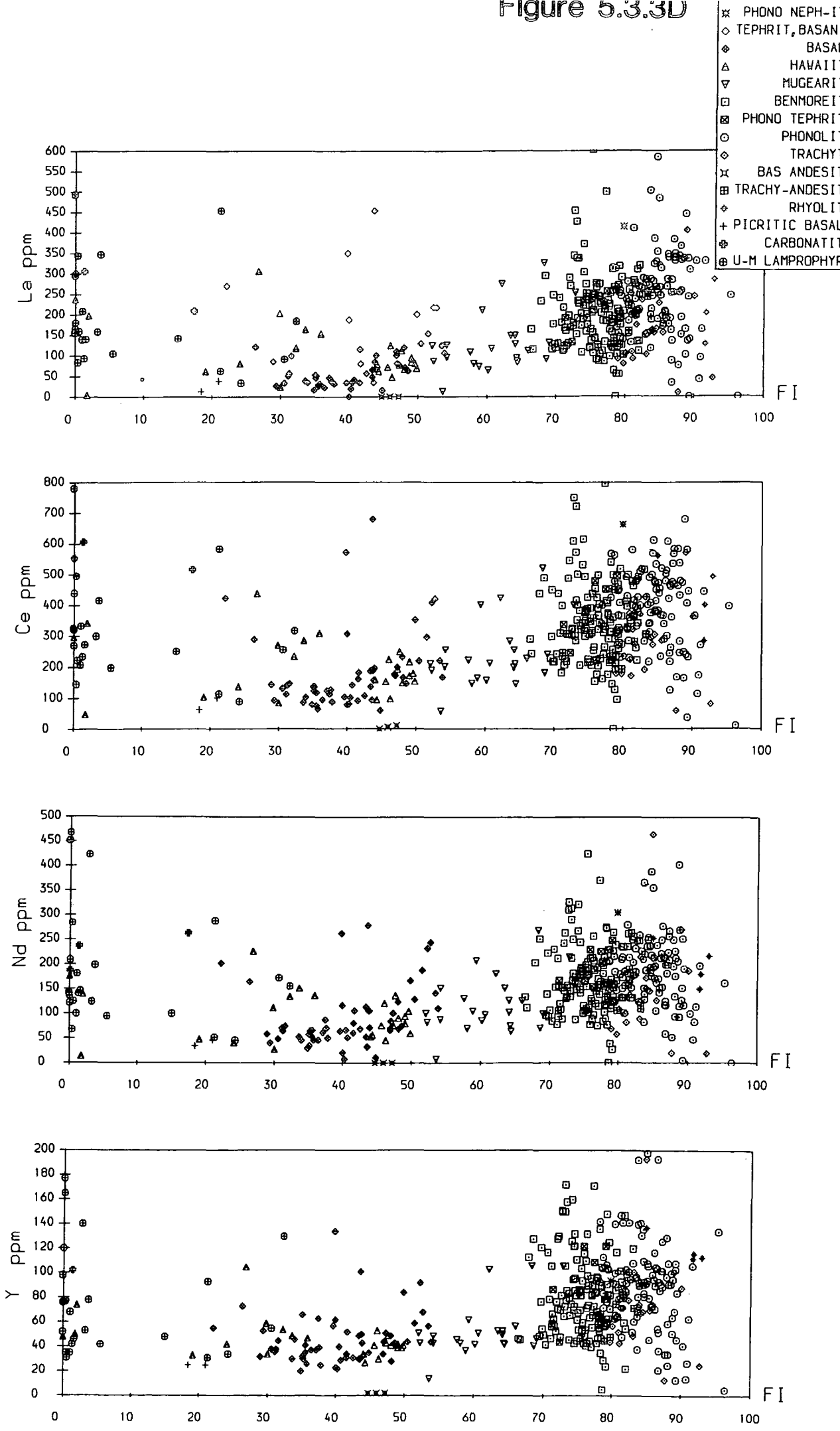
PHONO NEPH-I
TEPHRIT, BASAN
BASA
HAWAII
MUGEARI
BENMOREI
PHONO TEPHRI
PHONOLI
TRACHY
BAS ANDESI
TRACHY-ANDESI
RHYOLI
PICRITIC BASAL
CARBONATI
U-M LAMPROPHYR
La ppm
Ce ppm
Nd ppm
Y ppm
FI

Figure 5.3.3E

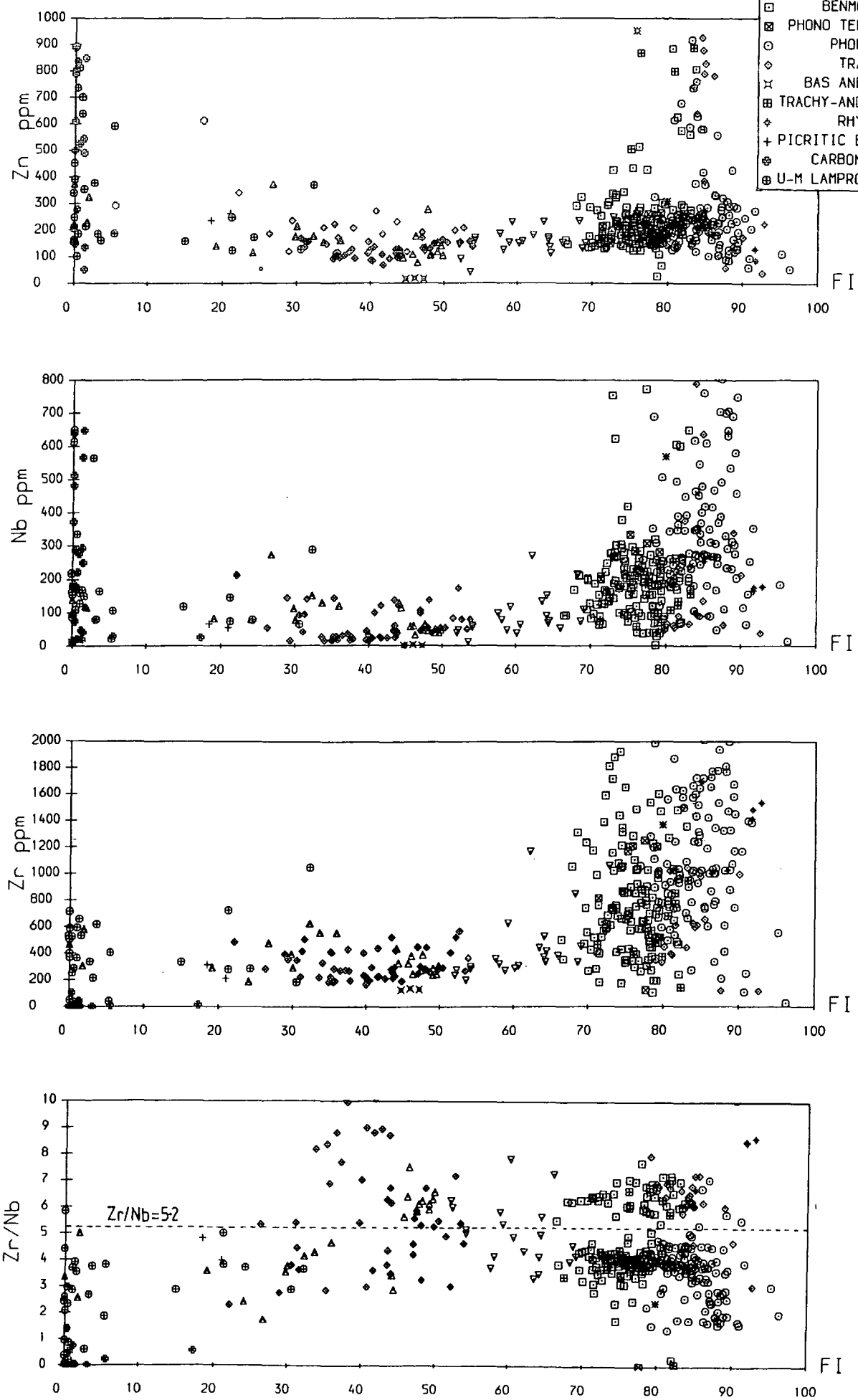
NEPHELINI
PHONO NEPH-I
TEPHRIT, BASAN
BASA
HAWAII
MUGEARI
BENMOREI
PHONO TEPHRI
PHONOLI
TRACHY
BAS ANDESI
TRACHY-ANDESI
RHYOLI
PICRITIC BASAL
CARBONATI
U-M LAMPROPHYR
Zn ppm
Nb ppm
Zr ppm
Zr/Nb
Zr/Nb=5.2
FI

Figure 5.3.3F

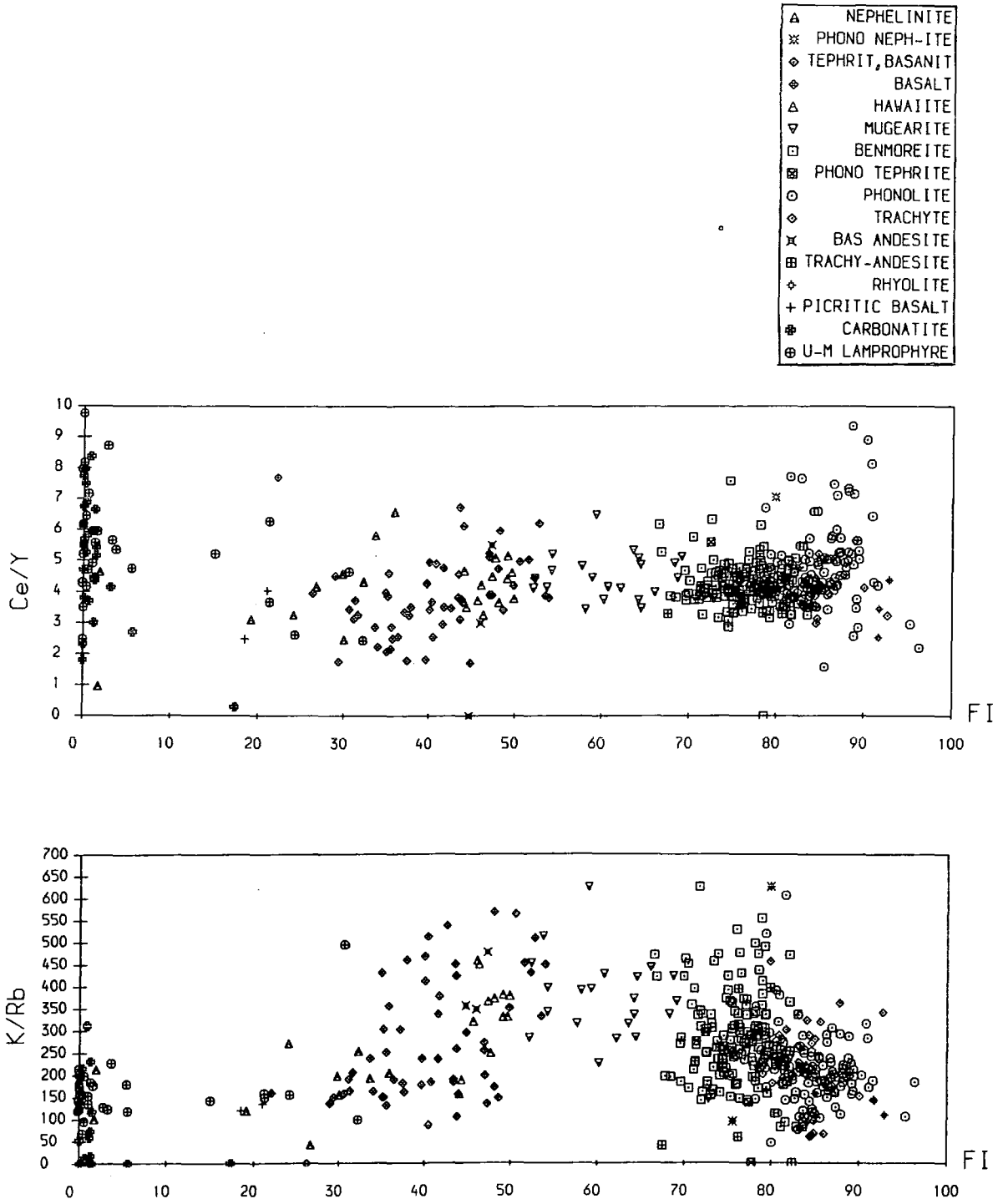
NEPHELINITE
PHONO NEPH-ITE
TEPHRIT, BASANIT
BASALT
HAWAIITE
MUGEARITE
BENMOREITE
PHONO TEPHRITE
PHONOLITE
TRACHYTE
BAS ANDESITE
TRACHY-ANDESITE
RHYOLITE
PICRITIC BASALT
CARBONATITE
U-M LAMPROPHYRE
Ce/Y
K/Rb
FI
FI

Figure 5.3.4

This figure presents trace element data for some elements which are above the range of the plots in Figure 5.3.3. They show the extreme enrichment of some incompatible elements in the phonolites, trachytes and trachy-andesites.

Figure 5.3.4A

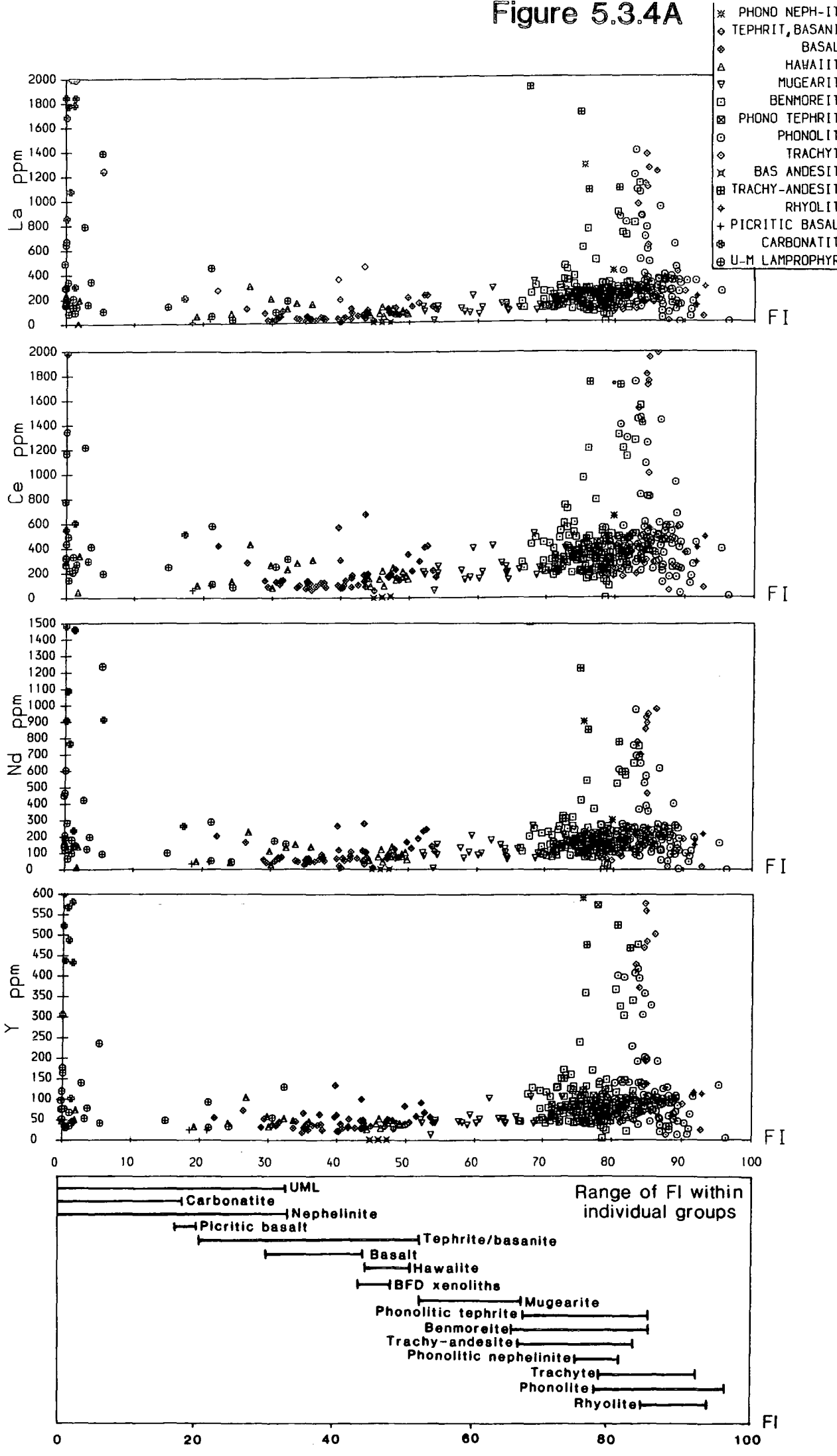
PHONO NEPH-IT
TEPHRIT, BASANI
BASAL
HAWAIIT
MUGEARIT
BENMOREIT
PHONO TEPHRIT
PHONOLIT
TRACHYT
BAS ANDESIT
TRACHY-ANDESIT
RHYOLIT
PICRITIC BASAL
CARBONATIT
U-M LAMPROPHYR
La ppm
Ce ppm
Nd ppm
Y ppm
FI
Range of FI within individual groups
UML
Carbonatite
Nephelinite
Picritic basalt
Tephrite/basanite
Basalt
Hawaiite
BFD xenoliths
Mugearite
Phonolitic tephrite
Benmoreite
Trachy-andesite
Phonolitic nephelinite
Trachyte
Phonolite
Rhyolite

Figure 5.3.4b

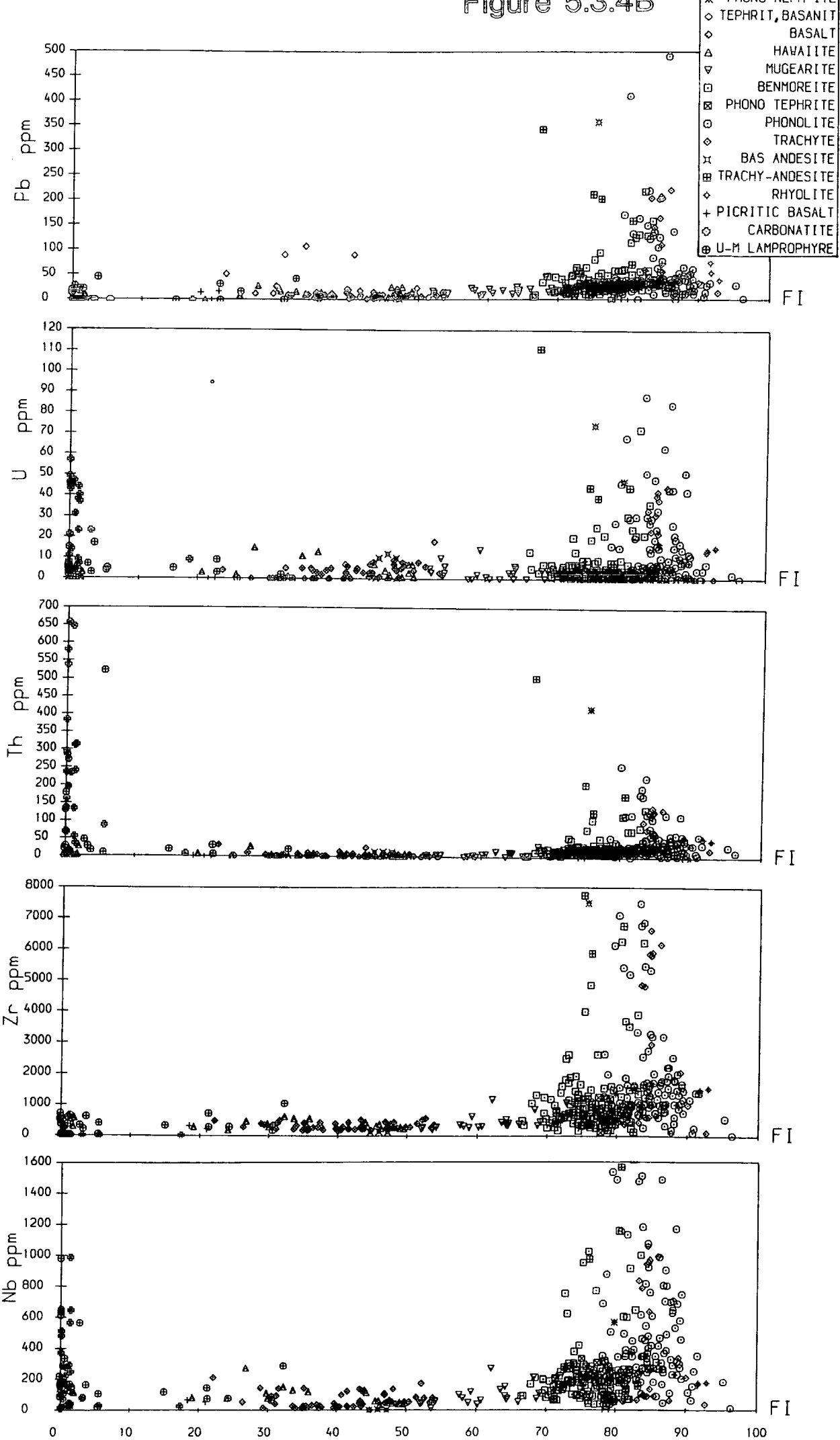
TEPHRIT, BASANIT
BASALT
HAWAIITE
MUGEARITE
BENMOREITE
PHONO TEPHRITE
PHONOLITE
TRACHYTE
BAS ANDESITE
TRACHY-ANDESITE
RHYOLITE
PICRITIC BASALT
CARBONATITE
U-M LAMPROPHYRE
Pb ppm
U ppm
Th ppm
Zr ppm
Nb ppm
FI

Bailey and Schairer (1964). Both of these processes would result in increasingly peralkaline residual liquids as fractional crystallisation proceeded. Once the peralkalinity has exceeded unity, the excess alkalis over Al become incorporated into ferro-magnesian minerals such as aegirine-augite and alkali amphiboles.

Trace Elements

The trace element data are all plotted against F.I. in Figure 5.3.3 and some of the data are presented in Figure 5.3.4. The former figure covers the majority of data, whilst the latter includes samples with unusually high trace element contents. This serves to illustrate the range of trace element concentrations observed. Correlation coefficients for trace elements are presented in Table 5.3.3. The analyses have been divided into 2 suites on their Zr/Nb ratios (see Chapter 5.4). Certain aspects of these tables are explained in the table heading.

Ni

Nickel shows a rapid decrease from basalts with contents from around 100ppm to hawaiite/mugearite where it has dropped to $\approx$ 25ppm or less. Ni is virtually absent from rocks more evolved than benmoreite. The highest Ni contents come from the UML and nephelinites where contents may range up to $\approx$ 600ppm with a hint of continuous trend into the basalts and tephrites/basanites.

Early crystallisation of olivine along with clinopyroxene will rapidly reduce the Ni content of the residual liquids as fractionation increases. (D_{Ni}^{ol}=14, D_{Ni}^{cpx}=2.6, Henderson 1982).

None of the Ni contents from the basalts or tephrites/basanites is high enough to be considered as 'primary' which would require Ni contents in the region of 200-450ppm and Ni/MgO between 23 and 39 (Basaltic Volcanism Study Project 1981).

Of the various field associations of basalt dykes observed Table 5.3.2 shows the Ni and Ni/MgO contents. Of these samples the Late Motzfeldt gabbro may be enriched in both Ni and MgO due to the presence of some cumulus olivine. None of these basalts however, appear to be primary and must be inferred to have undergone some olivine (and probably clinopyroxene) fractionation. The data for the Tugtutôq Younger

Table 5.3.2

Basalt Compositions

Basalt Type	Ni	Ni/MgO	
Possible BD_0	25.5ppm	6.07	Average of 2 samples
Giant Dyke	47ppm	9.14	Avg. excluding plag./apatite cumulate
Late Motzfeldt Gabbro	66ppm	13.75	Avg. of 5 samples - Ni (39-117ppm)
Basalt N of N.A.B	83ppm	13.07	One sample (highest Ni)
YGDC	66ppm	15	
OGDC	13ppm	≤ 5	

(YGDC) and Older (OGDC) Giant Dyke Complexes are taken from Martin (1985) for comparison. The YGDC data is similar to that of the basalts from north of Narssarssuaq (N.A.B.).

The only dykes that contain enough Ni (and also high Ni/MgO) to be possible candidates for primary magmas are the UML and nephelinites. These will be discussed later.

Cr

Cr shows behavior similar to that of Ni with a relatively rapid decline from F.I.$\approx$30 to F.I.$\approx$60, after which most samples are Cr free. There is a tendency for Cr to be higher in the tephrites/basanites than in most of the basalts. Again the UML and nephelinites show high Cr. Cr will partition into pyroxene (D_{Cr}^{cpx}=8.4, Henderson 1982) olivine (D_{Cr}^{ol}=2.1) and Cr-spinel (occasional xenocrysts seen in lamprophyres). Pyroxene and Cr-spinel would imply high pressure fractionation as neither of these phases are primary liquidus phases of these rocks at low pressure (Upton 1971). Primary magmas would be expected to contain in the region of 270ppm Cr (Basaltic Volcanism Study Project 1981).

Cu

The Cu data is less coherent than both Ni and Cr, but shows a similar behaviour with a rapid decline at low F.I. to low contents throughout the evolved rocks. Cu will be controlled in the main by the presence of any sulphide minerals, seen in many of the

more basic rocks. The tephrites contain more Cu than basalts at equivalent F.I. and this may imply a lower activity of sulphur in the tephrites. Cu was not analysed in the carbonatites and some of the lamprophyres which were analysed at Leicester (see Appendix III). Cu may also substitute for Mg in pyroxenes (D_{Cu}^{cpx}=1.5-2.4, Irving 1978).

V

V shows similar behavior to Ni, Cr, Cu as well as showing a similarity to TiO_2. V decreases steadily from both tephrites and basalts towards F.I.≈70 where its rate of decline decreases towards the most evolved rocks. Most rocks contain some V. Fractionation of Ti/Fe^{3+} bearing phases such as ilmenite and Ti-magnetite will preferentially remove V from the magmas (D_V^{mt} ≈3.9, Henderson 1982). Wilkinson (1957) reports high V^{3+} contents from clinopyroxenes and Ti-magnetite from an alkali gabbro sill, and thus fractionation of clinopyroxene will also help deplete V from the residual magmas. V contents of primary basaltic magmas should be in excess of 300ppm (Basaltic Volcanism Study Project 1981).

Ba

Ba increases from tephrites/basanites (F.I.≈35) to an ill defined maximum at F.I.≈60 where it starts a rapid decline to F.I.≈80. This peak in Ba will mark the onset of anorthoclase crystallisation (typically $An_{20}Ab_{58}Or_{20}Cn_2$, see Chapter 4.8). These feldspars are seen as phenocrysts in some mugearites but are most common in the benmoreitic rocks and are notably developed in the Rhomb Porphyries. Crystallisation of anorthoclase (containing 1-2 wt% of BaO in many cases) will rapidly deplete the residual magma in Ba.

Ba shows a fairly wide scatter within the early basalts, a scatter that would not be expected from the restricted range of compositions of other incompatible elements, eg. REE, Y etc. which show a fairly narrow range. Figure 5.3.5 shows Ba plotted against Ce in rocks with >3 wt% MgO, and this scatter in Ba content is particularly evident. A primary magmatic variation in such incompatible elements (for example, degree of partial melting or crystal fractionation) would be expected to produce a sympathetic variation in both elements. This is seen to some extent in the data from the ultramafic lamprophyres and some of the tephrites (a diagonal trend within a group

Figure 5.3.5

Ba vs. Ce for samples with MgO>3.0 wt%. Alteration produces a decrease in Ba (a mobile element) at relatively constant Ce (an immobile element). Ba is seen to be lost from basalts through alteration processes. Initial basaltic Ba content may have been ca. 2000ppm.

The lines indicating 'Increased Partial Melting' and 'Fractional crystallisation' are schematic only. The actual trend that Ba and Ce would follow (if affected by either of these processes) would depend on the bulk distribution coefficient for each element in the source of magma/crystallising assemblage (see text).

Figure 5.3.5

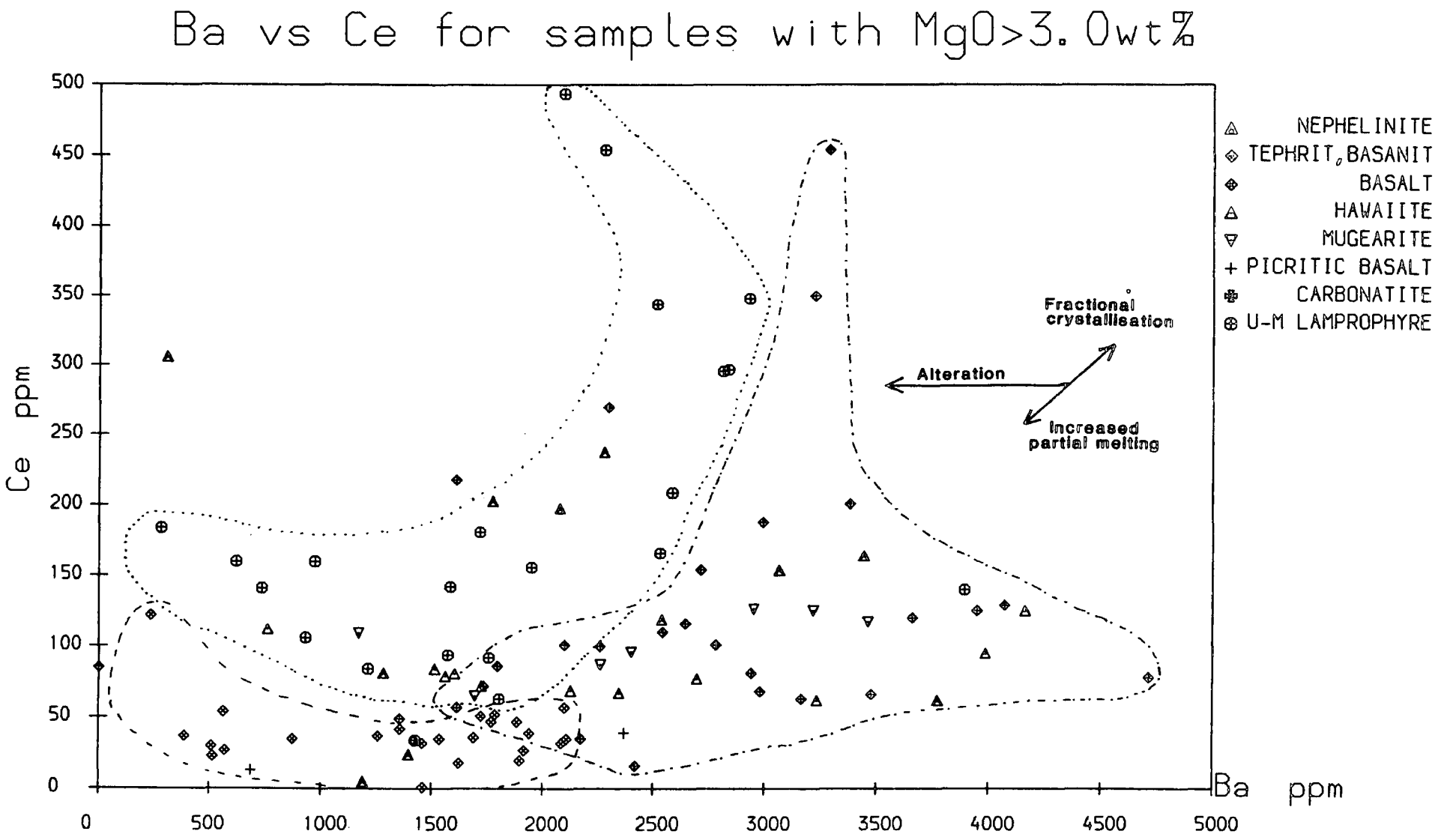
Ba vs Ce for samples with MgO>3.0wt%
Ce ppm
Ba ppm
0
50
100
150
200
250
300
350
400
450
500
0
500
1000
1500
2000
2500
3000
3500
4000
4500
5000
NEPHELINITE
TEPHRIT, BASANIT
BASALT
HAWAIITE
MUGEARITE
PICRITIC BASALT
CARBONATITE
U-M LAMPROPHYRE
Fractional crystallisation
Alteration
Increased partial melting

of analyses). However, no such trend is observed from the basalts which shows constant Ce at varying Ba. This is consistent with Ba loss due to alteration – Ba being relatively 'mobile' compared to Ce. Thus typical Ba contents in the fresh basalts may have been ≈2000ppm.

Sr

Sr rises from the tephrites to the basalts (peak at F.I.≈47) and then decreases as plagioclase becomes an important crystallising phase. Benmoreites and phonolites contain in the region of 100-200ppm Sr. Certain phonolites however contain very elevated Sr contents. Petrographic study of these high Sr phonolites shows them to invariably contain sodalite (implying high Cl) and cancrinite (high CO_2) along with, in one or two samples, free calcite. This high volatile content is an indication of the late stage origin of these Sr-rich phonolites, and the Sr content will be linked directly with the CO_2 content. Koster van Groos (1975) showed that Sr would partition preferentially into a carbonatite liquid that was immiscible with a coexisting phonolite. Thus it appears that the high Sr phonolites may contain a component of a carbonatitic magma. This will be discussed further in Chapter 7.

Rb

Rb shows a relatively gentle increase from tephrites/basanites, through basalts, to mugearites, when it starts to increase in concentration rapidly. The highest concentrations are seen in some of the trachytic (*s.s.*) rocks (≈600ppm). Rb is a highly incompatible element. The only major mineral phase into which it is concentrated is biotite, (D_{Rb} = 3.4, Henderson 1982). Biotite is not a major fractionating phase and thus Rb maintains its incompatibility over the whole range. Rb will be discussed in some more detail later.

La, Ce, Nd, Y

These highly incompatible elements all show similar behaviour. There is a steady increase in their concentrations with increasing F.I. The diagram Ce/Y Figure 5.3.3 shows a relatively gentle increase with increased fractionation, implying an increase in slope of chondrite-normalised REE data (see Chapter 5.4 and Chapter 6).

Table 5.3.3A

High Zr/Nb
F.I. <50

VARIABLE												
19.BA	1.0000											
20.NB	.4614	1.0000										
21.ZR	-.0013	.4445	1.0000									
22.Y	.2511	.4908	.5395	1.0000								
23.SR	.2934	-.1734	-.6682	-.4922	1.0000							
24.RB	.3279	.2147	.1287	.2276	-.2841	1.0000						
25.ZN	-.0518	.4485	.6365	.5442	-.6486	.2485	1.0000					
26.CU	-.2656	-.2227	.3805	.1532	-.3614	.0788	.3149	1.0000				
27.NI	-.2989	-.2746	-.0184	-.0942	-.3285	-.0099	.1157	.0952	1.0000			
28.PB	.0642	.1157	.1458	.1820	-.0205	-.0424	.4738	.0806	-.0473	1.0000		
29.U	.1248	-.2556	-.5691	-.5085	.8626	-.1982	-.5826	-.3155	-.3007	-.0457	1.0000	
30.TH	-.1730	-.0834	-.1891	.0993	.3187	-.3548	-.1238	-.2344	-.3077	.1677	.3831	1.0000
31.V	-.0459	.0545	.3927	.4566	-.6790	.2616	.4568	.2969	.4842	.0116	-.6726	-.5202
32.CR	-.1594	-.1554	.2396	.0761	-.4080	.1352	.1862	.3428	.6643	-.0745	-.3775	-.2792
33.ND	.3499	.7147	.3830	.8746	-.2700	.2291	.4749	-.1090	-.2804	.1610	-.3204	.1347
34.GA	-.4175	.2211	.5326	.3846	-.6429	.0274	.6059	.2111	-.0273	.1120	-.4831	.1279
35.LA	.4391	.6050	.2287	.8498	-.0543	.0798	.3391	-.1708	-.2774	.1828	-.1479	.2983
36.CE	.4190	.6771	.3207	.8875	-.1759	.1412	.4274	-.1328	-.2542	.1546	-.2429	.2420
	19 BA	20 NB	21 ZR	22 Y	23 SR	24 RB	25 ZN	26 CU	27 NI	28 PB	29 U	30 TH

31.V	1.0000					
32.CR	.4138	1.0000				
33.ND	.1992	-.1673	1.0000			
34.GA	.2720	.0401	.3234	1.0000		
35.LA	.1003	-.1762	.9119	.1145	1.0000	
36.CE	.1889	-.1397	.9454	.2268	.9765	1.0000
	31 V	32 CR	33 ND	34 GA	35 LA	36 CE

High Zr/Nb
F.I. 50-70

VARIABLE												
19.BA	1.0000											
20.NB	-.3774	1.0000										
21.ZR	-.4379	.9880	1.0000									
22.Y	-.4784	.9470	.9549	1.0000								
23.SR	.8996	-.2695	-.2970	-.3980	1.0000							
24.RB	-.6369	.7873	.8091	.8470	-.5846	1.0000						
25.ZN	-.2777	.9242	.9118	.9455	-.2171	.7988	1.0000					
26.CU	-.4121	-.2424	-.2313	-.1582	-.4203	.0990	-.3420	1.0000				
27.NI	-.2020	-.5220	-.5067	-.3927	-.1989	-.0820	-.4802	.6692	1.0000			
28.PB	-.7599	.8120	.8416	.8825	-.7127	.9122	.7476	.1144	-.1148	1.0000		
29.U	.6190	.1600	.1555	.0193	.8548	-.2548	.1412	-.5047	-.3762	-.3146	1.0000	
30.TH	-.7198	.7830	.8153	.7734	-.6440	.8037	.6185	.0997	-.1843	.9145	-.2231	1.0000
31.V	.2962	-.6511	-.7040	-.5449	.1985	-.4980	-.5269	.4445	.7160	-.5233	-.0997	-.6073
32.CR	.1531	.2133	.1443	.1184	.2341	.1056	.2715	-.1003	-.0972	.0003	.2861	-.1143
33.ND	.0024	.8059	.7913	.8427	.0667	.5755	.9210	-.3920	-.5412	.5333	.3792	.3825
34.GA	-.6952	.8704	.8972	.9041	- 6285	.9293	.8307	-.0459	-.3158	.9443	-.2314	.8593
35.LA	-.1089	.9052	.8847	.9069	-.0080	.6451	.9435	-.3730	-.5076	.6351	.3697	.5160
36.CE	-.0960	.8905	.8789	.8956	.0239	.6455	.9416	-.3503	-.5269	.6107	.3846	.4780
	19 BA	20 NB	21 ZR	22 Y	23 SR	24 RB	25 ZN	26 CU	27 NI	28 PB	29 U	30 TH

31.V	1.0000					
32.CR	.0858	1.0000				
33.ND	-.3833	.3191	1.0000			
34.GA	-.6645	.0222	.6125	1.0000		
35.LA	-.4414	.2737	.9585	.7015	1.0000	
36.CE	-.4652	.3065	.9717	.6928	.9876	1.0000
	31 V	32 CR	33 ND	34 GA	35 LA	36 CE

High Zr/Nb
F.I. > 70

VARIABLE												
19.BA	1.0000											
20.NB	-.1769	1.0000										
21.ZR	-.1857	.9958	1.0000									
22.Y	-.2163	.9245	.9468	1.0000								
23.SR	.8857	-.0834	-.1049	-.1755	1.0000							
24.RB	-.2780	.7414	.7694	.8350	-.2457	1.0000						
25.ZN	-.2068	.9269	.9274	.8977	-.0251	.7048	1.0000					
26.CU	.1247	-.3119	-.3101	-.3256	.3193	-.3285	-.0966	1.0000				
27.NI	-.0367	.6585	.6772	.6704	.0130	.5644	.5981	-.1440	1.0000			
28.PB	-.1661	.9305	.9197	.8096	-.0525	.6688	.8502	-.2638	.5634	1.0000		
29.U	-.0943	.9801	.9655	.9072	-.0164	.7532	.8819	-.2536	.6921	.9331	1.0000	
30.TH	-.1901	.8785	.9067	.9460	-.1572	.7765	.8512	-.2095	.7121	.7293	.8860	1.0000
31.V	.0954	-.4891	-.5088	-.4605	.0899	-.4017	-.4893	-.0024	-.3138	-.4170	-.5166	-.6069
32.CR	-.0339	-.0603	-.0567	-.0536	- 0307	-.1074	-.0763	.0087	-.0886	-.0415	-.0242	-.0237
33.ND	-.2418	.8469	.8789	.9768	-.2332	.8233	.8395	-.3310	.6124	.7158	.8331	.9311
34.GA	-.3337	.8861	.8996	.8990	-.2755	.7579	.8558	-.2860	.5950	.7624	.8212	.8794
35.LA	-.2277	.8440	.8772	.9687	-.2086	.8066	.8462	-.3009	.6662	.6768	.8200	.9526
36.CE	-.2407	.8630	.8931	.9762	-.2206	.8217	.8568	-.3177	.6299	.7224	.8451	.9481
	19 BA	20 NB	21 ZR	22 Y	23 SR	24 RB	25 ZN	26 CU	27 NI	28 PB	29 U	30 TH

31.V	1.0000					
32.CR	.0451	1.0000				
33.ND	-.4426	-.0554	1.0000			
34.GA	-.5820	-.0509	.8847	1.0000		
35.LA	-.4793	-.0750	.9861	.8862	1.0000	
36.CE	-.4746	-.0621	.9944	.8986	.9902	1.0000
	31 V	32 CR	33 ND	34 GA	35 LA	36 CE

Table 5.3.3B

Low Zr/Nb
F.I. <50

VARIABLE												
19.BA	1.0000											
20.NB	-.2464	1.0000										
21.ZR	.1561	.5828	1.0000									
22.Y	-.0271	.4134	.2063	1.0000								
23.SR	.6393	.0811	.4292	.0320	1.0000							
24.RB	.2677	-.0100	.0150	-.1979	-.1693	1.0000						
25.ZN	-.2072	.3122	.0677	.5442	-.3204	.0214	1.0000					
26.CU	-.0082	-.1420	-.0734	.0144	.1031	-.0672	-.0650	1.0000				
27.NI	-.0913	.1373	.1196	.2140	-.3871	.5275	.5771	-.0426	1.0000			
28.PB	-.2362	.0764	-.1602	.0031	-.1825	-.1375	.3345	.3974	-.1150	1.0000		
29.U	.1627	.3800	.3948	.3954	.6227	-.1123	.0233	-.0251	-.1486	-.1780	1.0000	
30.TH	.0288	.5086	.2528	.7450	.0380	.0751	.6419	-.0205	.3847	.0889	.4014	1.0000
31.V	-.4400	.0640	.0514	-.2984	-.2629	-.0569	.0241	.3251	-.0900	.2603	-.3891	-.4151
32.CR	-.2779	.1386	-.0560	-.0410	-.3528	.3280	.3474	-.0123	.6211	-.0890	-.1518	.0900
33.ND	.2527	.4571	.3712	.8394	.3603	-.2387	.5389	.0120	.1214	.0568	.4629	.7579
34.GA	.0223	-.2535	.2101	-.2267	.0580	-.2228	-.3375	.3381	-.3764	-.1122	-.0890	-.3242
35.LA	.2534	.3606	.2389	.8546	.3043	-.2050	.4950	.0537	.1545	.0051	.4332	.7706
36.CE	.2392	.3393	.2777	.8530	.3472	-.2502	.4669	.0828	.0798	.0595	.4837	.7889
	19 BA	20 NB	21 ZR	22 Y	23 SR	24 RB	25 ZN	26 CU	27 NI	28 PB	29 U	30 TH

31.V	1.0000					
32.CR	.2415	1.0000				
33.ND	-.3077	-.1180	1.0000			
34.GA	.3040	-.2234	-.2742	1.0000		
35.LA	-.4080	-.0536	.9639	-.2673	1.0000	
36.CE	-.3968	-.1557	.9672	-.2345	.9759	1.0000
	31 V	32 CR	33 ND	34 GA	35 LA	36 CE

Low Zr/Nb
F.I. 50-70

VARIABLE												
19.BA	1.0000											
20.NB	-.4596	1.0000										
21.ZR	-.4581	.9996	1.0000									
22.Y	-.4727	.9990	.9987	1.0000								
23.SR	.5905	-.3785	-.3849	-.3696	1.0000							
24.RB	-.2505	.6934	.6978	.6760	-.6606	1.0000						
25.ZN	-.4665	.9956	.9947	.9955	-.3682	.6789	1.0000					
26.CU	-.1014	-.1567	-.1507	-.1523	.0860	-.2526	-.1612	1.0000				
27.NI	-.4412	.4682	.4685	.4801	-.0768	.1336	.4406	.5391	1.0000			
28.PB	-.4690	.9941	.9936	.9935	-.4099	.6921	.9929	-.1718	.4356	1.0000		
29.U	-.4216	.9904	.9896	.9905	-.3341	.6673	.9918	-.1539	.4246	.9874	1.0000	
30.TH	-.4515	.9972	.9970	.9965	-.3942	.6978	.9946	-.1511	.4537	.9969	.9941	1.0000
31.V	.2753	-.4289	-.4307	-.4120	.7975	-.7845	-.4169	.4753	.2120	-.4599	-.4101	-.4462
32.CR	.1483	-.1082	-.1067	-.0951	.1786	-.1196	-.0954	.0325	.1910	-.1037	-.0913	-.0826
33.ND	-.5005	.9908	.9899	.9948	-.3461	.6412	.9926	-.1681	.4662	.9861	.9847	.9867
34.GA	-.6217	.8876	.8904	.8921	-.6022	.7576	.8831	-.1891	.4121	.8970	.8616	.8877
35.LA	-.4977	.9954	.9957	.9978	-.3901	.6778	.9928	-.1568	.4782	.9912	.9841	.9921
36.CE	-.5001	.9957	.9955	.9983	-.3792	.6716	.9944	-.1552	.4760	.9909	.9881	.9931
	19 BA	20 NB	21 ZR	22 Y	23 SR	24 RB	25 ZN	26 CU	27 NI	28 PB	29 U	30 TH

31.V	1.0000					
32.CR	.2503	1.0000				
33.ND	-.3864	-.1144	1.0000			
34.GA	-.6329	-.1289	.8966	1.0000		
35.LA	-.4252	-.1089	.9967	.9118	1.0000	
36.CE	-.4181	-.1035	.9978	.9060	.9993	1.0000
	31 V	32 CR	33 ND	34 GA	35 LA	36 CE

Low Zr/Nb
F.I. >70

VARIABLE												
19.BA	1.0000											
20.NB	-.1410	1.0000										
21.ZR	-.2137	.4403	1.0000									
22.Y	-.2101	.6703	.8375	1.0000								
23.SR	.6063	.2043	-.0050	.0047	1.0000							
24.RB	-.3964	.4111	.5453	.4853	-.1294	1.0000						
25.ZN	-.1145	.6877	.2287	.6022	.1011	.1853	1.0000					
26.CU	-.0657	-.2492	-.3002	-.2761	-.2101	-.1321	-.1889	1.0000				
27.NI	-.1708	.5188	.4418	.5568	.0486	.3939	.5089	-.1660	1.0000			
28.PB	-.1962	.4084	.8350	.8505	.0166	.4798	.4727	-.2294	.4794	1.0000		
29.U	-.0417	.7473	.4054	.6381	.3947	.2326	.8513	-.2767	.5079	.5932	1.0000	
30.TH	-.0910	.8719	.1243	.5365	.1345	.1944	.8808	-.1385	.4794	.2690	.7565	1.0000
31.V	.4249	-.2699	-.3558	-.3313	.1456	-.4823	-.1990	-.0628	-.2578	-.3069	-.2311	-.1783
32.CR	-.0462	.0670	.1007	-.0350	-.0473	-.0028	.0458	-.0310	.0379	.0862	.0512	.0039
33.ND	-.1455	.7034	.3635	.7329	.1051	.2437	.9702	-.2174	.5367	.5860	.8718	.8471
34.GA	-.3180	.2766	.4370	.5882	-.1082	.4207	.7204	-.1215	.4446	.6665	.6258	.3970
35.LA	-.1337	.6850	.3164	.6862	.1101	.2126	.9785	-.1972	.5301	.5467	.8712	.8510
36.CE	-.1272	.7574	.2706	.6678	.1204	.2262	.9832	-.1921	.5242	.4869	.8657	.9175
	19 BA	20 NB	21 ZR	22 Y	23 SR	24 RB	25 ZN	26 CU	27 NI	28 PB	29 U	30 TH

31.V	1.0000					
32.CR	-.0488	1.0000				
33.ND	-.2328	-.0245	1.0000			
34.GA	-.4486	.0343	.7499	1.0000		
35.LA	-.2288	-.0223	.9958	.7485	1.0000	
36.CE	-.2206	-.0130	.9858	.6782	.9877	1.0000
	31 V	32 CR	33 ND	34 GA	35 LA	36 CE

K/Rb

Figure 5.3.3 shows K/Rb plotted against F.I. and Figure 5.4.1 shows K_2O (wt%) plotted against Rb (ppm). From Figure 5.3.2 the K/Rb ratio can be seen to increase gradually from F.I.≈30 (K/Rb≈200) to F.I.≈55 (K/Rb ≈600). The K/Rb ratio then decreases through mugearites to low K/Rb (≈150-200 in phonolites and ≈150 in rhyolites).

This relationship is consistent with both K and Rb behaving as incompatible elements early in the fractionation history of these rocks (to DI≈55) after which a feldspar with appreciable K content starts to crystallise. Initially this will be anorthoclase which will give way to a binary alkali feldspar with continued evolution. Crystallisation of a K-rich feldspar will buffer K contents in the liquid (as D_K^{Fsp} will be around 1) whilst Rb is still excluded from the crystallising assemblage (D_{Rb}^{Fsp} ≈0.4 Larsen 1979), and thus cause a lowering of K/Rb in rocks fractionating an alkali-rich feldspar.

This relationship is also evident from Figure 5.4.1 where the relatively constant K_2O content in the benmoreites and phonolites can be seen whilst Rb continues to increase with evolution.

Rb, in a similar way to Ba, is relatively 'mobile' element and small amounts may be lost on alteration. This could account for the large amount of scatter at the more basic end of the compositional range in Figure 5.4.1.

Zr/Nb

Figure 5.4.2 shows histograms of Zr/Nb for all dykes excluding those from the Østfjordsdal swarm (Figure 5.4.2A) and for the Østfjordsdal swarm (Figure 5.4.2B). Clearly evident from this diagram is the fact that there are 2 marked ranges of Zr/Nb ratio with peaks at Zr/Nb=3.9 and at Zr/Nb=6.3. Both peaks have a 'Gaussian' distribution. The Østfjordsdal swarm (Figure 5.4.2B) has a lower Zr/Nb peak at 3.5. The large amount of data at Zr/Nb<0.2 are from carbonatites (and a few ultramafic lamprophyres) which are notably Zr-poor in actual terms – see later. From the whole data set (486 samples) only 11 analyses show Zr/Nb>10. Of these several are extremely evolved (Zr enriched) samples but this group also includes the possible BD_0 from Mellemlandet

These elements will be present in minerals such as rinkite, låvenite, monazite, allanite, as well as in solid solution in minerals such as sphene, apatite and zircon. Modal variation of these minerals may account for the range of concentrations seen for these elements in the coarse cumulates of the central complexes (cf. Jones 1980) but this will not be the case here with these concentrations representing 'true liquids'. REE elements were separated from a selection of these samples and analysed on an Inductively Coupled Plasma Spectrophotometer at Kings College, London/Royal Holloway and Bedford New College, Egham. These data will be discussed in Chapter 6.

U, Th

U and Th are both incompatible elements. Th rises from ≈5ppm in basaltic rocks to ≈100ppm or more in the phonolite samples. U shows slightly lower concentrations rising with only relatively few samples showing a strong increase in U. Data from Larsen (1979) may suggest that U would be incorporated into feldspar preferentially over Th. Amphibole may also have a 2-fold preference for U over Th (Henderson 1982). This will produce an overall lesser increase in U than in Th in the more evolved rock types.

Ga

Ga shows a fairly constant concentration at ≈25ppm up to F.I.≈65. This will reflect a bulk distribution coefficient of 1 in the tephritic, basaltic, hawaiitic and mugearitic rocks. From D.I.≈70. Ga starts to increase to typical contents of ≈50ppm (although it does reach slightly over 80ppm). This must reflect a lower distribution coefficient in these evolved rocks, and is probably due to a drop in the D_{Ga}^{Fsp} as the feldspar becomes less aluminous (from plagioclase $D_{Ga}^{Plag} \approx 1$ – Henderson 1982 – to a $D_{Ga}^{Ksp} < 1$).

Pb

Pb shows a gradual increase through basalts to mugearites (from ≈10ppm to ≈20ppm at D.I. ≈67) where its concentration increases rapidly. This coincides with the onset of abundant anorthoclase crystallisation. Data presented by Henderson (1982) would suggest that Pb should be more compatible in alkali feldspar in dacitic/rhyolitic ($D_{Pb}^{Ksp} \approx 1$) than in plagioclases from basalts ($D_{Pb}^{Plag} \approx 0.26$) and thus the Pb content may be expected to behave accordingly. However, data from Larsen (1979) show that the D_{Pb}^{Ksp}

in alkali silicic rocks is 0.208 and is thus less than that for plagioclase in basalt. Pb thus appears to become increasingly incompatible with fractionation in these undersaturated rocks and this may be a reflection of the a_{SiO_2}.

Zn

Zn shows little variation across most of the range of F.I. (≈200-300ppm) although a minor trend of strong Zn enrichment is seen from DI≈70-90 (300-1000ppm). Zn is strongly compatible only in amphibole (D_{Zn}^{Amp}=7) or in biotite (D_{Zn}^{Bi} ≈20, Henderson 1982). It is thus probable that crystallisation of amphibole (and probably some biotite) in these magmas 'buffered' the Zn content at late stages. Those magmas which show the highest Zn contents are some trachy-andesites and trachytes (along with a smaller number of undersaturated phonolites). These silica saturated magmas are characterised by low fo_2 and are probably drier (less H_2O). This may have inhibited late stage amphibole crystallisation in the magma reservoir and allowed a build up of Zn in these evolved fluids.

Nb, Zr

Nb and Zr are two highly incompatible elements (see Pearce and Norry 1979) and their concentrations across the range of dyke compositions reflects this aspect of their geochemistry.

Zr ranges from typical contents of 200ppm in basalts to in excess of 8000ppm in some phonolites (maximum 10899ppm in 41945, a trachy-andesite). Nb, which is present at about 30ppm in basalts increases to 1600ppm commonly. In the Zr enriched trachy-andesite 41945, Nb reached 3210ppm, however, one exceptional sample, 127064, is an altered (?carbonated) felsic rock (TAS classification as a phonolitic tephrite) which contains 8704ppm Nb, but only 125ppm Zr.

Zr is usually accommodated in pyroxenes or amphiboles and rarely as zircon. Jones (1980) recorded eudialyte from Motzfeldt, although none has been recorded from the Igaliko dykes. Larsen and Steenfelt (1974) reported Zr bearing silicates (other than zircon) from a micro-kakortokite dyke near Ilímaussaq.

Zr variation is similar to that observed by Macdonald and Parker (1970) from Tug-

tutôq who recorded up to 700ppm Zr at F.I.≈98. These authors concluded that Zr was probably present in sub-microscopic grains of Zr-rich accessory minerals disseminated through the groundmass. This was based on mass balance calculations between bulk rock Zr contents and those of riebeckite phenocrysts which could not account for the whole rock Zr content. However, in the light of data from Jones (1980) for pyroxenes, and this study for both pyroxenes and amphiboles, the high Zr concentrations are more easily explained. Sample 325986 contains 1884ppm of Zr (whole rock) and amphiboles which contain up to 4.13 wt% ZrO_2 (≡3.06 wt% Zr). The bulk rock Zr could be explained by 6% by weight of this enriched amphibole. Typically from this sample however, the Zr content of the amphibole is lower (2-3 wt%) and perhaps 9-12 wt% of this lower Zr-amphibole may be needed. Amphibole is present modally at around 10-15% and thus there is no difficulty accounting for the Zr content. Similar results are obtained for the Zr-aegirine bearing rocks also.

Nb contents are harder to account for than Zr. Larsen (1979) showed that Nb maintained its incompatibility even in the most evolved, alkaline rocks when Zr had started to be accepted into the pyroxene structure. Sphene, where present, may contain up to 0.1 atoms Nb (to 5 oxygens, Ribbe 1982) and Nb was detected in several grains although it was not analysed (see Chapter 4.12). In the central complexes important Nb-bearing phases such as pyrochlore are relatively abundant (Tukiainen *et al.* 1984) but these were not observed in the dykes. Nb may however be present in a similar manner to the Zr-rich accessories of Macdonald and Parker (1970), as sub-microscopic Nb-bearing phases. WDS microprobe analysis for Nb in the late crystallising grains may clarify the situation (as for Zr above).

5.4: K/Rb, Zr/Nb and Ce/Y

This section deals with the co-variance of the incompatible elements K/Rb, Zr/Nb and Ce/Y. Further discussion of other inter-element variation will be given later once some important points have been established on the basis of the Zr/Nb variation. Some discussion of sample bias and a 'sample numbers' against 'volume' approach to the quantities of certain magmas is also given.

Table 5.3.3 - 2 pages.

Correlation matrices for trace elements from the low and high Zr/Nb suites.

In both suites strong correlation coefficients exist between the incompatible elements Nb, Zr, Y, La, Ce and Nd, although the data is somewhat scattered at F.I.<50. Above F.I.=70, U and Th show strong correlations with the other incompatible elements in the high Zr/Nb samples.

In the evolved low Zr/Nb rocks (F.I.>70) the correlation coefficients between the incompatible elements are less strong than in the high Zr/Nb suite. This will reflect more scatter in the data, probably a result of 'individual liquid lines of descent' of small batches or pockets of magma (cf. Macdonald 1969, see Chapter 5.7).

In the undersaturated rocks (low Zr/Nb), Ga and Zn both show very similar behaviour to the REE etc. whereas this is less evident in the oversaturated (high Zr/Nb) rocks.

Elements typically associated with certain minerals (eg. Ba and Sr with feldspar, Ni and Cr with ferromagnesian minerals) show reasonably strong positive correlations.

If Zr increases 'linearly' with fractionation (cf. Clague 1978), comparison of other trace elements with Zr may give some indication of fractionating phases. V drops rapidly in both low and high Zr/Nb suites between F.I. 50 to 70 indicating the onset of opaque oxide extraction. Sr decreases with Zr increasing across all F.I ranges in the oversaturated rocks but only above F.I.=50 does it decrease in the undersaturated rocks indicating a later onset of feldspar fractionation in the low Zr/Nb suite. Similar variation is also noticed for Ba.

Figure 5.4.1 K_2O wt% vs. Rb ppm (log-log scale).

Both K and Rb are seen to increase from basic through to evolved rock types, where K becomes 'buffered' in the liquid by feldspar crystallisation whilst Rb continues to increase through to phonolites. The average K/Rb curve (solid line) and the normal limits of scatter (broken line) are taken from Ahrens *et al.* (1952).

Figure 5.4.1

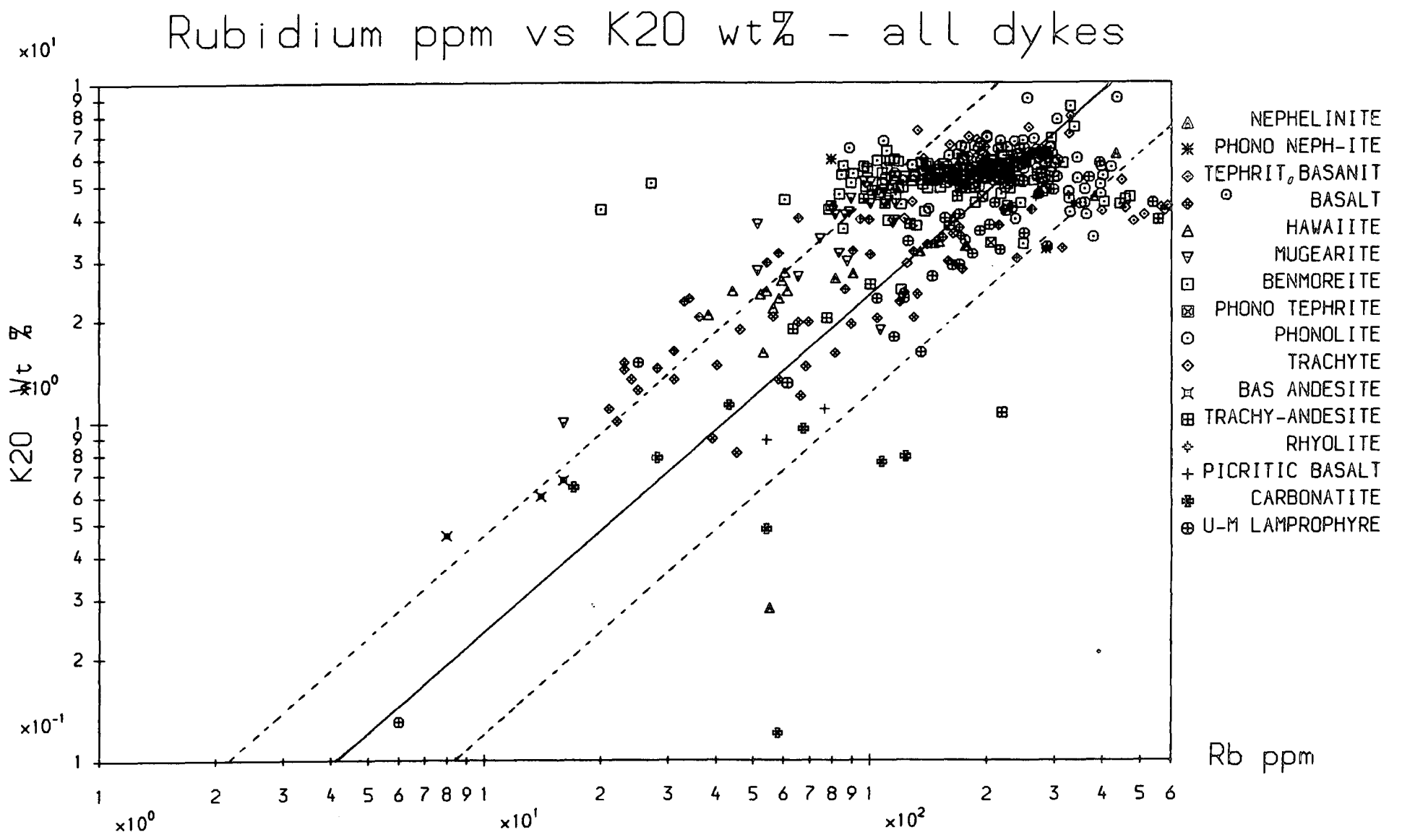
Rubidium ppm vs K20 wt% - all dykes
K20 Wt %
Rb ppm
NEPHELINITE
PHONO NEPH-ITE
TEPHRIT, BASANIT
BASALT
HAWAIITE
MUGEARITE
BENMOREITE
PHONO TEPHRITE
PHONOLITE
TRACHYTE
BAS ANDESITE
TRACHY-ANDESITE
RHYOLITE
PICRITIC BASALT
CARBONATITE
U-M LAMPROPHYRE

with Zr/Nb of 23.9-25.5 and the Alkali Gabbro Giant Dyke (also in Mellemlandet) with Zr/Nb from 10.1 to 12.1. Also, 325992, a basaltic dyke from North of Narssarssuaq has a Zr/Nb of 22.1, whilst a very similar dyke from almost the same locality possesses a Zr/Nb ratio of 6.88.

The minimumin the Zr/Nb distribution has been taken at 5.2 (see Figure 5.4.2A) and this has been used to discriminate high Zr/Nb samples from low Zr/Nb samples. Inevitably, some 'tailing off' of the (Gaussian) peaks will occur and thus some overlap is to be expected. This is illustrated schematically in Figure 5.4.2A, with samples belonging to the high Zr/Nb set becoming incorporated into the low Zr/Nb and *vice versa* when discriminating in this way.

The TAS data presented in Figure 5.2.1 (A, B and C) has been plotted with different symbols for the high and low Zr/Nb data. Two markedly different trends emerge. The low Zr/Nb samples, (tending to plot at higher total alkali contents than the high Zr/Nb samples for similar SiO_2 contents) evolve from tephrites (or possibly nephelinites) through benmoreite to phonolite. Conversely the high Zr/Nb samples evolve from basalt, through the trachy-basalts/trachy-andesites to trachyte and thence rhyolite. Certain exceptions to this trend are apparent – for example, the high Zr/Nb phonolites. This can be explained in terms of the overlap of the 'Gaussian' distributions, particularly as some of the more evolved phonolites may show the effects of crystallisation of appreciable quantities of Nb, Zr, etc. bearing phases. These anomalous samples can essentially be ignored when dealing with overall trends. Table 5.4.1 shows the relative abundance of rock types with differing Zr/Nb ratios.

In view of the data presented in Table 5.4.1 it is perhaps appropriate to consider the 'abundances' of certain rock types. Data here are presented as actual numbers of dykes and does not take account of their volumetric abundance. In view of the relatively straightforward nature of dyke morphology (on a gross scale) the volume of a dyke can be approximated by its width (assuming similar lengths and depths for all the dykes and no change in width with length/depth etc.). Martin (1985) considered this problem at some length, it being of particular importance in the Tugtutôq area where many of the dykes are the so called 'Giant Dykes' – several hundred metres across.

Figure 5.4.2

A. Histogram Zr/Nb data for all dykes excluding the Østfjordsdal dyke swarm. Two maxima are evident – one at Zr/Nb = 3.9, the other at Zr/Nb = 6.3. A minima, taken at Zr/Nb of 5.2 has been used to discriminate between samples with high and low Zr/Nb ratios. The dotted lines show presumed continuations of 'Gaussian' distributions across (underneath) the minima.

B. Histogram of Zr/Nb from dykes from the Østfjordsdal swarm. These data peak at Zr/Nb≈3.5, slightly lower than the lower Zr/Nb peak from the rest of the Igaliko dykes.

These data should be compared with the Zr/Nb ratios from Motzfeldt and South Qôroq in Figure 5.6.1.

volume of these magmas will be much less than this (perhaps only 1.5 times).

Martin (1985) concluded that with the majority of the narrow dykes from Tugtutôq and the Ilímaussaq Peninsula being on average around 5m wide, a 'numerical' approach (rather than a 'volumetric' approach) would make little difference to the overall interpretation. It is no surprise that a similar conclusion from the dykes in the vicinity of Igaliko can be reached, although the volumes involved should be borne in mind.

From Table 5.4.1 it can be seen that there are clear differences in the abundances of different compositions of dykes. Excluding the fact that the high Zr/Nb suite evolves to rhyolite and the low Zr/Nb suite to phonolite, the most striking differences are in the numbers of the more basic dykes. Whilst some 34% of the high Zr/Nb suite is less evolved than hawaiite, less than 7% of the low Zr/Nb suite (with the exclusion of UML's and carbonatites) are more basic than hawaiite – clearly a 'real' and not a 'sample bias' difference. This relationship is illustrated in Figure 5.4.3 where histograms of the F.I. of the low and high Zr/Nb data sets are shown. A clear bimodal distribution is evident in the high Zr/Nb data set, with a marked scarcity of compositions between F.I.≈55 to F.I.≈70. No such bimodal distribution is evident in the low Zr/Nb data where almost all samples cluster in the range F.I.>70. Discussion of the individual suites will be resumed in more detail later.

Both Zr and Nb are highly incompatible elements in almost all minerals (Pearce and Norry 1979, Henderson 1982). Assuming a fractional crystallisation model for the genesis of the evolved rocks from the more basic rocks (see later) and bulk distribution values of 0 for both Zr and Nb (typical $D_{Zr}^{mineral}$ or Nb≈0.01-0.1 – Pearce and Norry 1979), then the fractional crystallisation model

$$C_L^i/C_O^i = F^{D-1} \text{ approximates to } C_L^i/C_O^i = 1/F$$

where C_L^i is the content of trace element i in the magma at the time of observation, C_O^i is the content of trace element i in the initial magma, F is the fraction of liquid remaining and D is the bulk distribution coefficient (assumed to be 0). Thus, an approximation to the amount of liquid remaining can be made assuming an initial 'parent' composition. Figure 5.4.4 shows Zr plotted against Nb. 'F' has been calculated assuming the most abundant basic component from each suite may approximate to the parent (excluding

Figure 5.4.3A

Histogram of F.I. for the low and high Zr/Nb suites. The low Zr/Nb suite excludes the Østfjordsdal dykes. There is a clear difference in the relative amounts of varying compositions. The high Zr/Nb suite shows maxima at basaltic and benmoreitic/trachytic/rhyolitic compositions separated by a minima in the hawaiite/mugearite range ('Daly' gap). This is discussed in the text and may be due to the onset of magnetite crystallisation (Martin 1985).

The low Zr/Nb suite is mostly composed of benmoreites and phonolites with very small quantities of material less evolved than F.I.≈70. These compositions are closely similar to those exposed in all the central complexes of the Igaliko Nepheline Syenite complex.

Figure 5.4.3B (Overleaf)

Histogram of F.I. for dykes from the Tugtutôq–Ilímaussaq region (from Martin 1985). These data are clearly very similar to the high Zr/Nb suite of dykes.

Figure 5.4.3A

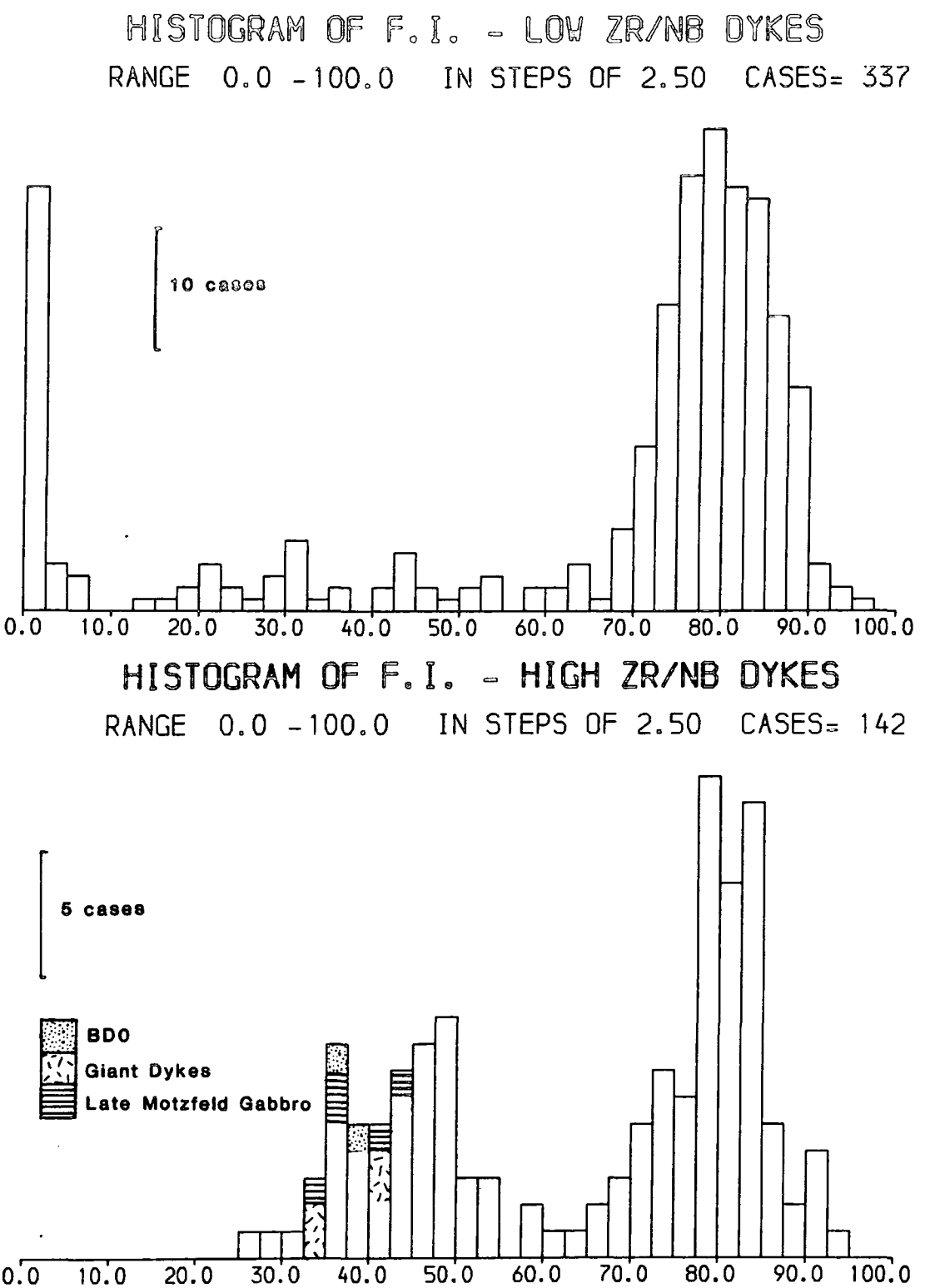
HISTOGRAM OF F.I. - LOW ZR/NB DYKES
RANGE 0.0 -100.0 IN STEPS OF 2.50 CASES= 337
10 cases
0.0 10.0 20.0 30.0 40.0 50.0 60.0 70.0 80.0 90.0 100.0
HISTOGRAM OF F.I. - HIGH ZR/NB DYKES
RANGE 0.0 -100.0 IN STEPS OF 2.50 CASES= 142
5 cases
BDO
Giant Dykes
Late Motzfeld Gabbro
0.0 10.0 20.0 30.0 40.0 50.0 60.0 70.0 80.0 90.0 100.0

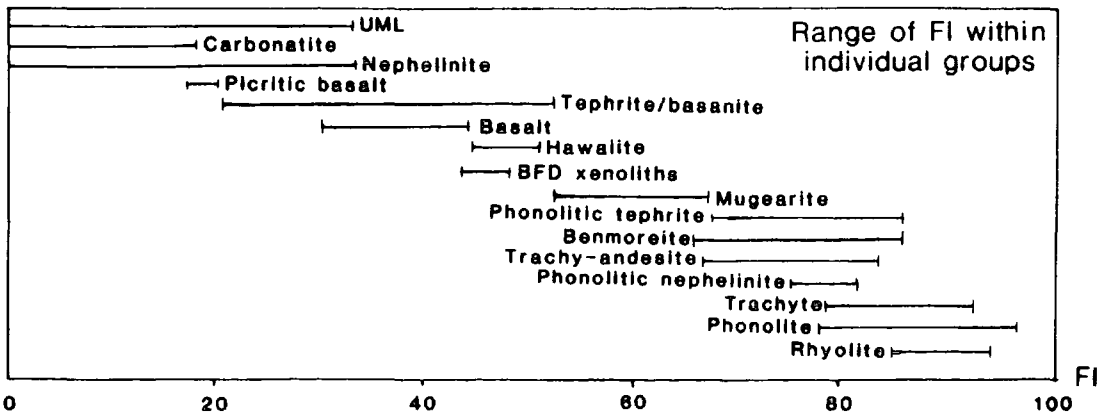
Range of FI within individual groups
UML
Carbonatite
Nephelinite
Picritic basalt
Tephrite/basanite
Basalt
Hawaiite
BFD xenoliths
Mugearite
Phonolitic tephrite
Benmoreite
Trachy-andesite
Phonolitic nephelinite
Trachyte
Phonolite
Rhyolite
0 20 40 60 80 100
FI

Figure 5.4.2A

HISTOGRAM OF ZR/NB, NOT ØSTFJ-DAL DYKES

RANGE 0.0 - 10.0 IN STEPS OF 0.20 CASES= 433

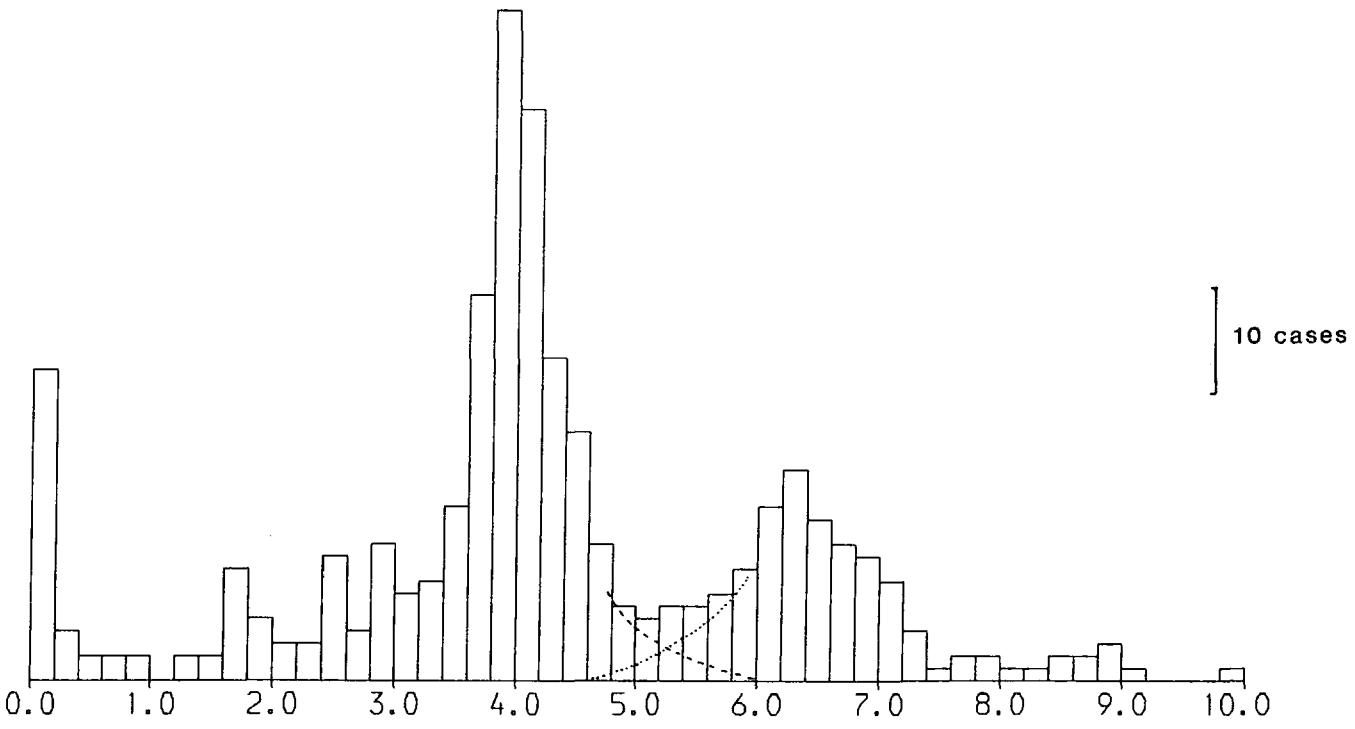

Figure 5.4.2B

HISTOGRAM OF ZR/NB FROM ØSTFJ-DAL DYKES

RANGE 0.0 - 10.0 IN STEPS OF 0.20 CASES= 34

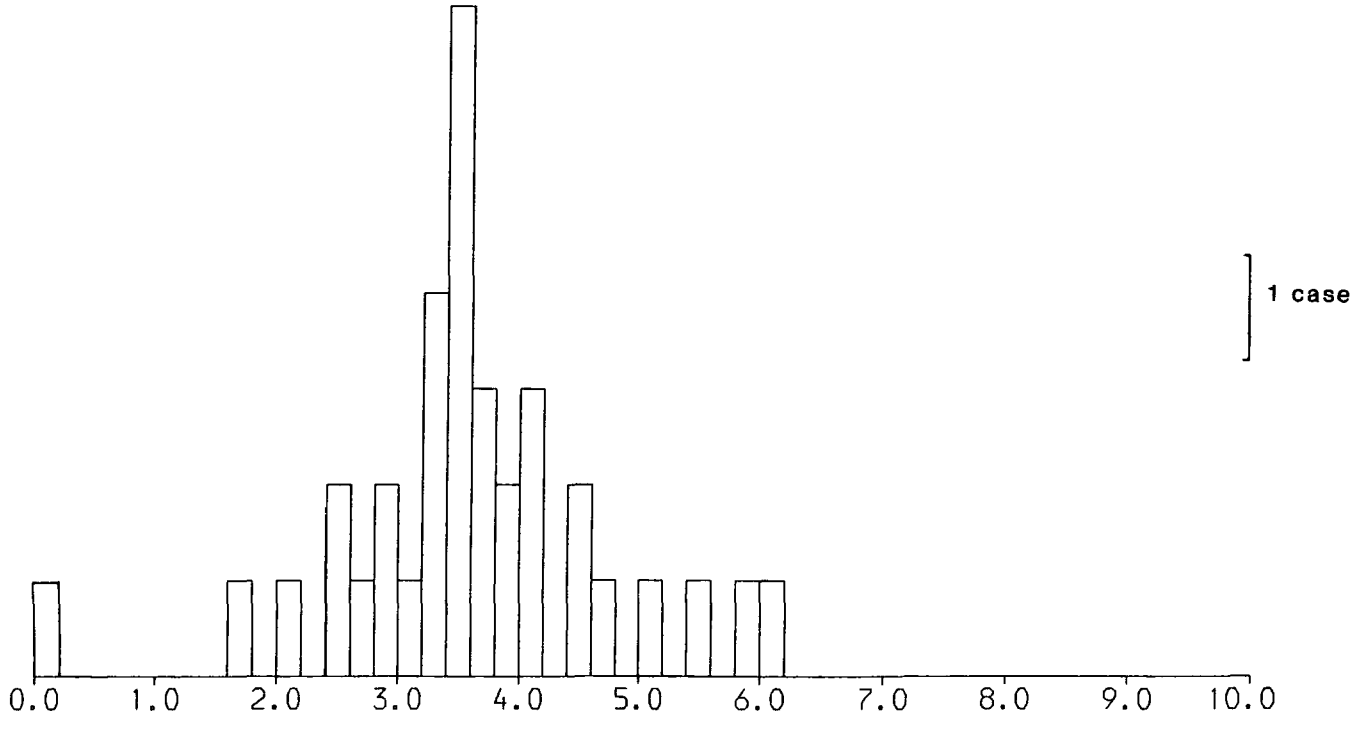

Table 5.4.1

Number of analysed samples of different rock types with differing Zr/Nb ratios. Figures in brackets are percentages excluding BFD xenocrysts.

Rock Type	Zr/Nb≤5.2	Zr/Nb>5.2	Østfjordsdal Swarm
Ultramafic Lamprophyre	21 (6.75)	0 (0.0)	6 (16.67)
Nephelinite	8 (2.57)	0 (0.0)	3 (8.33)
Tephrite/Basanite	9 (2.89)	15 (11.03)	6 (16.67)
Picritic Basalt	2 (0.64)	0.(0.0)	0 (0.0)
Basalt	2 (0.64)	23 (16.91)	0 (0.0)
Hawaiite	0 (0.0)	10 (7.35)	2 (5.56)
Mugearite	13 (4.18)	8 (5.88)	1 (2.78)
Benmoreite	99 (31.83)	42 (30.88)	2 (5.56)
Phonolitic Nephelinite	2 (0.64)	0 (0.0)	0 (0.0)
Phonolitic Tephrite	6 (1.92)	0 (0.0)	1 (2.78)
Phonolite	111 (35.69)	5 (3.68)	13 (36.11)
Trachyte	8 (2.57)	21 (15.44)	0 (0.0)
BFD xenocrysts	0 —	3 —	0 —
Trachy-andesite	4 (1.29)	8 (5.88)	1 (2.78)
Rhyolite	0 (0.0)	4 (2.94)	0 (0.0)
Carbonatite	26 (8.36)	0 (0.0)	1 (2.78)
Total	311 (100.0)	139 (100.0)	36 (100.0)

In general, the dykes from the Igaliko region tend to be less than 15 metres wide, most being in the region of 3-7m wide. Among the larger dykes, BFD's are the commonest (hawaiitic or mugearitic compositions) but these are relatively limited numerically. Of the thinner dykes, carbonatites are particularly abundant, tending not to exceed ≈2 metres. Thus, as with Table 5.4.1, where a purely numerical count of rock types is taken, the *volume* of carbonatite material will tend to be somewhat overestimated (perhaps 2.5 fold) and the hawaiitic/mugearitic component from BFD's will be underestimated (by perhaps 2-3 fold). However, BFD's are not the sole representatives among the high Zr/Nb dykes of hawaiitic and mugearitic magmas, these types occurring also as narrow (5m wide or so) dykes containing no foreign material. Thus, the underestimate of the

Figure 5.4.3B

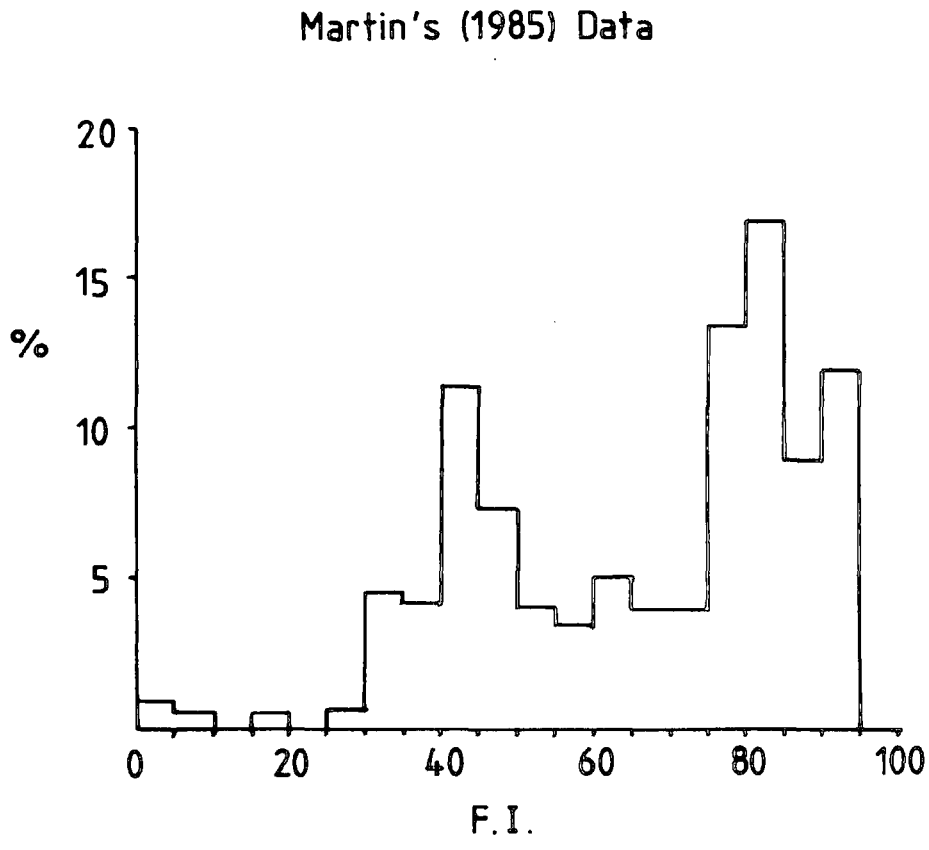

nephelinite, UML and carbonatites). Thus, an average of all tephrites with Zr/Nb$\leq$5.2 has been used as the parent for the low Zr/Nb suite and an average of all basalts with Zr/Nb>5.2 has been used for the high Zr/Nb suites. The average compositions for each group are tabulated later (Tables 5.5.1 and 5.6.1), and the average compositions of high Zr/Nb trachytes, and low Zr/Nb phonolites are plotted on Figure 5.4.4. There is a tendency for the early trend of Zr vs. Nb (at <2000ppm Zr) to be linear, and above this the low Zr/Nb trend tends to curve slightly to a less rapid increase in Nb with increasing Zr. This curvature essentially reflects a relative change in the bulk D for Zr and Nb between minerals and liquid, and is probably a direct result of the high solubility of Zr in peralkaline undersaturated liquids (Watson 1979). No such curvature of the Zr/Nb trend is seen in the high Zr/Nb which evolves to oversaturated compositions, and this would imply that both Nb and Zr maintain roughly equal solubilities in these oversaturated (peralkaline) residues.

From Figure 5.4.4, the average phonolite composition could be generated by about 65% crystallisation of the average low Zr/Nb basalt, but not from the tephrite without an increase in its Zr/Nb ratio with fractionation, whereby perhaps 68% crystallisation would produce phonolite.

The average basalt, with Zr/Nb at 10.9, has a Zr/Nb ratio about 75% higher than the majority of high Zr/Nb samples (Zr/Nb=6.3) whereas the high Zr/Nb tephrite has a Zr/Nb ratio of 6.38 and fits the observed trend more clearly. For the high Zr/Nb average trachyte, assuming crystallisation of a tephrite parent, about 88% crystallisation is required, and perhaps 89-90% if the basalt parent is assumed. The rhyolites however, pose a problem – plotting at about half the Zr and Nb contents of the average trachyte. As this suite becomes more acidic biotite and amphibole become increasingly important phases (Macdonald 1969, Martin 1985). Both of these minerals possess D_{Zr} and D_{Nb} greater than 1 (D_{Zr}^{Amph}=4, D_{Zr}^{Bi}=2, D_{Nb}^{Amph}=4, D_{Nb}^{Bi}=3, Pearce and Norry 1979), and as the content of these phases increase in the crystallising assemble the bulk D for Zr and Nb may exceed unity. This, with the similarity of D_{Zr} and D_{Nb} for amphibole and biotite would cause the trend to 'double back' on itself and this appears to have happened between the trachytes and the rhyolites. As some trachytes persist to F$\approx$0.04, the rhyolites can be assumed to be residues of less than 4% of the original parent.

Figure 5.4.4: Zr vs. Nb.

Two trends of data are clearly apparent at Zr less than 2000ppm. These can be seen to continue, more sparsely to higher contents of both Zr and Nb.

The straight lines are lines of constant Zr/Nb (as marked) taken from average basalts and tephrites from high (>5.2) and low (<5.2) Zr/Nb suites. These are likely to be parental to the more fractionated rock types. The dashed line is Zr/Nb=5.2.

The open stars marked on the solid lines represent residual liquid compositions assuming fractional crystallisation of the chosen parent (basalt or tephrite) with bulk D_{Zr} and bulk D_{Nb} both 0. Thus $C_l/C_o=1/F$ where F is the fraction of liquid remaining and is marked next to these stars. C_o is the content of a trace element in the original liquid, C_l is the content of the same trace element in the more evolved liquid.

The white stars on black grounds indicate average phonolite for the low Zr/Nb suite (P) and average trachyte for the high Zr/Nb suite (T). See text for discussion.

Figure 5.4.4

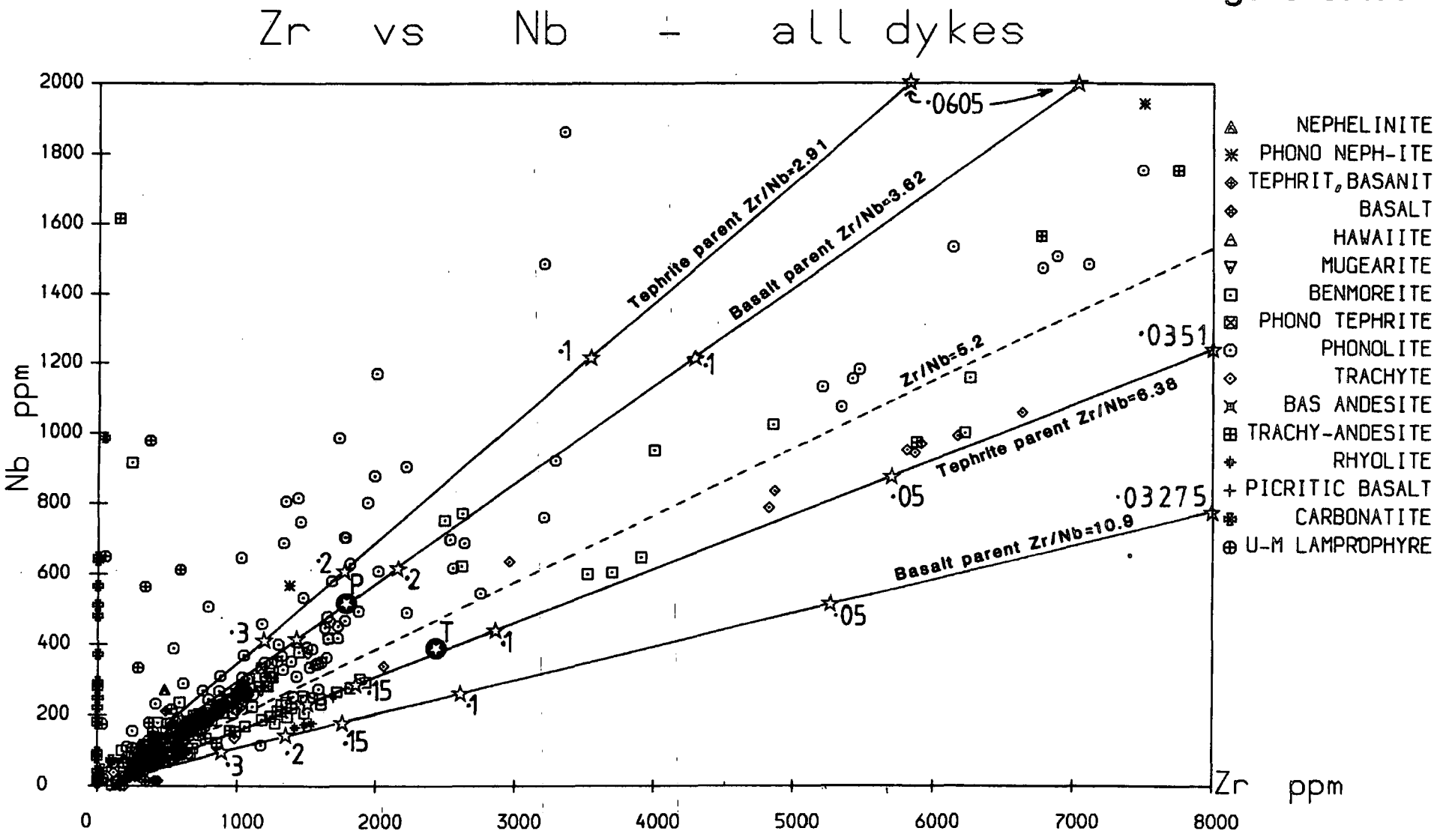
Zr vs Nb - all dykes
Nb ppm
Zr ppm
0
200
400
600
800
1000
1200
1400
1600
1800
2000
0
1000
2000
3000
4000
5000
6000
7000
8000
Tephrite parent Zr/Nb=2.91
Basalt parent Zr/Nb=3.62
Zr/Nb=5.2
Tephrite parent Zr/Nb=6.38
Basalt parent Zr/Nb=10.9
·0605
·0351
·03275
·05
·1
·2
·3
·15
P
T
NEPHELINITE
PHONO NEPH-ITE
TEPHRIT, BASANIT
BASALT
HAWAIITE
MUGEARITE
BENMOREITE
PHONO TEPHRITE
PHONOLITE
TRACHYTE
BAS ANDESITE
TRACHY-ANDESITE
RHYOLITE
PICRITIC BASALT
CARBONATITE
U-M LAMPROPHYRE

Ilmenites and Zr/Nb

A noticable feature of the Zr/Nb vs. F.I. plot (Figure 5.3.3) is a drop in Zr/Nb with increasing F.I. for basaltic rocks with Zr/Nb>5.2. Pearce and Norry (1979) quote $D_{Zr}^{Ilmenite}$ at ≈0.28 in basaltic melts. Ilmenite is a relatively common component of many of the basic rocks and two samples – a basalt, 325992, and a mafic syeno-gabbro (TAS classification as an ultramafic lamprophyre), 43867, both contain ilmenites with detectable Zr by EDS microprobe. Zr will substitute for Ti in the octahedral site in ilmenite. Due to the weak nature of the Zr peak, these were reanalysed by Dr A. Peckett using the WDS microprobe at Durham University, and gave the following results. $D_{Zr}^{Ilmenite}$ is calculated as Zr in ilmenite/Zr in whole rock.

Sample	43867	325992
Ilmenite, ppm Zr	≈1100	≈1700
Whole Rock, ppm Zr	187	332
$D_{Zr}^{Ilmenite}$	≈6	≈5.1
Normative Ilmenite, wt%	14.97	5.45

Figure 5.4.4 shows Zr/Nb against Nb for some of the high Zr/Nb basalts and shows that Zr/Nb decreases from about 12 to 6 over the range that Nb increases from 17 to 40ppm. This indicates a constant Zr content in the liquid, and assuming that fractional crystallisation is responsible for the increasing Nb, a bulk D of ≈0.85 is implied. The major phenocryst phases in the basaltic rocks are plagioclase, olivine, clinopyroxene and ilmenite. Taking a typical high Zr/Nb basalt as our example with ≈3.3 wt % TiO_2 corresponding to about 7 wt% ilmenite and assuming D_{Nb}=0 and D_{Zr} (for all phases other that ilmenite)=0, then the bulk D_{Zr} ≈0.07×5.5 ≈0.385. This is approximately half of the bulk D calculated from Zr/Nb vs. Nb of ≈0.85. It would thus seem that crystallisation and extraction of ilmenite (with a $D_{Zr}^{ilm/liq}$ of 5.5) is largely responsible for the decline in the Zr/Nb in the basaltic rocks. As ilmenite gives over to other Fe-Ti oxides with increased fractionation, the bulk D for Zr/Nb will return to ≈0 and the Zr/Nb ratio will stabalize. It is interesting to note that the EDS analyses for Zr in ilmenites (at 3130ppm in 325992 and 1940ppm in 43867) gives $D_{Zr}^{Ilmenite}$ of 9.4 and 10.4 respectively and would give a calculated bulk D_{Zr} of ≈0.7, close to the observed bulk D from Zr/Nb vs. Nb.

Figure 5.4.5: Zr/Nb vs. Nb for selected basaltic rocks.

The trend of increasing Nb with decreasing Zr/Nb suggests that the bulk D for Zr in these basaltic rocks is ≈ 0.85. This may be a result of the fractionation of ilmenite (see text for discussion).

Figure 5.4.5

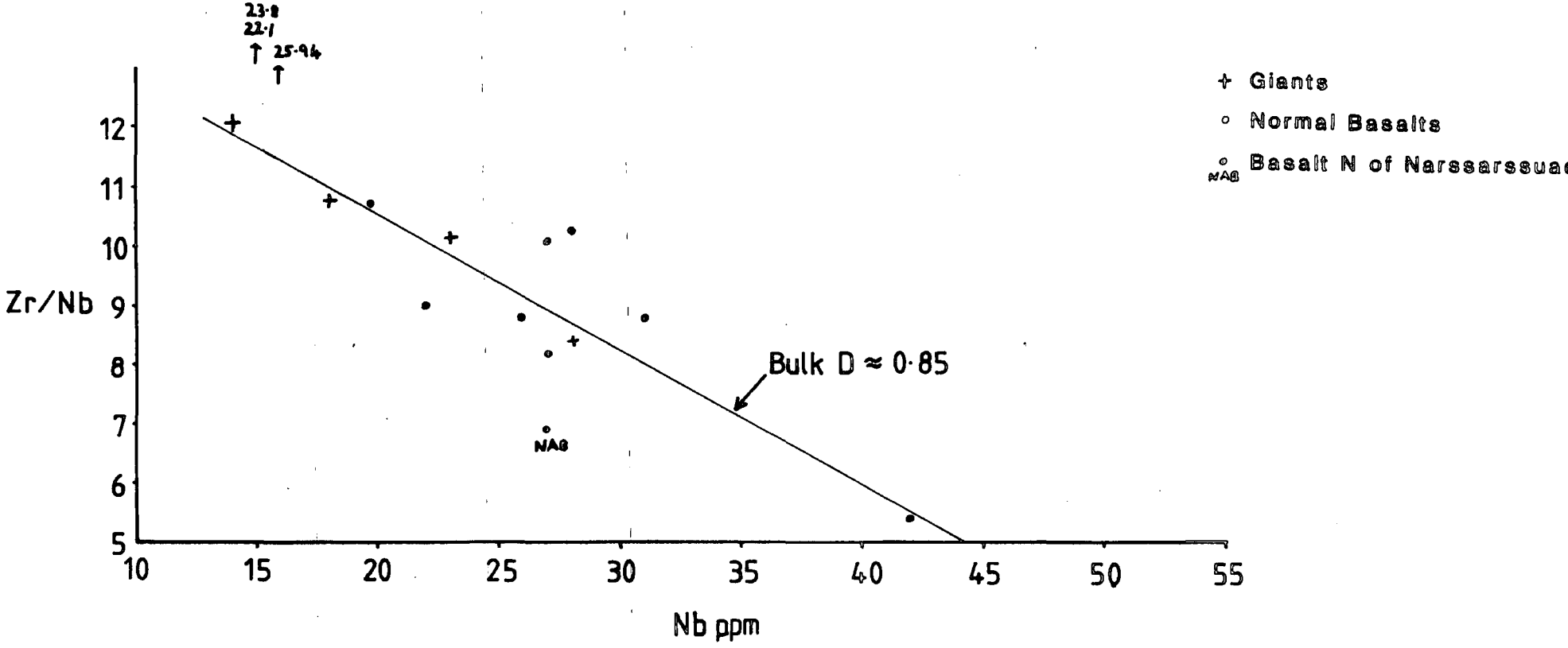
23·8
22·1
25·94
Giants
Normal Basalts
Basalt N of Narssarssuaq
NAG
Bulk D ≈ 0·85
Zr/Nb
Nb ppm
12
11
10
9
8
7
6
5
10
15
20
25
30
35
40
45
50
55

Ce/Y

A plot of Ce/Y is produced in Figure 5.3.1. Ce is a slightly more incompatible element than Y (Henderson 1982). These HFSE elements are relatively immobile on alteration and should reflect original compositions even in altered specimens. Ce/Y is approximately 3 in the basaltic rocks and is somewhat higher in the tephrites (≈5). From basalt through hawaiite there is a gradual rise in Ce/Y to ≈5 where it then remains essentially constant to F.I.≈85. From here it is perhaps noticeable that Ce/Y tends to be lower in the rhyolites and higher in the phonolites and that there is a slightly lower oversaturated trend. Y behaves in a similar manner to the HREE, and is incorporated into the structures of amphiboles and pyroxenes in preference to Ce. (D_{Ce}^{Amp} ≈0.34, D_{Y}^{Amp} ≈0.5?, D_{Y}^{cpx} ≈1.05 D_{Ce}^{Px} ≈0.34, Ce data from Henderson 1982, Y data taken as equivalent to Ho, Frey *et al.* 1978, and interpolated between Dy and Er from Henderson 1982). Plagioclase and alkali feldspar have a slight preference for the LREE, eg. Ce ($D_{Ce}^{Plag/basalt}$ ≈0.14 $D_{Y}^{Plag/basalt}$ ≈0.085?, $D_{Ce}^{Alk\ fsp/rhyolite}$ ≈0.04, $D_{Y}^{Alk\ fsp/rhyolite}$ ≈0.006, Henderson 1982, Y as Ho). Thus, feldspar fractionation will tend to slightly decrease Ce/Y, whilst increasing absolute Ce and Y contents, but clinopyroxene will tend to increase markedly Ce/Y, possibly 'buffering' Y but increasing absolute Ce. A combination of plagioclase/alkali feldspar and clinopyroxene fractionation will cause an increase in Ce/Y.

5.5: Magmatic Evolution

Having established in the previous section that the dykes in the vicinity of Igaliko include members of an oversaturated and an undersaturated suite which can be discriminated upon on the Zr/Nb ratio (see figures 5.2.1, 5.4.3 and 5.4.4), the following section will examine certain aspects of their chemistry independently, although many aspects of their evolution (particularly at early stages) can be regarded as essentially similar. Certain elements (eg. Si, Al, alkalis) show fairly distinct differences in behaviour between the low Zr/Nb suite (trending to Si-undersaturation) and the high Zr/Nb suite (showing a trend to Si-oversaturation). However, the majority of trace elements, when taken separately , show extremely similar behaviours and content for the low and high Zr/Nb groups, with the exception of Nb, not surprisingly lower in the high Zr/Nb group which trends to oversaturated compositions. All other trace elements show sim-

ilar behaviour in both suites indicating for both a relatively similar source/genesis and evolution.

5.5.A: High Zr/Nb suite

This suite evolves from basalt through to rhyolite. A histogram of F.I. for these rocks is presented in Figure 5.4.3A where a clear bi-modal distribution is evident. This represents a marked scarcity of rocks of mugearitic composition (see Table 5.4.1 for relative abundances of different compositional ranges). A noticable field characteristic of these dykes is their persistent outcrop. They tend to form larger dykes than the low Zr/Nb suite and on this basis have a more regional character. They also tend to be concentrated in the region of maximum extension, particularly to the north of Narssarssuaq. They also form some of the more prominent dykes running up through the South Qôroq Centre and south of Igaliko along the Igaliko-Julianehåb peninsula. Within the suite, there is a tendency for the basaltic dykes to be concentrated to the north of Narssarssuaq.

These dykes evolve to higher SiO_2 and lower Al_2O_3 contents than the low Zr/Nb suite, reflecting the presence of quartz instead of nepheline. These dykes also evolve to lower alkali contents. They tend to be *hy* or *q* normative. Figure 5.4.3B shows a histogram of F.I. for the data of Martin (1985) and this bears close similarity to that of the high Zr/Nb suite (Figure 5.4.3A). Both these data and Martin's (1985) show extremely similar Zr/Nb ratios and these are repeated to some extent in the data presented by Upton and Fitton (1985) from Mellemlandet and GF Holm Nunataq. Martin (1985) presents data from rocks similar to those studied by Macdonald (1969,1970); Macdonald and Edge (1970) and Macdonald and Parker (1970). Some of Martin's (1985) data is from dykes cropping out as close to the Igaliko Complex as 5km S of Qagssiarssuk, whereas Macdonald's data is limited to Tugtutôq. There can be no doubt that these high Zr/Nb dykes belong the main Tugtutôq - Ilímaussaq - Nunataq zone of dykes (Martin 1985, Upton and Fitton 1985, Upton and Emeleus 1987) with the exception of the possible BD_0, the late Motzfeldt alkali gabbro dyke and those phonolitic dykes with Zr/Nb>5.2 (which are only included in this group by virtue of the discriminating parameter). Although included in all plots, these phonolites can safely be ignored. The high Zr/Nb dykes are thus an 'along strike' continuation of those studied by Martin

(1985) and a 'down strike' continuation of those reported by Upton and Fitton (1985).

In the previous section it was noted that there is a compositional gap between basalts and benmoreites, a feature common to all traverses across the Tugtutôq - Ilímaussaq - Nunataq Swarm (see Martin 1985, Upton and Fitton 1985). This compositional gap is similar to the 'Daly Gap' common on oceanic islands and first described by Daly (1925) from Ascension.

Martin (1985) considered the effects of changing density and viscosity as a magma evolved from basalt to rhyolite. (calculated by the methods of Bottinga *et al.* 1982 and Shaw 1972 respectively) Modelling by these methods, Martin (1985) found no density or viscosity maxima which could account for a decreased abundance of a particular composition.

Clague (1978) argued that the reason for the 'Daly Gap', and not necessarily the gap itself, was important and questioned the fact that SiO_2, CaO, D.I. etc. varied directly with increased crystal fractionation (ie. are SiO_2, D.I. etc. inversely proportional to the fraction of remaining liquid). Clague (1978) obtained an estimate of the residual liquid from incompatible trace element concentrations where $D \approx 0$. Thus, $1/F \approx C_l/C_o$ and $F \approx 1/C_l$. Clague (1978) plotted SiO_2 against 1/Zr and found that SiO_2 varied little up to 55% crystallisation but showed a rapid increase between 55% and 70% crystallisation. This was seen to be coincident with a rapid change in both Fe and Ti and was equated with the onset of Ti-magnetite crystallisation. Martin (1985) noted similar behaviour from the Tugtutôq-Ilímaussaq dykes and this behaviour is also evident from the high Zr/Nb samples studied here, with the onset of Ti-magnetite crystallisation apparently at D.I.$\approx$50 (D.I.$\approx$F.I. at low D.I.). A relatively rapid change in D.I. is observed with a small increase in the amount of crystallisation and this can also be seen in the SiO_2 vs. F.I. plot (Figure 5.3.1).

5.5.B: Liquidus assemblages

Estimates of the compositions of liquidus mineral assemblages can be made using solutions to equations based on observed and experimental data for silicate liquid systems (Nathan and VanKirk 1978). This model assumes that the crystallisation temperature of a mineral is a smooth function of the composition of the magma and also that the

mineral compositions are 'simple'. The system only considers 8 major elements Si, Ti, Al, Fe, Mg, Ca, Na and K. A computer program produced by Geist *et al.* (1985) based on the Nathan and Van Kirk (1978) model was used to calculate the compositions of the liquidus assemblages. As with any model of this type inaccuracies are inherent and errors are cumulative. Thus the program was terminated after 20% crystallisation. Up to this stage errors are acceptable (Giest *et al.* 1985). The model is based on H_2O free, 1 atmosphere crystallisation. It is considered to be valid in predicting phenocryst phases in volcanic rocks and the sequence of events during crystallisation of shallow intrusions (Nathan and VanKirk 1978). Average compositions based on the Cox *et al.* (1979) TAS classification were used in the calculation and are listed in Table 5.5.1.

Table 5.5.2 shows the temperature at which the calculated mineral compositions appeared on the liquidus, their simplified compositions and their total weight% of the original liquid.

The range of mineral compositions generated by this model (particularly feldspar and oxide) agrees quite closely with observed mineral compositions from these rocks (see Table 3.12.1 – Summary mineralogy). The plagioclases of compositions An_{30-20} will represent the anorthoclases seen in many evolved samples. Olivines tend to be less magnesian in the rocks than those generated by the Nathan and VanKirk (1978) model. Liquidus mineral compositions can be used as a guide to the compositions used in the 'mineral extract' calculations (see below) but their use as the 'extracted minerals' is not necessarily valid due to the uncertainties in the model (see for example Cox 1980).

5.5.C: Mineral Extract Calculations

Modelling of fractional crystallisation can be achieved by a 'least squares' fitting of hypothetic extracted phases from a parent composition to produce a predetermined daughter composition. This is an iterative process which adjusts the proportions of the phases to be extracted to minimise the residual errors.

A computer program to perform this mass-balance calculation was written by Geist *et al.* (1985) and is based on the 'matrix inversion' procedure originally derived by Bryan *et al.* (1969). Caution should be exercised in the selection of mineral phases for extraction in that they must be geologically reasonable. The use of several mineral

TABLE 5.5.1 (2 pages)

Average composition of TAS classified high Zr/Nb rocks.

	TEPH	BAS	HAW	MUG	BEN
SIO2	44.37	45.87	47.63	50.24	58.11
TIO2	3.33	3.13	2.80	2.23	1.00
AL203	13.81	15.10	15.19	16.34	14.79
FE203	3.76	2.23	4.08	3.69	3.83
FEO	10.43	11.13	8.00	6.36	6.08
MNO	0.23	0.20	0.20	0.20	0.25
MGO	5.09	5.33	4.18	2.83	0.65
CAO	7.15	7.86	7.02	5.79	2.52
NA20	3.43	3.12	3.93	4.38	4.85
K20	3.11	1.51	2.31	3.64	5.15
H20+	nd	nd	nd	nd	nd
H20-	nd	nd	nd	nd	nd
P205	2.04	1.27	1.64	1.43	0.24
TOTAL	96.75	96.75	96.98	97.13	97.47
BA	3381	1377	2311	3364	685
NB	44.00	24.00	48.00	53.00	233
ZR	281	262	299	339	1439
Y	56.00	40.00	42.00	44.00	128
SR	1469	965	1187	1499	240
RB	111	64.00	54.00	82.00	212
ZN	140	133	140	135	288
CU	12.00	39.00	10.00	6.00	3.00
NI	20.00	52.00	17.00	7.00	2.00
PB	10.00	13.00	14.00	14.00	49.00
U	5.00	2.00	3.00	5.00	6.00
TH	3.00	2.00	4.00	6.00	28.00
V	267	330	239	156	40.00
CR	25.00	43.00	19.00	11.00	3.00
ND	121	60.00	89.00	98.00	236
GA	22.00	26.00	24.00	26.00	44.00
LA	121	40.00	83.00	96.00	284
CE	236	112	179	195	477
F	400	700	500	1400	1300
CL	300	300	500	300	600

TEPH - AVERAGE TEPHRITE
BAS - AVERAGE BASALT
HAW - AVERAGE HAWAIITE
MUG - AVERAGE MUGEARITE
BEN - AVERAGE BENMOREITE

continued...

TABLE 5.5.1 (continued)

	PHON	TR	BFD-XE	TR-AND	RHY
SIO2	56.81	60.73	53.46	60.93	72.37
TIO2	0.62	0.76	0.14	0.93	0.39
AL203	16.52	16.52	29.03	13.70	12.80
FE203	3.80	3.62	0.24	3.82	2.06
FEO	6.08	5.49	0.48	5.78	2.74
MNO	0.26	0.23	0.01	0.25	0.08
MGO	0.38	0.38	0.31	0.58	0.18
CAO	1.81	1.75	9.98	2.29	0.55
NA2O	6.21	5.33	4.53	4.85	3.98
K2O	6.79	5.38	0.58	4.50	4.53
H2O+	nd	nd	nd	nd	nd
H2O-	nd	nd	nd	nd	nd
P2O5	0.04	0.08	nd	0.13	nd
TOTAL	99.32	100.27	98.76	97.76	99.68
BA	314	177	851	171	121
NB	429	378	1.00	203	193
ZR	2383	2343	133	1250	1533
Y	121	205	2.00	118	120
SR	150	133	2143	107.00	31.00
RB	325	295	13.00	192	277
ZN	359	384	18.00	285	178
CU	5.00	3.00	2.00	8.00	10.00
NI	4.00	5.00	4.00	3.00	5.00
PB	123	86.00	2.00	56.00	60.00
U	15.00	13.00	11.00	6.00	15.00
TH	25.00	51.00	14.00	30.00	53.00
V	26.00	30.00	10.00	42.00	16.00
CR	nd	1.00	nd	3.00	7.00
ND	150	380	nd	227	200
GA	49.00	49.00	20.00	44.00	41.00
LA	157	278	nd	264	235
CE	323	765	6.00	450	435
F	2400	2000	4800	1600	2900
CL	1500	300	nd	200	200

PHON - AVERAGE PHONOLITE
TR - AVERAGE TRACHYTE
BFD-XE - AVERAGE BFD PLAG XENOCRYST
TR-AND - AVERAGE TRACHYANDESITE
RHY - AVERAGE RHYOLITE

Table 5.5.2

Liquidus mineral assemblages calculated from Nathan and VanKirk (1978) model.

Sample	Tephrite	Basalt	Hawaiite	Mugearite	Benmoreite	Trachyte
Mt %	5.28	0.32	3.96	3.43	4.39	3.33
Mt (Mt)	40-45	33-33	51-48	54-41	65-65	68-69
Mt Temp°C	1145.1	1140.7	1149.2	1134.9	1082.9	1084.0
Ol%	7.13	6.09	3.32	1.95	2.49	1.51
Ol (Fo)	73-73	73-66	77-76	74	39-27	29-24
Ol Temp	1163.9	1165.5	1144.7	1126.1	1074.6	1074.4
Plag %	7.64	13.64	12.78	14.68	11.78	15.21
Plag (An)	60-57	59-54	54-47	27-24	25-21	
Plag Temp	1142.3	1166.7	1148.8	1139.0	1075.4	1081.7
Aug %					1.40	
Aug (Di)					42-34	
Aug Temp					1068.5	
Final liquid after 20% crystallisation						
SiO_2	51.34	48.49	53.28	55.52	65.27	64.47
TiO_2	2.64	3.94	2.52	1.96	0.36	0.31
Al_2O_3	15.77	14.64	15.58	16.51	15.96	16.53
Fe_2O_3	2.37	2.78	3.06	2.70	1.52	1.86
FeO	7.33	12.26	6.55	5.10	2.68	3.39
MgO	3.74	4.47	4.01	2.86	0.22	0.25
CaO	8.47	8.09	7.50	5.78	2.16	1.34
Na_2O	4.16	3.38	4.44	4.76	5.09	5.07
K_2O	4.17	1.96	3.06	4.80	6.74	6.79
Final Temp°C	1131	1139.8	1131.2	1117.4	1066.9	1071.8
TAS Final Liquid	Mug	Bas	Mug	Ben	Trach	Trach

species will nearly always result in a good 'fit'. Addition of minerals of unusual composition into the crystallising assemblage solely to improve the fit may not have any significance. Modelling should be carried out in a series of small steps as it is unreasonable to expect mineral compositions to remain constant over a wide range of liquid composition.

Table 5.5.3

Results from Extract calculations – high Zr/Nb suite.

Parent	Ilmenite	Magnetite	Feldspar	Olivine	Pyroxene	Other	Daughter	R^2
Basalt	BAS-IL	TEP-OX	BA-PL2	BAS-OL	BA-PX2		Hawaiite	0.228
	1.2%	2.6%	16.2%	6.8%	6.4%		66.8%	
Hawaiite	BAS-IL	USP-60	HAW-PL	HAW-OL	HAW-PX		Mugearite	
	1.5%	1.4%	12.0%	5.9%	7.7%		71.5%	0.458
Mugearite	BA-IL2	TEP-OX	HAW-PL	HAW-OL	HAW-PX		Benmoreite	
	3.0%	0.5%	29.7%	6.9%	4.8%		55.2%	4.705
Benmoreite		USP-20			BE-PX2	APATIT	Trachyte	
		1%			4.6%	0.1%	94.2%	0.458
Trachyte		USP-20	ANT-1		TR-PX1		Rhyolite	
		8.2%	12.0%		3.3%		16.1%	0.623
			TRA-AF					
			28.9%					
			TR-AF					
			31.5%					
			=72.4%					
Total remaining liquid from basalt to rhyolite							4.0%	

Abbreviations: BA, BAS – Basalt; TEP – Tephrite; HAW – Hawaiite; PL, PL2 – Plagioclases; ANT – Anorthoclase; TRA – Trachy-andesite; TR – Trachyte; AF – Alkali Feldspar; BE – Benmoreite; APATIT – Apatite.

The results of mineral extract calculations for the high Zr/Nb dykes are given in Table 5.5.3 and the full calculations are presented in Appendix 4.

All minerals used in these above calculations, except those prefixed USP are actual analyses from dyke phenocryst phases. Those prefixed USP are theoretical ulvospinel compositions. 'Apatit' is an apatite selected from Deer *et al.* (1966, TAble 50, No.5, ignoring minor components). The extract calculation from trachyte to rhyolite was calculated using 3 different alkali feldspar analyses in an attempt to cover the observed compositional range of feldspar (from anorthoclase in the trachytes to binary alkali feldspar in the rhyolites) and that would be expected during 84% crystallisation of the parent. The stage from mugearite-benmoreite gives a bad fit to the observed

daughter (R^2=4.705), approximately half of this error being caused by the difference in K_2O between calculated and observed daughter. This may be a result of alkali loss from some of the samples. A more likely cause is the use of a K deficient feldspar compared to the actual crystallising feldspar (probably compositionally between $\approx An_{40}$ and $An_{20}Ab_{60}Or_{20}$ – or a gradation from one to the other). Rather than manufacturing a feldspar of such a composition the poor fit was tolerated. Accumulation of each 'step' indicates that the rhyolites may be residues after approximately 96% crystallisation of the initial basaltic parent. This is in reasonably good agreement with the conclusions drawn from the Zr–Nb data (Figure 5.4.4) and also agrees well with the conclusions of Martin (1985) who presented similar calculations (with generally lower R^2).

From basalt to trachyte the Zr–Nb data gives ≈88% crystallisation whereas the extract calculations gave about 76% crystallisation. This difference may be due to the extreme compositions attained by Zr and Nb in some of the trachytes, elevating the average composition. Assuming 76% crystallisation and the basalt parent (although Zr/Nb may have been modified by ilmenite crystallisation) the average 'trachyte' would have Zr≈1190 and Nb≈100. There is a distinct bi-modal distribution of the Zr (and Nb) contents of the trachytes. 12 samples have Zr between 333-658ppm, one at 982, one at 2054, and 7 samples show Zr between 4823-6628ppm. These high Zr samples correlate with high Fe_2O_3 and are highly fractionated trachytes. An average trachyte may thus not really exist amongst the dykes. The high Zr (and Nb) trachytes may possibly represent 97.5% crystallisation of a basalt parent (Nb=940ppm) and the low Zr (and Nb) trachytes may represent only 69% crystallisation. There are slight differences in the major element chemistry of the two groups, and this may be the result of continued fractional crystallisation.

5.5.D: Incompatible element variation

This section deals with the variation seen in the incompatible elements, ie. those elements that are not readily taken into (basaltic) mineral assemblages. Chondrite normalised incompatible element plots are shown for the high Zr/Nb suite in Figures 5.5.1 and 5.5.2 (chondrite compositions taken from Thompson 1982). The elements are laid out in the order used by Sun (1980) to produce smooth MORB patterns. This order correlates with increasing compatibility from Ba-Y when melting a lherzolite

Figure 5.5.1

Incompatible element 'spidergrams' from 4 field associations of basaltic rocks. All plots are rock/chondrite, with chondrite compositions taken from Thompson (1982), listed below as ppm.

Rb	0.35	La	0.328	Zr	6.84
Ba	6.9	Ce	0.865	Ti	620.0
Th	0.042	Sr	11.8	Y	2.0
K	120.0	Nd	0.63		
Nb	0.35	P	46.0		

See text for discussion.

Figure 5.5.1

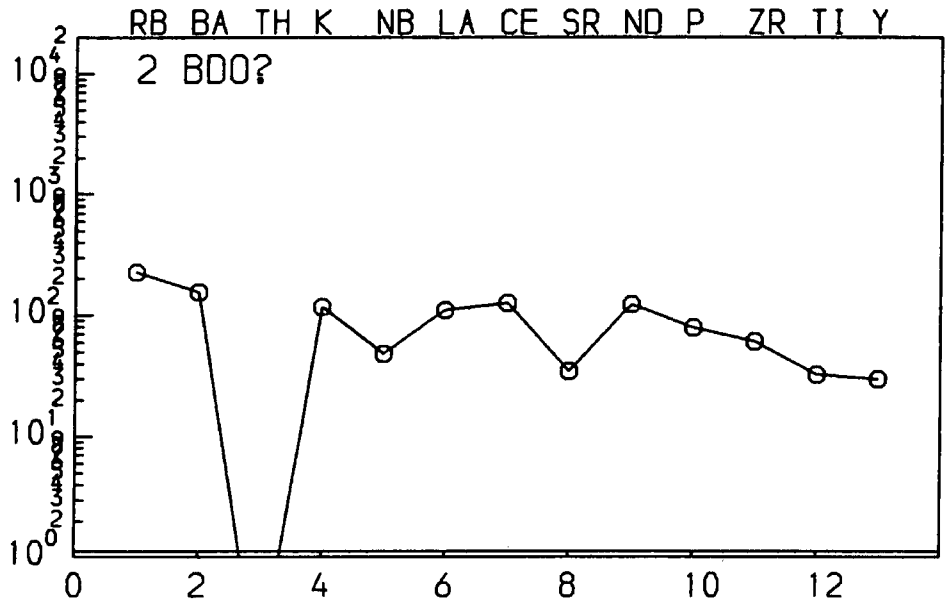
RB BA TH K NB LA CE SR ND P ZR TI Y
2 BDO?
10^4
10^3
10^2
10^1
10^0
0 2 4 6 8 10 12

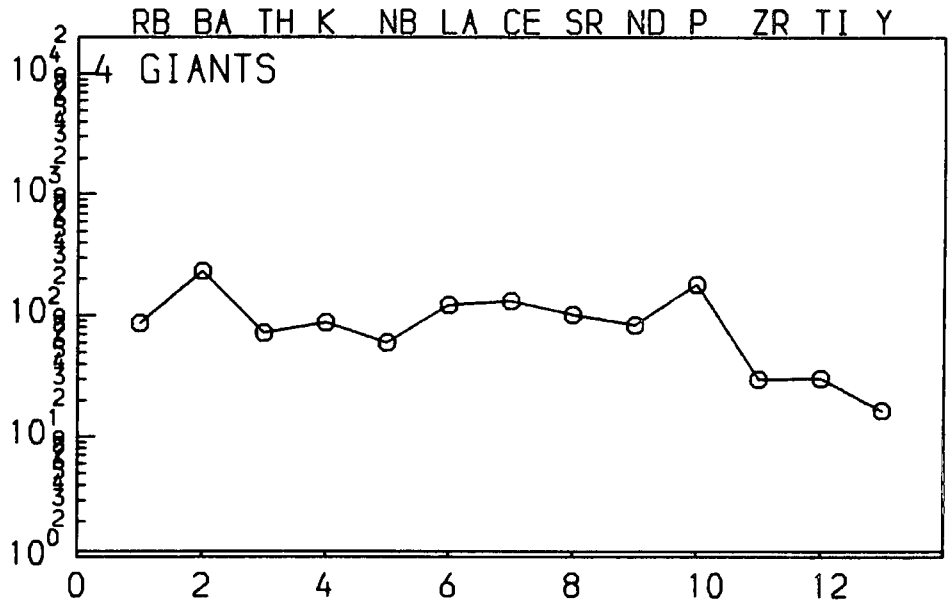
RB BA TH K NB LA CE SR ND P ZR TI Y
4 GIANTS
10^4
10^3
10^2
10^1
10^0
0 2 4 6 8 10 12

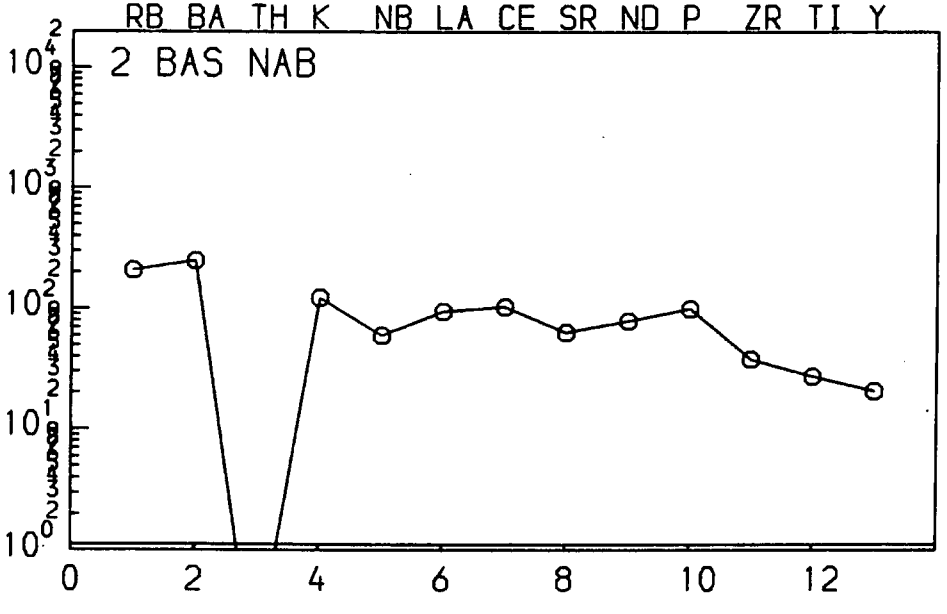
RB BA TH K NB LA CE SR ND P ZR TI Y
2 BAS NAB
10^4
10^3
10^2
10^1
10^0
0 2 4 6 8 10 12

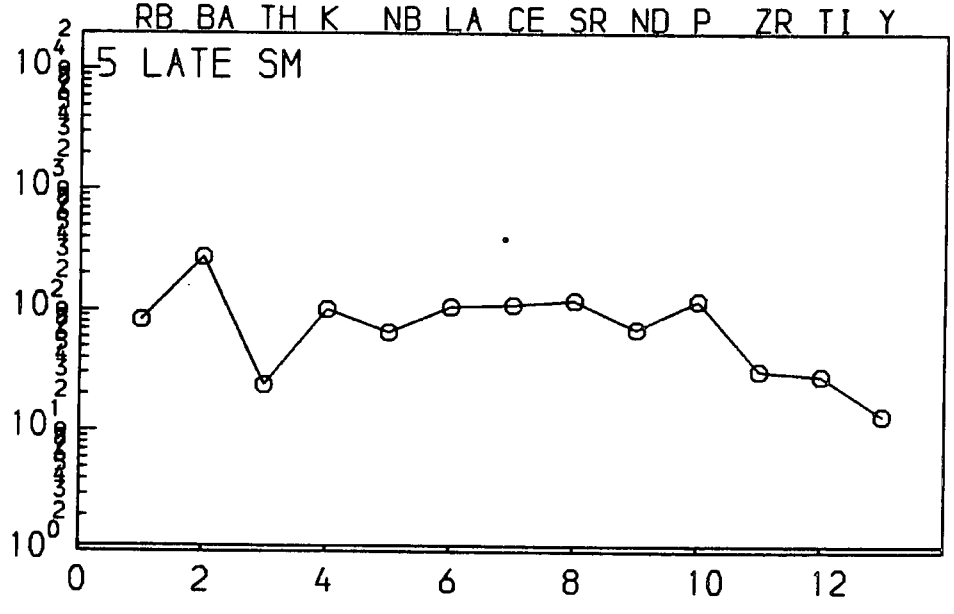
RB BA TH K NB LA CE SR ND P ZR TI Y
5 LATE SM
10^4
10^3
10^2
10^1
10^0
0 2 4 6 8 10 12

Figure 5.5.2

Incompatible element 'spidergrams' for the high Zr/Nb suite of dykes. All plots are rock/chondrite, with chondrite compositions taken from Thompson (1982). See Figure 5.5.1 for chondrite compositions. See text for discussion.

Figure 5.5.2

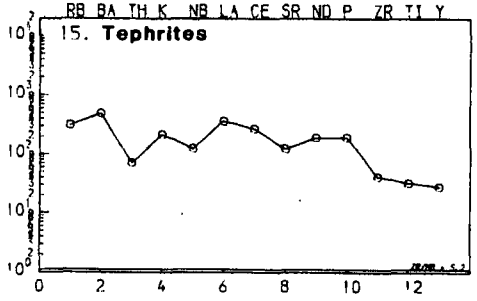
RB BA TH K NB LA CE SR ND P ZR TI Y
15. Tephrites

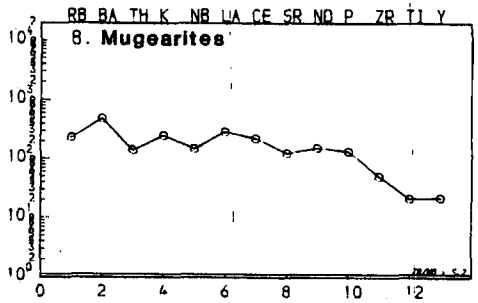
RB BA TH K NB LA CE SR ND P ZR TI Y
8. Mugearites

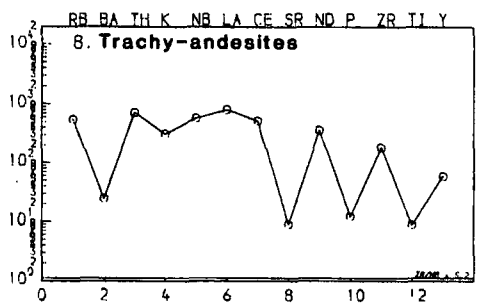
RB BA TH K NB LA CE SR ND P ZR TI Y
8. Trachy-andesites

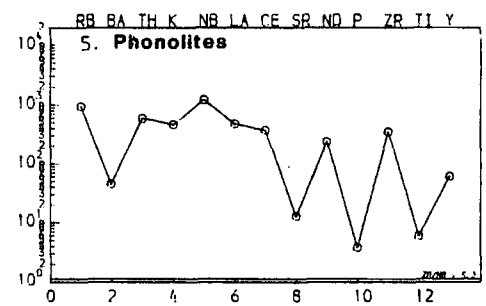
RB BA TH K NB LA CE SR ND P ZR TI Y
5. Phonolites

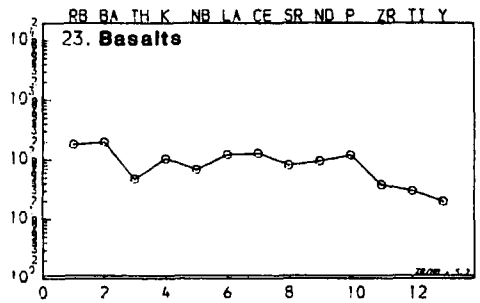
RB BA TH K NB LA CE SR ND P ZR TI Y
23. Basalts

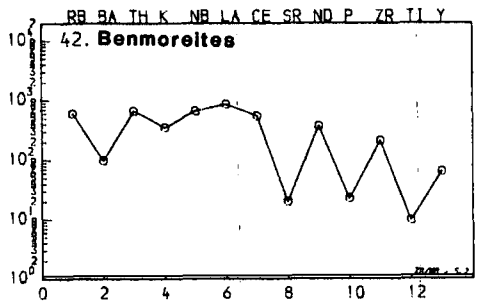
RB BA TH K NB LA CE SR ND P ZR TI Y
42. Benmoreites

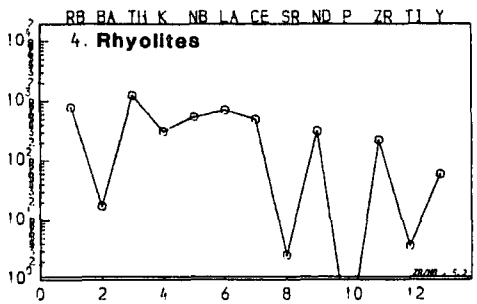
RB BA TH K NB LA CE SR ND P ZR TI Y
4. Rhyolites

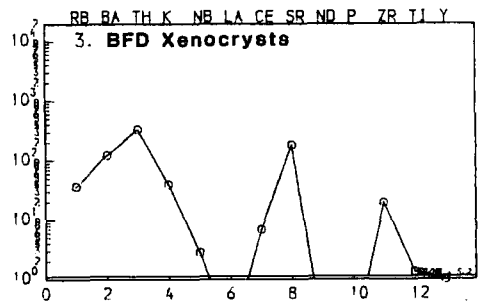
RB BA TH K NB LA CE SR ND P ZR TI Y
3. BFD Xenocrysts

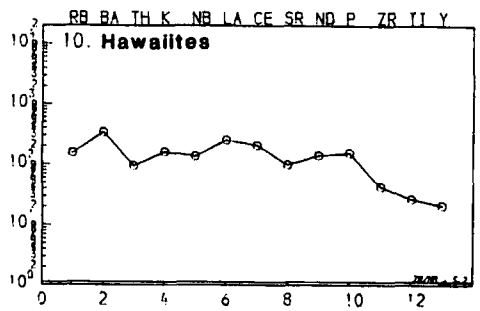
RB BA TH K NB LA CE SR ND P ZR TI Y
10. Hawaiites

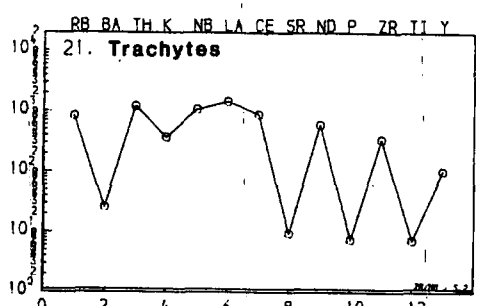
RB BA TH K NB LA CE SR ND P ZR TI Y
21. Trachytes

source (Sun 1980).

Table 5.5.1 shows the average compositions of each group of high Zr/Nb rocks plotted in Figure 5.5.2. In the following discussion of the chondrite normalised 'spidergrams' of the incompatible elements, an anomaly refers to an excess or deficiency of an elements normalised concentration relative to its neighbours, eg. a negative Sr anomaly is a deficiency of Sr compared to Ce and Nd.

Basalts

The basalts have been subdivided into several smaller groups on field associations. These are 2 samples from a possible BD_0, 2 narrow basalts from north of Narssarssuaq, 5 late alkali gabbros from the Motzfeldt Centre and 4 samples from a giant dyke. Spidergrams from these are shown in Figure 5.5.1 with the overall average 'basalt' shown in Figure 5.5.2, along with the other group averages. The BD_0 and the Narssarssuaq basalts show 0ppm of Th, compared to the Giant Dyke contents of $\approx$3ppm, and thus these show large, negative Th anomalies.

There are clear differences between the groups of basalts shown in Figure 5.5.1 although a common feature of all groups is a small negative Nb anomaly.

BD_0

These samples possess the largest negative Nb anomaly as well as a large depletion in Th (below the detection limit). They also have an apprec i able negative Sr anomaly which implies that they are derivative from a more basic magma that has fractionated some plagioclase. Ba is less enriched than Rb, probably due in part to some Ba loss by alteration, but Rb is higher in these basaltic samples than in any of the other basaltic groups illustrated. There is no positive P anomaly unlike all other high Zr/Nb basalts.

Giant Dykes

These giant dykes (3 from Mellemlandet, 1 from ca. 5km SW of Qagssiarssuk) show small negative anomalies at both Th and Nb and a relatively large positive P anomaly unlike the possible BD_0, and are similar to all other basalt dykes. Ba is more enriched than Rb. These giant dykes do not possess a negative Sr anomaly implying little or no

plagioclase fractionation has occurred. The enrichment in P is not a result of enrichment of the sample in cumulus apatite (although one sample –63777– is particularly rich in apatite). Apatite is typically present in contents of 2-3% modally, and the positive P anomaly presumably reflects some primary compositional control (see below).

Basalts from Narssarssuaq.

These basalts show a similar pattern of incompatible elements to the Giant dykes, although, rather obviously contain no Th. They however show similar negative Nb and positive P anomalies to the Giant Dykes. These samples also possess a very slight negative Sr anomaly. These basalts may have undergone small amounts of plagioclase fractionation whilst still retaining certain primary features (ie. the Nb, Th and P anomalies).

Late Motzfeldt gabbros

These dykes occur as large, late-stage intrusions of the Motzfeldt Centre in Upper Flinks Dal. They are presumed to be intimately related to the Motzfeldt Syenites occurring at the last stages of central complex evolution (Jones 1980, Bradshaw 1987). They however possess a Zr/Nb ratio (at $\approx$6) markedly higher than the bulk of the samples from Motzfeldt (with Zr/Nb$\approx$4-4.5, see Figure 5.6.1, data from Jones 1980). They possess some features typical of the above mentioned basalts with marked negative Th and Nb, and positive P anomalies. There are also slight positive Sr and Ti anomalies, indicative of a certain amount of cumulus plagioclase and Fe-Ti oxide. Normatively, these rocks contain $\approx$6 wt% of ilmenite (also seen in thin section in some samples), and this, if enriched in Zr (see Chapter 5.4 – *Ilmenites and Zr/Nb*), would have the effect of elevating the Zr/Nb ratio slightly.

It would seem from the above discussion of the characteristics of the various 'field associations' of the basalts that all, except the possible BD_0, are from a similar source which is deficient in Nb and Th and enriched in P. Thompson *et al.* (1983) suggest that both Th and Nb anomalies may be inherited by assimilation of Th and Nb depleted continental crust but the isotopic evidence (Blaxland *et al.* 1978, Martin 1985) indicates that no crustal contamination has occurred. However, considering the low relative Sr contents of granulite facies crustal rocks compared to the basalts (different by a

factor of 10 – see Thompson *et al.* 1983) a large amount of contamination would be necessary to produce a marked affect on the Sr isotopic composition. The Ketilidian granites/granodiorites in the region (perhaps only 470 million years older than the Late Gardar activity) may have relatively unevolved radiogenic Sr isotopic compositions and a minor amount of contamination may have a minimal effect on the isotopic composition of the magma. Contamination could thus go essentially unnoticed. Other isotopic studies (Sm-Nd, U-Pb) on these rocks and their inclusions would be very instructive.

Crustal contamination however could not account for the positive P anomaly apparent in these basalts (Martin 1985, Upton *et al.* 1985, Upton and Emeleus 1987) and these features are held to be inherited from the source. Apatite-rich mantle xenoliths have been reported from SE Australia, the Eifel District of Germany and Uganda (Lloyd and Bailey 1975). These have been attributed to the fractional crystallisation at depth of Si-undersaturated (or kimberlitic?) magmas. These magmas may have had a metasomatic effect upon the mantle source region of later alkali basalts, producing enrichment in P, LREE and other incompatible elements (see also Menzies 1983, Hawkesworth *et al.* 1984, Fitton and Dunlop 1985). Later magmas may then have been contaminated by such material, of which only a small amount would be required to produce a positive P anomaly (Exley 1982). This P anomaly is a feature common to both the OGDC and YGDC (Martin 1985). Residual Nb-bearing phases in the upper mantle, such as rutile, spinel or sphene may 'hold back' Nb on melting compared to other incompatible elements, and thus may be the cause of the negative Nb anomaly (Saunders *et al.* 1980, Saunders and Tarney 1984).

Also noticeable from the basaltic rocks (excluding the possible BD_0) is that Ba is more enriched than Rb. K (relative to Ba and La) is also less enriched than may be expected. Both these elements could be held back in a K-rich phase in the mantle, such as amphibole or phlogopite (cf. Sun and Hansen 1975) as partial melting takes place. Addition of water to a mantle source region may stabilise a Nb-bearing phase (possibilities include rutile? or sphene?) which is left as a residue on melt extraction (Saunders *et al.* 1980, Saunders and Tarney 1984). This would hold back Nb in the source causing a negative Nb anomaly. Addition of water may also cause stabilisation of other hydrous phases (mica or amphibole?) and these may also be residual on melting.

However these features were caused they are primary characteristics of the Late Gardar high Zr/Nb suite of basalts, but not necessarily of the earlier (Mid-Gardar?) possible BD_0. The possible BD_0 has a much higher Zr/Nb ratio ($\approx$22) than the Giant Dykes ($\approx$10) and shows no P anomaly, although it does possess negative Nb and Th anomalies. The higher Zr/Nb ratio would imply higher degrees of partial melting (Pearce and Norry 1979) and the lower Ce/Y ratio would suggest either less garnet in the mantle source (- as Ce/Y in the melt increases with increasing residual garnet in the source rocks, Kay and Gast 1973) or higher degrees of partial melting. Thus, the possible BD_0 shows very marked differences in its composition and possible source rocks to the Giant Dykes and other basalts of Late Gardar activity and is clearly unrelated to any of these late dykes. This is not altogether surprising when its age and structural setting are considered.

Tephrites

The high Zr/Nb tephrites show a more enriched, although overall very similar pattern to the average basalt with negative Sr, Nb and Th anomalies as well as a small positive P anomaly. The pattern is slightly more 'spiky' (evolved) than the basalts with higher absolute contents of many incompatible elements. This reflects their greater alkali content and is consistent with these having formed as a smaller degree partial melt from the same mantle source region. The small negative Sr anomaly may indicate some plagioclase fractionation has already occurred.

Hawaiites

The hawaiites also show a very similar pattern to the basalts with Th, Nb and P anomalies still clearly visible. The Sr trough is somewhat deeper than in the basalts indicative of continued feldspar fractionation. Overall there is a slight steepening of the pattern consistent with fractional crystallisation of feldspar, pyroxene, olivine and opaques.

Mugearites

Mugearites show a pattern extremely similar to the hawaiites with the exception of a notable negative Ti anomaly, indicating the onset of abundant Fe-Ti oxide crys-

tallisation between hawaiite and mugearite. This marked similarity of the hawaiite and mugearite pattern is consistent with limited chemical change due to fractionation over this compositional range and agrees with the contentions of Clague (1978) that opaque oxide crystallisation causes rapid compositional change across the 'Daly Gap' (see earlier).

Benmoreites

There is a marked change from the relatively smooth pattern of the mugearites to the evolved 'spiky' pattern of the benmoreites which shows large negative anomalies at Ba, K, Sr, P and Ti. By this stage of magmatic evolution Ba and K have become compatible in the crystallising feldspar (anorthoclase) along with Sr (which was compatible in plagioclase) and these become rapidly depleted in the residual liquid. Continued extraction of opaque oxides from mugearite to benmoreite pulls the Ti anomaly further down. Apatite extraction from mugearite for the first time becomes apparent from mugearitic magmas, rapidly depleting the benmoreitic residue in P. This is the same for the trachy-andesites, which are compositionally very similar to the benmoreites.

Trachytes

Evolution from benmoreite through to trachyte involved continued fractionation of feldspar (removing Ba, Sr and K), apatite and opaque oxide, producing deeper troughs and overall more elevated concentrations of Rb, REE, Th, Nb, Zr and Y.

Rhyolites

Continued apatite, feldspar and oxide extraction from trachyte to rhyolite produces the very evolved compositions seen in the rhyolites. Nb and Zr both have 'absolute' concentrations less than in the 'trachytes' indicating that some phase(s) involving Zr must have crystallised from these highly enriched compositions. Apatite crystallisation has occurred in sufficient quantity to completely remove P from the rhyolitic rocks.

The phonolites and BFD xenocrysts are included for completeness. The phonolites can effectively be ignored however and considered as members of the low Zr/Nb suite that have become Zr enriched (note high Zr compared to Nd and Y).

5.6: Low Zr/Nb Suite (excluding Østfjordsdal Swarm)

The data for the low Zr/Nb suite of samples is presented in a format similar to that for the high Zr/Nb suite, thus explanation of methods etc. will be excluded to avoid repetition. The dykes from the Østfjordsdal Swarm – mostly Zr/Nb less than 5.2 (see Figure 5.4.2) – have been excluded from this set of data and will be discussed later. Table 5.6.1 presents averaged compositions for each TAS classified rock type of the low Zr/Nb suite. This group of rocks (with the exclusion of ultramafic lamprophyres and carbonatites) is mostly composed of benmoreites and phonolites (see Table 5.4.1) with only minor amounts of rocks less evolved than these (see Figure 5.4.3). The compositional range exhibited by these dykes is almost identical to that observed in the central complexes of the Igaliko area with benmoreite ≡ augite syenite, and phonolite ≡ nepheline syenite (see Stephenson 1973, Chambers 1976, Powell 1978, Jones 1980, Bradshaw 1987). The Igaliko central complexes all tend to contain late dykes of alkali basaltic compositions, notably Motzfeldt and Igdlerfigssalik, although they are also recorded from South Qôroq. Unlike the high Zr/Nb suite, there is no compositional hiatus, rather the strong salic magma bias previously mentioned. Several of the 'late' basic intrusions from the central complexes are included in this data set as they provide some of the only clues as to the composition of a possible basic parent magma for the nepheline syenite complexes, and by inference the low Zr/Nb dykes.

Gill (1973) suggested a model for the salic magma bias of such intra-continental alkaline igneous provinces. Alkali basaltic magma generated from a mantle source may have a density of about 2.6-2.65g cm^{-3} (Bottinga and Weill 1970) which would be very bouyant compared to mantle densities of ≈3.4g cm^{-3}. These melts would rise through the mantle encountering lower crustal rocks of density ≈2.85 g cm^{-3} (Gumper and Pomeroy 1970). However, at higher levels, (10km or less) the crustal density falls as low as 2.61-2.70gcm^{-3} (Julianehåb granodiorite, Blundell 1978) or 2.65-2.7gcm^{-3} (Gumper and Pomeroy 1970) and thus the basalts, under non-dyking conditions, should be confined broadly to such depths. Here they will fractionate to produce salic residues. Trachyte and rhyolite glasses at room temperature have densities of 2.37-2.45g cm^{-3} (Tilley 1922) and thus at liquidus temperatures, may be expected to be less dense. They would thus be highly bouyant compared to crustal rocks and would rise by stoping to

TABLE 5.6.1 (2 pages)

Average composition of TAS classified low Zr/Nb rocks.

	NPH-IT	PH-NEP	TEPH	BASALT	MUG	BEN	PH-TH	PHON
SIO2	39.67	49.75	43.46	45.18	52.42	56.41	52.92	55.54
TIO2	3.61	0.74	3.21	3.45	1.91	1.06	1.08	0.56
AL203	9.70	16.05	12.38	13.78	15.79	15.79	16.17	17.92
FE203	3.69	3.54	3.75	2.19	3.80	3.17	4.35	3.72
FEO	10.24	7.08	10.43	10.98	6.55	5.04	6.29	4.13
MNO	0.31	0.62	0.26	0.24	0.24	0.27	0.46	0.28
MGO	10.74	0.71	6.90	7.38	2.45	0.92	1.10	0.44
CAO	11.08	4.58	8.24	7.35	4.52	2.62	3.14	1.85
NA20	2.08	8.44	2.59	2.42	4.42	5.01	6.76	7.16
K20	4.05	4.60	3.89	2.99	4.01	5.32	4.26	5.65
H20+	nd	nd	nd	nd	nd	nd	nd	nd
H20-	nd	nd	nd	nd	nd	nd	nd	nd
P205	1.07	0.29	1.44	0.64	1.05	0.33	0.38	0.09
TOTAL	96.24	96.40	96.55	96.60	97.16	95.94	96.91	97.34
BA	2175	3150	2414	1517	2509	995	834	380
NB	132	1257	121	121	125	219	1652	484
ZR	430	4439	439	352	521	825	867	1691
Y	56.00	343	55.00	30.00	61.00	80.00	177	124
SR	1457	4204	1771	856	766	290	699	356
RB	215	182	131	148	99.00	159	227	244
ZN	235	632	198	193	174	201	927	286
CU	10.00	nd	61.00	22.00	6.00	3.00	1.00	4.00
NI	301	6.00	141	54.00	4.00	1.00	3.00	2.00
PB	11.00	193	17.00	52.00	19.00	26.00	21.00	47.00
U	6.00	61.00	5.00	nd	2.00	4.00	28.00	12.00
TH	12.00	225	10.00	6.00	11.00	19.00	450	41.00
V	347	31.00	318	375	124	48.00	42.00	22.00
CR	279	nd	171	164	8.00	1.00	1.00	1.00
ND	117	606	140	59.00	131	167	649	251
GA	23.00	51.00	27.00	25.00	30.00	37.00	38.00	45.00
LA	151	845	176	47.00	155	202	957	339
CE	245	1377	290	140	271	348	1922	551
F	1700	6200	700	nd	800	1500	240	2800
CL	2800	200	200	200	200	300	1100	2100

NPH-IT - AVERAGE NEPHELINITE
PH-NEP - AVERAGE PHONOLITIC NEPHELINITE
TEPH - AVERAGE TEPHRITE/BASANITE
BASALT - AVERAGE BASALT
MUG - AVERAGE MUGEARITE
BEN - AVERAGE BENMOREITE
PH-TH - AVERAGE PHONOLITIC TEPHRITE
PHON - AVERAGE PHONOLITE

continued...

TABLE 5.6.1 (continued)

	UML	TR	TR-AND	PICBAS	CBT
SIO2	30.51	55.54	58.94	44.84	6.25
TIO2	4.65	0.56	0.29	3.55	0.11
AL203	6.65	17.20	17.20	10.17	0.62
FE203	13.62	2.38	4.94	1.44	5.63
FEO	6.63	3.61	7.49	14.43	2.82
MNO	0.64	0.22	0.74	0.25	2.14
MGO	11.63	0.41	0.36	8.35	1.49
CAO	15.71	1.49	1.42	10.46	41.37
NA20	0.53	5.76	7.02	1.63	0.40
K20	3.43	5.82	1.69	0.98	0.26
H20+	nd	nd	nd	nd	nd
H20-	nd	nd	nd	nd	nd
P205	1.71	0.04	0.10	0.58	2.07
TOTAL	95.71	93.03	100.19	96.68	63.16
BA	1985	230	132	1527	3559
NB	256	256	2037	60.00	242
ZR	386	1100	6389	266	8.00
Y	130	84.00	651	25.00	872
SR	2349	132	330	1037	27699
RB	210	239	105.00	65.00	25.00
ZN	442	191	2305	249	825
CU	33.00	5.00	nd	nd	nd
NI	283	1.00	9.00	111	23.00
PB	8.00	42.00	232	15.00	nd
U	4.00	4.00	101.00	nd	28.00
TH	110.00	28.00	582	nd	314
V	374	26.00	7.00	460	26.00
CR	281	nd	nd	371	6.00
ND	347	179	1960	40.00	1573
GA	25.00	42.00	95.00	28.00	4.00
LA	408	233	3014	26.00	2086
CE	790	375	4571	82.00	4093
F	2400	2900	1200	nd	15200
CL	200	300	100.00	1000	nd

UML - AVERAGE ULTRA MAFIC LAMPROPHYRE
TR - AVERAGE TRACHYTE
TR-AND - AVERAGE TRACHYANDESITE
PICBAS - AVERAGE PICRITIC BASALT
CBT - AVERAGE CARBONATITE

form the central complexes. Any fractures in the country rock would be exploited by these magmas and localised dyke swarms would ensue. This mechanism seems to have been operative in the Igaliko region, with the abundance of faults in the region possibly assisting magma ascent (Chambers 1976). Minor seepages along fractures above the deep (≈10km) fractionating chamber would allow minor amounts of basic and intermediate magmas to reach higher crustal levels, as too would tapping of deeper levels of a magma chamber with time (Stephenson 1973).

There is an overall similarity between the mugearite–phonolite dyke major and trace element data and data from the rocks of the South Qôroq Centre (Stephenson 1973). There are however many dykes whose compositions have become considerably more enriched in incompatible elements than the South Qôroq rocks (eg. Zr, Nb, REE, Th etc.).

Figure 5.6.1 shows histograms of Zr/Nb from both the South Qôroq and Motzfeldt centres (data from Stephenson 1973 and Jones 1980). The Motzfeldt centre shows a considerably more ragged pattern than South Qôroq, due mostly to Nb mineralisation considerably modifying the Nb contents of certain parts of the centre (see Tukiainen *et al.* 1984, Bradshaw 1987). The South Qôroq Centre however, shows an even, Gaussian distribution, very similar, and just slightly lower than the low Zr/Nb peak from the dykes (see Figure 5.4.2).

With the 2 marked phases of central complex activity in the Igaliko Complex (North Qôroq and Motzfeldt– Early Gardar; South Qôroq and Igdlerfigssalik–Late Gardar) separated by perhaps 140Myr (Blaxland *et al.* 1978), a model that assumes a close relationship between the dykes and the central complexes must therefore assume 2 phases of phonolite dyke injection. However, only 3 dykes are known that are contemporaneous with intrusions within the Motzfeldt Centre (325913-5). These are all trachytes (*s.s.*) with Zr/Nb ratios 4.62, 4.73 and 6.04, and La/Y ratios of 2.77, 2.83 and 4.01. These ratios are not distinct from the bulk of the dykes of the low Zr/Nb (undersaturated) suite and do not define criteria upon which dykes associated with Motzfeldt and North Qôroq can be distinguished from those related to South Qôroq or Igdlerfigssalik. The close similarity (physically and chemically) of all these complexes would imply similarity of the associated dykes. The fact that there is no obvious, marked difference in the

Figure 5.6.1

Histograms of Zr/Nb from the South Qôroq and Motzfeldt Centres (data from Stephenson 1973 and Jones 1980). The South Qôroq data is very similar to that from the low Zr/Nb dykes (see Figure 5.4.2). The Motzfeldt data is more scattered than the South Qôroq data, due most probably to a modification of the Zr/Nb ratio by Nb mineralisation (see Tukiainen *et al.* 1984, Bradshaw 1987).

Figure 5.6.1

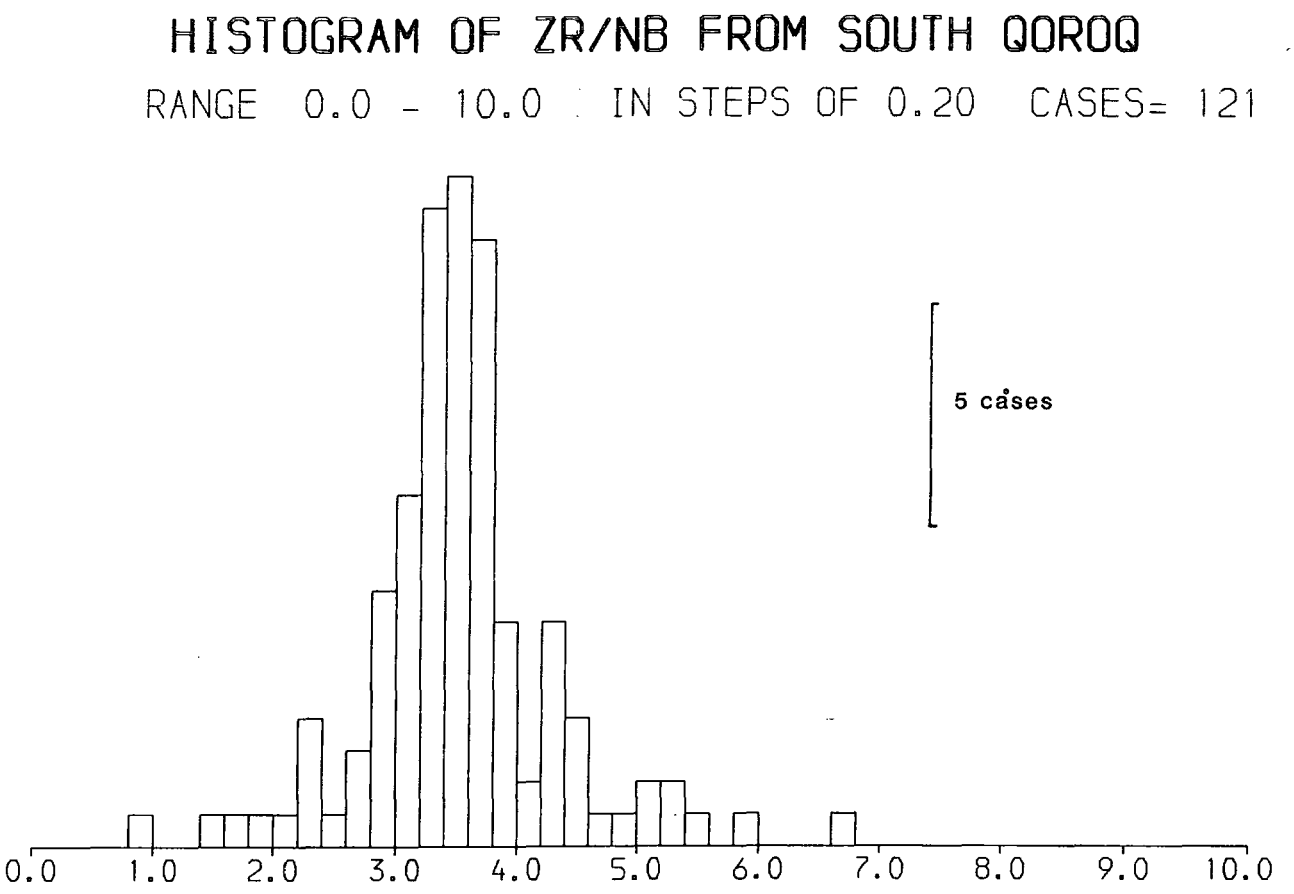
HISTOGRAM OF ZR/NB FROM SOUTH QOROQ
RANGE 0.0 - 10.0 IN STEPS OF 0.20 CASES= 121
5 cases
0.0
1.0
2.0
3.0
4.0
5.0
6.0
7.0
8.0
9.0
10.0

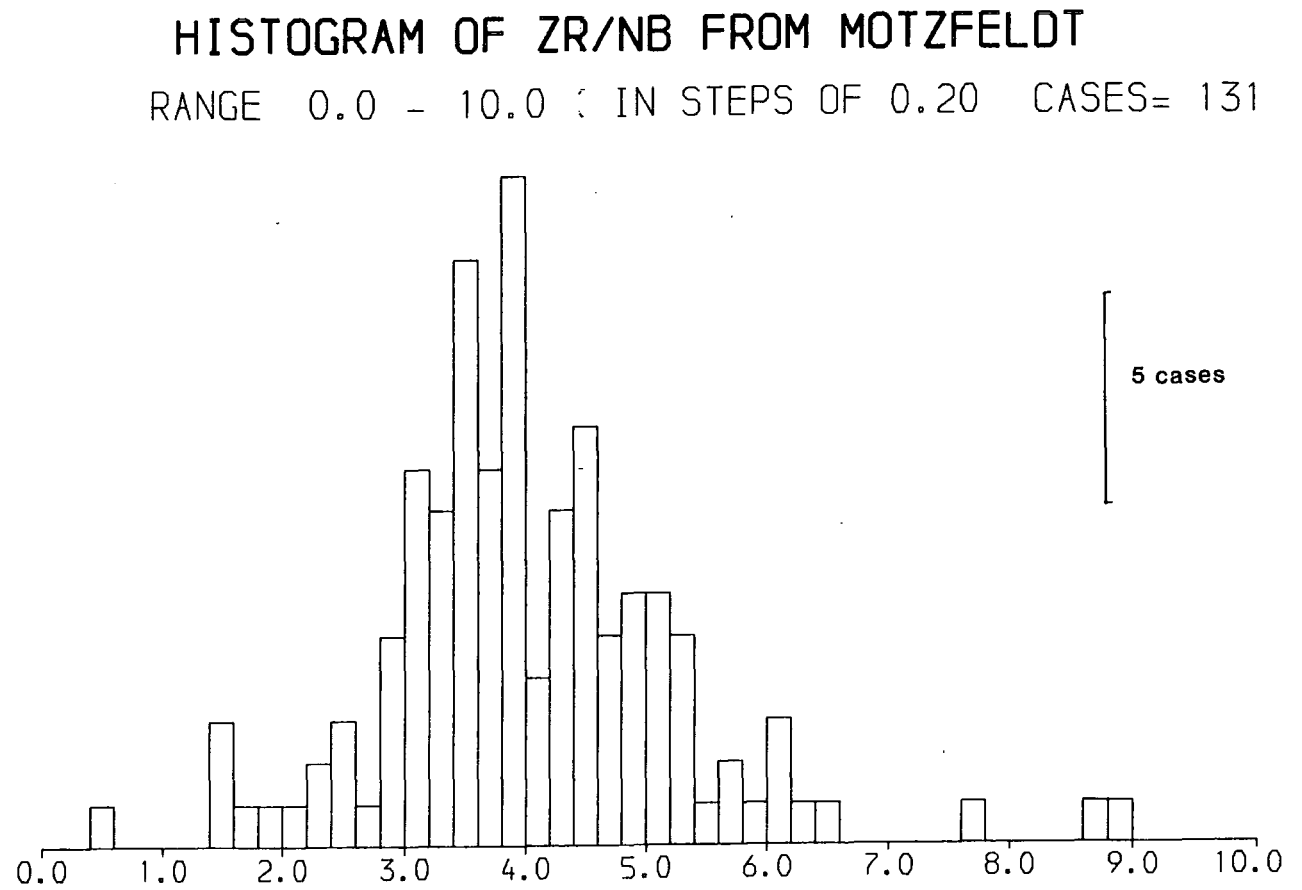
HISTOGRAM OF ZR/NB FROM MOTZFELDT
RANGE 0.0 - 10.0 IN STEPS OF 0.20 CASES= 131
5 cases
0.0
1.0
2.0
3.0
4.0
5.0
6.0
7.0
8.0
9.0
10.0

numbers of dykes cutting the Motzfeldt, North Qôroq or South Qôroq Centres, would imply that the local, central complex related dykes are mostly post-South Qôroq. They can all essentially be considered as one group, and most are probably related to the Late Gardar (South Qôroq–Igdlerfigssalik) activity.

5.6.B:Liquidus Assemblages

Nathan and Van Kirk (1978) modelling, as performed on the high Zr/Nb suite (see Chapter 5.5.B) to estimate liquidus mineral assemblages and compositions yielded the results shown in Table 5.6.2 for the low Zr/Nb suite of dykes.

Table 5.6.1 shows the average group compositions based on the TAS scheme of Cox *et al.* (1979) for the low Zr/Nb suite of dykes. These compositions were used as starting compositions for the liquidus assemblage calculations.

There are noticable differences in the liquidus assemblages between these samples and those of the high Zr/Nb suite, notably in the quantity of opaque oxide and olivine that crystallises. This reflects the differences in bulk chemistry (which may only be slight) of the different averaged groups. The overall trend of residual liquid evolution after 20% 'fractional crystallisation' is towards Si-undersaturation (decreasing SiO_2, increasing alkalis), whilst the same model for the high Zr/Nb data produced a trend towards Si-oversaturation and decreasing alkali content. The general compositional evolution of the liquidus mineral compositions follows closely that of the high Zr/Nb data and is in general agreement with the actual compositional data (see Table 3.12.1). It must be remembered that this model is for 1 atmosphere crystallisation and thus only approximates to the conditions prevailing at depth (around 2kb for the dykes, possibly 3-4kb or more for the parent, fractionating magma chamber).

5.6.C: Mineral Extract Calculations

Fractional crystallisation modelling was carried out to determine possible quantities and types of crystals that need to be extracted to alter the composition from an assumed 'parent' to its presumed 'daughter' (see Chapter 5.5.C for an explanation of the method etc.). As no major differences were evident in the mineral compositions related to the low and high Zr/Nb suites, the same mineral data base was used. Basalts and

Table 5.6.2

Liquidus mineral assemblages calculated from Nathan and VanKirk (1978) model.

Sample	Tephrite	Basalt	Mugearite	Benmoreite	Trachyte	Phonolite
Mt%	6.74	2.31	3.89	3.33	0.93	
Mt (Mt)	46.37	32-30	57-53	63-62	69-72	
Mt T°C	1153.6	1157.7	1122.2	1090.6	1081.7	
Ol%	10.52	11.08	2.60	2.62	2.52	
Ol (Fo)	80	81.73	70-69	50-43	34-21	
Ol T°C	1200.4	1210.9	1115.6	1085.3	1083.5	
Plag%	2.79	6.66	13.57	41.10	16.61	
Plag (An)	65-64	67-65	46-40	31-27	25-20	
Plag T°C	1148.5	1157.9	1120.5	1088.3	1092.6	
Aug%						
Aug (Di)						
Aug T°C						
Orth%						20.06
Or (Or)						45-42
Or T°C						1081
Final liquid after 20% crystallisation						
SiO_2	51.77	49.71	58.43	63.02	61.22	54.89
TiO_2	1.96	3.58	1.46	0.64	0.59	0.76
Al_2O_3	15.57	15.43	16.34	16.69	18.49	18.37
Fe_2O_3	1.60	2.03	2.44	1.78	2.42	4.78
FeO	5.59	9.46	4.70	2.71	2.28	5.31
MgO	4.34	4.59	2.13	0.46	0.14	0.57
CaO	10.60	8.47	4.48	2.44	1.06	2.38
Na_2O	3.34	2.84	4.75	5.22	5.59	7.60
K_2O	5.22	3.89	5.28	7.08	7.86	5.39
Final T°C		1153	1103.9	1076		1097
TAS Final Liquid	Mug	Haw	Ben	Trach	Phon	Phon

Table 5.6.3

Results of extract calculations – low Zr/Nb suite

Parent	Ilmenite	Magnetite	Feldspar	Olivine	Pyroxene	Other	Daughter	R^2
Basalt	BAS-IL	USP-80	AN-80	FO-80	BAS-PX		Mugearite	
	1.8%	4.7%	15.1%	11.2%	12.2%		54.9%	2.924
Tephrite		USP-60	AN-80	FO-80	TEP-PX	APATIT	Mugearite	
		6.3%	2.0%	0.005%	20.4%	2.5%	50.4%	0.491
						NE-BI2		
						18.3%		
Mugearite	BA-IL2	TEP-OX	ANT-44	BAS-OL	HAW-PX	APATIT	Benmoreite	
	1.4%	1.9%	16.1%	6.3%	0.7%	1.9%	71.7%	0.024
Benmoreite		BE-OX1	BE-AN1		BE-PX1	APATIT	Phonolite	
		2.8%	34.3%		13.2%	+1.8%	5.4%	1.654
Benmoreite	All solutions did not involve feldspar						Trachyte	
Trachyte		BE-OX1	BE-AN1		BE-PX1		Phonolite	
		1.4%	32.9%		0.7%		65.1%	0.767
Total remaining liquid Bas-Mug-Ben-Phon							20.2%	
Total remaining liquid Tep-Mug-Ben-Phon							18.5%	

Abbreviations: BA,BAS – Basalt; TEP – Tephrite; HAW –Hawaiite; BE – Benmoreite.

tephrites (the most abundant basic rocks) are relatively scarce from this suite and hawaiites are completely absent. Thus, modelling fractionation of basalt or tephrite necessitated the use of mugearite as a daughter. This is not wholly successful as the mineral phases assumed to crystallise will change significantly in composition across this range. However, the results of this, and other parent–daughter pairs, are presented in Table 5.6.3

The majority of minerals used in these calculations were actual analyses of appropriate composition for the parent. To obtain a better fit (lower R^2) certain hypothetical compositions, calculated from end member proportions were employed. These included magnetites (USP-80 and USP-60, with compositions $Mt_{20}Usp_{80}$ and $Mt_{40}Usp_{60}$ respectively), olivine (FO-80) and feldspar (AN-80) both with self explanatory compositions. BE-AN1 is real anorthoclase and ANT-44 is a real high-K andesine. NE-BI2 is a real

phlogopite from a nephelinite. APATIT is an apatite analysis selected from Deer *et al.* (1966).

Fractionation of feldspar, with lesser amounts of pyroxene, oxides and olivine seems to have controlled the evolution of the magma from mugearite through to phonolite. The poor fit of the basalt to mugearite data will be due largely to the changing mineral compositions with host rock evolution. However, if the magma was evolving at relatively high pressures spinel or garnet could produce the same effect as plagioclase and olivine. Inclusion of a mica would have improved the fit, and this was used in the case tephrite–mugearite. Some fine-grained tephrites contain micro-phenocrysts of a phlogopite mica or kaersutite along with pyroxene (similar to many nephelinites in that respect) and this may be a valid model. No reasonable solution could be obtained for tephrite–mugearite using kaersutite or by excluding both mica or amphibole. No solution involving feldspar could be obtained from benmoreite–trachyte. The TAS data (Figure 5.2.1) would suggest that trachyte is not an intermediate between benmoreite and phonolite.

The total remaining liquid, assuming a basalt parent and a phonolite daughter, is 20.2%, a tephrite parent producing 18.5% of daughter phonolite. This agrees very closely to the estimates of remaining liquid (F) obtained from the Zr/Nb data (Figure 5.4.4, Chapter 5.4) which gave a residue of ≈24% phonolite from the average basalt and ≈21% from the average tephrite. Thus, the phonolites would seem to constitute a much larger residue from their initial basic parent(s) than would the rhyolites (which represent a residue of ≈4%).

5.6.D: Incompatible Element Variation

Figure 5.6.2 shows chondrite normalised incompatible element spidergrams of the average group compositions for the low Zr/Nb suite of dykes (see Chapter 5.5.D for explanation). These should be compared with the patterns from the high Zr/Nb suite (Figures 5.5.1 and 5.5.2). There are marked differences in the patterns, particularly in the basic rocks. In general, the more basic samples show a 'smoother' pattern than their equivalent from the high Zr/Nb suite.

Figure 5.6.2

Incompatible element 'spidergrams' for the low Zr/Nb suit of dykes. All plots are rock/chondrite, with chondrite compositions taken from Thompson (1982). See Figure 5.5.1 for chondrite compositions.

Figure 5.6.2

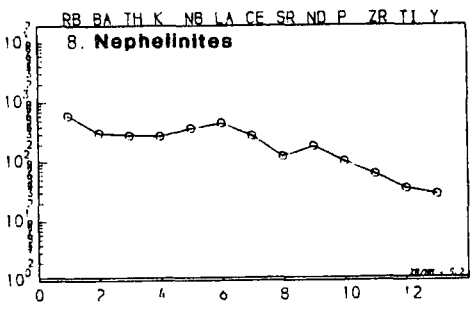
RB BA TH K NB LA CE SR ND P ZR TI Y
8. Nephelinites

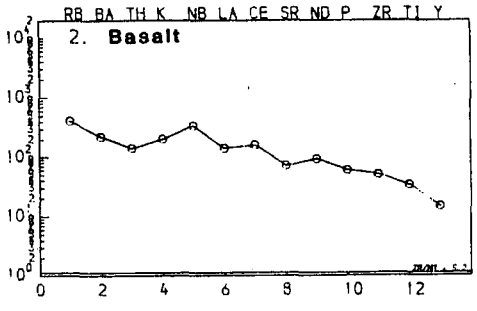
RB BA TH K NB LA CE SR ND P ZR TI Y
2. Basalt

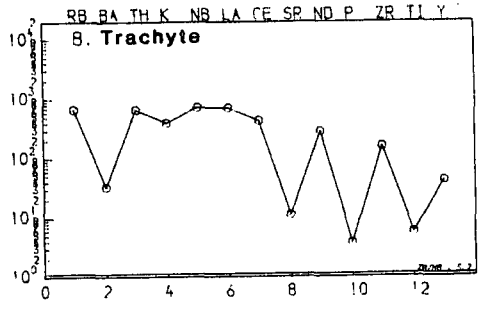
RB BA TH K NB LA CE SR ND P ZR TI Y
8. Trachyte

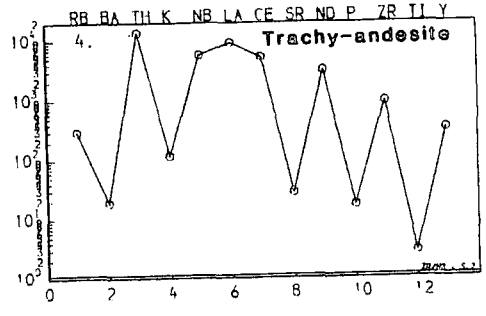
RB BA TH K NB LA CE SR ND P ZR TI Y
4. Trachy-andesite

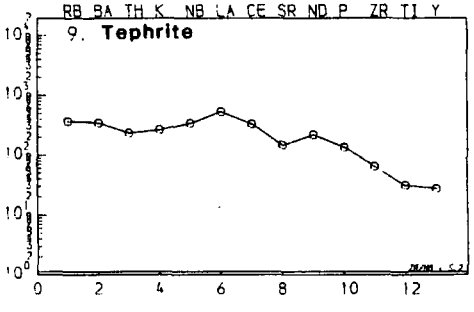
RB BA TH K NB LA CE SR ND P ZR TI Y
9. Tephrite

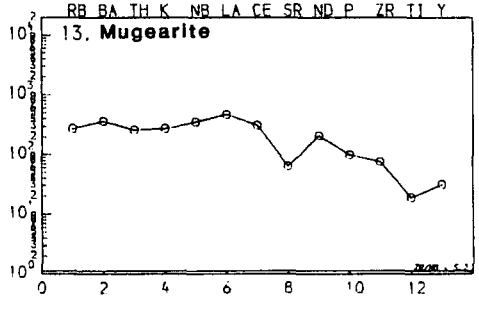
RB BA TH K NB LA CE SR ND P ZR TI Y
13. Mugearite

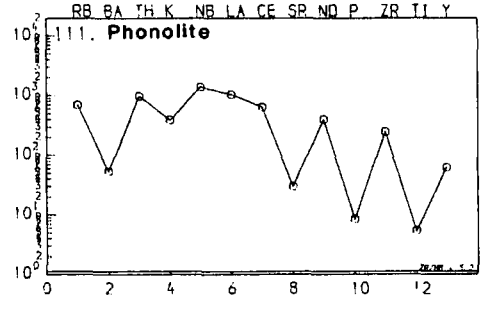
RB BA TH K NB LA CE SR ND P ZR TI Y
111. Phonolite

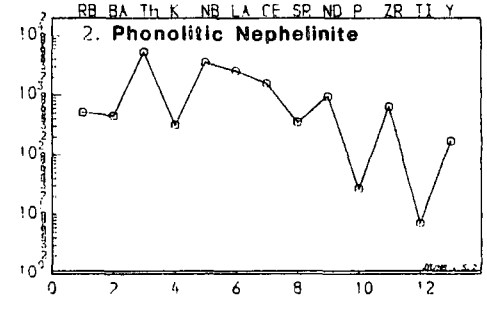
RB BA TH K NB LA CE SR ND P ZR TI Y
2. Phonolitic Nephelinite

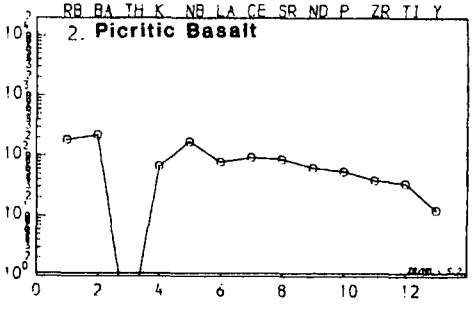
RB BA TH K NB LA CE SR ND P ZR TI Y
2. Picritic Basalt

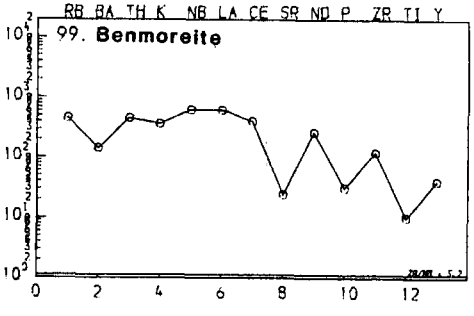
RB BA TH K NB LA CE SR ND P ZR TI Y
99. Benmoreite

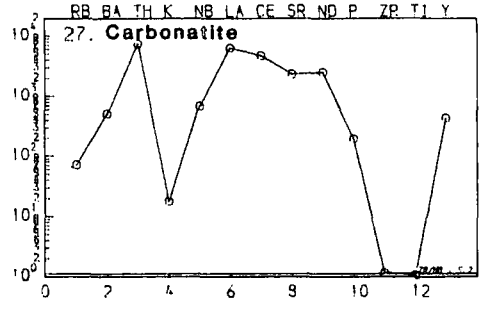
RB BA TH K NB LA CE SR ND P ZR TI Y
27. Carbonatite

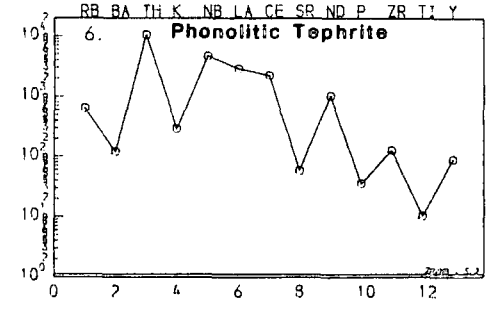
RB BA TH K NB LA CE SR ND P ZR TI Y
6. Phonolitic Tephrite

Basalts

There are only two basalts from this group and they show a markedly different pattern to the basalts of the high Zr/Nb suite. Noticable in these basalts, are small negative anomalies at Th and Sr and a positive anomaly at Nb. The Th anomaly is shown by the equivalent high Zr/Nb samples but the positive Nb anomaly is in strong contrast to a negative anomaly in the high Zr/Nb suite. Also, obviously lacking from these basalts is a positive P anomaly. Rb is also more enriched than Ba in contrast to the generally lower Rb enrichment compared to Ba in the high Zr/Nb suite. The low Zr/Nb basalts have a steeper slope to the pattern and are more enriched (in absolute terms) in Rb, Th, K and Nb, with similar contents of Ba and La-Y (except P). This overall steeper pattern would be consistent with a smaller degree of partial melting, and the marked differences in their source region chemistry (Norry and Fitton 1983). The positive Nb anomaly may be an artefact of averaging for just two samples, as no such anomaly is evident from the other 'basic' samples.

Tephrite

These show a 'smooth' pattern compared to their high Zr/Nb equivalents, with a relatively level portion from Rb-La where a decline starts towards Y. These tephrites show a small negative Sr anomaly but do not show the positive Nb anomaly seen in the basalts. This lack of an Nb anomaly would imply that no residual Nb-bearing phase has been left in the mantle on melting as with the high Zr/Nb suite (possibilities include rutile, sphene or spinel, Saunders *et al.* 1980). Thus, these rocks probably originated from a mineralogically different source region to the high Zr/Nb rocks, either as a previous or subsequent melt.

Nephelinite

These strongly undersaturated, basic rocks show incompatible element enrichments and an overall pattern extremely similar to that of the tephrites with the exception of slightly higher Rb. These nephelinites are all essentially 'lamprophyric' in character, and probably represent small degree partial melts from the mantle (perhaps as low as 0.1%, see Mackenzie 1985). Similarly tephrites/basanites may also represent small degrees of partial melting, and thus the characteristic patterns of these two groups of

rocks will be a reflection of their source – clearly different from the high Zr/Nb suite. The small negative Sr anomaly apparent in many basic rocks would thus appear to be a primary feature, and may represent either the retention of a Sr-bearing phase within the source region or a depletion in Sr (compared to La and Ce) in the source. Residual amphibole (with a $D_{Sr} \approx 2\times D_{Ce,Nd}$) may have such an effect, although any other Sr enriched (relative to Ce and Nd) residual phase would have a similar effect.

Picritic Basalt

These rather altered samples show a pattern similar to the basalts and tephrites, ignoring the lack of Th. K is lower than in the other basic rocks, as too is Rb, and this will be due to loss of these elements on alteration.

Mugearite

No hawaiitic samples from the low Zr/Nb suite (excluding two samples from Østfjordsdal) have been found, and there is a compositional gap from basalts to mugearite. In the mugearites, the small negative Sr anomaly has deepened, indicative of plagioclase fractionation, and a negative Ti anomaly has formed, a result of opaque oxide (Ti-magnetite) fractionation.

Benmoreites

Large negative anomalies exist at Sr, Ti and P indicating that feldspar and oxide crystallisation has continued from mugearite to benmoreite and been joined by apatite. The crystallising feldspar is now anorthoclase and has caused negative anomalies at K and Ba. Both of these elements have higher distribution coefficients into anorthoclase than plagioclase.

Phonolite and Trachyte

These rock types can essentially be considered together as immediate derivatives of the benmoreites. Their incompatible element enrichments are very similar. Continued fractionation of an alkali-rich feldspar (initially anorthoclase, ranging through to a binary alkali feldspar) has caused deepening of the negative anomalies at Ba, K and Sr. Further extraction of apatite and Fe-Ti oxide has produced larger negative anomalies

at P and Ti, giving these two groups highly evolved, 'spiky' patterns.

Phonolitic Nephelinites and Phonolitic Tephrites

These samples are very close (in TAS terms) to phonolite and show similar patterns. Noticable in these is the relatively strong enrichment of Th compared to Rb. In phonolitic rocks where alkali feldspar and nepheline are crystallising, Rb (with distribution coefficients of 0.38 and 0.44 respectively, Larsen 1979) becomes almost compatible, and will be almost 'buffered' by the crystallising assemblage. Thus, in both cases, Rb is higher than in the benmoreites, but by no means as enriched as (the still incompatible) elements such as Th, REE, Nb etc..

Trachy-andesites

These (4 samples) show some of the most enriched samples analysed, with one sample (127068) showing 11218ppm Ce, 7350ppm La, 4318ppm Nd, 213ppm Ga, 1446ppm Th, 205ppm U, 6302ppm Zn and another (41926) containing 3210ppm Nb, 10899ppm Zr and 964ppm Y. Although the other 2 samples (54286 and 54293) do not show such extreme enrichment, their compositions are none the less considerably more enriched than most phonolitic samples. The origins of such enrichment in trace elements is unclear petrographically. 127068 is a completely devitrified spherulitic felsic (trachytic) rock, 54286 and 54293 are iron-stained, probably slightly altered, feldspar, alkali amphibole and alkali pyroxene, trachytic rocks. 41926 is a carbonated trachytic rock now containing no fresh ferro-magnesian minerals but a large number of stained, almost opaque, patches in the groundmass. Phases such as zircon, monazite, allanite etc. are not visible in any samples. However, the complete (coarse grained) devitrification of 127068 and the carbonate patches visible in 41926 may point to the presence of a fluid phase, possibly (if late magmatic) a 'carrier' of large quantities of REE, Y, Zr, Nb and Th, but not of Rb, Ba, K, Sr, P and Ti which show enrichments similar to the phonolites and trachytes.

Carbonatites

The carbonatites are included in Figure 5.6.2 for comparison with the phonolites. They are thought to be formed by an 'immiscible' relationship to magmas of phonolitic

composition (Freestone and Hamilton 1980) and will be discussed in Chapter 7.

Summary

Incompatible element data from the low Zr/Nb suite shows a similar evolutionary pattern to the high Zr/Nb suite, governed largely by feldspar, oxide and apatite. Roughly similar degrees of enrichment are apparent from the intermediate and evolved samples of both suites. However, characteristic and obvious differences in the basic rocks have been described. These can not be attributed to any fractional crystallisation/assimilation process and must be regarded as primary features inherited from their (mantle?) source regions.

5.7: Further consideration of Incompatible Elements

The following discussion will concern itself mostly with the Large Ion Lithophile Elements (LILE) Zr, Nb, Y, La and Ce. These elements are all highly incompatible during both melting of a mantle source and crystal fractionation. These data are presented as x-y graphs, and as with the plots of element vs. F.I., all groups of rocks are included to show the range of all data although samples from the Østfjordsdal dyke swarm are not included. The Østfjordsdal data are however virtually indistinguishable from the low Zr/Nb (undersaturated) suite, although samples from Østfjordsdal do not evolve to such extreme compositions. Plots of an incompatible element against a slightly less incompatible element should, for fractional crystallisation, give near linear trends (in fact these will be slightly concave towards the axis of the element with lower bulk distribution coefficient; see for example Nb vs. Y, Figure 5.7.1 , where Nb is more incompatible than Y). Fractional melting (when considering x-y plots of incompatible elements) will also produce a curved trend. This will have a greater curvature concave towards the more incompatible element than the fractional crystallisation trend. Both of these trends should pass through the origin. Treuil and Varet (1973) suggest that near linear trends passing through (0,0) in such incompatible element plots are a "necessary and sufficient condition of fractional crystallisation".

Magma mixing will produce strongly curved trends, and these would not necessarily pass through the origin. Initial differences in magma composition or source region will be reflected in markedly different trends of incompatible element evolution, due to

Figure 5.7.1 (4 pages).

Incompatible element x–y variation. Each page shows the variation for one pair of elements for both the high and low Zr/Nb suites. The field of Martin's (1985) data from dykes on Tugtutôq and the Ilímaussaq Peninsula is shown on the plot for the high Zr/Nb (oversaturated) suite by a dashed line.

The data for the low Zr/Nb does not include the Østfjordsdal swarm data, although these are totally included by the scatter of this data set.

(i) Ce–Y

(ii) La–Y

(iii) Zr–Y

(iv) Nb–Y

A plot of Zr–Nb is presented in Figure 5.4.4.

Figure 5.7.1(i)

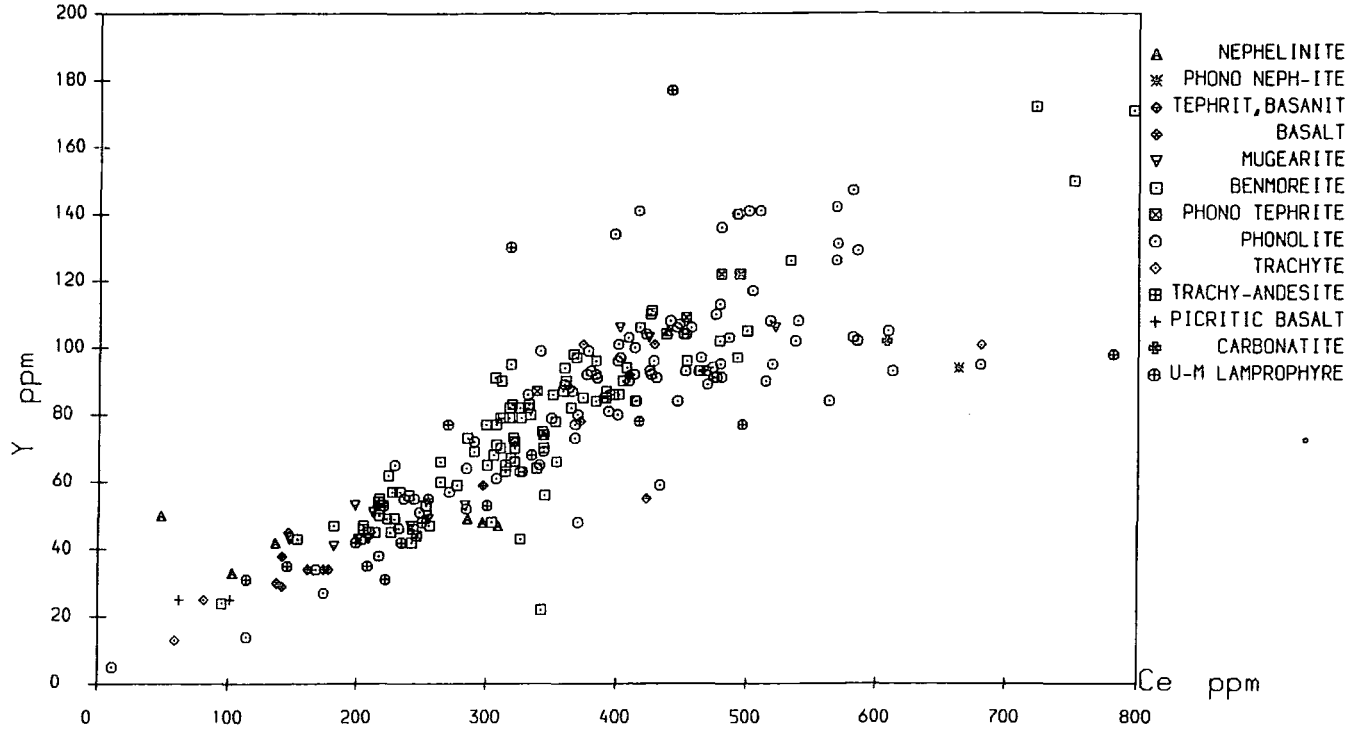
Y ppm
Ce ppm
NEPHELINITE
PHONO NEPH-ITE
TEPHRIT,BASANIT
BASALT
MUGEARITE
BENMOREITE
PHONO TEPHRITE
PHONOLITE
TRACHYTE
TRACHY-ANDESITE
PICRITIC BASALT
CARBONATITE
U-M LAMPROPHYRE

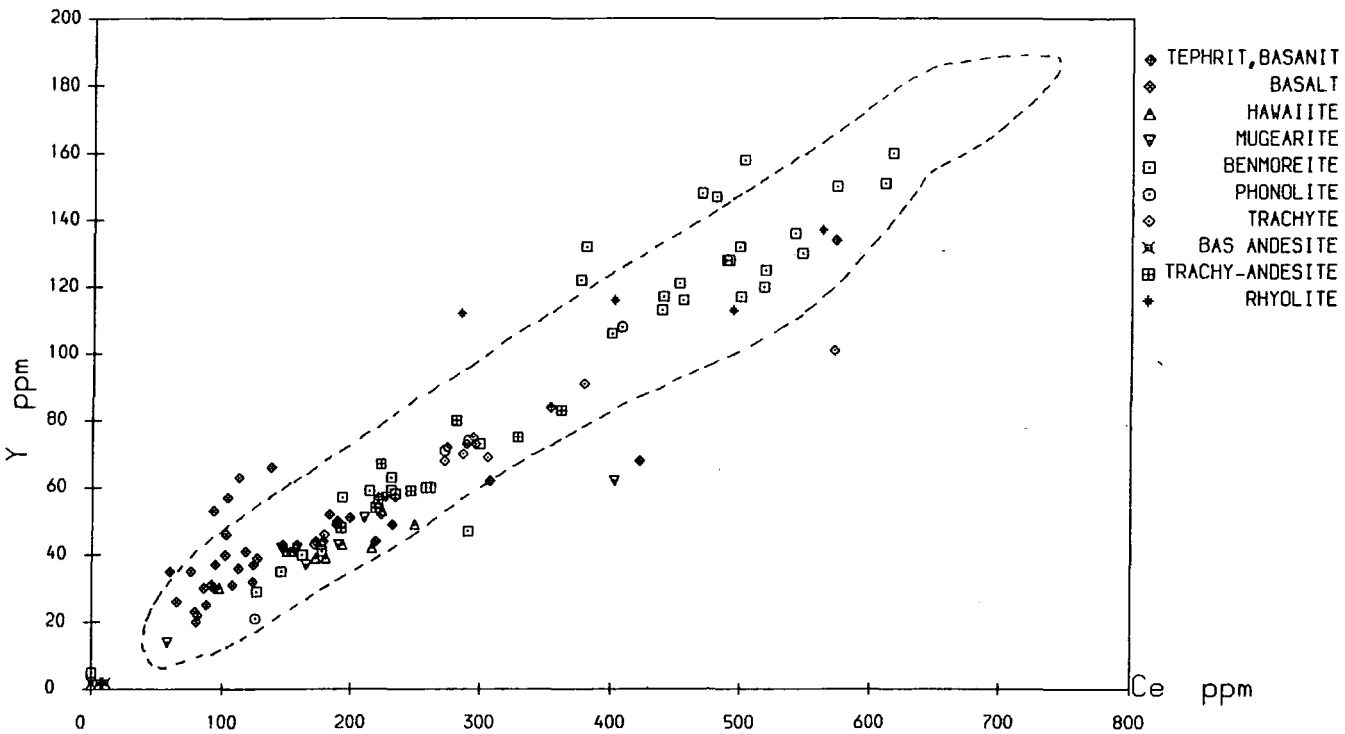
Y ppm
Ce ppm
TEPHRIT,BASANIT
BASALT
HAWAIITE
MUGEARITE
BENMOREITE
PHONOLITE
TRACHYTE
BAS ANDESITE
TRACHY-ANDESITE
RHYOLITE

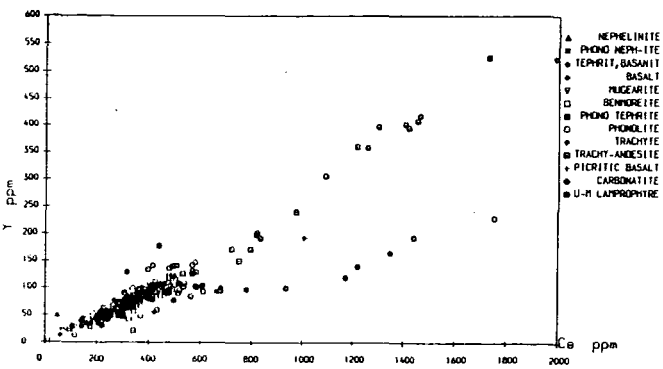

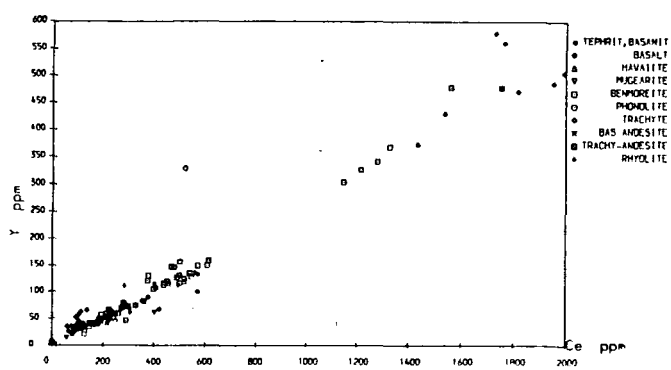

Figure 5.7.1(ii)

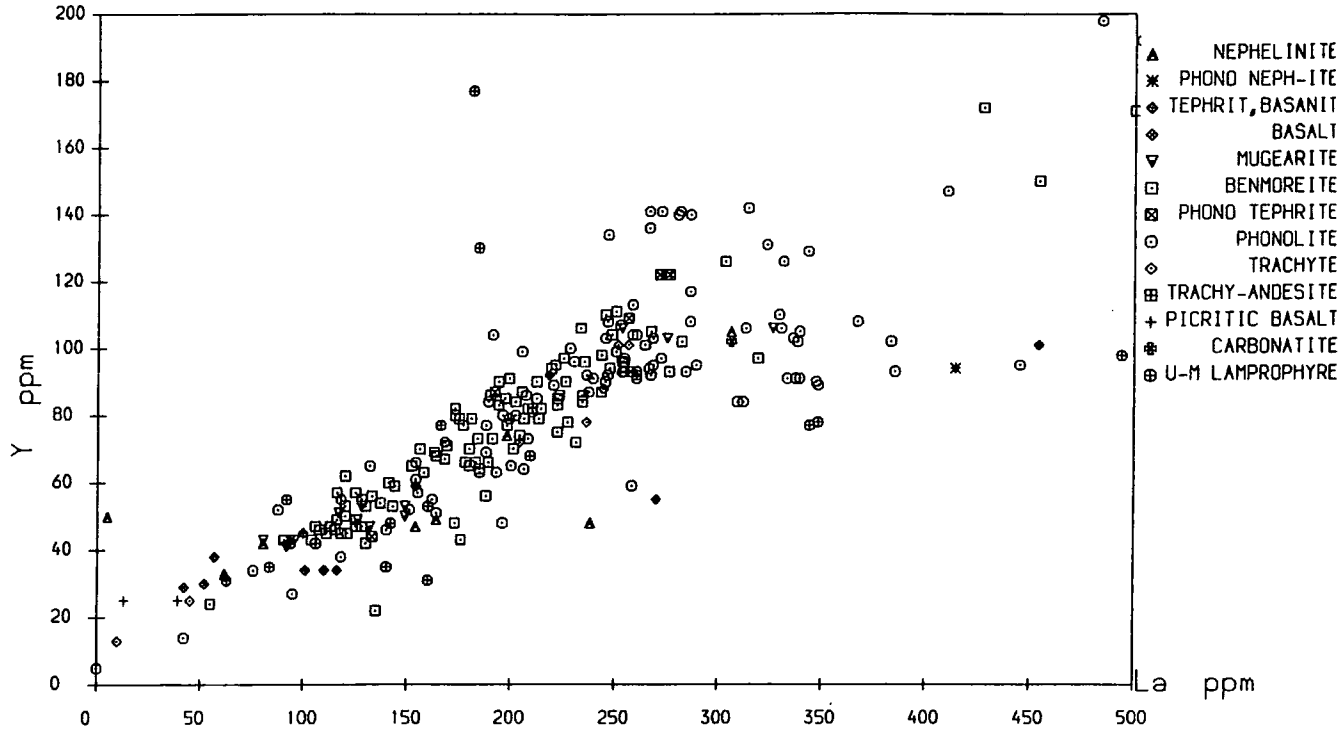

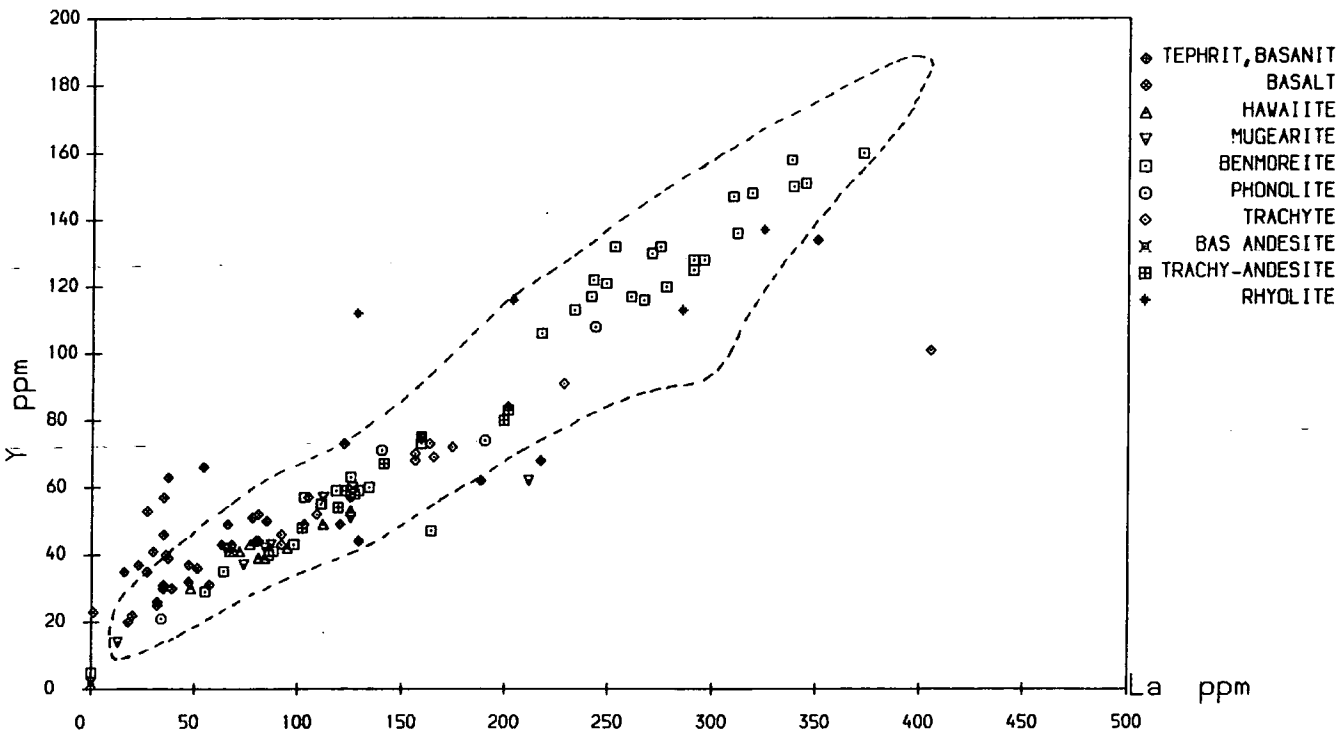

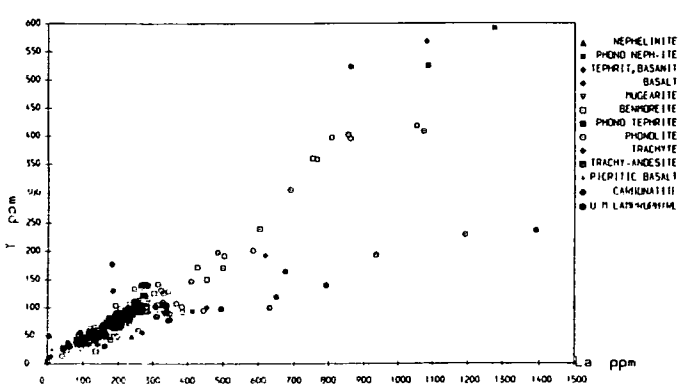

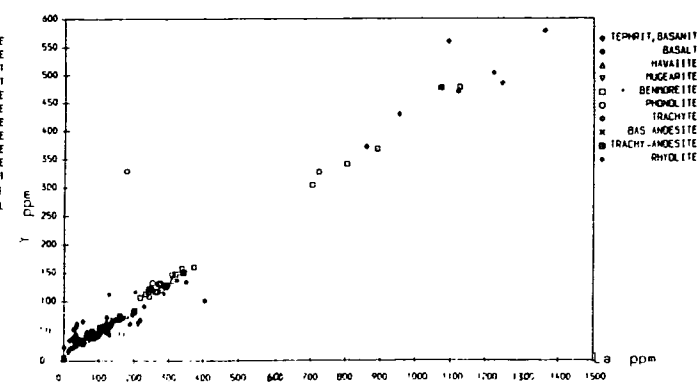

Figure 5.7.1(iii)

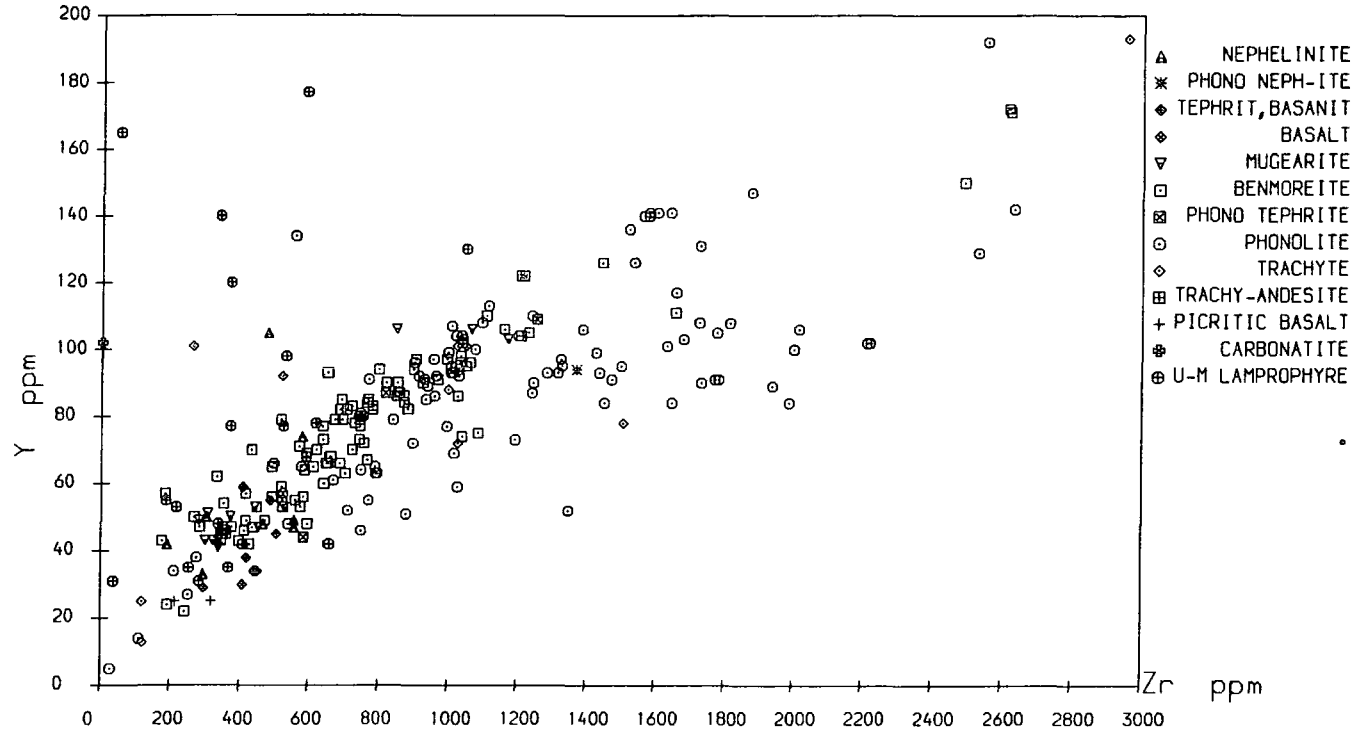

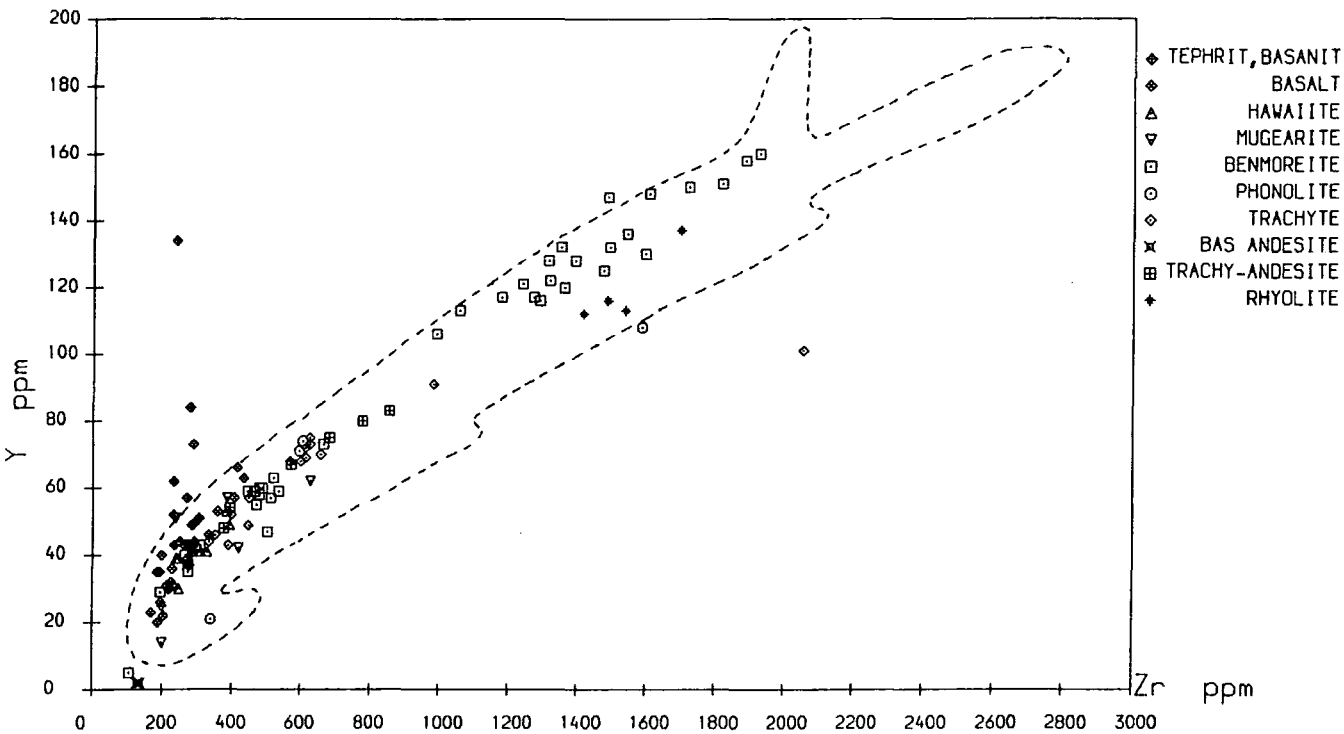

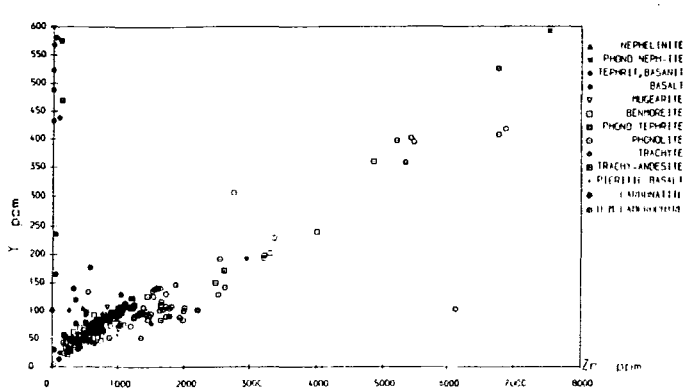

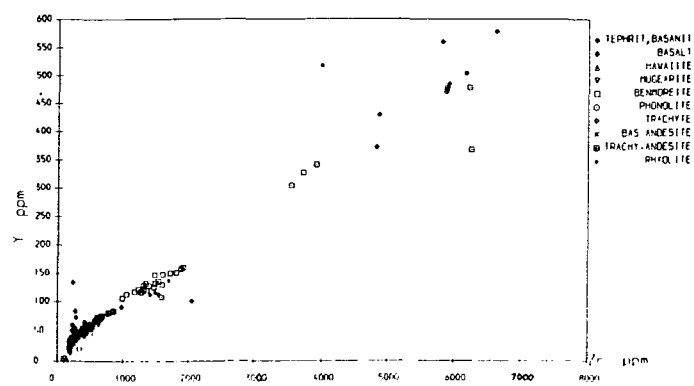

Figure 5.7.1(iv)

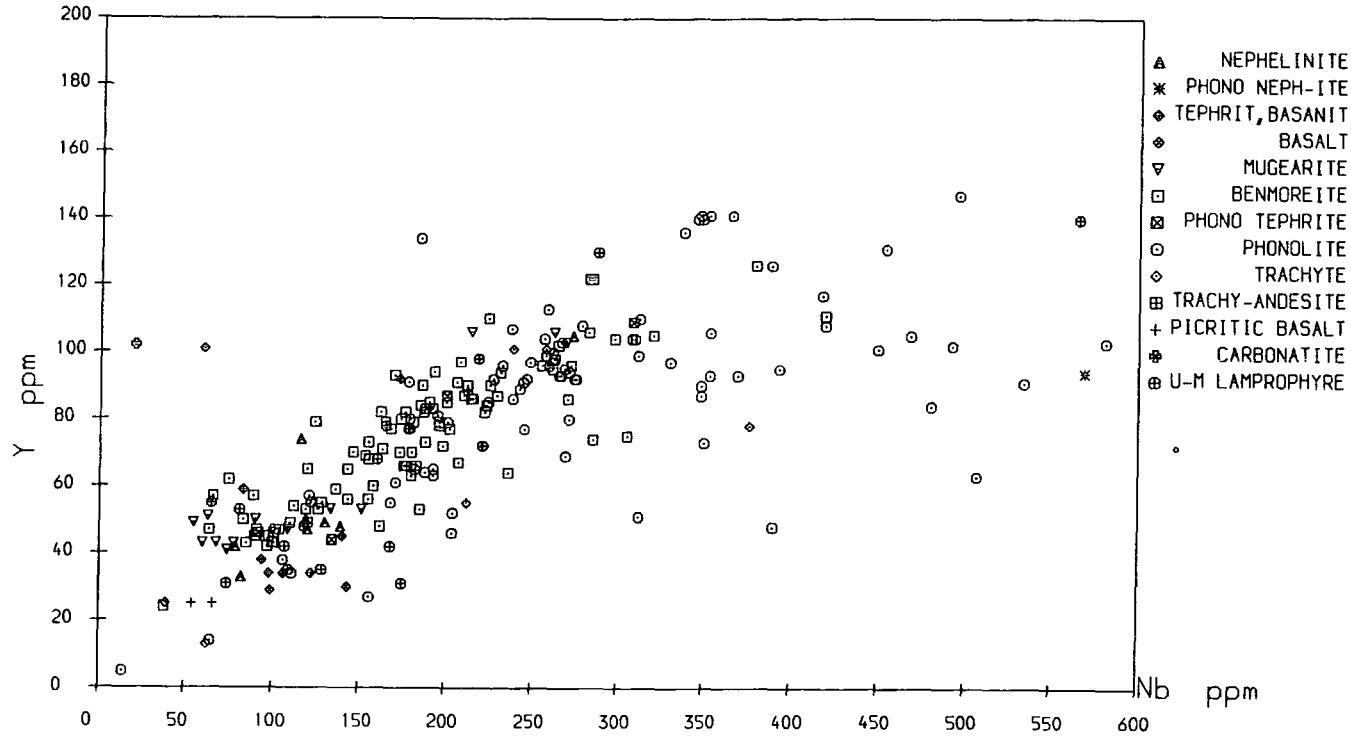

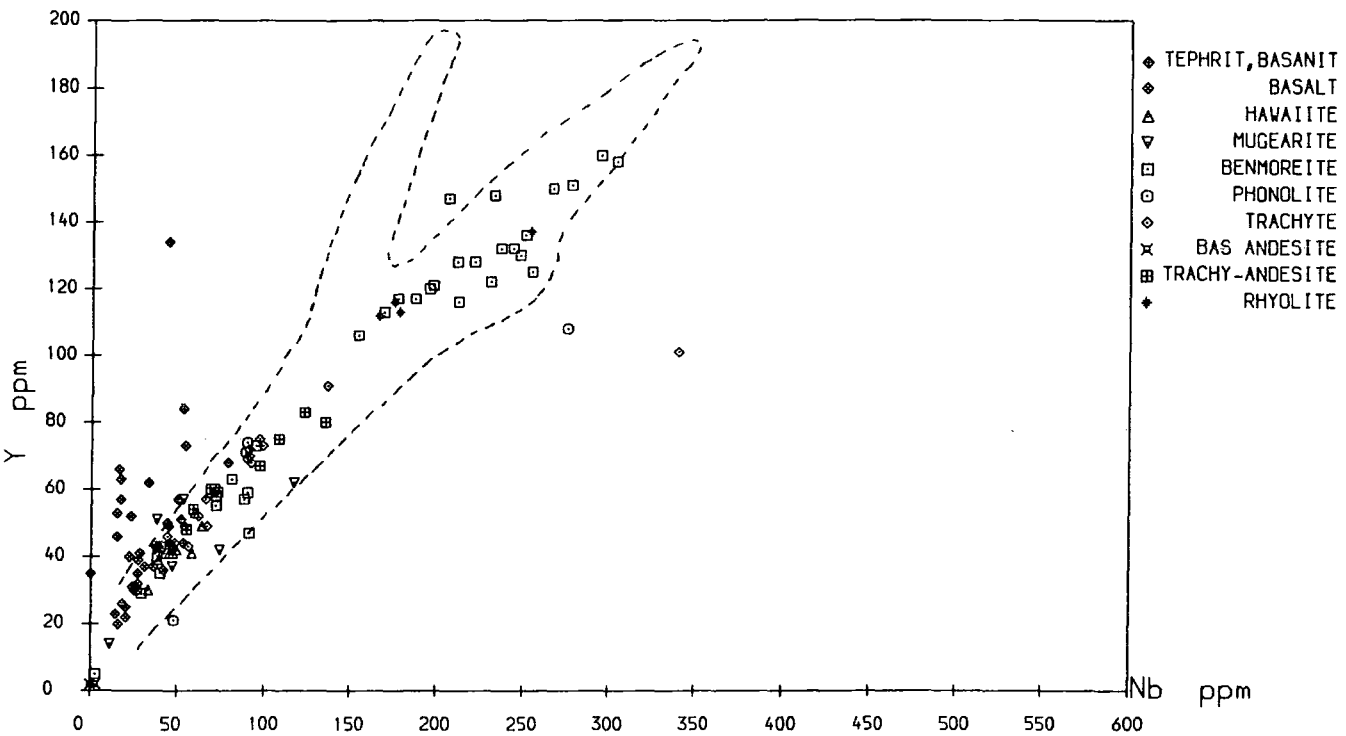

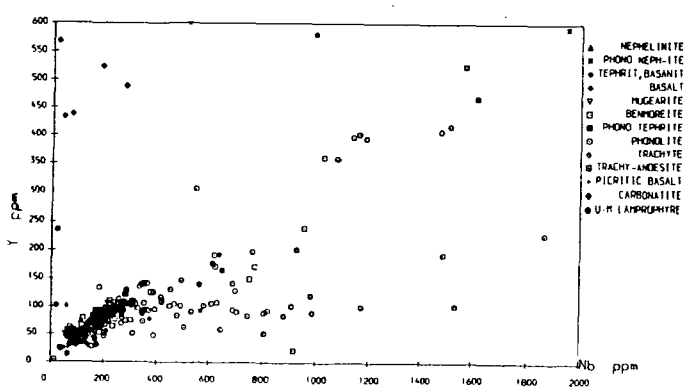

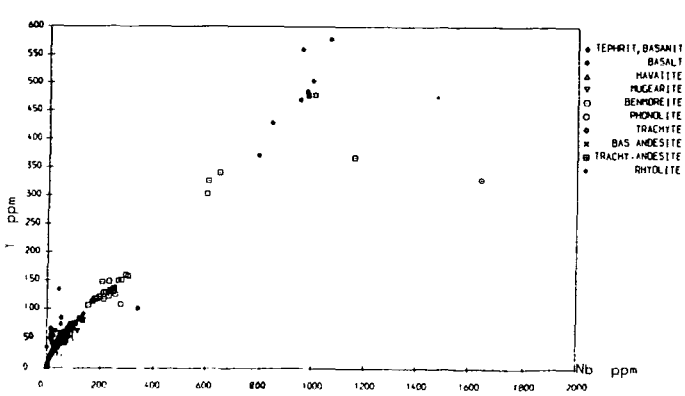

initial differences in the incompatible element ratios (eg. Zr/Nb). These early differences define initial 'parent' differences and imply differences in the source region or different degrees of partial melting from the same source.

Figure 5.7.1 shows plots of La/Y, Ce/Y, Nb/Y and Zr/Y for both the low and high Zr/Nb suites of dykes. With the exception of the Nb/Y plot, there is virtually no difference in the elemental concentration for the oversaturated (high Zr/Nb) and undersaturated (low Zr/Nb) suites. The low Zr/Nb data are however, much more widely scattered across the whole compositional range. This may in part be due to combinations of high and low pressure fractional crystallisation, particularly if an Y-bearing phase (such as garnet) is involved. Small pockets of magma evolving along different liquid lines of descent may produce a wide scatter of the data (cf. Macdonald 1969). The high Zr/Nb suite shows a particularly well defined, narrow range of composition on all plots. The data from both suites are consistent with a fractional crystallisation model, as all trends are gently curved and pass through (0,0). The plot of Nb/Y reflects the variation in Nb behaviour between the two suites of samples, with lower Nb seen at similar Y in the high Zr/Nb suite. This difference in Nb between the two suites is the only exploitable discriminator. Nb/Y would be less easy to use than Zr/Nb due to the more curved nature of the Nb/Y trends (see Zr/Nb, Figure 5.4.4).

Martin's (1985) data fields for these elements are shown on the high Zr/Nb plots, and confirm the fact that these dyke are members of the main Tugtutôq - Ilímaussaq - Nunataq swarm.

More information regarding partial melting and fractional crystallisation can be gained by plotting the ratio of a more incompatible element to a less incompatible element on the y-axis against the ppm concentration of the more incompatible element on the x-axis, eg. La/Y vs. La. From these plots, a trend governed by partial melting will produce a steep, straight line with a slope of D^a/C_o^a, and an intercept on y of $C_o^b(1\text{-}D^a)/C_o^a$, where C_o^b is the content in the source of the more incompatible element, C_o^a is the source concentration of the less incompatible element and D^a is the bulk distribution coefficient for the less incompatible element (Martin 1985). This assumes that $D^b \approx 0$. * For fractional crystallisation, a trend with a very slight positive slope,

* *The relationships described for the variation of incompatible elements plotted as*

more–or–less parallel to the x-axis would result. This is due to the very slight increase in the ratio of the more/less incompatible element (y-axis) against a steady increase in the concentration of the more incompatible element (x-axis) caused by fractional crystallisation.

Figure 5.7.2 shows plots of La/Y vs. La; Nb/Y vs. Nb; Zr/Y vs. Zr and Nb/Zr vs. Nb for the high and low Zr/Nb suites of rocks (making the Nb/Zr diagram slightly peculiar). As with the simple x-y plots, the low Zr/Nb data shows considerably more scatter than the very well constrained trends shown by the high Zr/Nb data. This is due probably to a combination of deep and shallow fractional crystallisation but may also be a reflection of different central complex sources for the undersaturated, local dykes (eg. South Qôroq or Igdlerfigssalik associated, and possibly some related to the Motzfeldt-North Qôroq activity, which may have inherent chemical differences).

However, certain general features of these trends are apparent, most notably a large difference in the observed trends followed by the high and low Zr/Nb suites.

(i) Generally, the low Zr/Nb suite show slightly higher values of the more/less incompatible element. This is consistent with smaller degrees of partial melting, assuming the same source chemistry.

(ii) Both trends show an initial steeply inclined section (through basic rock types) which levels off into a trend which is 'parallel' to the x-axis. This is consistent with an early control by partial melting which gives way to a control by fractional crystallisation. However, for Zr, the overall effect may also be controlled by some ilmenite fractionation (see Chapter 5.4).

---

simple x-y graphs or as a ratio of two incompatible elements against the concentration in ppm of the more incompatible elements are taken from Martin (1985). Martin (1985) calculated the behaviour of two incompatible elements, assuming one to be more incompatible than the other, by substitution of ratios of elements for C_o and C_l into the melting equation $C_l = C_o/(D+F(1-D))$, and the fractional crystallisation equation, $C_l = C_oF^{(D-1)}$, where C_l is the concentration in the liquid, C_o is the original concentration, F is the fraction of liquid and D is the element distribution coefficient – see Cox et al. (1979).

Figure 5.7.2 – 4 pages.

Plots of ratios of a more/less incompatible element against the same more incompatible element for both high and low Zr/Nb suites. See text for interpretation.

(i) Nb/Y–Nb

(ii) Zr/Y–Zr

(iii) La/Y–La

(iv) Nb/Zr–Nb

Figure 5.7.2(i)

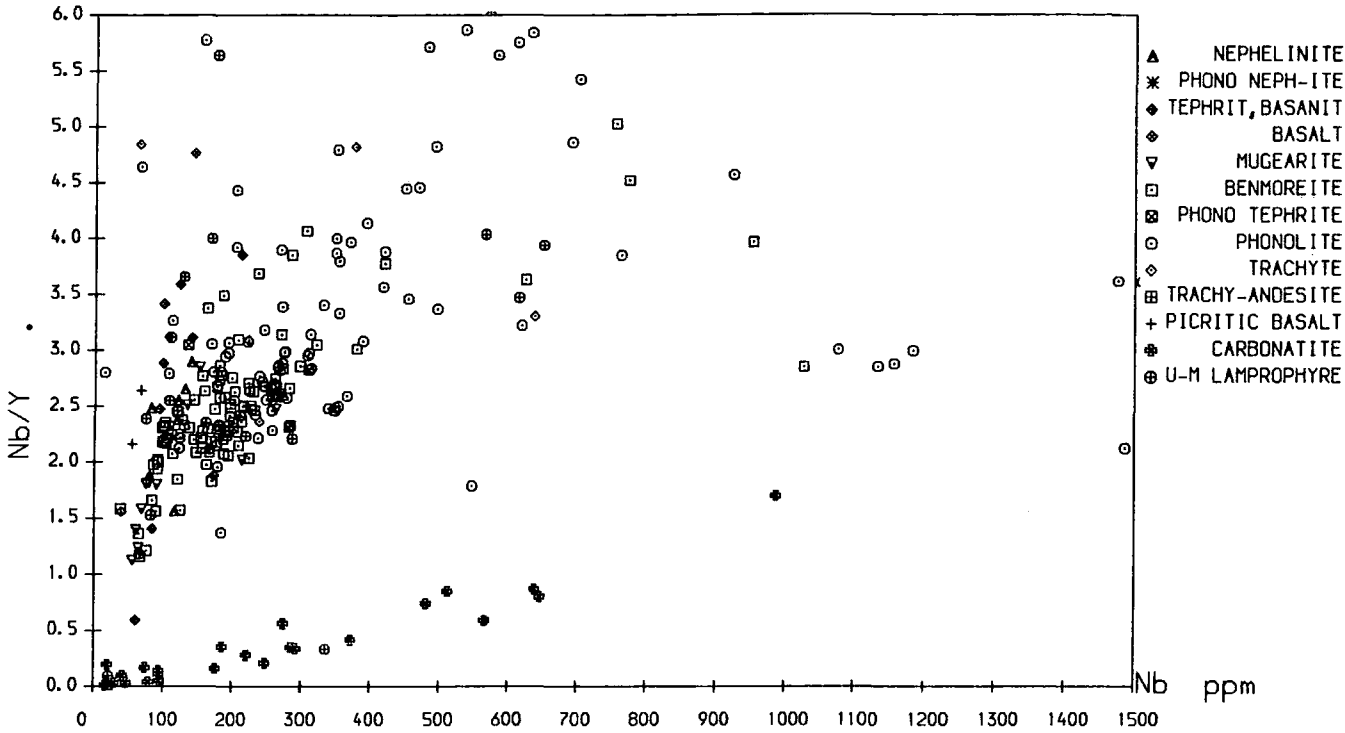
Nb/Y
Nb ppm
NEPHELINITE
PHONO NEPH-ITE
TEPHRIT, BASANIT
BASALT
MUGEARITE
BENMOREITE
PHONO TEPHRITE
PHONOLITE
TRACHYTE
TRACHY-ANDESITE
PICRITIC BASALT
CARBONATITE
U-M LAMPROPHYRE

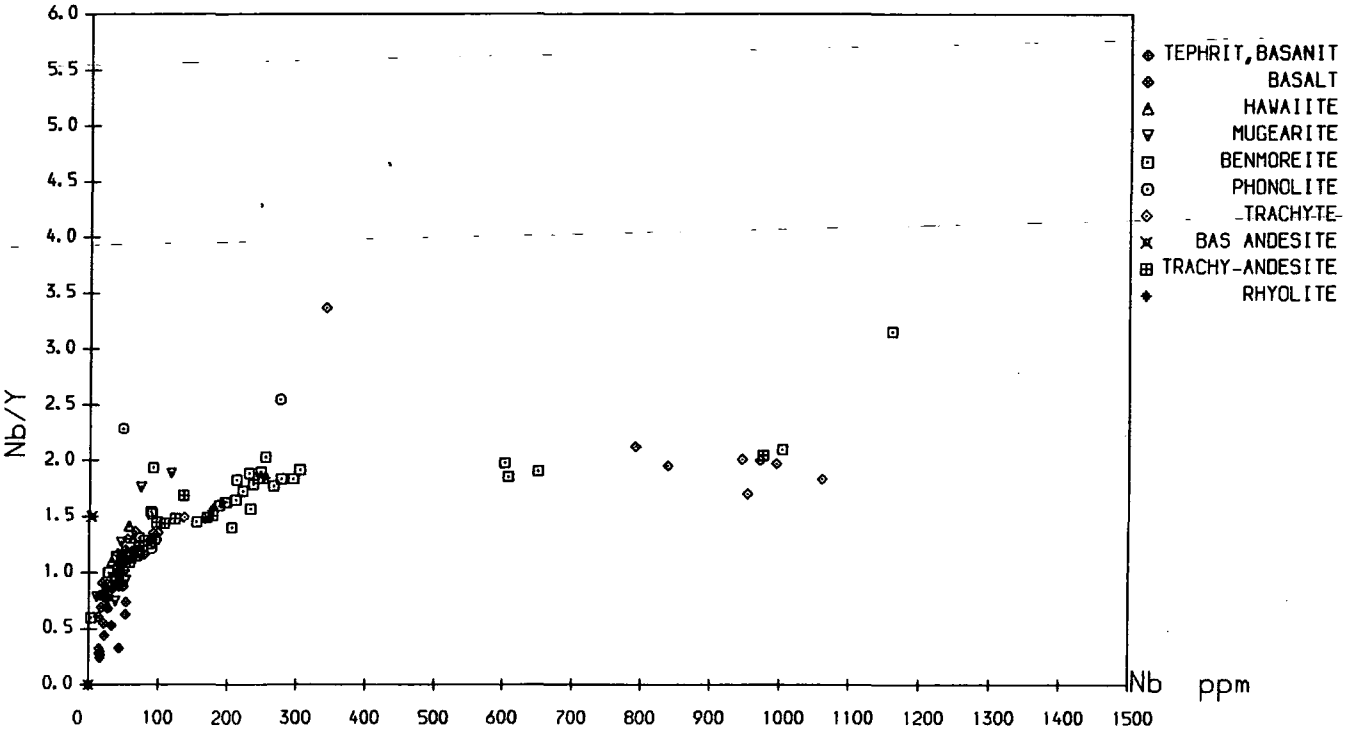
Nb/Y
Nb ppm
TEPHRIT, BASANIT
BASALT
HAWAIITE
MUGEARITE
BENMOREITE
PHONOLITE
TRACHYTE
BAS ANDESITE
TRACHY-ANDESITE
RHYOLITE

Figure 5.7.2(ii)

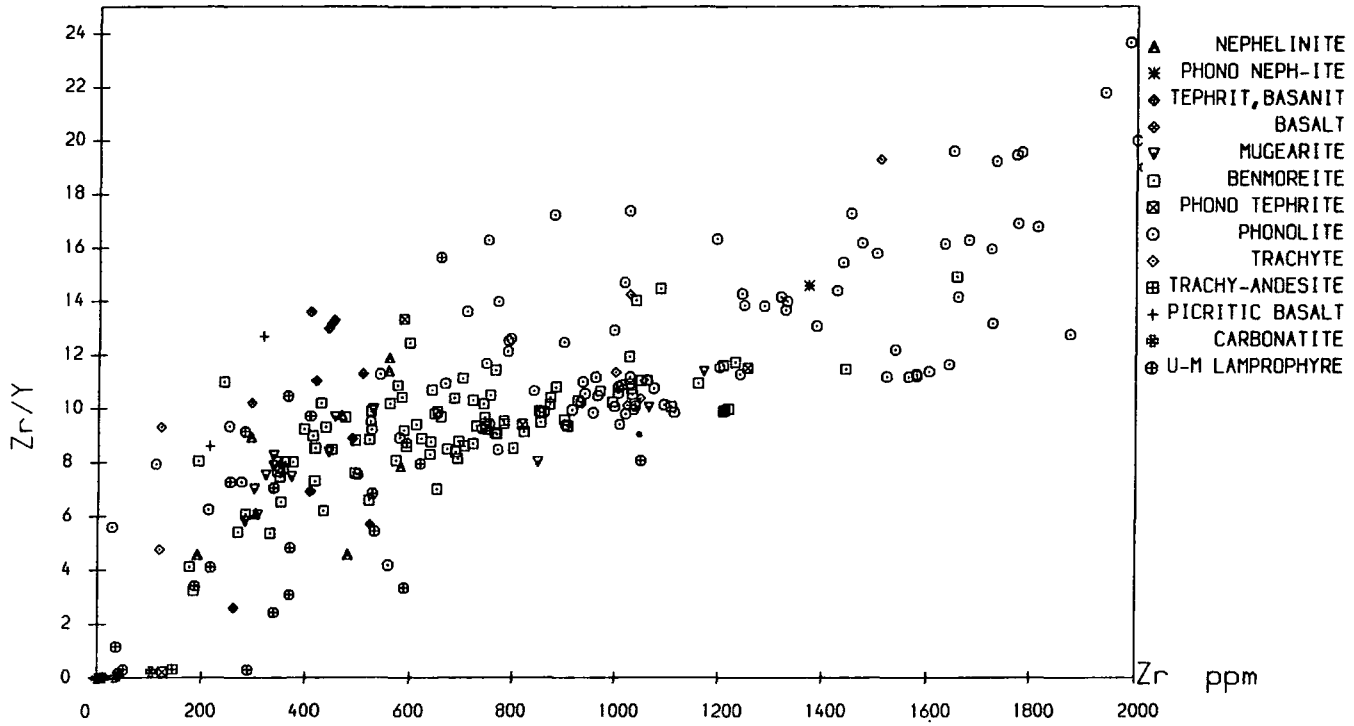

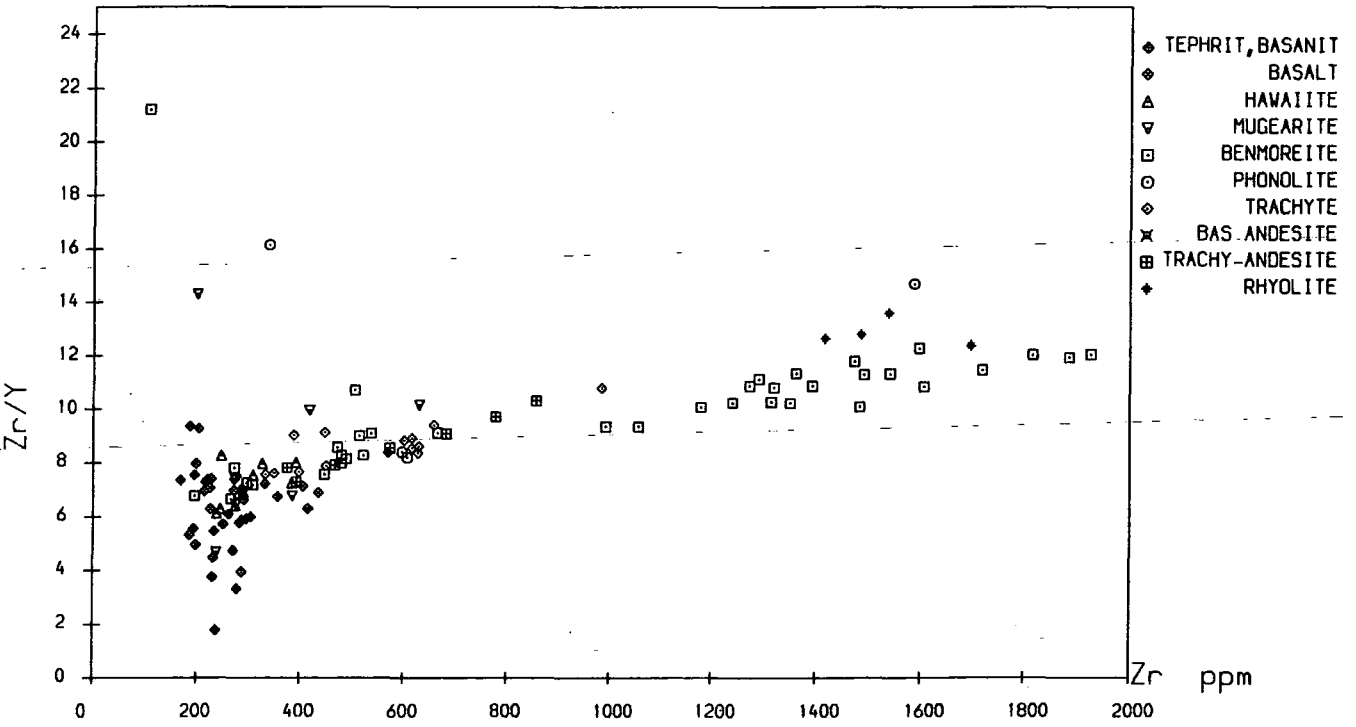

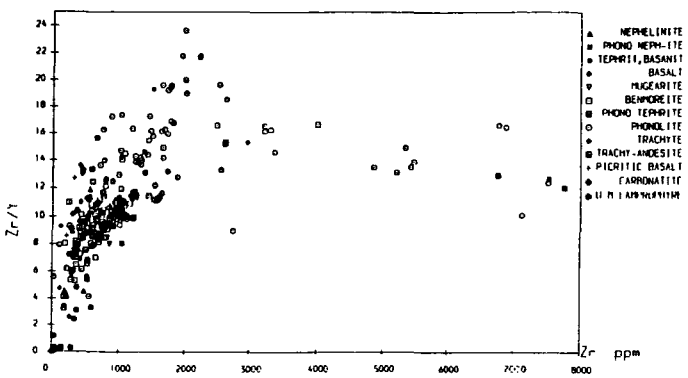

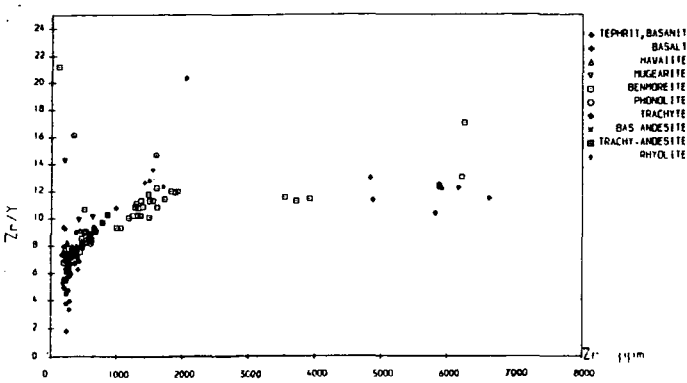

Figure 5.7.2(iii)

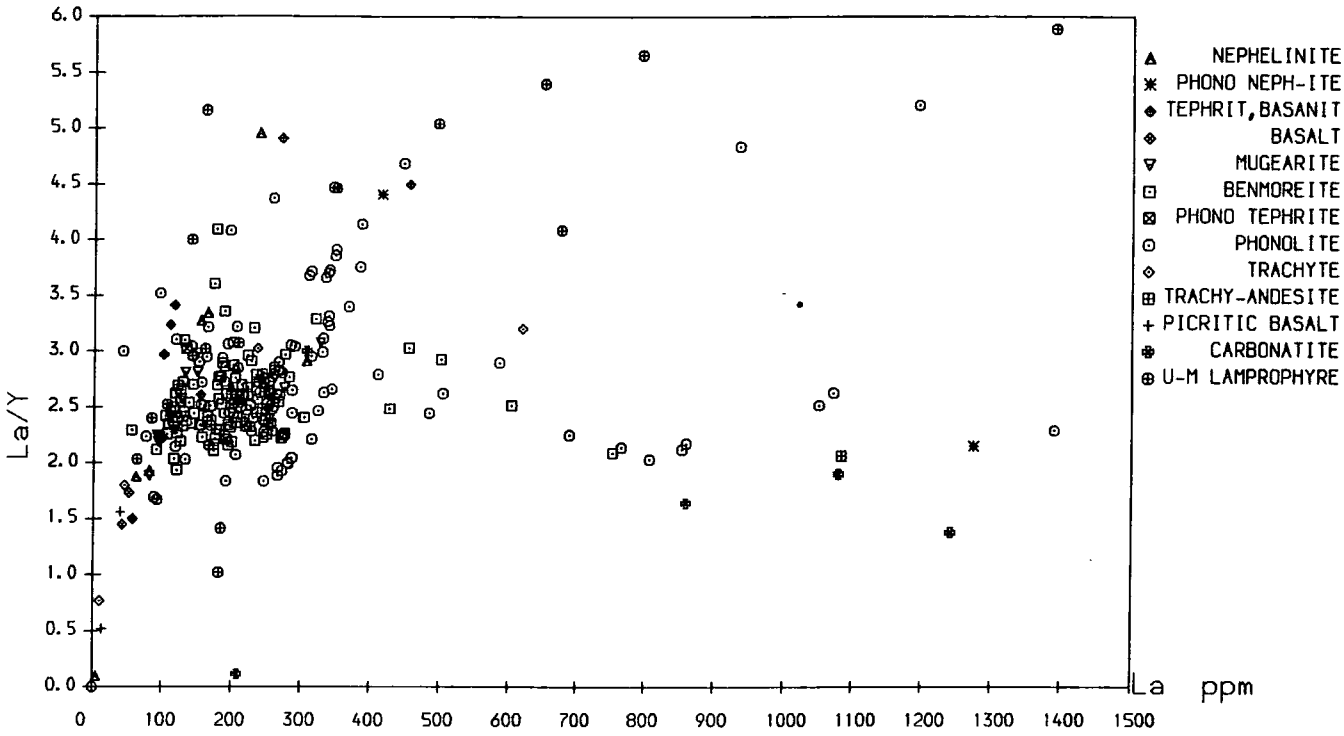

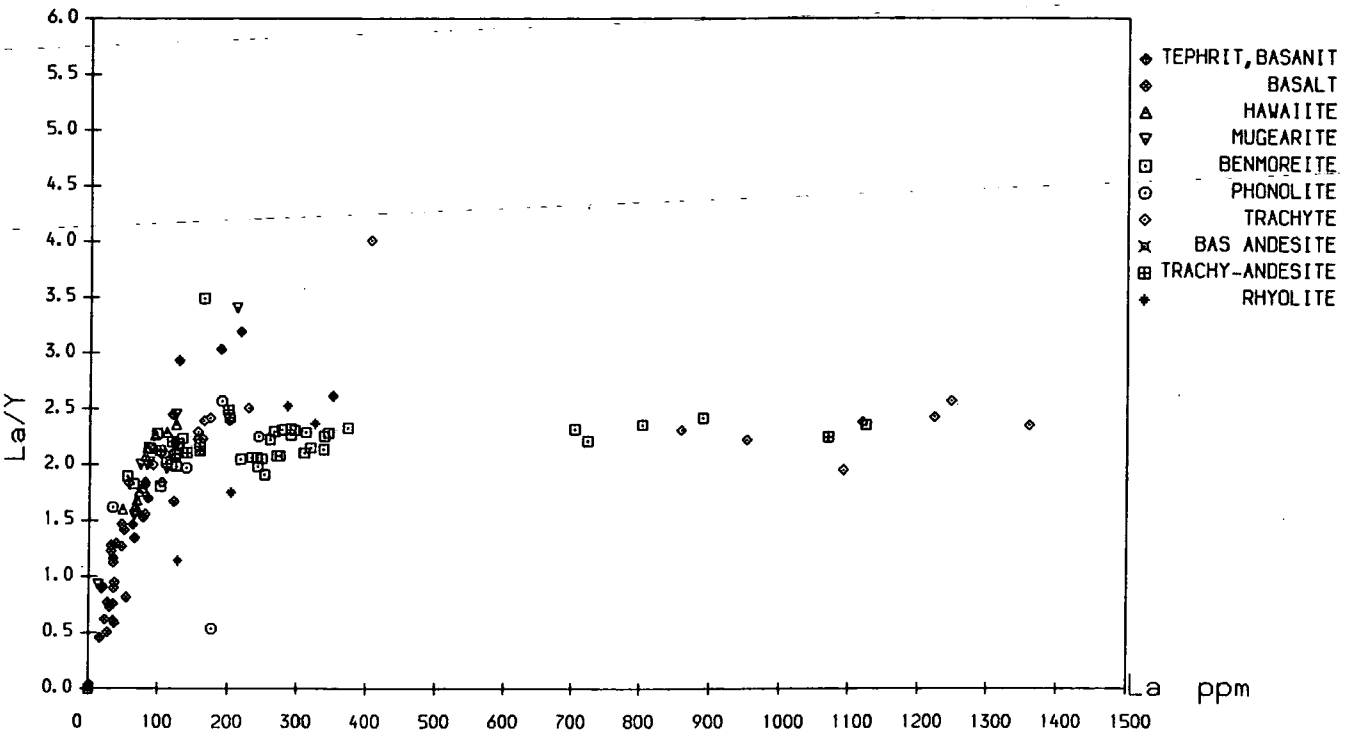

Figure 5.7.2(iv)

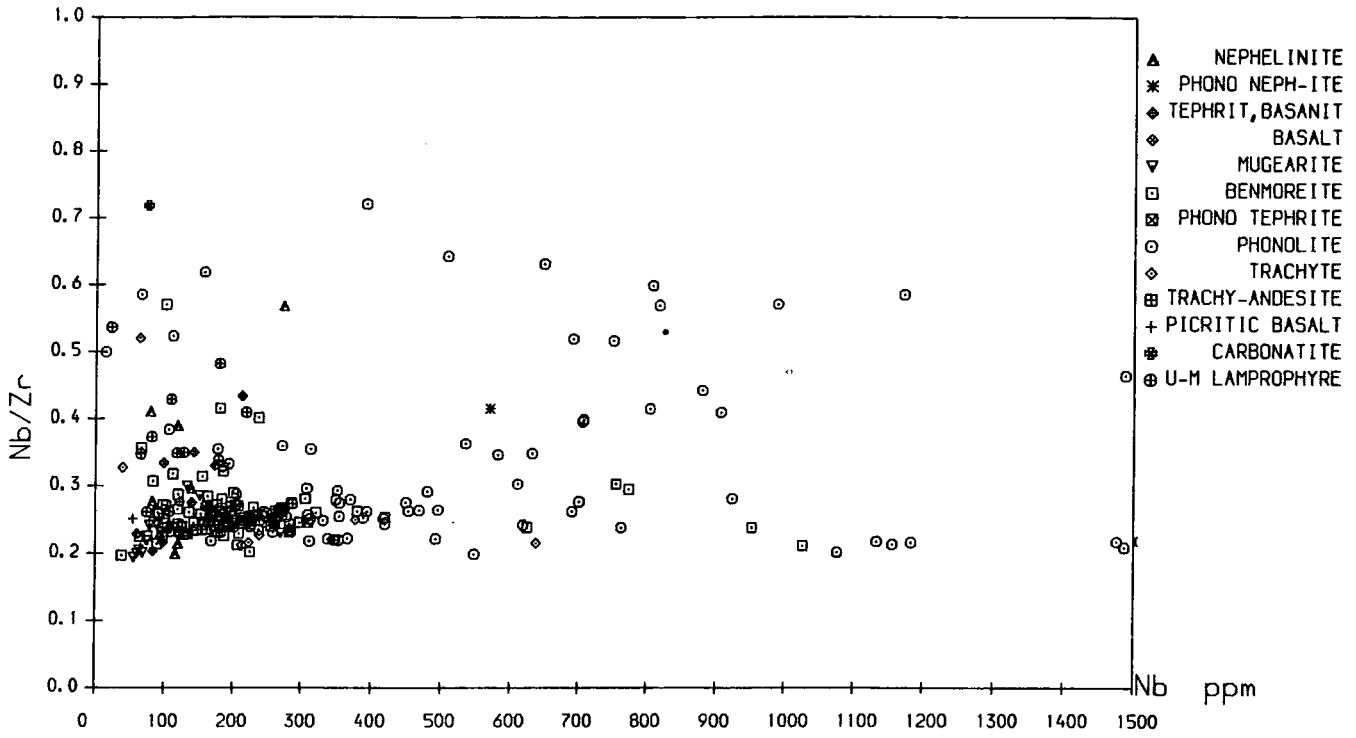

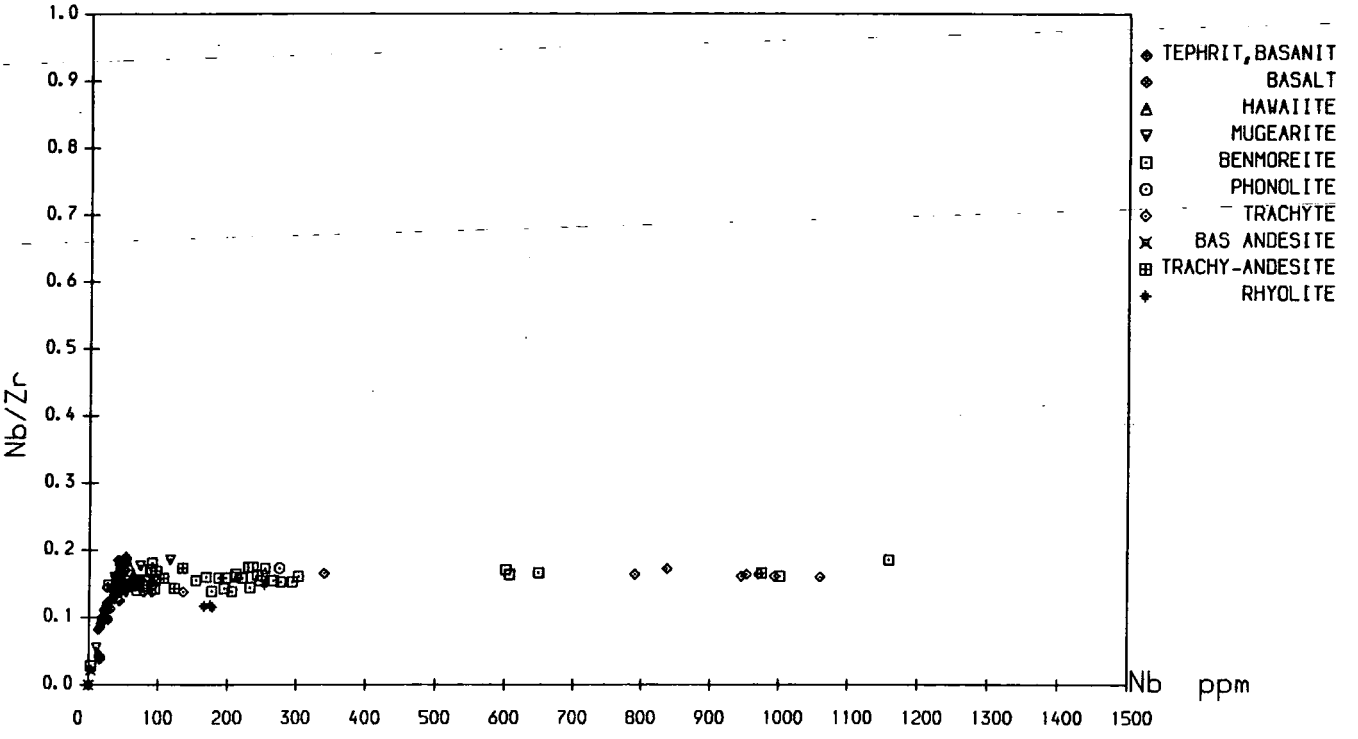

(iii) Differences in degree of fractional crystallisation cannot account for the differences in the low and high Zr/Nb suite.

(iv) The large amount of scatter evident in the low Zr/Nb suite may be due to individual liquid 'lines of descent' for small 'packets' of separate liquids. This is consistent with a source for these dykes as the highly fractionated central complexes, which, with varying degrees of fractional crystallisation of individual units, will have individual patterns of chemical evolution (see also Cox 1967, Macdonald 1969, Thompson *et al.* 1972). Magmas derived from a simpler source – a large fractionating magma chamber– would produce the tightly constrained trends observed from the high Zr/Nb suite.

Figure 5.7.3 shows histograms of the incompatible element ratios Nb/Y, Zr/Y, Ce/Y, La/Y from the low and high Zr/Nb suites and La/Nb for various (basaltic) igneous rock groups from Thompson *et al.* (1984). There are obvious similarities in La/Nb between the low Zr/Nb suite and the ocean island basalts (OIB) and continental alkali basalts of Thompson *et al.* (1984); and between the high Zr/Nb suite and the continental flood basalts (CFB). These similarities are also evident from the incompatible element 'spidergrams' in Figures 5.5.1, 5.5.2 and 5.6.1 in which the low Zr/Nb suite show patterns similar to OIB (see Thompson *et al.* 1984, cf. Fitton and Dunlop 1985, Fitton and James 1986, Fitton 1987) and the high Zr/Nb suite resembles CFB (with negative Nb, Th anomalies, see Thompson *et al.* 1983). Figure 5.7.3 includes all analyses (except those from Østfjordsdal) in the histograms. When only basic rocks are considered there is no significant difference in the data.

Zr/Nb vs. Ce/Y: Partial Melting

Assuming a 'homogenous' source region for a magma, the Zr/Nb ratio of the melt would increase with increased partial melting, and the Ce/Y ratio would decrease (as Nb and Ce are the most incompatible elements of each ratio in mantle phases, see Pearce and Norry 1979, Henderson 1982). If however, the source region was mineralogically heterogeneous, perhaps at the transition zone between spinel and garnet stability regions, the content of garnet in a chemically homogenous source would also effect the Ce/Y ratio (with Y being compatible in garnet). Smedley (1985) modelled Zr/Nb vs.

Figure 5.7.3

Histograms of various ratios of incompatible elements for both high and low Zr/Nb suite (oversaturated and undersaturated). Also included are histograms for La/Nb from various igneous rock groups taken from Thompson *et al.* (1984). Note the similarity between La/Nb from the low Zr/Nb suite with ocean island basalts (OIB) and between the high Zr/Nb data and continental flood basalts (CFB). These histograms are produced using data from all samples. There is essentially no difference when data for basic rocks only are used. The data from Thompson *et al.* (1984) is for basaltic rocks only.

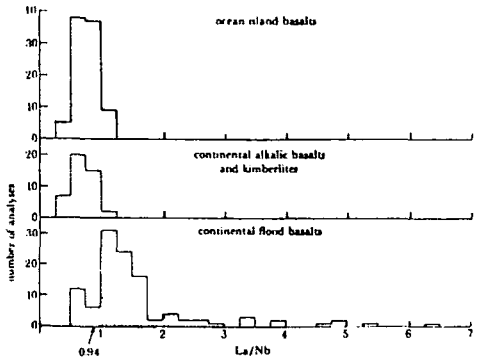

HISTOGRAM OF LA/NB - ALL LOW ZR/NB

RANGE 0.0 - 5.0 IN STEPS OF 0.20 CASES= 289

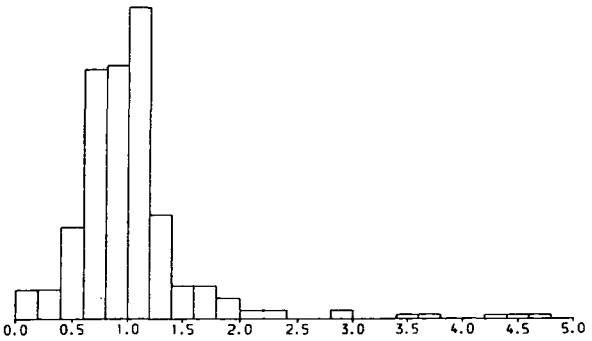

HISTOGRAM OF LA/NB - ALL HIGH ZR/NB

RANGE 0.0 - 5.0 IN STEPS OF 0.20 CASES= 136

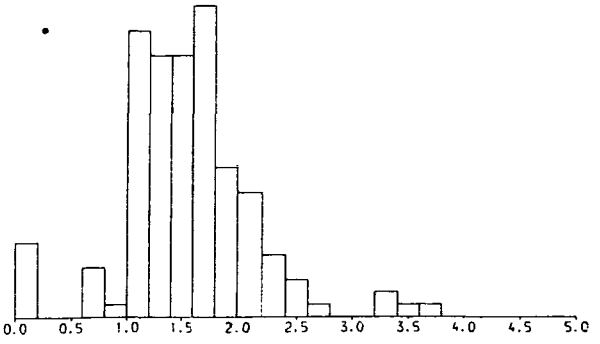

HISTOGRAM OF ZR/Y - ALL LOW ZR/NB

RANGE 0.0 - 20.0 IN STEPS OF 0.40 CASES= 305

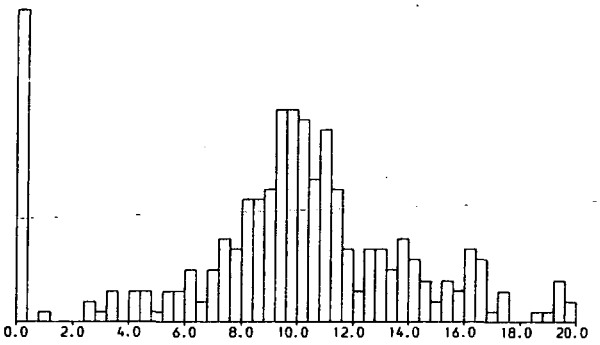

HISTOGRAM OF ZR/Y - ALL HIGH ZR/NB

RANGE 0.0 - 20.0 IN STEPS OF 0.40 CASES= 133

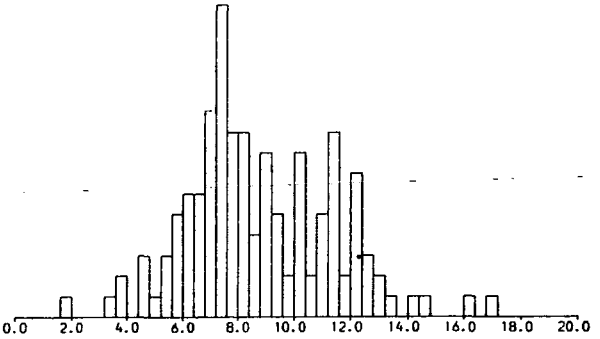

HISTOGRAM OF NB/Y - ALL LOW ZR/NB

RANGE 0.0 - 6.0 IN STEPS OF 0.20 CASES= 289

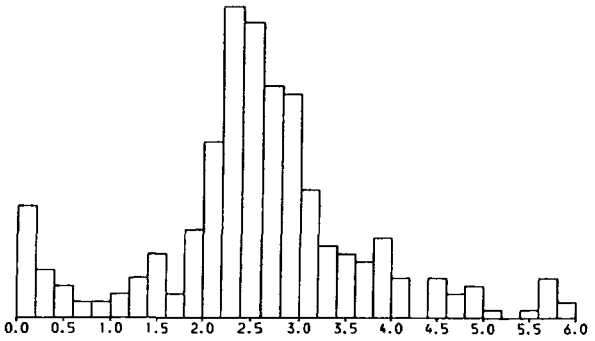

HISTOGRAM OF NB/Y - ALL HIGH ZR/NB

RANGE 0.0 - 6.0 IN STEPS OF 0.20 CASES= 139

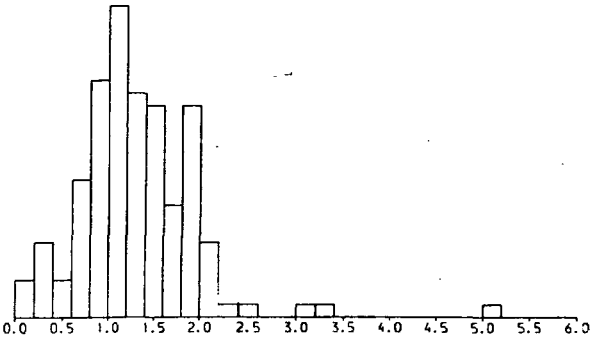

HISTOGRAM OF CE/Y - ALL LOW ZR/NB

RANGE 0.0 - 6.0 IN STEPS OF 0.20 CASES= 275

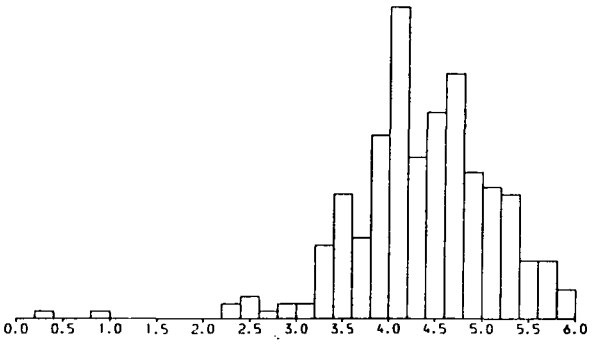

HISTOGRAM OF CE/Y - ALL HIGH ZR/NB

RANGE 0.0 - 6.0 IN STEPS OF 0.20 CASES= 136

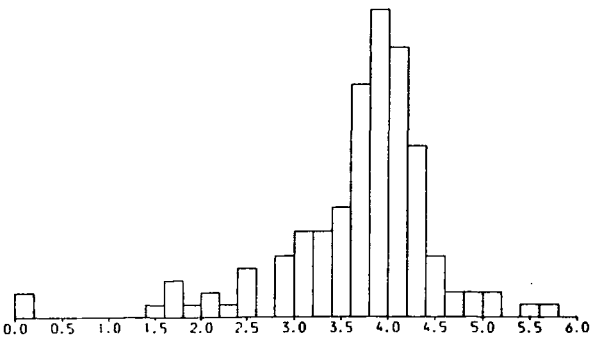

Ce/Y for Dinantian basalts from the Midland Valley of Scotland. A similar approach using slightly different parameters has been followed here.

Thus, taking the equilibrium batch melting curve;

$$C_l = C_o/(D_o + F(1-P_o))$$

where C_l = content of element in liquid

C_o = content of element in source

$D_o = D_iX_i + D_jX_j \ldots$

$P_o = P_iD_i + P_jD_j \ldots$

F = fraction of liquid

D_i is the distribution coefficient for mineral *i*.

X_i is the abundance of mineral *i* in the source.

P_i is the contribution to the melt made by mineral *i*.

Thus D_o is the bulk distribution coefficient 'weighted' for each element, and P_o is the weighted bulk distribution coefficient for the proportion of each mineral entering the melt. Taking a typical garnet lherzolite source of 58% olivine, 16% orthopyroxene, 17% clinopyroxene and 9% garnet (Frey *et al.* 1978) and assuming that garnet becomes more abundant with depth at the expense of clinopyroxene (Kay and Gast 1973) several hypothetical 'mantle' mineralogies can be calculated. A source composition of two-times chondrite has been assumed (Kay and Gast 1973) with chondrite compositions taken from Thompson *et al.* (1982). Smedley (1985) however chose a MORB source composition (see Fitton and Dunlop 1985). Distribution coefficients for the mantle phases considered are listed in Table 5.7.1.

Increased partial melting of a mineralogically and chemically homogeneous source causes a smooth variation in Ce/Y (decreasing) and Zr/Nb (increasing) and the results of the batch melting calculations are plotted on figure 5.7.4. It must be stressed that the melt fractions indicated, and also the amounts of garnet in the source are entirely model dependent, and thus no definite conclusions can safely be drawn from these. However, the model has been chosen to reflect a 'fertile' mantle source – comparable with an OIB source which has been inferred already as a source for these rocks.

It is immediately apparent that the low and high Zr/Nb suites of data plot in

Figure 5.7.4: Zr/Nb vs. Ce/Y.

Partial melting curves are shown for melt fractions indicated, using the equilibrium batch melting equation $C_l = C_o/(D_o+F(1-P_o))$, (see text for explanation). Partial melting curves have been calculated for 4 different, hypothetical garnet lherzolite sources, each with 58% olivine and 16% orthopyroxene plus 3%, 5%, 9% or 15% garnet and 24%, 21%, 17% or 11% clinopyroxene (Frey *et al.* 1978, Kay and Gast 1973). The source composition has been taken as twice-chondrite (Kay and Gast 1973, chondrite compositions from Thompson 1982).

Figure 5.7.4

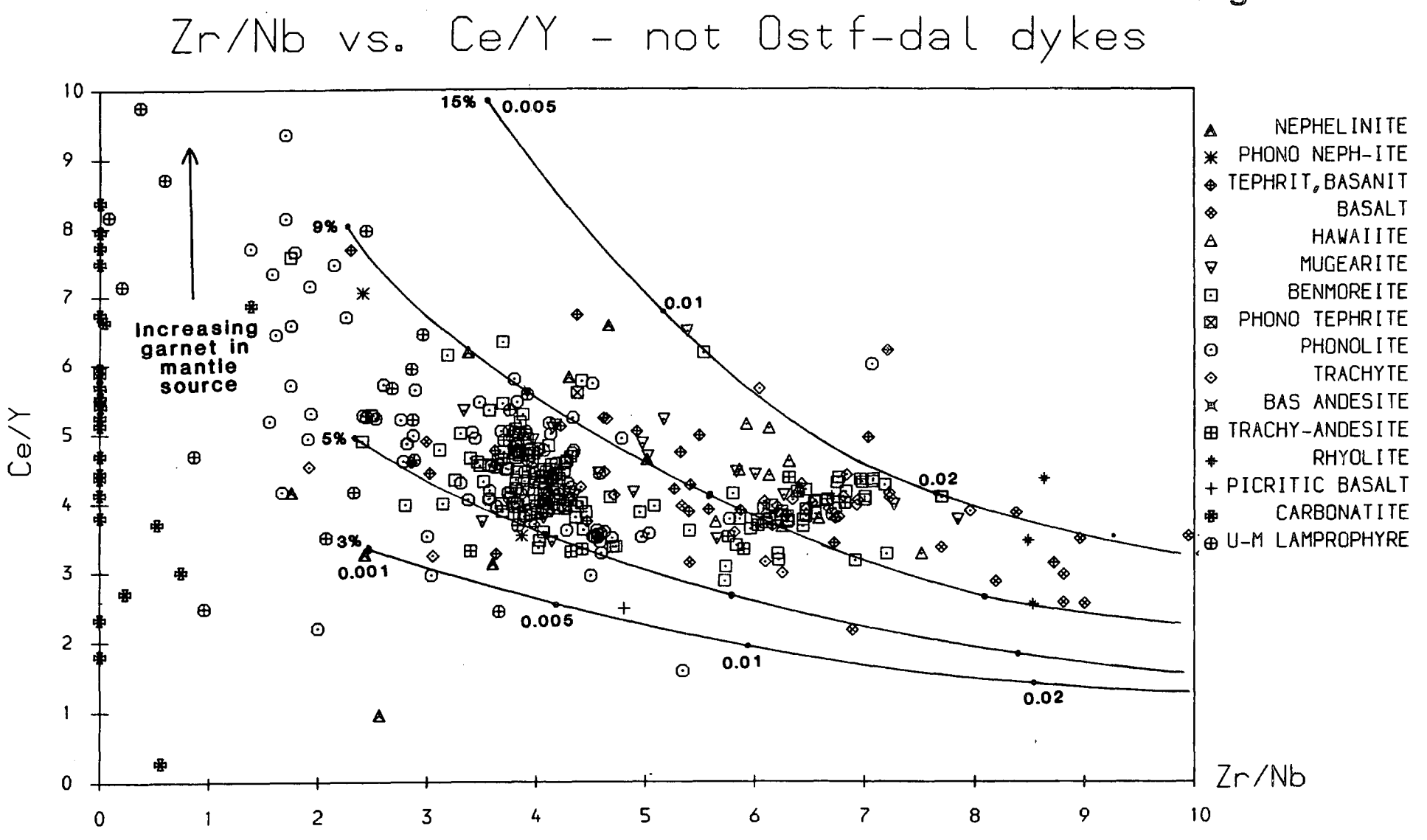
Zr/Nb vs. Ce/Y - not Ostf-dal dykes
Ce/Y
Zr/Nb
15%
0.005
9%
0.01
5%
0.02
3%
0.001
0.005
0.01
0.02
Increasing garnet in mantle source
NEPHELINITE
PHONO NEPH-ITE
TEPHRIT, BASANIT
BASALT
HAWAIITE
MUGEARITE
BENMOREITE
PHONO TEPHRITE
PHONOLITE
TRACHYTE
BAS ANDESITE
TRACHY-ANDESITE
RHYOLITE
PICRITIC BASALT
CARBONATITE
U-M LAMPROPHYRE

Table 5.7.1

Table of distribution coefficients for partial melting model.

	Ol	Opx	Cpx	Gt
Ce[1]	0.0008	0.0009	0.04	0.0033
Y[1]	0.002	0.009	0.2	1.4
Zr	0.001[2]	0.001[2]	0.12[3]	0.166[4]
Nb	0.001[2]	0.001[2]	0.01[3]	0.01[4]
P_i[5]	0.06	0.20	0.30	0.44

1. *Ce and Y data from Frey et al. (1978).* **2.** *Zr and Nb data an order of magnitude less than those given by Pearce and Norry 1979 (see also Smedley 1985).* **3.** *From McCallum and Charette (1978).* **4.** *Unpublished megacryst/basalt host data from the Biu Plateau, Nigeria of J.G. Fitton, data used in Smedley (1985).* **5.** *P_i–the contribution of each mineral to the melt – after M.J. Norry (pers. comm. 1986).*

two reasonably well defined clusters. Data from basic rocks (MgO>4%) is relatively scarce but, excluding the high Zr/Nb basalts (which have already been discussed with regard to ilmenite fractionation and partial melting effecting the Zr/Nb), there is no significant difference in the positions of the two clusters of data. If the Kay and Gast (1973) hypothesis is correct, and garnet/clinopyroxene does in fact increase with depth in the mantle, then the high Zr/Nb rocks were produced at greater depth than the low Zr/Nb rocks. They are also the products of higher degrees of partial melting. Assuming the model to be valid, the low Zr/Nb suite is perhaps the product of ca. 0.5% partial melting, and the high Zr/Nb suite (taking the cluster of basalts at Zr/Nb≈8.5) may be the result of 2-3% partial melting. These results are in reasonable agreement with amounts of partial melting to produce "alkali basalt" or similar by Kay and Gast (1973), Frey *et al.* (1978) and Fitton and Dunlop (1985) who all considered various aspects of source region–product trace element geochemistry in deriving their results. Melt fractions of less than those inferred by this model have been shown to be capable of separation from a mantle source in relatively short periods of time (McKenzie 1984, 1985) and thus are not unreasonably low.

Furthermore, higher degree partial melts may be expected to be more silica-saturated (see Thompson 1984, Figure 5.8.1) and this is consistent with the trend for the high Zr/Nb suite from basalt to rhyolite. The high Zr/Nb suite – forming the Giant Dykes

and many of the dykes in the Narssarssuaq region is related to relatively high amounts of crustal extension (up to 25% in Tugtutôq, see Chapter 2), whereas the low Zr/Nb dykes, local to the Igaliko area, represent perhaps as little as 3% crustal extension. Greater crustal extension may be expected to penetrate to greater crustal/mantle depths than lesser amounts of extension, and this may be borne out here with the high Zr/Nb, oversaturated suite from the more extensive rifting having been generated from greater depths than the low Zr/Nb suite (provided the Kay and Gast 1973 model holds true). This larger rifting event may also generate larger amounts of heat in the crust, and may induce some melting in the continental lithosphere. This could produce chemical characteristics in these magmas similar to continental flood basalts, rather than the ocean island basalt characteristics of magmas derived from the fertile mantle (?asthenosphere) such as the low Zr/Nb suite (cf. Thompson 1986).

5.8: Normative Mineralogy

CIPW norms have been calculated for all samples using the computer program NORMCAL written in PL1 by R.C.O. Gill at the University of Durham. Fe_2O_3/FeO ratios were assigned as described in Chapter 5.2.

Basic Rocks

The basic rocks are considered in terms of normative *Ne - Ol - Di - Hy - Q*. These can be related to magmas produced by partial melting of mantle phases in this compositional projection.

Recent experimental studies have shown that a melt extracted from a CO_2-rich lherzolite source is less silica saturated than an equivalent melt extracted from an H_2O-rich source (Eggler 1973; Eggler and Holloway 1977). Increased water content (provided $CO_2 < H_2O$) in a lherzolite source rock produces increased degrees of silica -(over) saturation in the melt (see Thompson 1984 for a brief summary of experimental work melting mantle rocks to generate basalts).

Anhydrous melting experiments are also summarised by Thompson (1984) and the compositions of melts from various mantle sources such as fertile lherzolite, MORB and the synthetic CMAS system are plotted on the exploded norm (normative *Ne - Ol - Di*

- *Hy* - *Q*) diagram which represents fairly simply basaltic rocks and emphasises their degree of silica saturation. Thompson (1984) considers this diagram only representative of rocks with >6.0% MgO. Figure 5.8.1 has been plotted for all samples with >3.0% MgO and thus the data from the hawaiites and mugearites are perhaps superfluous as these are likely to be the products of some fractional crystallisation and not melting.

In his summary, Thompson (1984) shows the effects of the addition of both H_2O and CO_2 on the composition of an initial melt produced from a 'fertile' lherzolite source at 20kb. These vectors and the anhydrous melt composition at various pressures of melting this source are shown on Figures 5.8.1A and B.

The low Zr/Nb data from Figure 5.8.1A can be seen to plot mostly on the *Ne* side of the primary, anhydrous melt compositions and this would be consistent with the addition of CO_2 to the source rock at these pressures. The picritic basalts, which plot in the *Ne* - *Ol* - *Hy* triangle are altered and thus not reliable in this context.

The high Zr/Nb rocks (Figure 5.8.1B) in contrast plot mostly on the *Hy* and Qz side of the primary, anhydrous melt compositions and this would be consistent with the presence of water in the source regions.

Additional weight is added to these suggestions by (i) the carbonatites which are solely associated with the Si-undersaturated suite of rocks (low Zr/Nb), with minor amounts of carbonate occurring in many of the nephelinites and ultramafic lamprophyres and (ii) hydration of the mantle which has been suggested to stabilise a Nb-bearing phase (Saunders *et al.* 1980, Saunders and Tarney 1984) and thus cause a negative Nb anomaly on chondrite normalised spidergrams. This behaviour is shown by the high Zr/Nb (oversaturated) suite of rocks.

Calcite is also a relatively common phase in both the North Qôroq and Motzfeldt centres (Chambers 1976, C. Bradshaw pers. comm. 1986) as too are CO_2 bearing phases such as cancrinite. There is also the possibility that, in the high Zr/Nb rocks, Rb and K have been held back in the mantle on melting by phlogopite or amphibole (see Chapter 5.5.C) hydrous phases possibly indicative of relatively high water contents.

Figure 5.8.1 (2 pages).

Normative *Ne* - *Ol* - *Di* - *Hy* - *Qz* plot for rocks with >3.0% MgO ('exploded norm' diagram). The curve marks the compositions of primary melts at varying pressures from a 'fertile' lherzolite source (from Thompson 1984). The vectors mark the effect of the presence of CO_2 and H_2O in the primary melt composition (at 20kb, also from Thompson 1984).

A. (Facing) Rocks with low Zr/Nb, ie. the undersaturated suite.

B. (Overleaf) Rocks with high Zr/Nb, ie. the oversaturated suite.

See text for interpretation.

Figure 5.8.1A

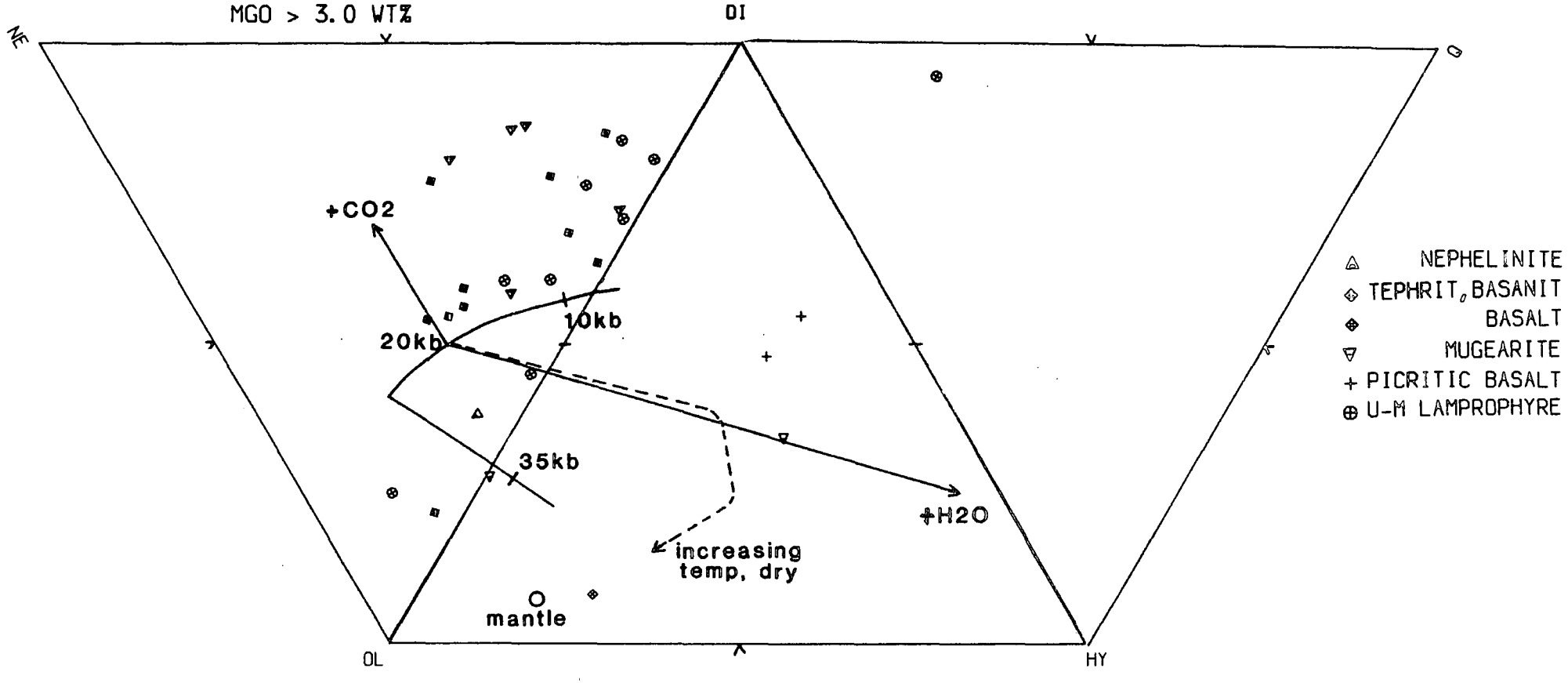
IGALIKO DYKE SWARM
'EXPLODED NORM'
LOW ZR/NB SUITE --
MGO > 3.0 WT%
DI
NE
Q
OL
HY
+CO2
20kb
10kb
35kb
+H2O
increasing
temp, dry
mantle
NEPHELINITE
TEPHRIT, BASANIT
BASALT
MUGEARITE
PICRITIC BASALT
U-M LAMPROPHYRE

Figure 5.8.1B

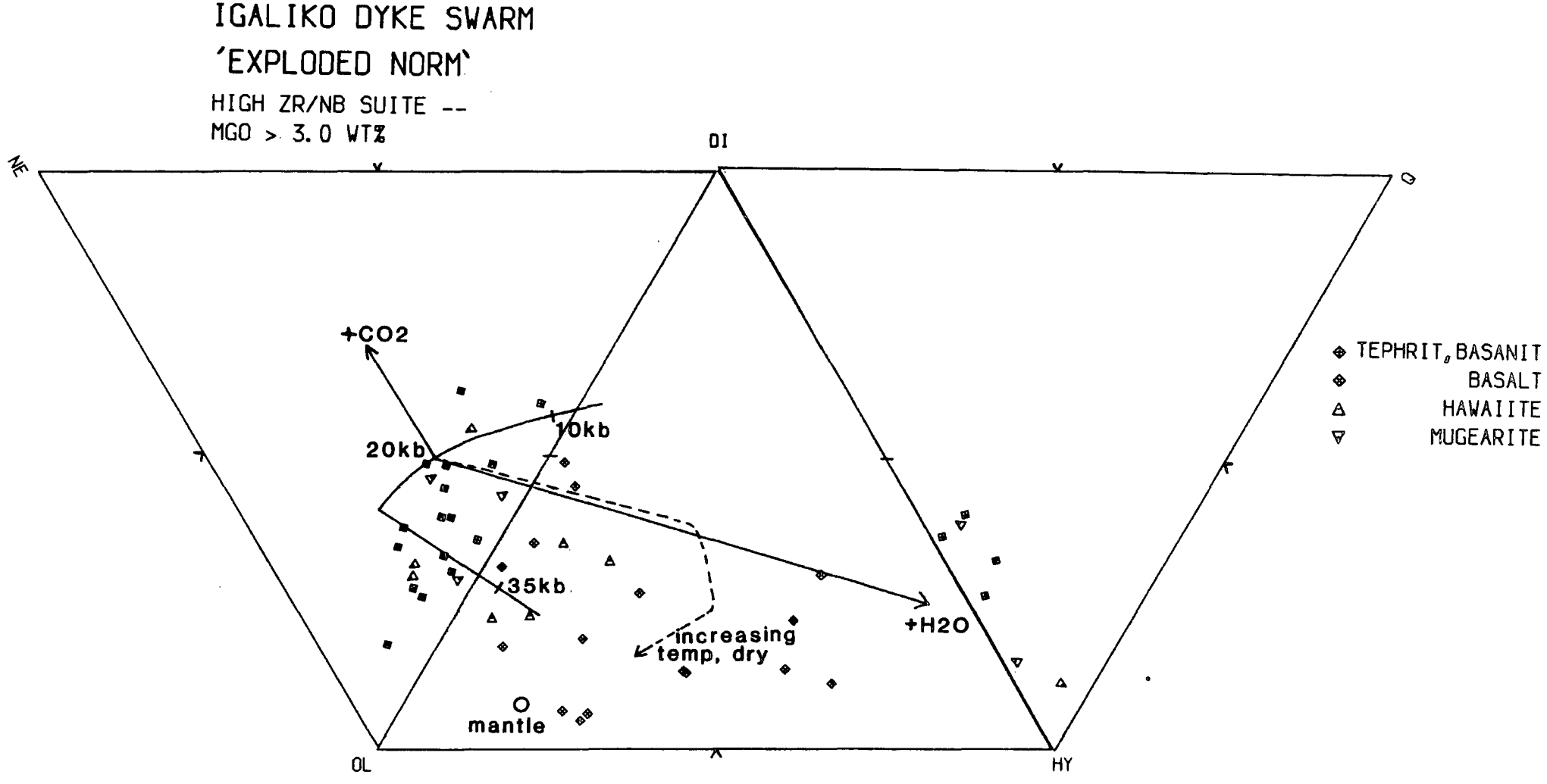
IGALIKO DYKE SWARM
'EXPLODED NORM'
HIGH ZR/NB SUITE --
MGO > 3.0 WT%
OI
NE
Q
OL
HY
+CO2
10kb
20kb
35kb
+H2O
increasing
temp, dry
mantle
TEPHRIT, BASANIT
BASALT
HAWAIITE
MUGEARITE

Evolved Rocks

The compositions of almost all evolved felsic rocks can be represented by the system Nepheline - Kalsilite - Quartz which cover both oversaturated and undersaturated compositions derived from more mafic magmas by crystal fractionation. Bowen (1937) aptly termed this condensed system 'Petrogeny's Residua System'.

Figure 5.8.2 shows rocks with a D.I.>70 (Thornton and Tuttle 1960) for the low and high Zr/Nb suites which are considered to be well represented by this system, although strongly peralkaline samples depart from this plane, being better represented by the 'Peralkaline Residua System', Na_2O - Al_2O_3 - Fe_2O_3 - SiO_2 (Bailey and Schairer 1964, 1966). However, for the moment the 'Residua System' will be assumed to represent the evolved dykes.

Figure 5.8.2A shows the low Zr/Nb samples and these all plot on the *Ne* - *Ks* (undersaturated) side of the feldspar thermal barrier (Hamilton and MacKenzie 1965) and evolve down the thermal valley towards the phonolitic minima composition. The phase relations are taken from Hamilton and MacKenzie (1965) for P_{H_2O} = 1kb. The presence of the thermal barrier along the alkali feldspar join persists from 1 atmosphere to at least 10kb (Morse 1969) and thus prevents the passage of granitic to nepheline syenitic liquids or *vice versa* by any process of equilibrium crystallisation or fractionation at crustal pressures (Gittins 1979).

Figure 5.8.2B shows the high Zr/Nb samples, and these (with the exception of 6 phonolites) show a clear trend of silica oversaturation with samples converging on the thermal valley and evolving towards the granite (rhyolite) minimum. These samples are effectively separated from the low Zr/Nb samples by the alkali feldspar thermal barrier.

There are only a few samples which are exceptions to this general rule caused by (i) the separation by Zr/Nb at 5.2 and the 'underlap' of the two gaussian Zr/Nb groups and (ii) uncertainties in the norm introduced by assignment of Fe_2O_3/FeO ratios, which in turn will effect the total *Q* or *Ne* in the norm. The carbonatites and ultramafic lamprophyres plotting near the *Ks* apex are spurious in as much as their compositions cannot be represented by a 'silicate' norm.

Figure 5.8.2 (2 Pages).

A. (Facing). Dykes of the low Zr/Nb suite with D.I.>70. Plotted in *Ne* - *Ks* - *Qz*, ie. Petrogeny's Residua System. Almost all dykes plot below the Ab - Or thermal divide and follow a trend towards the undersaturated minima at 1kb (Hamilton and MacKenzie 1965). Most samples cluster near the base of the thermal valley in this system.

B. (Overleaf). Dykes of the high Zr/Nb suite with D.I.>70 plotted in *Ne* - *Ks* - *Qz*. All but a few dykes plot above the Ab - Or thermal divide and follow a trend towards the oversaturated minima at 1kb (Hamilton and Mackenzie 1965). Most samples cluster near the base of the thermal valley, although dykes with compositions between trachyte/trachyandesite and rhyolite are scarce.

IGALIKO DYKE SWARM

Residua System.

Wt % Normative Comps

Zr/Nb < 5.2

Diffn. Index > 70

Figure 5.8.2A

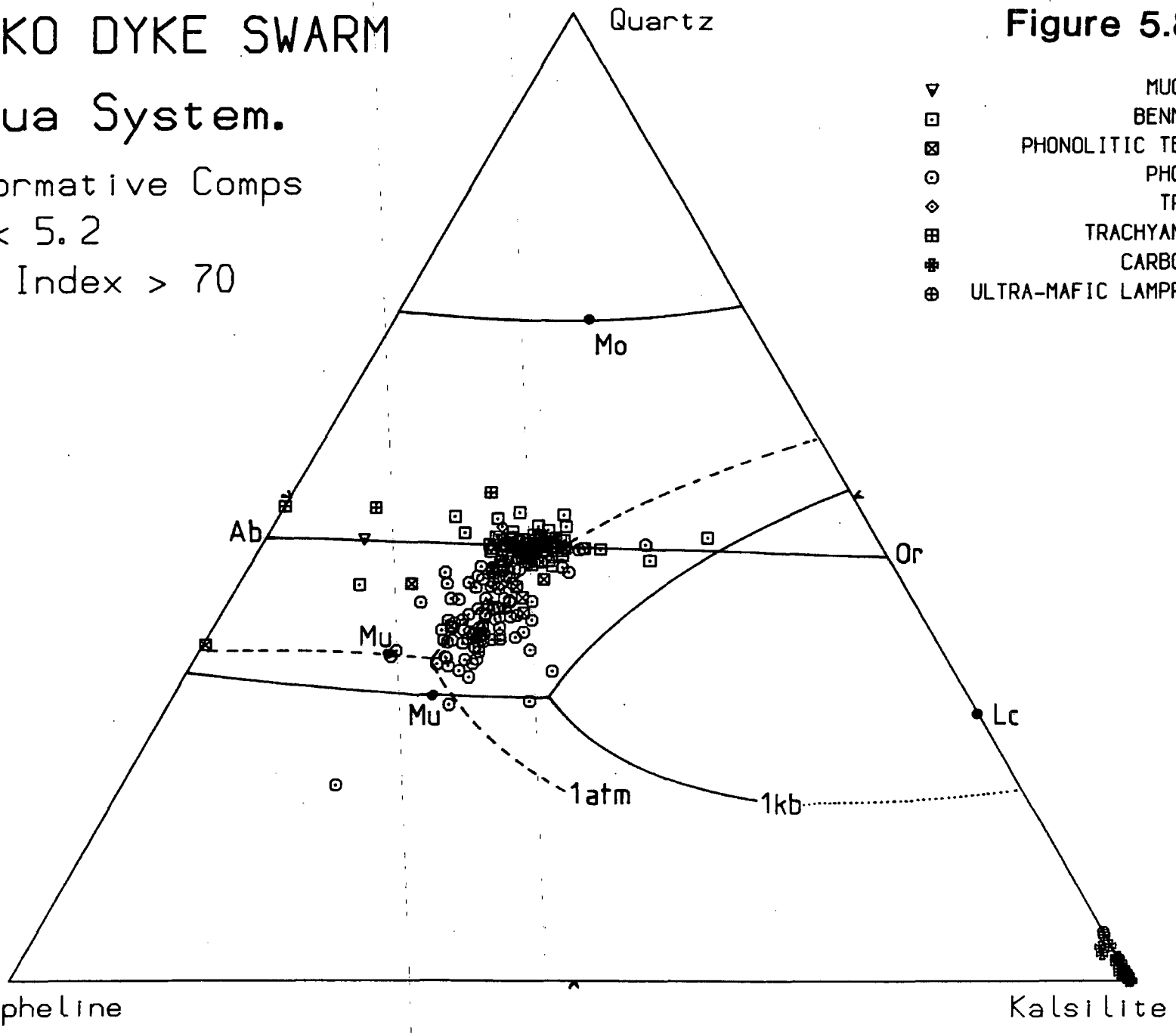

IGALIKO DYKE SWARM

Residua System.

Wt % Normative Comps

Zr/Nb > 5.2

Diffn. Index > 70

Figure 5.8.2B

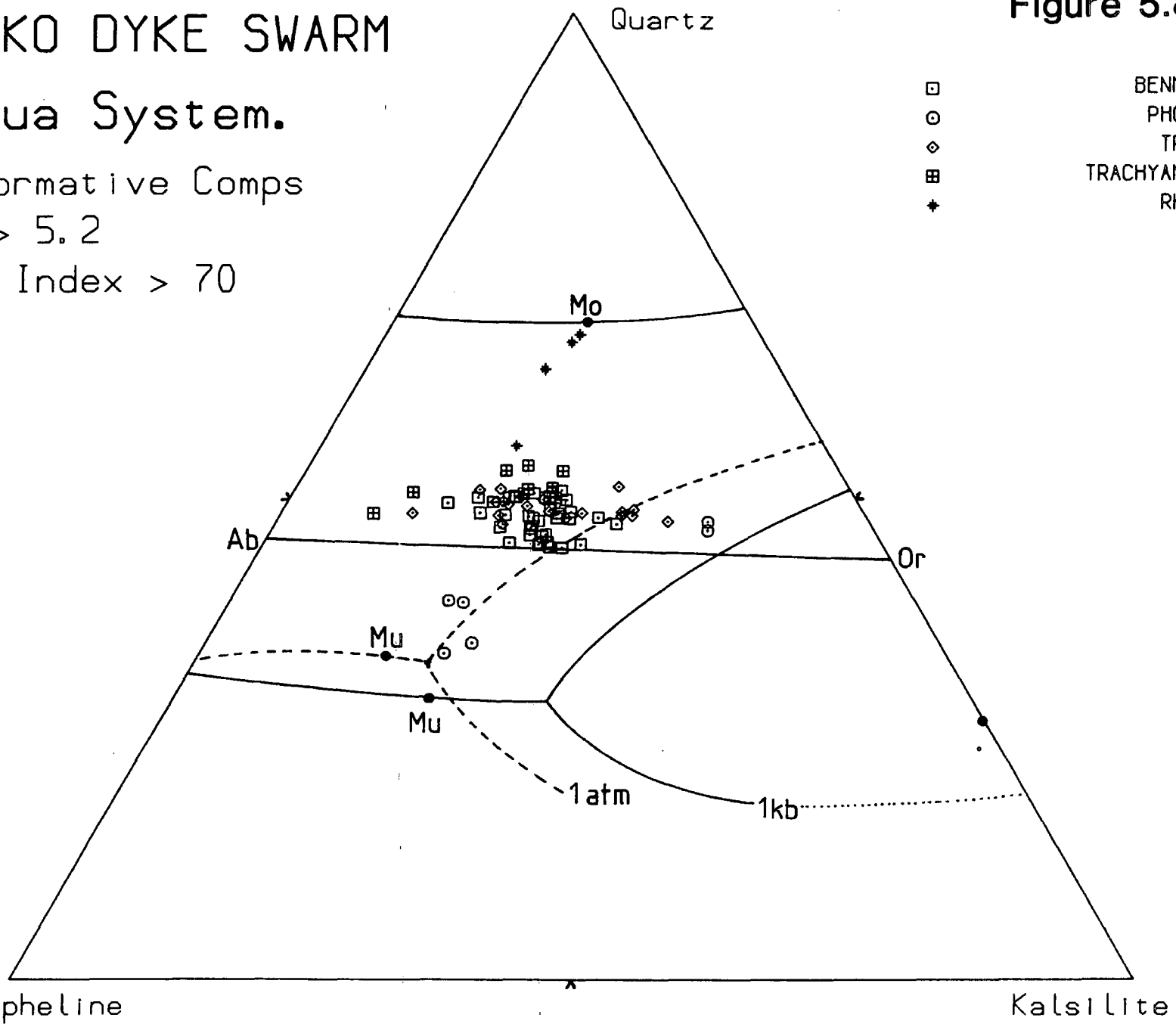

5.9: Peralkaline Residua System and AFM

Figure 5.9.1 shows the high and low Zr/Nb suites of rocks projected onto the planes Na_2O - Al_2O_3 - SiO_2 and NaO_2 - Al_2O_3 - Fe_2O_3 in the 'Peralkaline Residua System' (Na_2O - Al_2O_3 - Fe_2O_3 - SiO_2) at one atmosphere (Bailey and Schairer 1966). Following the procedure of Engell (1973) the Na_2O apex has been calculated as total alkalis equivalent to Na_2O (termed Na_2O^*). The plots show only peralkaline samples (ie moles Na+K>Al) with a D.I. (Thornton and Tuttle 1960) >70. Figure 5.9.1 also shows a simplified diagram of the system from Bailey and Schairer (1966), relevant to this part of the system.

Figure 5.9.1A shows the low Zr/Nb suites plotted in terms of Na_2O^* - Al_2O_3 - Fe_2O_3 and shows the field boundaries projected onto this plane by Engell (1973). The Si-oversaturated (high Zr/Nb suite) are not represented by this projection and are not plotted. Engell (1973) considered that addition of Ca to the system (to produce increased diopside in the pyroxenes) would enlarge the field of Acmite, moving the cotectic E-A towards Al_2O_3. Increased pressure would have a similar effect whereas decreasing fo_2 reduces the stability of acmite relative to albite and nepheline (and contracts the acmite field).

The low Zr/Nb data parallels the South Qôroq data (Stephenson 1973) at slightly higher alkali contents (see Figure 5.9.1A). The samples are clearly trending way from Fe_2O_3 and towards Ab and Ne. This is to be expected as these are end products of a solid solution series (Stephenson 1973). Liquids may only cross the Ab - Ne - Ac plane by precipitation of a peralkaline mineral (eg. sodalite). This is apparent from Ilímaussaq (Engel 1973) but not South Qôroq (Stephenson 1973), nor from the majority of the Igaliko dykes.

The majority of the dykes lie on a trend approximately parallel to the Ac - He cotectic (Figure 5.9.1A), at elevated Al_2O_3. The trend continues into the South Qôroq data near Ab, Ne and is closely parallel to the Ilímaussaq kakortokite and lujavrite data (Engel 1973). This parallelism at higher Al_2O_3, probably caused by the presence of Ca in the natural system enlarging the acmite field, and moving the reaction point E (the ijolite point, Bailey and Schairer 1966) across the Ab - Ne - Ac plane, to the top end

Figure 5.9.1

A. (Facing) Peralkaline rocks from both the low and high Zr/Nb suite projected projected onto the plane Na_2O^* – Al_2O_3 – Fe_2O_3 in the 'Peralkaline Residua System' of Bailey and Schairer (1966). Phase boundaries projected from SiO_2 apex by Engell (1973). Na_2O^* is Na_2O plus K_2O equivalent to Na_2O – the procedure adopted by Engell (1973).

The trends marked IL and SQ show the evolution of samples from Ilímaussaq(Engell 1973) and South Qôroq (Stephenson 1973) in this system.

E is the reaction point where albite, nepheline, acmite, hematite and liquid all coexist.

A is the eutectic point where albite, nepheline, acmite, sodium silicate (termed Ds) and liquid coexist.

B. – (Overleaf). Low and high Zr/Nb suites of rocks projected onto the plane Na_2O – Al_2O_3 – SiO_2. The oversaturated and undersaturated rocks cluster reasonably closely and may be separated by an alkali feldspar thermal barrier under these conditions (see above). The reaction point E may move to lie at the base of the undersaturated trend.

The flow diagram shows the part of the peralkaline residua system relevant to the above diagrams (from Gittins 1979, after Bailey and Schairer 1966). Invariant points in all diagrams are labelled to refer to this flow diagram. The figure heading below is from Gittins (1979) and relates to the flow diagram.

Simplified schematic flow diagram showing the univariant and invariant equilibria that involve liquids in the system Na_2O–Al_2O_3–Fe_2O_3–SiO_2. Ternary invariant points in the system Na_2O–Al_2O_3–SiO_2 are shown by triangles labeled *a*, *b*, and *c*; ternary invariant points in the system Na_2O–Fe_2O_3–SiO_2 are shown by triangles labeled *b'*, *c'*, and *d'*; quaternary invariant points are shown by octagons labeled *A*, *B*, *C*, *D* and *E*; ternary joins are shown as dashed lines labeled Ⓐ, Ⓑ, Ⓓ, and Ⓕ, that represent their projection onto the plane Na_2O–Al_2O_3–SiO_2 from the acmite composition that is a common apex of all the joins. Temperature maxima on the joins are shown as bars labeled with the appropriate temperature. Univariant lines, with three solid phases plus liquid, link the ternary invariant points of the bounding ternary systems and the quaternary invariant points. The direction of falling temperature along each line is indicated by arrows, and the solid phases crystallizing from the liquid are shown by abbreviations. In this type of schematic diagram the geometric arrangement is arbitrary, and so only the phase relations may be read. Abbreviations are: ab, albite; ac, acmite; cris, cristobalite; ds, sodium disilicate; hem, hematite; ne, nepheline; qu, quartz; trid, tridymite (after Bailey and Schairer, 1966).

Peralkaline Residua System

Figure 5.9.1A

Na2O=Na2O+equiv K2O

All peralkaline samples

Low Zr/Nb

Weight % oxide

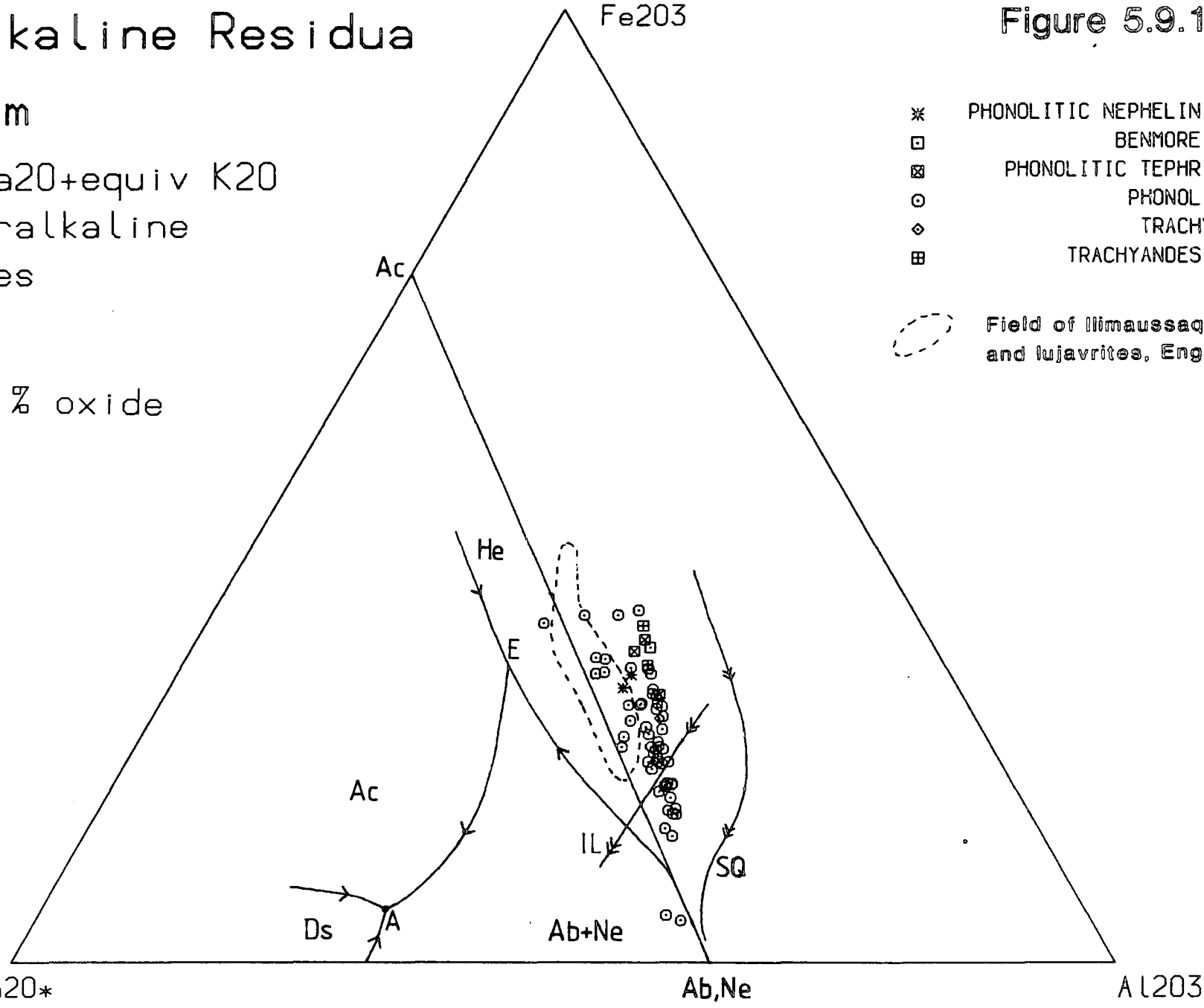

Figure 5.9.1B

Peralkaline Residua System

Weight % oxide
Na2O*=Na+K equiv Na

- NEPHELINITE
- PHONOLITIC NEPHELINITE
- BENMOREITE
- PHONOLITIC TEPHRITE
- PHONOLITE
- TRACHYTE
- TRACHYANDESITE

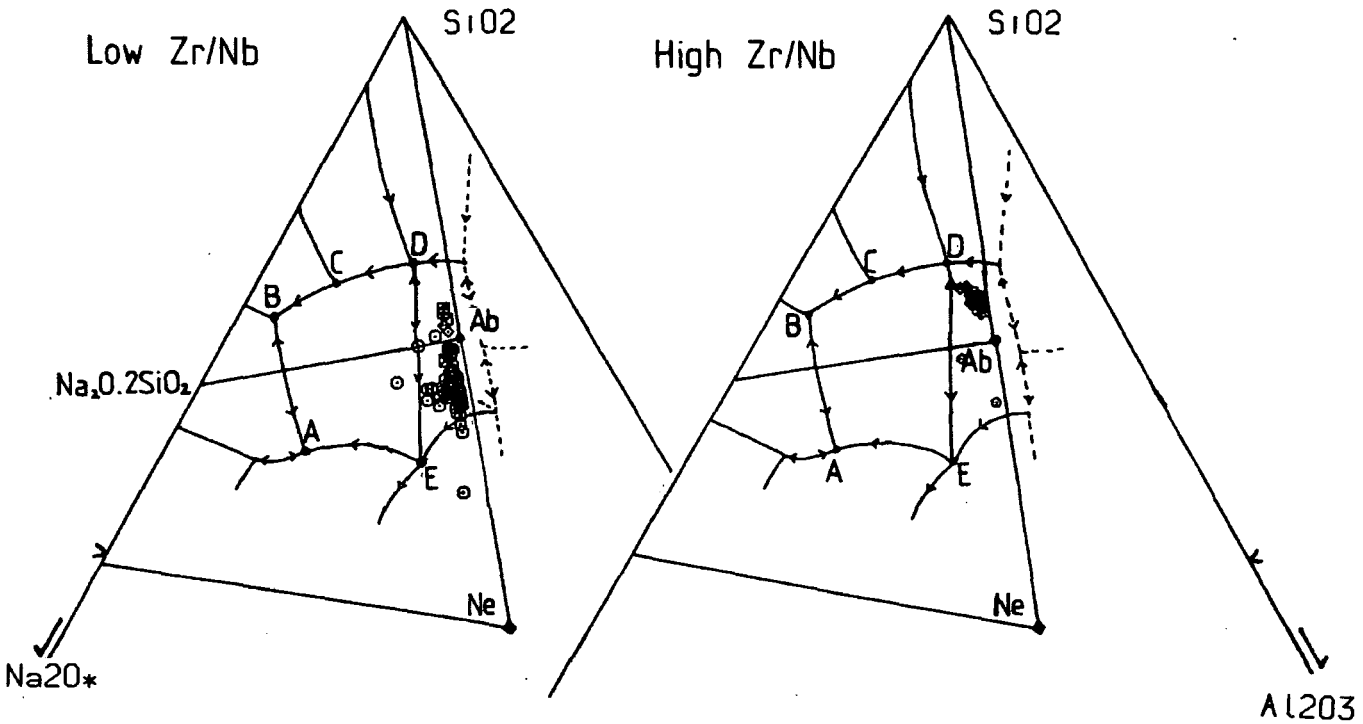

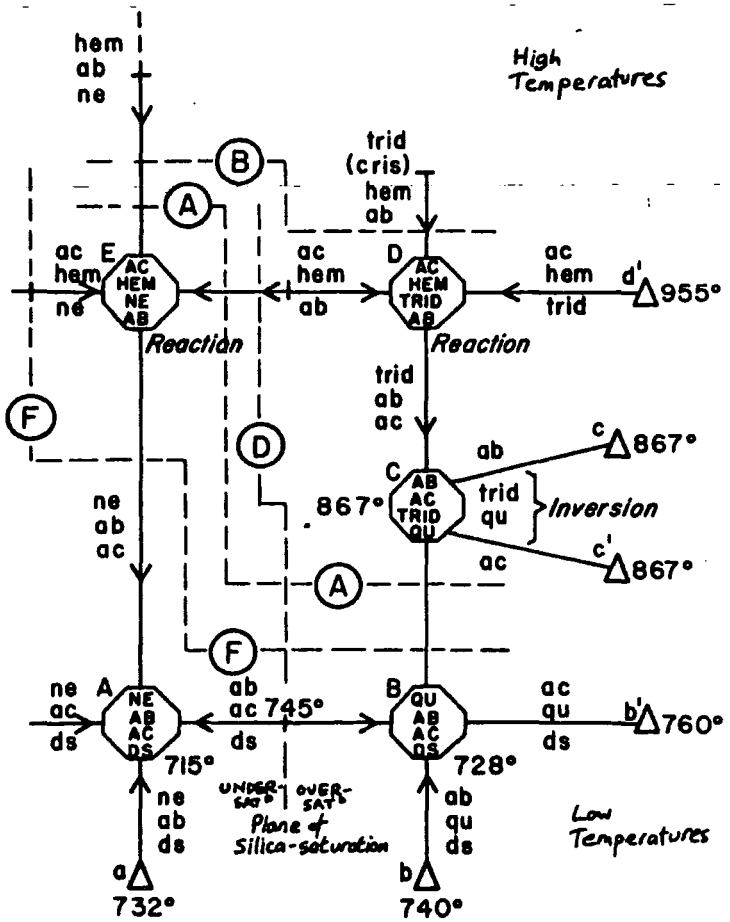

of the dyke trend. Some samples plotting to the left of the main dyke trend may be continuing from E along the cotectic E - A, by crystallising Ab, Ne and Ac. This agrees with observed mineralogies in some of the most 'evolved' alkali rich phonolitic rocks. Lower fo_2 in the natural system compared to the synthetic system (with fo_2=air) would lead to the presence of magnetite and/or olivine rather than hematite in the rocks.

Thus, the peralkaline, undersaturated liquids in this system appear to evolve via E (the ijolite reaction point) towards a minimum of albite, nepheline, acmite and sodium silicate (termed 'ds' by Bailey and Schairer 1966) by crystallisation of albite, nepheline and later acmite (aegirine). The oversaturated liquids are not represented by this projection, but are represented by $Na_2O^* - Al_2O_3 - SiO_2$, where they clearly separate from the undersaturated rocks, forming a cluster at higher SiO_2 (see Figure 5.9.1B).

As has been implied from the $Na_2O^* - Al_2O_3 - Fe_2O_3$ plot, the reaction point E becomes displaced under the conditions of crystallisation of the dykes, and would be displaced to the bottom of the trend for the low Zr/Nb undersaturated rocks in Figure 5.9.1B. This would imply, as the undersaturated rocks form a trend which continues across the Ab - $Na_2O.2SiO_2$ join into the oversaturated rocks, that reaction point D would be displaced towards the cluster of oversaturated rocks. The only 'rhyolites' found in the Igaliko region are not peralkaline and thus do not plot within this diagram. If E is moved towards the bottom of the trend of undersaturated rocks it is clear that some rocks move away (up and left) along a curved path towards A, confirming observations made from Figure 5.9.1A. If 'D' is moved to plot at the cluster of oversaturated (high Zr/Nb) rocks, there is a minor trend of trachytic rocks towards C. The rhyolitic rocks, if peralkaline, should plot somewhere along D - C - B. From the flow diagram (Figure 5.9.1B, from Gittins 1978) it would appear that these oversaturated rocks evolved by crystallisation of albite, acmite and quartz, consistent with observed petrographic details. The system Na_2O - Al_2O_3 - Fe_2O_3 - SiO_2 is greatly simplified compared to the natural system and it appears that even minor amounts of other elements (eg. Ca) in the system drastically affect its phase relations. For the undersaturated and oversaturated rocks to evolve by feldspar fractionation, the presence of other elements in the system may move the Ab – $Na_2O.2SiO_2$ join slightly to a point between the two suites, effectively providing a similar thermal barrier to that seen in

'Petrogeny's Residua System'.

AFM

Figure 5.9.2 shows AFM ($F=Fe_2O_3$) diagrams for the low and high Zr/Nb suites. These also include carbonatites and ultramafic lamprophyres (UML). Marked on these diagrams is the mean trend for rocks of the Gardar province taken from Watt (1966). Both swarms show fairly steady depletion in Mg and late stage enrichment in alkalis compared to Fe. Many of the UML lie on an extension to the trend of the low Zr/Nb suite towards more Mg-rich compositions. This also includes nephelinites and a tephrite. These very primitive (although incompatible element enriched) magmas may in some way be parental to the undersaturated magmas (cf. Rock 1987) although low pressure fractional crystallisation modelling could not derive basaltic rocks from these compositions. The carbonatites are typically alkali and magnesium poor.

The high Zr/Nb suite does not evolve to such high alkali contents and although superficially fairly similar to the low Zr/Nb suite, it shows a slightly 'flatter' evolutionary path. The higher numbers of basaltic rocks in this suite is clearly apparent, as too is the compositional gap at hawaiites and mugearites.

5.10: Mineralogical Differences

Having shown that there are two separate swarms of dykes in the area, are there any distinctive differences in the mineral phases found in both swarms? Clearly the phonolites are associated with the low Zr/Nb suite and the rhyolites with the high Zr/Nb suite and there are differences in their bulk mineralogy, but do their mineral trends evolve along different paths, particularly in the mafic minerals?

In the olivines (Chapter 4.3.3) we saw that a_{SiO_2} provided a control on the larnite (Ca) content of the olivine, with the highest Ca recorded from olivines in undersaturated rocks (see also Larsen 1976), these undersaturated rocks being the low Zr/Nb suite.

In the biotites higher fo_2 in the phonolites allowed more Mg rich micas to form than in the benmoreites. This however, does not really separate one suite from another as fo_2 will increase gradually with fractionation.

Figure 5.9.2: A–F–M

A–F–M diagram (Na_2O+K_2O – Fe_2O_3 – MgO) as cation proportions for both high and low Zr/Nb suites of rocks. Also shown on each is the mean Gardar trend for the province taken from Watt (1966). The relative differences in compositions between rock types from the two suites are clearly visible.

Figure 5.9.2

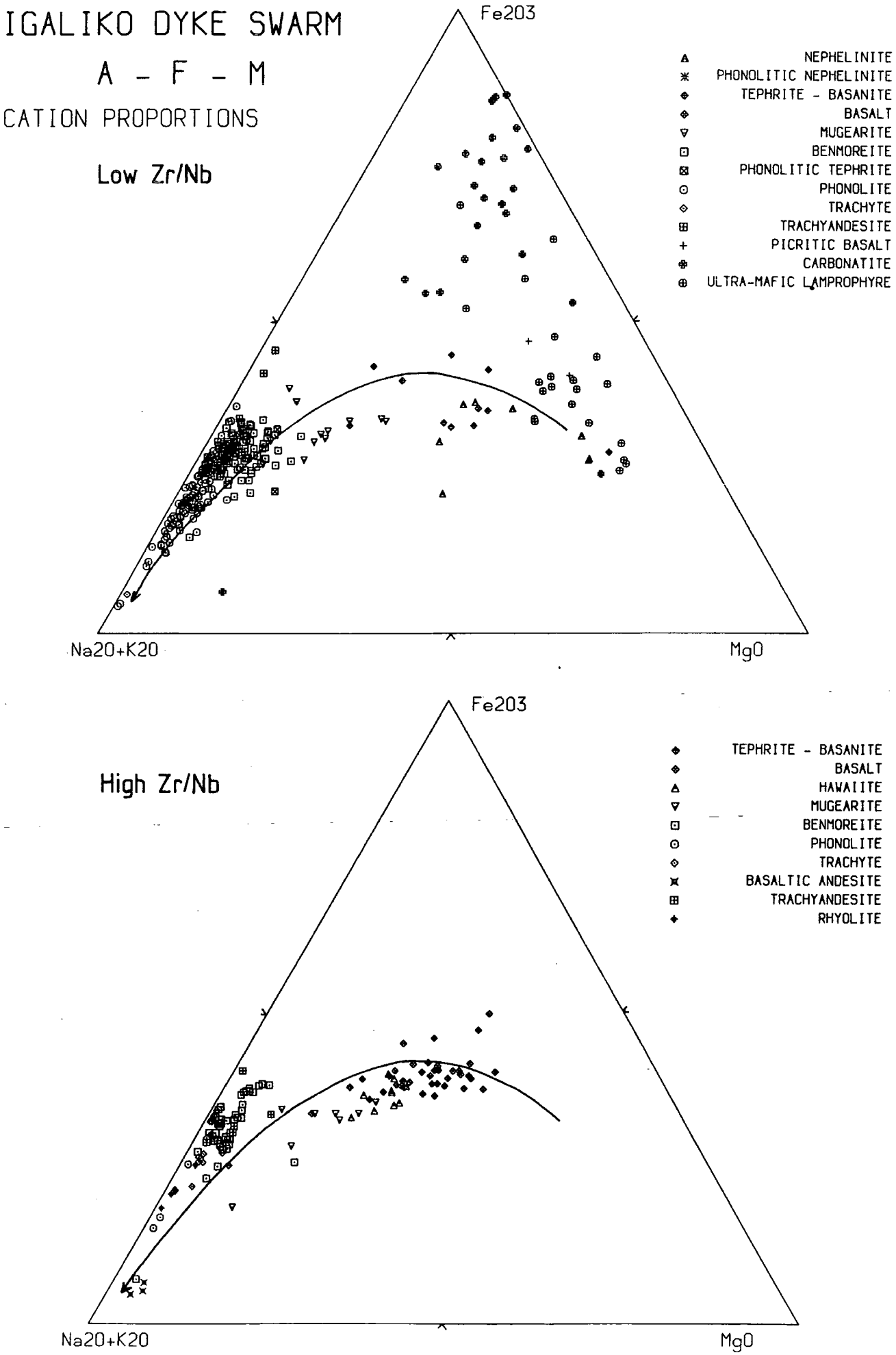
IGALIKO DYKE SWARM
A - F - M
CATION PROPORTIONS
Low Zr/Nb
Fe203
Na20+K20
MgO
NEPHELINITE
PHONOLITIC NEPHELINITE
TEPHRITE - BASANITE
BASALT
MUGEARITE
BENMOREITE
PHONOLITIC TEPHRITE
PHONOLITE
TRACHYTE
TRACHYANDESITE
PICRITIC BASALT
CARBONATITE
ULTRA-MAFIC LAMPROPHYRE
High Zr/Nb
Fe203
Na20+K20
MgO
TEPHRITE - BASANITE
BASALT
HAWAIITE
MUGEARITE
BENMOREITE
PHONOLITE
TRACHYTE
BASALTIC ANDESITE
TRACHYANDESITE
RHYOLITE

However, when the pyroxenes are considered, and plotted as Mg vs. (Na-Mg) atoms (with symbols to describe their Zr/Nb ratio, see Figure 5.10.1) there are clearly apparent differences in the evolutionary path of the low and high Zr/Nb suites. The bulk of the low Zr/Nb analyses do not exceed (Na-Mg)=0, zoning effectively ceasing at hedenbergite. Only the rhyolites contain acmite (Na-Mg>0.8) with only one high Zr/Nb analysis plotting between Na-Mg=-0.1 and Na-Mg=0.8. Similar results were obtained by Martin (1985) for pyroxenes from dykes elsewhere in the Tugtutôq-Ilímaussaq zone. The most likely control on this behaviour is fo_2, definitely higher in the phonolites than the benmoreites, but also more likely to be higher in the undersaturated benmoreites (low Zr/Nb) than in their oversaturated equivalents. Similar zoning from salite towards hedenbergite is reported by Stephenson and Upton (1982) for the Si-oversaturated Kûngnât complex.

There also appears to be a minor offshoot of a main trend in the amphiboles to Fe^{2+} + Mn enrichment (towards ferro-actinolite) and this may represent the oversaturated nature of its host (cf. Kûngnât,Stephenson and Upton 1982, and Nunarssuit Anderson 1974).

There thus appears to be a control on the mineralogical evolution by the bulk composition of the suite, ie. oversaturated and undersaturated, with the oversaturated suite apparently formed under conditions of lower fo_2 than the undersaturated suite.

Figure 5.10.1: Na-Mg vs. Mg (atoms per 6 oxygens) in pyroxenes.

Different symbols indicate different bulk rock chemistry. Pyroxenes from the low Zr/Nb suite clearly evolve differently from the high Zr/Nb suite, following a higher fo_2 trend through aegirine-augite to aegirine. The high Zr/Nb samples evolve to hedenbergite, with a few aegirine analyses.

Figure 5.10.1

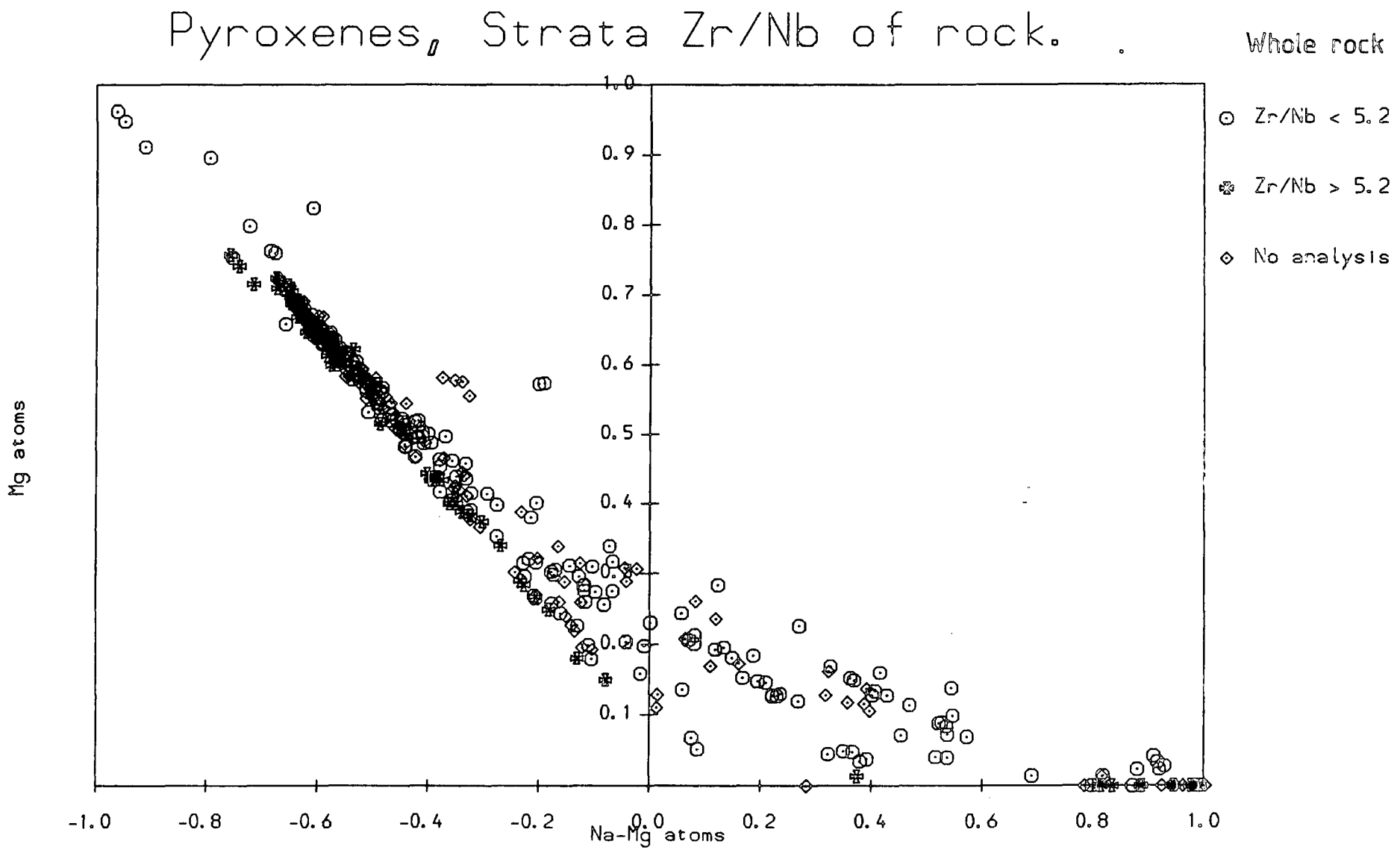
Pyroxenes, Strata Zr/Nb of rock.
Whole rock
Zr/Nb < 5.2
Zr/Nb > 5.2
No analysis
Mg atoms
Na-Mg atoms
1.0
0.9
0.8
0.7
0.6
0.5
0.4
0.3
0.2
0.1
-1.0
-0.8
-0.6
-0.4
-0.2
0.0
0.2
0.4
0.6
0.8
1.0

CHAPTER 6: RARE EARTH ELEMENT GEOCHEMISTRY

6.1: Introduction

A selection of samples from a wide range of dyke compositions was analysed for Rare Earth Elements (REE). Methods of analysis are described in Appendix V.

These analyses were undertaken with a view to;

(i) determining the concentration of the REE's in a selection of the dykes, particularly some of the more unusual compositions, (eg. carbonatites and lamprophyres).

(ii) in the trachytic/benmoreitic dykes, to determine any differences in REE concentrations and variation between the low and high Zr/Nb suites and the Østfjordsdal swarm, and thus any bearing this may have on the genesis and evolution of these groups.

(iii) determining the relative changes in Light REE (LREE) to Heavy REE (HREE) with fractionation of the dykes.

(iv) to define the role of feldspar fractionation within the evolving dyke swarms,

(v) and to see what constraints these data would place on fractional crystallisation/partial melting hypotheses for generation of these rocks.

In the following discussion the REE data are presented mostly as chondrite normalised 'spidergrams'. Chondrite concentrations have been taken from a recent compilation by Boynton (1984) and these are listed in Table 6.1.1 along with other commonly used chondrite REE estimates.

The slope of the chondrite normalised REE spidergrams gives an indication of the amount of LREE enrichment, and is measured in terms of $(La/Lu)_{cn}$ (cn=chondrite normalised). Figure 6.1.1 shows all REE data plotted in terms of $(La/Lu)_{cn}$ against Ce (ppm), and shows that the slope of the REE pattern increases fairly steadily with absolute REE enrichment (measured by Ce). Almost all data have $(La/Lu)_{cn} >> 1$, typical of alkali basalts and their derivatives (Cullers and Graf 1984), with maximum degrees of LREE enrichment (compared to HREE) being seen in the phonolites and

Figure 6.1.1: Ce ppm vs. $(La/Lu)_{cn}$.

As total REE content increases, measured by Ce a fairly steady rise in the chondrite normalised REE slope is seen (measured by $(La/Lu)_{cn}$). Some of these samples show exceptionally high total REE as well as very steep REE slopes (cf. Cullers and Graf 1984).

Figure 6.1.1

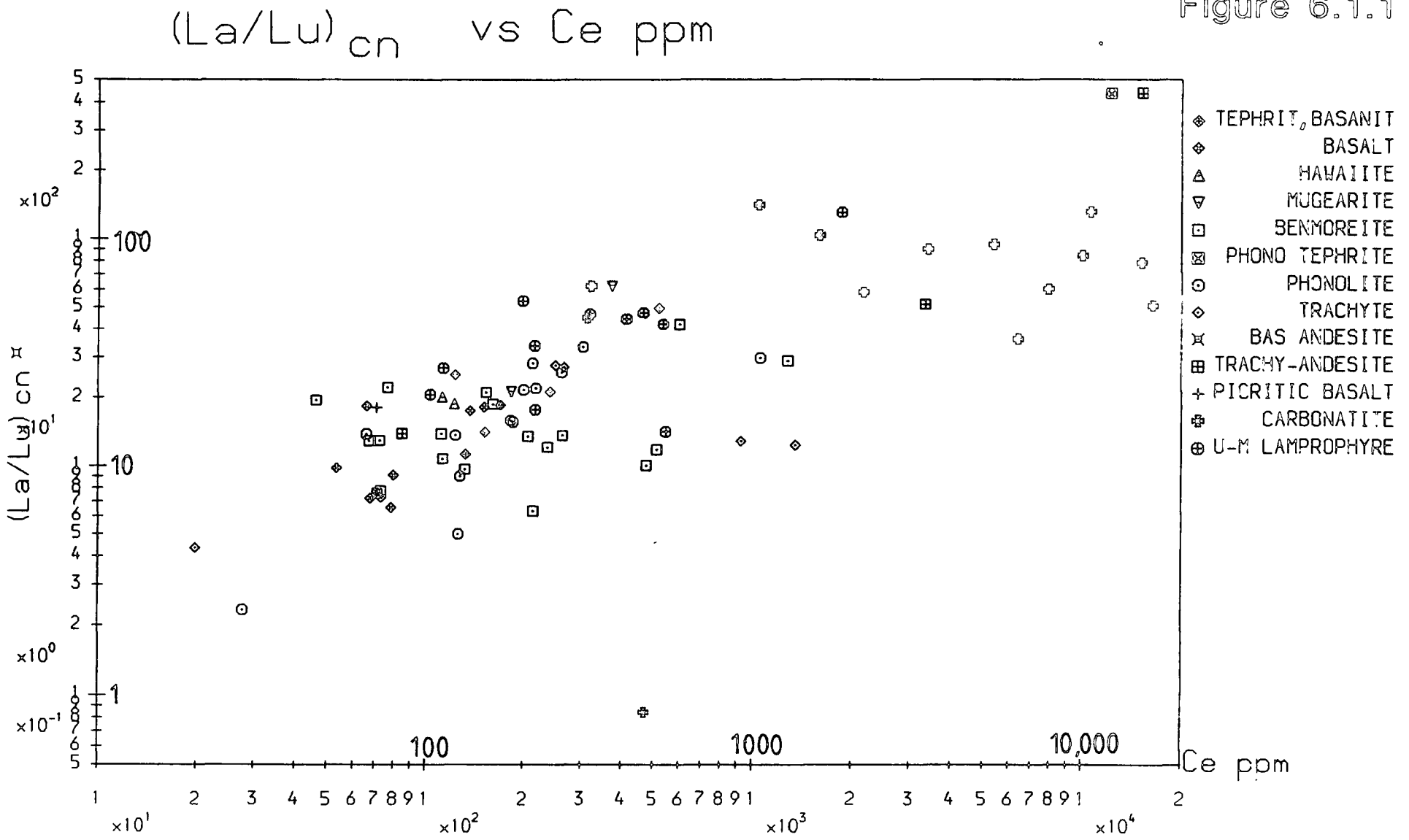
(La/Lu)cn vs Ce ppm
(La/Lu) cn
Ce ppm
100
1000
10,000
TEPHRITE, BASANITE
BASALT
HAWAIITE
MUGEARITE
BENMOREITE
PHONO TEPHRITE
PHONOLITE
TRACHYTE
BAS ANDESITE
TRACHY-ANDESITE
PICRITIC BASALT
CARBONATITE
U-M LAMPROPHYRE

Table 6.1.1

REE concentrations (ppm) in chondrites commonly used for normalisation.

	Haskin *et al.* (1968)	Nakamura (1974)	Boynton (1984)
La	0.33	0.329	0.310
Ce	0.88	0.865	0.808
Pr	0.112		0.122
Nd	0.60	0.630	0.600
Sm	0.181	0.203	0.195
Eu	0.069	0.0770	0.0735
Gd	0.249	0.276	0.259
Tb	0.047		0.0474
Dy		0.343	0.322
Ho	0.070		0.0718
Er	0.200	0.225	0.210
Tm	0.030		0.0324
Yb	0.020	0.220	0.209
Lu	0.034	0.0339	0.0322

carbonatites.

If the REE data are plotted as $\log_{10}(La/Sm)_{cn}$ vs. $\log_{10}$ $(Gd/Lu)_{cn}$, as in Figure 6.1.2, (ie. the degree of LREE/MREE enrichment against the MREE/HREE enrichment) many aspects of the REE spidergrams from a large data set can be represented clearly on one diagram. Taking logs of the REE_{cn} ratios means that ratios <1.0 plot as negative values. Steeper gradients plot further from the origin (see Figure 6.1.2 for illustration). Typical N-type MORB (Saunders 1984), for example, would plot at about ($\leq$ 0,-0.5) ie. on the left side of the lower right quadrant. MREE enriched and MREE depleted samples would plot in the lower right and upper left quadrants respectively.

From Figure 6.1.2 it is clear that almost all samples are LREE enriched, a feature typical of small partial melts from a 'fertile' garnet-bearing mantle source (Cullers and Graf 1984). As fractionation proceeds the degree of LREE enrichment can be seen to increase relatively steadily, measured by increasing $(La/Lu)_{cn}$.

Figure 6.1.2: $(Gd/Lu)_{cn}$ vs. $(La/Sm)_{cn}$ (log_{10}-log_{10} axes)

Presentation of REE data in this way can give a good indication of the chondrite normalised REE patterns of a large number of samples in 1 diagram. The sketch to the right of the plotted data indicates the REE spidergrams that are represented by various portions of the graph. The further from the origin ((0,0) on a log-log scale, (1,1) in numerical terms) that a point plots, the steeper will be its slope. The actual slope will be the product of its coordinates (in numerical terms) or the anti-log of the sum of its coordinates if they are given as logs. Thus, a phonolite plotting at (-0.2.0.3) (log-log) will have an overall slope of only 1.26, and has $MREE_{cn}$ <$HREE_{cn}$ (ie. a positive slope from Gd – Lu). However, the phonolitic tephrite, plotting at (1.2,1.1) (log-log) will have an overall slope of ≈200 with the slope for $(La/Sm)_{cn}$ and $(Gd/Lu)_{cn}$ being approximately equal. Only one sample from the dykes – a carbonatite, has a $(La/Lu)_{cn}$ <1. All other samples show overall LREE enrichment ($(La/Lu)_{cn}$ >1) with only 3 having $(Gd/Lu)_{cn}$ <1.

Figure 6.1.2

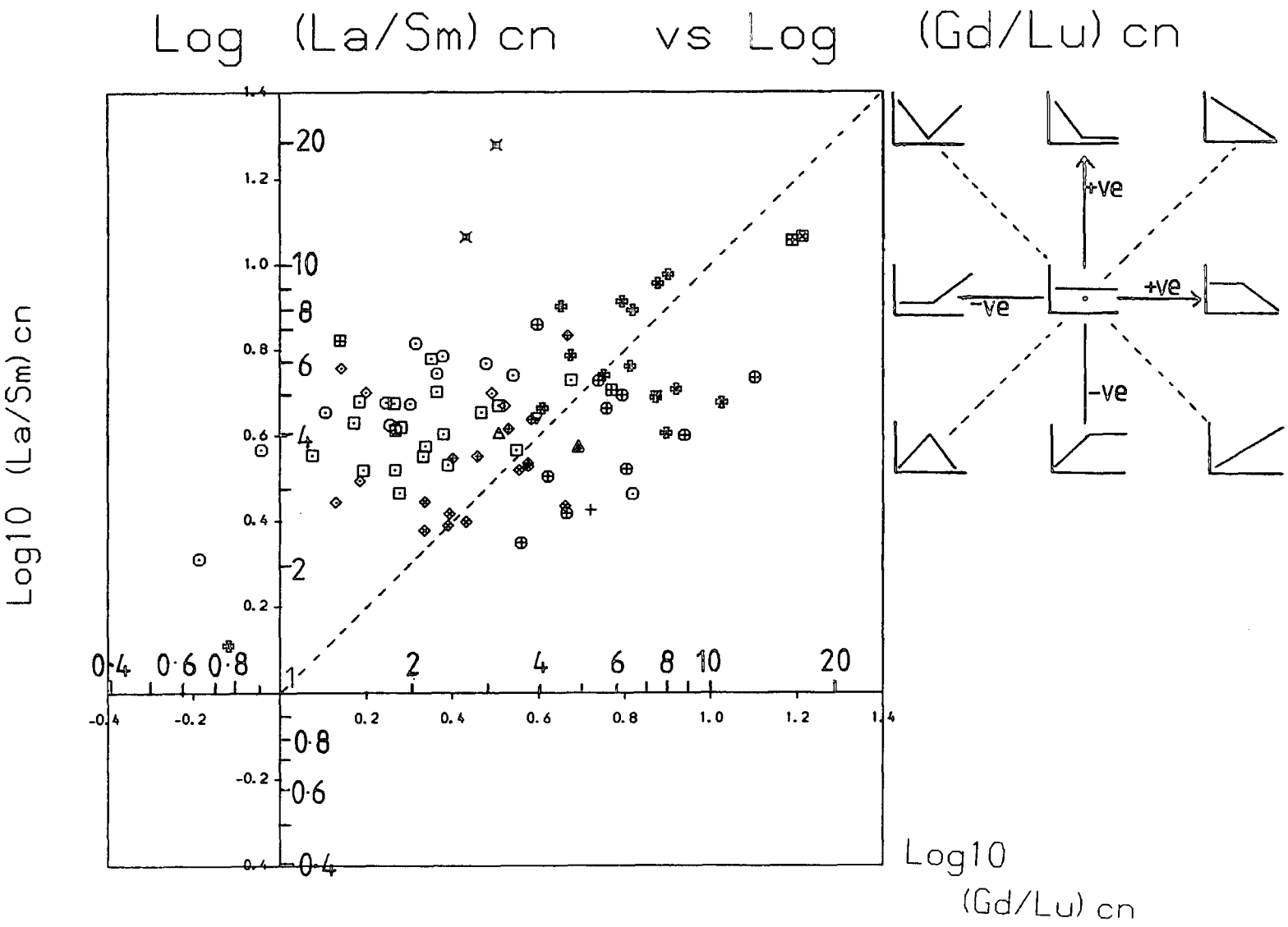
Log (La/Sm) cn vs Log (Gd/Lu) cn
Log10 (La/Sm) cn
Log10 (Gd/Lu) cn
+ve
-ve
+ve
-ve
NEPHELINITE
TEPHRIT, BASANIT
BASALT
HAWAIITE
MUGEARITE
BENMOREITE
PHONO TEPHRITE
PHONOLITE
TRACHYTE
BAS ANDESITE
TRACHY-ANDESITE
PICRITIC BASALT
CARBONATITE
U-M LAMPROPHYRE

However, (ignoring the carbonatite and lamprophyre data), as fractionation increases it becomes apparent that the MREE/HREE ratio gradually decreases ($(Gd/Lu)_{cn}$ is lower in phonolites, benmoreites and trachytes than in basalts and tephrites). This drop in $(Gd/Lu)_{cn}$ reflects a levelling off of the M-HREE portion of the spidergram and will be a result of fractionation of clinopyroxene and apatite (and probably also amphibole). MREE partition into pyroxene preferentially over HREE (D_{Gd}^{cpx}=3.1, D_{Lu}^{cpx}=2.3) the same being true for amphibole (D_{Gd}^{amph}=9, D_{Lu}^{amph}=4.5, Henderson 1982, dacite and rhyolite partition coefficients). This will have the effect of reducing the MREE/HREE ratio, and so flattening the M-HREE portion of the spidergram (see later). Apatite fractionation would have a similar effect (D_{Dy}=42, D_{Lu}=17, Henderson 1982)

In the following discussion, an anomaly represents a surplus or a deficiency of an element relative to its neighbours, typically Eu relative to Sm and Gd. The size of the Eu anomaly is measured by Eu/Eu* which equals measured Eu divided by Eu calculated from a chondrite normalised plot by interpolation between Sm and Gd (ie. Eu*).

6.2: Basaltic Rocks and 'Mantle Metasomatism'

Figure 6.2.1 shows REE spidergrams for two narrow dolerite dykes from north of Narssarssuaq and chill and core analyses of the possible BD_0 from Mellemlandet.

BD_0

The possible BD_0 shows marked LREE enrichment, with $(La/Lu)_{cn}$ of 6.58-7.77 Both analyses show very slight negative Eu anomalies (Eu/Eu* 0.88-0.95), indicative of minor plagioclase fractionation. The degree of LREE enrichment is typical of alkali basalts (see Cullers and Graf 1984). This is consistent with their formation by small degree partial melts of a fertile garnet-bearing mantle (Kay and Gast 1973) although, as will be shown later, a spinel bearing source is preferred.

Dolerites from Narssarssuaq

These chemically very similar rocks, although greatly varying in Zr/Nb, both have $(La/Lu)_{cn}$ ratios typical of alkali basalts (7.23-9.13). 325990 shows a slight positive Eu anomaly (Eu/Eu*=1.08) and this correlates with the presence of occasional plagioclase phenocrysts. The higher degrees of LREE/HREE enrichment compared to the possible

Figure 6.2.1

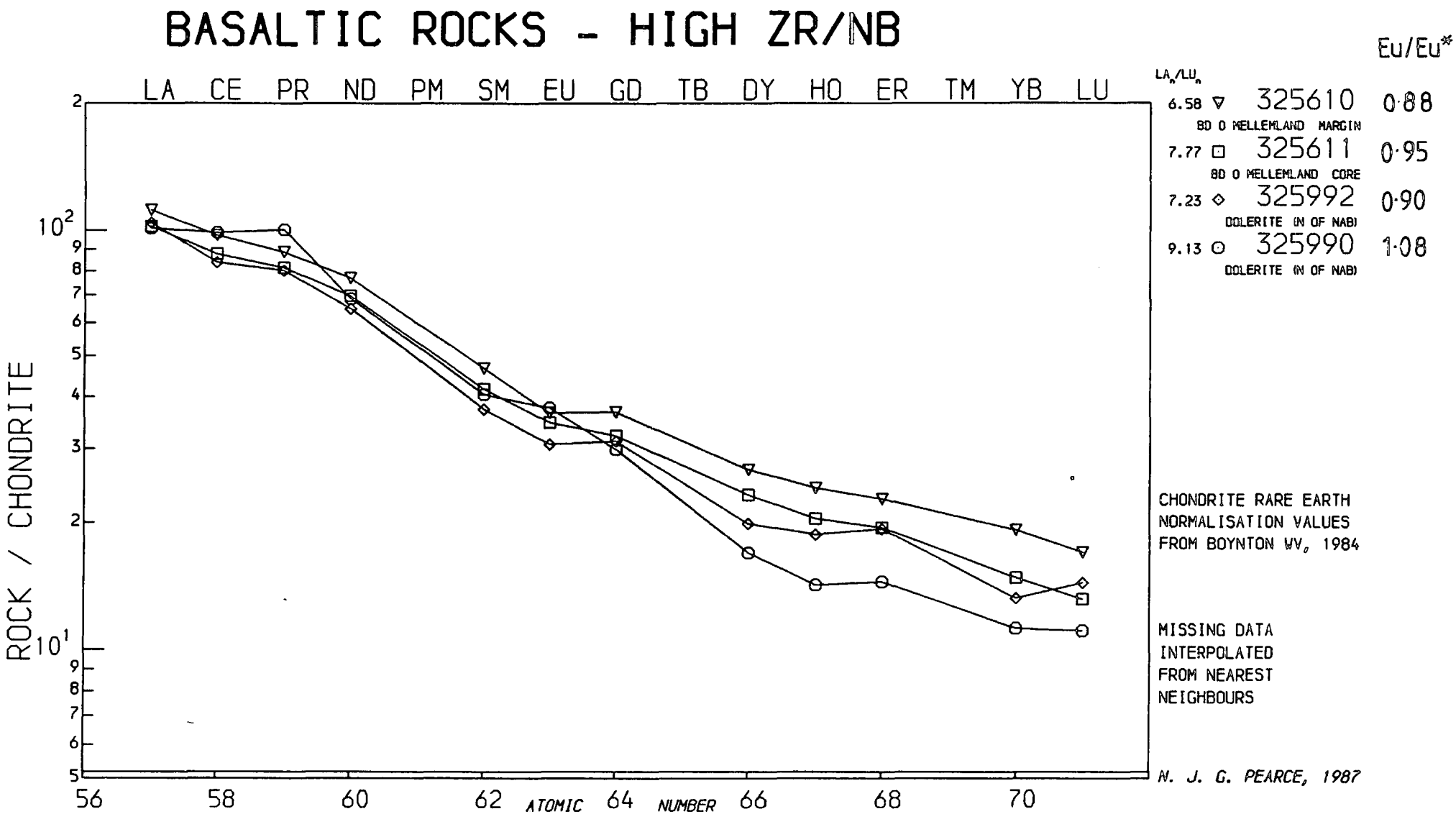
BASALTIC ROCKS - HIGH ZR/NB
LA CE PR ND PM SM EU GD TB DY HO ER TM YB LU
ROCK / CHONDRITE
ATOMIC NUMBER
Eu/Eu*
LA_n/LU_n
6.58 325610 0·88
BD 0 MELLEMLAND MARGIN
7.77 325611 0·95
BD 0 MELLEMLAND CORE
7.23 325992 0·90
DOLERITE (N OF NABI)
9.13 325990 1·08
DOLERITE (N OF NABI)
CHONDRITE RARE EARTH NORMALISATION VALUES FROM BOYNTON WV, 1984
MISSING DATA INTERPOLATED FROM NEAREST NEIGHBOURS
N. J. G. PEARCE, 1987

Table 6.2.1

Distribution coefficients and other parameters used in melting/fractional crystallisation modelling.

		Ol	Opx	Cpx	Gt	Sp	Pl
D_{La}		0.01	0.02	0.08	0.05	0.00003[z]	0.14
D_{Lu}	melting	0.02	0.11	0.8	5.7[2]	0.001[z]	
D_{Lu}	xtal^n	0.02	na	0.8	35	0.02	0.08
D_{Ni}		14	na	2.6	0.8[2]		0
D_{Cr}		2.1	na	8	na	na	0
D_{Rb}		0.01[2]	0.02[2]	0.05	0.02	0.02?	0.1
P[3]	melting(i)	0.06	0.20	0.30	0.44		
P[3]	melting(ii)	0.2	0.2	0.4		0.2	
X[4]	melting(i)	0.58	0.16	0.11,0.17,0.21	0.15,0.09,0.05		
X[4]	melting(ii)	0.58	0.16	0.17		0.09	

1 – calculated from $D^{sp/cpx}$ data from Stosch (1982) and $D^{cpx/liq}$ data from Henderson (1982). 2 – calculated from Frey et al. (1978). 3 – P proportion of mineral phase contributing to melt. 4 – X mineralogical composition of assumed mantle source (see Chapter 5.8). na – Not applicable. All other distribution coefficients from Henderson (1982, 1984).

BD_0 would imply slightly smaller degrees of partial melting of a similar source.

Melting Models

Model calculations involving mantle sources and melting proportions as used in Chapter 5.8 (for Zr/Nb and Ce/Y) were carried out to estimate the amount of partial melting required to yield the observed REE patterns. A 2× chondrite mantle source was assumed (Frey *et al.* 1978) and distribution coefficients for La and Lu in olivine, orthopyroxene, clinopyroxene and garnet were taken from Henderson (1982, 1984), except D_{Lu}^{garnet} which is from Frey *et al.* (1978). These are listed in Table 6.2.1.

The partition coefficients for a spinel/liquid were calculated from spinel/clinopyroxene partition coefficients given by Stosch (1982) by $D^{sp/liq} = D^{sp/cpx} \times D^{cpx/liq}$ where $D^{cpx/liq}$ is the value of Henderson (1982) for basaltic melts. Similar calculations treating olivine and orthopyroxene as unknowns gave results comparable to those cited by

Henderson (1982).

These basalts are very low in Ni and Cr and this must imply that their compositions have been substantially modified by fractionation of olivine and clinopyroxene (see Chapter 5.3). Small, negative Eu anomalies in some samples would imply that plagioclase has also been extracted. Bearing this in mind, theoretical primary magmas were generated and then fractionated. Crystal fractionation modelling was calculated from $C_l/C_o=(1\text{-}F)^{(D-1)}$ where D is the bulk distribution coefficient, F is the fraction of liquid remaining, C_o is the content of an element in the original liquid and C_l is the content in the remaining liquid.

The evolution of the Younger Giant Dyke magmas, equivalent to the high Zr/Nb (oversaturated) dykes in the Igaliko region, appears to be governed by early, deep clinopyroxene fractionation followed by shallower (10km) fractionation of olivine and plagioclase (see Upton and Thomas 1980). Clinopyroxene fractionation may have been important in producing the high Na/Ca and Al characteristic of both the OGDC (undersaturated) and the YGDC (oversaturated) basic magmas (Upton 1971).

Cr contents will be controlled largely by clinopyroxene fractionation with 'troctolitic' extracts of olivine (50%) and plagioclase (50%) only causing a slight increase in the Cr content (14% after extraction of 30% of mixture). Cr would also partition strongly into opaque oxides and if these were fractionating Cr would be reduced more rapidly than by clinopyroxene. REE would however have low partition coefficients into opaque oxides, and would thus not be greatly affected by its fractionation (Henderson 1982, 1984). Clinopyroxene would thus have a far greater effect upon the REE and opaque oxide fractionation can effectively be ignored. Cr thus puts a limit of around 20% fractionation of pyroxene on both the possible BD_0 and basalts north of Narssarssuaq (325990,2), if 270ppm of Cr is assumed for a parental magma (Basaltic Volcanism Study Project 1982). Assuming parental Ni at 500ppm (Basaltic Volcanic Study Project 1982) a further 30% extraction of 50:50 plagioclase:olivine (after the 20% clinopyroxene extract) will give Ni of around 40ppm – comparable to the basalts and possible BD_0. Back substitution for Rb, La and Lu gives parental magma compositions for La_{cn} of 58.5-61.5, Lu_{cn} of 8.8-10.1 and Rb_{cn} of 120-127 (first figure Narssarssuaq basalts, second figure possible BD_0).

Partial melting modelling for Rb, La and Lu was carried out for a 2-times chondrite mantle source containing garnet (15%, 9% and 5%, see Chapter 5.8) and sphene (9%) instead of garnet. No source containing garnet could produce Lu_{cn} comparable to the 'calculated parent' values at around 9 at partial melts up to 5%, (5% garnet, 5% partial melting gave Lu_{cn} 5.08). The spinel lherzolite source however produced melts with Lu_{cn} between 10 and 12 (5% to 0.1% melting) and a source with 1-2% garnet and 6-7% spinel produced Lu_{cn} concentrations very similar to the modelled values at 2% partial melting. 2% melting is consistent with the assumptions made from the Zr/Nb data in Chapter 5.8 for the high Zr/Nb basalts. From these calculations it would thus appear possible that melting of a twice chondrite source took place largely above the garnet/spinel transition zone, although some garnet may have been present in the source (1-2%).

However, this model does not generate the necessary La and Rb concentrations. To produce the 'calculated parent' Rb contents partial melts of less than 0.1% from a 15% garnet source would be necessary, already ruled out by the Lu data, as well as being in stark contrast to assumptions from the Zr/Nb data (Chapter 5.8). Similarly for La, partial melts of 0.1-0.5% (from any of the modelled sources) would produce the calculated parent compositions, again in contrast to the Zr/Nb data. Melts of such small proportions would be thoroughly undersaturated (probably nephelinitic) in composition (see McKenzie 1984, 1985). To generate the 'calculated parent' composition for La and Rb at 1-2% melting, source-region enrichment to 3× chondrite for La and 4× chondrite for Rb is necessary. This would also necessitate keeping the source Lu content near to twice chondrite.

Many workers have appealed to 'mantle metasomatism' as a source of enrichment in incompatible elements (eg. Lloyd and Bailey 1975, Frey *et al.* 1978, Menzies and Murthy 1980, Bailey 1982). These processes were a necessary requirement of the models employed as it was thought that small partial melts (of a few percent or less) would not be capable of migration and separation from the mantle. Thus, large melts (5-10%) were invoked by these authors to come from an enriched mantle source to account for observed chemical characteristics. Recently however, McKenzie (1984, 1985) has shown that melt fractions as low as tenths of a percent are capable of migration. Thus, the need for 'wholesale' mantle metasomatism is removed, and more recently some authors

have argued in favour of a 'streaked' mantle, selectively enriched in parts in LILE (such as LREE, Ba, Rb, K, Nb) (see Fitton and Dunlop 1985, Fitton and James 1986, Fitton 1987, Hawkesworth *et al.* 1984, Menzies *et al.* 1987).

The La and Rb data from the dykes would suggest that some mantle source enrichment in incompatible elements may have occurred, increasing La from 2- to 3-times chondrite and Rb from 2- to 4-times chondrite, but leaving Lu at about 2-times chondrite. It is apparent that the more incompatible the element, the more enriched it needs to be in the source. Streaking of the mantle to cause enrichments in LILE (see above) may be caused by the emplacement or metasomatising effect of magmas of kimberlitic/basanitic compositions rising through the lithospheric mantle (Hawkesworth *et al.* 1984, Menzies *et al.* 1987). Assuming that basaltic magmas are the cause of this process, then (with typical normalised concentrations of La at perhaps 500, $(La/Lu)_{cn}$ between 10 and 25 and Rb at 700-1000), as little as 0.2% by volume of this material in the source region would be enough to increase the source region compositions to the required calculated concentrations. This is by no means an unreasonable volume of magma to migrate to a higher level in the mantle.

It was noted in Chapter 5.8 that the low Zr/Nb (undersaturated) suite of rocks may have originated from a mantle source rich in CO_2; and H_2O may have been present in the source region for the oversaturated (high Zr/Nb) suite. The undersaturated suite is slightly more enriched in some LILE (higher K, Rb, Nb, LREE) and these may have been introduced by the fluid/CO_2 phase. These undersaturated rocks tend also to evolve to slightly higher F and Cl implying more volatiles in the source. These fluids/volatiles may act as transporting agents bringing other volatile/incompatible elements into the magma source regions (see for example Bailey 1980, 1982, 1987), producing a similar effect to the above mentioned 'streaks' with regard to magma chemistry. Bailey (1982, 1983) considers rift zones in analogous manner to 'pie funnels' tapping volatiles (particularly CO_2) from a large volume of sub-rift mantle. It is interesting to note the correlation between the only Gardar carbonatite occurrences at Grønnedal-Íka and Igaliko (C.H. Emeleus, pers. comm. 1987) and zones of major (pre-Gardar and Gardar) faulting (both N-S and E-W at Grønnedal, cf. Henriksen 1960; and ENE-WSW and roughly E-W at Igaliko, Emeleus and Harry 1970, Emeleus and Stephenson 1970).

If these zones of faulting penetrate into the upper mantle they may focus volatiles (particularly CO_2) into the area.

Picritic and Other Basalts

Figure 6.2.2 shows REE spidergrams of a picritic basalt from Mellemlandet (325618) and a late basalt which cuts Igdlerfigssalik Unit 7 (43916). Both samples have Zr/Nb <5.2, and both show $(La/Lu)_{cn}$ ≈18, twice that of the high Zr/Nb basalts. Both also show slight positive Eu anomalies, the result of some accumulation of plagioclase.

The REE are relatively immobile on weathering (Humphris 1984) and thus, despite the fairly altered nature of the picritic basalt, they probably represent closely its unaltered composition. In contrast Rb (and probably Ni and Cr) may have been modified by this alteration.

Both these basaltic rocks have La_{cn} ≈120, Lu_{cn} at ≈6.5. The picritic basalt has Ni at 73ppm and Cr at 245ppm. It is thus (even if modified by alteration) relatively primitive, with the Cr data suggesting little clinopyroxene extraction from a parental basalt, and the Ni data suggesting perhaps 10% olivine extraction (assuming parental Ni and Cr as suggested above).

Plagioclase may also have been involved in the fractionating assemblage. Assuming a model similar to that employed in modelling the evolution of the high Zr/Nb basalts, extraction of 25% of a 50:50 plagioclase - olivine mix would account for Ni and Cr contents. This would imply that initial REE contents were of the order of La_{cn} ≈85 and Lu_{cn} ≈4.6. The low HREE are consistent with a small degree of partial melting from a garnet-bearing source. If the degrees of partial melting suggested by the Zr/Nb - Ce/Y model in Chapter 5.8 are valid, the calculated parent data are reasonably consistent with a 5% garnet-bearing source and 0.5% partial melting from a fractionally greater than twice chondrite HREE source. The calculated LREE could be produced at such degrees of melting if the source was perhaps 2.5 to 3 times chondrite (ie. some degree of LREE enrichment). This degree of melting is not unreasonably small (cf. McKenzie 1984, 1985, Fitton and Dunlop 1985, for example) and would produce melts of undersaturated basaltic (basanitic, nephelinitic) compositions.

Figure 6.2.2

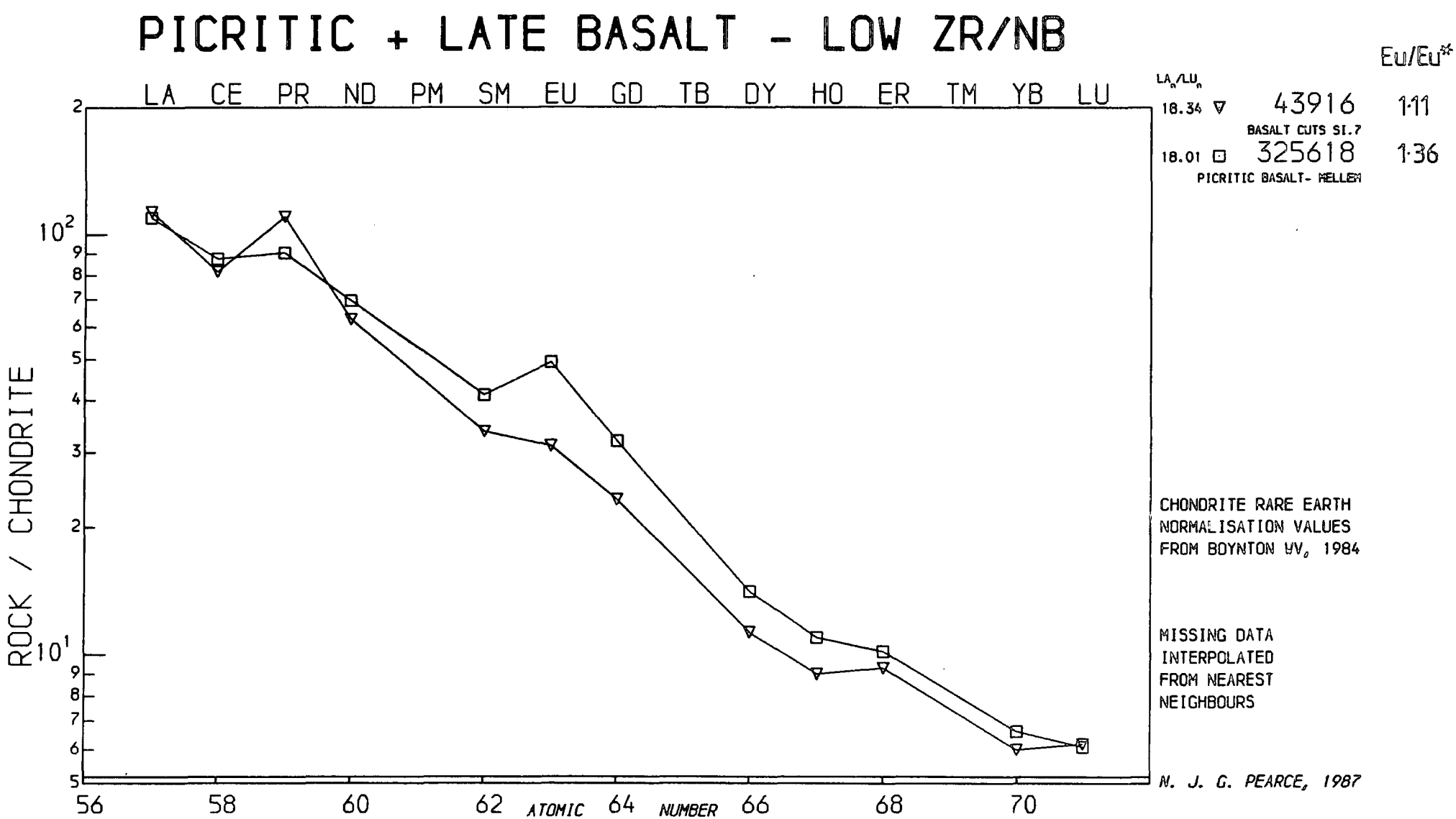
PICRITIC + LATE BASALT - LOW ZR/NB
LA CE PR ND PM SM EU GD TB DY HO ER TM YB LU
ROCK / CHONDRITE
ATOMIC NUMBER
Eu/Eu*
LA_n/LU_n
18.34 ▽ 43916 1·11
BASALT CUTS SI.7
18.01 □ 325618 1·36
PICRITIC BASALT- HELLEM
CHONDRITE RARE EARTH NORMALISATION VALUES FROM BOYNTON WV, 1984
MISSING DATA INTERPOLATED FROM NEAREST NEIGHBOURS
N. J. G. PEARCE, 1987

The late basalt which cuts SI.7 (43916) is also somewhat altered (although still contains fresh feldspar) and has Ni at 30ppm and Cr at 99ppm. Rb is high at 163ppm. The basalt would appear to have undergone fractionation including both clinopyroxene and olivine. Assuming the same model as for the high Zr/Nb basalts, extraction of about 13% of clinopyroxene and then 30% of 50:50 olivine:plagioclase would produce observed Ni and Cr contents. Calculated parental REE would thus be La_{cn} ≈72, Lu_{cn} ≈4.5 and Rb_{cn} ≈291. The REE data are similar to the above picritic basalt and could be generated directly by about 0.5% melting from a 5% garnet source of about twice chondrite composition with slight LREE enrichment (to perhaps 2.5-3 times chondrite).

In conclusion it would appear that these low Zr/Nb rocks fractionated from more basic parental magmas which were generated by smaller degrees of partial fusion of a garnet-bearing source (perhaps 0.5% melting) than the parent to high Zr/Nb basalts. By contrast these 'oversaturated' parental basalts appear to have been formed by greater amounts of partial fusion of a garnet-free (or very garnet-deficient) source, such as a spinel lherzolite.

Late Alkali Gabbro Dykes

Figure 6.2.2 shows the REE spidergrams of 3 'late alkali gabbro dykes'. These are considered in conjunction with 58130 discussed in the following section - another late gabbroic dyke cutting the South Qôroq centre although possessing tephritic/basanitic composition.

Sample 59622, from the late Motzfeldt Ring Dyke, shows a marked positive Eu anomaly (Eu/Eu*=1.51) a result of plagioclase accumulation. 43867, 127065 and 58130 in comparison only show smaller Eu anomalies (Eu/Eu* 1.01, 1.08 and 1.28 respectively. These rocks are typically olivine-rich but are all Ni (and Cr) poor. .They must have undergone substantial ferromagnesian mineral fractionation from some parental magma. They are however, still typically alkali basaltic/gabbroic, and all show Zr/Nb>5.2. This implies that (i) they have all been subject to ilmenite accumulation (see Chapter 5), or (ii) that the stratified magma chambers from which these late basaltic magmas were derived (see Stephenson 1973) have been subjected to addition of more melt with higher

Figure 6.2.3

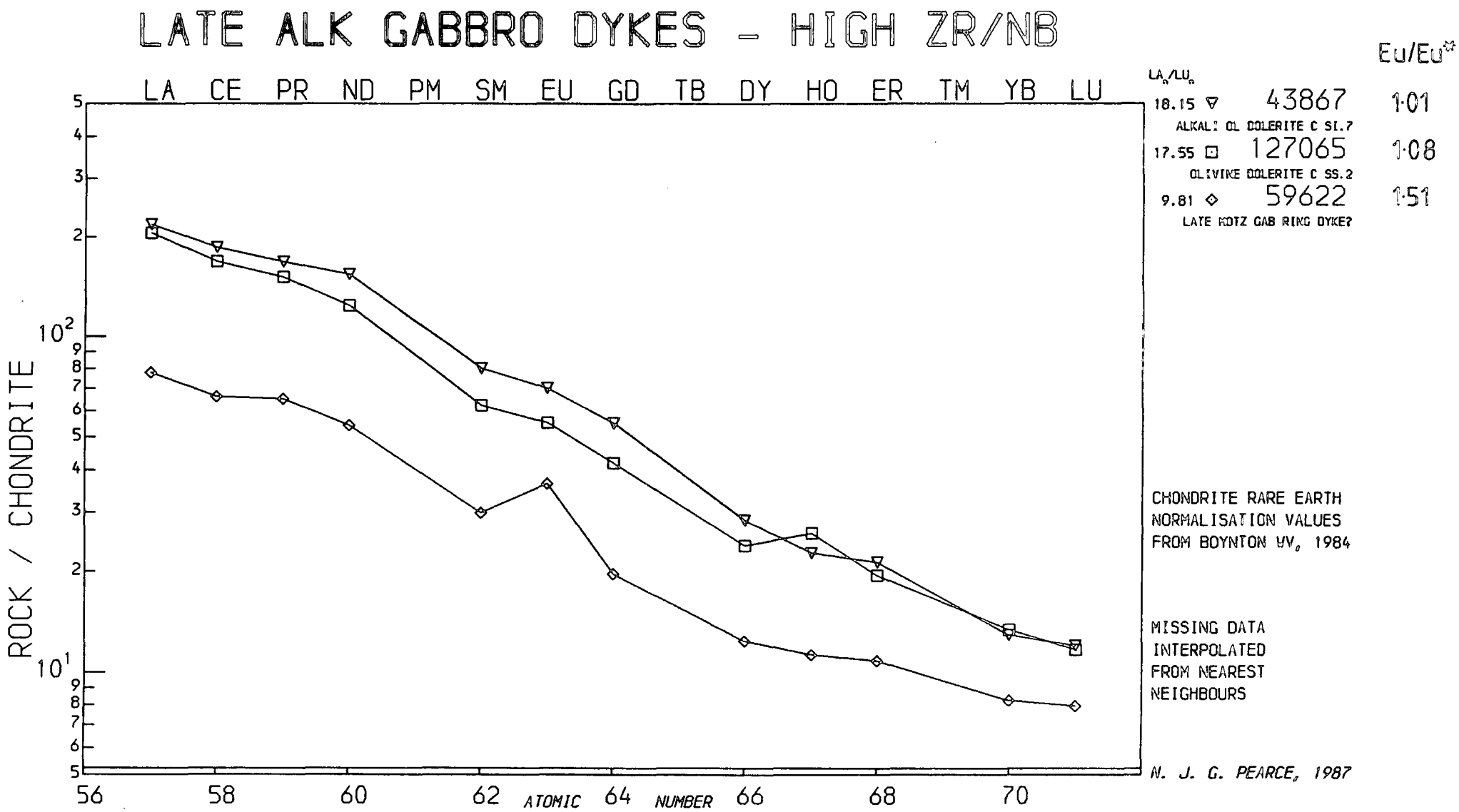
LATE ALK GABBRO DYKES - HIGH ZR/NB
LA CE PR ND PM SM EU GD TB DY HO ER TM YB LU
ROCK / CHONDRITE
ATOMIC NUMBER
Eu/Eu*
LA_n/LU_n
18.15 ▽ 43867 1·01
ALKALI OL DOLERITE C SI.7
17.55 □ 127065 1·08
OLIVINE DOLERITE C SS.2
9.81 ◇ 59622 1·51
LATE MOTZ GAB RING DYKE?
CHONDRITE RARE EARTH NORMALISATION VALUES FROM BOYNTON WV, 1984
MISSING DATA INTERPOLATED FROM NEAREST NEIGHBOURS
N. J. G. PEARCE, 1987

Zr/Nb. This additional material could be later magmas derived from the same melting event in the mantle, with the trace element characteristics of a higher degree of partial melting (see Chapter 5.7, Figure 5.7.4 - Zr/Nb vs. Ce/Y). These 'added' later melts should however be rich in Ni, Cr, V relatively poor in LREE compared to HREE. If this is the case, these magmas must still have undergone substantial olivine ± clinopyroxene extraction to reduce the compatible trace element and MgO content.

59622 is somewhat atypical of these rocks in being richer in plagioclase, leading to lower overall REE and a positive Eu anomaly. Ignoring 59622 they typically have La_{cn} ≈230, Lu_{cn} ≈13 and $(La/Lu)_{cn}$ ≈18. Ni averages ≈15ppm, Cr≈12ppm and Rb may typically be 27ppm (although 127065 has 261ppm). Assuming a model similar to the high Zr/Nb basalts for their derivation from a 'parent' basalt, then deep clinopyroxene fractionation probably removed most Cr and olivine at shallower levels will have accounted for loss of Ni. Plagioclase may also have been involved. 30% clinopyroxene fractionation at depth followed by a further 35% extraction of olivine and plagioclase (50:50) would produce the observed Ni and Cr assuming 500ppm and 270ppm respectively in the parent (Basaltic Volcanic Study Project 1981). This would imply parental La_{cn} at around 100 and Lu_{cn} at around 8 and $(La/Lu)_{cn}$ of 12.5. These values are generally consistent with generation by a smaller degree of partial melting than the high Zr/Nb basalts from a garnet-bearing source (although garnet may only be minor). Rb data do not agree however with any modelled values. The REE data would suggest that perhaps 3-4 times chondrite concentration of LREE and twice chondrite concentrations for HREE are required in the source to generate this hypothetical parent by 0.5% melting from a 1% garnet-bearing source, or about 4 times chondrite for all REE at 0.5%-1% melting of a 5% garnet-bearing source. Similarly a 0.5% melt of a spinel-lherzolite source with 3-times chondrite LREE and twice chondrite HREE could produce similar melts, particularly if garnet fractionation is considered at depth.

Any enrichment of LREE in the source should also lead to enrichment of other highly incompatible elements (eg. Rb) which casts further doubt upon the model by worsening the 'fit' of Rb. It appears that such a simple model produces no definitive and clear account of the origin of the late gabbroic dykes and perhaps a complex combination of fractional crystallisation, replenishment, more fractionation and cumulus enrichment is

ultimately responsible for their chemistries.

6.3: Tephrites/Basanites

Tephrites and basanites are relatively abundant basic rocks in the Igaliko area. In the low Zr/Nb suite they are considerably more abundant than basalts (TAS classification) and for this reason may have some parental status to the undersaturated suite. They occur in similar numbers to basalts in the high Zr/Nb suite although these include some samples from late 'alkali gabbro' dykes within the central complexes. REE spidergrams from these rocks are illustrated in Figure 6.3.1.

Samples 325943 and 52285, both classified as tephrites/basanites are in fact camptonitic lamprophyres (see Chapter 8 and Rock 1977). These alkaline lamprophyres may however grade into hawaiitic compositions with a loss of volatiles and decrease in Ti (Rock 1987a) and may thus be related, by some sort of fractional crystallisation process (including amphibole and oxides?) to the undersaturated suite of rocks. These samples both have Zr/Nb<5.2, Rb_{cn} ≈410 and Ni≈70ppm. They are thus relatively unfractionated but rich in incompatible elements (La_{cn} ≈225, Lu_{cn} 9.5-19, Rb 128-159ppm) compared to the high Zr/Nb basalts.

Samples 46236 and 58130 are both from a late alkali gabbro dyke which cuts unit 5 of the South Qôroq centre (SS.5) and is truncated by unit 2 of the Igdlerfigssalik centre (SI.2). 46236 has been recrystallised by the Early Igdlerfigssalik Syenites whereas 58130 is still fresh, containing abundant olivine. Both samples however contain no detectable Ni and only minor (<2ppm) Cr. They also, surprisingly, have different Zr/Nb ratios (46236, Zr/Nb=4.36; 58130, Zr/Nb=5.49). LREE and highly incompatible elements such as Rb and Pb are considerably more enriched in the thermally metamorphosed sample and this probably reflects addition of these elements to the sample by fluids escaping from the Igdlerfigssalik syenites. Martin *et al.* (1978) observed that LREE enrichment was more pronounced than HREE enrichment in pure Cambrian quartzites in the metasomatic aureole of the Loch Borrolan Alkali Complex by factors of up to 5. However, Humphris (1984) points out that secondary minerals must be capable of retaining a history of such changes in the rocks. Although 46236 consists mostly of biotite, feldspar and oxide mineral (all low D_{REE}, Henderson 1982, 1984), the many

Figure 6.3.1

TEPHRITE/BASANITE AND CAMPTONITE

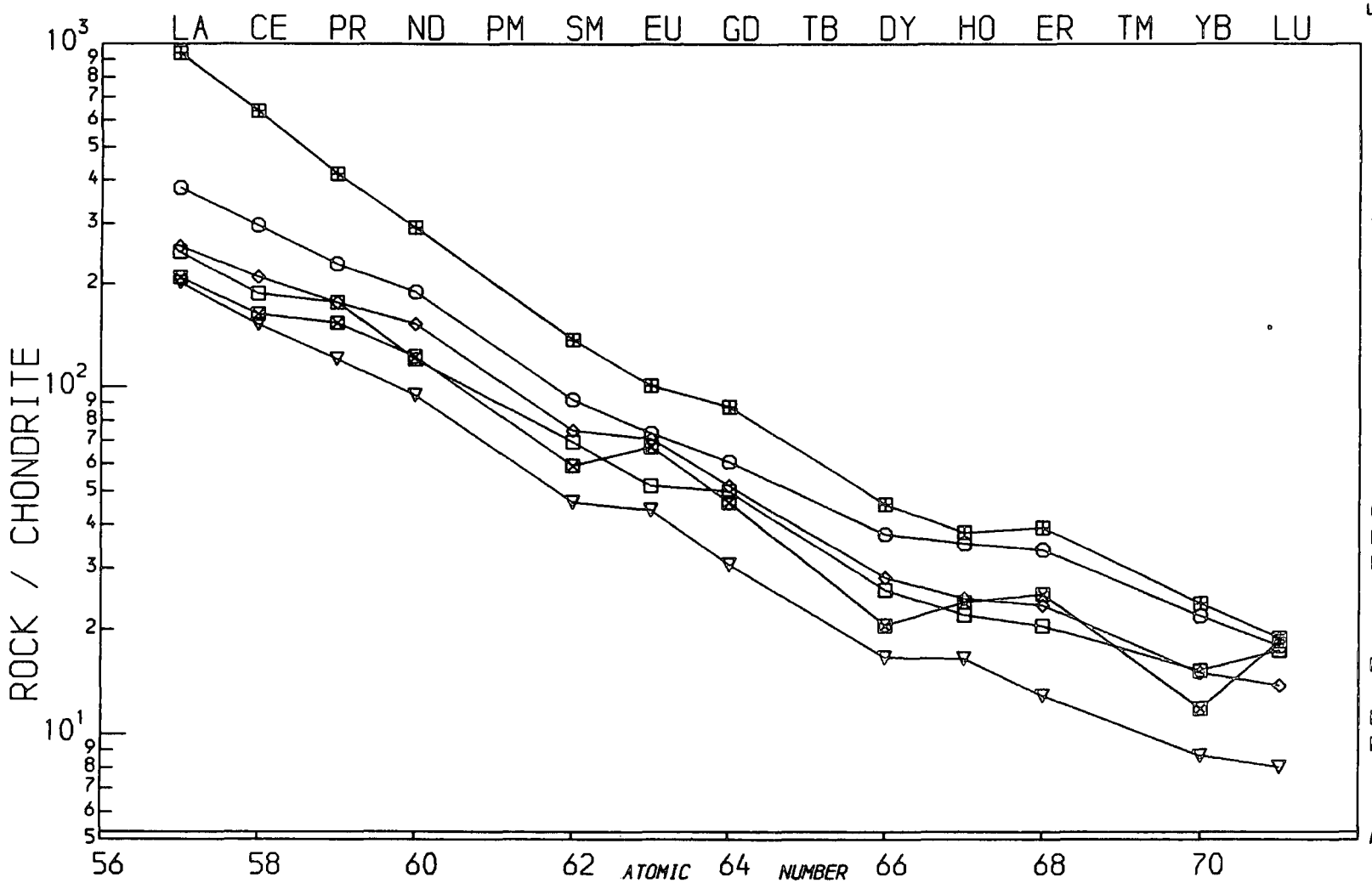

LA_n/LU_n			Zr/Nb	Eu/E
25.15	▽	52285	L	1·17
		CAMPTONITE (TEPHD C OSTFJ		
14.16	⊡	325943	L	0·88
		CAMPTONITE (TEPHD - KOTZ		
18.58	◇	59703	H	1·14
		BFD MATRIX (TEPHRITE)		
21.23	○	59708	H	0·9
		BFD MATRIX (TEPHRITE)		
49.57	⊞	46236	L	0·92
		TEPHRITE C SS.5,C BY S1.2		
11.29	⊠	58130	H	1·28
		TEPH, AS 46236, UN-KETAMD		

CHONDRITE RARE EARTH NORMALISATION VALUES FROM BOYNTON WV, 1984

MISSING DATA INTERPOLATED FROM NEAREST NEIGHBOURS

N. J. G. PEARCE, 1987

small apatites observed could easily account for the REE contents. Metasomatic addition of Nb, with perhaps slight reduction in Zr could also account for the differences in Zr/Nb ratio, although slight modifications in opaque mineralogy (especially ilmenite) could also modify Zr.

58130, the unmetamorphosed sample, has a relatively strong positive Eu anomaly (Eu/Eu*=1.28, whereas this is not evident from 46236 (Eu/Eu*=0.92), the metasomatism having effectively erased this. This would imply that these LREE-rich metasomatic fluids had a negative Eu anomaly sufficient to increase the overall Eu but to produce a small negative anomaly. This negative Eu in the metasomatising fluids would be consistent with the overall REE patterns of the evolved samples, assuming the fluids possessed a similar overall pattern to the magma from which they emanated.

The two other tephrites/basanites, 59703,8, are from a BFD, and are essentially free from xenolithic material, although both show small positive Eu anomalies, presumably the result of a minor amount of phenocrystic/xenocrystic plagioclase. These two samples both have Zr/Nb>5.2 and only 8ppm Ni.

Thus, of these rocks, only the two camptonites would appear to have any 'parental' status (based on Ni, Cr etc.) but even they are probably not 'primary' magmas. They probably suffered loss of ferromagnesian minerals (olivine, pyroxene and kaersutitic amphibole - xenocryst in 325943). These samples show the steep REE patterns $((La/Lu)_{cn}$ of 25.15 and 14.16), consistent with their generation by a small degree of partial melting from a garnetiferous source.

Both the 'alkali gabbros' (58130, 46236) and the BFD (59703,7) must have undergone appreciable extraction of ferromagnesian minerals to produce their typically low Ni and Cr compositions, from some more basic parent. In the case of the BFD, with HREE similar to high Zr/Nb basalts, but with 3-4 times higher LREE, the fractionating assemblage probably included clinopyroxene, olivine and garnet at depth followed by continued olivine and possibly plagioclase at shallow crustal levels. The inclusion of garnet in the assemblage is needed to 'buffer' the HREE content (D_{Lu}^{garnet}=35, Henderson 1982, 1984). Extraction of relatively large volumes of olivine and clinopyroxene could more-or-less buffer Si, whilst increasing alkalis thus generating hawaiites and/or

tephrites from basaltic compositions (see Figure 5.2.1). The 'alkali gabbro' (58130, 46236), rich in cumulus olivine (Fe-rich) is particularly Ni-poor and must have suffered prolonged olivine (± clinopyroxene) extraction. This was considered along with the late alkali gabbros in the previous section.

6.4: Intermediate Rocks

Figure 6.4.1 shows REE spidergrams of 2 mugearites and 2 hawaiites. Only one sample (63891), a mugearite which cuts SI.7, shows a negative Eu anomaly (Eu/Eu* = 0.46), caused by fractionation of feldspar. This sample is a fairly evolved mugearite and has Zr/Nb<5.2. Absolute degrees of REE enrichment are similar to those of the tephrites, with similar normalised REE slopes.

These rocks however, are some 2-6 times richer in LREE than the basalts although containing fractionally less HREE. $(La/Lu)_{cn}$ is thus typically 2-3 times that of the basalts (ranging from 18.78-62.21). The HREE data would suggest a bulk distribution coefficient of >1 assuming these rocks are the result of crystal fractionation from basalt. Mineral extract calculations produced a hawaiite from a basalt by extraction of 16.2% plagioclase, 6.8% olivine and 6.4% pyroxene. Fractionation of this mixture, assuming typical basaltic REE, would give 2.94-times the LREE contents and 2.8-times the HREE (D^{min}_{REE} from Henderson 1982). The calculated HREE data is thus not consistent with the observed HREE abundances. To increase the bulk D^{HREE} it is necessary to invoke garnet as a fractionating phase ($D^{garnet}_{Lu} \approx 35$). 2.6% garnet in addition to the above assemblage produces $D_{Lu}=1$. This would have a negligible effect on the bulk D_{La} ($D^{garnet}_{La} \approx 0.6$) and thus little effect on the observed LREE contents. The implication must be that a basaltic parent underwent some high pressure fractionation, involving minor amounts of garnet, before being emplaced higher in the crust to fractionate at lower pressures towards hawaiites and mugearites. High pressure fractionating assemblages would also probably include olivine and clinopyroxene and would in part be able to account for the observation in other trace elements (eg. Ni, Cr, V) if taken in conjunction with the low pressure fractionation (cf. Cox 1980). This would also be consistent with the density minimum at ca. 8% MgO (see Chapter 5.5, Sparks and Huppert 1984, Upton and Emeleus 1987). There is not sufficient data here to define any differences between the fractionation histories of the oversaturated and undersaturated

Figure 6.4.1

INTERMEDIATE ROCKS - LOW AND HIGH ZR/NB

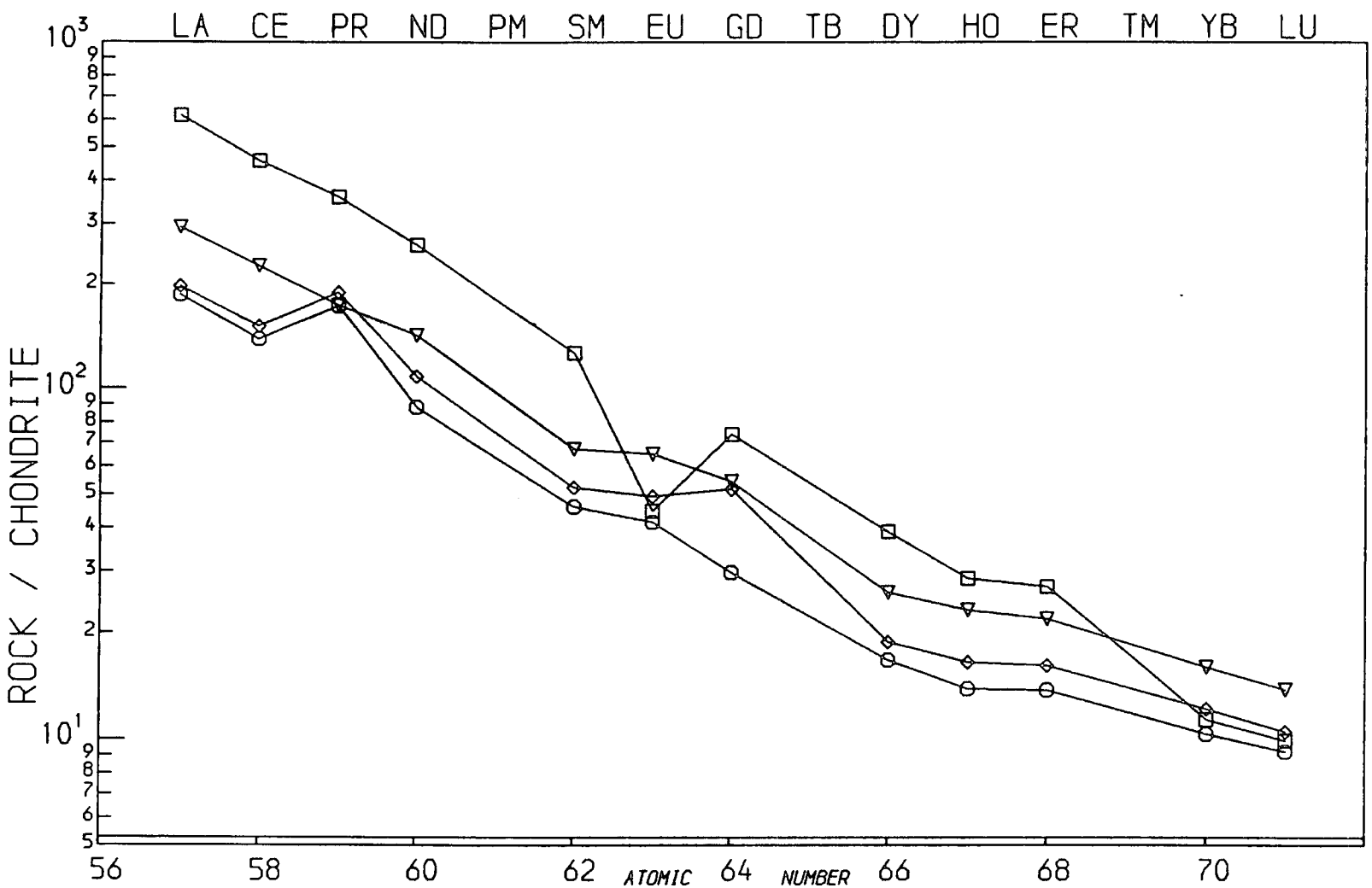

				Zr/Nb	Eu/Eu
LA_n/LU_n					
21.23	▽	326371	L		1·07
	BFD MATRIX (KUGEARITE)				
62.21	□	63891	L		0·46
	KUGEARITE CUTS SI.7				
18.78	◇	43887	L		1·12
	MINETTE (HAU) CUTS SI.7				
20.17	⊙	52274	H		0·95
	CAMPTONITE (HAU) CUTS SI4				

CHONDRITE RARE EARTH NORMALISATION VALUES FROM BOYNTON WV, 1984

MISSING DATA INTERPOLATED FROM NEAREST NEIGHBOURS

N. J. G. PEARCE, 1987

suites.

6.5: Benmoreites

Benmoreites from both the high and low Zr/Nb (over- and undersaturated) suites were analysed for REE. The analyses are plotted in Figure 6.5.1 (high Zr/Nb suite) and Figure 6.5.2A and B (low Zr/Nb rocks).

Mineral extraction calculations, along with incompatible element variation, indicates that for the magma to have evolved to benmoreitic compositions from intermediate composition (hawaiite/mugearite) substantial quantities of apatite and feldspar, along with lesser clinopyroxene, olivine and opaques, should have been removed from the liquid (see Chapters 5.5 and 5.6).

MREE will partition preferentially into apatite which has D_{Ce}=31, D_{Sm}=54, D_{Dy} =42 and D_{Lu}=17 (Henderson 1982). Similarly sphene, a common phase occurring as rims to opaque oxides, has a preference for MREE (D_{Ce}=53.3, D_{Dy}=102, D_{Lu}=26.9, Henderson 1984). Fractionation of 2% of apatite would thus cause depletion in many of the MREE relative to LREE and HREE. In the rocks of dacitic and rhyolitic compositions MREE would also partition preferentially into clinopyroxene (D_{La}=0.6, D_{Dy}=3.3, D_{Lu}=2.3, Henderson 1982). In these rocks the dominant feldspar is anorthoclase, grading into binary alkali feldspar with evolution to trachytes and phonolites. Eu partitions into alkali feldspar much more strongly than plagioclase (D_{Eu}^{plag}=0.32, $D_{Eu}^{alk\ fsp}$=1.13) whereas the rest of the REE prefer plagioclase to alkali feldspar (D_{Ce}^{plag}=0.14, $D_{Ce}^{alk\ fsp}$ =0.04, D_{Yb}^{plag}=0.07, $D_{Yb}^{alk\ fsp}$=0.012).

High Zr/Nb Benmoreites

Immediately obvious from Figure 6.5.1 are large negative Eu anomalies associated with all the high Zr/Nb benmoreites, becoming larger in the more evolved rocks. Also clearly evident is a marked flattening of the REE pattern from Dy to Lu.

The large Eu anomaly will be a result of increased (and more alkali-rich) feldspar fractionation, preferentially removing Eu, whilst the flattening of the pattern will result from the fractionation of MREE-rich phases, most probably apatite and clinopyroxene. Provided apatite is removed in quantities less than 2% (see Chapters 5.5 and 5.6 -

Figure 6.5.1

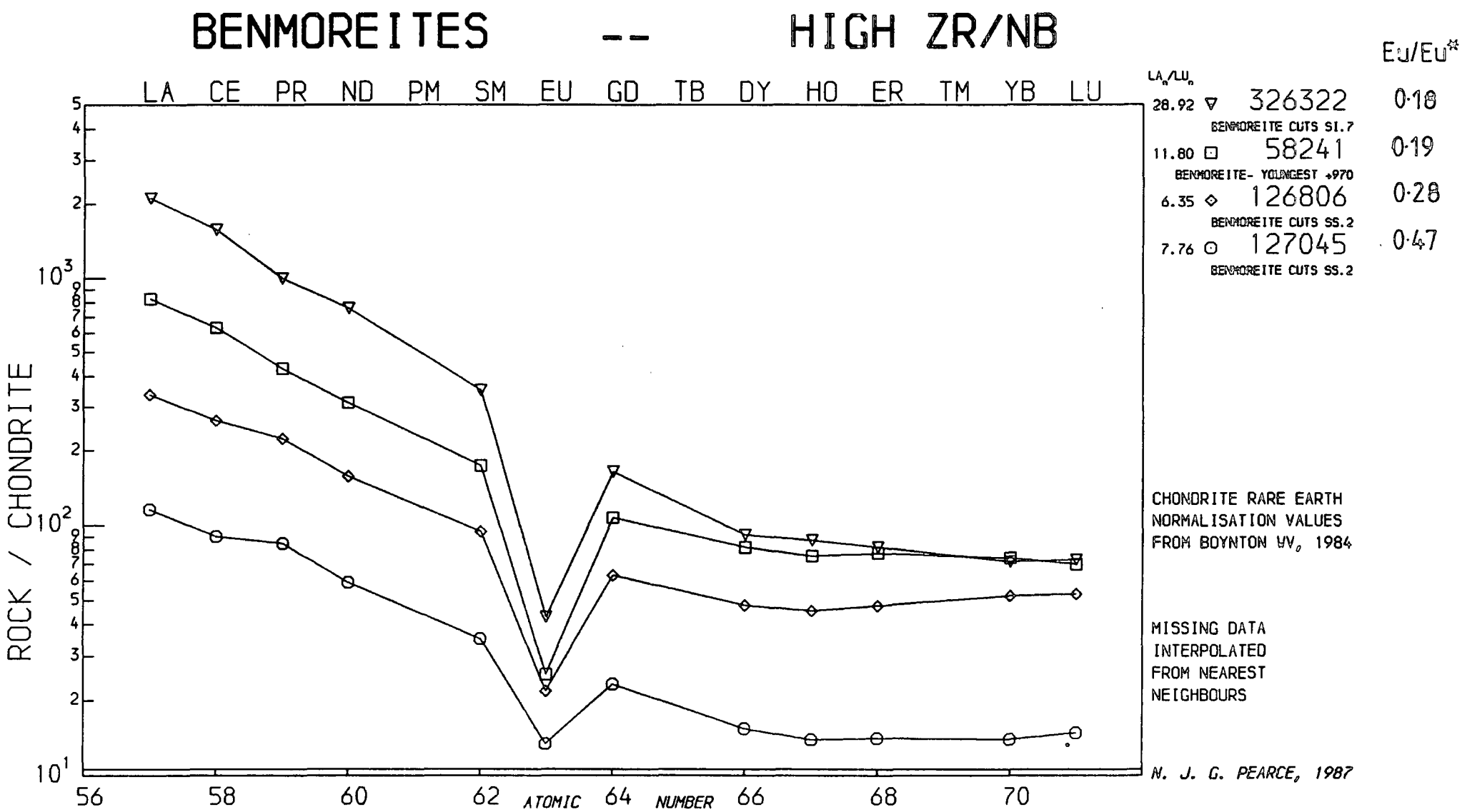
BENMOREITES -- HIGH ZR/NB
LA CE PR ND PM SM EU GD TB DY HO ER TM YB LU
ROCK / CHONDRITE
ATOMIC NUMBER
56 58 60 62 64 66 68 70
Eu/Eu*
LA_n/LU_n
28.92 326322 0·18
BENMOREITE CUTS SI.7
11.80 58241 0·19
BENMOREITE- YOUNGEST +970
6.35 126806 0·28
BENMOREITE CUTS SS.2
7.76 127045 0·47
BENMOREITE CUTS SS.2
CHONDRITE RARE EARTH NORMALISATION VALUES FROM BOYNTON WV, 1984
MISSING DATA INTERPOLATED FROM NEAREST NEIGHBOURS
N. J. G. PEARCE, 1987

mineral extract calculations), then only MREE will be depleted in the residua and LREE and HREE will continue to increase. Large extracts of clinopyroxene would have a similar 'flattening' effect. Apatite fractionation (with $D_{Ce} \approx 2 \times D_{Lu}$) will also cause a decrease in the overall slope of the pattern (reduce $(La/Lu)_{cn}$). This is seen in the benmoreites which have lower $(La/Lu)_{cn}$ than the intermediate rocks. Clinopyroxene fractionation would have the opposite effect on $(La/Lu)_{cn}$, causing it to increase (as $D_{Ce}^{cpx} \approx 0.4 \times D_{Lu}^{cpx}$). Thus, from the REE alone, it would appear that apatite is a major control between hawaiitic/mugearitic to benmoreitic compositions and this is backed up by the large reduction in P between these compositions. Continued feldspar fractionation would cause an absolute increase in all REE and cause deepening of the Eu anomaly.

Low Zr/Nb Benmoreites

Figures 6.5.2 A and B show REE spidergrams for the low Zr/Nb benmoreites. These are in many ways similar to the high Zr/Nb data in overall characteristics although what is immediately obvious is the lack of a negative Eu anomaly in many of the samples. Positive Eu anomalies are seen in 3 samples; 58138 ($Eu/Eu^* = 2.76$), 58240 ($Eu/Eu^* = 1.08$) and 58233 ($Eu/Eu^* = 1.17$). In the latter two cases these result from the presence of a small amount of entrained feldspar phenocrysts whilst the much more marked Eu anomaly in 58138 is a result of a relatively large modal quantity of feldspar phenocrysts. $(La/Lu)_{cn}$ is typically between 10 and 20 (average of 10 samples gave 17.8). As in the high Zr/Nb benmoreites there is a marked flattening of the Gd-Lu part of the curve. There is also development of a small negative anomaly at Ce in some samples. Of the 6 samples that show negative Ce anomalies, 2 have positive Eu anomalies, 2 have no obvious Eu anomaly and 2 have marked negative Eu anomalies.

Similar processes of fractional crystallisation to the high Zr/Nb suite will have acted to produce the low Zr/Nb suite (see Chapters 5.5 and 5.6); ie. feldspar, clinopyroxene and apatite fractionation. However, these processes have produced rather different results in these undersaturated rocks, notably a lack of negative Eu anomalies in many samples, and also some negative Ce anomalies. The absence of negative Eu anomalies is not a 'chance' effect caused by incorporation of just the right quantity of Eu enriched cumulus feldspar to balance the Eu defecit of the host magma, but is a real feature

Figure 6.5.2A

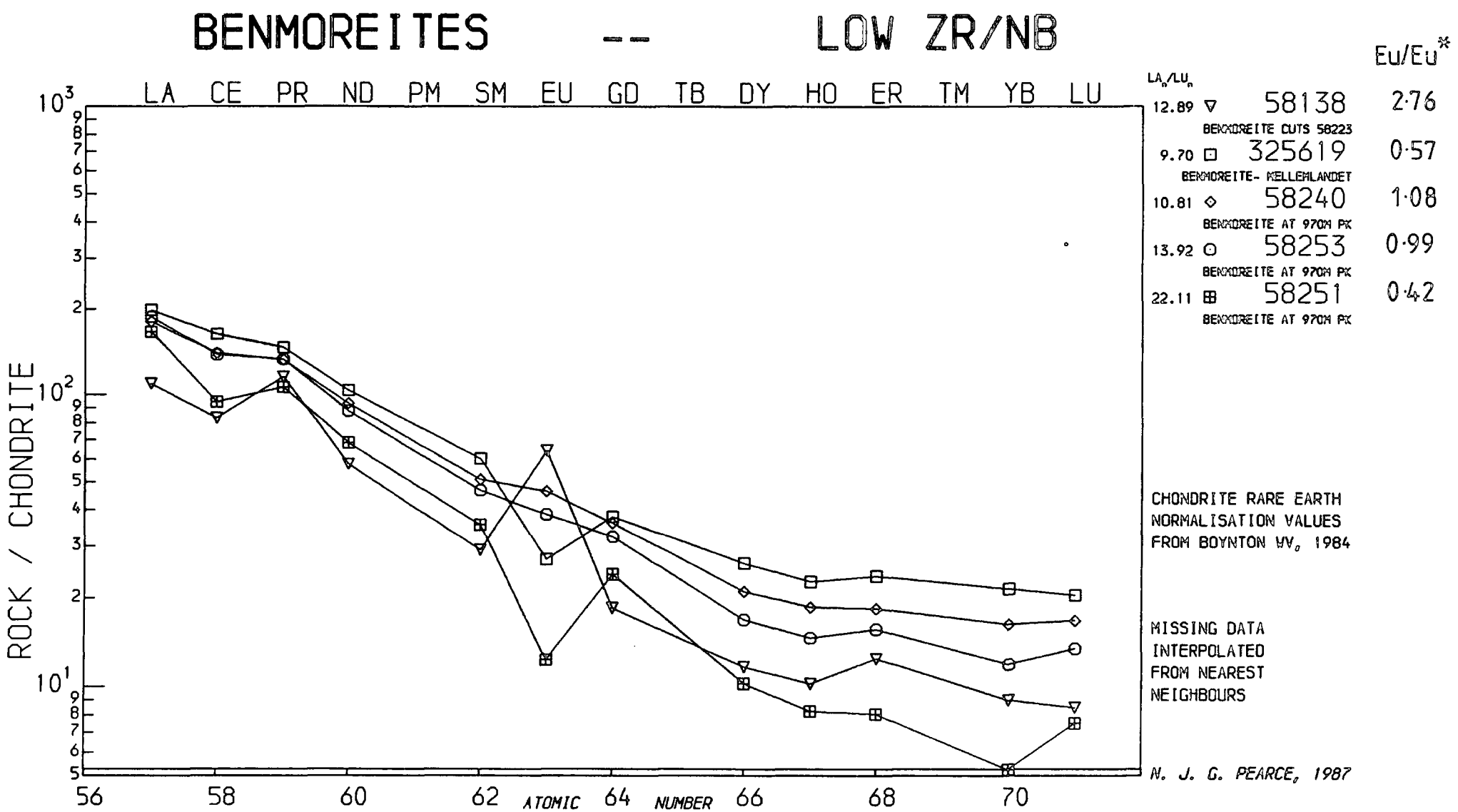
BENMOREITES -- LOW ZR/NB
LA CE PR ND PM SM EU GD TB DY HO ER TM YB LU
ROCK / CHONDRITE
ATOMIC NUMBER
Eu/Eu*
LA_n/LU_n
12.89 58138 2·76
BENMOREITE CUTS 58223
9.70 325619 0·57
BENMOREITE- KELLEHLANDET
10.81 58240 1·08
BENMOREITE AT 970M PK
13.92 58253 0·99
BENMOREITE AT 970M PK
22.11 58251 0·42
BENMOREITE AT 970M PK
CHONDRITE RARE EARTH NORMALISATION VALUES FROM BOYNTON WV, 1984
MISSING DATA INTERPOLATED FROM NEAREST NEIGHBOURS
N. J. G. PEARCE, 1987

Figure 6.5.2B

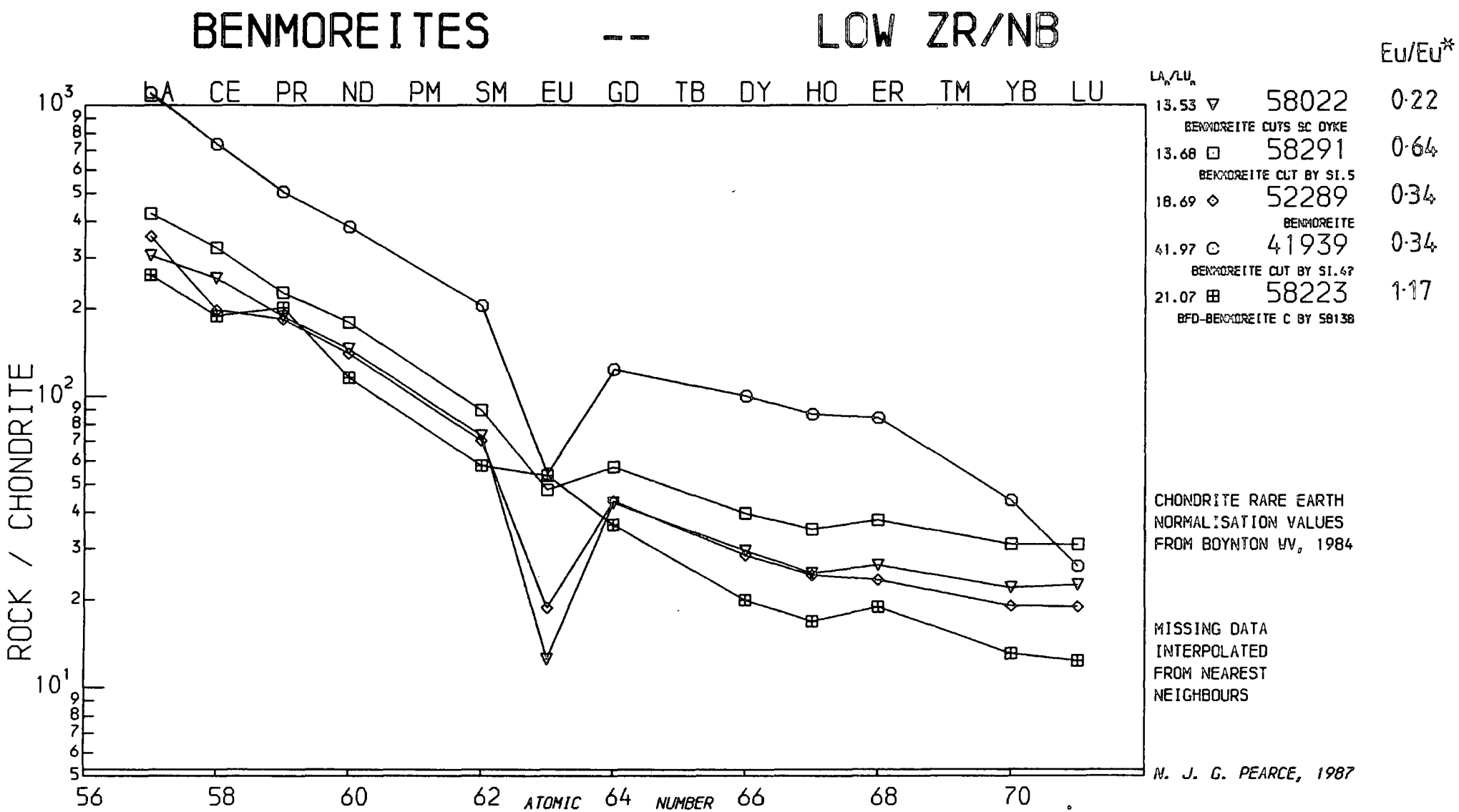
BENMOREITES -- LOW ZR/NB
LA CE PR ND PM SM EU GD TB DY HO ER TM YB LU
ROCK / CHONDRITE
ATOMIC NUMBER
56 58 60 62 64 66 68 70
LA_n/LU_n
Eu/Eu*
13.53 58022 0·22
BENMOREITE CUTS SC DYKE
13.68 58291 0·64
BENMOREITE CUT BY SI.5
18.69 52289 0·34
BENMOREITE
41.97 41939 0·34
BENMOREITE CUT BY SI.4?
21.07 58223 1·17
BFD-BENMOREITE C BY 58138
CHONDRITE RARE EARTH NORMALISATION VALUES FROM BOYNTON WV, 1984
MISSING DATA INTERPOLATED FROM NEAREST NEIGHBOURS
N. J. G. PEARCE, 1987

of these rocks. In natural silicate melts Eu exists as both Eu^{2+} and Eu^{3+}. Eu^{2+} will partition into feldspar in greater quantities than Eu^{3+}, with Eu^{2+} substituting for Ca^{2+} in plagioclase (as does Sr) or Na^{+} in alkali feldspar. Eu^{3+}, and other tri-valent rare earths will not however, substitute readily into feldspar structures, their large ionic radii (Shannon 1976) preventing substitution in most cases.

Sun *et al.* (1974) and Weill and McKay (1975) conducted experimental studies which showed the effect of variation of fo_2 on D_{Eu}. This is not a linear function but D_{Eu} decreases as fo_2 increases, due to the reduction of the Eu^{2+}/Eu^{3+} ratio in the liquid. There is thus less Eu^{2+} available at higher fo_2 to partition into feldspar. It was shown in Chapter 4 that there are distinct high and low fo_2 trends associated with different rock types and these were re-iterated in Chapter 5.10, which showed that the undersaturated suite has generally higher fo_2 than the oversaturated suite.

Thus, with higher fo_2, Eu^{2+}/Eu^{3+} will be lower in the undersaturated suite than in the oversaturated suite and this will manifest itself as a lack of (or smaller) negative Eu anomalies in these rocks. It also appears that Eu has become 'de-coupled' from Sr as a consequence of the higher fo_2. Figure 6.5.3 shows $(Sr/Ce)_{cn}$ plotted against Eu/Eu*. $(Ce/Sr)_{cn}$ represents the Sr-anomalies seen in the incompatible element spidergrams (Chapters 5.5 and 5.6), thus, Sr/Ce<1 indicates negative Sr anomalies. It is clear that Sr decreases rapidly relative to Ce with, in a lot of samples, no reduction in Eu/Eu*. Only when $(Sr/Ce)_{cn} \approx 0.15$ does Eu start to partition noticeably into the crystallising feldspar. As fo_2 increases D_{Eu}^{fsp} will fall, and presumably Eu will behave more and more incompatibly with increased fractionation. Eu anomalies may thus be formed relatively early in the fractionating history and remain little modified as evolution of the suite of rocks proceeds, although this may be countered to some extent by the increased D_{Eu} of alkali feldspar compared to plagioclase. The effect of CO_2 on Eu partitioning and fo_2 is discussed in Chapter 7.6 with regard to the genesis of carbonatites.

The presence of small negative Ce anomalies may be a reflection of a slight increase in bulk D_{Ce} caused by a higher Ce^{4+}/Ce^{3+} ratio at high fo_2. Goldschmidt (1954) cites examples of Ce bearing minerals with Ce wholly as Ce^{4+} in highly oxidised magmas, especially nepheline syenite pegmatites. However, ionic radii (Shannon 1976) show little difference (perhaps 10-12%) between Ce^{4+} and La^{3+} and Pr^{3+} in 6-fold coordination.

Figure 6.5.3

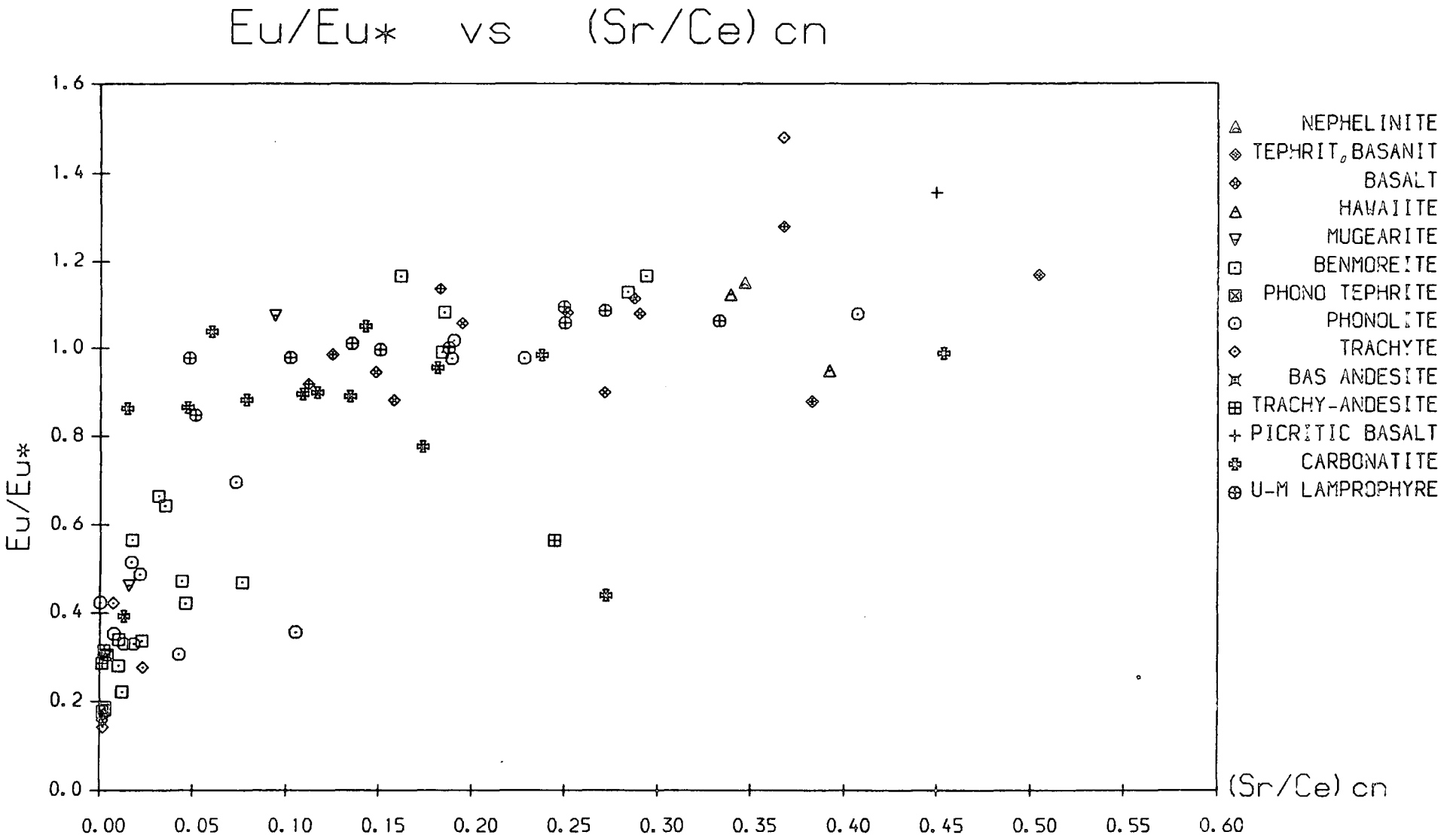
Eu/Eu* vs (Sr/Ce)cn
Eu/Eu*
(Sr/Ce)cn
0.0
0.2
0.4
0.6
0.8
1.0
1.2
1.4
1.6
0.00
0.05
0.10
0.15
0.20
0.25
0.30
0.35
0.40
0.45
0.50
0.55
0.60
NEPHELINITE
TEPHRIT, BASANIT
BASALT
HAWAIITE
MUGEARITE
BENMOREITE
PHONO TEPHRITE
PHONOLITE
TRACHYTE
BAS ANDESITE
TRACHY-ANDESITE
PICRITIC BASALT
CARBONATITE
U-M LAMPROPHYRE

This would make fractionation of Ce^{4+} relative to La and Pr more difficult to achieve, as they would have similar distribution coefficients.

In conclusion, the major differences between individual samples (particularly Eu/Eu*) are probably a result of the separate evolution of pulses of magma in high level magma chambers. Individual batches of magma may be intruded into the central complexes and undergo different degrees of fractionation, evolving along individual liquid lines of descent before injection as dykes. This may also be responsible for the large scatter of incompatible element data for the undersaturated suite (see Chapter 5.7) as well as different REE characteristics, caused by slightly different physico-chemical conditions during their evolution.

6.6: Trachytes

High Zr/Nb

Figure 6.6.1 shows spidergrams from the REE data from 3 high Zr/Nb trachytes. The general features are very similar to those of the high Zr/Nb benmoreites, with relatively low $(La/Lu)_{cn}$ between 7.29 and 12.85, as well as pronounced negative Eu anomalies (0.28-0.17). They show a similar range of absolute REE enrichment. Continued fractional crystallisation of feldspar, minor pyroxene and possibly some apatite from benmoreite will be responsible for their formation.

Low Zr/Nb

Two low Zr/Nb trachytes were found to be truncated by foyaite sheets within the Motzfeldt centre (at Camp 5, Lejrelv, 1984, see Figure 1.1.1). These were analysed for their REE contents and are shown in Figure 6.6.2. Major and trace element data suggest that these samples came from the same source, and the REE data backs this up. Eu, higher in 325915 is consistent with increased numbers of feldspar phenocrysts in this sample, erasing some of the negative Eu anomaly. These samples must have been contemporaneous with intrusions within the Motzfeldt centre, and are thus, in all probability, unrelated directly to the Late Gardar dyking events. Although their major and trace element chemistries are virtually identical to the Late Gardar dykes certain features of their REE chemistry differ. These dykes have a higher $(La/Lu)_{cn}$ than most

Figure 6.6.1

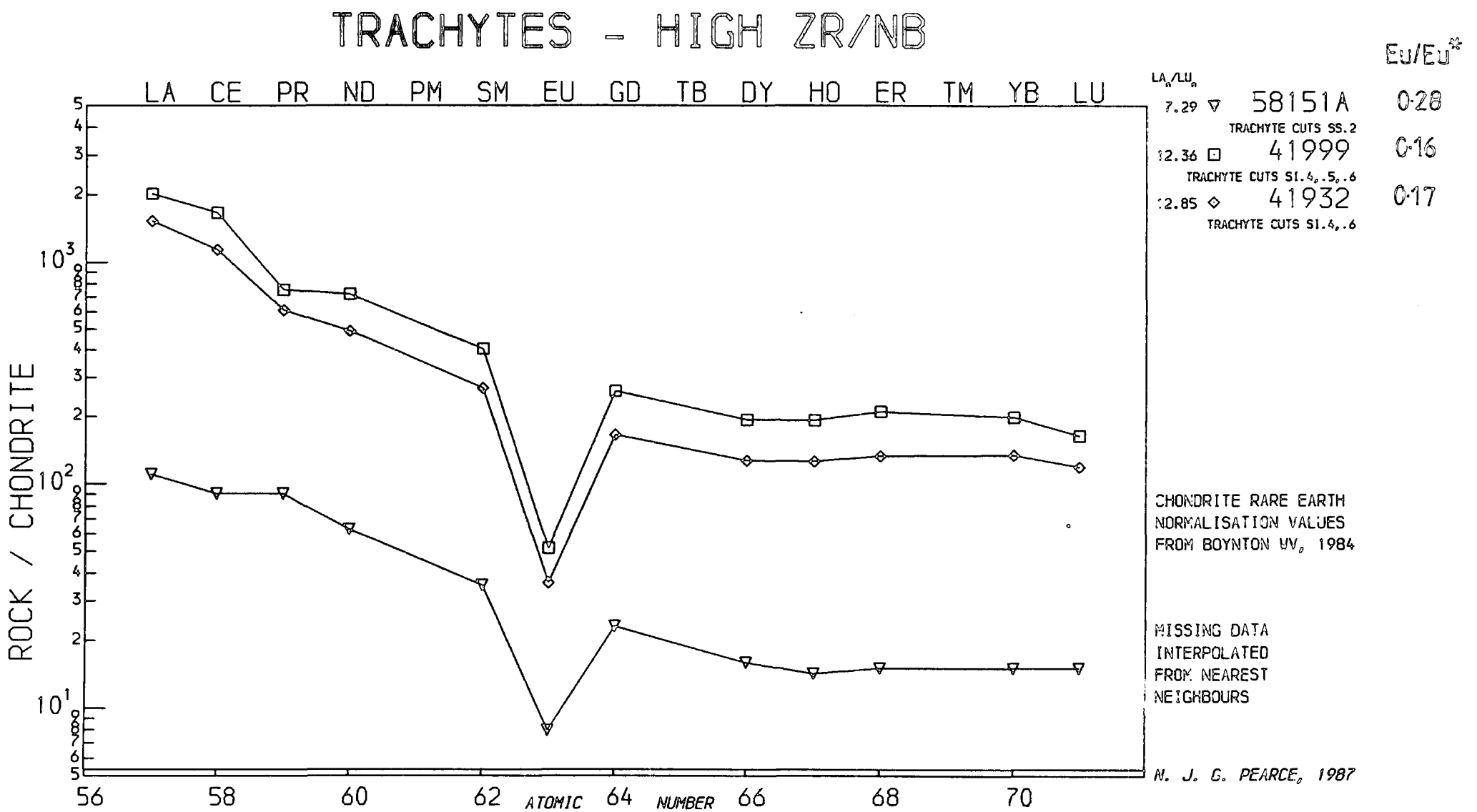
TRACHYTES - HIGH ZR/NB
LA CE PR ND PM SM EU GD TB DY HO ER TM YB LU
ROCK / CHONDRITE
ATOMIC NUMBER
56 58 60 62 64 66 68 70
LA_n/LU_n
Eu/Eu*
7.29 ▽ 58151A 0·28
TRACHYTE CUTS SS.2
12.36 □ 41999 0·16
TRACHYTE CUTS S1.4,.5,.6
12.85 ◇ 41932 0·17
TRACHYTE CUTS S1.4,.6
CHONDRITE RARE EARTH NORMALISATION VALUES FROM BOYNTON WV, 1984
MISSING DATA INTERPOLATED FROM NEAREST NEIGHBOURS
N. J. G. PEARCE, 1987

Figure 6.6.2

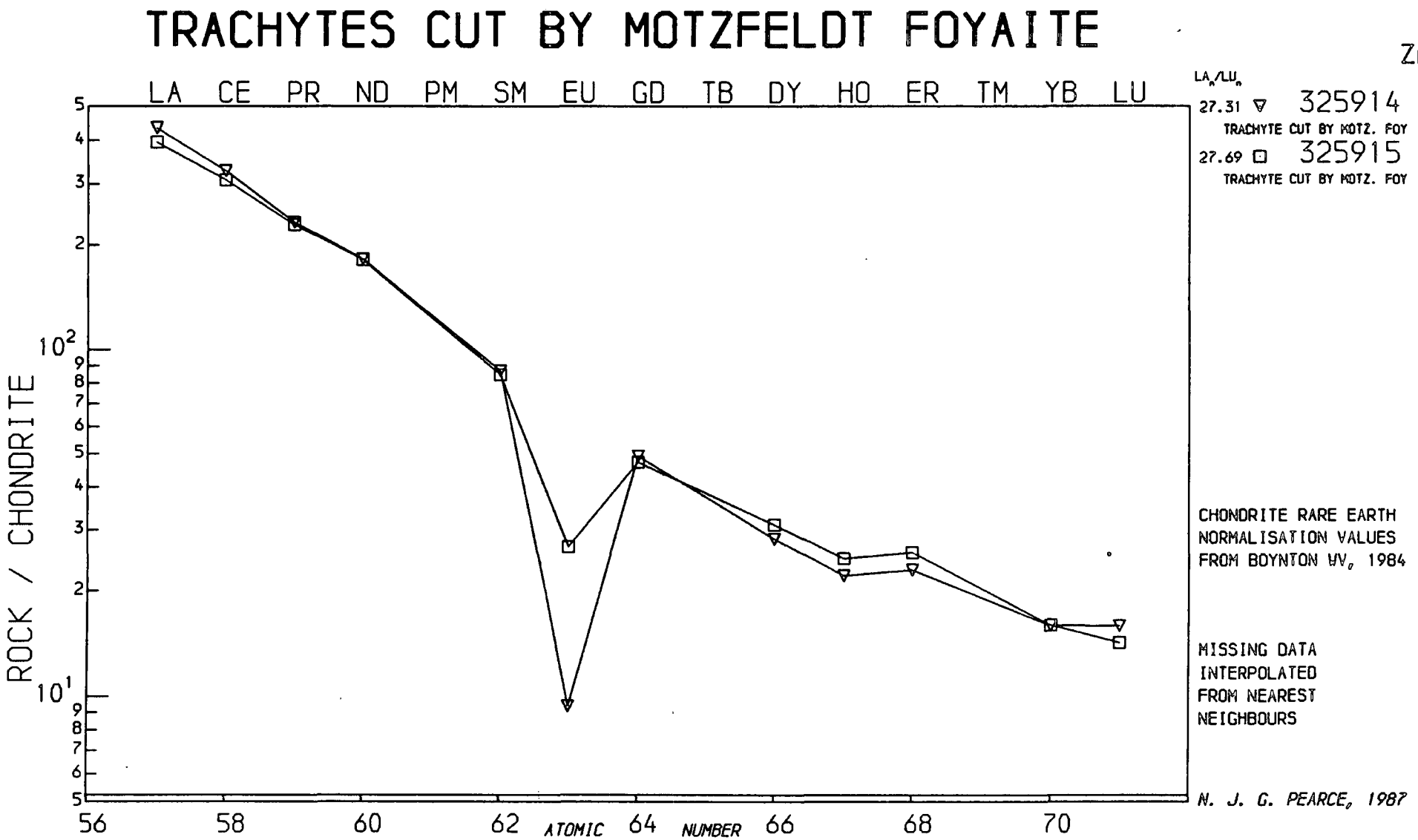
TRACHYTES CUT BY MOTZFELDT FOYAITE
LA CE PR ND PM SM EU GD TB DY HO ER TM YB LU
ROCK / CHONDRITE
ATOMIC NUMBER
56 58 60 62 64 66 68 70
Zr/Nb Eu/E
LA_N/LU_N
27.31 ▽ 325914 L 0·14
TRACHYTE CUT BY MOTZ. FOY
27.69 □ 325915 L 0·42
TRACHYTE CUT BY MOTZ. FOY
CHONDRITE RARE EARTH NORMALISATION VALUES FROM BOYNTON WV, 1984
MISSING DATA INTERPOLATED FROM NEAREST NEIGHBOURS
N. J. G. PEARCE, 1987

of the benmoreites, as well as being over twice that of the other trachytes. In absolute terms, they are less enriched in REE than most other benmoreites and trachytes, and show no flattening of the spidergram from Gd-Lu. These rocks have clearly fractionated feldspar and possibly pyroxene but probably only minor apatite (which would tend to flatten the MREE-HREE portion of the curve). There would thus appear to be some differences between the evolution of these early Gardar dykes and the majority of the (Late Gardar) dyke swarms.

6.7: Phonolites

Figure 6.7.1 shows spidergrams of REE from 6 phonolites, 3 of which show strong, negative Eu anomalies. None has a marked Ce anomaly (cf. benmoreites). They show a range of $(La/Lu)_{cn}$ from 2.33 to 33.28, but typical values are slightly over 20, slightly higher than $(La/Lu)_{cn}$ from typical low Zr/Nb (undersaturated) benmoreite. Absolute REE concentrations are similar to some of the more evolved benmoreites (see Figure 6.5.2B for comparison). An origin by fractionation of feldspar with minor pyroxene, olivine and perhaps some apatite from a benmoreite would produce the observed REE contents of the phonolites. Slightly steeper REE patterns may reflect lower contents of clinopyroxene and apatite in the fractionating assemblage. The lack of negative Eu anomalies is again a result of high fo_2, although 326380 and 326378 are both Sr and CO_2 rich samples. Philpotts (1970) suggests that due to the similarities in ionic radius of Sr and Eu^{2+}, they would show almost identical behaviour in natural rock systems. Koster van Groos (1975) showed Sr partitioned strongly into a carbonate phase that was immiscible with a phonolite and thus Eu^{2+} may be expected to follow suit. This would require a low fo_2 in the phonolite that yielded the CO_2-rich phase to reduce the Eu^{3+}/Eu^{2+} ratio. This carbonate-rich fluid would thus have to be enriched in Eu enough to exactly balance out the Eu anomaly of the rock which it subsequently invaded. This would seem unlikely and the lack of Eu anomaly is thus unrelated to the addition of a Sr and CO_2-bearing phase. CO_2 however will cause an increase in the a_{SiO_2} of a magma by depolymerising the melt (Mysen 1976). This in turn will cause an increase in fo_2 and maintain Eu mostly as Eu^{3+}, preventing the formation of substantial Eu anomalies. This is discussed further, with relation to carbonatite genesis in Chapter 7.

Figure 6.7.1

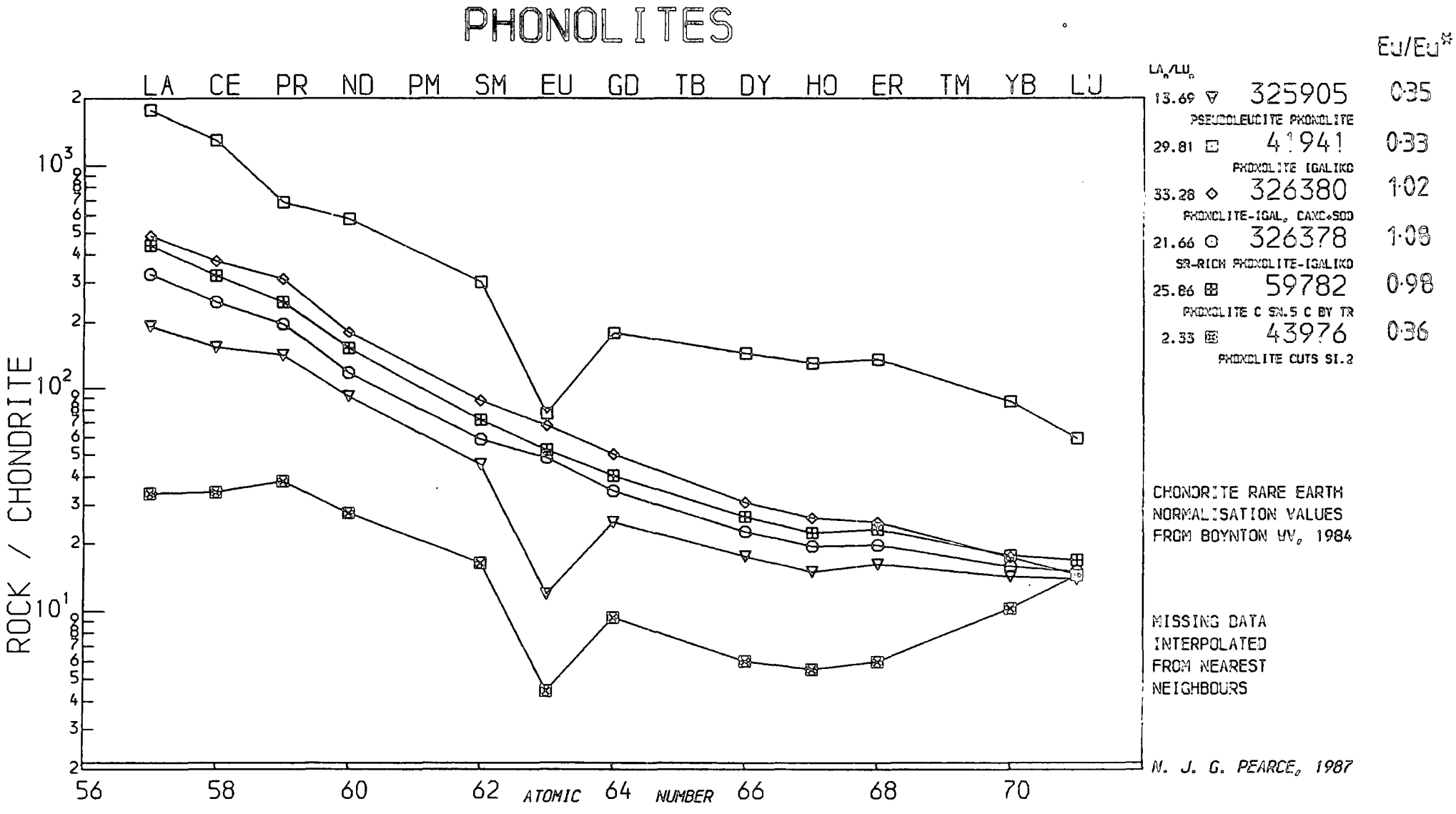
PHONOLITES
LA CE PR ND PM SM EU GD TB DY HO ER TM YB LU
ROCK / CHONDRITE
ATOMIC NUMBER
56 58 60 62 64 66 68 70
10^3 10^2 10^1
LA_n/LU_n
Eu/Eu*
13.69 ▽ 325905 0·35
PSEUDOLEUCITE PHONOLITE
29.81 □ 41941 0·33
PHONOLITE IGALIKO
33.28 ◇ 326380 1·02
PHONOLITE-IGAL, CANC+SOD
21.66 ○ 326378 1·08
SR-RICH PHONOLITE-IGALIKO
25.86 ⊠ 59782 0·98
PHONOLITE C SN.5 C BY TR
2.33 ⊠ 43976 0·36
PHONOLITE CUTS SI.2
CHONDRITE RARE EARTH
NORMALISATION VALUES
FROM BOYNTON WV, 1984
MISSING DATA
INTERPOLATED
FROM NEAREST
NEIGHBOURS
N. J. G. PEARCE, 1987

6.8: Igdlerfigssalik Syenite 6

For comparative purposes one REE analysis of a syenite from the Igdlerfigssalik centre was analysed, 41984, SI.6, a late ring dyke cropping out some 6km NE of Igaliko village (Emeleus and Harry 1970).

The sample has both low absolute REE concentrations and a very low normalised slope – $(La/Lu)_{cn} = 5.01$. The absolute concentrations of REE are similar to some of the lowest concentrations seen in phonolites and benmoreites. There is a marked upward curvature between Gd and Lu suggesting apatite and clinopyroxene fractionation as important processes (apatite fractionation could also account for the low absolute REE contents). A moderate negative Eu anomaly (0.42) is the result of feldspar extraction. Overall however, this is similar to many of the phonolite and benmoreite dykes, a result of the operation of similar processes during its genesis.

6.9: Conclusions

The REE data are consistent with the formation of parental basic melts by small degrees of partial melting of a 'fertile' and/or possibly incompatible element enriched mantle source. The high Zr/Nb rocks appear to have been generated from a garnet-free mantle source which may have become enriched by injection of small degrees of basanitic/kimberlitic magma (Hawkesworth *et al.* 1984). The low Zr/Nb suite was probably generated from a garnetiferous mantle source, by lesser degrees of partial melting than the high Zr/Nb suite. Some incompatible (LREE) element enrichment may have occurred in the source region of the low Zr/Nb suite but enrichment factors may have been less than for the high Zr/Nb suite.

Evolution of the swarm was achieved by fractional crystallisation of clinopyroxene at depth followed by olivine (which may be HREE enriched if Mg-rich – Schnetzler and Philpotts 1970 – although Henderson's 1982 data does not indicate this), plagioclase, lesser clinopyroxene (with a preference for MREE), and minor apatite at upper crustal levels. Oxides will have little effect on the REE contents. At later stages, apatite became a very important phase, fractionation of small quantities of which caused rapidly changing REE contents, and this, along with clinopyroxene, will cause a 'flattening off' of the MREE-HREE section of the normalised REE spidergram.

Figure 6.8.1

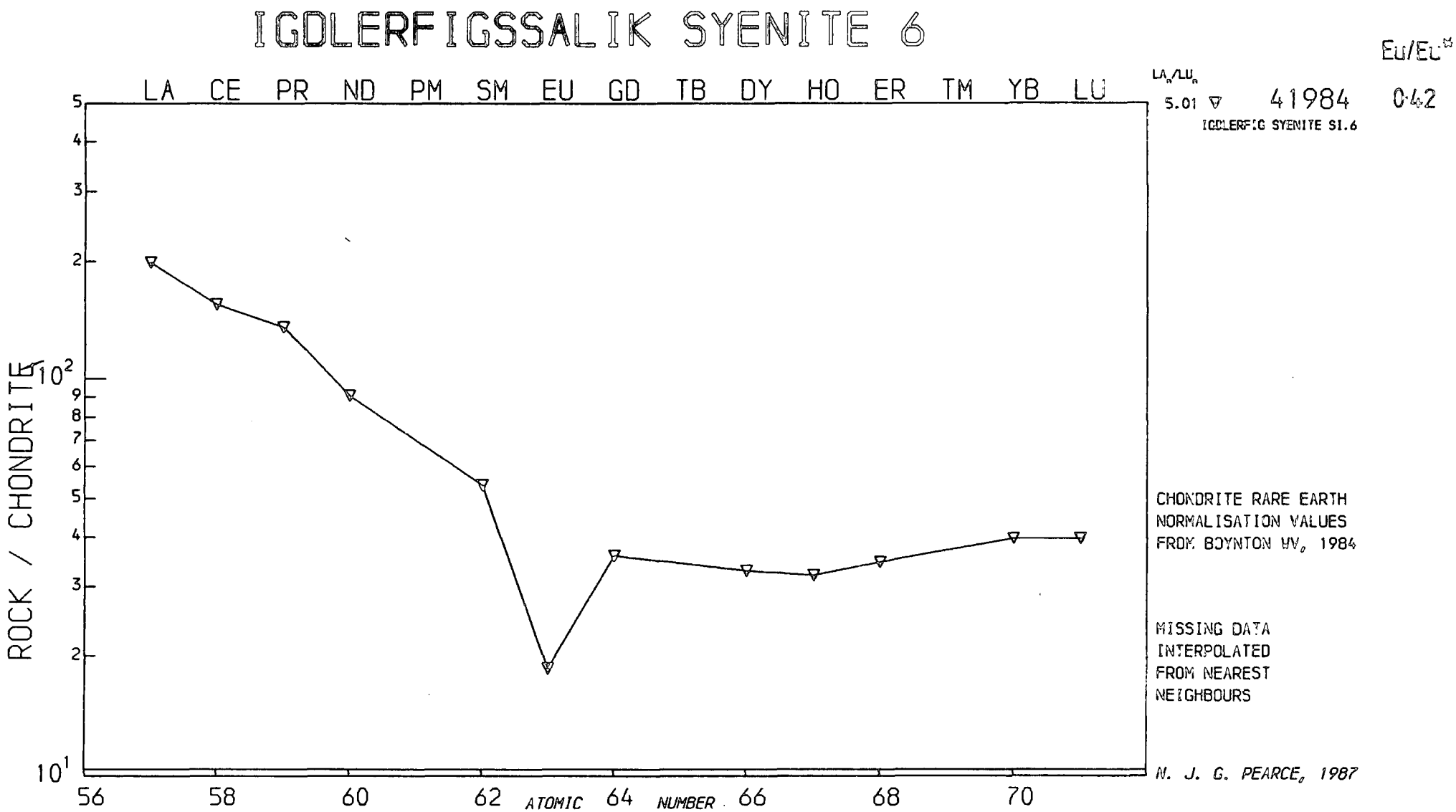
IGDLERFIGSSALIK SYENITE 6
LA CE PR ND PM SM EU GD TB DY HO ER TM YB LU
ROCK / CHONDRITE
10^2
10^1
5
4
3
2
9
8
7
6
56 58 60 62 ATOMIC 64 NUMBER 66 68 70
La_n/Lu_n
Eu/Eu*
5.01 41984 0·42
IGDLERFIG SYENITE SI.6
CHONDRITE RARE EARTH NORMALISATION VALUES FROM BOYNTON WV, 1984
MISSING DATA INTERPOLATED FROM NEAREST NEIGHBOURS
N. J. G. PEARCE, 1987

In low fo_2 conditions, where Eu^{2+}/Eu^{3+} is relatively high, large negative Eu anomalies develop. However, when fo_2 is high (as in the undersaturated suite of rocks) Eu^{2+}/Eu^{3+} will be low, Eu will not partition into feldspar preferentially over Sm and Gd, thus no Eu anomaly will develop.

High fo_2 may also have some effect on the behaviour of Ce, elevating Ce^{4+}/Ce^{3+} and possibly changing its bulk D characteristics compared to La and Pr. Thus, in high fo_2 suites of rocks Eu is not a good indicator of feldspar fractionation, $(Ce/Sr)_{cn}$ being a better indicator this process.

SECTION 3: OTHER OCCURRENCES

CHAPTER 7: CARBONATITES

7.1: Introduction and Field Occurrence

Carbonatites are defined as a group of igneous rocks which contain more than 50% of a carbonate mineral (Streckeisen 1980). Carbonatite is known from the Gardar province in a limited number of areas,

(i) Grønnedal-Íka (Emeleus 1964) – a carbonatite plug intrudes the central portion of a small nepheline syenite complex. This is currently being re-investigated by C. Bedford at Durham University.

(ii) Small occurrences of carbonatite occur as minor plugs and in volcanic breccias in the region of Qagssiarssuk (Stewart 1964) along with lamprophyric breccias. These occur at or near the base of the Eriksfjord Formation in this area. Numerous small carbonated diatremes/breccia pipes occur in the ground north of the river at Narssarssuaq, in Mellemlandet (Walton 1965), and a few cut the North Qôroq Centre.

(iii) Numerous small dykes and sheets of carbonatite occur in the Igaliko Nepheline Syenite complex, and form the basis of this chapter.

There are no other reports of carbonatite associated with any of the other central complexes in the Gardar province.

In the Igaliko area carbonatite dykes were initially described by Emeleus and Harry (1970). Relatively few samples were found by C.H. Emeleus and W.T. Harry during the 1960's. During the 1984 field season considerably more carbonatite material was encountered than had been expected, increasing its importance in the region. Carbonatite dykes tend to be among the latest representatives of igneous activity in the area, with many examples cutting the Late Igdlerfigssalik syenites. Several samples were also found in the Lower Flink's Dal area of the Motzfeldt centre (the author's Camp 2, 1984, see Figure 1.1.1). These Motzfeldt occurrences included a 1.5m thick sill of carbonatite and ultramafic lamprophyre extending laterally at least 200m.

As a general rule, carbonatite dykes are quite limited in their outcrop. They rarely exceed 2m in width and are usually traceable for only a few hundred metres. One example, the most persistent carbonatite dyke from this area (samples 325908 and 325910) was traced for 1.5km along strike with a typical width of 1.5-2m. Carbonatite dykes tend to be relatively soluble, hence a common feature of their outcrop is their occurrence in gullies. They can thus become overgrown and are not immediately obvious. Once this feature had been recognised these dykes were more easily located and it became apparent that they were more abundant than previously thought (see Emeleus and Harry 1970).

On the weathered surface carbonatite dykes are typically a deep, 'chocolate' brown or brown-green colour. These surfaces often show highly contorted flow-banding (see Plate 7.1). This is picked out by slight modal variation of the relatively soluble silicate minerals which stand proud of the surface on alteration (see Plate 7.2).

The carbonatites are for the most part very fresh, the newly broken surface often showing large, clear or white calcite crystals (up to 2mm across) with darker spots of silicate and opaque minerals (see Plate 7.6). Increased silicate content tends to darken the appearance of the fresh surface, as too does finer grain size. In some samples, fluorite is an important constituent, this occurring as distinct 'cubic' protrusions from the surface of sample 325910 (see Plates 7.3 and 7.4). 325908, a sample from the same dyke 1.5km away and about 200m lower, contains virtually no fluorite. The lighter F-rich fluids may have risen through the conduit during magma flow to accumulate at higher levels (possibly near to the top of the dyke).

Noticeably lacking from the country rock enclosing the dykes are obvious signs of fenitisation, this being commonly associated with carbonatite intrusions, (cf. Alnö, Von Eckermann 1948; Fen, Norway, Saether 1957 and Napak, E. Uganda, King 1949).

7.2: Petrography

The carbonate in the Igaliko dykes is most commonly calcite and thus these rocks are nearly all sövites or alvikites (coarse and medium-fine grained calcite carbonatites, nomenclature of Streckeisen 1980). Woolley (1982) has criticised this scheme, suggesting a classification based on whole rock CaO - MgO - ($FeO + Fe_2O_3$, + MnO)

contents. Using Woolley's scheme 14 carbonatites classify as sövites (or alvikites) and 13 as (calcium-rich) ferro-carbonatites (see Figure 7.4.1). Most of the carbonatites are coarse grained, with large, poly-synthetically twinned calcite crystals up to 4mm diameter in some cases (326333, see Plate 7.7 A and B). Carbonatites tend to have a granular texture with silicate minerals clustered along carbonate grain boundaries rather than being poikilitically enclosed by large calcites. No Mg or Fe carbonates have been found in any of the Igaliko carbonatites, although strontianite ($SrCO_3$) has been observed in minor amounts optically (326358, 325910; biaxial, negative, 2V=7°) and confirmed semi-quantitatively by microprobe analysis (325940). Strontianite has a similar birefringence to calcite, but seems to show less pronounced cleavage and twinning. It can thus be relatively easily discriminated from calcite in plane polarised light (see Plate 7.7A). No celestine ($BaCO_3$) has been recorded. Minor amounts of baryte ($BaSO_4$) have been detected in some samples (eg. 325910). No Ca-sulphates have been recorded.

Silicate mineralogies are varied, the major silicate phases being clinopyroxene and phlogopite. Pyroxene is typically pale green/brownish-green and weakly pleochroic, often rich in Mg and Mn (see later). Grain sizes rarely exceed 750μm. They are commonly rounded grains, often containing minor inclusions of apatite or opaque oxide (see Plate 7.8). Phlogopite forms as small grains (500μm as a maximum) scattered through many carbonatites (see Plates 7.10 and 7.11). It is almost colourless in some cases and at its most coloured is only a pale straw colour. There are no occurrences of deep red, reversely pleochroic tetraferriphlogopite (cf. Fen, where this is common in the sövite) although in one dyke (326329, 54243/4) pale straw-coloured, reverse pleochroic phlogopite does occur. The presence of pale, normally pleochroic phlogopite indicates sufficient Al_2O_3 in the magma to prevent substitution of Fe^{3+} for Al in the mica. In some cases phlogopite is the only silicate phase (eg. 326359).

Apatite is the most abundant non-silicate after calcite, occurring in many samples modally up to ≈5%, and occasionally more. It forms stubby euhedra/subhedra and is often enclosed poikilitically by either the calcite (see Plates 7.7 and 7.8) or the silicate phases. Apatite therefore appears to have been one of the first phases to crystallise.

Opaque oxides are also common, occurring in similar quantities to apatite. These form anything from small euhedral to rounded anhedral grains or aggregates. Occa-

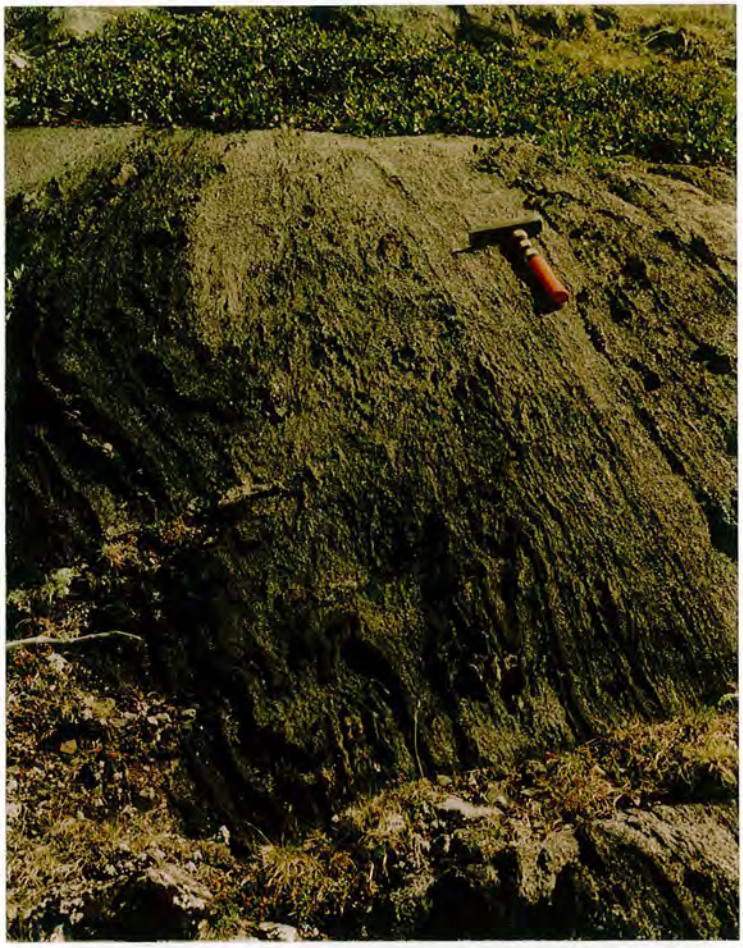

Plate 7.1: Flow-banding in carbonatite dyke (sample 54243, 54244, 326329). Contorted flow-banding is picked out on weathering by small modal variations in silicate content, increased silicate content producing the proud ridges. The deep 'chocolate' colour of the weathered surface is typical.

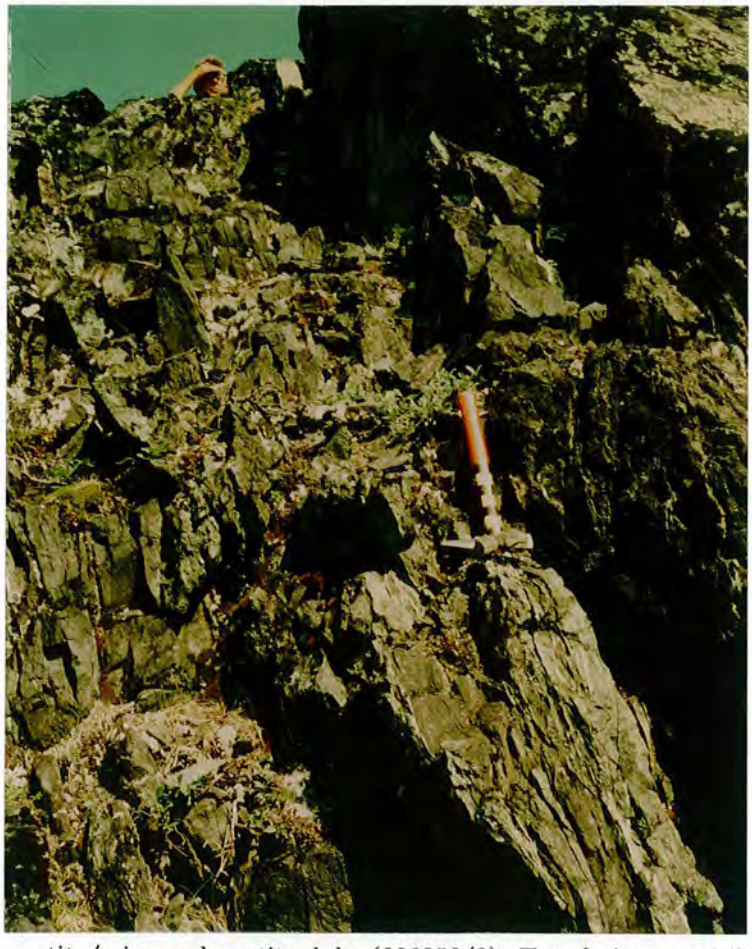

Plate 7.2: Carbonatite/mica carbonatite dyke (326358/9). Two facies are visible in this dyke, a silicate-poor facies (darker chocolate colour) and a silica-rich facies (pale green in colour, see Plate 7.10 and 7.11). The silicate rich portion of the dyke contains large amounts of phlogopite and iron oxide.

Plate 7.3: Flow banding in fluorite-carbonatite 325910. This carbonatite cuts through a trachytic dyke, parts of which can be seen on either side of the carbonatite.

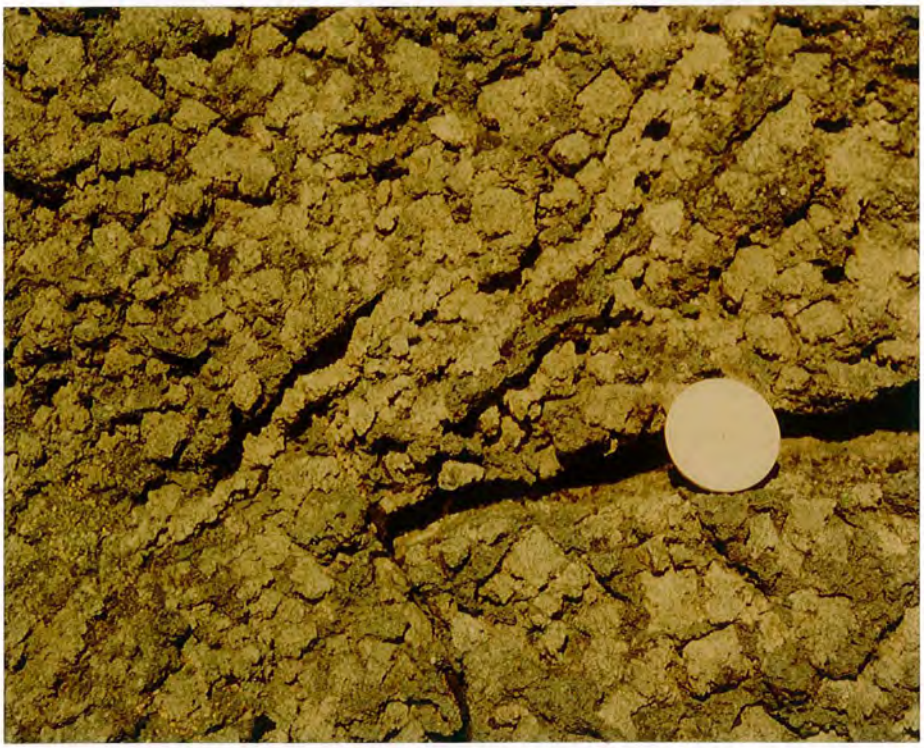

Plate 7.4: Close up of the surface of 325910 showing well developed fluorite cubes that weather to a pale yellow colour and stand proud of the surface.

Plate 7.5: 1.5m thick carbonatite/UML sill in the Lower Flinks Dal area, Motzfeldt centre, (326258-60).

Plate 7.6.: Hand specimen of 326333, fresh surface. This is a coarse grained carbonatite showing large plates of white calcite and darker spots of silicate and opaque oxide.

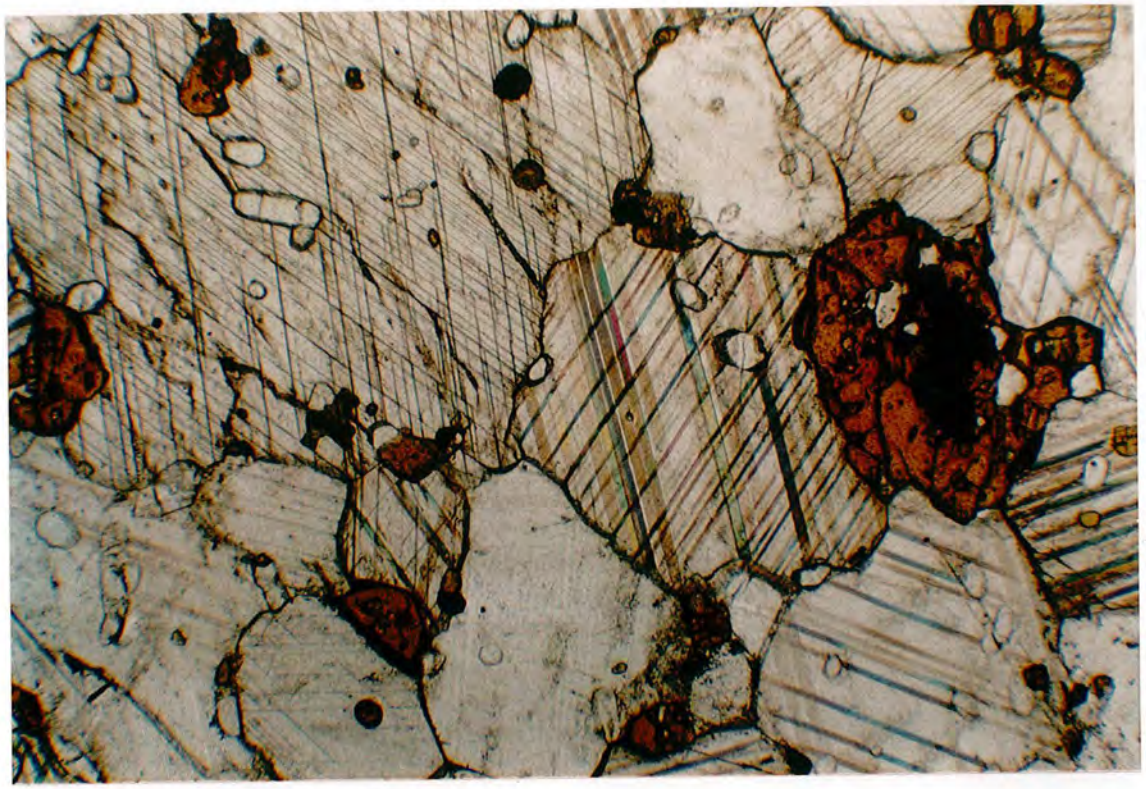

Plate 7.7A: 326333, Carbonatite, PPL ×35

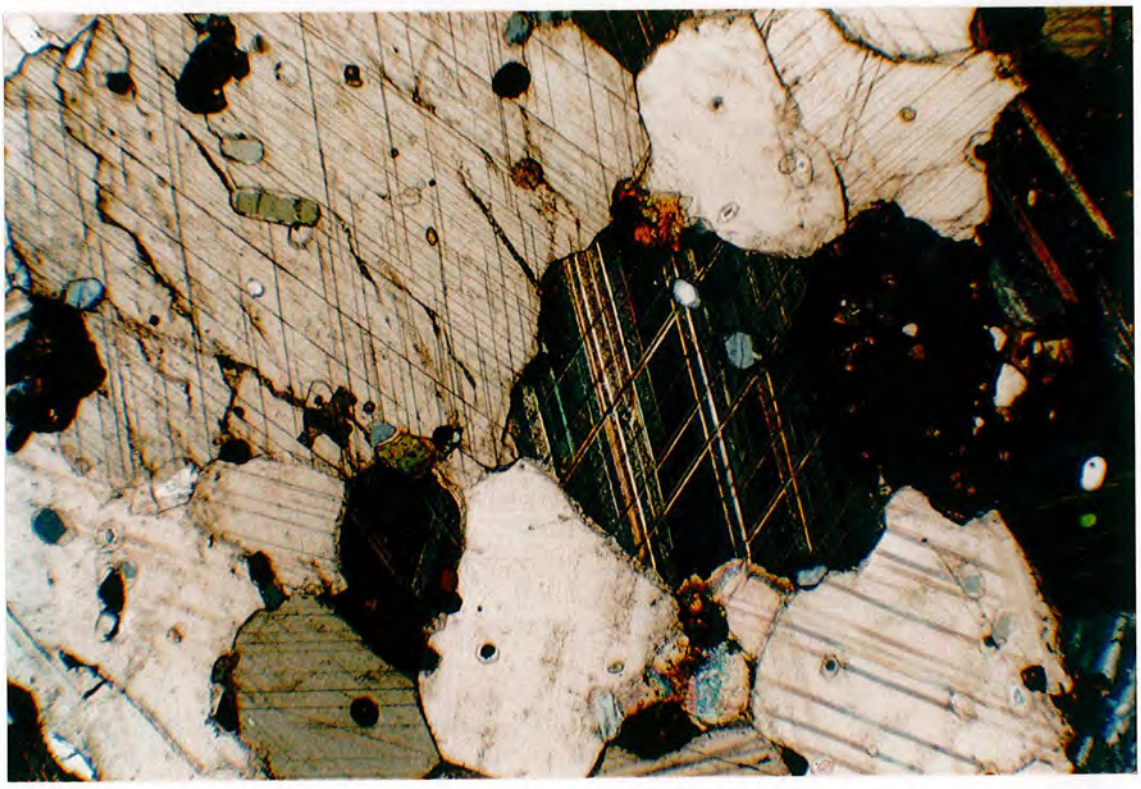

Plate 7.7B: Carbonatite 326333, XPL, ×35. The major mineral phase is calcite showing a good cleavage and polysynthetic twinning. A large garnet (greenish-brown andradite) is seen centre right with smaller garnets to the left. These rim(?) opaque oxides (see text) and often enclose small, stubby apatites. The clear, uncoloured, untwinned mineral to the to left of the largest garnet is strontianite, (biaxial, 2V≈7°). The small, greenish-birefringent minerals (green-brown in PPL) are Mn-rich clinopyroxenes).

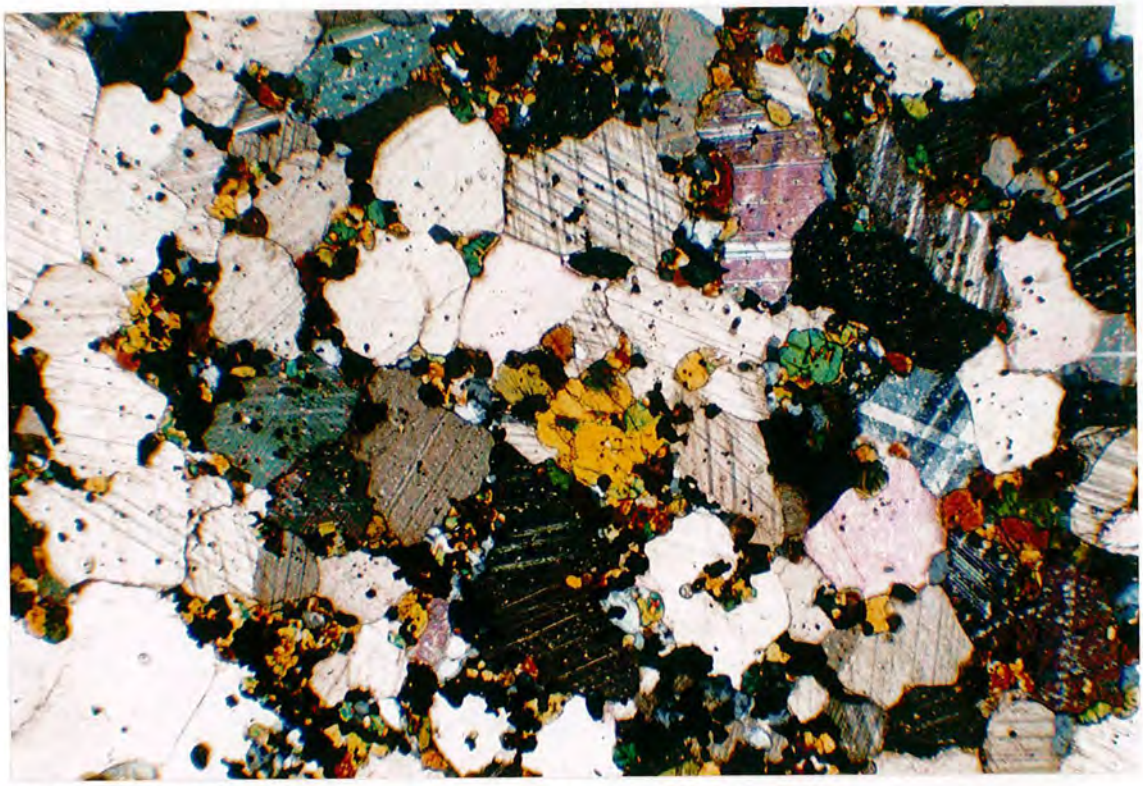

Plate 7.8: 326336, carbonatite, XPL, ×35. Mostly composed of calcite, this sample also contains clinopyroxene (blue-green-yellow interference colours) occasionally as granular aggregates, and opaque oxides. Apatite is a minor phase. This is a typical example of a carbonatite from the Igaliko area.

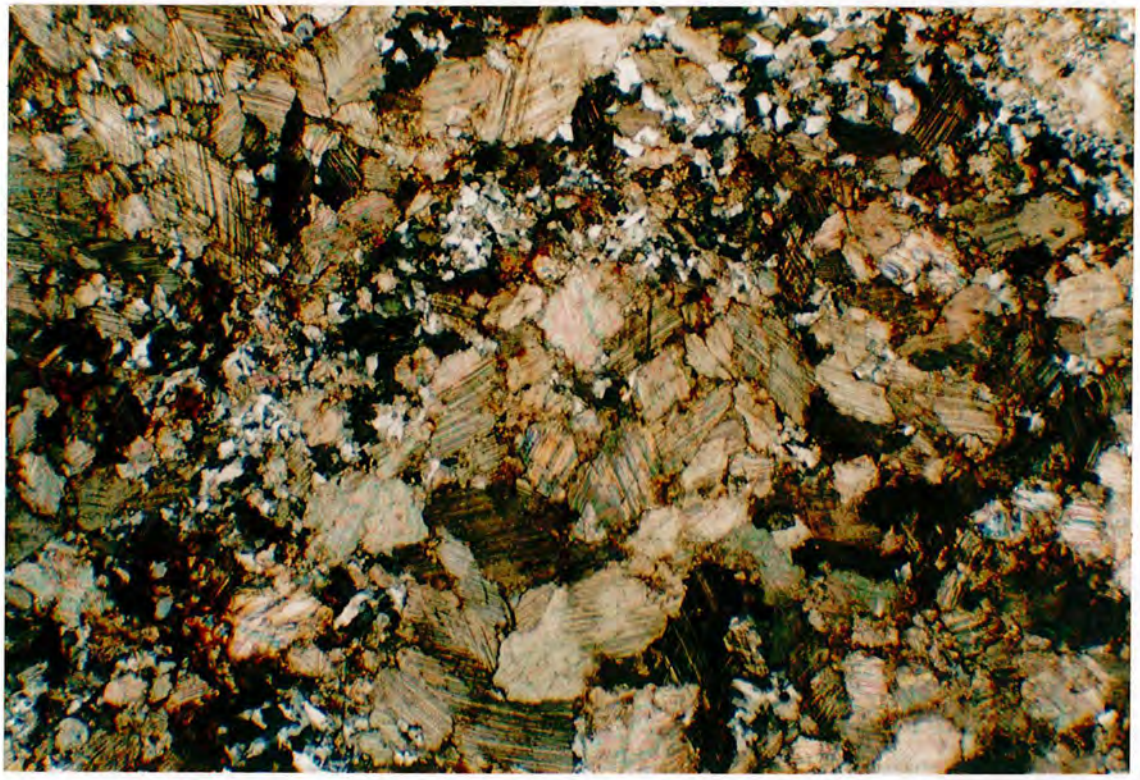

Plate 7.9: 326302, carbonatite, XPL, ×35. This carbonatite from Østfjordsdal is atypical, being the only sample from Igaliko to contain feldspar (albite, black/white interference colours). This is the most Si-rich carbonatite from the area. No silicates other than feldspar are seen. Opaque oxides are rare. The calcite also shows strain deformation of twin lamellae, and this may be a result of emplacement as a crystal 'mush'.

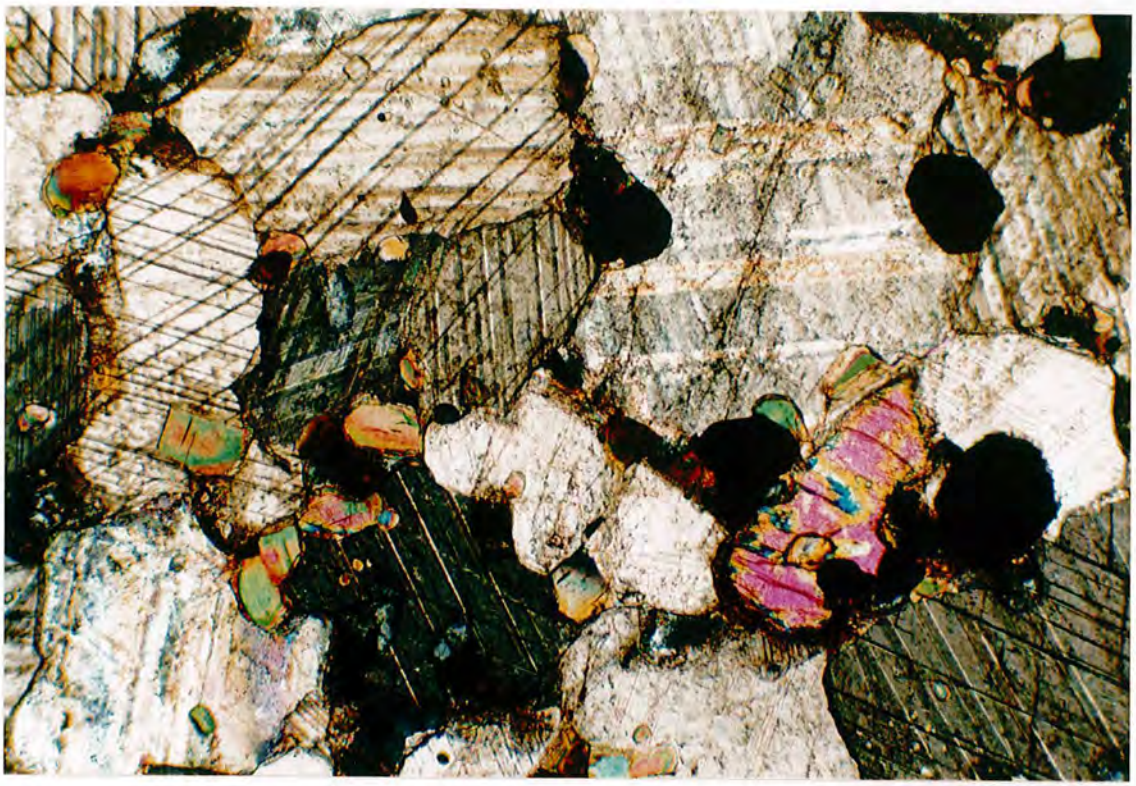

Plate 7.10: 326358, carbonatite, XPL, ×35.Predominantly calcite, this sample also contains Mn-rich pyroxene (large blue-pink grain, lower right) and small grains of phlogopite (greenish-brown, well cleaved, lower centre left). Euhedral iron oxides are scattered throughout the sample as too are small, stubby apatites.

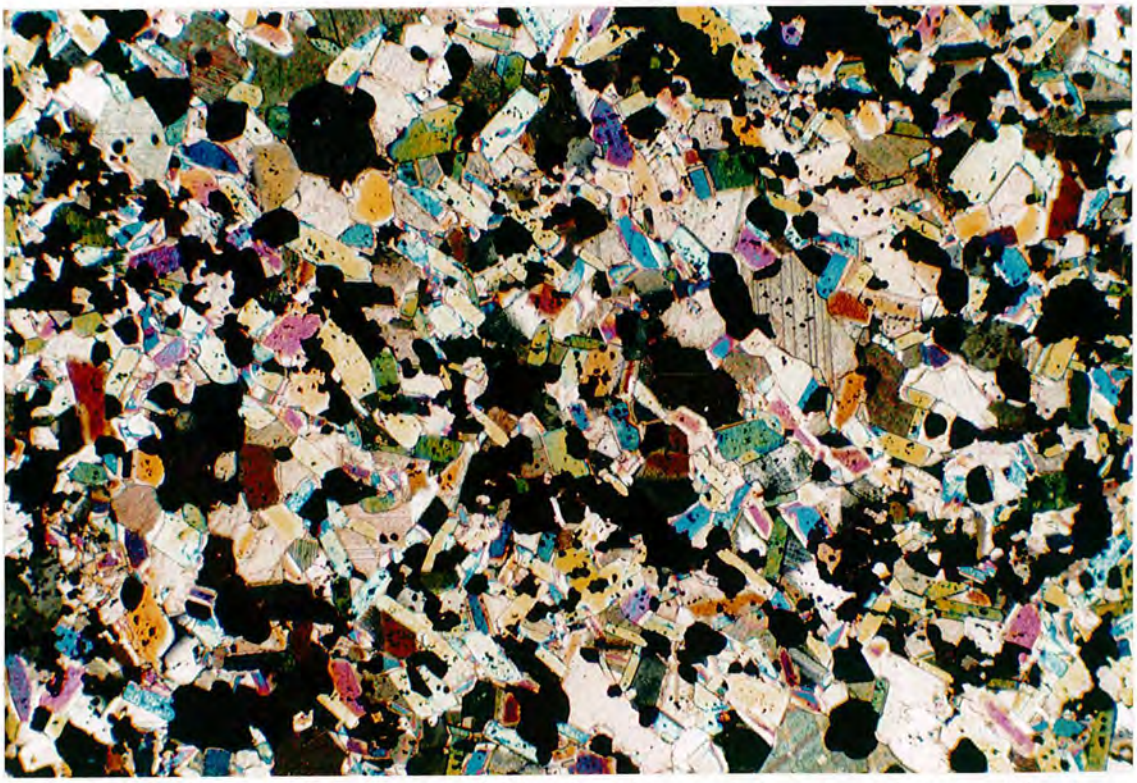

Plate 7.11: 326359, mica-rich carbonatite, XPL, ×35. This sample is a mica-rich facies of the above dyke (see also Plate 7.2). It lacks pyroxene and is composed mostly of Ba-rich phlogopite, iron oxide and carbonate. According to the classification of Streckeisen (1980) this sample is strictly not a carbonatite (<50% calcite), although is considered here due to its similarity to other carbonatites.

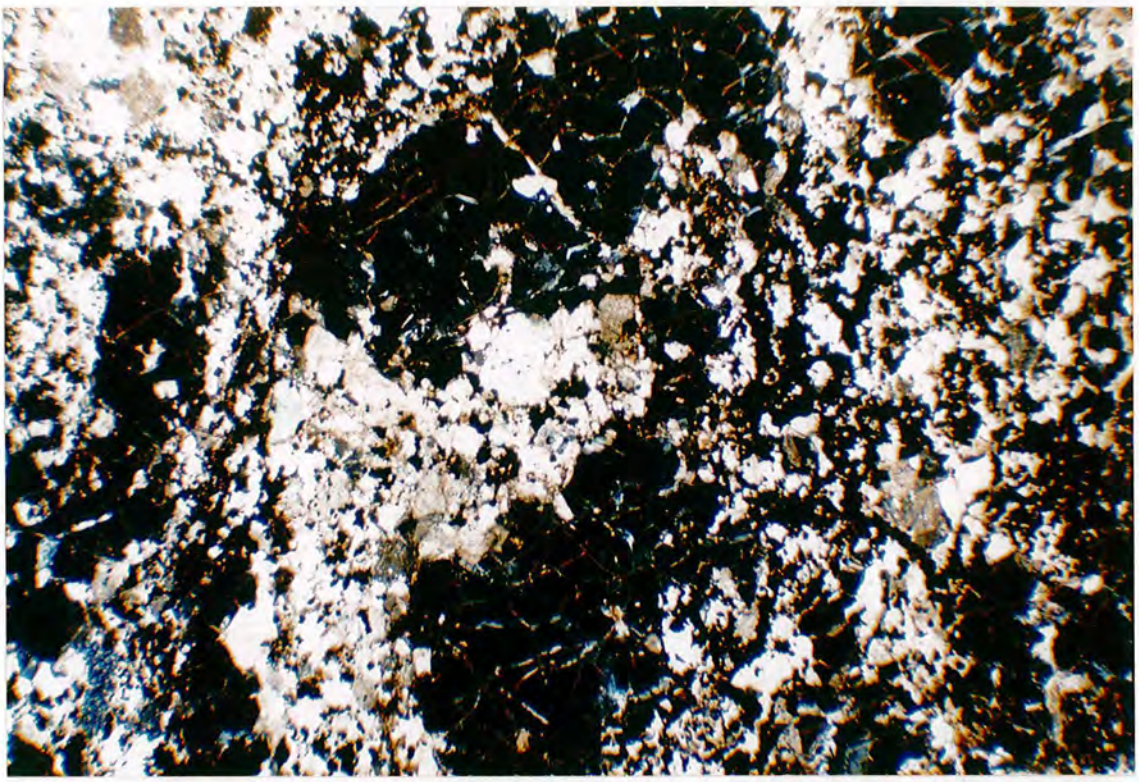

Plate 7.12: 326388, fluorite-carbonatite, XPL, ×35. This sample is composed of calcite (pale pink hues) and fluorite (large amorphous isotropic patches) in roughly equal proportion. Fine felted masses of altered opaque oxides are seen (reddish-browns). No fresh silicates are visible.

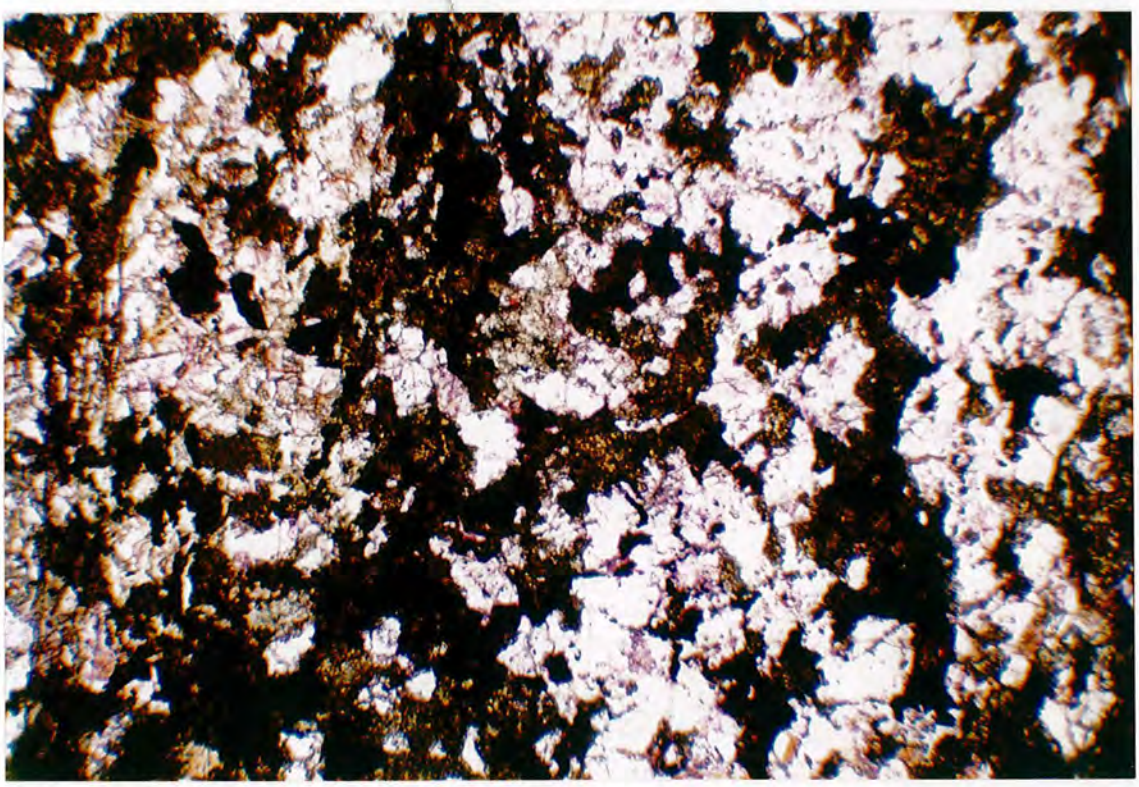

Plate 7.13: 326395, fluorite rock, PPL, ×35. Similar to a carbonatite in field appearance and chemistry, this sample contains no carbonate and is thus F-rich instead of CO_2-rich. Fluorite has a pale purple to clear colour. The dark minerals are chlorite (altered silicates?) and opaque oxides. In other similar F-rich samples baryte has been identified. These rocks represent late stage carbonatite activity.

sional skeletal crystals are also seen, comparing closely in appearance with the stratiform magnetite crystals described by Deans and Seager (1978).

There is a very wide range of accessory minerals which occur in the carbonatites. Fluorite forms up to about 50% modally in 325910 and 326338, either as irregular, large patches in the groundmass or as well formed cubes which weather proud of the surface (see Plates 7.4, 7.11, 7.12). Chlorite occurs commonly as a felted alteration product in the groundmass. In particularly altered samples chlorite may be the only silicate. Perovskite ($CaTiO_3$, deep brown, almost isotropic) is seen in a few samples, a testament, if it needs to be stressed, to the low a_{SiO_2} in these magmas. Olivine (and in many cases, iddingsite after olivine) have also been recorded from several samples. These are usually badly corroded, small and irregularly shaped crystals. Albite has only been observed in two samples. In 326302 (see Plate 7.9) it is the sole silicate phase, comprising about 25% of the mode. This sample must have had relatively high a_{SiO_2}, although it contains only $\approx$8.6 wt% SiO_2.

Amphiboles, of the iron - manganese - magnesium association (Leake 1978) have been observed in some samples. These too are often corroded, and are pleochroic in dark green-browns. In 326333, a very fresh sövite, pale, green-yellow andradite garnet ($Ca_3Fe_2^{3+}Si_3O_{12}$) is present, alongside pyroxene. The garnet often contains inclusions of apatite or iron oxide (see Plate 7.7 A and B) and is the most abundant silicate phase in this sample.

Due to the high contents of elements such as REE, U, Th, Nb, minor amounts of bastnäsite ((LREE)FCO_3, small, reddish grains, weakly pleochroic) and pyrochlore (deep red-brown pleochroic, needles/rhombs, $NaCa(Nb,Ta)_2O_6F$) can be identified with certainty. There are also many amorphous minerals with an altered, iron-stained appearance (possibly metamict) occurring between grains which could not be identified optically. No Zr-bearing phase was seen in any samples.

In contrast to the common granular texture, rarer, rather sheared samples are observed with deformed and bent twinning seen in all the groundmass calcite. These samples are often free from silicate minerals. This sheared appearance would be consistent with their emplacement as a crystal mush, lubricated by trapped pockets or thin

films of carbonatite magma.

7.3: Mineralogy

The mineralogy and mineral chemistry of carbonatites generally reflects the rather unusual bulk rock geochemistry. Sr, Ba, REE, Nb, Th, U may all substitute into many of the phases present in varying degrees, as well as being major constituents of certain minerals. High Ca, Mn, and low alkalis and Al are typical of the major element chemistry of most of the minerals present. It was hoped to present a reasonably complete picture of the carbonatite mineral chemistry. However, the EDS microprobe used at Manchester University was not standardised for Sr, Nb, Th, U, REE, with the WDS probe there not standardised for REE at the time of use. Thus many of the analyses made which showed the presence of these elements could not record their quantities. Consequently only partial analyses of many phases were obtained particularly for apatite (often REE-rich) and calcite (Sr-rich). Time did not permit reanalysing on the Durham WDS probe which, although accurately standardised for REE, Nb, U, Th (see Jones 1980) is very slow for these elements. Many of these partial analyses will be discussed and listed in this section and are not included in the analytical appendix. Regrettably a full and complete account of the mineralogy cannot be presented, although enough data exist to provide a reasonable cover.

7.3.A: Pyroxene

Pyroxene is the most abundant silicate phase in the carbonatites. It is often pale green/greenish-yellow and is usually weakly pleochroic suggesting the presence of some alkalis. Figure 7.3.1 shows all carbonatite pyroxenes plotted in terms of Mg – (Fe^{2+} + Mn) –Na and Mg – (Fe^{2+} + Fe^{3+}) – Mn. For comparison, the pyroxene trend from Ugandan alkali complexes and a field for Ugandan carbonatites reported by Tyler and King (1967) are shown. In general, the pyroxenes are diopsides or salites, with only a few aegirine-augites. They do not contain the alkali content that their green colour would suggest. The diopsidic pyroxenes are almost colourless.

The pyroxenes from the Igaliko carbonatites are significantly less alkali rich than those from Uganda (Tyler and King 1967), with some showing a very similar evolution to the early part of the pyroxene trend from the Igaliko phonolite dykes (see Chapter

4).

Almost all the pyroxenes have Ca + Na atoms $\approx 1 \pm 0.02$, and this implies almost no orthopyroxene component (Ca-poor) in solid solution, hardly surprising in such a calcic environment. No other pyroxenes were recorded from any samples.

Many of the pyroxenes are strongly enriched in Mn (see Figure 7.3.1) with MnO contents reaching 8.8 wt%. Of the 24 analyses for pyroxene only 6 have MnO<4 wt% with 9 analyses having MnO>6 wt%. Mn thus reaches 0.288 atoms per formula unit (representing 32 mol% of johannsenite, $CaMnSi_2O_6$). High Mn contents are achieved at low Fe enrichment, with Mn apparently entering the pyroxene in similar quantities to total Fe, both substituting for Mg. Deer *et al.* (1966, 1978) suggest that complete solid solution is likely between $CaFeSi_2O_6$ and $CaMnSi_2O_6$, and Winchell and Winchell (1951) indicate complete solid solution between diopside ($CaMgSi_2O_6$) and johannsenite, which is also stressed by Heubner (1980). The major substitution is thus probably $2Mg \rightleftharpoons Fe^{2+}+Mn$, with only minor substitution of $2Mg \rightleftharpoons Fe^{3+}+Na$. It is also possible that Mn may enter pyroxene as $NaMn^{3+}Si_2O_6$ – manganacmite – (see Heubner 1980). None of the analyses have $Fe^{3+} << Na$, which may imply the presence of another trivalent phase (Mn^{3+}?). Mn may also replace Ca as well as Mg (Vinokurov 1966).The high Mn content in these pyroxenes reflects an overall high MnO content in these rocks and they resemble Mn-rich pyroxenes from skarn rocks at Altan Topkan, Central Asia (Zharikov and Vlasova 1955). As a rule the pyroxenes were too small to check for zoning from core to rim. Zoning is not visible optically in any of the pyroxenes analysed and none was detected in the few core and rim analyses made.

None of the pyroxenes contain detectable Ti (ie. $TiO_2 \leq 0.25$ wt %), and all contain less than 0.65 wt% Al_2O_3. The lack of Ti reflects the highly evolved nature of the magmas, and both the low Ti and Al are reflections of their overall low bulk rock contents of these elements.

7.3.B: Phlogopite

After pyroxene, the second most abundant silicate is phlogopite mica. These all show normal pleochroism (pale straw-brown to almost colourless) with the exception of one sample where the pleochroism is reversed, although still pale in colour. All but one

Figure 7.3.1: Pyroxene analyses from carbonatite dykes.

A. Mg – (Fe^{2+}+Mn) – Na.

For comparison the carbonatite field of pyroxene analyses from Uganda (Tyler and King 1967) and their overall trend is shown. Pyroxenes from the Igaliko carbonatites are much less sodic than these African examples. Some of the more Fe(+Mn) rich pyroxenes seem to follow the early parts of the pyroxene trend observed in the Igaliko phonolites.

B. Mg – (Fe^{2+}+Fe^{3+}) – Mn.

Mn becomes very enriched in these pyroxenes. This data would suggest an overall exchange mechanism of 2Mg $\rightleftharpoons$ Fe+Mn.

Figure 7.3.1

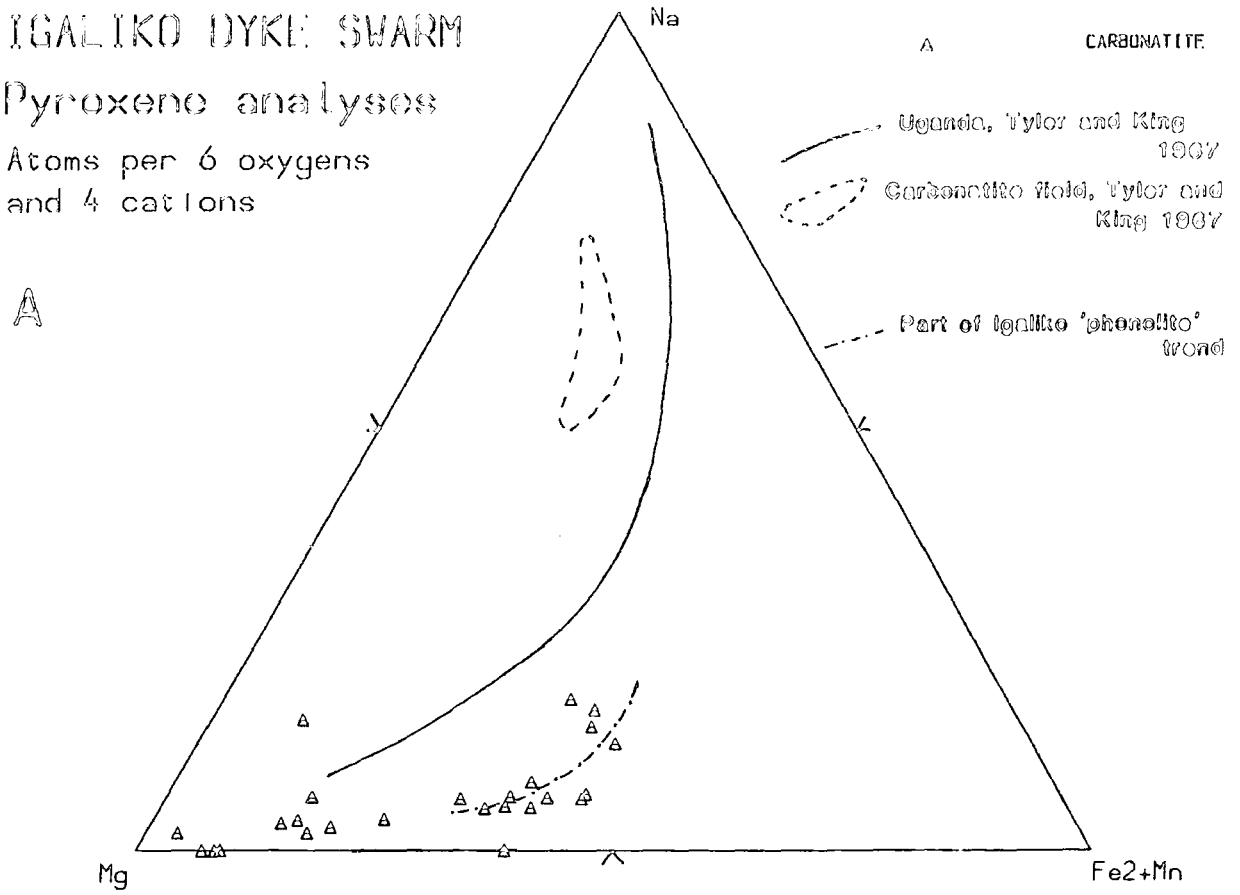
IGALIKO DYKE SWARM
Pyroxene analyses
Atoms per 6 oxygens
and 4 cations
A
Na
Mg
Fe2+Mn
CARBONATITE
Uganda, Tylor and King 1967
Carbonatite field, Tylor and King 1967
Part of Igaliko 'phonolite' trend

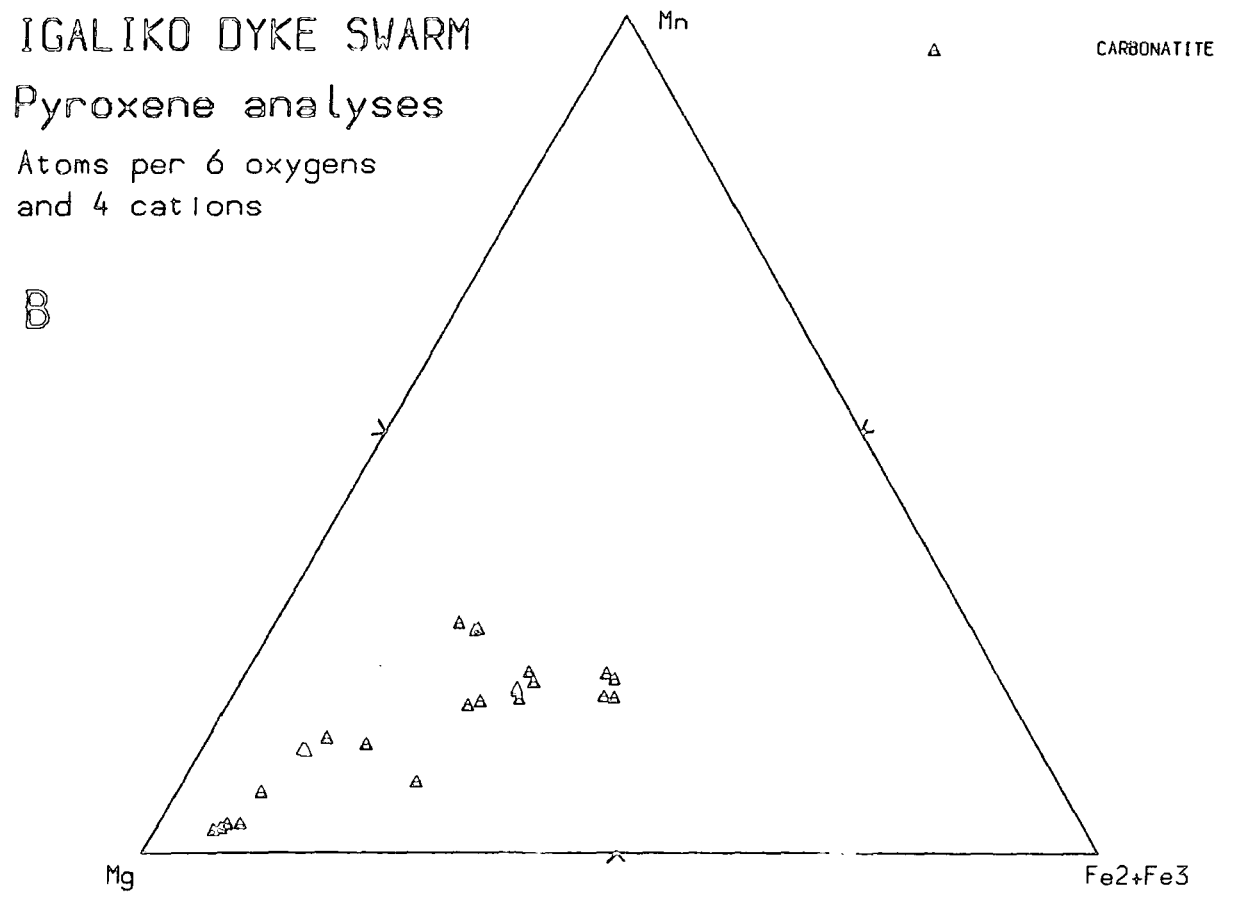
IGALIKO DYKE SWARM
Pyroxene analyses
Atoms per 6 oxygens
and 4 cations
B
Mn
Mg
Fe2+Fe3
CARBONATITE

of the mica analyses from carbonatites are phlogopites according to the classification of Deer *et al.* (1966), where Fe/Fe+Mg (atoms per 22 oxygens) <0.333 (see Figure 7.3.2A), and all but 2 having Fe/Fe+Mg (atoms) <0.2. These are thus all very Mg-rich micas, more so than any from the basalt to phonolite or rhyolite associations. They show similar degrees of MnO enrichment to the micas from the phonolites (maximum 2.10 wt%) but this is achieved at considerably lower Fe than the phonolite micas with substitution of (Fe,Mn) $\rightleftharpoons$ Mg occurring rather than Mn $\rightleftharpoons$ Fe, a result of the generally high activity if MnO in the magmas. Some micas however, contain no MnO. Smith *et al.* (1983) concluded that octahedral Mn^{2+} in conjunction with tetrahedral Fe^{3+} in phlogopites was the cause of the intense reverse pleochroism seen in the samples they studied. Normal pleochroism was a result of both Mn^{2+} and Fe^{3+} in octahedral coordination, and for the most part this would seem to be the case here, with most of the tetrahedral sites occupied by Si and Al.

The phlogopites are usually Ti-free although in a few samples Ti is present, reaching 2.13 wt% TiO_2. This is a result of the usually low bulk rock TiO_2. Phlogopites from the Safartôq carbonatite contain up to 1.79 wt% (Secher and Larsen 1980).

One of the more unusual aspects of the phlogopite compositions are their high content of Ba (up to 9.26 wt% BaO, see Figure 7.3.2C which shows BaO wt% vs. FeO/(FeO+MgO) as wt%). This compares closely with 10.03 wt% reported from the Jacupiranga carbonatite by Gaspar and Wyllie (1982). Other high BaO contents are recorded from a leucitite (7.32 wt%, Thompson 1977) and from a monticellite peridotite (8.62 wt%, Wendlandt 1977).

Both Wendlandt (1977) and Gaspar and Wyllie (1982) advocate a substitution mechanism of $Al^{3+} + Ba^{2+} \rightleftharpoons Si^{4+} + K^{+}$. It was suggested in Chapter 4.5 that Ba substitution may be achieved by $Ba^{2+} + \sqcup \rightleftharpoons 2K^{+}$ (where $\sqcup$ represents a vacancy in the large 12 coordinated site). Figure 7.3.2B shows K vs. Ba as atoms. A similar 2K:Ba relationship is evident at Ba$\leq$0.3 and the above mechanism $Ba^{2+} + \sqcup \rightleftharpoons 2K^{+}$ may still operate. Above Ba $\approx$0.3 atoms, $K^{+} \rightleftharpoons Ba^{2+}$ with charge balancing by $Si^{4+} \rightleftharpoons Al^{3+}$ may be dominant as K and Ba exchange in a near 1:1 ratio. In some samples (eg. 127052, which shows phlogopites with Ba at 0.548, 0.48, 0.402, 0.207 and 0.076 atoms per 22 oxygens) the most Ba-rich examples have highest Al and lowest Si, sug-

Figure 7.3.2 (2 pages)

A. Mica compositions in terms of Al^{iv} vs. Fe/Fe+Mg as atoms per 22 oxygens. The dashed horizontal line marks the suggested boundary between phlogopite and biotite of Deer *et al.* (1966). It is clear that almost all micas from carbonatites are very Mg-rich and thus phlogopites.

B. K vs. Ba in phlogopites. At relatively low Ba contents, substitution may be governed by $2K \rightleftharpoons Ba^{2+}+\sqcup$ (ie. 2K:Ba) where $\sqcup$ represents a vacancy (cf. Chapter 4). However, at higher Ba contents the relationship between K and Ba (ie. K:Ba) may suggest a coupled substitution of $Ba^{2+}+Al^{3+} \rightleftharpoons K^{+}+Si^{4+}$ (cf. Gaspar and Wyllie 1982).

C. (Overleaf). Ba wt% vs. FeO/FeO+MgO. The highest Ba contents occur in the most Mg rich micas. The dashed field shows the compositional range for phlogopites from Jacupiranga (Gaspar and Wyllie 1982).

Figure 7.3.2A

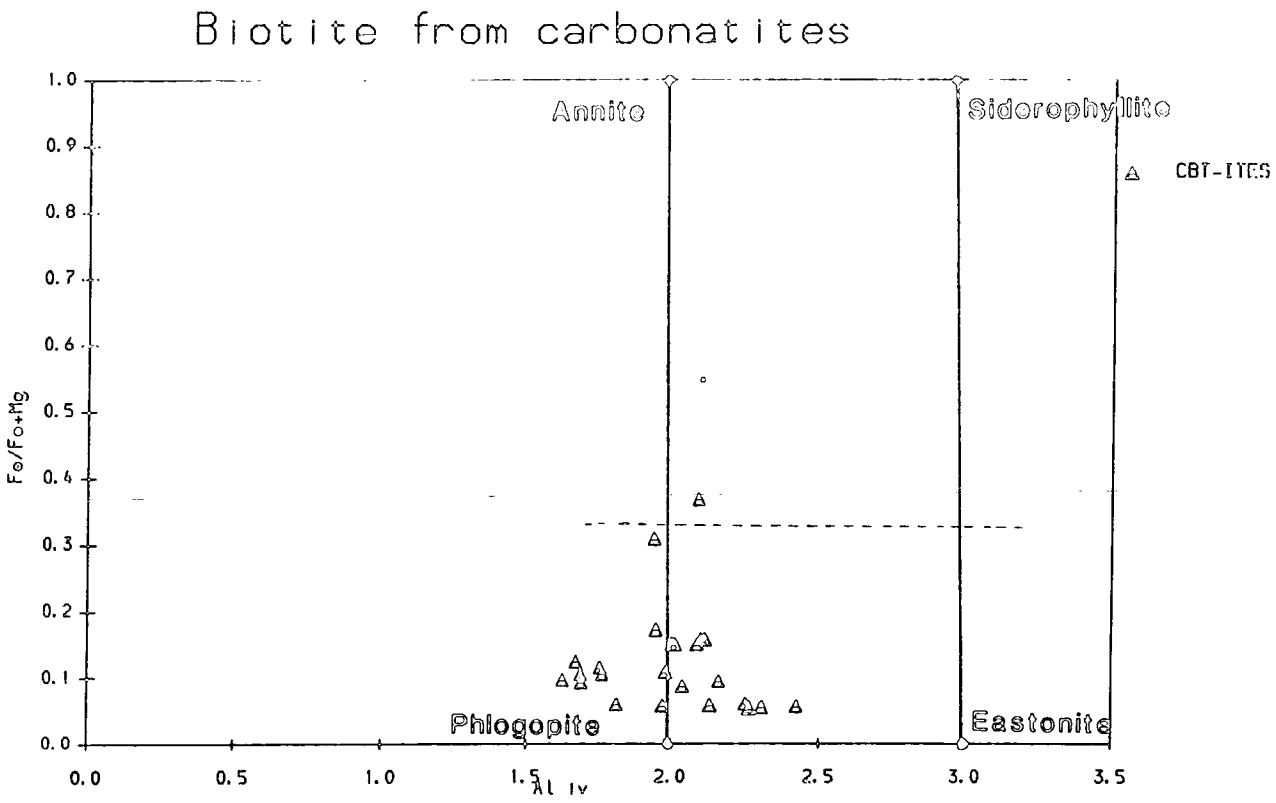

Figure 7.3.2B

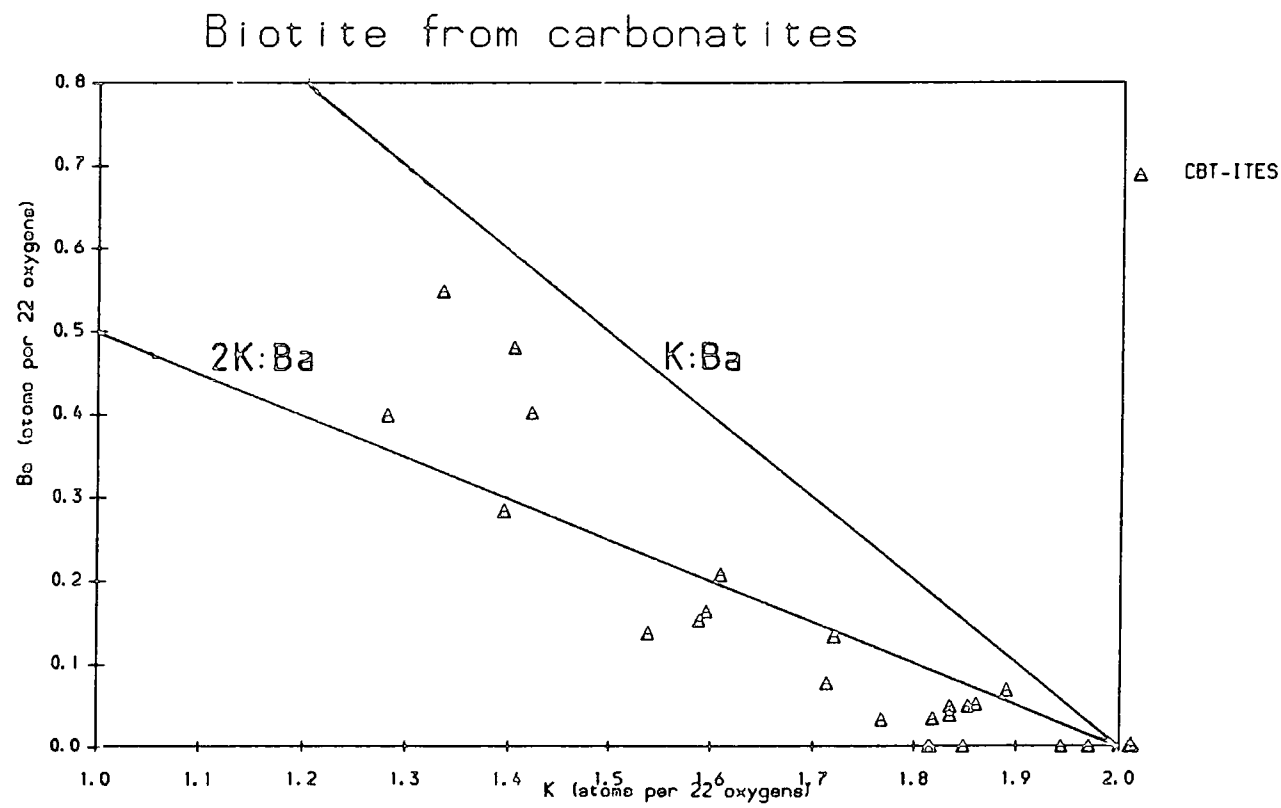

Figure 7.3.2C

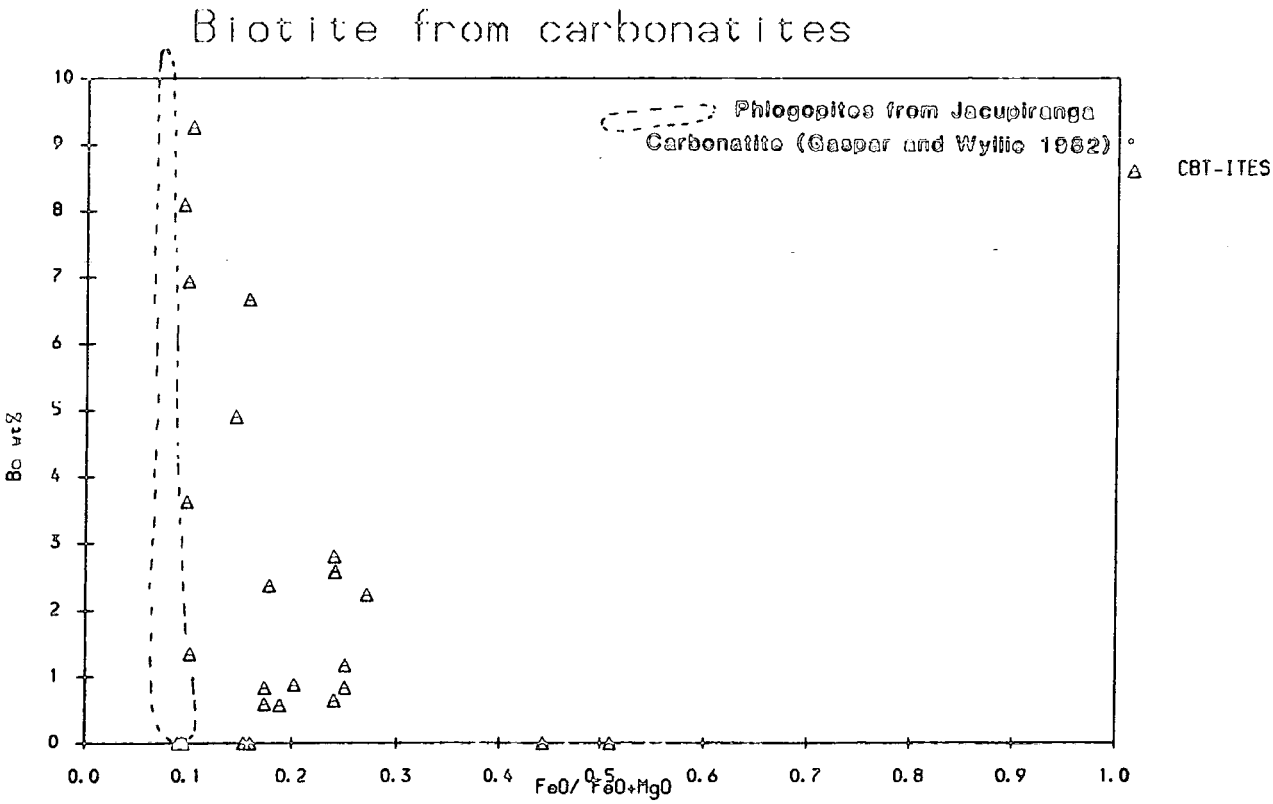
Biotite from carbonatites
Phlogopites from Jacupiranga Carbonatite (Gaspar and Wyllie 1982)
CBT-ITES
BaO wt%
FeO/FeO+MgO
0
1
2
3
4
5
6
7
8
9
10
0.0
0.1
0.2
0.3
0.4
0.5
0.6
0.7
0.8
0.9
1.0

gesting this coupled substitution operates at least for the high Ba micas. Ba contents of the mica reflect bulk rock Ba contents (127052, 6011ppm Ba, up to 9.26 wt% BaO in phlogopite, 46257, 187ppm Ba, no detectable BaO in phlogopite). Due to the small size of these grains, none was checked for zoning.

7.3.C: Oxides

All opaque oxides analysed are members of the magnetite–ulvospinel solid solution series. All but two samples have compositions in the range Mt_{100} – $Mt_{95.6}$. These other 2 samples (from 326359, a phlogopite – oxide – carbonatite) have the composition $Mt_{79.4}$–$Mt_{77.6}$. This sample is perhaps borderline between carbonatites (petrographically classified, ie. 50% carbonate) and ultramafic lamprophyres – ≈15% SiO_2, 18.5% CaO, 3.8% K_2O, 12.12% MgO). It occurs in a dyke with two distinct facies – this phlogopite-perovskite-carbonatite and a normal sövite (chemically and petrographically). For present purposes it will be regarded as a fine grained, calcite carbonatite (alvikite). This sample also contains the most magnesian oxides (up to 4.63 wt%, ≡0.213 atoms per 4 oxygens). Others contain MgO contents between 0.0 and 1.45 wt%, (0-0.08 atoms/4 oxygens). In this respect the bulk of these samples contain considerably less MgO than magnetites from Jacupiranga (where only 11 analyses from 48 contain less than 4 wt% MgO, reaching a maximum of 9.94 wt%, Gaspar and Wyllie 1983). MgO is similar to those of magnetites from the Safartôq carbonatite (Secher and Larsen 1980).

As with the other minerals mentioned thus far, Mn is an important component of many magnetites, reaching 6.74 wt% MnO in 54244 (≡ 0.214 atoms/4 oxygens, see Figure 7.3.3). Mn^{2+} occurs in a simple exchange for Fe^{2+}.

MnO is considerably higher in these magnetites than those from Jacupiranga (all <1.52 wt%, Gaspar and Wyllie 1983) and Safartôq (Secher and Larsen 1980). This once again reflects high bulk rock MnO although magnetite MnO contents are no higher than those from the silicate dykes. TiO_2 is typically low in magnetites. In all samples except 326359, the phlogopite and oxide-rich carbonatite, TiO_2 is less than 1.32 wt%. In 326359 however, TiO_2 reaches 2.01 wt%. This reflects the generally low TiO_2 contents of these carbonatite rocks.

Figure 7.3.3

$Fe^{2+}+Fe^{3+}$ vs. Mn in magnetites. There is a general antithetic relationship between total Fe and Mn in the magnetites from carbonatites.

Figure 7.3.4

Olivine compositions from carbonatite 41958. 2 analyses of olivine are plotted in terms of Ca - Fe - Mn. Their composition can be represented by the molecules fayalite, kirschsteinite ($CaFeSiO_4$ – the iron equivalent of monticellite), and glaucochroite ($CaMnSiO_4$). See text for discussion.

Figure 7.3.3

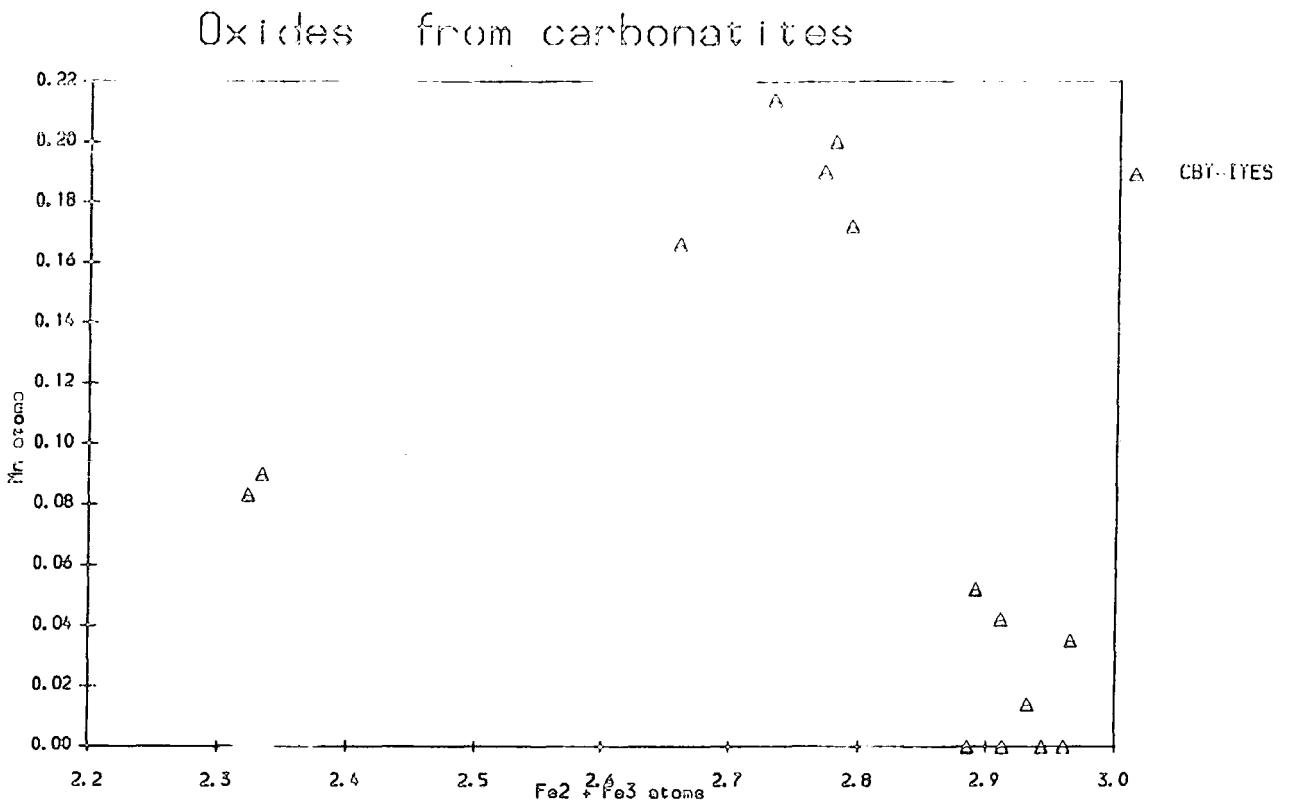

Figure 7.3.4

Olivine compositions

from 41958 in terms of Fe-Mn-Ca

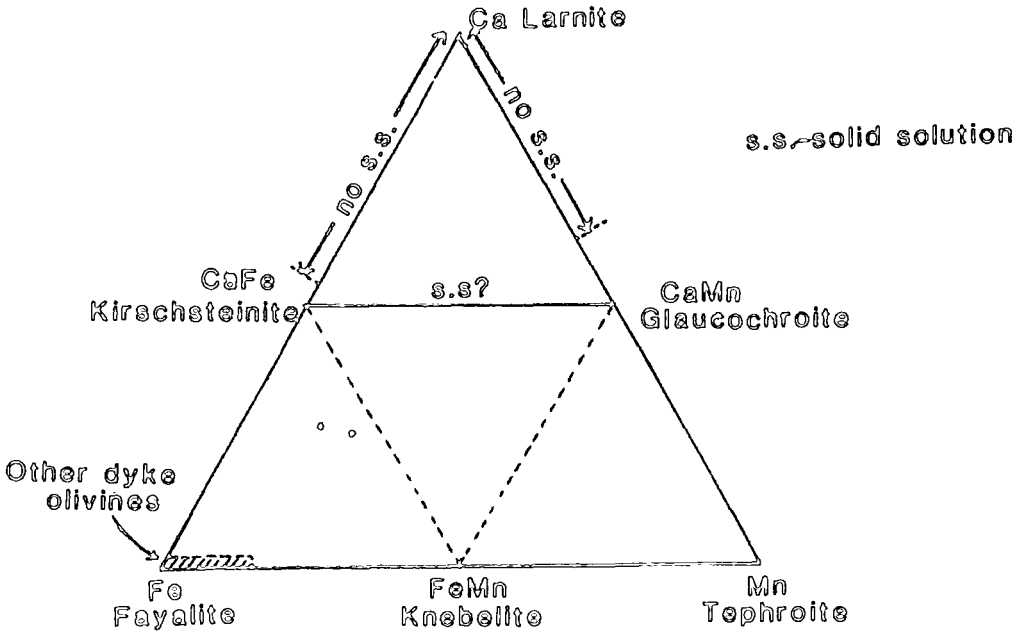

No ilmenites were recorded in any samples, unlike many other carbonatite complexes where ilmenite is a relatively common phase (Safartôq, Jacupiranga and Fen – Von Eckermann 1948).

7.3.D: Amphibole

Although amphibole is an important mineral in many carbonatite complexes (see for example Le Bas 1977, 1981, 1987; Twyman and Gittins 1987), often occurring to the exclusion of pyroxene (eg. Safartôq, Secher and Larsen 1980), it is only encountered in a very small number of the Igaliko carbonatites. 5 analyses of amphibole have been made, 3 from 326323 and 2 from 54275.

Those from 326323 are members of the iron – magnesium – manganese group of amphiboles (Leake 1978) and are manganese magnesio-anthophyllite according to the Leake classification. Recalculation of total Fe to Fe^{3+}/Fe^{2+} by the T+C=13 method (see Chapter 4.4) requires almost all Mn to be assigned to Mn^{3+} along with all Fe to Fe^{3+} to balance the calculation. These are thus almost devoid of Fe^{2+}. The two analyses from 54275 are manganoan subcalcic silicic edenite and manganoan richterite.

Once again Mn is an important constituent of these minerals (8.75-9.01 wt% MnO in 326323, 3.38-3.8 wt% MnO in 54275). They contain no Ti, with low total alkalis (≈1 wt% Na_2O+K_2O) in 326323 and low K_2O, moderate Na_2O in 54275 (0-78-0.81 wt% and 4.86-5.29 wt% respectively). This generally low alkali content reflects a general deficiency in alkalis in these carbonatite rocks.

7.3.E: Garnet

Pale yellow-green andradite garnet ($Ca_3Fe_2^{3+}Si_3O_{12}$) was recorded in carbonatite 326333, occurring alongside Mn-rich pyroxene, apatite and opaque oxides with apatite and rarely iron oxide occurring as inclusions in the garnets (see Plates 7.7A and B). Fe^{3+} ranges from 1.939-2.010 atoms/12 oxygens, and Ca from 2.766-2.817. Fe^{3+} is present in (and almost fills) the 6-coordinated Y site (garnet general formula, $X_3Y_2Z_3O_{12}$). Ca and Mn will both occupy (and together fill) the 8-coordinated X site, implying the presence of a small component of the calderite end member (up to 12.5 mol% of $Mn_3Fe_2^{3+}Si_3O_{12}$, see Deer *et al.* 1962). Minor quantities of Al and Ti are recorded and

these will reside, along with Si, in the 4-coordinated Z site. MgO was recorded up to 0.20 wt% in 2 of the analyses.

Melanite (Ti-rich andradite) is commonly reported as a constituent mineral of carbonatites (see Le Bas 1977). However, andradite from carbonatite is (as far as the author is aware) reported from only one other occurrence (Dixon and Collins in Le Bas 1977, p183). In this occurrence (an alvikite from the Ruri complex, Western Kenya) andradite occurs as rims to magnetite crystals, probably a late reaction product. This relationship is not apparent from 326333, although numerous apatites and rare (as in Plate 7.7) iron oxide inclusions are evident. Texturally, in the Igaliko case andradite would appear to be a primary mineral.

7.3.F: Chlorite

Chlorite forms as an abundant silicate in several samples. 3 analyses were made from 326247. They show MgO/(MgO+FeO) of 0.52 to 0.59 and are thus generally more magnesian than chlorites from the rest of the dykes. MnO contents are relatively high (2.25-3.44 wt%). K_2O and Na_2O are very low (both less than 0.43 wt% in all analyses).

7.3.G: Olivine

Fresh olivine was analysed in 2 samples; 41958 and 127052. From 127052, a composition of $Fo_{87}Fa_6Tp_5$ was recorded, high Mn for such low Fe, suggesting exchange of $2Mg \rightleftharpoons Fe+Mn$, similar to the pyroxenes. The olivines from 41958 were however considerably different. They are magnesium free and contain 13.48-14.13 wt% CaO, and 8.79-11.25 wt% MnO, giving cell formulae of $Fe_{59.3}Mn_{16.1}Ca_{24.5}$ and $Fe_{60.6}Mn_{12.6}Ca_{25.7}$ representing end members of fayalite, tephroite and larnite.

Complete solid solution at 1 atmosphere pressure has been shown to exist for Mg_2SiO_4–Mn_2SiO_4 (Glasser and Osborn 1960). Limited solid solution occurs between Ca_2SiO_4 and Fe_2SiO_4 (with up to 63% substitution of Ca for Fe, Bowen *et al.* 1933). The high Ca content of these olivines is obviously a result of extreme bulk rock CaO, their lack of Mg possibly a result of no solid solution existing between Ca_2SiO_4 and Mg_2SiO_4 (see Brown 1982). These olivines may indicate the existence of solid solution

between kirschsteinite , the natural analogue of iron-monticellite ($CaFeSiO_4$, Sahama and Hytonen 1957), glaucochroite ($CaMnSiO_4$, Palache 1937) and fayalite (Fe_2SiO_4), although their compositions are resolvable in terms of $CaFeSiO_4$ – Fe_2SiO_4 – $FeMnSiO_4$ (knebelite). This still implies Ca ⇌ Mn. Figure 7.3.4 shows the composition of these olivines in terms of Fe–Mn–Ca, plotted with a field showing all other olivines analysed from the dykes. A dark brown alteration product, tentatively identified as a Mn-rich iddingsite, has been analysed from one sample (54275) and contains 27.77 wt% MnO.

7.3.H: Perovskite

3 analyses of perovskite ($CaTiO_3$) were made from 326359. They have the composition $Ca_{1.005-0.982}Ti_{0.984}Fe_{0.011-0.025}O_3$. A minor exchange of Ca ⇌ Fe would appear to operate. Their presence attests to the thoroughly Si-deficient nature of these magmas. Many cases of perovskite occurrence are reported from nephelinite and other rocks of the nephelinite-carbonatite association, but none actually from carbonatite (sövites etc.) by Le Bas (1977).

7.3.I: Partially analysed minerals

The following section deals with a qualitative account of some other mineral species encountered in carbonatites which, due to the elements available for analysis on the probe, were only partially analysed. Time did not allow complete analyses for these minerals to be performed at Durham and these should provide scope for some interesting studies in the future.

Carbonates

Calcite, hitherto unmentioned, is the most abundant mineral in the carbonatites. The calcites almost always contain appreciable Sr (not analysed) along with Fe, Mg and Mn in solid solution. Le Bas (1987) reports ≈0.7 wt% SrO in calcites from natrocarbonatites from Kerismasi, E. Africa. Strontianite also occurs as a primary carbonate in many samples, containing some Ca, minor Ba (1.8 wt% BaO) and Na (0.42 wt% Na_2O) in solid solution.

Some partial analyses of calcites are given in Appendix II. Table 7.3.1 shows selected analyses in terms of Ca, Mg, Mn, Fe and Ba as atoms per formula unit. Sr is usually

Table 7.3.1

Partial analyses of calcite – atoms per formula unit.

	325910	326358	326358	326336	326336	54244	54244	46257
Ca	0.932	0.993	0.990	0.976	0.977	0.968	0.968	0.950
Mg	0.006	0.000	0.005	0.000	0.000	0.008	0.007	0.000
Fe	0.000	0.000	0.000	0.000	0.000	0.000	0.000	0.015
Mn	0.057	0.007	0.005	0.017	0.016	0.020	0.021	0.035
Ba	0.005	0.000	0.000	0.007	0.007	0.004	0.004	0.000
Sr	mod	high	high +Zn	mod	mod	high	high	low
	46256	326323	326388	41958	58254	326347	54275	326333
Ca	0.994	0.977	0.958	0.975	0.974	0.968	0.967	0.992
Mg	0.006	0.000	0.008	0.000	0.011	0.005	0.008	0.000
Fe	0.000	0.000	0.004	0.000	0.004	0.013	0.000	0.000
Mn	0.000	0.023	0.026	0.025	0.005	0.014	0.020	0.008
Ba	0.000	0.000	0.003	0.000	0.005	0.000	0.005	0.000
Sr	high	low	high	low	mod	high	high	high

Sr contents are guessed purely from the Sr peak observed on the real-time display of X-ray spectra whilst analysing. They are relative abundances, not absolute.

present and often in appreciable amounts. Recalculation of the analyses to cell formulae has taken no account of the presence of Sr, and because of this the number of atoms per formula unit of the elements reported will be an over estimate.

The most important analysed element after Ca is clearly Mn, reaching 0.056 atoms per formula unit (3.84 wt% MnO) in 325910. It is more commonly present in quantities up to ≈2 wt% MnO in most other calcites. BaO reaches just over 1.10 wt% in calcites from 326336. Fe is generally low in these calcites, always present in lesser amounts than Mn, and often subordinate to Mg, which reaches only 0.008 atoms (0.34 wt% MgO). All the above elements will readily substitute for Ca, as too will rare Na, (encountered in amounts up to ≈0.25 wt% Na_2O), and all are capable of forming carbonates in their own right. None however was recorded as a free carbonate, with calcite and strontianite being the only two carbonates observed. Emeleus (1964) records both calcite and siderite from Grønnedal-Íka. No Na-K carbonates (such as nyerereite –

$Na_2Ca(CO_3)_2$ or fairchildite -$K_2Ca(CO_3)_2$) were observed.

Apatites

Apatite occurs commonly in carbonatites in modal contents similar to or slightly less than pyroxene. They are thus one of the most important phases in the carbonatites. Typically they are rich in Sr and REE and for this reason have only been partially analysed. They will also host most of the whole rock F in the absence of fluorite as an accessory phase.

Table 7.3.2 lists certain elements of the analysis and indicates the other detected elements. The total of these other elements can be estimated if perhaps 4% of F, Cl and H_2O are assumed to be unanalysed (ie. total 96%, see Deer *et al.* 1966). Some apatites (eg. francolite) may contain appreciable CO_2, bringing the total of unanalysed elements (F, Cl, CO_2, H_2O) to $\approx$10%, and thus an analysed total of 90% may be expected.

Apatites are capable of accepting many different elements into their crystal structures. Minor amounts of S and Si appear together in apatites substituting as $Si^{4+} + S^{6+} \rightleftharpoons 2P^{5+}$ (McConnel 1937). This is however of limited importance with S occurring in only one sample. The most obvious feature of these is the low totals associated with high REE contents and incorporation of up to 8.9 wt% SiO_2 into the structure. These REE-apatites are essentially members of the apatite-britholite solid solution series with REE and Si exchanging for P in the coupled substitution;

$$3Si^{4+} + 3(REE,Y)^{3+} + 2Ca^{2+} \rightleftharpoons 3P^{5+} + 5Ca^{2+}$$

(Speer and Ribbe 1982). Complete solid solution has been synthesized between britholite–Y and apatite, but only incomplete solid solution exists between britholite-La and apatite (Ito 1968). Due to the extreme LREE enrichment of these carbonatites they are most likely members of the apatite - britholite-La partial solid solution series.

LREE enrichment in apatites from other carbonatites is reported by many workers (Leushe, NE Zaire, by Maravic and Morteani 1980; Fen by Mitchell and Brunfelt 1975; Alnö, by Kresten 1979 for example).

Table 7.3.2

Partial analyses of apatites from the carbonatite dykes.

	325910	326358	326358	325358	326336	54244	326333	326333
SiO_2	0.0	8.71	8.96	4.91	3.37	3.33	3.63	4.01
CaO	55.90	42.59	41.168	46.24	48.71	49.00	49.33	49.26
P_2O_5	40.17	23.75	22.47	29.86	31.35	32.31	30.99	29.75
BaO	0.22	nd	nd	nd	nd	nd	nd	nd
Na_2O	nd	nd	nd	nd	nd	nd	nd	nd
S	nd	nd	nd	nd	nd	nd	0.592	0.555
Sr	yes	*	*	*	*	*	*	*
REE	no	yes	yes	yes	yes	yes	yes	yes
Total	96.32	75.05	72.59	81.00	83.43	84.64	84.54	83.58
	326388	41958	58254	58254	326347	54275	46257	
SiO_2	1.17	0.745	0.556	0.77	0.34	4.13	nd	
CaO	51.05	54.52	54.86	54.11	53.43	47.61	54.208	
P_2O_5	35.15	38.76	39.27	38.07	38.16	30.61	39.144	
BaO	nd	nd	nd	nd	nd	0.63	nd	
Na_2O	nd	nd	nd	0.50	0.25	0.31	0.38	
S	nd	nd	nd	nd	nd	nd	nd	
Sr	yes	no	no	no	no	*	no	
REE	yes	no	v.low	no?	no	yes	v.low	
Total	87.61	94.03	95.04	93.63	92.35	83.47	94.05	

*nd – not detected. REE abundances estimated from magnitude of REE spectra. Peaks clearly visible were La, Ce, Nd, Pr and occasionally Eu. Sr from presence of Sr peak. * – Sr peak may be present but would be masked by Si peak.*

Fluorite

Fluorite was analysed in 325910, 46257, 326388, 326347. It is generally close to stoichiometric CaF_2, although all analyses reported the presence of minor Na (0.175-0.262 wt% Na – not Na_2O). From 46257, small peaks indicating the presence of some Y and Sr were observed. Samples 325910 and 326388 are both extremely F-rich carbonatites as well as being enriched in REE, Nb, Ba and Sr. Some of these elements may form complexes with F, particularly REE (see later).

Table 7.3.3

Partial analyses of Allanite (wt%).

	326323.40	326323.42	326323.44	326247.48	326247.50
SiO_2	29.50	29.31	29.59	28.64	29.73
Al_2O_3	8.48	9.45	8.80	11.85	11.09
FeO	23.67	11.18	23.24	12.79	15.57
MnO	1.44	1.43	1.24	3.55	4.28
MgO	0	0	0	0.79	0.55
CaO	12.11	11.16	11.06	8.70	8.89
Na_2O	0	0.46	0	0.32	0
K_2O	0	0	0	0	0
BaO	0	0	0.975	0	0
Total	75.21	69.99	74.9	66.63	70.11
	326247.51	326247.56	41958.28	41958.31	41958.33
SiO_2	28.26	20.66	29.12	29.55	18.03
Al_2O_3	10.78	8.34	8.83	8.73	0.471
FeO	15.54	11.62	22.92	21.51	2.22
MnO	1.62	0.49	0.932	1.82	0
MgO	0	0	0	0	0
CaO	8.91	16.68	11.00	10.66	7.80
Na_2O	0.40	0.44	0	0	0
K_2O	0	0	0	0	0
BaO	0	0	0	0	0
Total	65.49	63.57	72.80	72.27	30.22*

* *includes 0.92 wt% P_2O_5.*

Allanite

From 3 samples (326247, 326323 and 41958) a silicate mineral bearing optical and chemical characteristics similar to allanite were analysed. Allanite has the general formula $(Ce,Ca,Y)_2(Al,Fe^{2+},Fe^{3+})_3(SiO_4)_3OH$, and is sometimes referred to as orthite. Allanite is essentially a member of the epidote group of minerals.

These samples appear to contain of the order of 20-30 wt% of REE's (assuming

97-total $\approx$ REE content, Deer *et al.* 1962). The lower totals also appear to correlate with a reduction in Fe+Mn+Ca for which REE may be substituting.

Optically, these minerals are fairly deep red-brown, pleochroic to paler brownish-yellow and showing a poorly developed cleavage. They have slightly inclined extinction and low to moderate birefringence. Some samples appear to be metamict, a result of radioactive decay of some of their constituent elements.

Their chemical analyses compare favourably with those given by Deer *et al.* (1962), although the allanites from the dykes have universally lower Al_2O_3 and higher Fe_2O_3. This may imply $Fe^{3+} \rightleftharpoons Al^{3+}$, along with the major substitution of $Ca^{2+} + Al^{3+} \rightleftharpoons REE^{3+} + Fe^{2+}$. In these Al-deficient rocks replacement of Al^{3+} by Fe^{3+} would not seem unlikely.

Baryte

Baryte was detected in 325910 and 58254. It generally approximates closely to stoichiometric $BaSO_4$ although contains some Sr in solid solution eg. in 58254). Partial analyses are reproduced in Table 7.3.4. Sr will be present as $SrSO_4$. The presence of baryte indicates a build up of S in these magmas, and in the case of 325910, F. Le Bas (1981) describes late stage fluorite-baryte mineralisation associated with carbonatite magmatism due to a build up of F and S during evolution of the magma.

REE Minerals

As well as the presence of REE in allanite and apatite, REE may be present in reasonable amounts in calcite (see for example Maravic and Morteani 1980) and in fluorite (especially HREE).

REE also occur in exclusively REE bearing phases, and although they could not be analysed their most likely phase will be bastnäsite (LREE CO_3F). Pyrochlore, (Nb, Ta,U and REE bearing) was also seen (deep red, acicular lozenge shaped crystals, slightly metamict) and this will be another important host for the REE.

Table 7.3.4

Partial analyses of baryte from carbonatites.

	325910	58254	58254
BaO	67.60	64.91	63.74
SO_3	34.35	35.10	34.43
Na_2O	0.80	0.75	0.77
Cl	0	0.12	0.0
CaO	0	0.32	0.22
SiO_2	0	0.30	0.33
Al_2O_3	0	0.33	0.24
MgO	0	0.28	0.0
Sr	no	yes	yes
Total	102.75	102.11	99.73

7.3.J: Mineralogical Conclusions

In conclusion, the mineralogy records many of the peculiar chemical aspects of these magmas. High Mn contents in almost all mafic silicate phases give an indication of high a_{MnO} in the magmas and, in the olivines, provide evidence of hitherto speculated solid solution series. Many minerals are relatively Mg-rich, and carry high Mn, often in similar quantities to Fe, implying $2Mg \rightleftharpoons Fe+Mn$ as a dominant exchange process. Al deficiency along with a complete lack of Ti is characteristic of many phases (pyroxene and phlogopite typically), again a reflection of bulk rock deficiency in these phases. Sr, Ba and REE all occur commonly in the non-silicates along with REE occurring in allanite. Nb (U, Th) appears occasionally in pyrochlore and minor REE fluor-carbonate is also probably recorded (bastnäsite). These phases all attest to the generally high incompatible element contents, although peculiarly, no Zr-bearing phase has been detected in any sample (cf. Le Bas 1977, Secher and Larsen 1980).

7.4: Geochemistry

7.4.A: Introduction

Carbonatites as a group of igneous rocks show very unusual major and trace element chemistry. They are obviously dominated by Ca and CO_2 but are extremely enriched

in many of the incompatible trace elements (Sr, Ba, Nb, Th, U, REE, Y), often to economic concentrations (for example Mountain Pass, California and Barreiro, Minas Gerias, Brazil). All carbonatites were analysed by XRF on a Phillips PW1400 X-ray spectrometer at Leicester University with the help of N. Hodgson (now at BP) and N. G. Marsh. Analytical techniques are described fully by Hodgson (1986) who used wet chemically analysed carbonatites as standards to calibrate XRF analyses. All analyses were run for major elements (ie. Si, Al, Fe, Mg, Ca, Na, K, Ti, Mn, P) using fused beads and trace elements using pressed powders. Mass absorption procedures were applied for the effects of the major element composition on the or the trace trace elements but no absorption correction was made for the trace element concentrations. Cu and Pb were not analysed. F and Cl were analysed on pressed powders at Durham.

7.4.B: Chemical Variation

Woolley (1982) suggested a classification of carbonatites based upon whole rock CaO, $FeO+Fe_2O_3$ and MgO. All carbonatites from Igaliko are plotted on this basis in Figure 7.4.1. It is clear that most are sövites with slightly fewer ferrocarbonatites. They are chemically similar to carbonatites from West Kenya (Le Bas 1977). Also shown are fields from Oka and Alnö carbonatites.

All major and trace element data are plotted against SiO_2 (wt%) in Figure 7.4.2. This gives an idea of the total range of elemental variation observed and also indicates whether a particular element is associated primarily with the silicate or carbonate phases present. Si itself varies from 0 to 17.54 wt%. A total alkalis - silica basis was used to separate silica-rich carbonatites from a group termed ultramafic lamprophyres (UML, see Figure 5.2.1), a distinction based primarily on petrographic evidence. There are thus 3 samples which classify as UML by TAS methods which are carbonate rich and silica poor. They tend also to be Fe-rich and all contain less than 25.6% CaO. They are essentially mica-oxide-carbonate rocks, but not strictly carbonatites (according to Streckeisen 1980). The remainder of the UML contain >28.5% SiO_2, and are probably unrelated to these mica-oxide-carbonate rocks.

From Figure 7.4.2 it is clear that there is a very wide scatter of data with no obvious correlation of any element against SiO_2. There are however general trends associated

Figure 7.4.1

Carbonatite whole rock analyses in terms of CaO – Fe_2O_3+MnO – MgO showing the classification scheme proposed by Woolley (1982). Also shown are fields of carbonatites from other well known areas. The Igaliko carbonatites resemble most clearly those from West Kenya (Le Bas 1977).

Figure 7.4.1

Carbonatites

CaO- Fe2O3+MnO - MgO

Weight % whole rock

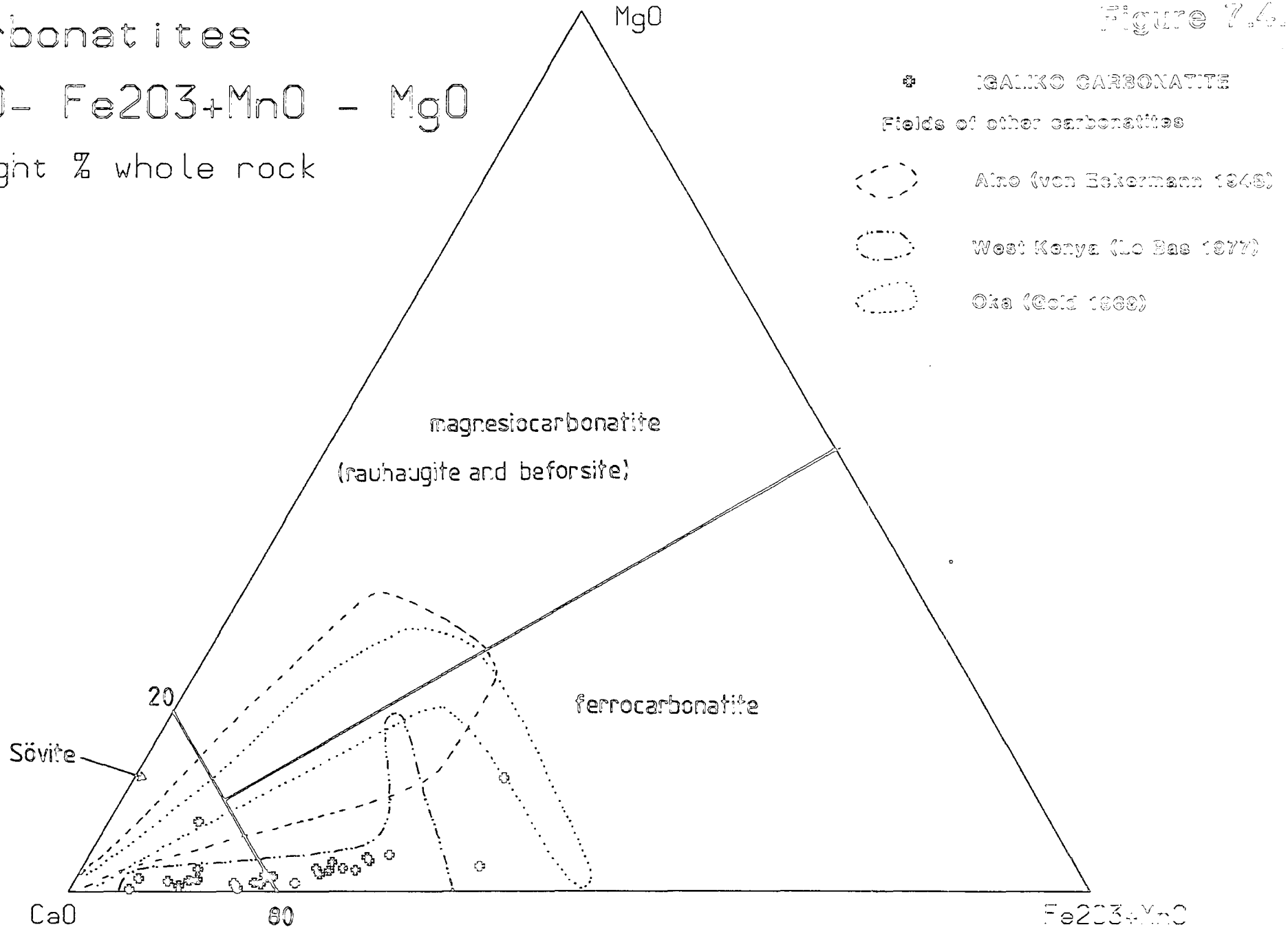

Figure 7.4.2 (3 pages).

Major (wt%) and trace element (ppm) data for carbonatites plotted against SiO_2 wt%. Cl was only detected in 6 samples and was always less than 0.02 wt%. Pb and Cu were not analysed.

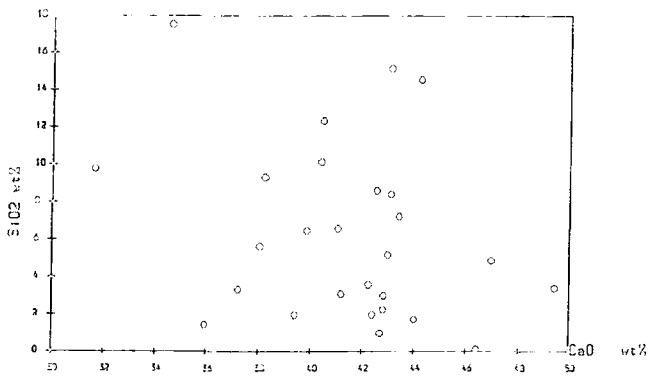
SiO2 wt%
CaO wt%

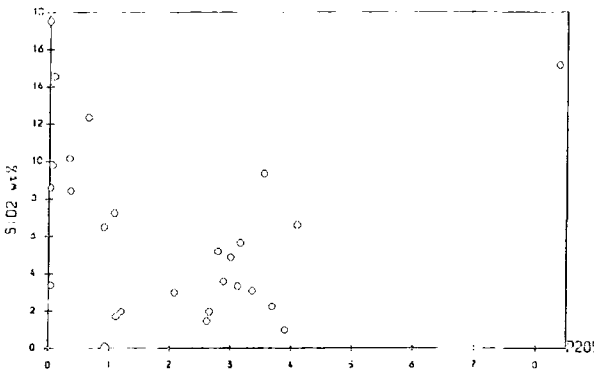
SiO2 wt%
P2O5

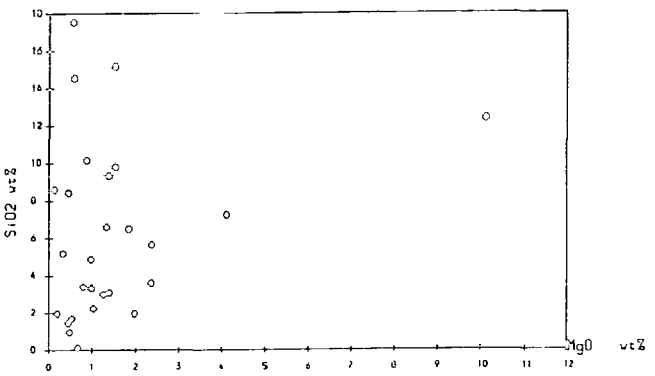
SiO2 wt%
MgO wt%

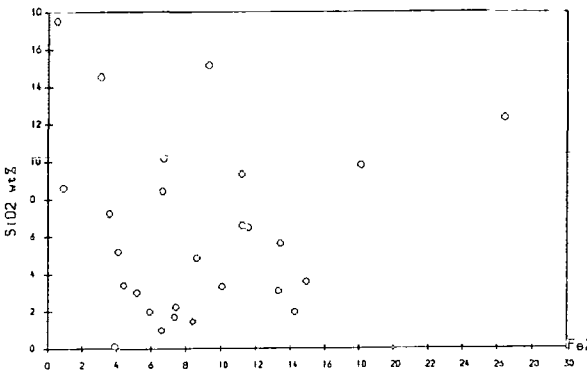
SiO2 wt%
Fe2O3

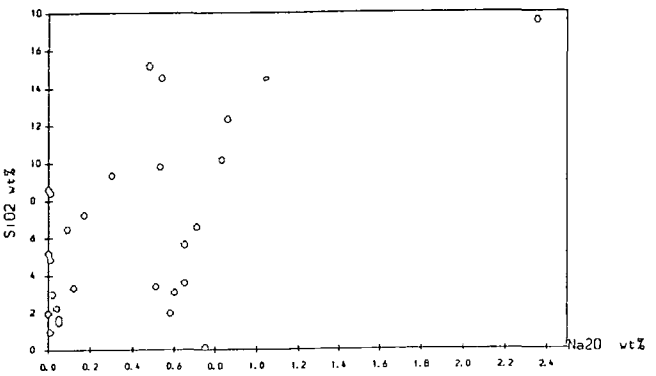
SiO2 wt%
Na2O wt%

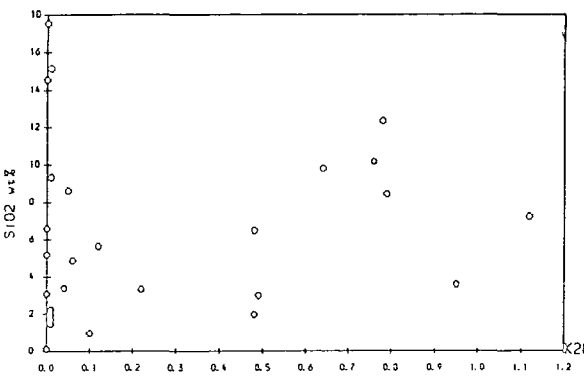
SiO2 wt%
K2O

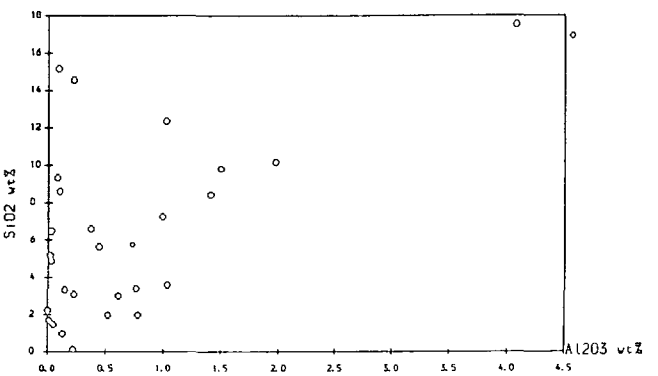
SiO2 wt%
Al2O3 wt%

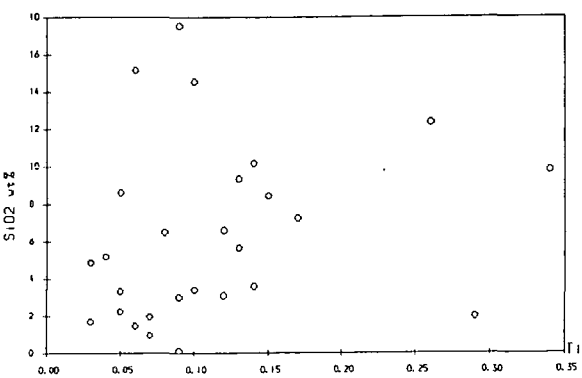
SiO2 wt%
TiO2

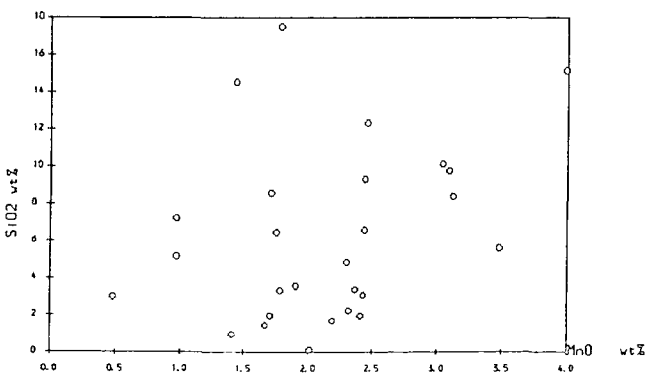
SiO2 wt%
MnO wt%

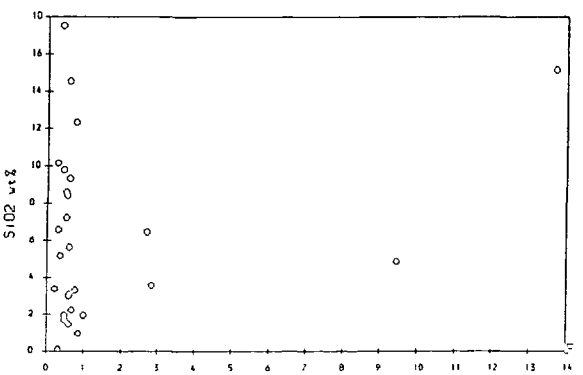
SiO2 wt%
wt%

Figure 7.4.2(ii)

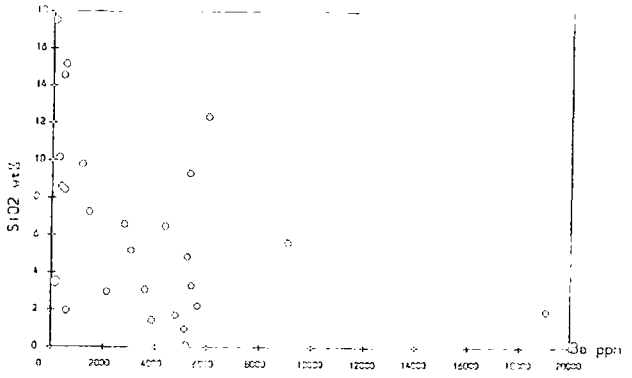

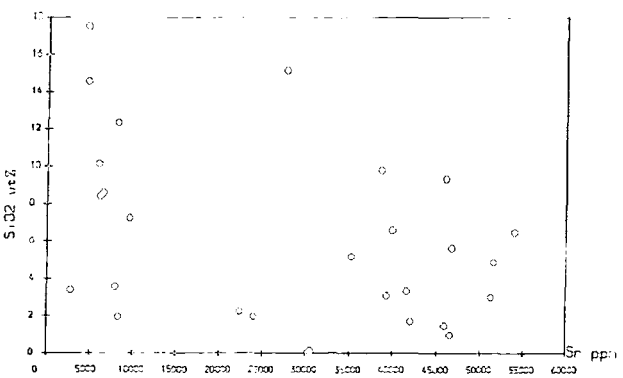

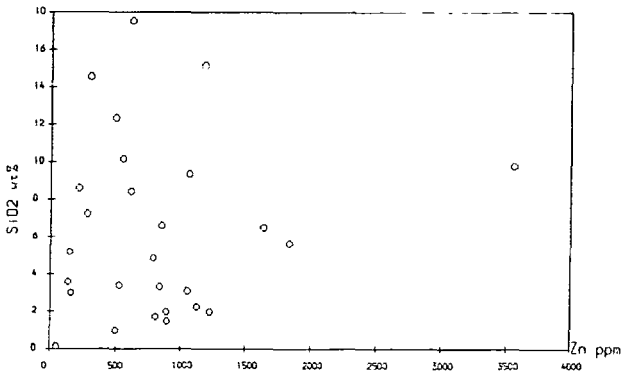

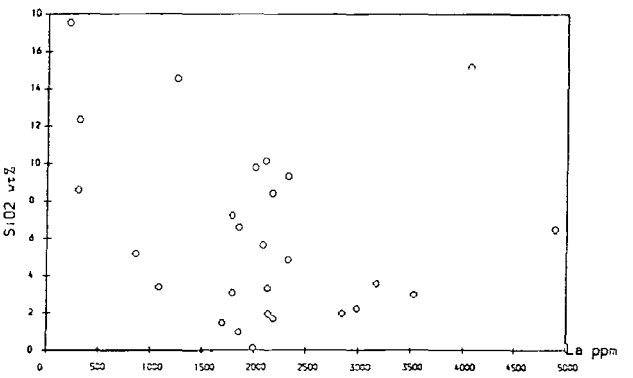

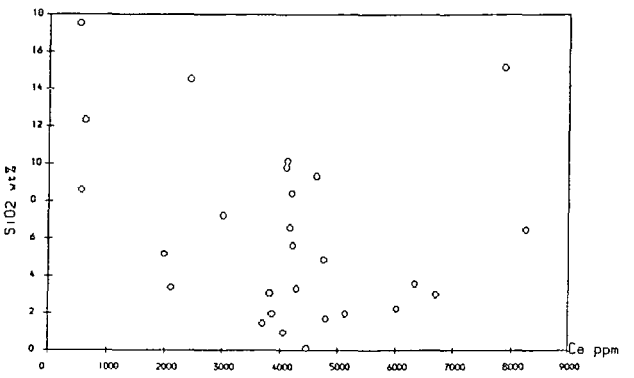

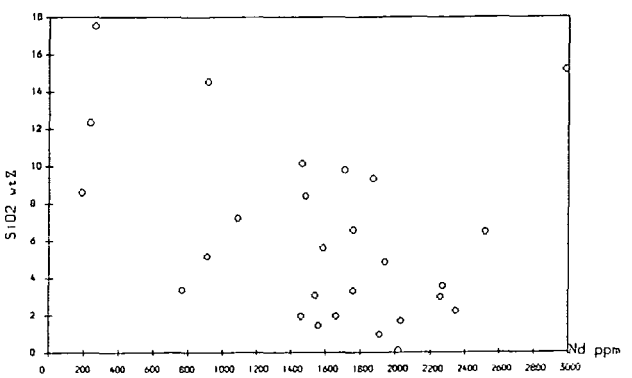

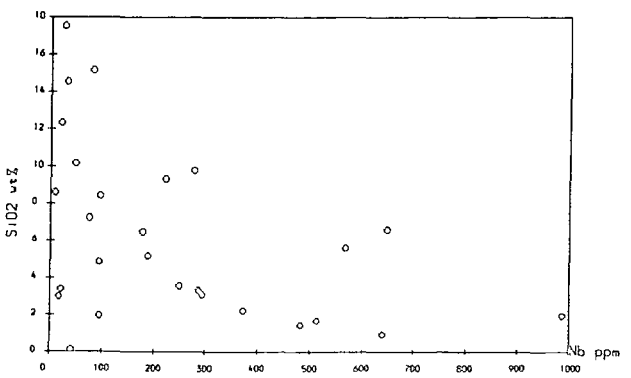

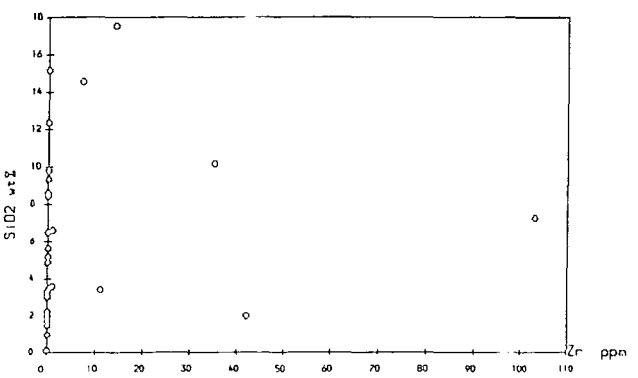

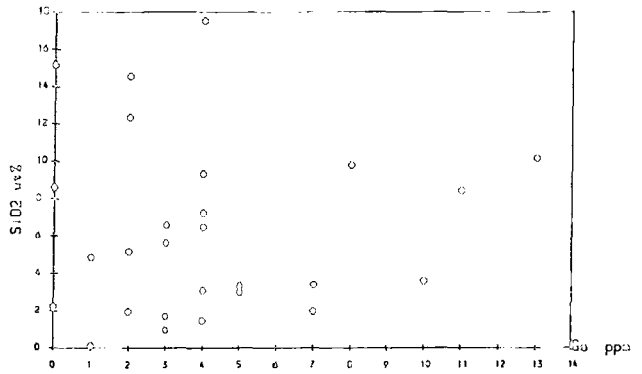
SiO2 wt%
Ga ppm

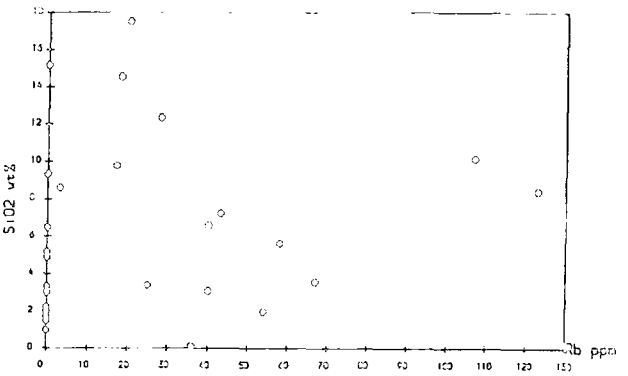
SiO2 wt%
Rb ppm

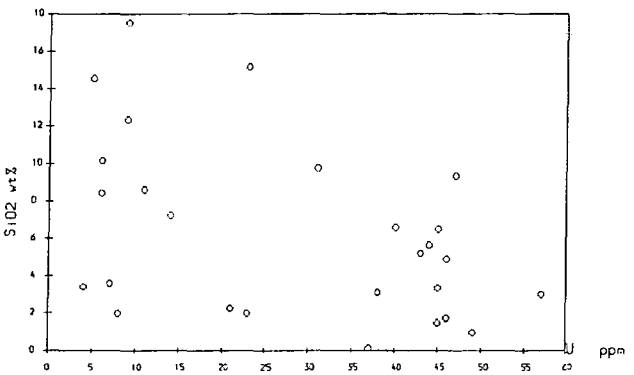
SiO2 wt%
U ppm

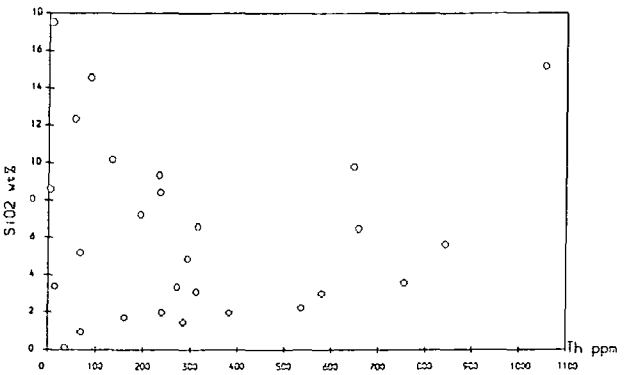
SiO2 wt%
Th ppm

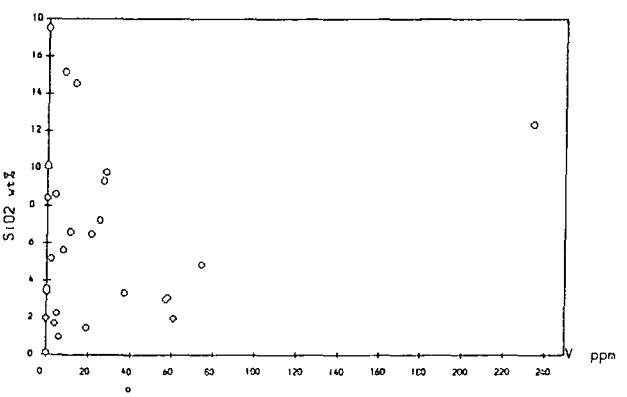
SiO2 wt%
V ppm

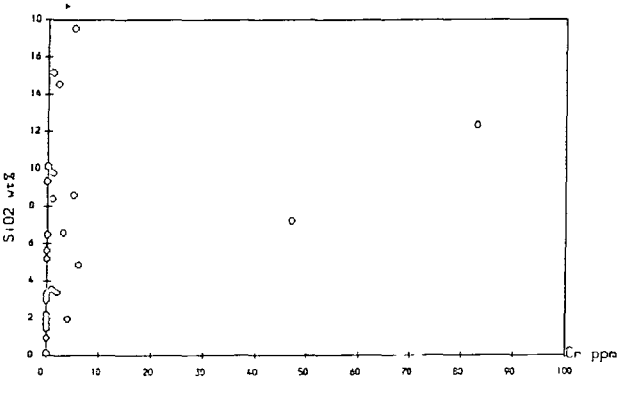
SiO2 wt%
Cr ppm

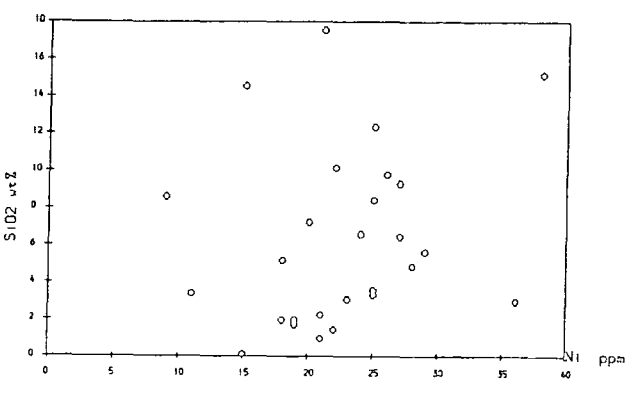
SiO2 wt%
Ni ppm

with the silicate or carbonate phase preference of an element.

Si -prefering:-The following elements would appear to be associated with the silicate phase:- Al, Fe, Mg, Na, K, Ti, V, Cr, Ni, Ga. These are the elements typically incorporated into the silicate minerals described in the previous section and their positive correlation (overall) is not surprising.

CO_3 *-prefering*:- Ca, P, Mn, F, Ba, Nb, Sr, Th, Zn, Nd, La, Ce, U, Rb, Zr(?). These elements are typically those occurring either in solid solution in carbonates (Mn, Sr, Ba, Zn(?)), apatite (REE, Th) or occurring as minor accessory phases (pyrochlore, allanite etc.).

There is a notable exception to these generalisations. Sample 326395 at 15.16 wt% SiO_2 is a fluorite-chlorite-iron oxide rock (13.7 wt% F) but has many if the attributes (both field and geochemical) of a carbonatite. It is also the most Th-rich (1175ppm) and Y-rich (1903ppm) sample. Its content of REE, Sr and Zn are however indistinguishable from carbonatites and is thought to be associated with late stage carbonatite activity (cf. Le Bas 1981). Fractionation of calcite, apatite and minor silicate would all tend to increase contents of F, alkalis, some incompatible trace elements and possibly silica, producing the late stage fluorite - baryte type mineralisation (or natro-carbonatite magmatism - cf. Twyman and Gittins 1987). Upward migration of volatiles may also account for F enrichment in some cases – and this can be seen in a carbonatite dyke near Igaliko village (325908, 325910) where the F content rises from less than 2 wt% to about 10 wt% over a 200m increase in altitude. Cl however is typically below detection in almost all samples. This accords with the observations of Heinrich (1966) who states that "Cl in carbonatites is very rare". Dawson and Fuge (1980) analysed a range of African carbonatites and found that Cl was typically subordinate to F (F/Cl ratios from 0.69 to 255), with the highest Cl contents from the 1960 natrocarbonatite eruption of Oldoinyo Lengai in Tanzania. Iodine contents reported by Dawson and Fuge (1980) are all extremely low (<2ppm).

Zr is surprisingly low or absent from most samples. This is not an analytical problem caused by overlap of Sr K_β on Zr K_α (a serious problem in such high Sr samples) as all analyses were carried out using the Zr K_β line. Zr (and Zr bearing minerals)

are reported frequently from carbonatites (Gold 1966, Le Bas 1977, 1980, Maravic and Morteani 1980, Secher and Larsen 1980), but generally not in excessive whole rock quantities (tens to hundreds of ppm typically). Gold's (1966) average carbonatite contains 641ppm Zr. This will be discussed further in a later section.

Figure 7.4.3 shows all analyses plotted in terms of CaO–Fe_2O_3–MgO. Woolley (1982) used this scheme to classify carbonatites. On this basis, there are roughly equal numbers of sövites and (calcium rich) ferrocarbonatites but no magnesium-rich carbonatites (beforsites). Also shown on this diagram are analyses of carbonatites from other well known localities. The Igaliko carbonatites are extremely similar to the West Kenyan carbonatites cited by Le Bas (1977) and are less magnesian than both Oka and Alnö.

7.4.C: Incompatible Element Variation

Figure 7.4.3 shows incompatible element 'spidergrams' of all 27 carbonatites. These are labelled to give a rough idea of their location within the complex.

Certain features are common to all carbonatites. Most obvious is their extreme enrichment in elements such as Th, REE, Y, Sr with typically slightly less enrichment in Ba, Nb and P. Generally very low K, Ti and Zr give low normalised contents and thus large dips in the patterns occur at these elements. Despite these broad similarities between all samples there are clearly differences between individual samples.

(i) The overall degree of enrichment of each element between individuals.

(ii) Presence or absence of negative Sr anomaly compared to Ce and Nd.

(iii) Variation in overall 'shape' of the pattern (cf. 326302 with 41982 and 325908 – 3 fairly typical sövites in thin section but with markedly different patterns).

From Figure 7.4.3 there would appear to be regional compositional groups, with certain features of the chemistry being characteristic of carbonatites from a particular area. The Igaliko occurrences for example show a large peak at Th, are often Rb, K, Zr and Ti deficient, with a relatively flat plateau between Nb and P. Ba_{cn} (cn=chondrite normalised) is typically less than 10% Th_{cn}. Carbonatites from the Lower Flink's Dal area are quite different however, Ba_{cn} is generally $\approx$ 1% Th_{cn}, and the REE slope

Figure 7.4.3 (3 pages).

Incompatible element 'spidergrams' of all carbonatites arranged in rough geographical groupings indicated in each diagram. The ordinate axis is rock/chondrite (see Figure 5.5.2 for chondrite concentrations from Thompson 1982). Certain differences in incompatible element chemistry are visible on a regional scale (eg. Igaliko, Iganaq, Østfjordsdal show different overall patterns). See text for discussion. The dykes marked 'Igaliko' are from the area to the west of the author's Camp 4, near the 45m lake, 4km North of Igaliko village (see Map 2 and Figure 1.1.1). Those from Iganaq are to the east of this camp in the vicinity of the small peak, Iganaq.

Figure 7.4.3(i)

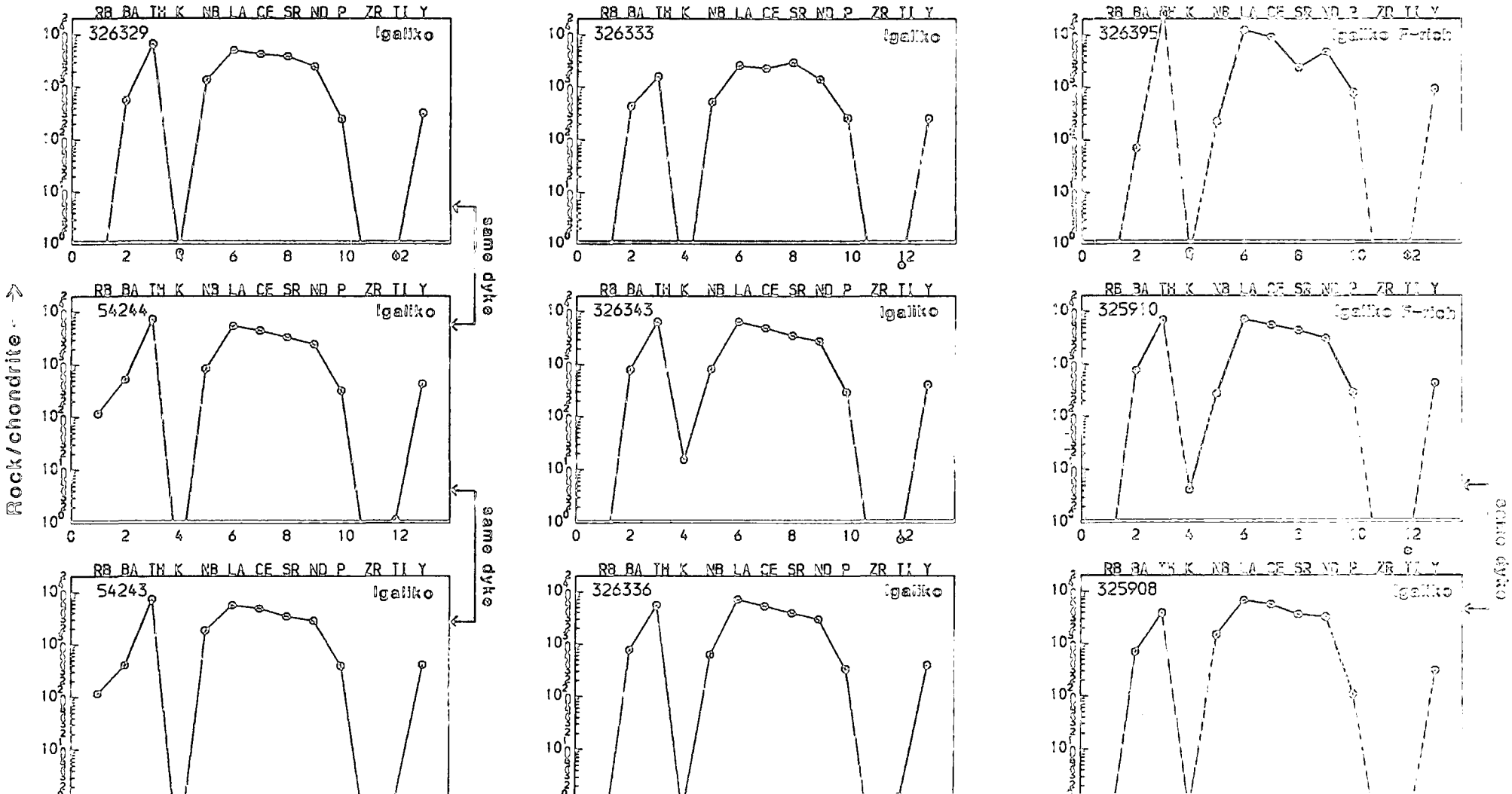
Rock/chondrite
RB BA TH K NB LA CE SR ND P ZR TI Y
326329
Igaliko
326333
Igaliko
326395
Igaliko F-rich
54244
Igaliko
326343
Igaliko
325910
Igaliko F-rich
54243
Igaliko
326336
Igaliko
325908
Igaliko
same dyke
same dyke
same dyke

Figure 7.4.3(iii)

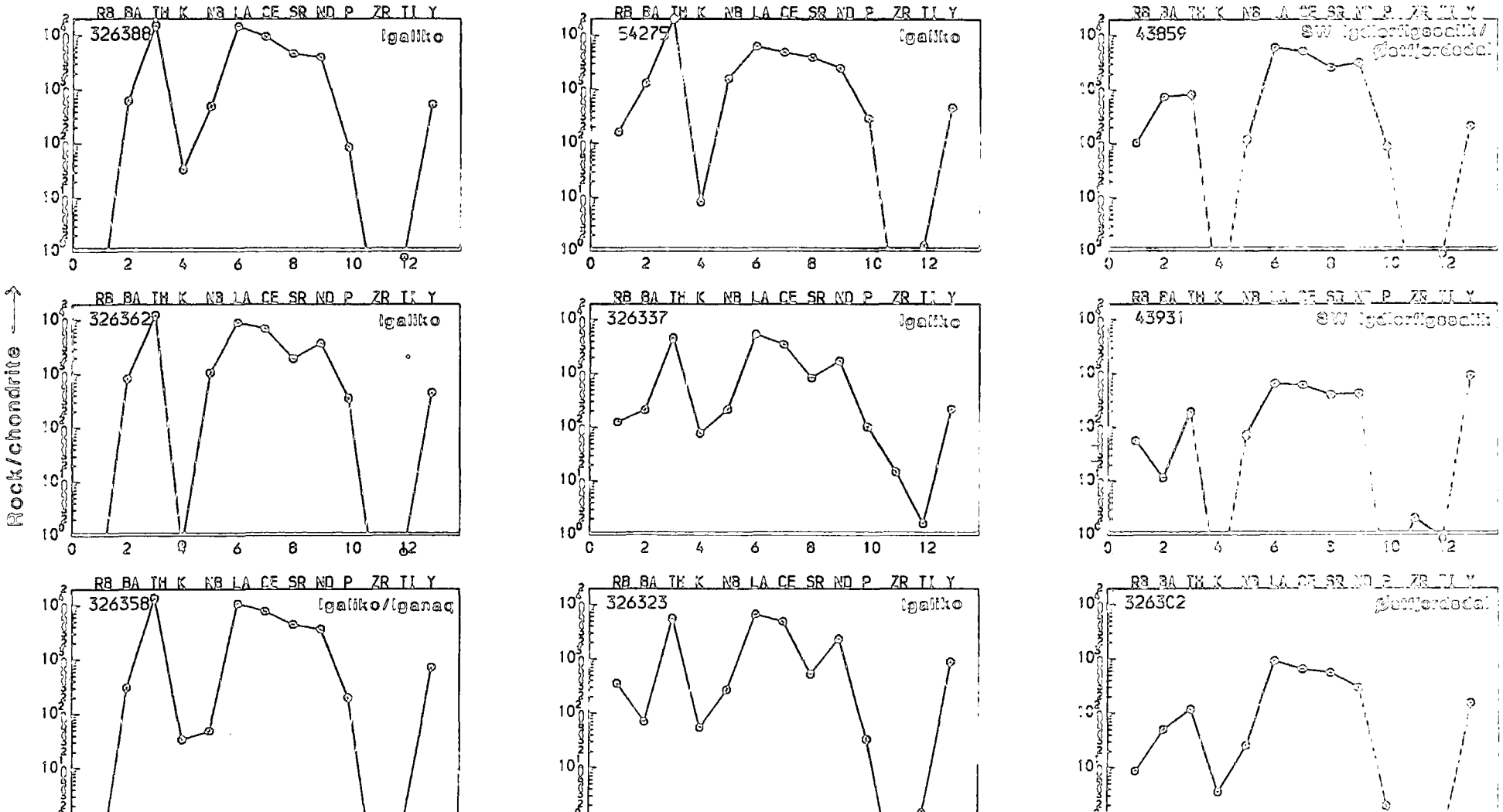

Figure 7.4.3(iii)

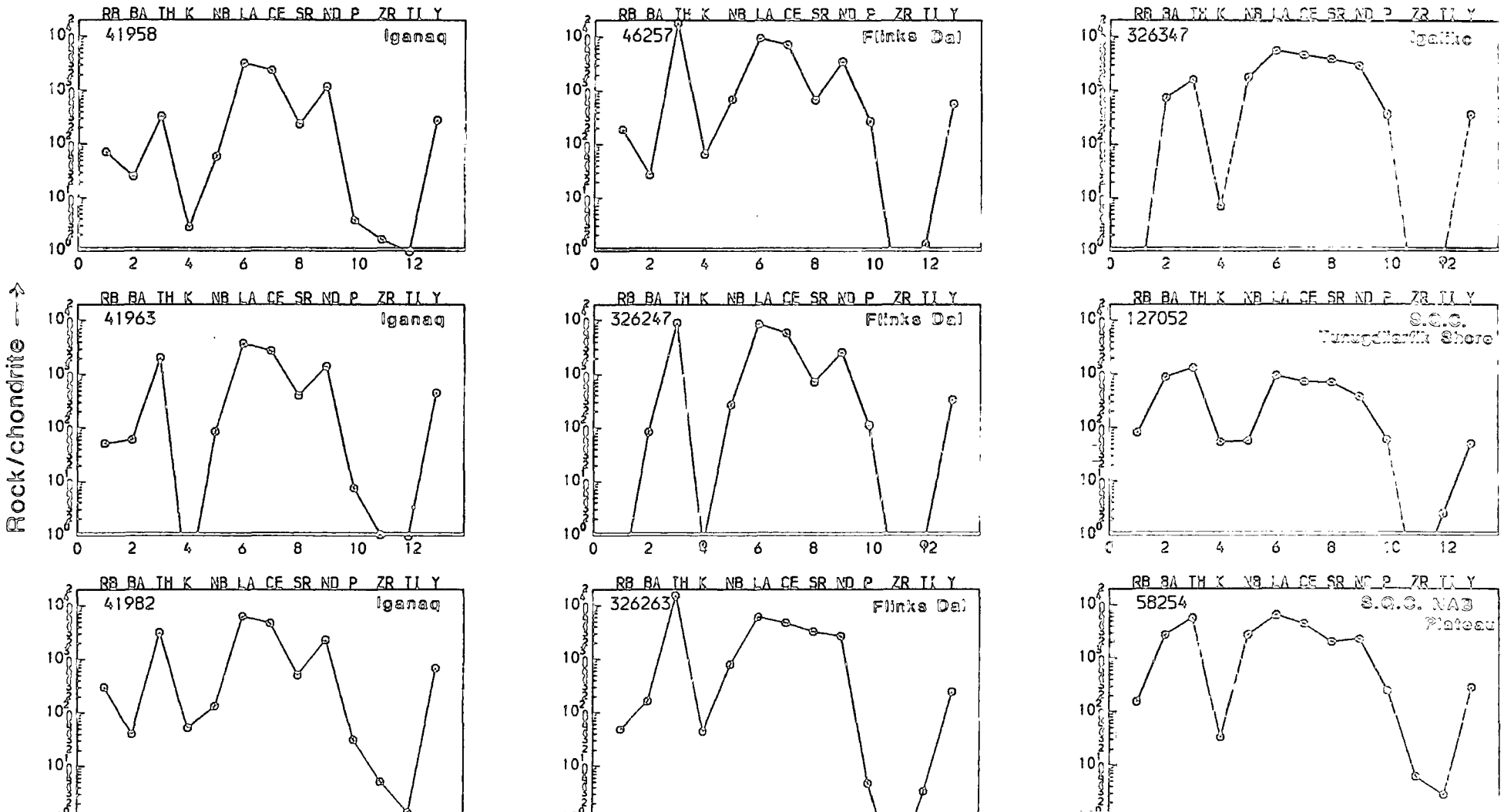

(measured by La_{cn}/Y_{cn}) is steeper than the Igaliko samples, despite similar degrees of enrichment in La, Ce, Nd. Two of the 3 Lower Flink's Dal samples also show negative Sr anomalies, which are not so pronounced in the Igaliko occurrences.

Carbonatites from the Iganaq area tend to be less P and Th enriched than typical 'Igaliko' carbonatite and show negative Sr anomalies. 326302, a carbonatite from Østfjordsdal is different again, having very low Ba, Rb and Th enrichments.

It would thus seem that carbonatites from different parts of the Igaliko complex have localised chemical characteristics. This would imply several carbonatite sources and dyking events, and would be consistent with localised, 'late' occurrences of these dykes. The main groups that can be identified are from Igaliko, Iganaq, Lower Flink's Dal, and minor occurrences from Østfjordsdal, the Narssarssuaq plateau and south-west Igdlerfigssalik, all slightly different in composition.

Further discussion of the geochemistry will be given after a discussion of carbonatite petrogenesis.

7.5: Models of Carbonatite Petrogenesis

Before considering REE data, and discussing trace element behaviour in carbonatite magmas it is worth briefly discussing the various models of carbonatite petrogenesis proposed by workers in this field. It is now universally accepted that carbonatites are igneous in origin, and not limestones etc. metamorphosed in the vicinity of volcanic centres. As a rule carbonatites are alkali-poor rocks comprising essentially Ca (and Fe and Mg) carbonates with minor silicates. They occur most commonly with undersaturated igneous rocks (eg. West Africa – Le Bas 1977; Alnö – Von Eckermann 1948; Grønnedal-Íka – Emeleus 1964) or occassionally with kimberlites (mainly as carbonate blebs in the ground mass exemplified by the Benfontein kimberlite, S. Africa, Dawson and Hawthorn 1973, or as dykes, eg. the Premier Mine, Pretoria, C. H. Emeleus pers. comm. 1987).

Early workers doubted the magmatic nature of carbonatites as pure calcite does not melt below 1339°C. However, experimental studies of the system CaO - CO_2 - H_2O by Wyllie and Tuttle (1960) showed that in the presence of a few percent of water, calcite

would be molten at more reasonable magmatic temperatures. The minimum liquidus temperature in this system was measured at 675°C at 1kb. Thus, carbonatites could quite easily have been molten. Also in 1960, the Tanzanian volcano, Oldoinyo Lengai erupted a peculiar Na and K rich carbonatite magma (Dawson 1962) termed natrocarbonatite. This lava contained up to 30 wt% Na_2O and 7 wt% K_2O, the remainder being made up essentially of CaO and CO_2. This alkali carbonatite contains minerals such as nyerereite ($Na_2Ca(CO_3)_2$), fairchildite ($K_2Ca(CO_3)_2$) and gregoryite (approximately anhydrous $NaHCO_3$ with a small amount of $CaCO_3$) which are all extremely soluble. Their occurrence is thus not commonly recorded elsewhere due to this fact although Deans and Roberts (1984) have observed pseudomorphs after nyerereite in similar tuffs from the Tinderet foothills in Kenya. They also suggest that pseudomorphs thought to be after melilite at Qagssiarssuk by Stewart (1970) may in fact be pseudomorphs after nyerereite.

The discovery of the Oldoinyo Lengai magma led to the idea that this was a primary carbonatite magma which, when intruded at sub-volcanic levels lost volatiles to produce alkali metasomatism in the surrounding rocks, as typified at Fen (viz. fenitisation), in Norway and Napak (King 1949), a locality presumed to be the eroded roots of a volcano similar to Oldoinyo Lengai.

More recently liquid immiscibility has been advocated as a method of producing carbonatite magma from a CO_2-rich silicate liquid (see for example Middlemost 1974, Cooper *et al.* 1975, Mitchell and Brunfeldt 1975, Le Bas 1977). This provides a process which would account for the often bimodal association of carbonatite with nephelinite with a lack of intermediate compositions (see Le Bas 1987). However, there is a considerable difference of opinion on this subject.

Le Bas (1987) envisages natrocarbonatite as an immiscible product from nephelinite/phonolite magmas at sub-volcanic depths and argues in favour of these as primary carbonatite magmas. Twyman and Gittins (1987) however, consider sövitic magmas to be primary, formed by liquid immiscibility from nephelinitic melts at ≈27kb, with natrocarbonatite magmas developing by fractional crystallisation of this alkali-poor sövite. Woolley and Jones (1987) propose that carbonatite and nephelinite magmas are derived as separate melts more or less at the same time from a mantle source. Experimental

work by Wyllie (1978, 1980) and Eggler (1978) has shown that carbonatite melts could be derived from mantle rocks and this would probably be associated with melilititic or kimberlitic magmas. Treiman and Essene (1983) point out that carbonatites generated by partial melting of mantle peridotite would be Na-poor.

If the identification of pseudomorphs after melilite at Qagssiarssuk by Stewart (1970) was correct, and they are not the nyerereite pseudomorphs of Deans and Roberts (1984), the above models of carbonatite - melilitite volcanism formed as primary melts or deep immiscibility may fit the Qagssiarssuk occurrences. Mackenzie (1984, 1985) considers that primary carbonatite melts from very small degrees of mantle fusion could migrate rapidly. They could thus be precursors to more extensive silicic (basaltic/nephelinitic) melt generation and volcanism as seen at higher structural levels in the Eriksfjord Formation.

Various experimental studies have been conducted on both natural and synthetic systems aimed at defining the limits (pressure, temperature and composition) of liquid immiscibility in silicate - carbonatite systems.

Liquid immiscibility (between carbonate and silicate) has been detected;

(i) in the system Na_2O - Al_2O_3 - SiO_2 - CO_2 (Koster van Groos and Wyllie 1966)

(ii) in the join $NaAlSi_3O_8$ - Na_2CO_3 - H_2O (Koster van Groos and Wyllie 1968)

(iii) in the join $NaAlSi_3O_8$ - $CaAl_2Si_2O_8$ - Na_2CO_3 - H_2O (Koster van Groos and Wyllie 1973)

(iv) along the join $KAlSi_3O_8$ - K_2CO_3 (Wendlandt and Harrison 1979)

(v) in the system Na_2O - $Al_2O_3.SiO_2$ - CaO - CO_2 (Freestone and Hamilton 1980) – natural phonolite and natrocarbonatite starting materials, *

but immiscibility has not been detected;

(vi) in the system CaO - MgO - SiO_2 - CO_2 (to 40kb – Wyllie 1977b, Eggler 1978)

(vii) in the join $NaAlSiO_4$ - $CaCO_3$ - H_2O (Watkinson and Wyllie 1971).

The most significant and unifying of the above are the experiments of Freestone and Hamilton (1980). They melted together samples of a natural silicate (one of either Oldoinyo Lengai phonolite, phonolitic nephelinite or nephelinite) with either synthetic natrocarbonatite or calcite carbonatite (sövite). Their results are illustrated in Figure 7.5.1B. In summary, Freestone and Hamilton (1980) found that increased pressure causes an increase in the size of the 2-liquid field, as too does increasing temperature. More calcic silicates (nephelinitic) are immiscible with more calcium rich carbonatites, whilst the phonolitic rocks show an immiscible relationship with natrocarbonatites. Twyman and Gittins (1987) have criticised the experiments of Freestone and Hamilton (1980). According to Twyman and Gittins, many people assume that the model proposed by Freestone and Hamilton, and their experimental results, provide the definitive solution to natrocarbonatite petrogenesis. Twyman and Gittins (1987) however propose a very different model for the evolution of the Oldoinyo Lengai magmas, and point out that the Freestone and Hamilton (1980) experiments may be applicable, but are not necessarily the only solution.

Twyman and Gittins (1987) propose that sövitic magmas are parental to natrocarbonatite having separated immiscibly from nephelinite at ≈27kb. These sövites are essentially anhydrous, and alkali loss occurs to produce fenites when they become water saturated. They suggest that the Oldoinyo Lengai natrocarbonatite was initially very 'dry' and never achieved water saturation, thus at a late stage this still retains its alkalis.

Work currently in progress at Manchester university by B. Kjaersgaard has extended the limits of the Freestone and Hamilton (1980) 2-liquid field to intersect the (SiO_2 + Al_2O_3) – CaO join. These experiments are run 'dry' (ie. H_2O-free systems) unlike those experiments by Watkinson and Wyllie (1971) and Koster van Groos and Wyllie (1968, 1973). Watkinson and Wyllie's (1971) data (under water saturated conditions) had forced Freestone and Hamilton (1980) to close the 2-liquid field above the nepheline - calcite join (D. L. Hamilton, pers. comm. 1987) indicating complete solid solution extended along the SiO_2+Al_2O_3 - CaO join. Bedson (1983) hinted at an increase in the Freestone and Hamilton (1980) 2-liquid field at lower temperatures. Preliminary results from Kjaersgaard's experiments are also shown in Figure 7.5.1A. From these

Figure 7.5.1

A. (Facing). Average dyke compositions based on TAS classification plotted with all carbonatite data in the system $SiO_2+Al_2O_3$ – CaO – Na_2O+K_2O. This system was studied by Freestone and Hamilton (1980) and is being re-investigated by B. Kjaersgaard at Manchester University, under anhydrous conditions (ie. $P_{CO_2}=P_{total}$). Kjaersgaard's preliminary results indicate an extension of the Freestone and Hamilton (1980) 2-liquid field to intersect the $SiO_2+Al_2O_3$ – CaO join. Kjaersgaard's 2-liquid field boundary is marked. The average TAS classified whole rock data roughly parallel the silicate liquid – 2-liquid field boundary and may reflect a lower temperature or higher pressure equivalent of this phase boundary. The results of the experimental runs are shown with silicate melt as solid circles and carbonate melt as open circles. X marks the bulk composition of the run. Note how the tie lines rotate more rapidly as compositions of the silicate approach the $SiO_2+Al_2O_3$ –Na_2O+K_2O join.

B. (Overleaf). 2-liquid field from Freestone and Hamilton (1980) for comparison, showing the effect of varying pressure on the position of the solvus.

Average Dyke Comp.

Si+Al - Ca - Na+K

Weight % oxide
whole rock

2-liquid field at
1250°C, P_{CO_2} = 5kb
Dry

× - Bulk composition
of experimental run

Figure 7.5.1A

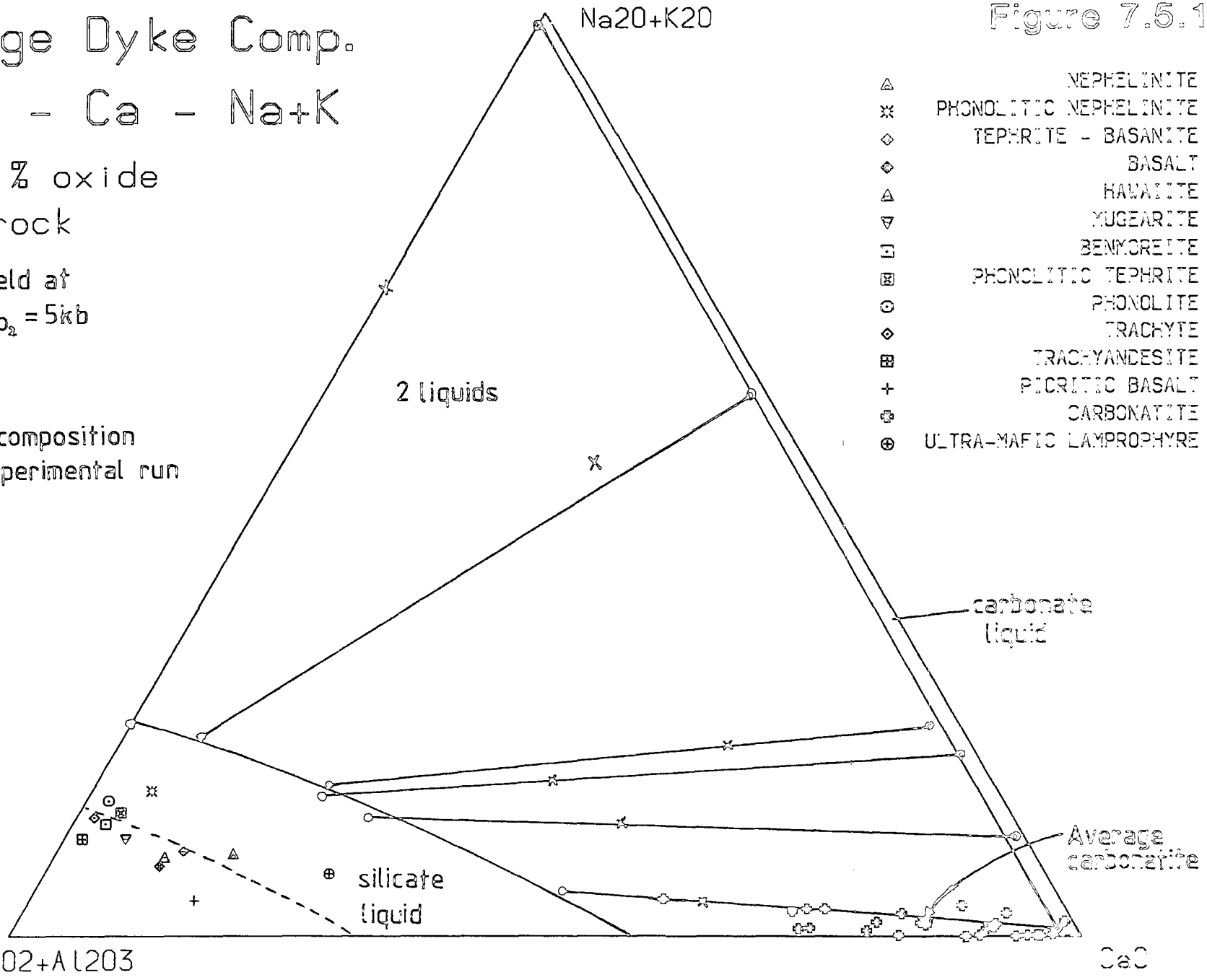

△ NEPHELINITE
⋇ PHONOLITIC NEPHELINITE
◇ TEPHRITE - BASANITE
◈ BASALT
△ HAWAIITE
▽ MUGEARITE
⊡ BENMOREITE
⊠ PHONOLITIC TEPHRITE
⊙ PHONOLITE
◈ TRACHYTE
⊞ TRACHYANDESITE
\+ PICRITIC BASALT
✿ CARBONATITE
⊕ ULTRA-MAFIC LAMPROPHYRE

Figure 7.5.1B

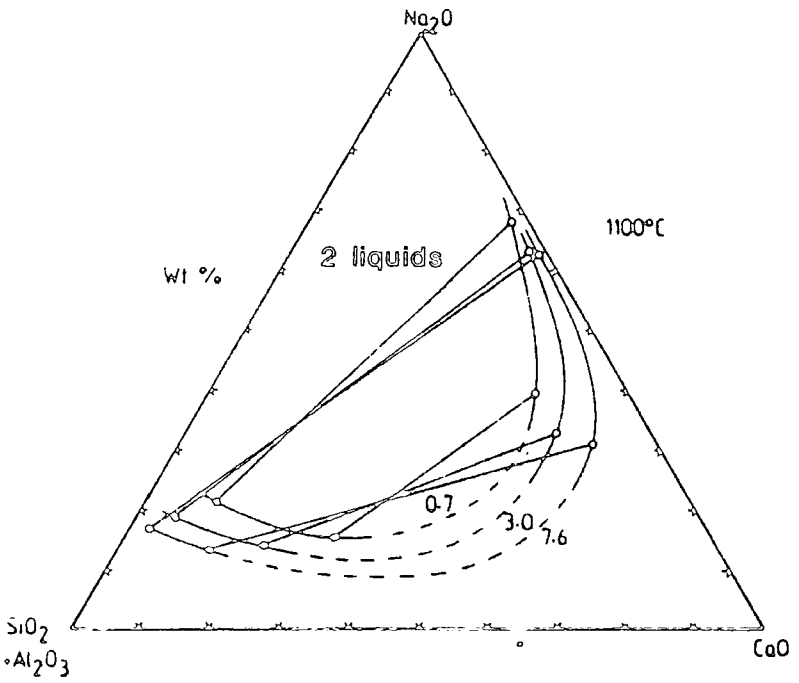

Effect of pressure on solvus at 1,100° C. $P_{total} = P_{CO_2}$ is indicated in kb

results calcite carbonatites could form as primary carbonatites by immiscibility from 'nephelinitic' melts (ie. high Ca compared to SiO_2 + Al_2O_3) with natrocarbonatite forming immiscibly from phonolitic rocks. Lowering temperature, or increasing pressure increases the size of the 2-liquid field and forces the phase tie lines to become packed closer together on the silica-rich 2-liquid field boundary. More calcic carbonatites will thus form from less Ca-rich (ie. more evolved) magmas. At temperatures as low as 800-900°C nepheline syenite magmas would still be partly liquid (Powell 1978), the 2-liquid field would be greatly enlarged, (from the 1250°C field of Kjaersgaard) and only a minor change in bulk rock composition could cause a major change in the composition of an immiscible carbonatite phase (due to the rapid rotation of the phase tie lines). Thus, variation in any of pressure, temperature and bulk composition would affect the bulk rock chemistry, and at low temperature (or high pressure) only a minor change in bulk (silicate phase) chemistry would be needed to produce a relatively large change in the composition of an immiscible carbonatite liquid.

Studies of trace element partitioning between immiscible silicate - carbonatite pairs have been conducted to try to explain some of the often excessive quantities of 'incompatible' elements occurring in carbonatites.

Koster van Groos (1975) investigated Sr distribution between silicate solid, silicate liquid and carbonatite liquid and concluded that Sr was not significantly enriched in the carbonate liquid relative to the silicate liquid. However, between a silicate solid and a carbonate liquid, Sr partitions strongly into the carbonate phase. Wendlandt and Harrison (1979) studied the behaviour of Ce, Sm and Tm between immiscible liquids in the $KAlSi_3O_8$ - K_2CO_3 (- CO_2) system. The carbonatite melt was enriched some 2-3 times in LREE and 5-8 times the HREE than the silicate. Thus, a carbonatite would be expected to have overall higher REE contents but a shallower slope (lower $(La/Lu)_{cn}$).

Recently, Bedson (1983, 1984), has investigated the distribution of REE and other elements (Cr, Mn, Cu, Zr, Ba, Hf, Ta) between natrocarbonatite - phonolite and nephelinite - calcite carbonatite immiscible pairs at a variety of temperatures and pressures. Figure 7.5.2A (i) shows Bedson's (1983) major element distribution between phonolite and natrocarbonatite immiscibility fields ($D^{sil/cbt}$). Figures 7.5.2A (ii) and 7.5.2A (iii) show Bedson's distribution data ($D^{cbt/sil}$) for Ba, Mn, Zr and Ta for phonolite - natro-

Figure 7.5.2A

(i) Selected major element distribution coefficients between phonolite and natrocarbonatite immiscible liquids as a function of pressure at 1150°C (ie. $D^{sil/cbt}$, from Bedson (1983) after Freestone and Hamilton (1980)).

(ii) Distribution coefficients between natrocarbonatite and phonolite immiscible liquids ($D^{cbt/sil}$) for Ba, Zr, Mn and Ta as a function of pressure at 1150°C (after Bedson 1983).

(iii) Distribution coefficients between nephelinite and calcite-carbonatite immiscible liquids for Ba, Zr, Mn and Ta as a function of pressure at 1150°C (after Bedson 1983).

Figure 7.5.2B (Overleaf).

(i) and (ii). Distribution coefficients between natrocarbonatite and phonolite immiscible liquids ($D^{cbt/sil}$) for Ba, Zr, Ta, Mn, La, Eu, Sm and Lu as a function of temperature at 3kb pressure (after Bedson 1983).

(iii) and (iv). Distribution coefficients between calcite-carbonatite and nephelinite immiscible liquids ($D^{cbt/sil}$) for Ba, Zr, Ta, Mn, La, Eu, Sm and Lu as a function of temperature at 3kb pressure (after Bedson 1983).

Figure 7.5.2A

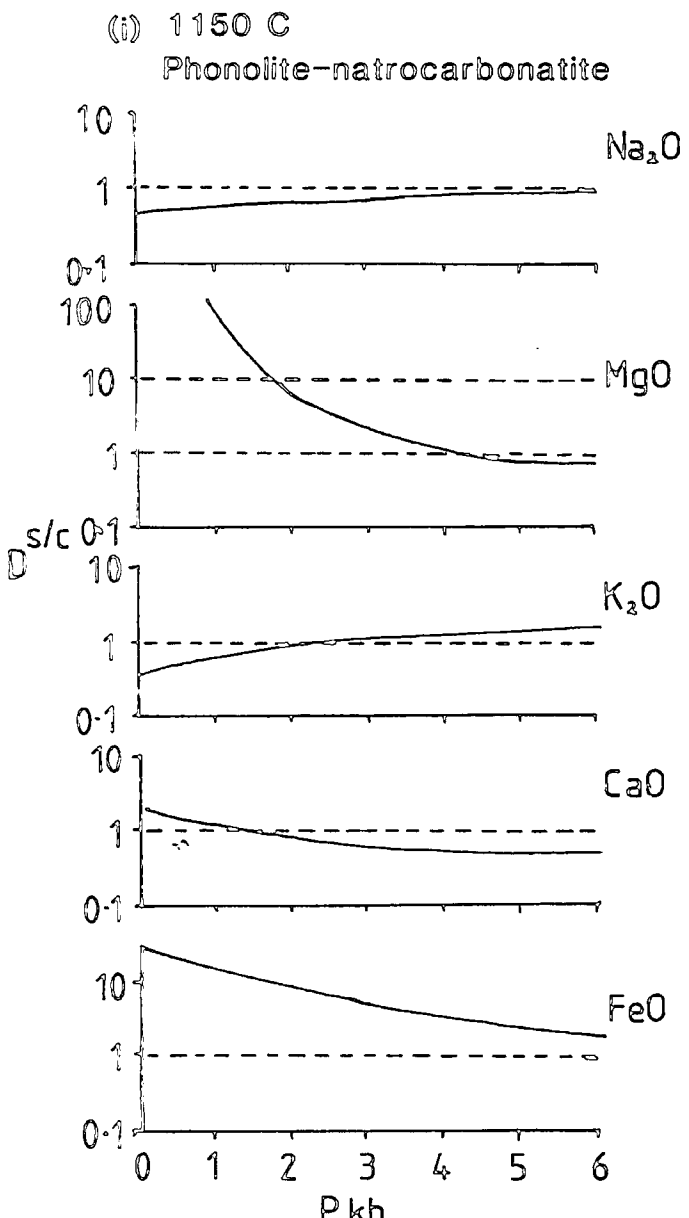
(i) 1150 C
Phonolite–natrocarbonatite
Na_2O
MgO
K_2O
CaO
FeO
D s/c
P kb

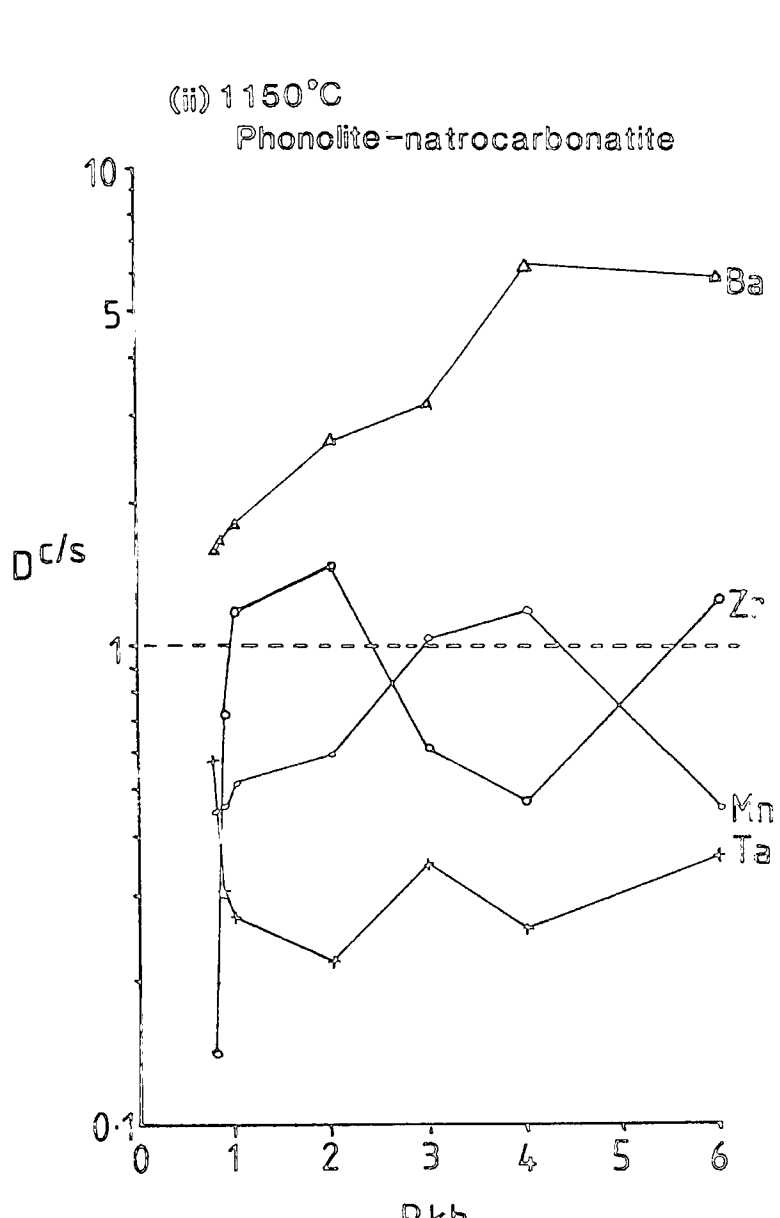
(ii) 1150°C
Phonolite–natrocarbonatite
Ba
Zr
Mn
Ta
D c/s
P kb

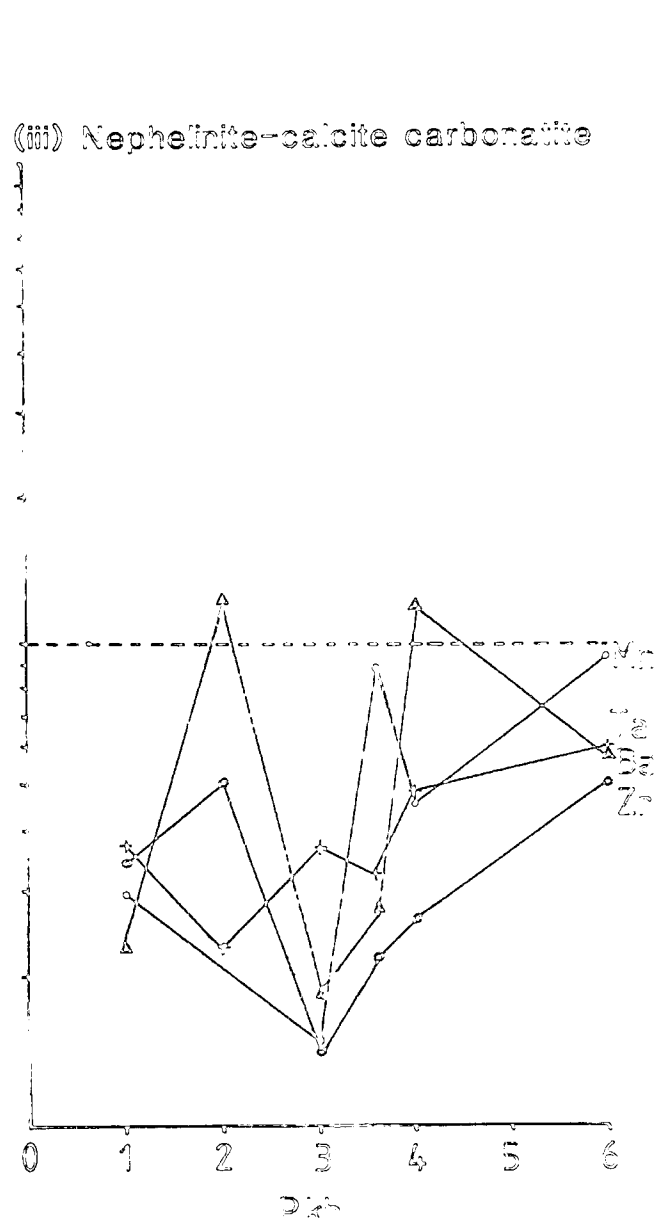
(iii) Nephelinite–calcite carbonatite
P kb

Figure 7.5.2B

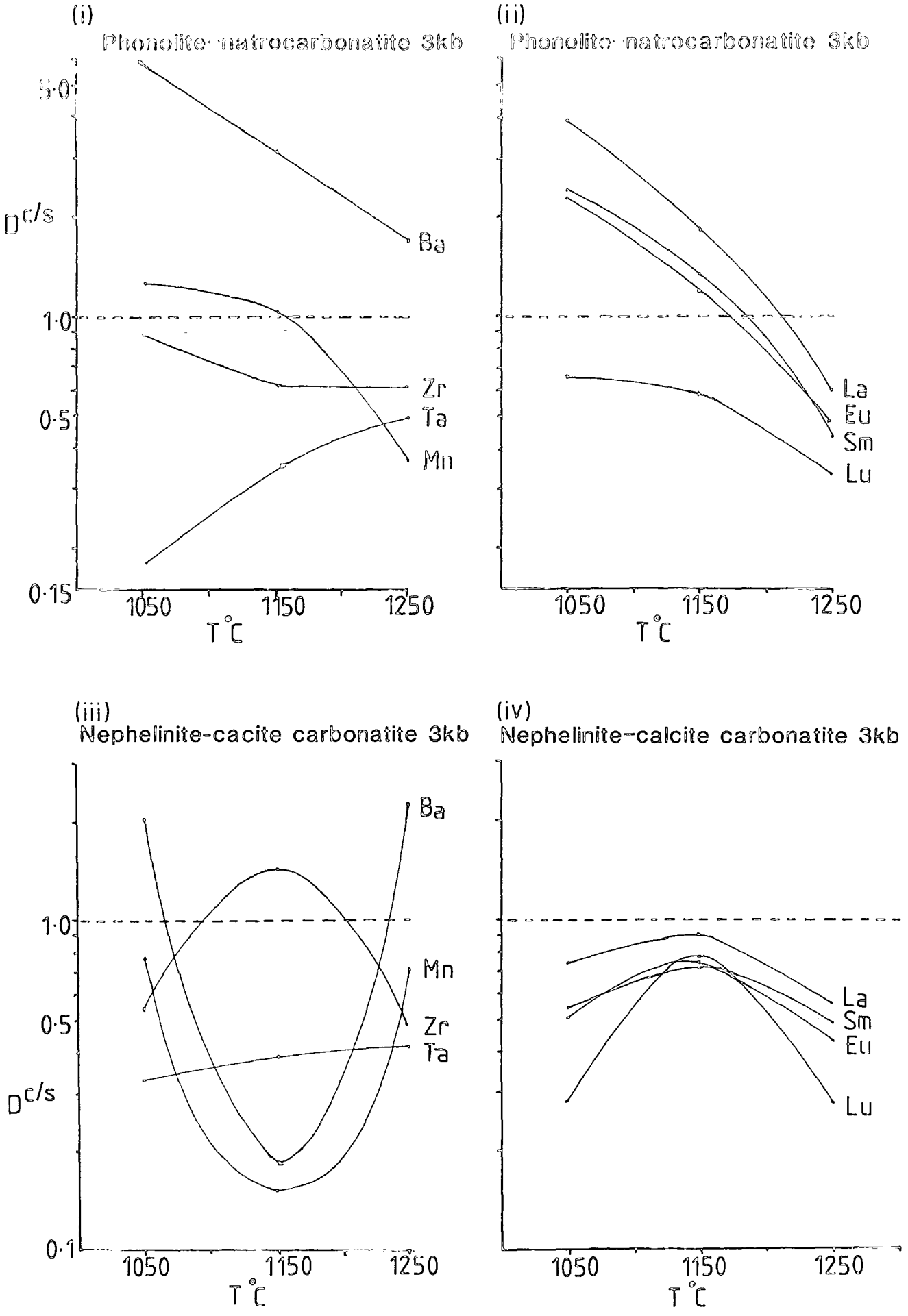
(i)
Phonolite-natrocarbonatite 3kb
5·0
1·0
0·5
0·15
D c/s
Ba
Zr
Ta
Mn
1050
1150
1250
T °C
(ii)
Phonolite-natrocarbonatite 3kb
La
Eu
Sm
Lu
1050
1150
1250
T °C
(iii)
Nephelinite-cacite carbonatite 3kb
1·0
0·5
0·1
D c/s
Ba
Mn
Zr
Ta
1050
1150
1250
T °C
(iv)
Nephelinite-calcite carbonatite 3kb
La
Sm
Eu
Lu
1050
1150
1250
T °C

carbonatite and nephelinite - calcite carbonatite immiscible pairs at varying pressures from 1-6kb. Figure 7.5.2B shows $D^{cbt/sil}$ for Ba, Mn, Zr, Ta, La, Sm, Eu and Lu for phonolite - natrocarbonatite and nephelinite - calcite carbonatite at 3kb. Figures 7.5.3A and B show the distribution coefficients for REE ($D^{cbt/sil}_{REE}$) between phonolite - natrocarbonatite and nephelinite - calcite carbonatite immiscible pairs after Bedson (1983). Figure 7.5.3C shows the REE distribution data calculated by Wendlandt and Harrison (1979) in the system sanidine - K_2CO_3. Bedson's data for the phonolite - natrocarbonatite pair is much less erratic than his data for the nephelinite - carbonatite pair. The former may be more applicable to the late stage occurrence of the Igaliko phonolites and the bulk composition of the Igaliko complex (see Chapter 7.6).

What is clear from this data is that, as well as the LREE prefering the carbonatite liquid over the HREE, increasing pressure causes an increase in $D^{cbt/sil}_{REE}$, as too does decreasing temperature. Ba and Mn show similar behaviour to the REE (ignoring the 6kb, 1150°C Mn data) and partition preferentially into carbonatite at lower temperatures/higher pressures. Zr data are erratic, being strongly enriched in the silicate at low pressure (<1kb) and showing no strong affinities to either silicate or carbonate liquids between 1-6kb. Ta (and thus, presumably Nb) is enriched in the silicate ($D^{cbt/sil}_{Ta} \approx 0.3$ between 1-6kb).

Bedson's (1983) major element distribution coefficients are also shown for phonolite - natrocarbonatite (note these are plotted as $D^{sil/cbt}$ not $D^{cbt/sil}$). At low pressures Mg, Fe (and surprisingly Ca) prefer the silicate liquid, whereas Na and K prefer the carbonate. Above about 4kb this reverses and Mg, Fe and Ca become enriched in the carbonate melt whilst Na and K partition into the silicate.

Wendlandt and Harrison (1979) conducted their experiments on REE partitioning at higher pressures than Bedson (1983) in a sanidine - K_2CO_3 system. Their 5kb data are however in stark contrast with the data of Bedson (1983, 1984) with Wendlandt and Harrison finding that HREE partition into the carbonatite ≈3 times more strongly than LREE. Their data are shown for comparison with Bedson's (1983) data in Figure 7.5.3. Bedson's (1983, 1984) data are considered to be more representative of the bulk compositions involved in the Igaliko dykes.

Figure 7.5.3

A. Distribution coefficients for REE between natrocarbonatite and phonolite immiscible liquids ($D^{cbt/sil}$) for pressures between 1 and 6kb at 1150°C (after Bedson 1983).

B. Distribution coefficients for REE between calcite-carbonatite and nephelinite immiscible liquids ($D^{cbt/sil}$) for pressures between 1 and 6kb at 1150°C (after Bedson 1983).

In the phonolite - natrocarbonatite pair the LREE above 2kb partition preferentially into the carbonate liquid, which always shows a preference for LREE rather than HREE (between 2.29 to 4.29 fold).

At these pressures in the nephelinite - calcite-carbonatite pair, the data appears more erratic (no smooth progression with increasing P) and there is a much weaker preference for the REE exhibited by the carbonatite than in the phonolite - natrocarbonatite case.

C. (Overleaf). REE partitioning for Ce, Sm and Tm determined by Wendlandt and Harrison (1980) in the system K_2O - Al_2O_3 - SiO_2 CO_2. Their figure captions are included under each diagram.

Figure 7.5.3A

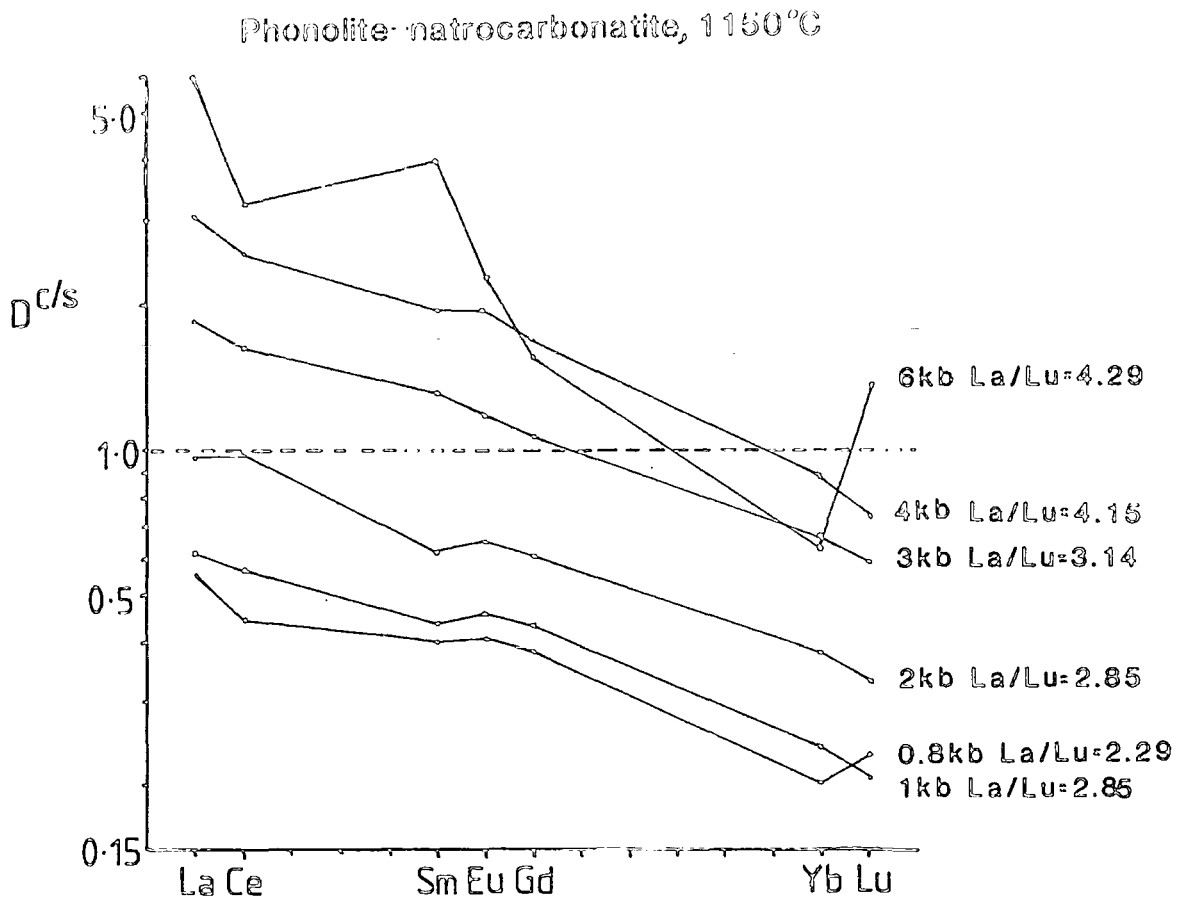

Figure 7.5.3B

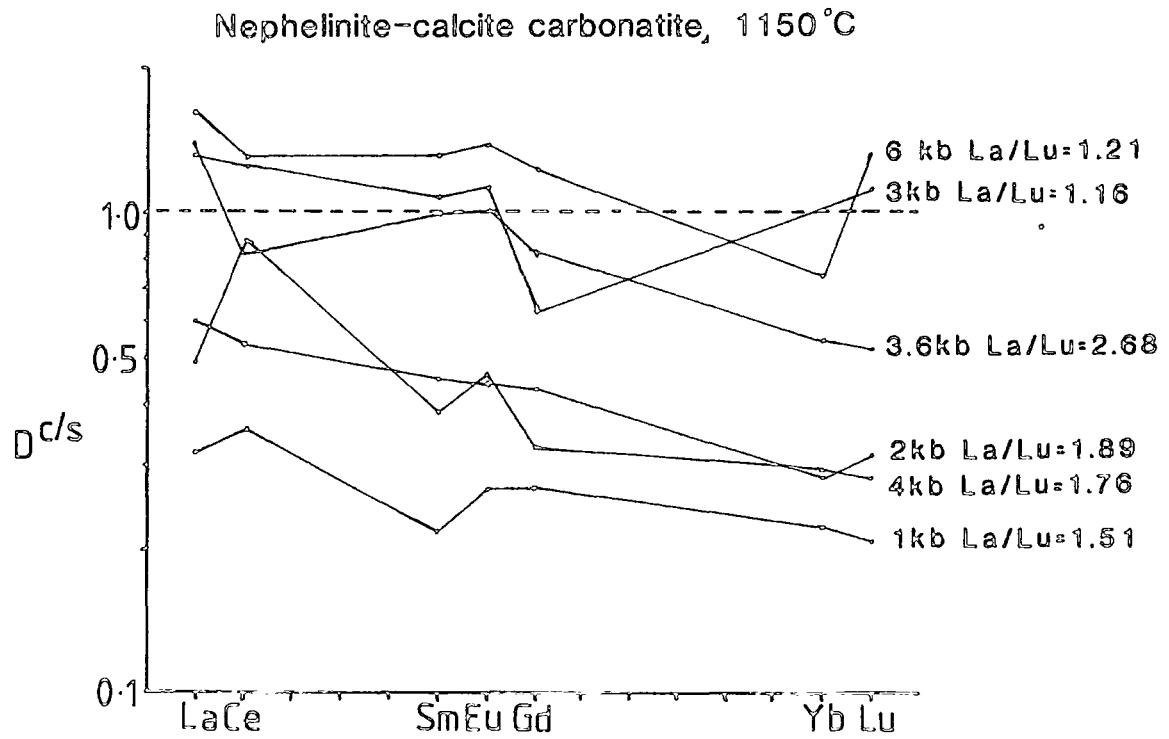

Figure 7.5.3C

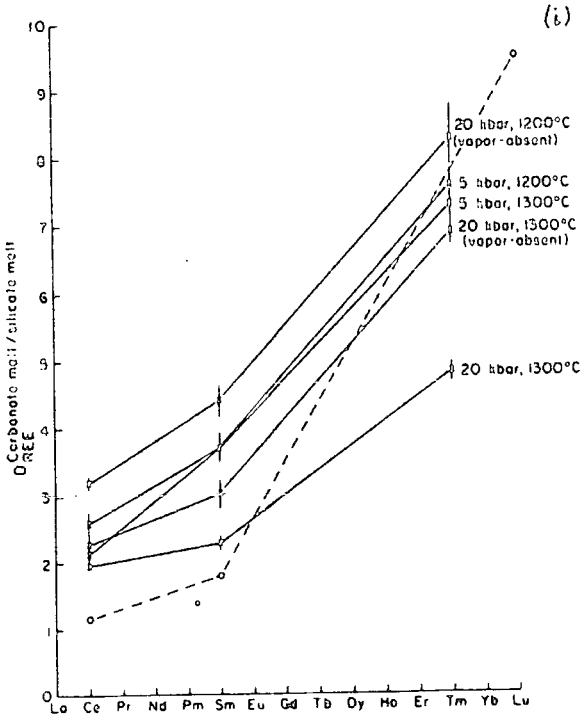

Fig. i. Partition coefficients for Ce, Sm, and Tm between coexisting carbonate and silicate melts at 1,200° and 1,300 °C, at 5 and 20 kbar. Ratios for Ce, Sm, and Lu from coexisting immiscible fractions from the Fen Complex (Mitchell and Brunfelt, 1975) are connected by *dashed line*. Error bars $\pm 1\sigma$

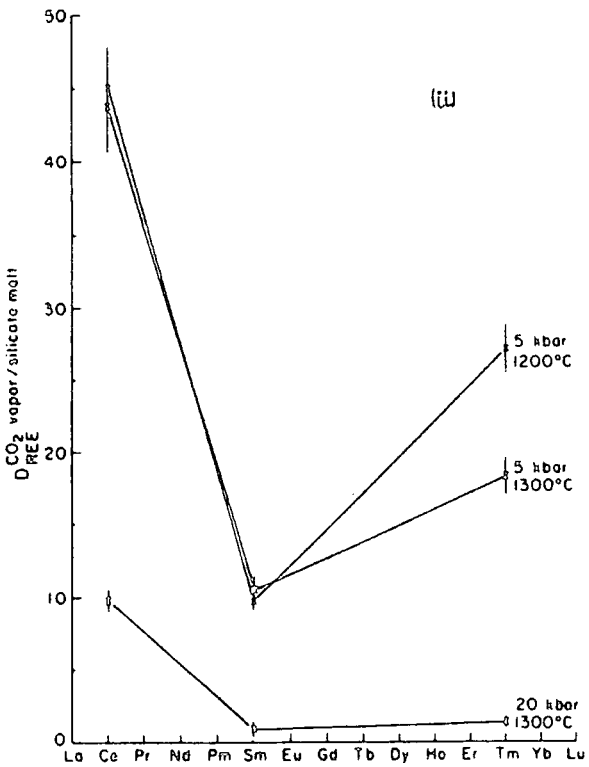

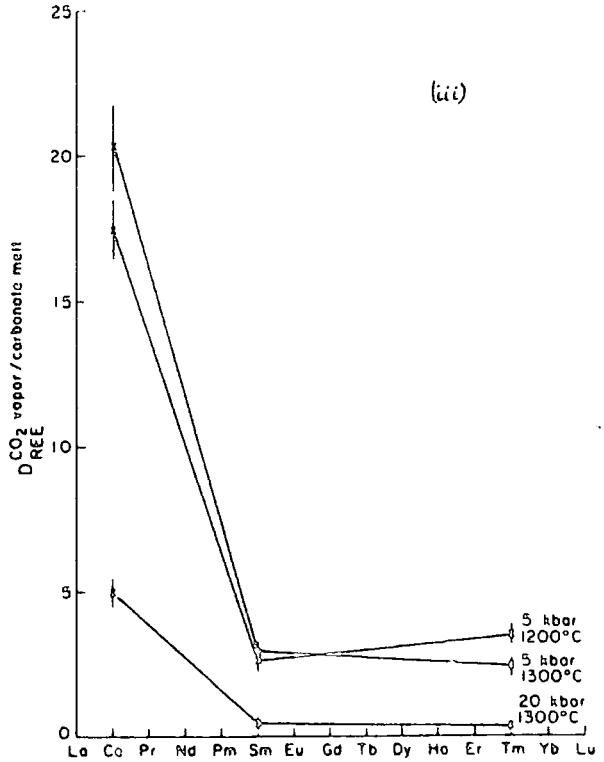

Fig. ii. and iii. Enrichment of REE in CO_2 vapor A relative to silicate melt at 5 and 20 kbar, and B relative to carbonate melt at 5 and 20 kbar. Partition coefficients are minimum values. Error bars $\pm 1\sigma$

7.6: Geochemistry, REE and Petrogenesis

In Chapter 7.4 a brief discussion of the geochemistry of the Igaliko carbonatites was presented. In the light of the various models proposed for the petrogenesis of carbonatites in the previous section (including trace elements partitioning), further consideration will be made of the geochemical data, including the REE.

It is generally accepted that carbonatites form by liquid immiscibility from a CO_2-rich silicate melt, although the compositions of both/either are ferociously debated (see Le Bas 1987, Twyman and Gittins 1987 for opposing opinions).

Figure 7.5.1A shows all analyses of carbonatites plotted in terms of $SiO_2+Al_2O_3$ - CaO - Na_2O + K_2O (analogous to the projection used by Freestone and Hamilton 1980 to show their 2-liquid field, Figure 7.5.B.

Also shown in Figure 7.5.1 are the average analyses for all TAS-classified groups. The scatter of data fall on a curve roughly parallel to the 1250°C, 5kb 2-liquid field boundary of Kjaersgaard. This may represent a 2-liquid boundary at lower temperature or higher pressure with the packing of all the tie lines onto such a short field boundary, a small change in silicate-liquid composition could produce a large change in carbonate-liquid composition. It may be possible, depending on the exact position of the tie lines, to produce relatively calcic carbonatites from 'evolved' rock types. Thus, relatively alkali-poor carbonatites (compared to Oldoinyo Lengai magmas) may be the primary carbonatites formed in Igaliko, and these would not have a great 'fenitising' effect upon the country rock. Fenitisation is not an obvious feature of the dyke walls in the field.

The incompatible element spidergrams (Figure 7.4.2) clearly indicated local occurrences of chemically distinct carbonatites. These show varying enrichment in incompatible elements, but relatively little variation in major element composition. Implicit in Figure 7.5.1A is that if CO_2 saturation is achieved in more basic magmas an immiscible carbonate liquid that forms will be more calcic and less alkali rich. It will generally possess chemical characteristics (major and trace) which are dependant upon the bulk chemistry of the system from which it formed (ie. the CO_2-saturated silicate). Thus, the time at which CO_2 saturation is achieved will govern the chemistry of the carbonatite as well as P and T playing important roles. If water saturation is achieved

in the carbonate melt prior to emplacement, it may lose alkalis away from its final place of rest (cf. Twyman and Gittins 1987 who suggest the Oldoinyo Lengai magmas never achieved water saturation), and may be emplaced as an alkali-poor sövite melt.

Trace Element Data - Implications

Bedson (1983) produced partition coefficients for an assortment of trace elements between silicate and carbonate immiscible melts. These are plotted in Figures 7.5.2 and 7.5.3. Table 7.6.1 shows average compositions for carbonatite, phonolite, nephelinite, ultra-mafic lamprophyre and tephrite for major and selected trace elements. The actual average for the carbonatites, due to local variations may not be truly representative, but it does illustrate many of the typical chemical features (enrichment in Sr, Ba, REE, Mn, P, F, Ca) compared to any of the other rock types from Igaliko.

From Bedson's (1983) data (see Figures 7.5.2 and 7.5.3), for a carbonatite forming immiscibly from a phonolite or nephelinite, the effect of pressure and temperature can be seen. Taking the enrichment factors from Table 7.6.1, the data would suggest that carbonatite contents of Ba and Mn could easily be obtained at ≈1050°C and 4-6kb, assuming phonolite - natrocarbonatite immiscibility. La, Ce and possibly Zr (although Zr appears to be lower in carbonatite than Bedson's data may suggest) would also fit this model. The distribution of these elements is not consistent with carbonatite immiscibility from a nephelinitic magma. Similarly, assuming nephelinitic distribution coefficients for the UML, and despite the occurrence of carbonate blebs in some UML, the carbonatites could not have formed as an immiscible liquid from the UML magmas.

REE

Several carbonatites were analysed for their total REE contents. Chondrite normalised spidergrams are shown in Figure 7.6.1. Pr has been omitted from these plots as correction factors for peak overlap on Pr become inaccurate at such high total REE (N. G. Walsh, pers. comm. 1986).

All but one of the carbonatites show extreme LREE enrichment -$(La/Lu)_{cn}$ ranging between 58.8 and 94.49, with La_{cn} exceeding 20,000 in 2 samples (326395 – a fluorite-bearing, late stage 'carbonatite' and 46257 – a 'normal sövite).

Figure 7.6.1A and B(overleaf).

REE spidergrams of carbonatite from the Igaliko Complex. Note how all but one (43931) show strong LREE enrichment. $(La/Lu)_{cn}$ ranges up to 140.4 from 58.39 with the exclusion of the HREE enriched sample 43931 with $(La/Lu)_{cn}$ of 0.84. Eu anomalies are virtually absent (except in 43931). Weight % F is indicated for each sample. Note the differences in HREE contents between individual samples, particularly in the 3 F-rich carbonatites (overleaf). Also notable are the very strong HREE enrichments achieved by some samples (eg. 43931, up to 700 times chondrite).

Figure 7.6.1A

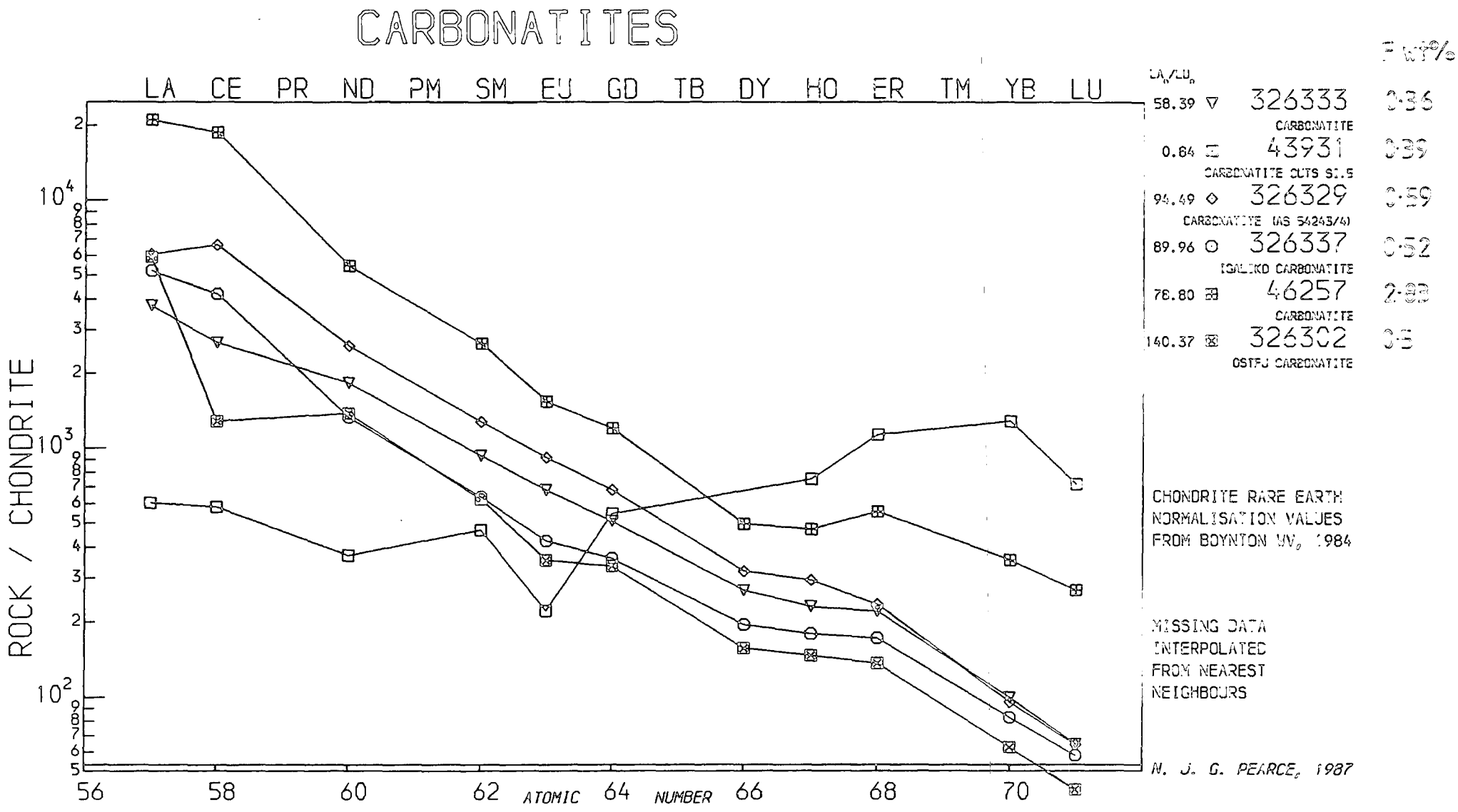
CARBONATITES
LA CE PR ND PM SM EU GD TB DY HO ER TM YB LU
ROCK / CHONDRITE
10^4
10^3
10^2
56 58 60 62 ATOMIC 64 NUMBER 66 68 70
La_n/Lu_n
58.39 ▽ 326333 CARBONATITE
0.84 □ 43931 CARBONATITE CUTS S1.5
94.49 ◇ 326329 CARBONATITE (AS 54243/4)
89.96 ○ 326337 IGALIKO CARBONATITE
78.80 ⊞ 46257 CARBONATITE
140.37 ⊠ 326302 OSTFU CARBONATITE
F wt%
0·36
0·39
0·59
0·52
2·33
0·3
CHONDRITE RARE EARTH NORMALISATION VALUES FROM BOYNTON WV, 1984
MISSING DATA INTERPOLATED FROM NEAREST NEIGHBOURS
N. J. G. PEARCE, 1987

Figure 7.6.1B

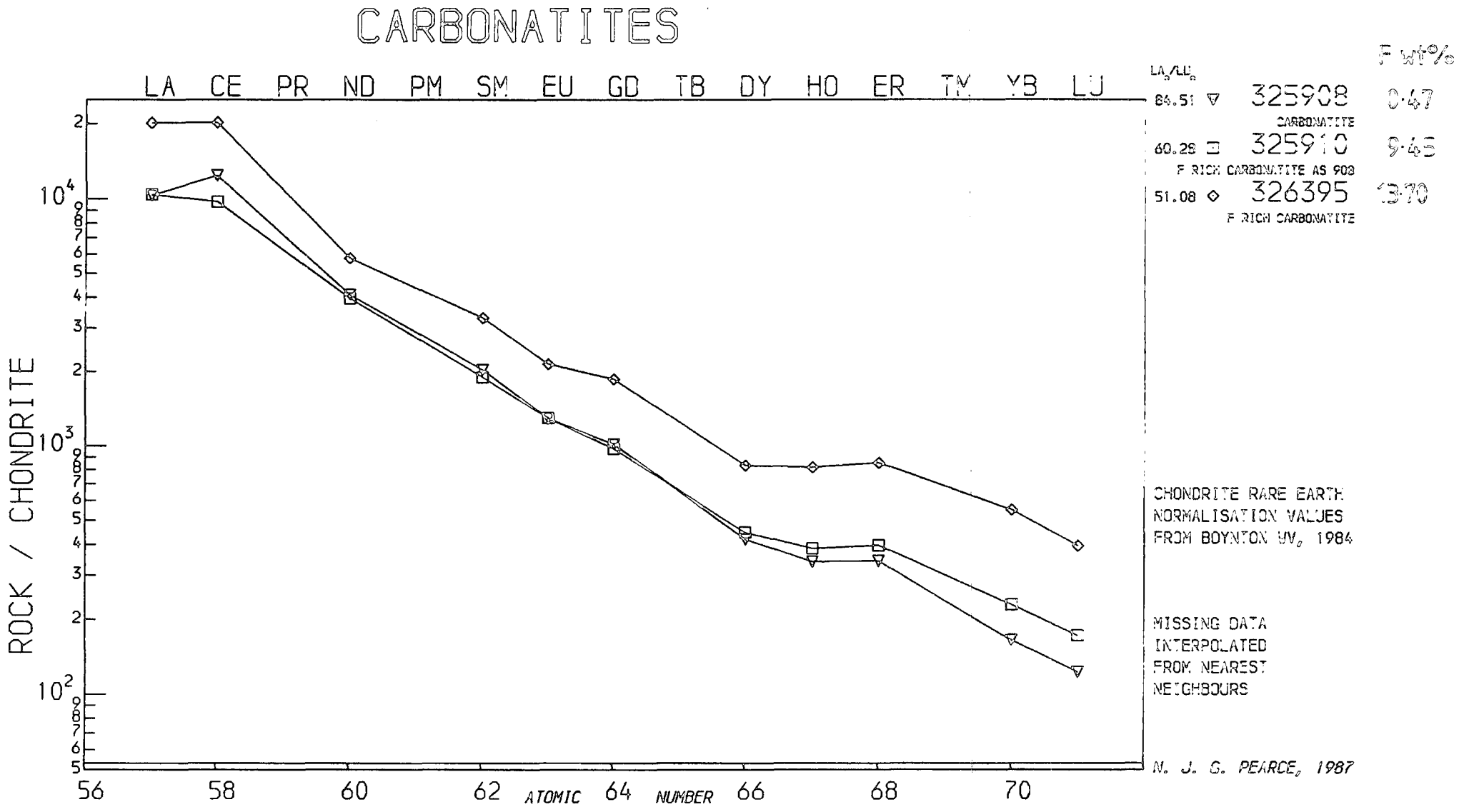
CARBONATITES
LA CE PR ND PM SM EU GD TB DY HO ER TM YB LU
ROCK / CHONDRITE
ATOMIC NUMBER
56 58 60 62 64 66 68 70
F wt%
LA_n/LU_n
84.51 ▽ 325908 0·47
CARBONATITE
60.28 □ 325910 9·45
F RICH CARBONATITE AS 903
51.08 ◇ 326395 13·70
F RICH CARBONATITE
CHONDRITE RARE EARTH NORMALISATION VALUES FROM BOYNTON WV, 1984
MISSING DATA INTERPOLATED FROM NEAREST NEIGHBOURS
N. J. G. PEARCE, 1987

Table 7.6.1

Average major and selected trace element data (unscaled).

	Cbt-ite	Phon	Neph-ite	UML	Cbt/Phon	Cbt/Neph	Cbt/UML
Major elements (wt%)							
SiO_2	6.25	55.54	39.67	35.76	0.113	0.158	0.175
Al_2O_3	0.62	17.92	9.70	7.68	0.035	.064	0.081
Fe_2O_3	8.79	8.30	15.08	16.94	1.05	0.583	0.519
MgO	1.49	0.44	10.74	13.61	3.39	0.139	0.109
CaO	41.37	1.85	11.08	13.14	22.36	3.73	3.14
Na_2O	0.4	7.16	2.08	0.52	0.056	0.192	0.769
K_2O	0.26	5.65	4.05	3.95	0.046	0.064	0.066
TiO_2	0.11	0.56	3.61	3.99	0.196	0.030	0.028
MnO	2.14	0.28	0.31	0.30	7.64	6.90	7.13
P_2O_5	2.07	0.09	1.07	1.30	23.0	1.93	1.59
F	1.52	0.28	0.17	0.21	5.43	8.94	7.23
Cl	0.00	0.21	0.28	0.07	0.0	0.0	0.00
Trace elements (ppm)							
Ba	3559	370	2175	2347	9.62	1.64	1.43
Nb	242	484	132	141	0.500	1.83	1.72
Zr	8	1691	430	459	0.005	0.061	0.017
Sr	27699	356	1457	2182	77.8	19.0	12.69
La	1573	339	151	214	4.64	10.4	7.35
Ce	2068	551	245	316	3.75	8.44	6.54
Y	872	124	56	58	7.03	6.71	15.03

One sample (43931) shows HREE enrichment – $(La/Lu)_{cn}$=0.84. This is the most Si-rich of the carbonatites and is essentially composed of calcite and albitic feldspar. Minor ?allanite (<1% modally) is observed along with an unidentified, brownish (altered?) mineral. One of these may be HREE enriched. Unlike all of the other carbonatites this shows a distinct negative Eu anomaly (Eu/Eu^*=0.44). Eu anomalies are generally lacking from most carbonatites although Eby (1975) has reported both positive and negative Eu anomalies from Oka, Quebec.

Several studies on REE of carbonatites and associated silicate rocks have been pub-

lished (eg. Eby 1975, Mitchell and Brunfeldt 1975, Cullers and Medaris 1977, Maravic and Morteani 1980, Secher and Larsen 1980). All of these studies report strong LREE enrichment in the carbonatites and generally high $(La/Lu)_{cn}$.

Figure 7.6.2 shows the range of late carbonatites in the region of Igaliko village compared to phonolites (with and without Eu anomalies) and to ultramafic lamprophyres. Using Bedson's (1983) data for REE partitioning it is apparent that the lamprophyres could not have been in an immiscible relationship with the carbonatites (at less than 6kb). The REE data as a whole are consistent with the formation of the carbonatites by liquid immiscibility from a CO_2-rich phonolite, at perhaps 5kb and 1050-1150°C (see Figure 7.5.1). They could however have formed at temperatures of less than 1050°C and pressures of 2-3kb, to produce similar REE results. Whatever the exact P-T conditions, immiscibility at low temperature (1000°C?) and low/moderate pressures (3-5kb?) seems to have governed their REE and trace element chemistry.

REE patterns of F-rich carbonatites are shown in Figure 7.6.2, where their F contents are indicated. 325908 and 325910 are from the same dyke separated by about 1.5 km horizontally and 200m vertically. Although these samples show very similar LREE and MREE contents there is a marked divergence in their HREE contents probably caused by preferential concentration of the HREE by F-bearing complexes. Mineyev (1963) showed similar complexing in a chemically zoned metasomatised granite, and correlated the REE content with F and pH of the metasomatic fluid. In this fluid LREE complexes were shown to be less stable than HREE complexes and thus would precipitate earlier. Thus, F-rich fluids would become preferentially enriched in HREE and this mechanism would seem to apply to the carbonatite dyke 325908, 325910. Experimental studies on REE stability in acidic solutions rich in Cl^- or F^- identified the most stable complexes as $RE(Cl,F)_2^+$ for most REE and $RE(Cl,F)_3$ for La (Sillén and Martell 1964).

Bedson's (1983, 1984) data suggest no strong fractionation of Eu relative to Sm and Gd between carbonate/silicate liquids. The lack of negative Eu anomalies in the carbonatites would therefore suggest that they separated from Eu-anomaly free phonolites (see Figure 7.6.3 and Chapter 6.7). Undersaturated benmoreites and phonolites (due to high fo_2) often show no En anomaly as a result of feldspar fractionation, thus the lack

Figure 7.3.2

REE contents from late carbonatite dykes in the vicinity of Igaliko village compared to phonolite dykes with or without Eu anomalies (A) or ultramafic lamprophyres (B). The UML, often containing calcite may be regarded as similar to the nephelinite used in Bedson's (1983) experiments. These diagrams should be compared with the REE distribution coefficients illustrated in Figures 7.5.2 and 7.5.3 (after Bedson 1983).

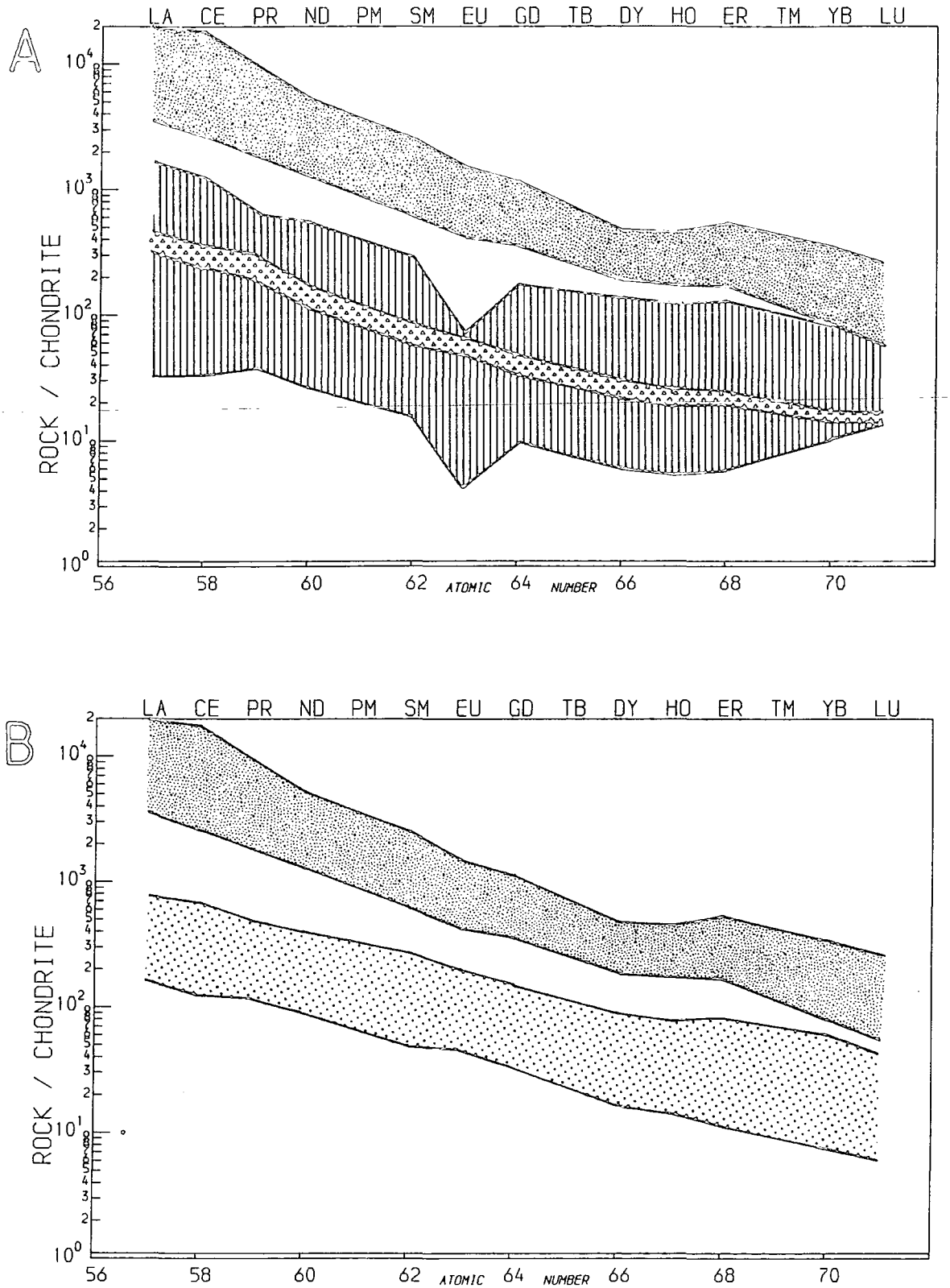

CHONDRITE RARE EAR
NORMALISATION VALU
FROM BOYNTON WV, 1

of an Eu anomaly in carbonatites formed by immiscibility from a phonolite presents no genetic problem.

Effect of CO_2 on Silicate Melts

The presence of substantial CO_2 in a felsic silicate melt will have a strong depolymerising effect (Mysen 1976). In a melt of albite composition, Mysen (1976) observed an increase in $CO_3^{2-}/(CO_2+CO_3^{2-})$ of about 100% between 20 and 30kb. This he attributed to a change in melt polymerisation producing an increase in the number of non-bridging oxygens. This yields higher $a_{O^{2-}}$ and high $X_{CO_3^{2-}}$, thus higher solubility of CO_2. An increase in $a_{O^{2-}}$ would lead directly to an increase in fo_2 (see Wood and Fraser 1977, p55). This in turn leads to Eu^{3+} complexes and reduction of Eu^{3+}/Eu^{2+} in the melt (Wood and Fraser 1977, p186), and reduces the $D_{Eu}^{feldspar}$. Thus Eu anomalies will either be small or absent in CO_2-rich rocks. Loss of a CO_2-rich phase (such as carbonatite melt) would cause some reduction in fo_2, would decrease Eu^{3+}/Eu^{2+}, and allow Eu to partition into feldspar. This would allow the development of negative Eu anomalies in the silicate melt by subsequent feldspar fractionation.

The presence of CO_2 in the undersaturated suite of rocks may thus account for the high fo_2 and the lack of negative Eu anomalies in many samples. CO_2 saturation, followed by loss of a carbonate phase could allow subsequent development of Eu anomalies. If this is the case, it appears that a carbonatite phase may have been lost from magmas of both benmoreitic and phonolitic compositions. This would be consistent with the differences in major and trace element geochemistries observed in different regional groups of carbonatites, these having formed at different stages of 'parental' silicate melt evolution.

Those phonolites without Eu anomalies tend to contain cancrinite and all have very high Sr contents (average 2373ppm), whilst those with Eu anomalies have Sr at $\approx$ 210ppm (average of 3) and no CO_2-bearing phases. Sr partitions into a carbonate-rich phase and it has already been suggested that these Sr-rich phonolites may contain a carbonatite component (see Chapter 5.3, *Sr*). The REE evidence would also support this, although some Sr may have been lost from the phonolites showing negative Eu anomalies by feldspar fractionation. Mn, which is not removed by feldspar, and strongly

preferred by a carbonatite phase (Bedson 1983) is noticeably higher in the phonolites with no negative Eu anomaly (0.41 wt % MnO) compared to those with an Eu anomaly (0.29 wt% MnO). This is consistent with the above argument relating to the loss of a CO_2-rich phase from a phonolite (or possibly benmoreite) melt that showed no Eu anomaly.

The lack of obvious fenitisation in such low T, moderate P conditions, could mean,

(i) that calcic carbonatite, with low alkali contents formed and thus had no fenitising effect on the country rock,

(ii) alkalis were lost at depth with early water saturation, the residue being an alkali-poor sövite crystal mush,

(iii) fenitisation was simply not apparent in the field, but was present (although this seems less likely than the other possibilities).

7.7: Melting Studies

To check that a late phonolite and carbonatite from the Igaliko region would not mix, 3 samples were sent to B. Kjaersgaard at Manchester University for experimental study.

Phonolite 43802 was run together in a 50:50, weight:weight mix with 325908 and 326333. These mixtures were sealed in Ag-Pd alloy tubes and run at ≈1200°C and 5kb in internally heated, argon medium pressure vessels (see Bedson 1984 for experimental techniques). Plates 7.14 and 7.15 show the quenched products of these charges. Both runs are interpreted as consisting of a CO_2-saturated silicate liquid (dark glass) a carbonate liquid (pale lining to vesicles – not a sublimate from a gas phase) and a vapour phase (producing the vesiculation). It was hoped to be able to analyse the separate phases but time did not allow. Comparison of the products of the melt run with those of the starting products would have been useful. The results of these runs show at least that it is possible for these samples to have formed by an 'immiscible-pair' relationship, although this does not necessarily mean that they could not have had somewhat different origins. Further experimental work on these samples would be instructive.

Plate 7.14: Product of experimental run of 43802 and 325908 in 50-50 w/w mix. Run conditions 5kb, 1200°C. The white coating to the vesicles is a quenched carbonate liquid. The dark glass is silicate. Magnification ×30.

Plate 7.15: Product of experimental run of 43802 and 326333. Interpretation as above. Magnification ×30.

CHAPTER 8: LAMPROPHYRES

8.1: Introduction

Lamprophyres are a group of rocks which are readily identified in the field and are characterised by many mafic phenocrysts. They are relatively abundant in the Igaliko Nepheline Syenite complex forming many small dykes of varied composition. Until recently lamprophyres have had little systematic treatment and this has led to widespread confusion in the literature. Streckeisen (1979) clarified the situation by proposing a nomenclature for the lamprophyres, and over the last 10 years Rock has tried to reconcile the many, often inconsistent, views proposed by various workers (see Rock 1977, 1984, 1986, 1987a). It is these studies that provide the basis for the nomenclature and classification employed in this chapter.

The lamprophyres can be divided into 5 'branches' (see Rock 1987a), (i) ultramafic lamprophyres (*UML*, see Rock 1986), (ii) alkaline lamprophyres (*AL*, see Rock 1977), (iii) calc-alkaline lamprophyres (*CAL*, see Rock 1984, although in his 1977 paper he prefers 'shoshonitic', implying K>Na), (iv) lamproites (*LL*, see Bergman 1987) and (v) kimberlites (see Rock 1987b and Hughes 1982). Although petrographically and mineralogically distinct it is not always possible to discriminate easily between different branches of the lamprophyre clan by chemical parameters. Similarly, certain branches of the lamprophyres are chemically very similar to more normal igneous rocks such as tephrites/basanites or alkali basalts/hawaiites. Rock (1987a) suggests that variations in mineral chemistry may be one of the most useful methods for distinguishing between individual groups of lamprophyres.

The mineralogy of lamprophyres forms the basis of their nomenclature and this is summarised below. Essential constituents are micas and/or amphiboles typically occurring alongside clinopyroxene, feldspar (alkali or plagioclase), olivine and, with the general exception of CAL, feldspathoid. Lamprophyres are thus typically mafic rocks although often contain abundant alkali feldspar/feldspathoid.

Table 8.1.1 (taken from Rock 1987a) gives certain features characteristic of different branches of the lamprophyre clan (excluding kimberlites).

Table 8.1.1.

Summary of major petrological contrasts between the four lamprophyre branches (excluding kimberlites). Taken from Rock 1987a.

	Calc-alkaline lamprophyres (CAL)	Alkaline lamprophyres (AL)	Ultramafic lamprophyres (UML)	Lamproites (LL)
Contrasts in cognate mineralogy				
Mafic index	33–67	>67	>90	33–67
Quartz	*Common* (but <10%)	Absent	Absent	*Occasional*
Nepheline, sodalite group	Absent	*Present to abundant*	*Present to abundant*	Absent
Armalcolite, pseudobrookite	*Occasional*	Absent	Unknown	*Common*
Leucite, wadeite, jeppeite, priderite, shcherbakovite etc.	Absent	Absent	Absent	*One or more almost always present*
Melilite, Ca-Ti-Zr-garnet	Absent	Absent	*Common*	Absent
Perovskite	Absent	Absent	*Ubiquitous*	Sometimes present
Plagioclase ($An_{<10}$)	Minor to essential	Minor to essential	Absent	Absent
Albite	Occasional	Common	Rare accessory	Absent
Contrasts in 'typical' compositions of common minerals found in all four lamprophyre branches (see also Figs 2–4; Tables 4 and 5)				
Ilmenites	May carry high Mn, moderate Mg[1]	Normal	*Rich in Mg and Mn*	*Normally absent*, but may be rich in Mg; Mn-poor
Carbonates[1]	Calcite	Calcite, dolomite	Calcite, dolomite, breunnerite	Dolomite, breunnerite
Ca-pyroxenes[2]	Al-bearing diopsidic augite; zoning minor	*Al-rich titanaugite, nearly always complexly and strongly zoned*	Al-Ti-salite; Fe^{3+}-salite; zoning minor	*Nearly pure diopside; practically unzoned*
Amphiboles	*Hastingsite; tschermakite*; Mg-riebeckite/arfvedsonite	*Kaersutite*; Ti-pargasite	Groundmass arfvedsonite; occasionally hoersutite/hastingsite megacrysts	*Potassium (titanian) richterite*; Mg-riebeckite/arfvedsonite
Micas	High Al-Ti phlogopite	High-Al-Ti *biotite*	*High-Ba* Ti phlogopite; *some tetraferriphlogopite*	*Al-poor tetraferriphlogopite*; rich in F, low in Cr, Ba-bearing
Olivine (%Fo)	80–90	Typically 80–86	Typically 84–90	Typically 88–92
Alkali feldspar	Fe-Ba-bearing orthoclase; zoning slight	*Fe-poor orthoclase to albite; usually strongly zoned*	Generally absent (<10%); Fe-orthoclase if present; unzoned[1]	Sometimes absent; *Ba-Fe-rich*, Na-poor orthoclase if present; unzoned
Contrasts in typical whole-rock composition ('typical' defined by >80% of analyses) (see also Figs 6 and 7; Table 8)				
SiO_2	46–57	36–46	20–35	48–58
Al_2O_3	11–18	10–16	2–12	6–12
MgO	3–10	4–10	8–20	6–14
CaO	4–9	7–15	10–20	2–7
Na_2O	1.5–4	2–5	<3	<2
K_2O	3–7	1–3	1–3	6–11
CO_2	1–5	1–6	2–12	<6
K/(Na+K) (atomic %)	30–60 (potassic)	15–40 (sodic)	30–80 (sodipotassic)	70–95 (ultrapotassic)
Contrasts in typical normative composition (see also Table 8)				
Q	<10	0	0	<10
Ne	<10	High	High	<10
Lc	Rarely, and <10	Occasionally, <20	Often >0	Usually >0
An	Generally 0	High	Often 0	Generally 0
Ns (Na_2SiO_3)	Rarely, and <10	0	Generally 0	Generally >0
Ks (K_2SiO_3)	0	0	0	*Often* >0
Lo	0	0	*High*	0
Ru	Rarely, and <2	Very rarely, and <2	0	Often, up to 5
Contrasts in mineralogy of 'globular structures'				
Quartz	Common	Rare	Absent	?Absent
Alkali feldspar	Common	Common	Absent	Common
Plagioclase	Common	Rare	Absent	Absent
Nepheline	Absent	Common	Occurs	Absent
Analcime	Rare	Common	Occurs	Occurs
Amphibole[1]	Rare	Rare	?Occurs	Common
Pyroxene[1]	Rare	Rare	?Occurs	Occurs
Biotite	Minor	Common	Occurs	?Occurs
Carbonate	Common	Common	*Dominant*	?Occurs
Epidote	Common	Rare	?Occurs	?Occurs
Serpolite[1]	?Occurs	Occurs	?Occurs	?Occurs

* The most useful diagnostic features are in italics. [1] Based on limited data; [2] aegirines in various relationships may be present in all four branches.

Table 8.1.2

Mineralogical classification of lamprophyres, excluding LL. (Compiled from Rock 1977, 1983, 1986). Rock names in italics.

Alkaline lamprophyres

	Ol	Ti-augite (Al-rich)	Kaers/ mica	Fsp	G-mass
Camptonite	Y	Y	e	Lab/And>AF	Fsp>Foid
Sannaite	Y	Y	e	AF>Plag	Fsp>Foid
Tannbuschite	Y	Y	e	any fsp	FSP<Foid (Ne)
Monchiquite	Y	Y	e	a	Amorphous/glass
Fourchite	a	Y	e	a	2° foid +/or zeolites

Calc-alkaline lamprophyres (Shoshonitic lamprophyres).

Cpx + altered ol +	Quartz (accessory) + alkali feldspar	plagioclase
Biotite	*Minette*	*Kersantite*
Green-brown Hbl	*Vogesite*	*Spessartite*

Ultramafic lamprophyres (modal %).

	Melilite	Foid	Cbt	AFsp	Cpx	Amp	Phlog	Ox	Glass
Aillikite	a	a (m)	5-90 e	a	4-30	<25	16-68 e	1-22	a
Alnöite	3-35 e	m/a	<10	a	5-24	32†	5-30	1-18	<6
Damkjernite	a	3-10 m/e	<3 e	6-7	30-49	a	5-24	9-22	<13
Ouachitite	<6	12-17 e	8-23 e	a	0-39	a	22-41	<6	a
Polzenite	13-35 e	11-35 e	<13	a	<20	32‡	8-22	5-12	5-19

Y – present; m – minor; a – absent; e – essential; † 1 example from 6 all others 0; ‡ 1 example from 7 all others 0; Kaers – kaersutite; Ol – olivine; Cbt – carbonate.

None of the dykes from Igaliko is lamproitic or kimberlitic, all being members of the UML, alkaline (AL) or calc-alkaline (CAL) lamprophyre branches. Table 8.1.2 present certain essential mineralogical data for petrographic classification within UML, AL or CAL branches, and has been compiled from Rock (1977, 1983, 1986).

8.2: Petrography

All the lamprophyres from the Igaliko region fall into the alkaline (AL), calc-alkaline (CAL) or ultramafic (UML) branches of the lamprophyre clan. These will be considered separately below.

8.2.A: Alkaline Lamprophyres (AL)

Alkaline lamprophyres are represented in the Igaliko area by several camptonites and a possible sannaite dyke. They are typically mafic rocks with around 30% modally of felsic minerals. Camptonites are porphyritic rocks which almost always contain large, euhedral phenocrysts of pinkish, Ti-rich augite/salite. These may be up to 5mm in diameter in some samples, (eg. 325943, see Plate 8.4). This pyroxene is usually very fresh although may become altered in some cases. Clinopyroxene may be present as glomeroporphyritic clusters up to 2.5mm across (see Plate 8.2). Sector zoning is visible occasionally in the pyroxene.

Olivine is an essential constituent of camptonites but is typically altered to serpentinite/chlorite assemblages (see Plates 8.1, 8.2, 8.3) which often preserve the outline of the former olivine crystal. Complete replacement of the olivine by calcite is also seen (eg. 52274, Plate 8.3).

Iron oxide is a common phenocryst phase occurring in crystals up to 5mm in diameter (eg. 325943). Occasionally, deep reddish-brown to bronze (or fox-coloured) kaersutite phenocrysts are seen (eg. 325943) which are strongly pleochroic to almost colourless. Typically however, kaersutite is confined to the groundmass, where it occurs as small, lath shaped crystals, between 0.5 to 1mm long. These often show a crude alignment (trachytic texture), flowing around phenocrysts (see Plate 8.1). Kaersutite forms about 20-25% of the mode typically, although is almost absent from the groundmass of some samples.

Pink, salitic pyroxene also forms as small, (500μm diameter or less) groundmass crystals, often euhedral and compositionally similar (ie. high Ti, Al) to the phenocrysts. Groundmass pyroxene may occupy up to 20% of the mode. Iron oxides are abundant in the groundmass as small, blocky euhedra, making up perhaps 10% of the mode. Chlorite

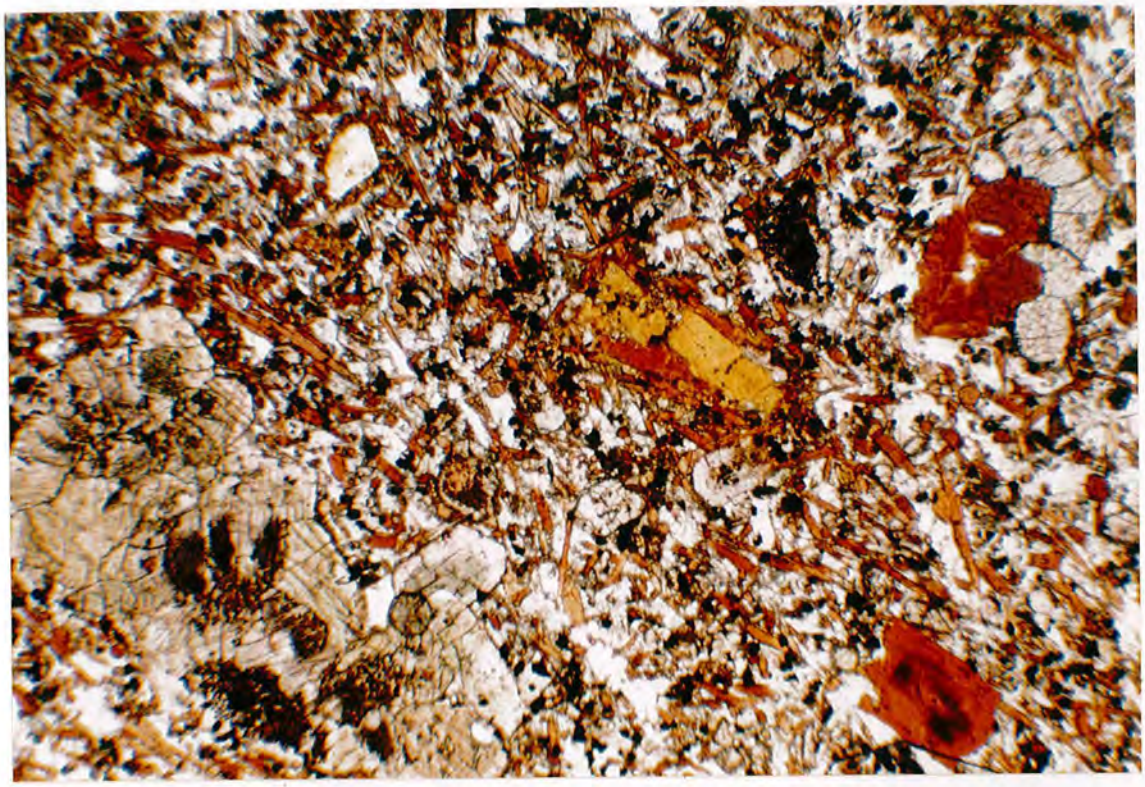

Plate 8.1A 52285 Camptonite. PPL. ×35.

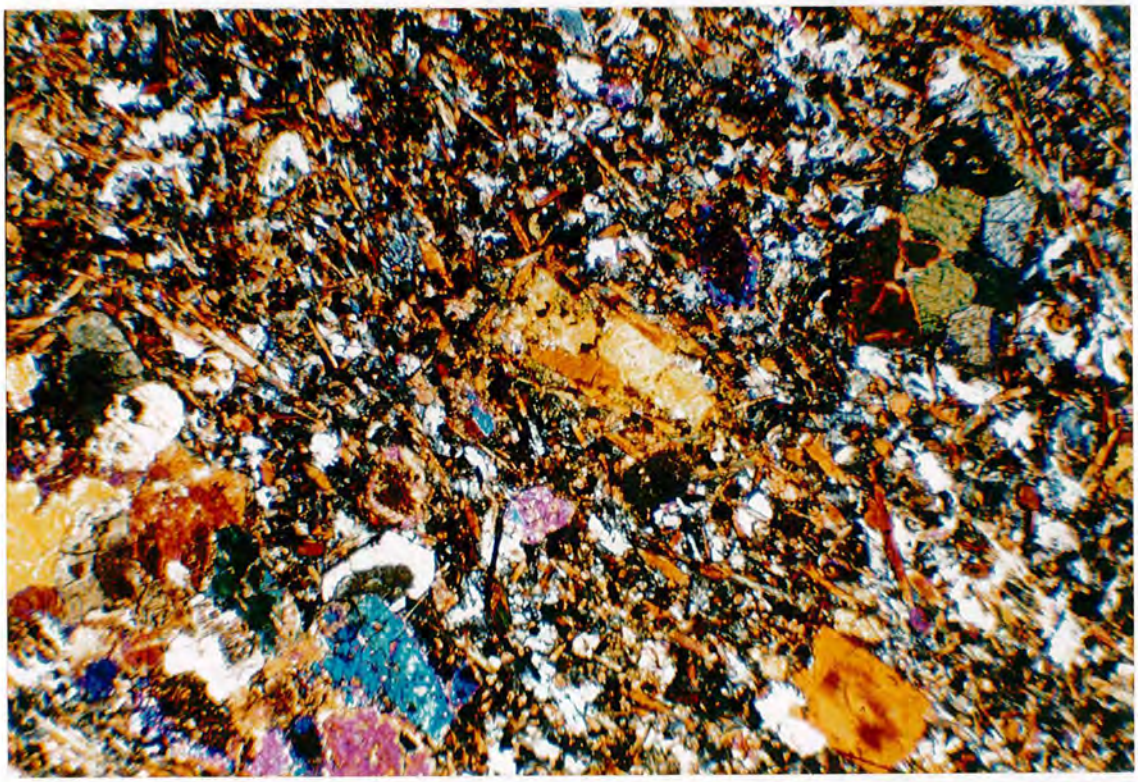

Plate 8.1B 52285 Camptonite. XPL. ×35. These alkaline lamprophyres are typified by the presence of deep reddish-brown kaersutite as either groundmass or phenocryst crystals. Large glomeroporphyritic crystals of Mg-rich clinopyroxenes are seen (bottom left). The groundmass is essentially kaersutite, opaque Fe-Ti oxide, plagioclase, feldspathoid (analcite?) and rare carbonate. The yellow-brown patch just right of centre is chlorite, an alteration product, probably of olivine. There is a hint of trachytic texture in the groundmass.

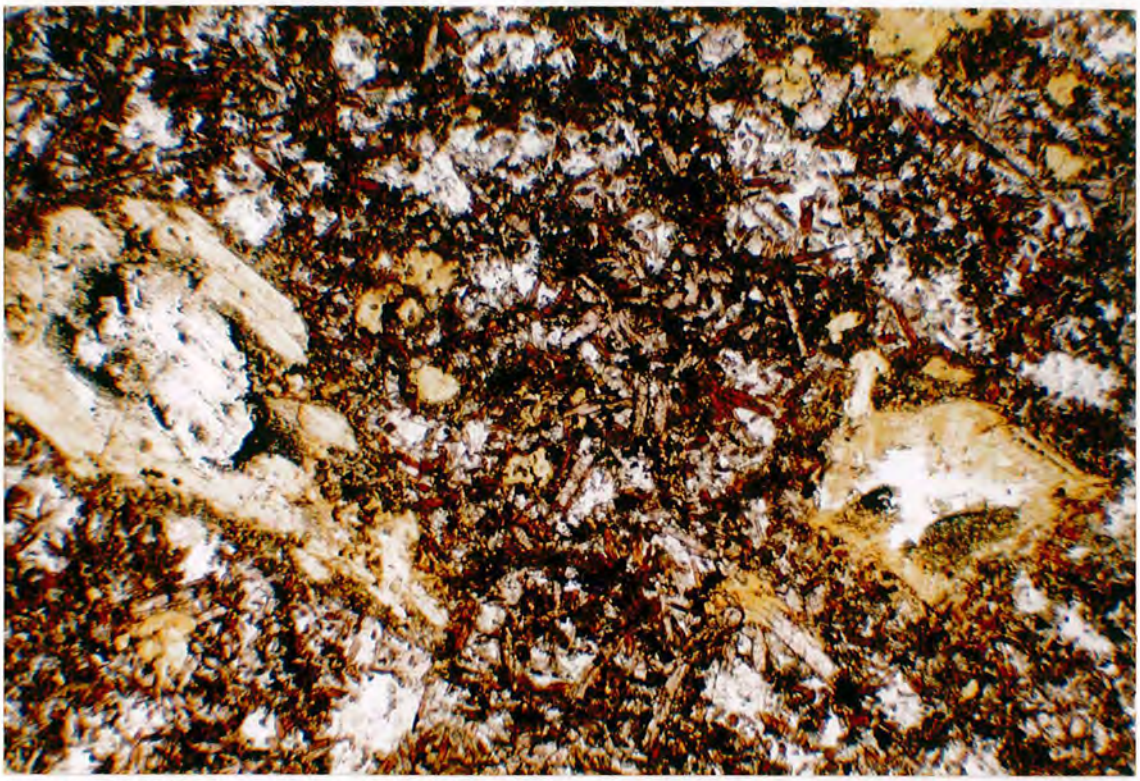

Plate 8.2 326308 Camptonite. PPL. ×35. The large yellow/clear patches (centre left and lower right) are chlorite/serpentine aggregates after olivine (note hexagonal outline). The groundmass is composed of kaersutite (red-brown), Ti-augite (pinkish) and opaque oxides with felsic minerals (plagioclase and analcite?) occurring in colourless ocelli, (eg. bottom, left of centre).

Plate 8.3 52274 Camptonite. XPL. ×35. A large augite phenocryst is visible at the centre of this plate, showing a vermicular exsolution of opaque Fe-Ti oxide. A large patch of calcite is visible (bottom left) and possibly replaces olivine. The groundmass is composed of kaersutite (orange-brown), plagioclase, chlorite (greenish-yellow speckles) opaque oxides and small pyroxenes (orange-pink). Flow-banding is visible at the centre of the plate.

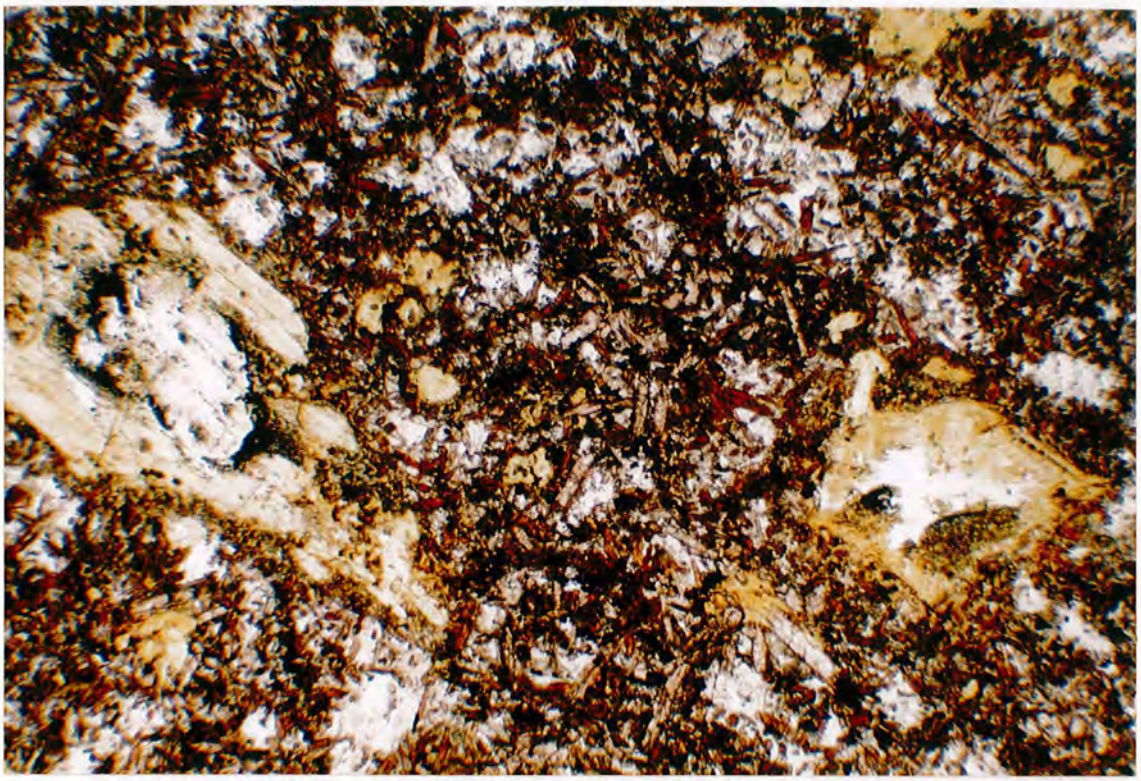

Plate 8.2 326308 Camptonite. PPL. ×35. The large yellow/clear patches (centre left and lower right) are chlorite/serpentine aggregates after olivine (note hexagonal outline). The groundmass is composed of kaersutite (red-brown), Ti-augite (pinkish) and opaque oxides with felsic minerals (plagioclase and analcite?) occurring in colourless ocelli, (eg. bottom, left of centre).

Plate 8.3 52274 Camptonite. XPL. ×35. A large augite phenocryst is visible at the centre of this plate, showing a vermicular exsolution of opaque Fe-Ti oxide. A large patch of calcite is visible (bottom left) and possibly replaces olivine. The groundmass is composed of kaersutite (orange-brown), plagioclase, chlorite (greenish-yellow speckles) opaque oxides and small pyroxenes (orange-pink). Flow-banding is visible at the centre of the plate.

is a relatively common component of the groundmass occurring as a breakdown product of olivine and, in rarer cases, pyroxene.

The remainder of the groundmass is composed of very fine-grained felsic minerals. Optical identification of these is not very easy, however, most samples appear to contain plagioclase > alkali feldspar and feldspar tends to be more abundant than feldspathoid, hence 'camptonite' – see Table 8.1.2. One sample clearly contained alkali feldspar and no plagioclase, but was otherwise similar to the camptonites, and is thus a sannaite. Apatite was observed in many samples forming thin needles a few hundred microns long in the groundmass There is however, a great deal of mineralogical heterogeneity, even on a thin section scale. In one extreme case the feldspar present changes almost completely from plagioclase in one field of view to alkali feldspar in another.

A common feature of camptonites are felsic ocelli, up to 5mm by 2mm. These are composed almost entirely of light coloured minerals, although their mineralogy is unclear. Minor amounts of alkali feldspar are visible, along with small quantities of carbonate set in an almost isotropic groundmass. This may be either zeolite or feldspathoid. Some highly birefringent, colourless minerals are present resembling mica (altered feldspar/nepheline?) and cancrinite. These ocelli contain only minor amounts of ferro-magnesian minerals. Their genesis is thought by Rock (1977) to be one of liquid immiscibility. He considers that an ocellar texture may be sufficient to classify a rock as an alkaline lamprophyre. Homogenous glasses prepared from natural ocellar rocks can be made to split into 2 liquids resembling the original matrix and ocelli (Fergusson and Currie 1971, Philpotts 1971). Samples from the Monteregian Hills provide clear evidence of immiscibility where the original magma splits into essexitic and monzonitic rock types (Philpotts and Hodgson 1968, Philpotts 1976). The ocelli from the Igaliko camptonites conform to this general mode of origin.

Chemically these rocks are similar to alkali basalts, tephrites/basanites and hawaiites.

8.2.B: Calc-alkaline Lamprophyres (CAL)

Rock (1984) reviewed the calc-alkaline lamprophyres, although he prefers the term 'shoshonitic lamprophyres' (Rock 1977) as this conveys the typically greater abundance

of K than Na in these rocks. Calc-alkaline lamprophyres are present in the Igaliko region as minettes and vogesites.

Minettes

Minettes are composed essentially of biotite mica and alkali feldspar with clinopyroxene and altered olivine, although these may be absent. They may contain either quartz or analcite less than 10% modally (Rock 1984).

The minettes from Igaliko are typically fine grained (100-300μm), often somewhat granular in appearance, suggesting some degree of recrystallisation in certain samples. The 'granularity' of many samples is however most likely a reflection of an even grain size (see Plate 8.5) and may be a result of crystallisation under high water pressures.

Biotite is the most abundant phase (typically 30% modally), although often coexists with lesser amounts of brown amphibole, sometimes difficult to distinguish due to the fine grain size. Altered phenocrysts of olivine (now aggregates of chlorite and serpentine) are evident in some samples. Phenocrysts of clinopyroxene are also evident which show a small scale (100μm) granularity, possibly a porphyroblastic texture. Pyroxene is a relatively minor component of the Igaliko minettes, always <20% modally, often <10%. The groundmass is composed primarily of alkali feldspar, with only minor quantities of plagioclase in any of the specimens, it is usually fairly fresh and contains in some cases minor primary calcite. No analcite or quartz has been detected in any of the minettes (although it may be difficult to tell apart from feldspar in minor amounts at small grain sizes). Opaques are relatively scarce, not exceeding 5% modally in any of the studied samples. Apatite is a common groundmass crystal occurring as small (50-100μm) needles which crowd the groundmass feldspar. Occasionally, blocky apatite crystals are seen with dimensions similar to those of the rest of the crystals in the rock, although these are relatively scarce.

Minettes (and CAL in general) do not possess ocelli and in this respect they are unlike the AL. They do however carry some xenocrystic material, which includes a large plagioclase 2cm in breadth by several cm in length in one sample (43887) and clusters of altered clinopyroxene in another (41904).

Vogesites

Vogesites are particularly abundant in the Østfjordsdal region but are relatively scarce across the rest of the Igaliko Dyke Swarm. They will be considered here and not with the rest of the Østfjordsdal dyke swarm (Chapter 9).

These calc-alkaline lamprophyres are composed of essential green brown hornblende and alkali feldspar with clinopyroxene and altered olivine. They are thus the hornblende equivalent of the minettes. With increasing plagioclase vogesites grade into spessartites, of which only one example is recorded from Igaliko.

The Igaliko vogesites vary from fine to medium grained. Amphibole is the dominant mafic mineral, comprising up to 60% of the mode in some cases. This is either a brown pleochroic or a dark olive green - greenish brown pleochroic hornblende occurring as primary crystals (see Plate 8.6) or overgrowing relics of pyroxene (see Plate 8.7), usually pinkish augite/salite. In the majority of samples, pyroxene is relatively scarce (usually <10% modally) although rarely it may equal amphibole in abundance (Plate 8.7). Deep brown biotite is a relatively abundant mafic mineral in the vogesites with amphibole > biotite > pyroxene. The mica often contains many small inclusions of apatite. No fresh olivine is seen, although rare pseudomorphs after olivine of chlorite and serpentine are evident.

The groundmass is composed mainly of alkali feldspar although in one sample (46279) microprobe analysis detected nepheline and sodalite. Rock (1987a) contends that nepheline and sodalite should be absent in CAL. However, the chemistry of the other minerals in this sample, and its petrography (based on Table 8.1.2) indicate it is a CAL and specifically a vogesite. Minor feldspathoid/zeolite (low relief, low birefringence, uniaxial negative), most probably analcite, is also seen in a few examples. No quartz was identified. Apatite is a common component of the groundmass occurring commonly as fine needles or as blocky crystals (up to 1mm in length) in rare cases.

Opaque oxides are relatively scarce in these rocks, contents of which range from 0% to about 10% modally. This is often rimmed, or almost completely replaced by granular aggregates of sphene, a reflection of the relatively high fo_2 of these rocks (Carmichael and Nicholls 1969). Minor groundmass calcite is also seen in some samples, perhaps

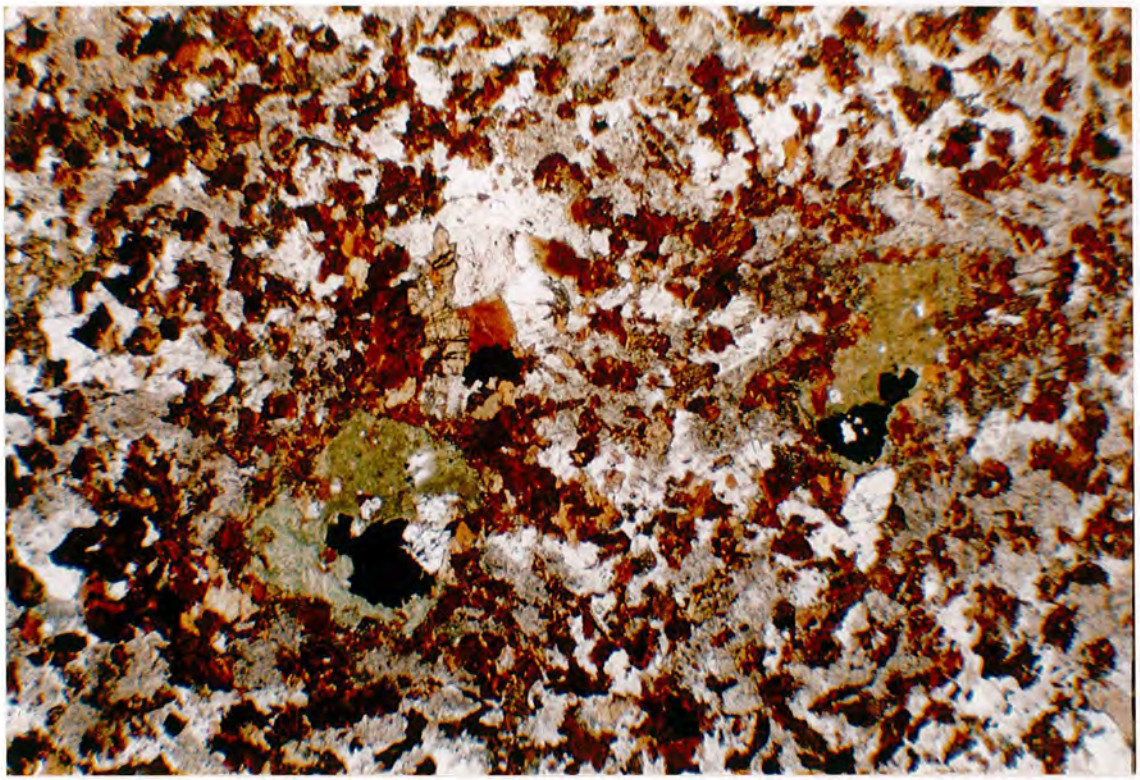

Plate 8.5 43887 Minette. XPL. ×35. This calc-alkaline lamprophyre is composed mostly of biotite (brown) and alkali feldspar (clear or altered to a cloudy pink/brown colour). Iron oxides are relatively scarce and in this case occur in association with dark green chlorite patches (alteration after olivine?). The high relief minerals near the oxides are apatites and although not clearly visible, (secondary?) carbonate is present in the groundmass.

Plate 8.6A 326281 Vogesite. Hand specimen. This coarse grained CAL shows large, dark flakes of mica (black), dark green, slightly finer grained amphibole and pyroxene. The white patches in the ground mass are feldspar.

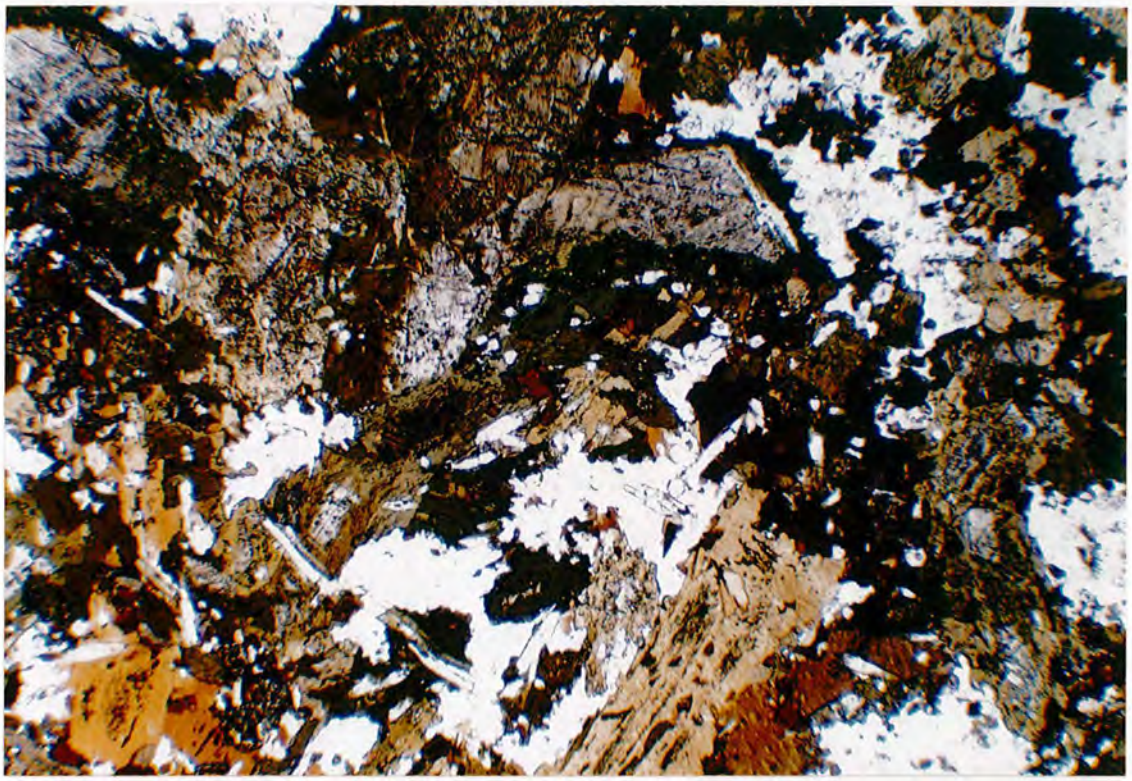

Plate 8.6B 326281 Vogesite. PPL. ×35.

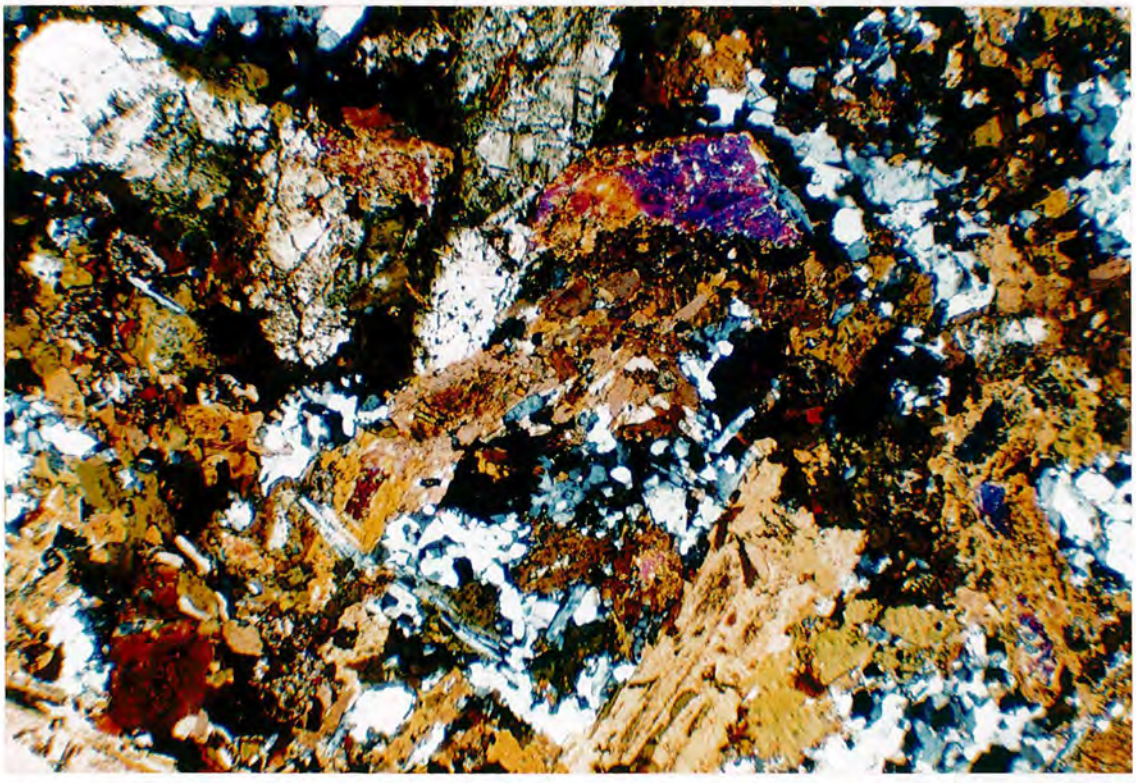

Plate 8.6C 326281 Vogesite. XPL. ×35. This coarse grained, calc-alkaline lamprophyre contains clinopyroxene (greyish pink in PPL, top centre) which is rimmed by deep green/brown amphibole (the most abundant mafic mineral). Amphibole also occurs as smaller discrete groundmass grains. Amphibole compositions range from ferroan pargasite to magnesian hastingsite. Biotite (Mg-rich) is slightly less abundant than amphibole occurring as large plates (centre bottom for example). Plagioclase is subordinate to alkali feldspar in the groundmass. Apatite is common as long, thin, high relief needles (lower centre left). Sphene is present in place of opaque oxides (lower centre left, speckley high relief aggregates).

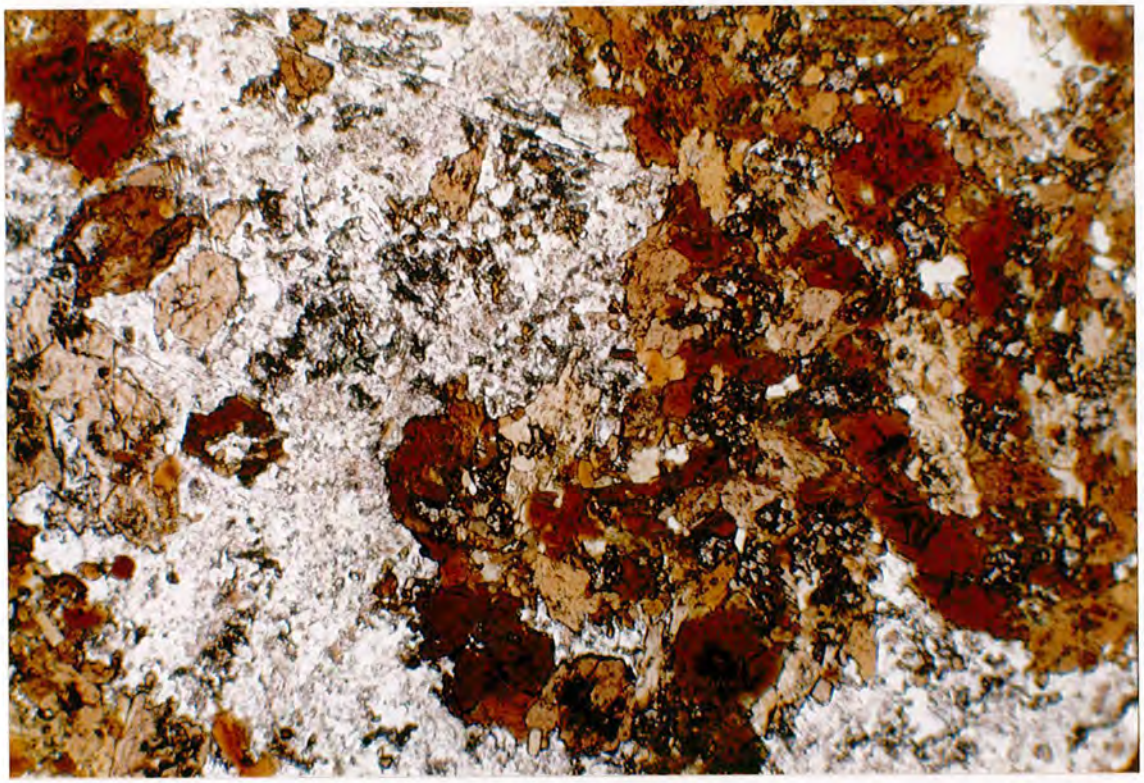

Plate 8.7A 326318 Vogesite. PPL. ×35.

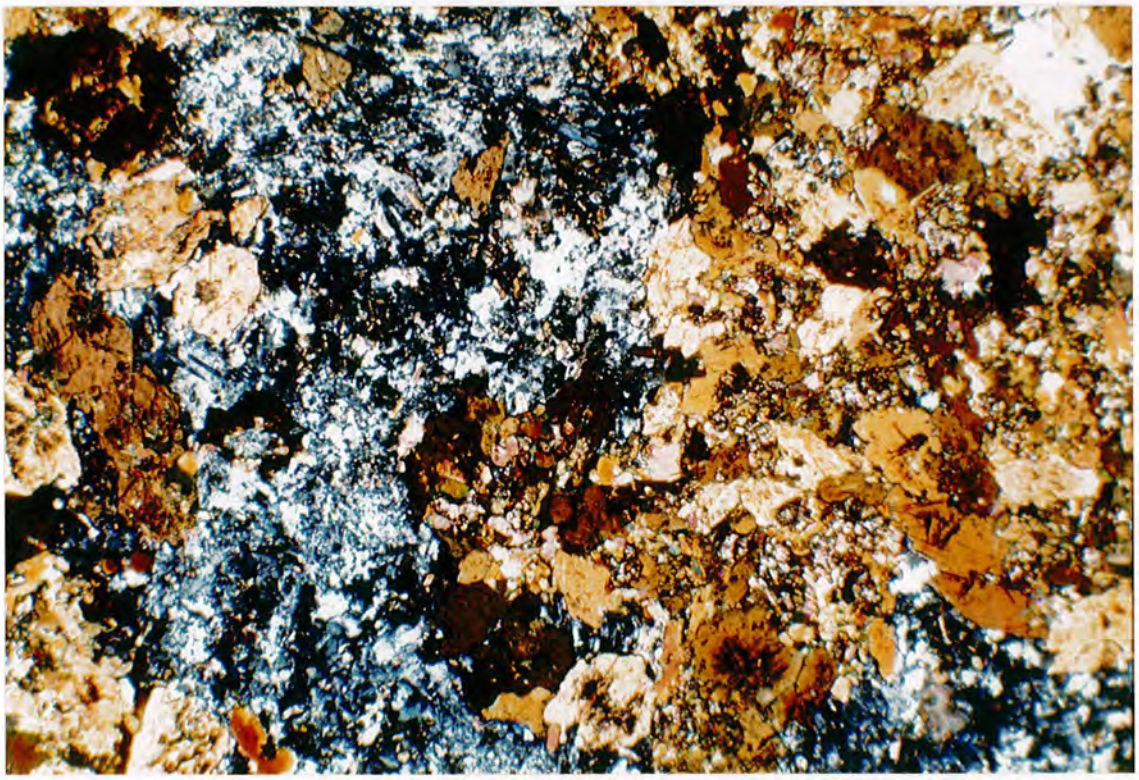

Plate 8.7B 326318 Vogesite. XPL. ×35. This calc-alkaline lamprophyre is composed mostly of brown hornblende, alkali feldspar and near isotropic patches of feldspathoid (analcite?). Long, thin, high relief apatites are visible in the felsic patches (top centre left). Granular sphenes are seen to be confined mostly to the mafic areas, as too are very small biotite crystals (left of lower centre, pink/green birefringence colours).

only 1-2% of the mode.

It is clear that both vogesites and minettes have hydrous mafic mineralogies which are K-rich rather than Na-rich (amphibole and mica). K-dominance is also reflected in the groundmass feldspar which is typically orthoclase with only minor albite visible in any given specimen.

8.2.C: Ultramafic Lamprophyres (UML)

Throughout this thesis reference has been made to ultramafic lamprophyres which have been classified upon their total alkalis - silica contents (see Figure 5.2.1). This field agrees reasonably closely with a field for ultramafic lamprophyres in TAS space given by Rock (1987a, see Figure 8.4.2C) which overlaps slightly the nephelinite field of Cox *et al.* (1979). Rock (1986) has reviewed the UML, and the nomenclature employed here is based on his suggestions.

UML are particularly abundant from the Østfjordsdal area, but unlike vogesites, are not confined to this swarm being fairly evenly spread across the whole region.

None of the UML contains melilite and they can thus be considered as either aillikites or damkjernites, although the general term mica-pyroxenite describes them equally well. Aillikites will grade, with increasing modal carbonate, into carbonatites (see Table 8.1.2).

Mica-pyroxenites

These ultramafic rocks are composed almost entirely of diopsidic pyroxene, phlogopitic mica and opaque Fe-Ti oxide. They are dark, sparkling rocks which are very dense and often exert a strong magnetic effect upon a compass needle (see Plate 8.8). Coppery-coloured plates of phlogopite are clearly visible on the fresh surface. They weather to pale or dark browns (similar to peridotite weathered surfaces). Occasionally they contain small patches (ocelli?) of light material which turns out to be carbonate on further examination. They are usually fine to medium grained and do not show a great deal of internal structure such as flow alignment or xenoliths.

Microscopic examination shows these rocks to have a granular texture on a 500μm

scale in a large number of cases (see Plate 8.9). Strongly pleochroic phlogopite is the most common mineral, occupying between 30-60% of the mode. This often contains inclusions of apatite or opaque oxides. Generally subordinate to this is a pale green or colourless diopsidic pyroxene (see Plates 8.9, 8.10). Both the pyroxene and mica are invariably fresh. Amphibole often reaches high modal contents (up to 30%, in 326314, Plate 8.11) where it occurs in slightly higher abundance than mica. The amphibole is generally a deep brown, pleochroic hornblende. Amphibole also tends to dominate over pyroxene and the term mica-hornblendite is a more accurate description. No olivine is seen in any of these samples, nor is melilite, the crystallisation of which may be suppressed by crystallisation at depths of a few kilometres (cf. Upton and Thomas 1973). This contention is supported by experimental studies of Tilley and Yoder (1968) who found that melilite-bearing eruptive rocks (in this case a monticellite-alnöite) may be represented by melilite-free clinopyroxene-rich assemblages when crystallised at depths of a few kilometres. Magmas of similar chemical composition were erupted at Qagssiarssuk in Early Gardar times and appear to contain pseudomorphs after melilite (Stewart 1970) although Deans and Robert (1984) suggest that these may be pseudomorphs after the Na-Ca carbonate mineral, nyerereite.

Opaque oxides – both magnetite and ilmenite – are abundant, often exceeding 15% modally (see Plate 8.9). The large volumes of magnetite will be responsible for the magnetic effects exerted by these samples. The small amount of groundmass is composed principally of felsic minerals. These include minor amounts of alkali feldspar (rare), analcite and fine grained aggregates of muscovite (altered feldspar?). Apatite is common in these rocks, occurring as acicular crystals up to $\approx 500\mu$m in length. Calcite is a fairly common constituent of the groundmass although rarely exceeds 10% modally. This often occurs as 'vughs' which appear to be the result of liquid immiscibility. This is particularly evident from 326303 (Plate 8.10) where carbonate patches 1cm by 3-4mm are visible. Groundmass phlogopites coarsen towards these patches of which all examples observed in this section, contain large, euhedral sphene crystals (see Plate 8.10). Geochemical evidence presented in Chapter 7 however showed that the typical late carbonatites of the region are the result of liquid immiscibility from a CO_2-rich phonolite and not ultramafic lamprophyre (or chemically similar nephelinite) magmas. These carbonate patches also contain blocky apatite crystals, morphologically distinct

Plate 8.8 326301 Ultramafic Lamprophyre. Hand specimen. UML are all dense, dark greenish-black rocks when fresh. Typically UML are micaceous and sparkle on freshly broken surfaces. Weathered surfaces are a fawn-brown colour. Thin section illustrated below.

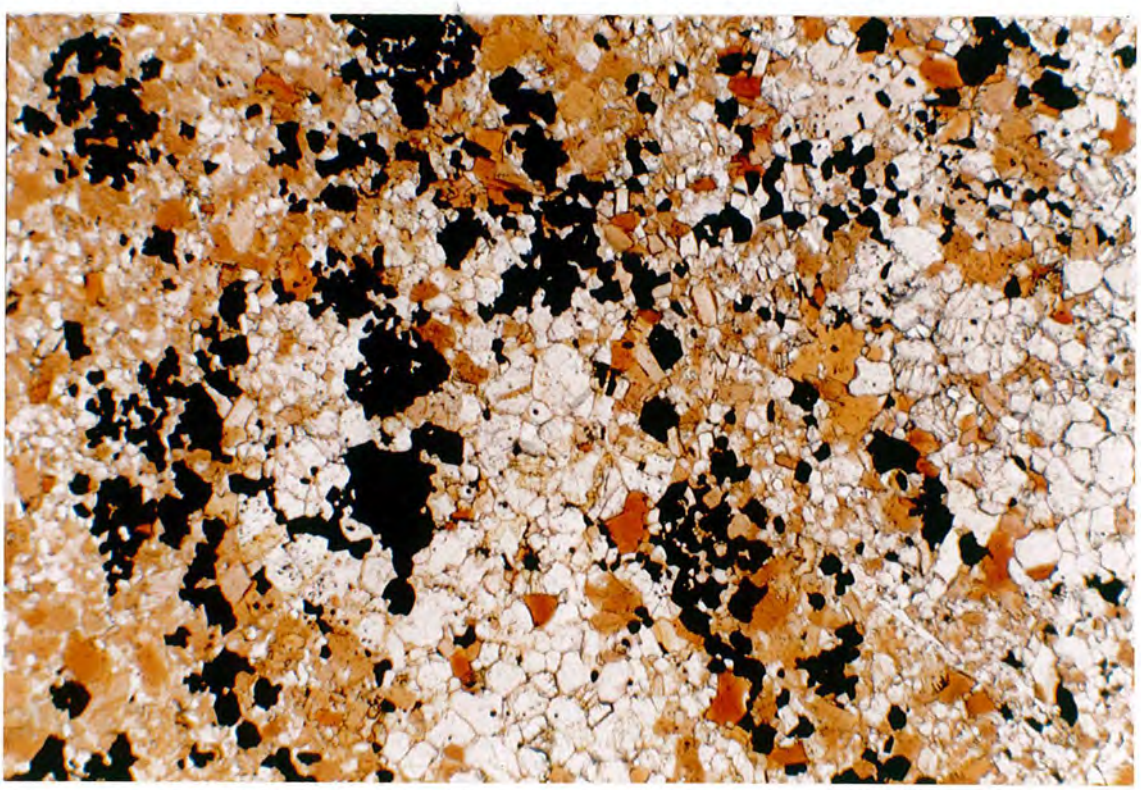

Plate 8.9 326301 UML PPL. ×35. This granular mafic rock is composed entirely of phlogopite mica, amphibole (ferroan pargasite), diopsidic pyroxene and opaque oxides (ilmenite and Ti-magnetite). The granular texture maybe related to the high volatile content of these rocks (Upton and Thomas 1973). This sample is very typical of this group of rocks.

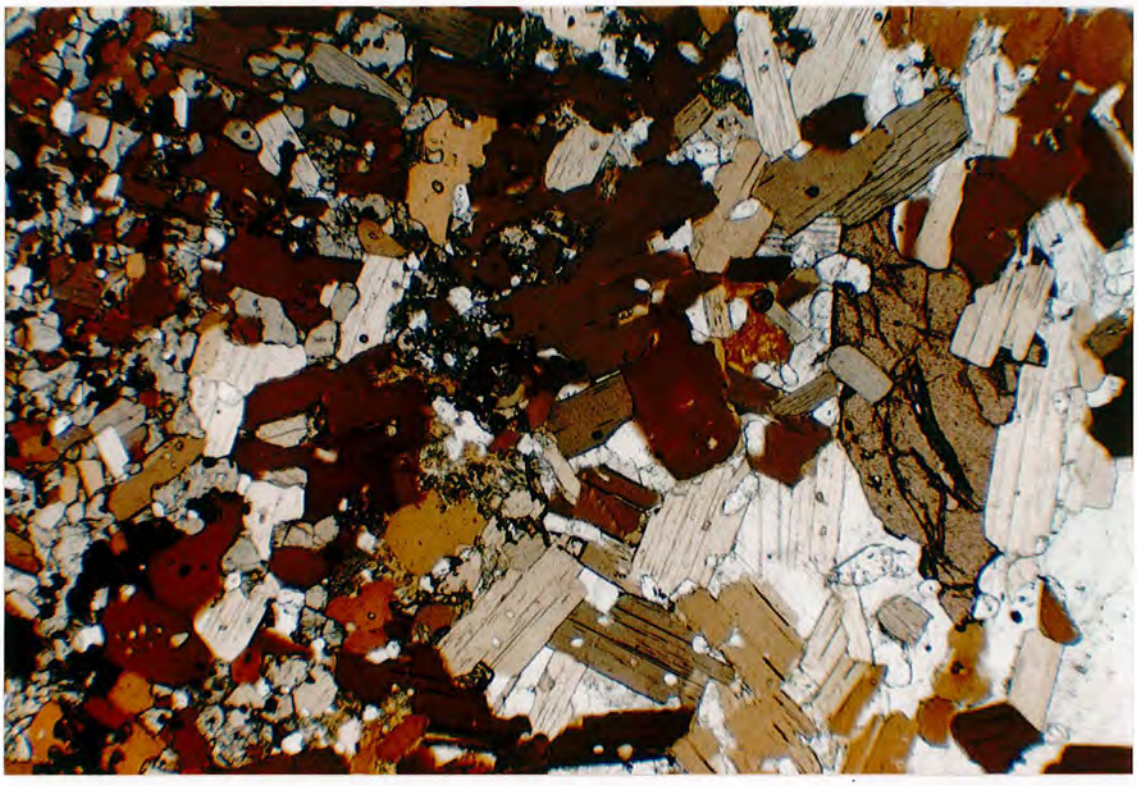

Plate 8.10A 326303 UML. PPL. ×35.

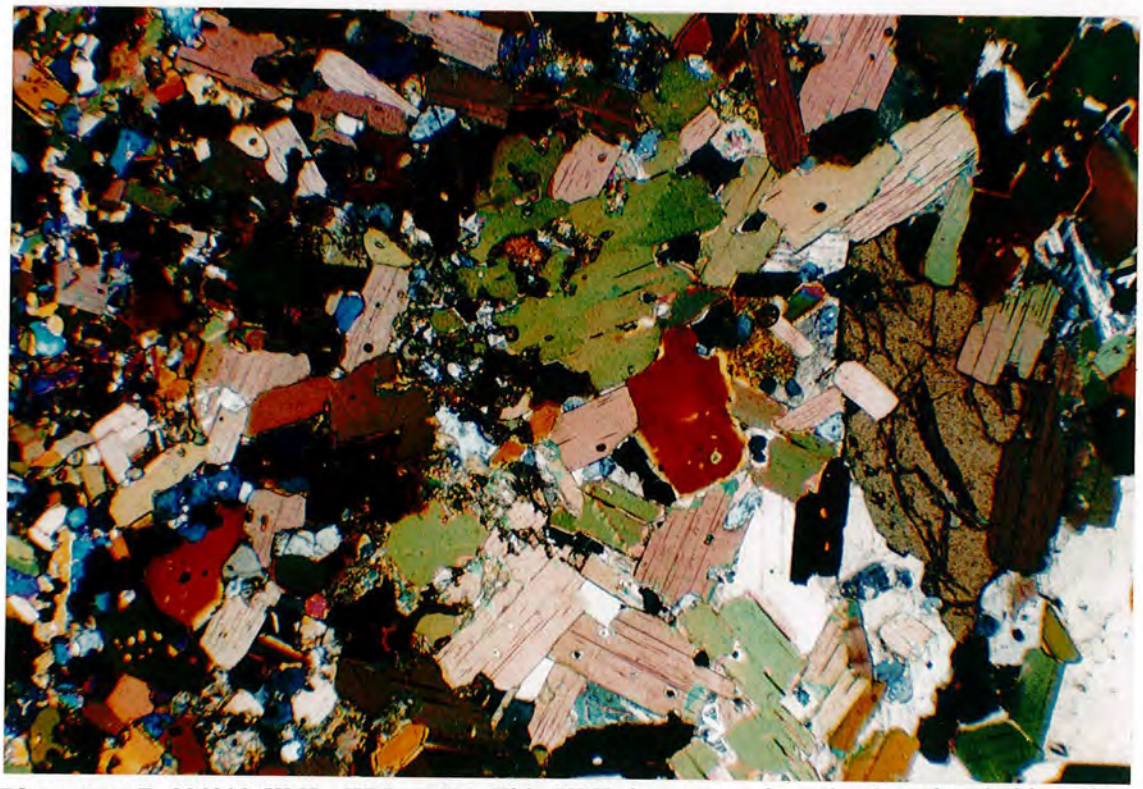

Plate 8.10B 326303 UML. XPL. ×35. This UML is composed predominantly of phlogopite mica, diopsidic pyroxene and opaque oxides which are often rimmed by sphene (granular, high birefringence). The grain size increases to the right of the plate as a carbonate-rich vugh (immiscible liquid?) is approached. Large phlogopites protrude into this patch. A large lozenge-shaped, high relief, pinkish-brown sphene is clearly seen, and is enclosed in calcite. Moderate to high relief apatites (against calcite) are also present in this carbonate vugh (bottom left of sphene).

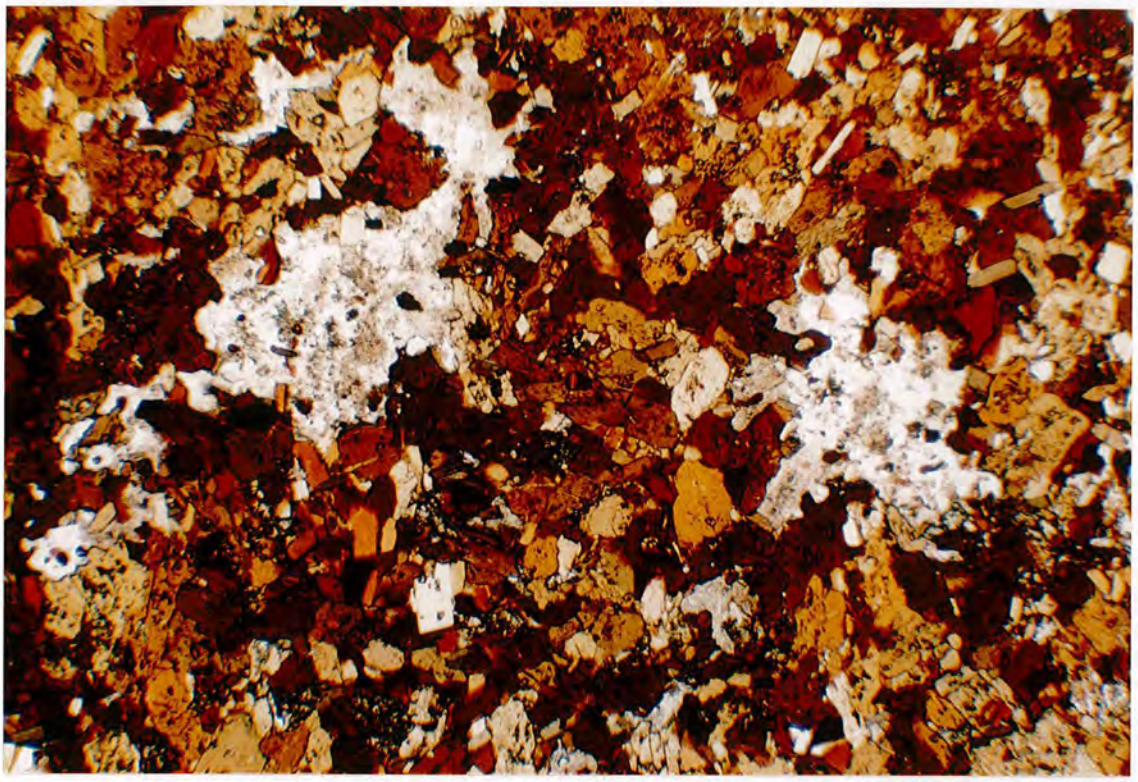

Plate 8.11 326314 UML. PPL. ×35. This ultramafic lamprophyre is composed predominantly of deep brown amphibole (probably hastingsite/pargasite) with lesser amounts of phlogopite mica (laths in upper right). Pyroxene is a minor component. The felsic ocelli are mostly altered (carbonated) feldspar and some fresh relics of plagioclase can be seen. Some free carbonate is seen. Elongated lines of apatite can be seen enclosed in some of the amphiboles. Sphene is present in place of Fe-Ti oxide.

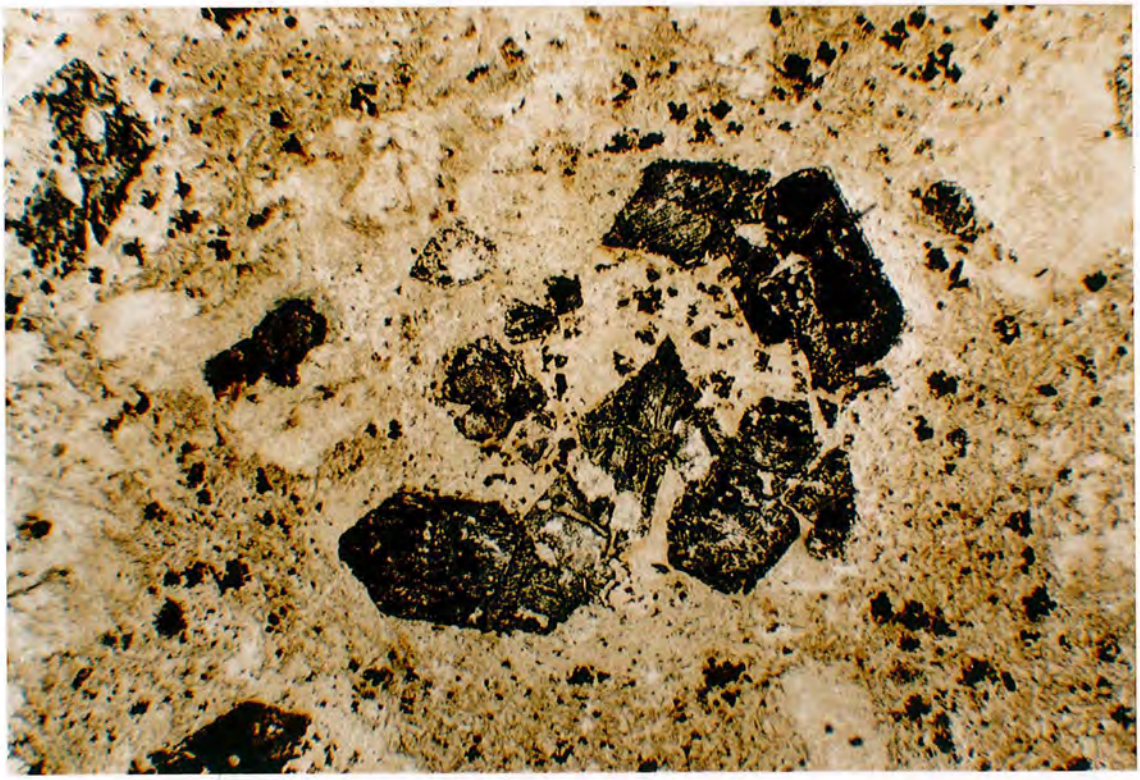

Plate 8.12 326222 Altered Ultrabasic Lamprophyre. PPL. ×35. This low SiO_2 rock contains hematite pseudomorphs after euhedral olivine, set in a ground mass of chlorite, phlogopite, calcite, some serpentine and opaque oxides. There appears to be some residual alignment of groundmass minerals around the pseudomorphed olivines.

from the apatites in the silicate phase.

Minerals occasionally observed in minor amounts in these rocks include a deep red brown, isotropic garnet - melanite - which occurs as small subhedra (200μm across) in 41906. This sample also contains minor quantities of deep red brown, near isotropic perovskite ($CaTiO_3$) reflecting the thoroughly silica-undersaturated nature of this sample. Sphene ($CaTiSiO_5$) is relatively common as an overgrowth on many opaque oxides in some of the ultramafic rocks. Upton and Thomas (1973) interpret sphene as a reaction of ilmenites with Ca-rich liquids at a relatively late stage. The textural evidence from the Igaliko samples is in agreement with this mode of origin. The presence of sphene must also reflect relatively high fo_2 (Carmichael and Nichols 1969). Sulphides are a relatively minor opaque phase. These are generally pyrite although pentlandite and sphalerite have also been recorded.

In general, the amphibole bearing UML described above can be classified as aillikites, as too can carbonate-rich, feldspar- and amphibole-free examples. Those samples that are free of carbonate and contain some feldspar (rare) are best described as damkjernites. No samples contain a glass phase (or its presumed breakdown product). Upton and Thomas (1973) consider the granular texture of similar rocks from the Narssaq-Tugtutôq area to be a result of high water contents leading to reaction of mineral phases present with late stage liquids and/or recrystallisation of mineral phases present.

With increasing carbonate and decreasing silicates (particularly feldspar/feldspathoid) aillikites grade into carbonatites (carbonate - phlogopite - pyroxene - oxide assemblages typically). Four TAS (Cox *et al.* 1979) classified UML with $\approx$15% SiO_2 (see Figure 5.2.1) are carbonate - phlogopite - oxide rocks, strictly not carbonatites (as calcite < 50% modally, Streckeisen 1979) but are more akin to ferro-carbonatites than to UML petrographically.

Altered Basic/Ultrabasic Rocks

Several dykes from the Lower Flink's Dal area (Motzfeldt Centre) consist of highly altered basic/ultrabasic rock. They are distinctive in hand specimen, often having a dark olive weathered crust, which is often pitted suggesting preferential erosion of a particular mineral (olivine?). Fresh surfaces are typically dark grey.

These samples are composed principally of chlorite/serpentinite, carbonate and opaque oxides. Clear pseudomorphs after olivine are visible in this section. These pseudomorphs are typically serpentine/chlorite aggregates up to 5mm in diameter. Occasionally the outline of the former olivine is picked out in hematite (see Plate 8.12). A felted groundmass of chlorite, phlogopite, carbonate and opaque oxides enclose these pseudomorphs, and this is typically very fine grained. Minor quantities of sphene, often surrounding the opaque oxides, are visible.

The highly altered nature of these samples is interpreted as late magmatic alteration of a volatile (H_2O, CO_2)-rich alkali basic/ultrabasic magma, and not post consolidation deuteric alteration, their host syenites being relatively fresh.

8.2.D: Breccia Dykes

A relatively common feature of lamprophyre dykes is their content of xenoliths and/or xenocrysts (Rock 1987). Although many of the lamprophyres described thus far are xenolith-free, several samples with dominantly mafic mineralogies contained abundant xenoliths of country rock. These are exemplified by samples 41947, 326250, a sandstone breccia dyke in the Igaliko area illustrated in Plate 2.10; and 325960, a granite breccia dyke from the Motzfeldt Sø area illustrated in Plate 8.13. A thin section from 41947 is shown in Plate 8.14. These dykes consist mostly of clinopyroxene (Na-rich salites in 41947, Na-poor ferro-salite – hedenbergites in 325960) in excess of 75-80% modally.

Other minerals present include sphene, sodalite, fluorite and very minor feldspar, all generally interstitial to euhedral or subhedral pyroxene. These rocks were probably intruded as crystal mushes charged with volatiles (water, F, Cl) and the presence of sphene indicates a relatively high fo_2.

A certain amount of disintegration of the xenoliths can be observed with granular margins showing partial consumption of the xenolith by its host magma/crystal mush (see Plate 8.14). Similar relationships are visible in 325960, which has entrained granite xenoliths which appear to show some degree of melting (embayed margins, occasional granophyric intergrowths - eutectic mixtures?).

Plate 8.13 325960-1 Breccia Dyke, SW end of Motzfeldt Sø. This dyke contains many xenoliths of Julianehåb Granite set in a groundmass of green ferro-salite/hedenbergitic pyroxene. The country rock to this dyke is the outer syenite of the Motzfeldt centre. Scale on hammer shaft in inches.

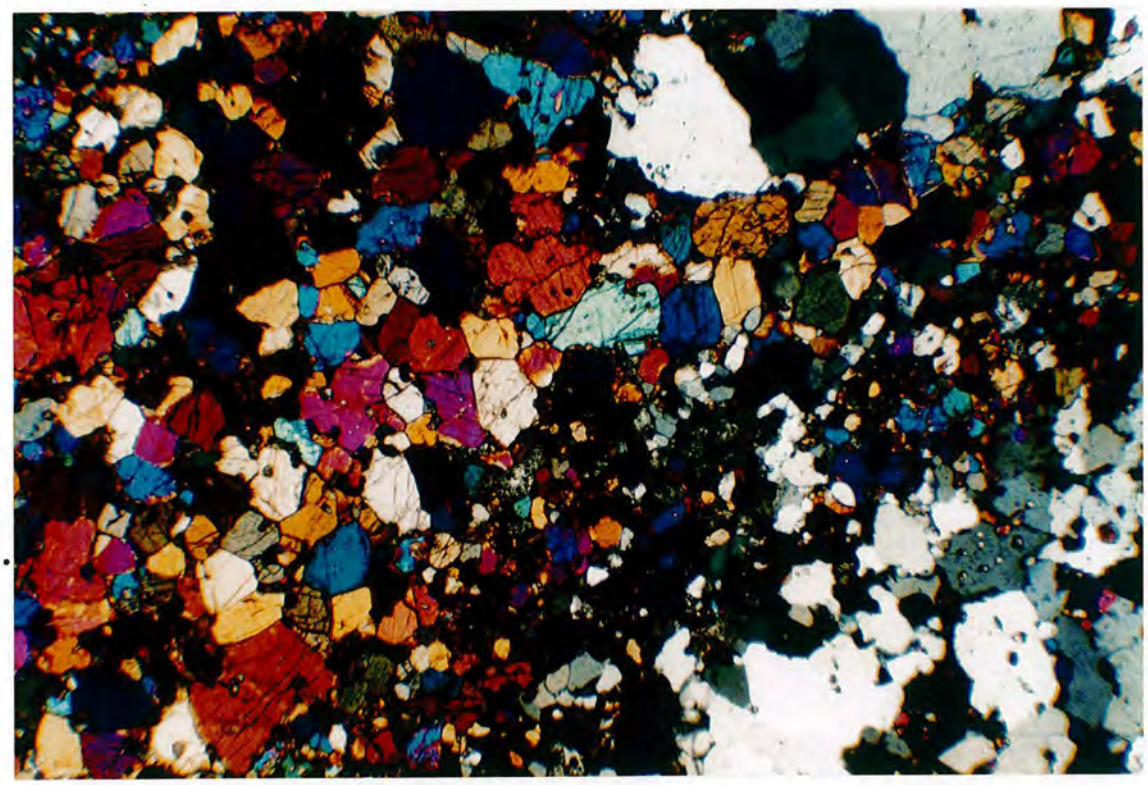

Plate 8.14 41947 Breccia Dyke, Iganaq. XPL. ×35. This dyke is also illustrated in Plate 2.10. The groundmass to this dyke is composed principally of salitic pyroxene with minor opaque oxides. Eriksfjord Formation sandstone xenoliths are seen at upper and lower right, with finer grained quartz crystals near the rims, due to partial disaggregation.

More 'typical' lamprophyres (particularly UML rich in carbonate) tend to be free from xenolithic inclusions, although on rare occasions relatively abundant (≈10% by volume) of xenolithic material (usually granite) is observed. Alkaline and calc-alkaline lamprophyres would appear to be free from xenoliths, although occasional large plagioclases several centimetres in length are seen in minettes and camptonites. In the latter case the feldspar is rounded and has a marked reaction rim. It is also sericitised in patches.

8.3: Mineralogy

In general, lamprophyre mineralogy is more basic (magnesian, calcic etc.) than that of the main series of dykes (basalts to phonolite/rhyolite), a reflection of generally higher Mg, Ca, etc. in these magmas. Although UML have been excluded in any discussion on mineralogy until now, a group entitled 'Other Lamprophyres' was included in the majority of diagrams from Chapter 4: Mineralogy. This group includes the alkaline and calc-alkaline lamprophyres and in certain cases mineralogical trends through these rocks are seen to grade into the main basic trends (eg. Ti and Al in pyroxenes, Mg number and Ti in amphiboles etc. see Chapter 4). For this chapter the lamprophyres have been divided into UML, AL and CAL, and also included are the Breccia Dykes, and Altered Ultrabasic dykes. Recently, Rock (1987a) proposed that a mineralogical classification may be one of the best ways to discriminate between various branches of the lamprophyre clan. Rock (1987a) described compositional fields typical of these various groups for pyroxene, amphibole, biotite/phlogopite and feldspar. These have been used in the following section.

8.3.A: Pyroxenes

Figure 8.3.1 shows all pyroxene analyses plotted in terms of Mg – (Fe^{2+}+Mn) – Na and Mg – (Fe^{2+}+Mn) – Ca, recalculated as atoms per 6 oxygens and 4 cations. It is clear that these pyroxenes are mostly Mg-rich salites and diopsides, typically having Mg/Mg+Fe^{2+} >0.6, with only 5 analyses (3 from breccia 325960 and 2 analyses from 325943) having Mg/Mg+Fe^{2+} <0.6. All other analyses from 325943 have Mg/Mg+Fe^{2+} >0.75) No orthopyroxene has been recorded.

Figure 8.3.2 shows pyroxenes plotted in terms of SiO_2/Al_2O_3 weight % against

Figure 8.3.1

Lamprophyre pyroxene composition in terms of Mg - (Fe^{2+}+Mn) - Ca (upper) and Mg - (Fe^{2+}+Mn) - Na (lower) as atoms per 6 oxygens. Clearly most pyroxenes are very Mg-rich, being either diopsides or salites with only a few ferro-salites. There is a tendency for Mg to decrease in pyroxenes in the order Altered Ultrabasic > UML > AL > CAL > Breccias. The high Al content will be accommodated in molecules such as Ca-Tschermaks ($CaAl_2SiO_6$). Exchange of $NaFe^{3+}$ (aegirine) for $MgFe^{2+}$ is of minor importance.

IGALIKO DYKE SWARM

Lamprophyre Dykes

Pyroxene Analyses

Atoms per 6 oxygens

△ ULTRA-MAFIC LAMPROPHYRE
▽ ALKALINE LAMPROPHYRE
◈ CALC-ALKALINE LAM-PHYRE
◈ BRECCIA
△ ALTERED ULTRABASICS

Figure 8.3.1

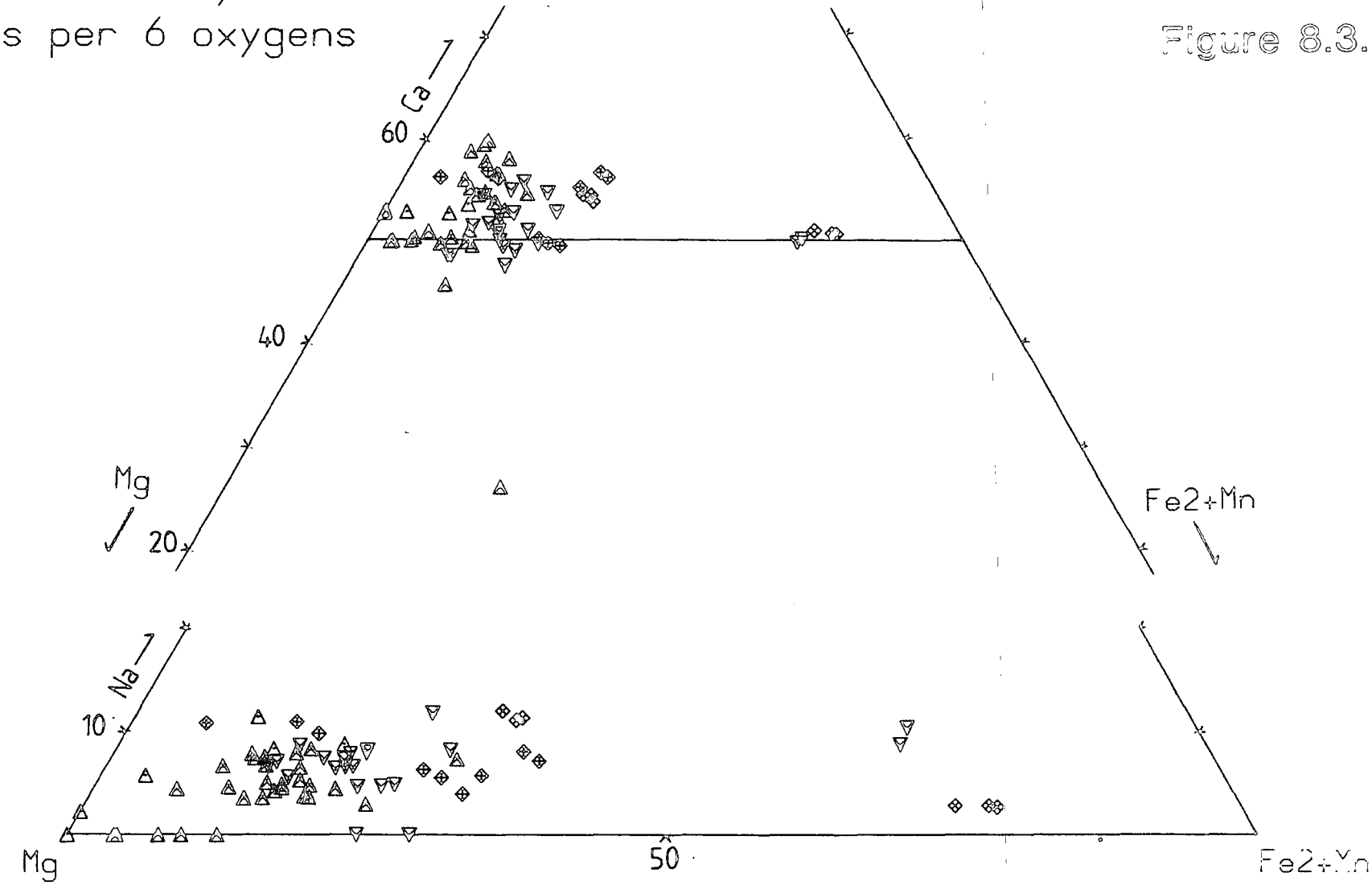

Figure 8.3.2

Pyroxenes from Igaliko lamprophyres plotted in terms of SiO_2/Al_2O_3 (wt %) vs. Mg/ $Mg+Fe^{2+}$ (atomic), compared to the suggested lamprophyre fields of of Rock (1987a). In general the Igaliko lamprophyre pyroxenes plot close to the fields suggested by Rock (1987a) although some scatter is evident (see text).

Figure 8.3.2

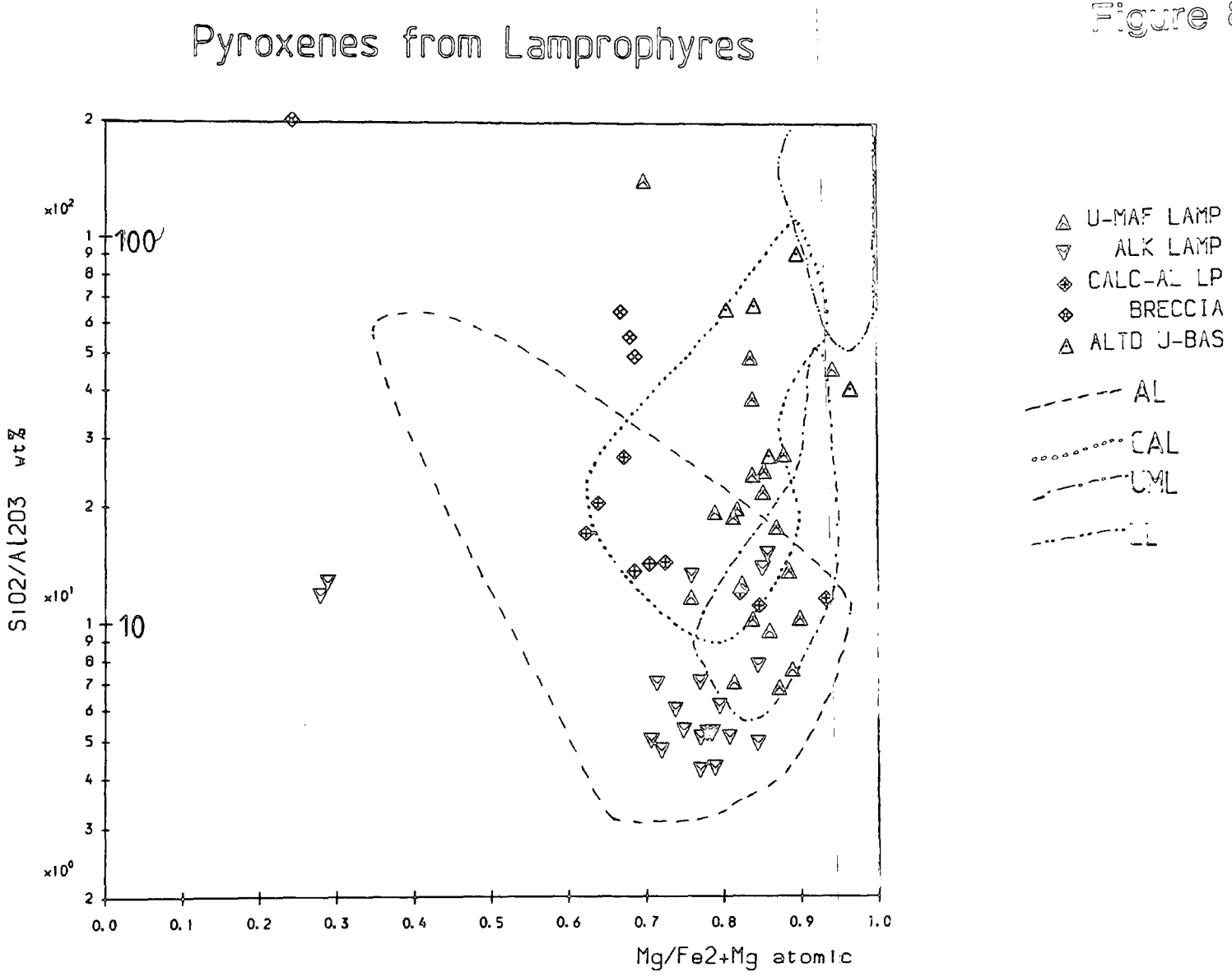
Pyroxenes from Lamprophyres
SiO2/Al2O3 wt%
x10²
100
x10¹
10
x10⁰
0.0
0.1
0.2
0.3
0.4
0.5
0.6
0.7
0.8
0.9
1.0
Mg/Fe2+Mg atomic
U-MAF LAMP
ALK LAMP
CALC-AL LP
BRECCIA
ALTD U-BAS
AL
CAL
UML
LL

$Mg/Mg+Fe^{2+}$ atomic and shows the fields given by Rock (1987) for various groups of lamprophyres. No analyses fall into the LL (lamproite) field. In general the analyses behave roughly as expected, although notably the UML occupy a larger field than Rock (1987) defines. These UML pyroxenes extend to lower $Mg/Mg+Fe^{2+}$ at higher SiO_2/Al_2O_3, and thus overlap more with the CAL field suggested by Rock. The altered ultrabasics' pyroxenes have compositions within the CAL field approaching lamproitic compositions.

One of the most striking features of the analyses of the lamprophyre pyroxenes is their high content of both Al and Ti (see Figure 8.3.3). Ti imparts a general pinkish hue to many of the pyroxenes and is particularly enriched (up to 0.149 atoms per 6 oxygens - 4.39 wt% TiO_2) in many of the AL. Al too is unusually high in pyroxenes from AL, reaching a maximum of 0.454 atoms per 6 oxygens (10.37 wt% Al_2O_3). Ti and Al tend to show a sympathetic behaviour. Both Ti and Al are at their highest contents in AL, with contents decreasing in the order UML then CAL. The pyroxenes from breccias and altered ultrabasics tend to be poor in both Ti and Al (see Figure 8.3.3).

Fassaite

Fassaite, similar to analyses by Deer *et al.* (1978) was detected in the UML 326303 (see Plate 8.11). Typical features of fassaites are high CaO (≈25 wt%), leading to >1 Ca atom per 6 oxygens and assignment of some Ca to the M2 site (Deer *et al.* 1978), high Al contents and high Fe^{3+}/Fe^{2+} ratio. Analysis 326303.19 and other pyroxenes from this sample have typically fassaitic composition. Those analyses quoted from 41906 and 326271 are however less aluminous than the typical fassaites cited by Deer *et al.* (1978) but show high Ca, Fe^{3+} , Al and Fe^{3+}/Fe^{2+} compared to many other pyroxenes. These also contain high Fe^{3+} contents for their Mg contents and Ca at ≈1 atom per 6 oxygens. It would appear that, with a decreasing Al content fassaites grade into calcic diopsides (rich in Al). This involves a reduction in the CaTs molecule ($CaAl_2SiO_6$).

The high Fe^{3+} content in these pyroxenes indicates that they are highly oxidised and would imply high fo_2 in th UML magmas (Huckenholz *et al.* 1969). This is also borne out by the presence of sphene in many of the UML.

Figure 8.3.3

Pyroxene variation in terms of Ti and Al against $Fe^{2+}/Fe^{2+}+Mg$ as atoms per 6 oxygens. The pyroxenes from the AL are typically very rich in both Al and Ti. These decrease into more 'normal' Ti and Al contents into the CAL and the remainder of the dyke swarm (cf. Chapter 4.2).

Figure 8.3.3

PYROXENES FROM LAMPROPHYRES

(Atoms per 6 oxygens)

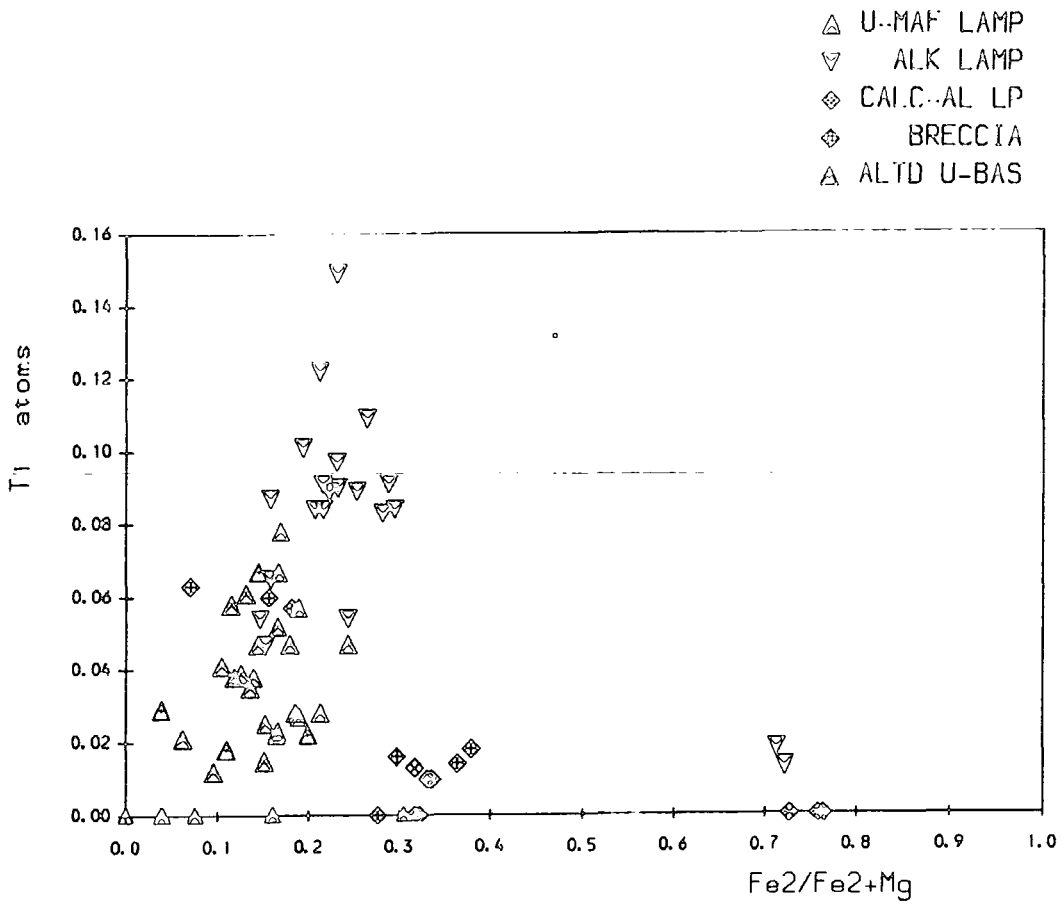

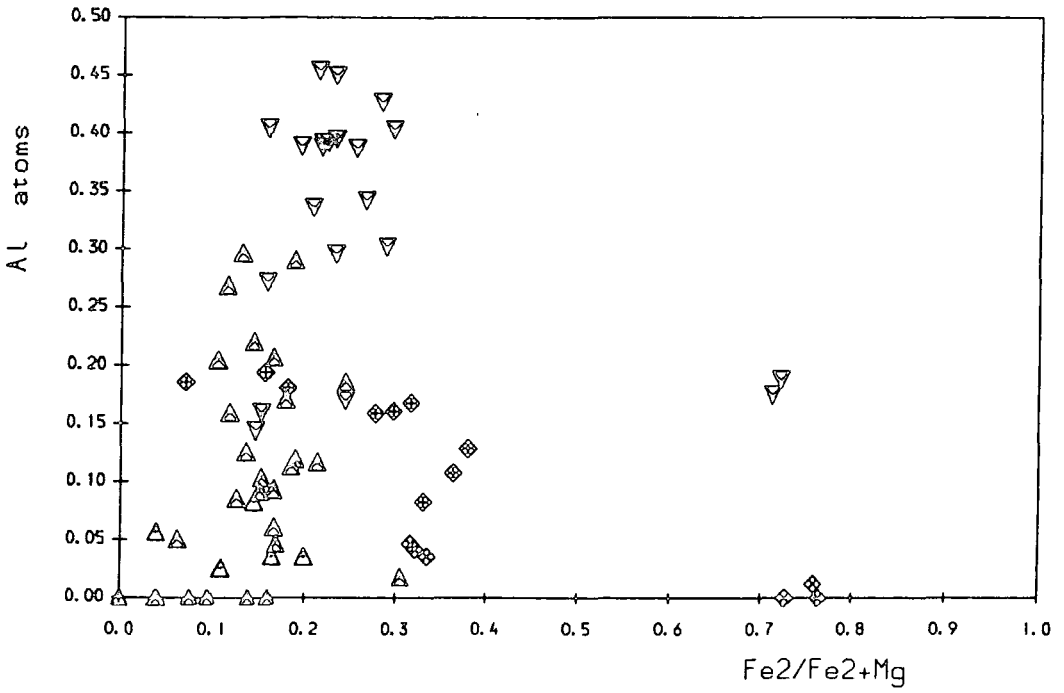

The major exchange in fassaites is $(Mg,Fe^{2+})Si \rightleftharpoons (Al,Fe^{3+})Al$, with most fassaites having been reported from metamorphic zones. Igneous fassaites are rare but have been reported from alkali basalts and nepheline basalts from the Hocheifel area, West Germany (Huckenholz 1973). These are more aluminous and sodic than the UML pyroxenes, although other characteristics are similar.

Certain of the highest Al analyses from the alkaline lamprophyres have characteristics similar to some fassaites described by Deer *et al.* (1978), despite CaO<25 wt % and Fe^{3+}/Fe^{2+} ≈0.8 (less than 1). These are from sample 325943 and tend to be rims to the large pink (Ti-rich) pyroxene phenocrysts (see Plate 8.4). The cores are generally less aluminous with considerably less Fe^{3+} despite overall similar total Fe contents. These are similar to fassaites reported by Huckenholz (1973) in terms of Fe/Mg, but are considerably richer in Al. These must attest to high fo_2 in these alkaline lamprophyre magmas.

Upton and Thomas (1973) describe Al and Ti rich pyroxenes from K-rich ultramafic rocks cropping out near Narssaq. These are exremely similar to the fassaites from the UML. Although Upton and Thomas (1973) do not use the term fassaite, the general outline given by Deer *et al.* (1978) would describe some of Upton and Thomas's analyses as such (eg. 40407 and 85941, Table 2).

Zoning

Pyroxenes were generally too small to analyse at core and rim positions with the exception of those from the camptonite 325943 (see Plate 8.4). The variation from core to rim (and overgrowth) of 3 pyroxene phenocrysts from this sample is shown in Figure 8.3.4. Zoning is complex, often showing rapid compositional change very close to the rim of the crystal. Ti and Al behave sympathetically. This is also seen for Al and Fe^{3+}, suggesting that some compositional variation is controlled by the ferri-calcium Tschermaks molecule ($Ca(Fe^{3+},Al)_2SiO_6$) to/from fassaitic compositions. There is a tendency also for zoning to be 'reversed' in 2 of the 3 phenocrysts with an increase in Mg and Ca being seen from core to rim, increasing the diopside content. Na contents (not shown) are low and thus substitution of Na as aegirine (with Fe^{3+}) is not an important process.

Figure 8.3.4

Zoning in 3 pyroxene phenocrysts from AL 325943 as atoms per 6 oxygens (see Plate 8.4). The same line type is used for each crystal. Zoning is irregular with a tendency for Al, Mg, Ca and Ti to increase towards the margin/overgrowth of the crystal. Distance from the core is arbitrary with the rim on the margin of the crystal unless an obvious overgrowth (optically discontinuous in colour etc.) is visible, this is marked as 'og'. The high Fe^{3+}, Al and Ca in one phenocryst rim (solid line) may be an overgrowth of fassaite.

Zoning in Pyroxenes from Al. 325943
(atoms per 6 oxygens)

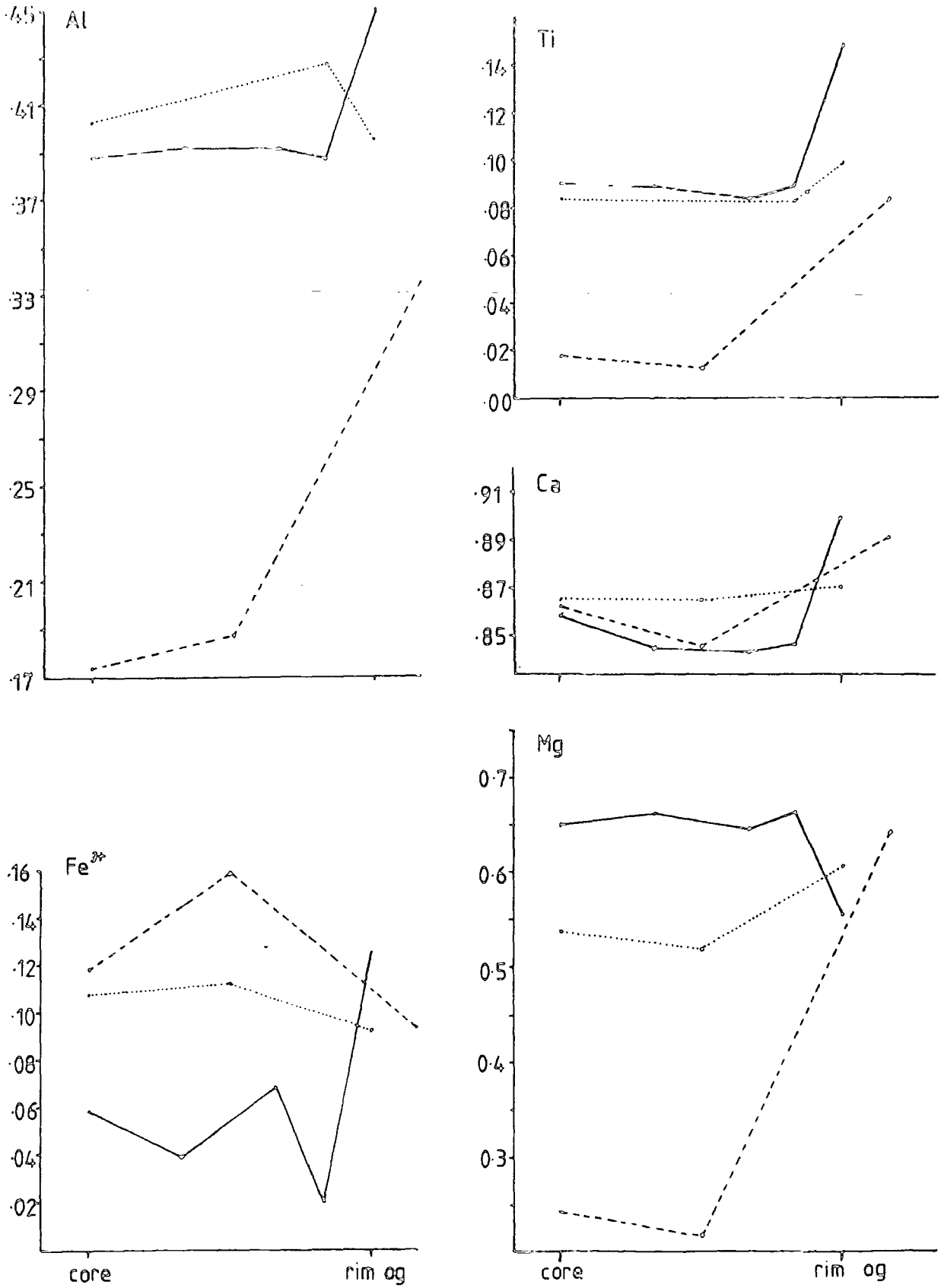

Table 8.3.1

Selected fassaites from UML and AL

Wt% oxide	326303.15	326303.19	41906.41	326271.41	325943.22
SiO_2	45.68	44.58	47.31	49.26	41.61
TiO_2	1.99	2.13	1.64	1.37	5.19
Al_2O_3	6.53	6.59	3.78	3.65	9.97
FeO	9.58	9.80	9.07	7.59	9.13
MgO	10.50	10.22	11.12	12.61	9.68
CaO	24.68	24.20	24.36	25.15	21.90
Na_2O	0.38	0.71	0.58	0.53	0.84
Total	98.34	99.23	95.86	97.16	94.32
Atoms per 6 oxygens					
Si	1.728	1.703	1.813	1.829	1.594
Ti	0.057	0.061	0.047	0.038	0.149
Al	0.291	0.297	.0171	0.167	0.450
Fe^{3+}	0.167	0.226	0.152	0.143	0.126
Fe^{2+}	0.137	0.087	0.138	0.093	0.166
Mg	0.592	0.582	0.635	0.698	0.553
Ca	1.001	0.991	1.000	1.001	0.899
Na	0.028	0.053	0.043	0.038	0.063
Rock	UML	UML	UML	UML	AL

One camptonite, unfortunately not probed, was seen to show sector zoning in its clinopyroxenes. This may be due to variation in Ti and Al contents in these different sectors (cf. Downes 1974, augites from Mt. Etna) and is possibly also related to growth rates and equilibration/diffusion processes (Hollister and Gancartz 1971).

8.3.B: Amphiboles

Amphiboles are an important component of all groups of lamprophyres from the Igaliko area. Their presence (along with mica) attests to the generally hydrous nature of the lamprophyre magmas.

Figures 8.3.5A and B show amphiboles from the various lamprophyre groups plotted in the relevant parts of Leake's (1978) classification scheme. Not shown on the diagrams

Figure 8.3.5 2 pages.

A. (Facing) Calcic amphibole composition in terms of Si atoms per standard cell against $Mg/Mg+Fe^{2+}$, classified according to Leake (1978). Only the relevant fields have been labelled, for others see Figure 4.4.1.

B. (Overleaf) Alkali amphibole compositions in terms of $Fe^{3+}/Fe^{3+}+Al^{c}$ against $Mg/Mg+Fe^{2+}$ classified according to Leake (1978).

In general, all amphiboles are Mg-rich. AL amphiboles are all Ti-rich kaersutites, UML amphiboles are ferroan-pargasite or alkali-rich (magnesio-arfvedsonite or magnesio-riebeckite). CAL amphiboles range from ferroan pargasite, through hastingsite to ferroan-kaersutite and are typically among the more Fe-rich lamprophyre amphiboles. This reflects the more Fe-rich nature of the CAL.

Figure 8.3.5A

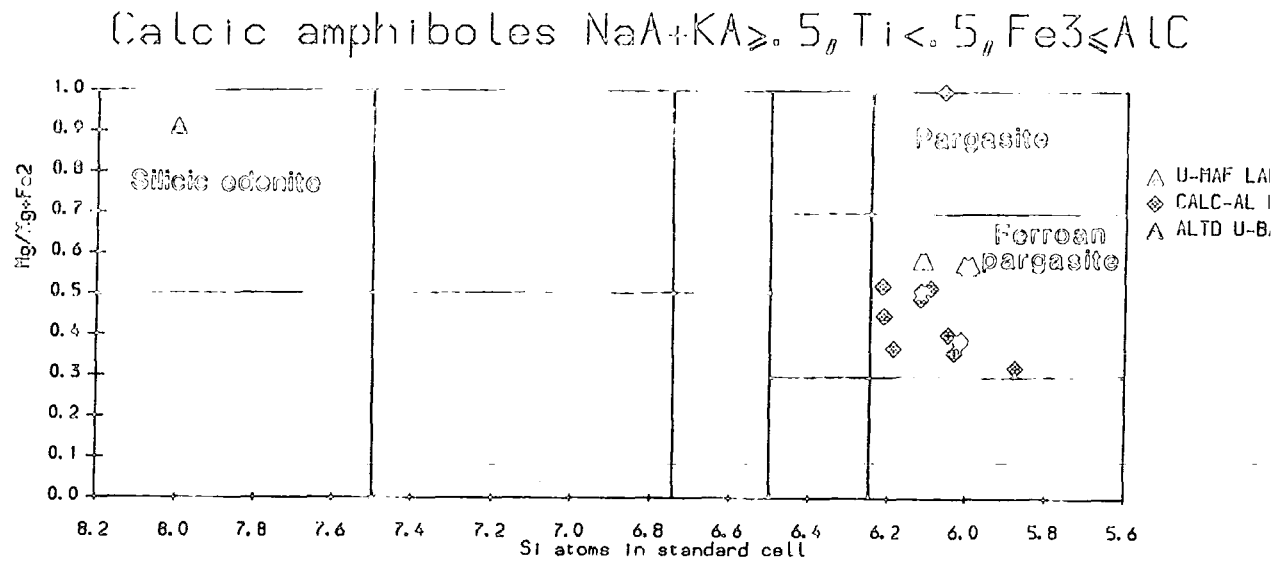
Calcic amphiboles NaA+KA≥.5, Ti<.5, Fe3≤AlC
Mg/Mg+Fe2
Silicic edenite
Pargasite
Ferroan pargasite
U-MAF LAI
CALC-AL I
ALTD U-B
8.2 8.0 7.8 7.6 7.4 7.2 7.0 6.8 6.6 6.4 6.2 6.0 5.8 5.6
Si atoms in standard cell

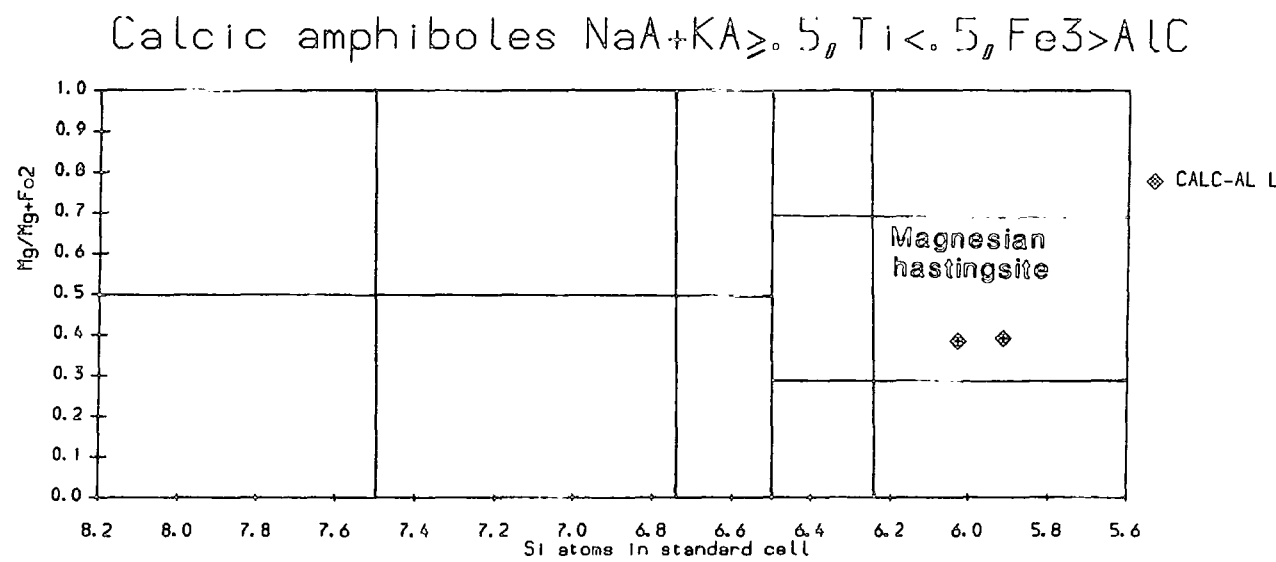
Calcic amphiboles NaA+KA≥.5, Ti<.5, Fe3>AlC
Mg/Mg+Fe2
Magnesian hastingsite
CALC-AL L
8.2 8.0 7.8 7.6 7.4 7.2 7.0 6.8 6.6 6.4 6.2 6.0 5.8 5.6
Si atoms in standard cell

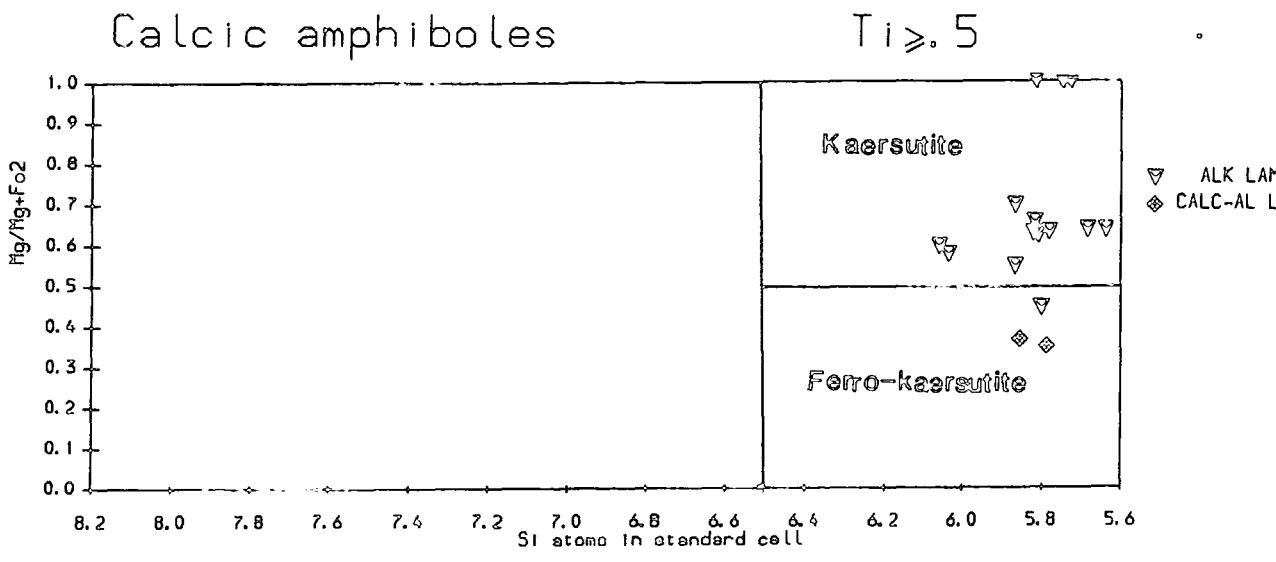
Calcic amphiboles Ti≥.5
Mg/Mg+Fe2
Kaersutite
Ferro-kaersutite
ALK LAM
CALC-AL L
8.2 8.0 7.8 7.6 7.4 7.2 7.0 6.8 6.6 6.4 6.2 6.0 5.8 5.6
Si atoms in standard cell

Figure 8.3.5b

Alkali amphiboles

△ U-MAF LAMP
△ ALTD U-BAS

NaA+KA≥0.5

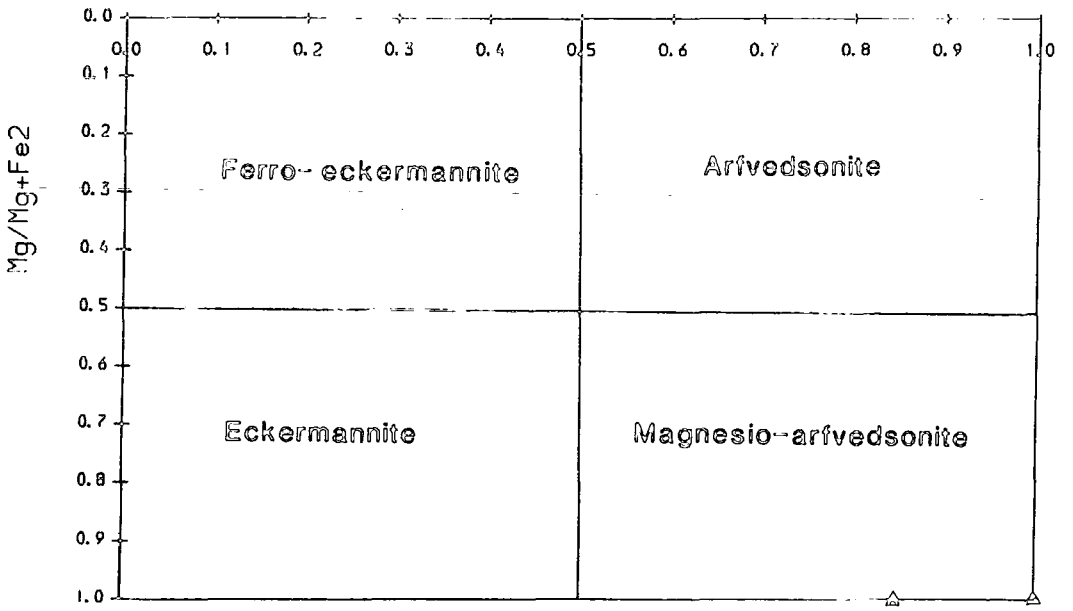

NaA+KA<0.5

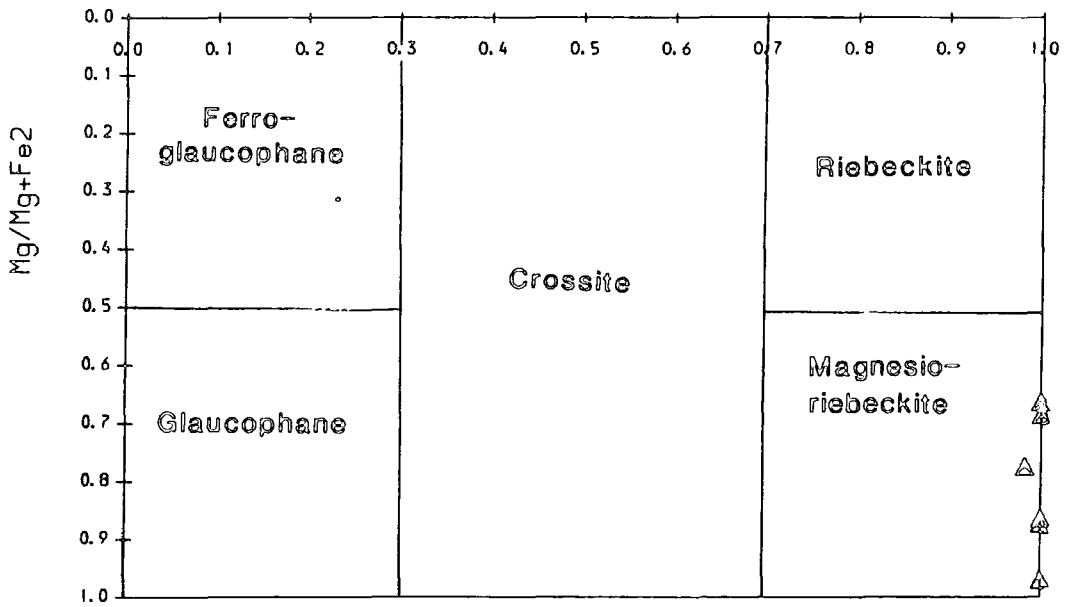

Figure 8.3.6

Amphibole compositions in terms of CaO/NaO_2 vs. Al_2O_3/TiO_2 as weight per cent compared to fields for various lamprophyre groups suggested by Rock (1987a). Both AL and UML amphiboles plot in roughly the same field, as too do some of the CAL. None plot within the lamproite (LL) fields.

Figure 8.3.6

Amphiboles from Lamprophyres

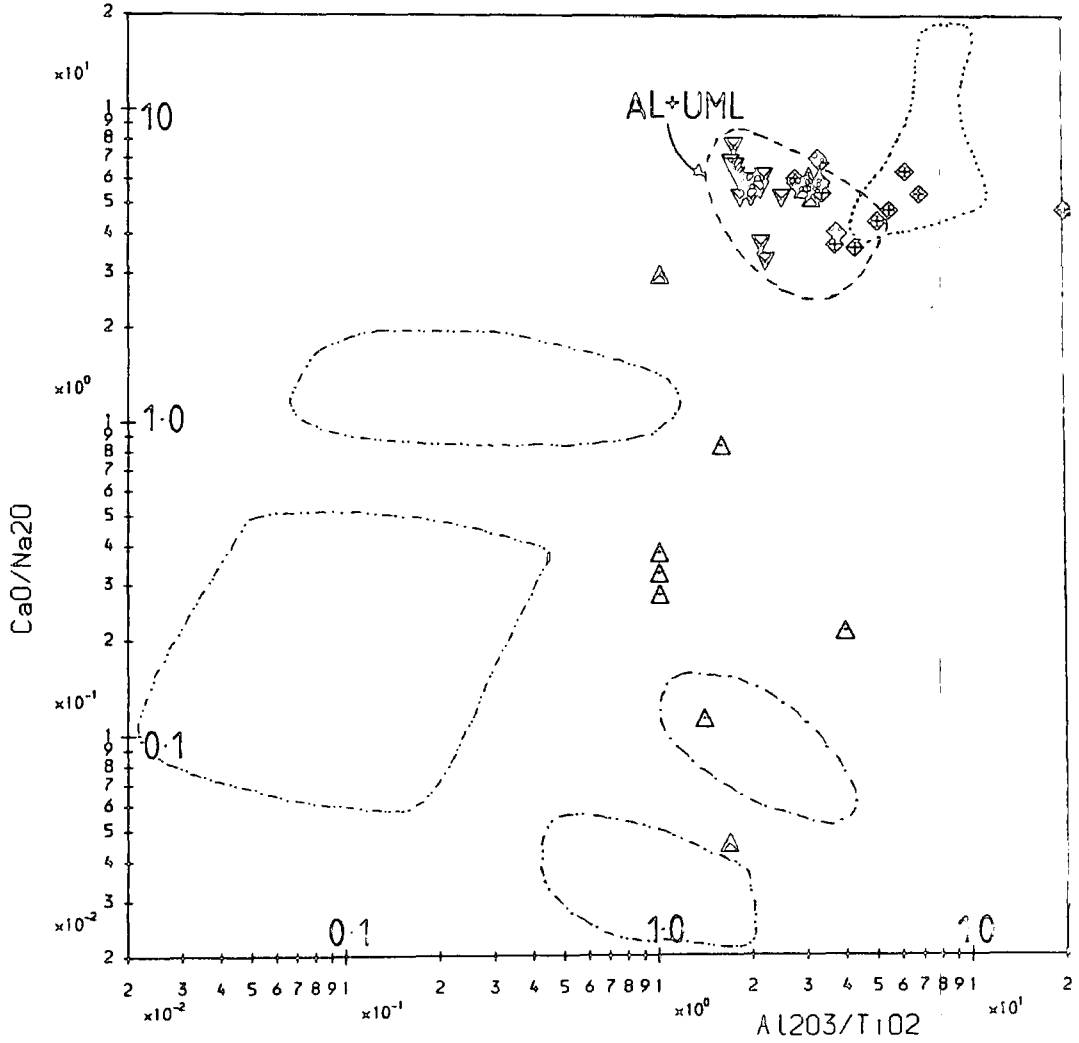

Figure 8.3.7: Amphibole composition from lamprophyres.

(A). Mg - (total Fe as Fe^{2+} + Mn) - Na+K. Also shown is the field of amphiboles from the remainder of the dykes. The trend of amphibole composition from UML through AL to CAL runs into the main swarm amphibole trend. A more alkali rich trend is seen in the altered ultrabasics, from Mg-rich alkali amphibole compositions.

(B). Mg - (Fe^{2+}+Mn) - Ti. There is a gradual reduction in Ti from AL through UML to CAL, reflecting the change from kaersutites to pargasitic amphiboles.

Figure 8.3.7A

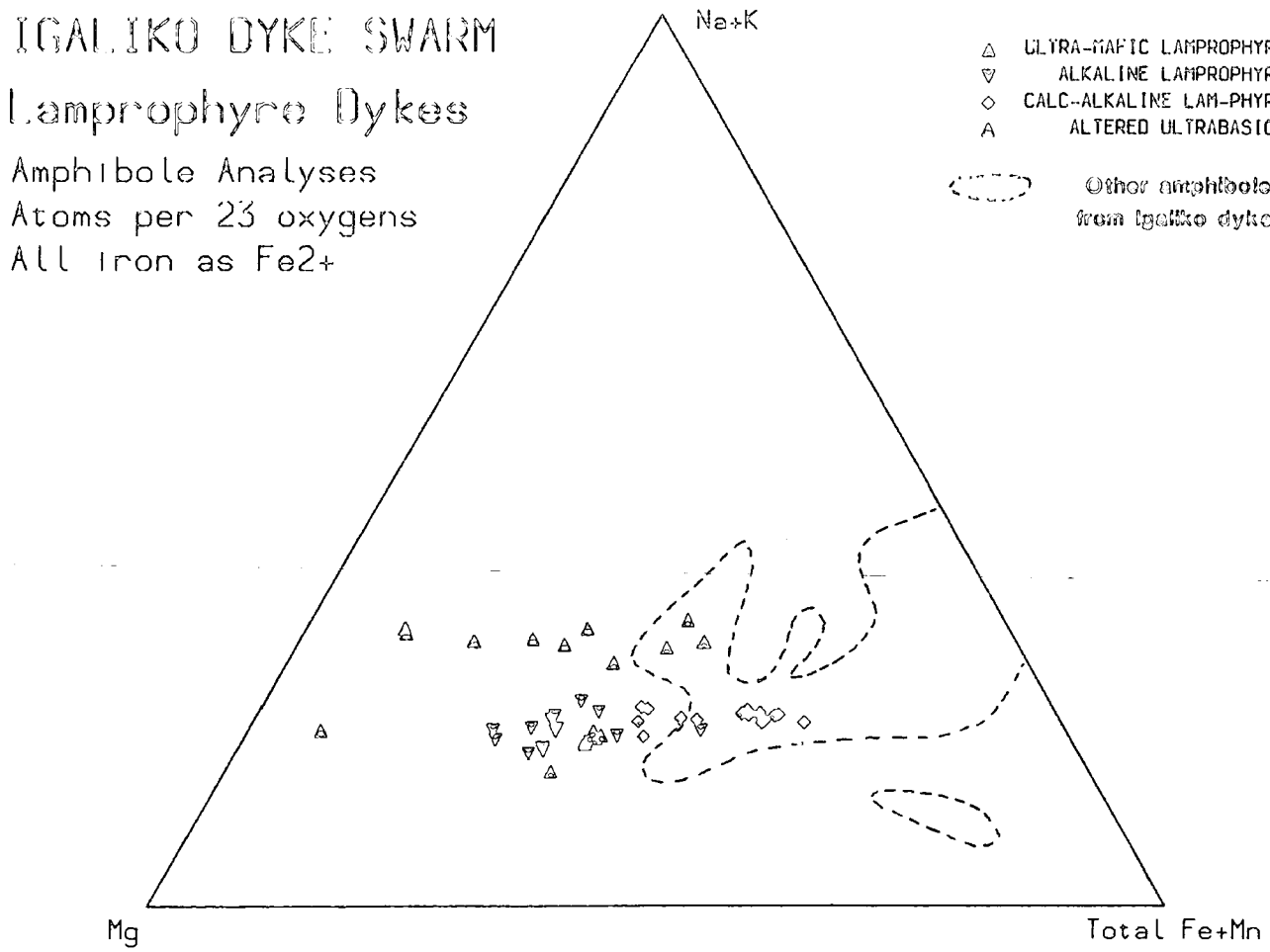

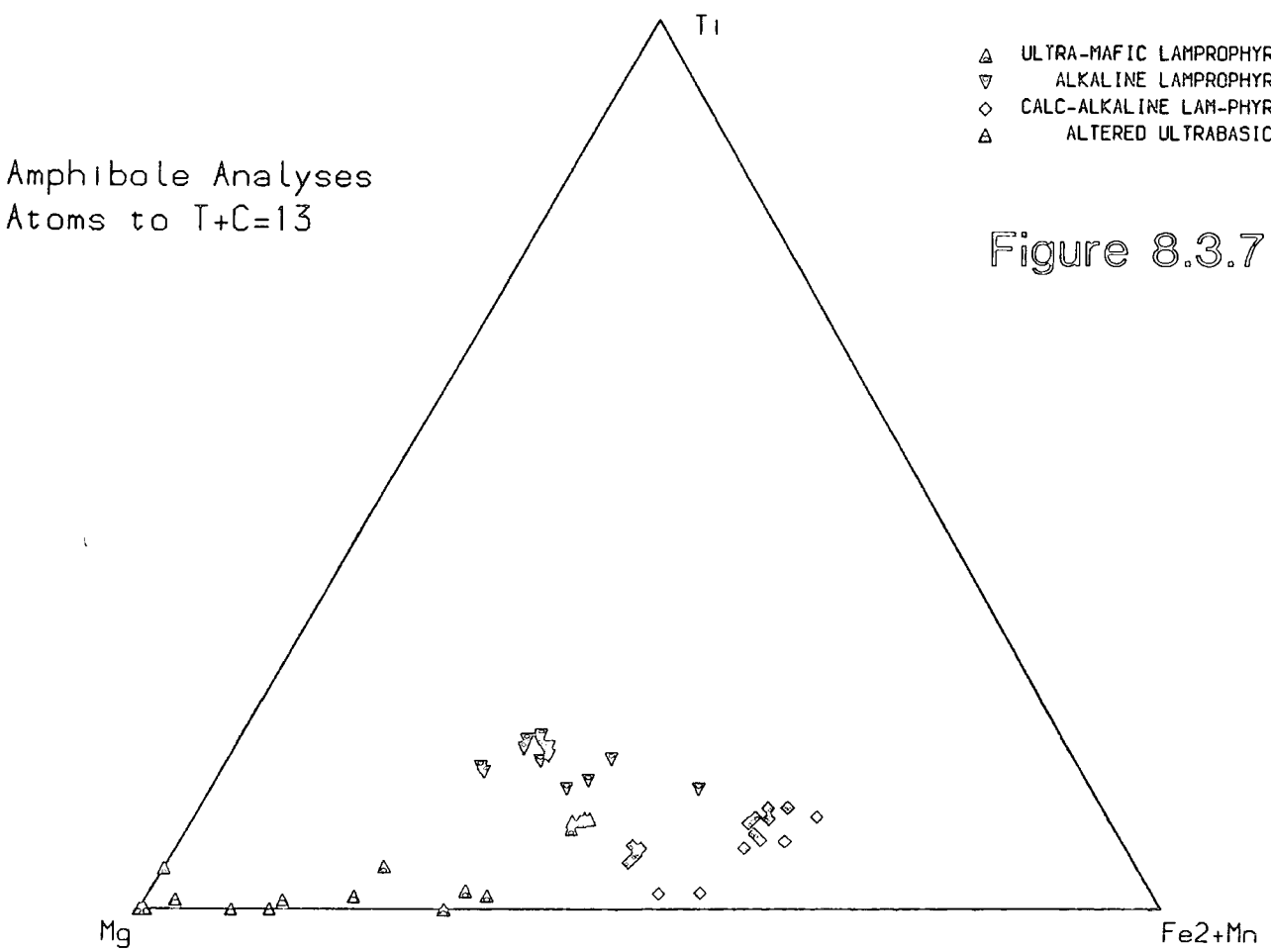

Figure 8.3.7

are two analyses of sodic-calcic amphiboles – a winchite from a UML and a K-richterite from an altered ultrabasic dyke. No amphiboles of the iron - manganese - magnesium series were recorded.

From Figure 8.3.5 it can be seen that the majority of the amphiboles are either ferroan pargasite or magnesio-riebeckite/manesio-arfvedsonite. CAL amphiboles are typically ferroan pargasite, although with minor compositional variation in terms of Ti and Fe^{3+} /Al ratio, small numbers pass through magnesian hastingsite to ferro-kaersutite. AL amphiboles are exclusively kaersutite or ferro-kaersutite reflecting the general Ti-rich mineralogy of this group.

Cawthorn (1976) noted that Ti in amphiboles was inversely proportional to total pressure. Although some kaersutites appear to be phenocrystic the high Ti would imply that they are not entrained from any great depth. The majority of kaersutites (including larger phenocrysts seen in some samples) will have grown *in situ* (cf. Campbell and Schenk 1950 who concluded that large – 4-inch – kaersutites grew *in situ* in camptonitic dykes from Arizona). Large crystals would grow rapidly in these volatile rich magmas. Fractionation of these kaersutitic amphiboles, with typically Ne-normative compositions, will tend to increase Si in the residual magmas as well as reducing Ti, volatiles and perhaps K (see Wones and Gilbert 1982), and they may thus grade into alkali basaltic rocks.

Figure 8.3.6 shows all amphibole analyses from lamprophyres plotted as CaO/Na_2O against Al_2O_3/TiO_2 used by Rock (1987a) to distinguish various lamprophyre fields. These generally conform to the data fields defined by Rock (1987a) to discriminate between various lamprophyre branches. Once again (cf. pyroxenes) no analyses plot in the LL fields. From Figure 8.3.7A it can be seen that the trend of amphibole evolution from the lamprophyres grades into the main amphibole trend with some overlap of the CAL. It is also apparent that Ti decreases with increased evolution (ie. with increased Fe+Mn).

8.3.C: Phlogopite/Biotite

Phlogopite is an important constituent of several groups of lamprophyres, particularly UML and CAL but also occurs in lesser amounts in AL and altered ultrabasics.

Figure 8.3.8: Mica compositions from lamprophyres.

(A). Al^{iv} vs. Fe/Fe+Mg.
End members abbreviated: An - Annite

Sdp - Siderophyllite

Phl - Phlogopite

Eas - Eastonite

Almost all UML micas are phlogopites, AL micas – relatively scarce – are more Fe-rich than those from UML, being biotites. All CAL micas have Fe/Fe+Mg>0.33 and are also biotites. CAL micas overlap the field of micas from other Igaliko dykes (excluding carbonatites).

(B). Al^{iv} vs. Ti.

Ti decreases with decreasing Al^{iv} (ie. increasing Si in the tetrahedral site). The most Ti-rich (and also the most Ti-poor) micas come from the AL. Generally the CAL have more Ti-rich micas than the UML, and this may reflect the presence of abundant Fe-Ti oxide (a sink for Ti) in the UML.

Figure 8.3.8A

Biotite/Phlogopite from Lamprophyres

Atoms per 22 oxygens

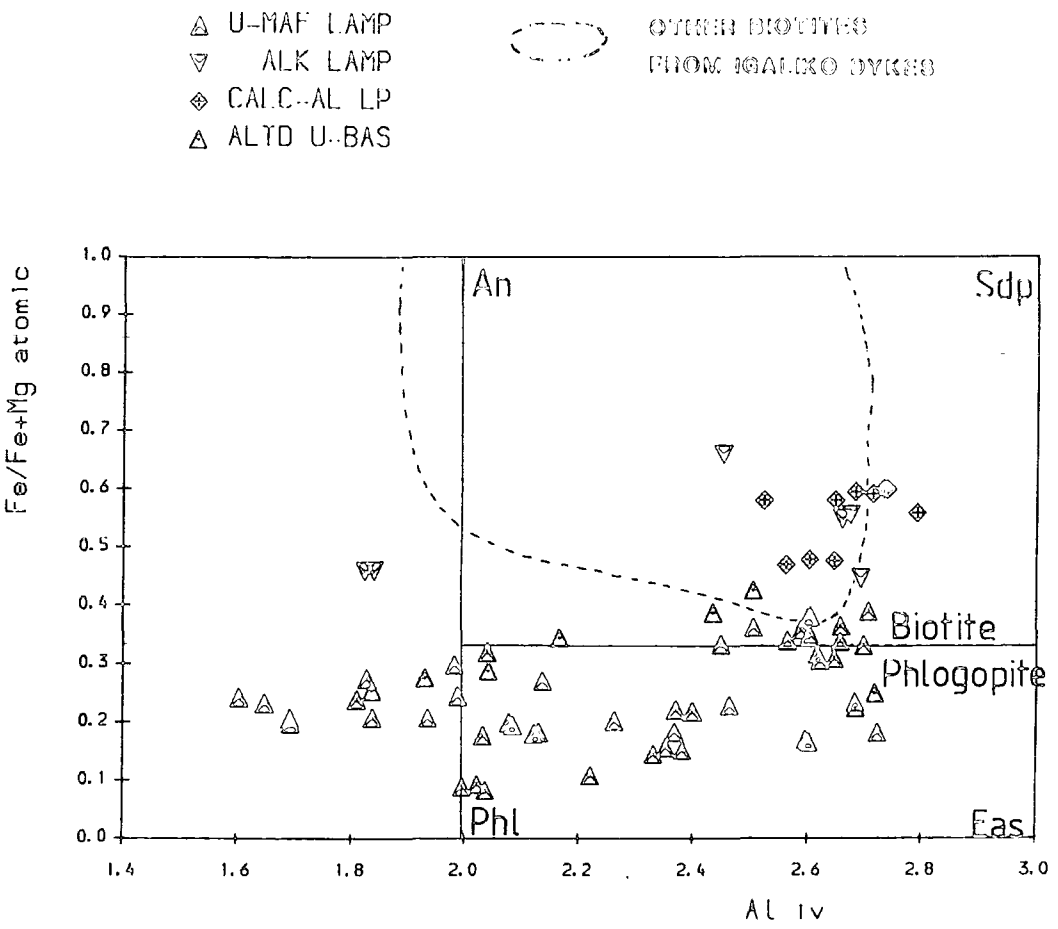

Figure 8.3.8B

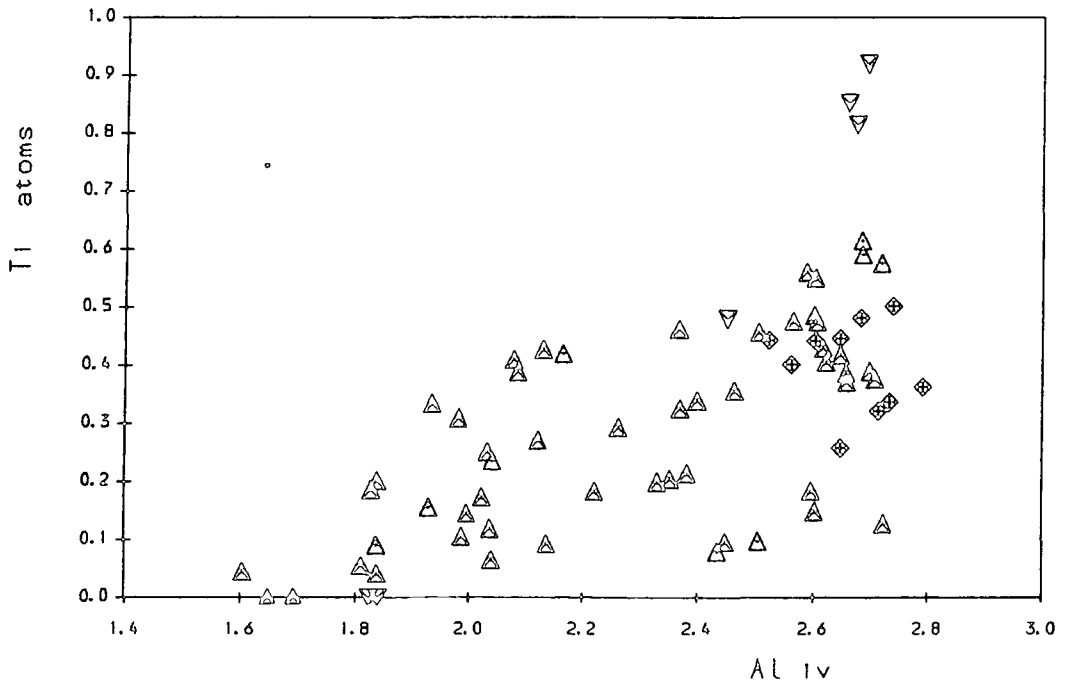

From Figure 8.3.8A it can be seen that the majority of micas from UML are phlogopites and that all the micas from the CAL are biotites (Deer *et al.* 1966). Biotites from the AL have Fe/Fe+Mg of ≈0.5 typically, whilst the micas from the altered ultrabasics tend to be transitional between phlogopite and biotite. This generally reflects the change in bulk rock Mg/Fe between these different groups of lamprophyres. Micas from the AL and CAL are similar to the most magnesian micas from the remainder of the Igaliko dykes (excluding the carbonatites).

Many micas are particularly rich in Ti (up to 0.95 atoms per 22 oxygens, 8.12 wt% TiO_2 in AL 52287), although Ti tends to decrease with Al^{iv} (see Figure 8.3.8B). There is however no distinct clustering of Ti and Al^{iv} with the exception of the CAL which all cluster around Al^{iv}=2.7 atoms, Ti=0.4 atoms.

Mn is generally low (<0.36 wt% MnO) in UML, AL and altered ultrabasics (AUB) but is recorded from most analyses of micas from CAL reaching 1.03 wt% as MnO.

Ba contents are erratic and are recorded in varying amounts from each group (UML up to 2.11 wt% BaO, AL up to 2.15 wt%, CAL up to 2.3 wt% and AUB up to 2.84 wt%).

Figure 8.3.9 shows all lamprophyre micas in terms of Mg – Fe+Mg –Ti and Mg – Fe+Mn –Al. Also shown are fields for biotites from the remainder of the Igaliko dyke swarm excluding carbonatites. The two trends roughly grade into one another, although the most basic micas from the main swarm are more titaniferous than the bulk of the lamprophyre micas.

Rock (1987a) described fields of mica compositions in terms of Fe/Fe+Mg vs. Al_2O_3 wt% from varying groups of lamprophyres. These are shown in Figure 8.3.10 along with all mica analyses from Igaliko lamprophyres. There is generally reasonable agreement with Rock's (1987a) scheme for AL and UML (although Igaliko UML extend to higher Al_2O_3 than Rock indicates). CAL consistently plot outside the suggested field of Rock (1987a) at higher Fe/Fe+Mg ratios, although may be within the scatter of Rock's original data set.

The UML micas show similar Ba and Fe/Mg ratios to those from K-rich ultramafic

Figure 8.3.9: Mica compositions from lamprophyres.

(A). Mg - total Fe+Mn - Al.

(B). Mg - total Fe+Mn - Ti.

Also shown are fields of other mica analyses from the remainder of the dykes. In both cases the lamprophyre trend grades into the more basic end of the main swarm mica trend.

IGALIKO DYKE SWARM

Lamprophyre Dykes

Biotite Analyses
Atoms to 22 oxygens
All iron as Fe2+

△ ULTRA-MAFIC LAMPROPHYRE
▽ ALKALINE LAMPROPHYRE
◈ CALC-ALKALINE LAM-PHYRE
△ ALTERED ULTRABASICS
OTHER BIOTITES FROM IGALIKO DYKES

Figure 8.3.9

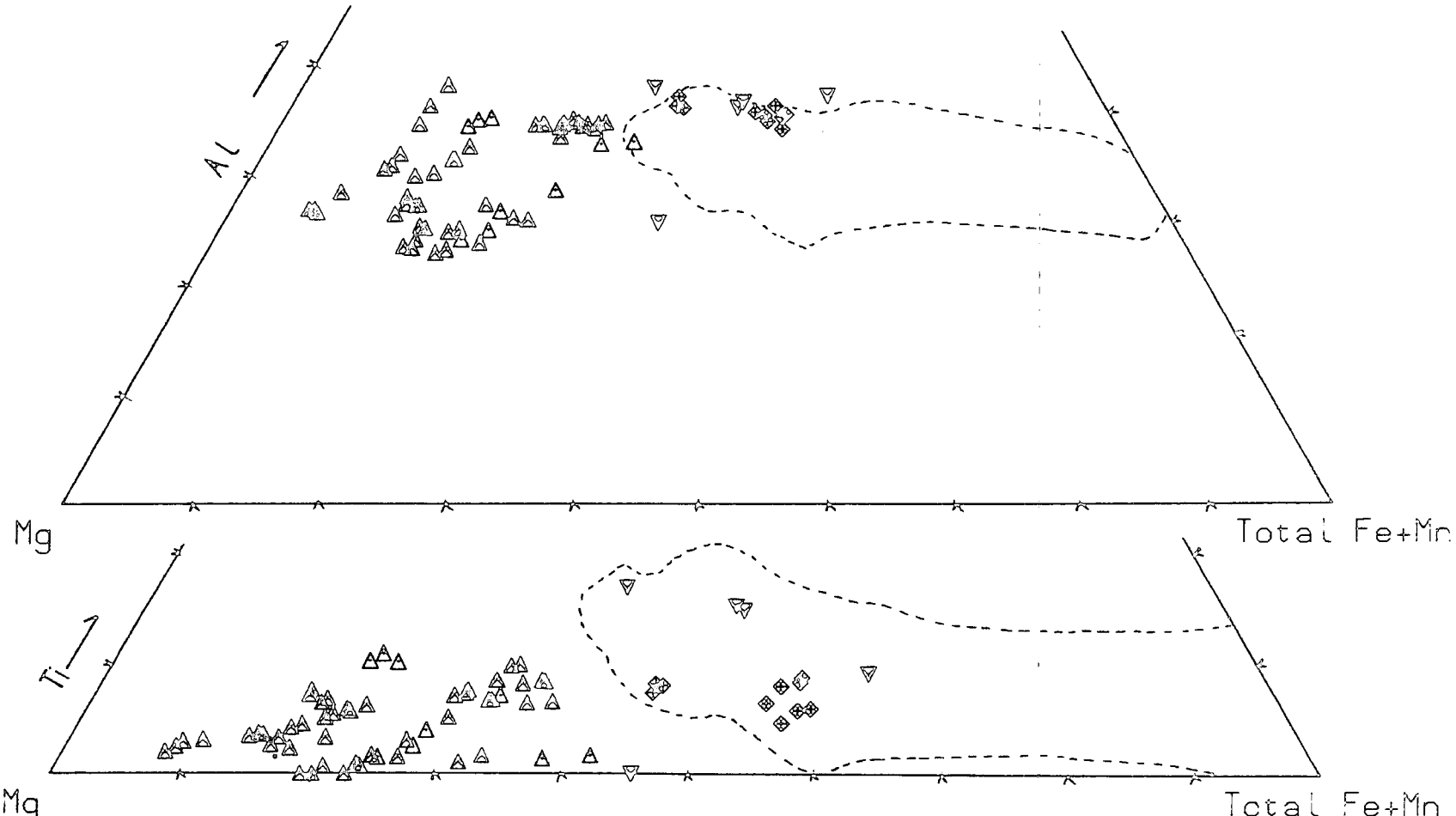

Figure 8.3.10

Lamprophyre mica compositions in terms of Fe/Fe+Mg (atoms per 22 oxygens) vs. Al_2O_3 wt%, compared to fields suggested for various lamprophyre groups by Rock (1987a). In general, UML and AL micas fall within the fields suggested by Rock, however, the CAL micas all plot at higher Fe/Fe+Mg ratio. UML are scattered around the field of Rock (1987a) and extend to higher Al_2O_3. No micas are typically 'lamproitic'.

Figure 8.3.10

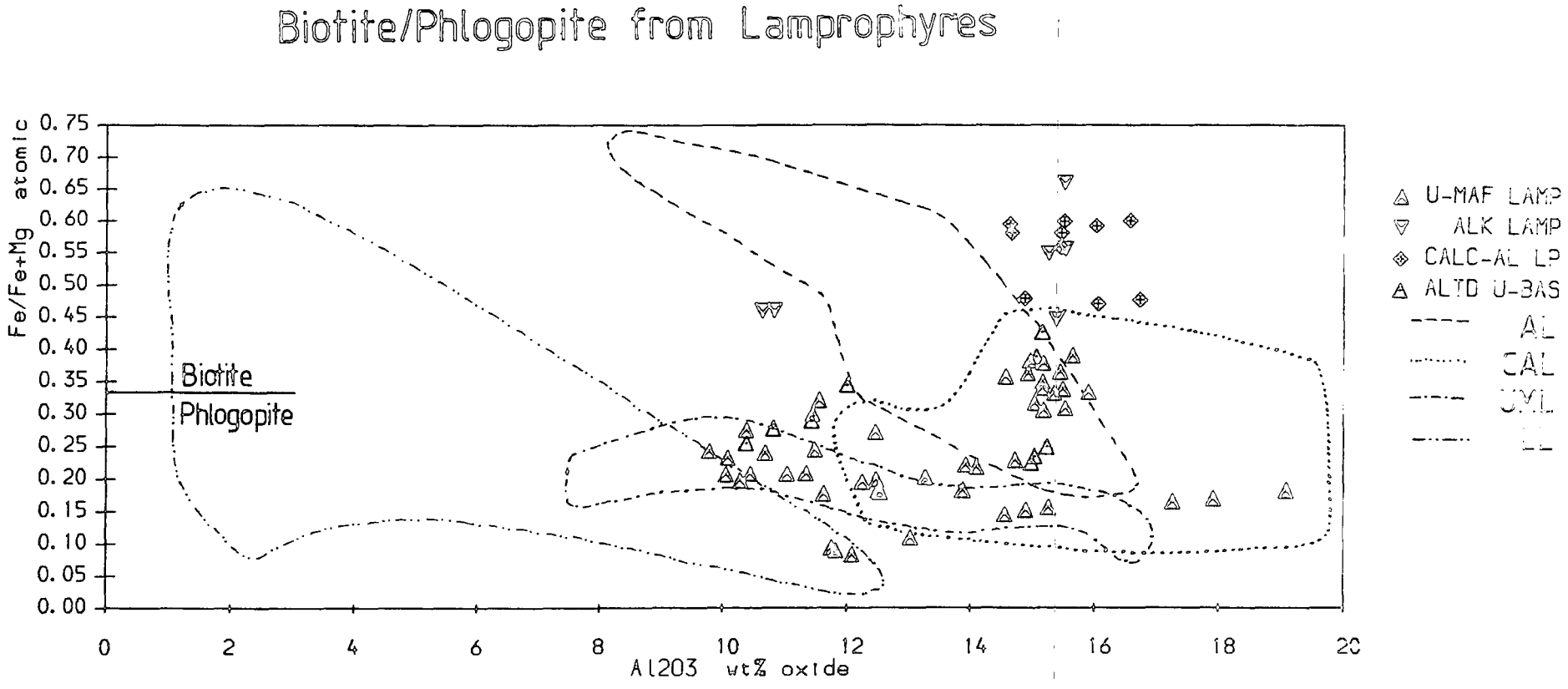
Biotite/Phlogopite from Lamprophyres
Fe/Fe+Mg atomic
0.75
0.70
0.65
0.60
0.55
0.50
0.45
0.40
0.35
0.30
0.25
0.20
0.15
0.10
0.05
0.00
Biotite
Phlogopite
0
2
4
6
8
10
12
14
16
18
20
Al2O3 wt% oxide
U-MAF LAMP
ALK LAMP
CALC-AL LP
ALTD U-BAS
AL
CAL
UML
LL

rocks from near Narssaq reported by Upton and Thomas (1973). They typically show much lower TiO_2 than the Narssaq examples which range from 6.14 to 9.13 wt% TiO_2. Mica chemistry in general reflects the basic (Mg-rich) nature of these rocks, with high Mg contents perhaps also a reflection of high fo_2 (Wones and Eugster 1967).

Zoning

Large micas from UML 326303 which protrude into a carbonate patch (immiscible liquid?, see Plate 8.11) were analysed to see if any compositional zoning was evident. The cores of the crystals were very similar to the bulk of the groundmass micas and zoning was only detected towards the rims of the crystals protruding into the carbonate patch. This involved a consistent increase in Al, (+0.4 atoms) and Fe (+0.2 atoms); and a decrease in Ti (-0.02 atoms), Mg (-0.25 atoms) and K (-0.1 atoms) from core to rim. Si and Na showed erratic behaviour. No Ca was detected in these micas. The large increase in Al was unexpected if these micas grew in place as carbonatitic magmas (and 'blebs' of carbonate such as this) are usually deficient in Al, however, all other variation would be expected knowing carbonatite chemistries.

8.3.D: Oxides and Sphene

Ilmenite and Magnetite

Figure 8.3.11 shows opaque oxide analyses from lamprophyres plotted in terms of molecular FeO – Fe_2O_3 –TiO_2 recalculated by the method of Carmichael (1967). Tie lines join analyses of ilmenites and magnetites from the same sample. Neither sample which contains both ilmenite and magnetite is within the range of any iron - titanium oxygen barometer - geothermometers (Buddington and Lindsley 1964, Powell and Powell 1977, Spencer and Lindsley 1981). The 'pairs' imply overall high temperature (>1000°C) and high fo_2 (perhaps $\approx 10^{-10}$).

Unlike the ilmenite/magnetites from the main dyke swarm, these are all low in Mn but often high in Mg (up to 8.48 wt% MgO in UML ilmenites and 1.54 wt% MgO in UML magnetites). Ilmenite MgO contents are similar to those reported by Smith and Dawson (1975) for ilmenites from an ilmenite glimmerite, and to the lower range for ilmenites reported by Shee (1984) from the Wesselton Mine Kimberlite, Kimberley.

Figure 8.3.11

Opaque oxides from lamprophyres, recalculated by the method of Carmichael (1967). Tie lines join analyses of ilmenites and magnetites from the same sample. Some 'ilmenites' tend to high Ti contents, approaching $FeO.2TiO_2$.

IGALIKO DYKE SWARM

Lamprophyre Dykes

Ilmenite and Magnetite
Molecular proportions

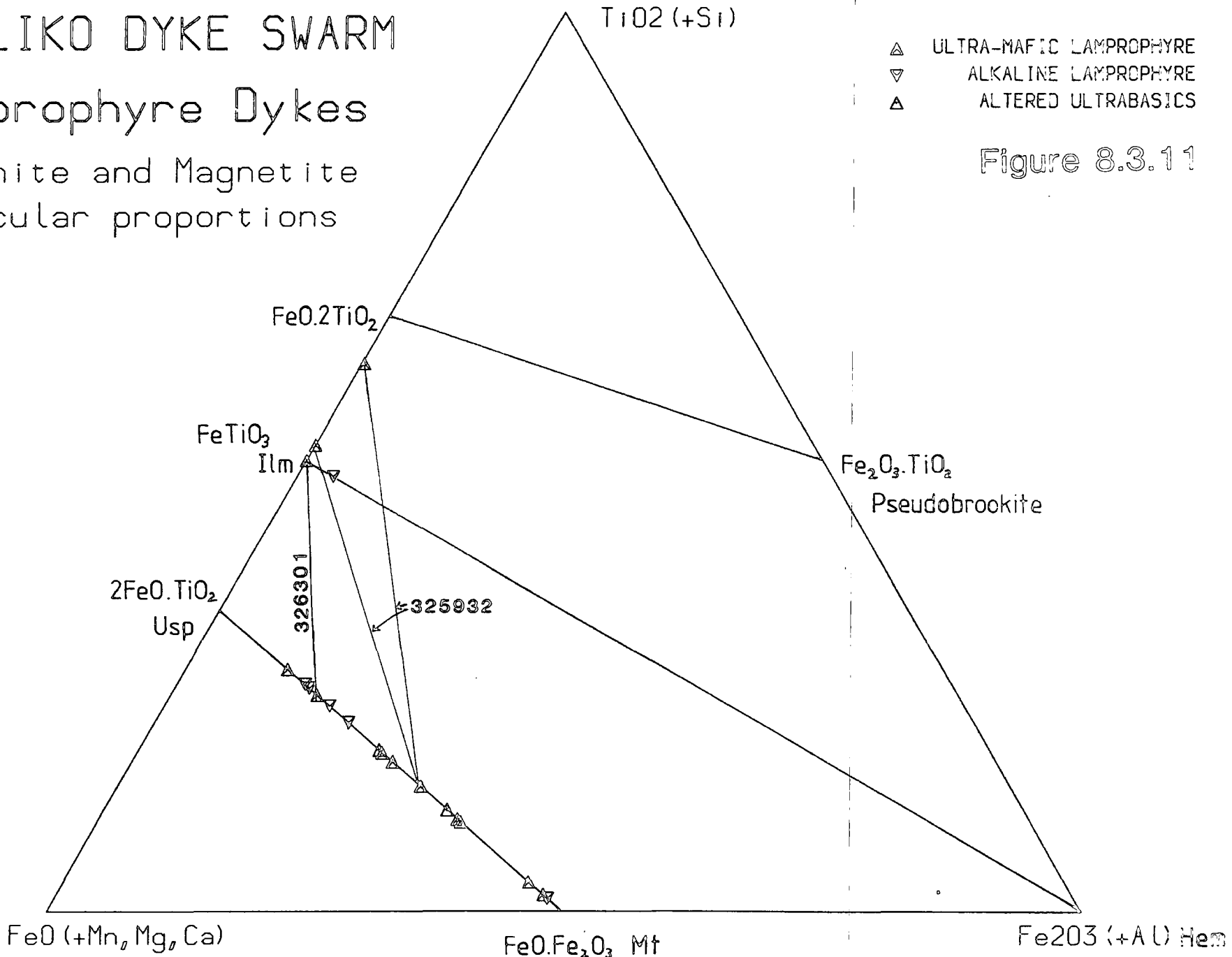

△ ULTRA-MAFIC LAMPROPHYRE
▽ ALKALINE LAMPROPHYRE
△ ALTERED ULTRABASICS

Figure 8.3.11

These analysts also reported high Cr_2O_3, but this was not analysed in the Igaliko examples. Rock (1986, 1987) contends that high Mn and Mg in ilmenites from UML is characteristic and that either high Mn or Mg apply to CAL and AL. Rock (1986) cites ilmenites from Alnö UML with up to 7.3 wt% MgO, marginally less than the Igaliko UML maximum. MnO is reported at 6.3 wt% from Fen UML ilmenites by Rock (1986) and this is considerably higher than any Igaliko UML analyses.

Ti enriched opaques approach the $FeO.2TiO_2$ end member of the pseudobrookite series (eg. 325932, UML). This may be a continuous compositional zonation from ilmenite or could be caused by minor (invisible) exsolution of a TiO_2 mineral (rutile, anatase) in ilmenite affecting the analysis.

Perovskite

Although Rock (1986) describes perovskite ($CaTiO_3$) as 'almost ubiquitous' in UML it has only been recorded from very few of the Igaliko UML, and analysed from only one sample – 41906. These range between $Ca_{0.908-0.921}Ti_{0.937-0.977}Fe_{0.030-0.045}Mg_{0.027-0.057}$ with minor Si (0.020-0.070) and Al (0.009-0.015) atoms per 3 oxygens. The presence of perovskite implies low a_{SiO_2} and lower fo_2 than required to form sphene (Haggerty 1976). The presence of Nb and LREE (Ce) was recorded from the analysed perovskites.

Sphene

Sphene is a relatively common phase in the lamprophyre dykes, particularly the UML where its presence reflects relatively high fo_2 (Carmichael and Nicholls 1967). Sphene occurs as rims to titaniferous magnetites or occasionally as large, lozenge-shaped euhedra, 2-3mm in length (see Plate 8.11). It is more typically confined to granular aggregates in the groundmass. One CAL (326281 – a vogesite) also contains sphene that has been analysed. Table 8.3.1 shows ranges of sphene analyses from various samples as atoms per 20 oxygens.

There is a noticable difference in sphene chemistry between the groundmass and phenocryst grains from UML 326303. The groundmass crystals contain less Ti, higher Fe, Mn and Mg. This may reflect changes in composition of the late stage liquids as crystallisation proceeds (increased a_{SiO_2} promotes sphene growth around oxides, lower

Table 8.3.1

Analyses of sphene from lamprophyres as atoms per 20 oxygens.

	CAL	UML phenocryst	UML g-mass	UML g-mass
Spl	326281	326303	326303	54168
Si	3.84-3.88	3.91-3.92	3.96-3.99	3.73
Ti	3.84-3.93	3.91-3.92	3.96-3.99	3.73
Al	0.15-0.20	0.12-0.18	0.51-0.52	0.16
Fe	0.09-0.13	0.09-0.13	2.32-2.35	0.05
Mn	0	0	0.031	0
Mg	0	0	0.22-0.27	0
Ca	4.07-4.09	4.11-4.14	5.14-5.16	3.96
Zr	0.031-0.032	0.048-0.161	0.047	0
Na	0	0	0.076-0.079	0

Ti and higher Fe in residual liquid lead to higher Fe/Ti ratio). Typically however, sphenes are close to stoichiometric $CaTiSiO_5$. They may contain some Nb and REE.

Smith (1970) observed that perovskite and sphene rarely coexist. At any given fo_2, a_{SiO_2} will govern whether sphene or perovskite form (Haggerty 1976) with sphene forming at higher a_{SiO_2}. The presence of sphene and perovskite thus both reflect high fo_2 and their respective occurrence is governed by a_{SiO_2} of their particular host magmas. fo_2 and a_{SiO_2} will also have an effect on the compositions of magnetite and ilmenite solid solution series in the rock.

Spinel

Cr-spinel was observed in UML 325932 and 2 analyses were made. These are reproduced in Table 8.3.2. This single grain of spinel occurs as a corroded core surrounded by ilmenite/magnetite, and is probably of xenocrystic origin. No other spinels have been seen in any other of the lamprophyre dykes.

8.3.E: Felsic Mineralogy

Feldspar

Feldspar compositions from lamprophyres are shown in Figure 8.3.12 in terms of

Figure 8.3.12

Feldspar analyses from lamprophyres in terms of Ca - Na - K as atoms per 8 oxygens.

IGALIKO DYKE SWARM

Lamprophyre Dykes

Feldspar analyses

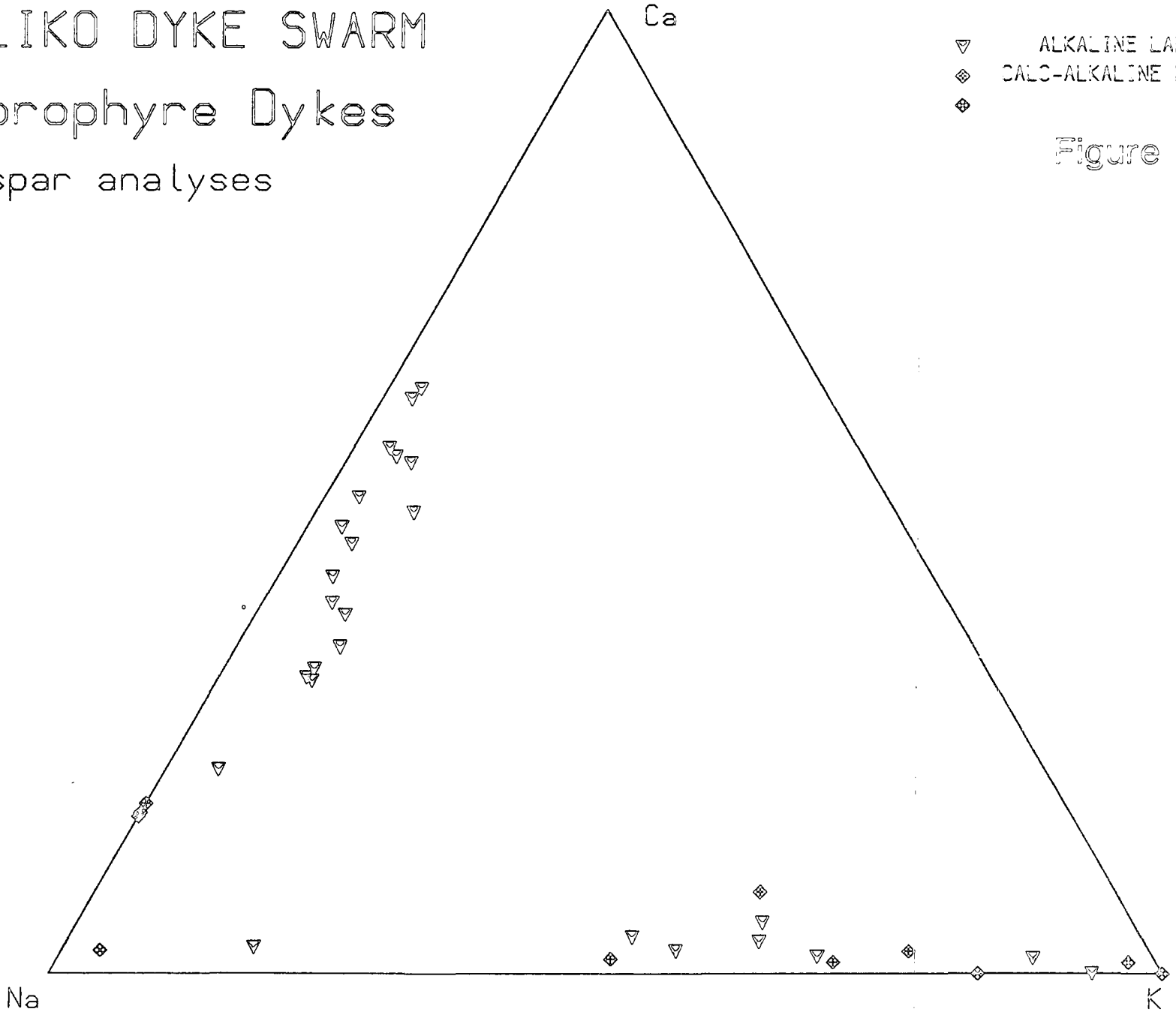

ALKALINE LAMPROPHYRE
CALC-ALKALINE LAM-PHYRE
BRECCIA

Figure 8.3.12

Table 8.3.2

Cr-spinel analyses from UML 325932.

	325932.44	325932.45
SiO_2	0.49	0.33
Al_2O_3	42.14	42.51
FeO	16.01	16.00
MnO	0.0	0.21
MgO	17.72	17.54
Cr_2O_3	25.37	24.60
Total	101.73	101.19

Ca, Na and K. Feldspar has been analysed from AL, CAL and the breccia dykes 325960 and 41947. No feldspar has been analysed from UML although minor amounts of alkali feldspar have been seen in some thin sections.

AL contain both plagioclase and alkali feldspar and this distinguishes between camptonite and sannaite respectively. The CAL from Igaliko are restricted to relatively Ca-poor feldspars with compositions from oligoclase to sanidine being recorded. Feldspars from the breccia dykes are binary alkali feldspars. Plagioclases from AL show a relatively early tendency towards K enrichment (K-labradorite and K-andesine according to the nomenclature of Smith 1974 – see Figure 4.8.1).

Rock (1987a) suggests that high Fe and Ba may be characteristic of lamprophyre feldspars. FeO reaches 0.89 wt% in AL, but 3.05 wt% in CAL and 0.58 wt% in the breccias. Rock (1987a) suggests Fe_2O_3 is greater in AL than CAL.

BaO contents are typically below detection in AL but one sample (326283) produced one analysis of Ba at 4.40 wt%. The only other AL feldspars with any Ba contained less than 0.67 wt% BaO. CAL feldspars are more consistently rich in BaO than AL with up to 2.29 wt% and feldspars from breccias contained up to 2.05 wt%. These data are in accord with Rock (1987a) who suggests that BaO in feldspars is typically greater in CAL than AL.

Analcite

Analcite is a relatively common mineral in the AL where several analyses have been

made. It is also seen in some thin sections of CAL although not analysed. Analcite analyses from lamprophyres (all from AL) are shown in Figure 4.10.1. Rock (1987a) reports that most analcites show little deviation from the standard formula. Several analyses cluster around 'analcite' but many fall between albite and analcite in *Ne - Ks - Qz*, possibly due to incomplete reaction of albite (Henderson and Gibb 1983, see Chapter 4.9).

Nepheline and Sodalite

Nepheline and sodalite were both analysed from one sample only, 46279, which appears petrographically to be a CAL. Rock (1987a) however states that 'nepheline and sodalite minerals occur only in AL and UML'. This sample is composed mostly of green-brown amphibole, lesser amounts of plagioclase, pyroxene, alkali feldspar and biotite, with nepheline and sodalite being subordinate to the feldspar. It would thus appear that this sample can be classified, using the suggestions of Rock (1984) as a spessartite (see Table 8.1.2).

Nepheline compositions are illustrated in Figure 4.7.1 and some features of the sodalite chemistry are shown in Figure 4.9.1. Nepheline compositions plot close to the Morozewicz composition or at lower *Qz*. Nephelines are discussed in Chapter 4.7. Sodalite contains between 5.69 and 7.40 wt% Cl and is similar to sodalites from the remainder of the dykes. One analysis with low Na (14.04 wt% Na_2O, cf. 21-26 wt%) and 1.3 wt% CaO may be from an altered grain which has lost alkalis.

Muscovite

Muscovite mica is recorded as an alteration product after feldspar/feldspathoid from UML 41906. It has the formula $Na_{0.09-0.21}K_{1.86-1.92}Ca_{0-0.04}Al_{5.77-5.94}Si_{6.06-6.11}O_{22}$. Its general appearance is of clear to murky patches showing low birefringence due to an extremely small grain size. It probably formed at late magmatic stages.

8.3.F: Garnet

Melanite garnet has been recorded from one sample 41906, where it occurs as sieve textured, ?poikiloblasts up to 1mm in diameter. The analyses are listed in Table 8.3.3.

Table 8.3.3

Garnet analyses from 41906 as atoms per 12 oxygens.

	41906.37	41906.38	41906.39
Si	2.246	2.275	2.326
Ti	1.002	1.023	0.952
Al	0.215	0.235	0.226
Fe^{3+}	1.332	1.128	1.281
Fe^{2+}	0.067	0.202	0.076
Mn	0.022	0.028	0.076
Mg	0.152	0.143	0.137
Ca	2.921	2.946	2.938
Na	0.043	0.0	0.046
K	0.00	0.00	0.00
Zr	0.000	0.021	0.00

The garnet general formula can be written as $X_3^{2+}Y_2^{3+}Z_3^{4+}O_{12}$ with X^{2+} being 8-fold coordinated, Y^{3+} is octahedrally coordinated and Z^{4+}, tetrahedrally coordinated. Si and probably Al will partly occupy the tetrahedrally coordinated site, leaving a defecit of about 0.5 atoms. Fe^{3+} , Fe^{2+} , Ti, Al have been recorded from the tetrahedral sites of natural garnets (Huggins *et al.* 1977a). Based on a study of synthetic garnets Huggins *et al.* (1977b) concluded that Al would enter the tetrahedral site in preference to Fe^{3+} and then Ti^{4+} and this agrees with the conclusions of Hartman (1969). Enough Fe^{3+} exists in these garnets to fill, along with Si and Al the tetrahedral site and thus all Al will be accommodated in the tetrahedral site. It is unlikely that any Ti^{4+} will occupy the tetrahedral site. For Ti^{4+} to occupy the octahedral site Huggins *et al.* (1977a) proposed coupled substitution of $Y^{2+}+Ti^{4+} \rightleftharpoons 2Y^{3+}$ (where Y^{2+} is Mg^{2+} or Fe^{2+} entering the octahedral site, and Y^{3+} will be Fe^{3+} or Al^{3+} in the octahedral site). Ca will occupy the X^{2+} site, the deficit being composed of minor Fe^{2+}, Mg and Mn.

Zr, detected in one analysis at 0.51 wt% ZrO_2, will occupy the Y site with coupled substitution of Al into Z, as the endmember kimzeyite ($Ca_3Zr_2(Al_2Si)O_{12}$) which has been found naturally in a carbonatite at Magnet Core, Arkansas (Milton *et al.* 1961). Upton and Thomas (1973) reported minor amounts of andradite ($Ca_3Fe_2^{3+}Si_3O_{12}$) from the ultramafic rocks around Narssaq, these being the Ti-poor equivalents of melanite.

8.4: Geochemistry

Lamprophyres cover a large compositional range and are unusual in being rich in both compatible and incompatible elements (eg. Mg, Ni, Cr, V, Rb, Ba, REE, Nb, Zr, etc.). Major and trace element composition are plotted in Figure 8.4.1 against MgO wt%. Also plotted are Zr/Nb and Ce/Y against MgO.

Lamprophyres have been classified upon petrographic grounds into UML, CAL and AL. Breccias and altered ultrabasics have been included in this group due to their chemical and petrographic similarities to the UML. A further sub-division of UML has been included – 'Carbonatite/UML' – which are a series of dykes with $SiO_2 \approx 15$ wt% and $CaO \approx 25$ wt%. These have petrographic and certain chemical affinities with both carbonatites and UML.

Major Elements

All lamprophyric rocks studied have SiO_2 <50 wt%, and there is a general increase in SiO_2 from UML<CAL<AL. Excluding the very Si-poor carbonatite/UML associations, UML typically contain 30-40 wt% SiO_2, CAL≈40-45 wt% SiO_2 and AL≈42-47 wt% SiO_2. The carbonatite/UML association are all < 16 wt% SiO_2. Al_2O_3 shows very similar behaviour to SiO_2. MgO decreases in the order UML>CAL>AL ranging from almost 18 to about 7 wt% in UML, from 8-6 wt% in CAL and about 8.5-4 wt% in AL. They are all thus mafic rocks, the most Mg-poor compositions being similar to many of the basaltic/hawaiitic samples from the main Igaliko dyke swarm. Fe_2O_3 increases gradually with decreasing MgO from ≈14 wt% to ≈20 wt% and this will probably reflect the extraction of very Mg-rich silicates (olivine – although none is seen – and pyroxene are likely phases). Through the CAL and AL both Fe and Mg decrease together, again a ferromagnesian control. CaO shows a somewhat erratic behaviour in the UML and will reflect differences in modal diopside/salite, oxides and phlogopite along with any carbonate content in the sample.

K_2O is the only alkali present in many of the UML, Na_2O often being below detection. One analysis, 46279, reports Na_2O at 4.3 wt%, all others are <1.01 wt% with 8 (from 23) being below detection. Na_2O shows a gradual increase through CAL to about 4 wt% in AL. K_2O, between 3 and 6 wt% in UML decreases into CAL and AL (about

Figure 8.4.1

(A). (Facing). Major element variation from lamprophyres vs. MgO as weight %.

(B). (Overleaf). Trace element variation (ppm) from lamprophyres vs. MgO (wt%). Note the high contents of incompatible elements in all branches of the lamprophyre clan. Ni and Cr show a relatively steady decrease with decreasing MgO implying a ferromagnesian control. The decrease in REE with decreasing MgO may be a melting control (not a fractionation control – see text). Zr/Nb is typically low showing a gradual increase from UML to CAL and AL. Ce/Y shows a decrease in the same order.

Lamprophyres - Major element variation

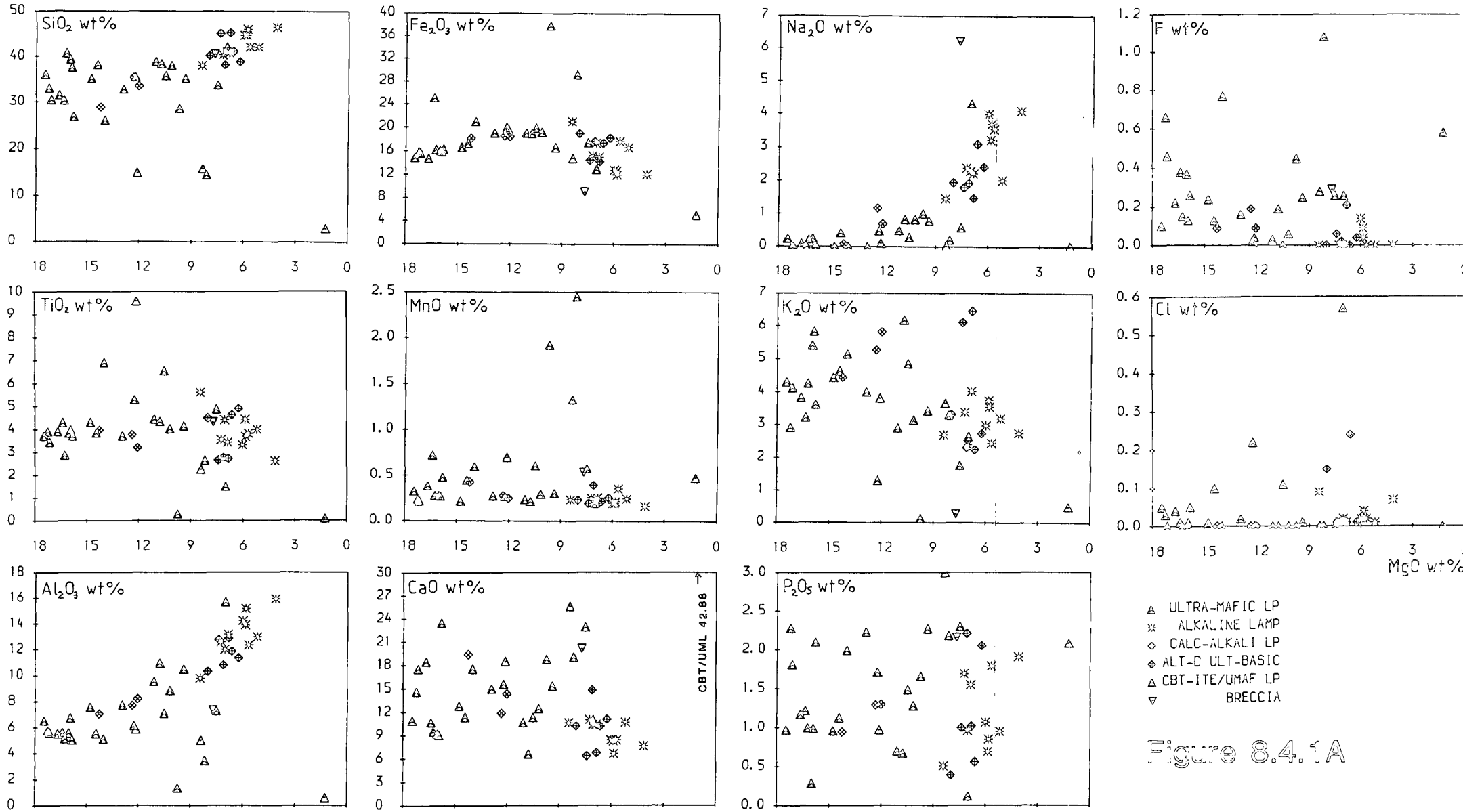

Figure 8.4.1A

Lamprophyres Trace element variation

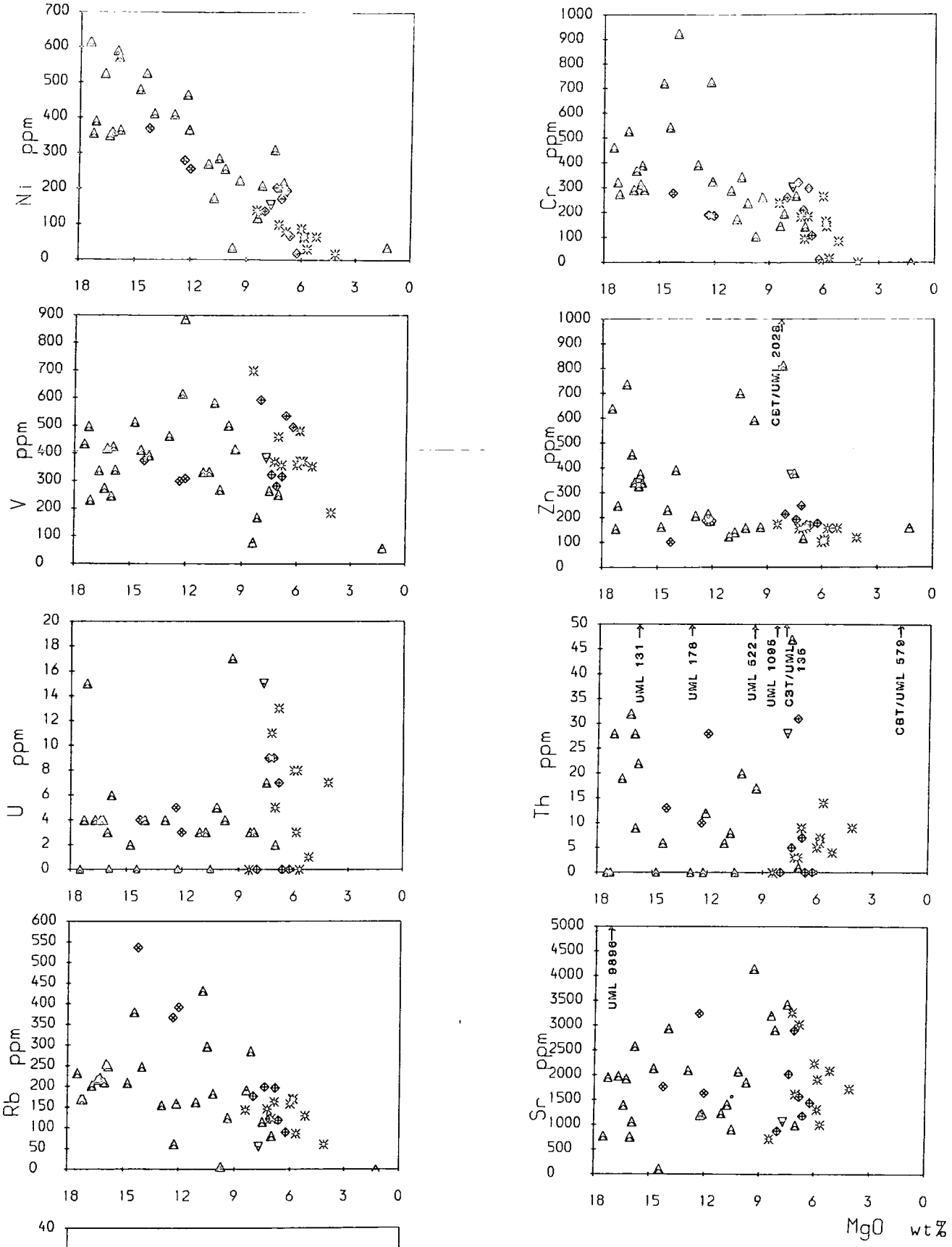

Figure 8.4.1B

Lamprophyres - Trace element variation

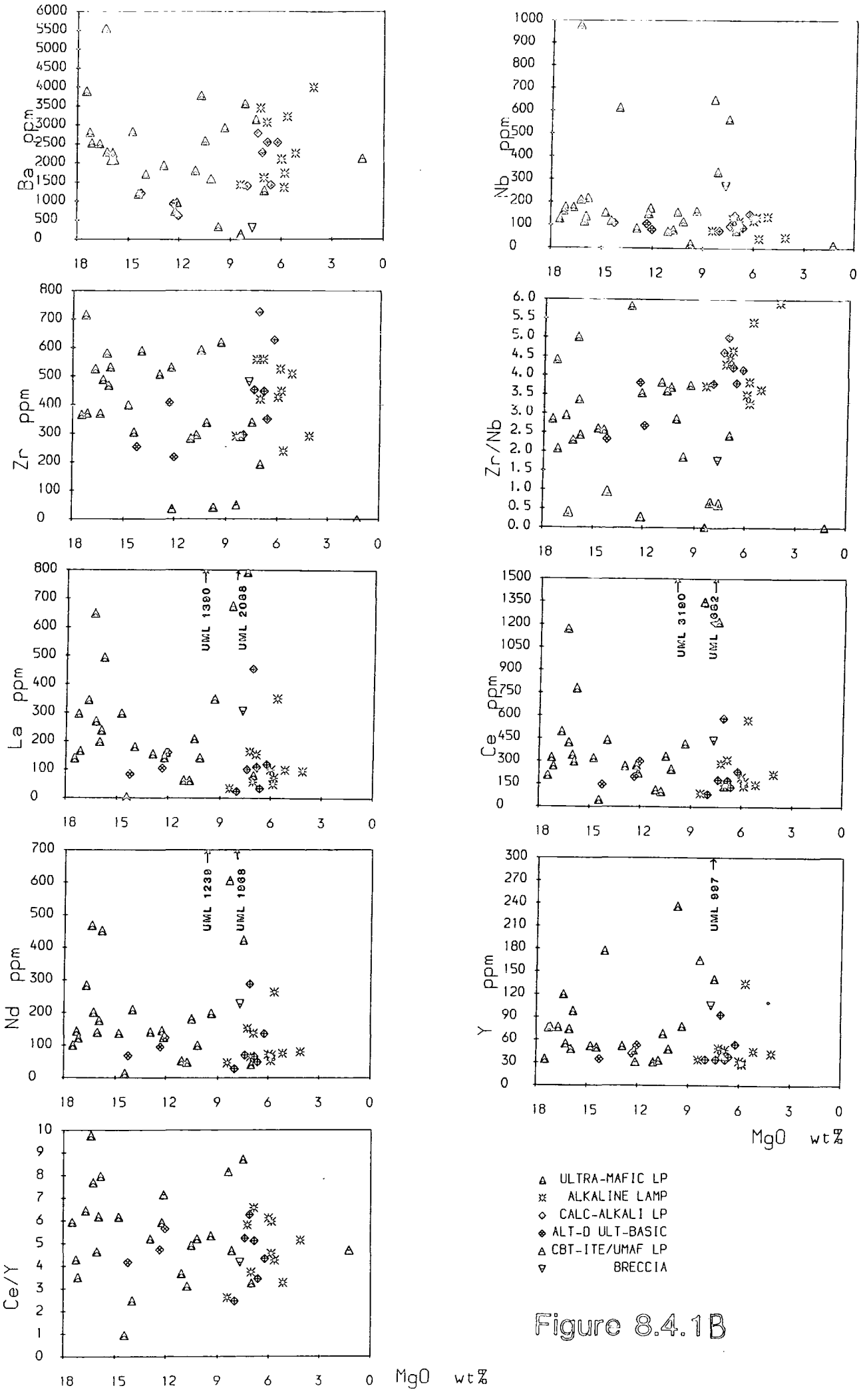

Figure 8.4.1B

3 wt%). Total alkali contents thus show a gradual increase from UML<CAL<AL, although there is some overlap (see Figure 4.8.2C). For equivalent MgO or SiO_2 contents in the main swarm, these lamprophyre dykes are much more alkali rich, leading to TAS (Cox *et al.* 1979) classification as nephelinites, tephrites/basanites or rarely hawaiites (see Figure 8.4.2C).

The presence of mica and amphibole as common phases in all groups of lamprophyres attests to their high volatile contents. F is much more abundant than Cl, and F shows a rough decrease with decreasing MgO (fractionation of phlogopite/amphibole?). Cl, typically less than 0.1 wt% increases very gradually with decreasing Mg. F/Cl thus decreases with decreasing MgO, with both F and Cl approaching typical basaltic levels in the AL. P_2O_5 shows a scattered distribution, reaching typical maximum contents of about 2.3 wt% in each lamprophyre group, about twice typical basalt contents.

TiO_2 is typically about 4 wt% although may reach nearly 7 wt% in UML and almost 10 wt% in a carbonatite/UML dyke. There is no marked decrease in TiO_2 with decreasing MgO or increasing SiO_2, thus TiO_2/SiO_2 ratio decreases from UML to AL. AL TiO_2 contents are typically 1 wt% greater than those from the basaltic rocks. MnO is generally between 0.2-0.3 wt% although in one UML rises to almost 2.5 wt%. There is a gradual decrease of MnO from UML to AL. AL MnO contents are similar to the basaltic rocks.

Normative Mineralogies

All the lamprophyres are undersaturated, falling on the alkaline side of the Hawaiian alkali/tholeiite boundary. They are all thus nepheline normative. Many of the UML are leucite rather than nepheline normative, reflecting the K-rich chemistries.

The AL are characterised by basanitic norms, ie. *ab+an+or+ol+di+ne*. CAL are similar with their high Fe and Ti contents reflected in relatively high contents of ilmenite, hematite and magnetite. Fe^{3+}/Fe^{2+} ratios were assigned on their TAS and peralkaline characteristics as described in Figure 5.2.1B.

Normative felsic minerals in UML, often very potassic (K>>Na), are dominated by orthoclase and/or leucite with anorthite a common normative component. Nepheline

may or may not be present, due to the general lack of Na. Diopside and olivine are common to all UML norms. An unusual and characteristic component of the UML norms is larnite (calcium orthosilicate), an indication of the silica-poor nature of these rocks. Normative opaques abound and occasionally perovskite is produced in the norm.

Major Element Discriminant Plots

In the above account of major element geochemistry several systematic differences have been noted between various groups such as (i) the range of Si, Al to be expected, (ii) Ti/Si ratio (iii) alkali content and (iv) the range of MgO to be expected. Rock (1987a) used certain of these criteria to produce a broad compositional classification for distinguishing between CAL, AL and UML. Figure 8.4.2 shows plots of CaO $-TiO_2 \times 4$ $- SiO_2/10$ (Figure 8.4.2A) which broadly separates CAL from AL and MgO - CaO - Al_2O_3 (Figure 8.4.2B) which separates Al from UML. In both cases there is generally good agreement between Rock's (1987a) fields and the Igaliko lamprophyres, classified petrographically into the various lamprophyre branches. At Igaliko, CAL however are not as rich in SiO_2 as the bulk of the lamprophyre data used by Rock would suggest, some appearing well inside the AL field. Similarly some Al_2O_3 rich UML plot within the AL field in MgO - CaO - Al_2O_3 terms, although most fall neatly within the fields defined by Rock (1987a).

Figure 8.4.2C shows all lamprophyres from Igaliko plotted in terms of total alkalis - silica, also showing the fields proposed by Rock (1987a) for these groups, and the Cox *et al.* (1979) TAS classification scheme for igneous rocks (see Figure 5.2.1). The UML field described here resembles the field of UML proposed in Chapter 5.2. Once again 4 of the 6 CAL plot outside the CAL field, although the AL and UML behave roughly as expected. The only breccia dyke analysed has chemical characteristics of an AL.

Trace Elements

Trace element analyses and Zr/Nb and Ce/Y are plotted against MgO in Figure 8.4.1B and 8.4.1C. Compatible elements (Ni, Cr) show a steady decrease with decreasing MgO and will reflect extraction of olivine and /or clinopyroxene. There is thus less Ni or Cr in CAL than UML, and less in AL than CAL. The AL contents of these elements approach basaltic and hawaiitic values.

Figure 8.4.2

(A). (Facing). Fields for discriminating between CAL and AL in terms of CaO - $4TiO_2$ - $SiO_2/10$ suggested by Rock (1987a) with Igaliko lamprophyres plotted. Most lamprophyres plot within the AL field, the CAL more often than not plotting outside the CAL field.

(B). (Facing). Fields for discriminating between UML and AL in terms of MgO - CaO - Al_2O_3 suggested by Rock (1987a) with Igaliko lamprophyres plotted. This discriminates very well between AL and UML of the Igaliko swarm.

(C). (Overleaf). Fields occupied by AL, UML and CAL in terms of Na_2O+K_2O vs. SiO_2 wt% (TAS) suggested by Rock (1987a). In general, the lamprophyres from Igaliko behave as predicted by Rock (1987a), although as with many other plots, the CAL do not fall well within their defined field. Lamproites (field not shown) plot at similar SiO_2 to AL and CAL, extending from about 4 to 12 wt% total alkalis, and are dominated by K.

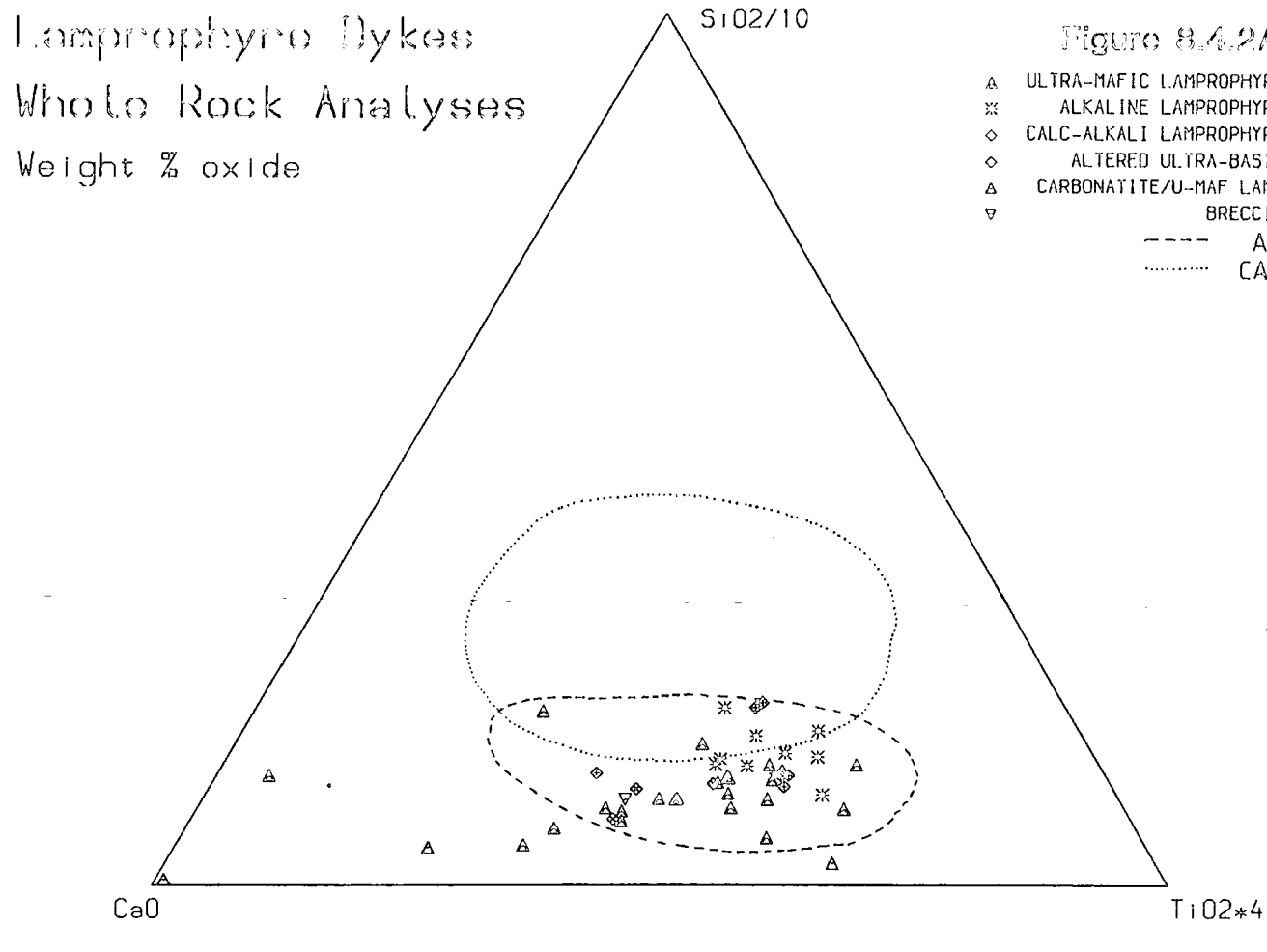

Figure 8.4.2A

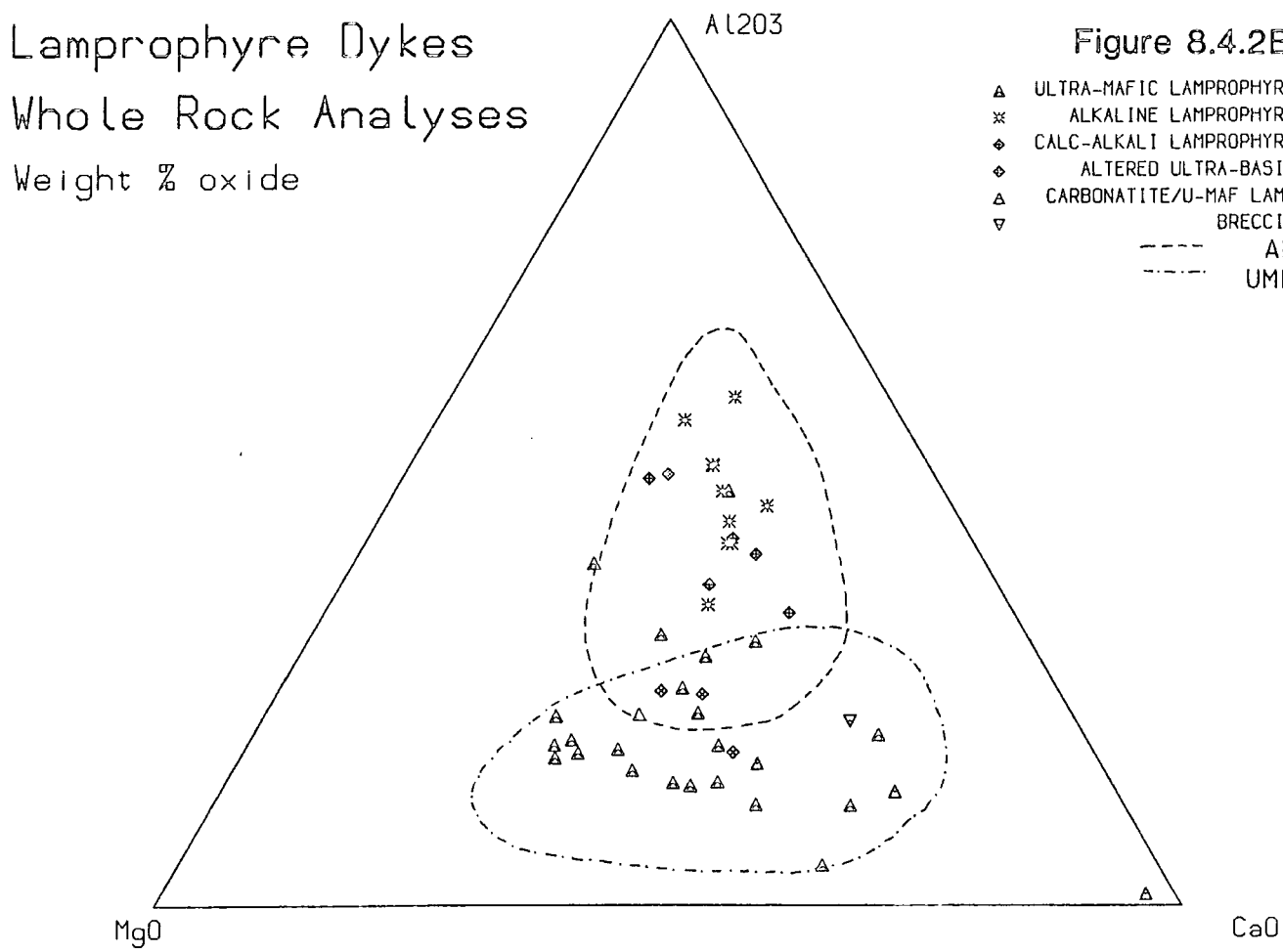

Figure 8.4.2B

Lamprophyres - Total alkalis-Silica

Figure 8.4.20

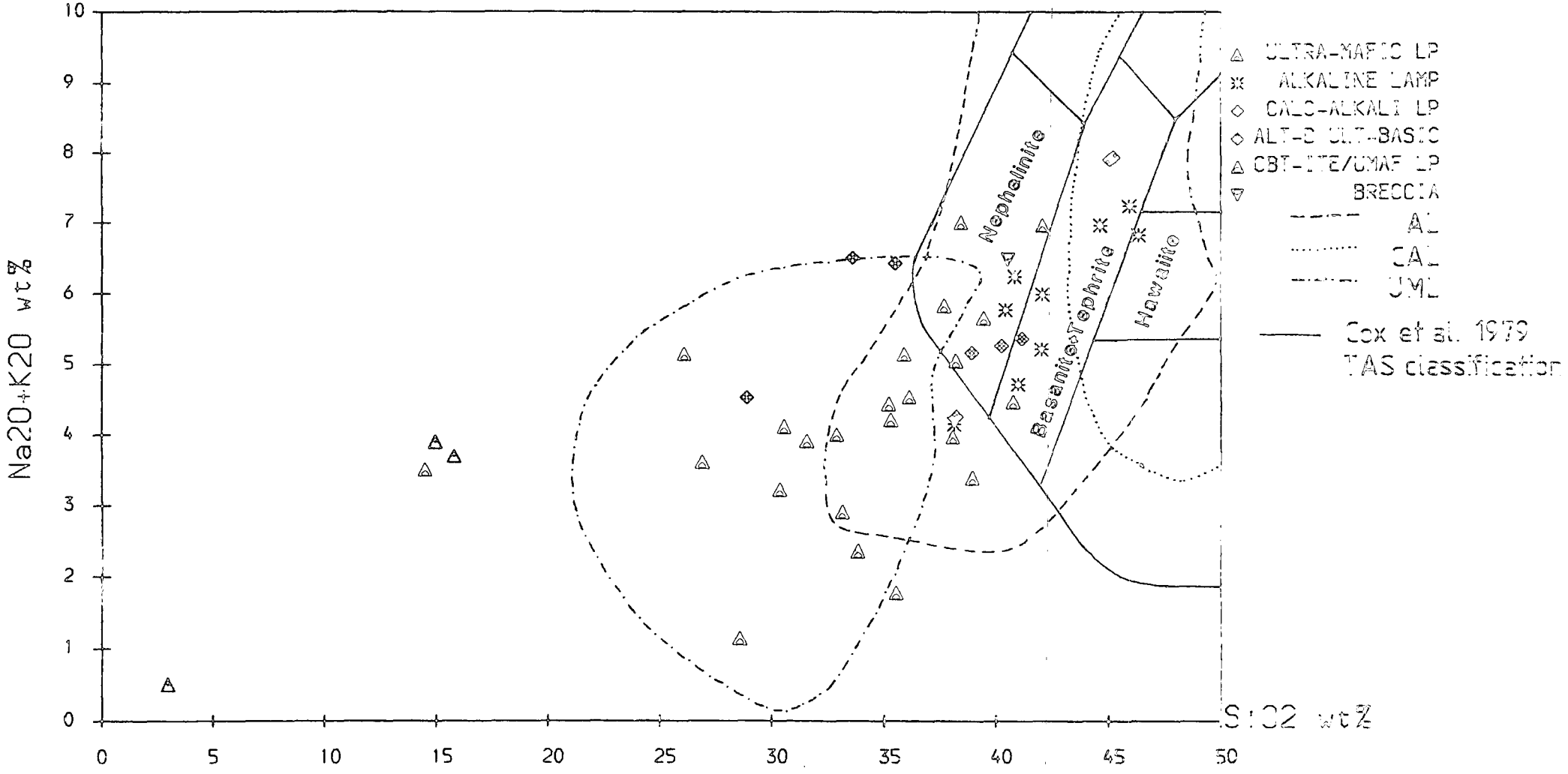

It is clear from these diagrams that many of the incompatible elements are also very enriched in the lamprophyric rocks. Typical LREE (La, Ce, Nd) contents for example in the UML are similar to many phonolites. These are thus several times higher their concentrations in basaltic rocks. Also noticable is a decrease in some incompatible elements (REE, Y, Ba, Th) with decreasing MgO between about 18 and 13 wt%. This is not a fractionation effect, which would increase increase incompatibles as MgO decreased but is probably a melting effect. Addition of more Fe-rich melt at higher degrees of partial melting would cause incompatible element contents to decrease. This is also seen in the Zr/Nb data, with higher Zr/Nb ratios from UML with lower MgO contents, increased Zr/Nb reflecting larger degrees of partial melting (see Chapter 5). A similar relationship may be evident from Ce/Y data for UML, reflecting larger degrees of melting from a similar source as Ce/Y decreases.

Figure 8.4.3 shows Nb/Y - Nb, Nb/Zr - Nb, La/Y - La and Zr/Y - Zr, ie. ratios of more/less incompatible elements against the more incompatible element. Chemical variation caused by melting will produce a steep positive slope whereas crystal fractionation will cause a trend roughly parallel to the x-axis (see Chapter 5.7 and Martin 1985). It would thus appear that a lot of the variation in AL and CAL is a melting effect, as too is variation in some of the UML. The UML however, also tend to show some degree of crystal fractionation producing a flattening of the trend (see especially La/Y - La).

Incompatible Element Variation

Figure 8.4.4 shows chondrite normalised spidergrams of all lamprophyres separated into certain field and/or chemical groupings within the UML, AL, CAL classification. Figure 8.4.4 shows averages of typical UML, AL, CAL and altered ultrabasic (AUB) samples compared to the averages for UML, AL and CAL presented by Rock (1987a). These averages, along with Rock's (1987a) averages are presented in Table 8.4.1.

Certain features are apparent from all lamprophyre groups, and certain aspects are characteristic of individual or regionally associated samples. These features are now summarised:

UML – Many UML show negative Sr anomalies but none show strong negative Eu

Figure 8.4.3: Incompatible element variation in lamprophyres.

(i) Nb/Zr vs. Nb.

(ii) Nb/Y vs. Nb.

(iii) Zr/Y vs. Zr.

(iv) La/Y vs. La.

Trends resulting from fractional crystallisation fall roughly parallel the x-axis. Trends resulting from melting effects will form steep slopes near the origin.

Figure 8.4.3

Lamprophyres - Incompatible Elements

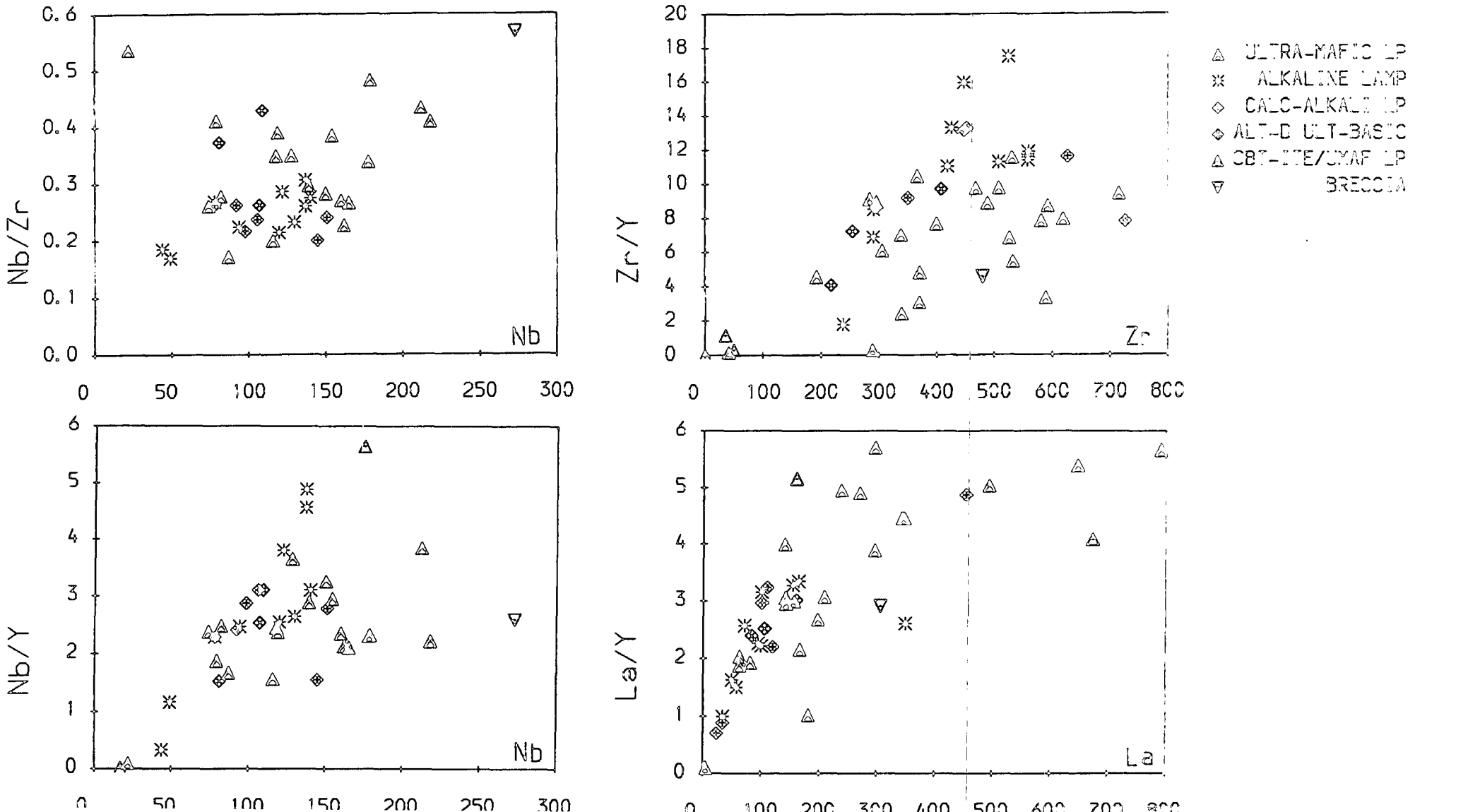

Figure 8.4.4 (6 pages)

Incompatible element chondrite normalised spidergrams of all lamprophyres from various lamprophyre groups.

(i) and (ii). UML – All show a steep slope from Rb to Y. Some show a negative Sr anomaly. One sample shows a negative P anomaly. It seems unlikely that feldspar has been lost from these UML (no feldspar as phenocrysts etc.), although feldspar (orthoclase) is the only liquidus phase of many UML using Nathan and Van Kirk (1978) modelling. Certain regional characteristics are evident, eg. the Østfjordsdal dykes are similar, as too are some of the 'Hotel Motzfeldt' dykes (from SW corner of Motzfeldt Sø). Some 'Harry's Dal' and 'Hotel Motzfeldt' UML are also similar.

(iii) 3 chemically unusual UML with very strongly enriched patterns (127051, 326345) or lacking LREE (325955).

(iv) AL – Most AL show similar patterns – typically with dips at Th and K. They are generally smooth, lacking negative Sr anomalies. Again, some regional similarities are seen as well as a general similarity between Østfjordsdal and 'Harry's Dal' dykes.

(v) One AL, from 'Harry's Dal' (compare with (iv)).

Breccia 325961 from Motzfeldt showing certain similarities to some AL and some UML.

CAL – similar in many respects to AL, all but one show negative Th anomalies. Rarely negative Sr anomalies are present. K tends to be more enriched relative to Th and Nb than in the AL and thus there is not the marked concave upwards appearance to the curve between Ba and Nb.

(vi) Altered ultrabasics. These dykes are carbonate - phlogopite - chlorite - oxide - pyroxene - assemblages. Occasionally (eg. 326222) pseudomorphed olivines are seen. These show a general similarity to UML although are extremely enriched in Rb.

Carbonatite/UML sill from Motzfeldt. Different facies of this sill show more or less carbonatite like features (cf. Chapter 7) especially 326259, one of the most Th rich samples from the region. The variation reflects modal differences with height in the sill of carbonate and silicate minerals, with 326259 being the most carbonate-rich example.

Carbonatite/UML dykes. 326358-9 Dykes from Iganaq. 326385 – sövite facies, 326359 – calcite - phlogopite - oxide - pyroxene facies (aillikite). The sövite shows incompatible element contents similar to carbonatites, whereas the aillikite has a chemistry similar to many UML. 326249 – a low SiO_2, carbonate-rich UML. This has incompatible element enrichments in many elements similar to the UML/carbonatite sill 326258-60 from Lower Flink's Dal.

Figure 8.4.4(3)

Ultramafic Lamprophyres

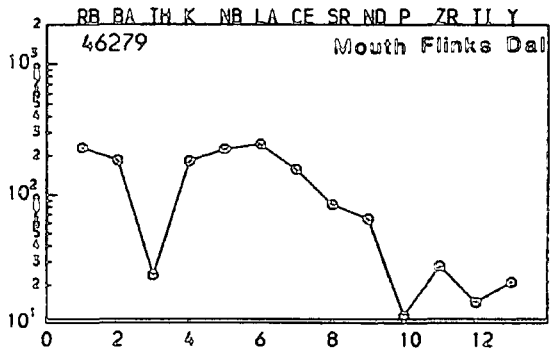

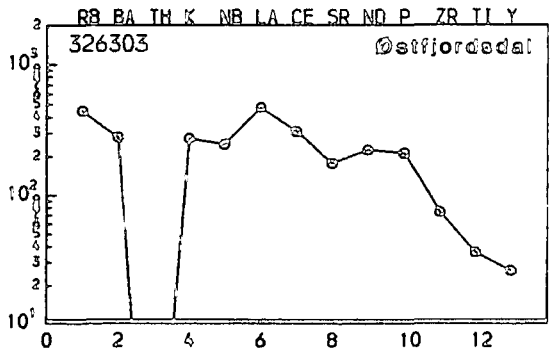

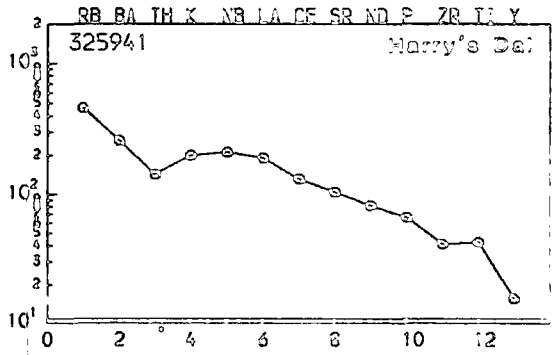

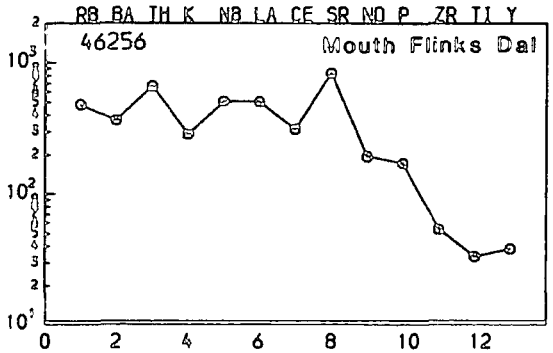

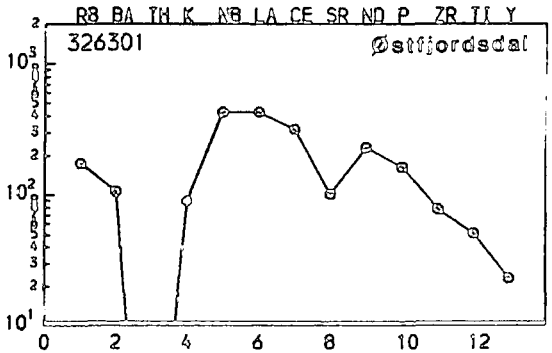

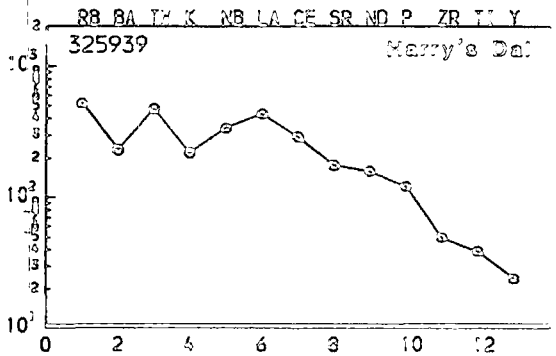

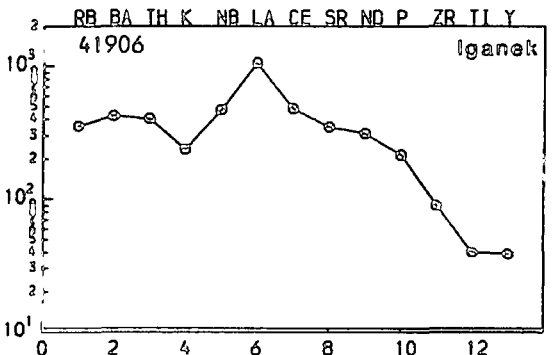

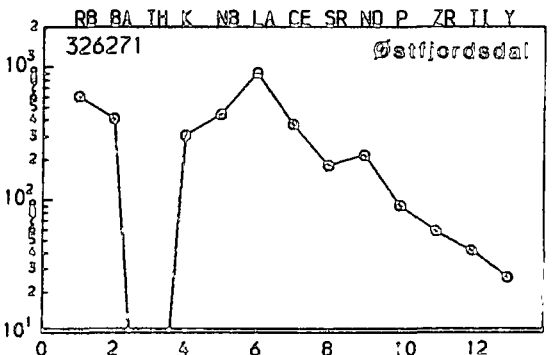

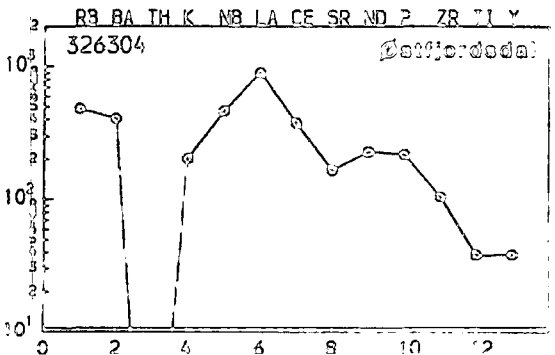

Ultramafic Lamprophyres

Figure 8.4.4(ii)

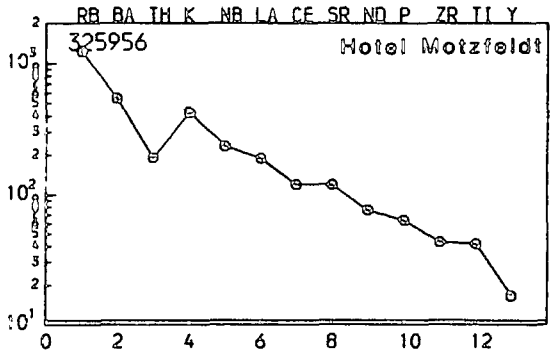

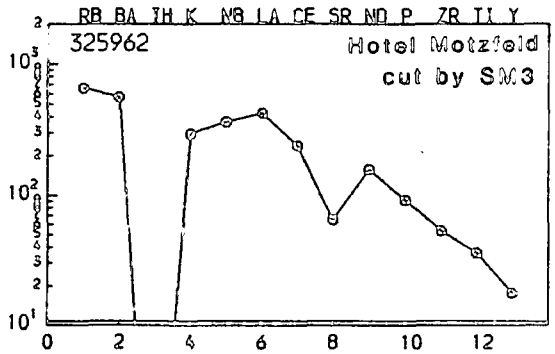

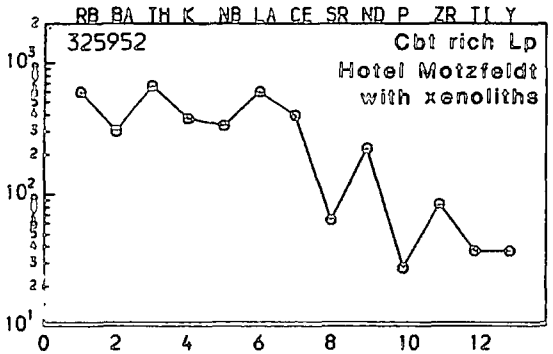

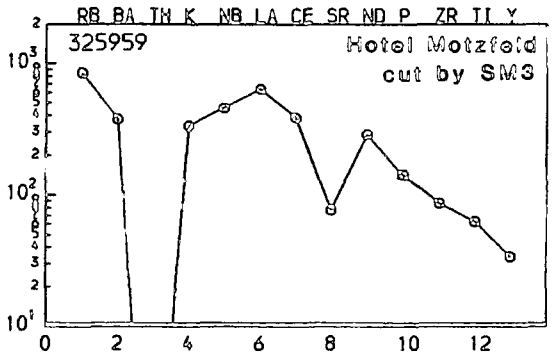

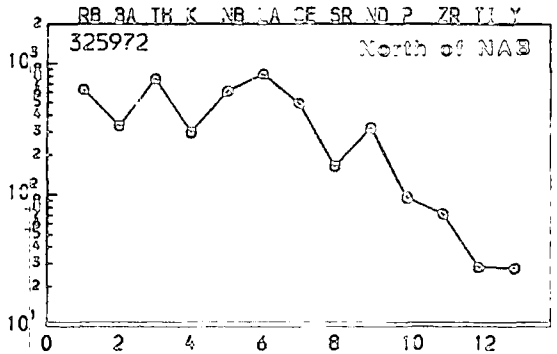

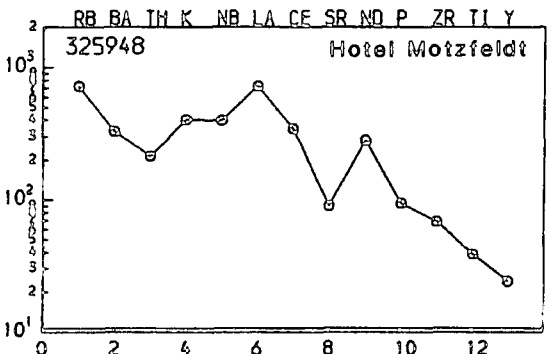

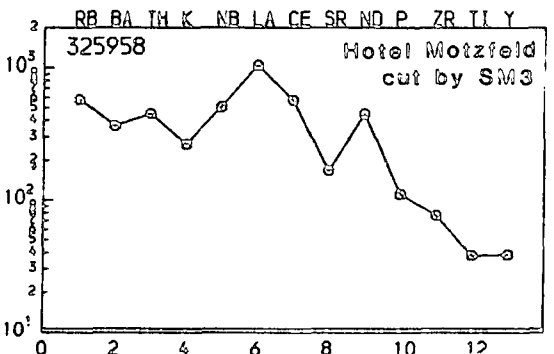

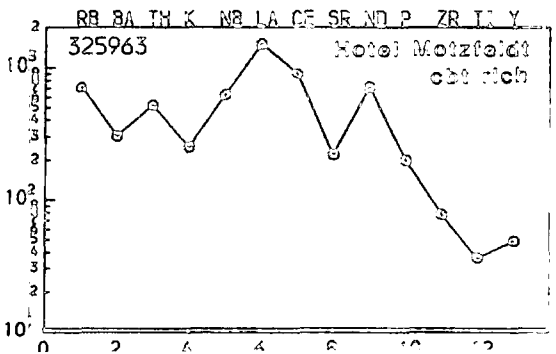

Unusual UML

Figure 8.4.4(iii)

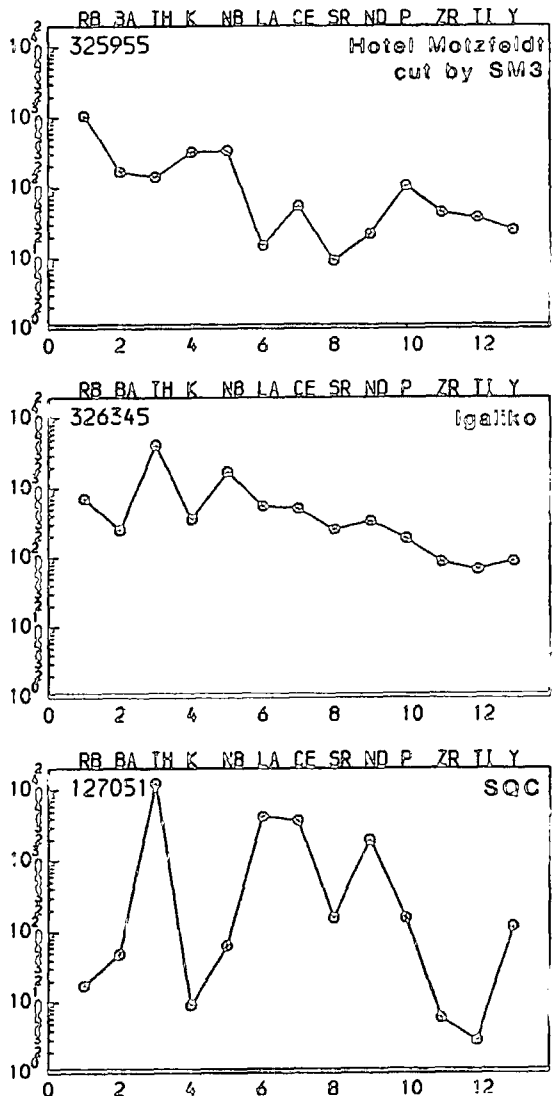

Alkaline Lamprophyres

Figure 8.4.4(iv)

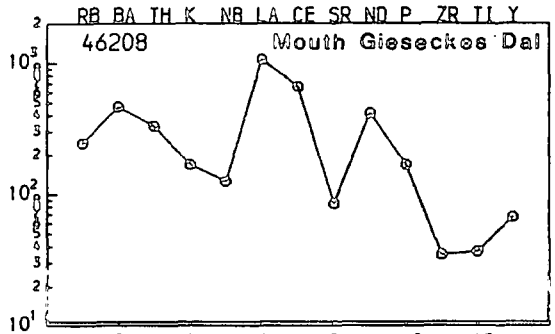

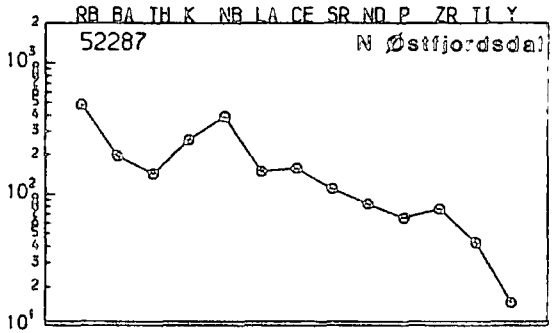

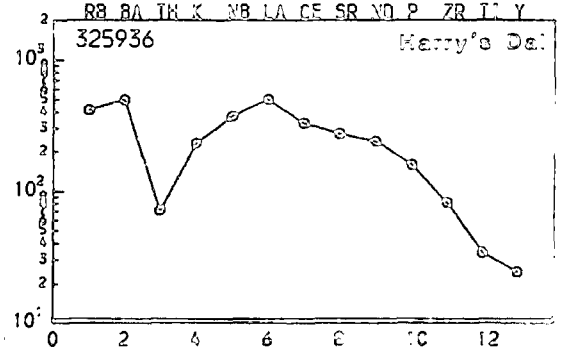

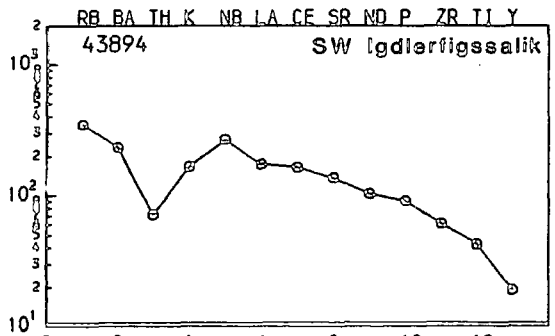

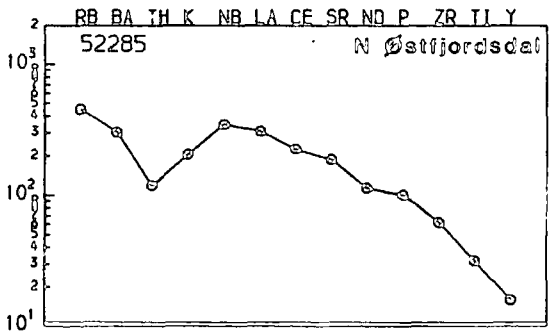

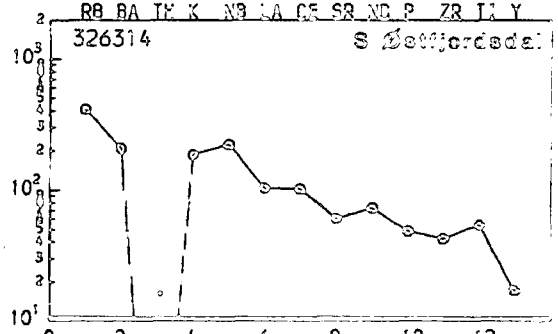

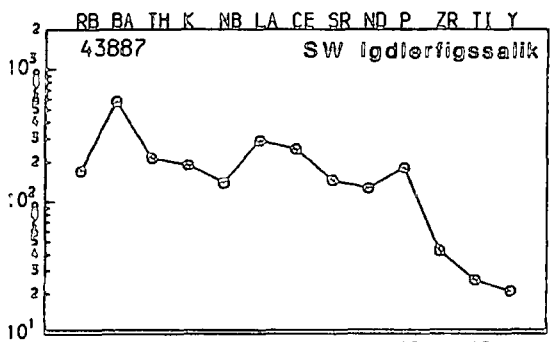

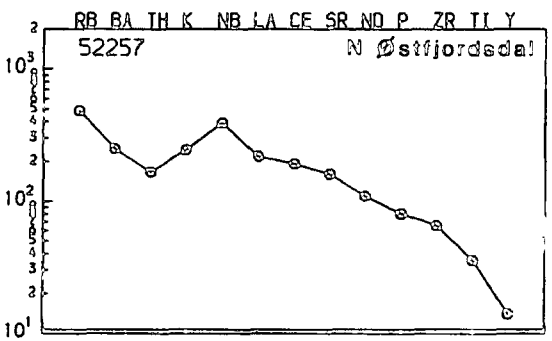

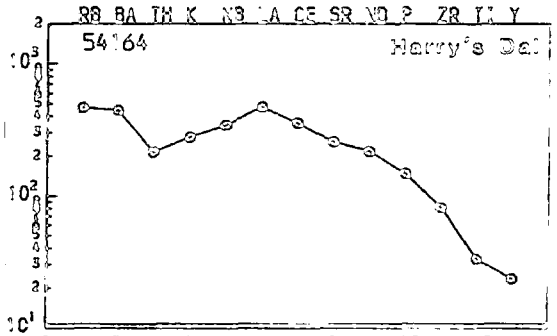

Calc-alkaline Lamprophyres

Figure 8.4.4(

Alkaline Lamprophyres

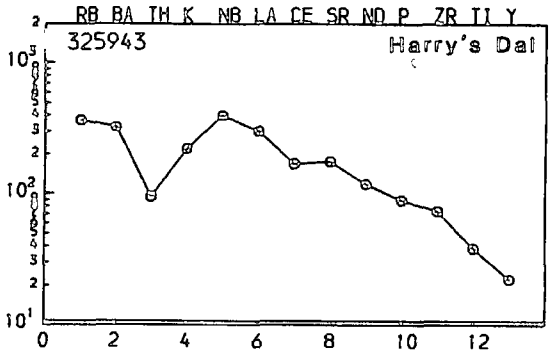

Breccia

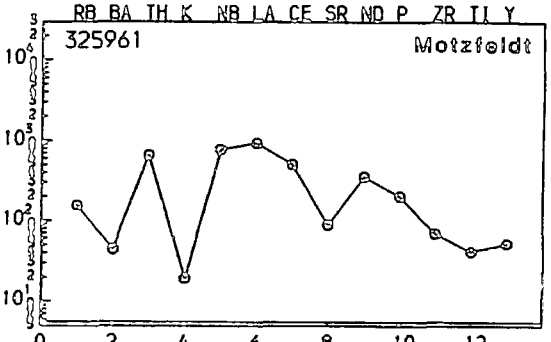

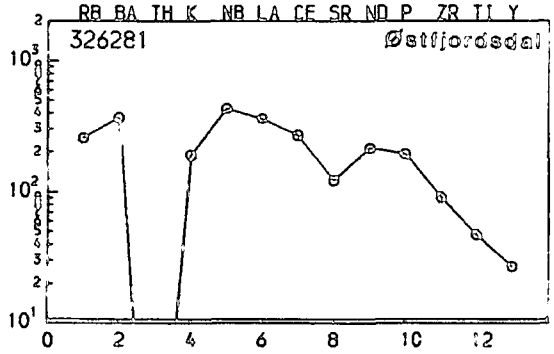

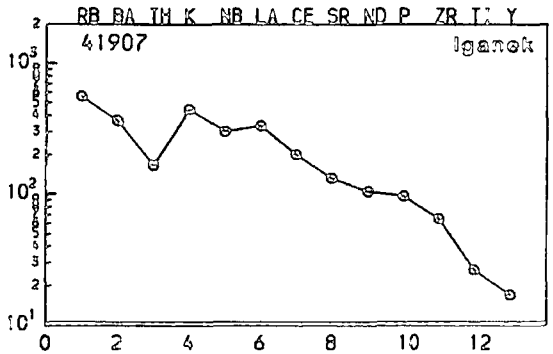

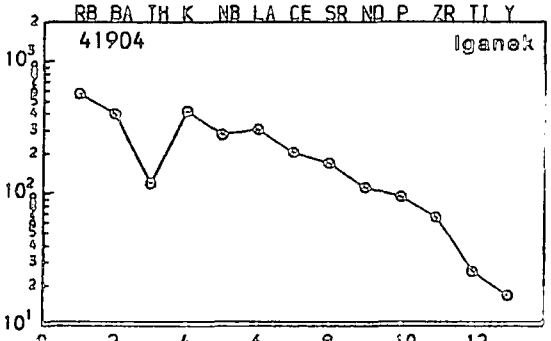

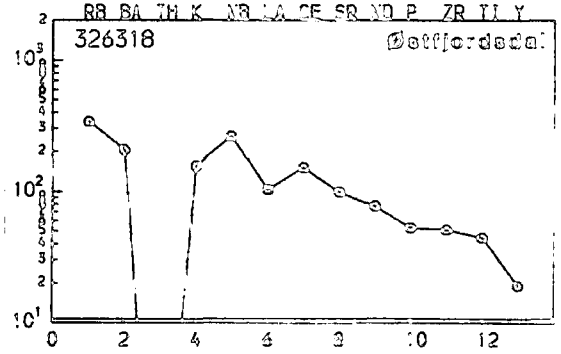

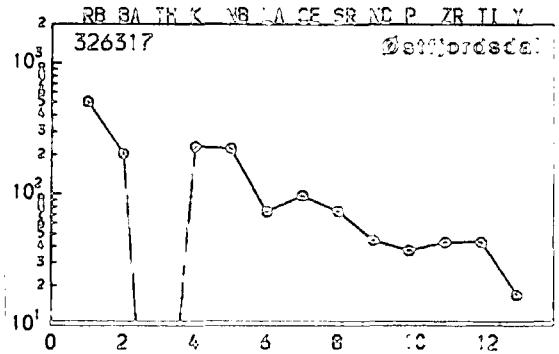

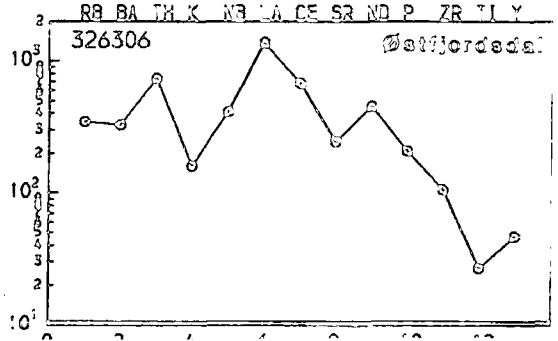

Figure 8.4.4.(v)

Altered Ultrabasics

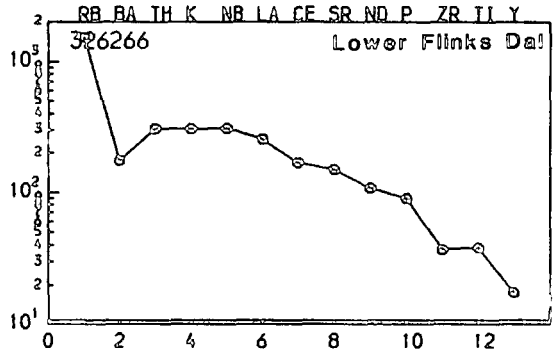

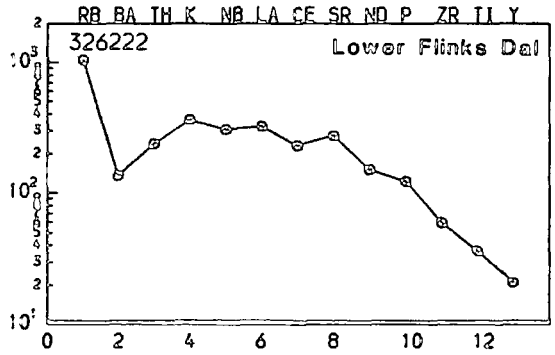

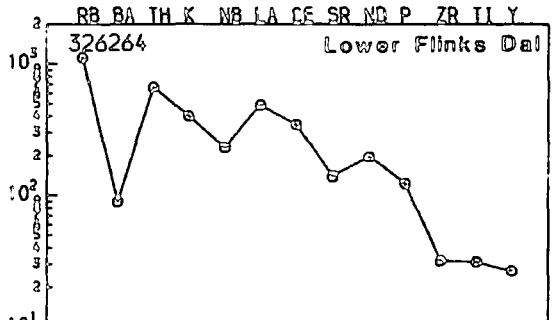

Carbonatite/UML sill

Lower Flinks Dal

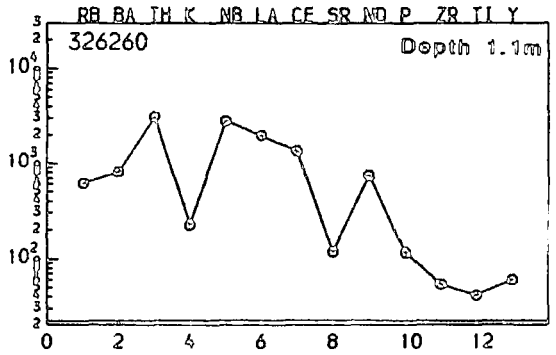

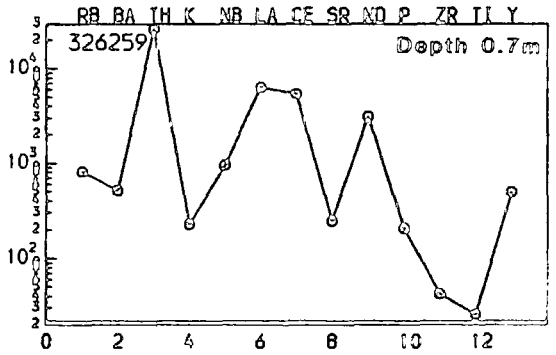

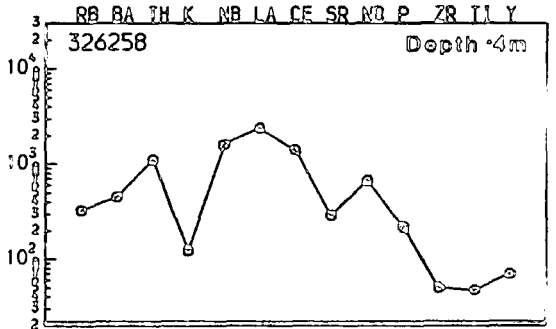

Carbonatite/UML dykes

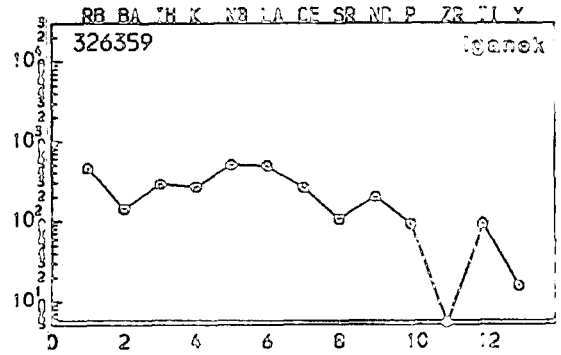

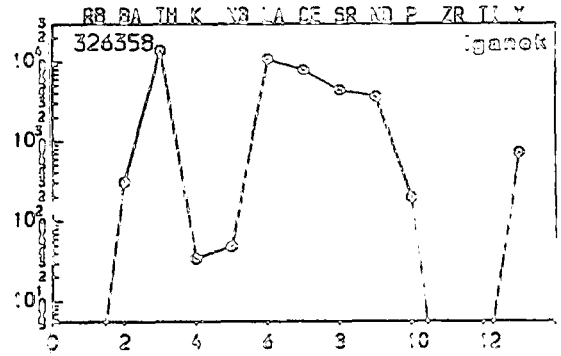

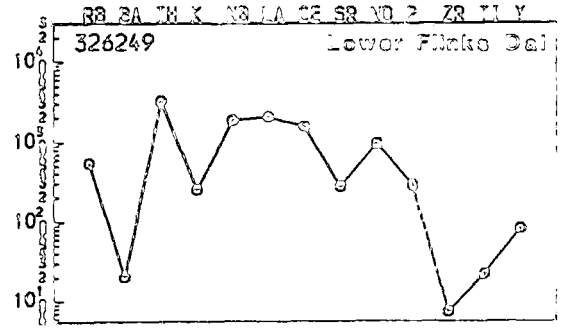

Table 8.4.1

Average lamprophyre compositions compared to averages from Rock (1987a).

Major elements wt%

	Igaliko UML	Rock UML	Igaliko AL	Rock AL	Igaliko CAL	Rock CAL	Igaliko AUB
SiO_2	35.76	30.9	42.59	41.9	41.46	51.5	32.62
Al_2O_3	7.68	6.8	13.21	13.7	11.67	14.0	7.6
Fe_2O_3	16.94	15.43	15.32	12.1	16.89	8.21	18.40
MgO	13.61	15.1	6.23	7.2	7.04	6.9	12.88
CaO	13.14	15.0	9.25	10.6	9.92	6.6	15.21
Na_2O	0.52	1.1	2.89	3.2	2.11	2.7	0.65
K_2O	3.95	1.8	3.12	2.3	3.87	3.8	5.17
TiO_2	3.99	3.6	3.89	3.0	3.70	1.3	3.66
MnO	0.30	0.26	0.24	0.21	0.25	0.15	0.32
P_2O_5	1.30	1.2	1.20	0.85	1.20	0.71	1.18
Trace elements ppm							
Ba	2347	1322	2419	1064	2159	1900	920
Nb	141	116	105	102	112	18	99
Zr	459	351	426	344	483	276	293
Y	58	31	48	34	48	25	43
Sr	2182	1146	1885	1089	1663	896	2217
Rb	201	73	135	70	151	124	432
Zn	303	107	140	104	195	82	159
Ni	385	485	84	88	132	186	302
Rb	4	8	6	5	4	5	4
Th	11	9	6	13	7	20	17
U	394	330	400	341	424	167	328
Cr	367	487	138	162	203	462	218
Ga	23	7	26	23	30	21	31
La	214	151	118	83	140	113	11
Ce	316	256	226	151	231	216	215
Nd	157	131	101	64	106	122	96
$n=$	17		10		6		3

anomalies (see later). It would appear unlikely that they fractionated feldspar, although Nathan and Van Kirk (1978) modelling would suggest that orthoclase is the first phase to appear on the liquidus. They all show steep patterns with high incompatible element enrichments. On a more local scale, the pre SM-3 UML from the 'Hotel Motzfeldt' area (authors camp 7, see Chapter 1) and the Østfjordsdal UML tend to show a complete lack of Th. In many cases also the low field strength elements (LFSE ie. Rb, Ba, Th, K) are less enriched than the less mobile elements (high field strength) such as LREE and this may reflect loss/alteration by a volatile phase. In the Østfjordsdal area where the phonolite dykes appear thoroughly recrystallised this must be a strong possibility, and Rock (1987a) considers that lamprophyres are unlikely to survive even low grade metamorphism. The same must be true for UML in the 'Hotel Motzfeldt' area which cut rafts of granite within SM-3. None however shows a negative Nb anomalies, and the high La/Y ratios may imply small degree melts from garnet bearing sources (cf. Cullers and Graf 1984). On a broad scale, as with carbonatites, there appear to be regional associations. UML from the 'Hotel Motzfeldt' area, internally very similar, show differences from 'Harry's Dal' UML and Østfjordsdal UML although there are general similarities between all groups. Within the UML is a carbonatite/UML sill 325258-60 from the Lower Flink's Dal area of the Motzfeldt centre which has incompatible element characteristics of both UML and carbonatites (see Chapter 7) and 3 chemically unusual lamprophyres: (i) 127051 – although a silicate, this sample possess carbonatite incompatible element characteristics and is extremely enriched, (ii) 326345, a UML with high LFSE, especially Th, compared to other UML and (iii) 325955, a very erratic spidergram with very low LREE and high Rb compared to other UML.

AL – These tend to have somewhat smoother incompatible element spidergrams than UML, although showing roughly similar degrees of enrichment. Sr anomalies are rare. The AL 326314, from SW of the Østfjordsdal Syenite, like the Østfjordsdal UML contains no Th (a result of alteration) otherwise it resembles the AL from NE of the Østfjordsdal Syenite (52257-87) and AL 43894 from SW Igdlerfigssalik. The 3 'Harry's Dal' AL are also similar to the dykes from NE of the Østfjordsdal Syenite although certain regional differences are evident (such as the depth of

Th spike and overall smoothness of the curve). No negative Nb anomalies are seen in any samples. 4388/ shows an enrichment in P compared to Nd and Zr. There is a general overall similarity between spidergrams from the AL and some tephritic/basanitic and alkali basaltic samples, to which they may be related. AL however are typically more enriched in incompatible elements than these alkali basaltic samples.

CAL – CAL show similar incompatible element patterns to AL and UML, often with negative Th spikes (?alteration/recrystallisation). Negative Sr anomalies are visible in some samples and this may reflect fractionation of feldspar in these more Si-rich lamprophyres. None shows a negative Nb anomaly.

Altered Ultrabasics – These highly altered rocks show very similar patterns to the UML except for their general enrichment in Rb compared to Ba and Th. This may have been added to these samples by late stage (igneous) hydrothermal fluids, rich in mobile incompatible elements which affected the alteration of these samples.

Others – The carbonatite/UML samples 326358-59 are from the same dyke which contains two distinct facies. 326358 – the carbonate rich facies is typical of carbonatites from Igaliko. 326359 however, enriched in phlogopite, has incompatible element contents more akin to UML, although like carbonatites, is Zr deficient. This may imply an origin for some low SiO_2 lamprophyres similar to that for carbonatites, ie. formed by late stage immiscibility processes, although a primary melt origin (cf. Qagssiarssuk, Stewart 1970, Mackenzie 1985) may also be responsible. 326249, another carbonatite/UML as incompatible element contents characteristic of carbonatites and is probably thus a Si-rich carbonatite. This may be formed by liquid immiscibility or by assimilation of counrty rock. The breccia dyke 325961 shows a similar chemistry to some AL/UML and may be related to either of these groups.

The above section has described various aspects of the different lamprophyre types encountered in Igaliko. Table 8.4.1 gives average compositions for these and for lamprophyres cited by Rock (1987a). These are presented as spidergrams in Figure 8.4.5.

Immediately obvious is the distinct similarity between the averages of different

groups from the Igaliko area, the only major difference between incompatible elements in UML, AL, and CAL being the depth of the negative Th anomaly, a likely product of alteration. Rock (1987a) contends that UML may grade into AL, and that most lamprophyres have a similar origin (the lamprophyre clan), using similarities in their chemistries to reinforce the group to group connections. Certain differences between various groups of lamprophyric rocks, even within one complex, have however been recorded by Vollmer *et al.* (1984), even from the same magmatic event. Systematic differences across the Igaliko complex would seem to suggest that small-scale compositional heterogeneity exists in the area, and may reflect slight differences in source region/melting history etc. It is worth noting that most AL and UML are from the south and east of the complex and, as has been noted above, there are distinct similarities between the Østfjordsdal and 'Harry's Dal'/'Hotel Motzfeldt' occurrences.

A comparison with the average data from Rock (1987a) shows the UML and AL to be very similar, with small to moderate negative Sr anomalies and similar overall degrees of enrichment. There is some difference in the elements Rb to K and this may be an alteration effect. The most noticable difference between the Igaliko lamprophyres and Rock's (1987a) averages is in the CAL, where Rock's average shows a large negative Nb anomaly, not seen in his average AL and UML. This may imply some crustal contamination (cf. Thompson *et al.* 1983), a residual Nb bearing phase in the source (cf. Saunders *et al.* 1980, Saunders and Tarney 1984) or may be characteristic of destructive plate magmatism (Pearce 1982, 1983). Rock (1987a) considers that the crust plays a large part in the genesis of CAL. The lack of a Nb anomaly in the Igaliko CAL would however imply none of the above processes was operative during their evolution and that they are clearly related to UML and AL in this area.

It is also noticable that there exists a broad similarity between AL and the low Zr/Nb basalts (see Chapter 5), and this may imply some genetic link between AL and the basaltic rocks (cf. Rock 1987a).

REE

Figures 8.4.6-8.4.9 show REE spidergrams of lamprophyres from the Igaliko complex. A feature common to all is their strong LREE enrichment and high $(La/Lu)_{cn}$ from

Figure 8.4.5

Average lamprophyre compositions from the Igaliko complex compared to average lamprophyres cited by Rock (1987a).

Immediately obvious is a remarkable similarity between the UML, AL and CAL from Igaliko, and must imply a similar source/petrogenesis for these lamprophyres. There are also general similarities between the Igaliko averages and those cited by Rock (1987a). A notable difference exists in the CAL, Rock's average showing a strong negative Nb anomaly. See text for explanation.

In general the Igaliko lamprophyres are slightly more enriched than Rock's (1987a) averages, possibly reflecting a more incompatible element enriched source region than 'average'.

Also shown are averages for the 3 'Altered Ultrabasics' which show some similarities to the Igaliko UML; and the breccia 325961.

The carbonatite/UML associations have been excluded as their average is meaningless.

Average Lamprophyre compositions

Figure 8.4.5

Igaliko Averages

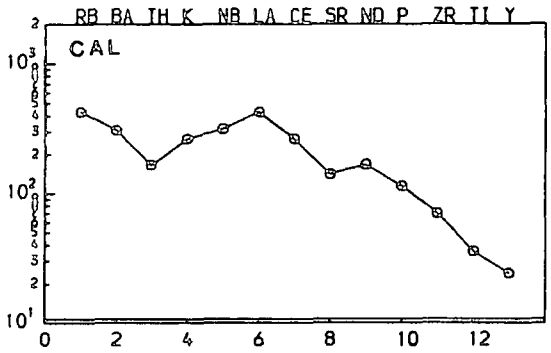

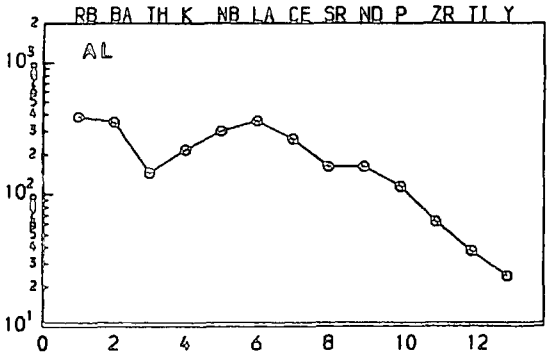

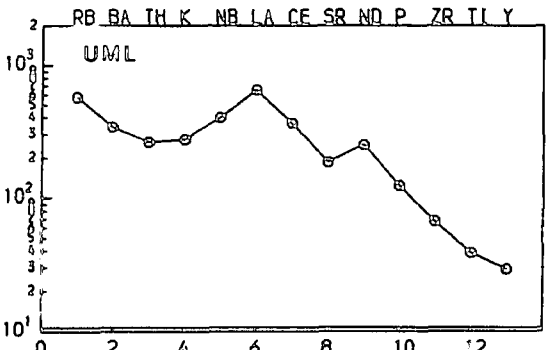

Rock(1987a) Averages

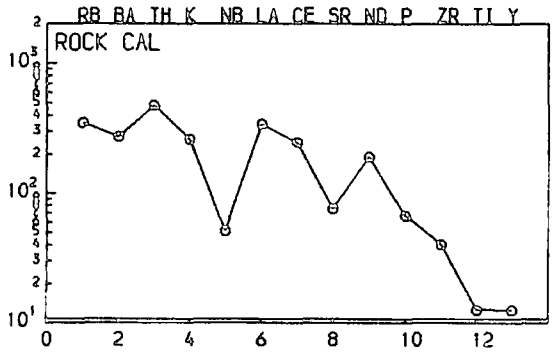

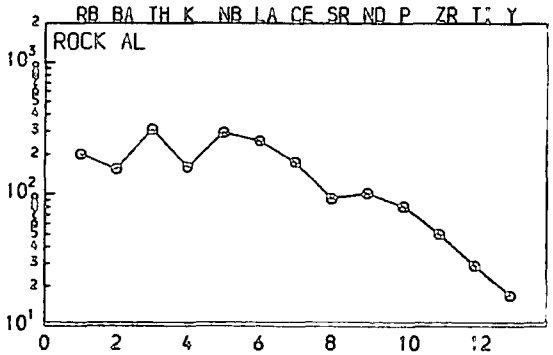

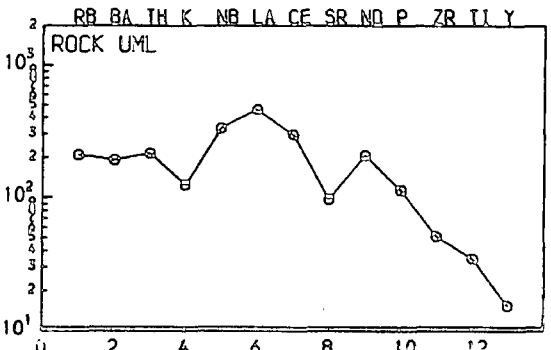

Igaliko Others

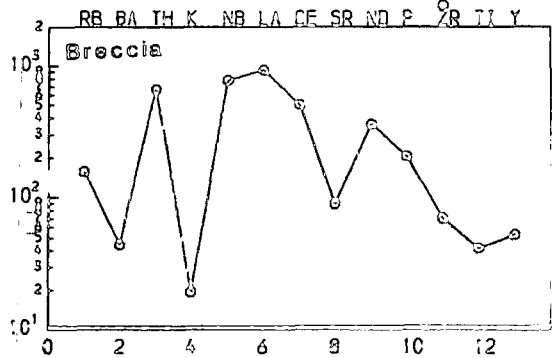

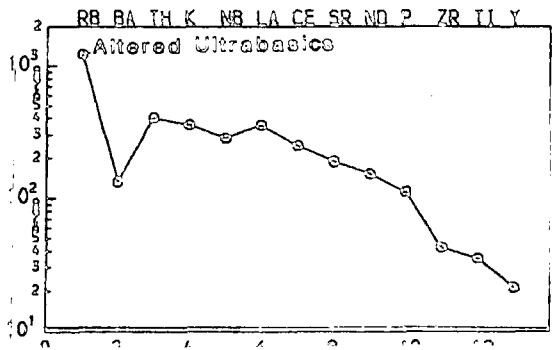

14.16 to 103.5 (excluding carbonatite 326358 with $(La/Lu)_{cn}$ of 131.0) as well as high overall REE contents. Noticeably lacking are Eu anomalies from all but one sample.

UML (Figure 8.4.6)

The UML show $(La/Lu)_{cn}$ from 14.17 to 47.33, with and average of 34.5. La_{cn} ranges from about 180-800 and Lu_{cn} from about 7 to 50. The high Ni, Cr and MgO contents of these rocks mean that they must in many cases be relatively unfractionated. The very high values of $(La/Lu)_{cn}$ would imply that these magmas were the result of very small degrees of partial melting of a garnetiferous source (Cullers and Graf 1984). However, the HREE contents in many cases are extremely high for primitive small degree melts and may require that large amounts of garnet enter the melt relative to the other mantle (source region) phases. However, at the small degrees of melting implied by the high degrees of incompatible element enrichment, assuming a fertile (twice chondrite) source, the HREE contents could not be modelled, even from a spinel (and not garnet) bearing source. Zr/Nb data (Chapter 5.8) would suggest degrees of melting of the order of tenths of a percent or less. The $(La/Lu)_{cn}$ values of the UML can be generated at about 0.2% partial melting of a 15% garnet, twice chondrite source (see Chapter 5.8) but the modelled contents are about one seventh of the observed REE contents (observed contents typically $La_{cn} \approx 500$, $Lu_{cn} \approx 14.3$).

Similar batch melting models, assuming a twice chondrite source can nearly produce the observed HREE contents at <0.1% partial melting of a spinel-bearing mantle source. This however gives $(La/Lu)_{cn}$ of ≈ 6, roughly one sixth that of the observed slope. Thus a 12-times chondrite LREE and slightly over twice-chondrite HREE source region is needed assuming a spinel lherzolite mantle source.

The above would imply that some form of source region enrichment process must be advocated to account for the extreme REE contents.

Similar problems are encountered in kimberlite petrogenesis where extreme REE enrichments are observed (Cullers and Graf 1984). Mitchell and Brunfelt (1974) calculated that <1% melting could generate La/Yb seen in kimberlites but not the observed REE abundances. REE contents in kimberlites can only be approached by using extreme parameters in the selected models, ie. lowest D, highest REE's in source, very

Figure 8.4.6

ULTRA-MAFIC LAMPROPHYRES

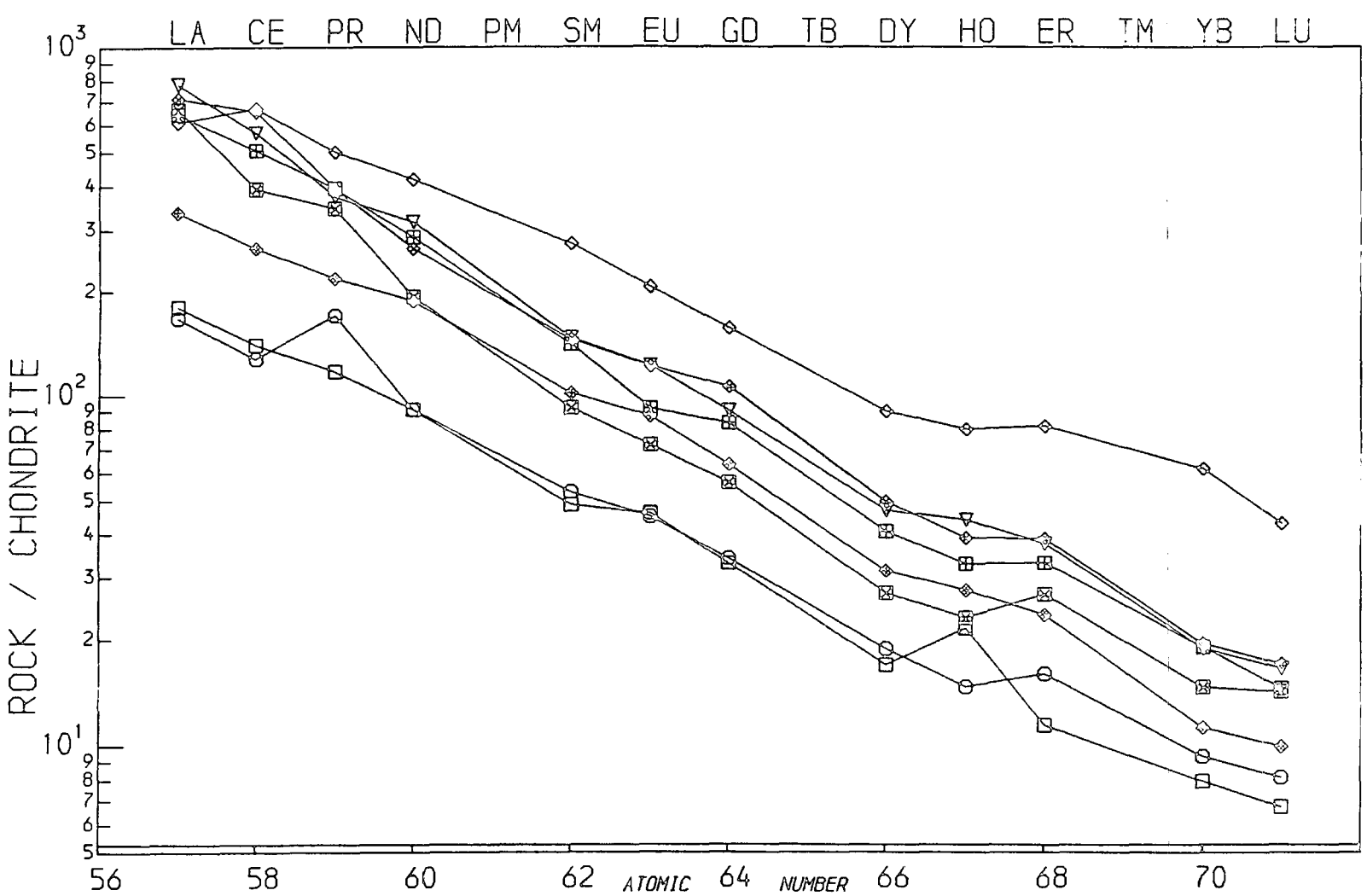

LA_n/LU_n

47.33 ▽ 41906
IGANEK U M L

26.87 □ 325956
U M L/NEPHELINITE IGALIKO

14.17 ◇ 326345
UNLOUT BY TR DYKE IGALIKO

20.63 ○ 325941
U M L C JKG XENO IN SM.1

44.37 ⊞ 325952
UML SE CORNER OF MOTZ SC

46.90 ⊠ 326271
OSTFJ U M L - PKL+DIOP

33.78 ◈ 326303
OSTFJ U M L - OGT VLOS

42.05 ◈ 326304
OSTFJ U M L- PKL+DIOP

CHONDRITE RARE EARTH NORMALISATION VALUES FROM BOYNTON WV, 1984

MISSING DATA INTERPOLATED FROM NEAREST NEIGHBOURS

N. J. G. PEARCE, 1987

small degrees of melting (Cullers and Medaris 1977, Cullers *et al.* 1982).

Partial melting at these levels, involving a mantle phase rich in REE which melts completely at early stages of melting, may cause the necessary enrichment in REE (disequilibrium partial melting). A mineral such as monazite or fluor-apatite may be present, and P-rich mantle xenoliths have been reported occasionally (eg. Exley 1982). This may however, cause an enrichment of P in the melt which is not clearly seen in the Igaliko UML relative to other incompatible elements (cf. Martin 1985, Upton *et al.* 1985 where P is enriched relative to Nd and Zr in the YGDC magmas). If some variety of apatite is responsible, distribution coefficient data (Henderson 1982, 1984) may suggest that a negative Eu anomaly would be present in the spidergrams – a feature that is completely lacking.

Modelling using either *zone refining* or *Rayleigh melting* which assume equilibrium melting, both have limiting enrichments of 1/D and thus neither could produce either the LREE or HREE contents observed. Galer and O'Nions (1986) discuss the variation of incompatible element contents from MORB in terms of mixing between extremely small partial melts (<0.1%) with more voluminous melts giving rise to the observed chemical differences. The high contents of compatible elements in the UML may indicate larger degrees of melting than the incompatible (particularly RE) elements would suggest. Mixing of a very small degree melt, rich in incompatibles and volatiles, perhaps the product of some disequilibrium melting process, with a more voluminous Mg, Ni, Cr rich melt, may thus produce the peculiar chemistry of the UML.

The presence of volatiles would also assist the migration of small amounts of melt within their source regions (McKenzie 1985), and this highly enriched, extremely small volume melt may be capable of separation.

Fesq *et al.* (1974), believe that stable REE (and in particular LREE complexes) may migrate with volatile phases and cause enrichments in incompatible elements in kimberlites (and by analogy lamprophyres). Volatile transfer may thus also be an important process in these H_2O, F, CO_2 rich rocks. Models such as that of Hawkesworth *et al.* (1984) or Menzies *et al.* (1987) for enrichment of a mantle source region by injecting and solidifying a small degree melt from a different area of the mantle, or

models such as those of Bailey (1980, 1982, 1984, 1987) may also be relevant to the petrogenesis of these UML. The presence of small grains of Cr-spinel in one UML may hint at a spinel-lherzolite source region, and thus perhaps at no need for substantial HREE enrichment in the source, the melting models requiring only that LREE be enriched from twice-chondrite to about 12-14 times chondrite. This may be achieved by addition of a few percent of basanitic or kimberlitic melt (cf. Hawkesworth *et al.* 1984). Analogy with both kimberlites and lamproites would suggest that deep melting of the mantle was operative and a garnet-bearing source would seem more likely. The role of fractional crystallisation is difficult to define as Ni, Cr and MgO are all very high in these UML. However Upton and Thomas (1973) consider the K-rich ultramafic rocks near Narssaq to be derivative from a 'kimberlitic' melt. This process may have been operative in the UML and will have increased $(La/Lu)_{cn}$ as well as increasing absolute REE contents. Extraction of about 12% clinopyroxene and 7% olivine would give observed Ni and Cr (assuming parental kimberlitic Ni of 1050ppm and Cr of 1100ppm, Wedepohl and Muramatsu 1979). This would only cause a 20% increase in La and a 10% increase in Lu, still requiring the parent to have had extreme REE contents and high $(La/Lu)_{cn}$.

AL and CAL (Figure 8.4.7)

These lamprophyres have REE spectra typified by $La_{cn} \approx 210$ and $Lu_{cn} \approx 10$ with $(La/Lu)_{cn} \approx 21.3$ (see Figure 8.4.7). These patterns are very similar to the picritic and alkali basalts of the low Zr/Nb (undersaturated) suite of dykes, although about twice as rich in REE. They do however bear a closer resemblance to some of the alkali gabbro dykes.

The AL and CAL show slight Eu anomalies, either positive or negative, and these will represent varying degrees of feldspar fractionation. Their overall chemistries are consistent with an origin by small degrees of partial melting (0.5-0.1%) of a 5% garnet-bearing source followed by fractionation of olivine and clinopyroxene, a model similar to that proposed for the origin of the basalts. There is no real difference between the camptonite REE and the minette REE profiles. The vogesite (326281) is however slightly more enriched in REE than the other AL and CAL and shows the greatest degree of LREE enrichment. Fractionation of amphibole and/or pyroxene from the AL

Figure 8.4.7

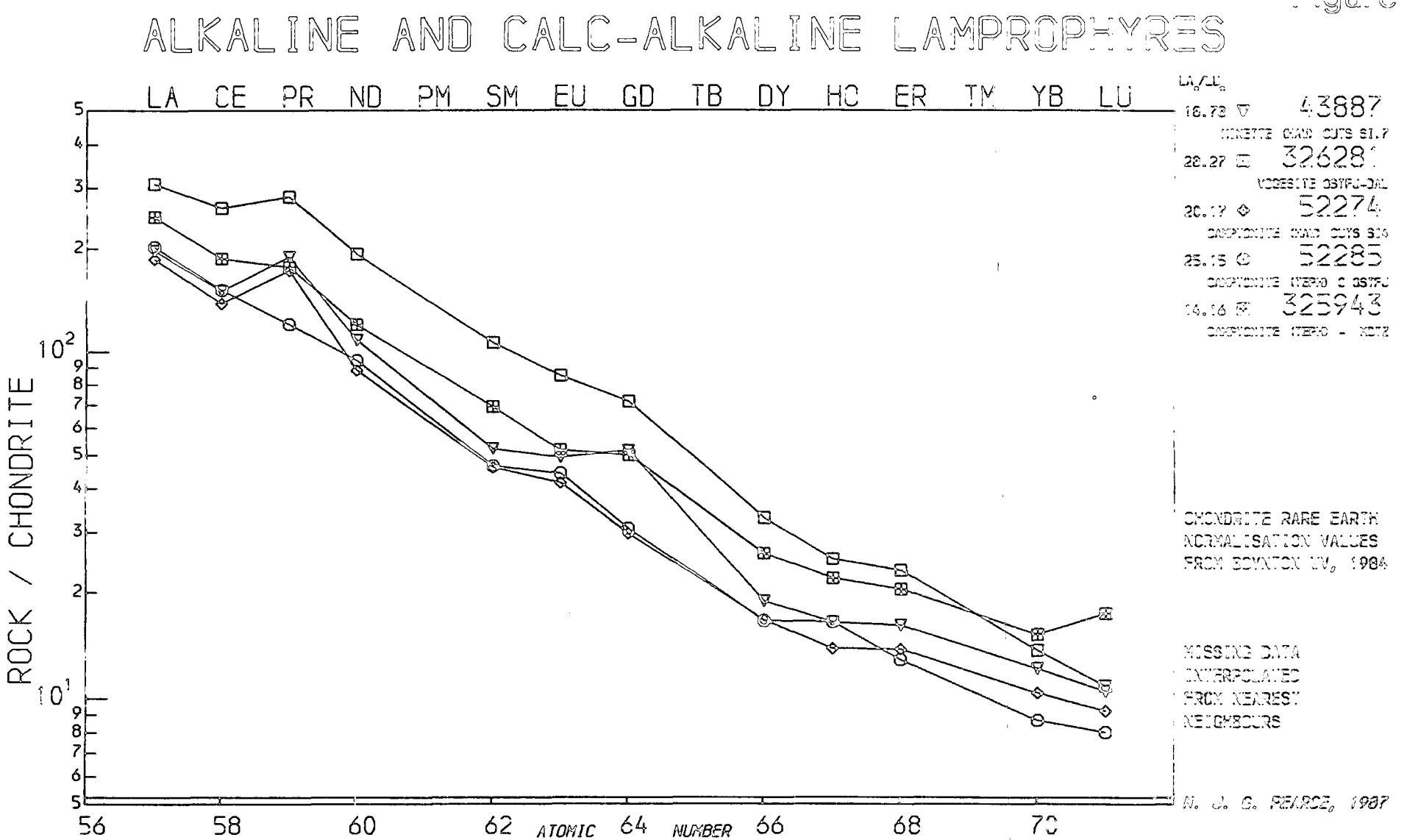
ALKALINE AND CALC-ALKALINE LAMPROPHYRES
LA CE PR ND PM SM EU GD TB DY HO ER TM YB LU
ROCK / CHONDRITE
ATOMIC NUMBER
56 58 60 62 64 66 68 70
5 4 3 2 10^2 9 8 7 6 5 4 3 2 10^1 9 8 7 6 5
La_n/Lu_n
16.73 ▽ 43887
MINETTE (SAUD CUTS S1.7
28.27 ▣ 32628
VOGESITE (STFJ-DAL
20.17 ◆ 52274
CAMPTONITE (SAUD CUTS S10
25.15 ⊙ 52285
CAMPTONITE (TERRO C (STFJ
14.16 ⊠ 325943
CAMPTONITE (TERRO - KOTZ
CHONDRITE RARE EARTH NORMALISATION VALUES FROM BOYNTON W., 1984
MISSING DATA INTERPOLATED FROM NEAREST NEIGHBOURS
N. J. G. PEARCE, 1987

may be capable of producing REE contents characteristic of alkali basalts/hawaiites which may be related. Extraction of these Ti-rich ferromagnesian minerals may reduce Ti to more normal basaltic levels.

Carbonatite/UML (Figure 8.4.8)

Carbonatite/UML associations have been recorded from a sill in Lower Flink's Dal in the Motzfeldt centre (326258-9) and a dyke on Iganaq, near Igaliko Village (326358-9). Both contain SiO_2-rich and SiO_2-poor facies.

326358-9: Here a sövite and a calcite - phlogopite - oxide rock (aillikite) are found as distinct facies to the same dyke (see Plate 7.2, 7.10 and 7.11). The sövite (3.0 wt% SiO_2) has $(La/Lu)_{cn}$ of 131 whereas the aillikite (14.94 wt% SiO_2) has $(La/Lu)_{cn}$ of 44.85, and overall REE contents some 30 times less than the sövite.

326258-9: Large chemical variations are seen throughout the thickness of the sill. 326258 with 33.78 wt% SiO_2 has $(La/Lu)_{cn}$ of 103.51 and 326259, with 14.47 wt% SiO_2, shows $(La/Lu)_{cn}$ of 36.09, with 3-10 times greater overall REE contents. This sample also shows a marked negative Eu anomaly ($Eu/Eu^* = 0.39$) whereas none of the others do.

In both cases the more carbonate-rich facies always contain greater REE contents than the more silica-rich phase. The degree of LREE enrichment varies however from the two occurrences as to whether the silica-rich or carbonate-rich phase is more LREE enriched. The data from the dyke 326358-9 may be consistent with liquid immiscibility (cf. Bedson 1983, 1984) although it may alternatively reflect a modal difference in carbonate (cf. Möller *et al.* 1980).

The sill data (326258-9) are more difficult to reconcile. Wendlandt and Harrison's (1979) REE partitioning data at high pressures (20kb) between immiscible carbonate and silicate would produce the observed REE contents, although their data are from very different bulk compositions, and may not apply. Jones (1980) considers the Motzfeldt centre to have crystallised at depths of 6-7km (ie. $\approx$2kb) and the data of Wendlandt and Harrison (1979) may not apply at such low pressures. The difference may simply reflect modal differences in diopside, carbonate and oxides resulting from

Figure 8.4.8

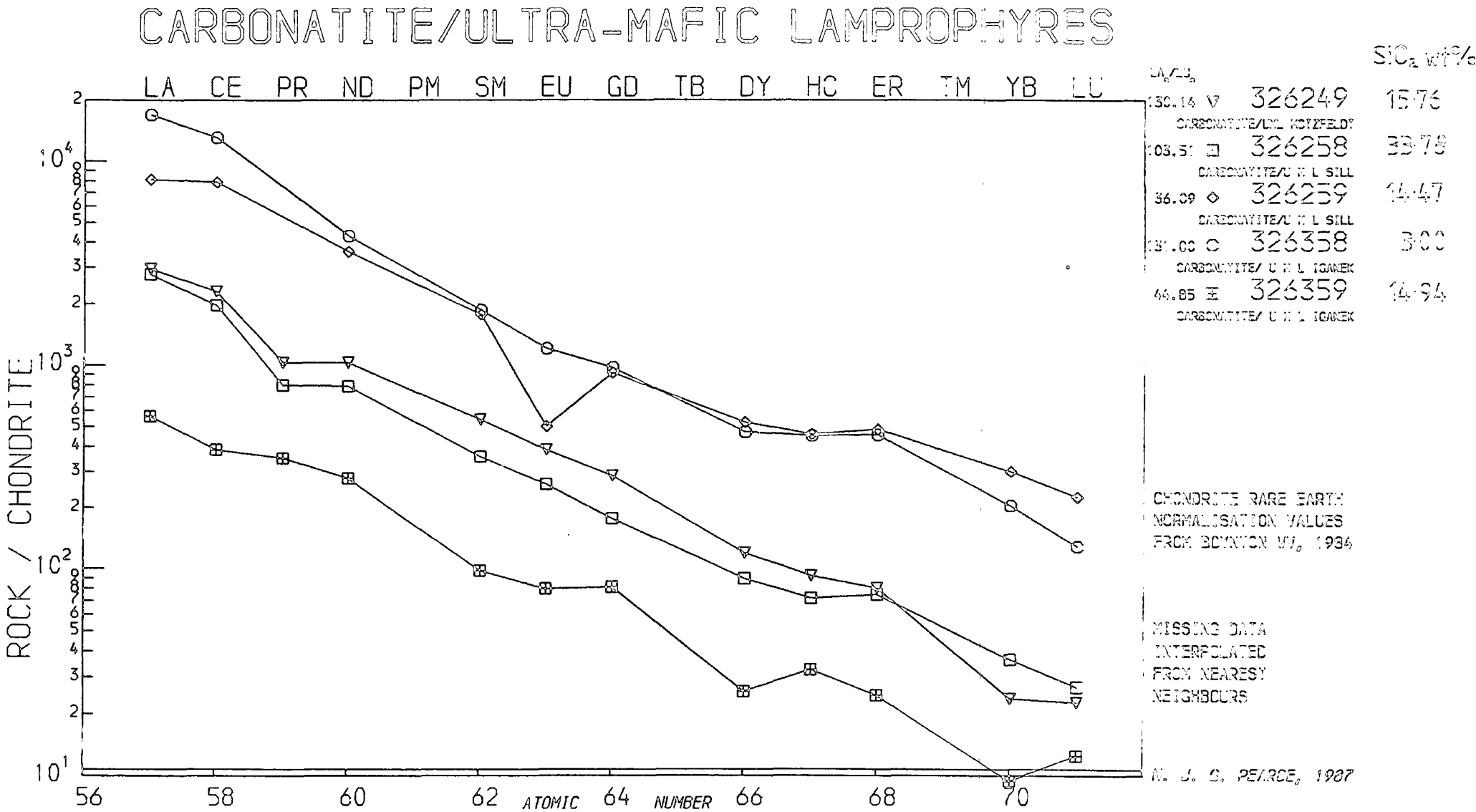
CARBONATITE/ULTRA-MAFIC LAMPROPHYRES
LA CE PR ND PM SM EU GD TB DY HO ER TM YB LU
ROCK / CHONDRITE
ATOMIC NUMBER
SiO2 wt%
326249 15.76
326258 33.78
326259 14.47
326358 3.00
326359 14.94
CHONDRITE RARE EARTH NORMALISATION VALUES FROM BOYNTON W., 1984
MISSING DATA INTERPOLATED FROM NEAREST NEIGHBOURS
N. J. G. PEARCE, 1987

crystal accumulation processes within the sill.

326249, from the Lower Flink's Dal area is technically an UML and not a carbonatite (Streckeisen 1980) although closely resembles a carbonatite petrographically and chemically (high Ca, Sr, low total). It has a REE pattern similar to many of the carbonatites from near Igaliko village. There are also many similarities between this and the more carbonate rich facies of the UML sill 326258-60, also from the Lower Flink's Dal area of Motzfeldt.

Altered Ultrabasics (Figure 8.4.9)

These low Si, ultramafic samples, similar in many respects to UML (mineralogy and chemistry if not petrography), have REE profiles indistinguishable from the more abundant UML *sensu stricto*. General problems of the origin of the UML apply equally to these samples, which may have undergone late magmatic alteration. They are almost certainly related to the more abundant (and fresher) UML.

8.5: Conclusions and Occurrence

There can be little doubt as to the primitive or unevolved nature of lamprophyres from their high contents of compatible trace elements, MgO, etc.. However, their parental or primary status may cause controversy and this too is questioned by the high contents of incompatible elements seen in all branches of the lamprophyre clan. These high incompatible element contents and their implications for small degrees of partial melting (steep REE patterns etc.) have however become easier to reconcile recently since McKenzie (1984, 1985) suggests that melt fractions of the order of tenths of a percent are capable of migration and escape from their source regions. Even at 0.1% partial melting however it is necessary to postulate limited mantle metasomatism to produce the observed REE contents of the UML as no melting models could produce the required enrichments.

The UML with high Mg/Fe ratios, Ni, Cr may fall in 'primary' ranges (Basaltic Volcanism Study Project 1981). Similarly Hart and Davis (1978) suggested 11-13% MgO as a primary range, and this covers all but 5 of the 23 UML. However, O'Hara *et al.* (1975) regarded picritic magmas with 20-25 wt% MgO as the only primary magmas

Figure 8.4.9

ALTERED ULTRA-MAFIC LAMPROPHYRES

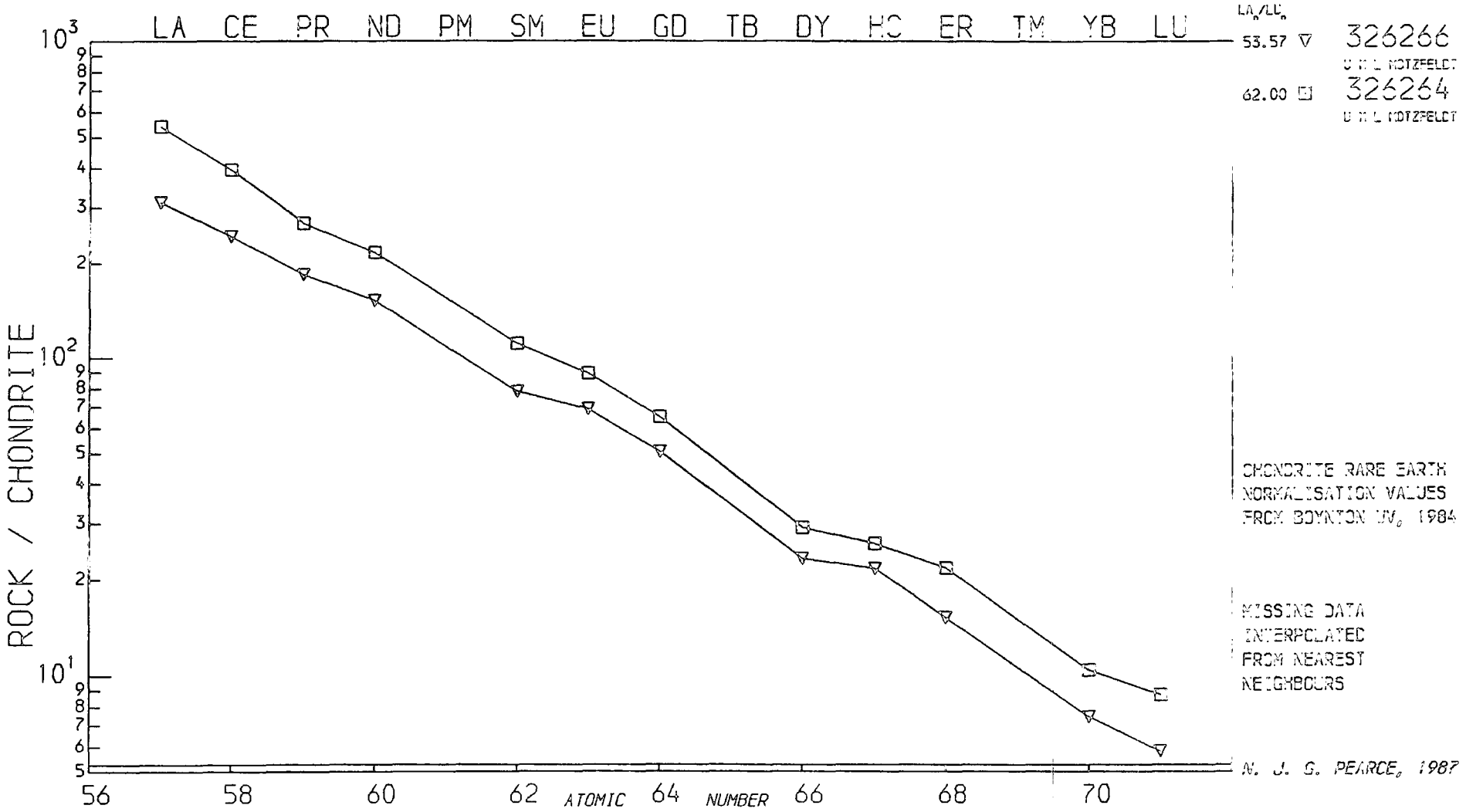

and on this criterion none of the lamprophyres from the Igaliko Complex are contenders. All AL and CAL are below any of the primary ranges suggested above, although are typically rich in MgO, Ni, Cr compared to rocks of similar SiO_2 from the main swarm.

The possible parental status of the AL to the alkali basalts and hawaiites has been hinted at throughout this chapter and has been stressed by others (Rock 1977, 1987a, Philpotts 1974, Bedard *et al.* 1985). In the Monteregian Province there is a gradual change in lamprophyre composition from camptonites in the east, through monchiquite (also AL) to alnöite in the west. Associated plutonic rocks change from gabbro-syenite through to essexite-foyaite and ijolite-carbonatite (Philpotts 1974). There is little doubt that there is a genetic link between the lamprophyres and the plutonic rocks (Eby 1987) although the view of Philpotts (1974) that the lamprophyres directly generated the plutons may be oversimplified. Nonetheless, in view of the general chemical similarities between AL and alkali basalts it seems likely that they may have some parental status to the basic dykes and thus the remainder of the undersaturated suite.

In conclusion the volatile-rich incompatible and compatible element rich rocks probably originated from small (to very small) degrees of partial melting, from an enriched garnet-bearing mantle source (even UML by analogy to lamproites, Bergmann 1987 and kimberlites, Dawson 1987). In the case of AL, and possibly CAL, they may have been parental to undersaturated alkali basalt/hawaiite magmatism. To quote Rock (1987a) 'lamprophyres are almost always primitive, frequently primary and sometimes parental'. The evidence from Igaliko is in accord with these generalisations.

Occurrence

It is noticable that many of the lamprophyric rocks outcrop to the southwest of the province (see Map 1), and this is particularly true for UML. Many UML occur around Østfjordsdal and are seen to be truncated by many dykes in this area and none cut the Østfjordsdal Syenite. Chemically similar UML are seen cutting the Julianehåb Granite in 'Harry's Dal' and also as dykes cutting rafts of granite within the outer units of the Motzfeldt Centre, but none of this type of UML are seen cutting the syenites themselves. These two areas are separated by the Gieseckes Dal fault which shows about 1km of post-South Qôroq sinistral displacement (Emeleus and Harry 1970). If

the Østfjordsdal and Motzfeldt UML are part of a continuous swarm from pre-Motzfeldt times, projection of the swarms onto the Gieseckes Dal fault may imply as much as 4-5km of offset over the period of Gardar activity (with 3-4km pre-South Qôroq). This is however poorly constrained elsewhere and is only speculative.

If a UML magmatic event occurred prior to major Gardar activity in the region, magmas of this type (chemistry) emplaced into the lithosphere, mantle and crust could have had an important metasomatic/enriching effect (cf. Hawkesworth *et al.* 1984, Fitton and Dunlop 1985, Fitton and James 1986, Menzies *et al.* 1987). They may well have been produced as extremely small degrees of melting at the onset of Gardar rifting and could have been the cause of the enrichments necessary to model the bulk of the basalt to phonolite/rhyolite magmatism. There may be some relationship between this activity and the carbonatite/lamprophyre activity at the base of the Eriksfjord Formation near Qagssiarssuk (Stewart 1970).

CHAPTER 9: ØSTFJORDSDAL DYKE SWARM

9.1: Introduction

The Østfjordsdal dyke swarm is a petrographically distinct group of dykes cropping out to the south east of the Igdlerfigssalik syenites and bounded by the Østfjordsdal valley and gravel flats (see Map 2). There is no record of their outcrop in the vicinity of the Si-oversaturated Klokken syenite on the south side of Østfjordsdal.

Dykes from the Østfjordsdal region have been sampled to the north east of the Østfjordsdal syenite by C. H. Emeleus in 1963 (sample numbers 52257-52291) and by this author to the south west of the Østfjordsdal syenite in 1984 (sample numbers 326271-326320). These mostly cut the country rock (Julianehåb Granite) surrounding the syenite, although samples 52265, 52285-52289 and 326308-326312 cut the Østfjordsdal syenite.

Many of those dykes which cut the Julianehåb Granite are not seen to continue along strike into the Østfjordsdal syenite. They are thus assumed to pre-date the Østfjordsdal syenite and it is these dykes which form the Østfjordsdal Dyke Swarm. Those dykes that cut the syenite (which include several AL and a few phonolites) are not members of the Østfjordsdal Dyke Swarm but are probably related to the main, Si-undersaturated dyke swarm.

The Østfjordsdal Dyke Swarm pre-dates the Østfjordsdal syenite, which is in turn cut by the South Qôroq and Igdlerfigssalik centres. There is no constraint on the older age limit of these dykes, which are tentatively assigned to part of the mid-Gardar activity. The average strike of the Østfjordsdal Dyke Swarm is approximately 043°, and this is about 10° less than the more typical 050°-055° for the bulk of the Igaliko dykes (see Figure 2.6.1). This may be a reflection of a slightly different tectonic regime in the area during the period of Østfjordsdal Dyke Swarm emplacement, or could be an effect of 'country rock grain' (see Chapter 2.6 for discussion).

The Østfjordsdal Dyke Swarm is distinctive in the granular texture of its component types, particularly the phonolitic examples. Included in the Østfjordsdal Dyke Swarm are a group of large (20m) porphyritic syenite dykes. These are equated with the Fox

Bay Porphyry Syenites described by Ussing (1912).

This chapter will concentrate on the petrographic differences (both in the field and in thin section) that differentiate these dykes from the main dyke swarm. Their mineralogy has been largely considered under 'Recrystallised Phonolites' in Chapter 4. Certain aspects of their geochemistry will be discussed, although they are essentially indistinguishable from the undersaturated dykes of the main swarm.

9.2: Petrography and Field Occurrence

Basic Dykes

The most abundant basic dykes in the Østfjordsdal area are lamprophyres. These are either AL (camptonites), CAL (vogesites) or UML and occur across the area. The UML often appear to be early, being cut by the trachytic and porphyritic syenite dykes. The AL tend to be later than the UML and several cut the Østfjordsdal syenite. These AL may be related to the late Gardar activity and not the Østfjordsdal activity. The CAL are only seen cutting the Julianehåb Granite, and show no cross-cutting relationships with one another or with other dykes.

Berrangé (1966) describes the occurrence and petrography of many lamprophyres from the Vatnahverfi area to the south east of Sønde Igaliko. These would appear to be AL (camptonites?). This ground is more or less along strike from the Østfjordsdal area and may be a continuation, beyond Fox Bay, of the same swarm. Berrangé (1966) however does not report any large porphyritic syenite dykes from the area.

The UML, CAL and AL have been described in Chapter 8, examples being 52285, 52274, 326308 (camptonites, Plate 8.1, 8.3 and 8.2 respectively), 326301, 326303 (UML, Plates 8.8, 8.9 and 8.10) and 326281, 326318 (vogesites, Plates 8.6 and 8.7 respectively).

Intermediate Rocks

Intermediate rocks are scarce, although chemical analyses and TAS classification (Cox *et al.* 1979) revealed a mugearite (326292). This is a fine grained, rather altered rock with an appearance similar to some calc-alkaline lamprophyres. It is composed of groundmass plates of alkali feldspar 1mm in diameter, enclosing many small (150μm)

fawn to greenish-brown biotite laths and small (10-20μm) apatite needles. The feldspar is weakly perthitic and typically 'orthoclase'. Discrete grains of albite are relatively rare, perhaps only 10-15% of the feldspar. Sphene is a relatively abundant groundmass phase, occurring as small, granular aggregates up to about 80μm diameter. Opaque Fe-Ti oxides are present in similar quantities to sphene ($\approx$3% modally). This sample is amygdaloidal, the amygdales, 5mm in diameter, typically being concentrically zoned. They are rimmed with green aegirine-augite and, rarely, sphene, which give way inward to albite and calcite.

Rather than being classified as a CAL (minette), this rock is considered to be a recrystallised mugearite which, from the presence of sphene and green biotite (Fe^{3+} -rich, Deer *et al.* 1966), underwent metamorphism at relatively high fo_2.

Phonolitic Dykes

These are the most common members of the Østfjordsdal Dyke Swarm. They are typically 2-5m in width. They are generally a blue-grey colour on their weathered surfaces and when broken show a speckled 'salt and pepper' fresh surface with small, granular clusters of dark, mafic minerals enclosed in a very fresh felsic groundmass. Rarely, large black specks of opaque oxides develop and are surrounded by a well defined rim free from ferromagnesian minerals. These oxides may be up to 2-3mm in diameter, and are enclosed entirely by felsic minerals to a distance of 1-2mm. They often contain platy alkali feldspar laths, the morphology of which is typical of phonolites (see Chapter 4.8). These feldspars may be up to 1.5cm by 2-3mm in size.

The granular speckling present in most samples may develop to such an extent that a marked banding is visible in the sample in hand specimen (eg. 326309, see Plate 9.1). This involves a concentration of the ferromagnesian minerals into thin (1-2mm) bands leaving the intervening felsic areas almost devoid of mafic minerals. The mafics, usually aegirine-augite (or more rarely amphibole) are large poikiloblastic crystals, optically continuous over 10-15mm in many cases, although the band may be only 1mm or so in width.

In the more common, unbanded examples the ferromagnesian minerals occur either as small grains scattered throughout the sample, or as larger, poikiloblastic/sub-

poikiloblastic crystals (part-) enclosing groundmass feldspar, nepheline etc. These textures are essentially very similar to those shown in Plates 3.6 and 3.7. In several cases a similar poikiloblastic texture is shown by opaque oxide minerals. Relic cores of aegirine-augite are sometimes seen to be totally enclosed and corroded by amphibole overgrowths, suggestive of recrystallisation in the presence of water.

Relic porphyritic textures are sometimes seen, with 'phenocrysts' of alkali feldspar (see Plate 9.2). In this case relic morphology resembling 'anorthoclase' type feldspars is visible. These often show only weakly defined perthitic textures. Tabular relic feldspars are often seen in the phonolites and are invariably coarsely exsolved. Many of these larger feldspars show a sieve texture, being peppered with small holes/inclusions (see Plate 9.2).

In one sample, 326289, large, poikiloblastic andradite garnets have developed (see Plates 9.3 and 9.4). These are sparingly developed in small clusters throughout this sample (see Plate 9.3). The andradites reach maximum diameters of about 8-10mm, although they are typically about 5-6mm across. On a cut surface they appear to sit within a pale, felsic zone, free from any mafic material and this resembles a pressure shadow. This is also evident in thin section, where a band of perhaps 1-2mm free from mafic material surrounds each garnet. These andradites are straw yellow - green in colour and are poikiloblastic. They enclose large numbers of small nepheline and feldspar crystals along with minor inclusions of cancrinite and, rarely, sodalite. These are all in the range 50-100μm in diameter (see Plate 9.4). A rough mineral alignment in the groundmass feldspar is evident and may be either a relic trachytic texture, enhanced by recrystallisation or a pressure-induced alignment, although no other fine-grained samples show strongly aligned textures. To some extent this mineral alignment is paralleled by felsic veins and patches throughout the rock and this may imply a tectonic control.

Pressure shadows, filled with cancrinite and nepheline (see Plate 9.4) bound all of the garnets seen in thin section. These thin out to become parallel with the overall mineral alignment. It seems difficult to escape the conclusion that, at least in some samples, recrystallisation was effected under moderate pressures. In most cases however, where aligned textures of groundmass minerals are seen, a relic trachytic origin is favoured.

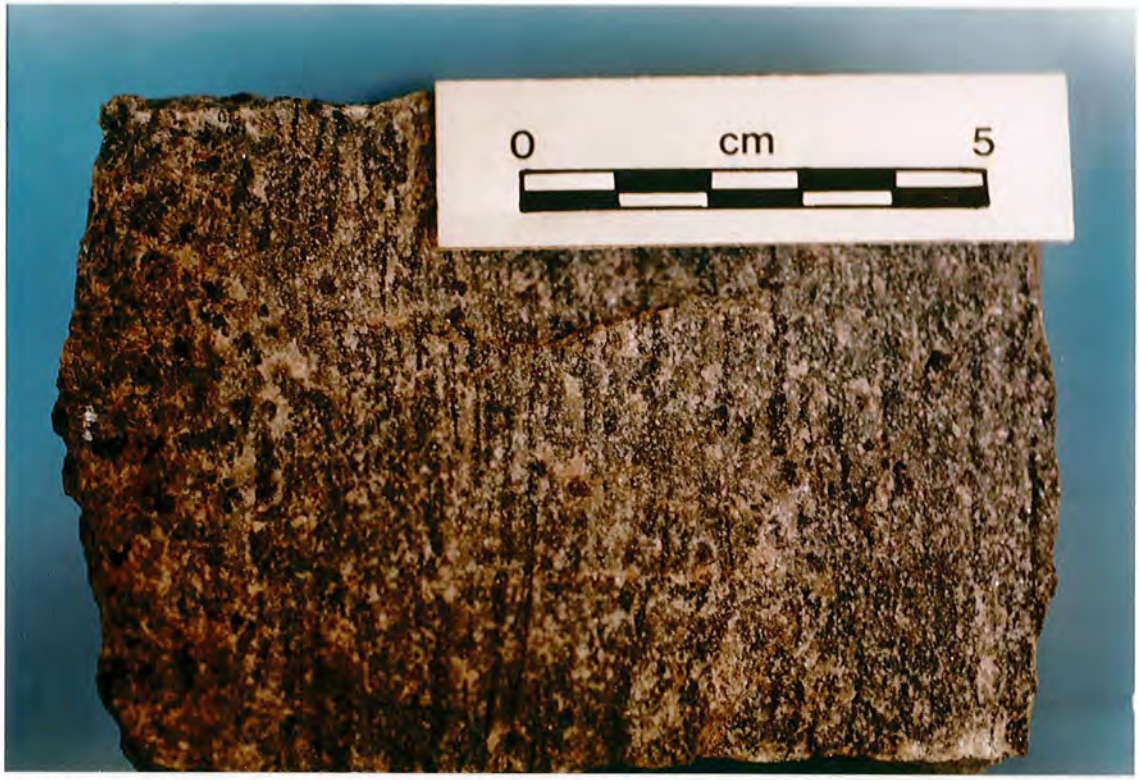

Plate 9.1 Recrystallised phonolite. 326309. This is a banded, recrystallised, phonolite, with mafic minerals tending to aggregate in 2-3mm scale bands, as poikiloblastic crystals. The sample coarsens to the left into a more normal nepheline syenite.

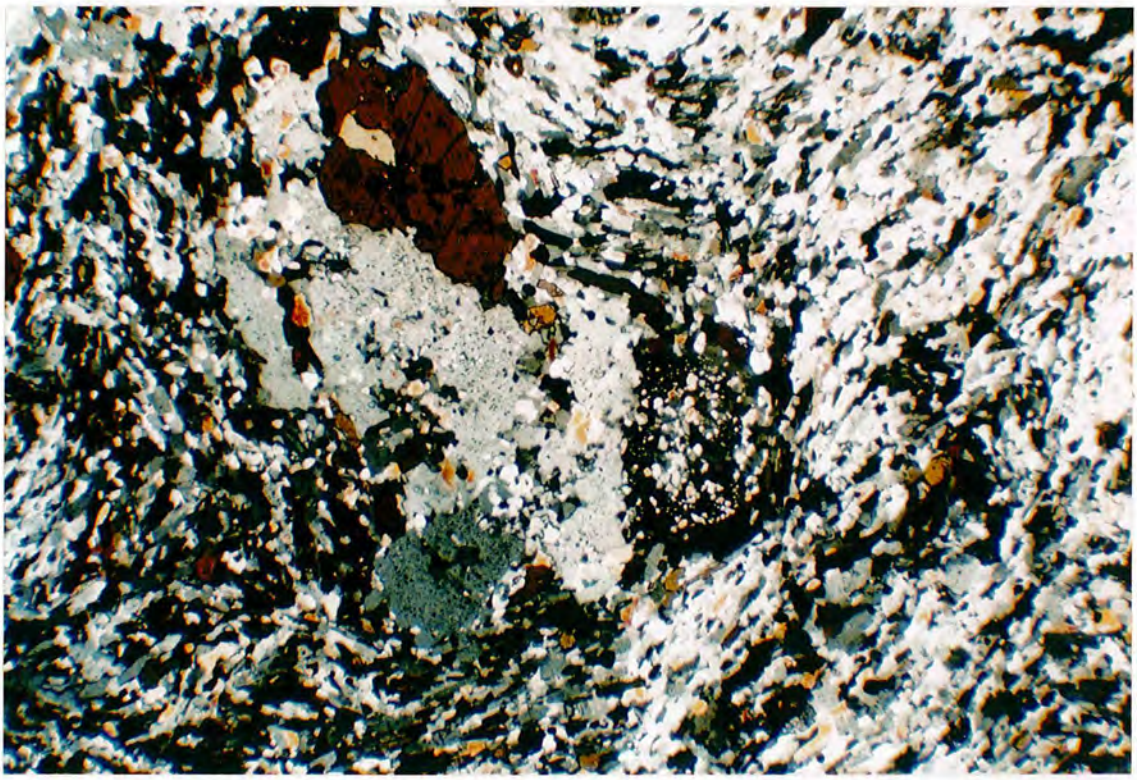

Plate 9.2 Recrystallised phonolite. 326275. ×35. XPL. This sample shows a well defined, granoblastic texture developed over a relic trachytic texture (trachy-blastic texture, see Chapter 3). Relic feldspar phenocrysts, now showing sieve textures, are seen at the centre, with an isotropic sodalite crystal (right of centre). A large, hastingsitic amphibole is seen top centre. The groundmass is composed of alkali feldspar, nepheline, sodalite and cancrinite (yellow/orange birefringence).

Plate 9.3 Recrystallised phonolite. 326289. The pale weathering recrystallised phonolite shows clusters of poikiloblastic garnets. These show hexagonal outlines, and are surrounded by patches of mafic-depleted material.

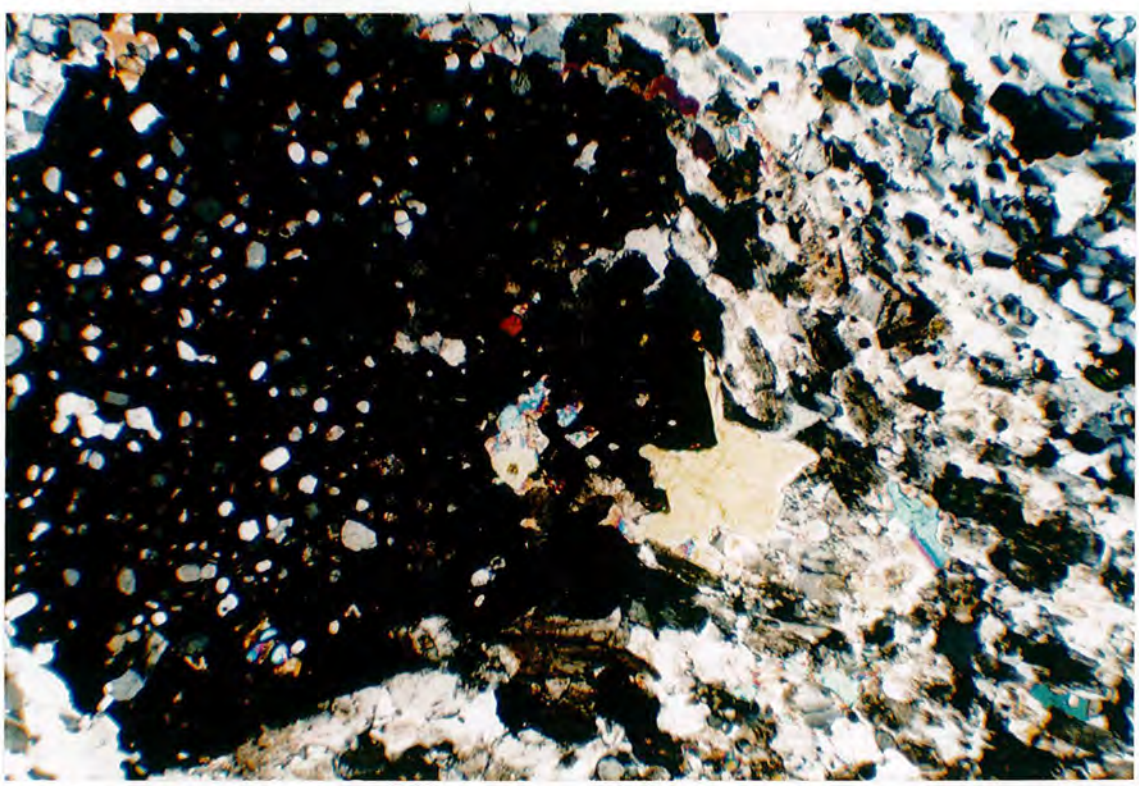

Plate 9.4 326289. Recrystallised Phonolite. ×35. XPL. A poikiloblastic, isotropic, andradite garnet occupies the left of the field, and contains many inclusions of nepheline, feldspar and cancrinite (blue/yellow birefringence). The andradite is pale yellowish-green in PPL. The groundmass (top right) is composed essentially of alkali feldspar and nepheline close to the garnet with aegirine augite seen no closer than ≈2mm. Cancrinite forms in 'pressure shadows' on either side of the garnet (large yellow patch) and these are parallel to the overall mineral alignment of the groundmass (bottom right - top left). This has been deformed by the garnet as it grew. There is some groundmass cancrinite.

'Aligned' samples are less common than those not showing any mineral alignment, and minerals such as mica, the growth of which is sensitive to any confining pressures, do not show any preferred orientations.

Typical felsic groundmass minerals are feldspar, nepheline, sodalite (isotropic) and cancrinite (low relief, bright first and second order polarisation colours). Groundmass mafic minerals include aegirine-augite, amphiboles (hastingsitic to alkali), opaque oxides (typically magnetite), biotite and chlorite (retrograde from biotite in many cases). These all occur as small grains, typically 100-200μm in diameter. Several of the more highly recrystallised samples show well developed granoblastic textures with 120° grain boundaries.

Feldspar in all samples is either coarsely perthitic or completely exsolved to separate grains of albite and orthoclase. In rarer cases microcline is seen in some perthitic feldspars.

In several cases, exemplified by 326282, the feldspars, recrystallised to a medium grained granoblastic texture, show 'pleated' grain boundaries under cross polars (Parsons 1978). These are illustrated in Figure 9.2.1. The pleating is caused by a coarsening of perthitic exsolution lamellae from micro- (or even crypto-) perthities at the grain core ('braid' microperthites) to coarser braid perthites at the rims. The braid microperthites at the cores are probably the result of 'coherent' exsolution on cooling, with a later coarsening of the exsolution lamellae towards the grain boundaries. These samples typically contain sodalite and some cancrinite (ie. volatile-rich) and the 'pleating' is almost certainly a result of volatiles (water etc.) being present at grain boundaries (cf. Parsons 1978). This fluid will have facilitated grain boundary modification, including the peculiar 'dovetailed' interlocking of some grains where one phase of the perthite appears to protrude into the neighbouring grain (see Figure 9.2.1).

The presence of volatiles thus appears to have been quite important during the recrystallisation of these samples.

There is evidence of alkali metasomatism surrounding some of these fine grained phonolitic dykes. This generally involves growth of light blue alkali amphibole (glaucophane, riebeckite) on joint surfaces within the country rock granite (see Plate 9.9).

Figure 9.2.1: Sketches of alkali feldspar exsolution textures from 326289.

Key: Biotite – vertical ruling
Opaque oxides – black
Alkali feldspar – shaded or black and white

A. Coarsening of the perthitic exsolution lamellae towards the crystal margin leads to a pleated texture (Parsons 1978). There is often a band of clear feldspar at the crystal margin. Microperthitic exsolution is often visible at the centre of individual feldspars.

B. Enlargement from centre of A showing a 'dovetailed' intergrowth of adjacent crystals. Exsolution textures often terminate in this 'dovetailed' intergrowth which protrudes into the adjacent crystal.

C. Pleated perthitic exsolution. Note the relatively homogenous rim to the feldspar crystal to the right of the field, giving way towards pleated perthites the crystal core.

D. Enlargement from left of centre of C. Complex dovetailed intergrowth at termination of pleated exsolution lamellae in adjoining crystals. These dovetailed intergrowths produce a band 'exsolution'-free boundary between adjacent feldspars and often have a 'horses-head' shape.

Figure 9.2.1

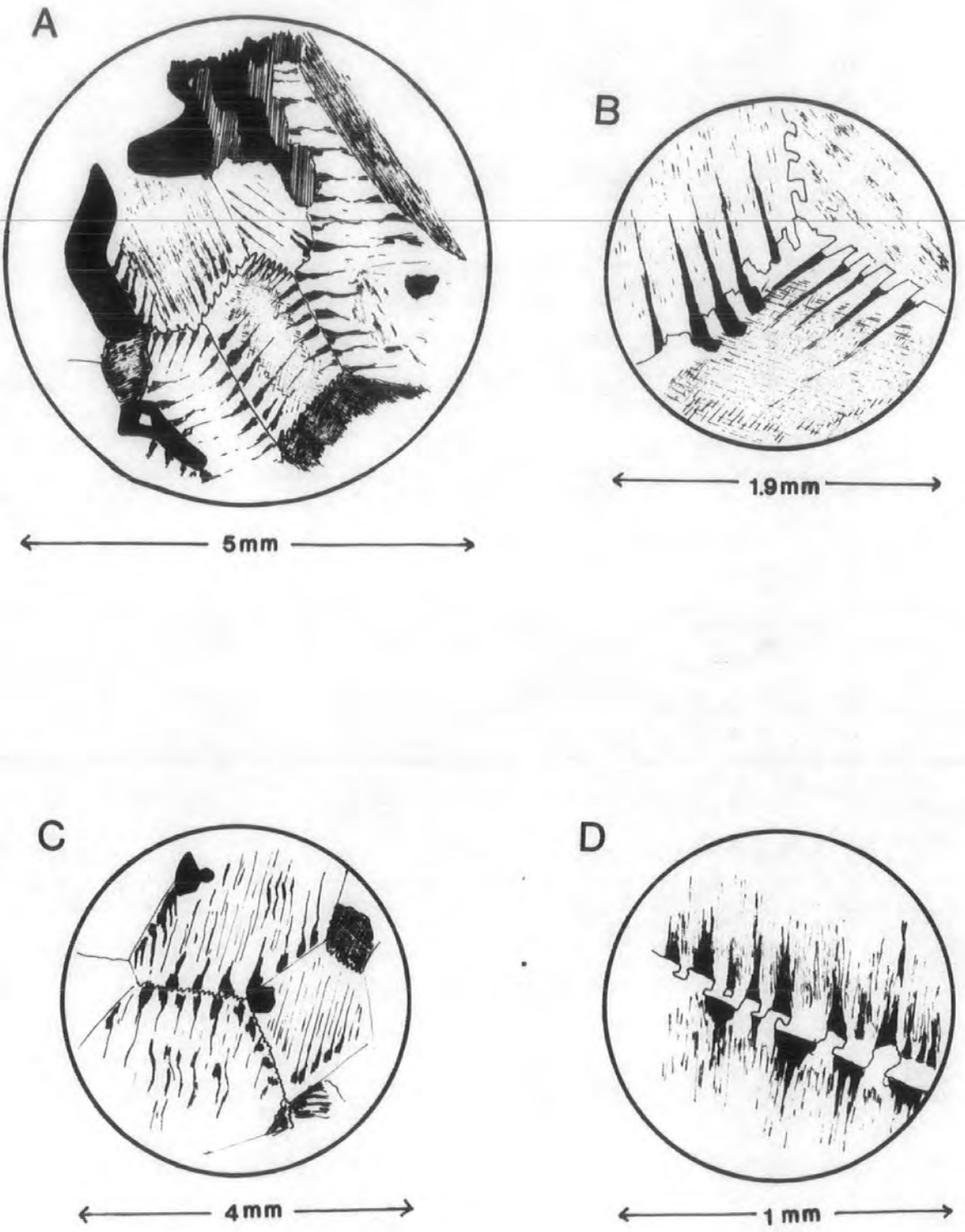

This involves introduction of Na and K by the dyke into the surrounding granite, presumably in an aqueous solution or possibly as aqueous halide solutions (Cl must be present to form the sodalite so commonly encountered).

A few phonolite dykes cut the Østfjordsdal syenite and are thus not members of the Østfjordsdal Dyke Swarm. They show none of the recrystallisation textures described above for the blue-grey phonolite dykes, but resemble very clearly typical phonolites of the main undersaturated swarm. These are described in Chapter 3.

Syenitic Dykes

Cropping out in the Østfjordsdal area is a swarm of large (5-25m wide) porphyritic, nepheline syenite dykes. Similar dykes were first described by Ussing (1912) from Fox Bay some 10km to the SW of the Østfjordsdal syenite, and subsequently by Emeleus and Harry (1970) to the NE of the Østfjordsdal syenite. The outcrop of these dykes is shown in Figure 2.7.1 to the immediate SW of the Østfjordsdal syenite (authors camp 3, 1984). Dykes of this type only occur in this region of the Igaliko Nepheline Syenite complex.

These are highly porphyritic dykes, containing large euhedra of both nepheline (1-1.5cm diameter) and alkali feldspar (2-3cm by 1cm). On the fresh surface (see Plate 9.5) they have an overall grey colour with a slight pinkish hue imparted by the alkali feldspar. The groundmass is dark and has a sparkling appearance caused by the presence of abundant, small flakes of biotite mica occasionally appearing as small aggregates in a more felsic area of the groundmass. On the weathered surface (Plate 9.6) the characteristic square or hexagonal outline of nepheline is clearly visible where this has been weathered out to give a pitted surface. The large alkali feldspars are also clearly seen as long white blocks. Phenocrysts of nepheline are modally slightly more abundant than feldspar.

In the area to the SW of the Østfjordsdal syenite these large dykes have been recrystallised. The large phenocrysts have often become aggregates of smaller grains of feldspar or nepheline, showing well developed 120° triple junctions (granoblastic textures). The groundmass is composed of albite and orthoclase, nepheline, sodalite, opaque Fe-Ti oxides and biotite with no other ferromagnesian minerals. Cancrinite

Plate 9.5 Porphyritic syenite, fresh surface. 326285–type. Phenocrysts of alkali feldspar (rectangular blocks) and nepheline (hexagonal) are clearly visible in this highly porphyritic sample. Large mafic clusters of biotite sit in a fine-grained pinkish groundmass to the dyke. The coin is approximately 1.5cm in diameter. It is difficult to distinguish between feldspar and nepheline.

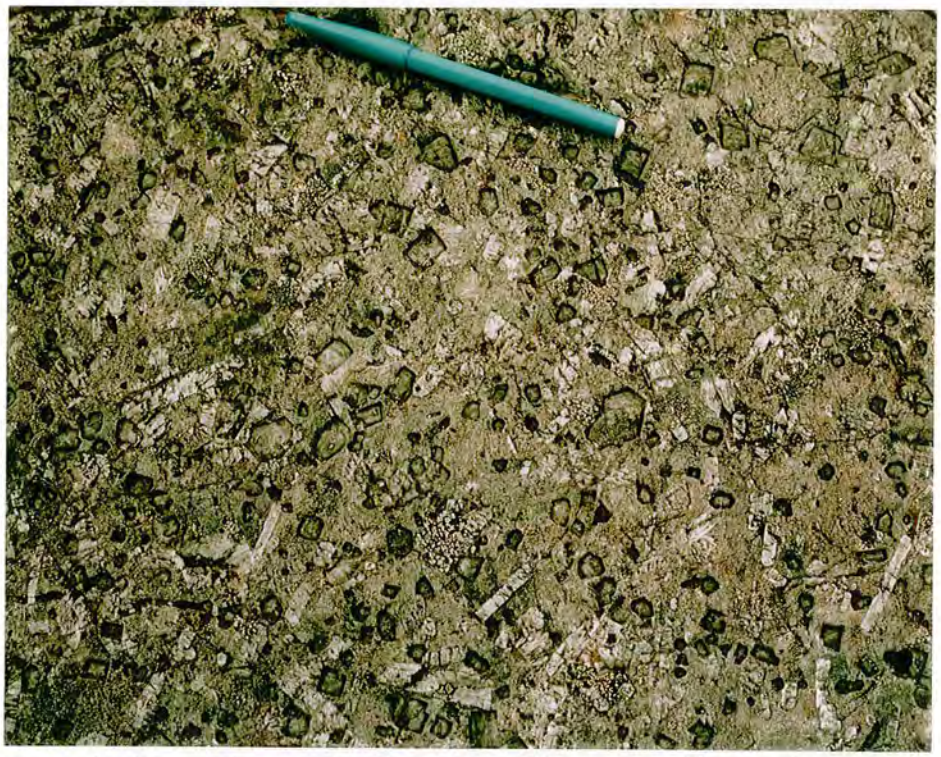

Plate 9.6 Porphyritic syenite, weathered surface. 326385–type. The weathered surface of the dyke enables nepheline to be distinguished from feldspar with relative ease. Nepheline weathers into the surface of the dyke producing well defined hexagonal (and square) pits in the surface. Feldspar weathers to a white colour (?clays) and is flush with the surface. The pen is approximately 14cm long.

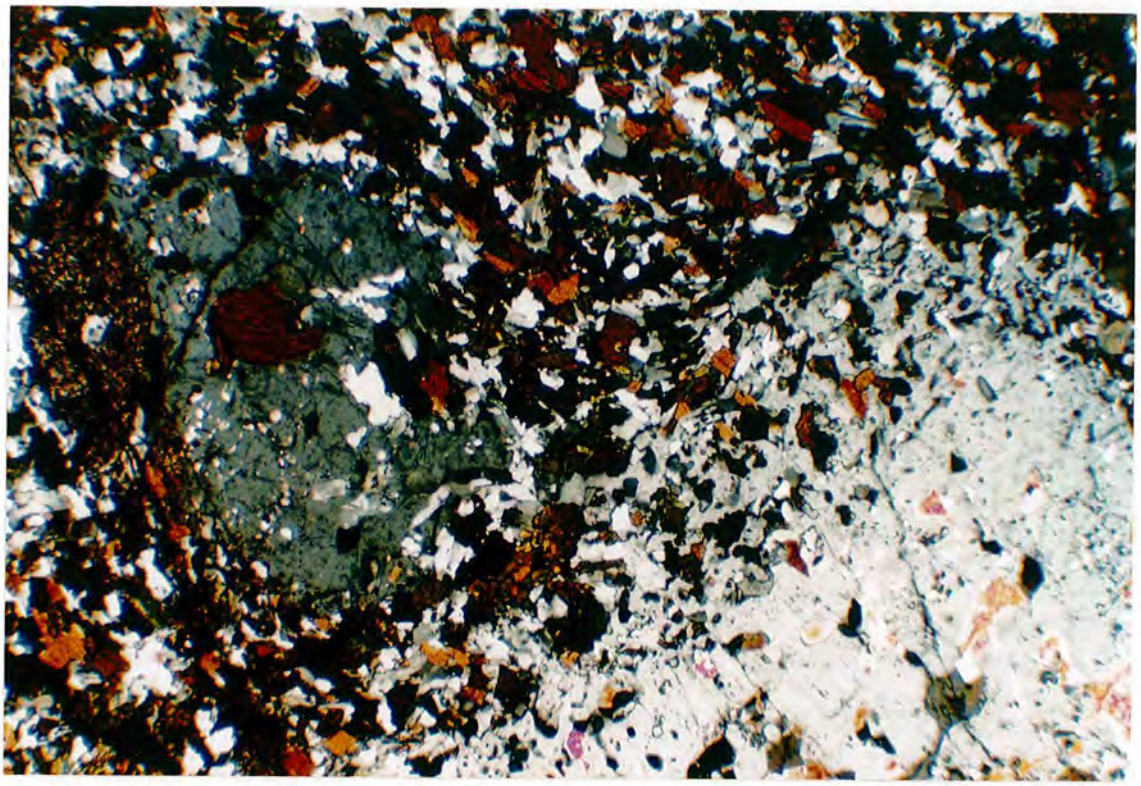

Plate 9.7 52267. Porphyritic syenite. XPL. ×35. This sample is from NE of the Østfjordsdal syenite and is a continuation of the dykes from the SW of the Østfjordsdal syenite. It contains large nephelines with sieve textured margins often containing intergrowths of cancrinite (bottom right). Alkali feldspar is the other main phenocryst phase (centre left). The groundmass consists of granular alkali feldspar (often exsolved to albite and orthoclase), nepheline, aegirine-augite and biotite. Some sodalite is also present. In 326285, no aegirine-augite is present, the only ferromagnesian mineral being biotite, and the feldspars and nephelines have been recrystallised to a granoblastic aggregate of smaller minerals.

Plate 9.8 Sheared porphyritic syenite. This porphyritic syenite dyke has been sheared, possibly whilst still at high temperature and thus plastic. This has caused the phenocrysts to become streaked out and thoroughly recrystallised to fine-grained, granoblastic aggregates.

Plate 9.9 Alkali metasomatism at dyke margins. Pale blue amphibole (riebeckite) is developed along joint faces in the Julianehåb Granite immediately around a recrystallised phonolite dyke. The dyke shows a well developed chilled margin and is sparsely porphyritic,also containing some felsic inclusions (eg. near lens cap). The production of amphibolein the granite will be a result of alkali loss from the phonolite dyke. Scale on hammer shaft in inches.

occurs as small patches in the groundmass. The nepheline is often altered to micaceous aggregates of gieserkite, often stained to a muddy pink-brown colour. One of these dykes is illustrated in Plate 9.7 (sample 326385).

To the NW of the Østfjordsdal syenite however, these large porphyritic syenite dykes have a different appearance in thin section, although appearing very similar in hand specimen (see Emeleus and Harry 1970, Figure 32). There is no developement of granoblastic texture in the phenocrysts, although what appear to be large grains of nepheline are typically composed of 2-3 separate grains. This is probably a recrystallisation effect which has not proceeded to the same extent as to the SW of the Østfjordsdal syenite. The nepheline phenocrysts have vermicular growths of cancrinite penetrating their margins. Cancrinite is also developed along fractures in these nephelines and rare, large (2mm diameter) sodalites are seen in the groundmass. The feldspar phenocrysts have exsolved to coarse braid or patch perthites.

The groundmass contains abundant albite, orthoclase, sodalite, nepheline and cancrinite and shows a well developed granular texture. Iron oxides are abundant and biotite is the most common ferromagnesian mineral, occurring singly or as clusters of crystals. Unlike the same dykes from the SW of the Østfjordsdal syenite, those to the NE contain appreciable fresh, bottle-green aegirine-augite. Rare, large (500μm) zircons are seen, again absent from those dykes to the SW of the Østfjordsdal syenite. Only rarely is biotite seen enclosing the aegirine-augite.

The mineralogical differences between these dykes in these two areas will have been caused by differences in the conditions operative during recrystallisation (temperature and water content probably being the most important).

In the area SW of the Østfjordsdal syenite some of the large, porphyritic syenites are seen to be sheared, and show elongated and deformed feldspars and nephelines (see Plate 9.8, sample 326313). This sample has a mineralogy very similar to that described above although contains dark green (alkali) amphibole in place of biotite or aegirine which are both absent. Cancrinite is also absent. There is a distinct lineation to the groundmass minerals. The phenocrysts have been converted to fine-grained, granoblastic aggregates and substantial alteration of nepheline has occurred, producing

gieseckite and in some cases large flakes of muscovite (up to 400μm). Large aggregates of sodalite are visible in this sample unlike any of the others as granoblastic patches 2-3cm in length by 5mm in breadth. These may represent primary phenocryst phases peculiar to this one sample although are more likely to be the product of substantial alteration of nepheline by Cl-rich fluids during deformation.

In general, the outcrop of these porphyritic syenite dykes is complex, bifurcating and merging along their length, they occupy a zone perhaps 200m wide of which aggregate widths of 40-50m may be dykes. In some cases these large porphyritic syenites appear to grade, either marginally or longitudinally into fine-grained, blue-grey recrystallised phonolites. This involves rapid gradational changes and there are no abrupt, chilled internal contacts. These finer-grained, blue-grey, phonolitic dykes may thus be a chilled, aphyric facies of the coarser, porphyritic syenites although they are not restricted to the margins of these larger porphyritic syenite dykes. The longitudinal extension of these porphyritic syenites into finer-grained, blue-grey phonolites may suggest more of a genetic link between the two. Despite differences in grain size their compositions and mineralogies are very similar.

9.3: Mineralogy

In general the mineralogy has been discussed in Chapter 4 with the dykes considered as 'Phonolites/Syenites' or 'Recrystallised Phonolites'. There are no systematic differences in the mineralogy of dykes from the Østfjordsdal area when compared to similar dykes from the rest of the Igaliko Province.

The presence of sphene in some samples, and the composition of many of the alkali pyroxenes (often very rich in Mn) from the recrystallised phonolites (ie. the blue-grey phonolites) attest to metamorphism at relatively high fo_2. Discussion of the mineralogy is mostly confined to Chapter 4 although some points of interest will be mentioned here.

Feldspars

Most alkali feldspars in the phonolitic rocks show some form of perthitic exsolution. Thus, only a small amount of alkali feldspar data from these samples is available due to difficulties of analysis by microprobe.

Alkali feldspars from the recrystallised phonolites (see Chapter 4) tend to have low Ca and low Ba, these elements having been driven out on recrystallisation/exsolution. Where homogenous feldspars have been analysed in the phonolitic rocks, compositions range from about $Ab_{60}Or_{40}$ to $Ab_{30}Or_{70}$ and are more potassic than the binary minimum (Deer *et al.* 1966). Where recrystallisation has produced two feldspars compositions range from Ab_{88} to Ab_{100} for the Na-rich feldspar and Or_{88} to Or_{100} for the K-rich feldspar.

Figure 9.3.1 shows all feldspar analyses plotted on the Smith and Parsons (1974) alkali feldspar solvus. Following the approach adopted in Chapter 4.8.E, 326289 probably equilibrated between 400°C and 600°C, 326273 equilibrated close to 300°C and 326286 finally equilibrated at below 200°C. These temperatures at or below ≈300°C may however be too low to cause substantial modification to the crystal structure unless a volatile phase is present (cf. Parsons 1978). 326273 is from the N edge of the Østfjordsdal gravel flats (not shown on Figure 2.7.1), 326286 and 326289 are from near the author's camp at Østfjordsdal, and thus their recrystallisation temperatures and position give no indication of a thermal gradient in the area. The most obvious source of heat to affect the recrystallisation is the Igdlerfigssalik syenite which effectively truncates the Østfjordsdal dyke swarm, and temperatures of perhaps 300°C may be expected some 2.5km from the contact (ie. at the margin of the Østfjordsdal gravel flats). This is comparable with the thermal gradient calculated in Chapter 4.8 moving along the length of a dyke away from the Igdlerfigssalik syenites, directly N of Igaliko village. At the latter locality however, recrystallisation occurred only above about 450°C although this appears to have been a less volatile-rich environment than that prevailing during recrystallisation in the Østfjordsdal area.

McDowell (1986) discusses low temperature growth of authigenic alkali feldspars and concludes that both albite and orthoclase form in the Salton Sea hydrothermal system at temperatures of 250-360°C. The composition of these feldspars compare well with experimental solvus for microcline - low albite of Bachinski and Muller (1971) and less well with the Smith and Parsons (1974) solvus. Plotting the Østfjordsdal feldspar on the Bachinski and Muller (1971) solvus gives higher temperatures of equilibration at slightly over 400°C for 326273 and about 250°C for 326286. The equilibration temperatures

Figure 9.3.1

Alkali feldspar compositions from Østfjordsdal phonolites ploted on the 2-feldspar solvii at 1kb of Smith and Parsons (1974) and Bachinski and Muller (1971).

Where Na- and K-rich feldspars coexist from the same sample they have been joined by tie-lines (dash-dot and dash-dot-dot lines for the Bachinski and Muller 1971 solvus, dash or dot lines for Smith and Parsons 1974).

Recrystallisation may have taken place at temperatures as low as about 250°C - 350°C in some of these dykes.

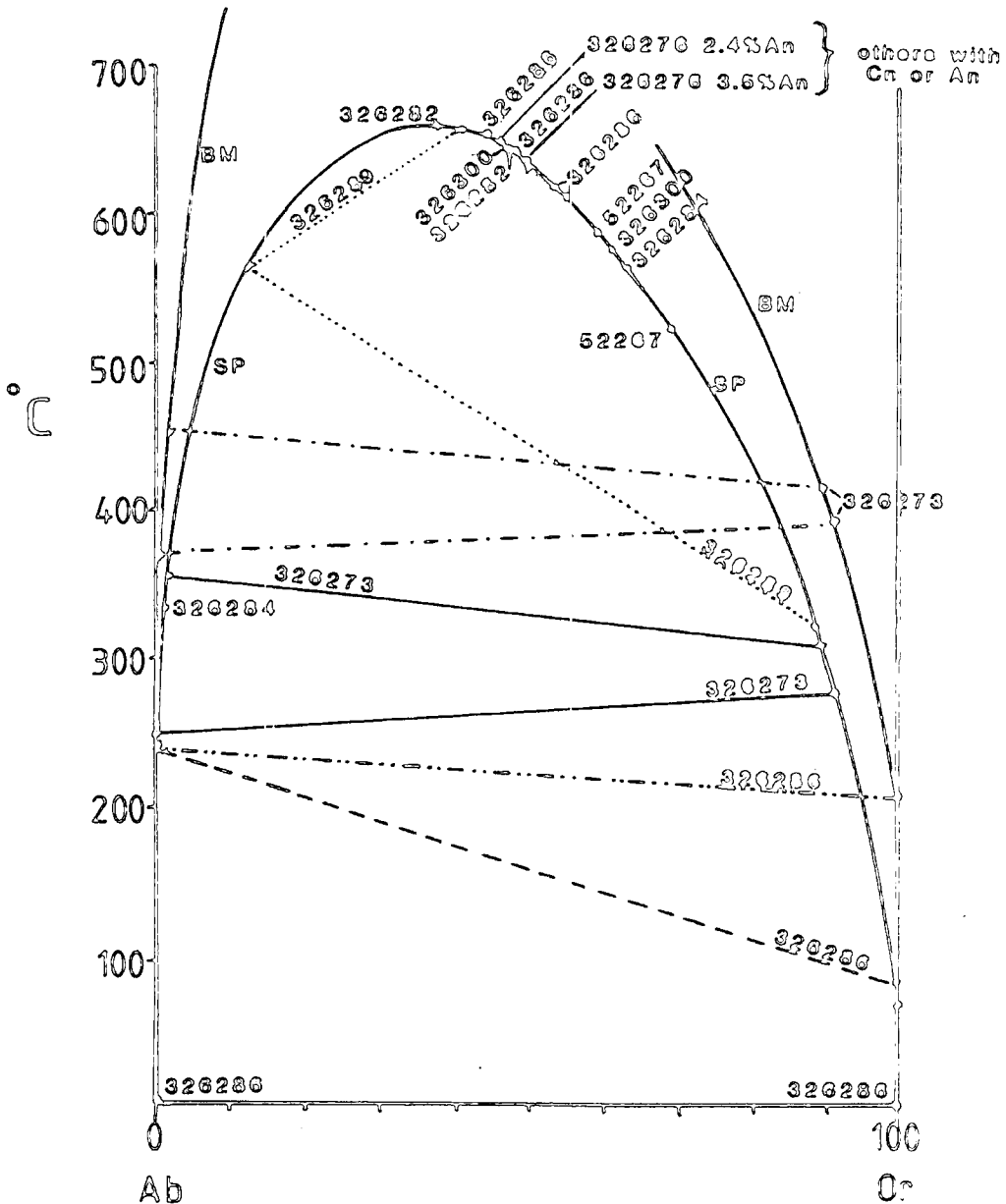

Figure 9.3.1

Østfjordsdal Dykes

Feldspar solvi at 1kb

BM-Bachinski and Muller 1971
Low Albite Microcline

SP-Smith and Parsons 1974

for 326289 on this solvus become elevated to between about 500°C and 800°C if this solvus represents the conditions operative during recrystallisation.

Garnet

Andradite garnet was found in one recrystallised phonolite (326289) from the Østfjordsdal area. Analyses of this are presented in Table 9.3.1. They are all Mg-free and are recalculated to all Fe as Fe^{3+}. They approximate very closely to $Ca_3Fe_2^{3+}Si_3O_{12}$ with only minor amounts of Al and Ti substituting for Si and Fe^{3+}, and minor Mn ($\approx$1.8 wt% MnO) replacing Fe^{3+}. Zr was detected in one analysis and will represent minor substitution of the end-member kimzeyite.

Andradite is a common skarn mineral produced by hydrothermal metamorphism of calcareous sandstones. It generally forms by the reaction:

$$3CaCO_3 + Fe_2O_3 + 3SiO_2 \rightleftharpoons Ca_3Fe_2Si_3O_{12} + 3CO_2$$

(Deer *et al.* 1962 vol.1). Fe_2O_3 and SiO_2 are both components of aegirine/aegirine-augite which may be consumed in the recrystallisation process to provide some Ca and Fe^{3+}. There is abundant evidence in these rocks of the presence of CO_2 (in cancrinite), which occurs in great abundance surrounding the andradite. A reaction of the form:

$$\text{nepheline} + \text{aegirine-augite} + \text{calcite} \rightleftharpoons \text{andradite} + \text{cancrinite} + SiO_2$$

$$\text{ie. } Na_6Al_6Si_6O_{24} + 3(Ca,Fe^{3+},Na)_2Si_2O_6 + CaCO_3 \rightleftharpoons$$

$$Ca_3Fe_2^{3+}Si_3O_{12} + Na_6Al_6Si_6O_{24}.Na_2CO_3 + 3SiO_2$$

appears to be analogous to the above reaction. The excess SiO_2 generated would react with nepheline to form albite. There are also no ferromagnesian minerals within 1-2mm of the poikiloblastic andradites. Similar reactions could be produced for the generation of andradite by consumption of an alkali amphibole, although this would produce more SiO_2 and thus more albite. The major mafic mineral in this sample is aegirine-augite. In hand specimen it is noticeable that the garnets occur on small fractures which may have acted as pathways for a CO_2-bearing fluid. The garnets also appear to post-date the fractures and, in thin section, are seen to deform the dominant mineral alignment (see Plate 9.4).

Table 9.3.1

Andradite analyses from 326289

326289.11	326289.14	326289.15	
SiO_2	34.76	35.36	35.15
TiO_2	1.09	0.90	0.46
Al_2O_3	1.62	1.83	2.01
FeO_{tot}	27.78	28.19	28.02
MnO	1.77	1.70	1.94
MgO	nd	nd	nd
CaO	32.18	32.98	32.91
Na_2O	0.33	0.27	0.0
K_2O	nd	nd	nd
ZrO_2	0.0	0.	0.38
Total	99.53	101.23	100.86
Atoms per 12 oxygens			
Si	2.86	2.86	2.86
Ti	0.07	0.05	0.03
Al	0.15	0.17	0.19
Fe^{3+}	1.92	1.90	1.91
Mn	0.12	0.12	0.13
Mg	—	—	—
Ca	2.83	2.85	2.87
Na	0.05	0.04	0.0
K	—	—	—
Zr	0.0	0.0	0.02

nd – not detected

9.4: Geochemistry

The major and trace element geochemistry of these samples has largely been considered in Chapter 5. They show no significant differences from the undersaturated (low Zr/Nb) suite of dykes. The relative abundance of sodalite in the phonolitic dykes only causes a minor increase in Cl when compositions are averaged. Zr/Nb ratios for

these dykes peak at about 3.5 and are very similar to the South Qôroq data (Stephenson 1973, see Figure 5.4.2B) and this is fractionally less than the remainder of the low Zr/Nb suite (at 3.9).

In general the average Østfjordsdal phonolites are less enriched in the incompatible trace elements than the low Zr/Nb main swarm phonolites (eg. La, Ce, Nd, Nb, Zr, etc, see Table 9.4.1). The Østfjordsdal phonolites have distinctly lower Fe_2O_3 and higher Al_2O_3 than the main swarm phonolites. The Østfjordsdal phonolites also have slightly higher total alkalis and thus the most evolved samples plot closer to the Na_2O+K_2O apex of an A-F-M diagram than most of the main swarm phonolites (see Figure 9.4.1A, cf. Figure 5.9.2). They thus tend to have higher F.I. than typical main swarm phonolites.

There is little difference between the compositions of the porphyritic nepheline syenite dykes and 'Average Østfjordsdal phonolites', although the porphyritic syenites are slightly more Mg-rich and alkali-poor than an average phonolite. The porphyritic syenites are also slightly more enriched in REE and considerably richer in Ba, Zr, and Nb although poorer in Sr.

Ussing (1912) quotes analyses of two porphyritic syenite dykes from the Akiliaruseq area (Fox Bay), Igaliko Fjord. Petrographically these appear similar to the Østfjordsdal porphyry syenites with Ussing (1912) reporting aegirine breaking down to biotite. These analyses are similar to 326285, from SW of the Østfjordsdal syenite, particularly the Nuk type porphyritic syenite, which also resembles quite closely the average Østfjordsdal phonolites.

Figure 9.4.2 shows some incompatible element data plotted in terms of a ratio of a more incompatible element/less incompatible element against the more incompatible element (cf. Figures 5.7.2 and Chapter 5.7). These are plotted for those dykes that cut the Julianehåb Granite and those that cut the Østfjordsdal syenite. The dykes that cut the Julianehåb Granite are not all necessarily older than the Østfjordsdal syenite however, no UML, nor any recrystallised phonolites (ie. all phonolites cutting the basement granite) cut the Østfjordsdal syenite. The AL and most CAL commonly cut the Østfjordsdal syenite and by inference most AL and CAL cutting the Julianehåb Granite will also be younger than the Østfjordsdal syenite.

Table 9.4.1

Selected chemical analyses from Østfjordsdal phonolitite dykes

	326285 Porp Sy	326288 Typical Phonolite	Avg Østfj Phonolite	Avg IDS Phonolite	Porphyry Syenites Ussing (1912) Fox Bay	Nuk
Major elements wt%						
SiO_2	56.09	56.42	56.56	55.54	51.31	54.58
Al_2O_3	21.30	20.36	20.05	17.92	21.54	20.43
Fe_2O_3	5.53	5.14	5.65	8.30	7.42*	5.84*
MgO	0.67	0.14	0.31	0.44	0.18	trace
CaO	1.54	1.40	1.36	1.85	1.39	1.56
Na_2O	7.89	8.63	8.03	7.16	9.25	10.70
K_2O	4.20	5.54	5.44	5.65	5.49	5.74
TiO_2	0.43	0.07	0.29	0.56	1.20	0.62
MnO	0.20	0.20	0.20	0.28	0.41	trace
P_2O_5	0.13	0.0	0.05	0.09	trace	trace
F	0.32	0.50	0.41	0.28	—	—
Cl	0.02	0.36	0.24	0.21	0.17	—
O≡F,Cl	0.14	0.29	0.23	0.21	0.04	—
Total	98.18	98.47	98.36	98.10	98.94	100.24
Trace elements ppm						
Ba	1144	213	525	370		
Nb	465	302	293	484		
Zr	1667	1075	1022	1691		
Y	81	69	55	124		
Sr	571	112	683	356		
Rb	223	203	215	244		
Zn	164	130	156	286		
Cu	3	3	6	4		
Ni	5	0	3	2		
Pb	41	18	21	47		
U	13	1	7	12		
Th	50	17	24	41		
V	18	4	11	22		
Cr	0	5	0	1		
Nd	129	127	121	251		
Ga	42	42	43	45		
La	214	136	183	339		
Ce	313	240	278	551		
Zr/Nb	3.58	3.56	3.48	4.05		
Ce/Y	3.86	3.47	5.05	4.44		
K/Rb	156.3	226.5	210.0	192.2		

* *total Fe calculated as Fe_2O_3, IDS – Igaliko dyke swarm.*

Figure 9.4.1 A - F - M variation (cation proportions) in dykes from Østfjordsdal.

Marked on both diagrams is the trend from Watt (1966) for the Gardar province.

A. Dykes that cut the Julianehåb Granite.

B. Dykes that cut the Østfjordsdal syenite.

The dykes that cut the granite may be pre-Østfjordsdal syenite, although it is likely that the AL and CAL are post-Østfjordsdal syenite. Almost all the phonolites which cut the Julianehåb Granite have been recrystallised, whereas none cutting the Østfjordsdal syenite is recrystallised. It is likely that most phonolites predate the Østfjordsdal syenite, as too do the UML.

Figure 9.4.1

Ostfjordsdal Dykes
Cation Proportions
Na2O+K2O - Fe2O3 - MgO

A

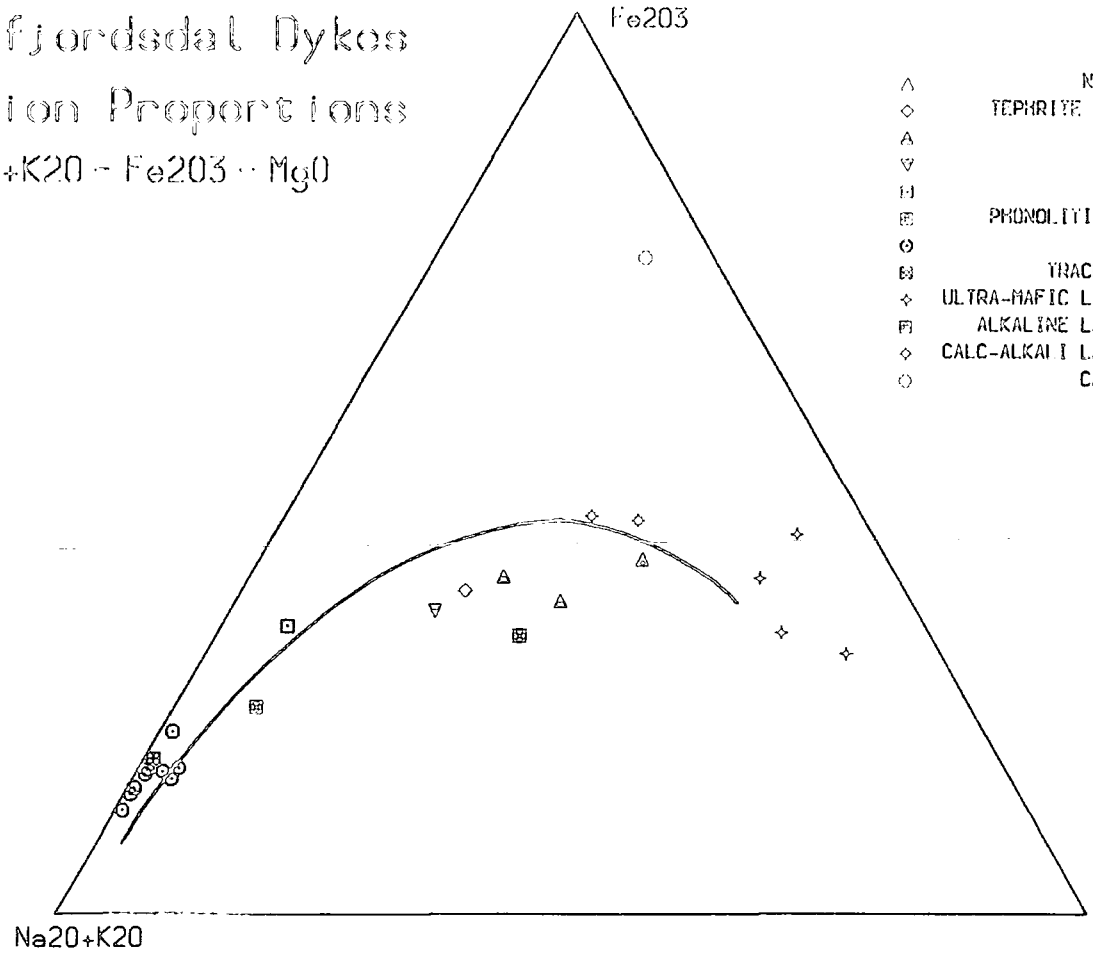

Ostfjordsdal Dykes
Cation Proportions
Na2O+K2O - Fe2O3 - MgO

B

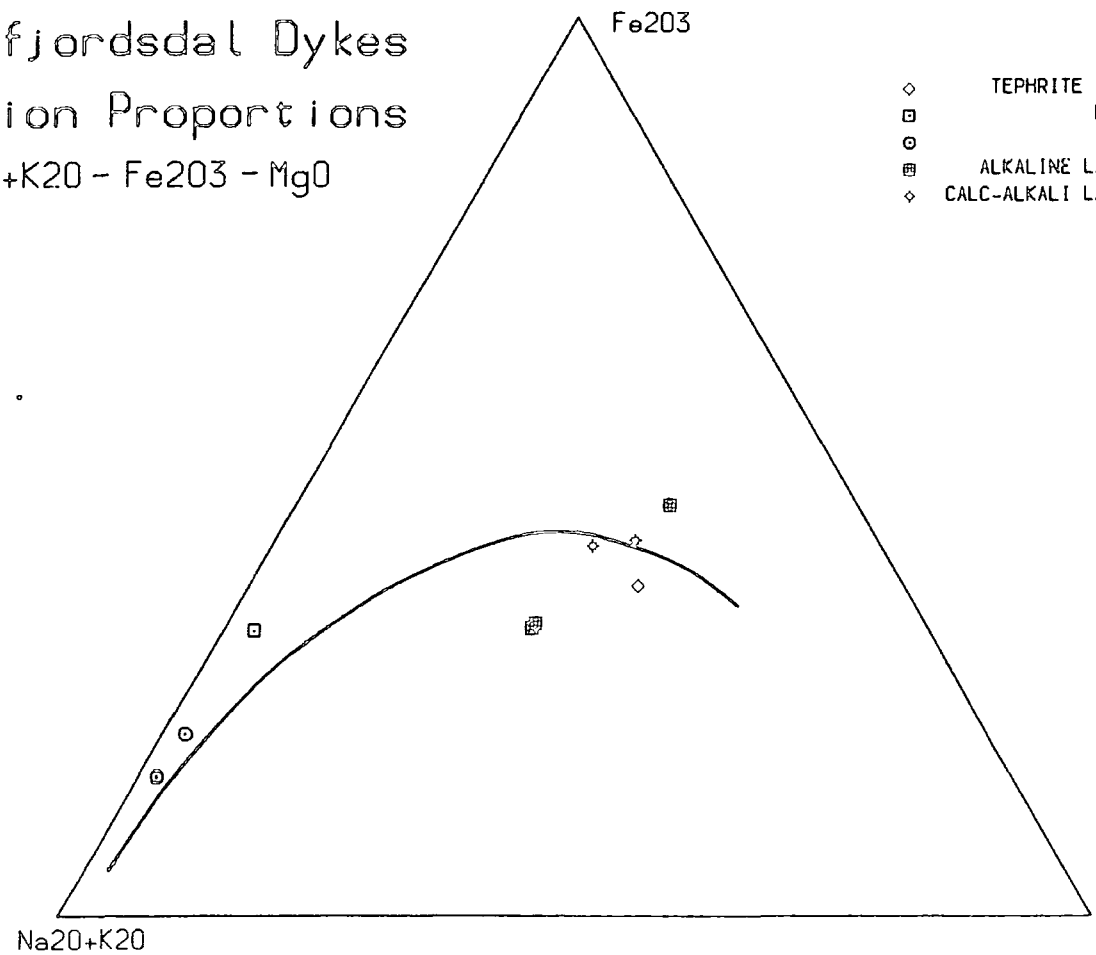

Figure 9.4.2 2 pages.

Incompatible element variation from the Østfjordsdal dykes in terms of:

Nb/Y – Y ppm

La/Nb – Nb ppm

La/Y – La ppm

Nb/Zr – Nb ppm

A. (Facing page). Dykes which cut the Julianehåb Granite.

Marked on these diagrams, where appropriate, are the fields for the main swarm low Zr/Nb dykes (cf. Figure 5.9.2). The Østfjordsdal dykes have a slightly lower Zr/Nb ratio than the main undersaturated swarm, but it is not possible to discriminate between the two swarms by this, or by and other ratio of incompatible elements.

B. (Overleaf). Dykes which cut the Østfjordsdal syenite.

Ostfjordsdal Dykes- Incompatible Elements

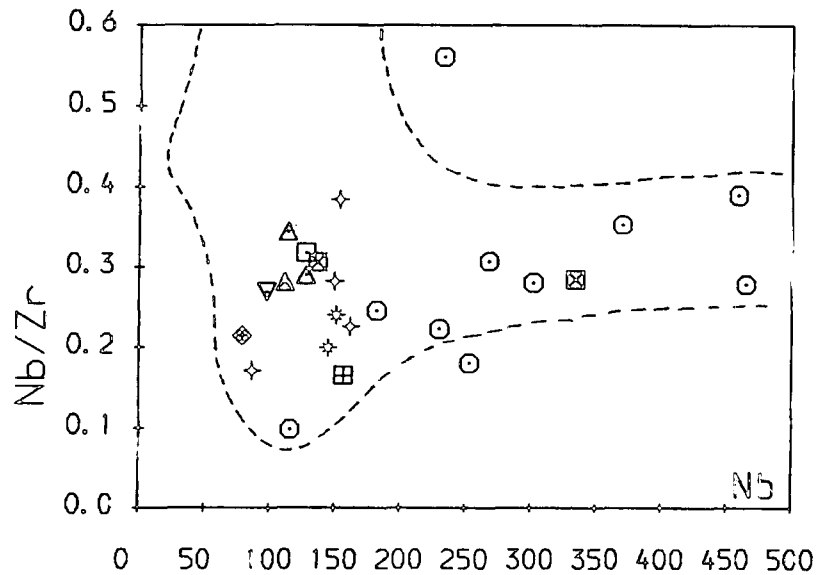

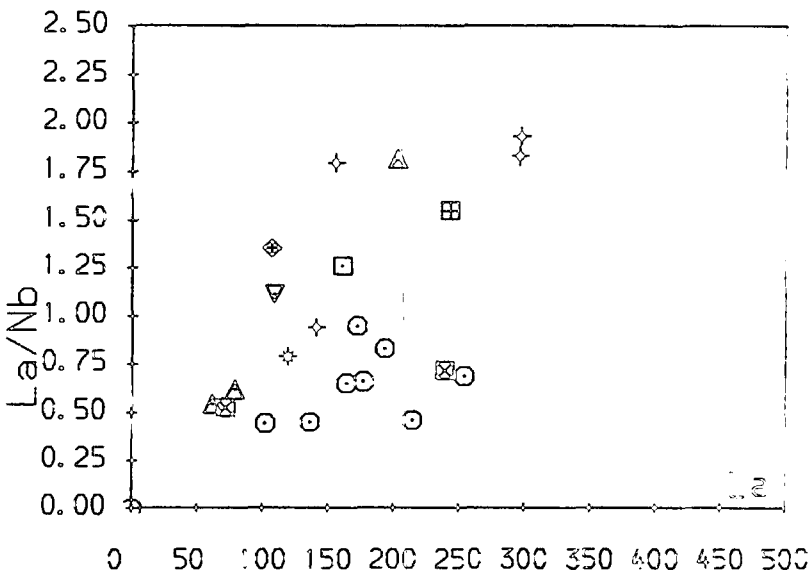

Figure 9.4.2A

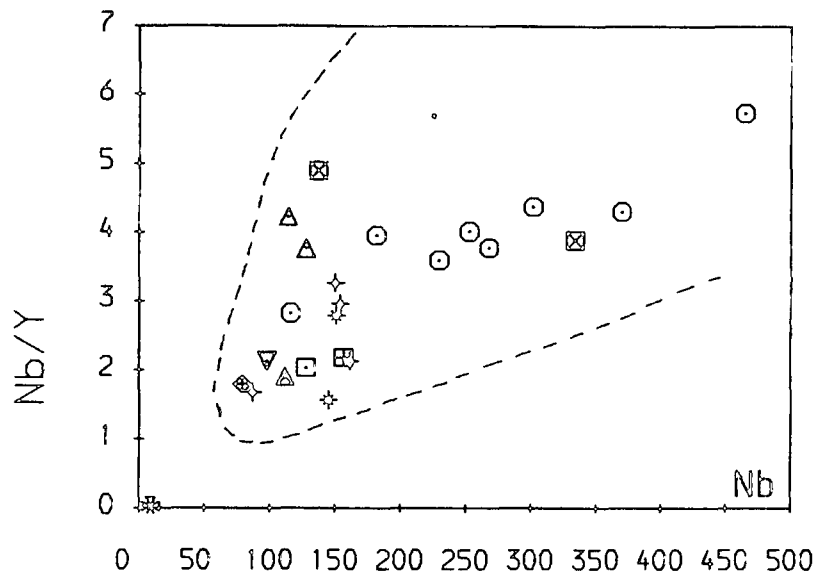

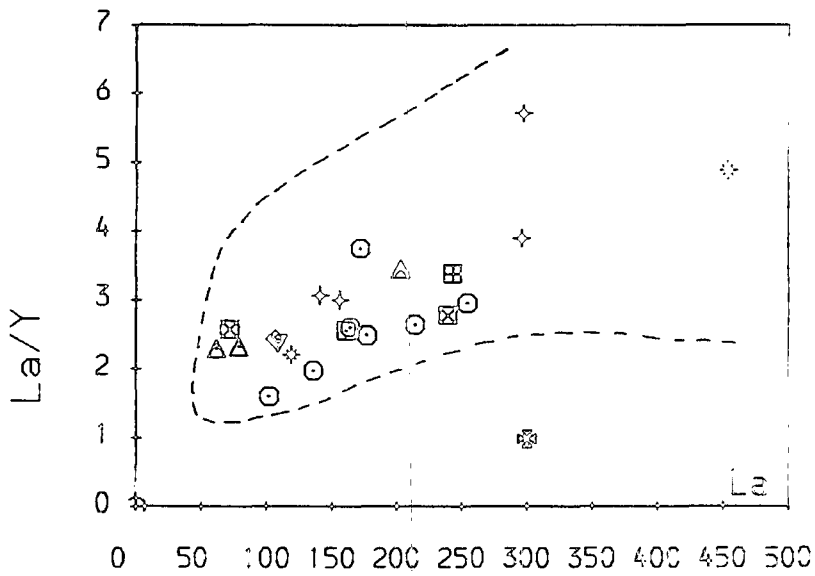

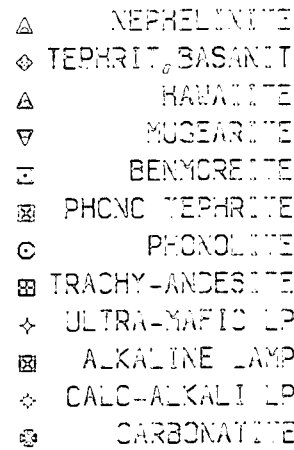

Ostfjordsdal Dykes- Incompatible Elements

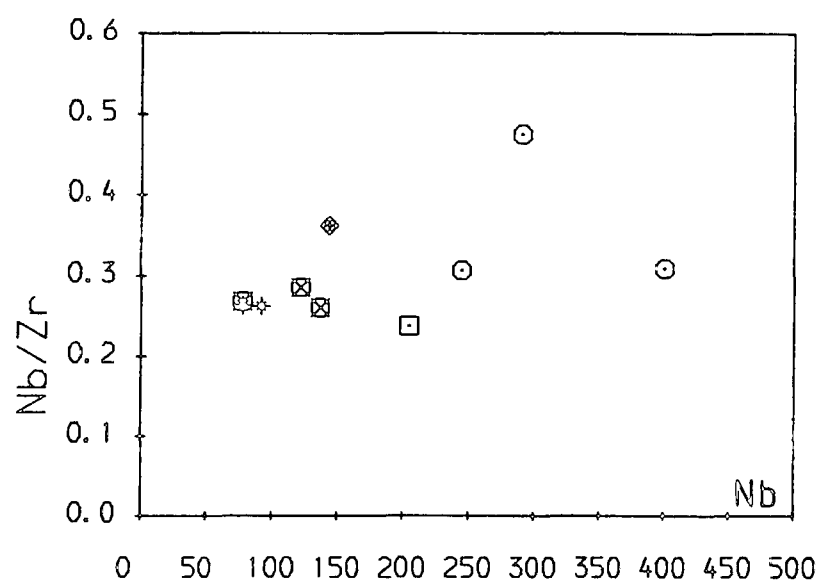

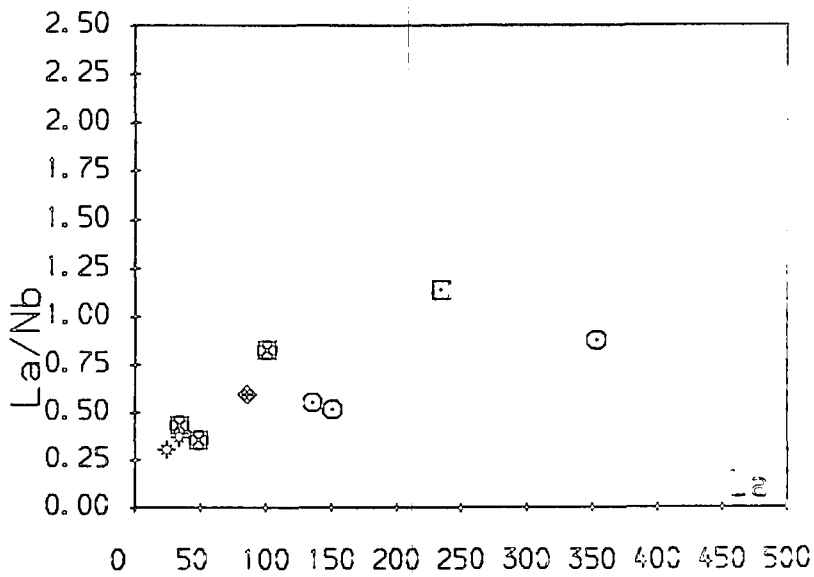

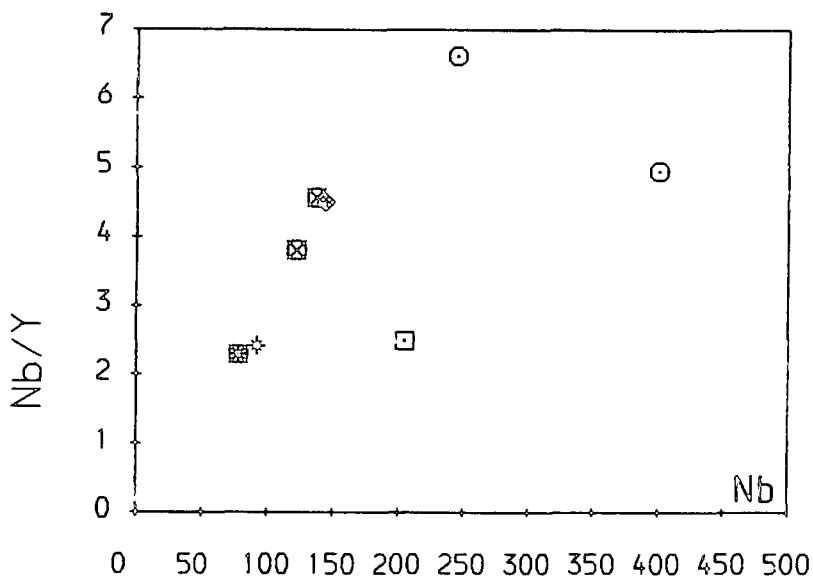

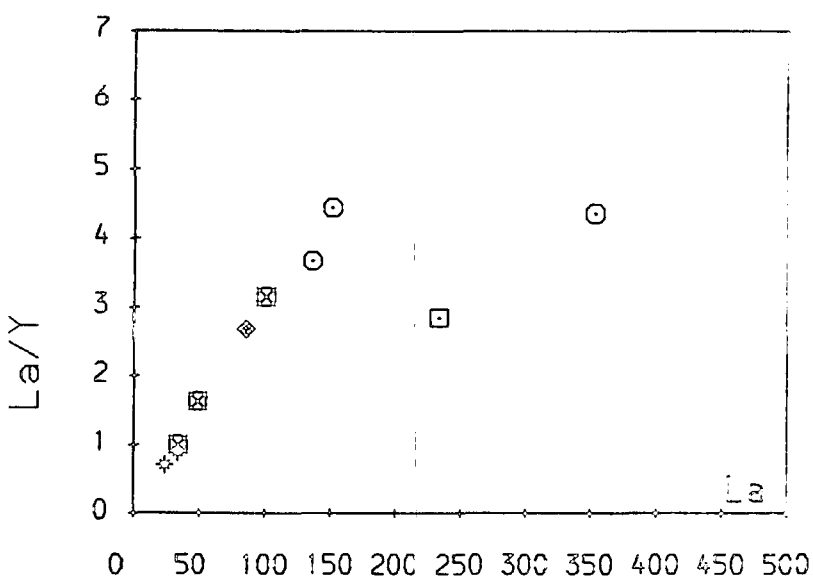

◇ TEPHRIT, BASANIT
⊡ BENMOREITE
⊙ PHONOLITE
⊠ ALKALINE LAMP
✧ CALC-ALKALI LP

Figure 9.4.2

Also shown on Figure 9.4.2 are the fields for the low Zr/Nb, undersaturated main swarm of dykes. The Østfjordsdal dykes plot within these fields and must suggest similar source/genesis etc. In general however, the Østfjordsdal dykes do not achieve such high incompatible element enrichments as the main swarm dykes with the phonolites especially containing comparatively low REE, Nb, Zr, Y, etc. for rocks with such highly fractionated major element chemistries.

REE

Figure 9.4.3 shows REE spidergrams of evolved dykes from Østfjordsdal (5 phonolites and one trachy-andesite by TAS classification). These include recrystallised phonolites and the large porphyritic syenites (326285).

All samples show well developed negative Eu anomalies ranging from $Eu/Eu^* = 0.7$ to 0.31, a result of extensive feldspar fractionation. All samples show relatively flat portions of the spidergrams between Gd and Lu. This flattening will be the result of fractionation of either clinopyroxene or apatite. Low P in these samples may imply that apatite has been lost from the precursors to the phonolites (cf. Chapter 6).

In general the deeper Eu anomalies are associated with samples containing lower REE, Extraction of alkali feldspar ($D_{Eu} = 1.13$, Henderson 1982) will cause the Eu anomaly to become larger as fractionation proceeds, but feldspar fractionation should cause an overall increase in REE. Apatite extraction could cause the reduction in overall REE, and there is a general correlation between P and Ce (ie. lower P, lower Ce).

There are marked similarities between the REE from the Østfjordsdal Dyke Swarm phonolites and phonolites from the main swarm, with steep La-Sm, flatter Gd-Lu and some negative Eu anomalies. In general the Østfjordsdal dykes are slightly less enriched than those of the main swarm, reaching REE contents slightly lower than the Eu-anomaly-free main swarm phonolites. The major difference between the two sets is that the Østfjordsdal phonolites all possess negative Eu anomalies, and this may indicate that they evolved under lower fo_2 than the main swarm dykes, producing higher Eu^{2+}/Eu^{3+} and thus higher D_{Eu}^{Fsp}. The Østfjordsdal phonolites tend to have slightly flatter patterns between Gd and Lu than the main swarm phonolites, and this may reflect more apatite fractionation in the evolution of the Østfjordsdal dykes, which have

Figure 9.4.3

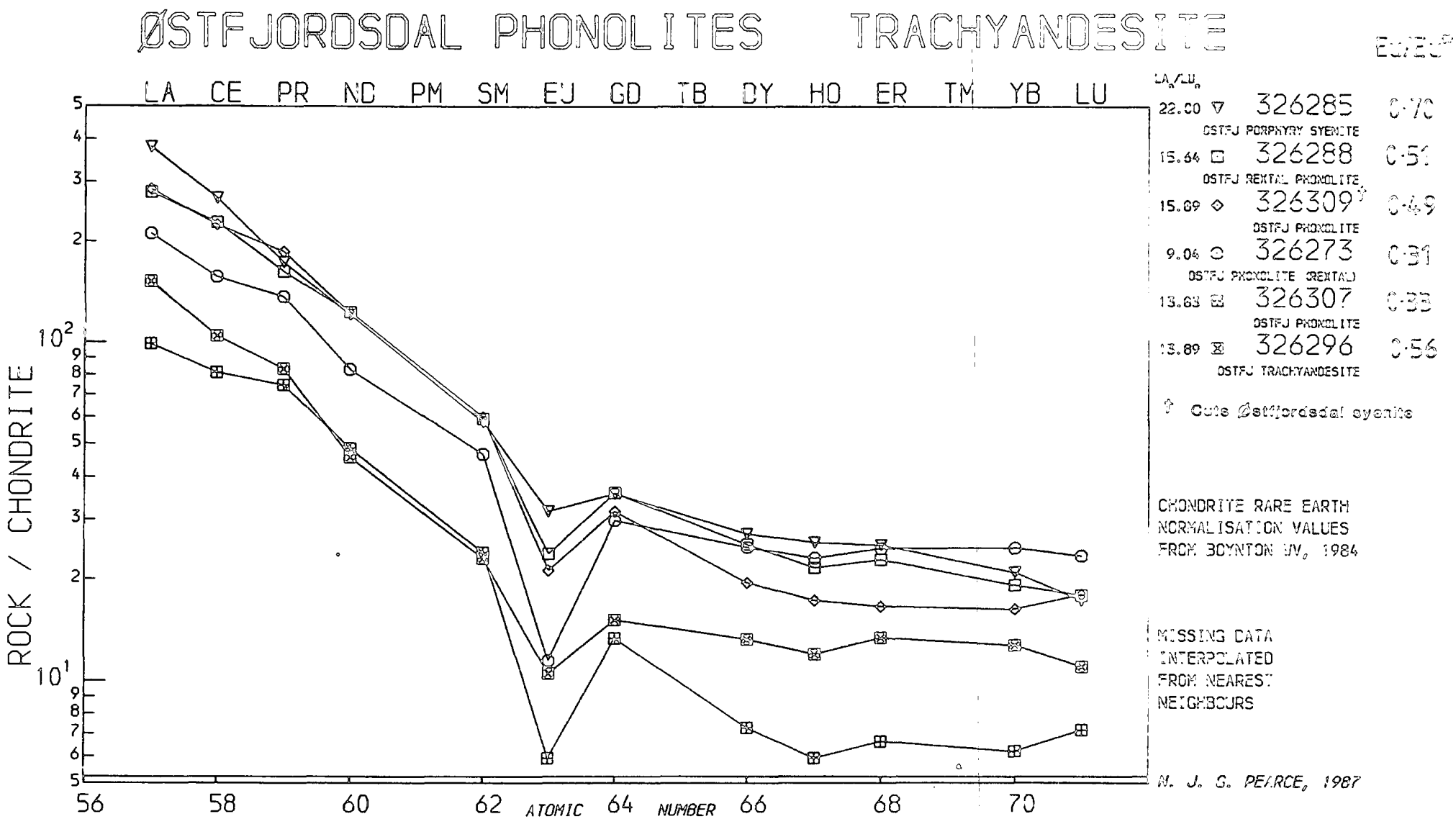
ØSTFJORDSDAL PHONOLITES TRACHYANDESITE
LA CE PR ND PM SM EU GD TB DY HO ER TM YB LU
ROCK / CHONDRITE
ATOMIC NUMBER
22.00 326285 0·70
ØSTFJ PORPHYRY SYENITE
15.64 326288 0·51
ØSTFJ REXTAL PHONOLITE
15.69 326309† 0·49
ØSTFJ PHONOLITE
9.04 326273 0·31
ØSTFJ PHONOLITE (REXTAL)
13.63 326307 0·35
ØSTFJ PHONOLITE
13.89 326296 0·56
ØSTFJ TRACHYANDESITE
† Cuts Østfjordsdal syenite
CHONDRITE RARE EARTH NORMALISATION VALUES FROM BOYNTON WV, 1984
MISSING DATA INTERPOLATED FROM NEAREST NEIGHBOURS
N. J. S. PEARCE, 1987

lower P_2O_5 contents on average (0.05 wt% cf. 0.09 wt%).

Extraction of clinopyroxene (or amphibole) may also be responsible for this flattening of the REE pattern (see Chapter 6). The considerably lower Fe_2O_3 and MgO in the Østfjordsdal phonolites compared to the main swarm phonolites may indicate more ferromagnesian mineral fractionation.

9.5: Conclusions

The Østfjordsdal dykes form a petrographically unique swarm in the Igaliko Nepheline Syenite complex, although geochemically they are almost indistinguishable from the main swarm, undersaturated dykes. The Østfjordsdal swarm includes many phonolite dykes and includes the large (20m wide), porphyritic, nepheline syenite dykes, which pre-date the Østfjordsdal satellitic syenite. This syenite is cut by several AL and CAL but no UML. The UML are similar to many UML which cut granite rafts in the outer units of the Motzfeldt centre. They may be related to these and be very early Gardar, or to the phonolites and porphyritic syenite of the Østfjordsdal Dyke Swarm and be Mid-Gardar. They are almost certainly pre-Østfjordsdal syenite, whereas the AL and CAL are likely to be related to the Late Gardar phase of magmatism. The more evolved, pre-Østfjordsdal syenite dykes, seen to cut several UML (see Figure 2.7.1) are probably either Early or Mid-Gardar.

The overall granular texture of these dykes is a result of thermal metamorphism and recrystallisation which was accompanied by an influx of volatiles, notably CO_2 and Cl (producing cancrinite and sodalite respectively). The heat source (and probable volatile source) is most likely to have been the Igdlerfigssalik central complex, which truncates the swarm to the NW. Recrystallisation may have occurred down to temperatures as low as 250°C.

The large porphyritic nepheline syenite dykes are a continuation of the porphyritic syenites described by Ussing (1912) at Fox Bay and Nuk, Akilaruseq, Igaliko Fjord. These dykes thus persist for some 20km inland from Fox Bay, and are confined (in the area SW of the Østfjordsdal syenite) to a relatively narrow zone.

CHAPTER 10: BIG FELDSPAR DYKES

10.1: Introduction

The Big Feldspar Dykes (BFD) are so called because of their content of large feldspar phenocrysts/xenocrysts. They are thus very easily identified in the field and are relatively common across the Igaliko Nepheline Syenite complex. They tend to occur as wide (10-15m) dykes and often can be traced for many kilometres. A very detailed account of BFD petrography has been given by Bridgwater and Harry (1968) which describes many dykes from the Gardar province. It is not proposed to give a detailed account of the BFD in this chapter, but rather a very broad description of the dykes, some aspects of their chemistry and a discussion of their relationship to the main swarm dykes.

10.2: Petrography

The most characteristic feature of these dykes is their content of large plagioclase crystals and/or anorthosite xenoliths. Throughout the province the plagioclase megacrysts may reach lengths in excess of 50cm and the large anorthosite xenoliths may have surface areas of tens to hundreds of square metres (Bridgwater and Harry 1968). In extreme cases this foreign material may comprise 80% of the volume of the dyke (Bridgwater and Harry 1968).

In the Igaliko area several large BFD's crop out, although the main concentration of BFD (and other basic dykes) in the late Gardar swarm is to the north of Narssarssuaq (cf. Walton 1965). Large plagioclase megacrysts are recorded from the Igaliko BFD's and these may reach 30-40cm in length (see Plate 10.1). Moderate sized anorthosite rafts are also relatively common and these range from granular textured to coarse pegmatitic anorthosite (see Plate 10.2, cf. Bridgwater and Harry 1968). Coarser xenolithic/xenocrystic material tends to become concentrated towards the centre of the BFD's by processes of flow differentiation (see Chapter 2; Komar 1972a,b) although magma chamber stratification may also be responsible for some of the size-grading across a BFD (Bridgwater 1968). BFD's thus often have almost aphyric chilled margins and occasionally show abrupt changes of xenocryst/xenolith content across their width.

The groundmass of the BFD is typically hawaiitic or mugearitic and is composed mostly of plagioclase, clinopyroxene, minor olivine, opaque oxides and rarely biotite. Hawaiite and mugearite petrographies are described in Chapter 3. Many BFD's are altered and their groundmasses have become chloritised and/or sericitised. Some have been recrystallised and abundant biotite is developed in the groundmass (see Plate 10.3). Other than alteration, the groundmasses of these rocks are unremarkable. Obviously their most striking feature is the abundance of included materials. These are usually large plagioclase xenocrysts with compositions typically An_{50-60} (see Plates 10.4-10.8). They may range in size from 50cm to 1-2cm euhedra and many smaller, rather corroded crystal fragments (see Plate 10.4). In many cases these have been altered, either partly or wholly to sericite (see Plates 10.4, 10.7). In some instances the larger plagioclase xenocrysts (eg. Plate 10.1) have altered margins but cores of clear, glassy, unaltered feldspar, with a very pale yellow or greenish-brown hue. In some of these crystals coarse, millimetre scale albite twinning is clearly visible in hand specimen. Some pericline twinning is also rarely developed perpendicular to the albite twins (cf. Bridgwater and Harry 1968).

The anorthosite inclusions contain plagioclase of similar compositions to the xenocrysts. The feldspar is typically converted partly or wholly to sericite, although albite twinning is still evident. The other major mineral is clinopyroxene (20-30% of the mode in some cases, see Plate 10.2), which has been converted to chlorite in many instances. The presence of serpentine may indicate that olivine was originally present in some of these rocks. Accessory minerals include apatite (often 2-3mm in length) and similar sized opaque oxides. Texturally these xenoliths vary from coarse gabbroic (grain sizes 5mm-10mm typically) rocks, to granular textured anorthosites and rarely pegmatitic facies (see Plate 10.2).

In some areas xenoliths of BFD material are found in the syenites (eg. in SI.4 of the Igdlerfigssalik centre), and in microsyenite dykes of the undersaturated swarm (eg. 304150 – see Plate 10.8). These xenoliths are commonly altered and metamorphosed, with prominent large patches of yellow - green epidote developed (see Plates 10.7, 10.8) as well as sericitised feldspar, chlorite etc.

Plate 10.1 BFD. 325901-3. Large and small plagioclase xenocrysts and smaller pieces of granular anorthosite (above left of lens cap) crowd this BFD from near Igaliko village. Note the clear glassy patches at the core of the large feldspar to the right. Lens cap 5cm in diameter.

Plate 10.2 BFD. 325901-3. Coarse grained, pegmatitic anorthosite xenolith in BFD from near Igaliko village. This xenolith is composed principally of plagioclase and interstitial clinopyroxene. The groundmass to the dyke is crowded with small plagioclase xenocrysts. Lens cap 5cm in diameter.

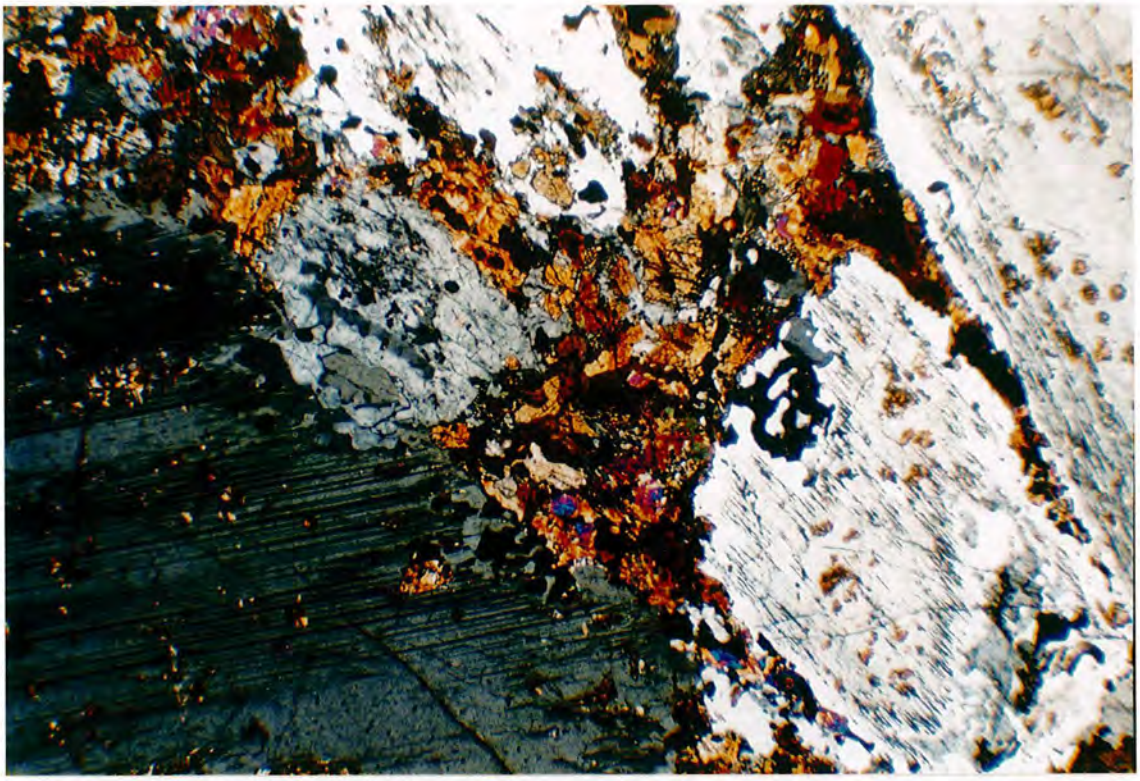

Plate 10.3 63828. BFD. XPL. ×35. This recrystallised BFD is composed of large plagioclase xenocrysts which show faint sieve textures, set in a groundmass of clinopyroxene and biotite mica. Well developed albite twinning is visible in the plagioclase to the left of the picture.

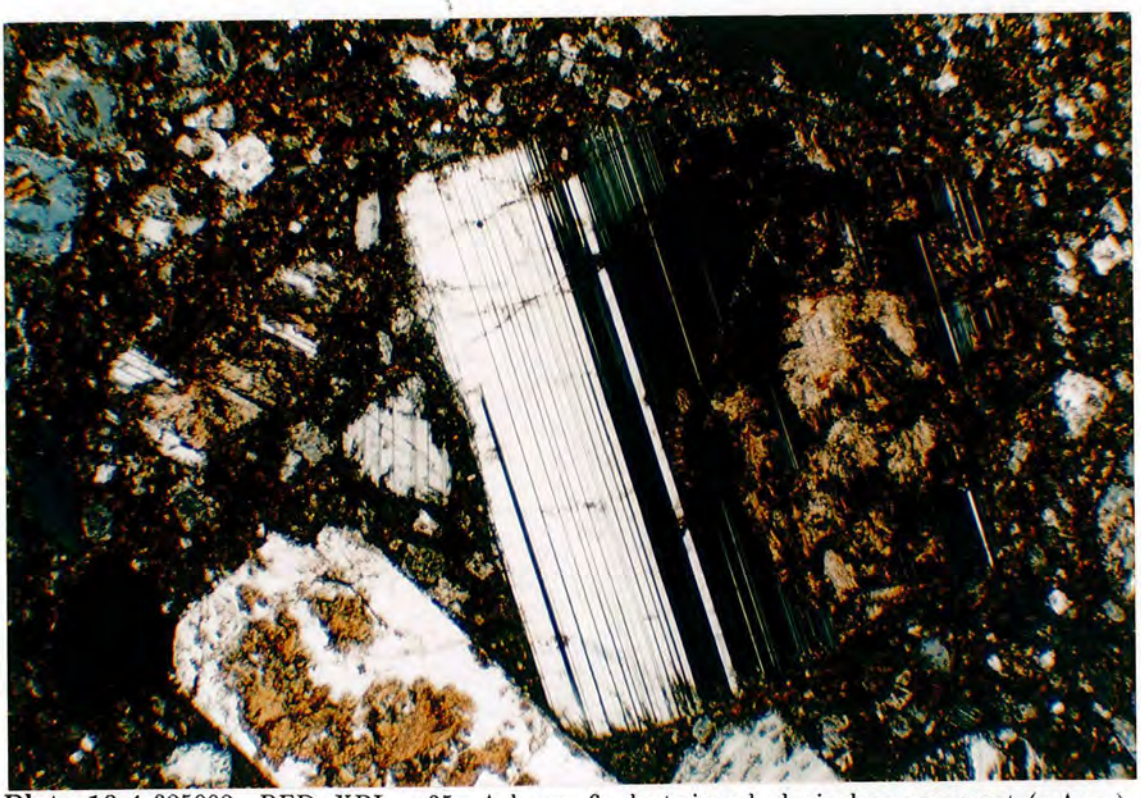

Plate 10.4 325902. BFD. XPL. ×35. A large, finely twinned plagioclase xenocryst ($\approx An_{52}$) occupies the centre of this plate. No compositional zoning is evident. Smaller, granular plagioclases reside in the groundmass, the product of mechanical disaggregation of granular anorthosite xenoliths. Alteration has produced pale brown aggregates of sericite in many feldspars. The groundmass is also highly altered.

Plate 10.5 BFD's. A selection of BFD's showing the range of grain size encountered in the xenocrysts, from relatively fine grained examples (back right) to large, individual crystals (front left and right).

Plate 10.6 325903. BFD. The range of grain size within one sample is clearly seen in this example with xenocrysts ranging from several centimetres to 1-2mm. This will be a result of the mechanical breakdown of granular anorthosite bodies.

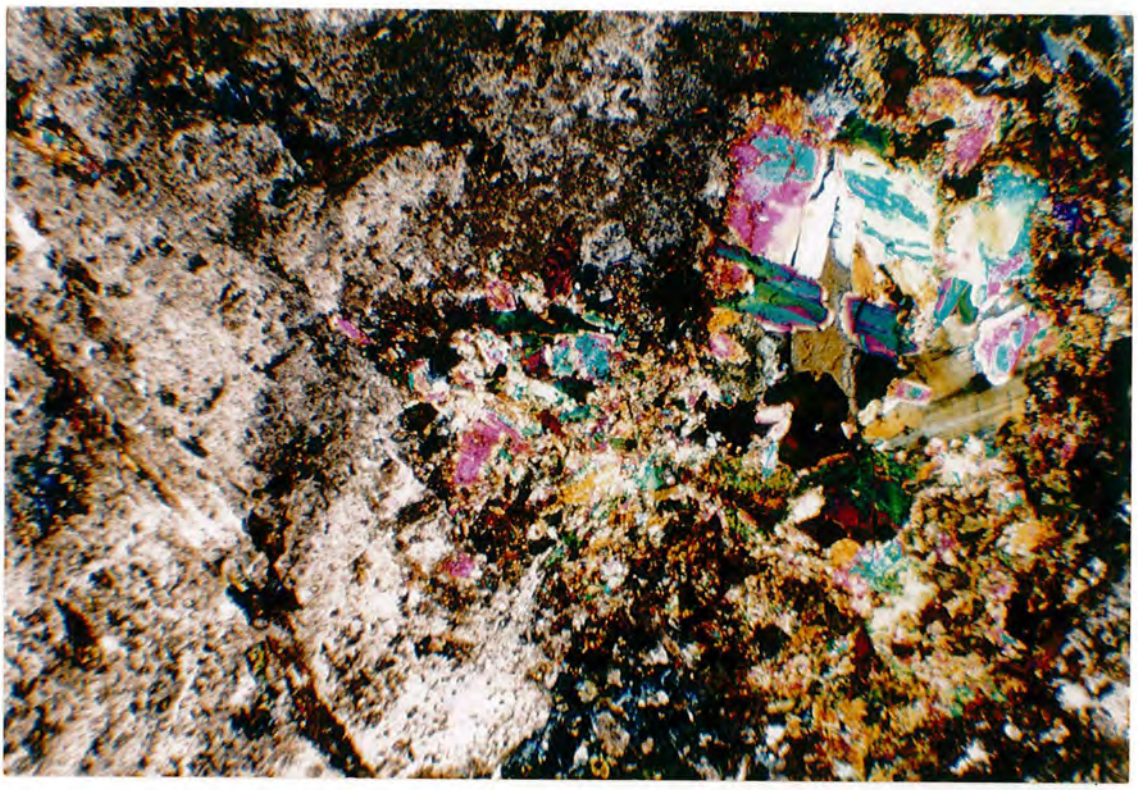

Plate 10.7 326370/304150. BFD. XPL. ×35. This is a highly altered BFD, the result of low grade metamorphism. The plagioclase (left) has been wholly altered to sericite (pale cream brown - dark grey) and large patches of epidote (bright birefringence colours) several millimetres in diameter have developed. The groundmass has been altered to chlorite and sericite.

Plate 10.8 304150. BFD. Hand specimen of the above sample. BFD xenoliths have been entrained in an aphyric microsyenite dyke. Clearly visible in the cut surface are patches of yellow-green epidote and turbid (white) plagioclase xenocrysts set in a dark, altered matrix.

10.3: Geochemistry

The matrix from several BFD's and 3 plagioclase xenocrysts have been analysed for major and trace elements.

The matrix to these BFD's is typically hawaiitic or mugearitic although some benmoreitic and tephritic/basanitic hosts are observed. These are chemically indistinguishable from 'normal' (ie. inclusion-free) dykes of similar composition, whose evolution has been considered in Chapter 5. They may belong to either the oversaturated or undersaturated suite of dykes. 4 BFD matrices were also analysed for their REE contents. Of the inclusions, 3 plagioclase megacrysts were analysed for major and trace elements. These samples had been previously crushed by D. Stephenson and thus their overall 'freshness' was not known. Two plagioclase xenocrysts were cut into thin slabs, broken and hand picked to select clear, glassy feldspar for REE analysis. No anorthosite xenoliths were analysed as those available are all altered. The analyses of the plagioclases are extremely similar for major, trace and RE elements. Their major and trace element contents are presented in Table 10.3.1.

The plagioclase xenocrysts have fairly sodic compositions (labradorites of ca. An_{53}) and will have crystallised from relatively Na-rich magmas. Taking distribution coefficients from Henderson (1982) certain aspects of the parental magma to these xenocrysts can be calculated. This may have been relatively K-rich (3.5 wt%) with Sr at $\approx$1200ppm, Ba$\approx$3700ppm and Rb$\approx$130ppm.

Feldspars of a sodic composition such as this could crystallise from hawaiitic magmas similar to those of the high Zr/Nb suite (see Chapter 5.5, liquidus mineral composition modelling, Nathan and Van Kirk 1978). Hawaiitic magmas of this composition also possess similar contents of Al, K, Mn, Sr and Ga (as calculated above). However, compared to the high Zr/Nb hawaiites, the calculated parent for the plagioclase phenocrysts would have been much richer in Ba and Rb. Tephritic/basanitic magmas could also crystallise a feldspar of similar composition although this would appear on the liquidus after olivine and magnetite. Tephritic/basanitic to hawaiitic magmas would have chemistries very similar to the calculated parent for the plagioclase xenocrysts (for all elements where D^{el}_{plag} is cited in Henderson 1982). The data for U would suggest that

Table 10.3.1

Analyses of plagioclase xenocrysts from BFD's

	58262	58276	58332	Average	Parent*
Major elements wt%					
SiO_2	53.89	53.06	53.43	53.46	—
Al_2O_3	28.94	29.19	28.96	29.03	15.28
Fe_2O_3	0.67	0.74	0.94	0.78	—
MgO	0.25	0.35	0.32	0.31	—
CaO	9.80	10.29	9.86	9.98	—
Na_2O	4.71	4.45	4.42	4.53	—
K_2O	0.46	0.60	0.67	0.58	3.41
TiO_2	0.13	0.14	0.16	0.14	—
MnO	0.01	0.01	0.01	0.01	0.2
F	0.52	0.50	0.42	0.48	—
O≡F	-0.22	-0.21	-0.18	-0.20	—
Total	99.16	99.12	99.02	99.10	—
Trace element ppm					
Ba	792	678	1083	851	3700
Nb	0	0	3	1	—
Zr	132	128	138	133	—
Y	2	2	2	2	—
Sr	2118	2059	2253	2143	1190
Rb	8	14	16	13	130
Zn	17	17	19	18	—
Cu	4	0	1	2	—
Ni	8	3	1	4	—
Pb	1	3	3	2	—
U	10	10	12	11	1222
Th	13	14	14	14	—
V	8	10	13	10	—
Ga	19	20	20	20	20
Atom per cent					
Ca	0.519	0.541	0.528	0.529	—
Na	0.451	0.422	0.429	0.434	—
K	0.030	0.037	0.043	0.037	—

** Parent calculated composition from average distribution coefficients for plagioclase - basalt from Henderson 1982). La, Nd both below detection limits.*

either the analysis or the D^{U}_{plag} is considerably in error.

Microprobe analyses of BFD feldspar xenocrysts reveal a range of compositions from about $An_{60}Ab_{38}Or_0$ to about $An_{20}Ab_{75}Or_5$, although a large number of analyses cluster at around $An_{50}Ab_{45}Or_5$ (see Figure 4.8.3A). The crystals show very little zoning (see Figure 4.8.4) with core - rim variation of only 1-2 mol% of any end member. This lack of zoning is a remarkable feature of many plagioclase megacrysts from such anorthositic bodies (Philpotts 1981) and poses certain petrogenetic problems. For such large, unzoned crystals to form either, (i) magma volumes must have been immense for removal of plagioclase to have had no effect upon the residual liquid composition or (ii) equilibration must have erased any zoning. However, this would require billions of years using known diffusion coefficients. Philpotts (1981) proposes a model involving liquid immiscibility in the genesis of these anorthosite bodies. In this he suggests an Fe-rich silicate liquid separates immiscibly from an andesitic parent magma. This Fe-rich liquid removes Na and Si and effectively buffers the composition of plagioclase crystallising from the 'andesite' liquid. This could be responsible for the constancy of plagioclase compositions.

REE

Figure 10.3.1 show REE spectra of 4 BFD hosts and 2 plagioclase xenocrysts. The xenocrysts show LREE enrichment and strong positive Eu anomalies (Eu/Eu^*=17.23 and 18.55, $(La/Lu)_{cn}$=31.22 and 56.96). The marked Ho anomaly will be the result of inaccuracies in analytical correction procedures at such low concentrations (Walsh *et al.* 1981). Taking an average of the REE for both feldspars and using the basalt - plagioclase distribution coefficients of Henderson (1982, 1984), REE profiles for the parent liquid to these xenocrysts can be calculated. These are shown for the maximum, average and minimum values of D^{REE}_{plag} cited. The average D^{REE} would suggest that the parent magma had La_{cn} of ≈57, Lu_{cn} ≈2.5 and $(La/Lu)_{cn}$ ≈22.8, with the maximum and minimum D^{REE} giving lower and higher overall REE contents respectively. The D^{Eu} data would also suggest that the parental liquid was Eu enriched. If this is the case it would point to an origin which involved melting of a feldspar-rich source, or metasomatic enrichment of the source region in Eu. Isotopic evidence from Martin (1985) suggests that the BFD xenoliths crystallised from magmas derived from a source very similar

Figure 10.3.1

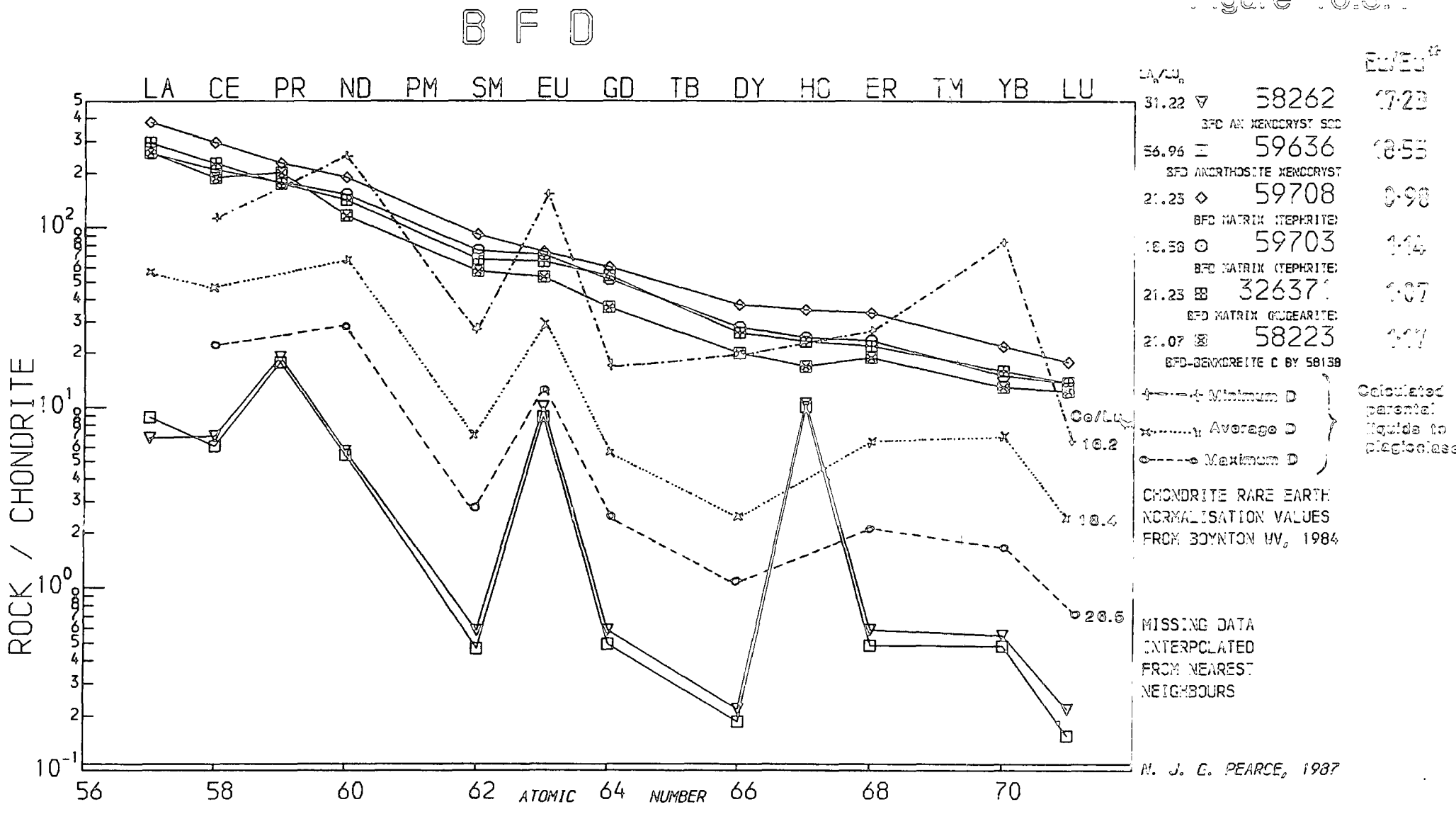
B F D
LA CE PR ND PM SM EU GD TB DY HO ER TM YB LU
ROCK / CHONDRITE
ATOMIC NUMBER
56 58 60 62 64 66 68 70
Ce/Lu
16.2
18.4
20.6
Minimum D
Average D
Maximum D
CHONDRITE RARE EARTH NORMALISATION VALUES FROM BOYNTON WV, 1984
MISSING DATA INTERPOLATED FROM NEAREST NEIGHBOURS
N. J. G. PEARCE, 1987

to the YGDC magmas and were uncontaminated (ie. no crustal assimilation). This may militate against melting of a feldspar-rich crustal component (such as a granulite, cf. Thomas and Nixon 1987) which could also cause Eu enrichment. Enrichment in the source region in Eu alone relative to other REE may seem unlikely, and thus the D^{Eu}_{plag} given by Henderson (1982) appear not to apply to these feldspars.

The host rocks to these xenoliths show no negative Eu anomalies. This is not an effect of cancelling out a negative Eu anomaly by including some Eu-enriched xenocrystic material in the analysis: all these samples were free from plagioclase xenocrysts. The lack of a negative Eu anomaly suggests that these host samples could not have fractionated substantial amounts of plagioclase. Other chemical features (Sr, Ba, Rb. total REE) also suggest that there is no genetic relationship between the host dykes and their inclusions.

The xenocryst REE contents would also suggest that they crystallised from some type of alkali basaltic magma (LREE enriched, Cullers and Graf 1984). Bridgwater and Harry (1968) noted that more basic plagioclases occurred in the less evolved hosts and this led them to conclude a genetic relationship between the xenoliths/xenocrysts and their host rocks. Bridgwater (1967) however, pointed out that density equilibration in a stratified magma chamber may also account for the compositional relationship between host and inclusions, more basic (and thus denser) hosts being able to suspend denser (more Ca-rich) feldspars (cf. Bridgwater and Harry 1968).

10.4: Anorthosites – General Statement

Massif type anorthosites are mostly confined to Mid-Proterozoic times, with most examples dating from 1.8-1.1Ga and many clustering at around 1.4Ga. They are generally intrusive bodies of immense proportions. They may form as flotation cumulates (cf. granular anorthosites of the Gardar province, Bridgwater 1967) and are typically composed of relatively unzoned plagioclase. Many large anorthosite bodies crop out in Labrador and these would appear to be related to the massif anorthosites which underlie the Gardar province (Bridgwater 1967). Anorthosites of this type are thought to form in a broad belt from Canada (Labrador), through (under) South Greenland and across into Scandinavia, which were all part of one continent in Gardar times (Bridgwater

1967, Piper 1982). Morse (1977) contends that 'massif anorthosites are the products of aborted continental rifts' and are restricted to such rift zones. He argued that Proterozoic rifting was confined to 1.2-1.8Ga. For the anorthosites of the Nain area Morse (1977) considered many magmas were involved rather than a single pulse, with relatively high Fe, high Al, low K basaltic parentage, and that these were emplaced at depths of between 13-22km.

Emslie (1977) also considers that the North American anorthosites were emplaced at the beginning of mantle activity which eventually matured into continental rifting. Magmas parental to these occurrences were thought to have been tholeiitic in character and possibly evolved from olivine tholeiites. Weibe (1980) defended the idea of high Al basalts being parental to anorthosite magmas.

Fractionation of plagioclase may cause an increase in the peralkalinity of a magma by increasing Na and K whilst reducing Al in the residual liquids ('the plagioclase effect', Bowen 1945). This forces the residual liquid onto an alkaline trend and has been widely proposed as a method of generating alkaline magmas (eg. Bailey and Schairer 1966). The presence of large quantities of anorthosite xenoliths and labradorite xenocrysts entrained in Gardar magmas makes this an appealing process. This however forces a genetic link between the anorthosite xenoliths and the undersaturated and/or oversaturated Gardar magmas, which may not exist.

10.5: Conclusions

Anorthosite xenoliths and plagioclase megacrysts occur in rocks of all compositions (from gabbros to nepheline syenites) throughout Gardar time (plagioclase megacrysts seen in the Motzfeldt syenites, xenoliths and xenocrysts of both types in Late Gardar dykes). There is however a complete lack of BFD's in the Østfjordsdal area, although Berrange (1966) reports some xenocrystic material from a dyke in the Vatnahverfi area on the south shore of Igaliko Fjord. This in itself may hint at a different origin for the Østfjordsdal Dyke Swarm compared to the main swarm dykes.

Geochemical evidence from the plagioclase xenocrysts suggests that they could not have crystallised directly from their present host magmas, nor could they have crystallised from any other basic magmas represented by intrusions in the Igaliko area

(including Giant Dykes and BD_0). The parental magmas to these xenocrysts may have had Sr at ≈1200ppm, Ba at 3700ppm and K_2O at ≈3.5 wt%. They may have been hawaiitic or even mugearitic in composition, with $(La/Lu)_{cn}$ at about 17. The parental magmas were therefore LREE enriched with La_{cn} of perhaps 50-60. These parental magmas (assuming that they had fractionated to intermediate compositions, cf. Emslie 1977) would have been LREE enriched (La_{cn} ≈40?, $(La/Lu)_{cn}$ ≈13-15?) and would have been the products of considerably more partial melting from a twice-chondrite garnet-lherzolite mantle source than either the undersaturated or oversaturated suites of the Igaliko area (with lower La and La/Lu). The parental material may have been similar to magmas which formed the Keweenawan, Seal Lake and Coppermine Bay flood basalts which, although being tholeiitic in character, were relatively rich in large ion lithophile elements, sometimes verging to alkaline compositions (Baragar 1977).

Martin (1985) concluded that there was no genetic link between the anorthosite inclusions found in the YGDC and their host magmas. This too was the conclusion of Upton and Thomas (1980) and Blaxland and Upton (1978). Martin (1985) did however conclude that the parent magmas to the anorthosites came from an isotopically similar source to the YGDC magmas.

The massif anorthosite bodies that must underlie the Gardar province probably formed before the onset of Gardar magmatic activity. These large intrusive bodies will have been continually disrupted by various magmatic events throughout Gardar times, resulting in the removal of xenoliths and xenocrysts. The compositional relationship between host and inclusions observed by Bridgwater and Harry (1968) may be a result of density equilibration, with less dense (more Na-rich) feldspars being suspended by more evolved (less basic) magmas (cf. Upton and Emeleus 1987).

The massif type anorthosites may have deveolped at the onset of Gardar (or even pre-Gardar) rifting, a result of plate motion between the North American and Grenville plates. These may have formed at more or less the same time as many North American anorthosites (1400-1260Ma for Labrador intrusions, Collerson 1982). Dykes from the Nain province, dating from 1450-1040Ma, of Fe-rich troctolitic compositions and have alkaline to transitional normative characteristics (Weibe 1985). There are thus clear (compositional and temporal) relationships between the magmatism in Labrador and

South Greenland, and anorthosite magmatic activity was probably related to pre- to Early Gardar plate movements in this general area (see Chapter 2, cf. Morse 1977).

CHAPTER 11: CONCLUSIONS

11.1: Introduction

This chapter essentially reiterates the conclusions reached in the previous chapters and draws them together in a petrogenetic scheme for the dyke swarm. This involves integrating the structural, petrological, mineralogical and geochemical data into a framework applicable to the component dyke swarms seen in the Igaliko Nepheline Syenite complex.

11.2: Component Dyke Swarms

There is clear evidence in the Igaliko Nepheline Syenite complex for 3 distinct dyke swarms (i,ii,iii), with several more minor occurrences (iv, v, vi). These are:

(i) a major Si-oversaturated swarm related to the Tugtutôq - Ilímaussaq - Nunataq zone of dykes of Late Gardar age,

(ii) a major Si-undersaturated swarm related to the central complex activity in the Igaliko area, of Late Gardar age,

(iii) a smaller Si-undersaturated swarm which pre-dates the Østfjordsdal syenite, cropping out from Fox Bay on Igaliko Fjord to NE of the Østfjordsdal syenite (the Østfjordsdal Dyke Swarm), possibly of Mid-Gardar age,

(iv) a large, gabbroic dyke (possibly BD_0) cropping out in Mellemlandet which is truncated by the Early Gardar Motzfeldt centre,

(v) early UML dykes seen in granite rafts in the Motzfeldt centre,

(vi) trachytic dykes cut by porphyritic syenite sheets in the Motzfeldt centre.

There is no apparent difference in orienation between the Si-oversaturated swarm and the main Si-undersaturated swarm (both approximately 053° as the major direction). The Østfjordsdal swarm however strikes at about 043°, and this reflects different tectonic stresses operative during its emplacement.

Crustal dilation due to dykes varies across the region from about 3% in the Østfjords-

dal and Igaliko village areas, to nearly 10% in the region north of Narssarssuaq, where there is the greatest concentration of basic dykes. One 'Giant Dyke', related to the YGDC (Upton and Fitton 1985) crops out to the north of the complex in Mellemlandet. Extensions across Giant Dykes of up to 25% have been recorded from Tugtutôq (see Upton and Fitton 1985). No Giant Dykes occur in any of the measured traverses from the Igaliko Nepheline Syenite complex.

Minor differences in the orientation of the larger giant dykes and the smaller ones of more evolved compositions were observed (Upton and Fitton 1985) and are of the order of a few degrees. The geometry of these dykes varies, with the giant dykes being predominantly *left stepping* whereas the majority of the smaller dykes appear to have a *right stepping* geometry (see Chapter 2.9). It is proposed that a right stepping geometry would be favoured by simple sinistral shear, whereas the left stepping geometry would need the shear zone to undergo transtensional extension to develop.

The size of these giant dykes attests to a vigorous extension regime. The Tugtutôq - Ilímaussaq - Nunataq zone is probably the only area of the Gardar province where major graben structures developed and is a localised zone of major crustal extension.

Emplacement Mechanisms

The dykes in the Igaliko Nepheline Syenite complex were emplaced as arrays of echelon cracks formed in a sinistral shearing environment. Fractures propagated into the country rock as near vertical sheets growing both vertically and horizontally from the magma source. Individual fractures were separated by *bridges* of country rock which bent and eventually fractured leaving steps or *offsets* in the dyke margins. Once the bridge has broken, dilation proceeds more rapidly (Nicholson and Pollard 1985). Rarely, where crack tips interfered, curved propagation paths developed. These produce rotation of the intervening bridge. In general, dykes were emplaced along straight propagation paths. The overall geometry of the dykes on both a large, regional scale and on a small, individual scale can be related to the overall tectonic regime operative at the time of their emplacement.

11.3: Chemical Evolution

Dykes cropping out in and around the Igaliko Nepheline Syenite complex cover a very wide range of composition. More normal rock types range from tephrite/basanite and basalt, via benmoreite to either phonolite or rhyolite, these being the residual products of the undersaturated and oversaturated magmas respectively. In addition minor occurrences of carbonatite and lamprophyre are seen across most of the region and are associated with the Si-undersaturated volcanism.

The oversaturated and undersaturated suites can be distinguished by their Zr/Nb ratios. Those rocks that evolve to phonolites have a Zr/Nb ratio of about 3.9, whilst those evolving to quartz-trachytes and rhyolites have a Zr/Nb ratio of about 6.4 with a minima separating the two groups at about 5.2. The division between the two swarms on this basis is extremely good with only a few undersaturated rocks being included with the oversaturated suite and *vice versa.*

Dykes from the Si-undersaturated Østfjordsdal Dyke Swarm have Zr/Nb ratios around 3.5 and are chemically very similar to the main undersaturated dyke swarm.

The high Zr/Nb, oversaturated suite is part of the more major, Tugtutôq - Ilímaussaq - Nunataq dyke swarm (cf. Upton and Fitton 1985) cropping out in the region. They show a pronounced basaltic and benmoreitic/trachytic rock types with a marked 'Daly Gap'. The low Zr/Nb, undersaturated main swarm of dykes (excluding carbonatites and lamprophyres) are mostly benmoreites and phonolites, with very few samples of F.I.<65 (MacDonald 1969). These rocks are compositionally extremely similar to the augite syenites/nepheline syenites of the Igaliko central complexes, particularly South Qôroq (Stephenson 1973) and are clearly related to this Late Gardar activity.

The basaltic and tephritic rocks of both the low and high Zr/Nb suites are generally low in Mg, Ni and Cr. They have low *mg* numbers and high Al_2O_3/CaO ratios (see Table 11.3.1).

The general Fe-rich nature of these rocks is regarded as a result of fractional crystallisation from a more basic parent by extraction of both olivine and clinopyroxene at depth (see Upton and Emeleus 1987). This would also reduce Ni and Cr as well as Mg.

Table 11.3.1

Major element ratios of average basic rocks from the Igaliko Dyke Swarm.

	Low Zr/Nb		High Zr/Nb	
	Teph	Basalt	Teph	Basalt
Al_2O_3/CaO	1.50	1.87	1.93	2.16
MgO wt%	6.90	7.38	5.09	5.33
Fe_2O_3 tot.	15.35	14.40	15.35	14.59
mg number*	0.287	0.315	0.229	0.249
Ni	20	52	141	54
Cr	15	43	171	164

* *mg number, calculated as* $Mg/Mg+Fe^{2+}$ *atomic with* $Fe_2O_3/FeO=0.15$

Extraction of clinopyroxene would also result in an increase of the Al_2O_3/CaO ratio whereas plagioclase fractionation would not. A general increase in Sr with fractionation in the basic rocks and the lack of a negative Eu anomaly also suggests that plagioclase was not an early fractionating phase.

Similar basaltic compositions could be generated from an abnormally Fe-rich mantle source region with high garnet/clinopyroxene or spinel/clinopyroxene ratios to produce such Mg-poor, high Al_2O_3/CaO magmas (see Upton and Emeleus 1987). However, a model involving deep/sub-crustal fractionation of parental magmas to produce the basaltic magmas seen is favoured.

From these basic compositions each suite can be shown to evolve by fractional crystallisation. There are general similarities in the fractionating assemblages for both low and high Zr/Nb suites, involving opaque, Fe-Ti oxides, olivine, clinopyroxene and feldspar, with olivine and pyroxene becoming less important as evolution of the magmas proceeds (see Chapters 5.5 and 5.6).

Assuming that basalt is the parent for the high Zr/Nb, oversaturated suite, the rhyolitic rocks represent a residue of about 4% of the original basalt. For the low Zr/Nb, undersaturated suite of rocks, the phonolite represents a residue of about 20% from a basaltic parent or 18.5% from a tephritic parent. These figures are in close agreement with the enrichments achieved in some trace elements (eg. Zr, Nb).

The trace element data for the oversaturated suite is tightly constrained, plotting in a narrow field (see Figures 5.7.1, 5.7.2, 5.7.3). The undersaturated data however, show considerably more scatter. This scatter is a reflection of many individual liquid lines of descent (cf. Cox 1967) with individual, small batches of magma evolving slightly differently. This will cause slightly different behaviour of certain trace elements, and cause the large scatter of data. Individual batches of magma may be pulses injected to high levels, for example, into the central complexes, where they may evolve slightly differently from the magmas retained at depth (different P-T-X conditions etc.).

Magnetite (Ti-rich) crystallisation may be important in the evolution from hawaiite to benmoreite. Extraction of magnetite could cause a rapid increase in SiO_2 in the residual liquid and may account for the 'Daly Gap' apparent in the oversaturated suite (cf. Clague 1978, Martin 1985). Incompatible element spidergrams would suggest that a Ti-rich phase (magnetite) has not been removed from the hawaiitic magma, but fractionation of this has occurred in magmas which evolved to mugearite.

Apatite fractionation appears to start between mugearitic and benmoreitic compositions, continuing through to phonolites and rhyolites producing very low P_2O_5 in the most evolved rocks.

Major differences are noticable between the basic rocks from the oversaturated and undersaturated groups of rocks. Most obvious are a positive anomaly at P and a negative anomaly at Nb in the oversaturated (high Zr/Nb) suite which are not seen in the undersaturated, basic rocks. Thompson *et al.* (1983) consider negative Nb anomalies to be a result of assimilation of Nb-poor crustal rocks in the genesis of the Tertiary lavas of NW Britain. However, this process would not cause an increase in P (cf. Upton *et al.* 1985, Martin 1985, Upton and Emeleus 1987) and should also cause an increase in the initial $^{87}Sr/^{86}Sr$ isotopic ratio, which is not seen in Gardar rocks (Blaxland *et al* 1978, Martin 1985). Most Gardar rocks have Sr-isotopic ratios typical of mantle derived melts and there can be little doubt as to their mantle origins. Apatite-rich mantle xenoliths have been reported (Exley 1982) and magmas derived from these could be enriched in P.

Basic rocks of the undersaturated (low Zr/Nb) suite show no marked anomalies,

having very smooth incompatible element spidergrams enriched in LILE. These undersaturated basic rocks resemble ocean island basalts (OIB) whereas the oversaturated suite has chemical characteristics similar to continental flood basalts (CFB, cf. Thompson *et al.* 1984). The undersaturated rocks would thus appear to be melts of a fertile, asthenospheric source whereas the oversaturated samples may have involved melting of continental lithosphere (as opposed to contamination by continental crustal material).

Normative mineralogy for the basic rocks suggests that the undersaturated rocks were produced from a mantle source region containing CO_2, whereas the oversaturated rocks may have been formed by melting in the presence of H_2O (Thompson 1984). The presence of H_2O in a mantle source region may stabilise a Nb bearing phase (Saunders *et al.* 1980,Saunders and Tarney 1984) and thus cause the depletion in Nb seen in the high Zr/Nb basic rocks (negative Nb anomaly).

Rocks of both suites are typically rich in F and Cl, with F>Cl in most cases. F/Cl ratios in the basic rocks are typically around 2 and rise to nearly 10 in some evolved compositions. Melting may have been accompanied or initiated by an influx of volatiles caused by continental rifting (cf. Upton and Emeleus 1987). In general, the oversaturated suite is slightly poorer in F and Cl than the undersaturated suite.

Melting modelling has been conducted in an attempt to generate melts of the observed basaltic compositions. This also involved a consideration of early fractional crystallisation (of clinopyroxene and olivine to generate observed Ni, Cr and Rb). The oversaturated rocks, which have high contents of HREE appear to be the products of a spinel-bearing mantle source region, whereas the undersaturated rocks can only be modelled by generation from a garnet-bearing mantle source. The oversaturated rocks also appear to be the products of larger degrees of melting than the undersaturated suite from both REE and Zr/Nb modelling (2-3% cf. 0.5-1%). In both cases however it is necessary to invoke some source region enrichment in the LILE (eg. Rb, LREE) whilst the HREE remain at a primitive, twice-chondrite concentration (Frey *et al.* 1978).

For the undersaturated suite, LREE contents in the source would need to be elevated to $\approx 2.5 - 3\times$ chondrite, for the oversaturated rocks source LREE may be about $3\times$ chondrite and Rb about $4\times$ chondrite. Metasomatism, required to achieve

the LREE enrichment may be a result of the passage or emplacement of kimberlitic/basanitic magmas through the source region of these basalts prior to the melting event (cf. Hawkesworth *et al.* 1984, Menzies *et al.* 1987, see later).

11.4: Mineralogical Evolution

The mineral chemistry essentially reflects the chemical evolution of the magmas with the most basic (Mg-rich, Si-poor) pyroxenes and amphiboles occurring in the most basic magmas, grading through to more Mg-poor, Fe and Si-rich compositions in the more evolved rocks. Zr, highly soluble in peralkaline magmas (Watson 1979), is incorporated into late stage, interstitial amphiboles and pyroxenes in the evolved rocks such as some benmoreites and phonolites.

Aegirine-augite Zr contents reach levels similar to those reported by Jones and Peckett (1980). ZrO_2 in amphiboles reaches 4.13 wt% ZrO_2 from sample 325986, which represents 33% of the newly defined end member zirconian-arfvedsonite ($Na_3(Fe^{2+},Mg)_4ZrSi_7AlO_{22}(OH)_2$). This crystallises from highly peralkaline (per-sodic), Ti and Al-poor interstitial liquids, residual from solidification of the rock and enriched in Zr (and presumably many other incompatible elements). Zr enters the amphibole structure in a coupled substitution:

$$Zr_C^{4+} + Al_T^{3+} \rightleftharpoons Si_T^{4+} + Fe_C^{3+}$$

The Ca content of olivine reflects its hosts overall a_{SiO_2}. Distinct trends are observed from the oversaturated and undersaturated suites with olivines from nepheline normative dykes having higher Ca contents. Mn becomes very enriched in olivines in the phonolites ≈16 mol% Tp) and carbonatites (≈20 mol%Tp). In the undersaturated benmoreites and phonolites in particular, olivine is often corroded to rims of opaque oxide. This implies that the fo_2 had risen above the QMF synthetic buffer by this stage of magmatic evolution. Higher fo_2 in the undersaturated rocks is also implied by the pyroxene evolution, with alkali-enrichment in these undersaturated examples starting at higher Mg/Fe ratios than in the oversaturated rocks which evolve towards hedenbergite before significant alkali enrichment. Sphene, as reaction rims to opaque oxides, also indicates high fo_2 (Carmichael and Nicholls 1969) with fo_2 increasing from benmoreites into phonolites.

Mineral - mineral geothermometry indicated liquidus temperatures in the range of 1050°C for basic rocks to 1020°C for phonolites (from olivine - clinopyroxene compositions, Powell and Powell 1978) and solidus temperatures of about 800°C for phonolites (from nepheline - alkali feldspar compositions, Powell and Powell 1977). This, and the geothermometer of Hamilton (1961) for nephelines, suggests that little sub-solidus reequilibration at low temperatures occurred. This is supported by structural data from the alkali feldspars which, in several cases, maintain fully disordered, high temperature crystal structures. In one case (58003) no exsolution textures are recorded (on a scale resolvable by X-rays). This must attest to extremely rapid cooling and to the stability of the South Greenland region since Gardar times, with not even slight heating/metamorphism having occurred in the area since about 1120Ma.

11.5: Significance of Carbonatites

Many sövite dykes are seen in the Igaliko Nepheline Syenite complex. In contrast only one example is recorded by Martin (1985) from the north-eastern end of the Ilímaussaq peninsula and none is seen on Tugtutôq. They are clearly associated with the Si-undersaturated magmatism in the Gardar province (cf. also Grønnedal-Íka, Emeleus 1964; West Kenya, Le Bas 1977; Alnö, Von Eckermann 1948). They are notably abundant in the area north of Igaliko village, although they are also widely scattered across the rest of the province. They are invariably late stage occurrences with many dykes cutting the Late Igdlerfigssalik syenites (see Map 1). A late stage origin for the Grønnedal-Íka carbonatite is advocated by Emeleus (1964) after a build up of CO_2 in the syenitic magmas during fractional crystallisation.

Recent work (Freestone and Hamilton 1980, Bedson 1983, 1984) has shown that liquid immiscibility exists between phonolitic and natrocarbonatitic magmas and current experimental work is extending the limits of the 2-liquid field to give immiscibility between anorthosite and calcite under 'dry' conditions, (ie. $P_{tot}=P_{CO_2}$, B. Kjaersgaard, pers. comm. 1987).

Major and trace element data suggest that the Igaliko carbonatites formed by liquid immiscibility from CO_2-enriched phonolites and benmoreites at temperatures of perhaps 900-1000°C (or possibly less) and pressures of around 3-5kb. Unmixing of the carbonate

phase was achieved on CO_2 saturation in the parental silicate. This occurred at different stages of magmatic evolution and led to regional differences in carbonatite geochemistry (cf. Iganaq-type, Igaliko-type, Østfjordsdal-type, Chapter 7, see below).

The presence of CO_2 in mantle source regions has been cited as necessary to produce Si-undersaturated magmas (see Gittins 1979) whereas the presence of H_2O will encourage Si-saturation/oversaturation in the melts produced (Gittins 1979, cf. Thompson 1984). It is not surprising then that carbonatites are frequently associated with evolved Si-undersaturated rocks, fractionation having led to a build up in CO_2.

It is also notable that only recorded occurrences of Gardar carbonatites are in areas of intense faulting ie. the Igaliko complex (Emeleus and Harry 1970, this study), Qagssiarssuk (Stewart 1964, 1970) and Grønnedal-Íka (Emeleus 1964). In the Grønnedal area, major faulting has been shown to be pre-Gardar (Henriksen 1960). Bailey (1983) considers that continental rifts may act in a manner analogous to 'pie-funnels' and channel volatiles from a large mantle source region into a small surface fracture. If these intensely faulted areas have disruptive effect to mantle depths (see Chapter 11.9) they may focus volatiles, and particularly deep mantle-derived CO_2, into the sub-rift mantle. This will not only generate alkaline, undersaturated rocks, but will provide them with the wherewithall to evolve to produce carbonatite.

Early CO_2-rich eruptives are recorded as carbonatitic and lamprophyric tuffs and breccias from Qagssiarssuk at the base of the Eriksfjord Formation (Stewart 1964, 1970), These may have formed as precursors to more extensive basaltic magmatism. They may represent early, volatile-rich melts (low viscosity) which were generated at the earliest stages of partial melting (cf. McKenzie 1984, 1985).

The point at which CO_2 saturation is achieved in igneous rocks is variable and depends on the interplay of several different factors. Saturation is achieved at the lowest CO_2 contents in highly polymerised siliceous liquids. Solubility of CO_2 in igneous melts increases with increasing basicity, temperature and pressure. In leucocratic nepheline syenite magmas the level of CO_2 saturation is at its lowest at about 1kb (Eggler 1973, Mysen 1975). Fractionation of normal igneous assemblages (eg. feldspar, pyroxene, olivine etc.) will not only cause CO_2 to increase in the residual liquids but will also

reduce the amount of CO_2 the liquid is able to dissolve and thus increase the chances of CO_2 saturation being achieved. A reduction in pressure will also increase the likelihood of CO_2 becoming saturated in the magma, as too would a drop in temperature. Emplacement of a nearly saturated CO_2-rich magma as a relatively small pulse from deep to a shallower crustal level may cause CO_2 saturation and thereby loss of a carbonatite phase. The magma left at depth may still evolve etc. to be emplaced later (different composition), again becoming CO_2 saturated but exsolving a carbonatite of markedly different composition (related to the higher pressure bulk composition of the system). In this way a variety of carbonatite compositions may be produced from essentially one magmatic event, and this may be the cause of the variation of carbonatite compostitions seen in the Igaliko area.

The presence of CO_2 in the felsic melts causes the melt structure to depolymerise producing an increase in a_{SiO_2} (Mysen 1976) leading to an increase in fo_2 (Wood and Fraser 1977). This in turn causes much (if not all) of the Eu present in the sample to be present as Eu^{3+}. In this valency state it shows no preferential entry into feldspar crystal structures compared to the other REE. Several phonolites from the Igaliko complex show no negative Eu anomalies although their genesis must have involved substantial feldspar fractionation. These examples contain abundant CO_2 (in cancrinite) which must have caused high fo_2 and suppressed the developement of an Eu anomaly. These samples are also relatively rich (compared to average phonolites) in both Mn and Sr, elements which become enriched in carbonatite magmas. It would appear that these Eu anomaly-free phonolites contain (in solution) a carbonate component which, if CO_2 had been allowed to increase to saturation, would have exsolved as an immiscible carbonate liquid. The absence of negative Eu anomalies in some phonolites and all (but one) carbonatites thus presents no genetic problem.

11.6: Significance of Lamprophyres

Lamprophyric dykes are fairly common across the Igaliko Nepheline Syenite complex although many appear to be concentrated in the SE of the area (especially CAL).

The ultramafic lamprophyres (UML) are rich in both compatible and incompatible elements and are the most basic (Mg, Ca-rich, Si, Al-poor) silicate rocks from the Igaliko

Nepheline Syenite complex. They are frequently early and several examples occur in rafts of granite within the outer units of the Motzfeldt complex. Chemically they are very similar to lamprophyric breccias and tuffs from the Qagssiarssuk area (Stewart 1964, 1970). The UML contain no melilite which may be a reflection of crystallisation at depth (cf. Upton and Thomas 1973). This is in contrast to the Qagssiarssuk occurrences which contain possible melilite pseudomorphs (Stewart 1964, 1970, but see also Deans and Roberts 1984).

The UML are probably the products of extremely small degrees of partial melting in a fertile (or enriched) mantle source. Melting may have involved a disequilibrium process involving phlogopite (leading to high K, Mg, Rb) and apatite (Ca, P, REE, F, H_2O) as well as contributions from other typical mantle phases. If source region enrichment can be achieved by emplacement of enriched melts into, or metasomatism by their passage through, an area of mantle (cf. Hawkesworth *et al.* 1984, Menzies *et al.* 1987), the UML have compositions similar to those required by melting - modelling to enrich the source region for the Late Gardar basaltic magmatism in incompatible elements. Small amounts of UML magma retained in the source regions of these later basalts may be the cause of source region enrichment which is necessary to model their trace element contents. Their presence as early intrusives may also reinforce this. The chemical similarity between these UML and the breccias and tuffs cropping out at the base of the Eriksfjord Formation at Qagssiarssuk may imply a similar origin for both suites in Early Gardar times.

The alkaline lamprophyres (AL) have many chemical similarities with basanites/-tephrites and hawaiites, although they are typically much richer in incompatible elements. They contain Ti and Al-rich ferromagnesian minerals such as kaersutite and Ti-augite. Fractionation of kaersutite and possibly Ti-augite from AL would cause an increase in SiO_2; reduce Ti and K; and may buffer incompatible elements such as Rb and REE. This may produce magmas of hawaiitic/mugearitic compositions. It is notable that in the undersaturated suite of rocks, the AL are amongst the most abundant basic rocks. In this way the AL may have some parental status to the main, undersaturated suite of rocks (cf. Rock 1978a).

The calc-alkaline lamprophyres (CAL) are chemically quite similar to the AL, but

lack the Ti and Al-rich mineralogy. They are equally abundant in the Mid-Gardar Østfjordsdal swarm where, with UML, they are the only basic rocks. These CAL tend to be less Si-rich than the typical CAL cited by Rock (1987a). Their abundance in the Østfjordsdal region may suggest a parental status for these rocks to the abundant phonolitic dykes seen in the Østfjordsdal area.

11.7: Relationship of BFD's

Large plagioclase xenocrysts and granular anorthosite xenoliths occur in many basic to intermediate dykes of both the oversaturated and undersaturated suites, but are absent from dykes of the Østfjordsdal swarm. Chemical evidence suggests that the xenoliths and xenocrysts could not have crystallised from their present host magmas but have been entrained from a disrupted anorthosite body at depth. This may have crystallised from 'hawaiitic' magmas which were LREE (and possibly Eu) enriched. They are however not related to the Late Gardar activity in the Igaliko region or Tugtutôq - Ilímaussaq - Nunataq area (see also Upton and Thomas 1980, Upton and Blundell 1978, Martin 1985) but may be related to massif type anorthosites of similar type to those which crop out in Labrador (Bridgwater 1967, Morse 1977, Upton and Emeleus 1987). Their origins may be related to pre- to Early Gardar plate movements (cf. Morse 1977).

11.8: Stratigraphy

Dyke intersections are relatively rare in the Igaliko Nepheline Syenite complex, as a result of the marked parallelism of the dykes. Appendix I contains all cross cutting information from the region. Table 11.8.1 shows a summary of the cross cutting relationships of all dykes that have been chemically analysed.

There are only 2 recorded cases where high Zr/Nb (oversaturated) rocks intersect low Zr/Nb (undersaturated) rocks. In both cases the oversaturated rocks are younger. Several cases of more evolved rocks cutting less evolved rocks are recorded. There are also a few cases of less evolved rocks cutting more evolved rocks, eg. benmoreite cutting phonolite. These occurrences attest to the availability of more basic magmas at later stages of evolution and support Stephenson's (1973) idea of stratified magma chambers of which deeper, more basic levels are tapped with time. Dykes of both the low and

Table 11.8.1

Cross cutting relationships from analysed dykes

4 cases of low Zr/Nb benmoreite cutting low Zr/Nb benmoreite

4 cases of high Zr/Nb benmoreite cutting low Zr/Nb phonolite

1 case of high Zr/Nb trachyte cutting low Zr/Nb phonolite

1 case of high Zr/Nb benmoreite cutting low Zr/Nb mugearite

1 case of high Zr/Nb benmoreite cutting low Zr/Nb benmoreite

1 case of high Zr/Nb benmoreite cutting high Zr/Nb mugearite

4 cases of low Zr/Nb phonolite cutting low Zr/Nb phonolite

2 cases of low Zr/Nb benmoreite cutting low Zr/Nb mugearite

1 case of low Zr/Nb benmoreite cutting low Zr/Nb basalt

1 case of carbonatite cutting low Zr/Nb phonolite

high Zr/Nb suite cut the Late Igdlerfigssalik syenites, showing that both suites were active until the end of Gardar times: most of the dykes of both suites will however have been emplaced between the South Qôroq/Early Igdlerfigssalik syenites and the Late Igdlerfigssalik syenites. Both the oversaturated and undersaturated systems may have been active more-or-less simultaneously.

11.9: Fault Geometry and Rifting

In areas of crustal extension heat flow will be elevated as a result of crustal thinning (cf. McKenzie 1978). In areas of strike slip faulting earthquake foci tend to be no deeper than 20km (typically less than 12-15km, Chen and Molnar 1983). Similar focal depths are recorded from zones of continental rifting. Heat flow measurements from California (strike slip) and the Basin and Range province, Western U.S.A (continental extension) suggest that at depths of 12-15km crustal temperatures may be 350±100°C (Lachenbruch and Sass 1978). Below this depth (at higher temperatures) the continental crust will undergo ductile deformation. Below the Moho the upper (lithospheric) mantle, with relatively high strength at higher temperatures than the crust, may undergo brittle deformation to temperatures of perhaps 800°C (35km?, Chen and Molnar 1983, Wernicke 1986).

Higher heat flow during Proterozoic times would produce steeper thermal gradients

than those cited above and the brittle - ductile deformations would occur at shallower crustal (or lithospheric) depths.

In extensional areas normal faults from a horst - graben environment may, at depth, have listric geometries and flatten out into zones of detachment above the ductile region of the lower crust. Conversely the faults may not flatten into listric geometries and instead grade into zones of foliation/deformation in the lower crust. Which ever process operates, continental extension would still cause disruptions in the brittle upper mantle with the shearing being transmitted through the ductile lower crust (see Wernicke 1986).

Thus, regardless of the fault geometry, it would appear that there is some disturbance of the upper (lithospheric) mantle. There is no direct evidence that this may continue as ductile deformation into the deeper, weaker (asthenospheric) mantle. In zones of intense faulting such as the Igaliko Nepheline Syenite complex or in the Grønnedal-Íka area, these zones of deformation/dislocation may penetrate to mantle depths act as fluid pathways and focus volatiles, especially CO_2, into the area (cf. Bailey 1983, see later).

11.10: Rifting and Magma Genesis

The Gardar period is characterised by repeated episodes of intra-continental rifting and associated alkaline magma genesis (Upton 1974, Emeleus and Upton 1976, Upton and Emeleus 1987). These alkaline rocks may be saturated, oversaturated or undersaturated with respect to silica and appear to have evolved from basic (basaltic) parents. Basic magmas persist to a late stage and, in the syenites of the Igaliko area, crop out as large, dyke-like intrusions.

Magmas were generated in the Gardar province in passive response to rifting caused by continental plate motions, possibly between the North American and Grenvillian plates, (Bradshaw 1987, see Chapter 2) and not in response to mantle upwelling above a hot spot (cf. Burke and Dewey 1973).

Dyking events appear to have occurred throughout Gardar times, with examples of trachytes from Early Gardar, phonolites at Østfjordsdal from Mid(?)-Gardar and the main swarms of oversaturated and undersaturated dykes from Late Gardar times.

Crustal thinning due to rifting will be accompanied by asthenospheric upwelling and an increase in the geothermal gradient (cf. McKenzie 1978). This would induce decompressive partial melting in the asthenosphere (McKenzie 1984, 1985). More melt is produced when the upwelling asthenosphere is hotter and is dependant upon the amount of decompression, with more melting occurring where the lithosphere thinning is greatest (White *et al.* 1987).

Dyke geometry and the quantity of crustal extension attest to different tectonic regimes controlling the emplacement of the oversaturated and undersaturated suites of rocks. The oversaturated rocks (with YGDC-type parental magmas) are associated with amounts of crustal extension of between 10-25% (this study and Upton and Fitton 1985), and probably associated with fairly vigorous transtensional extension of the shear zone. The undersaturated suites (both those of the Late Gardar main swarm and those of the Mid-Gardar Østfjordsdal swarm) appear to be related to crustal extensions of about 3% associated with normal, sinistral shear of the region.

As crustal extension appears to be related to the degree of partial melting (eg. White *et al.* 1987), larger percentage melts would be expected from the rifting episode leading to the YGDC and related magmas than from the smaller rifting episode related to the undersaturated dykes (and central complexes) around Igaliko. More alkaline, undersaturated melts would be expected as the result of smaller degrees of partial melting, larger melting episodes producing more transitional to Si-saturated melts (cf. McKenzie 1984, 1985, Harris 1969).

The UML which are interpreted as extremely small volume melts from a garnet-rich mantle source (steep $(La/Lu)_{cn}$) often occur early and may have been formed at the onset of crustal extension (from a deep source?). With further extension, hotter, asthenospheric material would rise to shallower depths and melt decompressively to give rise to the Si-undersaturated suites of Motzfeldt and North Qôroq in Early Gardar times. It appears necessary for the Greenland/North American continent to have been moving relative to the underlying mantle to produce fresh, fertile mantle sources for subsequent (Late-Gardar) magmatic events (cf. Bailey 1982, 1983).

Late Gardar extension and magmatism produced both an undersaturated suite

(South Qôroq, Igdlerfigssalik and the undersaturated dykes) and a transitional to oversaturated suite (YGDC to rhyolite/comendite dykes and Tugtutôq central complex, cf. Martin 1985, Upton and Thomas 1980).

REE data suggest that the oversaturated rocks were the product of melting of spinel-lherzolite mantle whereas the undersaturated rocks were produced from a garnet-lherzolite source. The larger rifting event will have caused more crustal thinning and a higher thermal gradient by asthenospheric upwelling (McKenzie 1978) which may have induced melting at shallower mantle depths and involved partial fusion of spinel-lherzolite mantle (lithospheric?). The presence of substantial H_2O in the source may stabilise a Nb-bearing phase which is residual on melting (cf. Saunders and Tarney 1984) and lead to a negative Nb anomaly and also produce basalts of a transitional to Si-oversaturated character similar to CFB (cf. Thompson 1984, see Chapter 5.9). Negative Nb anomalies may also be produced by crustal contamination by Nb-poor lower crustal rocks (Thompson 1982) and the elevated thermal gradient associated with the genesis of these rocks may assist crustal fusion/assimilation. Sr-isotopic evidence (Martin 1985, Blaxland *et al.* 1978) however, provides no evidence of crustal contamination, although if the amount of material assimilated was small and had a fairly unevolved Sr isotopic composition, it would not necessarily be detected. Upton and Emeleus (1987) and Martin (1985) however, argue that crustal assimilation could not produce the positive P anomaly seen in these basic rocks and that these features (including the negative Nb anomaly) are primary characteristics of the parental magmas.

Recently however, Davis and MacDonald (1988) have shown from Pb isotopic studies that the oversaturated trend exhibited by some Kenyan central complexes (ie. from basalt to alkali rhyolite/comendite) is a result of contamination by F and Cl-rich crustal rocks. A detailed isotopic study of these Late Gardar oversaturated rocks would help unravel their origins.

The undersaturated Late Gardar rocks appear to be formed as smaller melts from a deeper (ie. garnet bearing) mantle source region with OIB-source characteristics (ie. asthenospheric source). Melting was induced by a smaller amount of crustal extension than in the case of the oversaturated rocks and was probably the result of decompression of upwelling mantle material (cf.McKenzie 1978) with only small volume of melt

being generated. They evolved by relatively simple process of fractional crystallisation to phonolitic residues with no apparent contamination. Rocks of lamprophyric nature (alkali lamprophyres) are among the most abundant basic rocks in the undersaturated suite. They may have some parental status to the undersaturated dykes through loss of volatiles, Ti, K and some incompatible elements by fractionation of Ti-augite, kaersutite and opaque oxides. In the Østfjordsdal Dyke Swarm calc-alkaline lamprophyres are abundant and these may also have some parental status to the Østfjordsdal phonolitic dykes.

The evolved, Si-undersaturated dykes have clear chemical affinities with the South Qôroq and Igdlerfigssalik centres. They have similar Ce/Y, Zr/Nb, F.I., major and trace element compositions and mineralogical evolution trends. These dykes are clearly related to the plutonic activity in the Igaliko Nepheline Syenite complex and are confined in outcrop to the area close to these centres with only a few undersaturated dykes being reported from the NE end of the Ilímaussaq peninsula (Martin 1985).

11.11: Summary

This section summarises the main order of events and major processes in the evolution of the dykes from the Igaliko region.

Stratigraphy

(i) Emplacement of many UML at onset of rifting. Possible BD_0 dyke truncated by Motzfeldt centre. UML related to Qagssiarssuk tuffs, breccias?

(ii) Some trachyte dykes emplaced in Motzfeldt centre and truncated by later Motzfeldt foyaite sheets.

(iii) Mid(?)-Gardar emplacement of CAL and phonolite dykes of the Østfjordsdal Dyke Swarm, including the large porphyritic syenite dykes (cf. Fox Bay Porphyritic Nepheline Syenites, Ussing 1912). This swarm subsequently metamorphosed by the Igdlerfigssalik central complex (Late-Gardar) at fairly low temperatures.

(iv) Late Gardar rifting and magmatism commenced.

(v) Emplacement of South Qôroq and Early Igdlerfigssalik centres. South Qôroq possibly related to Tugtutôq OGDC (Upton *et al.* 1985).

(vi) Emplacement of the main swarms of undersaturated and oversaturated dykes (in-

cluding many lamprophyres). Oversaturated dyke activity may be slightly younger than undersaturated dyke activity, although activity in both suites probably overlapped.

(vii) Emplacement of the Late Igdlerfigssalik centre.

(viii) Emplacement of late dykes including several phonolites, some alkali basalts and many carbonatite dykes in the Igaliko village area.

Main points in the evolution of the undersaturated suite of dykes (and, by inference, central complexes).

(i) Rifting associated with simple shear. Crustal extension small.

(ii) Asthenospheric upwelling (cf. McKenzie 1978).

(iii) Decompressive melting in garnet-bearing mantle source ($(La/Lu)_{cn} \approx 18$).

(iv) Fertile (or metasomatised) source similar to OIB source, rich in CO_2.

(v) Primary melts alkali basaltic or lamprophyric (camptonite) with smooth incompatible element profiles. Zr/Nb≈3.9.

(vi) Accumulation of magma in fairly shallow crustal magma chamber.

(vii) Crystal fractionation of pyroxene, feldspar, olivine (and perhaps early kaersutite and Ti-augite) to produce low density, benmoreitic residues. Magma chambers develop chemical stratification (cf. Stephenson 1973).

(viii) Ascent of low density liquids by cauldron/block subsidence to produce central complexes at late stages (cf. Gill 1973).

(ix) Injection of some material into fractures/fissures to form dykes.

(x) Ascent of more basic magma with successive, deeper tapping of magma chamber. More dyking. Many liquid lines of descent producing wide scatter of trace element data – magmas evolving at different P-T conditions – proliferation of liquid lines of descent (Cox 1967).

(xi) CO_2 saturation achieved in some cases with exsolution of carbonatite magma. The presence of high CO_2 contents in the silicate magmas suppresses the formation of negative Eu anomalies by maintaining high fo_2 (above QMF buffer). Carbonatites extremely rich in REE, F, Mn, Sr, Ba, poor in alkalis, may have formed as calcic carbonatites (not natrocarbonatites).

(xii) Ascent of late basic material within central complexes.

(xiii) Crustal dilation due to undersaturated dykes 2-3% typically.

Main points in the evolution of the oversaturated suite of dykes.

(i) Transtensional extension of shear zone/rift. Crustal extension large.

(ii) High thermal gradient leading to partial melting of spinel-bearing mantle source with little/no garnet (high HREE contents, low ($La/Lu_{cn} \approx 7$).

(iii) Fertile source, possibly enriched by metasomatism. Magmas generated similar to CFB (Thompson *et al.* 1984).

(iv) Accumulation of magma in deep (lower crustal) magma chamber.

(v) Fractionation of clinopyroxene and olivine, to ≈10 wt% MgO.

(vi) Ascent of magmas to shallower (10km?) magma chamber.

(vii) Fractionation of plagioclase, clinopyroxene, olivine, opaques.

(viii) Intrusion as basic to rhyolitic dykes as system evolves.

(ix) Basic rocks characterised by negative Nb and positive P anomalies. Zr/Nb≈6.4.

(x) Is negative Nb anomaly (a) primary feature of source region, (b) caused by Nb-rich residual phase on melting in presence of H_2O (Saunders and Tarney 1984) or (c) crustal contamination (cf. Thompson 1982). Sr isotopic evidence shows no crustal contamination (Martin 1985) and positive P anomaly could not be caused by crustal assimilation (Martin 1985, Upton and Emeleus 1987). Si-oversaturated trend could however be a result of assimilation (cf. Davis and Macdonald 1988, Fitton 1987).

(xi) Evolution to alkali rhyolite/comendite from basalt, via benmoreite and trachyte. Volatile enrichment in some cases (eg. trachytes) of incompatible elements by F, Cl complexes (Martin 1985). Lower fo_2 than undersaturated rocks (below QMF buffer).

(xii) Simple liquid evolution with tightly constrained trace element variation, ie. effectively one liquid line of descent.

(xiii) Clear association with YGDC magmas and part of main Tugtutôq - Ilímaussaq - Nunataq swarm (Upton 1962, 1964a, b, c, MacDonald 1969, 1970, Upton and Thomas 1980, Martin 1985, Upton and Fitton 1985).

REFERENCES

ABBEY, S. 1983. Studies in 'standard samples' of silicate rocks and minerals. Canadian Geological Survey Paper, 83-15.

AFONINA, G.G. and SHMAKIN, B.M. 1970. Inhibition of lattice ordering of potassic feldspar by barium ions. Doklady Akad Nauk, English translation, 195, 133-135. Translated from Doklady Akad Nauk, SSSR, 195, 929-931.

AHRENS, L.H., PINSON, W.H. and KEARNS, M. 1952. Association of rubidium and potassium and their abundance in igneous rocks and meteorites. Geochimica et Cosmochimica Acta, 2, 229-242.

ANDERSON, E.M. 1951. *The dynamics of faulting and dyke formation with applications to Britain*, London, Oliver and Boyd. 206pp.

ANDERSON, J.G. 1974. The Geology of Alângorssuaq, Northern Nunarssuit Complex, South Greenland. Unpublished PhD Thesis, University of Aberdeen.

AOKI, K. 1964. Clinopyroxenes from the alkaline rocks of Japan. American Mineralogist, 49, 1199-1223.

ARZI, A.A. 1978. Critical phenomena in the rheology of partially melted rocks. Tectonophysics, 44, 173-184.

BACHINSKI, S.W. and MULLER, G. 1971. Experimental determinations of the Microcline - Low albite solvus. Journal of Petrology, 12, 329-356.

BAER, J., EMSLIE, R.F., IRVING,E. and TANNER, J.G. 1974. Grenville Geology and Plate Tectonics. Geoscience Canada, 1, 54-61.

BAGNOLD, R.A. 1954. Experiments on a gravity-free dispersion of large solid spheres in a Newtonian fluid under shear. Proceedings of the Royal Society (London) Series A, 225, 49-63.

BAILEY, D.K. 1964. Crustal warping – a possible tectonic control on alkali magmatism. Journal of Geophysical Research, 69, 1103-1111.

BAILEY, D.K. 1980. Volcanism, Earth degassing and replenished lithospheric mantle. Philosophical Transactions of the Royal Society, London, A297, 309-322.

BAILEY, D.K. 1982. Mantle metasomatism – continuing chemical change within the earth. Nature, 296, 525-530.

BAILEY, D.K. 1983. The chemical and thermal evolution of rifts. In Morgan, P. and Baker, B.H. (Eds) *Processes of Continental Rifting*, Tectonophysics, 94, 585-597.

BAILEY, D.K. 1984. Kimberlite: 'The mantle sample' formed by ultrametasomatism. In Kornprobst, J. (Ed) *Kimberlites; I: Kimberlites and Related Rocks.* Elsevier, Amsterdam.

BAILEY, D.K. 1987. Mantle metasomatism – perspective and prospect. In Fitton, J.G. and Upton, B.G.J. (Eds) *Alkaline Igneous Rocks*, Geological Society Special Publication No. 30

BAILEY, D.K. and SCHAIRER, J.F. 1964. Feldspar - liquid equilibria in peralkaline liquids – The Orthoclase Effect. American Journal of Science, 62, 1198-1206.

BAILEY, D.K. and SCHAIRER, J.F. 1966. The system Na_2O - Al_2O_3 - Fe_2O_3 - SiO_2 at 1 atmosphere and the petrogenesis of alkaline rocks. Journal of Petrology, 7 114-170.

BAILEY, J. 1976. Trace element techniques in the Institute for Petrology, University of Copenhagen. In Bailey, J. and Sørensen, I. *X-ray fluorescence analysis*, Internal report, University of Copenhagen.

BARAGAR, W.R.A. 1977. Volcanic regimes in Canada. Geological Association of Canada Special Paper, 17.

BARRIÈRE, M. 1976. Flowage differentiation: Limitation of the *Bagnold effect* to the Narrow intrusions. Contributions to Mineralogy and Petrology, 55, 139-145.

BASALTIC VOLCANISM STUDY PROJECT. 1981. *Basaltic volcanism on the terrestrial plan-*

ets. Pergamon Press, New York.

BATTACHARJI, S. 1967. Mechanics of flow differentiation in ultramafic and mafic sills. Journal of Geology, 75, 101-112.

BATTACHARJI, S. and SMITH, C.H. 1964. Flowage differentiation. Science, 145, 150-153.

BÈDARD, J., LUDDEN, J. and DANIS, D. 1985. Silica oversaturated residua by fractionation - assimilation of a camptonitic parent magma, the Megantic Complex. The Geological Society of Canada Annual Meeting, Fredericton, New Brunswick, Program with Abstracts, A3.

BEDDOE-STEPHENS, B. 1977. The petrology and geochemistry of the Rossland Volcanic Rocks, Southern British Colombia. Unpublished PhD Thesis, University of Durham.

BEDSON, P. 1983. The origin of the carbonatites and their relation to other rocks by liquid immiscibility. Unpublished PhD Thesis, University of Manchester.

BEDSON, P. 1984. Rare earth element distribution between immiscible silicate and carbonate liquids. In *Progress in Experimental Petrology*, Volume 6. National Environment Research Council, Publications Series D, No. 25.

BERGMAN, S.C. 1987. Lamproites and other potassium-rich igneous rocks: a review of their occurence, mineralogy and geochemistry. In Fitton, J.G. and Upton, B.G.J. (Eds) *Alkaline Igneous Rocks*, Geological Society Special Publication No. 30

BERRANGÉ , J.P. 1966. The bedrock geology of Vatnahverfi, Julianehåb district, South Greenland. Rapport Grønlands Geologiske Undersøgelese, Nr3.

BERTHELSEN, A. and HENRIKSEN, N. 1975. Geological map of Greenland, 1:100,000, Ivigtut. 61 v.1 Syd. The orogenic and cratogenic geology of a Precambrian shield area. Descriptive text, 169pp. Geological Survey of Greenland.

BERTHELSEN, A. and NOE-NYGAARD, A. 1965. The Precambrian of Greenland. In RANKAMA, K. (ed.), *The Geologic System, The Precambrian.* 2, 113-262.

BILLINGS, M.P. 1972. *Structural Geology*: Englewood Cliffs, N.J., Prentice Hall, 606.

BLAXLAND, A.B. and UPTON, B.G.J. 1978. Rare earth distribution in the Tugtutôq younger giant dyke complex: evidence bearing on alkaline magma genesis in South Greenland. Lithos. **11**, 291-299.

BLAXLAND, A.B., VAN BREEMEN, O., EMELEUS, C.H. and ANDERSON, J.G. 1978. Age and origin of the major syenite centres in the Gardar Province of South Greenland: Rb-Sr studies. Geological Society of America Bulletin 89, 231-244.

BLUNDELL, D.J. 1978. A gravity survey across the Gardar Igneous Province, SW Greenland. Journal of the Geological Society, London, **135**, 545-554.

BONDAM, J. 1955. Petrography of a group of alkali-trachytic dyke rocks from Julianehåb district, South Greenland. Meddelelser om Grønland, Bd **135**, Nr2.

BOTTINGA, Y. and WEILL, D.F. 1970. Densities of liquid silicate systems calculated from partial molar volumes of oxide components. American Journal of Science, **269**, 169-182.

BOTTINGA, Y., WEILL, D.F. and RICHET, P. 1982. Density calculations for silicate liquids – revised method for alumino-silicate compositions. Geochimica et Cosmochimica Acta, **46**. 909-919.

BOWEN, N.L. 1928. *The Evolution of the Igneous Rocks.* Princeton University Press, 334pp.

BOWEN, N.L. 1937. Recent high temperature research on silicates and its significance in igneous geology. American Journal of Science, **33**, 1-21.

BOWEN, N.L. 1945. Phase equilibria bearing on the origin and differentiation of alkaline rocks. American Journal of Science, **243A**, 75-89.

BOWEN, N.L. SCHAIRER, J.F. and POSNJAK, E. 1933. The system Ca_2SiO_4 - Fe_2SiO_4. American Journal of Science, **25**, 273-297.

BOYNTON, W.V. 1984. Geochemistry of the Rare Earth Elements: Meteorite studies. In

Henderson, P. (Ed) *Rare Earth Element Geochemistry,* Developments in Geochemistry 2. Elsevier, Amsterdam.

BRADSHAW, C. 1985. The alkali rocks of the Motzfeldt centre – progress report on the 1984 field season. Rapport Grønlands Geologiske Undersøgelese No. 125, 62-64.

BRADSHAW, C. 1987. The petrology, geochemistry and mineralogy of the Motzfeldt Centre, South Greenland. Unpublished PhD Thesis, University of Durham (currently in prep.).

BRIDGWATER, D. 1967. Feldspathic inclusions in the Gardar Igneous Rocks of South Greenland and their relevance to the formation of major anorthosites in the Canadian Shield. Canadian Journal of Earth Science, 4, 995-1014.

BRIDGWATER, D. 1968. Mechanics of flow differentiation in ultramafic and mafic sills. Journal of Geology, 76, 596-599.

BRIDGWATER, D. and COE, K. 1970. The role of stoping in the emplacement of the giant dykes of Isatoq, South Greenland. In Newall, G. and Rast, N. (Eds) *Mechanisms of Igneous Intrusion.* Geological Journal Special Paper No.2, 67-78.

BRIDGWATER, D. and HARRY, W.T. 1968. Anorthosite xenoliths and plagioclase megacrysts in Precambrian intrusions of South Greenland. Meddelelser om Grønland, Bd.185, Nr2.

BROOKS, C.R. and GILL, R.C.O. 1982. Compositional variations in the pyroxenes and amphiboles of the Kangerdlugssuaq intrusion, East Greenland: further evidence for the crustal contamination of syenite magma. Mineralogical Magazine, **45**, 1-9.

BROUSSE, R. and RANÇON, J.P. 1984. Crystallisation trends of pyroxenes from agpaitic phonolites (Cantal, France). Mineralogical Magazine, **48**, 39-45.

BROWN, G.E. 1982. Olivines and silicate spinels. In Ribbe, P.H. (Ed) *Reviews in Mineralogy, Volume 5: Orthosilicates.* Mineralogical Society of America.

BRYAN, W.B., FINGER, L.W. and CHAYES, F. 1969. Estimating proportions in petrographic mixing equations by least-squares approximation. Science, **163**, 926-927.

BUDDINGTON, A.F. and LINDSLEY, D.H. 1964. Iron-titanium oxide minerals and synthetic equivalents. Journal of Petrology, **5**, 310-357.

BURKE, K. 1980. Intracontinental rifts and aulacogens. In *Continental Tectonics.* National Academy of Science, 42-49.

BURKE, K. and DEWEY, J.F. 1973. Plume generated triple junctions: key indicators in applying plate tectonics to older rocks. Journal of Geology, **81**, 406-412.

BURNS, R.G. and BURNS, V.M. 1971. Study of the crystal chemistry of titaniferous garnets by Mössbauer spectroscopy. Geological Society of America Abstract Programs 3. 519-520.

BØGGILD, O.B. 1906. On some minerals from Narsarsuk at Julianehåb, Greenland. Meddelelser om Grønland, Bd **33**, Nr 5.

CAMERON, M. and PAPIKE, J.J. 1982. Crystal chemistry of silicate pyroxenes. In Prewitt, C.T. (Ed) *Reviews in Mineralogy, Volume 7: Pyroxenes.* Mineralogical Society of America, 525pp.

CAMPBELL, I. and SCHENK, E.T. 1950. Camptonite dykes near Boulder Dam, Arizona. American Mineralogist, **35**, 671.

CARMICHAEL, I.S.E. 1967. The iron-titanium oxides of salic volcanic rocks and their associated ferromagnesian silicates. Contributions to Mineralogy and Petrology, **14**, 36-64.

CARMICHAEL, I.S.E. and NICHOLLS, J. 1967. Iron-titanium oxides and oxygen fugacities in volcanic rocks. Journal of Geophysical Research, **72**, 4655-87.

CAWTHORN, R.G. 1976. Some chemical controls on igneous amphibole compositions. Geochimica et Cosmochimica Acta, **40**, 1319-1328.

CAWTHORN, R.G. and COLLERSON, K.D. 1974. The recalculation of pyroxene end member parameters and the estimation of ferrous and ferric iron content from electron probe analysis. American Mineralogist, **59**, 1203-8.

CHAMBERS, A.D. 1976. The petrology and geochemistry of the North Qôroq Centre, Igaliko Complex, South Greenland. Unpublished PhD Thesis, University of Durham.

CHASE, C.G. and GILMER, T.H. 1973. Precambrian plate tectonics: the mid-continental gravity high. Earth and Planetary Science Letters, 21, 70-78.

CHEN, W.P. and MOLNAR, P. 1983. Focal depths of intracontinental and intraplate earthquakes and their implications for the thermal and mechanical properties of the lithosphere. Journal of Geophysical Research, 88, No. B5, 4183-4214.

CLAGUE, D.A. 1978. The oceanic basalt - trachyte association: An explanation of the Daly Gap. Journal of Geology, 86, 739-743.

COOMBS, D.S. and WILKINSON, J.F.G. 1969. Lineages and fractionation trends in undersaturated volcanic rocks in the East Otago Volcanic Province (New Zealand) and related rocks. Journal of Petrology, 10, 441-501.

COOPER, A.F., GITTINS, J. and TUTTLE, O.F. 1975. The system Na_2CO_3 - K_2CO_3 - $CaCO_3$ at 1 kilobar and its significance in carbonatite petrogenesis. American Journal of Science, **275**, 534-560.

COX, K.G. 1967. Proliferation of liquid lines of descent. Proceedings of the Geological Society, London, **1637**, 49.

COX, K.G. 1980. A model for flood basalt volcanism. Journal of Petrology, **21**, 629-650.

COX, K.G., BELL, J.D. and PANKHURST, R.J. 1979. *The Interpretation of Igneous Rocks.* George, Allen and Unwin, London, 450pp.

CULLERS, R.L. and GRAF, J.L. 1984. Rare earth elements in igneous rocks of the continental crust: Predominantly basic and ultrabasic rocks. In Henderson, P. (Ed) *Rare Earth Geochemistry.* Elsevier, Amsterdam.

CULLERS, R.L. and MEDARIS, G.Jr. 1977. Rare earth elements in carbonatite and cogenetic alkaline rocks: Examples from Seabrook Lake and Callander Bay, Ontario. Contributions to Mineralogy and Petrology, 65, 143-153.

CULLERS, R.L., MULLENAX, J., DEMARCO, M. and NORDENG, S. 1982. Trace element content and petrogenesis of kimberlites, Riley County, Kansas. American Mineralogist, **67**, 223-233.

CURRIE, K.L. and FERGUSON, J. 1970. The mechanism of intrusion of lamprophyre dykes indicated by 'offsetting' of dykes. Tectonophysics, **7**, 525-535.

DALY, R.A. 1925. The geology of Ascension Island. Proceedings of the American Academy of Arts and Sciences (Philadelphia), **60**, 3-124.

DANA, J.D. 1892. *Descriptive Mineralogy,* 6^{th} Edition by E.S. Dana. John Wiley and Sons, New York.

DAVIS, G.R. and MACDONALD, R. 1988. Crustal influences in the petrogenesis of the Naivasha basalt-rhyolite complex: combined trace element and Sr-Nd-Pb isotope constraints. Journal of Petrology, **28**.

DAWSON, J.B. 1962. The geology of Oldoinyo Lengai. Bulletin Volcanologique, **24**, 349-87.

DAWSON, J.B. 1987. The kimberlite clan: relationship with olivine lamproites and inferences for upper mantle metasomatism. In Fitton, J.G. and Upton, B.G.J. (Eds) *Alkaline Igneous Rocks*, Geological Society Special Publication No. 30.

DAWSON, J.B. and FUGE, R. 1980. Halogen content of some primary African carbonatites. Lithos, **13**, 139-143.

DAWSON, J.B. and HAWTHORN, J.B. 1973. Magmatic sedimentation and carbonatite differentiation in kimberlite sills at Benfontein, South Africa. Journal of the Geological Society, London, **129**, 61-85.

DE LA ROCHE, H., LETERRIER, J., GRAND CLAUD, P. and MARCHAL, M. 1980. A classification of volcanic and plutonic rocks using R_1R_2 - diagram and major element

analyses - its relationships with current nomenclature. Chemical Geology, 29, 183-210.

DEANS, T. and ROBERTS, B. 1984. Carbonatite tuffs and lava clasts of the Tinderet foothills, Western Kenya - a study of calcified natrocarbonatites. Journal of the Geological Society, London, 141, 563-580.

DEANS, T. and SEAGER, A.F. 1978. Stratiform magnetite crystals of abnormal morphology from volcanic carbonatites in Tanzania, Kenya, Greenland and India. Mineralogical Magazine, 42, 463-475.

DEER, W.A., HOWIE, R.A. and ZUSSMAN, J. 1962. *Rock Forming Minerals, volume 1: Ortho- and Ring-silicates.* John Wiley and Sons, New York.

DEER, W.A., HOWIE, R.A. and ZUSSMAN, J. 1966. *An Introduction to the Rock Forming Minerals.* Longman, London, 528pp.

DEER, W.A., HOWIE, R.A. and ZUSSMAN, J. 1978. *Rock Forming Minerals, 2A. Single Chain Silicates.* London: Longman Group Ltd..

DELANEY, P.T. and POLLARD, D.D. 1981. Deformation of host rocks and flow of magma during growth of minette dikes and breccia-bearing intrusions near Ship Rock, New Mexico. United States Geological Survey Professional Paper 1202. United States Government Property Office, Washington.

DELANEY, P.T. and POLLARD, D.D. 1982. Solidification of basaltic magma during flow in a dyke. American Journal of Science, 282, 856-885.

DONALDSON, J.A. and IRVING, E. 1972. Grenville front and rifting of the Canadian Shield. Nature (London) Phys. Sci. 237, 139-140.

DOWNES, M.J. 1974. Sector and oscillatory zoning in calcic augites from Mt. Etna. Contributions to Mineralogy and Petrology, 47, 187-196.

DREVER, H.I. and JOHNSTON, R. 1958. The petrology of picritic rocks in minor intrusions, a Hebridean group. Transactions of the Royal Society of Edinburgh, 63, 459-499.

DUNCUMB, P. and JONES, E.M. 1969. Tube Investments Company Report, No. 260.

DUNCUMB, P. and REED, S.J.B. 1968. Quantitative electron probe micro-analysis. National Bureau of Science Special Publication, 298, 133-154.

EBY, G.N. 1975. Abundance and distribution of the rare earth elements and yttrium in the rocks and minerals of the Oka carbonatite complex, Quebec. Geochimica et Cosmochimica Acta, 9, 597-620.

EBY, G.N. 1987. The Monteregian Hills and White Mountains alkaline igneous provInces, Eastern North America. In Fitton, J.G. and Upton, B.G.J. (Eds) *Alkaline Igneous Rocks*, Geological Society Special Publication No. 30.

EDGAR, A.D. and PARKER, L.M. 1974. Comparison of melting relationships of some plutonic and volcanic peralkaline undersaturated rocks. Lithos, 7, 263-273.

EGGLER, D.H. 1973. Role of CO_2 in melting processes in the mantle. Annual report of the Director of the Geophysical Laboratory, Washington, 73, 457-467.

EGGLER, D.H. 1978. The effect of CO_2 upon partial melting of peridotite in the system Na_2O - CaO - Al_2O_3 - MgO - SiO_2 to 35kb with an analysis of melting in a peridotite - H_2O - CO_2 system. American Journal of Science, 278, 305-343.

EGGLER, D.H. and HOLLOWAY, J.R. 1977. Partial melting of peridotite in the presence of H_2O and CO_2: principles and review. In *Magma Genesis.* Oregon, Department of Geological and Mineralogical Industries Bulletin, 96, 15-35.

EMELEUS, C.H. 1964. The Grønnedal-Íka alkaline complex, South Greenland. Grønlands Geologiske Undersøgelese Bulletin No.45 (also Meddelelser om Grønland, Bd 172, Nr 3.)

EMELEUS, C.H. and HARRY, W.T. 1970. The Igaliko Nepheline Syenite complex. Bulletin Grønlands Geologiske Undersøgelese, 85 (also Meddelelser om Grønland, 186, Nr 3) 116pp.

EMELEUS, C.H. and STEPHENSON, D. 1970. Field work between Tunugdliarfik and Tasiussaq. Rapport Grønlands Geologiske Undersøgelese No.28.

EMELEUS, C.H. and UPTON, B.G.J. 1976. The Gardar Period in Southern Greenland. In Escher, A. and Watt, W.S. (Eds) *The Geology of Greenland.* 153-81. Grønlands Geologiske Undersøgelese, København.

ENGELL, J. 1973. A closed system crystal fractionation model for the agpaitic Ilímaussaq intrusion, South Greenland, with special reference to lujavrites. Bulletin of the Geological Society of Denmark, **22**, 334-362.

ERNST, W.G. 1968. *Minerals, rocks and inorganic materials, 1, Amphiboles.* Springer – Verlag, New York.

EXLEY, R.A. 1980. Microprobe studies of REE-rich accesory minerals: implication for Skye granite petrogenesis and REE mobility in hydrothermal systems. Earth and Planetary Science Letters, **48**, 97-110.

EXLEY, R.A. 1982. The role of mantle enrichment processes in the petrogenesis of some alkali basalt suites. Geochimica et Cosmochimica Acta, **46**, 1375-1384.

FERGUSON, J. and CURRIE, K.L. 1971. Evidence of liquid immiscibility in alkalic ultrabasic dykes. Journal of Petrology, **12**, 561-585.

FESQ, H.W., KABLE, E.D.J. and GURNEY, J.J. 1974. Aspects of the geochemistry of kimberlites from the Premier mine and other selected South African occurrences with particular reference to the rare earth elements. Physics and Chemistry of the Earth, **9**, 687-707.

FLINK, G. 1898. Be rättalse om en Mineralogisk Resa i Syd-Grönland sommaren 1897. Meddelelser om Grønland, **14**, Nr 2.

FLINK, G. BØGGILD, O.B. and WINTHER, C. 1899. Undersøgeleser af mineraler fra Julianehåb indsamlede af G. Flink 1897 (in English). Meddelelser om Grønland, **24**, Nr 1.

FITTON, J.G. 1987. The Cameroon Line, West Africa: a comparison between oceanic and continental alkaline volcanism. In Fitton, J.G. and Upton, B.G.J. (Eds) *Alkaline Igneous Rocks*, Geological Society Special Publication No. 30.

FITTON, J.G. and DUNLOP, H.M. 1985. The Cameroon Line, West Africa, and its bearing on the origin of oceanic and continental alkali basalt. Earth and Planetary Science Letters, **2**, 23-38.

FITTON, J.G. and JAMES, D. 1986. Basic volcanism associated with intraplate linear features. Philosophical Transactions of the Royal Society, London, **A317**, 253-266.

FLOYD, P.A. and WINCHESTER, J.A. 1975. Magma type and tectonic setting discrimination using immobile elements. Earth and Planetary Science Letters, **27**, 211-218.

FREESTONE, I.C. and HAMILTON, D.L. 1980. The role of liquid immiscibility in the genesis of carbonatites. An experimental study. Contributions to Mineralogy and Petrology, **73**, 105-117.

FREY, F.A., GREEN, D.H. and ROY,S.D. 1978. Integrated models of basalt petrogenesis; A study of quartz tholeiites to olivine melilitites from South Eastern Australia utilising geochemical and experimental petrological data. Journal of Petrology, **19**, 463-513.

GAMOND, J.F. 1983. Displacement features associated with fault zones; a comparison between observed examples and experimental models. Journal of Structural Geology. **5**, 33-45.

GASPAR, J.G. and WYLLIE, P.J. 1982. Barium phlogopite from the Jacupiranga Carbonatite, Brazil. American Mineralogist, **67**, 997-1000.

GASPAR, J.G. and WYLLIE, P.J. 1983. Magnetite in carbonatites from the Jacupiranga Complex, Brazil. American Mineralogist,**68**, 195-213.

GEIST, D.J., BAKER, B.H. and McBIRNEY, A.R. 1985. GPP: A program package for creating and using geochemical data files. (Version for IBM PC and compatible microcomputers).

Centre for Volcanology, University of Oregon, Eugene, Oregon 97403.
GIBB, F.G.F. 1968. Flow differentiation in ultrabasic dykes of the Cullins and the Strathaird Peninsula, Isle of Skye, Scotland. Journal of Petrology, 9, 411-443.
GIBB, F.G.F. 1973. The zoned clinopyroxenes of the Shiant Isles Sill, Scotland. Journal of Petrology, 14, 203-30.
GIESECKE, K.L. 1910. Karl Ludwig Gieseckes Mineralogisches Reisejournal über Grönland, 1806-1813. Meddelelser om Grønland, 35.
GILL, R.C.O. 1972. Chemistry of peralkaline phonolite dykes from the Grønnedal-Íka area, South Greenland. Contributions to Mineralogy and Petrology, 34, 87-100.
GILL, R.C.O. 1972b. The geochemistry of the Grønnedal-Íka alkaline complex, South Greenland. Unpublished PhD Thesis, University of Durham.
GILL, R.C.O. 1973. Mechanism for the salic magma bias of continental alkali provinces. Nature Physical Science, 242, 41-42.
GITTINS, J. 1979. The Feldspathoidal Alkaline Rocks. In Yoder, H.S.Jr. (Ed) *The Evolution of the Igneous Rocks*, Princeton University Press.
GITTINS, J. and McKIE, D. 1980. Alkalic carbonatite magmas: Oldoinyo Lengai and its wider applicability. Lithos, 13, 213-215.
GLASSER, F.P. and OSBORN, E.F. 1960. The ternary system MgO - MnO - SiO_2. Journal of the American Ceramic Society. 43, 132-140.
GOLD, D.P. 1966. The average and typical chemical composition of carbonatites. International Mineralogical Association, 1964 meeting, India, 83-91.
GOLD, D.P. 1969. In *Geology of the Monteregian Hills*. Geological Association of Canada and Mineralogical Association of Canada Guidebook, Montreal, 43-62.
GOLDSCHMIDT, J.V. 1954. *Geochemistry.* Clarendon Press, Oxford.
GORDON, S.G. 1924. Minerals obtained in Greenland on the second Vaux-Academy expedition, 1923. Proceedings of the Academy of Natural Science, Philadelphia, 76, 249-268.
GORDON, S.G. 1927. On arfvedsonite, riebeckite and crocidolite from Greenland. Proceedings of the Academy of Natural Science, Philadelphia, 79, 193-205.
GRAPES, R., YAGI, K. and OKUMURA, K. Aenigmatite, sodic pyroxene, arfvedsonite and associated minerals from Morutu, Sakhalin. Contributions to Mineralogy and Petrology,69, 97-103.
GREEN, J.C. 1983. Geologic and geochemical evidence for the nature and developement of the Middle Proterozoic (Keweenawan) mid-continent rift of North America. Tectonophysics, 94, 413-437.
GREENWOOD, R.C. and EDGAR, A.D. 1984. Petrogenesis of the gabbros from Mt. St. Hilaire, Quebec, Canada. Geological Journal, 19, 353-376.
GUMPER, F. and POMEROY, P.W. 1970. Seismic wave velocities and earth structure on the African continent. Bulletin of the Seismological Society of America, 60, 651-668.
HAGGERTY, S.E. 1976. Opaque mineral oxides in terrestrial igneous rocks. In Rumble, D III (Ed) *Reviews in Mineralogy Volume 3: Oxide Minerals*, Mineralogical Society of America.
HALLS, H.C. 1978. The Late Precambrian Central North American Rift System – a survey of recent geological and geophysical investigations. In Ramberg, I.B. and Neumann, E.R. (Eds) *Tectonics and Geophysics of Continental Rifts.* Reidel, Dordrect, 111-123.
HAMILTON, D.L. 1961. Nephelines as crystallisation temperature indicators. Journal of Geology, 69, 321-329.
HAMILTON, D.L. and MACKENZIE, W.S. 1965. Phase equilibrium studies in the system $NaAlSiO_4$ (nepheline) - $KAlSiO_4$ (kalsilite) - SiO_2 - H_2O. Mineralogical Magazine, 34, 214-231.
HANSEN, K. 1980. Lamprophyres and carbonatitic lamprophyres related to rifting in the

Labrador Sea. Lithos 13, 145-152.
HARKER, A. 1909. *The natural history of igneous rocks.* [1965 facsimilie of original edition]. Hafner, New York. 384pp.
HARRIS, P.G. 1969. Basalt type and rift valley tectonism. Tectonophysics, 8, 427-36.
HARRISON, S. and HESSELBO, S.P. (Eds) 1983. Aberdeen University Geological Expedition to South Greenland. Report of Activity 1983. Unpublished Report, University of Aberdeen.
HART, S.R. 1964. The petrologic and isotopic mineral age relations of a contact zone in the Front Range, Colorado. Journal of Geology, 72, 493-526.
HART, S.R. and DAVIS, K.E. 1978. Nickel partitioning between olivine and silicate melt. Earth and Planetary Science Letters, 40, 203-219.
HARTMAN, P. 1969. Can Ti^{4+} replace Si^{4+} in silicates? Mineralogical Magazine, 37, 366-369.
HASKIN, L.A., FREY, F.A., SCHMITT, R.A. and SMITH, R.H. 1963. Meteoritic, solar and terrestrial rare earth distributions. In Ahrens, L.H., Press, S.K., Runcorn, S.K. and Urey, H.C. (Eds) *Physics and Chemistry of the Earth, 7.* Pergamon Press, Oxford, 167-321.
HAWKESWORTH, C.J., ROGERS, N.W., VAN CALSTEREN, P.W.C. and MENZIES, M.A. 1984. Mantle enrichment processes. Nature, London, **311**, 331-5.
HEINRICH, E.W. 1966. *The Geology of Carbonatites.* Rand-McNally, Chicago.
HEINRICH, K.F.J. 1967. Second national conference on electron probe microanalysis. Boston, USA. Paper No.7.
HELZ, R.T. 1973. Phase relationships of basalts in their melting range at P_{H_2O}=5kbar as a function of oxygen fugacity. Part 1: mafic phases. Journal of Petrology, **14**, 249-302.
HENDERSON, C.M.B. and GIBB, F.G.F. 1977. Formation of analcime in the Dippin Sill, Isle of Arran. Mineralogical Magazine, **41**, 534-7.
HENDERSON, C.M.B. and GIBB, F.G.F. 1983. Felsic mineral crystallisation trends from differentiating alkaline basic magmas. Contributions to Mineralogy and Petrology, **84**, 355-364.
HENDERSON, P. 1982. *Inorganic Geochemistry.* Pergamon Press, Oxford, 353pp.
HENDERSON, P. 1984. General geochemical properties and abundances of the Rare Earth Elements. In Henderson, P. (Ed) *Rare Earth Element Geochemistry*, Elsevier, Amsterdam.
HENRIKSEN, N. 1960. Structural analysis of a fault in south-west Greenland. Bulletin Grønlands Geologiske Undersøgelese, **26**, 40pp. (also Meddelelser om Grønland, **162**, No.9).
HESSELBO, S.P. 1983. Petrography and origin of feldspathic balls in a trachyte dyke. In Harrison, S.M. and Hesselbo, S.P. (Eds) *Aberdeen University Geological Expedition to South Greenland.* Unpublished Report of activities, University of Aberdeen.
HESSELBO, S.P. 1986. Pseudoleucite from the Gardar of South Greenland. Bulletin of the Geological Society of Denmark. **35**, 11-17.
HEUBNER, J.S. 1980. Pyroxene phase equilibria at low pressure. In Prewitt, C.T. (Ed) *Reviews in Mineralogy; volume 7: Pyroxenes.* Mineralogical Society of America.
HILLS, R.C. 1901. Description of the Spanish Peaks Quadrangle, Colorado. United States Geological Society Geological Atlas Folio **71**, 7p.
HODGSON, N.A. 1985. Carbonatites and associated rocks from the Cape Verde Islands. Unpublished PhD Thesis, University of Leicester.
HOLLISTER, L.S. and GANCARTZ, A.J. 1971. Compositional sector-zoning in clinopyroxene from the Narce area, Italy. American Mineralogist, **56**, 959-979.
HUCKENHOLZ, H.G. 1973. The origin of fassaite augite in the Hocheifel area, West Germany. Contributions to Mineralogy and Petrology, **40**, 315-326.
HUCKENHOLZ, H.G., SCHAIRER, J.F. and YODER, H.S. 1969. Synthesis and stability of ferri-diopside. In *Pyroxenes and Amphiboles: Crystal Chemistry and Phase Petrology.*

Mineralogical Society of America Special Paper No.2. 163-177.

HUGGINS, F.E., VIRGO, D. and HUCKENHOLZ, H.G. 1977a. Titanium containing silicate garnets II. The crystal chemistry of melanites and schorlomites. American Mineralogist, 62, 646-665.

HUGGINS, F.E., VIRGO, D. and HUCKENHOLZ, H.G. 1977b. Titanium containing silicate garnets I. The distribution of Al, Fe^{3+} and Ti^{4+} between octahedral and tetrahedral sites. American Mineralogist, 62, 475-490.

HUGHES, C.J. 1982. *Igneous Petrology.* Elsevier, Amsterdam.

HURLBURT, C.S. and GRIGGS, D.T. 1939. Igneous rocks of the High Wood Mountains, Montana. Geological Society of America Bulletin. 50, 1032-1112.

HUMPHRIS, S.E. 1884. The mobility of rare earth elements in the crust. In Henderson, P. (Ed) *Rare Earth Element Geochemistry*, Elsevier, Amsterdam.

IRVING, A.J. 1978. A review of experimental studies of crystal/liquid trace element partitioning. Geochimica et Cosmochimica Acta, 42, 743-770.

ITO, J. 1968. Silicate apatites and oxyapatites. American Mineralogist, 53, 890-907.

JAKES, P. and WHITE, A.J.R. 1972. Hornblendes from calc-alkaline volcanic rocks of island arcs and continental margins. American Mineralogist, 57, 887-902.

JONES, A.P. 1980. The petrology and structure of the Motzfeldt Centre, Igaliko, South Greenland. Unpublished PhD Thesis, University of Durham.

JONES, A.P. 1984, Mafic silicates from nepheline syenites of the Motzfeldt Centre, South Greenland. Mineralogical Magazine, 48, 1-12.

JONES, A.P. and PECKETT, A. 1980. Zirconium-bearing aegirines from Motzfeldt, South Greenland. Contributions to Mineralogy and Petrology, 75, 251-255.

JORGENSEN, D.B. 1971. Origin of patchy zoning in plagioclase from gabbroic rocks of southwestern Oregon. Bulletin of the Geological Society of America, 82, 2667-2670.

KAY, R. and GAST, P.W. 1973. The rare earth content and origin of alkali-rich basalts. Journal of Geology, 81, 653-682.

KEMPE, D.R.C. and DEER, W.A. 1970. The mineralogy of the Kangerdlugssuaq alkali intrusion, East Greenland. Meddelelser om Grønland, 190 (3), 95pp.

KIM, K.T. and BURLEY, B.J. 1971. Phase equilibria in the system $NaAlSi_3O_8$ - $NaAlSiO_4$ - H_2O with special emphasis on the stability of analcite. Canadian Journal of Earth Science, 8, 311-337.

KING, B.C. 1949. The Napak area of southern Karamoja, Uganda. Geological Survey of Uganda, Memoir V.

KIRK, R.D. 1955. The luminescence and tenebrescence of natural and synthetic sodalite. American Mineralogist, 40, 22.

KNIGHT, J.L. 1976. The classification and interpretation of the amphiboles. Unpublished PhD Thesis, University of Durham.

KOMAR, P.D. 1972a. Mechanical interactions of phenocrysts and flow differentiation of igneous dykes and sills. Bulletin of the Geological Society of America, 83, 973-988.

KOMAR, P.D. 1972b. Flow differentiaiton in igneous dykes and sills: Profiles of velocity and phenocryst concentration. Bulletin of the Geological Society of America, 83, 3443-3448.

KOSTER VAN GROOS, A.F. 1975. The distribution of Sr between coexisting silicate and carbonatite liquids at elevated pressures and temperatures. Geochimica et Cosmochimica Acta, 39, 27-34.

KOSTER VAN GROOS, A.F. and WYLLIE, P.J. 1966. Liquid immiscibility in the system Na_2O - Al_2O_3 - SiO_2 - CO_2 at pressures to 1kb. American Journal of Science, 264, 234-255.

KOSTER VAN GROOS, A.F. and WYLLIE, P.J. 1968. Liquid immiscibility in the join $NaAlSi_3O_8$

– Na_2CO_3 – H_2O and its bearing on the genesis of carbonatites. American Journal of Science, 266, 932-967.

KOSTER VAN GROOS, A.F. and WYLLIE, P.J. 1973. Liquid immiscibility in the join $NaAlSi_3O_8$ – $CaAlSi_2O_8$ – Na_2CO_3 – H_2O. American Journal of Science, 273, 465-487.

KRESTEN, P. 1979. The Alnö Complex. Discussion of the main features, bibliography, excursion guide. Nordic Carbonatite Symposium/Alnö. 21-26.5.

LACHENBRUCH, A.H. and SASS, J,H, 1978. Models of extending lithosphere and heat flow in the Basin and Range province. In Smith, R.B. and Eaton, G.P. (Eds) *Cenozoic and Regional Geophysics of the Western Cordillera.* 209-250. Geological Society of America Memoir 152.

LARSEN, L.M. 1976. Clinopyroxenes and coexisting mafic minerals from the alkaline Ilímaussaq intrusion, South Greenland. Journal of Petrology, **17**, 257-290.

LARSEN, L.M. 1977. Aenigmatites from the Ilímaussaq intrusion, South Greenland: Chemistry and petrological implications. Lithos, **10**, 257-70.

LARSEN, L.M. 1979. Distribution of REE and other trace elements between phenocrysts and peralkaline undersaturated magmas exemplified by rocks from the Gardar Igneous Province, South Greenland. Lithos, **12**, 303-315.

LARSEN, L.M. and STEENFELT, A. 1974. Alkali loss and retention in an iron-rich peralkaline dyke from the Gardar Province, South Greenland. Lithos, **7**, 81-90.

LAUBE, G.C. 1873. Geologische Beobachtungen, gesammelt während der Reise auf der 'Hansa' und gelegentlich der Aufenhaltes in Süd-Gronland. Sber. Akad. Wiss. Wien, maths-natural. Kl. **68**, 1, 1-93.

LAVES, F. 1952. Phase relations of the alkali feldspars. I. Introductory remarks. II. The stable and pseudostable phase relations in the alkali feldspar system. Journal of Geology, **60**, I. 436-450. II. 549-574.

LEAKE, B.E. 1978. Nomenclature of the amphiboles. Mineralogical Magazine, **42**, 533-563.

LE BAS, M.J. 1977. *Carbonatite - Nephelinite Volcanism.* John Wiley and Son, New York.

LE BAS, M.J. 1981. Carbonatite magmas. Mineralogical Magazine, **44**, 133-140.

LE BAS, M.J. 1987. Nephelinites and carbonatites. In Fitton, J.G. and Upton, B.G.J. (Eds) *Alkaline Igneous Rocks*, Geological Society Special Publication No. 30.

LE BAS, M.J., LE MAITRE, R.W., STRECKEISEN, A. and ZANETTIN, B. 1986. A chemical classification of volcanic rocks based on the Total Alkali - Silica diagram. Journal of Petrology, **27**, 745-750.

LLOYD, F.E. and BAILEY, D.K. 1975. Light element metasomatism of the continental mantle: The evidence and the consequences. Physics and Chemistry of the Earth, **9**, 389-416.

LOVERING, T.S. 1935. Theory of heat conduction applied to geological problems. Bulletin of the Geological Society of America, **46**, 69-94.

LUTTON, R.J. 1971. Tensile fracture mechanics from fracture surface morphology. In Clark, G.B. (Ed) *Dynamic Rock Mechanics.* Proceedings of the 12^{th} Symposium on Rock Mechanics, Port City Press, Baltimore, 561-571.

LE MAITRE, R.W. 1982. *Numerical Petrology.* Elsevier, Amsterdam. 281pp.

MACDONALD, R. 1969. The petrology of alkaline dykes from the Tugtutôq area, South Greenland. Meddelelser fra Dansk Geologisk Forening, **19**, 257-282.

MACDONALD, R. 1970. Mid-Gardar feldspathoidal dykes in the Tugtutôq region, South Greenland. Bulletin of the Geological Society of Denmark, **20**, 64-66.

MACDONALD, R. and EDGE, R.A. 1970. Trace element distribution in alkali dykes from the Tugtutôq region, South Greenland. Bulletin of the Geological Society of Denmark, **20**, 38-58.

MACDONALD, R. and PARKER, A. 1970. Zirconium in alkaline dykes from the Tugtutôq

region, South Greenland. Bulletin of the Geological Society of Denmark, 20, 59-63.
MACDONALD, R., UPTON, B.G.J. and THOMAS, J.E. 1973. Potassium- and fluorine-rich hydrous phases coexisting with peralkaline granite in South Greenland. Earth and Planetary Science Letters, 18, 217-222.
MAKAGON, V.M. and SHMAKIN, B.M. 1971. Triclinicity and barium content of potassium feldspars from muscovite pegmatites. International Ecological Review, 13, 1647-1679.
MARSH, J.S. 1973. Relationship between transform directions and alkaline igneous rock lineaments in Africa and South America. Earth and Planetary Science Letters, 18, 317-323.
MARAVIC, H. and MORTEANI, G. 1980. Petrology and geochemistry of the carbonatite and syenite complex of Leushe (NE Zaire). Lithos, 13, 159-170.
MARTIN, A.R. 1985. The evolution of the Tugtutôq - Ilímaussaq Dyke Swarm, Southwest Greenland. Unpublished PhD thesis, University of Edinburgh.
MARTIN, R.F., WHITLEY, J.E. and WOOLLEY, A.R. 1978. An investigation of rare earth mobility: fenitised quartzites, Borrolan Complex, NW Scotland. Contributions to Mineralogy and Petrology, 66, 69-73.
MAUDE, A.D. and WHITMORE, R.L. 1956. The wall effect and the viscosity of suspension. British Journal of Applied Physics, 7, 78.
McCALLUM, I.S. and CHARETE, M.P. 1978. Zr and Nb partition coefficients: Implications for the genesis of mare basalts, KREEP and seafloor basalts. Geochimica et Cosmochimica Acta, 42, 859-869.
McCONNEL, D. 1937. The substitution of SiO_4– and SO_4– groups for PO_4– groups in the apatite structure; ellestradite, the end member. American Mineralogist, 22, 977-986.
McDOWELL, S.D. 1986. Composition and structural state of co-existing feldspars, Salton Sea geothermal field. Mineralogical Magazine, 50, 75-84.
McKENZIE, D.P. 1978. Some remarks on the development of sedimentary basins. Earth and Planetary Science Letters, 40, 25-32.
McKENZIE, D.P. 1984, The generation and compaction of partially molten rock. Journal of Petrology, 25, 713-765.
McKENZIE, D.P. 1985. The extraction of magma from the crust and mantle. Earth and Planetary Science Letters, 74, 81-91.
MENZIES, M. 1983. Mantle and ultramafic xenoliths in alkaline magmas: Evidence for mantle heterogeneity modified by magmatic activity. In Hawkesworth, C.J. and Norry, M.J. (Eds) *Continental Basalts and Mantle Xenoliths.* Shiva, Nantwich, Cheshire.
MENZIES, M.A. and MURTHY, V.R. 1980. Nd and Sr isotopic geochemistry of hydrous mantle nodules and their host alkali basalts: Implications for local heterogeneities in metasomatically veined mantle. Earth and Planetary Science Letters, 46, 323-334.
MENZIES, M.A., ROGERS, N., TINDLE, A. and HAWKESWORTH, C.J. 1987. Metasomatic and enrichment processes in lithospheric peridotites, an effect of asthenosphere lithosphere interaction. In Menzies, M.A. and Hawkesworth, C.J. (Eds) *Mantle Metasomatism*, Academic Press, London.
MIDDLEMOST, E.A.K. 1974. Petrogenetic model for the origin of carbonatite. Lithos, 7, 275-278.
MILTON, C., INGRAM, B.L. and BLADE, L.V. 1961. Kimzeyite, a zirconium garnet from Magnet Cove, Arkansas. American Mineralogist, 46, 533-548.
MINEYEV, D.A. 1963. Geochemical differentiation of the rare-earths. Geochemistry (USSR) 12, 1129-1149.
MITCHELL, R.H. and BRUNFELT, A.O. 1974. Rare earth element geochemistry of kimberlites. Physics and Chemistry of the Earth, 9, 671-686.
MITCHELL, R.H. and BRUNFELT, A.O. 1975. Rare earth element geochemistry of the Fen

Alkaline Complex, Norway. Contributions to Mineralogy and Petrology, 52, 247-59.

MITCHELL, R.H. and PLATT, R.G. 1978. Mafic mineralogy of ferro-augite syenite from the Coldwell alkaline complex, Ontario, Canada. Journal of Petrology, 19, 627-51.

MÖLLER, P., MORTEANI, G. and SCHLEY, F. 1980. Discussion of REE distribution patterns of carbonatites and alkalic rocks. Lithos, 13, 171-179.

MORSE, S.A. 1969. Syenites. Annual Report of the Director of the Geophysical Laboratory, Washington. 67, 112-120.

MORSE, S.A. (Ed). 1977. The Nain anorthosite project, Labrador: Field Report 1976. Contribution No.26, Department of Geology and Geography. University of Massachusetts, Ambers, Mass. USA.

MYSEN, B.O. 1975. Solubility of volatiles in silicate melts at high pressure and temperature: the role of carbon dioxide and water in feldspar, pyroxene and feldspathoid melts. Annual Report of the Director of the Geophysical Laboratory, Washington, 74, 454-468.

MYSEN, B.O. 1976. The role of volatiles in silicate melts: Solubility of carbon dioxide and water in feldspar, pyroxene and feldspathoidal melts to 30kb and 1625°C. American Journal of Science, **276**, 969-996.

NAKAMURA, N. 1974. Determination of REE, Ba, Fe, Mg, Na and K in carbonaceous and ordinary chondrites. Geochimica et Cosmochimica Acta, **38**, 757-775.

NASH, W.P., CARMICHAEL, I.S.E. and JOHNSON, R.W. 1969. The mineralogy and petrology of Mt. Suswa, Kenya. Journal of Petrology, **10**, 409-439.

NASH, W.P. and WILKINSON, J.F.G. 1970. Shonkin Sag laccolith, Montana. I. Mafic minerals and estimates of temperature, pressure, oxygen fugacity and silica activity. Contributions to Mineralogy and Petrology, **25**, 241-269.

NATHAN, H.D. and VAN KIRK, C.K. 1978. A model of magmatic crystallisation. Journal of Petrology, **19**, 66-94.

NEUMANN, E.R. 1974. The distribution of Mn^{2+} and Fe^{2+} between ilmenites and magnetites in igneous rocks. American Journal of Science, 274, 1074-88.

NICHOLLS, G.D. 1971. Geochemical sampling problems in the analytical laboratory. Transactions/Section B of the Institution of Mining and Metallurgy, 80, B299-B304.

NICHOLLS, J., CARMICHAEL, I.S.E. and STORMER, J.G. 1971. Silica activity and P_{total} in igneous rocks. Contributions to Mineralogy and Petrology, **33**, 1-20.

NICHOLSON, R. 1985. The intrusion and deformation of Tertiary minor sheet intrusions, West Suardal, Isle of Skye, Scotland. Geological Journal, **20**, 53-72.

NICHOLSON, R. and POLLARD, D.D. 1985. Dilation and linkage of echelon cracks. Journal of Structural Geology, **7**, 583-590.

NIELSEN, T.F.D. 1979. The occurrence and formation of Ti-aegirines in peralkaline syenites. Contributions to Mineralogy and Petrology, 69, 235-244.

NORRISH, K. and HUTTON, J.T. 1969. An accurate X-ray spectrographic method for the analysis of a wide range of geological samples. Geochimica et Cosmochimica Acta, **33**, 431-453.

NORRY, M.J. and FITTON, J.G. 1983. Compositional differences between oceanic and continental basic lavas and their significance. In Hawksworth, C.J. and Norry, M.J. (Eds) *Continental Basalts and Mantle Xenoliths.* Shiva, Nantwich, Cheshire.

O'HARA, M.J., SAUNDERS, M.J. and MERCY, E.L.P. 1975. Garnet - peridotite, primary ultrabasic magma and eclogite: interpretation of upper mantle processes in kimberlite. Physics and Chemistry of the Earth, **9**, 571-604.

ORVILLE, P.M. 1963. Alkali ion exchange between vapour and feldspar phases. American Journal of Science**261**, 201-237.

PALACHE, C. 1937. The minerals of Franklin and Sterling Hill, Sussex County, New Jersey.

United States Geological Society Professional Paper, 180.

PAO, R.H.F. 1961. *Fluid Mechanics.* John Wiley, New York.

PARSONS, I. 1978. Feldspar and fluids in cooling plutons. Mineralogical Magazine, 42, 1-18.

PARSONS, I. 1979. The Klokken Gabbro - Syenite Complex, South Greenland: Cryptic variation and the origin of inversely graded layering. Journal of Petrology, 20, 653-694.

PATCHETT, P.J., BYLUND, G. and UPTON, B.G.J. 1978. Palaeomagnetism and the Grenville orogeny: New Rb-Sr ages from dolerites in Canada and Greenland. Earth and Planetary Science Letters, 40, 349-364.

PEARCE, J.A. 1982. The role of the subcontinental lithosphere in magma genesis. In Hawkesworth, C.J. and Norry, M.J. *Continental Basalts and Mantle Xenoliths*, Shiva, Nantwich, Cheshire.

PEARCE, J.A. 1983. Trace element characteristics of lavas from destructive plate boundaries. In Thorpe, R.S. (Ed) *Andesites*, Wiley, New York.

PEARCE, J.A. and CANN, J.R. 1973. Tectonic setting of basic volcanic rocks determined using trace element analyses. Earth and Planetary Science Letters, 19, 290-300.

PEARCE, J.A. and NORRY, M.J. 1979. Petrogenetic implications of Ti, Zr, Y and Nb variations in volcanic rocks. Contributions to Mineralogy and Petrology, 69, 33-47.

PEARCE, N.J.G. and EMELEUS, C.H. 1985. Geological investigations of the Igaliko Dyke Swarm, South Greenland. Rapport Grønlands Geologiske Undersøgelese, 125, 60-61.

PHILIBERT, J. 1963. X-ray optics and x-ray microanalysis. 3^{rd} International Symposium, Academic Press, 379-392.

PHILLIPS, R. Amphibole compositional space. Mineralogical Magazine, 35, 945-52.

PHILPOTTS, A.R. 1971. Immiscibility between feldspathic and gabbroic magmas. Nature Physical Science, 229, 107-109.

PHILPOTTS, A.R. 1976. Liquid immiscibility: Its probable extent and petrographic significance. American Journal of Science, 276, 1147-1177.

PHILPOTTS, A.R. 1981. A model for the generation of massif-type anorthosites. Canadian Mineralogist, 19, 233-253.

PHILPOTTS, A.R. and HODGSON, C.J. 1968. Liquid immiscibility in alkali rock genesis. 23^{rd} International Geological Congress, 2, 175-188.

PHILPOTTS, J.A. 1970. Redox estimation from a calculation of Eu^{2+} and Eu^{3+} concentrations in natural phases. Earth and Planetary Science Letters, 257-268.

PHILPOTTS, J.A. 1974. The Monteregian Hills. In Sørensen, H. (Ed) *The Alkaline Rocks*, Wiley, New York.

PINGEL, C. 1843. Om den, af Porphyrygange gjennembrudte Røde Sansten; det Sydlige Grøland. Kgl. Danske Vidensk, Selsk. Skr. 10, 19pp.

PIOTROWSKY, J.M. and EDGAR, A.D. 1970. Melting relations of undersaturated alkaline rocks from South Greenland. Meddelelser om Grønland, 181, Nr.9, 62pp.

PIPER, J.D.A. 1982. The Precambrian palaeomagnetic record. The case for the Proterozoic Supercontinent. Earth and Planetary Science Letters, 59, 61-81.

PLATT, R.G. and MITCHELL, R.H. 1982. The Marathon Dykes. Ultrabasic lamprophyres from the vicinity of McKellar Harbour, NW Ontario. American Mineralogist, 67, 907-916.

PLATT, R.G. and WOOLLEY, A.R. 1986. The mafic mineralogy of peralkaline syenites and granites of the Mulanje Complex, Malawi. Mineralogical Magazine, 50, 85-99.

POLDERVAART, A. and HESS, H.H. 1951. Pyroxenes in the crystallisation of basaltic magma. Journal of Geology, 59, 472-489.

POLLARD, D.D. 1973. Derivation and evaluation of a mechanical model for sheet intrusions. Tectonophysics, 19, 233-269.

POLLARD, D.D., MULLER, O.H. and DOCKSTADER, D.R. 1975. The form and growth of fingered sheet intrusions. Geological Society of America Bulletin, 86, 351-363.

POLLARD, D.D., SEGALL, P. and DELANEY, P.T. 1982. Formation and interpretation of dilatant echelon cracks. Geological Society of America Bulletin, 93, 1291-1303.

POULSEN, V. 1964. The sandstones of the Precambrian Eriksfjord Formation in South Greenland. Rapport Grønlands Geologiske Undersøgelese, Nr.2.

POWELL, M. 1978. The crystallisation history of the Igdlerfigssalik nepheline syenite intrusion, Greenland. Lithos, 11, 99-120.

POWELL, M. and POWELL, R. 1974. An olivine - clinopyroxene geothermometer. Contributions to Mineralogy and Petrology, 48, 249-263.

POWELL, R. and POWELL, M. 1977. Geothermometry and oxygen barometry using coexisting iron-titanium oxides: a reappraisal. Mineralogical Magazine, 41, 257-63.

RAMSAY, J.G. 1967. *Folding and Fracturing of Rocks.* McGraw-Hill, New York, 83-91.

REED, S.J.B. 1965. Characteristic fluoresence corrections in electron-probe microanalysis. British Journal of Applied Physics, 16, 913-926.

RHODES, J.M. 1969. On the chemistry of potassium feldspars in granititc rocks. Chemical Geology, 4, 373-392.

RIBBE, P.H. 1982. Titanite (sphene). In Ribbe, P.H. (Ed) *Reviews in Mineralogy, volume 5: Orthosilicates.* Second edition. Mineralogical Society of America, 450pp.

RICKARDS, M.J. and RIXON, L.K. 1983. Stress configuration in conjugate quartz vein arrays. Journal of Structural Geology, 5, 573-578.

ROCK, N.M.S. 1977. The nature and origin of lamprophyres: Some definitions, distinctions and derivations. Earth Science Reviews, 13,123-169.

ROCK, N.M.S. 1978. Petrology and petrogenesis of the Monchique Alkaline Complex, Southern Portugal. Journal of Petrology, 19, 171-214.

ROCK, N.M.S. 1984. The nature and origin of calc-alkaline lamprophyres: Minettes, vogesites, kersantites and spessartites. Transactions of the Royal Society, Edinburgh: Earth Sciences, 74, 193-227.

ROCK, N.M.S. 1986. The nature and origin of ultramafic lamprophyres: Alnöites and allied rocks. Journal of Petrology, 27, 155-196.

ROCK, N.M.S. 1987a. The nature and origin of lamprophyres: An overview. In Fitton, J.G. and Upton, B.G.J. (Eds) *Alkaline Igneous Rocks*, Geological Society Special Publication No. 30.

ROCK, N.M.S. 1987b. Kimberlites as varieties of lamprophyres. Proceedings of the 4^{th} International Kimberlite Conference, (in press).

ROSCOE, R. 1952. The viscosity of suspensions of rigid spheres. British Journal of Applied Physics, 3, 267-269.

ROSENBERG, P.E. 1974. Compositional variations in synthetic sphene (abstract). Geological Society of America Abstract with Program, 6, 1060.

ROUX, J. and HAMILTON, D.L. 1976. Primary igneous analcite – an experimental study. Journal of Petrology, 17, 244-257.

ROWBOTHAM, G. 1973. Hydrothermal synthesis and mineralogy of the alkali amphiboles. Unpublished PhD Thesis, University of Durham.

SAETHER, E. 1957. The alkaline rock province of Fen area in Southern Norway. Kge. naske Videns. Selsker. Skr. 1957 (1).

SAFFMAN, P.G. and TAYLOR, G. 1958. The penetration of a fluid into a porous medium or the Hele-Shaw cell containing a more viscous liquid. Royal Society fo London, Proceedings Serial A, 245, 312-329.

SAHAMA, Th.G. and HYTONEN, K. 1957. Kirschteinite, a natural analogue to synthetic

iron-monticellite, from the Belgian Congo. Mineralogical Magazine,31, 698-9.
SANDERSON, D.J.A. and MARCHINI, W.R.D. 1984. Transpression. Journal of Structural Geology, 6, 449-58.
SAUNDERS, A.D. 1984. The rare earth element characteristics of igneous rocks from the ocean basins. In Henderson, P. *Rare Earth Element Geochemistry*, Elsevier, Amsterdam.
SAUNDERS, A.D. and TARNEY, J. 1984. Geochemical characteristics of basaltic volcanism within back arc basins. In Kokelaar, B.P. and Howells, M.F. (Eds) *Marginal Basin Geology*, Geological Society of London Special Publication No.16.
SAUNDERS, A.D., TARNEY, J. and WEAVER, S.D. 1980. Transverse geochemical variations across the Antarctic Peninsula: Implications for the genesis of calc-alkaline magmas. Earth and Planetary Science Letters, 46, 344-360.
SCHARBERT, H.G. 1966. The alkali feldspars from microsyenite dykes of Southern Greenland. Mineralogical Magazine, 35, 903-919.
SCHARBERT, H.G. 1968. Microsyenite dykes from the northern part of the Ilímaussaq peninsula, Southern Greenland. Tschermaks Mineralogische und Petrographische Mittelungen, 12, 443-462.
SCHNETZLER, C.C. and PHILPOTTS, J.A. 1970. Partition coefficients of rare earth elements between igneous matrix material and rock forming mineral phenocrysts II. Geochimica et Cosmochimica Acta, 34, 331-340.
SECHER, K. and LARSEN, L.M. 1980. Geology and mineralogy of the Safartoq carbonatite complex, Southern West Greenland. Lithos, 13, 199-212.
SEGALL, P. and POLLARD, D.D. 1980. Mechanics of discontinuous faults. Journal of Geophysical Research, 85, 4337-50.
SHANNON, R.D. 1976. Revised effective ionic radii and systematic studies of interatomic distances in halides and chalcogenides. Acta Crystallographica Section A, 32, 751-767.
SHAW, H.R. 1972. Viscosities of magmatic silicate liquids – an empirical method of prediction. American Journal of Science, 272, 870-893.
SHEE, S.R. 1984. The oxide minerals of the Wesselton Mine Kimberlite, Kimberley, South Africa. In Kornprobst, J. (Ed) *Kimberlites I: Kimberlites and Related Rocks.* Proceedings of the Third International Kimberlites Conference, Elsevier, Amsterdam.
SHMAKIN, B.M. 1967. Barium orthoclase from Southern Yakutia and importance of barium as an indicator element. International Geological Review, 9, 1135-1137.
SILLÉN, L.G. and MARTELL, A.E. 1964. Stability constants of metal-ion complexes. Chemical Society of London Special Publication, 17, 754pp.
SIMKIN, T. 1967. Flow differentiation in the picritc sills of Northern Skye. In Wyllie, P.J. (Ed) *Ultramafic and Related Rocks.* J. Wiley, New York.
SIMKIN, T. and SMITH, J.V. 1970. Minor element distribution in olivine. Journal of Geology, 78, 304-325.
SMEDLEY, P. The petrochemistry of Dinantian volcanism in Northern Britain. Unpublished PhD thesis, University of Edinburgh.
SMITH, A.L. 1970. Sphene, perovskite and co-existing Fe-Ti oxide minerals. American Mineralogist, 55, 264-269.
SMITH, G., HÅLENIUS, U., ANNERSTEN, H. and ACKERMANN, L. 1983. Optical and Mössbauer spectra of manganese-bearing phlogopites: Fe^{3+}_{iv} – Mn^{2+}_{vi} pair absorbtion as the origin of reverse pleochroism. American Mineralogist, 68, 759-768.
SMITH, J.V, 1974. *Feldspar Minerals – I. Crystal Structure and Physical Properties.* Springer Verlag, Heidelberg, 627pp.
SMITH, J.V. 1982. Some chemical properties of feldspars. In Ribbe, P.H. (Ed) *Reviews in Mineralogy, Volume 2: Feldspar Mineralogy, second edition.* Mineralogical Society of

America.

SMITH, J.V. and DAWSON, J.B. 1975. Chemistry of Ti-poor spinels, ilmenites and rutiles from peridotite and eclogite xenoliths. Physics and Chemistry of the Earth, 9, 309-322.

SMITH, N.J. 1987. The age and structural setting of limestone and basalt on the Main Ring Fault of southeast Rhum, Inner Hebrides, Scotland. Unpublished MSc Thesis, University of Durham.

SMITH, P. and PARSONS, I. 1974. The alkali feldspar solvus at 1kb water-vapour pressure. Mineralogical Magazine, **39**, 747-767.

SMITH, R.P. 1973. Age and emplacement structures of Spanish Peaks Dykes, south-central Colorado. Geological Society of America Abstrascts with Program (Cordilleran Section), 5, No.1, 513.

SOOD, M.K. and EDGAR, A.D. 1970. Melting relations of undersaturated rocks. Meddelelser om Grønland, **181**, Nr.12, 125pp.

SPARKS, R.S.J. and HUPPERT, H.E. 1984. Density changes during fractional crystallisation of basaltic magmas: Fluid dynamic implications. Contributions to Mineralogy and Petrology, **85**, 300-309.

SPEER, J.A. and RIBBE, P.H. 1982. Miscellaneous orthosilicates. In Ribbe, P.H. (Ed). *Reviews in Mineralogy, Volume 5: Orthosilicates.* Mineralogical Society of America.

SPENCER, K.J. and LINDSLEY, D.H. 1981. A solution model for co-existing iron-titanium oxides. American Mineralogist, **66**, 1189-1201.

SPRY, A. 1969 *Metamorphic Textures.* Pergamon Press, Oxford, 350pp.

STEENSTRUP, K.V.J. 1909. Geologiske og antikvariske Iagttagelser; Julianehåb Distrikt. Meddelelser om Grønland, **34**, Nr.5.

STEENSTRUP, K.V.J. and KORNERUP, A. 1881. Beretning om Expeditionen til Julianehåbs Distrikt; 1876. Meddelelser om Grønland, **2**, Nr.1.

STEIGER, R.H. and JÄGER, E. 1977. Subcommision on geochronology: Convention on the use of decay constants in geo- and cosmology. Earth and Planetary Science Letters, **36**, 359.

STEPHENSON, D. 1972. Alkali clinopyroxenes from the nepheline syenites of the South Qôroq Centre, South Greenland. Lithos, **5**, 187-201.

STEPHENSON, D. 1973. The petrology and mineralogy of the South Qôroq Centre, Igaliko Complex, South Greenland. Unpublished PhD Thesis, University of Durham.

STEPHENSON, D. 1974. Mn and Ca enriched olivines from the nepheline syenites of the South Qôroq Centre, South Greenland. Lithos, **7**, 35-41.

STEPHENSON, D. 1976a. The South Qôroq Centre nepheline syenites, South Greenland, (petrology, felsic mineralogy and petrogenesis). Bulletin Grønlands Geologiske Undersøgelese, **118**.

STEPHENSON, D. 1976b. A simple shear model for the ductile deformation of high level intrusions in South Greenland. Journal of the Geological Society, London, **132**, 307-318.

STEPHENSON, D. and UPTON, B.G.J. 1982. Ferromagnesian silicates in a differentiated alkaline complex: Kûngnât Fjeld, South Greenland. Mineralogical Magazine, **46**, 283-300.

STEWART, D.B. and WRIGHT, T.L. 1974. Al/Si order and symmetry of natural alkali feldspars and the relationship of strained cell parameters to bulk composition. Bulletin Societé Français de Mineralogie et Crystallographie, **97**, 356-77.

STEWART, J.W. 1964. The Early Gardar igneous rocks of the Ilímaussaq area, South Greenland. Unpublished PhD Thesis, University of Durham.

STEWART, J.W. 1970. Precambrian alkaline – ultramafic/carbonatite volcanism at Qagssiarssuk, South Greenland. Bulletin Grønlands Geologiske Undersøgelese, **84**, (also Med-

delelser om Grønland, **186**, 4) 70pp.
STORMER J.C. 1972. Mineralogy and petrology of the Raton - Clayton volcanic field, Northeastern New Mexico. Bulletin of the Geological Society of America, **83**, 3299-3322.
STORMER J.C. 1973. Calcium zoning in olivine and its relationships to silica activity and pressure. Geochimica et Cosmochimica Acta, **37**, 1815-1821.
STORMER J.S. Jr. 1983. The effects of recalculation on estimates of temperature and oxygen fugacity from analyses of multicomponent iron-titanium oxides. American Mineralogist, **68**, 586-592.
STORMER J.S and CARMICHAEL, I.S.E. 1971. The free energy of sodalite and the behaviour of chloride, fluoride and sulphate in silicate magmas. American Mineralogist, **56**, 292-306.
STOSCH, H.G. 1982. Rare earth element partitioning between minerals from anhydrous spinel peridotite xenoliths. Geological Society of America, **46**, 793-811.
STRECKEISEN A.L. 1967. Classification and nomenclature of igneous rocks. Neues Jahrbuch für Mineralogie, Abhandlungen, **107**, 144-240.
STRECKEISEN A.L. 1976. To each plutonic rock its proper name. Earth Science Review, **12**, 1-33.
STRECKEISEN A.L. 1979. Classification and nomenclature of volcanic rocks, lamprophyres, carbonatites and melilitic rocks. Geology, **7**, 331-335.
STRECKEISEN A.L. 1980. Classification and nomenclature of volcanic rocks, lamprophyres, carbonatites and melilitic rocks: IUGS subcommision on the systematics of igneous rocks. Geol. Rundsch, **69**, 194-207.
SUN, C-O., WILLIAMS, R.J. and SUN, S-S. 1974. Distribution coefficients of Eu and Sr for plagioclase - liquid and clinopyroxene - liquid equilibria in oceanic ridge basalt: an experimental study. Geochimica et Cosmochimica Acta, **38**, 1415-1433.
SUN, S-S. 1980. Lead isotopic study of young volcanic rocks from mid ocean ridges, oceanic islands and island arcs. Philosophical Transactions of the Royal Society, London A297, 409-445.
SUN, S-S and HANSON, G.N. 1975a. Evolution of the mantle: geochemical evidence from alkali basalt. Geology, **3**, 297-302.
SUN, S-S. and HANSON, G.N. 1975b. Origin of Ross Island basanites and limitations upon the heterogeneity of mantle sources for alkali basalts and nephelinites. Contributions to Mineralogy and Petrology, **52**, 77-106.
SYKES, L.R. 1978. Intra-plate seismicity, reactivation of pre-existing zones of weakness and other tectonism post-dating continental fragmentation. Review of Geophysics and Space Physics, **16**, 621-688.
SØRENSEN, H. 1970. Internal structures and geological setting of three agpaitic intrusions – Khibina, and Lovozero of the Kola Peninsula and Ilímaussaq, South Greenland. Canadian Mineralogist, **10**, 299-334.
TCHALENKO, J.S. and AMBRASEYS, N.N. 1970. Structural analysis of Dasht-e Bayaz (Iran) earthquake fractures. Bulletin of the Geological Society of America, **81**, 1625-40.
TILLEY, C.E. and YODER, H.S. 1968. The pyroxenite facies conversion of volcanic and sub-volcanic melilite-bearing and other alkali ultramafic assemblages. Yearbook of the Carnegie Institution, Washington, **66**, 457-60.
THOMAS, C.W and NIXON, P.H. 1987. Lower crustal granulite xenoliths in carbonatite volcanoes of the Western Rift of East Africa. Mineralogical Magazine, **51**, 621-634.
THOMPSON, J.B. and WALDBAUM, D.R.. 1969. Mixing properties of sanidine crystalline solutions III. Calculations based on two-phase data. American Mineralogist, **54**, 811-838.
THOMPSON, R.N. 1977. Primary basalts and magma genesis III. Alban Hills, Roman Comagmatic Province, Central Italy. Contributions to Mineralogy and Petrology, **60**, 91-108.

THOMPSON, R.N. 1982. Magmatism of the British Tertiary Volcanic Province. Scottish Journal of Geology, **18**, 49-107.

THOMPSON, R.N. 1984. Dispatches from the basalt front, I. Experiments. Proceedings of the Geological Association, **95**, 249-262.

THOMPSON, R.N. 1986. Sources of basic magmas. Nature, London, **319**, 448-449.

THOMPSON, R.N. , ESSON, J. and DUNHAM, A.C. 1972. Major element chemical variation in the Eocene lavas of the Isle of Skye, Scotland. Journal of Petrology, **13**, 219-235.

THOMPSON, R.N., MORRISON, M.A., DICKIN, A.P. and HENDRY, G.L. 1983. Continental flood basalts ...Arachnids rule OK? In Hawkesworth, C.J. and Norry, M.J. (Eds) *Continental Basalts and Mantle Xenoliths.* Shiva, Nantwich, Cheshire.

THOMPSON, R.N., MORRISON, M.A., HENDRY, G.L. and PARRY, S.J. 1984. An assessment of the relative roles of crust and mantle in magma genesis: An elemental approach. Philosophical Transactions of the Royal Society, London, **A310**, 549-590.

THORNTON, C.P. and TUTTLE, O.F. 1960. Chemistry of igneous rocks: Part 1. Differentiation Index. American Journal of Science, **258**, 664-684.

TILLEY, C.E. 1922. Density, refractivity and composition relations of some natural glasses. Mineralogical Magazine, **19**, 275-294.

TILLEY, C.E. 1954. Nepheline - alkali feldpar paragenesis. American Journal of Science, **252**, 65-75.

TREIMAN, A.H. and ESSENE, E.J. 1983. Mantle eclogite and carbonate as sources of sodic carbonatites and alkali magmas. Nature. London, **302**, 700-703.

TREUIL, M. and VARET, J. 1973. Critères volcanologiques, pétrologiques et géochemiques de la genèse et de la différenciation des magmas basaltiques: Example de l'Afar. Bulletin de la Societie Geologique de France, 7^{em} series, **15**, 506-540.

TUKIAINEN, T., BRADSHAW, C. and EMELEUS, C.H. 1984. Geological radiochemistry of the Motzfeldt Centre of the Igaliko Complex, South Greenland. Rapport Grønlands Geologiske Undersøgelese, **120**, 78-83.

TWETO, O. 1951. Form and structure of sills near Pando, Colorado. Geological Society of America Bulletin, **62**, 507-532.

TWYMAN, J.G. and GITTINS, J. 1987. Alkalic carbonatite magmas: Parental or derivative. In Fitton, J.G. and Upton, B.G.J. (Eds) *Alkaline Igneous Rocks*, Geological Society Special Publication No. 30.

TYLER, R.C. and KING, B.C. 1967. The pyroxenes of the alkaline igneous complexes of Eastern Uganda. Mineralogical Magazine, **36**, 5-22.

UPTON, B.G.J. 1962. Geology of Tugtutôq and neighbouring islands, South Greenland. Part 1. Meddelelser om Grønland, **169**, Nr.8.

UPTON, B.G.J. 1964a. The geology of Tugtutôq and neighbouring islands, South Greenland. Part II. Nordmarkitic syenites and related alkaline rocks. Meddelelser om Grønland, **169**, Nr.3.

UPTON, B.G.J. 1964b. The geology of Tugtutôq and neighbouring islands, South Greenland. Part III. Olivine gabbros, syenogabbros and anorthosites. Meddelelser om Grønland, **169**, Nr.38.

UPTON, B.G.J. 1964c. The geology of Tugtutôq and neighbouring islands, South Greenland. Part IV. The nepheline syenites of the Hviddal Composite Dyke. Meddelelser om Grønland, **169**, No.3, 50-80. (Also Bulletin of the Grønlands Geologiske Undersøgelese, No.48).

UPTON, B.G.J. 1971. Melting experiments on chilled gabbros and syenogabbros. Yearbook of the Carnegie Institution, Washington, **70**, 112-118.

UPTON, B.G.J. 1974. The alkaline province of south-west Greenland. In Sørensen, H. (Ed),

The Alkaline Rocks, 221-238. Wiley, New York.

UPTON, B.G.J. and BLUNDELL, D.J. 1978. The Gardar Igneous Province, evidence for Proterozoic rifting. In Neumann, E.R. and Ramberg, I.B. (Eds), *Petrology and Geochemistry of Continental Rifts.* 163-172. D.Reidel Publishing Company, Dordrecht, Holland.

UPTON, B.G.J. and EMELEUS, C.H. 1987. Mid-Proterozoic alkaline magmatism in Southern Greenland: The Gardar Province. In Fitton, J.G. and Upton, B.G.J. (Eds) *Alkaline Igneous Rocks*, Geological Society Special Publication No. 30.

UPTON, B.G.J. and FITTON, J.G. 1985. Gardar dykes north of the Igaliko Syenite Complex, Southern Greenland. Rapport Grønlands Geologiske Undersøgelese, 127.

UPTON, B.G.J. and THOMAS, J.E. 1973. Precambrian potassic ultramafic rocks, South Greenland. Journal of Petrology, 14, 509-534.

UPTON, B.G.J. and THOMAS, J.E. 1980. The Tugtutôq Younger Giant Dyke Complex, South Greenland; Fractional crystallisation of transitional olivine basalt magma. Journal of Petrology, 21, 167-198.

UPTON, B.G.J., STEPHENSON, D. and MARTIN, A.R. 1985. The Tugtutôq Older Giant Dyke Complex: Mineralogy and geochemistry of an alkali gabbro - augite syenite - foyaite association in the Gardar Province of South Greenland. Mineralogical Magazine, 49, 623-642.

UPTON, B.G.J., THOMAS, J.E. and MACDONALD, R. 1971. Chemical variation within 3 alkaline Complexes in South Greenland. Lithos, 4, 163-184.

USSING, N.V. 1894. Mineraligisk - petrografiske Undersøgeleser af Grønlandske Nefelinsyeniter og beslægtede Bjærgarter. Anden del: De Kiselsyrefattige Hovedmineraler. Meddelelser om Grønland, 14, Nr.1.

USSING, N.V. 1912. The geology of the country around Julianehåb, Greenland. Meddelelser om Grønland, 38.

VAN BREEMEN, O. and UPTON, B.G.J. 1972. Age of some Gardar intrusive complexes, South Greenland. Bulletin of the Geological Society of America, 83, 3381-3390.

VIALON, P. 1979. Les déformations continues - discontinues des roches anisotrope. Eclog. geol. Helv., 72, 531-549.

VINOKUROV, V.M. 1966. Electron paramagnetic resonance data on isomorphism of manganese and iron ions in certain minerals. Geochemistry International, 3, 996-1002.

VOLLMER, R., OGDEN, P., SCHILLING, J.G., KINGSLEY, R.H. and WAGGONER, D.G. 1984. Nd and Sr isotopes in ultrapottasic rocks from Leucite Hills, Wyoming. Contributions to Mineralogy and Petrology, 87, 359-368.

VON ECKERMANN, H. 1948. *The Alkaline District of Alnö Island.* Stockholm AB, Kartografiska Institutet (Sveriges Geologiska Undersökning, 36).

VRBA, K. 1874. Beiträge zur kenntniss der Gesteine Süd-Grönlands. Sber. Akad. Wiss. Wein. Math. - naturw. Kl., 69, 1, 91-123.

WAGER, L.R. and DEER, W.A. 1939. Geological investigations in East Greenland, Part III. Petrology of the Skaergaard Intrusion, Kangerdlugssuaq, East Greenland. Meddelelser om Grønland, 105.

WALSH, J.N., BUCKLEY, F. and BARKER, J. 1981. The simultaneous determination of the rare-earth elements in rocks using inductively coupled plasma source spectrometry. Chemical Geology, 33, 141-153.

WALTON, B.J. 1965. Sanerutian appinitic rocks and Gardar dykes and diatremes north of Narssarssuaq, South Greenland. Meddelelser om Grønland, 179, Nr.9.

WATKINSON, D.H. and WYLLIE, P.J. 1971. Experimental studies of the compositional join $NaAlSiO_4$ – $CaCO_3$ – H_2O and the genesis of alkali rock - carbonatite complexes. Journal of Petrology, 12, 357-378.

WATSON, E.B. 1979. Zircon saturation in felsic liquids; experimental results and application to trace element geochemistry. Contributions to Mineralogy and Petrology, 70, 407-419.

WATT, W.S. 1966. Chemical analyses from the Gardar Igneous Province, South Greenland. Rapport Grønlands Geologiske Undersøgelese, 5.

WEDEPOHL, K.H. and MURAMATSU, Y. 1979. The chemical composition of kimberlites compared with the average composition of three basaltic magma types. 300-312. In Boyd, F.R. and Meyer, H.O.A. (Eds) *Kimberlites, diatremes and diamonds: their geology, petrology and geochemistry.* Proceedings of the 2nd International Kimberlite Conference, American Geophysical Union, Washington D.C.

WEGMANN, C.E. 1938. Geological investigations in Southern Greenland. Part I. On the structural divisions of Southern Greenland. Meddelelser om Grønland, 158, Nr.4.

WEILL, D.F. and McKAY, G.A. 1975. The partitioning of Mg, Fe, Sr, Ce, Sm, Eu and Yb in lunar igneous systems and a possible origin of KREEP by equilibrium partial melting . Proceedings of the 6th Lunar Scientific Conference, 1143-1158.

WELLMAN, T.R. 1970. The stability of sodalite in a synthetic syenite plus aqueous chloride fluid system. Journal of Petrology, 11, 49-71.

WENDLANDT, R.F. 1977. Barium-phlogopite from Haystack Butte, Highwood Mountains, Montana. Carnegie Institution of Washington Yearbook 76, 534-539.

WENDLANDT, R.F. and HARRISON, W.J. 1979. Rare earth partitioning between immiscible carbonate and silicate liquids and CO_2 vapour: Results and implications for the formation of Light Rare Earth-enriched rocks. Contributions to Mineralogy and Petrology, 69, 409-419.

WERNICKE, B. 1986. Whole lithosphere normal simple shear: an interpretaion of deep-reflection profiles in Great Britain. In Barazangi, M. and Brown, L. *Reflection Seismology: The Continental Crust,* Geodynamics Series Volume 14. American Geophysical Union, Washington D.C.

WHITE, R.S., SPENCE, G.D., FOWLER, S.R., McKENZIE, D.P., WESTBROOK, G.K. and BOWEN, A.N. 1987. Magmatism at rifted continental margins. Nature, **330**, 439-444.

WIEBE, R.A. 1980. Anorthositic magmas and the origin of Proterozoic anorthosite massifs. Nature, **286**, 564-567.

WIEBE, R.A. 1985. Proterozoic basalt dikes in the Nain anorthosite complex, Labrador. Canadian Journal of Earth Science, **22**, 1149-1157.

WILCOX, R.E., HARDING, T.P. and SEELY, D.R. 1973. Basic wrench tectonics. American Association of Petroleum Geologists' Bulletin, **57**, 74-96.

WILKINSON, J.F.G. 1957. The clinopyroxenes of a differentiated teschenite sill near Gunnedah, New South Wales. Geological Magazine, **94**, 123-134.

WILLS, K. 1974. The geological history of Southern Dominica and plutonic nodules of the Lesser Antilles. Unpublished PhD Thesis, University of Durham.

WINCHELL, A.N. and WINCHELL, H. 1951. *Elements of optical mineralogy. An introduction to microscopic petrography. Part II. Descriptions of Minerals.* Fourth edition. John Wiley and Sons, New York.

WONES, D.R. and EUGSTER, H.P. 1965. Stability of biotite: Experiments, theory and application. American Mineralogist, **50**, 1228-1272.

WONES, D.R. and GILBERT, M.C. 1982. Amphiboles in the igneous environment. In Velben, D.R. and Ribbe, P.H. *Reviews in Mineralogy Volume 9B. Amphiboles: Petrology and experimental phase relations.* Mineralogical Society of America.

WOOD, B.J. 1976. An olivine - clinopyroxene geothermometer. Contributions to Mineralogy and Petrology, **56**, 297-303.

WOOD, B.J. and FRASER, D.G. 1977. *Elementary Thermodynamics for Geologists.* Oxford

University Press, Oxford.

WOOLLEY, A.R. 1982. A discussion of carbonatite evolution and nomenclature and the generation of sodic and potassic fenites. Mineralogical Magazine, 46, 13-17.

WRIGHT, T.L. 1968. X-ray and optical study of alkali feldspar: II. An X-ray method for determining the composition and structural state from measurement of 2θ values for three reflections. American Mineralogist, 53, 88-104.

WRIGHT, T.L. and STEWART, D.B. 1968. X-ray and optical study of alkali feldspar: I. Determination of composition and structural state from refined unit cell parameters and 2V. American Mineralogist, 53, 38-87.

WYLLIE, P.J. 1977a. Effect of H_2O and CO_2 on magma generation in the crust and mantle. Journal of the Geological Society, London, 134, 215-234.

WYLLIE, P.J. 1977b. Mantle fluid compositions buffered by carbonates in peridotite - CO_2 - H_2O. Journal of Geology, 85, 187-208.

WYLLIE, P.J. 1978. Silicate - carbonatite systems with bearing on the origin and crystallisation of carbonatite. *Proceedings of the 1st International Symposium on Carbonatites*, Ministerio das Minas e Energia, Departmento Nacional da Produçao Mineral, Poços de Caldas, Minas Gerias, Brazil. 61-78.

WYLLIE, P.J. 1980. The origin of Kimberlites. Journal of Geophysical Research, 85, 6902-6910.

YAGI, K. 1953. Petrochemical studies on the alkalic rocks of Morotu District, Sakhalin. Bulletin of the Geological Society of America, 64, 769-810.

YAGI, K. 1966. The system acmite - diopside and its bearing on the stability of natural pyroxenes of the acmite - hedenbergite - diopside series. American Mineralogist, 51, 976-1000.

YAKOWITZ, H., MYKLEBUST, R.L. and HEINRICH, K.J.F. 1973. Frame: An on line correction procedure for quantitative electron probe microanalysis. National Bureau of Science Technical Note, 796.

YODER, H.S. Jr., STEWART, D.B. and SMITH, J.R. 1957. Ternary feldspars. Carnegie Institute of Washington Yearbook, 56, 206-214.

ZHARIKOV, V.A. and VLASOVA, D.K. 1955. The diagram: composition - properties for pyroxenes of the isomorphous series diopside - hedenbergite - johannsenite. Doklady Akad Nauk USSR, 105, 814-817.

ØDUM, H. 1927. Geologiske Iag Hagelser; Landet Øst for Igaliko Fjord. Meddelelser om Grønland, 74, Nr.4.